



University
of Glasgow

Bowey, Alan William (1996) *Predictions of soil behaviour using finite element analysis*. PhD thesis.

<http://theses.gla.ac.uk/1920/>

Copyright and moral rights for this thesis are retained by the author

A copy can be downloaded for personal non-commercial research or study, without prior permission or charge

This thesis cannot be reproduced or quoted extensively from without first obtaining permission in writing from the Author

The content must not be changed in any way or sold commercially in any format or medium without the formal permission of the Author

When referring to this work, full bibliographic details including the author, title, awarding institution and date of the thesis must be given

UNIVERSITY OF GLASGOW
DEPARTMENT OF CIVIL ENGINEERING

PREDICTIONS OF SOIL BEHAVIOUR USING
FINITE ELEMENT ANALYSIS

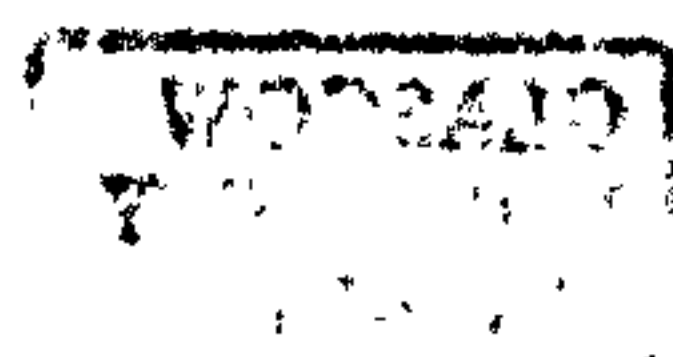
ALAN WILLIAM BOWEY M.Eng

JULY

1996

**A thesis submitted in fulfilment of the regulations governing the award of the
degree of Doctor of Philosophy.**

@ Alan William Bowey 1996



To Gillian.

ABSTRACT

Measured data from five geotechnical structures have been back analysed to determine, in each case, the set of material parameters that will permit a reasonable match to the observed pre-failure foundation response. Back analyses have been performed using simple constitutive soil models (Tresca, Mohr-Coulomb and modified Cam clay) as implemented in the finite element analysis package CRISP90.

Trial loading data are available from:

1. The rapid loading to failure of a soft clay soft foundation through a rigid reinforced concrete slab.
2. The loading to failure of a soft clay foundation via the rapid construction of a trial embankment.
3. The long-term behaviour of a soft clay foundation loaded via a stable trial embankment.
4. The behaviour of two long span, flexible culverts under (granular) backfill and imposed loads.

From comparison of the computed and observed responses conclusions have been drawn which have implications for the general application of finite element analysis to geotechnical problems; parameter selection for numerical analyses; and the essential requirements of the soil model for predicting soil behaviour.

In chapters 3, 4 and 5 the main concern of analyses was to reproduce the observed settlements, lateral displacements and excess pore water pressures induced within the soft clay foundations. Analyses primarily concentrated on the use of the modified Cam clay soil model. Particularly in chapter 3, the ability of modified Cam clay to predict the essential elements of the foundation behaviour was reasonable. However,

in chapters 4 and 5 predictions of lateral displacements and excess pore water pressures were poor. More accurate estimates of the observed lateral displacements and excess pore water pressures were obtained using empirical methods (hand calculations). The reason for the different quality of lateral displacements and excess pore water pressure predictions is thought, mainly, to be due to incomplete saturation of the soft clay at the trial embankment test site. The influence of incomplete saturation is thought to initially force a drained foundation response, which in the short term will give rise to smaller lateral displacements and excess pore water pressures than those predicted from fully undrained analyses. In the long term, further improvement of embankment lateral displacements and excess pore water pressures may be achieved through consideration of viscosity.

Accurate predictions of the observed surface settlement profiles were obtained using the modified Cam clay soil model for each of the soft clay studies. In each case, the surface settlement profiles were found to be significantly influenced by the selected elastic stiffness. To achieve an accurate description of the observed settlement response, values of elastic stiffness were selected from consideration of the anticipated deformations and stress changes induced within the foundation. This process of parameter selection was found to be more satisfactory than picking off the required parameters one by one from tests which have been performed in a traditional manner over ranges of deformation and stress change which are quite different from those expected. Despite the accurate prediction of surface settlements simultaneous prediction of settlements, lateral displacements and excess pore water pressures was not possible. The elements of soil behaviour thought necessary to be included within a numerical framework to allow simultaneous prediction of settlements, lateral displacements and excess pore water pressures are: anisotropy; degree of saturation; non-linear elasticity; and viscosity.

In chapters 8 and 9 the simple linear elastic, perfectly plastic Mohr-Coulomb soil model has been used to describe the behaviour of granular backfill surrounding two long span, flexible culverts under shallow cover conditions. Compaction and imposed live loads were modelled. In view of the soil parameters required to provide reasonable predictions of the observed behaviour, the simple Mohr-Coulomb soil

model is considered to be inappropriate for describing the culvert/backfill behaviour. From comparison of published flexible culvert case histories, the necessary elements of soil behaviour required within a soil model to predict the essential elements of flexible culvert behaviour (thrusts, bending moments and displacements) are thought to be: non-linear elasticity; a mean stress cap yield surface; and the inclusion of hysteresis. Further improvements may be achieved through improved modelling of the flexible culvert within the finite element mesh, e.g., use of curved beam elements or multi-noded isoparametric elements.

ACKNOWLEDGEMENTS

I would like to express my sincere thanks to my supervisor Professor David Muir Wood (formerly Cormack Professor, University of Glasgow) for his invaluable advice, encouragement and help throughout the course of this study.

I am grateful for the financial support extended by the Engineering and Physical Science Research Council (EPSRC) and the Transport Research Laboratory (TRL). Additionally, I am grateful to Fugro McClelland Ltd for kindly donating the trial loading data described in chapter 3.

I would also like to express my thanks to my friends and colleagues, both at Glasgow University and Fairhurst Geotechnical, for their support and encouragement.

Lastly, but not least, I acknowledge with humble gratitude the boundless patience, and encouragement of my wife and parents, without which this thesis would never have been completed.

TABLE OF CONTENTS

	Page
CHAPTER 1 INTRODUCTION	1
CHAPTER 2 NUMERICAL TOOLS	5
2.1. Introduction	5
2.2. Main program (CRISP)	6
2.2.1. Effective stress approach	6
2.2.2.1. Initial/In situ stress	9
2.2.2. Solution technique	14
2.2.3. Equilibrium check	15
2.3. Description of soil models used	16
2.3.1. Introduction	16
2.3.2. Postulate of normality	17
2.3.3. Elastic perfectly plastic soil models	18
2.3.3.1. Tresca yield criterion	19
2.3.3.2. Mohr-Coulomb yield criterion	22
2.3.4. Elasto-plastic soil model	24
2.3.4.1. Modified Cam clay soil model	25
2.3.4.2. Modified Cam clay and CRISP	29
CHAPTER 3 TRIAL LOADING ON SOFT CLAY	36
3.1. Introduction	36
3.2. Description of trial loading	37
3.3. Ground conditions	38
3.4. Soil parameters required for analyses	39
3.4.1. Parameters required for the isotropic elastic soil model	39
3.4.2. Parameters required for the linear elastic, perfectly plastic (Tresca) soil model	42
3.4.3. Parameters required for the elasto-plastic soil model, modified Cam clay.	46
3.4.4. Discussion	53
3.5. Modelling assumptions	53
3.6. Analyses	55
3.6.1. Introduction	55
3.6.2. Isotropic linear elastic analyses	56
3.6.2.1. Introduction	56
3.6.2.2. Initial analysis	56
3.6.2.3. Selection of elastic stiffness for analyses.	57
3.6.2.4. Undrained analyses	59
3.6.2.4. Discussion	61

	Page
3.6.3. Linear elastic, perfectly plastic (Tresca) soil model.	62
3.6.3.1. Introduction	62
3.6.3.2. Analyses	62
3.6.3.3. Discussion	64
3.6.4. Elasto-plastic (modified Cam clay) analyses	66
3.6.4.1. Introduction	66
3.6.4.2. Parameter selection	66
3.6.4.3. Discussion of results	71
3.6.4.4. Discussion	73
3.7. Conclusions	75
 CHAPTER 4 CUBZAC-LES-PONTS EMBANKMENT A	 119
4.1. Introduction	119
4.2. Details of trial loading and previous analyses	120
4.3. Ground conditions and parameters required for analyses	121
4.3.1. Introduction	121
4.3.2. Ground conditions	122
4.3.3. Elastic parameters κ and ν'	122
4.3.4. Compressibility, λ	124
4.3.5. Critical state parameters, e_{cs} and M	125
4.3.6. Preconsolidation stress	127
4.3.7. Permeability	129
4.3.7.1. Introduction	129
4.3.7.2. Selection of permeability for consolidation analyses	129
4.3.7.3. Review of some methods used to select permeability.	129
4.3.7.4. Discussion of permeability	132
4.4. Modelling assumptions	134
4.5. Results of analyses	135
4.5.1. Introduction	135
4.5.2. Undrained analyses	135
4.5.2.1. Displacements	135
4.5.2.2. Excess pore water pressures	136
4.5.2.3. Influence of the embankment	137
4.5.3. Discussion	138
4.6. Consolidation analyses	140
4.6.1. Alternative methods for excess pore water pressure predictions	141
4.6.2. Discussion of results	143
4.7. Discussion	145
4.8. Conclusions	146

	Page
CHAPTER 5 CUBZAC-LES-PONTS EMBANKMENT B	189
5.1. Introduction	189
5.2. Trial loading and numerical modelling	191
5.3. Material parameters for embankment B	192
5.4. Results and discussion	193
5.4.1. Introduction	193
5.4.2. Vertical displacements	194
5.4.3. Lateral displacement	196
5.4.4. Excess pore water pressure	200
5.5. Previous analysis	203
5.5.1. Introduction	203
5.5.2. Results and discussion	203
5.6. Conclusions	204
CHAPTER 6 SOFT CLAY; CONCLUSIONS	228
6.1. Trial loading	228
6.2. Embankment A	229
6.3. Embankment B	230
6.4. Necessary site investigation requirements for soft clay analyses	231
6.4.1. Elastic stiffness	231
6.4.2. Shear strength parameters	231A
6.4.3. Plasticity and preconsolidation parameters	231A
6.4.4. Permeability	231B
6.5. Empirical and semi-empirical methods	231B
CHAPTER 7 FLEXIBLE CULVERT ANALYSES	232
7.1. Introduction	232
7.2. Soil interaction; definition of the problem	233
7.2.1. Construction sequence	236
7.3. Review of flexible culvert design methods	237
7.3.1. Classical concepts	237
7.3.1.1. Spangler deflection theory	238
7.3.1.2. Ring compression theory	240
7.3.2. Closed-form analytical solutions	241
7.3.3. Duncan's design method	245
7.3.4. Constitutive soil models used to describe soil-culvert systems	247
7.3.4.1. Introduction	247
7.3.4.2. Constitutive soil models	247
7.3.4.3. Discussion	250
7.4. Finite element modelling	251
7.4.1. Modelling the culvert and backfill	252
7.4.2. Modelling of soil-culvert interface	252

	Page
7.4.3. Modelling the construction sequence	254
7.4.4. Representation of live loads	254
7.4.5. Determination of stresses around culvert	255
CHAPTER 8 MYTHOLMROYD CULVERT	267
8.1. Introduction	267
8.2. Mytholmroyd flexible culvert trial loading	268
8.3. Loading case A	269
8.3.1. Modelling of the soil-structure system	269
8.3.2. Initial parameter selection and analyses	270
8.3.3. Results, initial analyses	272
8.3.3.1. Thrust (ring compression forces)	272
8.3.3.2. Bending moment	274
8.3.3.3. Radial stress	275
8.3.3.4. Shear stress	276
8.3.3.5. Culvert displacements	277
8.3.3.6. Discussion	278
8.3.4. Parametric and back analysis studies	279
8.3.4.1. Introduction	279
8.3.4.2. Variation of the backfill modulus	279
8.3.4.3. Variation of Poisson's ratio	284
8.3.4.4. Variation of the angle of internal friction, ϕ'_f	288
8.3.4.5. Variation of the angle of dilation, ψ_f	290
8.3.4.6. Variation of the compaction pressure	292
8.3.4.6. Effect of no-fines concrete plinths	294
8.3.4.7. Discussion	296
8.4. Loading case B	299
8.4.1. Introduction	299
8.4.2. Initial analysis	299
8.4.2.1. Culvert thrusts	300
8.4.2.2. Bending moment distributions	301
8.4.2.3. Radial stress	302
8.4.2.4. Shear stress	303
8.4.2.5. Culvert displacements	303
8.4.2.6. Discussion	303
8.4.3. Case B; parametric study	304
8.4.3.1. Introduction	304
8.4.3.2. Effect of backfill Young's modulus, E'_f	305
8.4.3.3. Variation of Poisson's ratio	308
8.4.3.4. Variation of the angle of internal friction, ϕ'_f	309
8.4.3.5. Effect of compaction pressure	310

	Page
8.4.3.6. Effect of no-fines concrete plinths	312
8.4.3.7. Discussion	313
8.5. Trial loading, case C	314
8.5.1. Introduction	314
8.5.2. Description of analysis and parameters	315
8.5.3. Results of analyses	316
8.5.3.1. Case C; results	317
8.5.3.2. Comparison of case B and C	318
8.5.4. Discussion	319
8.6. Conclusions	322
 CHAPTER 9 QUY WATER CULVERT	 425
9.1. Introduction	425
9.2. Description of case history; Quy Water	426
9.3. Modelling of soil-culvert system	427
9.4. Initial analysis and results	429
9.4.1. Introduction	429
9.4.2. Results, construction behaviour	429
9.4.3. Results, live load behaviour	433
9.4.4. Discussion	434
9.5. Curved culvert elements	436
9.5.1. Introduction	436
9.5.2. Discretisation of the culvert using curved elements	436
9.5.3. Results with curved elements	438
9.5.3.1. Thrust behaviour	438
9.5.3.2. Radial stress, σ_r	439
9.5.3.3. Shear stress, $\tau_{r\theta}$	440
9.5.3.4. Bending moments and displacements	440
9.5.4. Discussion	442
9.6. Conclusions	446
 CHAPTER 10 CONCLUSIONS AND RECOMMENDATIONS	 476
10.1. Introduction	476
10.2. Conclusions	476
10.2.1. General application of finite element analysis and modelling assumptions	476
10.2.2. Soft clay; necessary requirements of a soil model	477
10.2.3. Site investigation and laboratory tests data	478
10.2.4. Flexible culvert analyses	479
10.2.5. Empirical and semi-empirical hand calculation methods	480

	Page
10.3. Recommendations	481
10.3.1. Soft clay	481
10.3.2. Flexible culverts	482
LIST OF REFERENCES	483

CHAPTER 1

1. Introduction

Geotechnical predictions are arguably the most important of civil engineering predictions. As a result geotechnical engineers are especially damned and blessed by the importance of their predictions (Lambe, 1973). The need for accurate geotechnical predictions, driven by increasingly demanding Employer's requirements, has therefore challenged geotechnical engineers and researchers to progressively improve their methods of prediction. Recently the increasing availability of digital computers has encouraged the development of advanced numerical techniques as design tools, the most publicised of which is finite element analysis. The reason for the attraction of finite element analysis to geotechnical engineers is that the method is versatile, and it has provided a platform for constitutive laws from which accurate numerical predictions of field behaviours previously thought of as intractable (e.g. plasticity, visco-plasticity, soil dynamics) have been made (Britto and Gunn, 1987). Published literature contains a great number of studies describing the successful application of finite element analysis to geotechnical problems, a few of which are contained within the references of this thesis.

As mentioned previously, finite element analysis only provides a platform from which numerical predictions of soil behaviour can be made. The relationship between the physical soil behaviour and predictions of this behaviour is bridged by the constitutive law (or soil model) implemented within a finite element framework. Over the past two decades the understanding of real soil behaviour has advanced considerably; consequently the race to research and develop increasingly complex soil models incorporating higher-levels of soil behaviour, has similarly increased apace. To date, many soil models are extremely complex requiring many soil parameters. The demands of these soil models typically go beyond the resources available for commercial site investigations; as a result, many of the high-level constitutive laws are very rarely used outside research institutions. Due to resource constraints constitutive laws commonly used in geotechnical engineering to describe monotonic

loadings, are simple linear elastic, perfectly plastic or elasto-plastic relationships employing an associated flow rule. Examples of soil models frequently used in practice which employ these simple constitutive laws are the classical soil models, Tresca and Mohr-Coulomb, and the critical state soil models, Cam clay and modified Cam clay (Roscoe and Schofield, 1963 and Roscoe and Burland, 1968). These soil models are well documented in published literature and are quite capable of predicting well some important aspects of soil behaviour, e.g., Indraratna et al. (1992) and Schnaid et al. (1993).

Irrespective of the level of complexity of the constitutive law used, accurate predictions of soil behaviour require effective selection and use of the adopted soil model. Essential features of a soil model required to provide accurate predictions; therefore need to be clearly understood. Deficiencies of simple models and consequently recommendations to use an alternative, more complex soil model are also widely documented in published literature. However, what is not clear, and is especially lacking within a commercial environment, is information describing which features of soil behaviour should be present within a soil model to provide accurate predictions. Such a data base should be useful to practising geotechnical engineers requiring an accurate but quick solution to a particular problem.

Further enhancement of the effectiveness of the chosen soil model can be achieved through careful selection of model parameters. This aspect of numerical modelling is fundamental to the accuracy of predictions (Lambe, 1973 and Gens, 1994). Despite the recognised importance of parameter selection, published literature is deficient in studies describing a framework of parameter selection for particular geotechnical problems. However, this weak link may be a result of limited soils data provided by modern-day site investigation practice.

In this thesis the fundamental themes associated with using a constitutive law within a finite element framework have been further investigated. These themes (essential elements of a soil model required to provide accurate predictions; and a framework of parameter selection for geotechnical problems) have been investigated through back analysis of trial loading data using simple constitutive laws incorporated within a

finite element system (CRISP90). Trial loading data were available for four common geotechnical problems:

1. The loading to failure of a soft clay foundation using a reinforced concrete slab.
2. The short-term behaviour of a soft clay foundation loaded to failure under embankment loading.
3. The long-term (consolidation) behaviour of a soft clay foundation under embankment loading.
4. The behaviour of two flexible, long span culverts under granular backfill and imposed loads.

The loading events are monotonic (the dynamic effects associated with compaction of the backfill around the flexible culverts were not considered). All analyses performed are autopsies or type C1 predictions (Lambe, 1973) of the loading event. Despite the continuation of the loading to failure, trial loadings (1) and (2), the main concern of analyses was to reproduce the observed pre-failure foundation response. This was achieved by repeatedly adjusting the soil model parameters. Particular care was taken to ensure the variation of soil model parameters was justifiable and within the bounds of available soil data. Using this process of trial and error optimum parameter sets were obtained, and hence a framework of parameter selection for each loading event suggested. Conclusions concerning the necessary features of a soil model to provide accurate predictions were obtained by comparing predictions of the loading event with those obtained by previous researchers using soil models (and finite element programs) of differing complexity from those used in this thesis. The finite element program and soil models (or tools) used in this thesis are briefly described in chapter 2.

The discussion commences with the trial loadings performed on soft clay; each is considered in a separate chapter (chapters 3-5), the order of which is the same as that presented above. For each trial loading, simple constitutive laws were used to describe the foundation response. The constitutive laws used were linear elastic, perfectly plastic, Tresca soil model, and an elasto-plastic law, modified Cam clay. These soil models were chosen because of their frequent use in practice for describing soft clay behaviour. Conclusions common to each of the soft clay studies are summarised and briefly discussed in chapter 6.

The flexible culverts are introduced to the discussion in chapter 7, which includes a brief review of flexible culvert behaviour and methods of analysis. Back analysis of the culvert trial loading data are described in chapters 8 and 9. Conclusions arising following back analysis of the observed flexible culvert behaviour are discussed at the end of chapter 9. The behaviour of the granular backfill was described using a simple linear elastic, perfectly plastic soil model with the onset of failure described by the Mohr-Coulomb failure criterion. A non-associated flow rule was employed.

Conclusions particular to the themes investigated in this thesis are briefly discussed in chapter 10. Additionally, recommendations for future work required to improve numerical modelling of problems of soil/structure interaction, similar to those presented in this thesis, are also briefly discussed in chapter 10.

CHAPTER 2

2.1 Introduction

In this chapter a brief description of CRISP and the soil models used in analyses described in this thesis is given. Details of CRISP and the constitutive soil models were extracted from Britto and Gunn (1987), Chen and Mizuno (1990) and Muir Wood (1990). The main elements of CRISP are described in section 2.2. The constitutive soil models used in analyses are described in section 2.3.

All analyses described within this thesis were performed using the standard version of the finite element computer program CRISP (Britto and Gunn, 1987). The program CRISP (the acronym of which stands for **CR**Itical State Program) was originally developed at Cambridge University starting as far back as 1975 (Zytynski, 1976) under the acronym of MZSOL. Since then the program has undergone many modifications and improvements to arrive in its current form.

The acronym CRISP is a banner name which represents a suite of FORTRAN programs which make up the finite element software package CRISP. The most important of these programs are the Geometry program and the Main program. The Geometry program processes and creates a store file of all the information describing the finite element mesh, which is subsequently read by the main program which performs all the numerical calculations for a given problem.

A number of constitutive relationships are available within CRISP, these include,

1. Elastic (isotropic and anisotropic)
2. Inhomogenous elastic (properties varying with depth)
3. Elastic perfectly plastic with a yield criterion defined by either von Mises, Tresca, Drucker-Prager or Mohr-Coulomb.
4. Critical state models: Cam clay, modified Cam clay and the Schofield soil model.

In this study most use was made of the elastic perfectly plastic Tresca and Mohr-Coulomb soil models and the critical state modified Cam clay soil model. These models are described in further detail in section 2.3.

Analyses may be undrained, drained or fully coupled (Biot) consolidation analyses of two dimensional plane strain or axisymmetric (with axisymmetric loading) solid bodies. The work described in this thesis was simplified to two dimensional plane strain analyses using undrained, drained and consolidation (coupled undrained/draind) behaviour.

In CRISP there are eight different element types, full details of which are not presented here. For the analyses described in this thesis, discretisation of the foundation soil was performed using linear strain triangular elements and linear strain quadratic elements. For consolidation analyses (chapter 5) the corresponding consolidation linear strain triangular and quadratic elements (with displacements and pore pressure unknown at the element corners) were used.

CRISP allows elements to be added or removed to simulate construction or excavation. The implied loadings for both these cases are automatically calculated by the main program. This feature of CRISP was used during the embankment and flexible culvert analyses (chapters 4, 5 and 8) to simulate embankment construction and backfilling around the culvert.

2.2 Main Program

2.2.1 Effective stress approach

Conventional finite element analyses of geotechnical problems use a total stress approach, assuming the soil to be a single-phase, incompressible material. This approach significantly limits the scope of computational modelling of soils and no account can be made of the developing pore pressures. CRISP uses a more

fundamental approach, assuming that the soil is a two-phase material comprising a porous, compressible solid (the soil skeleton) with the void spaces completely filled with water. Taking separate account of the soil skeleton and pore fluid requires the use of effective stress methods. The effective stress law is given in relation (2.1).

$$\sigma = \sigma' + mu \quad (2.1)$$

where σ is the total stress; σ' is the total effective stress; u is the pore water pressure and m is a vector indicating which stress terms participate in the effective stress relation. For example, for a two-dimensional plane strain condition;

$$\sigma = [\sigma_x \quad \sigma_y \quad \sigma_z \quad \tau_{xy} \quad 0 \quad 0]^T \quad (2.2)$$

$$\sigma' = [\sigma'_x \quad \sigma'_y \quad \sigma'_z \quad \tau_{xy} \quad 0 \quad 0]^T \quad (2.3)$$

and

$$m = [1 \quad 1 \quad 1 \quad 0 \quad 0 \quad 0] \quad (2.4)$$

The advantages of the effective stress approach to modelling are that a description of the soil effective stress anywhere within the soil can be obtained, i.e. a description of stress states with respect to the yield stress, and pore water pressure changes due to undrained loading are calculated. Additionally, this approach enables a description of the development of deformations and pore pressures with time for a consolidation analysis. To understand how CRISP does this first requires some description of the incremental effective stress-strain relations.

Suppose an element of soil undergoes an increment of total stress change $\delta\sigma$ resulting in a change of pore pressure δu and incremental strain $\delta\epsilon$. The resulting change in effective stress $\delta\sigma'$ can be related to the incremental strains by relation (2.5).

$$\sigma' = D'\delta\epsilon \quad (2.5)$$

The matrix D' is (in three dimensions) a 6x6 effective stress modulus matrix and may describe either an elastic-perfectly plastic or an elasto-plastic law.

Assuming that the volumetric strain experienced by the soil is due entirely to a change in volume of pore water, the volumetric strain experienced by the soil element, and the volumetric strain experienced by the pore water are given by relations (2.6) and (2.7).

$$\epsilon_{ps} = m^T \delta \epsilon \quad (2.6)$$

$$\epsilon_{pw} = \left[\frac{(1 + e_o)}{e_o} \right] m^T \delta \epsilon \quad (2.7)$$

where e_o is the current voids ratio.

The change in pore water pressure, δu , is given by,

$$u = K_w \left[\frac{(1 + e_o)}{e_o} \right] m^T \delta \epsilon \quad (2.8)$$

where K_w is the bulk modulus of the pore water, and for undrained analyses is normally set between 50 and 500 times the effective bulk modulus of the soil, K' .

Therefore, combining the incremental effective stress-strain relation (relation (2.8)) and the effective stress law (relation (2.1)) gives

$$\sigma = D' \delta \epsilon + m K_w \left[\frac{(1 + e_o)}{e_o} \right] m^T \delta \epsilon \quad (2.9)$$

Relation (2.9) forms the basis of the effective stress approach used by CRISP. For comparison the incremental constitutive relation in terms of total stress is presented in relation (2.9a).

$$\sigma = D \delta \epsilon \quad (2.9a)$$

where D is (in three dimensions) a 6×6 total stress modulus matrix and may describe either an elastic perfectly plastic or an elasto-plastic law.

CRISP uses relation (2.9) in the following way.

1. For an undrained analysis, material property data required for input into the main program must relate to changes in effective stress. This leads to more detailed and demanding testing procedures to obtain the appropriate parameters.
2. The volumetric stiffness of the pore water is added separately to the element stiffness matrices calculated by CRISP.
3. Following the solution of the finite element equations CRISP calculates the changes in effective stresses and pore water pressure separately.

The scope of computational modelling of soil using the constitutive soil models implemented in CRISP with an effective stress approach is significantly widened.

2.2.1.1 Initial/In situ stress

The in situ stresses are needed for non-linear material modelling, e.g. modified Cam clay (or any elasto-plastic soil model), since the stiffness matrix of a finite element will be dependent on the stress state within the element. Clearly, for an effective stress approach the in situ stress conditions must be specified in terms of effective stress. Alternatively, using a total stress approach the in situ stresses are specified in terms of total stress and no description of pore pressure is given. The effective stress approach also allows versatility in being able to take into account different ground water conditions. In two dimensions, plane strain, the initial stresses for an effective stress analysis comprise the vertical effective stress, σ'_y ($=\sigma'_v$), the horizontal effective stress, σ'_x ($=\sigma'_h$), the pore pressure, u , and the shear stress τ_{xy} . Shear stress τ_{xy} is zero.

Many soils have been deposited over areas of large lateral extent, and the deformations that these soils have experienced during and after deposition have been essentially one-dimensional, with little or no possibility for a soil element to have moved or deformed laterally. Hence, shear stresses on the vertical and horizontal planes, τ_{xy} are zero. Principal stress directions are therefore vertical and horizontal, horizontal stresses are equal, $\sigma'_x = \sigma'_z$; (convention, y-axis vertical (plane of page); x-axis horizontal (perpendicular to plane of page)).

Determination of the vertical effective stress is straightforward and is calculated from relation (2.10).

$$\sigma'_{vi} = \sigma_{vi} - u_i \quad (2.10)$$

where σ_{vi} is the in situ total vertical stress and is given by relation (2.11).

$$\sigma'_{vi} = \gamma y \quad (2.11)$$

where γ is the bulk density of the soil and y is the depth within the soil mass at which the total vertical stress is required.

The in situ pore water pressure is calculated using relation (2.12), assuming a static head of water within the soil.

$$u_i = \gamma_w (y - y_i) \quad (2.12)$$

where γ_w is the unit weight of water; y_i is the depth to water table from the ground surface and y is the depth at which the pore pressure is required.

The horizontal in situ effective stresses, σ'_{hi} were calculated from the vertical effective stresses using relation (2.13)

$$\sigma'_{hi} = K_o \sigma'_{vi} \quad (2.13)$$

where K_o is the coefficient of earth pressure at rest.

Experimental evidence does indicate that the coefficient of earth pressure, K_o , is dependent on the stress history or overconsolidation ratio, n , of the soil (Ladd, 1965, Schmidt, 1966; Meyerhof, 1976 and Muir Wood, 1990). Many methods have been proposed to estimate K_o (Mayne and Kulhawy, 1982; Muir Wood, 1990) researchers (Britto and Gunn, 1987) have found that most of these methods are not entirely satisfactory, but are dependent on the soil characteristics.

The complexity of estimating an appropriate value of K_o is evident from Fig 2.1 which represents the simplified stress history of a homogeneous soil deposit with horizontal ground surface. Stress path OA represents virgin loading of the soil (deposition) and the ratio of effective horizontal to vertical effective stress is constant,

$$\frac{\sigma'_{honc}}{\sigma'_{vonc}} = K_{onc} \quad (2.14)$$

where K_{onc} is the coefficient of earth pressure at rest and is given by relation (2.15)

$$K_{onc} = 1 - \sin\phi \quad (2.15)$$

Relation (2.15) proposed by Jaky (1948) is every engineer's favourite. Mayne and Kulhawy (1982) from examination of soil data from over 170 different sites determined that relation (2.15) was valid for cohesive soils but only moderately valid for cohesionless soils. This is evident from Fig 2.2 (Wroth, 1972 and Ladd, et al., 1977), which shows values of K_{onc} determined from triaxial compression tests. Relation (2.15) provides a good approximation of the measured values of K_{onc} for the clay. Values of K_{onc} for the sand are less well defined by relation (2.15). Consequently, throughout this study values of K_{onc} have been estimated using relation (2.15) for the soft clay analyses reported in chapters 3, 4 and 5.

Unloading and subsequent reloading of the soil generally results in a loop as shown in Fig 2.1; experimental measurements during one-dimensional unloading show significant curvature of the effective stress path BC. Therefore, the stress ratio σ'_h/σ'_v is not constant, the current value of σ'_h/σ'_v or K_o is dependent on the overconsolidation ratio or magnitude of unloading. Wroth (1975) suggests that if the degree of overconsolidation is small, $n < 2$, then a linear relationship can be assumed for the unloading process, ABC Fig 2.1, relation (2.16).

$$K_o = nK_o - (n-1)\frac{v'}{1+v'} \quad (2.16)$$

where v' is the effective stress value of Poisson's ratio. Schmidt (1966) determined a simple expression from plotting K_{onc} against overconsolidation ratio, n , relation (2.17).

$$K_o = K_{onc} n^a \quad (2.17)$$

where a is the rebound parameter.

Schmid (1966) proposed that parameter a was related to the effective angle of friction, ϕ' , of the soil, (Fig 2.3) (Schmidt, 1966 and Mayne and Kulhawy, 1982).

$$K_o = K_{onc} n^{\sin\phi'} \quad (2.18)$$

Meyerhof (1976) that the value of $a=0.5$, which appears to be an average of the data shown (corresponding to $\phi'=30$ degrees) in Fig 2.3, was reasonable to use for most soils, giving,

$$K_o = K_{onc} n^{0.5} \quad (2.19)$$

As can be seen from Fig 2.4(a) (Muir Wood 1990) relation (2.19) provides a good fit to the experimental observations of K_0 obtained for Boston Blue clay ($I_p=0.15$; $\phi'=32.75$ degrees) (Ladd, 1965). For comparison values of K_0 are also shown estimated using relation (2.16) (Wroth, 1975) for values of Poisson's ratio, $\nu'=0.2$ and 0.3 . Additionally, values of K_0 determined using relation (2.16) are significantly influenced by the chosen value of Poisson's ratio. It is evident therefore, that if this relation is going to be used to estimate K_0 values then values of Poisson's ratio will need to be accurately known. Very often this is not the case and values of Poisson's ratio are selected arbitrarily or from experience. Values of Poisson's ratio can be determined from an empirical link with plasticity index, I_p (Wroth, 1975) Fig 2.4(b). Values of Poisson's ratio were estimated from one-dimensional unloading data of a number of soils. The plasticity index of Boston blue clay is approximately, $I_p=15\%$, from Fig 2.4(b) this gives a Poisson's ratio of approximately 0.28 . As can be seen from Fig 2.4(a) this significantly underestimates the measured values of K_0 using relation (2.16). A value of Poisson's ratio, $\nu'=0.22$ was determined from experimental observations of the Boston blue clay, as can be seen from Fig 2.4(a) using relation (2.16) and assuming a $\nu'=0.22$ is only accurate from an overconsolidation range of $1 \leq n \leq 4$.

Mayne and Kulhawy (1982) determined from experimental observations of clays and sands for overconsolidation ratios of $4 \leq n \leq 10$ that variation of K_0 with n is approximately dependent on the effective angle of friction, ϕ' , as suggested by Schmidt (1966) relation (2.18).

Therefore, for the soft clays studied here relation (2.18) was used to estimate K_0 as far as was possible given the available data. In situations where available data were sparse (chapter 3) relation (2.19) was used in preference. Relation (2.15) was used throughout to determine K_{onc} .

Alternatively, when using the Cam clay models in situ stresses can be determined by performing an analysis (using CRISP) in which a soil mass is subject to the stress history which is believed to have been applied. This approach is theoretically consistent with the subsequent analysis but suffers from the disadvantage that modified Cam clay is not very successful in predicting values of K_{onc} (Britto and Gunn, 1987). This is also demonstrated in Fig 2.5 (Muir Wood, 1990) which presents

values of K_{onc} estimated using the modified Cam clay soil model for various values of Poisson's ratio, ν' , and critical state parameter $\Lambda = \frac{\lambda - \kappa}{\lambda}$; where κ and λ are the slopes of the unload-reload and normal compression lines in an oedometer test. As can be seen from Fig 2.5 the modified Cam clay model tends to overestimate the value of K_{onc} determined using relation (2.15). Experimental data seem to support the correctness of (2.15).

2.2.2 Solution technique

CRISP uses an incremental or tangent stiffness approach when analysing non-linear problems. In CRISP the small-displacement, small strain approach is used since this avoids the numerical complexity of incorporating geometric non-linearity. For most monotonic geotechnical problems small displacement theory is usually satisfactory (Carter et al., 1977 and Britto and Gunn, 1987). The non-linearity therefore arises from material non-linearity which arises when the stress-strain relation for the material is non-linear, e.g. the elasto-plastic models (section 2.3.3).

In order to use the tangent stiffness approach the applied loads (or displacements) are divided into a number of increments. For each increment the stiffness matrix of the system is based on the stress state at the beginning of the increment and is assumed to be constant throughout the increment. Unlike more advanced finite element programs e.g. ICFEP (Imperial College Finite Element Program) (Potts and Gens, 1984) and DIANA SWANDYNE II (Chan, 1988) no iteration is performed during the increment to ensure that the stress state at the end of the increment is consistent with the constitutive model. As a result, errors can accumulate as the CRISP analysis progresses unless a large number of increments is used implying a small load (or displacement) increase in each increment. Potts and Ganendra (1991) have found that the tangent stiffness approach is sensitive to increment size especially for analyses involving normally consolidated clay. Therefore, throughout this study checks have been performed to ensure that the solution is independent of increment size.

2.2.3 Equilibrium check

In the Main Program an equilibrium check has been incorporated to ensure that equilibrium is satisfied at the end of each increment. In this equilibrium check the stresses in the elements currently in the mesh are integrated over the volume to calculate the equivalent nodal loads and these are then compared with external loadings (self-weight loading of the soil is considered as part of the external loading). The difference is then expressed as a percentage of the applied loading, relation (2.20).

$$\%error = \frac{|(Q_{PL} + Q_{SW}) - Q_{ES}|}{Q_{ES}} \quad (2.20)$$

where Q_{PL} is the sum of pressure loads applied along an element boundary; Q_{SW} is the sum of self-weight or distributed loads; Q_{ES} is the sum of nodal loads equivalent to element stresses summed for all elements present in the current mesh.

CRISP attempts to correct any equilibrium errors (or out-of-balance loads) by adding these to the next load increment. Britto and Gunn (1987) suggest that small load (or displacement) increments are required in order to ensure that the stresses calculated at the end of each increment are consistent with the applied loading.

For the soft clay work equilibrium error was not typically a problem except when failure of the system had occurred (trial loadings to failure chapters 3 and 4). However, the pre-failure response of the foundation was of most interest throughout this study. Some large 'blips' in the equilibrium error (typically >20%) did occur during the consolidation analyses (chapter 5) when the drainage conditions were introduced into the analysis, however, these errors quickly dissipated within a few increments (usually less than 5). The equilibrium error posed a particular problem in the culvert analyses, particularly during the backfilling operation. Therefore, an incremental-iterative scheme was implemented (Davies et al., 1993) until no residual

nodal force was more than a given percentage of the maximum applied nodal force. In this work the tolerance was set at 20%.

2.3 Description of soil models used

2.3.1 Introduction

In this section a brief description of the constitutive soil models (tools) used in this study are described. Details of the soil models have been extracted from Britto and Gunn (1987), Chen and Mizuno (1990) and Muir Wood (1990).

The soil models implemented within the standard version of CRISP are models which are commonly used for most geotechnical analysis. Throughout this study most use was made of the elastic perfectly plastic Tresca and Mohr-Coulomb soil models and the elasto-plastic effective stress soil model, modified Cam clay (Roscoe and Burland, 1968).

A brief description of these models and their implementation within CRISP is given in section 2.3.3. Details of the models used have been included within the text to provide the reader with a reference of the models (or tools) used from which an engineering description of the given problems were obtained. The model text is by no means complete and if a more detailed description of these models is required then more detailed texts such as Schofield and Wroth (1968), Chen and Mizuno (1990) and Muir Wood (1990) should be sought.

For convenience the models have been divided into two groups; elastic perfectly plastic and elasto-plastic (modified Cam clay). The elastic perfectly plastic models are considered first.

Prior to the description of the models some discussion of flow rules is required as the soft clay and flexible culvert work employ differing concepts.

2.3.2 Postulate of normality

The models which have been implemented within the standard version of CRISP assume a postulate of normality. The postulate of normality assumes that the plastic strain increment vector induced due to an increment of stress, $\delta\sigma$, applied to a plastic material, is normal to the current yield locus. This implies that the plastic potential function, $g(\sigma_1, \sigma_2, \sigma_3)$, for the material is equal to the yield function, $f(\sigma_1, \sigma_2, \sigma_3)$,

$$f = g \quad (2.21)$$

and the plastic strain increment is given by (2.22)

$$\varepsilon_{ij}^p = \delta m \frac{\delta f}{\delta \sigma_{ij}} \quad (2.22)$$

where δm is known as the plastic multiplier (δm has been used instead of the more commonly used $\delta\lambda$ to avoid confusion with the use of λ in critical state soil mechanics).

This assumption of coincident plastic potential and yield functions is also known as "associated" flow. When the plastic potential and yield function are not equal the flow rule is described as "non-associated" and the plastic strain increment is normal to the plastic potential function, $g(\sigma_1, \sigma_2, \sigma_3)$, Fig 2.6(a) and (b). The plastic strain increment vector is then given by relation (2.23).

$$\varepsilon_{ij}^p = \delta m \frac{\delta g}{\delta \sigma_{ij}} \quad (2.23)$$

Investigations by Graham, Noonan and Lew (1983) on Winnipeg clay have found that the plastic strain increment vectors can be assumed to be approximately normal to the average yield locus. The deviation from normality was found to vary between

± 20 degrees, but given the uncertainty from which the average yield curve is drawn these deviations were assumed to be minor.

For clays the assumption of normality is reasonable and for most static loading situations on clays the postulate of normality will provide reasonable results (Britto and Gunn, 1987). However, the normality condition can significantly overestimate plastic strains when strain-softening behaviour (dilation or expansion) is occurring (Chen and Mizuno, 1990) e.g. reloading of heavily overconsolidated clays.

For sands and gravels the postulate of normality is not appropriate due to the highly dilational nature of these materials. Poorooshasb et al. (1966) using dense Ottawa sand have found that the assumption of normality, will result in greater negative plastic volumetric strains (volumetric expansion or dilation) than would actually be observed. Numerical predictions of the stress: strain response of sands using elastic-plastic models (Lade, 1977; Vermeer, 1984 and Chen and Mizuno, 1990) are most accurate assuming a non-associate flow rule. Consequently, analyses describing culvert behaviour (chapters 7-9) required the implementation of a non-associated flow rule (Davies et al., 1993) to the Mohr-Coloumb soil model to suitably describe the granular backfill behaviour. Implementation of the non-associated flow rule was not part of this study.

2.3.3 Elastic perfectly plastic soil models

Elastic perfectly plastic soil models are still successfully used in many practical geotechnical engineering problems. The concept of perfect plasticity is a much simplified assumption of the complex plastic behaviour of soils, and as will be shown in subsequent chapters can provide an accurate solution to some common loading situations. The attraction of the elastic perfectly plastic soil models, particularly in the presence of more rigorous and widely available elasto-plastic soil models, is primarily simplicity but also due to the fact that the few material parameters that define these models can usually be determined from standard, uncomplicated tests. The elastic perfectly plastic soil models used in this study were the Tresca soil model and the Mohr-Coulomb soil model, which are fully defined by three and four material

parameters respectively. A comparatively "simple" elasto-plastic model, e.g. modified Cam clay, requires five material parameters together with a description of stress history. Additionally, application of the more simple elasto-plastic models is not necessarily straightforward.

Fig 2.7 shows the idealisation known as elastic perfectly plastic. The first part of the curve is linear and isotropic elastic until the material yields, $\sigma = \sigma_{yd}$; where σ_{yd} is the yield stress of the material. Once yield has occurred the material continues to deform at a constant yield stress. The material exhibits no strain hardening. The onset of yield is defined by a yield criterion, classical descriptions of yield are given by the Tresca and Mohr-Coulomb yield criteria. Incremental plastic strains $\delta\epsilon$ are given by relation (2.22).

2.3.3.1 Tresca yield criterion

The Tresca model or maximum shear stress criterion dates back to 1864 and was originally proposed to describe a yield criterion for metals. The Tresca criterion (or maximum shear stress criterion) implies that metal yielding occurs when the maximum shear stress reaches a critical level. This occurs when the principal stress satisfy relation (2.24).

$$|\tau| = c \quad (2.24)$$

or

$$\text{Max} \left(\frac{|\sigma_1 - \sigma_2|}{2}, \frac{|\sigma_2 - \sigma_3|}{2}, \frac{|\sigma_3 - \sigma_1|}{2} \right) = c \quad (2.24a)$$

where τ is the shear strength of the material and c is the yield stress of the material determined from the pure shear test and $\sigma_1, \sigma_2, \sigma_3$ may be the major, minor or

intermediate principal stress. The Tresca model assumes that the material is frictionless, $\phi=0.0$.

The three-dimensional view of the Tresca yield criteria in principal stress space is shown in Fig 2.8. As can be seen relation (2.24) represents a prismatic surface, the cross section of which is a regular hexagon. The prism is centred on the hydrostatic axis, the line on which all three principal stresses are equal ($\sigma_1=\sigma_2=\sigma_3$). As already noted the Tresca criterion was developed primarily for metals, the yield strength of which is insensitive to the hydrostatic pressure. Hence the yield criterion involves only differences of principal stresses and is not dependent on the current value of mean stress, p , relation (2.25).

$$p = \left(\frac{\sigma_1 + \sigma_2 + \sigma_3}{3} \right) \quad (2.25)$$

This limits the application of the Tresca model to situations of loading of fully saturated soil (clays) using a total stress approach. Typically, the Tresca model is used in calculations of bearing capacity of soils.

The classical Tresca model as implemented in the standard version of CRISP requires the specification of three, total stress material parameters, Young's modulus, E_u , Poisson's ratio, ν_u , and the undrained shear strength, c_u . The data input format is the same for each of the four elastic perfectly plastic soil models implemented in CRISP and therefore includes the parameter ϕ , the angle of internal friction of the material, required for the Drucker-Prager and Mohr-Coulomb soil models. The Tresca model describes purely undrained shearing and does not include material friction, therefore ϕ must be set to zero. This also applies to the von Mises soil model, however this model was not used throughout this study.

In conventional plane strain axes, t : s ; where $t = \frac{\sigma_1 - \sigma_3}{2}$ and $s = \frac{\sigma_1 + \sigma_3}{2}$, the Tresca yield surface becomes a straight line parallel to the mean total stress axis, s , located at $t=c_u$, Fig 2.9. (Note that this surface is both a yield surface and failure surface.) For

stress states, $t < c_u$, the soil is described as isotropic elastic, the size of this region is controlled by the undrained shear strength, c_u .

In undrained analyses a condition of constant volume is imposed, hence the total stress undrained bulk modulus, K_u , must be infinite. This implies that the soil is incompressible and from relation (2.26), the undrained Poisson's ratio, $\nu_u = 0.5$.

$$K_u = \frac{E_u}{3(1-2\nu_u)} \quad (2.26)$$

To avoid numerical problems caused by a division by zero in relation (2.26), $\nu_u = 0.499$ is typically used in analyses. Elastic undrained total stress analyses were performed using the Tresca model in chapter 3 to investigate the initial stiff elastic foundation response to a trial loading. Elastic behaviour was ensured by inputting very high values of the undrained shear strength, c_u , such that the failure envelope was at stress states far higher than those produced by the trial loading. A value of $c_u = 5000 \text{ kPa}$ was found to be appropriate for this. Behaviour within the elastic region is controlled through variation of a single parameter, E_u . The model automatically calculates the remaining elastic parameters G_u and K_u using relations (2.27) and (2.28).

$$G_u = \frac{E_u}{2(1+\nu_u)} \quad (2.27)$$

$$K_u = \frac{E_u}{3(1-2\nu_u)} \quad (2.28)(2.26\text{bis})$$

Selection of the elastic parameter E_u is described in detail in chapter 3.

The implementation of the elastic perfectly plastic models with CRISP allows a linear variation with depth of the Young's modulus, E_u , and undrained shear strength, c_u , Fig 2.10. Undrained parameters E_u and c_u have been used here because it is the Tresca model which is being described, however the drained parameters E' and c' can also be made to vary linearly with depth as may be required for the Mohr-Coulomb or Drucker-Prager soil models. Poisson's ratio ν_u , is assumed to remain constant. Parameters m_e and m_c , specified directly by the user in the input file, describe the rate

of increase of Young's modulus and undrained shear strength with depth. It is recognised that Young's modulus E_u , is dependent on the induced strain level within the soil and does not exhibit an obvious linear variation with depth as does the undrained shear strength, c_u , (compare Fig 3.18 and Fig 3.16). However, use of this method enables the Young's modulus, E_u , to be tailored to the assumed depth profile of strain using a suitable relationship. This approach was most used in chapter 3 to describe the elastic stiffness of the clay foundation.

2.3.3.2 The Mohr-Coulomb yield criterion

The Mohr-Coulomb criterion is the most renowned failure criterion in soil mechanics. This criterion was proposed solely for geotechnical materials and takes into account, unlike the Tresca or von Mises criteria, the effects of hydrostatic pressure on the strength. This criterion states that if at a point on any plane within a soil mass the shear stress becomes equal to the shear strength of the soil defined by relation (2.29), failure will occur at that point.

$$\tau_f = \sigma'_f \tan \phi' + c' \quad (2.29)$$

where τ_f is the shear strength of the soil; σ'_f is the effective stress at failure normal to the failure plane and c' and ϕ' are the effective shear strength parameters.

At failure the straight line represented by relation (2.27). For the special case of frictionless materials for which $\phi=0$, relation (2.27) reduces to the Tresca, maximum shear stress criterion, $\tau_f=c$.

In three dimensional stress space the Mohr-Coloumb criterion is represented by relation (2.30) describing an irregular hexagonal pyramid, Fig 2.11.

$$(\sigma'_1 - \sigma'_3) = \sin \phi' (\sigma'_1 + \sigma'_3 + 2c' \cot \phi') \quad (2.30)$$

where σ'_1 and σ'_3 are the major and minor principal effective stresses respectively.

The Mohr-Coulomb failure criterion can also be represented in terms of conventional plane stress axes, σ : τ . This plot represents any state of stress as a stress point and the failure envelope is represented by relation (2.31).

$$\frac{1}{2}(\sigma'_1 - \sigma'_3) = a' + \frac{1}{2}(\sigma'_1 + \sigma'_3) \tan \alpha' \quad (2.31)$$

where a' and α' are modified shear strength parameters,

$$\alpha' = \tan^{-1}(\sin \phi') \quad (2.32)$$

and

$$a' = c' \cos \phi' \quad (2.33)$$

The simplicity of the Mohr-Coulomb criterion has led to its wide use to describe many practical geotechnical problems. However, although it is an improvement on the Tresca yield criteria and enables an effective stress approach to be adopted it is still too simple as an assumption of plasticity, as soils typically show evidence of volumetric yielding under isotropic stress changes, where the Mohr-Coulomb soil model suggests elastic behaviour.

Use of the Mohr-Coulomb model within CRISP requires the specification of four effective stress soil parameters, Young's modulus, E' , Poisson's ratio ν' , and the effective stress shear strength parameters c' and ϕ' . The Mohr-Coulomb criterion is best used within CRISP to describe, using an effective stress approach, drained and limited consolidation analyses. In this study the Mohr-Coulomb criterion was most used to describe the behaviour of granular backfill material during the flexible culvert work, Chapter 7. The criterion was also used to describe the behaviour of granular embankments, chapters 4 and 5, and for comparison with the more complex elastoplastic analyses using modified Cam clay. Modified Cam clay was used to describe the long term consolidation behaviour of a soft clay foundation under embankment loading, chapter 5.

2.3.4 Elasto-plastic soil model

The elastic perfectly plastic soil models described in the previous section provide a reasonable first approximation to soil behaviour. It is well known that actual soil behaviour is far more complex and during the process of increments of plastic deformation, the yield surface changes size, shape and location. Inclusion of these aspects of soil plasticity into elasto-plastic soil models is described using a hardening rule. In their simplest form the main difference between the elasto-plastic and elastic perfectly plastic soil models is the inclusion of a hardening law.

There are several types of hardening rules which are used to describe the growth of subsequent yield surfaces for strain-hardening (or softening) materials. The elasto-plastic model used, modified Cam clay, employs an isotropic hardening rule. For such a hardening rule the initial yield surface is assumed to expand or contract uniformly without any distortion during plasticity. The isotropic hardening rule is the most simple and is rarely used outwith simple monotonic loading situations (Chen and Mizuno, 1990) such as those described in this thesis. For more complex models hardening rules such as kinematic (the yield surface can translate as a rigid body in stress space) or mixed hardening (a combination of both isotropic and kinematic hardening) are required.

The inclusion of a hardening rule requires some adjustment of the plastic strain increment vector, $\delta\epsilon_{ij}^p$. As for the elastic perfectly plastic materials the plastic strain increment is given by relation (2.34).

$$\epsilon_{ij}^p = \delta m \frac{\partial f}{\partial \sigma_{ij}} \quad (2.34)(2.22\text{bis})$$

where δm is the plastic multiplier. Inclusion of a hardening rule forces δm to be a function of hardening, described as the hardening modulus, H' .

$$\delta m \propto \frac{1}{H'} \quad (2.35)$$

The hardening modulus depends on the stress and strain states and loading history.

Mathematical formulation of the elasto-plastic model is more complex than the elastic perfectly plastic soils models, and application of these models to geotechnical engineering can also be troublesome. Throughout this study a single elasto-plastic soil model has been used, the modified Cam clay soil model. A brief description of this model is given in the next section.

2.3.4.1. Modified Cam clay model

The modified Cam clay model (Roscoe and Burland, 1968) is an isotropic, non-linear elastic, strain-hardening plastic model. This model was developed at Cambridge University during the 1960s and the term "modified" was added to distinguish it from an earlier Cam clay model (Roscoe and Schofield, 1963), a description of which is not given here.

The modified Cam clay yield locus and coincident plastic potentials are described by ellipses centred on the effective mean stress axis, p' , Fig 2.12(a) relation (2.36).

$$\frac{p'}{p'_0} = \frac{M^2}{M^2 + \eta^2} \quad (2.36)$$

where η is a stress ratio and is equal to q/p' ; q is the deviator stress and p' is the current mean effective stress. Relation (2.36) describes a set of ellipses all having the same shape, controlled by the shape parameter M , all passing through the origin, and having sizes controlled by p'_0 . When the soil is yielding the yield locus expands or contracts isotropically with constant shape.

Stress states within the yield locus are described as isotropic, non-linear elastic, the elastic stiffness being dependent on the mean effective stress p' . Recoverable changes in volumetric strain, $\delta\epsilon_p^e$, accompany any changes in mean effective stress p' , relation (2.37)

$$\delta\epsilon_p^e = \kappa \frac{\delta p'}{v p'} \quad (2.37)$$

Relation (2.37) links changes in volumetric strain, ϵ_p^e , with changes in the logarithm of mean effective stress for elastic unloading-reloading of the soil and implies a linear relation in the compression plane, of slope κ , Fig 2.12(c). In CRISP the elastic stiffness properties of stress states within the yield locus are defined by specification of a single value of κ for all elastic stress states.

Estimates of κ are typically obtained from one-dimensional unloading, oedometer test data. Unloading in an oedometer test is not a constant stress ratio unloading process as required by the Cam clay model. This therefore, leaves the selection of appropriate values of κ open to some interpretation.

In the original formulation of the Cam clay models it is assumed that there are no elastic shear strains, ϵ_q^e . In terms of the conventional elastic parameters this means that the shear modulus G is infinite which forces Poisson's ratio, $\nu'=-1$. It is not possible to implement this in CRISP or any other displacement based finite element program. Therefore, to avoid numerical problems, (division by zero), and to achieve better modelling inside the yield surface, CRISP allows an extra elastic parameter, shear modulus G or Poisson's ratio ν' , to be specified and elastic shear strains are calculated, using relation (2.38), assuming a constant shear modulus.

$$\epsilon_q^e = \frac{\delta q}{3G} \quad (2.38)$$

where δq is the change in deviator stress.

If a constant value of Poisson's ratio is assumed then the shear modulus, G , can be deduced from the effective bulk modulus, K' .

$$G = \frac{3K'(1-2\nu')}{2(1+\nu')} \quad (2.39)$$

The effective bulk modulus, K' is pressure dependent and is obtained by differentiating the equation of the unload - reload line, relation (2.40).

$$K' = \frac{\nu p}{\kappa} \quad (2.40)$$

Then elastic shear strains are given by (2.41).

$$\varepsilon_{\theta}^e = \frac{2(1+\nu')\delta q\kappa}{(9(1-2\nu')\nu p')} \quad (2.41)$$

Use of relation (2.39) however, forces a link between the shear modulus and mean effective stress through (2.40). It can be shown that if both G and K' vary with mean stress, then the soil is not truly elastic and it is not strictly thermodynamically acceptable, as there is a possibility of work being created or dissipated on supposedly elastic closed stress cycles (Zytynski et al., 1978; Houlsby, 1985; Britto and Gunn, 1987). Theoretically, it is therefore preferable to ensure a constant value of shear modulus and calculate Poisson's ratio using relation (2.42).

$$\nu' = \frac{3K' - 2G}{2G + 6K} \quad (2.42)$$

Use of a constant shear strength can result in unrealistically low or negative values of Poisson's ratio occurring during the analysis. Experimental evidence indicates that the shear modulus does in fact vary with stress level. Typically, for static analyses, use of a constant Poisson's ratio and allowing the shear modulus to vary with mean stress does not introduce any significant error. Use of this method is numerically more convenient and Houlsby (1985) and Almeida et al. (1986) found that a mean stress dependent shear modulus provides a better estimate of observed test data. In view of this, analyses described here have been performed assuming a constant value of Poisson's ratio and a mean stress dependent shear modulus.

When plastic deformations are occurring it is assumed that the yield loci expand at constant shape, the size being controlled by the tip stress p'_0 , and that the expansion of the yield loci, the hardening of the soil, is linked with the normal compression of the soil, Fig 2.12(b). Normal compression of the soil assumes a linear relationship, at constant stress ratio, between specific volume, v , and the Logarithm of mean effective stress, relation (2.43)

$$v = v_\lambda - \lambda \ln p'_0 \quad (2.43)$$

where v_λ is a soil constant specifying the position of the normal compression line in the compression plane $p':v$, Fig 2.12(c). When yield occurs the soil exhibits a less stiff response, the stiffness of which is now controlled by λ . The parameter λ defines the slope of the normal compression line in the compression plane. Values of λ are typically selected from oedometer normal compression data. One-dimensional normal compression in an oedometer is a constant stress ratio loading process, therefore it is reasonable to use oedometer data to deduce a value of λ for use in the Cam clay model.

The plastic compliance relationships, describing plastic volumetric and plastic shear strains, which apply whenever there is a change in the size of the yield locus, are given by;

$$\varepsilon_p^p = \left(\frac{\lambda - \kappa}{v p' (M^2 + \eta^2)} \right) ((M^2 - \eta^2) \delta p' + 2\eta \delta q) \quad (2.44)$$

$$\varepsilon_q^p = \left(\frac{(\lambda - \kappa)}{v p' (M^2 + \eta^2)} \right) \left(2\eta \delta p' + \left(\frac{4\eta^2}{M^2 - \eta^2} \right) \delta q \right) \quad (2.45)$$

The assumption of coincident yield loci and plastic potentials, together with the assumption that the soil is volumetric hardening, in turn implies that the soil ends with critical states at the stress ratio, $\eta=M$. The critical state, point C Fig 2.12(a), is the point at which plastic shearing would continue indefinitely without changes in volume or effective stress.

$$\frac{\partial p'}{\partial \varepsilon_q} = \frac{\partial q}{\partial \varepsilon_q} = \frac{\partial v}{\partial \varepsilon_q} = 0 \quad (2.46)$$

The slope of the critical state is defined in the $p':q$ plane by specification of the critical state parameter M (Fig 2.12(a)).

The position of the critical state line in the compression plane $v: \ln p'$ is defined by the parameter, Γ (or e_{cs} in terms of void ratio as used in CRISP) the critical state void ratio

at $p'=1$, Fig 2.12(c). The critical state line is parallel to the normal compression line and therefore also has slope λ .

2.3.4.2 Modified Cam clay and CRISP

Within CRISP the modified Cam clay model is fully defined by the specification of five material parameters, κ , λ , v' , e_{cs} , M together with a description of stress history, p'_o . Parameters κ and λ are required to define the slope of the unload - reload and normal compression lines in the compression plane to relate changes of mean effective stress to changes in volume. Parameter e_{cs} is required to define the position of the critical state line in the compression plane but also to calculate the current voids ratio, e , from the known stress history of the soil, relation (2.47).

$$e = e_{cs} + (\lambda - \kappa) \ln 2 - \lambda \ln p'_o + \kappa \ln \left(\frac{p'_o}{p'} \right) \quad (2.47)$$

The position and slope of the critical state line in the $p': q$ plane is fully defined by parameter M .

Stress history of the soil is defined through specification of the size of the initial yield locus, p'_o . Stress history is not a material parameter and is specified with the initial stress conditions which are given in terms of effective stress.

Values of p'_o are determined from preconsolidation stress data, using relation (2.48)

$$p'_o = p'_c \left(1 + \frac{\eta_c^2}{M^2} \right) \quad (2.48)$$

where p'_c is the preconsolidation mean effective stress and is determined from relation (2.49)

$$p'_c = \frac{1}{3} (\sigma'_{vc} + K_o \sigma'_{vc}) \quad (2.49)$$

where σ'_{vc} is the vertical effective preconsolidation stress and K_o is the coefficient of earth pressure (discussed in section 2.2).

Parameter η_c is a stress ratio equal to,

$$\eta_c = \frac{3(1 - K_o)}{1 + 2K_o} \quad (2.50)$$

When using the modified Cam clay soil model as currently implemented in CRISP the user should exercise caution, particularly if the user is using modified Cam clay to generate the in situ stresses for problems of plane strain. Difficulties arise because CRISP assumes that the slope of the critical state line in the deviator-mean stress ($q:p'$) space is given by the gradient M . This gradient is independent of the intermediate stress σ'_2 and therefore the Lode angle θ .

$$\theta = \tan^{-1} \left(\frac{2b - 1}{\sqrt{3}} \right) \quad (2.51)$$

$$\text{where } b = \frac{\dot{\sigma}_1 - \dot{\sigma}_3}{\dot{\sigma}_1 - \dot{\sigma}_3} \quad (2.52)$$

The strength of a modified Cam clay soil changes according to a three dimensional stress field ($\sigma'_1, \sigma'_2, \sigma'_3$). However, because M is independent of σ'_2 , this forces the angle of internal friction, ϕ' , to be a function of the Lode angle, θ . Additionally, because the modified Cam clay soil model assumes associated plasticity, $\theta=0$ for plane strain failure (Potts and Gens, 1984) the angle of internal friction is given by,

$$\phi' = \sin^{-1} \left(\frac{M}{\sqrt{3}} \right) \quad (2.53)$$

If $\phi'=26$ degrees in triaxial compression, modified Cam clay gives 35 degrees in plane strain for an $M=1.0$. Clearly, this problem needs to be understood by prospective CRISP users and hence caution is require when selecting appropriate input parameters.

Fig 2.1 Typical path followed on one-dimensional unloading and reloading in (a) σ'_h : σ'_v and (b) p' : q effective stress planes (Muir Wood, 1990).

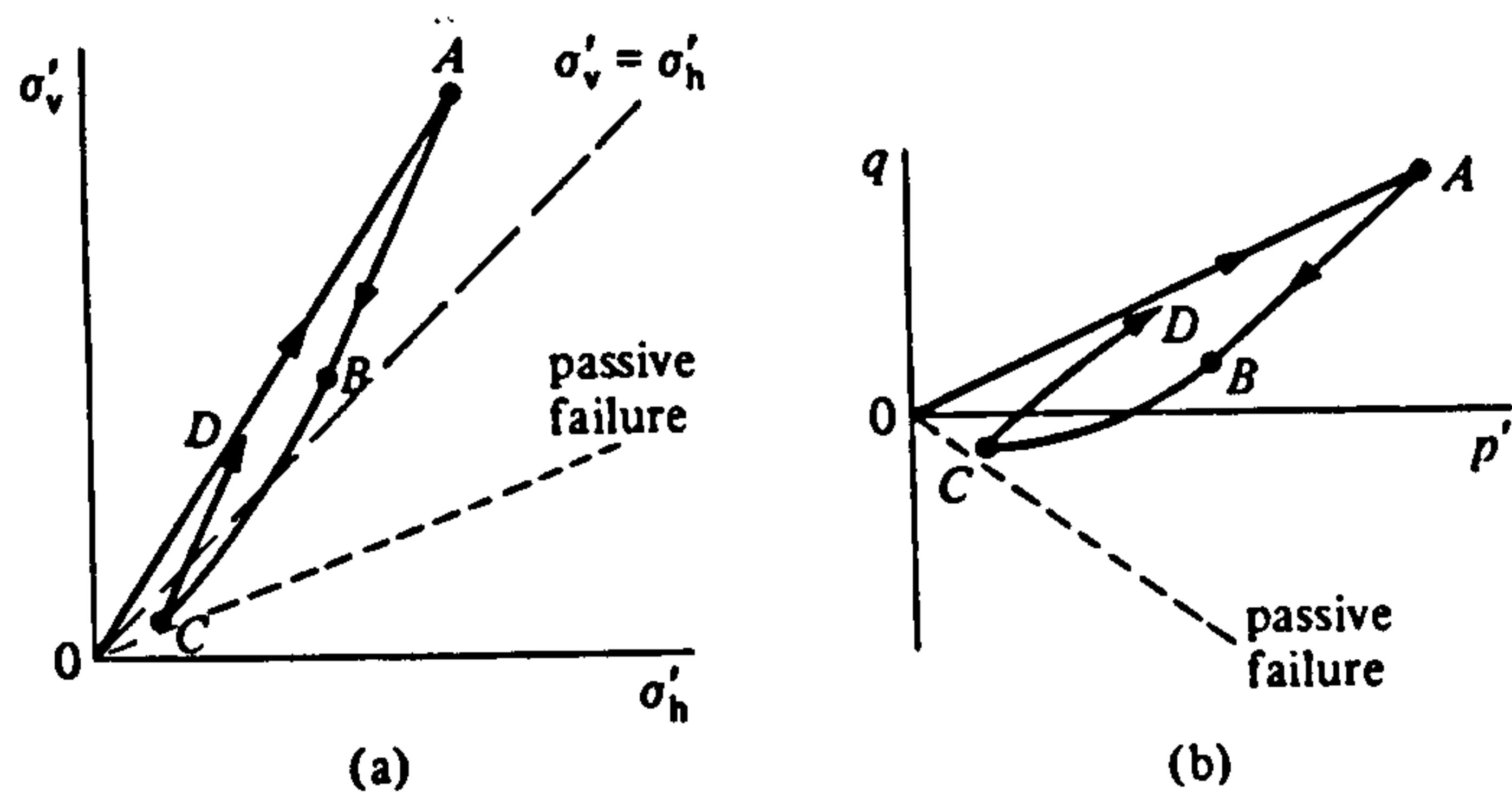


Fig 2.2 Dependence of the coefficient of earth pressure at rest for normally compressed soil, K_{0nc} , on angle of shearing resistance ϕ' (o, clays; + sands) (Wroth, 1972; Ladd, Foott, Ishihara, Schlosser, Poulos, 1977 and Muir Wood, 1990).

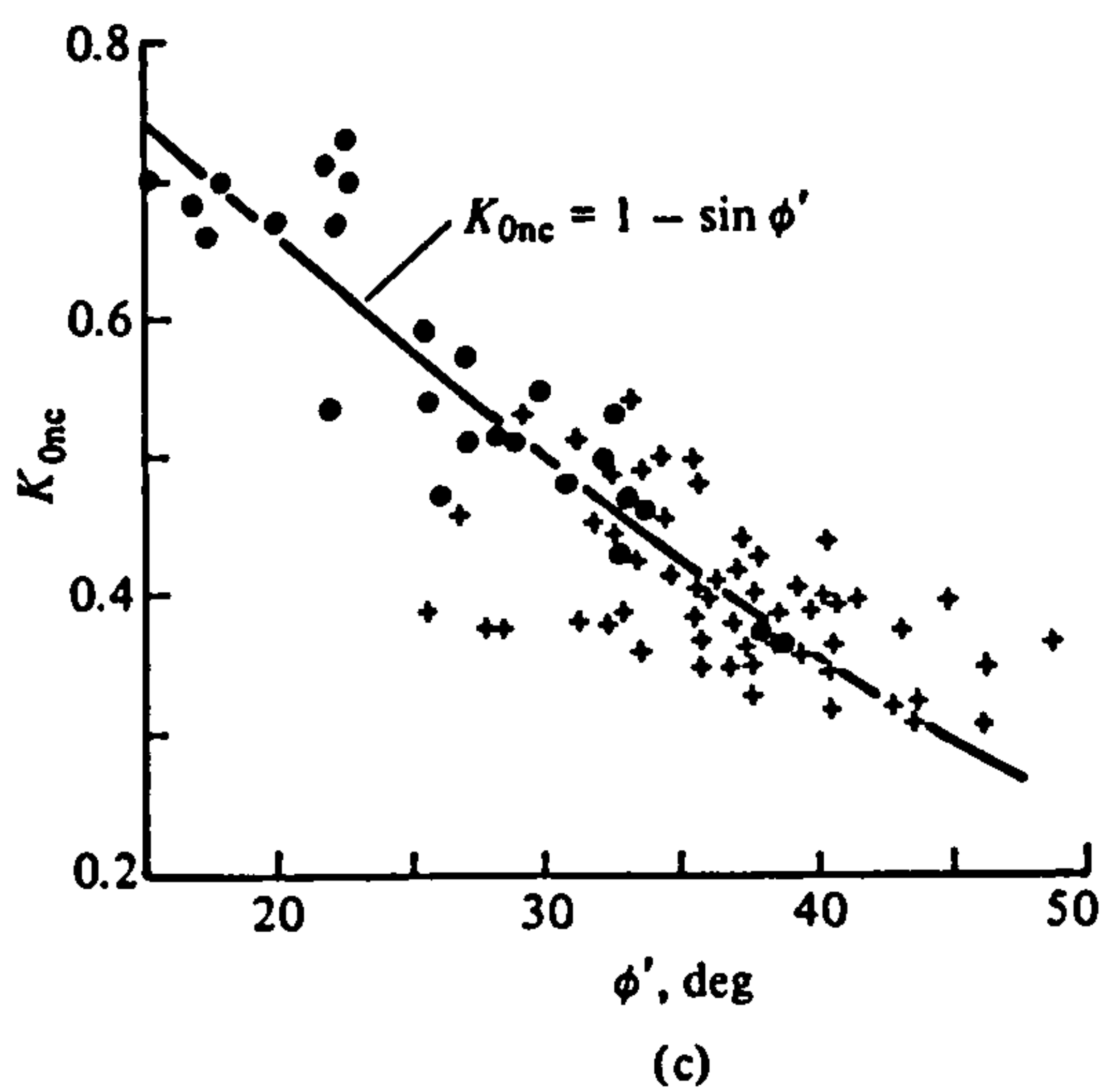


Fig 2.3 Relationship between at-rest rebound parameter, a , and $\sin \phi'$ for clays and sands (Mayne and Kulhawy, 1982).

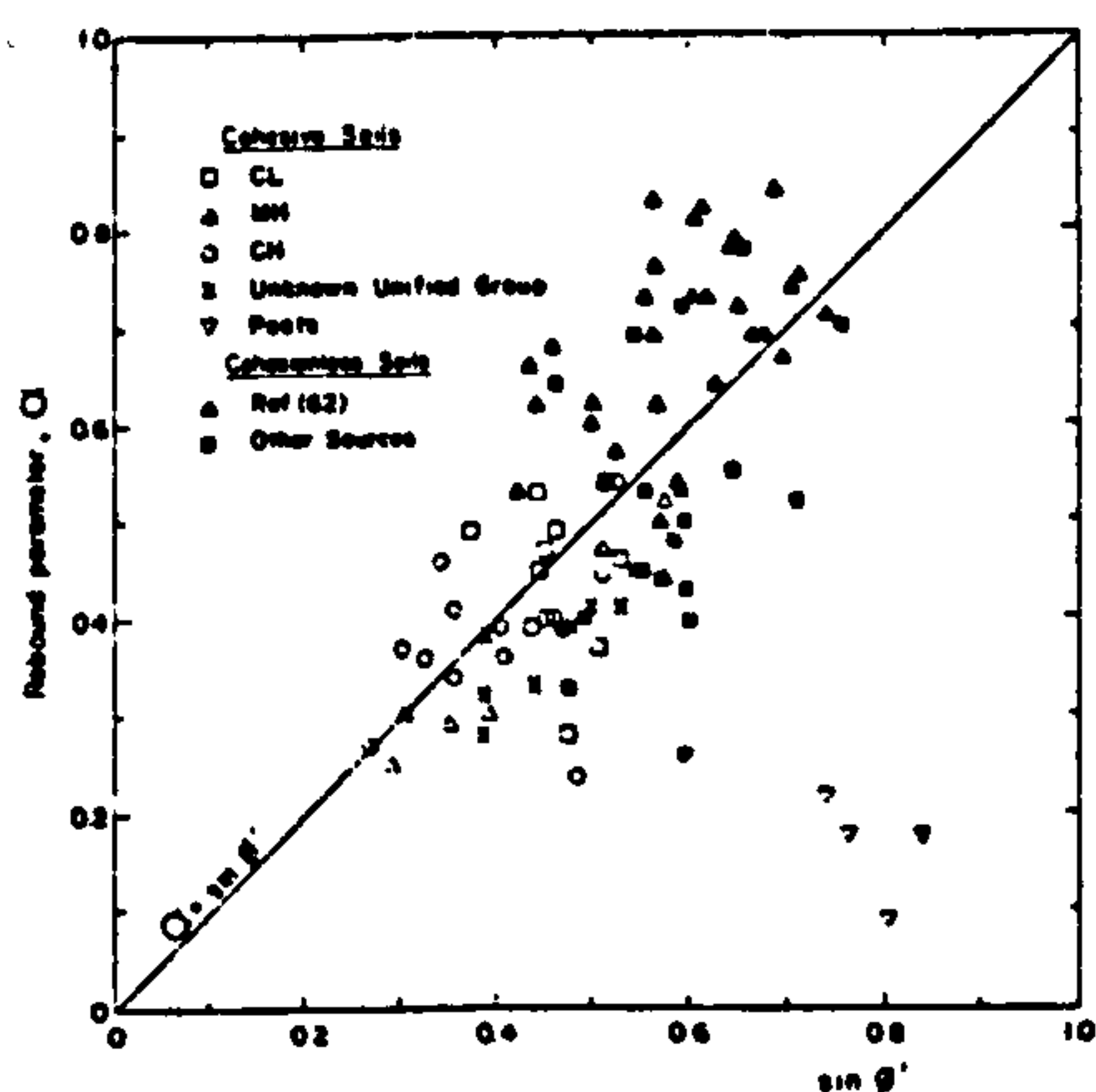


Fig 2.4(a) Observations and calculations of relationship between coefficient of earth pressure at rest K_0 and overconsolidation ratio n (Ladd, 1965 and Muir Wood, 1990).

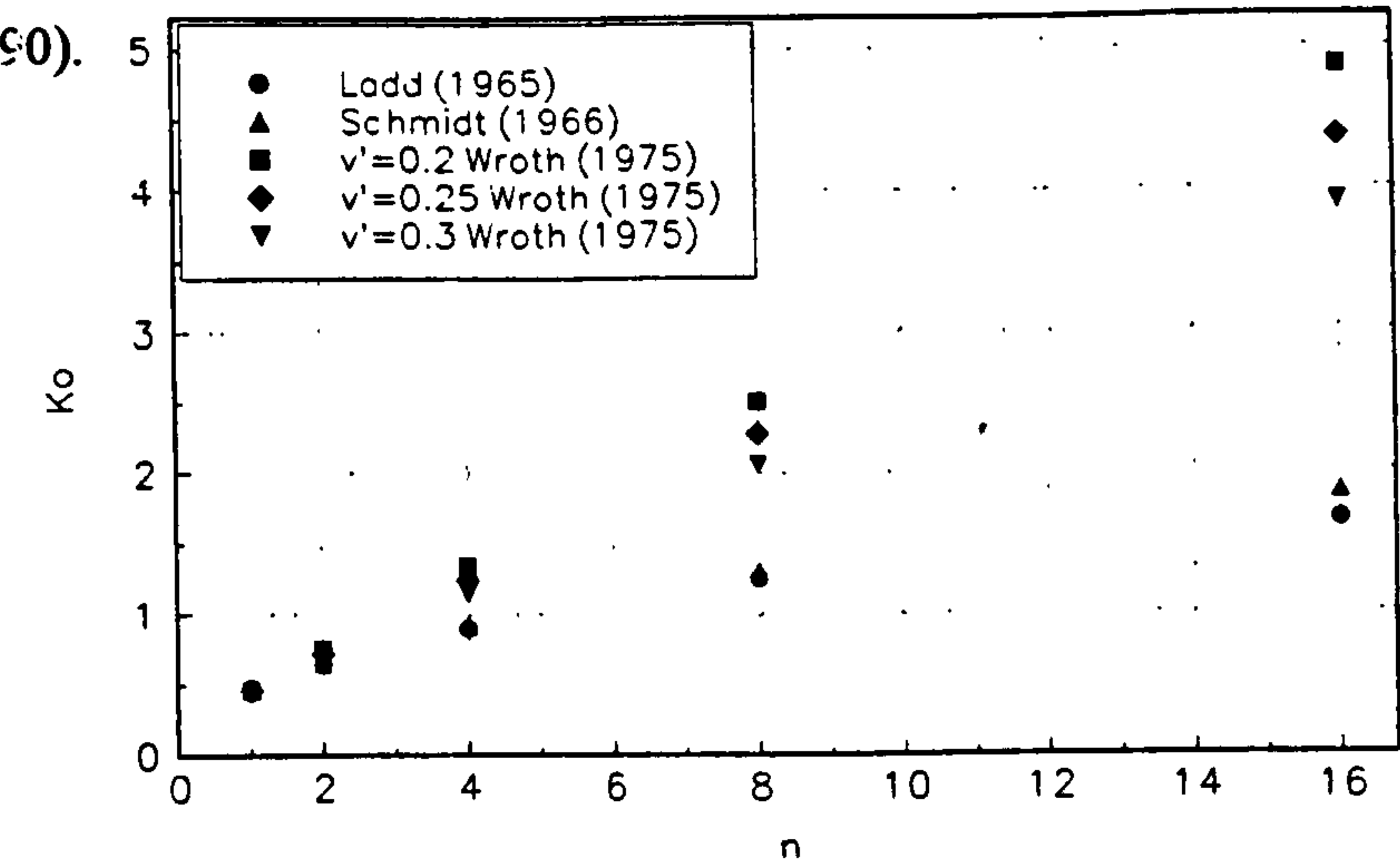


Fig 2.4(b) Dependence of Poisson's ratio v' on plasticity index I_p (Wroth, 1975 and Muir Wood, 1990).

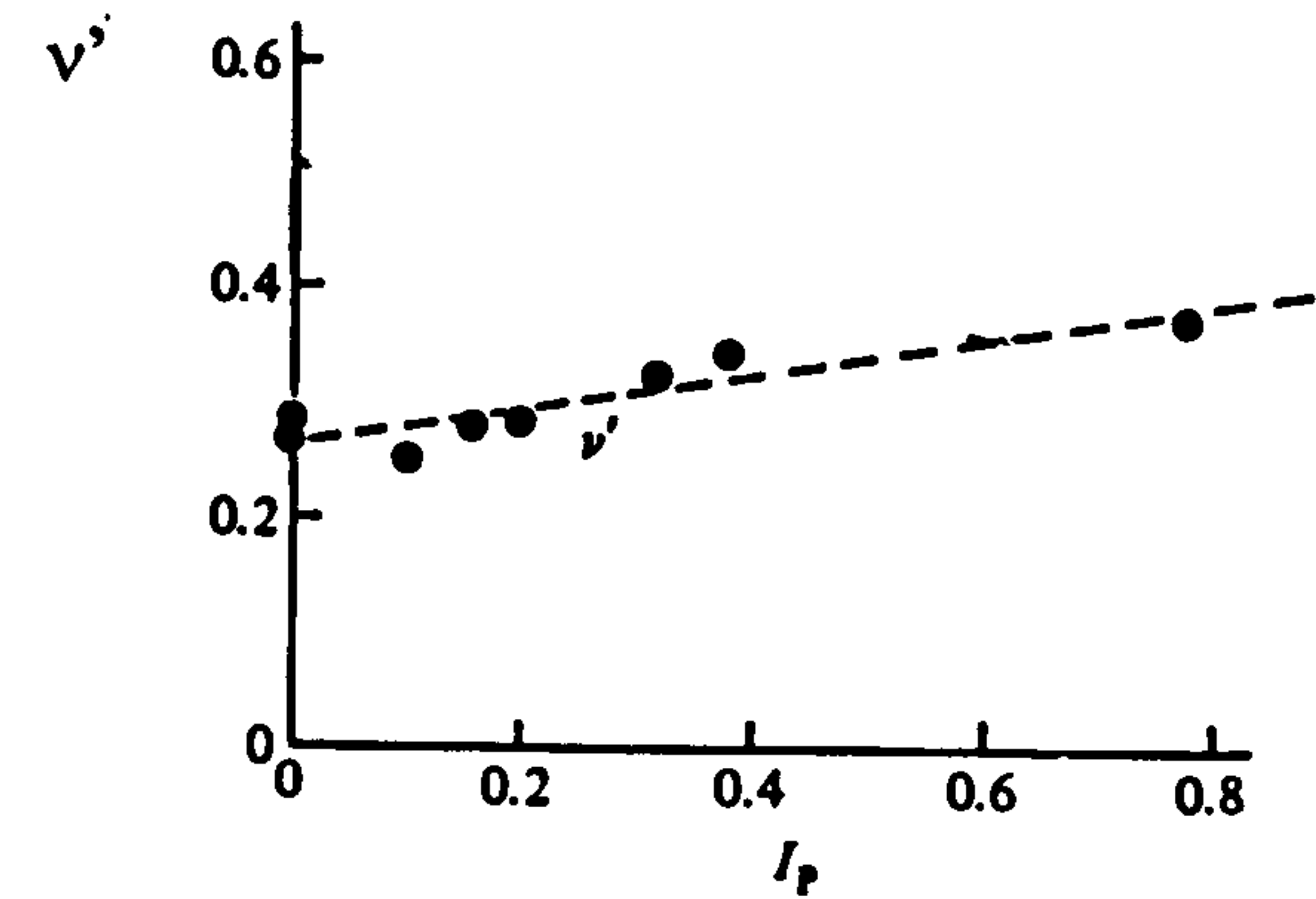


Fig 2.5 Dependence of the coefficient of earth pressure at rest for normally compressed soil, K_{onc} , on angle of shearing resistance ϕ' according to the Cam clay soil model (Muir Wood, 1990).

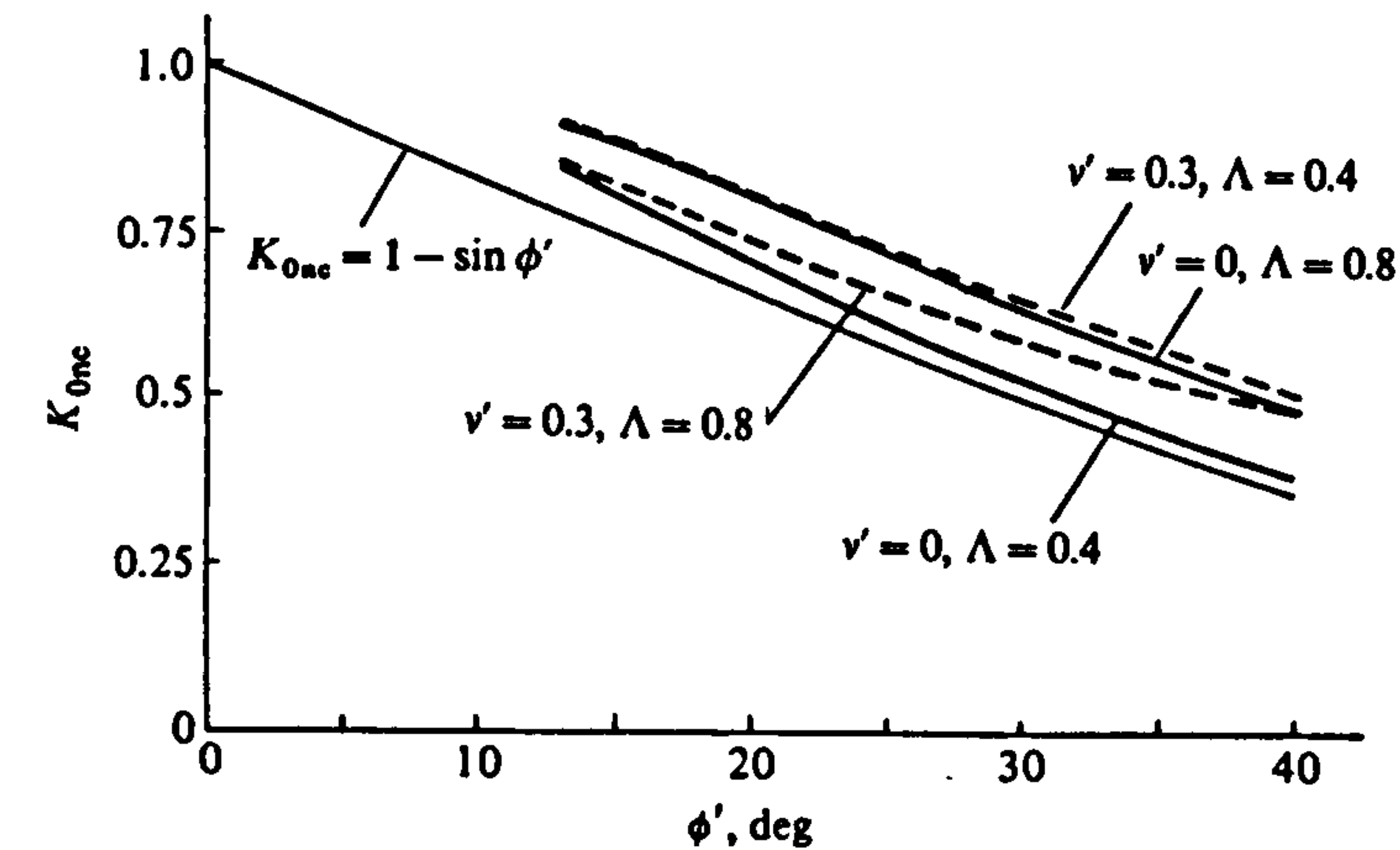


Fig 2.6 (a) Plastic strain increment vectors normal to family of plastic potential curves; (b) families of plastic potentials (--) and yield loci (—) (Muir Wood, 1990).

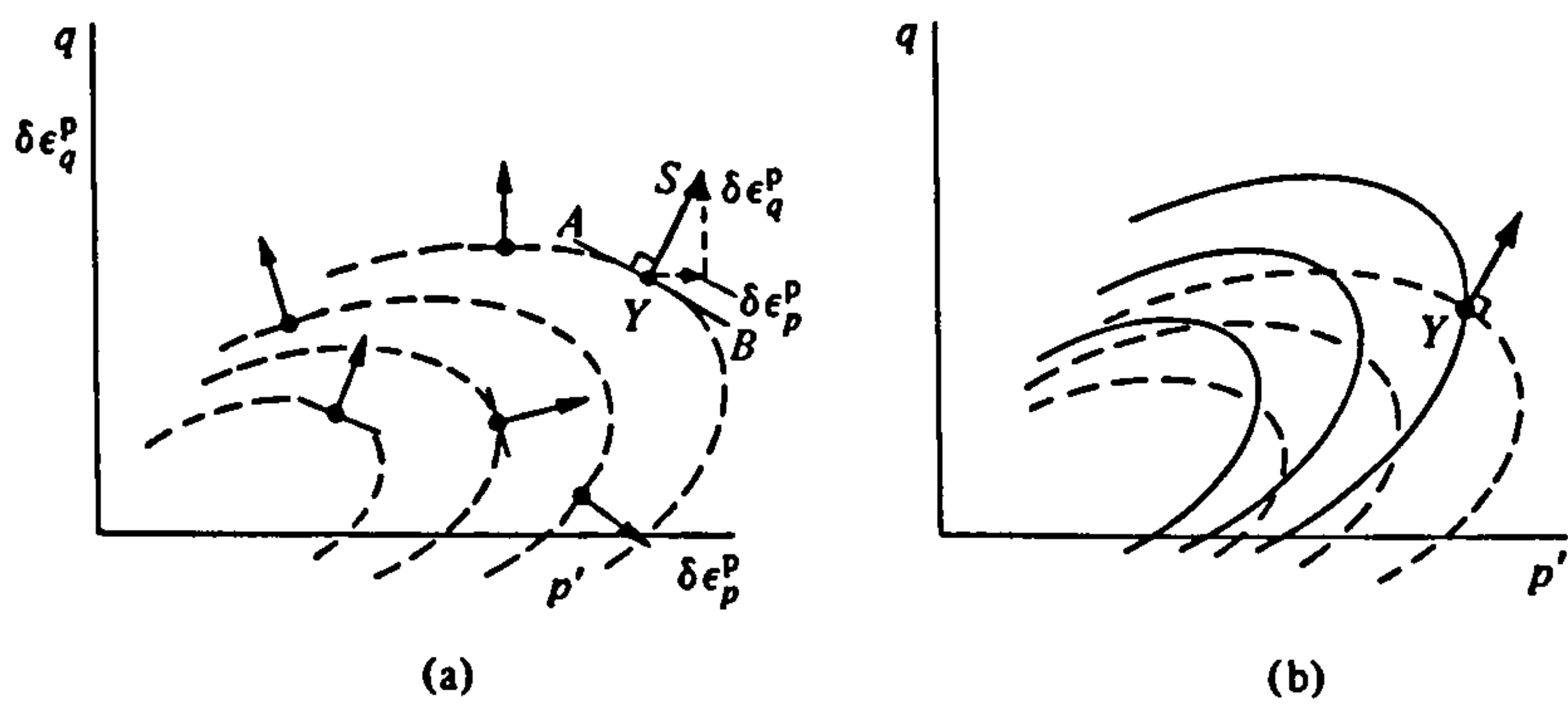
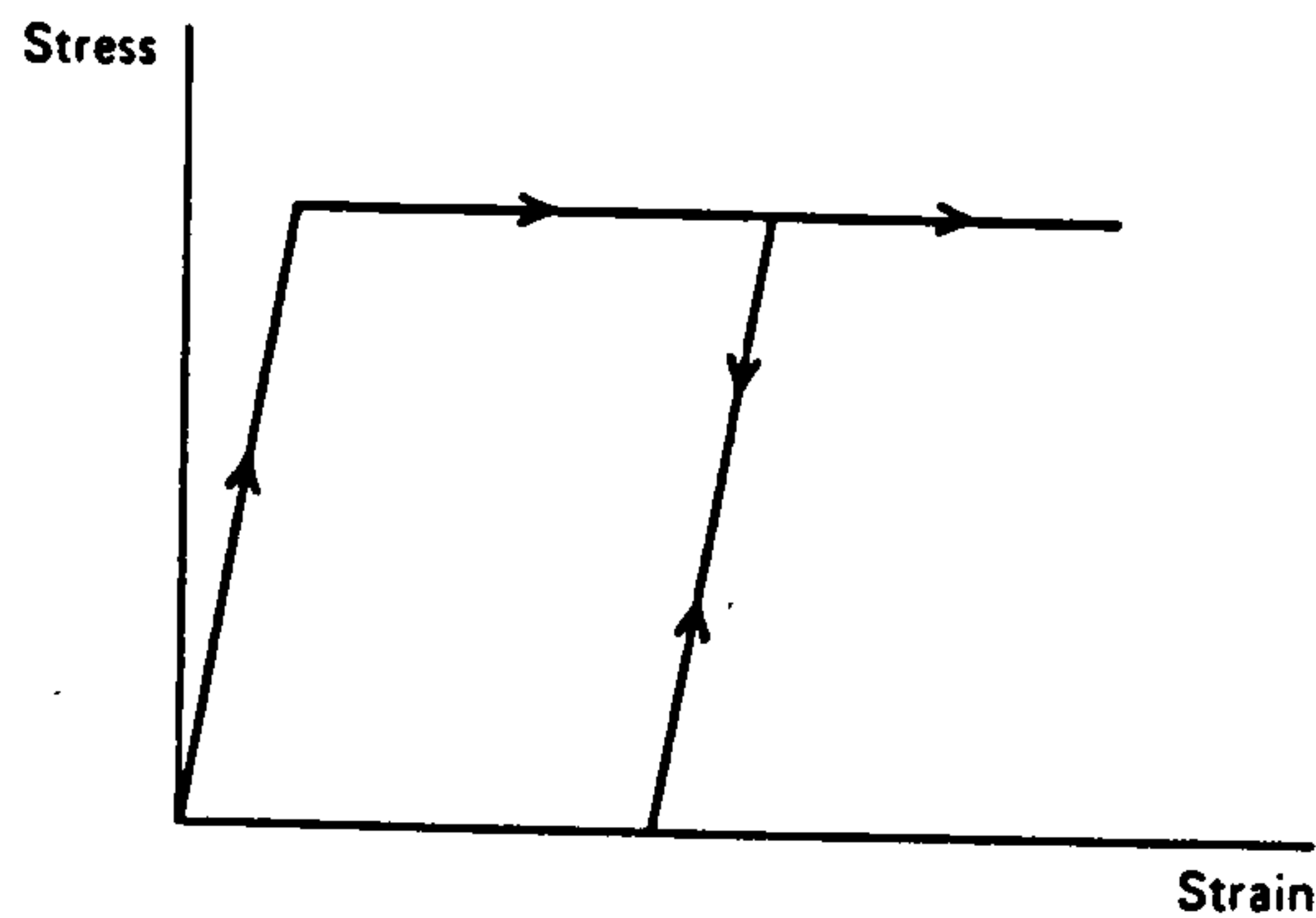
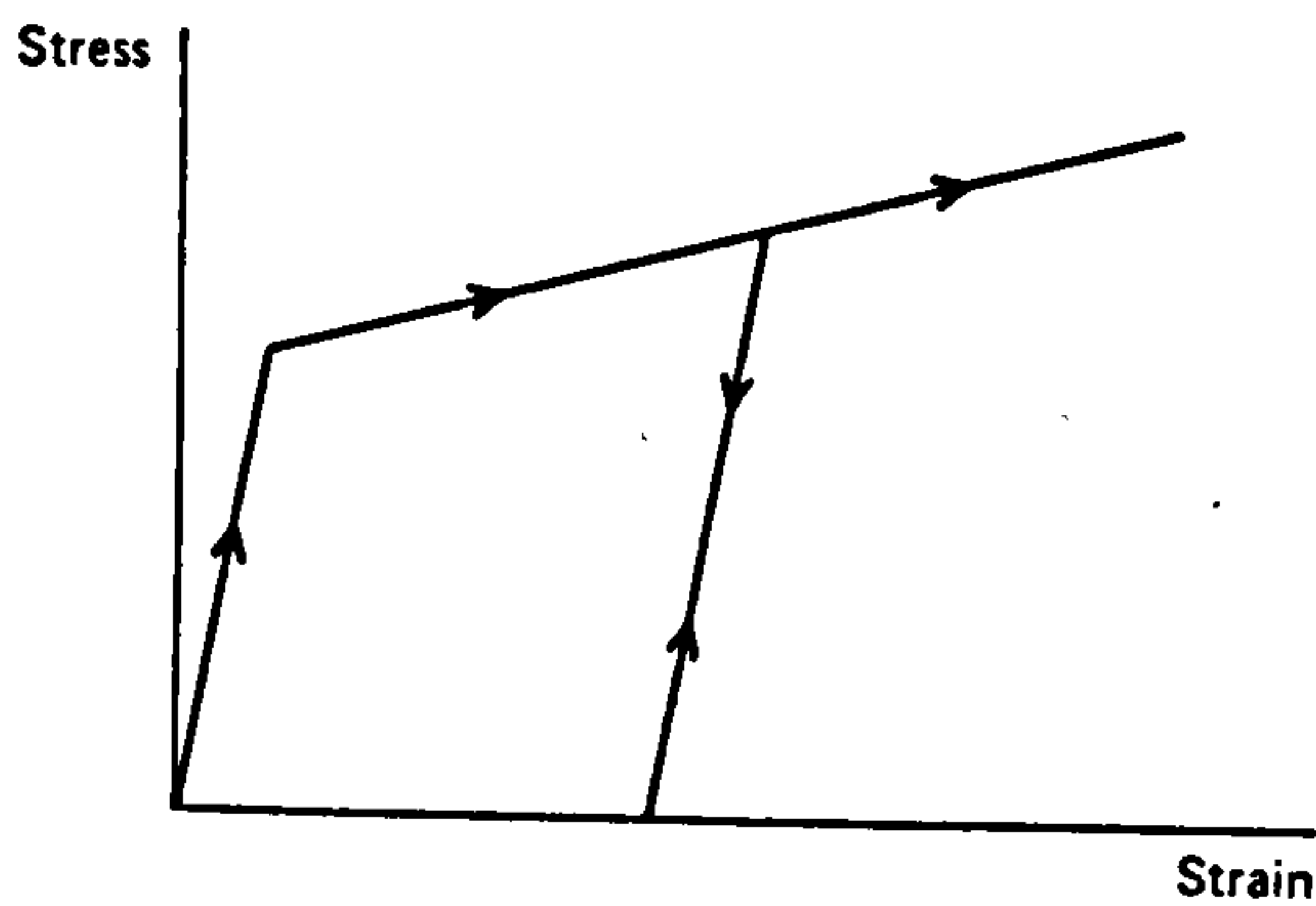


Fig 2.7 Idealisations of plastic behaviour (Britto and Gunn, 1987).

(a) Elastic–perfectly-plastic



(b) Elastic, strain-hardening plastic



(c) Rigid, perfectly-plastic

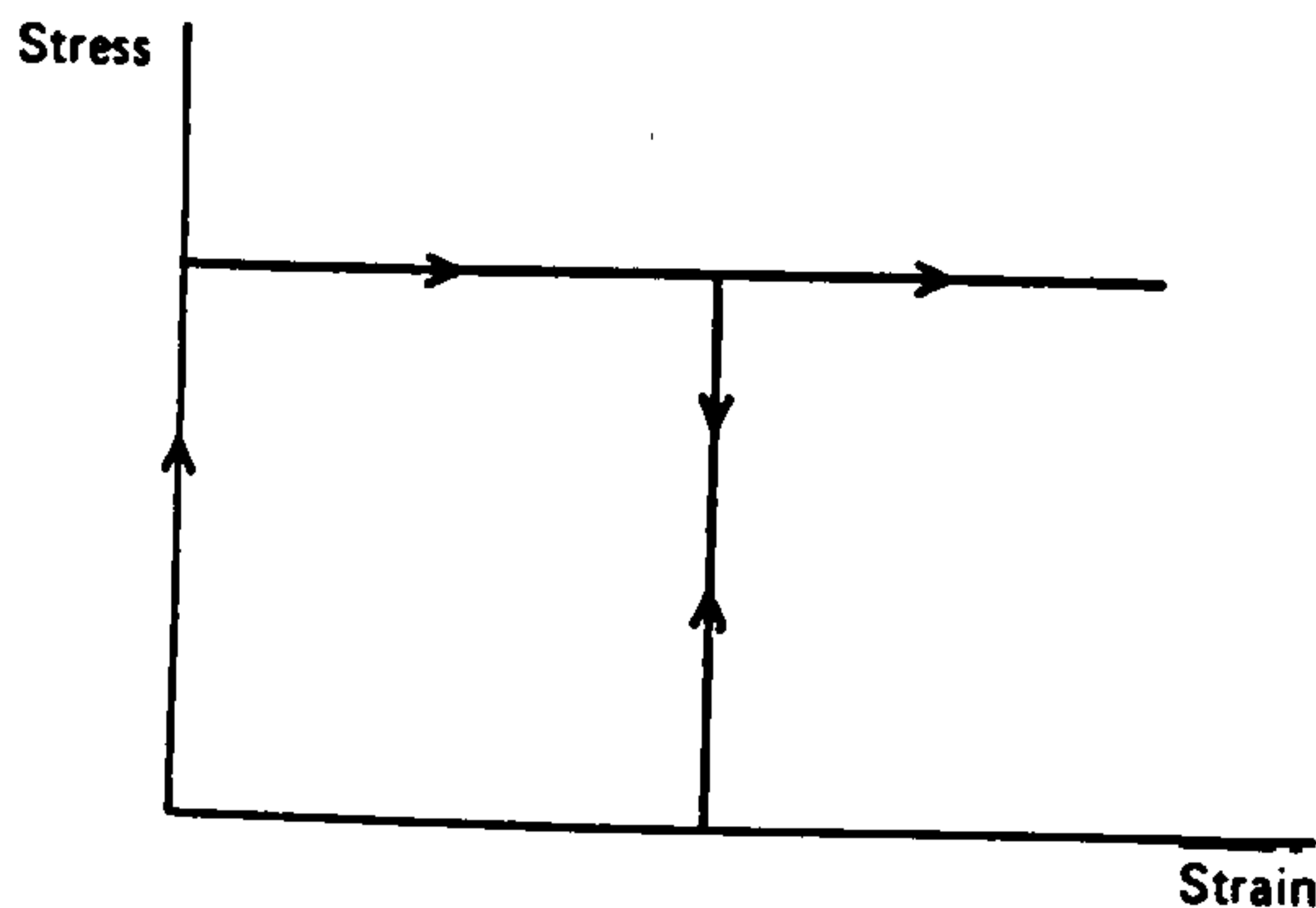


Fig 2.8 Yield surface according to the yield criterion of Tresca (Britto and Gunn, 1987).

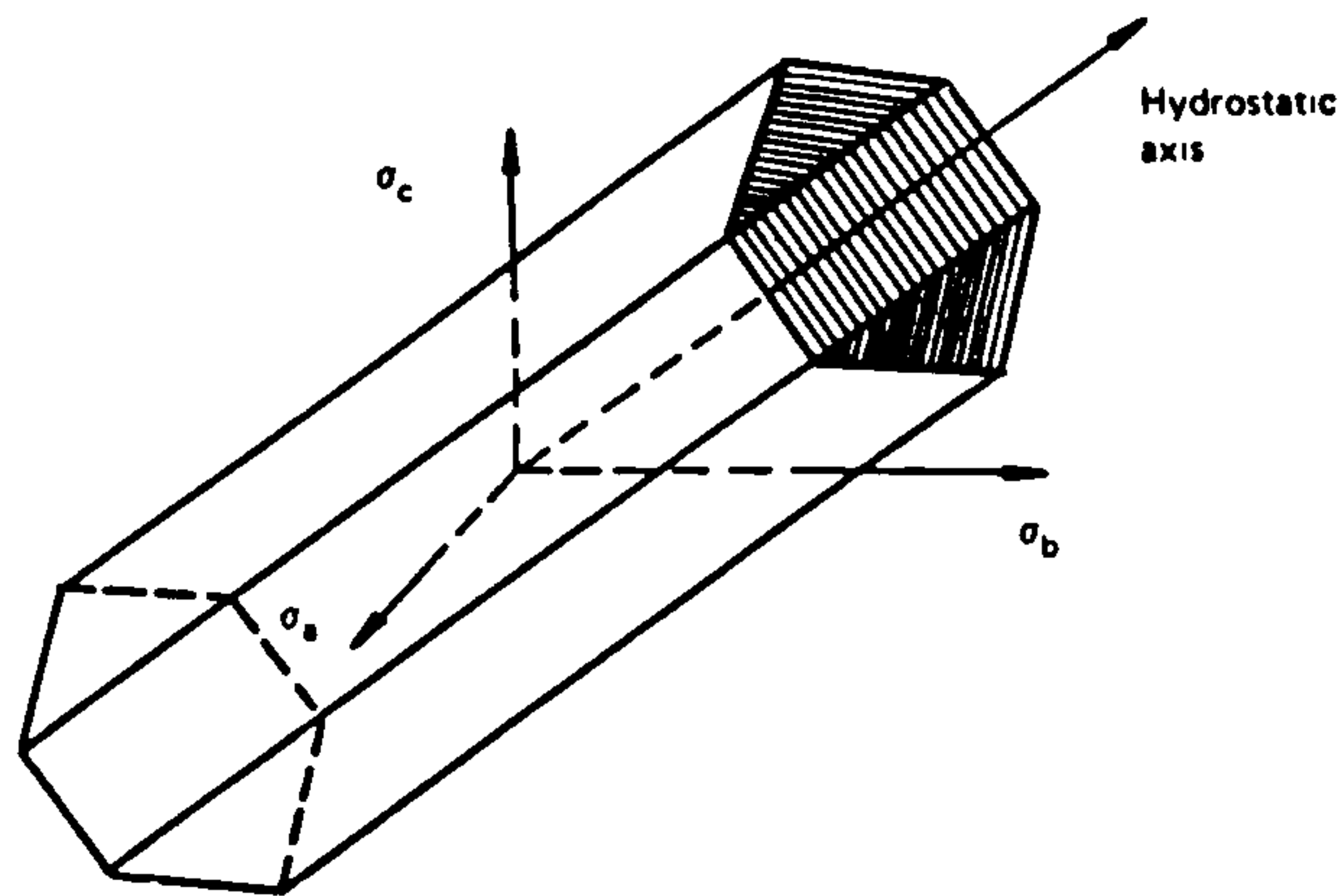


Fig 2.9 Tresca yield surface described in the plane of shearing $s : t$.

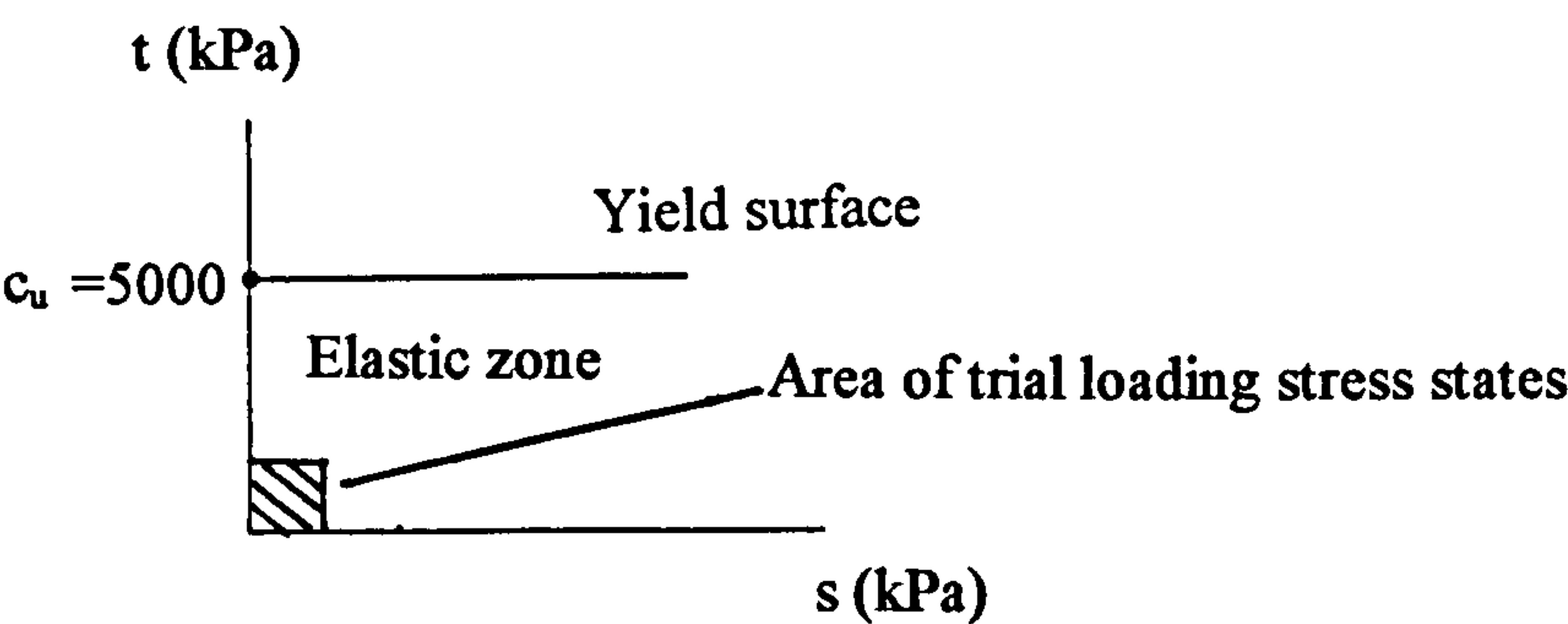
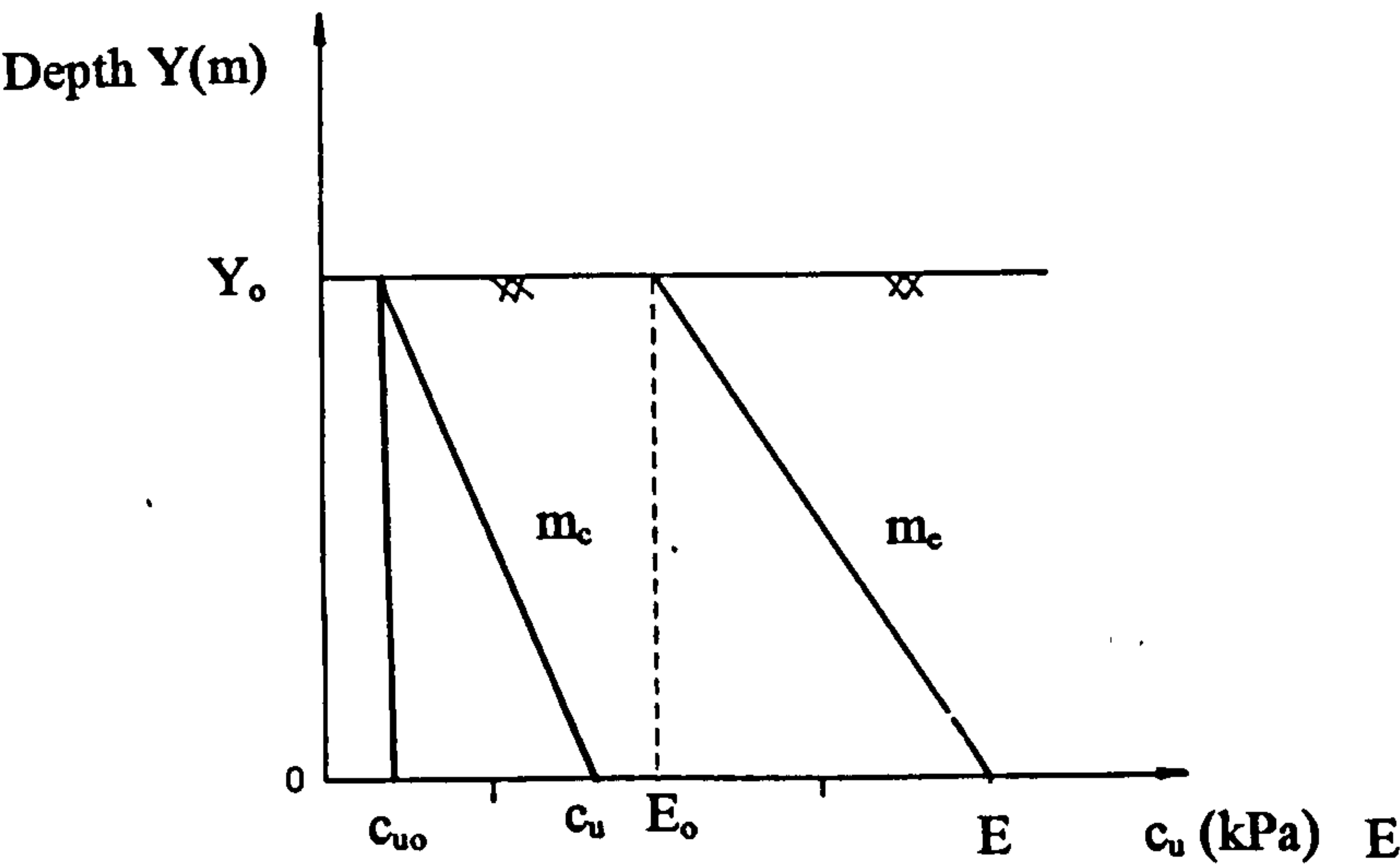


Fig 2.10 Variation of Young's modulus, E , and undrained shear strength, c_u , with depth for non-homogeneous elastic soil model.



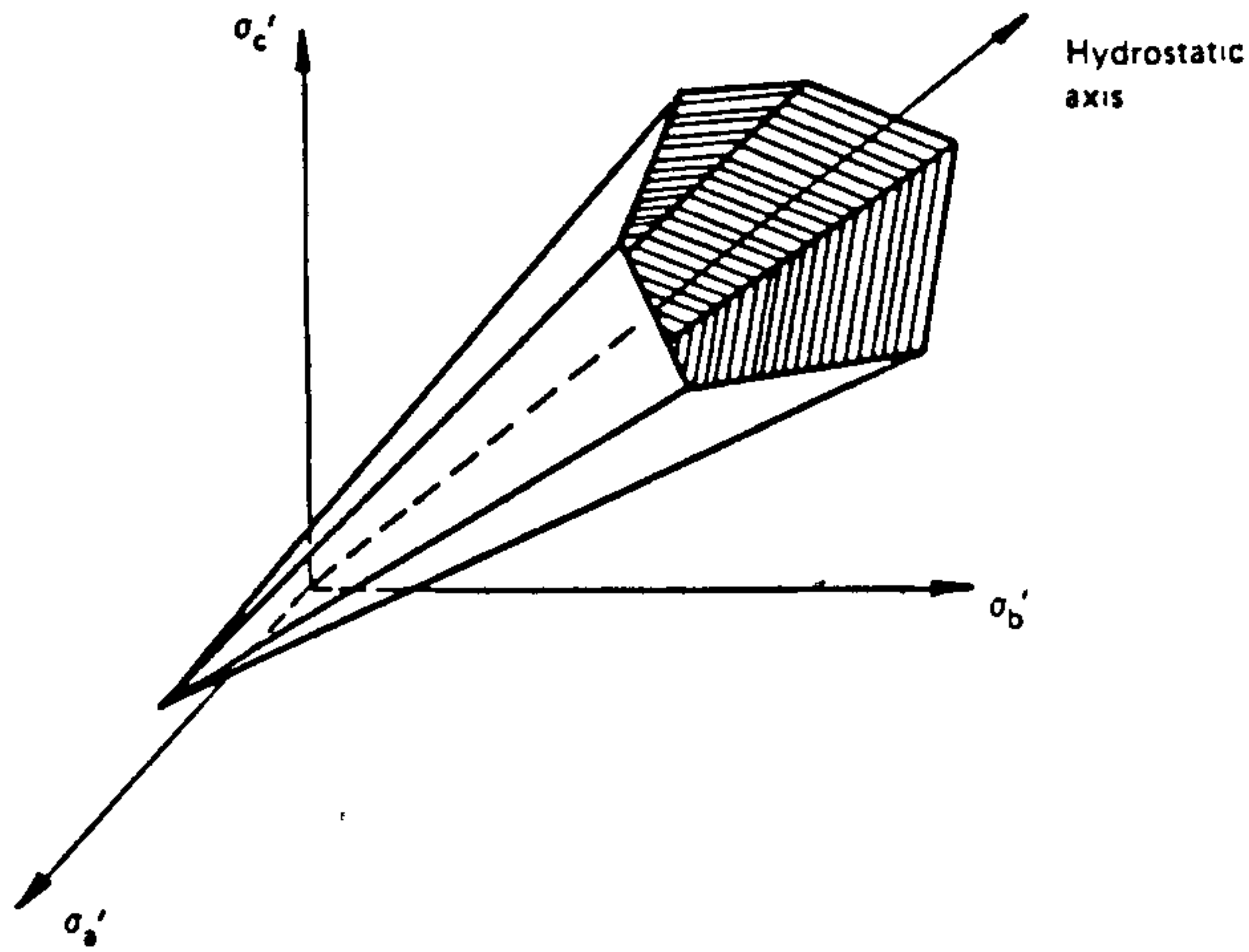


Fig 2.11 Yield surface according to the yield criterion of Mohr-Coulomb (Britto and Gunn, 1987).

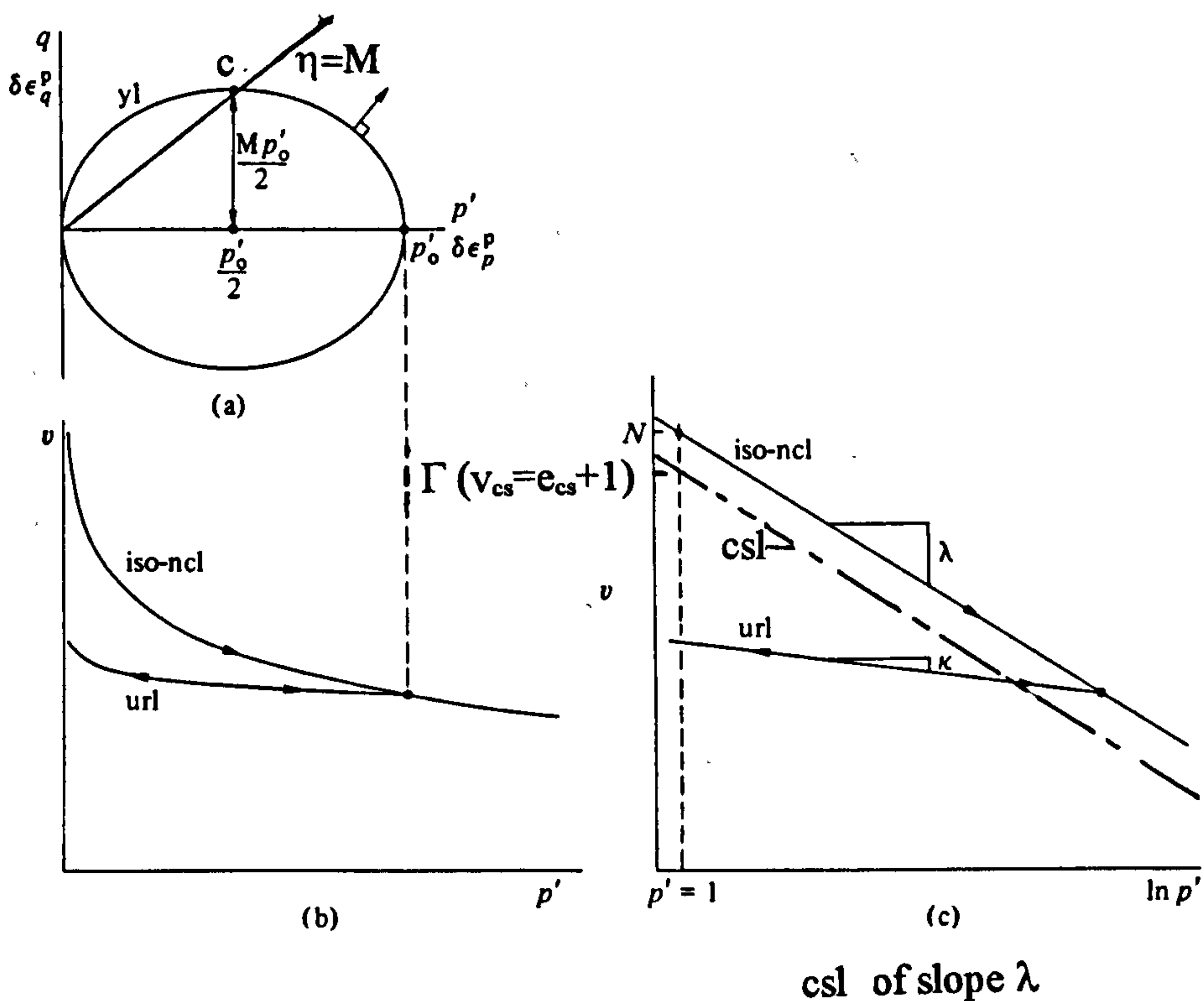


Fig 2.12 (a) Elliptical yield locus for Cam clay model in $p':q$ plane; (b), (c) normal compression line and unloading-reloading line in compression plane (Muir Wood, 1990).

CHAPTER 3

3. Trial loading on soft clay

3.1 Introduction

This chapter is the first of three chapters describing back analysis of trial loadings on soft clay foundations. Back analyses have been performed using finite element analysis and to resemble a typical design procedure a simple numerical approach has been adopted using established soil models commonly used for geotechnical analysis. In each case the object of the analyses was to determine a set of material parameters which gave a reasonable estimate of the observed behaviour, and hence provide a framework of parameter selection for similar loading situations. Particular concern was given to accurately reproduce the observed pre-failure behaviour, which is important in serviceability limit state design.

This chapter is concerned with the back analysis of observed data obtained from a trial loading at a soft clay site on the Thames estuary in England, Fig 3.1. The loading was performed in September 1990 and was part of a detailed investigation into the bearing capacity and settlement response of the foundation for the design of haulage routes required to transverse the site. Design recommendations for the haulage routes were made from back analysis of the trial loading data. The original back analysis study (Schnaid, Wood, Smith and Jubb, 1993) concentrated on the use of a linear elastic-perfectly plastic soil model with a Tresca failure criterion. Full details of the trial loading and ground conditions at the loading site are described in sections 3.2 and 3.3. Finite element modelling for this present study is described in section 3.4.

In this present study the original design requirements have been neglected and the trial loading has been re-analysed using three simple soil models, isotropic linear-elastic, linear elastic-perfectly plastic (Tresca) and modified Cam clay effective stress soil model (Roscoe and Burland, 1968). For each soil model a framework of parameter selection has been suggested. Each is based on available site investigation and laboratory test data, however empirical and semi-empirical methods are also

incorporated within the suggested framework to provide a check and/or a supplement to sparse or inaccurate soil data.

The three soil models mentioned above were used in this study as these are most commonly used in geotechnical analysis of soft clay foundations. The isotropic linear elastic and linear elastic-perfectly plastic soil models are typically used in serviceability limit state design where an estimation of displacements are required. Pore water pressures are not typically considered to be significant in the working range of stress. The Tresca soil model is typically used to provide a factor of safety on the working range of stresses. Here the Tresca soil model has been re-applied to the trial loading to provide a more systematic approach to parameter selection for use of this soil model. The trial loading has been re-analysed using the modified Cam clay soil model to resemble a design situation where a more complex method of analysis is required. Such a method of analysis may be required if the structure is to be located in a sensitive area, for example a congested urban area, in this case the influence of the structure on the foundation soil will need to be closely investigated. Due to sparse site investigation and laboratory site data parameter selection for this soil model depends largely on empirical and semi-empirical methods.

Material parameters required to describe the soil models noted above are briefly discussed in section 3.5. This section is subdivided into three subsections. The results of the finite element analyses using these models are presented and discussed separately in section 3.6. The main findings of the analyses are compared and discussed in section 3.7. Conclusions drawn from the analyses are presented in section 3.8.

3.2 Description of the trial loading

The trial loading was performed on an existing section of haulage road cut to form an isolated length of 14m. The road pavement consisted of a 175mm thick, 5m wide reinforced concrete slab founded on a 225mm thick compacted gravel sub-base. To ensure no influence from the adjacent sections of road a trench some 500mm wide was

excavated all round the slab to the base of the gravel sub-base and backfilled with clean sand.

The foundation response to the loading was measured using three piezometers, seven inclinometers, eight slip indicators and 45 surface markers. Vertical displacements of the slab, Fig 3.2(c) were measured using 16 survey targets located around the periphery of the slab. The instrumentation was placed predominantly in one transverse section of the slab as shown in Fig 3.2(a) and (b). Results from the numerical analyses are to be compared with the measurements obtained from this instrumented section.

Loading of the slab was performed rapidly by successively placing 20kN concrete blocks in layers, Fig 3.3, until failure occurred at an applied load of 84kPa, some 26 hours later. A total of 300 concrete blocks was placed in four layers. Failure occurred by rotation of the slab about the z-z axis, Fig 3.2. During failure some concrete blocks were displaced, destroying several surface markers and inclinometers I2, I3, I4 and I5.

The main results of the load test are presented in Figs 3.4-3.9. The most noticeable feature of the test results is the very stiff initial foundation response to the loading, Fig 3.4.

3.3 Ground conditions

The site is located on the post glacial marshes along the north bank of the Thames estuary (Fig 3.1). Since the 1950s the site has been subject to much industrial development. Site investigation work performed during the initial development is reported by Skempton and Henkel (1953).

Site investigations performed more recently for the haulage routes and subsequently for the trial loading determined that the geotechnical profile of the site, Fig 3.10, was relatively uniform and consists of a 1.0m-2.0m thick surface desiccated crust, overconsolidated by seasonal variation of the water table, underlain by soft normally consolidated clays with sand and peaty lenses to a depth of about 10m. These soft soils are underlain by a layer of Thames Gravel (predominantly flint), which in turn is underlain by deposits of Thanet Sand. The ground water level was found to vary

across the site between the ground surface and the base of the surface crust. The soil properties are summarised in Fig 3.11-3.19.

The site investigations performed for the haulage routes included boreholes, sampling, in situ vane, static cone penetration, piezocone and seismic cone tests. Additionally, oedometer tests, undrained triaxial tests and one drained triaxial test with internal strain measurement were performed in the laboratory on undisturbed samples.

From the site investigation and laboratory test data parameters required for the numerical analyses have been selected. Over the area in which much of the site investigation was concentrated the desiccated surface crust had been removed during previous site development. Additionally, in areas where some crust material still remained the necessity to excavate inspection pits to search for services prior to in situ testing has resulted in limited data for the crust material. As a result crust data, especially preconsolidation and stiffness data, have been obtained from published literature (Skempton and Henkel, 1953; Marsland and Powell, 1977; Nicholson and Jardine, 1986) describing ground investigations at adjacent sites.

3.4 Soil parameters required for analyses

From site investigation and laboratory test data material parameters required for the numerical analyses have been selected. In this section the material parameters required to describe the soil models used in this study and how these parameters are selected from available site investigation and laboratory test data are discussed.

This section is divided into three subsections (3.4.1, 3.4.2 and 3.4.3) within which parameters required for the isotropic linear elastic, linear elastic-perfectly plastic (Tresca) and elasto-plastic (modified Cam clay) soil models are discussed.

3.4.1 Parameters required for the isotropic linear elastic soil model

Isotropic linear elastic analyses were performed using a linear elastic, perfectly plastic soil model with a Tresca failure criterion. Elastic behaviour was ensured in the Tresca

model by inputting very high values of the undrained shear strength, c_u , forcing the failure envelope to be located at stress states far higher than those produced by the trial loading. A value of $c_u=5000\text{kPa}$ was found to be appropriate for this. The Tresca soil model is a frictionless model therefore the angle of internal friction, ϕ_u is equal to zero. Details of the Tresca soil model are given in chapter 2. Using this model to perform elastic analyses requires the specification of three material parameters (excluding undrained shear strength parameters c_u and ϕ_u). These parameters are Young's modulus, E_u , Poisson's ratio ν_u and the unit weight of the soil, γ_s . Undrained, total stress analyses were performed therefore parameters E_u and ν_u are in terms of total stress.

Values of γ_s (unit weight of the soil) were estimated from available laboratory test data, Fig 3.13. In analyses the foundation was divided into layers (see section 3.5) and from available γ_s data an average value was assigned to each layer.

As previously noted in chapter 2, in undrained total stress analyses Poisson's ratio is equal to 0.5 to produce a constant volume response. However, directly inputting $\nu_u=0.5$ results in numerical problems (division by zero in relation (2.26). To avoid this a Poisson's ratio of 0.499 was used. Behaviour within the elastic region is controlled through variation of a single parameter, E_u . The model automatically calculates the remaining elastic parameters bulk shear modulus, G , and the bulk modulus, K_u using relations (2.27) and (2.28).

Estimates of the stiffness of the soft clay, presented in terms of shear modulus, G , Fig 3.18(a), have been estimated from conventional undrained unconsolidation (UU) tests and a single isotropically overconsolidated undrained triaxial test (CIU) with internal strain measurement, Fig 3.18(b). Stiffness has been presented in terms of shear modulus, G , because the value of G is not affected by the drainage conditions (either drained or undrained) of the test. For comparison values of shear modulus obtained using the seismic cone penetrometer are also shown in Fig 3.18(a). The value of stiffness obtained from internal strain measurement in the laboratory, at shear strains of 0.01-0.1%, is some seven times greater than that estimated from conventional triaxial test stiffness measurement (external strain measurement) at shear strains $\epsilon_q>0.5\%$, Fig 3.18(b). Internally measured strains provide a better measure of soil stiffness by removing errors arising from equipment compliance and sample end

effects (Clayton and Khatrush, 1986). The depth profile of the ratio of tangent shear modulus, obtained from conventional (external strain measurement) triaxial testing, to the in situ mean effective stress, G/p'_i , is shown in Fig 3.19. Values of p'_i were estimated assuming a water table depth of 0.5m below the ground surface. An alternative form of normalising the shear modulus is to use the undrained shear strength, c_u . However this form of normalisation is not entirely satisfactory as the undrained shear strength is known to be influenced by the type and rate of testing (Jardine et al., 1986 and Smith et al., 1992). Additionally, in this study the actual depth to the water table is not accurately known, consequently normalising G with respect to p'_i may also be ambiguous.

Internal strain measurement at 0.01%-0.1% strain gives a $G/p'_i=145$ or alternatively a $G/c_u=190$. These normalised stiffnesses, inferred from the single CIU test, are smaller than values determined from high quality triaxial tests incorporating low strain stiffness measurement performed on Bothkennar soft clay, $G/p'_i=200-400$ and $G/c_u=500-800$ (Smith et al., 1992 and Nash et al., 1992). This may be attributed to the greater care taken for testing on the Bothkennar tests rather than any significant difference in the geotechnical properties of the two sites. Bothkennar is a soft clay research site and consequently testing was free of the rigorous commercial constraints which were imposed on testing during the trial loading. The greater accuracy of testing performed on the Bothkennar soft clay is evident from Fig 3.20, which shows the secant shear modulus for the trial loading and Bothkennar sites, obtained from low strain measurement triaxial testing, normalised with respect to the in situ effective mean stress, G/p'_i and plotted against the triaxial axial strain (which is identical to triaxial shear strain in undrained tests). As can be seen from Fig 3.20 there is a significant amount of scatter of G/p'_i ratios for the trial loading soft clay. Additionally, reliable data are only available from internal strain measurement for shear strains greater than about 0.05% for the trial loading soft clay. Bothkennar testing has a lower strain resolution of approximately 0.005% and displays a smooth distribution of G/p'_i values, suggesting greater accuracy of testing.

Initial estimates of stiffness, E_u , for the elastic analyses were obtained from the results of the conventional triaxial tests. However, as shall be discussed in section 3.5 a more

accurate representation of the initial behaviour was obtained using E_u values of similar magnitude to those inferred from the CIU test performed with internal strain measurement.

3.4.2 Parameters required for the linear elastic, perfectly plastic (Tresca) soil model

Linear elastic, perfectly plastic (Tresca) analyses were performed to resemble a design which requires a consideration of plasticity (irrecoverable deformations) and an estimation of the factor of safety against failure. Such a check may be incorporated into the design of a foundation which may be subject to occasional loading outwith the normal working range of working loads. Use of this model is typically associated with situations where the main concern of analyses is vertical displacements.

In CRISP the linear elastic, perfectly plastic Tresca soil model requires the selection of four material parameters, E_u , ν_u , c_u and γ_s , where symbols have the same meaning as described previously in section 3.4.1. As for the elastic analyses undrained total stress analyses have been performed therefore, as described previously, $\nu_u=0.499$. Values of γ_s for the foundation layers were selected as discussed previously in section 3.4.1. The value of γ_s was unchanged throughout these studies. Analyses therefore only requires the selection of two parameters: Young's modulus, E_u , is required to describe the stiffness properties of stress states within the yield locus and the undrained shear strength, c_u , is required to define the location of the yield/failure locus. In elastic, perfectly plastic soil models the yield and failure loci are coincident.

Values of elastic stiffness, E_u , were selected from manipulation of available stiffness data and reference to empirical methods (see section 3.6).

Values of the undrained shear strength, c_u , have been estimated from in situ vane, static cone penetrometer, piezocone and triaxial tests. Values of undrained shear strength obtained from these tests are shown in Fig 3.16. Also shown in Fig 3.16 are the values of undrained shear strength obtained by Skempton and Henkel (1953) using the in situ vane test and triaxial test.

In situ vane undrained shear strengths have been adjusted to exclude the effects of testing rate and anisotropy and ageing effects using a correction factor μ empirically related to the plasticity index, I_p (Bjerrum, 1973).

The undrained shear strength has also been estimated from manipulation of static cone penetrometer and piezocone test data. Three static cone penetration tests were performed at the load test site and a full description of the foundation, including the crust was obtained at each test location. Three piezocone tests were performed at locations distant from the load test site.

Using static cone penetration test data values of the undrained strength can be estimated from relation (3.1),

$$c_u = \frac{q_c - \sigma_v}{N_k} \quad (3.1)$$

Where $(q_c - \sigma_v)$ is the nett cone resistance for the cone penetrometer; q_c is the measured cone tip resistance, σ_v is the total vertical stress (in situ overburden pressure) and N_k is the cone factor.

Similarly, values of c_u can be estimated from piezocone data using relation (3.2),

$$c_u = \frac{q_t - \sigma_v}{N_{kt}} \quad (3.2)$$

Where $(q_t - \sigma_v)$ is the nett cone resistance for the piezocone; q_t is the corrected cone resistance such that $q_t = q_c - \lambda u$; u is the water pressure that acts on the shoulder of the cone tip at its joint within the sleeve and λ is an area correction factor equal to the ratio of the area of the groove behind the cone head, A_g , to the projected base area of the cone, A_c . Typically, λ is in the range of 0.15-0.25; N_{kt} is the piezocone factor.

The cone factors N_k and N_{kt} are estimated by plotting the nett cone resistance $(q_c - \sigma_v)$ and $(q_t - \sigma_v)$ against the corrected in situ shear vane undrained shear strength, Figs 3.21 and 3.22.

The gradients of the best fit lines passing through the origin, determined using linear regression, give estimates of N_k and N_{kt} of 15 and 11 respectively. The spread of nett cone resistance data, from which N_k is estimated, is wide leaving room to interpretate an appropriate value of N_k . The spread of data shown in Fig 3.21 gives a range of N_k

of 8-35. The large range of N_k values may be attributed to the wide range of plasticity index, I_p , Fig 3.12. Data presented by Lunne and Kleven (1981) show that for normally consolidated marine clays using corrected field vane strengths the cone factor N_k ranges between 11 and 19, with an average of 15. O'Riordan et al (1982) report an N_k range of 12 to 18 for three soft clay sites in Northern Ireland. Robertson and Campanella (1983) suggest the use of N_k equal to 15 for soft normally consolidated clays. For sensitive clays the value of N_k should be reduced to 10 or less depending on the degree of sensitivity. The soft clay at this site has a sensitivity, S_t , typically less than 5; however, some thin layers of silty clay were found at approximately 9m depth to have a sensitivity of 5-7 (Skempton and Henkel, 1953). It was thought that these sensitive layers were sufficiently remote so as not to influence the foundation behaviour. In view of the reviewed data for similar soft clay sites, a value of N_k equal to 15 was adopted for this study and as can be seen from Fig 3.21 an N_k equal to 15 provides a reasonable fit to the q_c : c_u data.

Some check on the estimated value of N_{kt} can be made using relation (3.3) (Mayne, 1992) assuming that the spherical cavity expansion theory of Vesic (1977) applies to the penetration of the cone tip.

$$N_{kt} = \frac{4}{3}(\ln I_r + 1) + \frac{\pi}{2} + 1 \quad (3.3)$$

where I_r ($=G/c_u$) is the rigidity index and G is the shear modulus of the soil.

As described previously the value of shear modulus is dependent on the magnitude of strain induced during testing. This is evident from Fig 3.18, as shear moduli estimated from seismic cone test, measured at strains of approximately 0.001% (Smith et al., 1992) are approximately 2.5 and 8 times larger than those measured from triaxial testing with internal and external strain measurement respectively. As a result, the rigidity index, I_r , will also be sensitive to the magnitude of strain over which the shear modulus is measured. Vesic (1977) does not give any indication as to the appropriate level of strain the shear modulus should be measured for use in relation (3.3). Values of N_{kt} determined from relation (3.3) and using values of G obtained from triaxial

testing (with internal and external strain measurement) and seismic cone tests are presented in Table 3.1.

As can be seen from Table 3.1 the value of N_{kt} is influenced by the magnitude of strain at which the shear modulus is measured. Values of N_{kt} estimated using values of shear modulus obtained from the seismic cone tests are slightly larger than that obtained from Fig 3.22. Conversely values of N_{kt} estimated from values of shear modulus estimated from triaxial testing at strains of 0.5-1.0% (external strain measurement) are typically lower than that estimated from Fig 3.22. The value of N_{kt} estimated from the single value of shear modulus obtained from the triaxial test with internal strain measurement agrees with that estimated previously from Fig 3.22, and provides a reasonable average of Table 3.1 values.

The ratio of the nett piezocone resistance and the uncorrected vane strength, N_{kt} , measured at an experimental soft clay site at Bothkennar gives a range of 12-14 (Nash et al., 1992). Using corrected vane strengths (Bjerrum, 1973) this range is increased to 14-19. The difference between "corrected" N_{kt} ratios for the two sites can be attributed to the larger undrained shear strength and lower organic content of the Bothkennar clay. In view of the available data a value of N_{kt} equal to 11 was adopted for this study.

Undrained shear strengths obtained from the undrained unconsolidated (UU) triaxial tests are generally lower than those obtained from the vane tests. This is particularly evident at 7-11m depth and may be due to the higher sensitivity of the soft clay within this depth range (Schnaid et al., 1993).

No significant difference exists between the results of the triaxial and vane tests reported by Skempton and Henkel (1953) throughout the foundation depth. The reason for this is unclear.

An initial estimate of the undrained shear strength profile for the soft clay was obtained by using the average profile of available undrained shear strength data.

3.4.3 Parameters required for the elasto-plastic soil model, modified Cam Clay

Analyses using the modified Cam clay soil model were performed to replicate a design situation where a more complex method of analysis is required. Such a design may be required if the structure were constructed in a sensitive area, i.e., a typical urban environment which is congested with surface and buried structures. In this case, a serviceability limit state design may require more than an estimate of displacements, both vertical and horizontal, but also an estimate of the increase in excess pore water pressure and effective stress states within the foundation.

A description of the modified Cam clay effective stress soil model is given in section 2.3.4. In this section a brief review of the material parameters required to describe the modified Cam clay soil model and how they are selected from available site investigation and laboratory data is discussed. Parameter selection for the modified Cam clay soil model was not straightforward but was frustrated by sparse and inaccurate data (see section 3.6). Therefore, for these analyses parameter selection depended greatly on empirical and semi-empirical methods and the results of earlier analyses performed using the Tresca soil model. As noted previously in chapter 2 (section 2.3.4.2.), the modified Cam clay effective stress soil model requires the selection of five material parameters; κ , λ , v' , e_{cs} and M together with a description of stress history, p'_o . Symbols have the same meaning as described previously in chapter 2.

Parameters κ and λ are required to define the slope of the unload-reload and normal compression lines in the compression plane $v: \ln p'$ (where v is the specific volume and p' is the effective mean stress) and are estimated from oedometer test data. Typically, the unload-reload line is assumed to be linear and a value of κ estimated from the average slope of the entire unloading process (variation of K_o on unloading ignored). Rarely however, is the unloading process linear (Muir Wood, 1990) and as can be seen from Fig 3.23 the unloading process in this case of the trial loading soft clay is not strictly linear. This feature of the unloading data does leave room for interpretation in selecting a value of κ . Here, values of κ have been estimated assuming an average slope of the entire unloading process and from the slope of the unloading line

immediately after a change in the loading direction in an oedometer. However, due to the resolution of the oedometer tests (which is rarely low enough to measure low strain elastic stiffness) neither assumptions provided values of κ which gave elastic stiffnesses high enough to accurately model the initial stiff elastic response of the trial loading. As a result, values of κ were selected indirectly from the result of the single CIU test with internal strain measurement and reference to published data and empirical methods (see section 3.6).

Once a stress state lies on the yield locus plastic strains will occur, the magnitude of which are controlled by the parameter λ . Values of λ are typically determined from the slope of the line drawn through the oedometer normal compression data, Fig 3.23. As can be seen from Fig 3.23, the normal compression line is approximately linear and is described well by the “best fit” line. In section 3.6 empirical methods are also used to check and supplement sparse oedometer test data.

As described previously in chapter 2, throughout this study analyses have been performed assuming a constant value of Poisson’s ratio, ν' and hence a mean stress dependent shear modulus, G . The shear modulus is calculated automatically within the soil model and only Poisson’s ratio is specified in the input.

Poisson’s ratio, which gives the ratio of elastic horizontal strain to vertical strain, is also required to describe the elastic response of the soil. Values of Poisson's ratio are typically arbitrarily selected and often assumed equal to either 0.3 or 0.2 for soft clays (Magnan et al., 1983 and Hird, 1994). Very often in numerical analyses a value of Poisson's ratio is selected for numerical convenience rather from considerations of the foundation soil properties (Almeida et al., 1986). Wroth (1975) indicates some dependence of Poisson's ratio on the Plasticity Index, I_p , Fig 3.24. Therefore, assuming an average plasticity index of 45-50% gives an estimate of Poisson's ratio of approximately 0.25-0.3. Here, following the trend of published data, a value of 0.2 was assumed for Poisson’s ratio.

Values of the critical state parameter M , which defines the slope of the critical state line in the $q: p'$ stress plane and also controls the shape of the Cam clay yields locus,

were primarily obtained using relation (3.5). Values of M obtained using relation (3.5) are shown in Fig 3.25.

$$M = \frac{6 \sin \phi'}{3 - \sin \phi'} \quad (3.5)$$

where ϕ' is the effective angle of internal friction.

Values of the angle of internal friction, ϕ' , were estimated using an empirical link with plasticity index, Fig 3.26 (Mitchell, 1976 and Muir Wood, 1990). Some corroboration of estimated ϕ' values was made using published data from an adjacent soft clay site (Nicholson and Jardine, 1986) Fig 3.15.

A single value of M , equal to 1.1 ($\phi'=28$ degrees), has been obtained from the results of a single isotropically consolidated undrained triaxial test (CIU) performed on a single undisturbed sample of soft clay obtained from a depth of approximately 3.2m depth. No triaxial testing was performed on the crust material and as a result values of M selected for the crust relied entirely on the use of relation (3.5). Estimates of M estimated from relation (3.5) are shown in Fig 3.25.

As described previously in chapter 2 the critical state line in the $v: \ln p'$ plane is defined by specification of parameters e_{cs} (void ratio at the critical state, where $e_{cs}=v_{cs}-1$) and λ . Values of e_{cs} were obtained by re-arranging terms for e_{cs} in relation (3.6) and substituting $p'=p'_{cs}$.

$$e_{cs} = e - (\lambda - \kappa) \ln 2 - \lambda \ln 2 p'_{cs} + \kappa \ln 2 \quad (3.6)$$

Relation (3.6) is in terms of void ratio e , to express relation (3.6) in terms of specific volume, v , substitute $e=v-1$.

Values of the void ratio, e , of the soil were obtained from moisture content tests. Estimates of the in situ void ratio are shown in Fig 3.14.

Stress history of the soil is defined through specification of the size of the initial yield locus, p'_o . Values of p'_o are determined from preconsolidation pressure, σ'_{vc} , data,

which were deduced from oedometer tests, manipulation of piezocone test data and semi-empirical methods based on the vane undrained shear strength. Values of preconsolidation pressure are shown in Fig 3.17.

Five oedometer tests were performed on selected undisturbed samples. The preconsolidation pressure was estimated using Casagrande's method (Casagrande, 1936). Preconsolidation pressures reported by Skempton and Henkel (1953) also estimated from the oedometer test using Casagrande's method, were used to supplement the more recent oedometer data, particularly for the surface crust.

Estimates of the preconsolidation pressure, σ'_{vc} , have also been obtained from an empirical correlation between overconsolidation ratio, n , and the ratio of the vertical effective yield stress, σ'_{yc} , determined from manipulation of piezocone test data, to the preconsolidation pressure, σ'_{vc} , obtained from conventional oedometer tests (Konrad and Law, 1987) Fig 3.27. This method assumes that the value of preconsolidation pressure obtained in conventional oedometer tests is representative of the actual in situ preconsolidation pressure (Morin et al., 1983; Crooks et al., 1984; Leroueil, 1988 and Leroueil et al., 1985). The relation shown in Fig 3.27 is therefore based on conventional oedometer test preconsolidation pressures.

The effective yield stress, σ'_{yc} , is determined from manipulation of the piezocone test data using relation (3.7).

$$\sigma'_{yc} = \frac{q_t - \alpha u}{1 + F_s \tan \phi' \cot \theta} \quad (3.7)$$

Where σ'_{yc} is the yield stress of the soil beneath the centre of the cone tip; q_t is the corrected cone resistance; u is the pore water pressure measured above the base of the cone; α is a correction factor typically in the range of 1.0-1.1 so that αu is the pore water pressure in the failure zone; θ is the apex angle of the cone (60 degrees); ϕ' is the effective friction angle of the soil and F_s is the friction factor for the soil acting on the cone surface, typically assumed equal to 1.0. (Konrad and Law (1987) used the symbol M to describe this friction quantity. The symbol F_s has been used here to avoid confusion with the Cam clay critical state parameter M).

Relation (3.7) was developed from interpretation of piezocone penetration based on cavity expansion theory as used by Gibson (1950) for the problem of bearing capacity of deep foundations.

Konrad and Law (1987) have defined the "preconsolidation" stress as σ'_{yc} so as not to confuse this value with the preconsolidation pressure, σ'_{vc} , determined from an oedometer test. The authors also emphasise that σ'_{yc} and σ'_{vc} should not be expected to be equal because these stresses have been obtained from tests with different stress paths as well as different strain rates. However, the two stresses relate to a yield condition of the same soil and consequently the features displayed by the oedometer overconsolidation profile should also be evident in the piezocone overconsolidation profile.

To determine the overconsolidation ratio, n , and consequently σ'_{vc} , without prior knowledge of stress history, an iterative procedure may be used. The ratio $\sigma'_{yc}/\sigma'_{vi}$ provides the first value of n , where σ'_{vi} is the initial in situ effective stress. Using Fig 3.27 the ratio $\sigma'_{yc}/\sigma'_{vc}$ can be obtained. A new n is obtained by dividing the original $\sigma'_{yc}/\sigma'_{vi}$ by $\sigma'_{yc}/\sigma'_{vc}$. This procedure is repeated until satisfactory convergence of the value of n is obtained. Values of n and σ'_{vc} obtained using this procedure are presented in Figs 3.29 and 3.30.

In soft soils the cone tip loads are often about 2-4% of the design capacity of the cone therefore, considerable care is required during the testing procedure to ensure suitable precision. The variation of σ'_{yc} , Fig 3.28, and σ'_{vc} , Fig 3.30, may be attributed to this.

The empirical relation (3.7) is based on information of preconsolidation history obtained from five eastern Canadian soft clay deposits (Gloucester (Ontario), Saint-Marcel (Quebec), Varennes (Quebec), Ottawa Campus and Ottawa Sewage treatment plant (Ontario)). Typical properties of the Canadian clays are very different from those at the trial loading site, the most obvious being sensitivity, S_t , which is in the range of 10-500. Plasticity index, I_p , of the Canadian clays is also lower, typically 25-40%.

Despite the different clay properties from which Fig 3.27 was derived, the empirical relationship has produced reasonable results which agree with the preconsolidation pressures obtained from the oedometer tests. Nevertheless, this method should be used

with caution and only if additional preconsolidation data exist with which to check the results.

Use of the piezocone method has the advantage that a continuous record of preconsolidation stress can be deduced throughout the test depth, enabling significant variations of σ'_{vc} to be identified throughout the foundation soil. Very often however, piezocones are not used in land site investigation practice. Conventionally, estimates of preconsolidation pressures are obtained from a few oedometer tests and some interpolation between the test results is required. Variations of σ'_{vc} , which would be easily identified from a piezocone test, can be missed. An appropriate check on the results in Fig 3.30 and a supplement to typically sparse oedometer data can be obtained from a semi-empirical correlation between the in situ field vane undrained strength c_{uFV} and the preconsolidation pressure, σ'_{vc} , relation (3.7) (Hansbo, 1957; Larsson, 1980 and Mayne and Mitchell, 1988).

$$\sigma'_{vc} = \alpha_{FV} c_{uFV} \quad (3.7)$$

where c_{uFV} is the undrained shear strength estimated from the field vane and α_{FV} is an adjustment coefficient which depends on the overconsolidation ratio. The parameter α_{FV} has been found to typically range from approximately 2 to 20 (Mayne and Mitchell, 1988) and is related to the plasticity index.

An expression which is widely used in practice to assess undrained shear strength data for normally consolidated clays is relation (3.8) (Skempton, 1954 and 1957) which links the preconsolidation pressure, σ'_{vc} to undrained shear strength, c_u , as a function of the plasticity index, I_p .

$$\sigma'_{vc} = \frac{1}{(0.11 + 0.37 I_p)} \cdot c_u \quad (3.8)$$

Mayne and Mitchell (1988) from a data base of 263 individual data points from 96 clay sites, have plotted α_{FV} , estimated from relation (3.8), against plasticity index I_p

and found that relation (3.9) provides a reasonable estimate to the apparent trend of the data. Scatter of the data is however quite wide.

$$\alpha_{FV} = 22(I_p)^{-0.48} \quad (3.9)$$

Muir Wood (1990) suggests an approximate link between the strength ratio c_u/σ'_{vc} , as described by relation (3.10), for normally compressed clays.

$$\frac{c_u}{\sigma'_{vc}} = 0.25 \quad (3.10)$$

Here the factor $\alpha=0.25$ is an average number arising from a calculation made using the Cam clay model (Muir Wood, 1990) linking plasticity index, I_p and the angle of friction, ϕ' , with the parameter Λ Fig 3.31. The parameter Λ describes the relative slopes of the normal compression and unloading-reloading lines for the soil, relation (3.11).

$$\Lambda = \frac{\lambda - \kappa}{\lambda} \quad (3.11)$$

Parameter Λ also emerges as a link between the undrained shear strength and overconsolidation ratio, Fig 3.32 (Ladd et al., 1977; Andresen et al., 1979 and Muir Wood, 1990) which is in fact how relation (3.10) emerges.

In relation to the choice of the factor α in relation (3.10) the parameter Λ is not a fundamental parameter and as can be seen from Fig 3.31 a higher or lower value of Λ could have been assumed.

Choice of a suitable relation with which to estimate the preconsolidation pressure from the in situ vane undrained shear strength was investigated by plotting computed and observed values of c_u/σ'_{vc} as a function of the plasticity index, I_p , Fig 3.33. As can be seen from Fig 3.33 observed values of c_u/σ'_{vc} do not exhibit any obvious trend. Relations (3.8) and (3.9) compare reasonably with observed ratios at values of $I_p > 40\%$. For lower values of I_p neither relation (3.8) or (3.9) compares well with

observations. This suggests that relations (3.8) and (3.9) may provide more accurate estimates of σ'_{vc} for higher values of plasticity index $I_p > 40\%$.

Observed values of c_u/σ'_{vc} tend to plot above values of c_u/σ'_{vc} computed using relation (3.10). However, at values of plasticity index, $I_p < 40\%$ relation (3.10) may provide a more accurate estimate of c_u/σ'_{vc} . This behaviour is evident from Fig 3.34 where values of σ'_{vc} computed using relation (3.10) are closer to those estimated using the oedometer test over the depth range of 0-1.5m. Below this depth values of σ'_{vc} computed using relations (3.8) and (3.9) are more accurate.

The final depth profile of preconsolidation was primarily obtained by trial and error. However, the final profile was approximately coincident with the average depth profile of preconsolidation.

3.4.4 Discussion

In this section a brief description of how the required model material parameters were selected from available site investigation and laboratory data has been presented. However these methods, generally relate to the selection of initial or first-estimate parameters and as has been suggested throughout this section final, justifiable parameters giving the most accurate solution were obtained by adjusting the initial parameters using established empirical and semi-empirical methods and some element of trial and error. This was particularly the case for the modified Cam clay analyses.

Analyses and selection of the final parameter sets for the soil models used are discussed in section 3.6.

3.5 Modelling assumptions

In this section the numerical modelling of the trial loading is discussed.

Throughout this study plane strain, undrained analyses were performed. The finite element mesh symmetric about the centre line, used to describe the trial loading is shown in Fig 3.35. The mesh consists of 86 linear strain quadrilateral (eight noded)

elements. The vertical boundaries are assumed to be perfectly smooth allowing vertical movement to occur freely, but lateral movement is fully restrained. The bottom boundary is assumed to be perfectly rough, hence fully restraining vertical and lateral movement.

From site investigation data (index properties, undrained shear strength and preconsolidation pressure) three distinct foundation layers were identified and have been included in the present analysis. For simplicity and to keep the material input to a minimum, the number of foundation layers was maintained at three throughout this study. For analyses an average crust thickness of 1.5m was assumed. The underlying soft clays were divided into two layers of 4.5m and 5m thick.

The condition of plane strain was assumed from examination of the observed displacements after failure had occurred. Surface vertical displacements of survey targets located around the edges of the loading slab, Fig 3.2(a), indicate that the failure was essentially two dimensional and consisted of rigid body rotation of the loading slab. Markers 27-8-2 and 21-28-7, Fig 3.37, are located at opposite ends of the loading slab and as can be seen vertical displacement at the ends of the slab are approximately equal. This suggests that the longitudinal tilt of the slab (tilt in the direction at right angles to the cross section shown in Fig 3.37) is negligible. No measured data are available for the displacement behaviour at the centre of the loading slab.

The assumption of plane strain is only applicable to a transverse section of the slab. During the load test the slab was seen to be predominantly rigid in the transverse section but flexible in the longitudinal section Fig 3.36. This dual behaviour is common in many geotechnical structures, such as rafts and retaining walls. To be able to apply the plane strain assumption the differing longitudinal behaviour must be neglected. The longitudinal flexible behaviour will induce some slip along the soil-structure interface and as a result, modify the pressure distribution towards something between a perfectly flexible and perfectly rigid footing. Analyses performed by Powrie and Li (1991) for long retaining walls, very stiff in the cross section but flexible in their longitudinal direction, using a hypothesis of plane strain for a typical transverse section, present reasonable results, and neglect of this flexible behaviour does not appear to be significant.

Loading of the slab was rapid (loading to 84kPa was complete after 24 hours). As a result, the response of the foundation soil was assumed to be undrained.

The loading of the foundation slab was simulated by applying uniform prescribed vertical displacements directly to the foundation. The loading slab was not modelled. Adoption of the displacement control method is a convenient and simpler method of modelling the perfectly rigid slab. An alternative method would have been to model the slab and gravel sub-base and apply a pressure loading directly onto the slab surface. However, previous researchers (Hooper 1974; Griffiths 1982) analysing similar problems have found this method, used in two or three dimensions, can numerically complicate the problem.

The bearing pressure mobilised at a given vertical displacement was obtained by averaging the vertical stress component occurring in the first row of integration points below the displaced nodes. Using the displacement control method failure is indicated by a levelling out of the average stresses beneath the footing, which having reached the bearing capacity, remain at that value despite further displacement increments.

3.6 Analyses

3.6.1 Introduction

In this section the results of analyses performed using the soil models presented in sections 3.1 and 3.4 are presented and discussed. The object of analyses, for each of the soil models used, was to represent some hypothetical design problem (section 3.1 and 3.4), and determine a set of material parameters which provided a reasonable estimate of the observed foundation response.

Parameter selection for the isotropic linear elastic soil model is considered first in section 3.6.2. Use of this model was included to represent a serviceability limit state design check. Analyses performed using the elastic, perfectly plastic (Tresca) soil model and modified Cam clay soil model are discussed in sections 3.3 and 3.4 respectively. These soil models were used to replicate design situations where more detailed methods of analysis are required.

The main findings of analyses presented in this section are discussed in section 3.7.

3.6.2 Isotropic linear elastic analyses

3.6.2.1 Introduction

In this section the intention of analyses is to reproduce the observed elastic displacement behaviour, replicating a simple serviceability limit state design. Predictions of excess pore water pressures are not usually the concern of serviceability limit state calculations and as a result are not included here.

3.6.2.2 Initial analysis

It is evident from Fig 3.4 applied load: vertical edge displacement profile that the initial response is approximately linear up to an applied load of 40kPa. This suggests that the foundation response is elastic up to an applied load of 40kPa. The average vertical edge displacement at an applied load of 40kPa is approximately 15mm.

An initial estimate of the observed vertical displacement has been made using a simple hand calculation based on Boussinesq elastic theory for a rectangular area, relation (3.12).

$$\delta = \frac{qa}{E_u} (1 - \nu_u) I_s, \quad (3.12)$$

where δ is the vertical displacement; q is the applied pressure loading; a is the lesser dimension of the rectangular area (cross section width) and I_s is an influence factor.

Dempsey and Li (1989) investigating the contact pressure distribution under a rigid rectangular footing on an elastic layer, using finite element analysis, have presented elasticity solutions for relation (3.12), Table 3.2. The average pressure distribution, p_{av} , under the loading slab was obtained from Table 3.3. For simplicity the foundation

was considered as a single layer. An average stiffness, $E_u=1.2\text{MPa}$, was obtained from values of stiffness presented in Fig 3.18 (where $E_u=3G$). The CIU test result, performed with internal strain measurement, was not included in the averaging process.

Using Dempsey and Li's elasticity solution a vertical displacement, $\delta=400\text{mm}$ was obtained. This is significantly larger than that observed and indicates that values of elastic stiffness estimated from triaxial testing performed with conventional strain measurement (0.2-0.5%) are too small. To obtain the observed magnitude of observed vertical displacement at an applied load of 40kPa an average elastic stiffness $E_u=8\text{MPa}$ ($G=2.4\text{MPa}$) is required. This value of E_u was back calculated using Dempsey and Li's elasticity solution and is of a similar magnitude as the elastic stiffness obtained from the CIU test measured at low strain (approximately 0.03%). Therefore, it is evident from this simple calculation that high (low strain) elastic stiffness values are required to accurately reproduce the observed elastic response.

Stiffness determined from the seismic cone test are very large and imply stiffness at low strains. It has been reported that strains induced by the seismic cone are typically less than 0.001% (Smith et al., 1992). Re-applying Dempsey and Li's elasticity solution and assuming a minimum seismic cone stiffness $E_u=12\text{MPa}$ gives a vertical edge displacement of approximately 9mm. This is significantly lower than that observed (=15mm) and suggests that seismic cone stiffnesses are too high for use here. This leaves the single CIU triaxial test from which to select suitable stiffness values.

3.6.2.3 Selection of elastic stiffness for analyses

In the previous section the limitations of available stiffness data have been highlighted. Preliminary investigations of the observed elastic response using a simple hand calculation found that the magnitude of elastic stiffness required to accurately reproduce the observed elastic response was similar to that measured in the CIU test at low strain (approximately 0.03%). No other triaxial tests with small strain measurement were performed. Selection of suitable elastic stiffness parameters, in the absence of more accurate data, predominantly relies on this single test result.

Values of the secant shear modulus, G_{secant} , determined from the CIU test performed with internal strain measurement have been normalised with respect to the undrained shear strength, c_u , and initial mean effective stress, p'_i , and plotted against axial strain, ϵ_a , which is identical to triaxial shear strain in undrained tests, Fig 3.38. Internal measurement of strain was only used for a single triaxial test. Reliable data are only available from internal strain measurement for strains greater than about 0.03%.

Assuming that this relationship between stiffness and shear strain can be applied generally to the whole foundation, values of stiffness, G , can be determined given a value of undrained shear strength or initial mean effective stress, and an estimated strain level. The greatest uncertainty with this method to obtain elastic stiffness data, is accurately estimating the magnitude of shear strain which will occur.

Finite element analyses performed for a rigid footing founded on a low plasticity clay to assess the influence of small strains (Jardine et al., 1986) determined that the axial strains beneath the centre of the footing were less than 0.1%, Fig 3.39. Therefore, for a first approximation of the strain distribution presented in Fig 3.39, can be assumed. The corresponding G/c_u profile is given from Fig 3.38. From Fig 3.38 a $G/c_u=170$ ($G/p'_i=71$) has been assumed from which to determine values of elastic stiffness. The depth profile of undrained shear strength, which plays no part in an elastic analysis but has been included to provide an alternative means of normalising the shear stiffnesses, is shown in Fig 3.16.

Some check on the value of G/c_u estimated from the above method is provided by an empirical correlation relating plasticity index, I_p , and overconsolidation ratio, n , to an elastic stiffness, Fig 3.40 (Duncan and Buchigani, 1976 and Meigh 1987).

The overconsolidation ratio of the soft clay is predominantly in the range of $n=1-1.5$. The plasticity index of the soft clay was seen to be very variable, Fig 3.12 and in the range of $30 < I_p < 80$ (average approximately 50%). This gives a G/c_u ratio range of 40-200. This range is large which for preliminary studies, type A predictions (Lambe, 1973) could be misleading. From back analysis of the loading event G/c_u ratios in the range of 125-250, as implied by the $30 < I_p < 50$ region of Fig 3.40, are most accurate. The high organic content of the soft clay, which accounts for the high values of plasticity index has forced the wide range of possible G/c_u values. Consequently, use

of Fig 3.40 may not be suitable for organic clays in the absence of detailed site or laboratory test data.

For comparison the empirical method described by Fig 3.40 was applied to the Bothkennar soft clay. Plasticity index of the soft clay is typically in the range of $30 < I_p < 50\%$ and the clay has an overconsolidation ratio of approximately 1.5-1.7, which gives a stiffness to strength ratio, G/c_u , of 100-200 (Nash et al., 1992). The soft clay found at Bothkennar has a small organic content, typically less than 5% (Hight et al., 1992). In situ measurements of stiffness at Bothkennar using the self-boring pressuremeter determined a G/c_u ratio of 100-200 for the soft clay. Values of shear moduli were determined over a strain range of 0.34%. Alternatively, small strain triaxial testing performed on undrained samples of Bothkennar clay (Smith et al., 1992) determined G/p'_o ratios of the order of 100-300, for $0.01 \leq \epsilon_a \leq 0.1\%$.

For the crust, values of plasticity index have been assumed from data reported by Nicholson and Jardine (1976) and Nash et al.(1992) for the Bothkennar clay. Typically, values of plasticity index are in the range of $30 < I_p < 50$. Values of overconsolidation ratio are in the range of 2-5, giving a G/c_u ratio of 85-170.

The values of G/c_u estimated from the CIU test data and an assumed strain profile are consistent with the trend of G/c_u ratios estimated from the empirical method. The G/c_u ratio assumed ($G/c_u=170$) is within the upper limit of the range of G/c_u ratios presented. Additionally, the estimated stiffness ratios are consistent with the range of those obtained from in situ and laboratory testing on Bothkennar clay.

The results of linear elastic finite element analyses using the stiffness ratio obtained are presented and discussed in the next section.

3.6.2.4 Undrained analyses

Elastic parameters selected to describe each of the foundation layers are presented in Table 3.4. Values of E_u are based on a $G/c_u=170$, values of undrained shear strength are shown in Fig 3.41. Results of analyses (vertical and horizontal displacements) are shown in Figs 3.42 to 3.45.

As can be seen from Fig 3.42 the selected elastic parameters have accurately reproduced the observed vertical edge displacements up to an applied load of 40kPa. The foundation response is assumed to be elastic up to an applied load of 40kPa. The initial stiff elastic response observed from vertical edge displacement data is also accurately reproduced.

Predictions of lateral displacements are also included in this study. Numerical predictions of lateral displacements, at inclinometers I4, I5 and I6 are compared with those observed in Figs 3.43-3.45. No information of observed lateral displacements at applied loads of less than 63kPa is available.

Except at inclinometer I6 predicted lateral displacements are considerably smaller than those observed between 0 and 6m depth. At inclinometer I6 lateral movements are concentrated between 0 and 3m depth. This behaviour suggests that over this depth range much of the observed lateral displacement is occurring after yield. Measured profiles show little movement is occurring below 6m depth, 3m depth for inclinometer I6 indicating a stiff lateral, predominantly elastic, response in these regions. Between 6-11m depth, 3-11m depth inclinometer I6, predicted lateral displacements are typically overpredicting those observed. To reproduce these small observed lateral displacements higher values of elastic stiffness are required, Fig 3.18. As can be seen from Figs 3.46-3.48 ratios of $G/c_u > 340$ are required. In practice the concern of analyses is to predict maximum or worst case behaviours. Therefore, to ensure accurate predictions of maximum lateral displacement low values of stiffness measured at high strains, 0.5-1% (as is performed in conventional triaxial testing), are required, Fig 3.49-3.51. To demonstrate this a $G/c_u = 85$ was used. However, displacement data have been measured at applied loads in excess of that assumed to represent the limit of elasticity. As a result, use of the elastic model to reproduce these displacements is not suitable and use of a plasticity model may be more appropriate.

3.6.2.4 Discussion

The results of the simple elastic study demonstrate that an accurate description of the low strain elastic stiffness is required if reasonable predictions of the observed initial elastic response are to be made. In this case an estimate of the elastic stiffness was obtained indirectly from manipulation of the small strain CIU test data and an estimated elastic strain level. Initial estimates of the anticipated elastic strain level were obtained from studies performed by Jardine et al. (1986); where shear strains were typically less than 0.1%. Values of elastic stiffness estimated from these assumed values of strain reproduced accurately the observed initial stiff foundation response. Stiffnesses obtained from conventional testing, triaxial and oedometer tests, measured at approximately 1-2% strain could not reproduce the stiff initial response. This demonstrates that optimisation of the elastic stiffness to stress/strain changes that are similar to those expected in the ground is more accurate than selecting elastic stiffnesses from tests which have been performed in a traditional manner over ranges of deformation and stress change which are quite different from those expected. Therefore, even for such simple loading situations laboratory testing to evaluate the stiffness properties of the ground will require measurements of strains of less than 0.1%, particularly if accurate serviceability limit state calculations are required. As shown in sections 3.6.2.2 and 3.6.2.3 this applies to a simple (hand) calculation and more complex (finite element) design approach.

Throughout the study described in this section, linear elasticity has been assumed to describe the foundation behaviour up to an applied load of 40kPa. Experimental studies (Smith et al., 1992) have shown that linear elasticity (constant stiffness with increasing strain) only applies to a very small part of the soil behaviour, strains less than 0.001%. This behaviour is defined by a plateau in the G/c_u or G/p' : $\log \epsilon_a$ plot. Such a behaviour is displayed by the G/c_u : $\log \epsilon_a$ plot presented in this study, Fig 3.38. However, high quality triaxial testing performed on Bothkennar clay does not support constant stiffness or true elastic behaviour over the range of strains shown, $\epsilon_a < 0.1\%$.

3.6.3 Linear elastic, perfectly plastic (Tresca) soil model

3.6.3.1 Introduction

In this section the object of analyses was to simulate a design situation where a more detailed description of the anticipated elastic and plastic displacement is required. The Tresca soil model is also very often used to provide estimates of the bearing capacity of a foundation. Parameter selection with which to perform bearing capacity analyses has also been included.

As for the elastic analyses the study has focused on reproduction of displacements.

3.6.3.2 Analyses

Suitable values of elastic stiffness have been selected previously in section 3.6.2. Therefore, Tresca analyses, incorporating plastic behaviour, require selection of a single parameter, the undrained shear strength, c_u .

The average c_u profile Fig 3.41 was described in analyses by using the facility in CRISP which allows the undrained shear strength to vary linearly with depth (see chapter 2). To do this the input requires the initial value of c_u at the top of each layer and the slope of the c_u profile through the layer, m_c . Initial values of these parameters are shown in Table 3.5. Results of analyses using these initial parameters are shown in Figs 3.52-3.55.

Predictions of vertical edge displacements compare reasonably well with those observed up to an applied load of approximately 60kPa. At applied loads greater than 60kPa computed displacements are underestimating those observed. The observed bearing capacity of 84kPa is accurately reproduced.

Predictions of lateral displacement at inclinometers I4 and I5 are underestimating those observed over the top 4-5m of foundation, but compare reasonably well with those observed below 5m depth. Predictions of lateral displacements at inclinometer I6 are in good agreement with those observed. Observed lateral displacements at

inclinometers I4 and I5 were measured at an applied load of 63kPa. Observed lateral displacements were measured at an applied load of 84kPa (failure) at inclinometer I6.

It is evident from Figs 3.52-3.55 that analyses have provided a reasonable estimate of the observed pre-failure behaviour. However, some adjustment of the selected undrained shear strength parameters is required in order to improve predictions, particularly lateral displacements at inclinometers I4 and I5.

Inaccuracies in the numerical predictions presented are generally associated with underestimating the observed displacements. More displacement (both vertical and horizontal) can be generated in analyses by increasing the magnitude of yield within the soil. Using the Tresca soil model this is done by reducing the undrained shear strength, c_u . Here, more displacement was generated by reducing the undrained shear strength of the surface crust.

The undrained shear strength of the crust was reduced to 20kPa and 15kPa respectively. The results of analyses are shown in Figs 3.56-3.63. For clarity predictions of lateral displacement for each solution are presented separately.

As can be seen from Figs 3.61-3.62, predictions of lateral displacement at inclinometers I4 and I5 performed with a crust $c_u=15\text{kPa}$ compare reasonably well with observations and are more accurate than those obtained using a crust $c_u=20\text{kPa}$. Similarly, predictions of vertical edge displacements performed with a crust $c_u=15\text{kPa}$, up to an applied load of 65kPa, are more representative of the behaviour than those obtained for a crust $c_u=20\text{kPa}$. However, for a crust $c_u=15\text{kPa}$ the predicted bearing capacity is some 1.2 times smaller than that observed at failure (84kPa). Using a crust $c_u=20\text{kPa}$ has underestimated the observed bearing capacity by approximately 1.1 times. Catastrophic failure occurred at an applied load of 84kPa, however at an applied load of 78kPa movements were seen to be occurring without increasing load suggesting a failure condition had already occurred under sustained load (Schnaid et al., 1993). The amount therefore that analyses have underestimated the bearing capacity may be lower.

3.6.3.3 Discussion

In this study analyses have been performed using an elastic perfectly plastic soil model to provide a more detailed description of the foundation displacement behaviour. A description of the plastic displacement and bearing capacity of the foundation soil was required. Selection of suitable elastic parameters was considered previously in section 3.6.2 therefore in this study only the selection of undrained shear strengths, c_u , was required. An initial estimate of the depth profile of undrained shear strength was assumed equal to the average profile of the available undrained shear strength data. From the results of the above study this profile was found to be reasonable for the soft clay underlying the surface crust. However, the resulting average value for the surface crust $c_u=30\text{kPa}$ was found to underestimate the observed plastic displacements. A better estimate of the crust undrained shear strength was obtained by trial and error, $c_u=15\text{-}20\text{kPa}$. These values of undrained shear strength are lower than those measured in the in situ vane test or inferred from static cone penetrometer tests, but are comparable with strengths obtained from triaxial compression tests. This is similar to the findings of Trak et al. (1980). Lefebvre et al. (1987) have found that the undrained shear strength of the crust which can be mobilised is significantly lower than that measured in the in situ vane test due to the occurrence of the local failure in the crust. During the trial loading the occurrence of local failure is evident at an applied load of 50kPa. At this applied load some rotation of the slab occurred, indicated by a sudden divergence of the two centre edge vertical displacement markers' profiles, Fig 3.4. Studies performed by Jardine et al. (1986) for a rigid circular footing on a soft clay foundation also determined that local failure under an edge will occur due to the higher magnitude of strain mobilised under the edges of a rigid loading platform. Lefebvre et al. (1987) suggest that the undrained shear strength assumed in analyses should be equal to the strength in the underlying clay. Applying this assumption to the trial loading gives a crust undrained strength of approximately 8kPa. As can be seen from Fig 3.60 (results obtained for a crust $c_u=15\text{kPa}$), a crust strength of 8kPa would further overestimate the observed plastic behaviour and hence underestimate the observed bearing capacity. Tavenas and Leroueil (1980) suggest that the crust undrained shear strength which should be used in calculations is approximately equal to a third of the

maximum crust undrained shear strength measured with the in situ shear vane. Here, the maximum crust vane undrained shear strength is approximately 30kPa and hence a shear strength of $c_u=10\text{kPa}$ should be used in calculations. Use of this magnitude of c_u in analyses will give a similar result as the method suggested by Lefebvre et al. (1987). Use of the empirical correlations suggested by Tavenas and Leroueil (1980) and Lefebvre et al. (1987) will introduce a high factor of safety into calculations.

. From the results of this simple study, crust undrained shear strengths selected from available triaxial compression tests will provide a reasonable estimate of the observed displacement behaviour and observed bearing capacity (Trak et al., 1980).

This simple study has shown that the undrained shear strength of the crust has a significant influence on the predicted plastic solution and hence bearing capacity. It would therefore be prudent to estimate the undrained shear strength from all the different methods outlined above in order that its effect on the solution can be seen and a final choice made.

From the use of this 'simple' model some important aspects of the plastic foundation behaviour have been identified which will assist in the parameter selection process for the Cam clay soil model. However, before progressing on to the use of this model it is worth noting that the simple elastic perfectly plastic, Tresca soil model has reproduced the essential behaviour of the foundation reasonably well. The original study was primarily concerned with the prediction of displacements, mainly vertical displacements, and an appreciation of the bearing capacity of the soil. As can be seen from the results of the analyses presented here, the model has predicted the behaviour for the design loading, 45kPa, well. Application of the more complex Cam clay model may therefore be academic rather than practical.

Use of finite element analysis to provide estimates of the bearing capacity of the foundation may also not be necessary. A suitable estimate of the bearing capacity can be obtained from a simple hand calculation performed using relation (3.13).

$$q_f = (2 + \pi) \bar{c}_u \quad (3.13)$$

where q_f is the ultimate bearing capacity and \bar{c}_u is the weighted average undrained shear strength of the foundation (weighted with respect to the thickness of each layer).

Values of bearing capacity using this relation and values of undrained shear strength used in this study (section 3.6.3.2) are presented in Table 3.6. As can be seen values computed using relation (3.13) are larger than those computed using finite element analysis by as much as 13%. For most simple design situations where an estimate of the bearing capacity of the foundation is required, relation (3.13) may suffice and the given difference of 13% may not be significant.

3.6.4 Elasto-plastic analyses; modified Cam clay

3.6.4.1 Introduction

In this section the trial loading has been re-analysed using the modified Cam clay effective stress soil model (Roscoe and Burland, 1968). Cam clay analyses have been performed to replicate a design situation where a significantly more detailed description of the foundation response to the trial loading is required.

The selection of material parameters for the modified Cam clay soil model is briefly described in section 3.6.4.2, the results of subsequent analyses are presented and discussed in section 3.6.4.3. The main findings of analyses are discussed in section 3.6.4.4.

3.6.4.2. Parameters selection

The modified Cam clay soil model requires the selection of five soil parameters; κ , λ , v' , M and γ_s (symbols have their usual meaning-see chapter 2) together with an assumption about the initial size of the yield locus, p'_o . Initial values of these parameters were selected from available site investigation and laboratory test data and adjusted to improve the match between computed and observed responses. Adjusted parameters are presented in Table 3.7. The results of the analyses are presented in

section 3.6.4.3. Prior to moving on to section 3.6.4.3, selection of the initial parameters is briefly discussed.

Back analysis of the loading event indicated that the elastic stiffness determined for the crust and soft clay from minimum κ values observed in oedometer tests was too low. Maximum values of elastic stiffness, G , obtained from minimum values of κ , are shown in Fig 3.64. Values of elastic stiffness G , were obtained using relation (3.14).

$$G = \frac{3(1 - 2\nu')(1 + e_o)p'_i}{2\kappa(1 + \nu')} \quad (3.14)$$

where ν' is the effective stress Poisson's ratio; e_o is the initial or in situ voids ratio and p'_i is the initial effective mean stress.

For comparison values of stiffness, G , obtained from triaxial testing are shown in Fig 3.64. As can be seen from Fig 3.64 values of G obtained from the oedometer tests are of the same magnitudes as those obtained from conventional triaxial testing at strains of approximately 0.5-1%. It was found previously in section 3.6.2, using elastic analyses, that the magnitude of stiffness estimated from conventional triaxial tests were too low to accurately reproduce the initial stiff foundation response. Oedometer values of stiffness are of the same order of magnitude and will therefore give a similar result. This also demonstrates that the strain resolution of conventional oedometer testing in this case is also inadequate. As a result, values of elastic stiffness, G , were obtained as described previously for the elastic analyses from the results of the single CIU test performed with internal strain measurement, Fig 3.18. Values of κ were determined from the selected values of G using relation (3.14) in terms of κ . Initial values of G were estimated assuming an initial value of Poisson's ratio equal to 0.2.

Values of κ estimated from relation (3.14) are small, especially for the crust. Additionally, values of κ estimated from the underlying soft clay are typically lower than those found at similar soft clay sites. Values of κ used to describe the elastic stiffness properties of a soft clay foundation at Willow Plantation (A414) England (Hird, 1994) were in the range of 0.043-0.05, with a Poisson's ratio, $\nu'=0.3$. Numerical analyses of the performance of a test embankment constructed on soft Malaysian

marine clay, using the modified Cam clay model, assumed values of κ of 0.03-0.06, with a Poisson's ratio, $\nu'=0.35$ (Chai and Bergado, 1993). The sensitivity, S_t , of the Malaysian clay is larger than that found at the trial loading site described in this chapter. Numerical analyses reported by Mouratidis and Magnan (1983) describing the construction to failure of a trial embankment on soft soils at Cubzac-les-Ponts, South West France, used values of $\kappa=0.013$ for the surface crust and 0.035-0.05 for the underlying soft clay. Poisson's ratio was assumed equal to 0.4 for the Cubzac-les-Ponts failure analyses. These values of κ are approximately 3 and 1.5-2 times greater than those assumed for the crust and soft clay.

Estimated values of κ required to describe the elastic stiffness of the soft clay foundation at Paimio, Finland (Naatanen and Lojander, 1994) were of the order of 0.01 for the overconsolidated surface crust and 0.015 for the underlying soft soils. For these studies Poisson's ratio was assumed equal to 0.3 and 0.1 for the crust and soft clay. These values are lower than those selected for the trial loading. The sensitivity, S_t , of these soft Finnish clays is typically very much greater than that found in the UK.

Values of λ for the soft clay were determined directly from oedometer normal compression data. Some check on λ values is provided by a correlation which links λ with plasticity index, I_p , relation (3.15), Fig 3.65 (Muir Wood, 1990).

$$\lambda = 0.586 I_p \quad (3.15)$$

Fig 3.65 has been compiled from a number of published sources describing the compressibility of soils from around the world.

From this relation estimates of λ can be made given a value of plasticity index, I_p . Plasticity index varies considerably with depth, Fig 3.12, consequently values of λ estimated using this relation also exhibit a wide variation. Despite this, values obtained from the average relationship compare well with values of λ estimated from the oedometer test.

Values of λ estimated from oedometer and triaxial tests at an adjacent site (Skempton, 1944 and Nicholson and Jardine, 1986) were in the range 0.22-0.46 for the surface crust and 0.26-0.57 for the underlying soft clay. Estimates of λ obtained from the soft clay test site Bothkennar, Scotland (Nash et al., 1992) are 0.04-0.4 for the

surface crust and 0.2-0.45 for the underlying soft clay. These data of compressibility tend to plot close to or on the line given by relation (3.15). The sensitivity, S_t , of these soils is low, typically, $S_t < 6$. Clays of a high sensitivity, $S_t > 16$, such as some Canadian or Scandinavian clays (Tavenas et al., 1986) tend to plot some distance above the line given by relation (3.15). This suggests that relation (3.15) is only applicable to clays of a low sensitivity. Values of λ selected for the analyses are comparable with those determined from adjacent sites and from similar UK soft clay sites.

A single value of Poisson's ratio $\nu' = 0.2$ was selected for the foundation. This value of Poisson's ratio was mainly obtained by trial and error, however some guidance as to a suitable value of ν' was obtained from published data (Nicholson and Jardine 1986; Hird, 1994 and Naatanen and Lojander, 1994). Additionally, field observations of embankment construction on soft soils (Tavenas et al., 1980) suggest that the ratio of maximum lateral movement to maximum vertical movement at the early stages of construction is approximately 0.2. Researchers have found that in order to obtain such a low movement ratio, low values of Poisson's ratio of the order of 0.1-0.2 are required (Poulos et al., 1989).

A description of the position of the critical state line in $e: \ln p'$ and $q: p'$ space is given through specification of parameters e_{CS} and M . Values of e_{CS} were estimated from relation (3.6), but were found to have little influence on the predicted result.

From the single undrained triaxial test an estimate of the critical state parameter M , equal to 1.1, was obtained from an undisturbed test sample obtained from 3.2m depth. From the same test the effective angle of internal friction, ϕ' , was estimated to be approximately 28 degrees.

For this study only a single value of $M = 1.1$, was determined for the soft clay, leaving a very vague description of the variation of the parameter M for the foundation. No triaxial data from which M can be estimated are available for the crust. Values of M for the foundation can be estimated from relation (3.5), section 3.4.3.

Values of the angle of internal friction, ϕ' , have been estimated from an empirical link with plasticity index, see section 3.4.3 and Fig 3.26. Estimated values of M are presented in Fig 3.25. As can be seen values of M are very variable throughout the foundation because of the high variability of the plasticity index, leaving some ambiguity as to an accurate description of M . A value of $M=1.2$ was initially assumed for the surface crust, which corresponds to a ϕ' of exactly 30 degrees.

Ideally the value of M should be estimated from a series of triaxial tests performed on samples obtained from various depths throughout the foundation. Here, however this is not possible, since only a single value for the soft clay exists. Initial values of M do compare reasonably well with values obtained from similar soft clay sites (Naatanen and Lojander, 1994) where M is of the range of 0.9-1.20. The sensitivity of these clays is, however, very much larger than the soft clay described here. Numerical analyses using the modified Cam clay model to describe the loading of a soft clay foundation at Willow Plantation (A414) England (Hird, 1994) estimated M equal to 0.97-1.20 for the soft clay and 1.25-1.70 for an overconsolidated crust (surface layer of peat).

The size of the initial yield locus, p'_o , is required to describe the stress history of the soil. The item, p'_o defines the size of the modified Cam clay ellipse and consequently defines the size of the elastic zone and the subsequent occurrence of plasticity. Choice of the p'_o , has a significant influence on the predicted solution and small variations of p'_o can be significant. Many analyses were performed to obtain the final depth profile of overconsolidation. The greatest difficulty throughout the study was the selection of the quantity p'_o , especially for the crust. An initial estimate of the depth profile of overconsolidation was provided by the consistency of measured and predicted undrained shear strengths, c_u , which can be determined from values of p'_o using Cam clay (Hird and Kwok, 1986 and Hird, 1994).

$$c_u = \frac{Mp'_i}{2} \left(\frac{p'_o}{2p'_i} \right)^\Lambda \quad (3.16)$$

where $\Lambda = 1 - \frac{\kappa}{\lambda}$

Initial values of p'_o were chosen so that something resembling the required profile of undrained shear strength (determined from back analysis, see section 3.6.3) was obtained. From back analysis, section 3.6.3, it was found that local yielding was occurring in the crust at shear stresses lower than the in situ vane strengths. In the Cam clay analyses this behaviour was modelled by inputting reduced p'_o values for the crust. As can be seen from Fig 3.66 the final crust p'_o is some 1.5-2.5 times lower than values of p'_o obtained from the piezocone and oedometer tests.

Material parameters are shown in Table 3.7 and analyses are described in the next section.

3.6.4.3 Discussion of results

As can be seen from Figs 3.67-3.72 computed and observed responses are in reasonable agreement. However, many analyses have had to be performed to obtain the current solution. For comparison vertical and lateral displacements solutions obtained from the elastic, perfectly plastic Tresca analyses (EP4 $c_u=20\text{kPa}$) are also shown. In each case an improved solution is provided by the modified Cam clay effective stress soil model.

Vertical edge displacements computed using modified Cam clay compare well with the maximum observed edge displacements (marker 24) up to an applied load of approximately 75kPa. Tresca analyses, compare better with vertical displacements measured at marker 4 up to an applied load of 60kPa. Lower vertical edge displacements were observed at marker 4 than marker 24 due to the tilt of the loading slab. The initial elastic responses of the two soil models are similar. For applied loads of greater than 20kPa the responses of the two models separate. At applied loads of greater than 30kPa the Tresca solution is underestimating the observed displacement response. The Cam clay model is displaying a less stiff response which is very similar to that observed. The initial divergent behaviour of the two model responses is due to the elliptical shape of the modified Cam clay yield locus, compared to the straight line yield locus of the Tresca model, causing yield to occur sooner in the Cam clay

analyses. Following yield a less stiff foundation response is observed. The Tresca stress path will remain longer within the elastic region displaying a stiffer response.

Predictions of lateral displacements using modified Cam clay are in good agreement with those observed at inclinometers I4, I5 and I6. However, at inclinometers I4 and I5 analyses are under predicting the observed response over the top 1m of foundation. Predictions obtained using the modified Cam clay soil model are more accurate than those obtained using the Tresca soil model particularly over the top 6m of foundation. This behaviour is due to the greater magnitude of plastic strains associated with the modified Cam clay soil model, as described previously.

Predictions of excess pore water pressures, Figs 3.71-3.72, are in reasonable agreement with those observed. However, excess pore water predictions at piezometers P1 and P2 are typically underestimating those observed. Predictions for P3 are overestimating those observed by a maximum of 8kPa.

Many analyses had to be performed to obtain the pore water pressure solution. During the course of analyses predictions of excess pore water pressure were found to be significantly influenced by the magnitude of p'_o selected to describe stress history at each piezometer location.

As can be seen from Fig 3.66 low values of p'_o , similar to those obtained from the oedometer test, were required to generate the required magnitude of excess pore water pressure. Excess pore water pressure, δu , is equal to the difference between total and effective mean stress, relation (3.16).

$$u = \delta p - \delta p' \quad (3.16)$$

where δp and $\delta p'$ are the change in total and effective mean stress respectfully.

The required magnitude of excess pore water pressure was obtained by ensuring that sufficient yielding was occurring on the subcritical or 'wet' side of the yield locus giving negative $\delta p'$, Fig 3.73. The tilt of the slab may have caused more yielding and therefore, generated larger excess pore water pressures than would have occurred had the loading slab not tilted. As a result, the final back analysed profile of overconsolidation may be lower than that actually in the field.

At piezometer location P3 excess pore water pressure predictions are overestimating those observed. From relation (3.16) this implies that the change in effective mean stress is too large and needs to be reduced to improve predictions at P3. Changes in effective mean stress only occur once yield has occurred, therefore the magnitude of excess pore pressure computed at P3 can be reduced by reducing the magnitude of yielding. This can be done by increasing the size of the yield locus, p'_o at the location of P3 (6m depth, edge). Estimates of preconsolidation stress obtained from the piezocone and in situ vane test indicate the presence of a stiff layer at approximately 6.0-7.9m depth. Additionally, borehole logs (Skempton and Henkel, 1953 and Schnaid et al., 1993) indicate the presence of a thin stiff layer of peat at approximately 6m depth. The presence of this peat layer may suggest that some drainage is occurring throughout this layer, causing the lower excess pore water pressures measured at P3.

As can be seen from Fig 3.67 modified Cam clay provided a reasonable estimate of the observed bearing capacity. The modified Cam clay soil model predicted a bearing capacity of approximately 80kPa.

3.6.4.4. Discussion

Use of the modified Cam clay soil model has provided a reasonable estimate of the observed foundation response. However, attaining this solution was not straightforward but was frustrated by sparse site investigation and laboratory test data. Empirical and semi-empirical methods have been presented with which to supplement and check available data required for Cam clay analyses.

The main problem was associated with the selection of values of κ required to describe the stiffness properties of stress states within the yield locus. Typically values of κ are estimated from oedometer unload-reload data. However, in this case the strain resolution of the oedometer tests was not small enough to permit selection of suitable values of κ . As a result, values of κ were estimated from the results of a single CIU test performed with initial strain measurement (from axial strains of 0.03%). To ensure a sufficiently high magnitude of elastic stiffness, G , these values of κ were used in conjunction with low values of Poisson's ratio, $\nu'=0.2$. A low value of

Poisson's ratio was also found necessary to provide accurate predictions of the observed lateral displacements.

For the soft clay values of λ were obtained from oedometer normal compression data. Values of λ for the crust were obtained using an empirical correlation between λ and the plasticity index. The empirical correlation was also used to check values of λ estimated for the soft clay.

Values of the critical state parameter M for the soft clay were selected from data available from a single CIU test. Based on an empirical link between M (through ϕ') and the plasticity index this value was assigned to the entire depth of soft clay. Values of M for the crust were estimated using the empirical correlation.

From the results of the analyses it is evident that the empirical methods used to estimate values of λ and M have provided reasonable estimates of these parameters. However, use of empirical methods with which to select suitable parameters should not be thought of as a substitute to laboratory testing from which the parameters should be obtained.

Despite the quality of preconsolidation stress data available many analyses had to be performed to obtain the final depth profile of overconsolidation. For the soft clay the final depth profile of overconsolidation is approximately equal to the average profile, Fig 3.66 (average of all methods used to estimate the preconsolidation stress). Low values of p'_o were assumed, implying values of undrained shear strength, c_u , approximately equal to strengths estimated in triaxial compression tests to model the occurrence of local failure in the crust.

It is evident from the parameter selection process previously discussed (sections 3.6.4.2 and 3.6.4.3) that site investigation and laboratory testing are more demanding in situations where from the outset Cam clay analyses are the intention. Investigations using the Tresca soil model are very much more straightforward and the small number of material parameters required to implement this model still makes it attractive to engineers. Additionally, the Tresca model was found to provide good results, especially for displacements. However, an improved solution was obtained using the modified Cam clay soil model, especially for predictions of lateral displacements. Clearly, modified Cam clay has a role to play in geotechnical design. However, the

demands of the parameter selection process do not make this soil model attractive in engineering practice.

3.7 Conclusions

Finite element analyses of the trial loading have been performed using the isotropic elastic, elastic-perfectly plastic Tresca and elasto-plastic modified Cam clay soil models. These soil models were used to replicate foundation design checks of some hypothetical foundation design situation. For each of the soil models used, especially modified Cam clay, many analyses had to be performed to obtain the presented solutions. Nevertheless, conclusions can be drawn from comparison of observed and computed foundation responses. During the trial loading the initial settlement response was observed to be stiff. As a result high values of elastic stiffness were required in order to accurately model the observed settlement response. Values of elastic stiffness were deduced from a single isotropically consolidated undrained triaxial test performed at low strain (typically, $\epsilon_a < 0.05\%$). Stiffnesses estimated from oedometer and conventional triaxial tests were too low implying that in this case the strain resolution of these tests was not small enough to provide an accurate estimate of elastic stiffness. Consequently, if accurate estimates of deformations are required (serviceability limit state) then it becomes important to match the strain range of the test data to the strains that develop in the ground. Studies performed by Jardine et al. (1986) suggest that the average strains induced under the centre line of a rigid loading platform are typically less than 0.1%. Conventional oedometer and triaxial tests are typically performed at strains of $\epsilon_a > 0.1\%$.

Estimates of elastic stiffness deduced from the single CIU test were checked using an empirical link between normalised elastic stiffness (normalised with respect to the undrained shear strength), plasticity index and the overconsolidation ratio (Duncan and Buchigani, 1976).

Elastic, perfectly plastic Tresca analyses showed that the most accurate description of the depth profile of undrained shear strength was obtained from triaxial compression

tests (for the surface crust) and the in situ shear vane (for the underlying soft clay). Local failure in the crust, occurring under an edge of the rigid loading platform, was found to be occurring at undrained shear strengths some 1.5-2 times smaller than the maximum undrained shear strengths measured using the in situ shear vane and static cone penetrometer. Back analysed crust shear strengths were comparable with strengths estimated from triaxial compression tests. This result is 'similar to the findings of Trak et al. (1980). The undrained shear strength of the surface crust was found to significantly influence the bearing capacity of the foundation.

The Tresca soil model provided a reasonable match to the observed behaviour, particularly settlements. However, an improved solution was obtained using the modified Cam clay soil model. Application of the Tresca soil model, was straightforward compared to the modified Cam clay soil model. Modified Cam clay analyses were frustrated by sparse soils data from which to select the required material parameters. The extent of the site investigation conducted at the trial loading site was probably greater than average. However, available site investigation and laboratory testing data are not necessarily directly applicable to Cam clay analyses. Parameter selection for the Cam clay model was dependent on empirical and semi-empirical methods.

Predictions using the modified Cam clay soil model were significantly influenced by parameters κ and p'_o . Values of κ were selected indirectly from the single CIU test performed with internal strain measurement. Values of p'_o were determined from the assumed undrained shear strength profile. Local failure in the crust was modelled by using reduced values of p'_o . Additional values of preconsolidation stress were estimated using an empirical link with undrained shear strength.

Reasonable estimates of the parameter λ were obtained from oedometer normal compression data. Some check on selected values of λ was provided by an empirical link with plasticity index (Muir Wood, 1990).

Values of the critical state parameter M were estimated using an empirical link with plasticity index (Mitchell, 1976 and Muir Wood, 1990). This method was thought to provide reasonable estimates of M . Data were only available from a single test from which to select values of M .

Despite the dependency of Cam clay parameters on empirical methods, the chosen parameter set provided reasonable predictions of the observed behaviour. A more systematic approach to parameter selection for the Cam clay model may be to tailor the site investigation and laboratory testing to suit these models. However, as mentioned previously, the complexity of the design would need to justify this approach. The original problem, for which the trial loading was performed (Schnaid et al., 1993) did not require use of the more complex Cam clay soil model. However, as will be seen in subsequent chapters, particularly chapter 5, even for some common loading situations use of more complex soil models, i.e., modified Cam clay, is necessary.

Table 3.1. Values of piezocone factor, N_{kt}, estimated from relation (3.3)
(Mayne, 1992)

Depth(m)	Rigidity		Index I _r	Cone		Factor N _{kt}
	Seismic cone	Triaxial (Conv)		Seismic cone	Triaxial (Conv)	
0.8	200	73		11	10	
2.3	1010	22		13	8	
2.3		116			10	
3.2	755	46	190	13	11	11
3.8	755	46		13	9	
5.6	400	82		12	10	
5.8	741	16		13	8	
7.4	312	174		11.5	11	
8.3	661	68		12.5	10	
8.4	846	78		13	10	
10.0	765	52		13	9	

Table 3.2. Centre contact pressure, p(0,0)/p_{av}(r=b/a) (Dempsey and Li, 1989)..

v _f	d/a	r = 1	r = 1.5	r = 2	r = 3	r = 5	r → ∞
0.1	0.3	0.7988	0.8301	0.8456	0.8597	0.8737	0.8950
	1.0	0.5385	0.5712	0.5997	0.6362	0.6660	0.7105
	3.0	0.4877	0.4935	0.5024	0.5210	0.5527	0.6466
	10.0	0.4850	0.4886	0.4947	0.5067	0.5241	0.6375
0.3	0.3	0.8366	0.8653	0.8792	0.8906	0.9020	0.9184
	1.0	0.5503	0.5880	0.6195	0.6574	0.6852	0.7229
	3.0	0.4884	0.4948	0.5044	0.5245	0.5588	0.6485
	10.0	0.4850	0.4886	0.4948	0.5068	0.5245	0.6377
0.5	0.3	1.0045	1.0612	1.0922	1.1164	1.1076	1.0327
	1.0	0.5819	0.6342	0.6756	0.7233	0.7555	0.7567
	3.0	0.4902	0.4981	0.5095	0.5337	0.5753	0.6536
	10.0	0.4850	0.4887	0.4950	0.5071	0.5254	0.6382
	∞	0.4849	0.4884	0.4945	0.5062	0.5227	0.6366

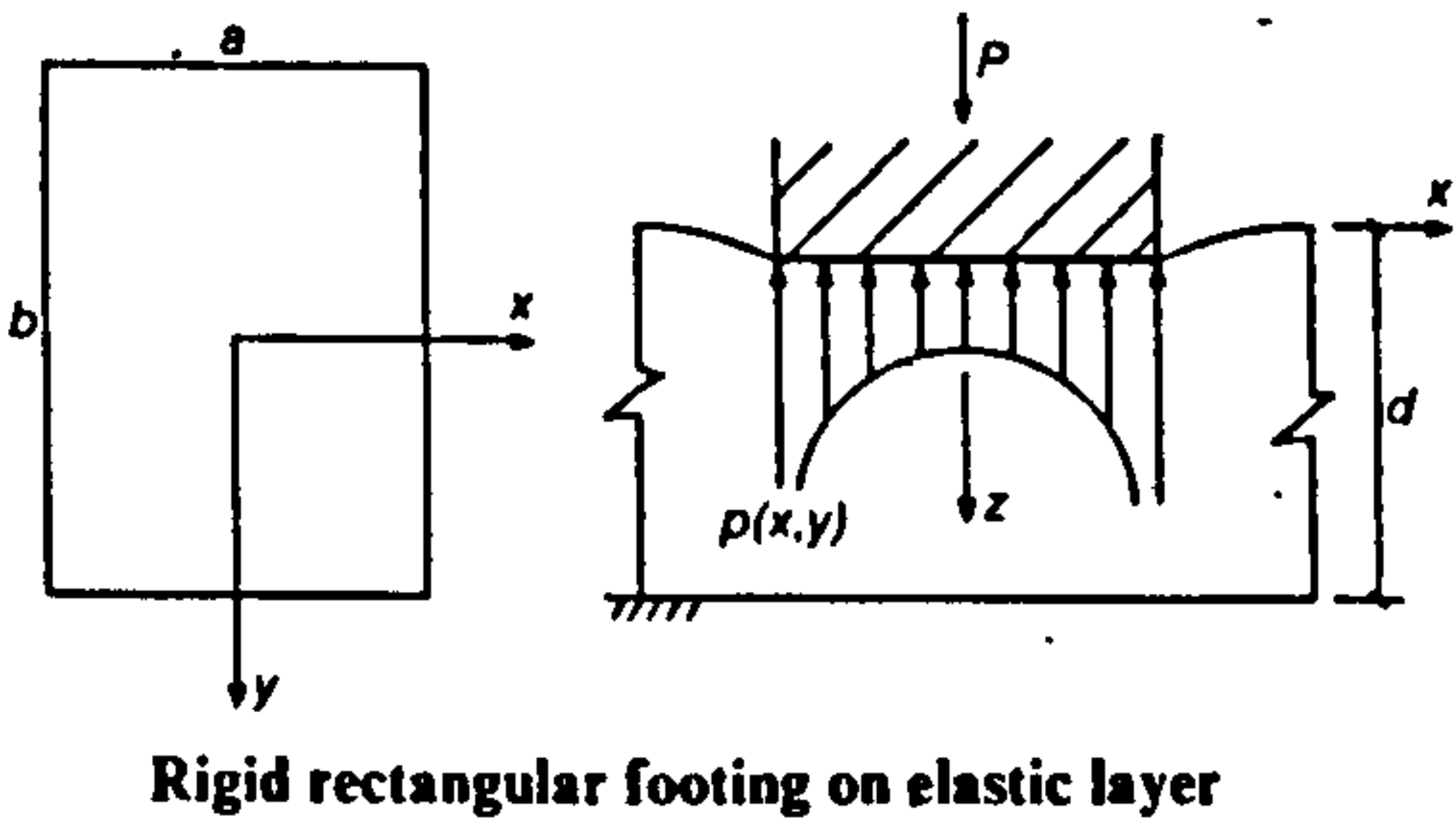


Table 3.3. Displacements, $\left(\frac{\delta}{a}\right) \frac{E_t}{(1-\nu_r^2)p_{av}\left(r=\frac{b}{a}\right)}$ (Dempsey and Li, 1989).

v _f	d/a	r = 1	r = 1.5	r = 2	r = 3	r = 5	r → ∞
0.1	0.3	0.2396	0.2479	0.2522	0.2567	0.2606	0.2668
	1.0	0.5292	0.5795	0.6078	0.6388	0.6659	0.7121
	3.0	0.7389	0.8625	0.9458	1.0496	1.1508	1.3437
	10.0	0.8284	0.9947	1.1183	1.2948	1.5088	2.1010
0.3	0.3	0.2112	0.2166	0.2195	0.2224	0.2252	0.2289
	1.0	0.4989	0.5404	0.5629	0.5869	0.6074	0.6418
	3.0	0.7252	0.8425	0.9200	1.0141	1.1022	1.2619
	10.0	0.8241	0.9883	1.1097	1.2821	1.4883	2.0175
0.5	0.3	0.1059	0.0959	0.0899	0.0835	0.0787	0.0725
	1.0	0.4075	0.4200	0.4217	0.4182	0.4099	0.3921
	3.0	0.6851	0.7839	0.8442	0.9089	0.9549	0.9822
	10.0	0.8116	0.9696	1.0849	1.2452	1.4283	1.7332
	∞	0.8678	1.0537	1.1968	1.4122	1.7020	∞

Table 3.4. Material parameters selected for isotropic linear elastic analyses (Tresca soil model).

Layer No	Depth (m)	E_u (kPa) ⁺	c_u (kPa) ⁺⁺	ν_u	ϕ_u (degrees)
1	0-1.5	30000	5000	0.499	0.0
2	1.5-6.0	6000	5000	0.499	0.0
3	6.0-9.0	13000	5000	0.499	0.0

E_u^+ values estimated from $G_u/c_u=170$.
 c_u^{++} significantly enhanced values of undrained shear strength to ensure elasticity for all stress states.

Table 3.5. Material parameters selected for linear elastic perfectly plastic (Tresca) soil model.

Layer No	Depth (m)	E_u (kPa)	c_{uo} (kPa) ⁺	ν_u	ϕ_u (degrees)	y_o	m_c
1	0.0-1.5	30000	60 (60)	0.499	0.0	0.0	0.0
2	1.5-6.0	6000	12 (15)	0.499	0.0	1.50	0.667
3	6.0-9.0	13000	15 (35)	0.499	0.0	6.0	6.667

c_{uo}^+ values estimated from Fig 3.16. Undrained shear strength at top of each layer
(c_u) undrained shear strength at the base of each layer.

Table 3.6. Ultimate bearing capacity q_f computed using relation (3.13).

Average undrained shear strength c_u (kPa)	18	16	15.5	15	14.5
Ultimate bearing capacity q_f (kPa) relation (3.13)	92	82	79	77	74
Ultimate bearing capacity (finite element analysis)	84	76	70	-	-

Table 3.7 Adjusted material parameters for modified Cam clay analyses.

DETAILS		MATERIAL PROPERTIES					
DEPTH (m)	LAYER No	κ	λ	e_{cs}	M	ν	$\gamma(\text{kN/m}^3)$
0-1.5	1	0.0045	0.20	2.52	0.95	0.2	16
1.5-3.0	2	0.025	0.35	2.57	0.95	0.2	16
3.0-4.5	3	0.025	0.35	3.02	1.10	0.2	15
4.5-6.0	4	0.025	0.35	2.31	1.10	0.2	15
6.0-9.0	5	0.02	0.25	2.54	1.10	0.2	15
9.0-11.0	6	0.02	0.25	2.02	1.10	0.2	15

**TEXT BOUND
INTO
THE SPINE**

Fig 3.1. Location of site.

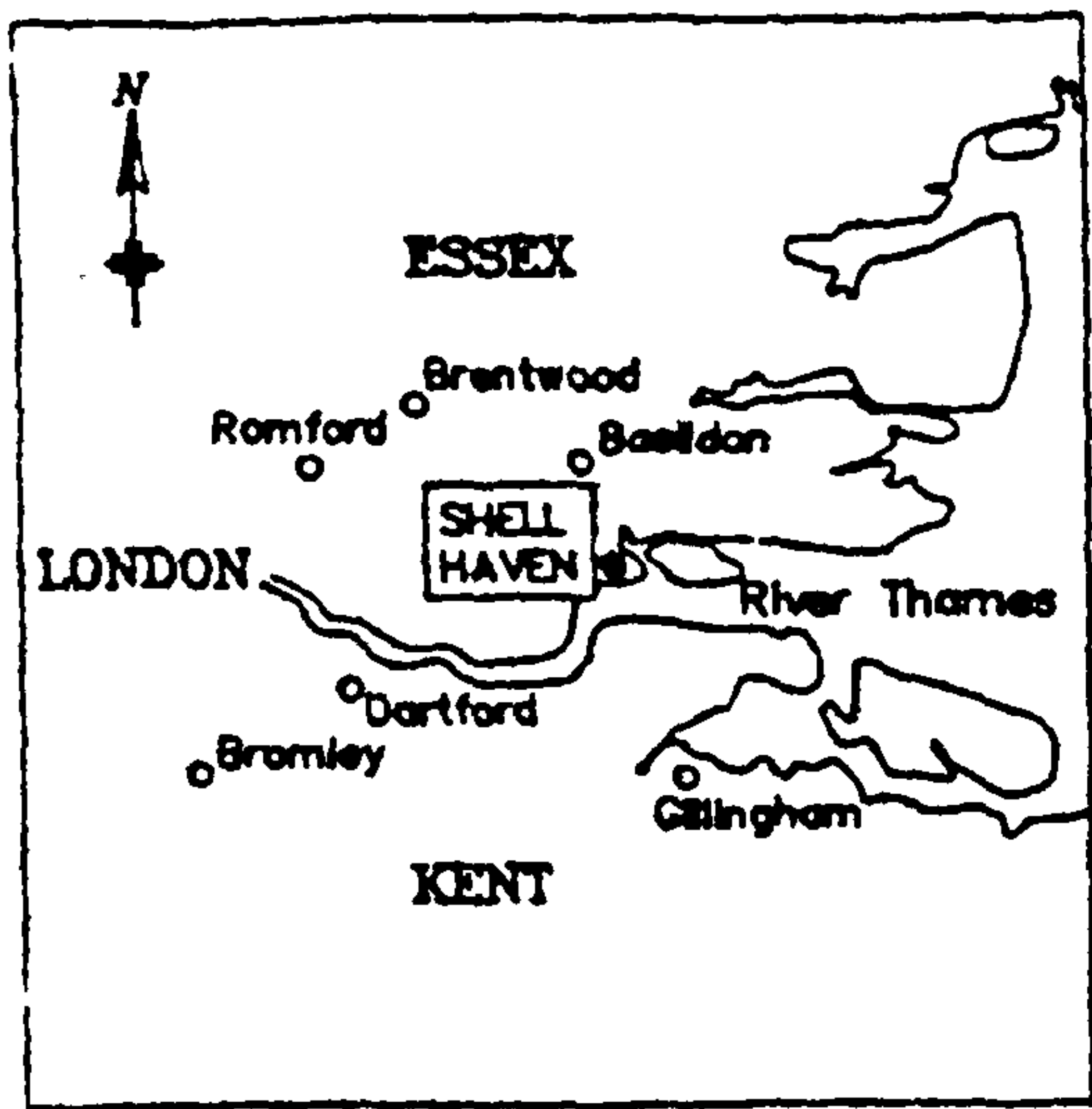
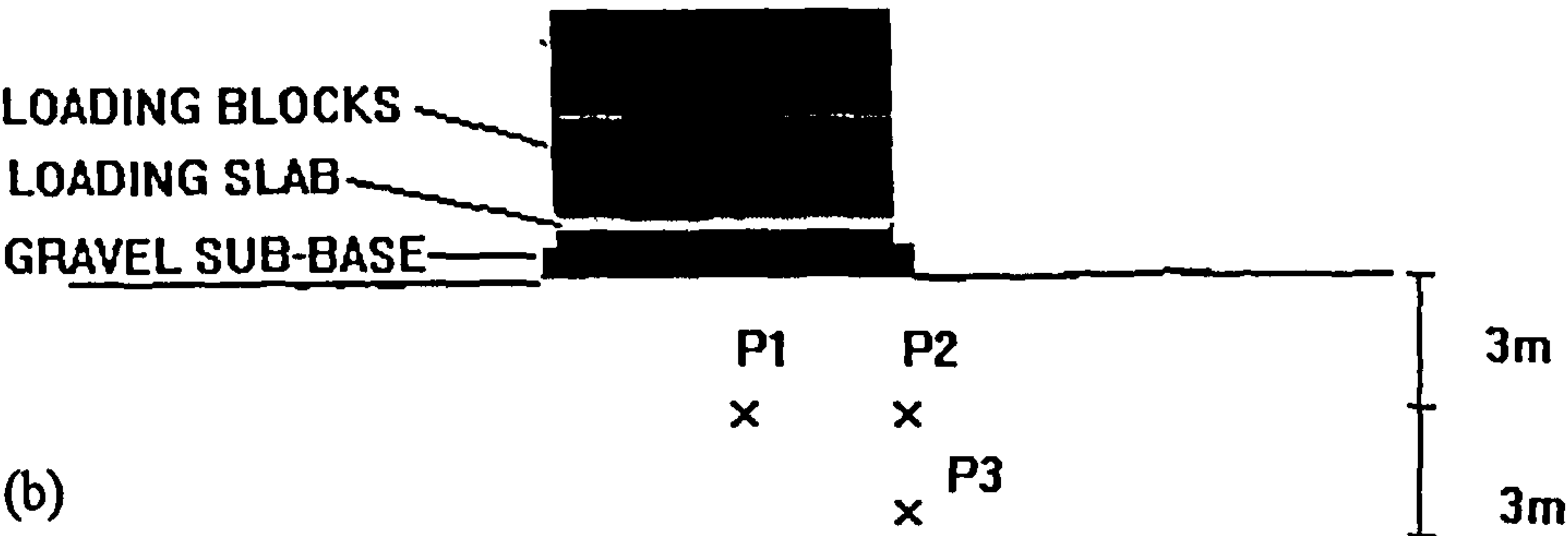
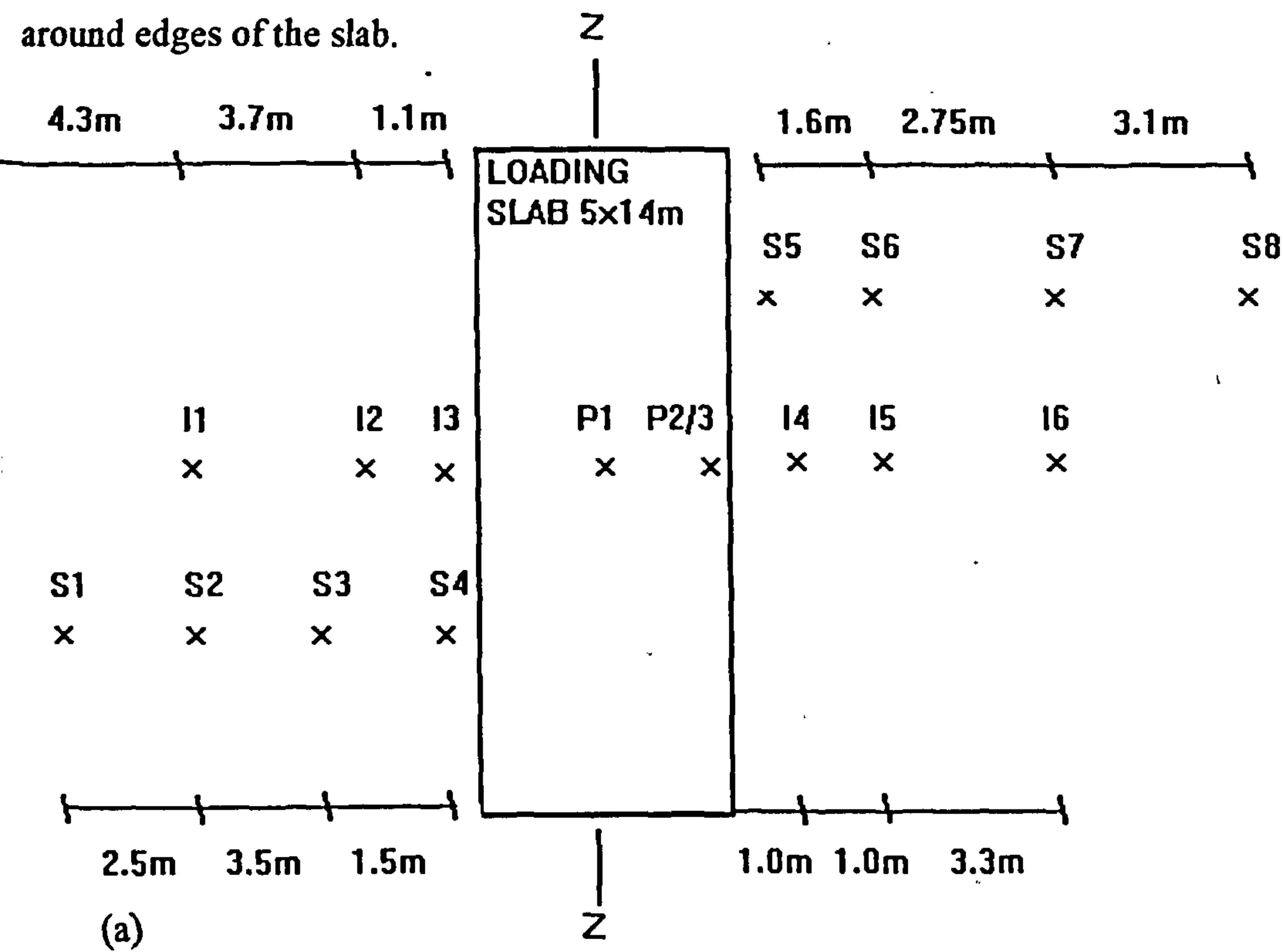


Fig 3.2. Instrumentation layout (a) inclinometers and slip indicators; (b) piezometers and (c) surface vertical displacement markers located around edges of the slab.



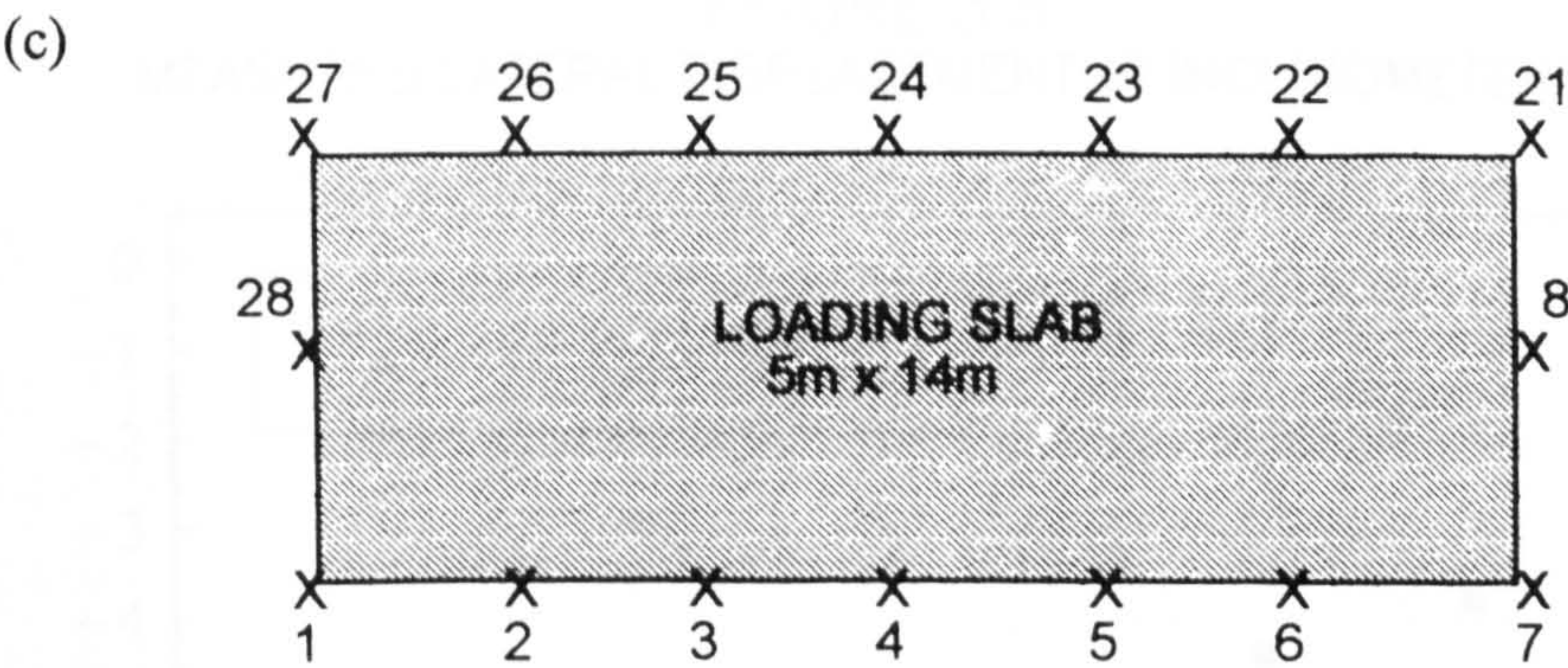


Fig 3.3. Typical loading sequence of concrete blocks on loading slab.

75	69	67	71	73
65	59	57	61	63
55	49	47	51	53
45	39	37	41	43
35	29	27	31	33
25	19	17	21	23
15	9	7	11	13
5	3	1	2	4
12	10	6	8	14
22	20	16	18	24
32	30	26	28	34
42	40	36	38	44
52	50	46	48	54
62	60	56	58	64
72	70	66	68	74

FIGURE 3.4
MEASURED CENTRE EDGE VERTICAL DISPLACEMENT

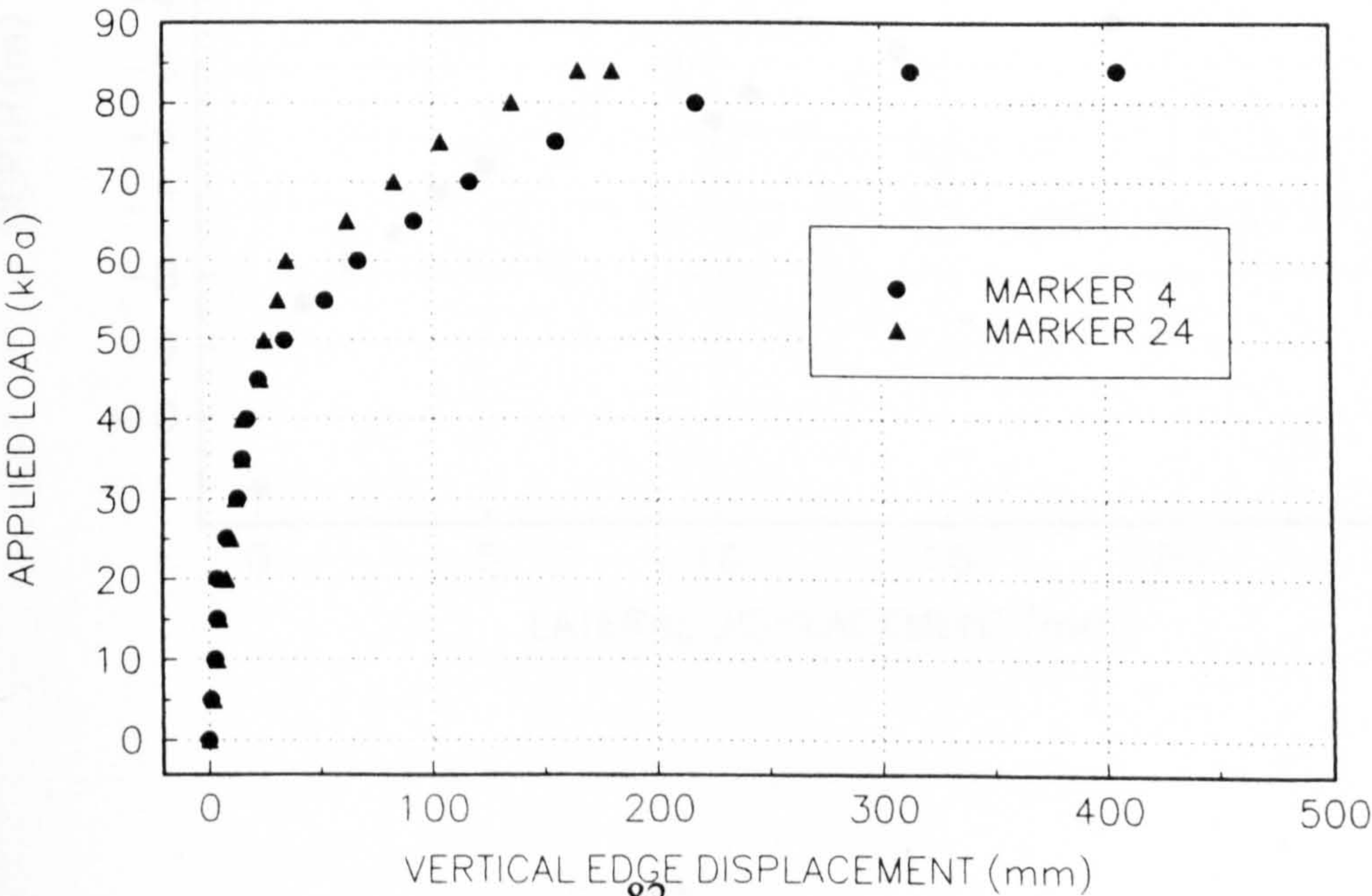


FIGURE 3.5
MEASURED LATERAL DISPLACEMENT AT INCLINOMETER 14

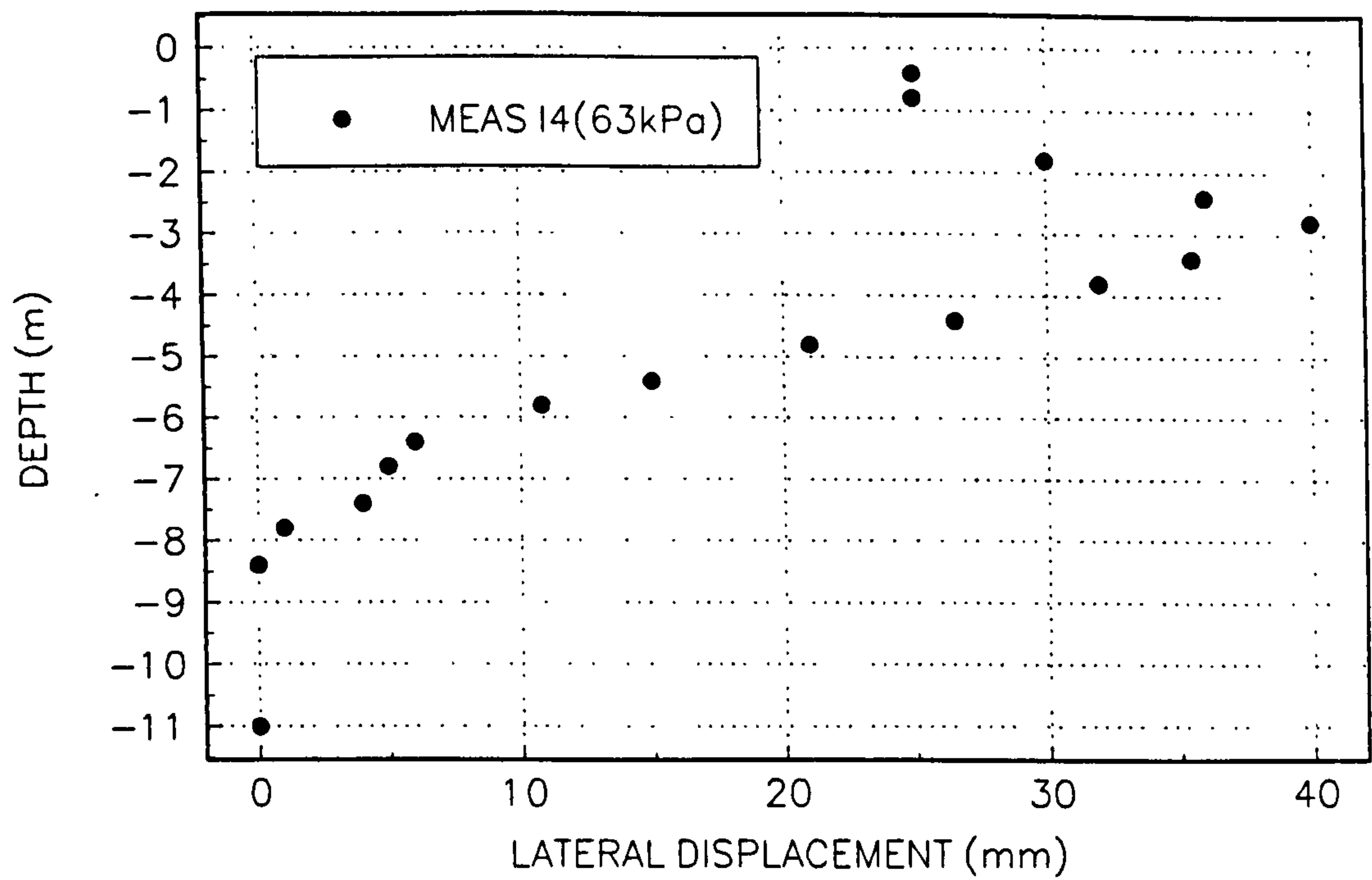


FIGURE 3.6
MEASURED LATERAL DISPLACEMENT AT INCLINOMETER 15

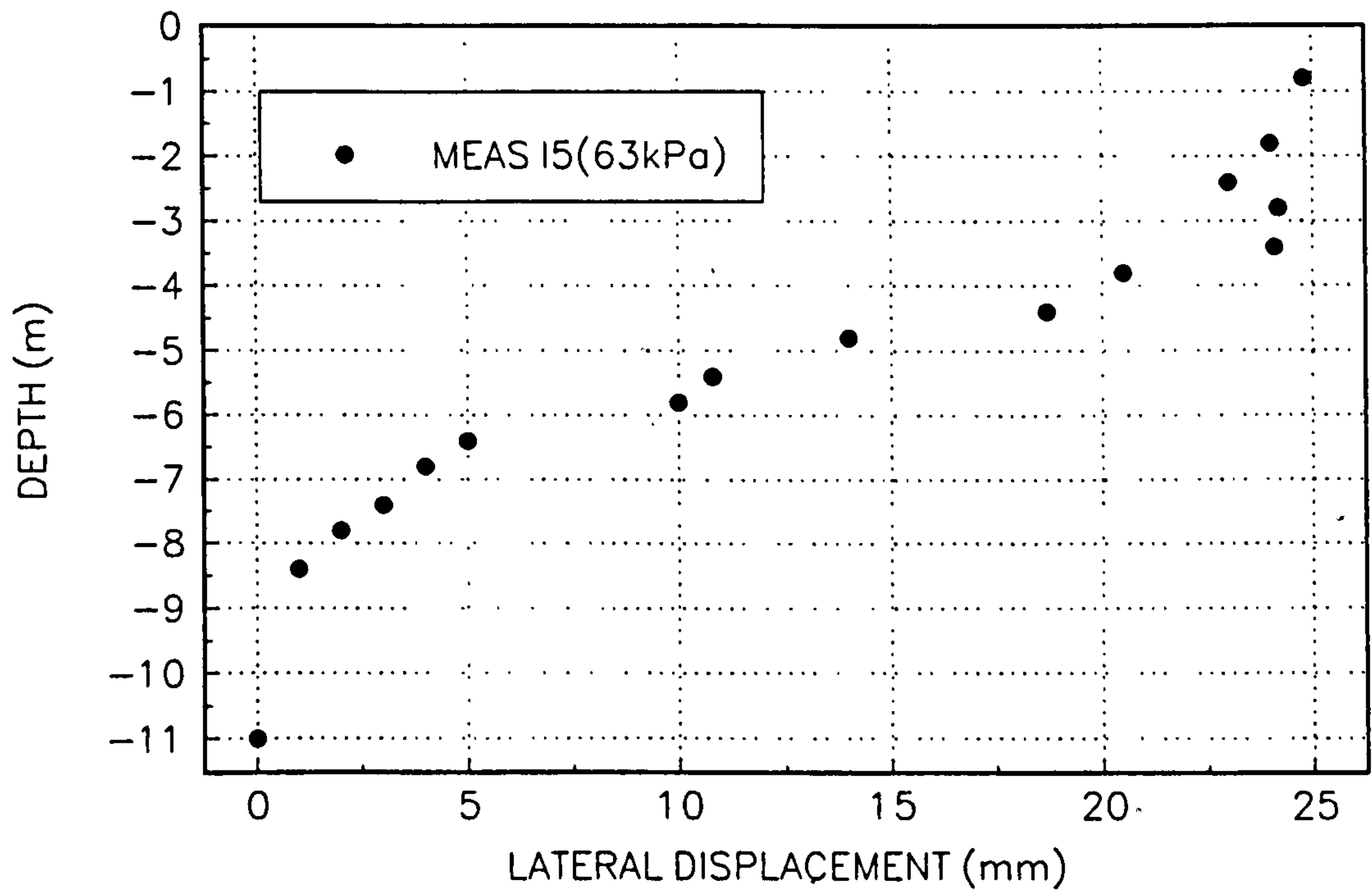


FIGURE 3.7
MEASURED LATERAL DISPLACEMENT AT INCLINOMETER I6

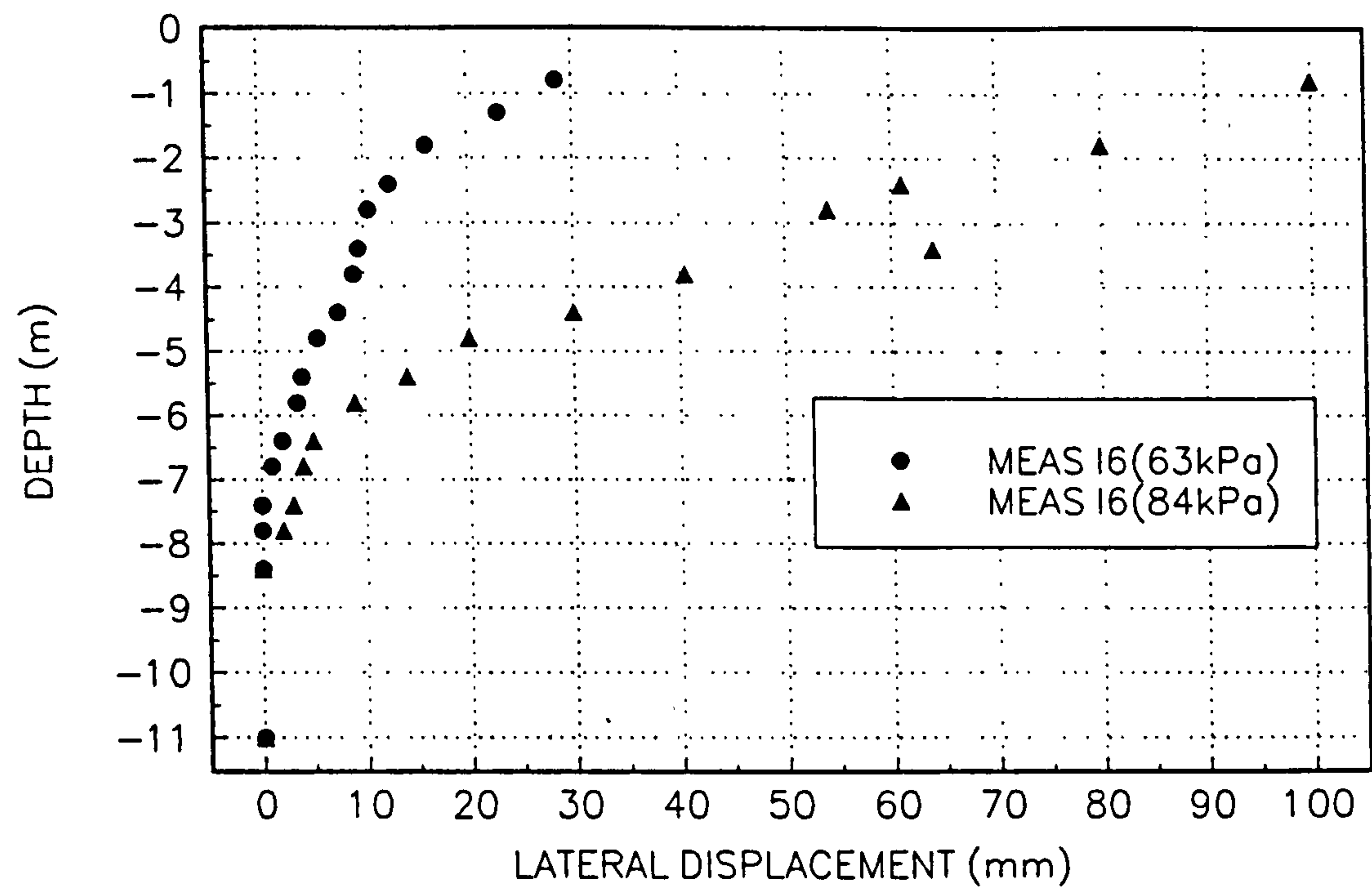


FIGURE 3.8
MEASURED LATERAL DISPLACEMENT AT INCLINOMETER I7

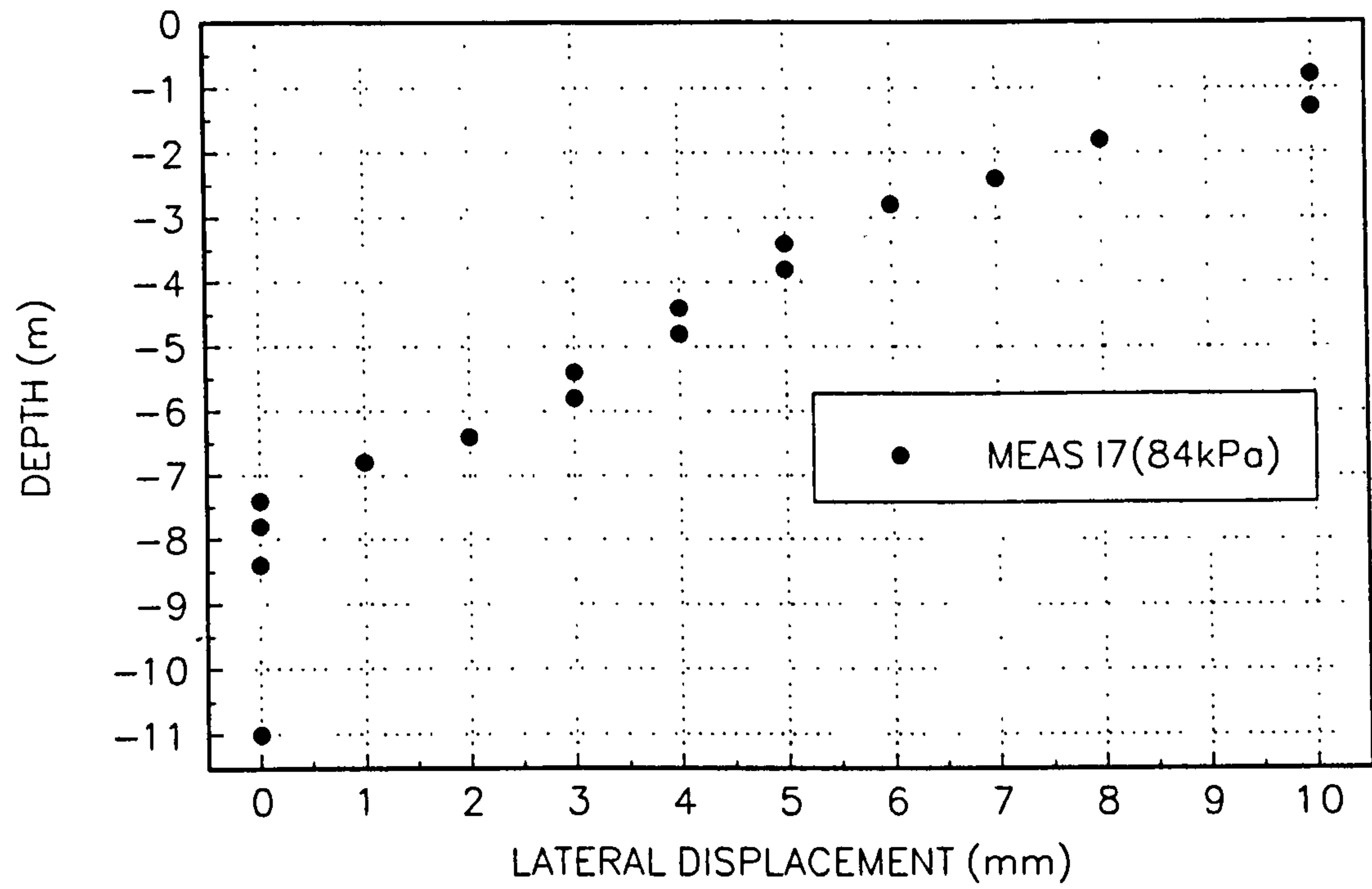


FIGURE 3.9
MEASURED EXCESS PORE WATER PRESSURES

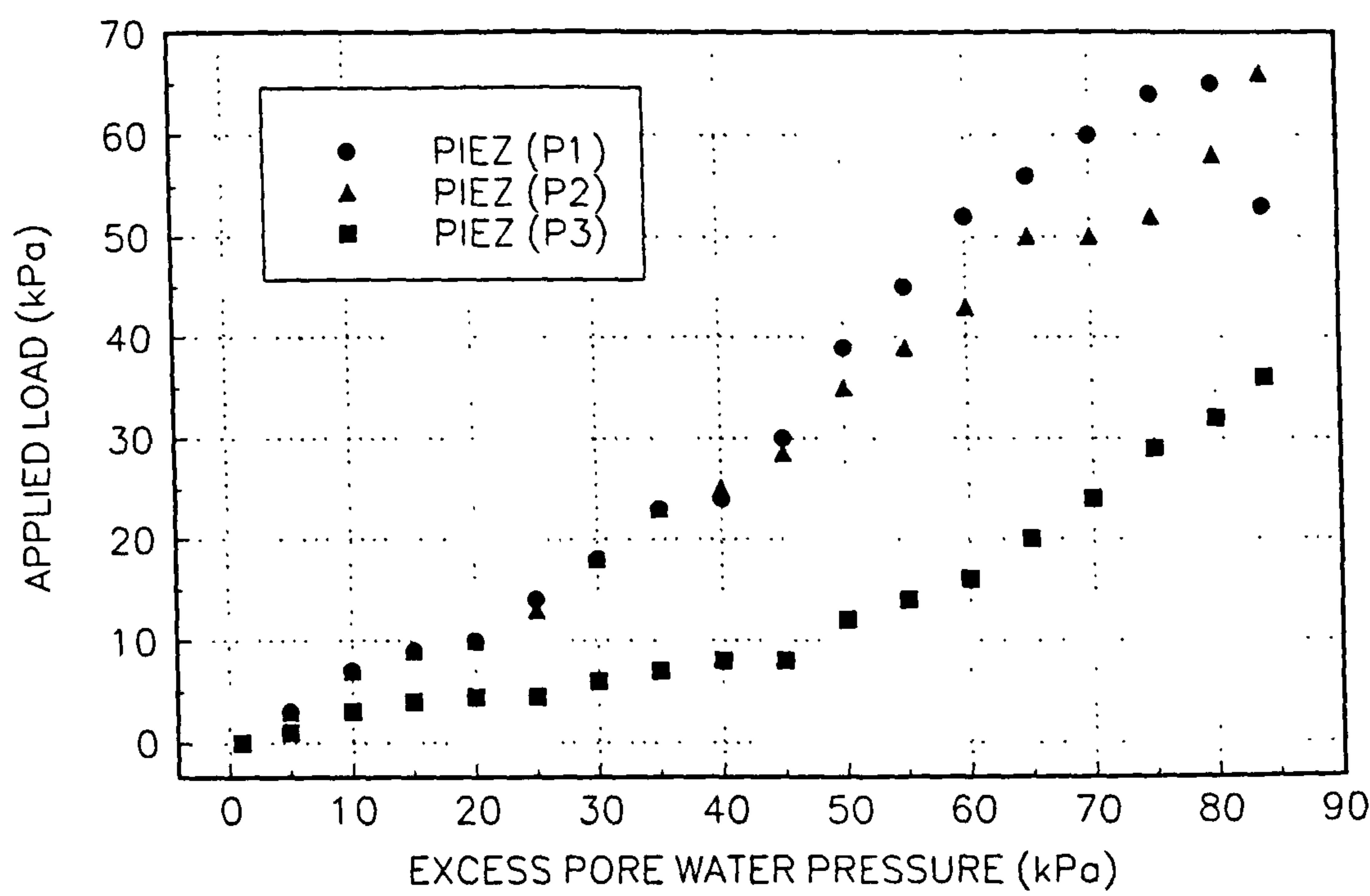


Fig 3.10. Typical geotechnical profile at site.

DEPTH	STRATA
0.0	Firm clay (Crust)
1.5	Soft to very soft CLAY
6.0	Firm PEAT
7.0	Soft becoming firm sandy CLAY
11.0	Dense GRAVEL

FIGURE 3.11
INDEX PROPERTIES

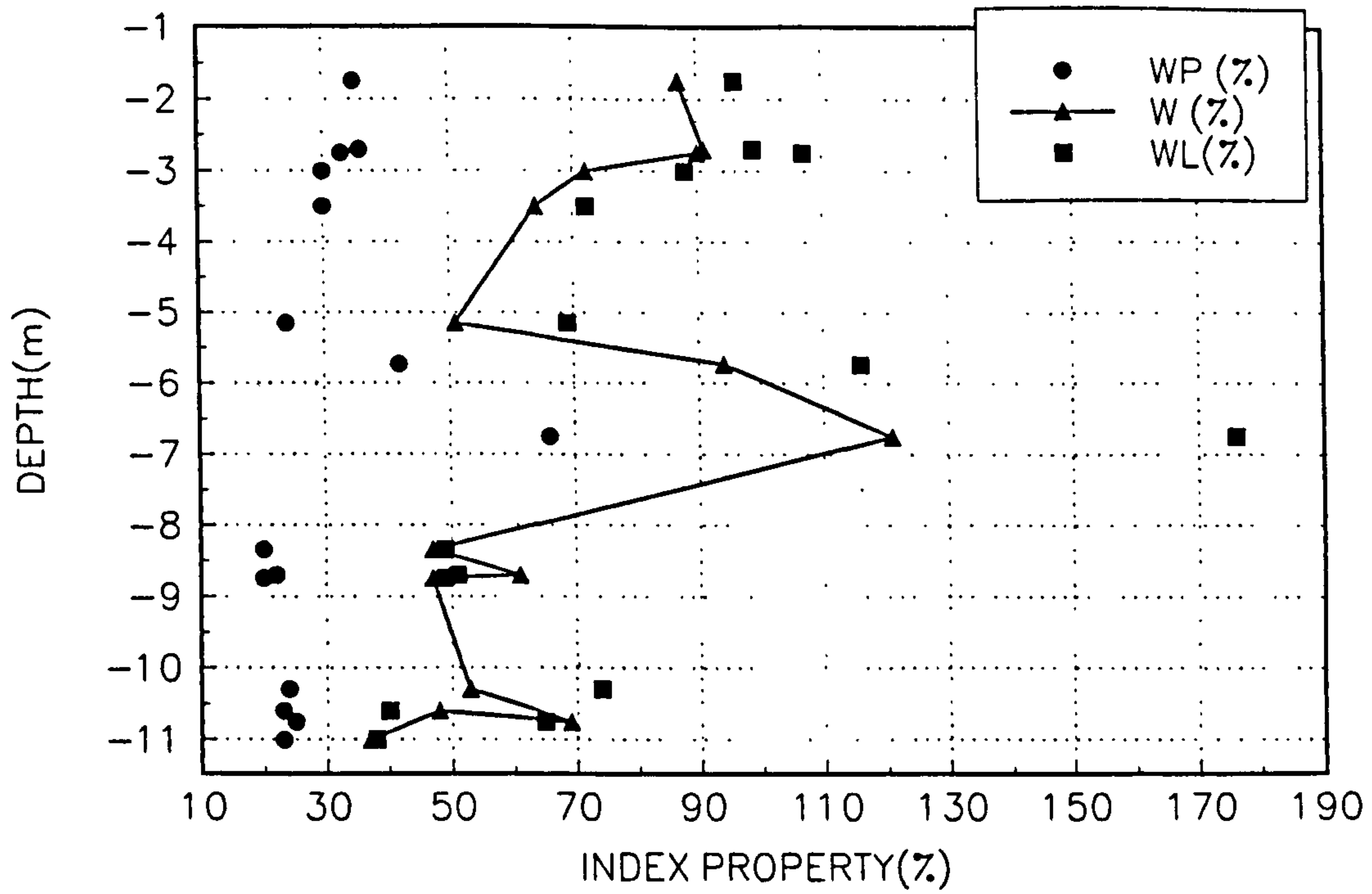


FIGURE 3.12
VARIATION OF PLASTICITY INDEX, I_p

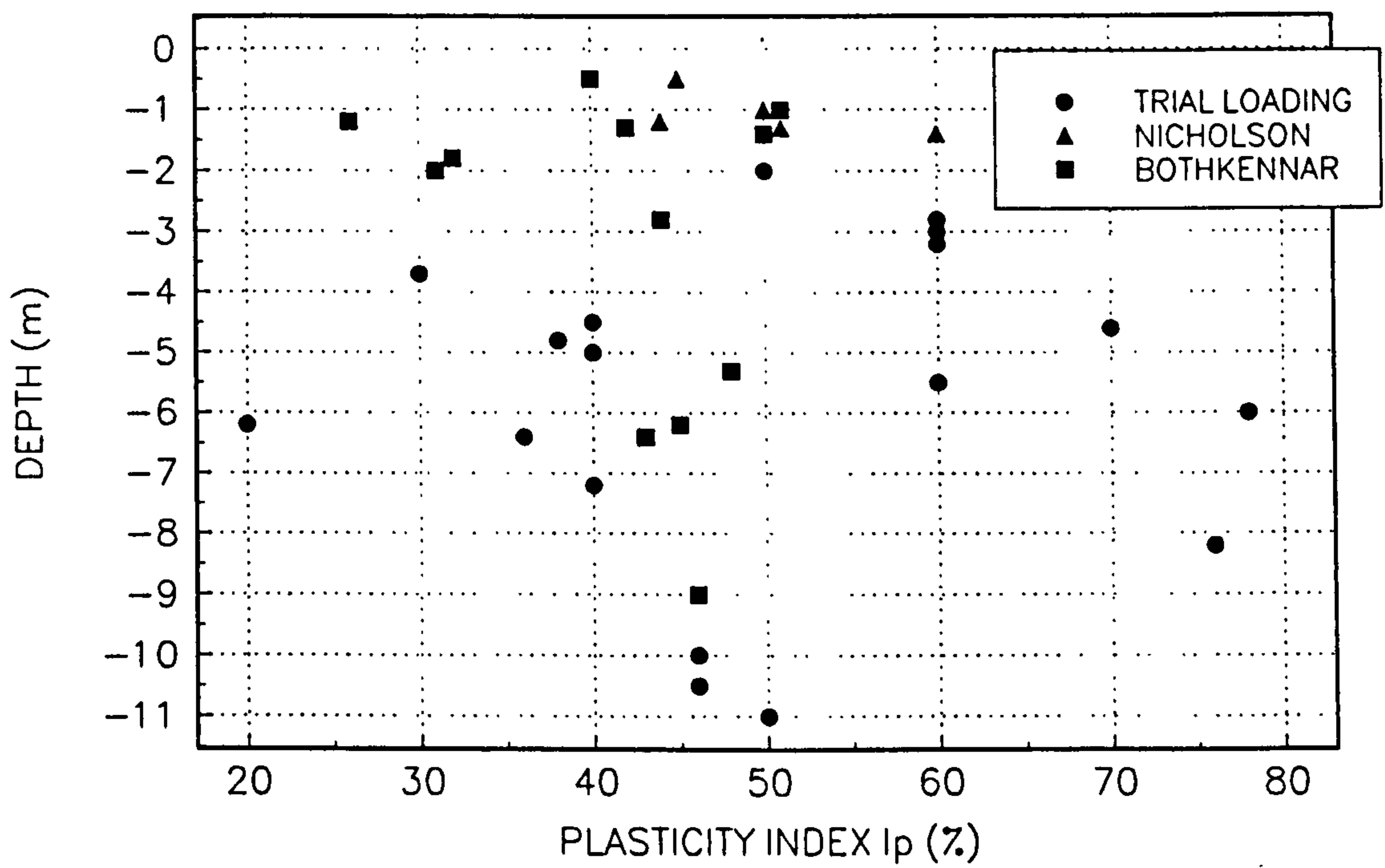


FIGURE 3.1 3
VARIATION OF UNIT WEIGHT WITH DEPTH

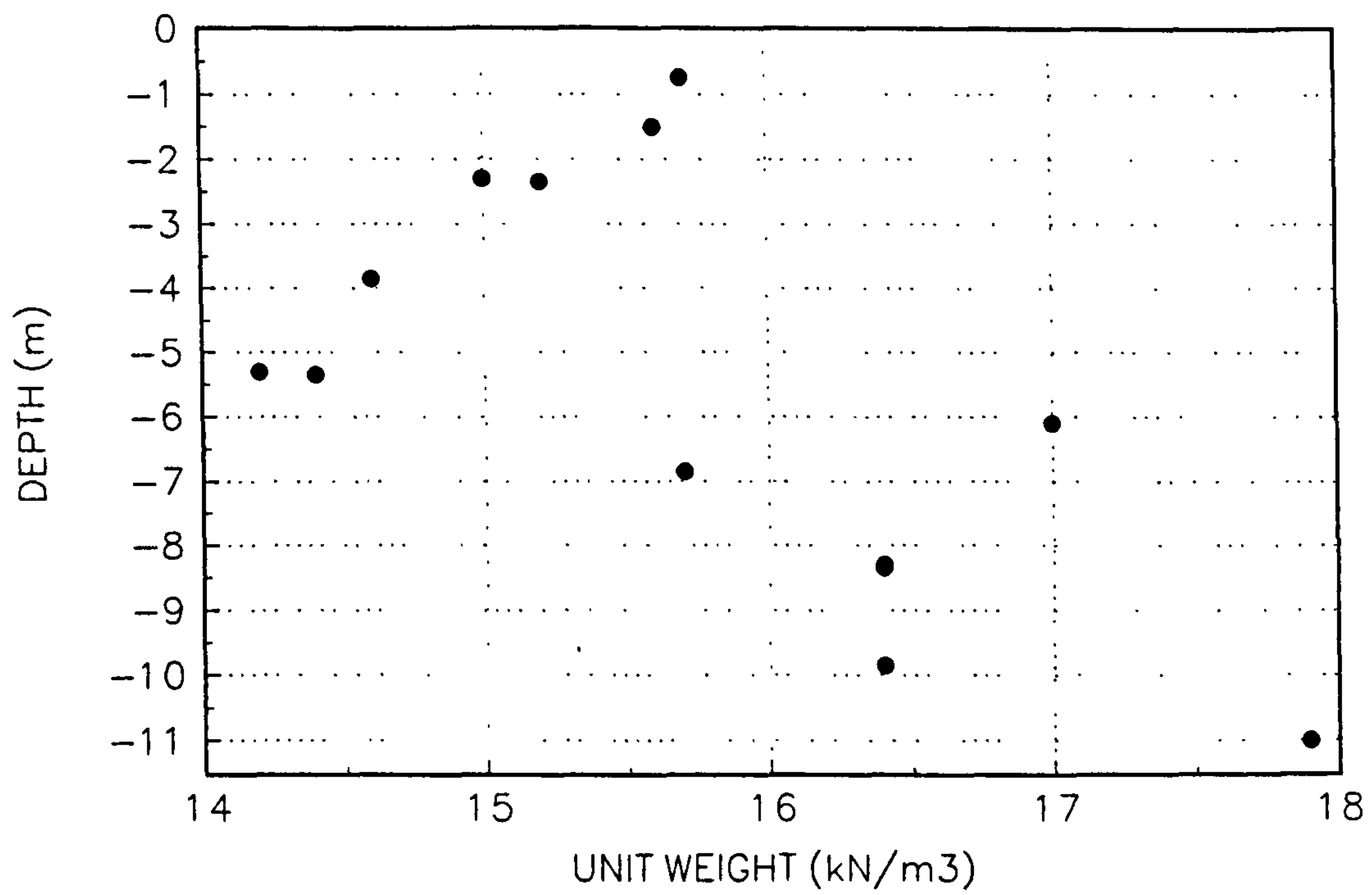


FIGURE 3.1 4
VARIATION OF VOID RATIO WITH DEPTH

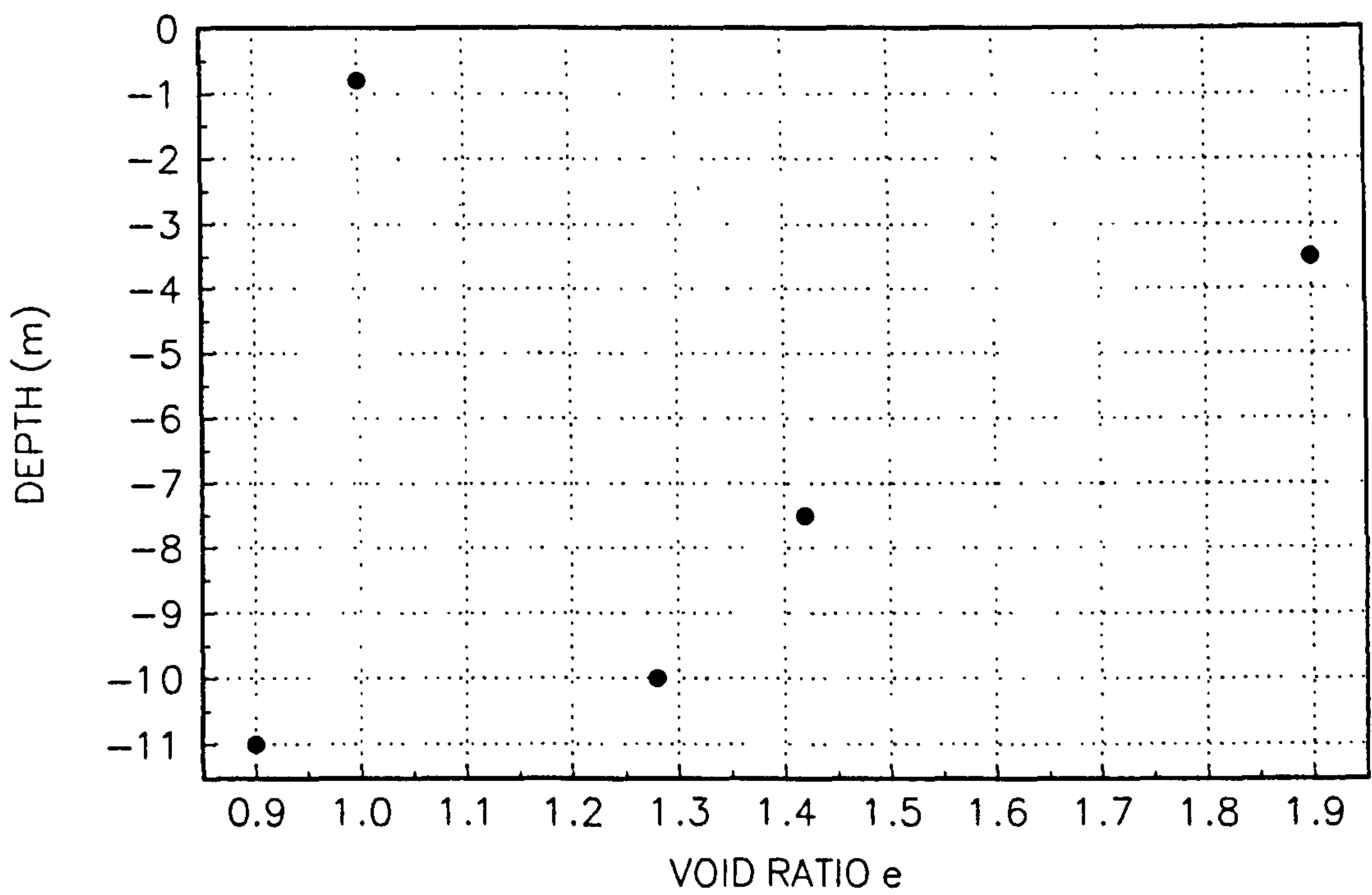


FIGURE 3.15
VARIATION OF PHI WITH DEPTH

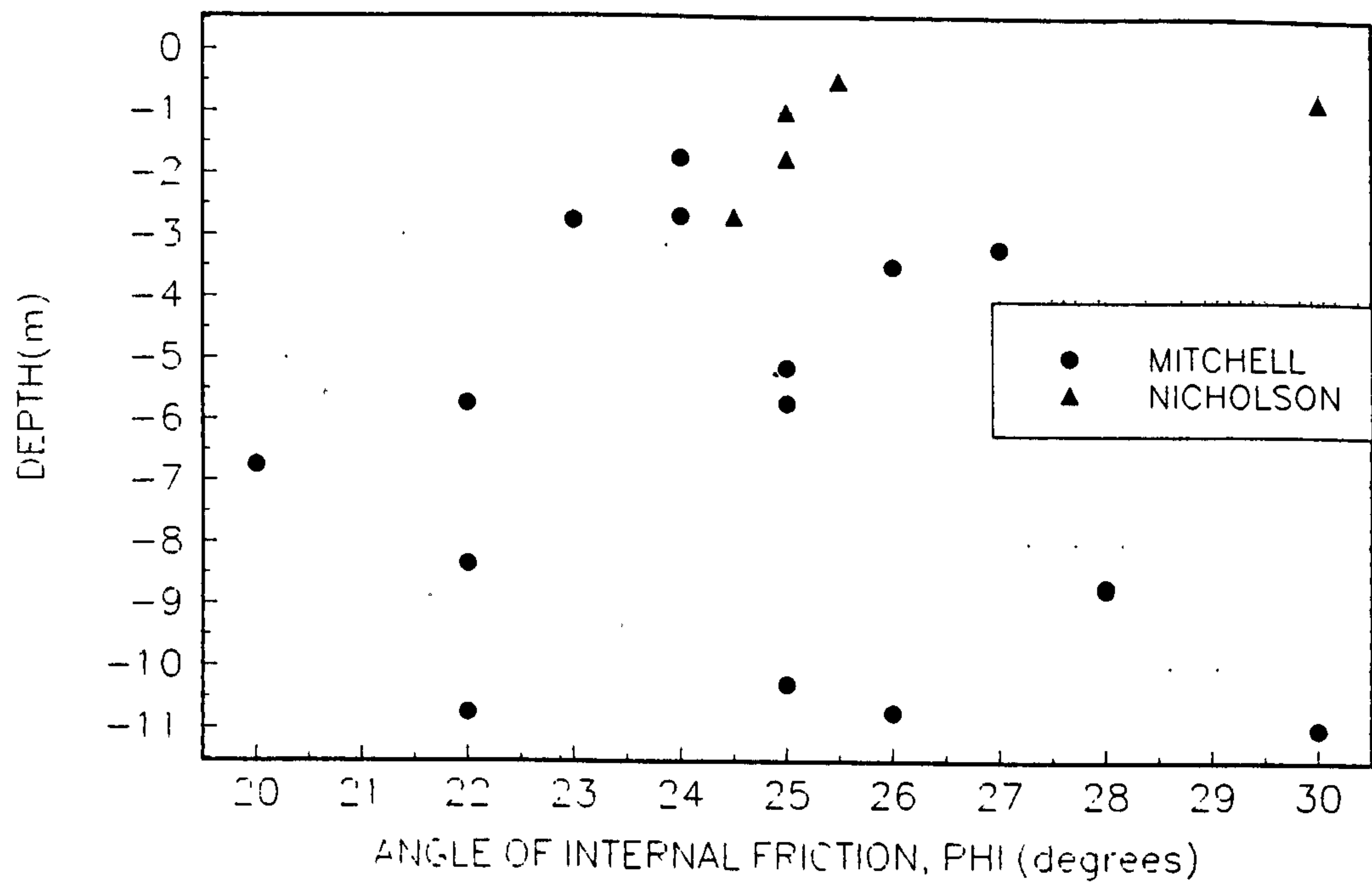


FIGURE 3.16
UNDRAINED SHEAR STRENGTH PROFILE

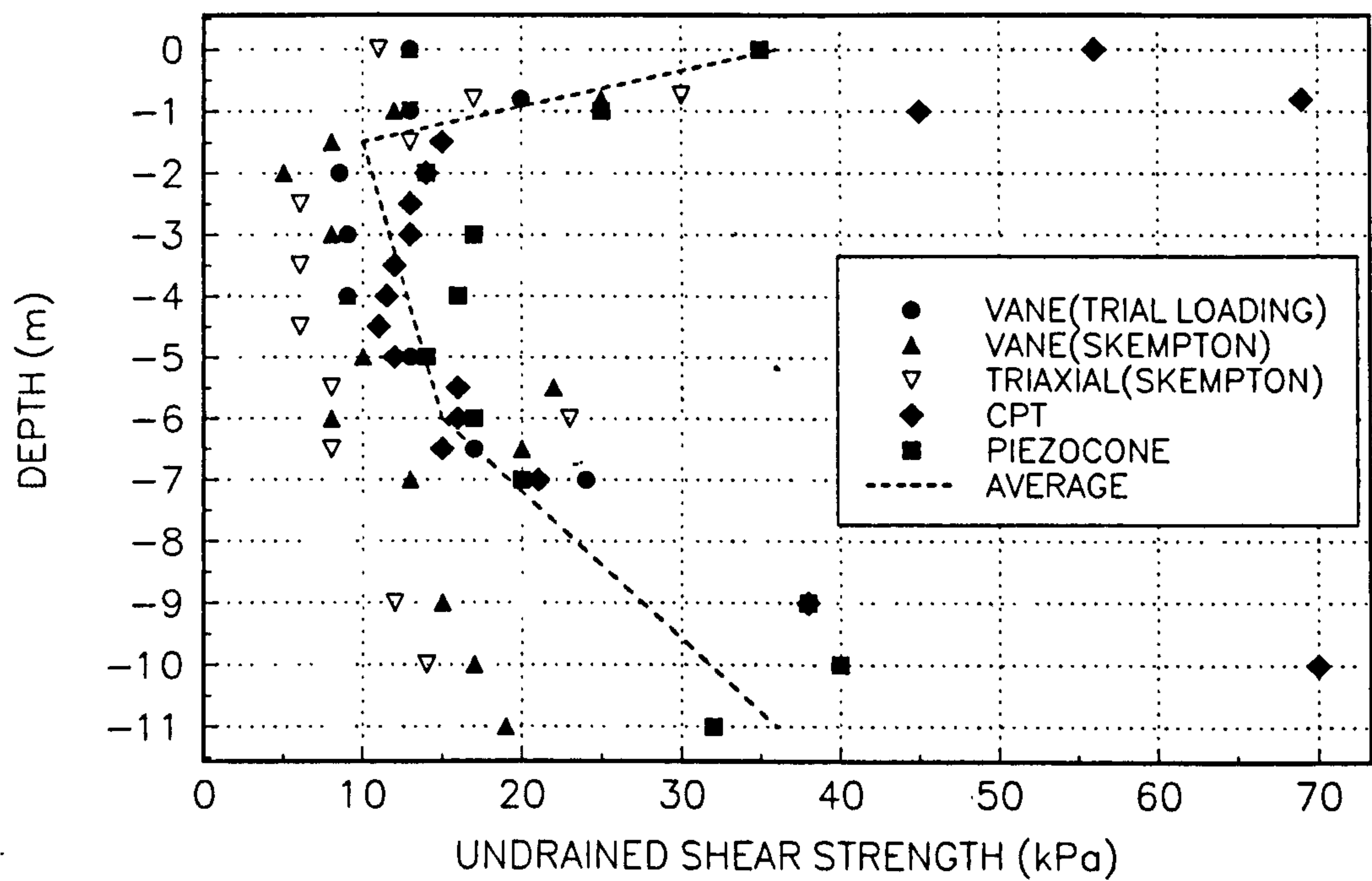


FIGURE 3.17
PRECONSOLIDATION STRESS

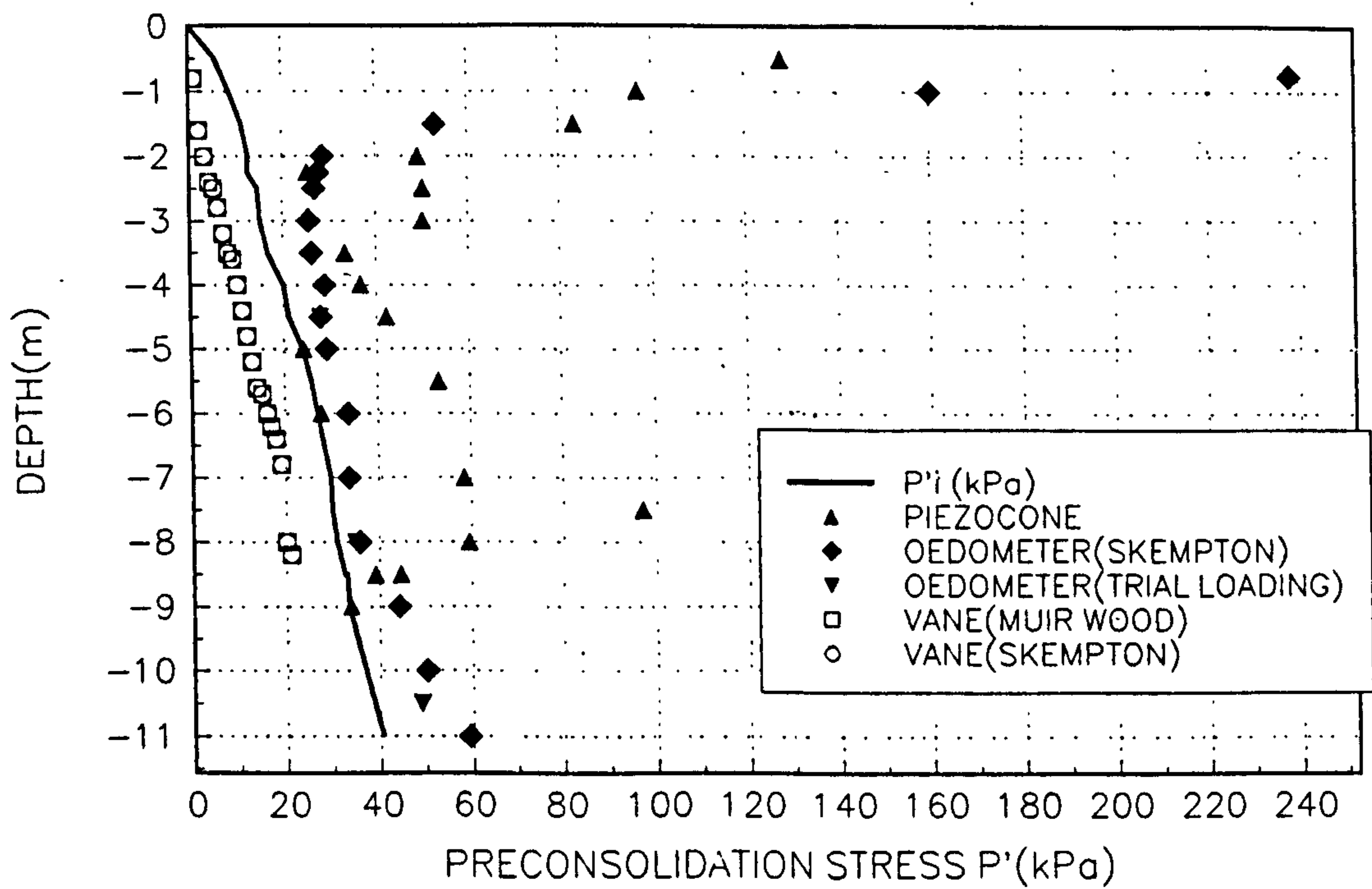


FIGURE 3.18(a)
VARIATION OF SHEAR MODULUS WITH DEPTH

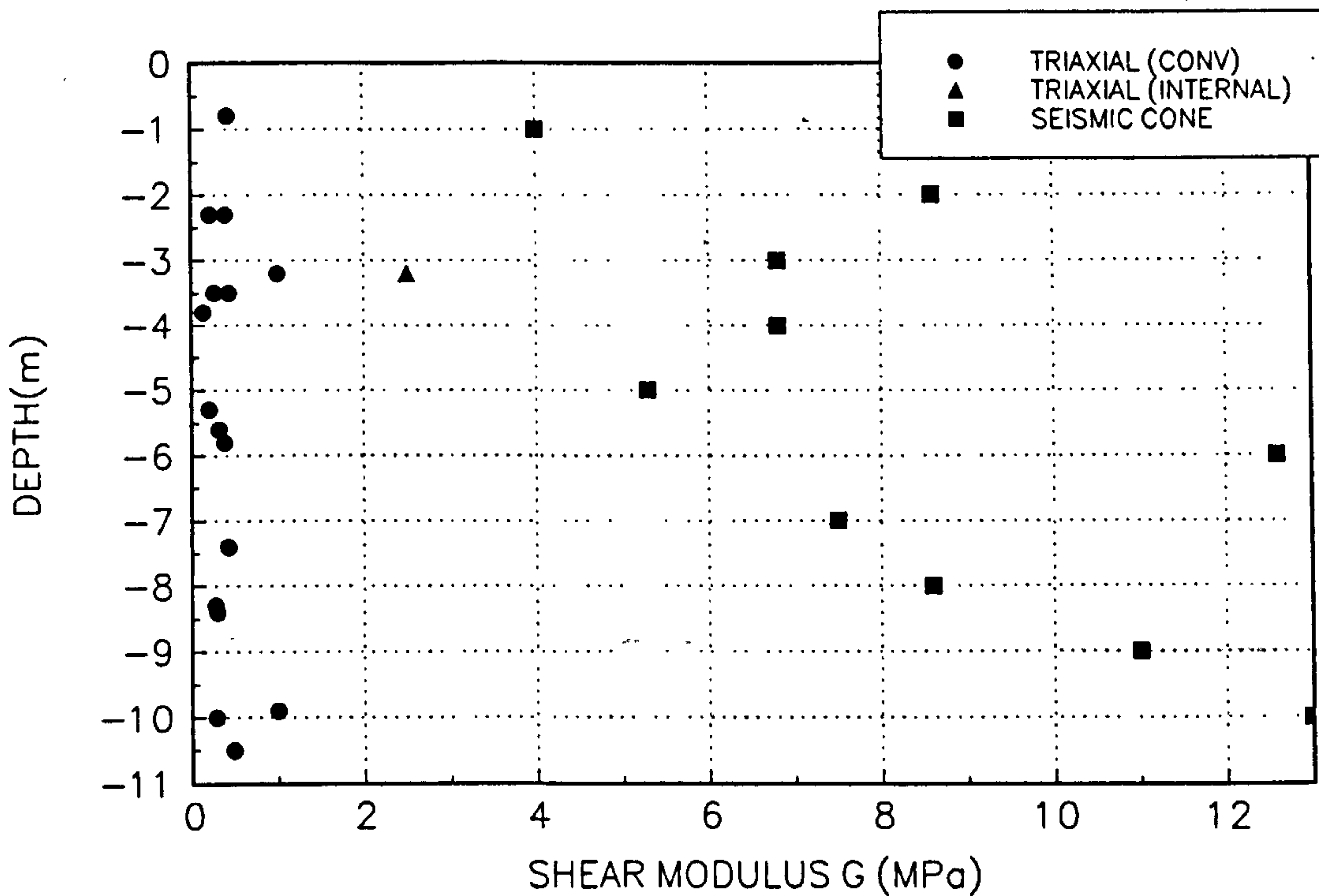
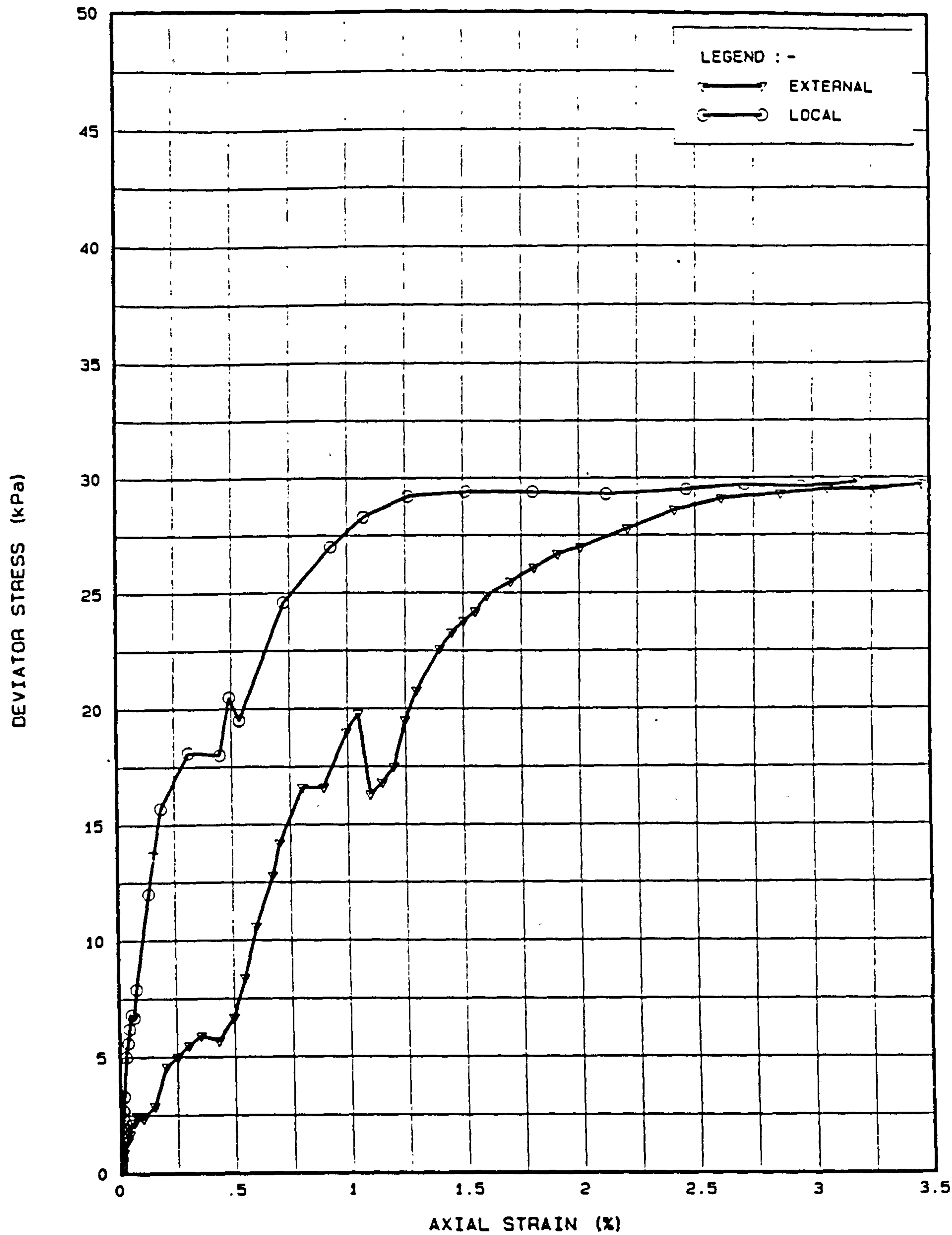


Fig 3.18(b). Comparison of soil triaxial testing using internal and external strain measurement.



DEVIATOR STRESS VERSUS AXIAL STRAIN
BOREHOLE GMF 1 @ 3.2m

FIGURE 3.19
DEPTH PROFILE OF STIFFNESS RATIO G/C_u AND G/P'_i

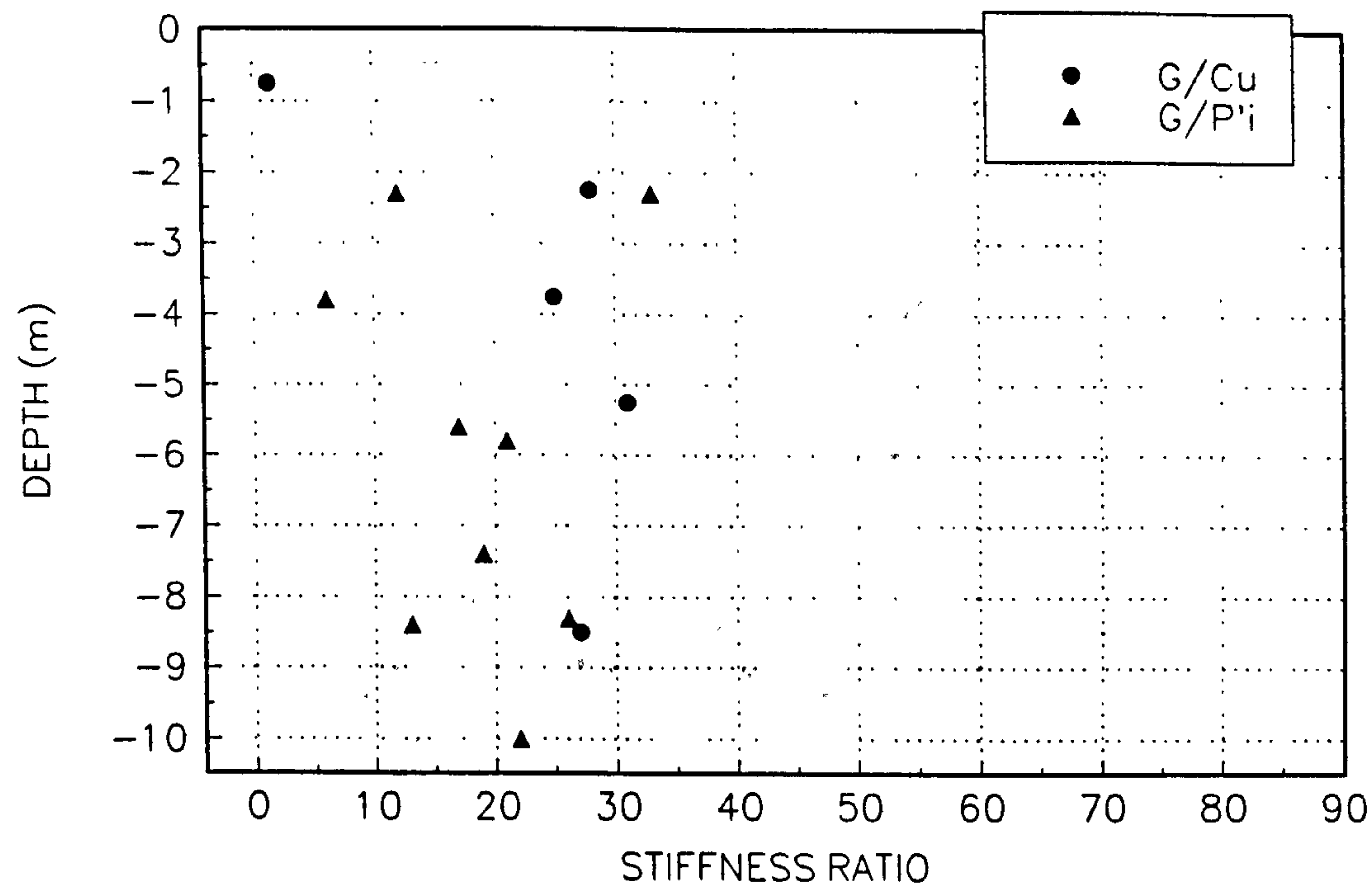


FIGURE 3.20
STIFFNESS RATIOS G/P'_i FOR TRIAL LOADING AND BOTHKENNAR COMPARED

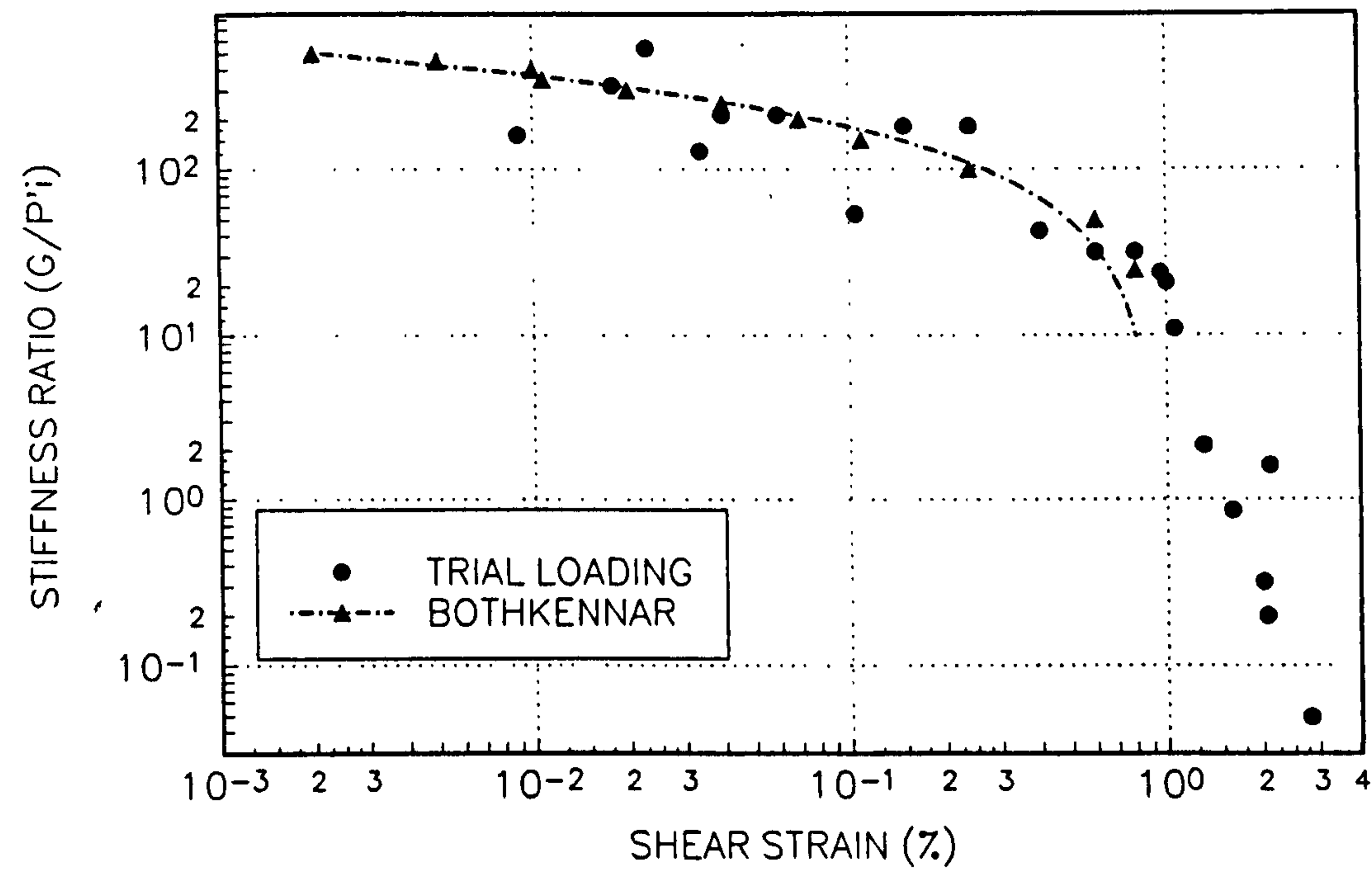


FIGURE 3.21
ESTIMATION OF CONE FACTOR N_k

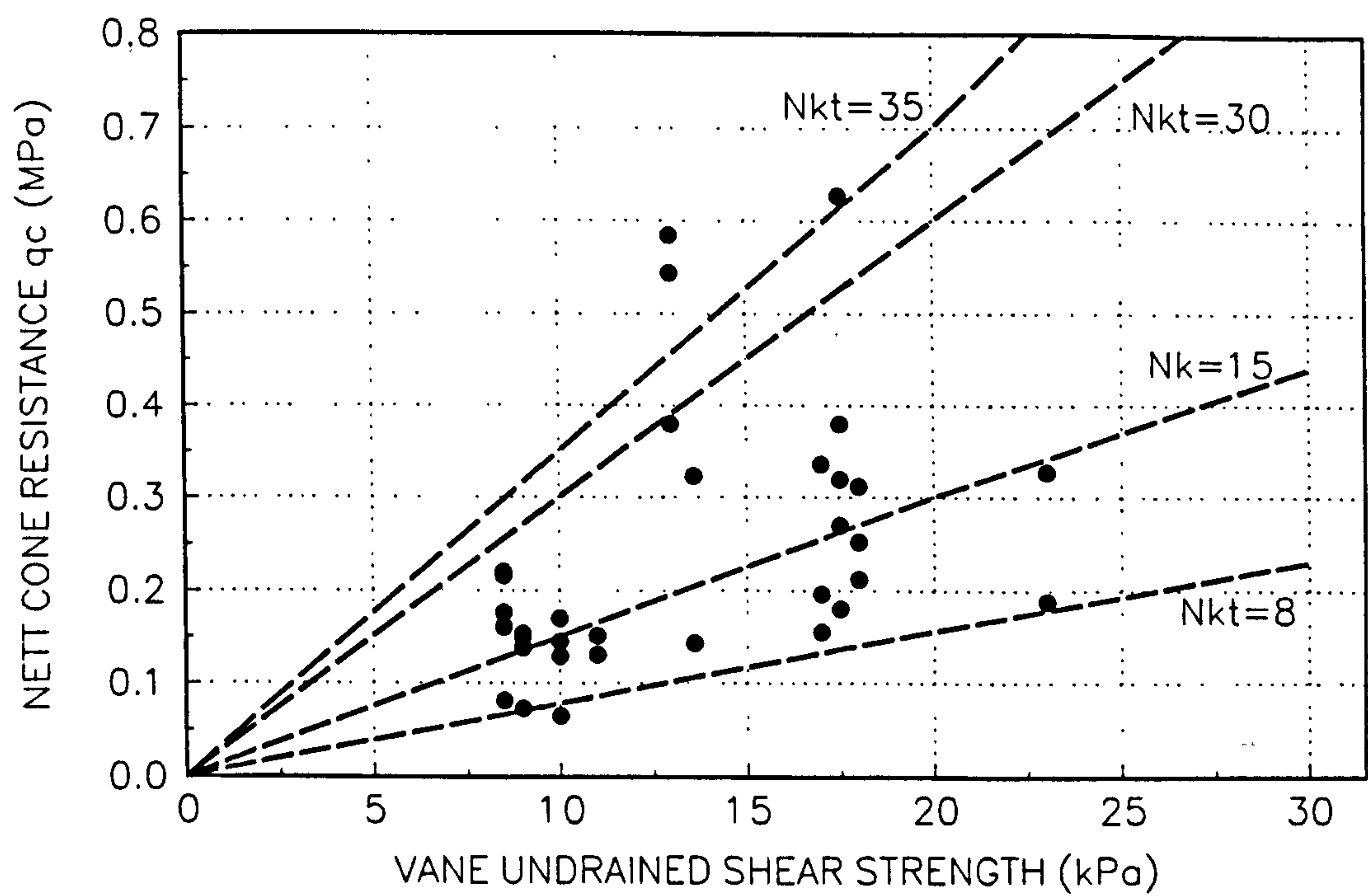


FIGURE 3.22
ESTIMATION OF PIEZOCONE FACTOR N_{kt}

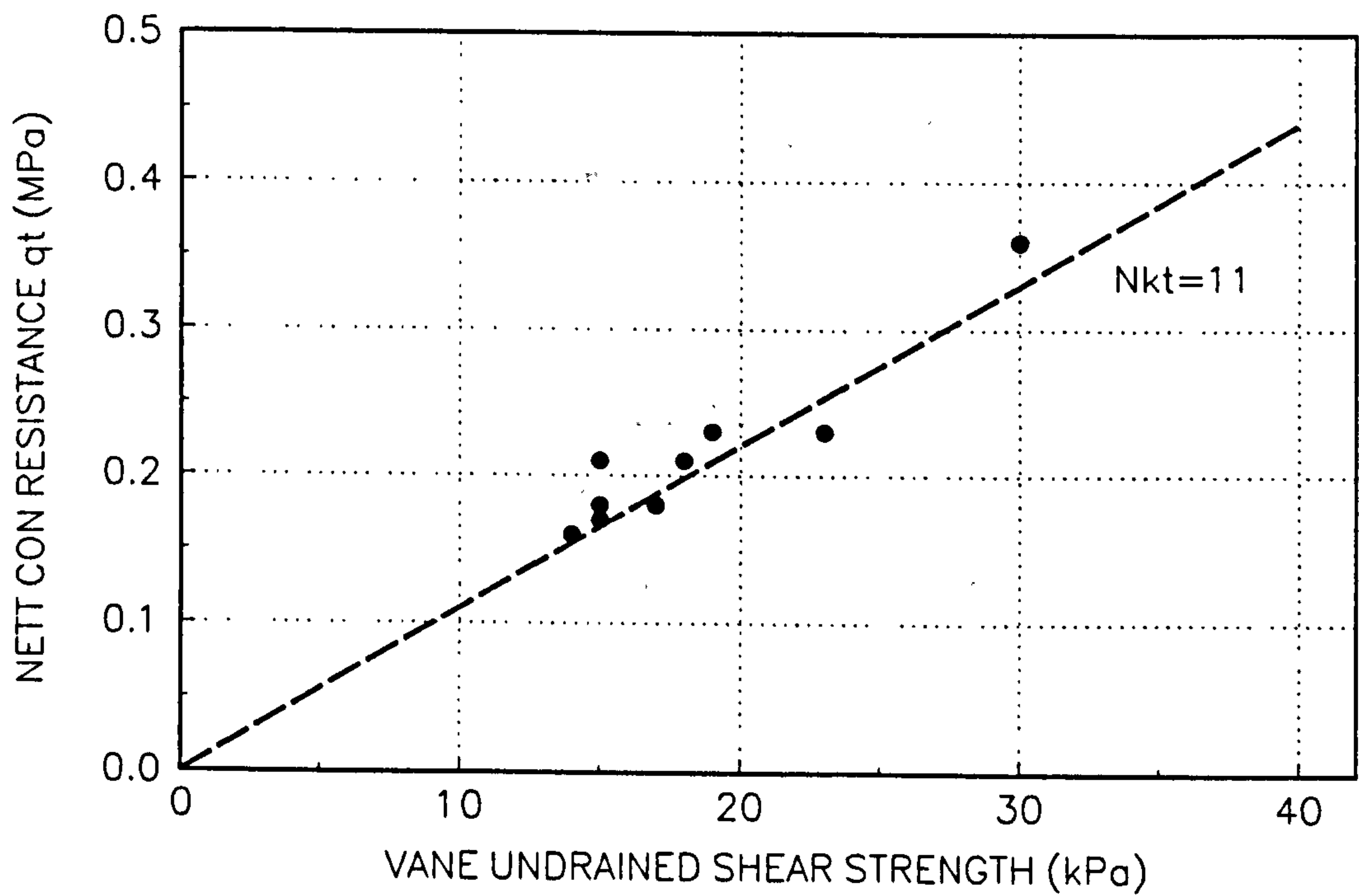


FIGURE 3.23
TYPICAL OEDOMETER TEST RESULT

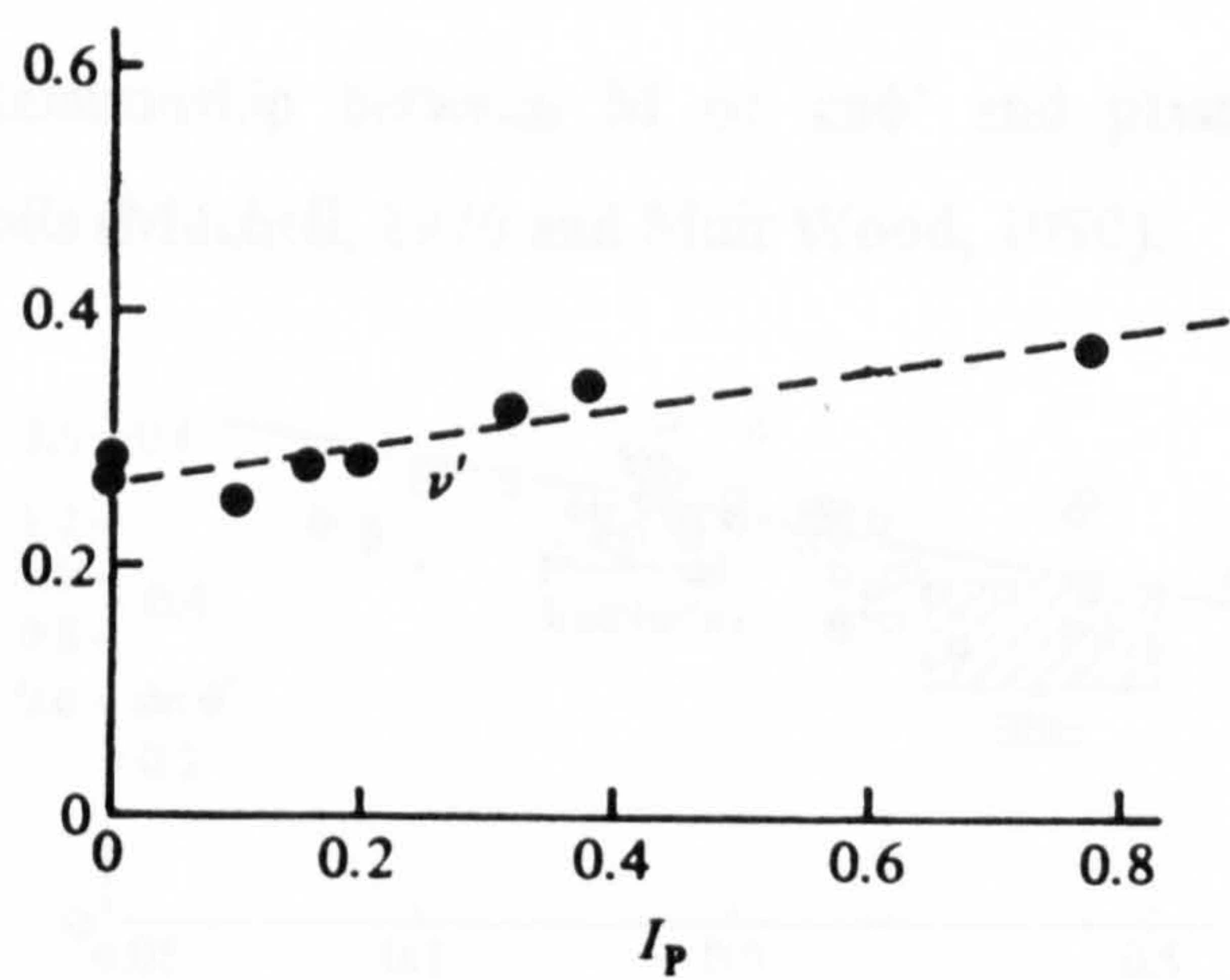
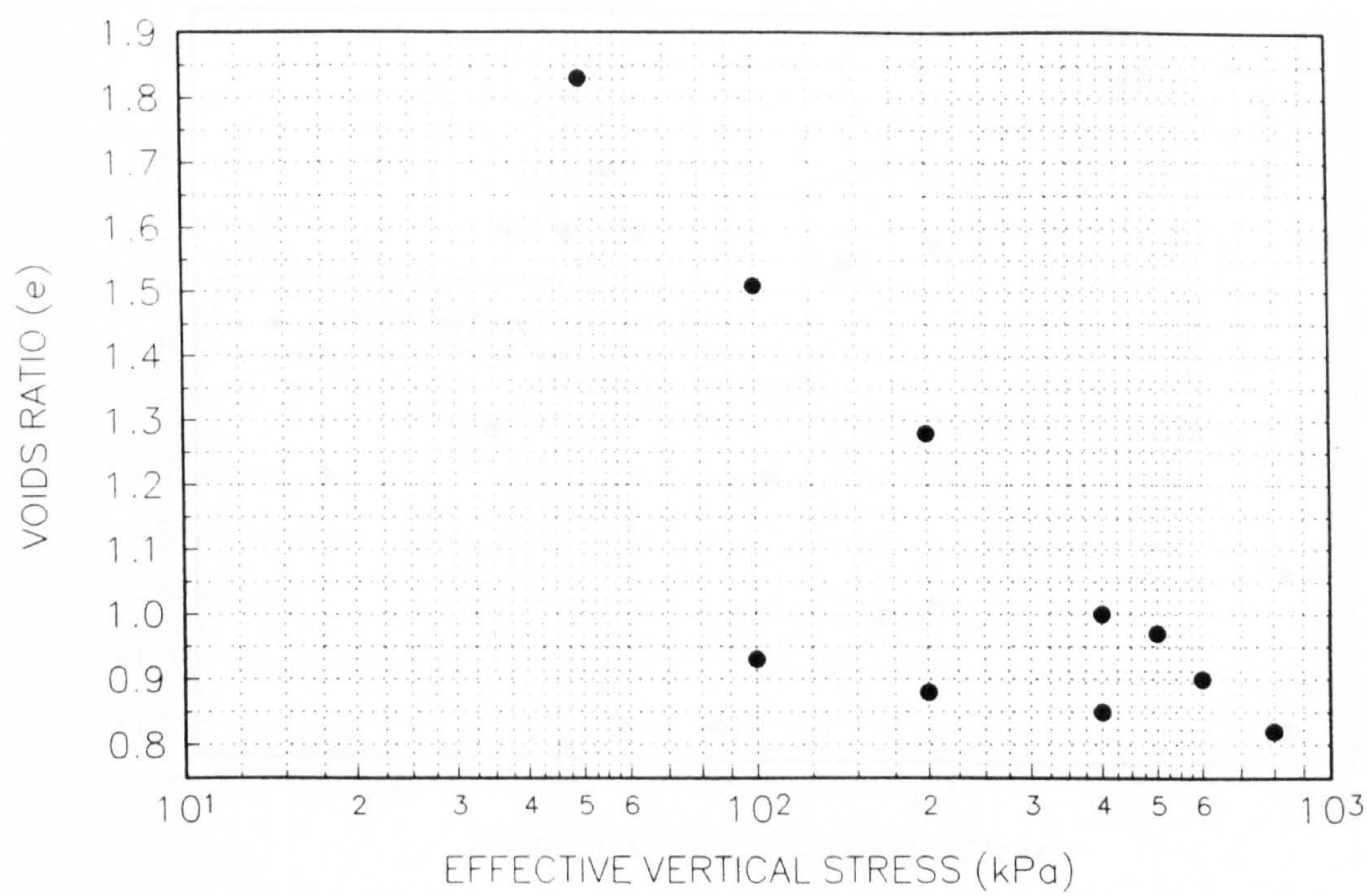


Fig 3.24. Dependence of Poisson's ratio ν' on plasticity index I_p
(Wroth, 1975 and Muir Wood, 1990)

FIGURE 3.25
VARIATION OF M WITH DEPTH

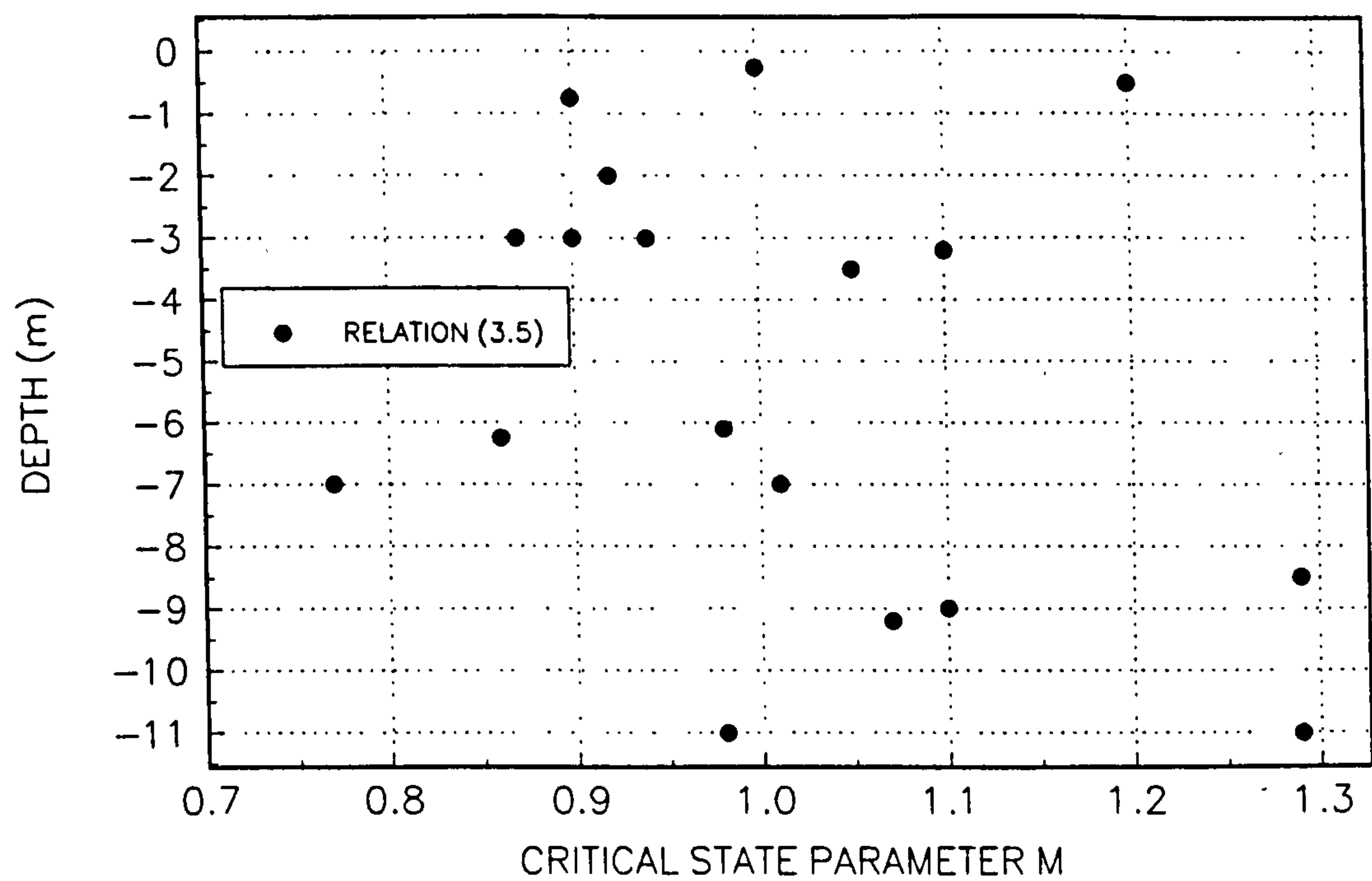


Fig 3.26. Relationship between M or $\sin\phi'$ and plasticity index, I_p , for normally compressed soils (Mitchell, 1976 and Muir Wood, 1990).

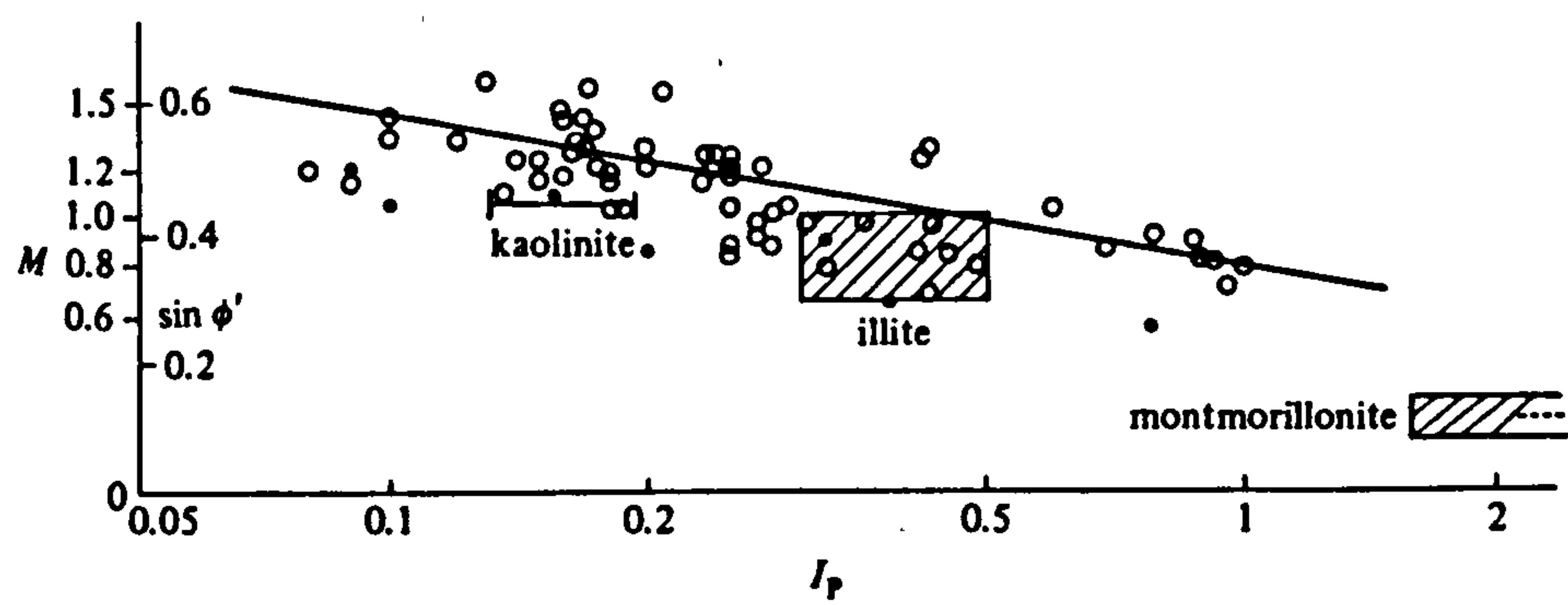


FIGURE 3.27
DETERMINATION OF n FROM PIEZOCONE DATA

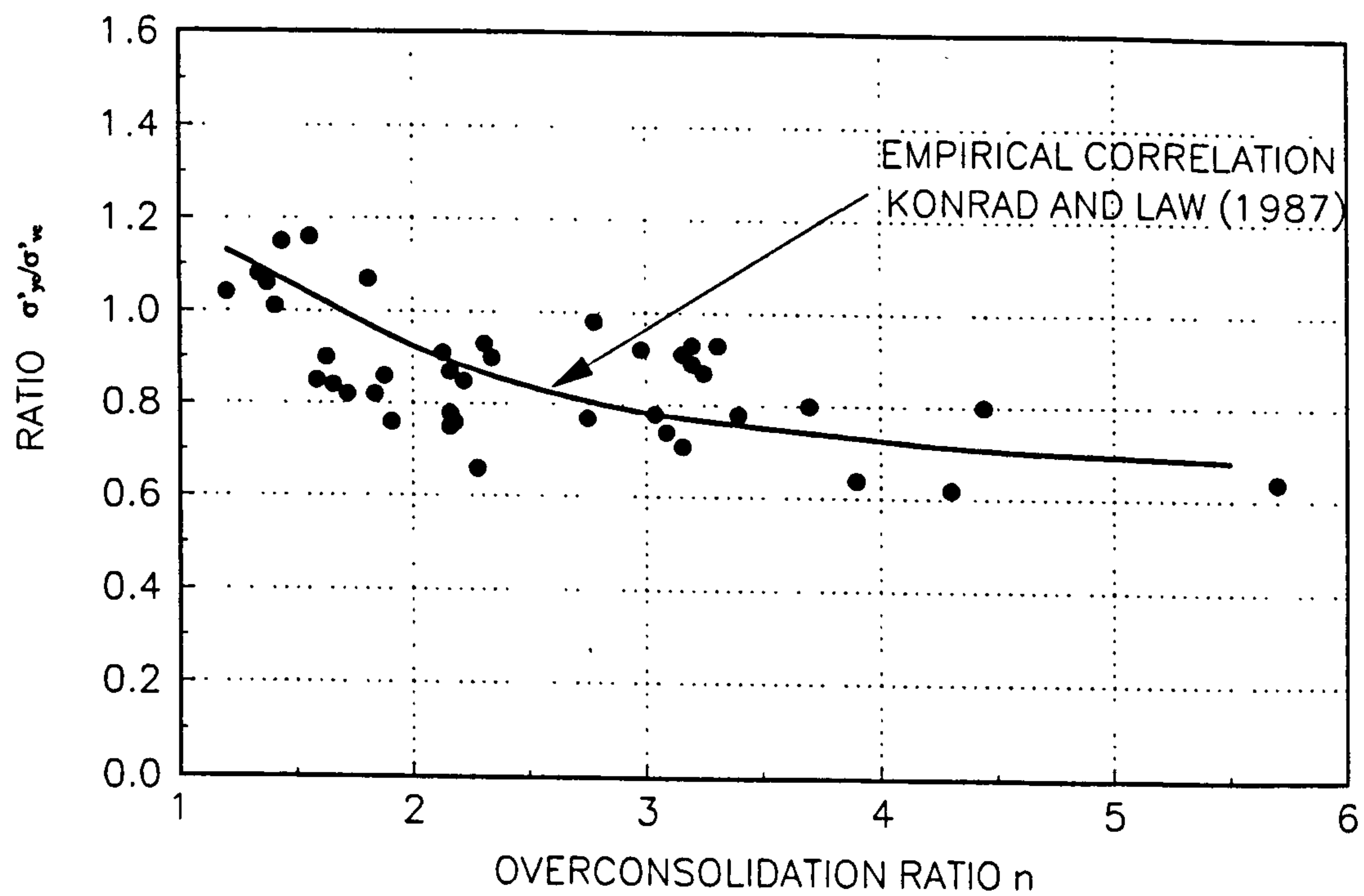


FIGURE 3.28
OEDOMETER AND PIEZOCONE PRECONSOLIDATION STRESS

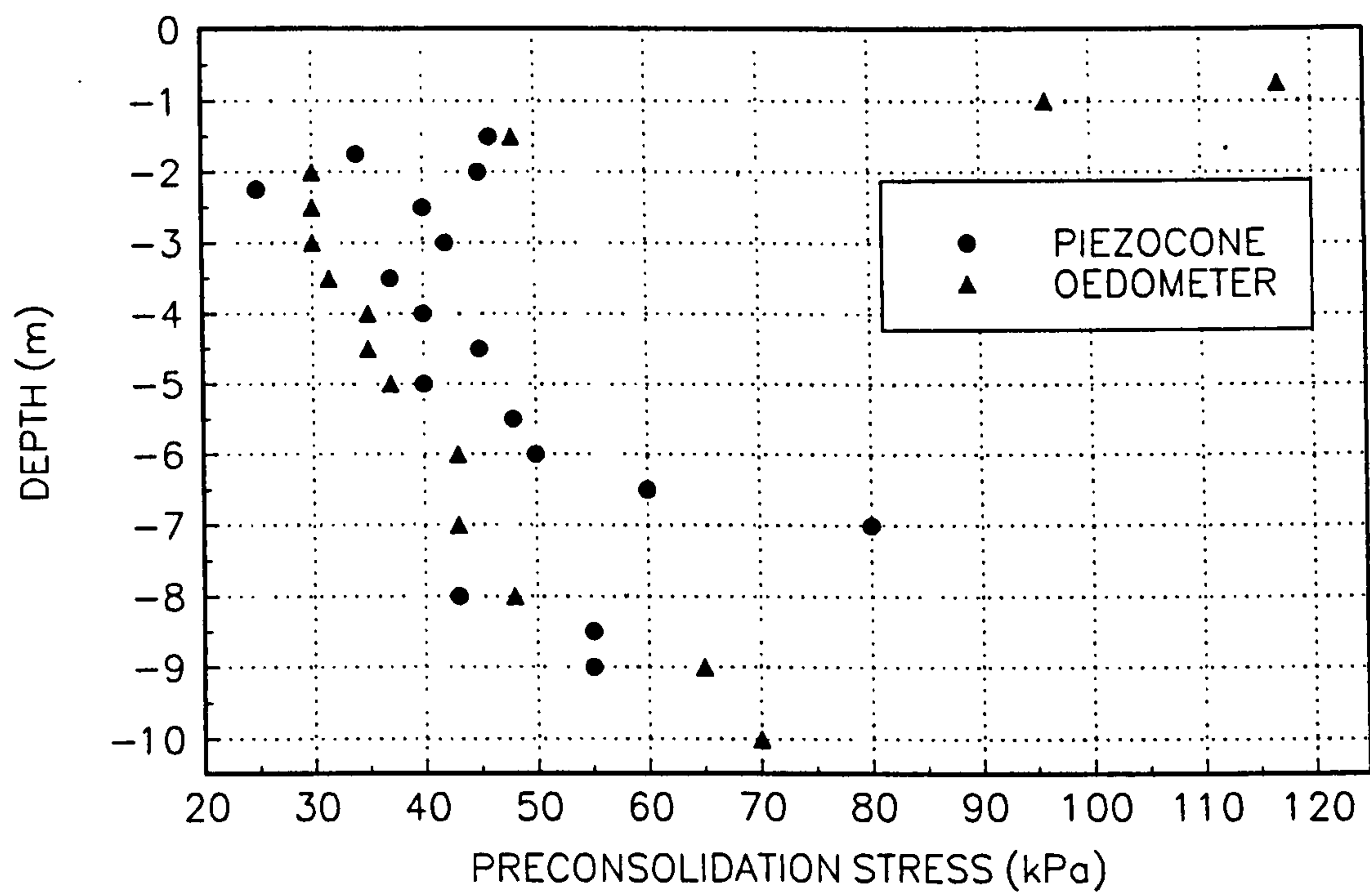


FIGURE 3.29
OEDOMETER AND PIEZOCONE OVERCONSOLIDATION RATIOS

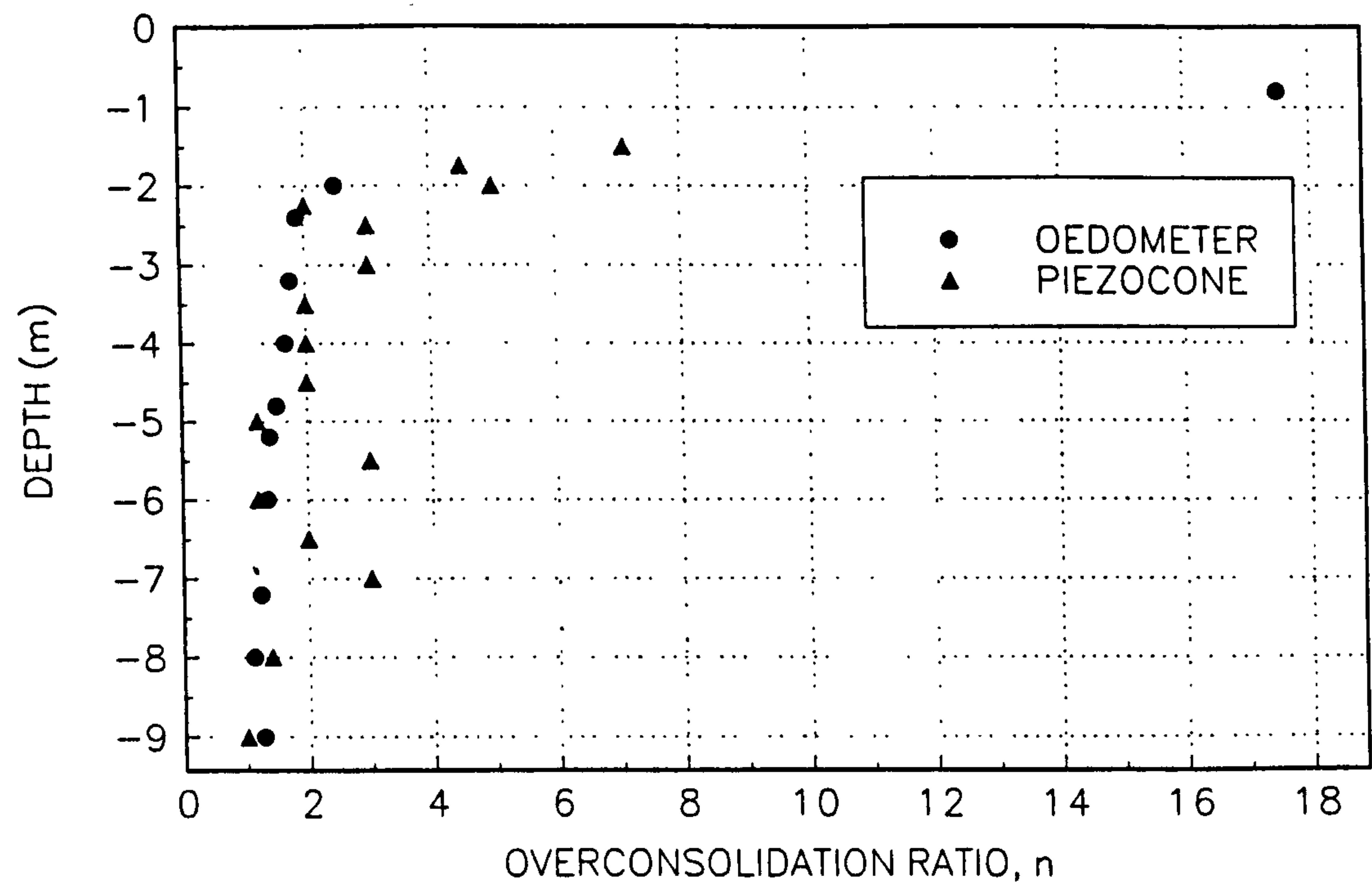


FIGURE 3.30
OEDOMETER AND PIEZOCONE PRECONSOLIDATION STRESS

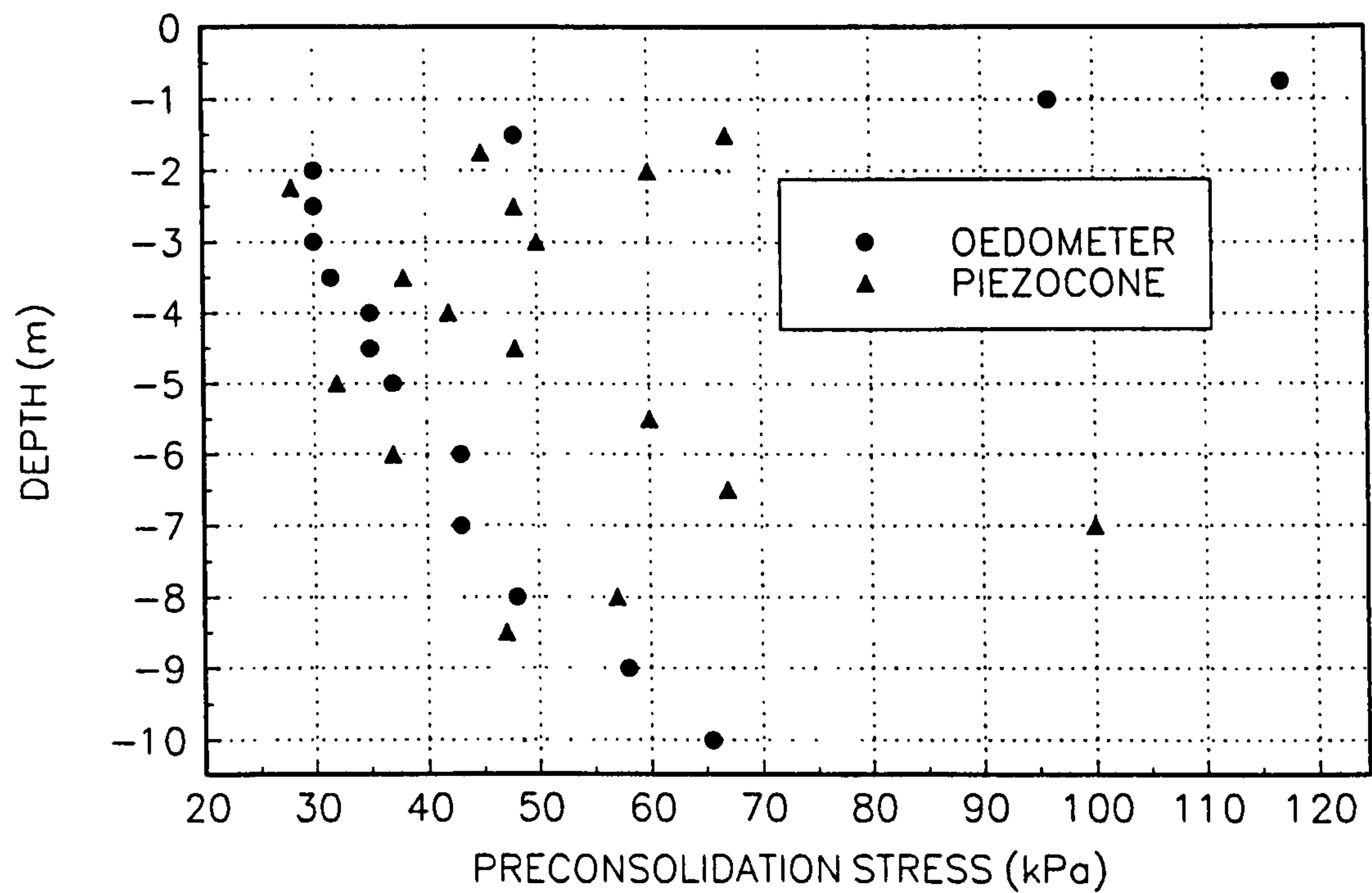


Fig 3.31. Ratio of undrained strength to initial mean effective stress (c_u/p'_i) varying with isotropic overconsolidation ratio (Muir Wood, 1990).

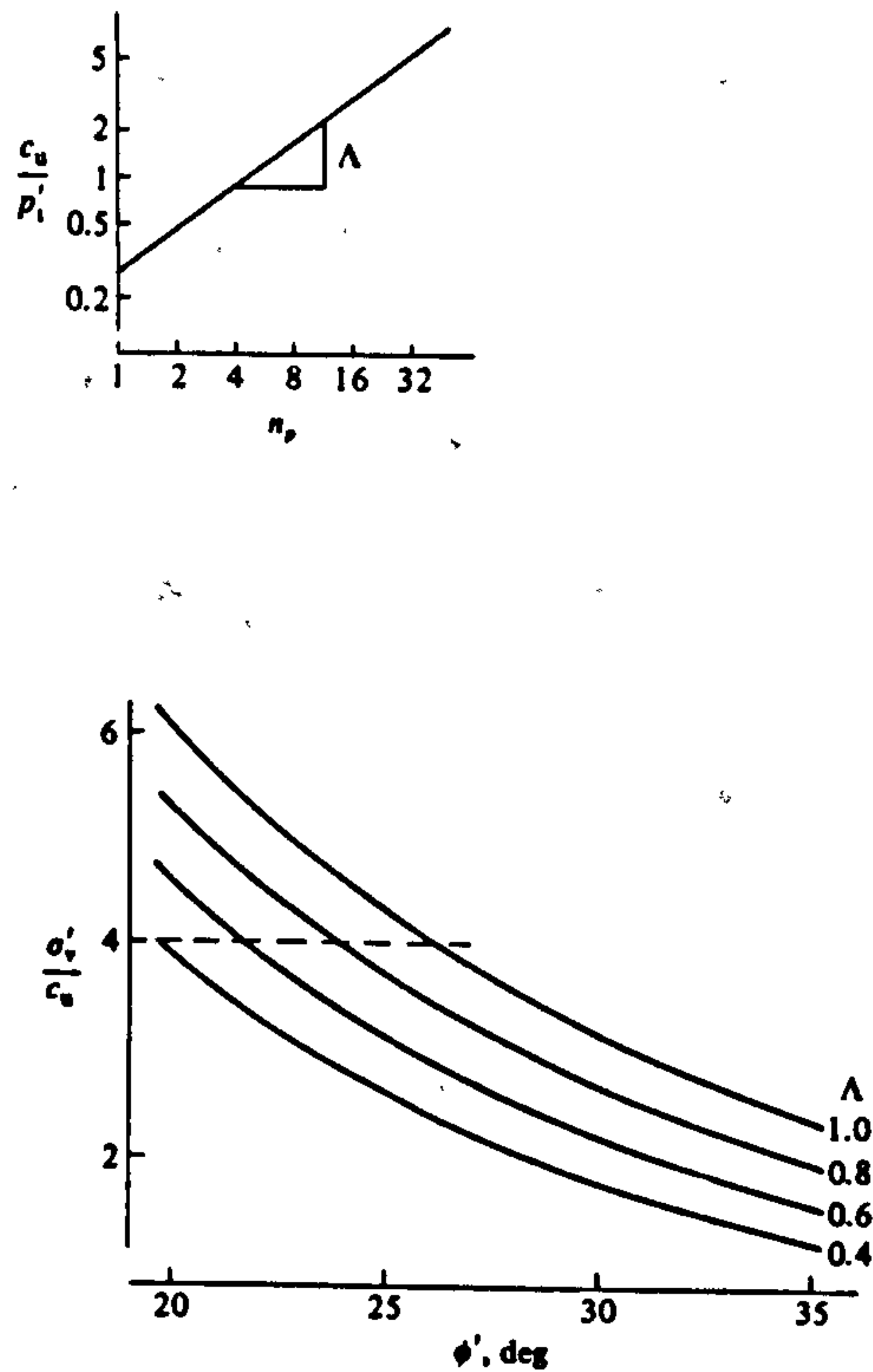


Fig 3.32. Ratio of vertical effective stress in one-dimensional normal compression and undrained strength at same specific volume as function of Λ and angle of shearing resistance ϕ' according to modified Cam clay soil model (Muir Wood, 1990).

FIGURE 3.33
VARIATION STRENGTH RATIO ($\frac{c_u}{\sigma'_v}$) WITH PLASTICITY INDEX I_p

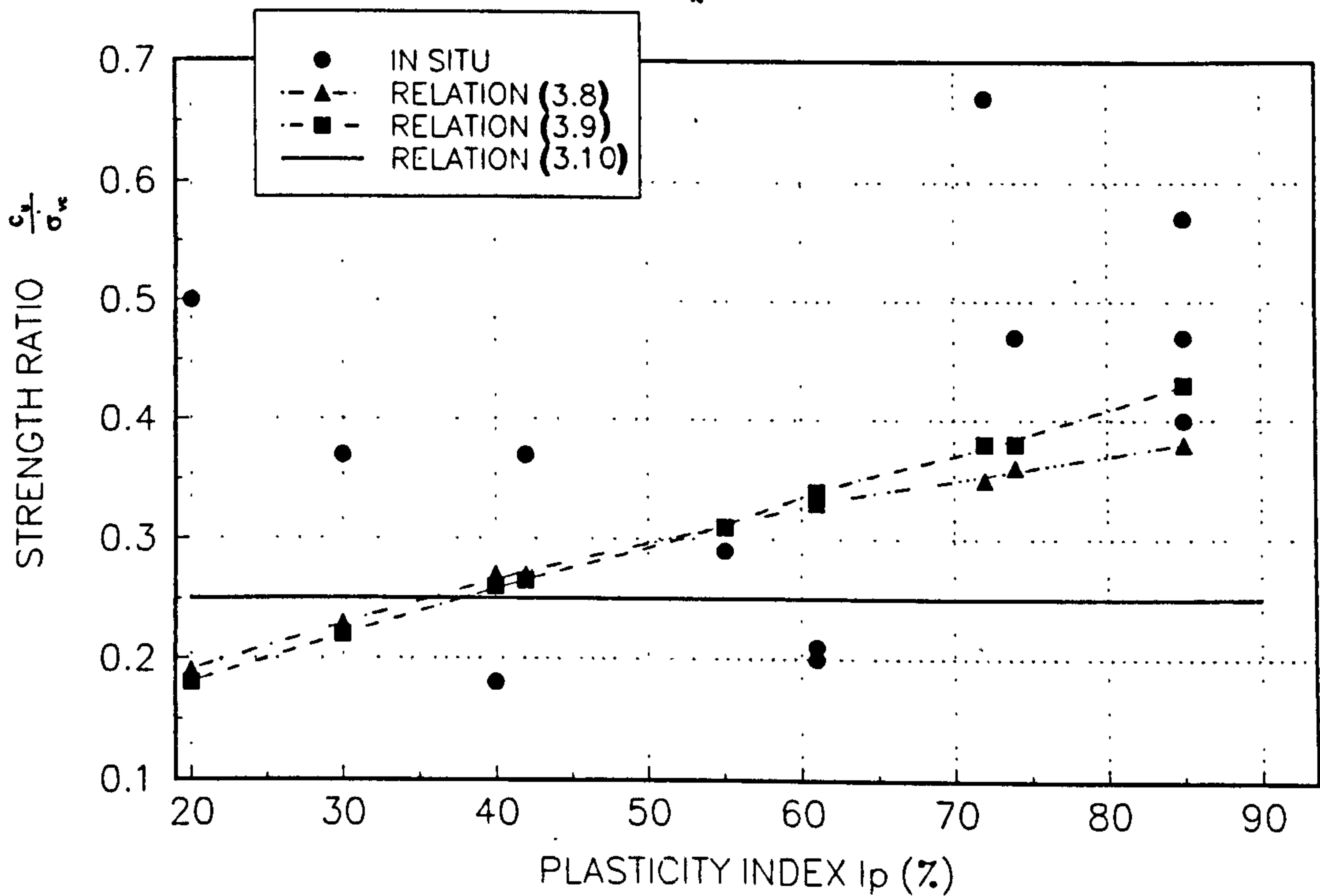
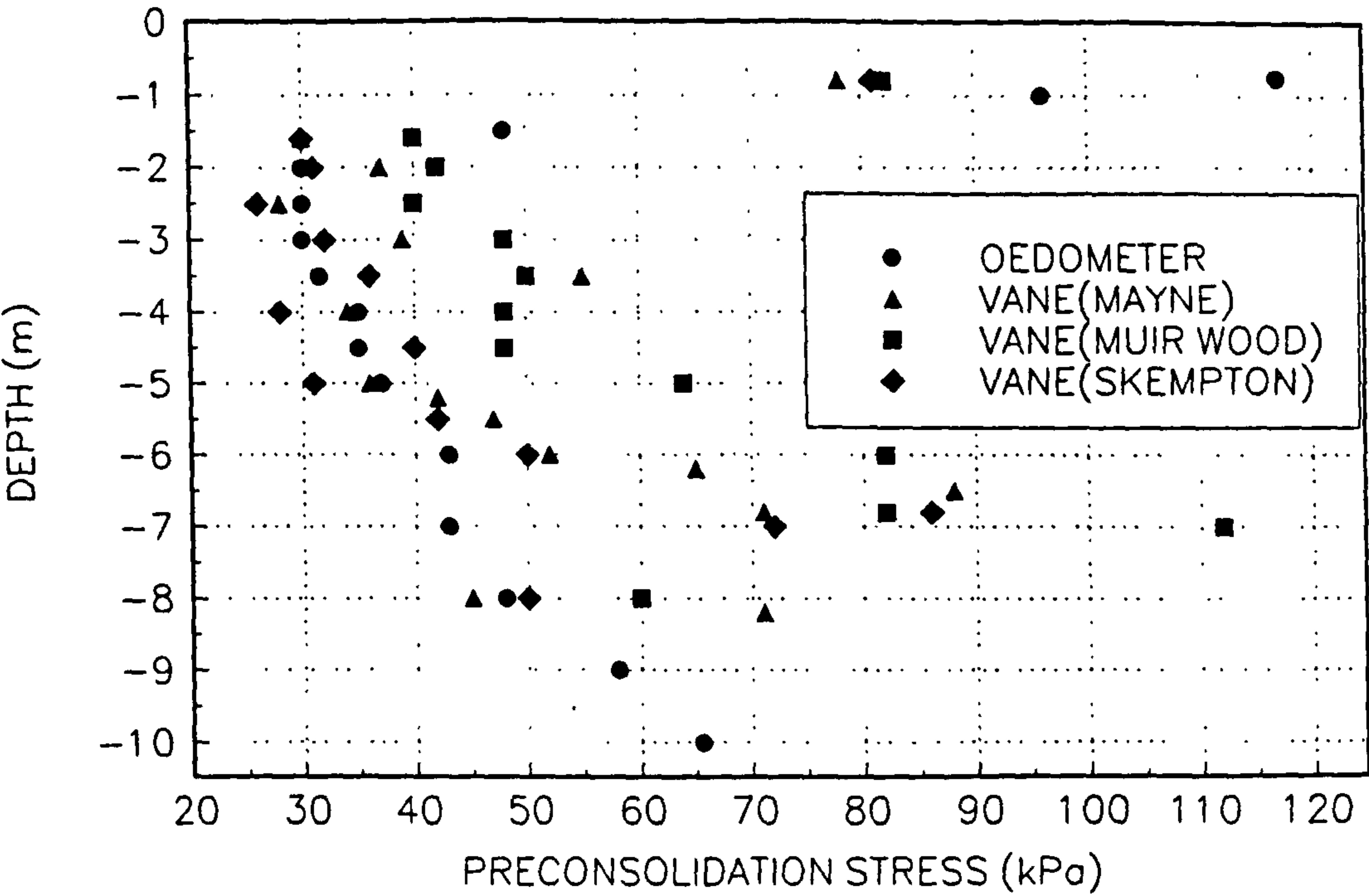


FIGURE 3.34
OEDOMETER AND FIELD VANE PRECONSOLIDATION STRESS



33	34	41	46	50	53	55	56
21	27	32	36	39	41	42	54
25	26	32	40	45	49	52	
15	20	25	31	35	38	40	51
18	19	24	31	39	44	48	
10	14	19	25	30	34	37	47
12	13	17	23	30	38	43	
6	9	13	18	24	29	33	42
7	8	11	16	22	29	37	
3	5	8	12	17	23	28	35
1	2	5	9	14	20	27	
1	2	4	7	11	16	22	36
3	4	6	10	15	21	28	

Fig 3.35. Finite element mesh used to describe the foundation soil.

FIGURE 3.36
VERTICAL EDGE DISPLACEMENT PROFILES

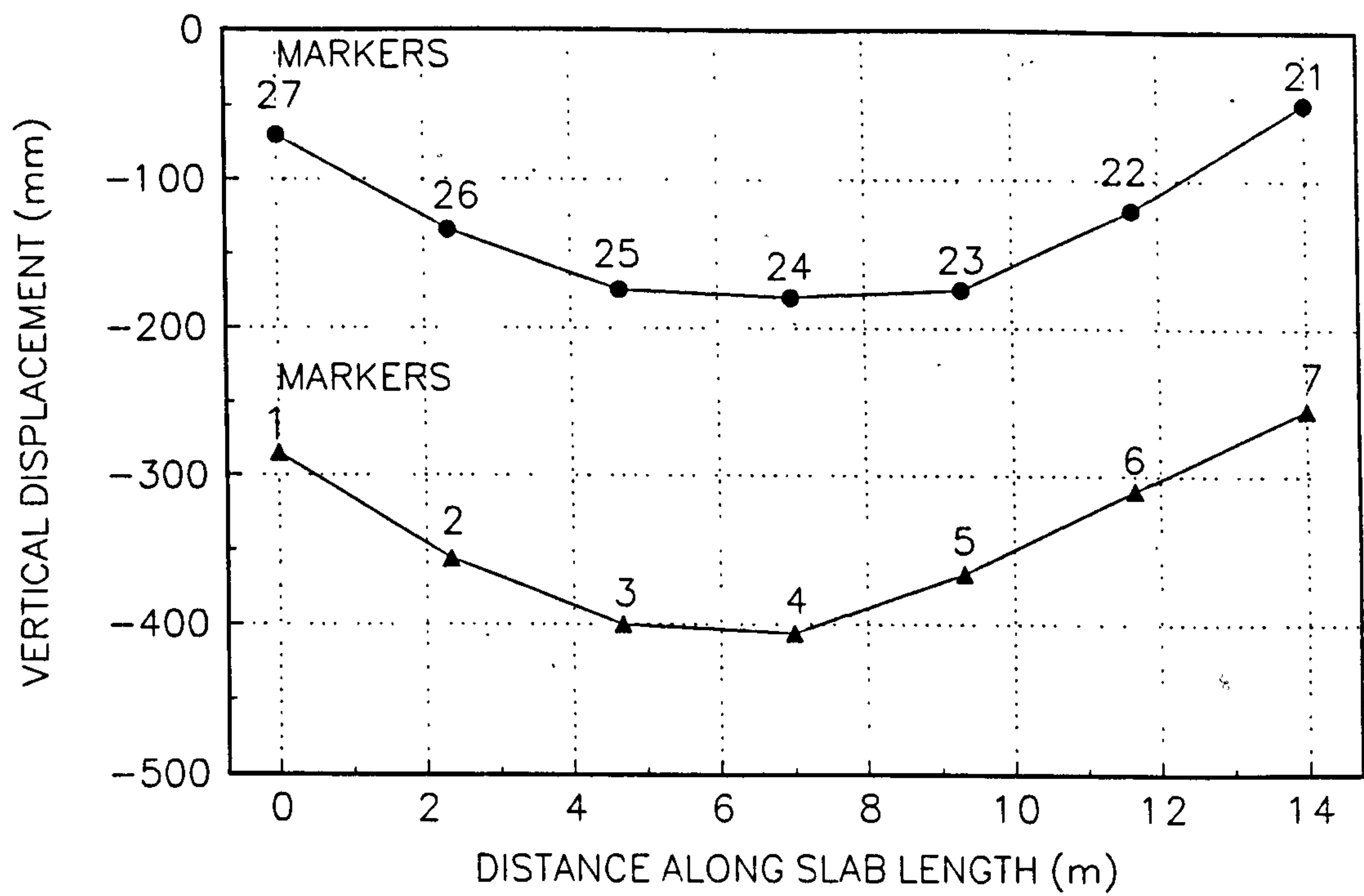


FIGURE 3.37
VERTICAL EDGE DISPLACEMENT PROFILE OF SLAB

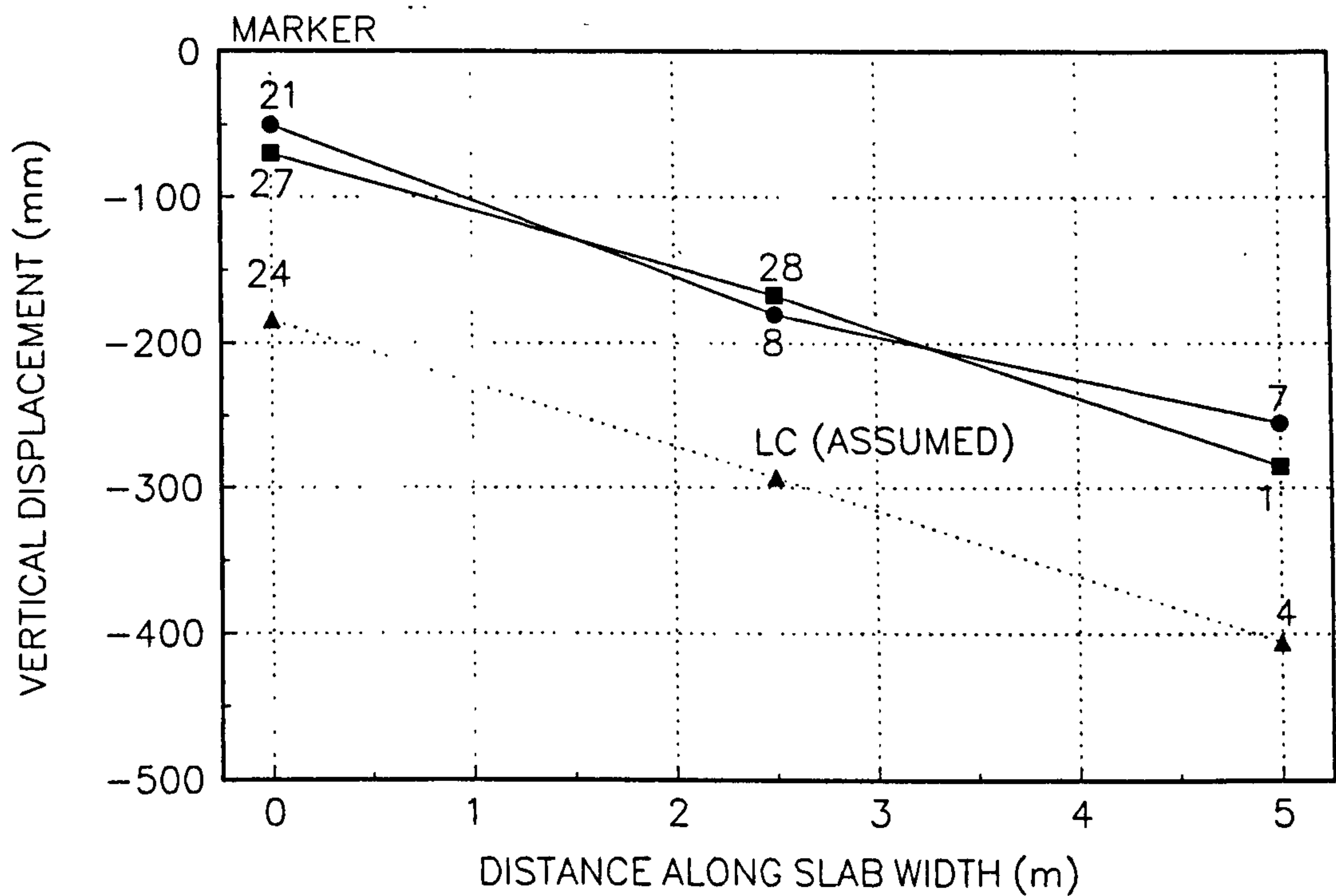


FIGURE 3.38
NORMALISED SECANT SHEAR MODULUS (G/C_u) AGAINST SHEAR STRAIN

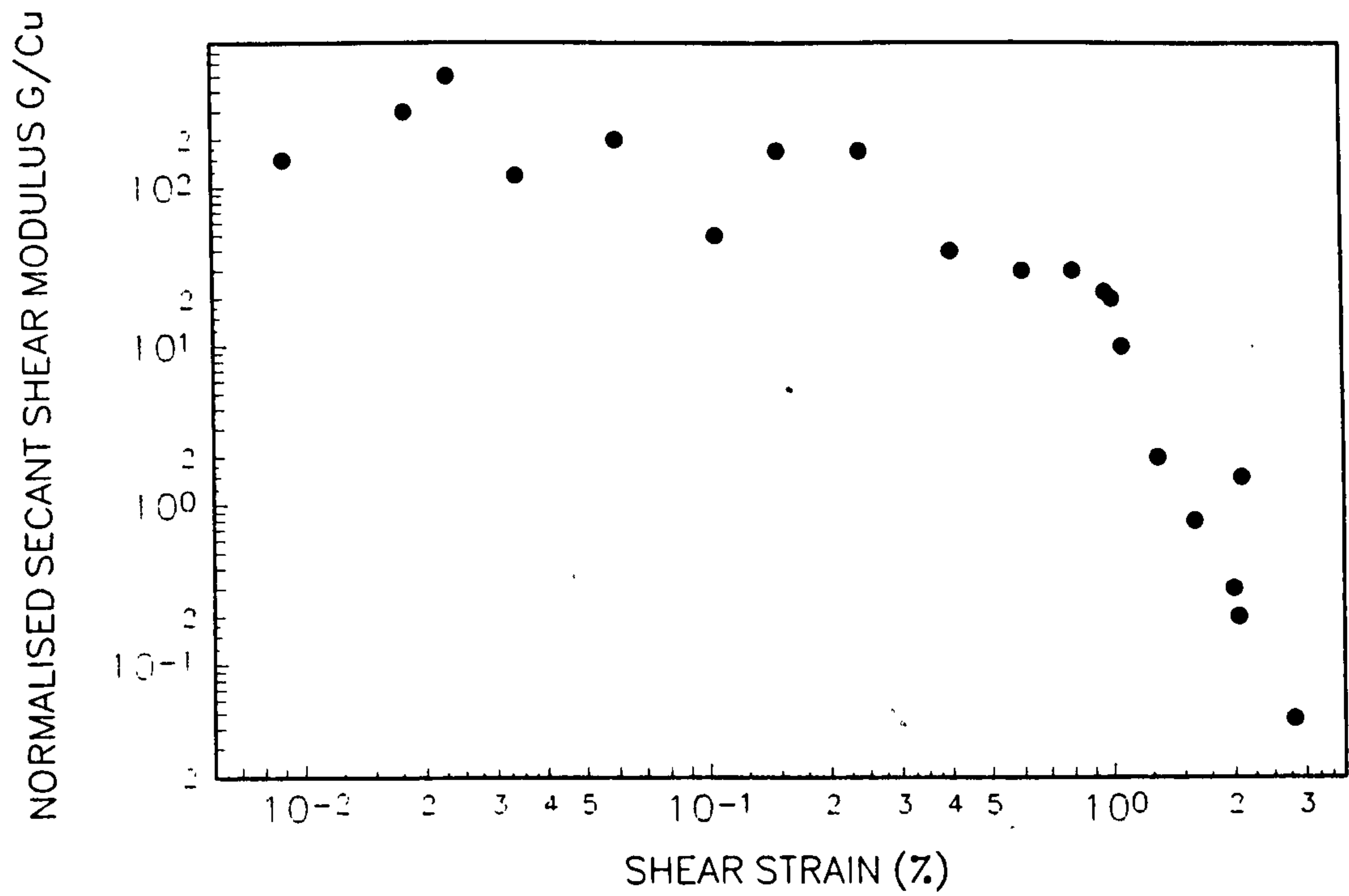
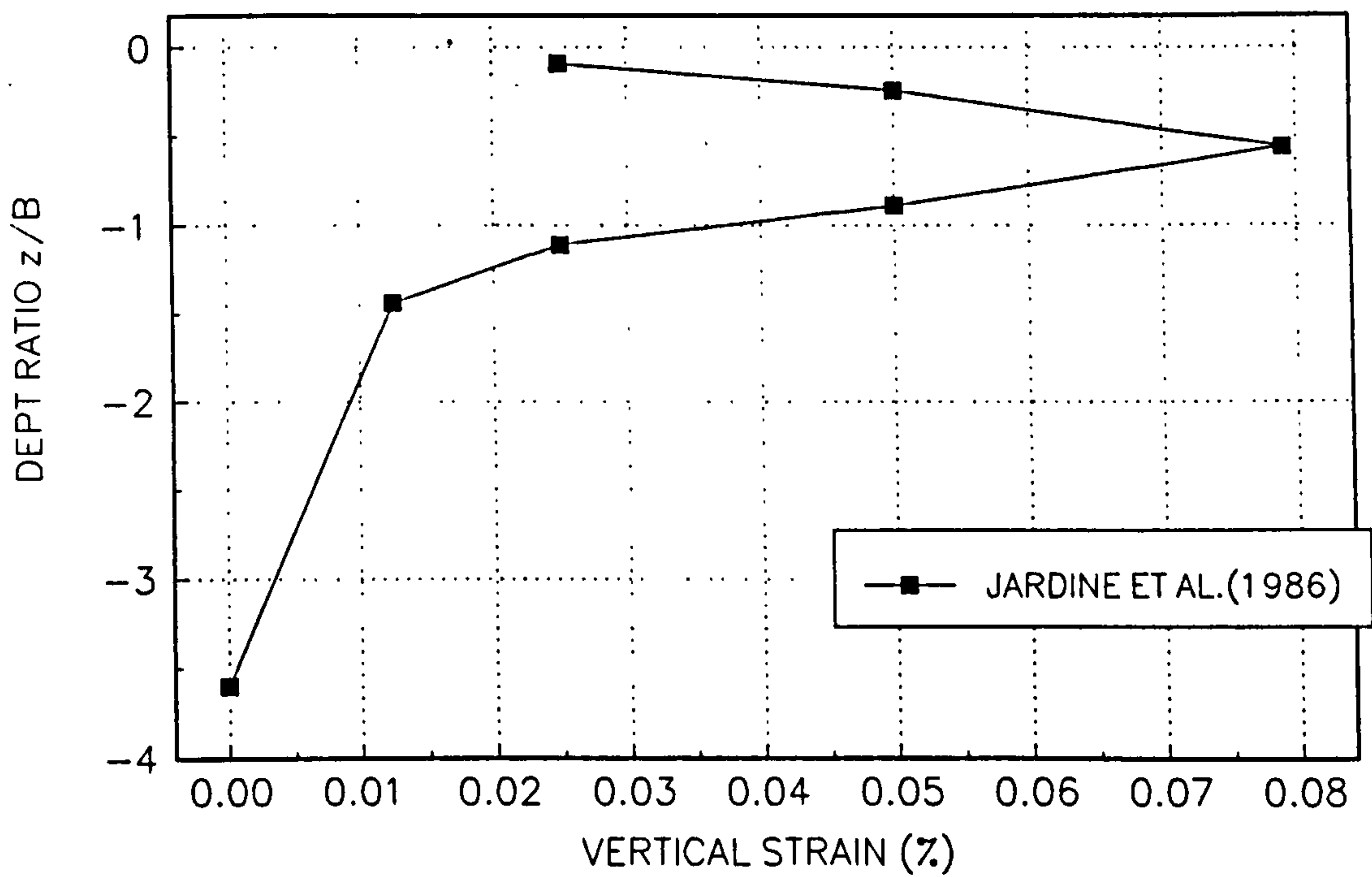


FIGURE 3.39
VERTICAL STRAIN PROFILE WITH DEPTH AT CENTRE LINE



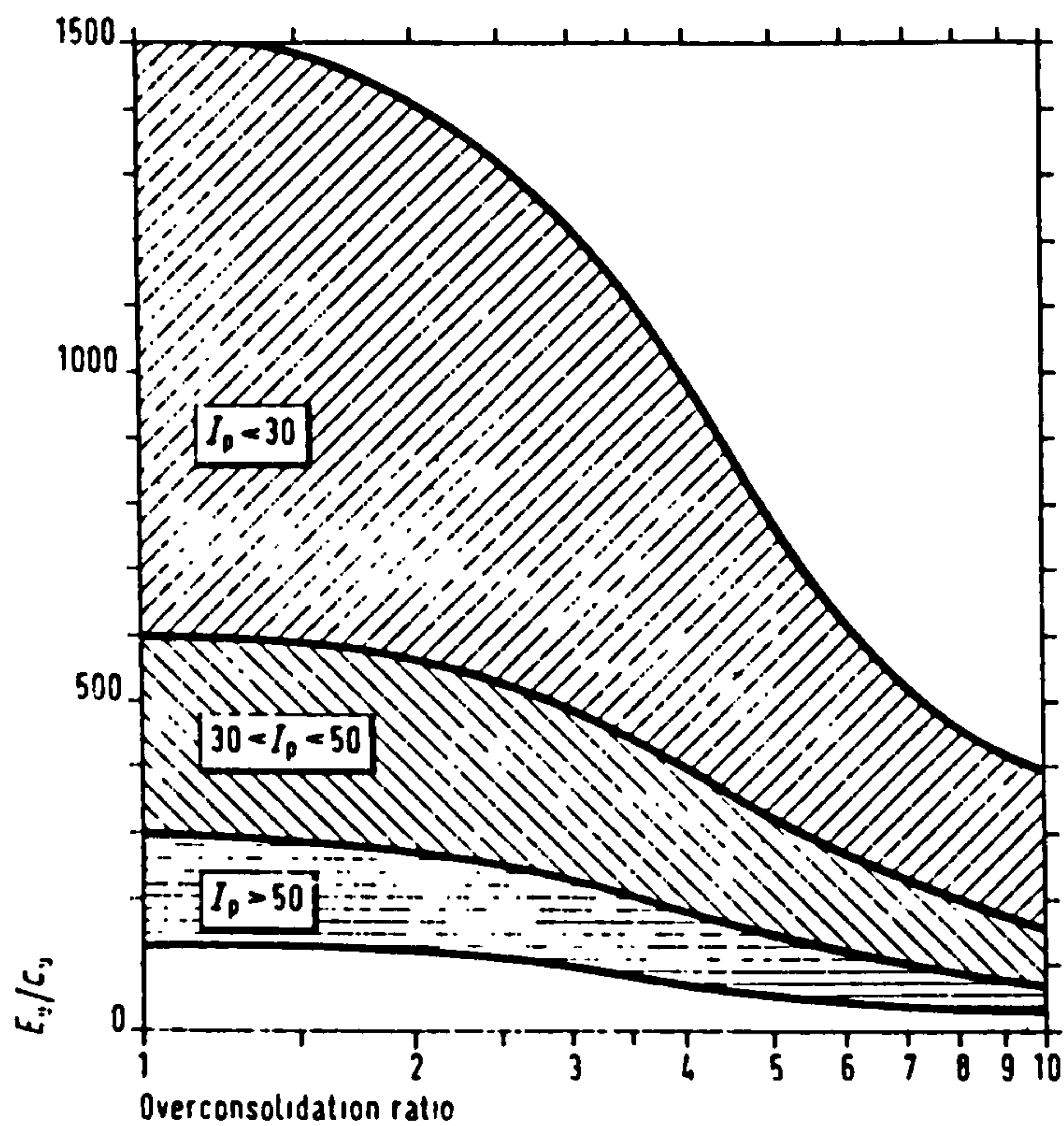


Fig 3.40. Ratio of undrained Young's modulus to shear strength against overconsolidation ratio for clays (Duncan and Buchignani, 1976 and Meigh, 1987).

FIGURE 3.41
UNDRAINED SHEAR STRENGTH DEPTH PROFILE ASSUMED TO SELECT ELASTIC STIFFNESS

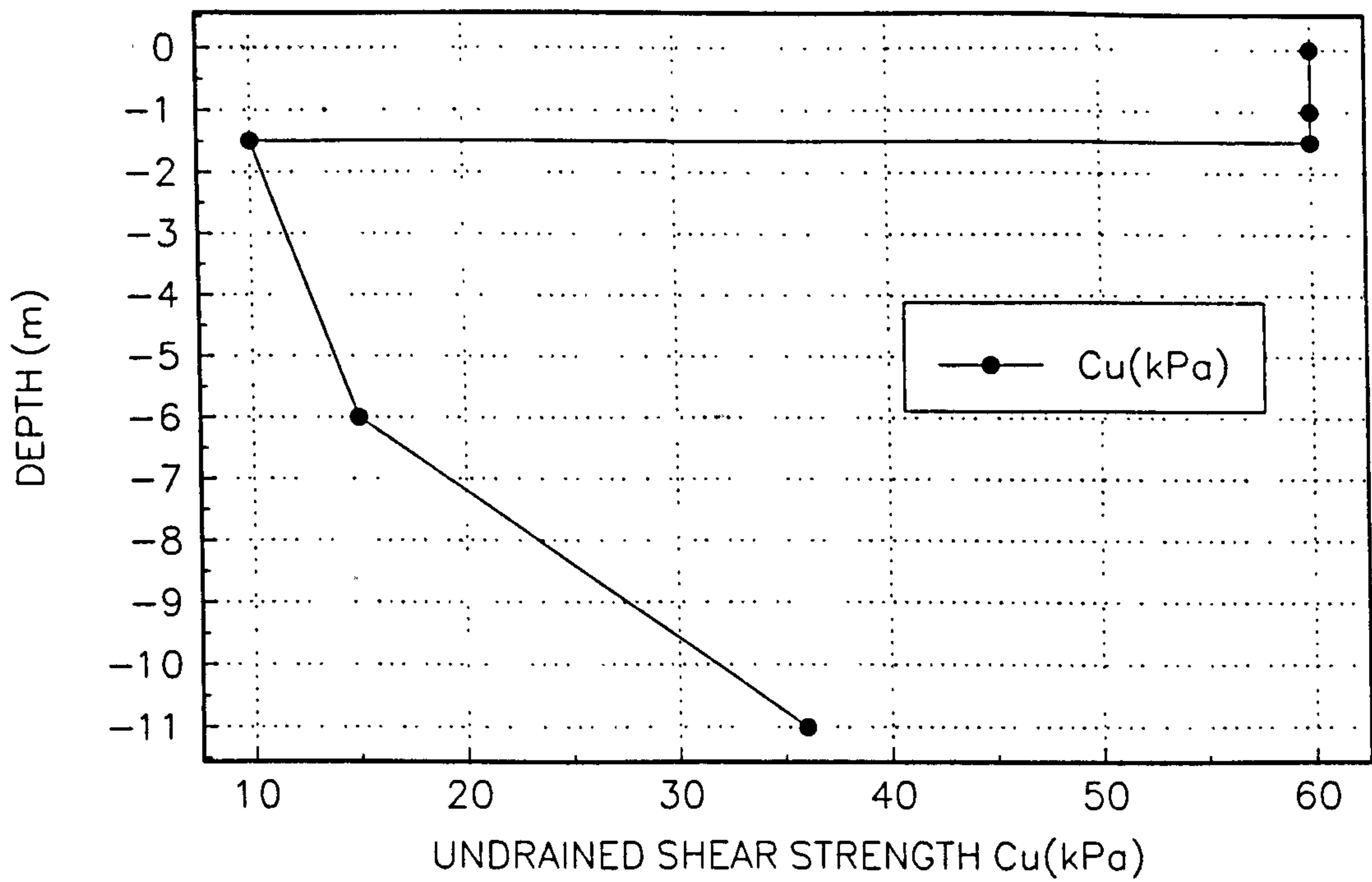


FIGURE 3.42
APPLIED LOAD AGAINST VERTICAL EDGE DISPLACEMENT

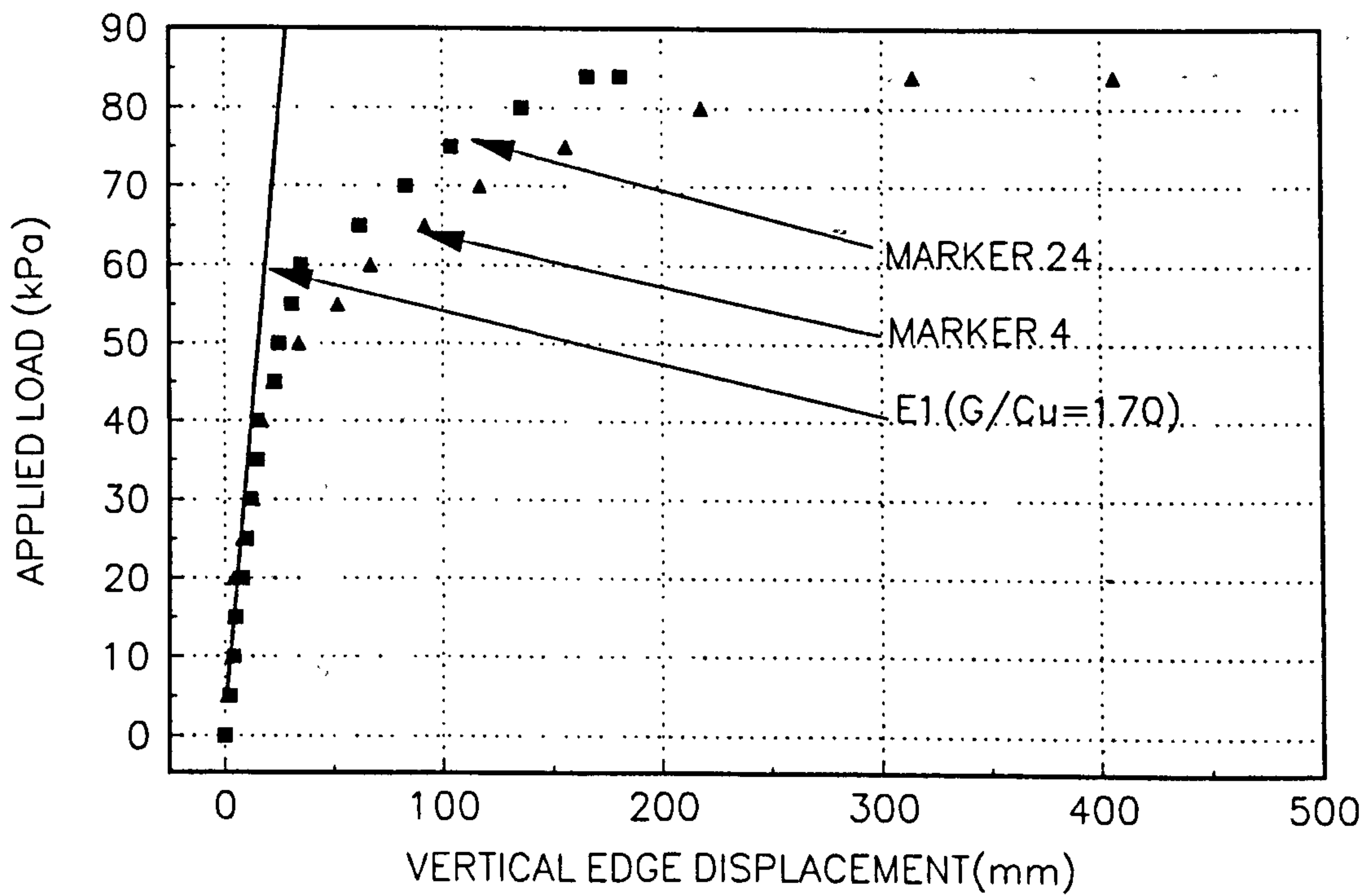


FIGURE 3.43
LATERAL DISPLACEMENT AT INCLINOMETER I4 AGAINST DEPTH AT LOAD 63kPa

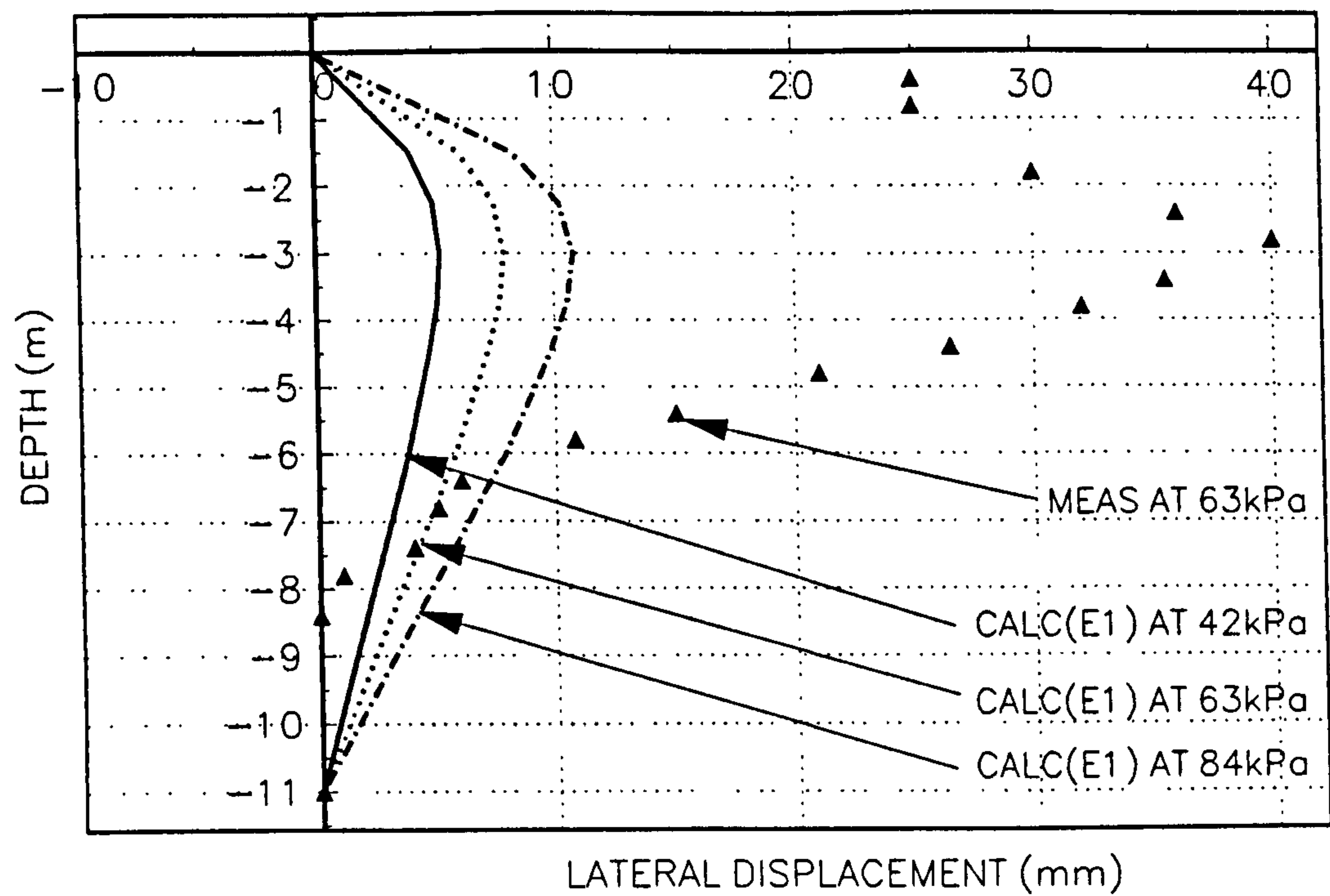


FIGURE 3.44
LATERAL DISPLACEMENT AT INCLINOMETER I5 AGAINST DEPTH

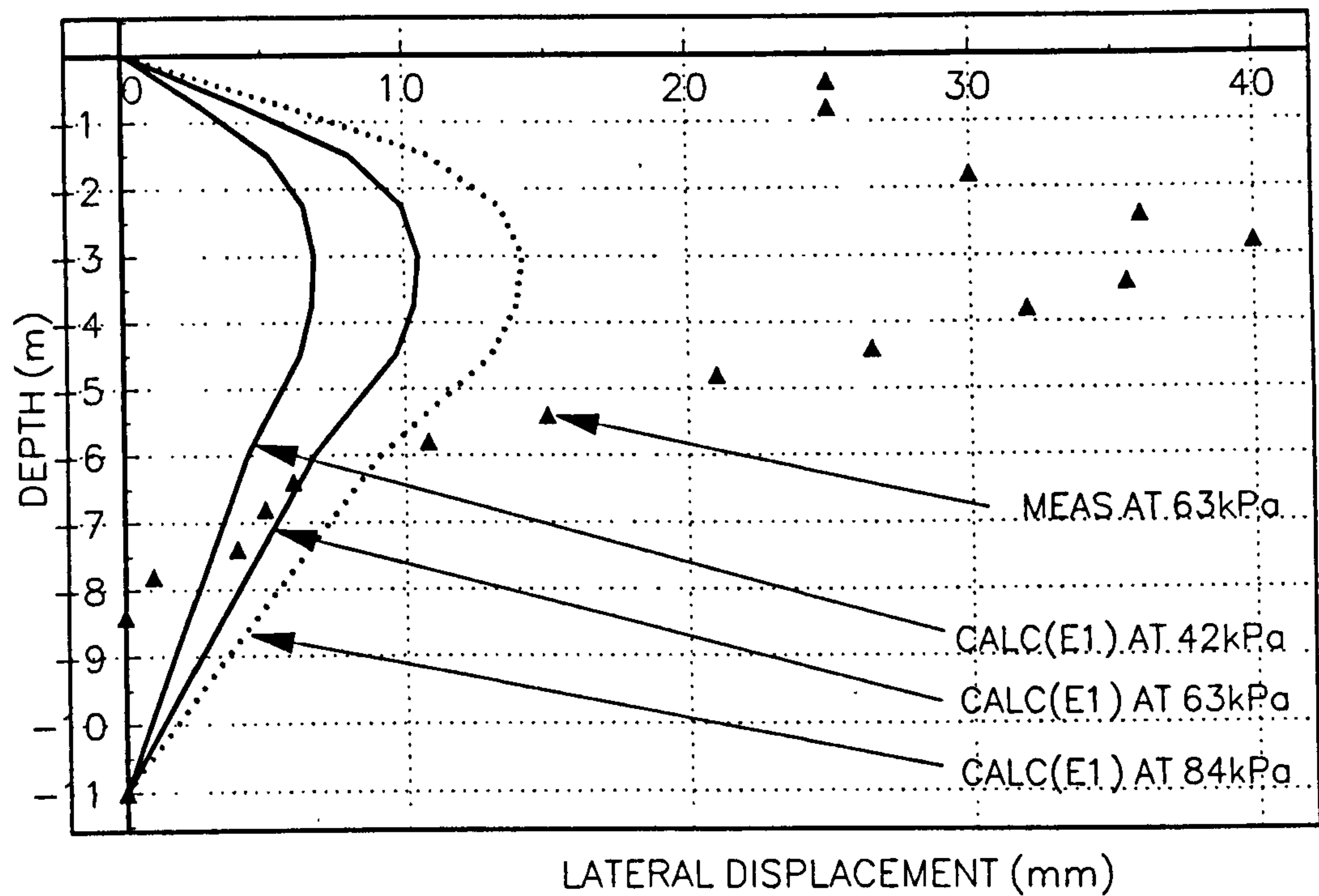


FIGURE 3.45
LATERAL DISPLACEMENT AT INCLINOMETER 16 AGAINST DEPTH

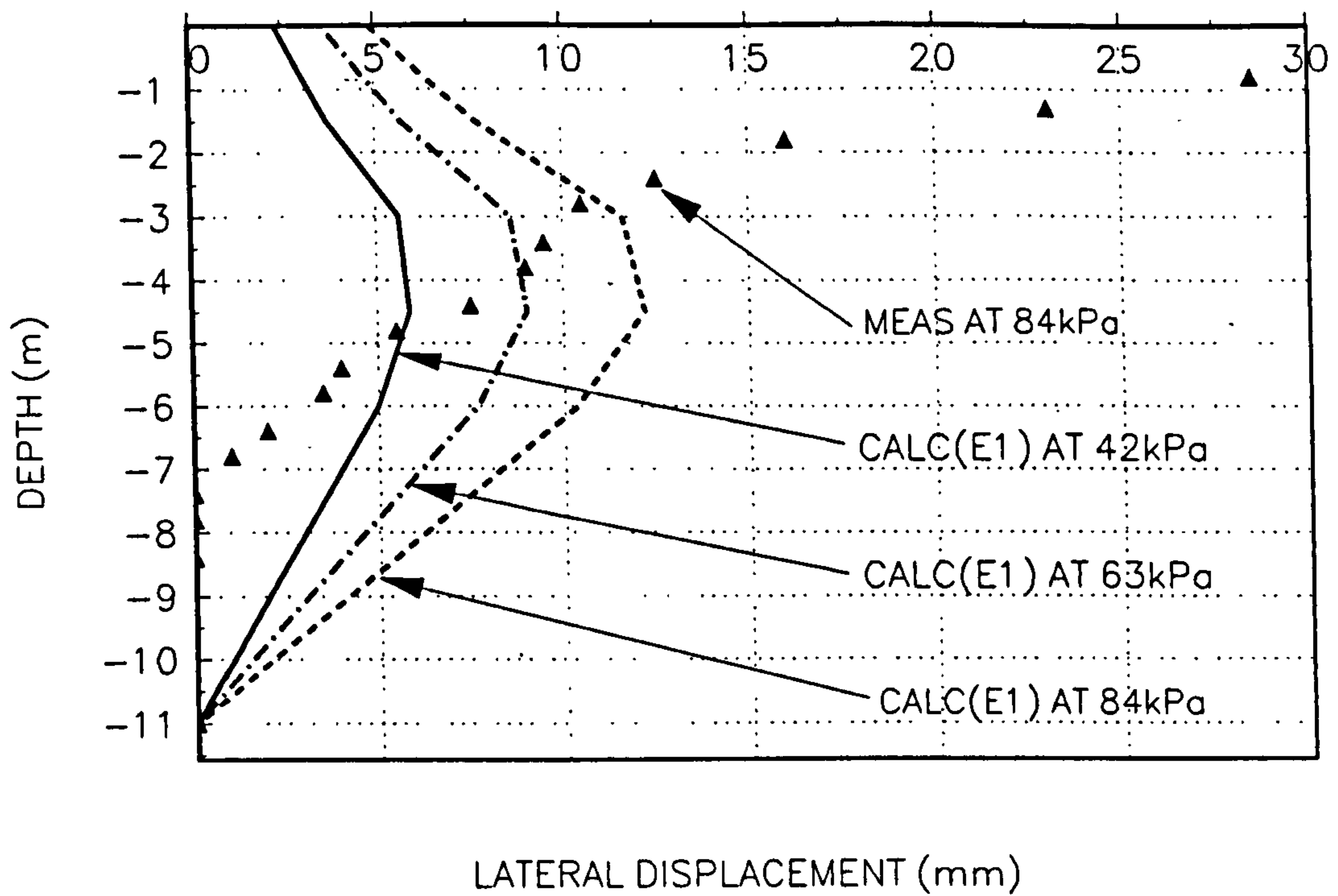


FIGURE 3.46
LATERAL DISPLACEMENT AT INCLINOMETER 14 AGAINST DEPTH AT LOAD 63kPa

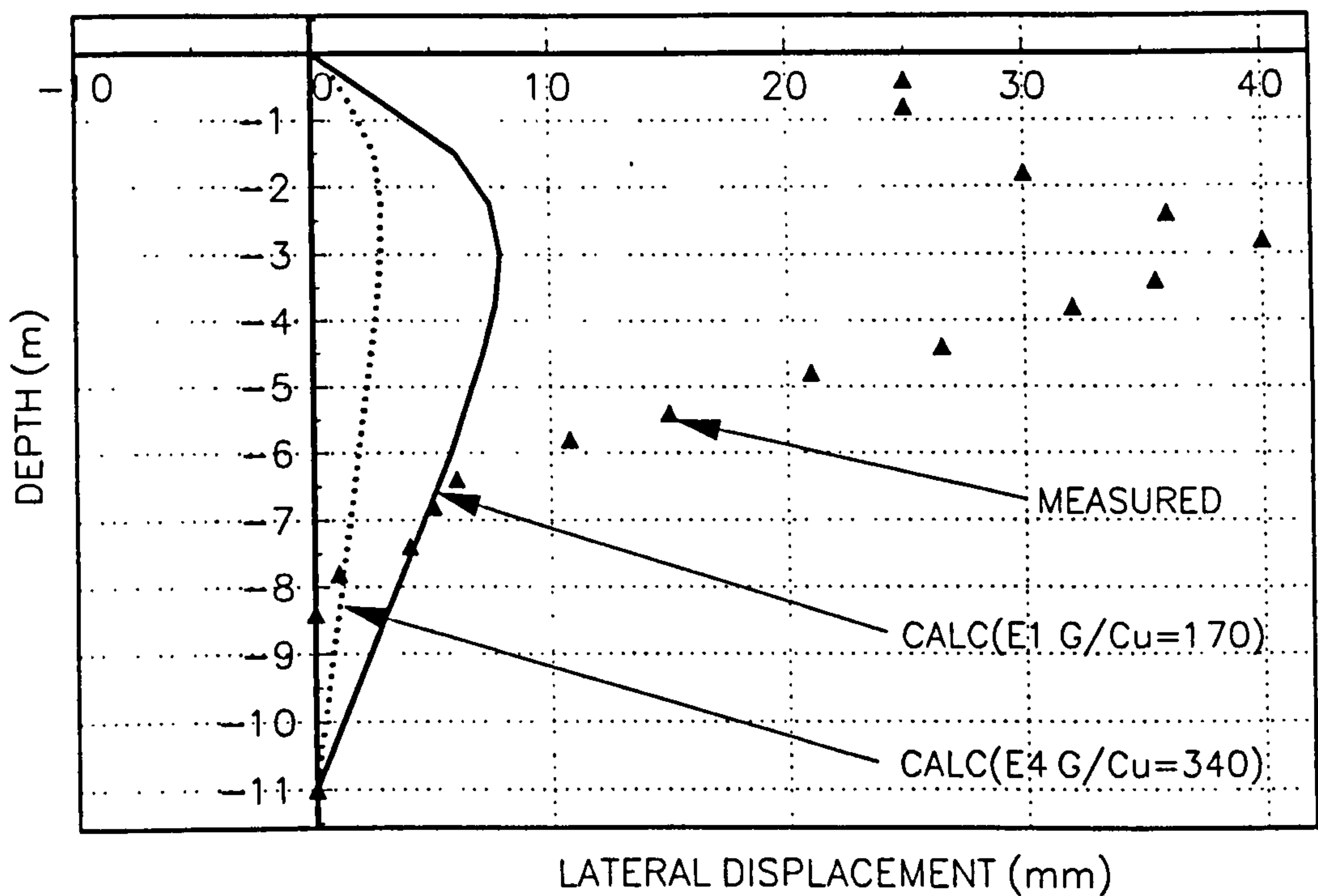


FIGURE 3.47
 LATERAL DISPLACEMENT AT INCLINOMETER 15 AGAINST DEPTH AT 63kPa

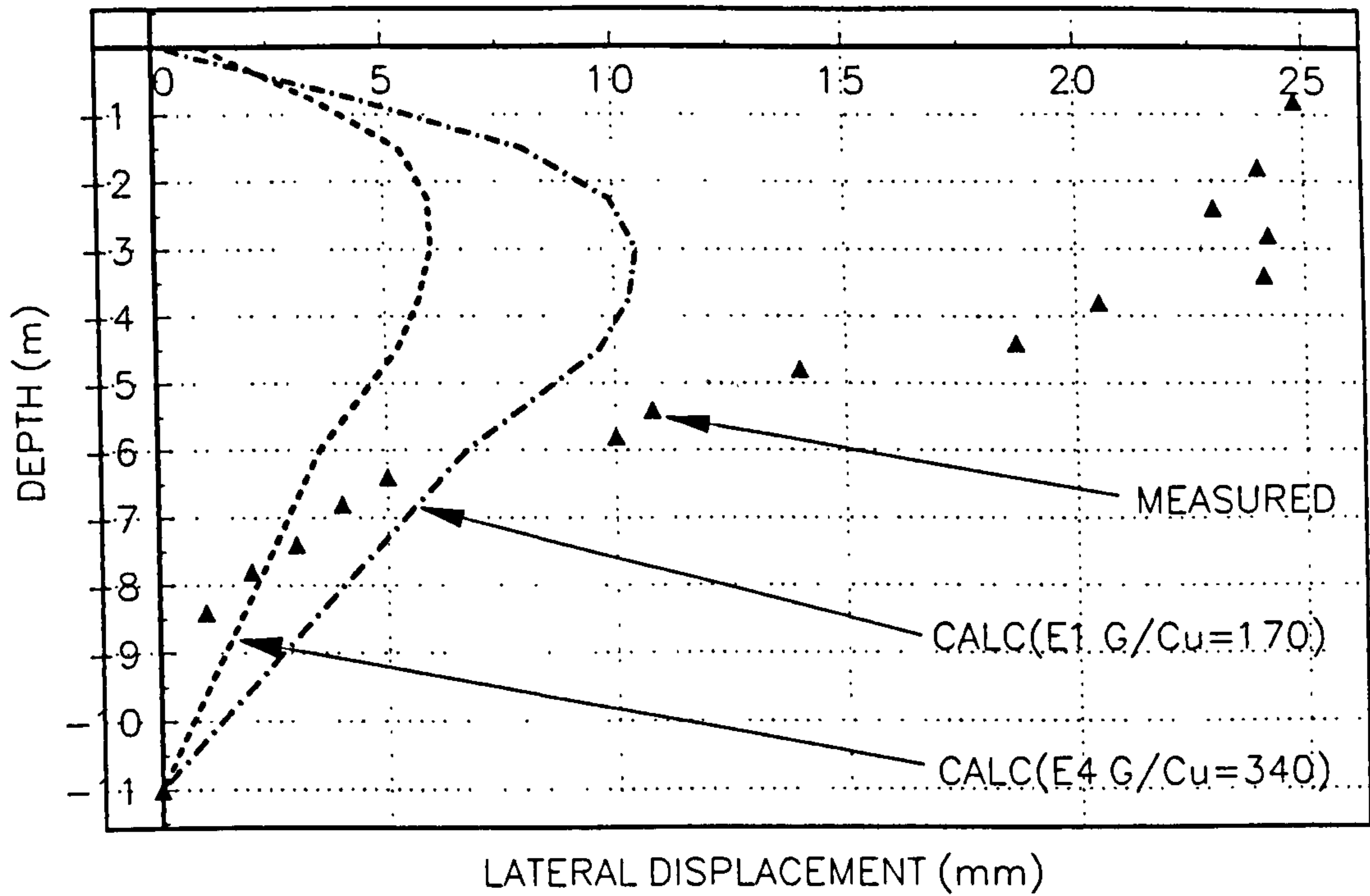


FIGURE 3.48
 LATERAL DISPLACEMENT AT INCLINOMETER 16 AGAINST DEPTH AT LOAD 84kPa

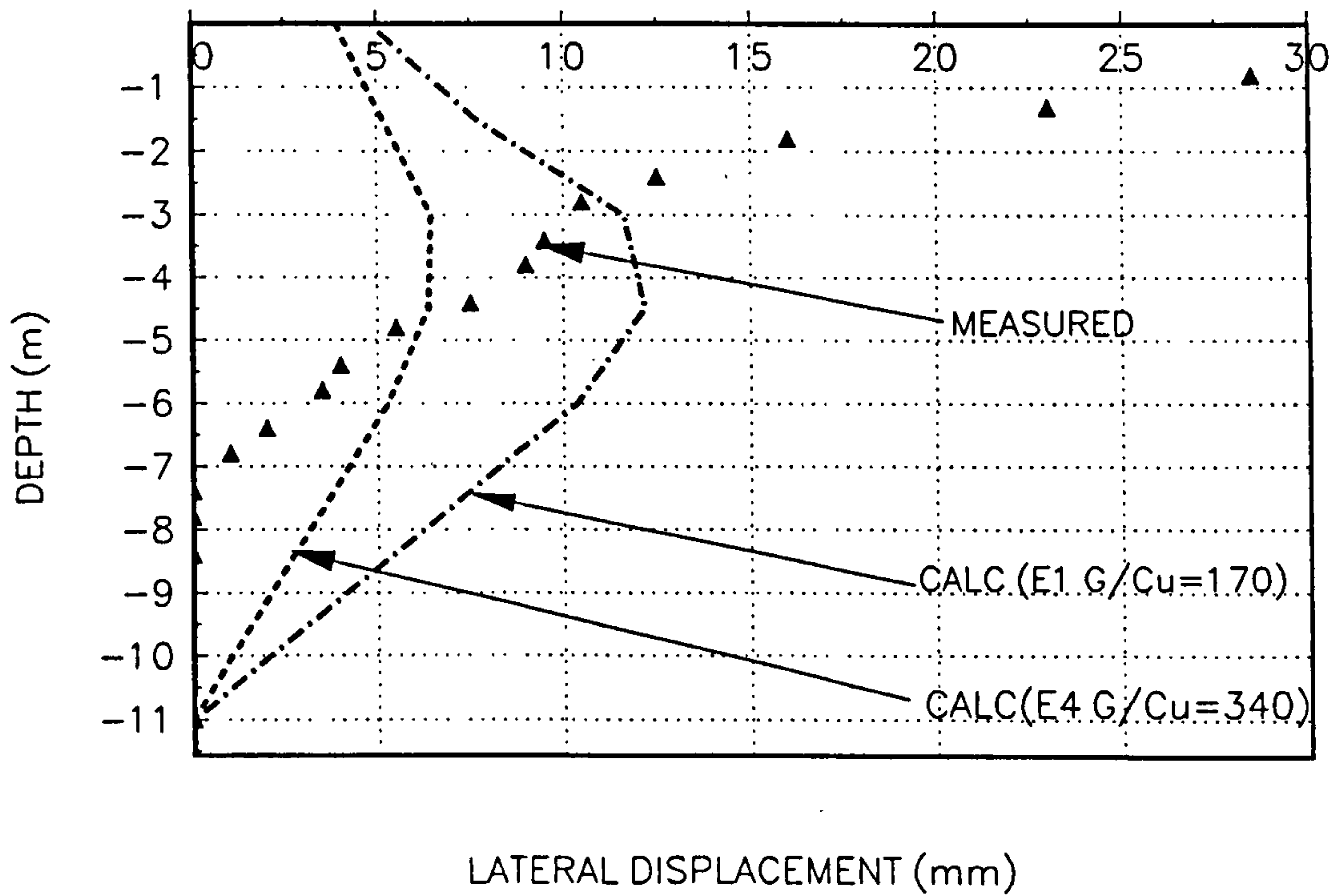


FIGURE 3.49
LATERAL DISPLACEMENT AT INCLINOMETER I4 AGAINST DEPTH AT LOAD 63kPa

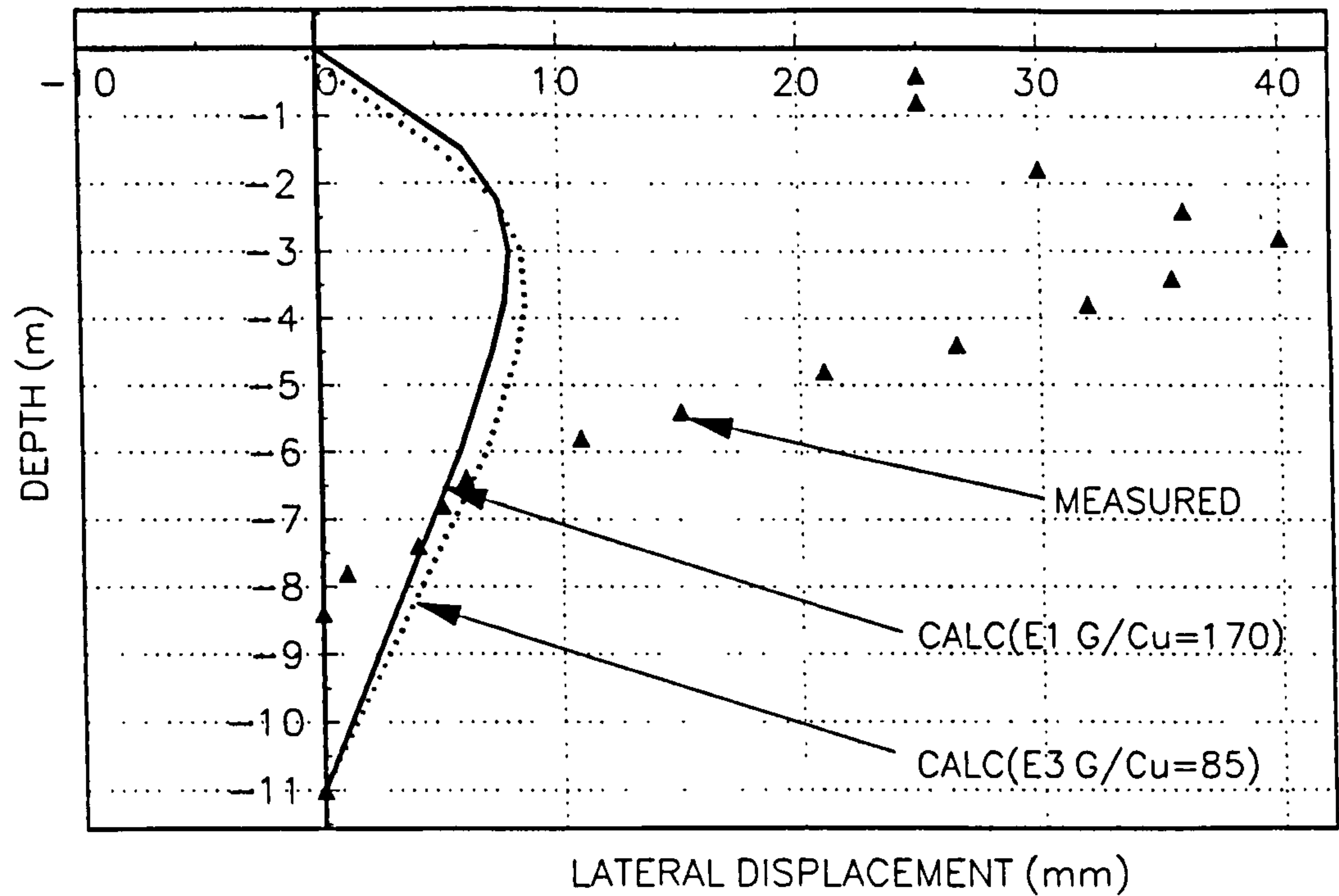


FIGURE 3.50
LATERAL DISPLACEMENT AT INCLINOMETER I5 AGAINST DEPTH AT 63kPa

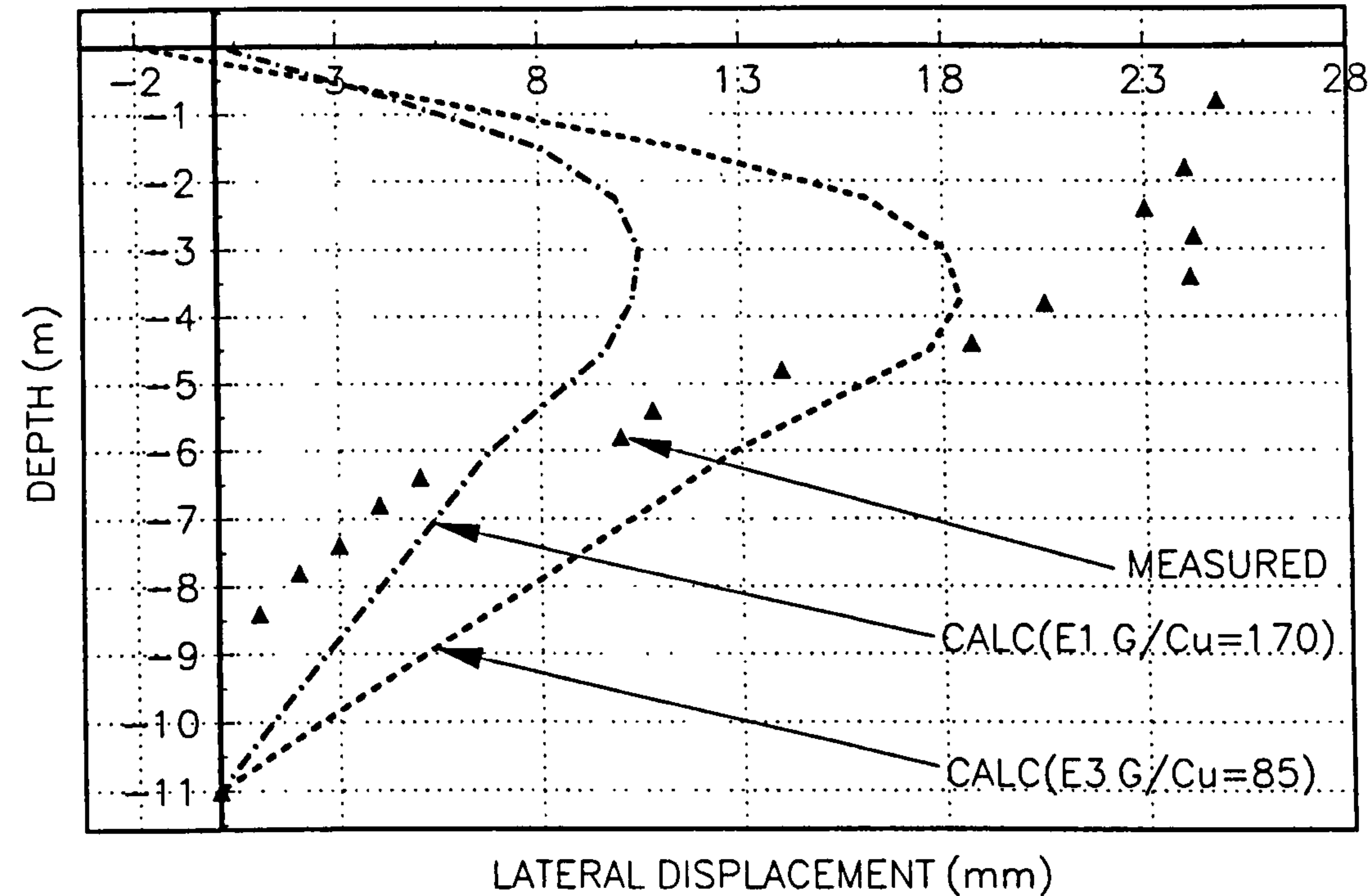


FIGURE 3.51
LATERAL DISPLACEMENT AT INCLINOMETER 16 AGAINST DEPTH AT LOAD 84kPa

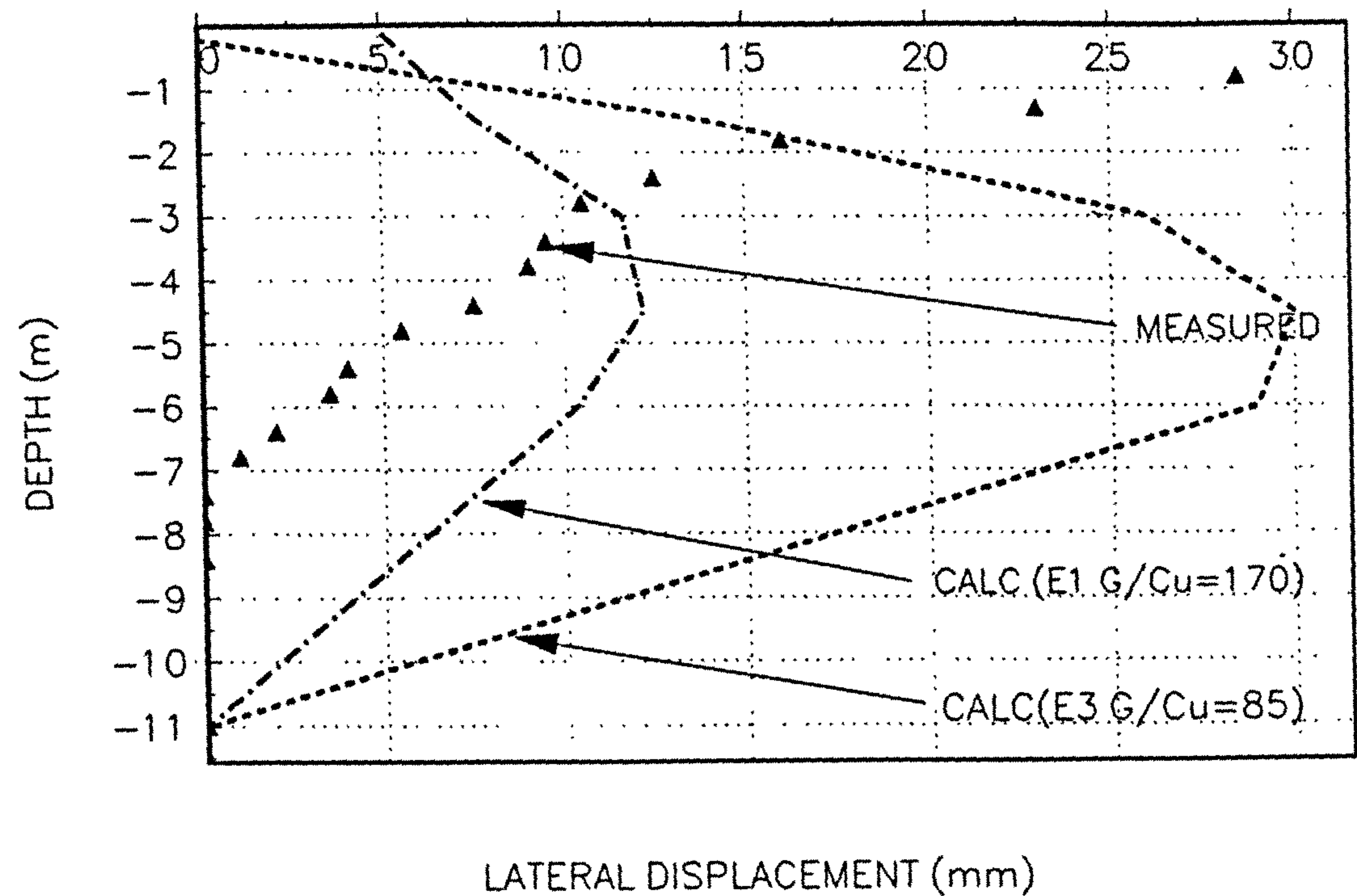


FIGURE 3.52
APPLIED LOAD AGAINST EDGE DISPLACEMENT

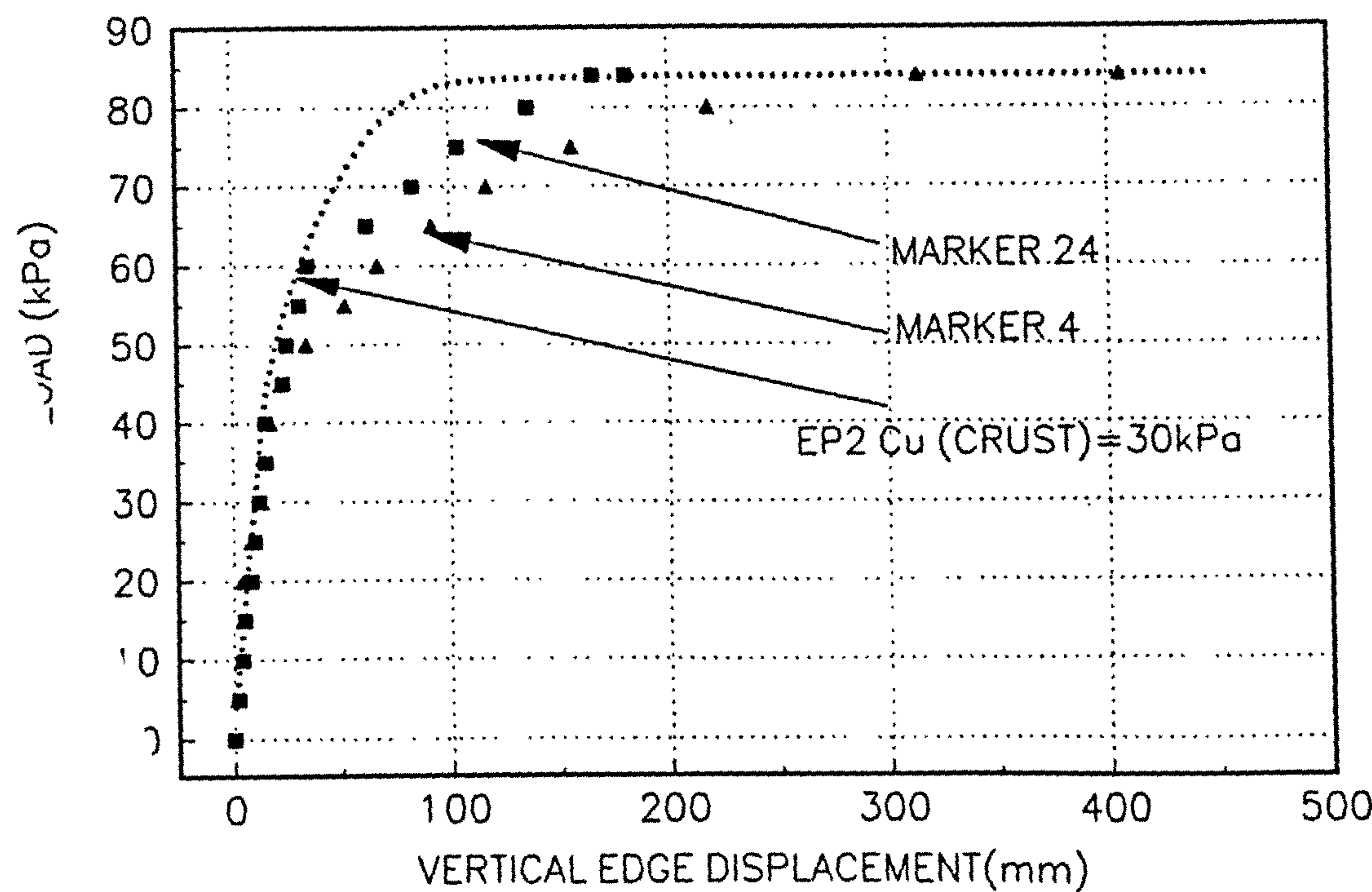


FIGURE 3.53
LATERAL DISPLACEMENT AT INCLINOMETER 14 AGAINST DEPTH.

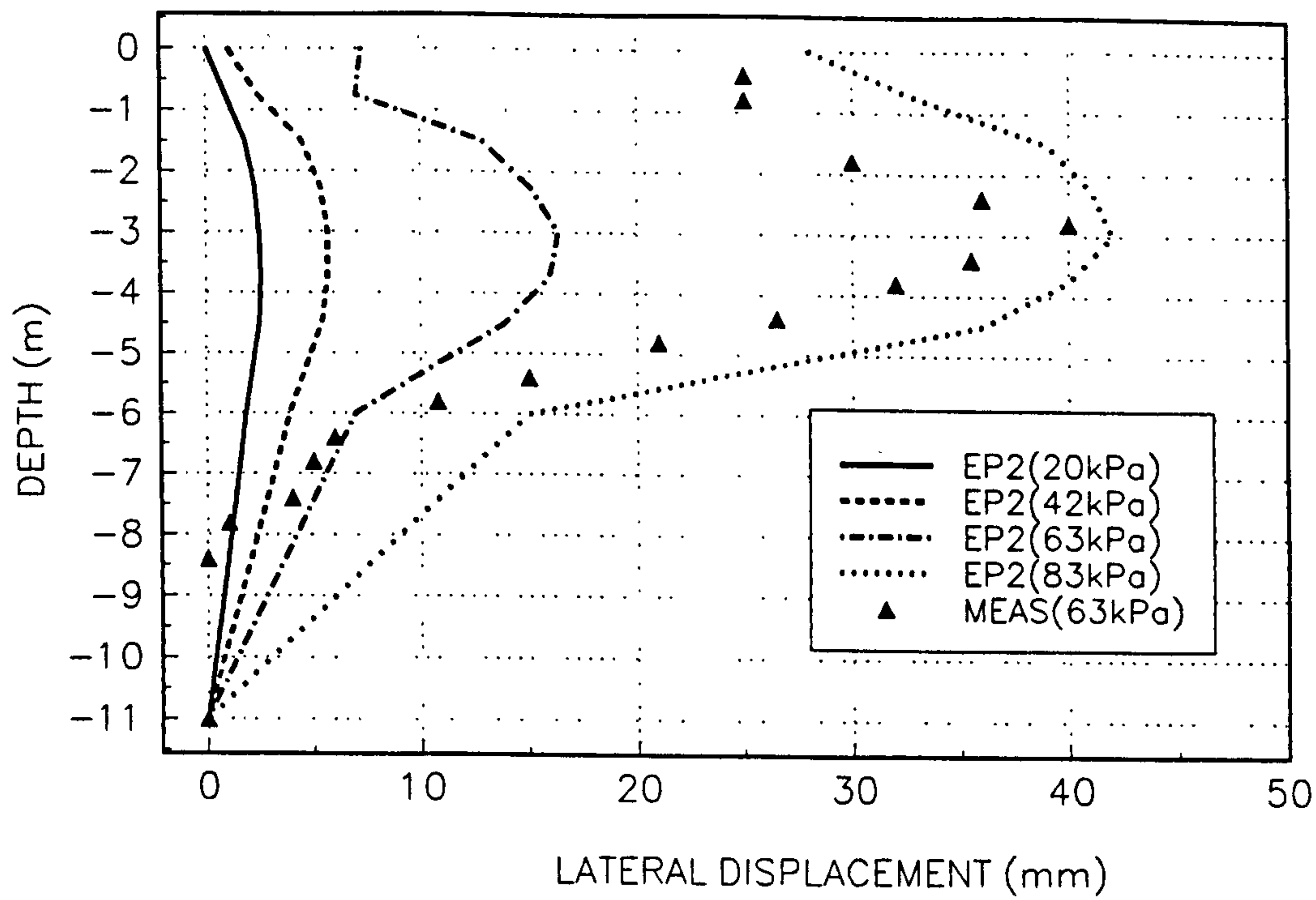


FIGURE 3.54
LATERAL DISPLACEMENT AT INCLINOMETER 15 AGAINST DEPTH.

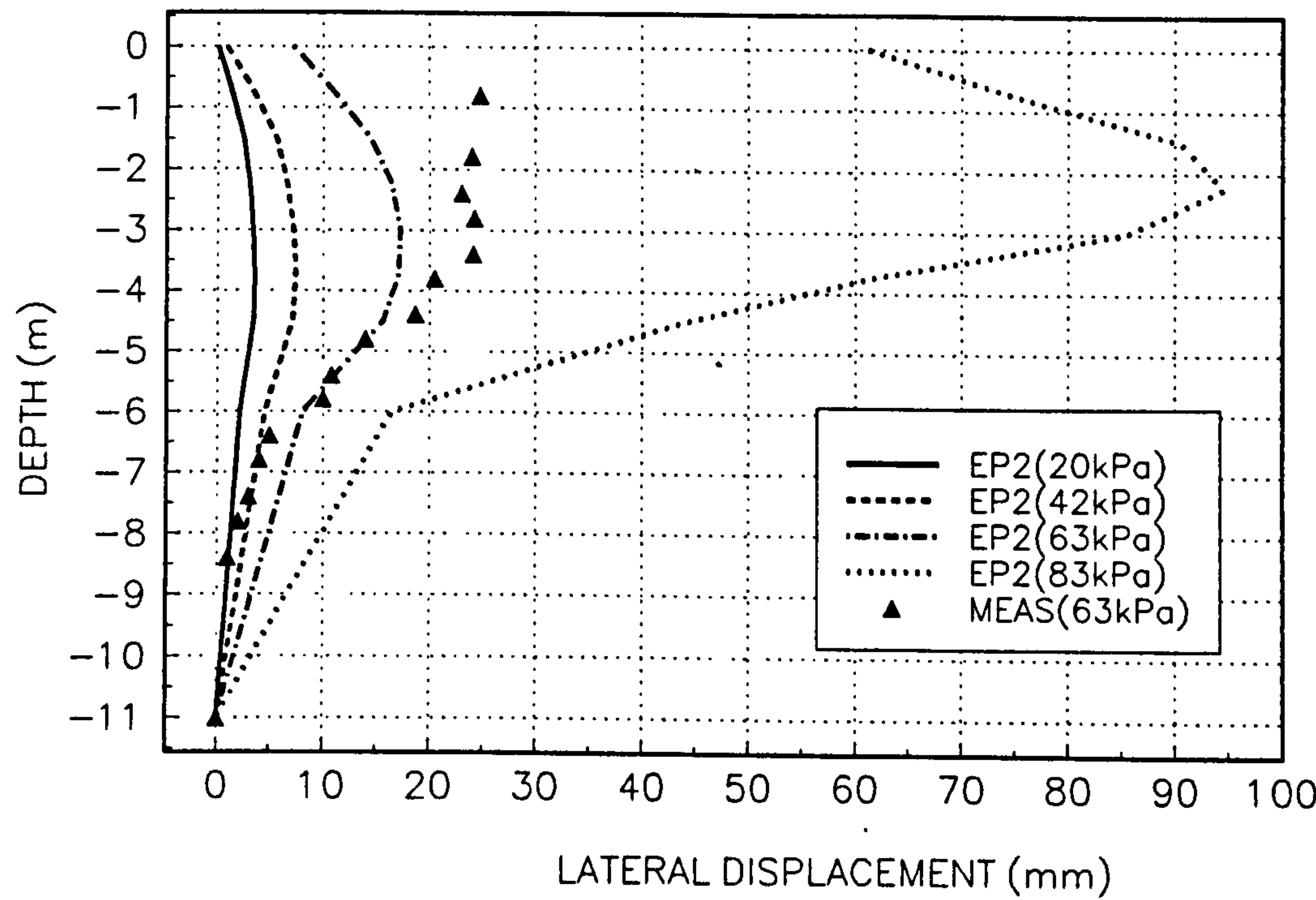


FIGURE 3.55
LATERAL DISPLACEMENT AT INCLINOMETER 16 AGAINST DEPTH.

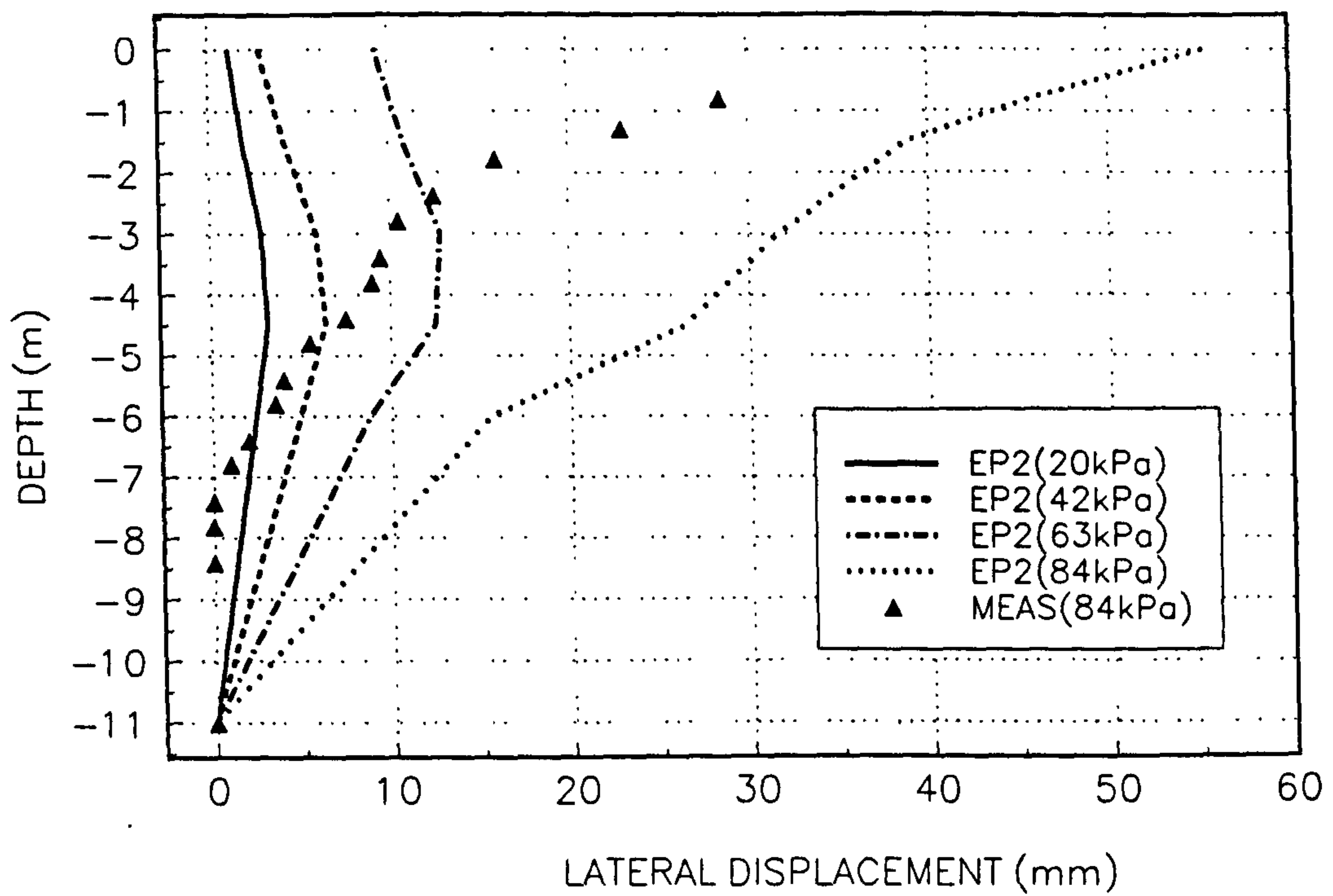


FIGURE 3.56
APPLIED LOAD AGAINST EDGE DISPLACEMENT

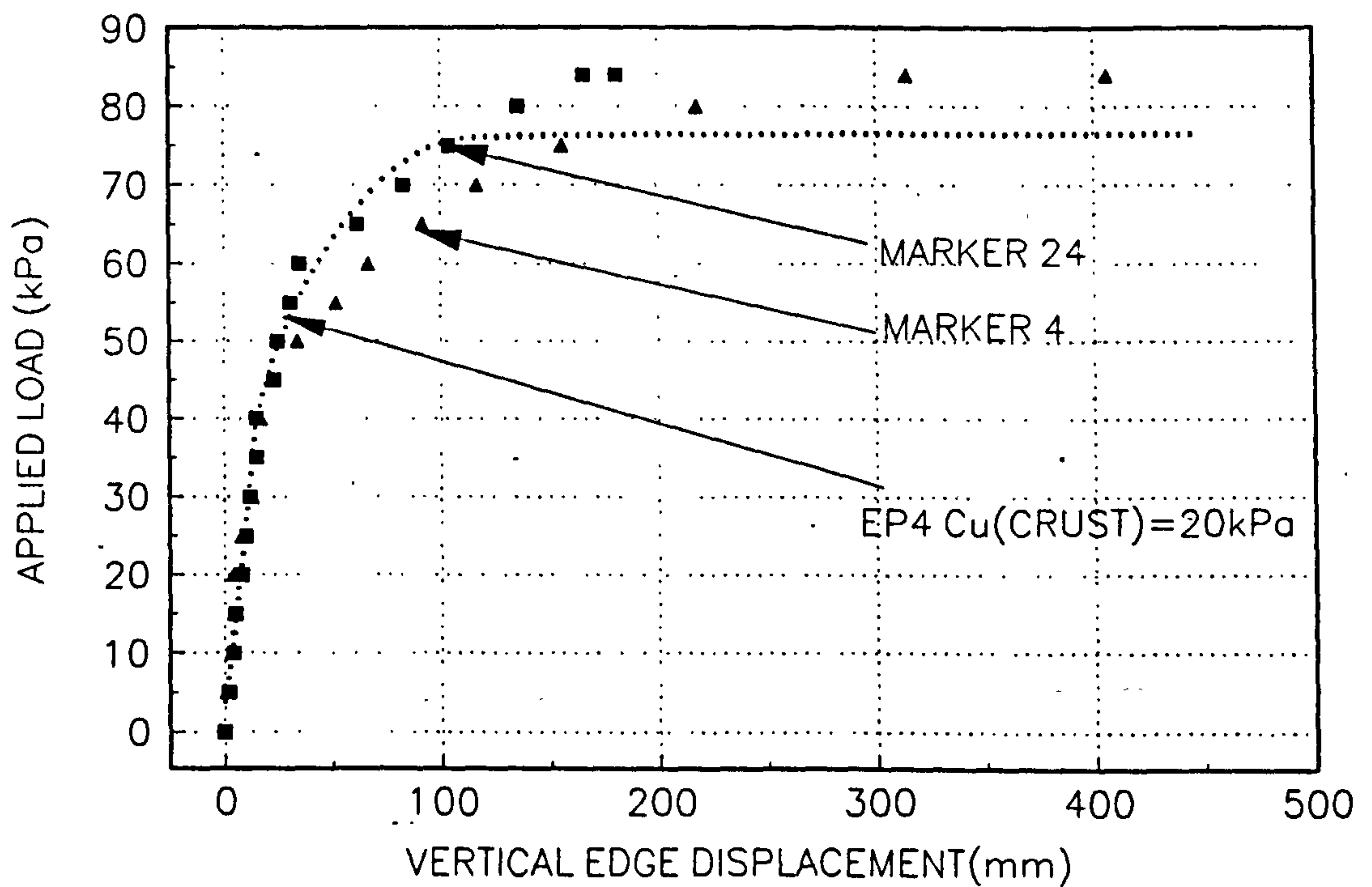


FIGURE 3.57
LATERAL DISPLACEMENT AT INCLINOMETER 14 AGAINST DEPTH.

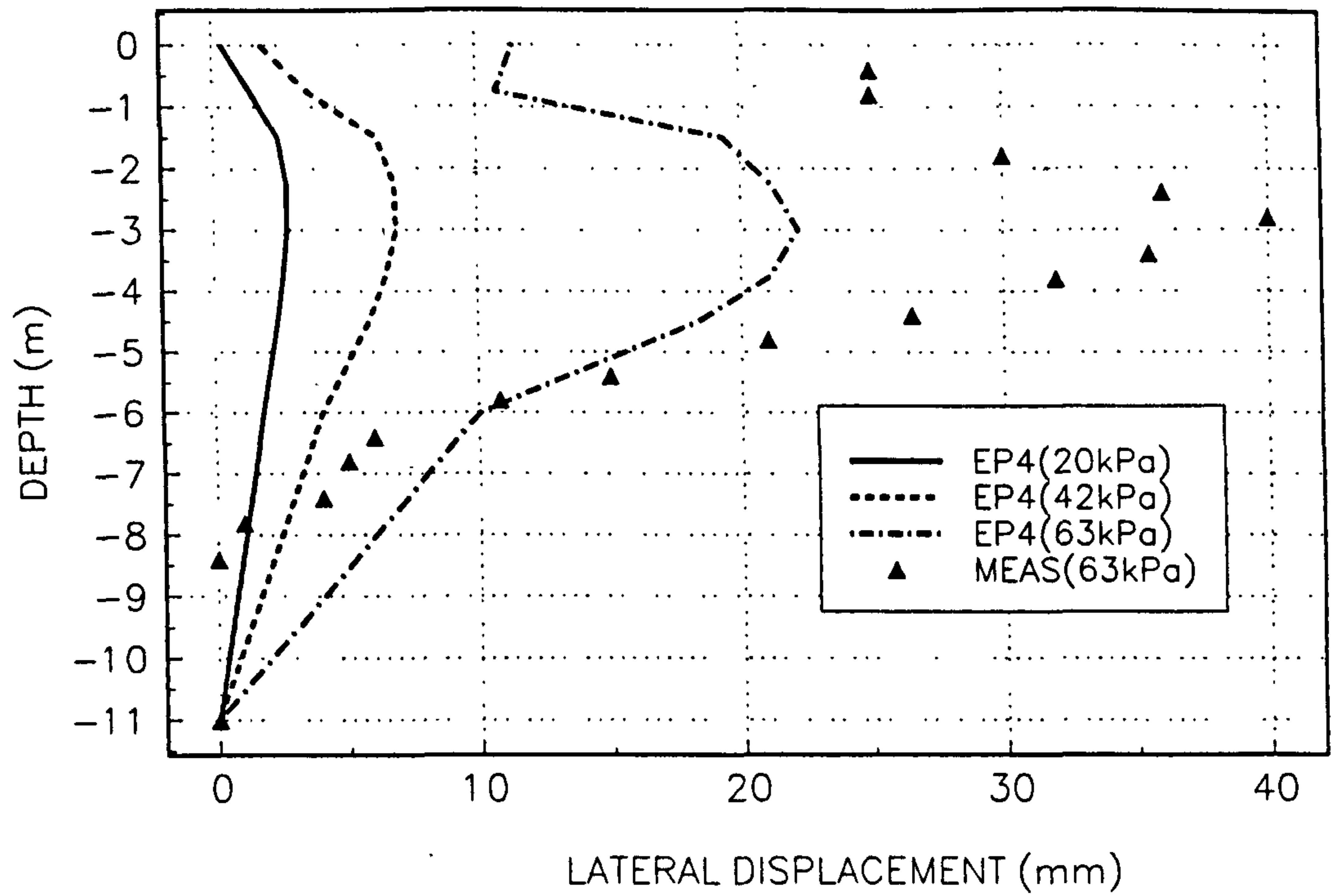


FIGURE 3.58
LATERAL DISPLACEMENT AT INCLINOMETER 15 AGAINST DEPTH.

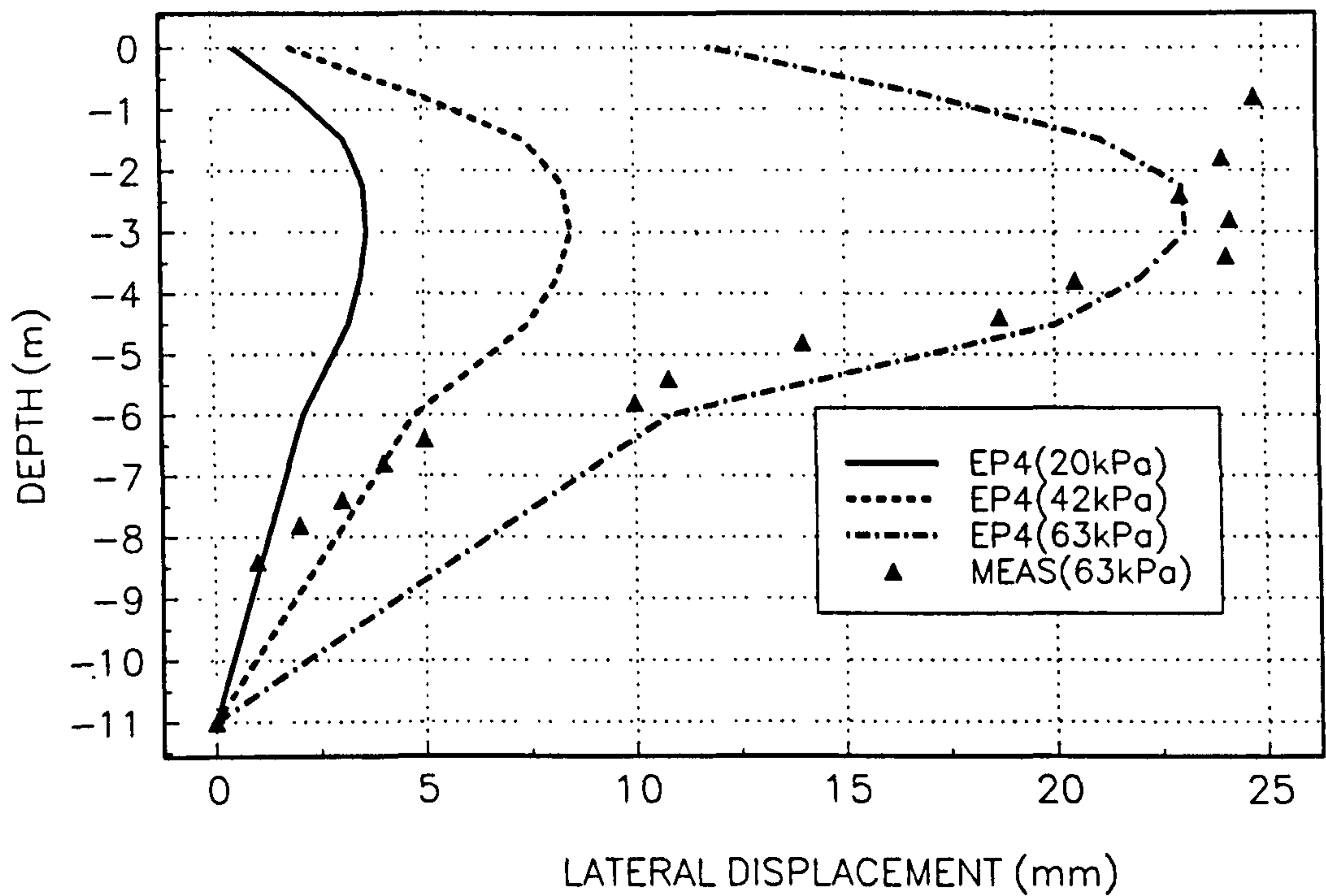


FIGURE 3.59
LATERAL DISPLACEMENT AT INCLINOMETER 16 AGAINST DEPTH.

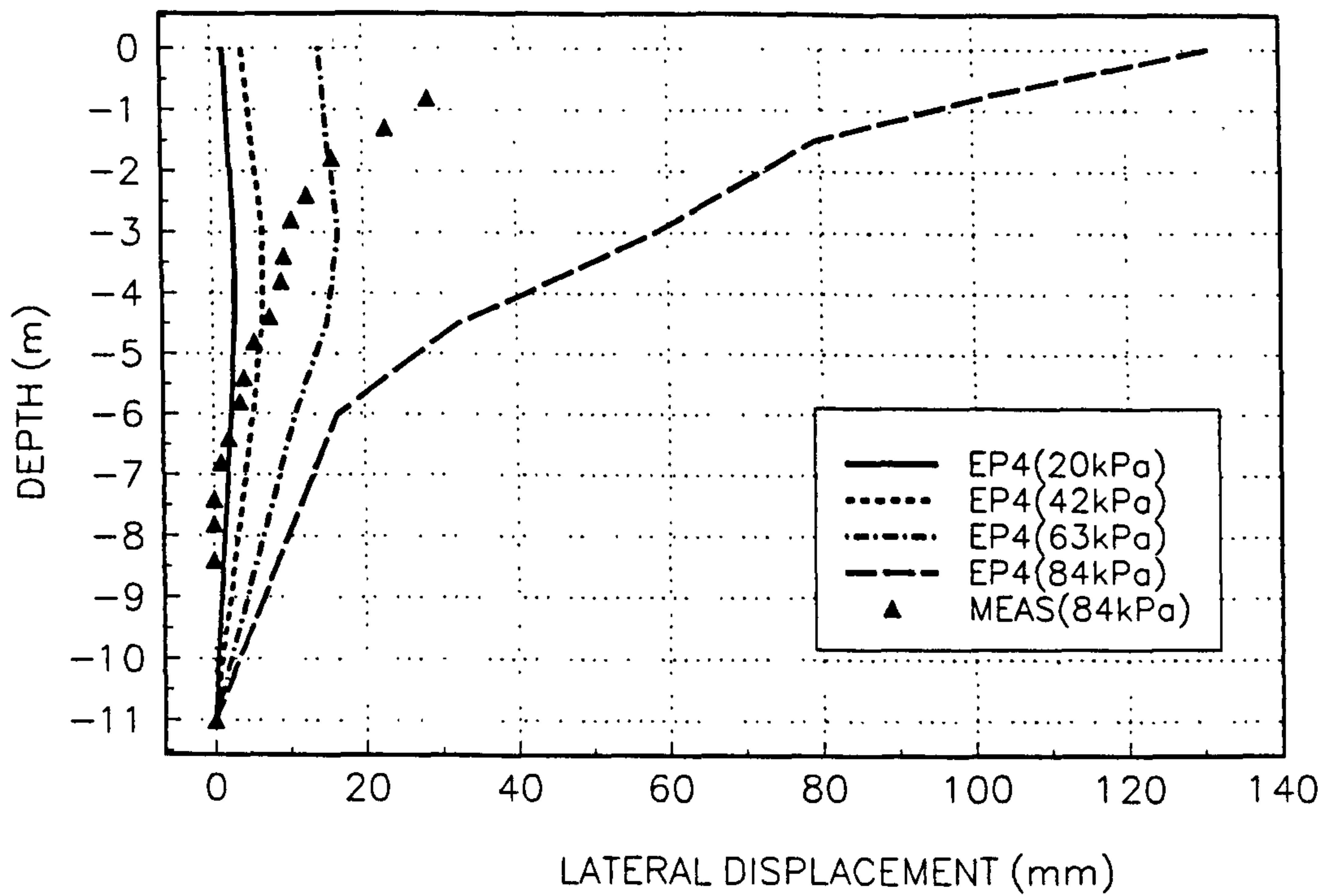


FIGURE 3.60
APPLIED LOAD AGAINST EDGE DISPLACEMENT

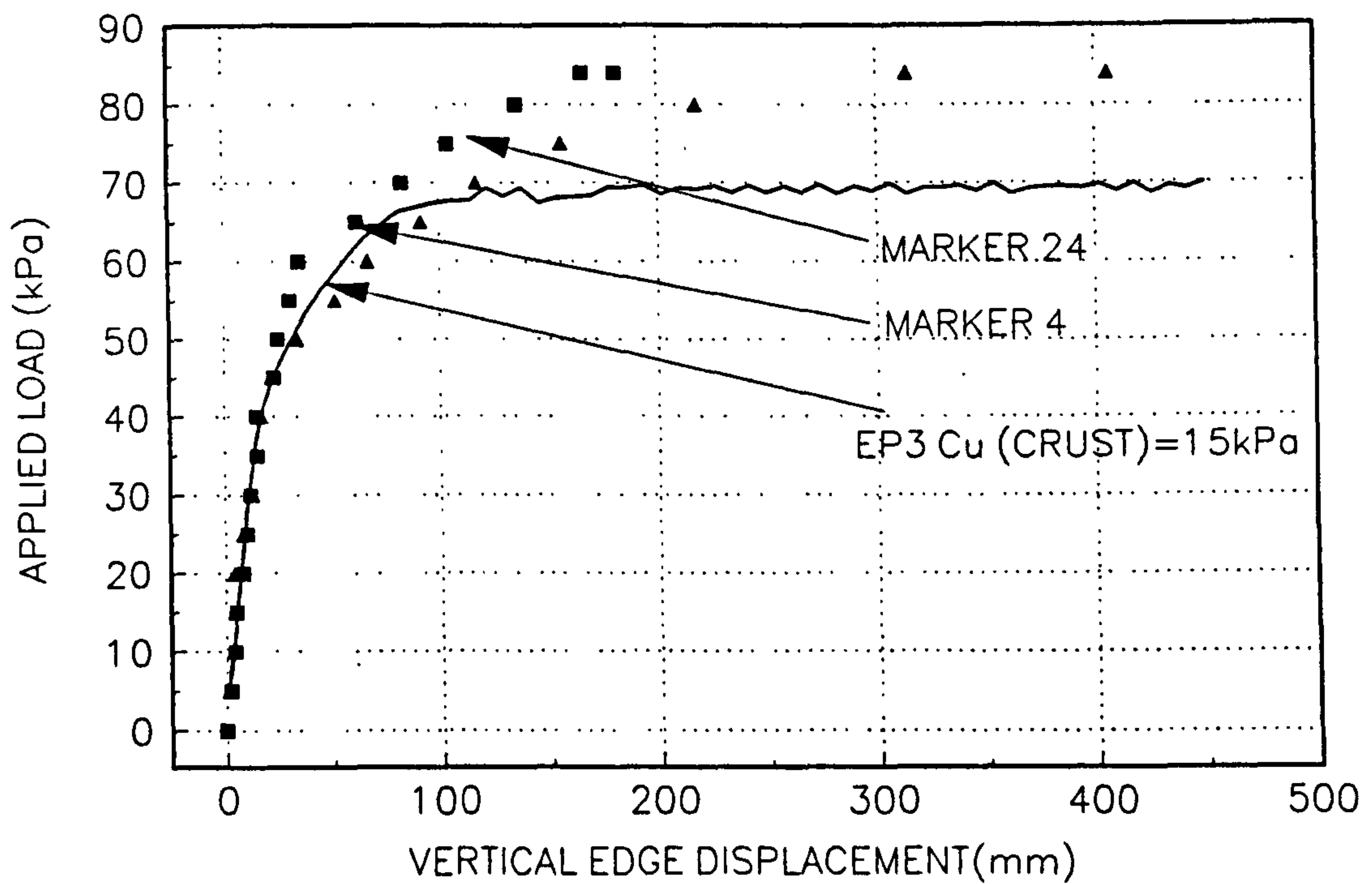


FIGURE 3.61
LATERAL DISPLACEMENT AT INCLINOMETER 14 AGAINST DEPTH.

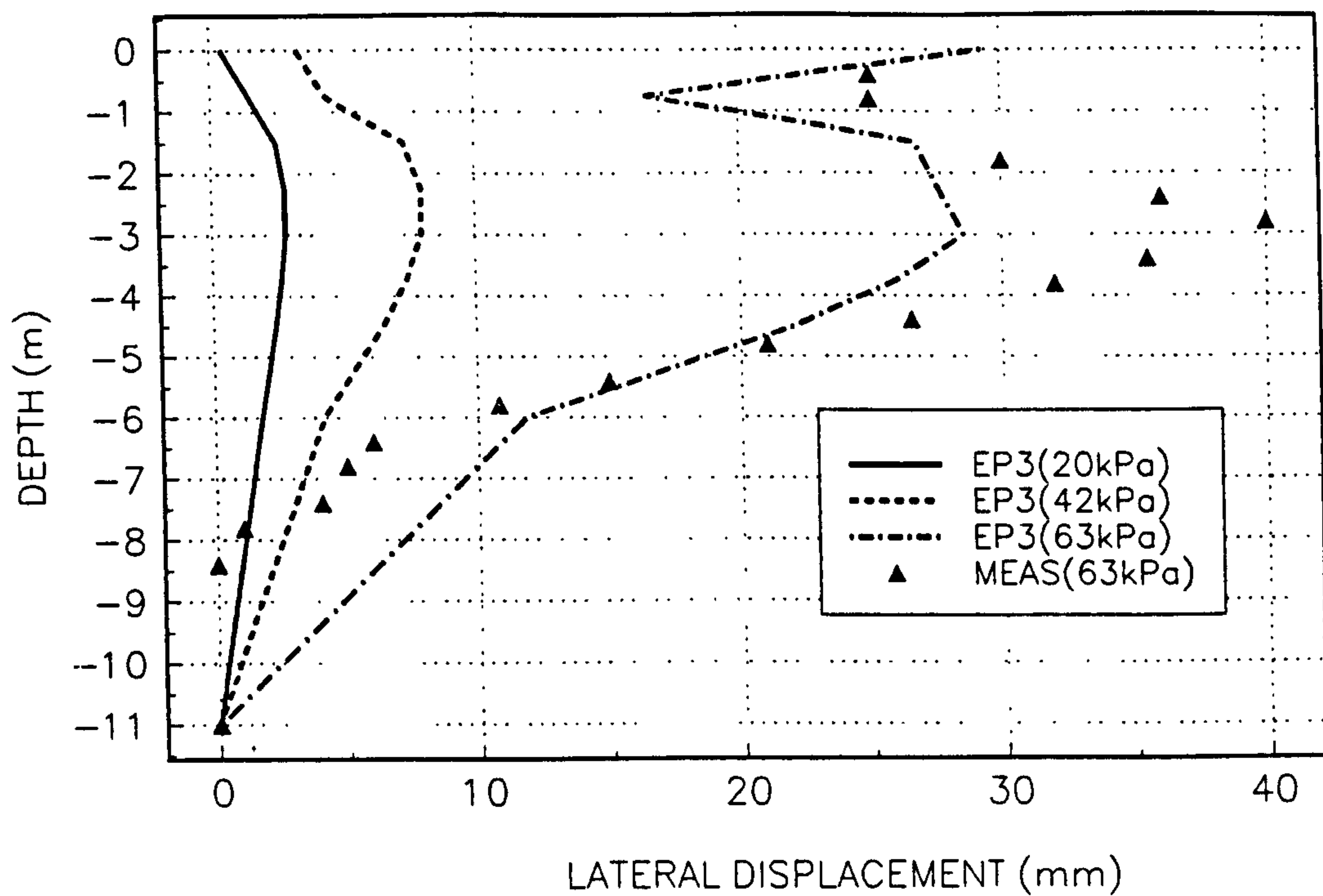


FIGURE 3.62
LATERAL DISPLACEMENT AT INCLINOMETER 15 AGAINST DEPTH.

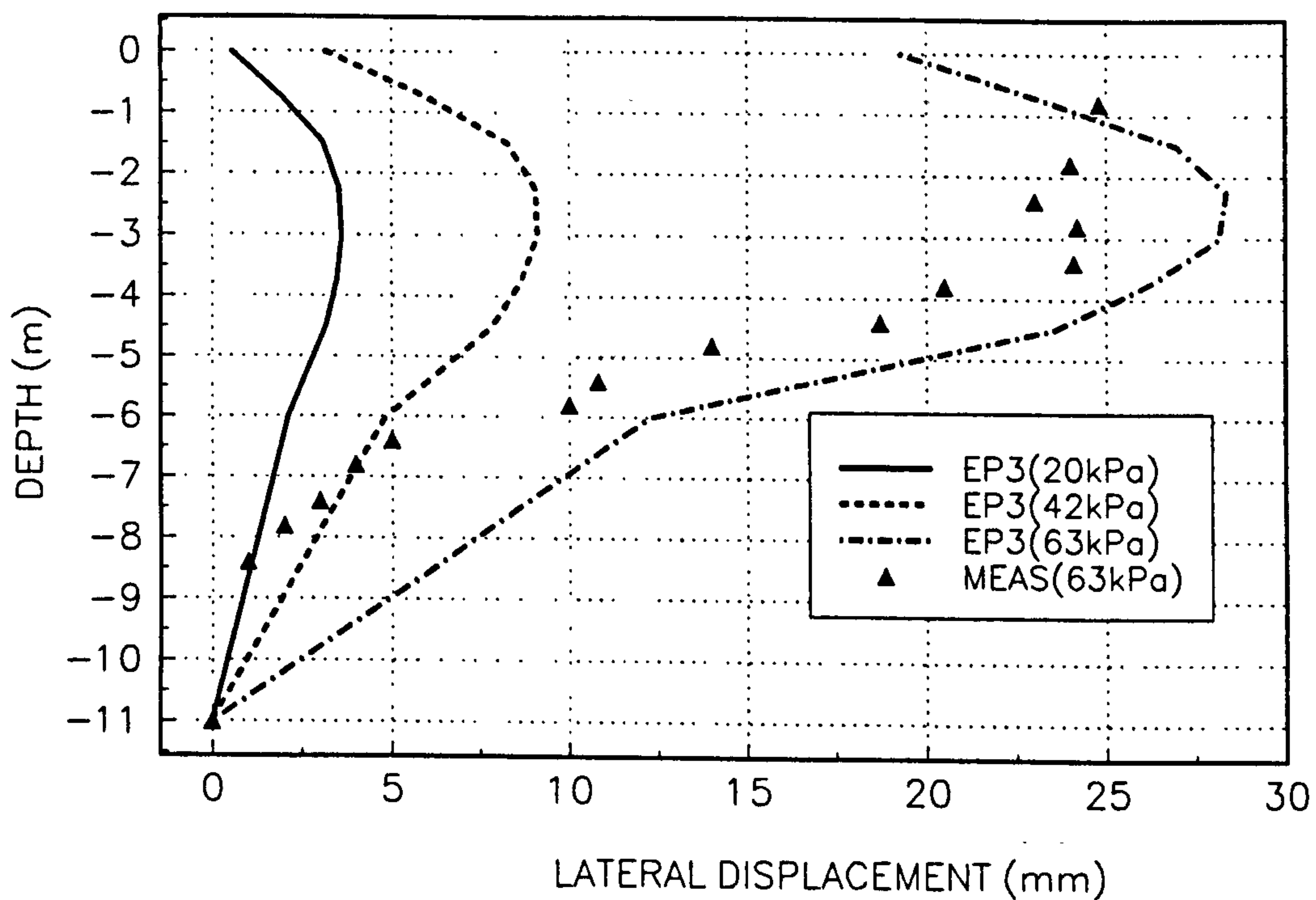


FIGURE 3.63
LATERAL DISPLACEMENT AT INCLINOMETER I6 AGAINST DEPTH.

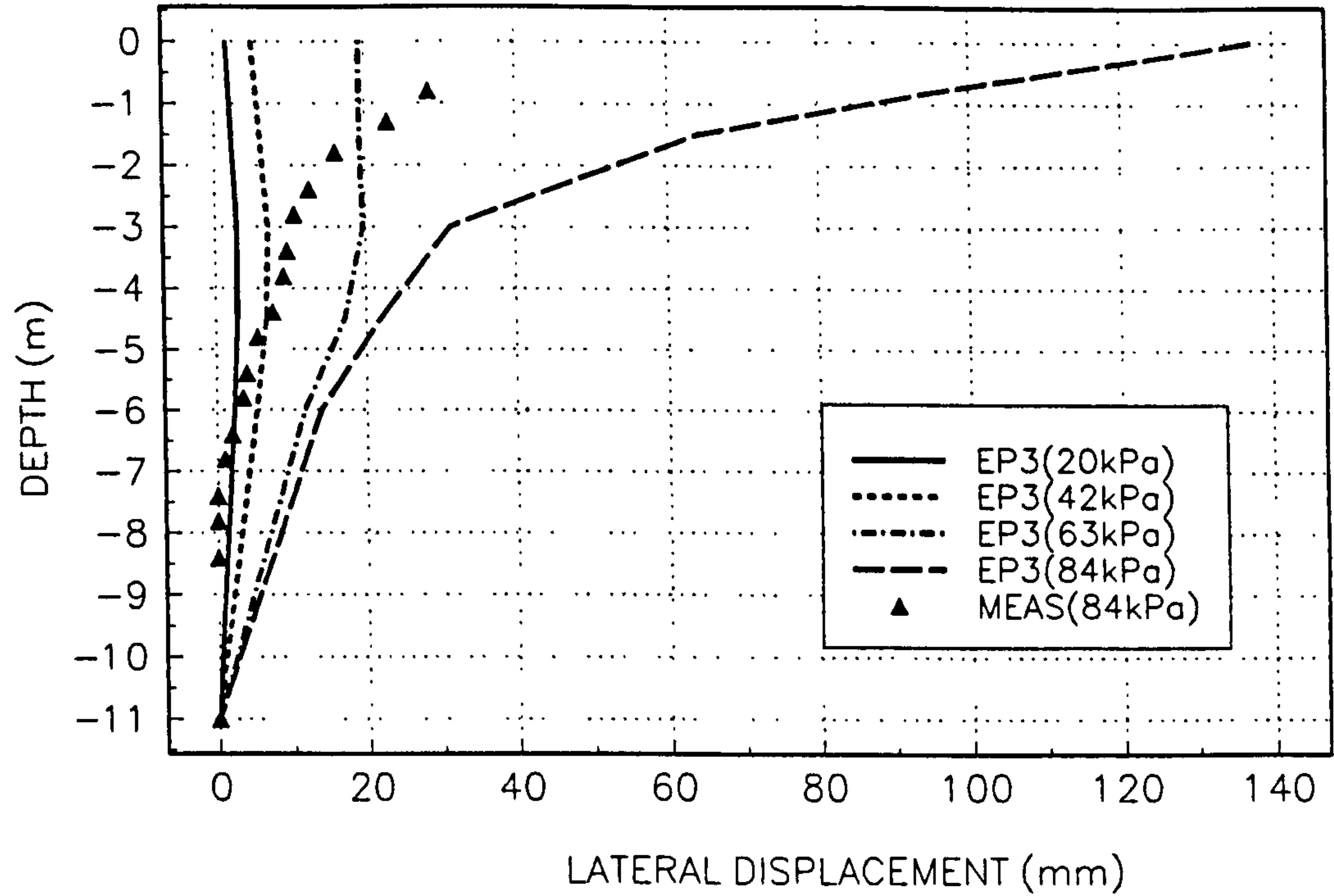


FIGURE 3.64
INCREASE IN STIFFNESS ASSOCIATED WITH A DECREASE IN KAPPA

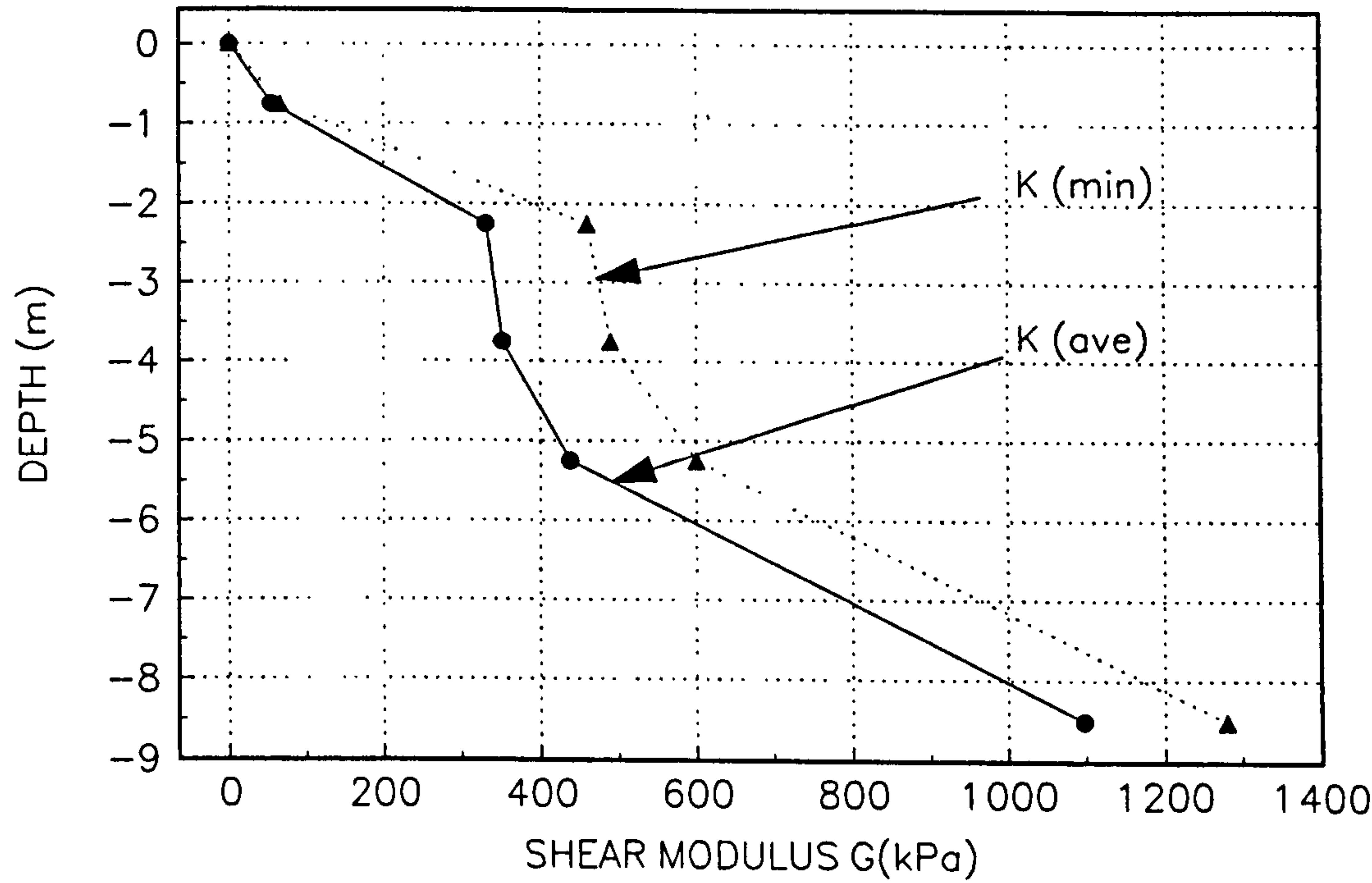
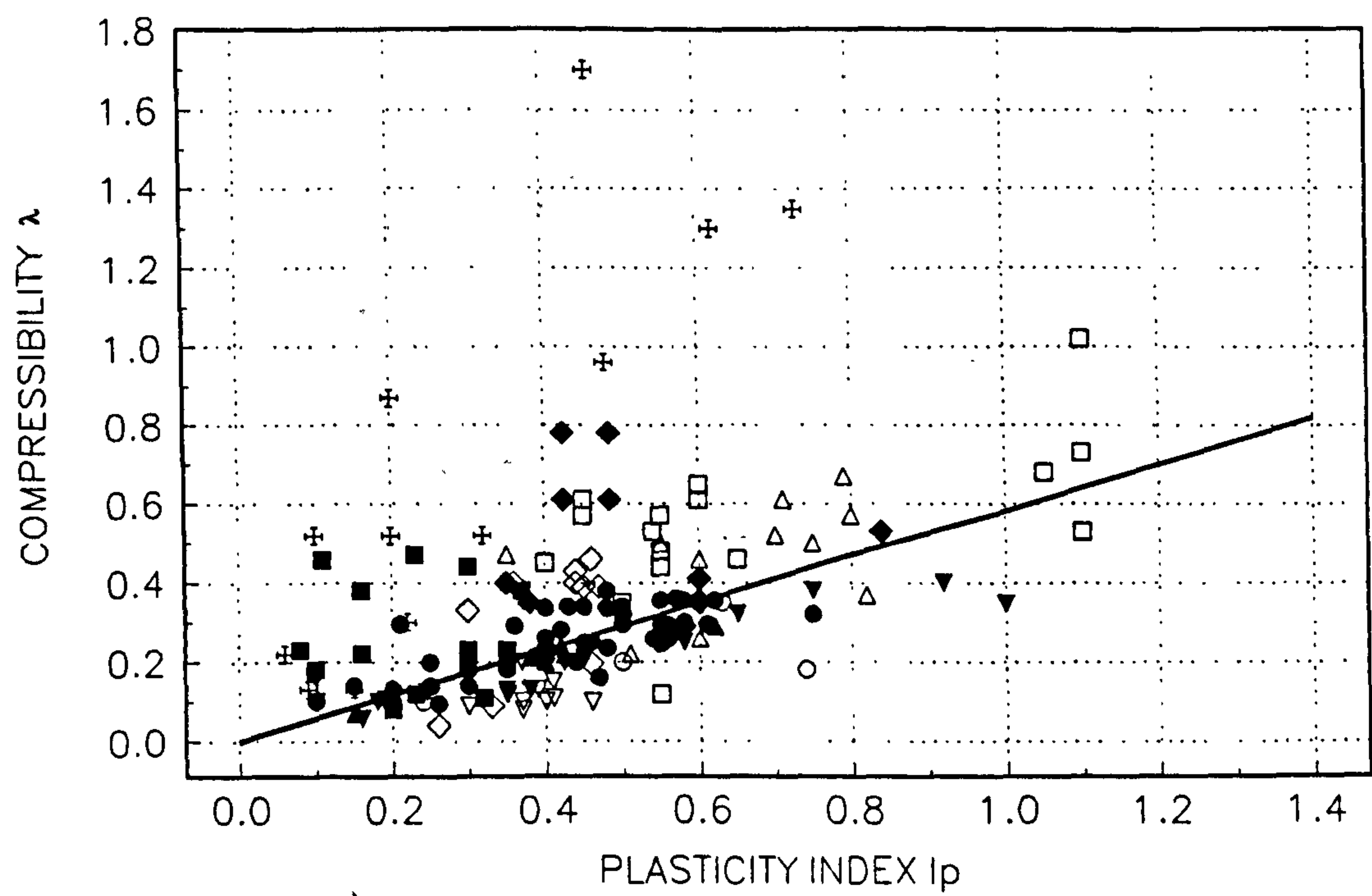


FIGURE 3.65
 COMPRESSIBILITY PLOTTED AGAINST PLASTICITY INDEX
 MUIR WOOD (1990)



Legend for Fig 3.65.

Data point (symbol)	Source
○	Trial loading (Schnaid et al., 1983)
●	Mississippi delta and Gulf of Mexico (Mc Clelland, 1967)
△	Isle of Sheppey (Nicholson and Jardine, 1986)
▽	Blaine Lake (Sauer and Christiansen, 1988)
▲	Egyptian soils (Youssef et al., 1965)
▼	Soils from Britain (skempton, 1944)
□	Cubzac-les-Ponts (Shahangiuan, 1981)
■	St Lawrence River (Samson and Gareau, 1973)
◇	Bothkennar (Nash et al., 1992)
◆	Seabed soils off Tel Aviv (Almagor, 1967)
✱	Champlain Sea clay (Tavenas et al., 1983)
—	Muir Wood (1990)

FIGURE 3.66
DEPTH PROFILE OF DEGREE OF OVERCONSOLIDATION

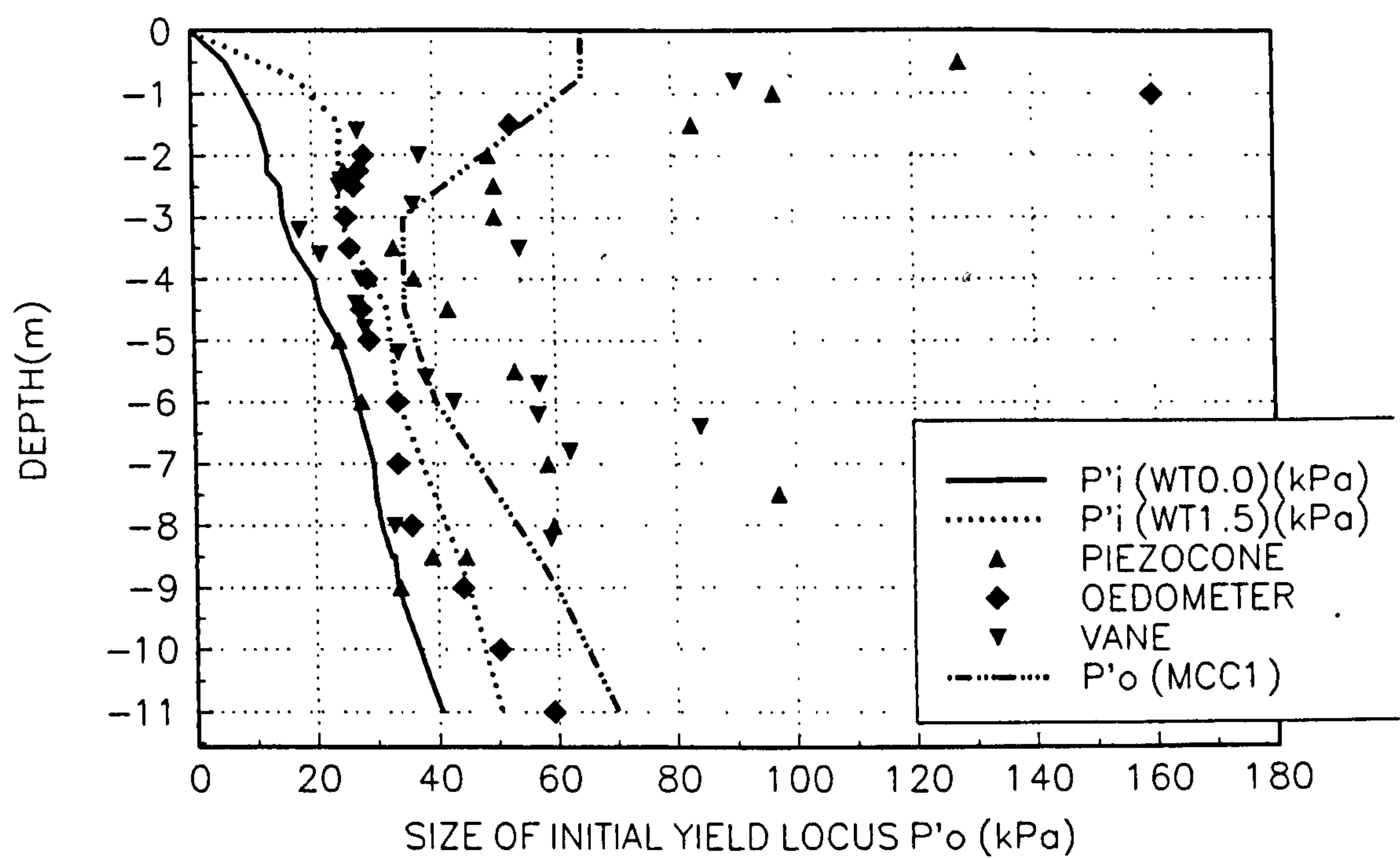


FIGURE 3.67
APPLIED LOAD AGAINST EDGE DISPLACEMENT.

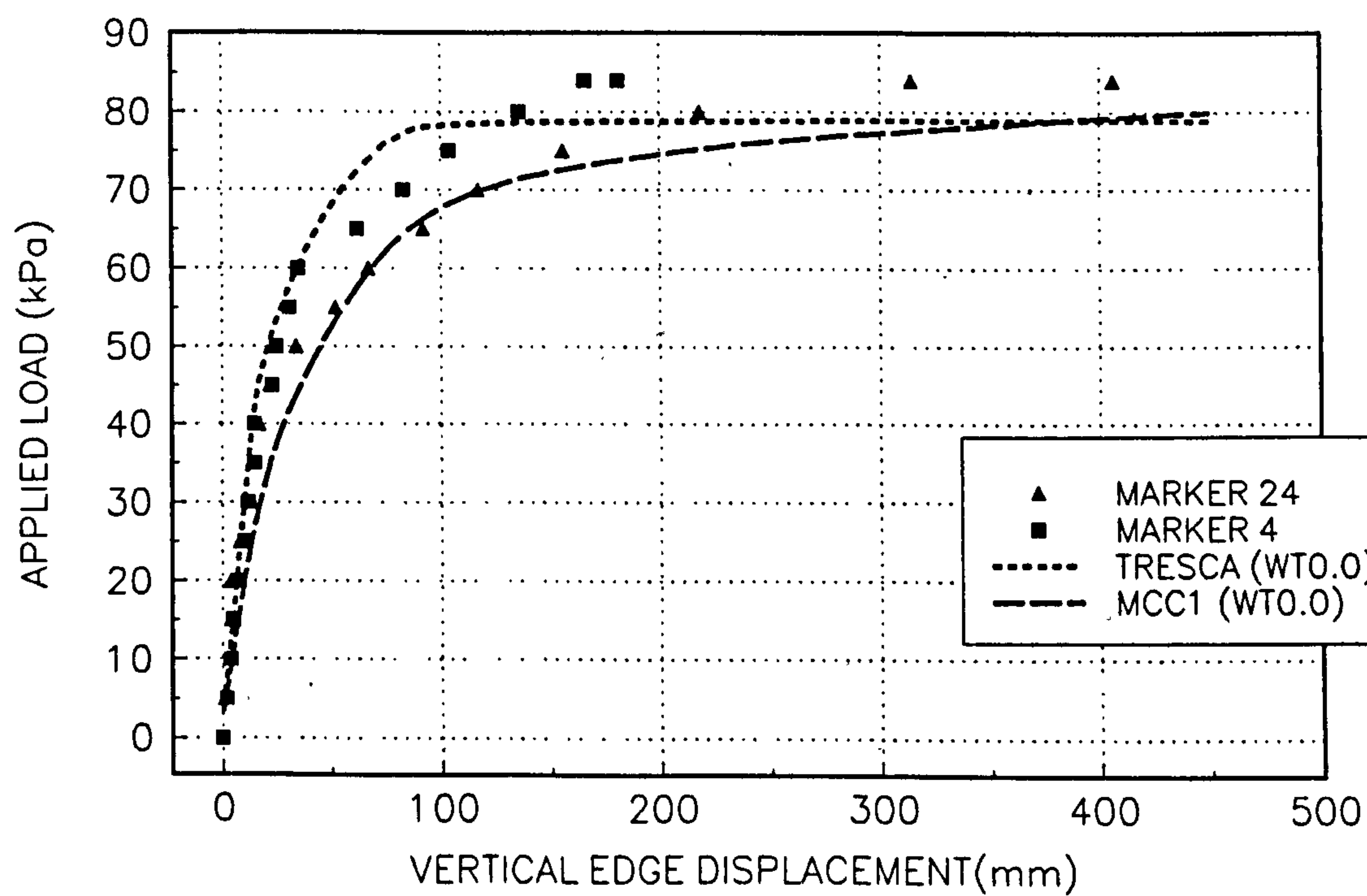


FIGURE 3.68
LATERAL DISPLACEMENT PROFILE AT INCLINOMETER 14

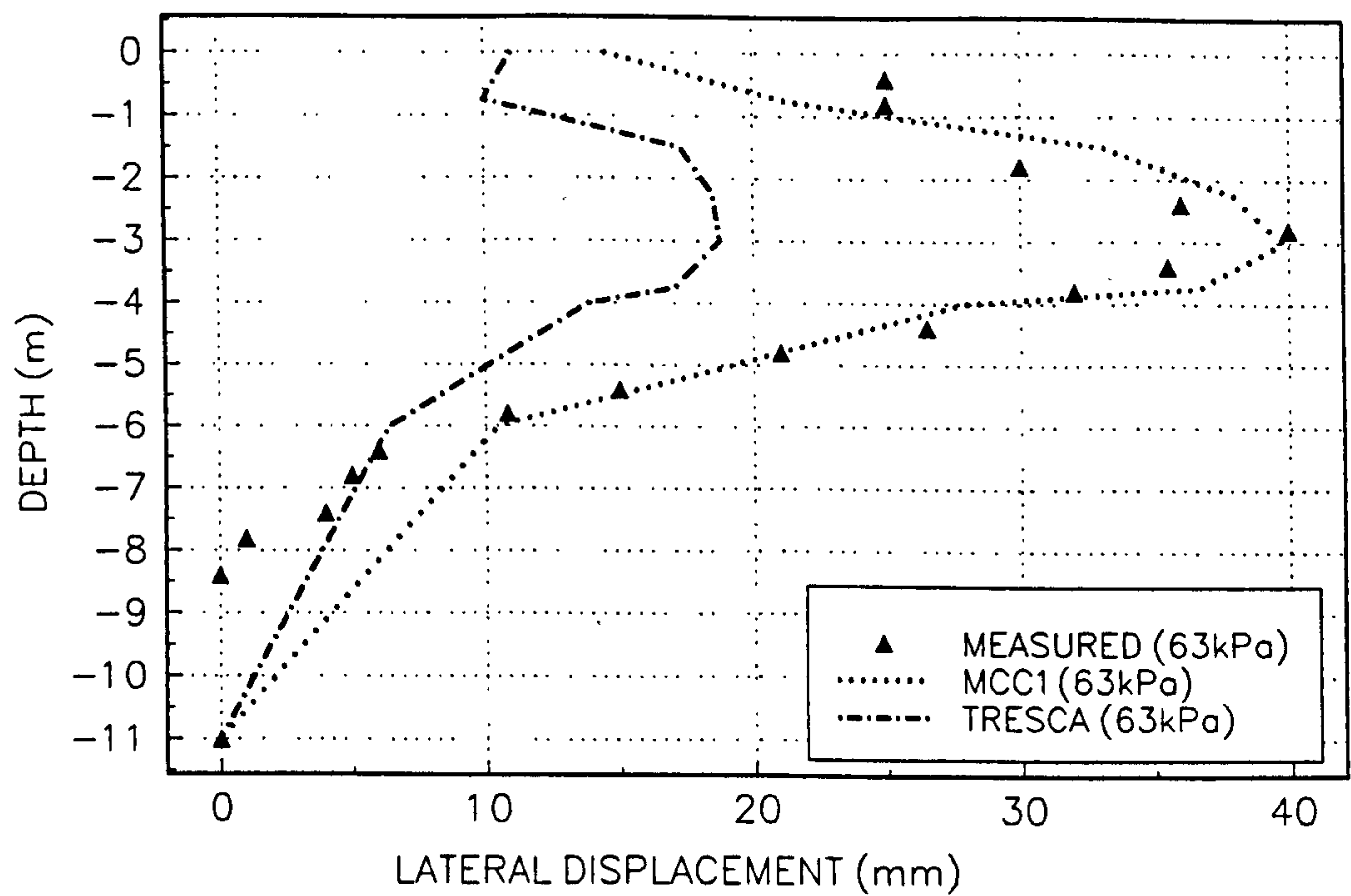


FIGURE 3.69
LATERAL DISPLACEMENT PROFILE AT INCLINOMETER 15.

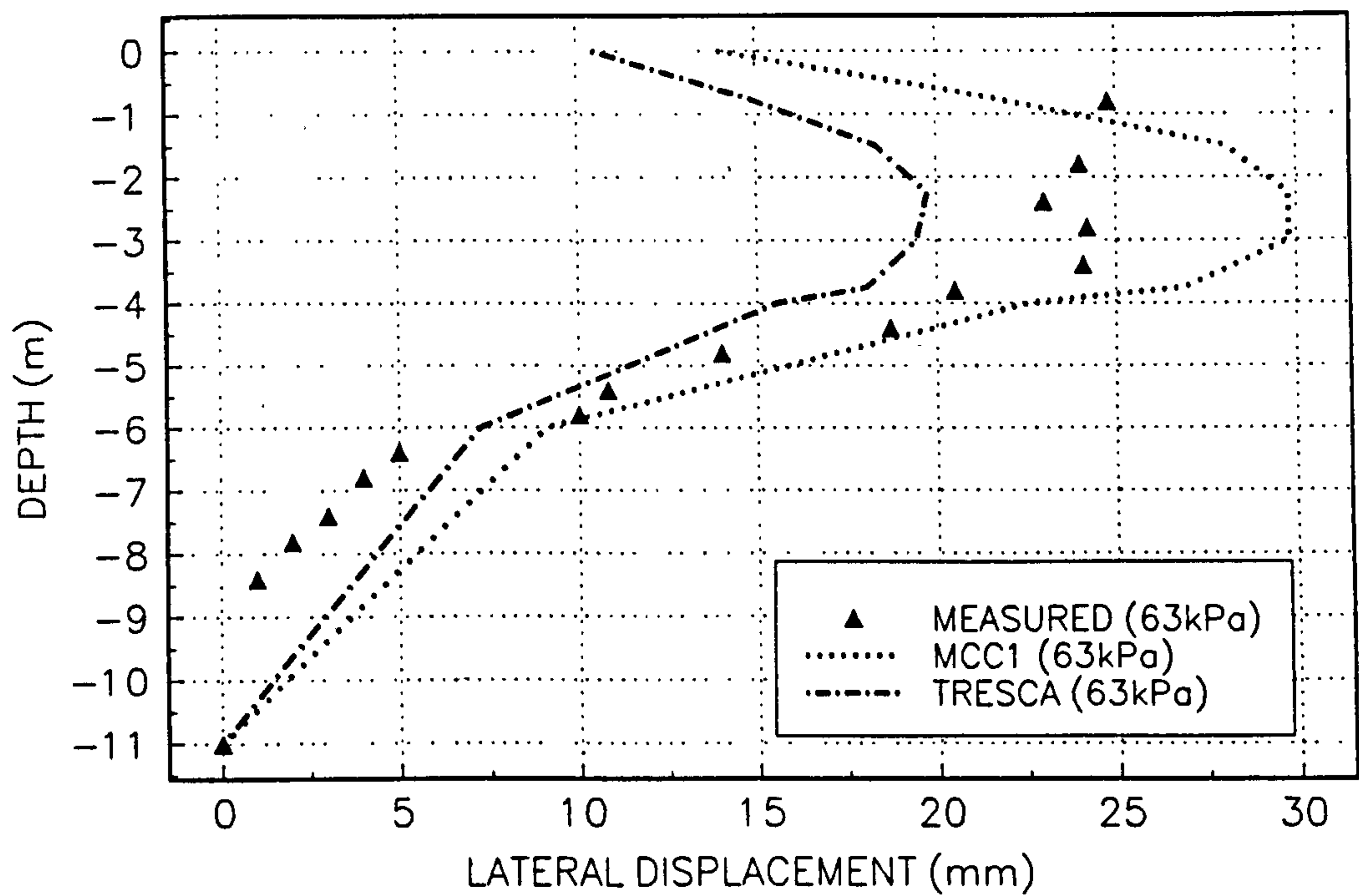


FIGURE 3.70
LATERAL DISPLACEMENT PROFILE AT INCLINOMETER 16.

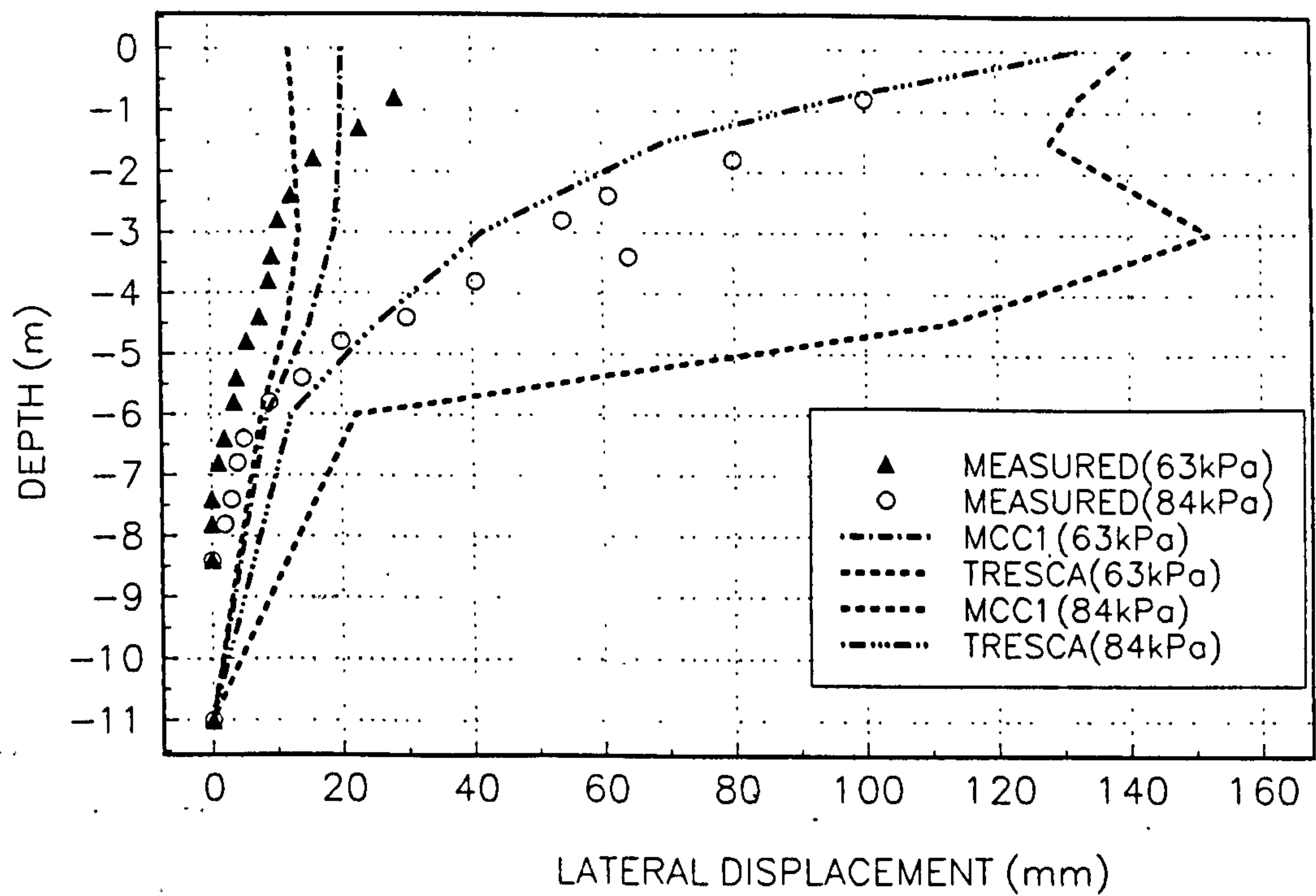


FIGURE 3.71
EXCESS PORE WATER PRESSURES AGAINST APPLIED LOAD AT A DEPTH OF 3.0m

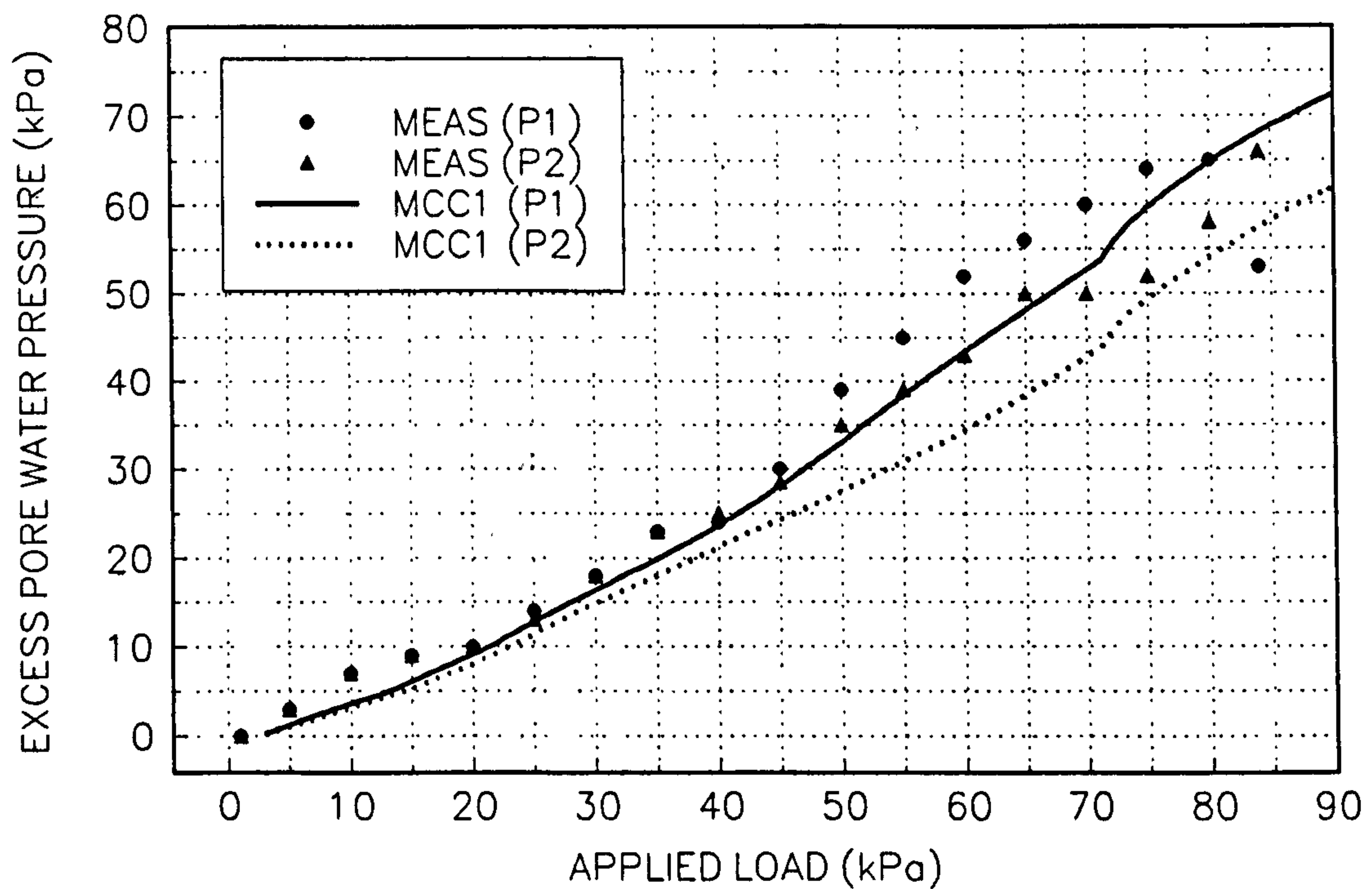


FIGURE 3.72
EXCESS PORE WATER PRESSURES AGAINST APPLIED LOAD AT A DEPTH OF 6.0m

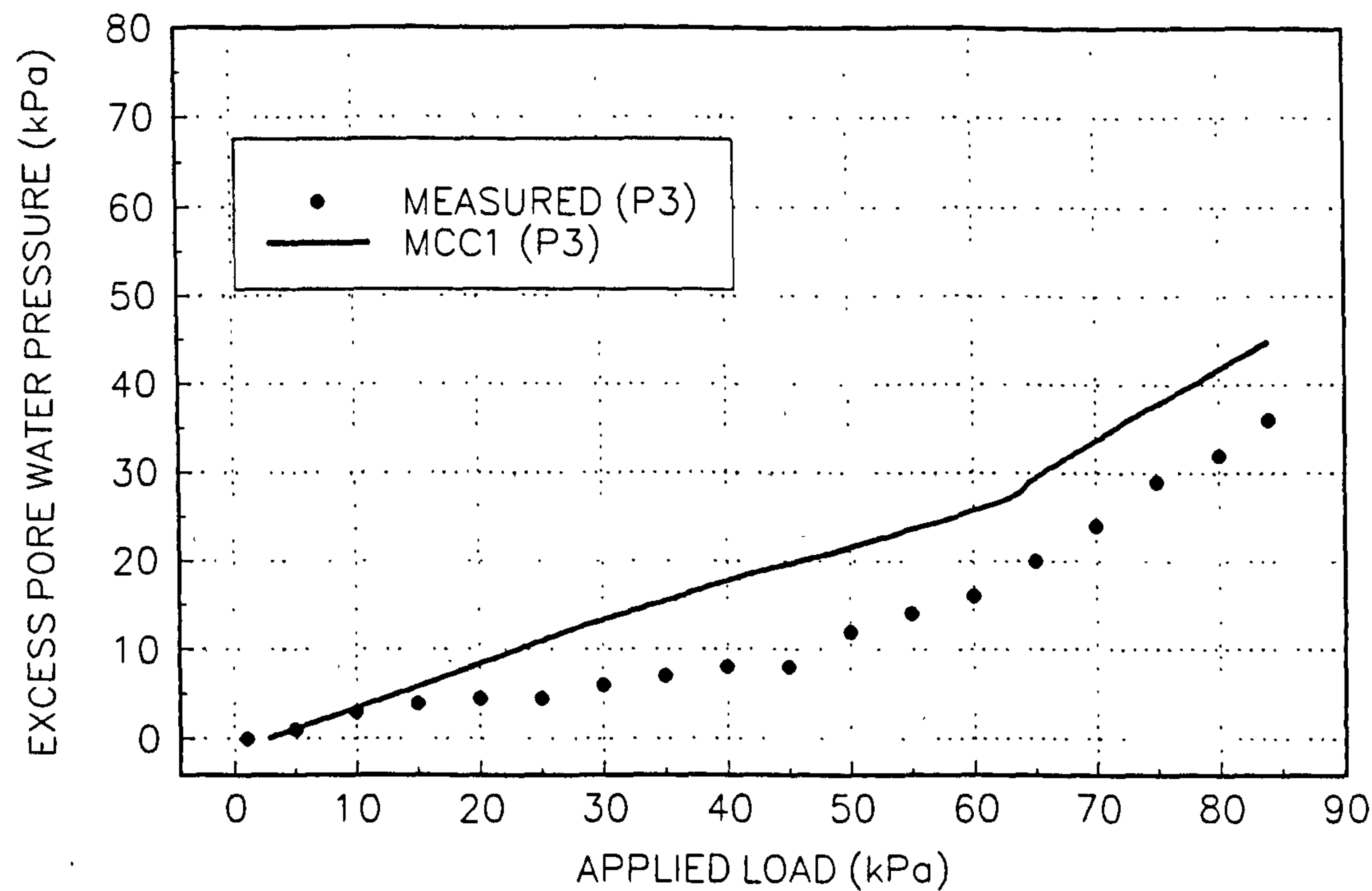
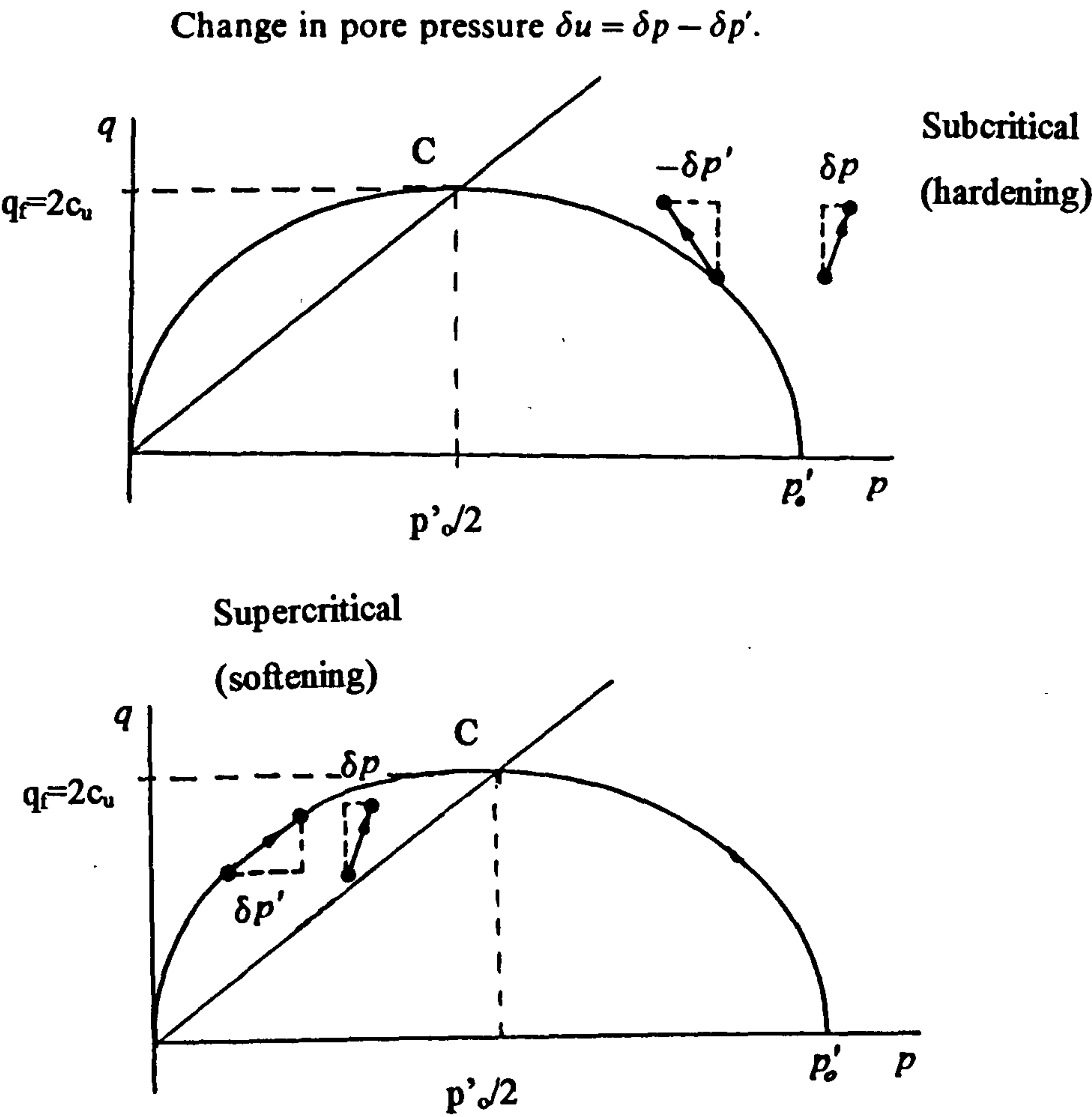


Fig 3.73. Total and effective stress paths for modified Cam clay analyses; (a) yield on subcritical side of yield locus and (b) yield on the supercritical side of the yield locus.



CHAPTER 4

4. Cubzac-les-Ponts, embankment A

4.1 Introduction

In this chapter the observed behaviour of a soft clay foundation loaded rapidly to failure via the construction of a trial embankment has been back analysed using finite element analysis. As for the trial loading described previously in chapter 3, the intent of analyses was to determine a set of material parameters which provided a reasonable estimate of the observed pre-failure foundation behaviour. A hypothetical design situation requiring an estimation of construction induced settlements, lateral displacements and excess pore water pressures at pre-failure embankment heights has been assumed.

The embankment trial loading described in this chapter was included in this thesis to test the findings and parameter selection process described for the trial loading described previously in chapter 3, and hence assess the applicability of this parameter selection process to embankment type loads. In practice the construction of embankments on soft clays is very often analysed using finite element analysis and the modified Cam clay soil model (Gens, 1994).

The embankment described in this chapter (embankment A) was the first of four trial embankments constructed on a soft clay research site at Cubzac-les-Ponts, some 30km north of Bordeaux on the north bank of the Dordogne, Fig 4.1. Construction of the trial embankments was started in 1972 by the French Laboratories des Ponts et Chaussees to study the behaviour of embankments constructed on soft clay foundations. Embankment A was constructed to failure in 1974; failure occurred at a height of approximately 4.5m. The failure of this embankment was used to guide the choice of heights of the subsequent embankments to give differing margins of safety against complete failure. Details of the embankment field tests are given in Shahanguian (1981), Mouratidis and Magnan (1983), Magnan, Mieussens and Queyroi (1983) and Leroueil, Magnan and Tavenas (1985). Details of embankment A and the trial loading are given in section 4.2. Details of previous analyses of embankment A (Mouratidis and Magnan, 1983; Magnan, 1984 and Babchia, 1984) are also included in section 4.2.

Here, plane strain, undrained and coupled undrained/drained consolidation analyses have been performed using the modified Cam clay soil model. Consolidation analyses were performed in an attempt to improve predictions of excess pore water pressures.

In this chapter, due to the wealth of soils data, use of additional empirical methods with which to check selected parameters is also explored.

A brief description of the soft clay site at Cubzac-les-Ponts is given in section 4.3. For comparison the main aspects of the trial loading site described in chapter 3 (mainly required Cam clay parameters) are also included. Parameter selection for the Cam clay analyses are also included in this section.

Numerical modelling of the embankment trial loading for both the undrained and consolidation analyses is described in section 4.4. The results of finite element analyses are presented and discussed in section 4.5. The results of analyses are also compared with alternative methods of analysis (hand-calculations). These methods are also described in section 4.6. The main findings of analyses are discussed in section 4.7. Conclusions are presented in section 4.8.

4.2 Details of trial loading and previous analyses

Embankment A was constructed from coarse sand and gravel ($\gamma=21\text{kN/m}^3$; $\phi'=35$ degrees, Mouratidis and Magnan, 1983) over a period of eight days, to a failure height of 4.5m. Details of the embankment dimensions are shown in Fig 4.2. The instrumentation, which consisted mainly of piezometers, settlement gauges and inclinometers, was placed predominantly in one transverse section of the embankment, section A-A, Fig 4.3. Measurements were taken at regular intervals during construction and after completion of the embankment. The results of the numerical predictions were compared with the measurements obtained from the transverse section. It was assumed that this section was sufficiently remote from the ends of the embankment to be deforming under conditions of plane strain. The condition of plane strain was imposed on the analyses.

Previous analyses of embankment A (Mouratidis and Magnan, 1983; Magnan, 1984 and Babchia, 1984) have been performed using the ROSALIE-Group 9 finite element program and the MELANIE soil model (Mouratidis and Magnan, 1983) to describe the soft clay foundation. The embankment was described as an elastic, perfectly plastic material with a Mohr-Coulomb failure criterion.

The MELANIE soil model is an anisotropic elasto-plastic strain hardening effective stress soil model. Development of the MELANIE soil model was inspired by the modified Cam clay effective stress soil model (Roscoe and Burland, 1968). The MELANIE soil model differs from the modified Cam clay model principally in three respects:

1. The elastic properties are assumed to be cross-anisotropic.
2. The yield locus is similar to those observed for natural clays (Shahanguian, 1981 and Diaz-Rodriguez et al., 1992) and is not symmetrical about the mean effective stress axis.
3. The plastic potential is not the same as the yield locus, hence a postulate of non-associated flow is assumed.

The main features of the model are shown in Fig 4.4.

The ROSALIE-Group 9 finite element program incorporates a feature which enables the incomplete saturation, presence of gas within the soil pores, of a soil foundation to be included in the analyses. Introduction of a certain amount of compressibility of the pore fluid has proven useful and very often has significantly improved predictions.

Full details of this model and previous analyses of the loading event can be found in Mouratidis and Magnan (1983) and Leroueil et al. (1985).

4.3 Ground conditions and parameters required for analyses

4.3.1 Introduction

In this section the ground conditions at Cubzac-les-Ponts are discussed in relation to the soil parameters required by the modified Cam clay soil model for undrained and consolidation analyses. Parameters required to describe undrained Cam clay analyses have been discussed at length previously in chapters 2 and 3. As a result only a very brief description is given here. In consolidation analyses of an extra two parameters describing horizontal, k_h ($=k_x$), and vertical, k_v ($=k_y$) permeability are required. In practice different methods are used to obtain suitable estimates of the permeability of the soil. A brief review of these methods is included in subsection 4.3.7.3. Permeability is considered in section 4.3.7. As in chapter 3 the final parameter set includes an element of trial and error required to improve the match between observed and computed responses. The final parameter set is presented in Table 4.1.

4.3.2 Ground conditions

The foundation soils at Cubzac-les-Ponts consist of approximately 8m of soft normally consolidated clay of variable organic content, overlain by a firm 1.75m thick desiccated surface crust. The soft clay is underlain by a layer of coarse sand and gravel some 5m thick. The ground water level was found to be at a depth of approximately 1.0m. A summary of the ground conditions is presented in Fig 4.5-4.10.

The site investigation included boreholes, sampling, in situ vane, static cone penetration, pressuremeter and in situ permeability tests. An extensive laboratory testing program was performed on undisturbed samples: this included oedometer tests, undrained and drained triaxial tests and permeability tests. Details of the site investigation and laboratory tests are given by Shahanguian (1981), Mouratidis and Magnan (1983) and Magnan, Mieussens and Queyroi (1983). The soft clay site at Cubzac-les-Ponts is an experimental research site, as a result, an extensive volume of soils data describing the ground conditions at this site is available.

4.3.3 Elastic parameters κ and ν'

Conventionally values of κ are selected from the slope of the unload-reload line in an oedometer. Because of the typically non-linear unloading process observed in an oedometer test there is room for interpretation as to the line which best describes the unloading process. The problem, therefore is which slope to use. Previously for the trial loading (chapter 3), analyses required the selection of very small values of κ , implying a high value of elastic stiffness, which corresponds to the slope of the unloading process immediately after the change in loading direction, i.e. a minimum value of κ . Assuming this to apply here, values of κ estimated from the slope of the unloading line immediately after a change in loading direction are presented in Fig 4.11. For comparison κ values of the average slope of the entire loading process are also shown. Corresponding values of shear modulus, G , estimated using relation (2.40) and using a Poisson's ratio, $\nu'=0.2$, are presented in Fig 4.12. Estimates of the in situ stiffness have also been obtained from the self-boring pressuremeter and triaxial tests. Values of stiffness obtained using these methods are also shown in Fig 4.12. As can be seen from Fig 4.12 shear moduli estimated from minimum values of κ compare approximately with the values of stiffness estimated from triaxial tests performed at low strains ($0.02\% < \epsilon < 0.05\%$) implying that minimum κ values are low strain values. Average κ values correspond to stiffnesses determined from standard triaxial tests at

conventional strain levels ($\epsilon > 0.5\%$) which are in turn comparable to shear moduli estimated from the self-boring pressuremeter tests. Shear moduli estimated using the self-boring pressuremeter tests were determined over a strain range of 0.3-0.4%. The maximum oedometer shear moduli give a ratio to the undrained shear strength, G/c_u , of 125-200. Fig 4.13.

Values of undrained shear strength, c_u , are shown in Fig 4.7. Estimates of the undrained shear strength have been obtained from in situ vane, self-boring pressuremeter and static cone penetrometer tests and undrained triaxial compression tests performed on undisturbed samples. Here a depth profile of undrained shear strength similar to those described by the corrected in situ vane strengths (Bjerrum, 1973) and triaxial compression tests, has been assumed.

Further estimates of foundation stiffness can be obtained from the empirical chart, Fig 3.40 (Duncan and Buchignan, 1976 and Meigh, 1987) previously discussed in chapter 3 relating the ratio of elastic stiffness to undrained shear strength to the overconsolidation ratio, n and plasticity index, I_p . The plasticity index of the clay foundation is presented in Fig 4.14 and is typically less than 50% for the crust, but greater than 50% for the soft underlying soft clay. The range of possible plasticity index, $25 \leq I_p \leq 50$ and overconsolidation ratios $1 \leq n \leq 20$, Fig 4.15, makes the chart difficult to interpret for the crust. For the soft clay a distinct range of G/c_u ratios emerges in the range of 35-100 for a plasticity index range of $I_p > 50\%$ and an overconsolidation ratio range of 1-3. The resulting G/c_u ratios are comparable with values obtained from manipulation of oedometer test data assuming an average slope of the entire unloading process to deduce the value of shear modulus.

Further guidance as to which slope to use to describe the oedometer unload-reload data can be obtained by comparing the minimum and average oedometer G/c_u ratios with those obtained from the small strain triaxial tests. The most convenient means of doing this is as follows. Values of secant modulus, G , determined from the low strain triaxial tests were normalised with respect to the undrained shear strength and plotted against axial strain, ϵ_a (which is the same as shear strain in undrained loading) Fig 4.16. Three low strain triaxial tests were used to compose the $G_{\text{secant}}/c_u: \epsilon_a$ relation presented. Assuming that this relationship between stiffness and strain can be applied generally to the whole foundation, values of G/c_u can be obtained given an estimated elastic strain level. Back analysis of the trial loading described in chapter 3 determined that the small strain stiffness properties of the clay foundation had a significant influence on the magnitude and form of the displacement response. Quantifying “small” is difficult without direct measurement of strains as they occur in

the ground however, Jardine et al. (1984), from triaxial testing at small strains of soft clay samples, found that the attainment of 0.1% axial strain generally coincided with a marked loss of stiffness which they assumed to be the limit of the small strain range or first yield. Therefore, assuming an initial elastic strain level of 0.1% gives a stiffness to strength ratio of approximately, $G/c_u=90$. This G/c_u ratio of 90 is typically not reproduced by either of the oedometer unloading slope assumptions, but corresponds approximately to the average of stiffness ratios inferred from the average and minimum oedometer unloading slope assumptions. The stiffness to strength ratio $G/c_u=90$, corresponds with the values estimated using the empirical chart (Duncan and Buchigani, 1976).

Values of κ estimated using this process are presented in Table 4.1. Initial values of κ for analyses were selected from Fig 4.11 with bias towards the average κ values, particularly over the depth range of 2-4m below ground level. Initial values of κ were adjusted mainly by trial and error to provide the current solution.

Based on the findings described in chapter 3, Poisson's ratio, ν' , was assumed equal to 0.2. A value of $\nu'=0.2$ was selected to ensure that the required initial stiffness profile with depth was compatible with that automatically calculated by CRISP90 from material input data and initial in situ stress conditions. Additionally, $\nu'=0.2$ was considered to be suitably small to ensure a low ratio of maximum lateral movement to maximum vertical movement (Poulos et al., 1989). From the results of drained triaxial test performed on selected undisturbed samples of soft clay, Poisson's ratio was estimated to be equal to $\nu'=0.12-0.46$ (Shahanguian, 1981). As can be seen the value selected is at the lower end of the measured range of values.

4.3.4 Compressibility λ

Values of λ were determined directly from oedometer normal compression data. Typically, the entire normal compression process observed in an oedometer test is approximated by a straight line. In this case normal compression data were represented reasonably well by a linear relationship. However, situations do arise where the amount of curvature of the normal compression line cannot be ignored (Samson and Garneau, 1973). In this case estimates of λ should be obtained from the slope of the line fitted to the normal compression data over the range of applied field pressures. Typically, expected field pressures are small compared to the pressures applied to the sample throughout the test. Selected values of λ are presented in Table 4.1.

As described previously in chapter 3 a check on the values of λ estimated from oedometer test data is provided by an empirical link between λ and plasticity index, I_p , (Muir Wood, 1990). Oedometer test values of λ , are plotted against plasticity index and are shown in Fig 4.17(a). As can be seen, oedometer values of λ plot reasonably close to the empirical relationship. This method can also be used to supplement sparse or inaccurate oedometer data for similar soft clay sites.

The parameter λ can also be used to guide or check the choice of κ values using relation (4.1).

$$\Lambda = \frac{\lambda - \kappa}{\lambda} \quad (4.1)$$

The parameter Λ describes the relative slopes of the normal compression and unloading-reloading lines for the soil. This implies that Λ can be treated as an alternative soil constant within the Cam clay model.

Available laboratory strength data indicate that for natural clays the parameter Λ is approximately equal to 0.75, 0.8 and 0.85 for triaxial compression, simple shear and triaxial extension (Kulhawy and Mayne, 1990). Under the embankment loading the foundation soil will be undergoing many modes of deformation, therefore an average of the above values $\Lambda=0.8$, could be used to evaluate values of κ , Table 4.2. As can be seen from Table 4.2 assuming $\Lambda=0.8$ estimated values of κ are larger than those assumed. Previous researchers studying the Cubzac-les-Ponts trial loadings (Mouratidis and Magnan, 1983) assumed $\Lambda=0.9$, giving values of κ which compare with those assumed for analyses.

Within the Cam clay model Λ is, through (4.1), a soil constant. However, plotting values of Λ determined experimentally from many forms of testing (Mayne, 1980 and Mayne and Swanson, 1981) against plasticity index, I_p (Muir Wood, 1990) no obvious trend emerges, Fig 4.17(b). Consequently, because of the uncertainty surrounding parameter Λ , estimating values of κ from values of λ should only be used as a check or rough guide to the selection of an appropriate slope of the oedometer unloading process.

4.3.5 Critical state parameters, e_{cs} and M

The position of the critical state line in the compression plane $e: \ln p'$ is defined by specification of the critical state void ratio, e_{cs} . Values of e_{cs} were determined as described previously in chapter 3.

Critical states are reached when the effective stress ratio $q/p'=M$, the slope of the critical state line in $q: p'$ space, provided plastic strains are occurring. Values of M were determined from values of the effective angle of shearing resistance, ϕ' using relation (4.2). Values of ϕ' were estimated from drained triaxial tests performed on undisturbed samples.

$$M = \frac{6 \sin \phi'}{3 - \sin \phi'} \quad (4.2)(3.5\text{bis})$$

Values of M estimated using relation (4.2) and measured values of ϕ' are shown in Table 4.1. Typically, data pertaining to ϕ' are sparse and some interpolation between test depths is required. Additional values of ϕ' can be estimated using an empirical link with plasticity index I_p (Mitchell, 1976 and Muir Wood, 1990) described previously in chapter 3.

This method was relied upon in the previous section for estimates of M for the clay foundation. However, the accuracy of the method could not be assessed due to the absence of ϕ' data. Comparing values of ϕ' , Fig 4.18, determined using relation (4.2) with values obtained from triaxial testing reveals that the empirical values of ϕ' provide a reasonable estimate of ϕ' for the crust, but significantly underestimate those for the soft clay. Observed values of ϕ' are higher than might be expected for a clay of an average plasticity index, I_p of 70%. Using the empirical relation this would give an average ϕ' of 23 degrees, smaller than that measured of 30 degrees. High values of ϕ' were also observed at Bothkennar (Nash et al., 1992) typically 34 degrees, for an average I_p of 40%, using the empirical relation gives a $\phi'=26$ degrees. The high values of ϕ' at Bothkennar were attributed to the angularity of silt particles and high organic content of the clay (Paul et al., 1992). Nothing is known of the macro structure of the Cubzac-les-Ponts clay. However, the clay has a high organic content and therefore it is feasible to assume that this is causing the poor match between measured and empirical values of ϕ' as for the Bothkennar clay.

Further estimates of ϕ' for the soft clay can be made using a empirical relationship linking the undrained shear strength c_u and the preconsolidation pressure σ'_{vc} , relation (4.3) (Diaz-Rodriguez et al., 1992).

$$\sin \phi' = \frac{c_u}{(\sigma'_{vc} - c_u)} \quad (4.3)$$

Relation (4.3) was deduced from the study of yield curves for many natural normally consolidated soft clays and gives an indication of the maximum shear strength of an intact clay, point F Fig 4.19. Diaz-Rodriguez et al. (1992), using measured maximum

strength data obtained from many sources, Table 4.3, have shown that relation (4.3) provides a reasonable estimate of measured maximum shear strength data, Fig 4.20. Values of ϕ'_f estimated using relation (4.3) are also presented in Fig 4.18, using the uncorrected and corrected in situ vane undrained shear strengths. As with most empirical methods a certain amount of ambiguity remains.

Parameter selection for the trial loading described in chapter 3 found that accurate selection of M was required if good predictions were required. Consequently if numerical predictions are required using Cam clay then M should be measured directly. In practice testing for critical state parameters is unlikely to occur at frequent intervals through the foundation and that was the case here. In general, typically a maximum of four tests would be performed. Therefore, some interpolation between test samples will be required. Application of the empirical methods presented may assist in this process.

4.3.6 Preconsolidation stress

From analyses performed for the trial loading (chapter 3) it was found that the choice of p'_o has a significant influence on the predicted solution and small variations of p'_o can be significant. For this study (embankment A) an initial estimate of the depth profile of the degree of overconsolidation was obtained using relation (3.16) such that the assumed values of p'_o gave an undrained shear strength, c_u , profile resembling that required. The assumed undrained shear strength profile is shown in Fig 4.7. The corresponding preconsolidation stress profiles are shown in Figs 4.21 (in terms of σ'_{vc}) and Fig 4.22 (in terms of p'_o). Several analyses were performed to obtain this final depth profile of preconsolidation.

For comparison estimates of the preconsolidation stress, σ'_{vc} , were also obtained using the empirical correlations linking σ'_{vc} and the in situ vane undrained shear strength previously described in chapter 3. Here the final depth profile of preconsolidation was found to approximately coincide with preconsolidation stress estimated using the correlation presented by Muir Wood (1990), relation (3.10).

A check of the assumed depth profile of the degree of overconsolidation is provided from consideration of the critical embankment height, H_{nc} . The critical embankment height, H_{nc} , is the embankment height at which a soil element under the embankment centre line becomes normally consolidated, $\sigma'_v = \sigma'_{vc}$, and is given by relation (4.4) (Leroueil et al., 1985).

$$H_{nc} = \frac{\sigma'_{vc} - \sigma'_{vi}}{I\gamma_r(1 - \bar{B}_1)} \quad (4.4)$$

where σ'_{vc} is the vertical effective preconsolidation pressure; σ'_{vi} is the initial in situ vertical effective stress; I is a stress influence factor (Osterberg, 1957); γ_r is the unit weight of the embankment and \bar{B}_1 is a pore water pressure coefficient and is deduced from Fig 4.23 (Tavenas and Leroueil, 1980).

Fig 4.23 has been compiled from pore water pressure observations under the centre line of many embankments during the first stage of construction (Tavenas et al., 1979 and Tavenas and Leroueil, 1980). The assumed average relationship between $\bar{B}_1 = \frac{\Delta u}{\Delta \sigma_v}$, where Δu is the increase in pore water pressure and $\Delta \sigma_v$ is the increase in total vertical stress, and \bar{B}_1 is given by relation (4.5).

$$\bar{B}_1 = 0.6 - 2.4\left(\frac{z}{D} - 0.5\right)^2 \quad (4.5)$$

where z is the depth beneath the ground surface to the point under consideration and D is the depth of the clay layer. Fig 4.23 assumes that a clay layer is free draining at the top and bottom boundaries (an open-layer); as is assumed in this study for embankment A.

The height to which an embankment can be constructed on the soft soils found at Cubzac-les-ponts is unlikely to be high in view of the shallow depth and characteristics of the soft clay. Yield would therefore start to occur at small embankment heights. Using the average relationship shown in Fig 4.23 estimates of the critical embankment height, H_{nc} , calculated for the assumed preconsolidation stress profile, are presented in Table 4.4 for a water table at 1.0m depth.

As can be seen from Table 4.4 estimates of H_{nc} indicate that yield of the soft clay foundation will occur at small embankment heights, typically less than 3m. The description of yield given by these "average" critical embankment heights corresponds with that observed and implies that failure will be initiated at an embankment height of the order of that observed (4.5m).

In this case the actual embankment height which could be supported by the foundation was known. For design situations where this knowledge is not known at the outset, critical embankment heights estimated from this method used in conjunction with the results of stability analyses and/or experience of embankment construction on similar soft clay sites will facilitate the selection of a suitable depth profile of the degree of overconsolidation.

4.3.7 Permeability

4.3.7.1 Introduction

This section is divided into three subsections. The first section 4.3.7.2 explains how values of permeability (horizontal and vertical) were selected from available data for use in the consolidation analyses. The second section 4.3.7.3 describes some of the alternative methods successfully used to obtain values of permeability for use in embankment consolidation analyses. The final subsection discusses these methods and describes why these methods are not favoured here.

4.3.7.2 Selection of permeability for consolidation analyses

For consolidation analyses CRISP requires values of permeability in the horizontal, $k_h(=k_x)$, and vertical, $k_v(=k_y)$, directions. In the standard version of CRISP, as used here, the coefficients of permeability are assumed to remain constant throughout the analysis. Estimates of the in situ permeability are available from in situ and laboratory tests. Laboratory permeability testing was performed on small soil specimens in an oedometer cell with either vertical, horizontal or radial drainage.

Values of horizontal permeability, $k_h(=k_x)$, estimated in situ are much lower than those obtained from oedometer tests. This is due to sample disturbance arising from smearing and reconsolidation of the sample on retrieval from the ground (Leroueil et al., 1992 and Hight et al., 1992). From permeability studies performed on Bothkennar clay (Leroueil et al., 1992) the self-boring permeameter was found to provide the most representative values of horizontal permeability. Therefore, for analyses estimates of the horizontal permeability, k_x , were obtained from the in situ permeability tests and estimates of the vertical permeability, k_y , determined from k_x/k_y ratios estimated from laboratory tests, Fig 4.24. Selected permeabilities are presented in Table 4.5. The values of permeability were not changed at any stage throughout the analysis.

4.3.7.3 Review of some methods used to select permeability

In this section a brief description of some of the more common methods of selecting values of permeability is given. However, prior to this a brief description of soft clay behaviour, in relation to excess pore water pressure, under embankment loading is required.

It has long been recognised from observations of pore water pressures generated beneath trial embankments that during the early stages of construction some drainage of pore pressure takes place and the soft clay foundation behaves as if partially drained (Ramalho-Ortagio et al., 1983; Leroueil et al., 1985 and Leroueil and Tavenas, 1986). This partially drained behaviour is thought to be attributed to incomplete saturation arising from some overconsolidation of the clay. Therefore, during the initial loading of the foundation the behaviour follows approximately a drained response, Fig 4.25 and consequently observed vertical displacements are typically larger. Additionally, observed lateral displacements and excess pore water pressures are significantly smaller than those predicted from undrained analyses. It is thought that the actual foundation response does not follow an undrained response until yield occurs, point P' Fig 4.25.

Consolidation and the effect of incomplete saturation are also evident from comparison of the observed displaced volumes of soft soil, horizontally (V_h) and vertically (V_v), Fig 4.26; presented data are compiled from many embankment studies (Johnston, 1973 and Leroueil et al., 1985). As can be seen from Fig 4.26, observations show that the volume changes associated with settlements, V_v , are significantly larger than the volume changes, V_h , associated with lateral deformations during construction. The fully undrained response assumes that these two volumes are equal, $V_h = V_v$.

To model this behaviour during the numerical simulation of embankment construction on soft clay using conventional finite element programs, e.g. CRISP90, researchers have tended to vary the coefficients of permeability (Poulos et al., 1989; Balasubramanian et al., 1989 and Chai and Bergado, 1993). Details of these methods are given below.

Poulos et al. (1989) determined estimates for an anisotropic description of permeability, $k_h (=k_x)$ and $k_v (=k_y)$, using relations (4.6 and 4.7) for a 5m high embankment constructed over a period of 100 days to failure on a soft Malaysian marine clay at the Muar test site.

$$k_v = 3m_v c_v \gamma_w \quad (4.6)$$

and

$$k_h = 1.5k_v \quad (4.7)$$

where k_v is the vertical coefficient of permeability; m_v is the vertical coefficient of consolidation; c_v is the vertical coefficient of compressibility; γ_w is the unit weight of water and k_h is the horizontal coefficient of permeability.

The field value of the coefficient of consolidation, m_v , was assumed equal to three times the laboratory value, hence the occurrence of the factor 3 in relation (4.6). The horizontal permeability was assumed equal to 1.5 times the vertical permeability. Pre-yield permeability was assumed to be twenty times higher than that given by relations (4.6) and (4.7) on the basis of published field observations from similar soft clay sites. No details of these similar sites are given. This method provided good predictions of excess pore water pressures, but was less successful at predicting displacements.

For the same embankment, in contrast to Poulos et al. (1989), Balasubramanian et al. (1989) assumed throughout an isotropic field permeability, $k_v=k_h$, some fifty times higher than the measured laboratory values on the basis of the authors' experience with soft Bangkok clay. A single value of permeability was assumed throughout the analyses. This method provided good predictions of the vertical surface and lateral displacements. However, excess pore water pressure predictions were not very accurate and tended to underestimate those observed, particularly over the top 5m of foundation. Pore pressures and movements were measured over a depth of approximately 24m, predictions were typically made over a depth of approximately 13m.

Chai and Bergado (1993) investigating the behaviour of embankments on soft ground during construction assumed that the foundation permeability varied with void ratio according to relation (4.8).

$$k = k_i \exp\left(\frac{e - e_i}{c_k}\right) \quad (4.8)$$

where k_i and e_i are initial reference values of permeability and void ratio and c_k is a permeability constant, typically assumed equal to $0.5e_i$ (Tavenas et al., 1983 and Leroueil et al., 1992). The embankment was constructed to a stable height of 8.5m over a period of approximately 400 days at the Muar soft clay test site, Malaysia. Some grid reinforcement was placed at the embankment base to help to sustain stability. The problem is further complicated by the presence of vertical band drains within the foundation. These were included to minimise excess pore water pressures and hence promote consolidation of the clay foundation. The embankment was constructed in three lifts 4m, 2m and 2.5m up to a height of 8.5m, a period of approximately 100 days was allowed between lifts to allow some dissipation of excess pore water pressure.

Numerical analyses were performed using a finite element program CRISP-AIT (Chai and Bergado, 1993) which is a hybrid of the finite element program CRISP90 (Britto and Gunn, 1987). The foundation soil was described using the modified Cam clay effective stress soil model (Roscoe and Burland, 1968). In analyses vertical permeability of the soft ground, k_v , was assumed to vary with void ratio, e , (relation (4.8)) before and after yield. However, initial estimates of the vertical permeability, k_v , to estimate pre-yield behaviour were five times higher than those used to estimate post-yield behaviour. Post-yield vertical permeability was assumed equal to that used by Poulos et al. (1989), which was some three times the laboratory oedometer test value. The horizontal permeability, k_h , was assumed equal to twice the vertical permeability. Using this procedure the results of the analyses compared well with observations of vertical and lateral displacements and excess pore water pressures generated during the construction procedure. Analyses performed using a constant permeability, equal to the initial values, k_{vi} and k_{hi} , assumed for pre-yield consolidation behaviour provided a reasonable description of displacements (both vertical and lateral) throughout the entire construction process. Excess pore pressures were only accurately reproduced up to an embankment height of approximately 4m. Thereafter, up to completion of the embankment at a height of 8.5m excess pore pressures were underestimated.

4.3.7.4 Discussion of permeability

Values of permeability used to describe the pre-yield behaviour of the Malaysian trial embankments' foundations were determined from available laboratory test data and linked by an arbitrary factor which depends primarily on the authors' experience or background. The surprise expressed by Poulos et al. (1989) at the accuracy of their predictions further reflects this.

Experimental evidence (Barry and Nicholls, 1982) does not support the drastic decrease in permeability used in analyses as the preconsolidation pressure, σ_{vc} , is passed. The permeability of the soil is largely governed by the size of the pores through which the water flows and is consequently primarily dependent on the void ratio, e . As can be seen from Fig 4.27 and Fig 4.28 (Barry and Nicholls, 1982 and Davies and Humpheson, 1986) as the preconsolidation pressure is passed there is not a significant decrease in the void ratio, and consequently, through relation (4.8), the permeability also does not significantly change. However, as the preconsolidation pressure is passed there is a significant decrease in the coefficient of consolidation, c_v ,

Fig 4.27 and Fig 4.28, because of an increase in the coefficient of volume compressibility, m_v , relation (4.9).

$$c_v = \frac{k}{m_v \gamma_w} \quad (4.9.)$$

where k is the permeability and γ_w is the unit weight of water.

The coefficient of volume compressibility m_v , is estimated from oedometer test data, relation (4.10).

$$m_v = \frac{\delta v}{v \delta \sigma'_v} \quad (4.10)$$

where v is the specific volume ($=1+e$).

Changes in volume during loading of a soil are given by

$$v = v_k - \kappa \ln p \quad (4.11)$$

for unloading, reloading or reconsolidation and

$$v = v_\lambda - \lambda \ln p \quad (4.12)(2.43\text{bis})$$

for normal compression.

Hence, for unloading and reloading m_v is given by relation (4.13) and during normal compression given by relation (4.14).

$$m_v = \frac{\kappa}{v \sigma'_v} \quad (4.13)$$

$$m_v = \frac{\lambda}{v \sigma'_v} \quad (4.14)$$

As the preconsolidation pressure is passed there is not a change in the rate of which pore water can flow to dissipate excess pore pressures, but there is an increase in the rate at which pore pressure is being expelled from the soil, due to an increase in the

coefficient of volume compressibility m_v , as the soil tries to collapse under continued loading.

Therefore, assuming a marked decrease in the permeability of the clay to describe the post yield consolidation behaviour is not consistent with the actual observed soil response. This procedure appears to be numerically convenient to obtain good results rather than based on experimental observations. As a result, for the embankment study described in this chapter, (Cubzac-les-Ponts, embankment A) selection and subsequent adjustment of permeability values is consistent with experimental observations. Numerical convenience should not be considered as an aspect of the geotechnical design process.

4.4 Modelling assumptions

Undrained and coupled undrained/drained consolidation analyses were performed using the finite element mesh shown in Fig 4.29. The lateral boundary of the mesh was defined by approximately four times the vertical depth from the toe of the embankment. This is consistent with finite element predictions performed for trial embankments constructed on soft Malaysian marine clays (Balasubramaniam et al., 1989; Poulos et al., 1989; Indraratna et al., 1992 and Chai and Bergado, 1993) which were typically performed assuming a ratio of lateral boundary distance, from the embankment toe, to vertical depth of approximately three. Horizontal displacements are fully restrained on the lateral boundaries. Both horizontal and vertical movements are fully restrained along the base of the finite element mesh. Pore water pressure boundary conditions required for consolidation analyses are: zero excess pore water pressures at the top surface for a water table at the ground surface, and zero excess pore water pressures at the base of the finite element mesh, justified by the underlying gravel layer. The embankment was assumed to be fully drained throughout the analysis.

The embankment was assumed to be constructed in three layers each of approximately 1.5m height. The embankment loading was applied to the foundation by the self weight of the embankment elements when they are introduced into the mesh. The Mohr-Coulomb elastic perfectly plastic soil model was used to describe the embankment. For the embankment fill the shear resistance is represented by $c'=2\text{kPa}$ and $\phi'=35$ degrees, obtained from laboratory tests (Mouratidis and Magnan, 1983). The clay foundation was divided into five layers simulating the variable characteristic properties of the soil. The foundation soil was described using the modified Cam clay soil model.

4.5 Results of analyses

4.5.1 Introduction

In this section the results of analyses are presented and discussed. Undrained analyses are considered first in sections 4.5.2-4.5.3. Consolidation analyses are presented in section 4.5.4. In each case analyses were performed assuming a water table at 1.0m depth.

4.5.2 Undrained analyses

4.5.2.1 Displacements

The results of the undrained analyses are presented in Figs 4.30-4.39. As can be seen from Figs 4.31-4.33 calculated and observed displacement responses are in reasonable agreement. Additionally, the general shapes of predicted and observed displacement profiles are in agreement. Measured vertical displacement data are available from markers 160 and 162 located at the main embankment centre line and midway between the centre line and main embankment edge, Fig 4.3, respectfully. Horizontal displacement data are available from marker 197 located at 4m depth beneath the right hand toe of the embankment.

Predictions of vertical displacement at marker 160, up to embankment heights of approximately 3m, are underestimating those observed. However, predictions of vertical displacement at marker 162 are typically overestimating those observed. At marker 162 the difference between predictions and observations is typically small. At an embankment height of 1.5m the computed settlement at the centre is smaller than at the edges of the embankment: approximately 11mm at the centre and 44mm at the edges. This pattern of vertical displacement has arisen because the wide lateral extent of the surface loading has caused lateral confining stresses to develop within the top two layers of the mesh immediately beneath the embankment, Fig 4.40. Consequently, elements beneath the central region of the embankment are being prevented from displacing by the lateral stresses imposed on them by neighbouring elements. This behaviour is also evident from the depth profile of mobilised shear stress at the embankment centre line and edges, Fig 4.41. Shearing at the edges is some 1.5 times larger than at the centre line. As can be seen from Fig 4.42 this problem diminishes as the width of the embankment, L (or loaded area) decreases.

This suggests that this problem will tend to occur at ratios of embankment cross section width to foundation depth, B/D , of greater than approximately 2.5.

At marker 160, Fig 4.31 the difference between computed and observed vertical displacement is large and predictions are underestimating those observed, up to an embankment height of 3.5m, by as much as 50%.

For comparison lateral displacements at 'marker' 197 are also shown, Fig 4.33, for a fully drained analysis. As can be seen fully drained lateral displacements provide a more accurate description of lateral displacements than the undrained analyses. This behaviour is consistent with the findings of Poulos et al. (1989) and Indraratna et al. (1992) for numerical analyses of a test embankment constructed on a deposit of soft Malaysian marine clay.

The lateral displacement 'marker' 197 was located at 4m depth to coincide approximately with the assumed occurrence of maximum lateral displacement Fig 4.43, $z/D=0.3$. Fig 4.43 has been compiled from field observations of lateral displacements occurring under the toe of several embankments constructed on soft soils (Tavenas et al., 1979) and assumes that the distribution of lateral displacement with depth depends directly on the consolidation state (overconsolidated or normally consolidated) of the clay beneath the embankment. Several different lateral displacement profiles, arising from various consolidation states of the foundation (1 overconsolidated state; 2 varying, part normally consolidated and part overconsolidated; and 3 normally consolidated), are shown in Fig 4.43. Here a consolidation state of 3, equivalent to a normally consolidated foundation, was assumed and corresponds to a maximum lateral displacement occurring at a normalised depth of 0.3.

4.5.2.2 Excess pore water pressures

Predictions of centre line excess pore water pressures, Figs 4.34-4.39 do not compare well with those observed, typically predictions are 1.5-2 times larger. As can be seen from Figs 4.34-4.37 the shapes of predicted and observed excess pore water pressure profiles, except predictions at an embankment height of 1.5m (Fig 4.34) are in reasonable agreement.

4.5.2.3 Influence of the embankment

To investigate the contribution and influence of the embankment material on the foundation the embankment was modelled as isotropic elastic, giving the embankment infinite strength. Analyses were performed for a water table at 1.0m and are presented in Figs 4.44-4.46; analyses E2. The result of the undrained analysis described previously with limiting embankment strength (embankment parameters are shown in Table 4.1) are also shown; analyses E1. As can be seen from the Figs 4.44-4.45 there is little difference between the vertical displacement solutions up to an embankment height of 3.5m. As embankment heights become greater than 3.5m, the increase in vertical displacement for analysis E1 is significantly greater than that observed for E2 (isotropic elastic embankment). Lateral displacements at marker 197 Fig 4.46 for analysis E1 are approximately twice as large as those computed for analysis E2 up to an embankment height of 3.5m. The increase in lateral displacement associated with analysis E1, once failure is initiated, is approximately 5 times larger than that computed for analysis E2. It is also interesting to note that predictions of lateral displacement for E2 compare significantly better with those observed than lateral displacements predicted by analysis E1. This suggests that the embankment is restraining the foundation from pushing out laterally under the applied loading. Examination of horizontal stress, σ_h developed within the embankment Fig 4.47-4.49, indicates that high tensile stresses are mobilised, particularly within the base layer of the embankment, elements 180-192, Fig 4.29, and the central core element 199 of layer 2, where the mobilised tensile stress is in the range 40 to 150kPa. These tensile stresses are larger than the embankment could sustain. The influence of these high tensile stresses is evident from comparison of displacement vectors for analyses E1 and E2, Figs 4.50-4.57. It is evident from the form and magnitude of displacement vectors that the high lateral stresses developed within the isotropic elastic embankment, analysis E2, are tightly holding the embankment together and resisting any lateral spread of the embankment under its self weight. Additionally, modelling the embankment as isotropic elastic has pushed the failure mechanism deeper within the foundation. For analysis E1, the failure mechanism is shallow.

Suitable modelling of the embankment strength and its contribution to foundation stability within the analysis is beneficial, especially for predictions of lateral displacements. However, some caution is required to ensure that the stress states generated within the embankment do not become unrealistic, hence forcing an equally unrealistic embankment deformation response.

4.5.3 Discussion

It is evident from the results presented, that the selected parameters have provided a reasonable estimate of the observed vertical displacements, but not of the observed lateral displacements and excess pore water pressures.

For comparison an estimate of the lateral displacement at an embankment height of 2.5m was estimated using the classical Boussinesq equations for a surface strip loading of width B . The strip influence factors, I_{st} , were estimated from the solution presented by Poulos (1967). Using this method a maximum lateral displacement of approximately 45mm was estimated. At the same embankment height (2.5m) finite element analysis estimated an approximate maximum lateral displacement of 100mm. A more accurate estimate of the minimum lateral displacement, in this case, is provided by the Boussinesq solution. This result indicates inaccuracies in the finite element results for lateral displacements.

This behaviour may partially be attributed to incomplete saturation and/or some overconsolidation of the clay. Initially the clay is in an overconsolidated state and therefore has a high coefficient of consolidation. It is expected that the effect of incomplete saturation will be greatest within the top 3-4m of foundation where the degree of overconsolidation, n , is typically greater than 2, Fig 4.15. As described previously (section 4.3.7.3), the effect of incomplete saturation and some overconsolidation during the initial loading of the foundation will force the effective stress path to follow a drained response. It is not thought that the foundation follows a fully undrained response until yield occurs (Leroueil and Tavenas, 1986 and Leroueil et al., 1985). As can be seen from values of critical embankment height, H_{nc} , Table 4.4, for the bottom 3m of clay, 6-9m, yield is thought to have occurred prior to completion of the second layer. However, in the upper 4m of the foundation yield will not occur until an embankment height of approximately 3.5-4.5m. Critical embankment heights for the top 1-1.5m of clay indicates that yield will not occur until after completion of the embankment. As a result, the top 2m of the foundation will be following an approximately drained response throughout the trial loading. This will give rise to larger vertical displacements but smaller lateral displacements than would be expected from fully undrained analyses (see section 4.3.7.3 and Fig 4.26). Computed lateral displacements assuming a fully drained response compare well with those observed. However, computed fully drained vertical settlements are significantly larger than those computed from undrained analyses or observed.

As previously noted predictions of vertical displacements at marker 160 underestimate those observed by as much as 50%. An improved vertical displacement solution at this marker which coincides with the embankment centre line can be

obtained by increasing the values of κ and λ , controlling the magnitude of elastic and plastic strains respectfully. In section 4.3 it was assumed that values of κ equivalent to the average of the average and minimum slopes of oedometer test data were required. This assumption was based on use of Fig 4.16 (G/c_u vs ϵ_a) and assuming an elastic strain level of 0.1%. The level of strain assumed, $\epsilon_a=0.1\%$, was based on the results of experimental studies performed by Jardine et al. (1984) to investigate the low strain stiffness of low plasticity clays. The attainment of 0.1% axial strain generally coincided with a marked loss of stiffness and was assumed (Jardine et al., 1984) to be the limit of the small strain range. In chapter 3 adoption of 0.1% strain with which to estimate values of elastic stiffness provided good results. However, as can be seen from Fig 4.14 the plasticity of the soft clay at Cubzac-les-Ponts is typically greater than 60% and as high as 120% between 2 and 4m depth. Clearly the clay at Cubzac is not of a low plasticity and assuming 0.1% strain is providing too stiff a foundation response. Improved values of κ were obtained by using the average slope of the entire unload-reload data, Fig 4.11. This corresponds to an average $G/c_u=60-70$, Fig 4.13, implying a strain of 0.2-0.3%. Improved values of λ were obtained mainly by trial and error, however final values correspond to the maximum values of λ obtained, Fig 4.17. Adjusted values of κ and λ are shown in Table 4.6 and the improved vertical displacement solution is shown in Fig 4.58.

For embankment A, to improve the predictions of lateral displacements using undrained analyses requires a significant increase in the elastic stiffness. From comparison of computed and observed lateral displacements, Fig 4.33, the elastic stiffness may need to be increased by 3-4 times. Using modified Cam clay, this implies that to select the appropriate value of κ requires a G/c_u ratio 240-320 which is beyond the limit of available stiffness data. However, it does suggest that to improve the lateral displacement predictions minimum values of κ giving maximum elastic stiffness should be used. Using values of κ giving $G/c_u=240-320$, will give an excessively stiff vertical displacement response and consequently predictions of vertical displacements will significantly underestimate those observed. In view of the above discussion two very different elasticity solutions have emerged from which to obtain accurate predictions of vertical and lateral displacements. This demonstrates that simultaneous accurate reproduction of the observed vertical and lateral displacement responses using undrained analyses is not possible. This behaviour is consistent with the findings of Hird (1994) determined from numerical studies performed to investigate the behaviour of a soft clay foundation at Willow Plantation (A414).

As previously noted, excess pore water pressure predictions do not compare with those observed. In an attempt to improve excess pore water pressure predictions

consolidation analyses have been performed. These analyses are described in the next section.

4.6 Consolidation analyses

In the previous sections numerical analyses describing the embankment loading assumed a fully undrained response. The results of these analyses were of mixed success. Centre line vertical displacements tended to under-predict the observed behaviour, particularly at embankment heights less than the critical embankment height, $H_r < 2.5\text{m}$. Predictions of lateral displacements and excess pore water pressures overestimated the observed behaviour. Excess pore water pressures were overestimated heights by a factor of 1.5-2 times.

From the results of the undrained analyses it is evident that even for a rapid loading the fully undrained condition is not an accurate representation of the actual soil behaviour, particularly for predictions of excess pore water pressures.

Results of the consolidation analyses performed for a water table depth of 1.0m are presented in Fig 4.59-4.68 using the initial parameter set Table 4.1. The adjusted parameter set, Table 4.6 (see section 4.5.3) was not used in this study as it was anticipated that use of consolidation analyses would provide the necessary improvement to the vertical displacement solution at marker 160.

As can be seen from Figs 4.59-4.61 consolidation analyses have increased both the vertical and lateral displacement predictions. This behaviour was anticipated from analyses performed by Indraratna et al. (1992) for an embankment constructed on soft clay.

Using consolidation analyses predictions of excess pore water pressures Fig 4.62-4.67, except at an embankment height of 4.5m, have not provided a significant improvement by comparison with undrained analyses. At embankment heights of 1.5 and 2.5m predictions of the excess pore water pressure using consolidation and undrained analyses are approximately equal. Consolidation analyses start to improve undrained predictions at an embankment height of 3.5m. Predictions of excess pore water pressure using consolidation analyses are in reasonable agreement with those observed at an embankment height of 4.5m. Failure occurred at an embankment height of 4.5m, therefore accurate prediction at this embankment height is meaningless for a design situation. For design accurate predictions of excess pore water pressures are required at stable embankment heights, i.e. $H_r < H_{nc}$.

In order to provide a more accurate excess pore water pressure solution at pre-failure embankment heights further predictions of excess pore water pressures have been made using three "traditional" methods (D'Appolonia et al., 1971) and a semi-empirical method based on field observations of pore pressures generated under the centre line of embankments constructed on soft clay (Leroueil et al., 1985). These methods are described in the next section.

4.6.1 Alternative methods for excess pore water pressure predictions

The three "traditional" methods used to provide further estimates of the observed excess pore water pressures from total stress changes are briefly described below.

1. One dimensional case, the increase in excess pore water pressure, δu , is equal to the change in vertical total stress, $\delta\sigma_v$.
2. Three dimensional case the soil is assumed to be a porous elastic material subject to a general three-dimensional stress change and δu is equal to the change in total mean stress, δp .
3. Henkel's semi-empirical equation which considers that the excess pore water pressure has two components, one due to the change in mean stress and one due to the change in deviatoric stress. The deviatoric component is related to the change in octahedral shear stress. Hence,

$$\delta u = \delta p + a\delta\tau_{oct} \quad (4.15)$$

where a is Henkel's pore pressure parameter (Henkel, 1956) and is related to Skempton's parameter A (Skempton, 1954) (determined from triaxial tests) through relation (4.16)

$$a = \frac{3A-1}{\sqrt{2}} \quad (4.16)$$

For normally consolidated clays Skempton and Bjerrum (1957) suggest values of $A=0.5-1$. Here, Skempton's pore pressure parameter A was assumed equal to 0.75, average of the proposed range of values.

The octahedral shear stress, τ_{oct} , is given by relation (4.17).

$$\tau_{oct} = \frac{1}{3} \sqrt{(\delta\sigma_1 - \delta\sigma_2)^2 + (\delta\sigma_2 - \delta\sigma_3)^2 + (\delta\sigma_1 - \delta\sigma_3)^2} \quad (4.17)$$

The total stress changes within the soil due to the embankment loading have been estimated from Osterberg's (1957) solution. This solution assumes the soil to be isotropic and elastic and the applied embankment load is assumed to have a trapezoidal distribution equal to the weight of the embankment fill above each point of the loaded surface.

The fourth method used to provide further predictions of the excess pore water pressure is semi-empirical method (Leroueil et al., 1985) based on Skempton's pore pressure relation, relation (4.18) (Skempton, 1954).

$$u = B(\delta\sigma_3 + A(\delta\sigma_1 - \delta\sigma_3)) \quad (4.18)$$

From measurements of excess pore water pressures generated under the centre line of large trial embankments (Leroueil and Tavenas, 1980 and Leroueil et al., 1985) the behaviour is essentially one dimensional and the horizontal principal stress $\delta\sigma_3 (= \delta\sigma_h)$ is assumed to have negligible influence on the excess pore pressure generated. Additionally, Leroueil et al., (1985) assume $A=1$ for soft normally consolidated clay which reduces relation (4.18) to relation (4.19).

$$\delta u = B\delta\sigma_1 \quad (4.19)$$

where B is Skempton's pore water pressure coefficient (Skempton, 1954) and $\delta\sigma_1 = \delta\sigma_v$ is the increase in total vertical stress beneath the centre line of an embankment.

For saturated clays $B=1$ (Skempton, 1954) however, from field measurements of centreline excess pore pressures caused by embankment construction (Tavenas and Leroueil, 1980) it is thought that B does not equal 1.0 until yield of the clay occurs. Field measurements indicate that prior to yield B is less than 1.0. The pore pressures generated during construction of an embankment can be related to the increasing vertical load of the embankment as shown in Fig 4.68 (Tavenas and Leroueil, 1980 and Leroueil et al., 1985). As can be seen from Fig 4.68, initially δu is much lower than $\delta\sigma_v$ and the pore pressure coefficient, $\bar{B} = \frac{\delta u}{\delta\sigma_v}$, varies with depth in the clay according to Fig 4.23. Once the clay becomes normally consolidated, $\sigma'_v = \sigma_{vc}$ the excess pore water pressure, $\delta u = \delta\sigma_v$, and the pore pressure coefficient, $\bar{B} = 1.0$. Normal consolidation or yield of the soft clay occurs once the height of the embankment

critical, H_{nc} , relation (4.4). Above the critical embankment height, excess pore water pressures are given by relation (4.20).

$$\delta u = I\gamma_r H_r - (\sigma'_{vc} - \sigma'_{vi}) \quad (4.20)$$

where I is a stress influence factor (Oesterberg, 1957); γ_r is the unit weight of the embankment; H_r is the height of the embankment; σ'_{vc} is the vertical effective preconsolidation pressure and σ'_{vi} is the initial in situ vertical effective stress.

Estimates of δu using these methods are shown in Figs 4.69-4.72, the excess pore pressure solution obtained from the consolidation analyses is also shown. As can be seen, there are significant differences in the stress fields calculated using the three "traditional" methods. Using the "traditional" methods observed excess pore water pressure are typically overestimated, especially in the upper few metres of soil. However, in general the "traditional" methods have provided more accurate predictions of the observed excess pore pressure and, at embankment heights greater than 1.5m, are in reasonable agreement with those observed.

Excess pore water pressures for all pre-failure embankment heights are most accurately predicted using the empirical method after Tavenas and Leroueil (1980). Not only does this method accurately reproduce the observed magnitude of excess pore water pressures but it also accurately reproduces the shape of the observed pore pressure profile. Additionally excess pore pressure predictions obtained using this semi-empirical method are a significant improvement on the finite element solution. However, the success of the semi-empirical method should not be surprising as field measurements obtained from the Cubzac-les-Ponts embankments were used to compile Fig 4.68. Nevertheless this method does demonstrate that careful consideration of the actual physical state of the in situ clay is required if accurate predictions of its behaviour are to be made.

4.6.2 Discussion of results

The intent of consolidation analyses was to provide an improved excess pore pressure solution. As discussed, this was not achieved. Selected values of permeability were at their maximum, therefore further increases in permeability could not have been justified from available data. As described previously in section 4.3 variation of the permeability to suit the pre-yield and post yield behaviour was not considered consistent with experimental observations.

An improved solution of excess pore water pressure was obtained using the methods described in section 4.6.5. Of these methods the semi-empirical method (Leroueil and Tavenas, 1980 and Leroueil et al., 1985) gave the most accurate solution at all embankment heights considered. The accuracy of this semi-empirical method and the "traditional" methods compared with the solution obtained from undrained and consolidation analyses demonstrates that use of conventional finite element analysis to predict excess pore water pressures for such loading situations may not be the most accurate method.

As mentioned in section 4.2 previous researchers of this loading event (Mouratidis and Magnan, 1983) used the MELANIE soil model to describe the soft clay foundation. In their study use was made of the feature which allows variation of the degree of saturation of the soft clay. Initially analyses were performed assuming a fully saturated clay foundation and the results of excess pore water pressures for these analyses were similar to those obtained from the consolidation analyses described in section 4.6.1. A second study performed by Mouratidis and Magnan (1983) in which the pore fluid was assumed to be compressible, modelled by reducing the degree of saturation of the clay foundation to 98% (this value was close to the average degree of saturation measured at the site), therefore introducing some compressibility of the pore fluid significantly improved excess pore pressure predictions, Figs 4.73-4.75. As can be seen, taking account of incomplete saturation of the clay in numerical analyses has given excess pore water pressures which are in good agreement with those observed. Additionally, using this model reasonable simultaneous prediction of the vertical and lateral displacements was achieved. This was also attributed to taking account of incomplete saturation of the clay, but may also be due to the incorporation of anisotropy into the soil model.

In view of the above discussion, if finite element analyses are to be used to provide an accurate solution of all elements of the foundation behaviour considered in this section, i.e. vertical and lateral displacements and excess pore water pressures, then careful consideration of the actual in-field characteristics of the soft clay are required. To obtain the required accuracy use of more complex finite element programs, such as that described by Mouratidis and Magnan (1983), will be necessary. However, for most design situations the level of complexity afforded by the more complex soil models may not be required and simple undrained analyses, providing a serviceability (displacement) check, and hand calculations giving predictions of excess pore water pressures may be sufficient.

4.7 Discussion

It is evident from the results presented in sections 4.5 (undrained analyses) and 4.6 (consolidation analyses) that using the modified Cam clay soil model to describe the soft clay foundation at Cubzac-les-Ponts has only provided a reasonable estimate of the observed vertical displacements induced during construction of embankment A. Predictions of lateral displacements and excess pore water pressures have significantly overpredicted those observed. The current solution (both undrained and consolidation analyses) do not provide support for the suggested parameter selection process. However, the selected parameters have provided, for both the undrained and consolidation analyses, reasonable vertical displacement estimates. Back analysis has determined that very high, low strain, elastic stiffness values are required to accurately reproduce the lateral displacements using the Cam clay model. Such high values of elastic stiffness could be estimated from the triaxial test performed with low strain stiffness measurement and/or from seismic tests. The seismic cone test is thought to measure the elastic stiffness at strains of 0.001%. It has been suggested in section 4.5 that the minimum values of κ (giving high elastic stiffness) should be used when estimating lateral displacements using the Cam clay soil model. Here, approximately average values of κ were selected. These values have provided a reasonable estimate of the vertical displacements. In addition to the effect of incomplete saturation and/or some overconsolidation (see section 4.6), the apparent need to select differing values of elastic stiffness to obtain reasonable predictions of the vertical and lateral displacements suggests that to simultaneously predict vertical and lateral displacements requires the inclusion of anisotropic elasticity in analyses. Elasticity in the modified Cam clay soil model is isotropic, i.e. the elastic properties are same in vertical and horizontal directions. Anisotropic elasticity is a standard feature of the MELANIE soil model and may account for the accurate predictions of lateral displacement at marker 197, Fig 4.76(c), before the effects of incomplete saturation were included in analyses (Mouratidis and Magnan, 1983). The special form of anisotropy known as cross-anisotropy is included in the MELANIE soil model. The Cubzac-les-Ponts soil demonstrates a high degree of elastic anisotropy, Table 4.7 (Shahanguian, 1981). As can be seen from Table 4.7 the elastic stiffness in the horizontal direction at low effective stress is considerably larger than the vertical elastic stiffness of the soil.

In design situations where an estimation of the construction induced displacements is important then use of a soil model incorporating anisotropic elasticity should be considered. Simpler designs may not warrant this level of complexity as incorporation of anisotropy requires extra soil testing to provide the necessary parameters.

Additionally, a simple check involving Boussinesq's elastic equation (section 4.5) suggests that less complex designs may suffice.

It is recommended that in situations where only conventional finite element programs are available predictions of excess pore water pressures should be made using the simple hand-calculations described in section 4.6. Use of the simple hand-calculations are limited to predictions of excess pore pressures under the centreline of the embankment. For designs requiring estimates of excess pore water pressures at various sections under the embankment, a more complex method of analysis, such as that performed by Mouratidis and Magnan (1983), may be necessary.

Throughout this chapter the concern of analyses has been to reproduce the observed construction induced foundation behaviour. In practice however, embankment design is primarily concerned with the prediction of the long-term foundation response to the loading. Typically the design is primarily concerned with the accurate prediction of displacements over the life span of the embankment. Parameter selection for such a design situation is described in chapter 5.

4.8 Conclusions

Undrained and consolidation analyses have been performed using the modified Cam clay soil model to describe the response of the soft clay foundation to the embankment loading. From comparison of the computed and observed responses conclusions can be drawn concerning the analysis of similar loading situations using finite element analysis and the modified Cam clay soil model.

Undrained and consolidation analyses provided a reasonable estimate of the observed settlement behaviour. Neither provided accurate predictions of the observed pre-failure lateral displacements or excess pore water pressures. A more accurate description of the construction induced lateral displacements was obtained by performing drained analyses. An empirical method (Tavenas et al., 1979) based on the degree of overconsolidation also provided a reasonable estimate of the observed maximum lateral displacement under the embankment toe. The construction induced excess pore water pressures were most accurately estimated using hand-calculations, particularly a semi-empirical method (Tavenas and Leroueil, 1980) based on Skempton's pore water pressure parameter B .

Comparing the results of the modified Cam clay and MELANIE analyses (Mouratidis and Magnan, 1983) with the observed behaviour indicates that the elements of the MELANIE soil model (see section 4.2) are providing a more accurate description of the physical in situ state of the Cubzac-les-Ponts soft clay. The ability to vary the degree of saturation in the MELANIE soil model was found to be a significant feature of this model. Additionally, this feature of the MELANIE soil model is its main strength enabling simultaneous accurate predictions of the observed settlements, lateral displacements and excess pore water pressures induced during construction (Mouratidis and Magnan, 1983).

The inclusion of anisotropic elasticity within a soil model is also considered to be an important feature of a soil model (Poulos, 1972; Mouratidis and Magnan, 1983 and Leroueil et al., 1985). Here, studies performed using the modified Cam clay soil model determined that significantly enhanced values of elastic stiffness were required to provide accurate predictions of lateral displacements. Values of elastic stiffness were 3-4 times larger than those required to provide accurate settlement predictions, however available data could not justify use of such high values of elastic stiffness.

Values of elastic stiffness, providing reasonable estimates of the observed settlements, were selected from the average slope of available oedometer unload-reload data. Plotting values of G/c_u against shear strain ϵ_q (values of elastic stiffness G were obtained from available triaxial test data) indicated that optimum values of elastic stiffness implied an average strain of 0.2-0.3%. Previously in chapter 3 values of elastic stiffness were selected assuming a strain of 0.1%.

Values of compressibility, λ , were determined from the slope of oedometer normal compression data. Oedometer test values of λ were in reasonable agreement with those estimated using the empirical link with plasticity index (Muir Wood, 1990). It has also been suggested that values of λ could be used to guide or check the choice of κ values using parameter Λ . The parameter Λ describes the relative slopes of the normal compression and unloading-reloading lines for the soil.

A low value of Poisson's ratio, $\nu'=0.2$, was selected to ensure a suitably low ratio of maximum lateral movement to maximum vertical movement (Poulos et al., 1989). Values of Poisson's ratio estimated from drained triaxial tests were in the range $\nu'=0.12-0.46$ (Shahanguian, 1981).

The depth profile of the degree of overconsolidation was obtained from available preconsolidation stress data. Some check on the assumed profile was obtained from the depth profile of undrained shear strength (see section 4.3.6.) and consideration of the critical embankment height H_{nc} , relation (4.4) (Leroueil et al., 1985).

Values of the critical state parameter M were determined from values of the effective angle of shearing resistance, ϕ' . Here, values of ϕ' were available from drained

triaxial tests. For comparison values of ϕ' were also estimated using empirical correlations (Mitchell, 1976; Muir Wood, 1990 and Diaz-Rodriguez et al., 1992). From back analysis it was found that optimum predictions of ϕ' , using the empirical correlations, were obtained using the empirical link with plasticity index (Mitchell, 1976 and Muir Wood, 1990) to estimate values of ϕ' for the surface crust and using the link with the undrained shear strength and preconsolidation stress (Diaz-Rodriguez et al., 1992) to estimate values of ϕ' for the underlying soft clay.

For consolidation analyses values of the horizontal permeability, k_x , were selected from self-boring permeameter data. Values of vertical permeability, k_y , were estimated from k_x/k_y ratios estimated from laboratory tests. Selected values of permeability were kept constant throughout analyses. Available permeability data did not justify current practice to significantly vary pre-yield and post-yield permeabilities (Poulos et al., 1989 and Balasubramanian et al., 1989).

As mentioned previously accurate predictions of the observed foundation behaviour was observed using the MELANIE soil model. However, given the level of complexity associated with this soil model (in relation to the greater number of material parameters) its use for most design situations may not be necessary. Consequently, use of the modified Cam clay soil model in addition to the semi-empirical methods described in this chapter may therefore suffice.

Table 4.1 Material input parameters for undrained analysis

DETAILS		MATERIAL PROPERTIES					
DEPTH (m)	LAYER No	κ	λ	e_{cs}	M	ν	$\gamma(\text{kN/m}^3)$
0-1.0	1	0.015	0.10	1.56	1.00	0.2	17
1.0-2.0	2	0.030	0.40	3.08	1.00	0.2	16
2.0-4.0	3	0.060	0.50	5.32	1.00	0.2	14
4.0-6.0	4	0.040	0.40	3.07	1.15	0.2	15.5
6.0-8.0	5	0.050	0.50	3.54	1.15	0.2	15
8.0-9.0	6	0.050	0.60	4.67	1.15	0.2	15.5

DETAILS	EMBANKMENT PARAMETERS				
LAYER	E' (MPa)	c' (kPa)	ϕ' (degrees)	ν'	$\gamma(\text{kN/m}^3)$
ALL	15	2	35	0.4	21
LAYERS					

Table 4.2. Estimation of κ from values of Λ and λ using relation (4.1).

Depth (m)	λ	κ_{assumed}	$^+\kappa_{\text{cal}} (\Lambda=0.8)$	$^{++}\kappa_{\text{cal}} (\Lambda=0.9)$
1	0.1	0.015	0.02	0.01
2	0.4	0.02	0.08	0.04
3	0.5	0.06	0.1	0.05
4	0.5	0.06	0.1	0.05
5	0.4	0.035	0.08	0.04
6	0.4	0.035	0.08	0.04
7	0.5	0.04	0.1	0.05
8	0.5	0.04	0.1	0.05
9	0.6	0.04	0.12	0.06

$^+ \kappa_{\text{cal}}=0.2\lambda$ for $\Lambda=0.8$; average from values proposed by Mayne (1992).

$^{++} \kappa_{\text{cal}}=0.1\lambda$ for $\Lambda=0.9$; after Mouratidis and Magnan (1983).

Table 4.3. Natural clays from which yield curves have been determined with geotechnical characteristics (Diaz-Rodriguez et al., 1992).

Site (1)	Depth (m) (2)	ω (%) (3)	I_p (%) (4)	σ'_p (kPa) (5)	ϕ'_{inc} (degrees) (6)
Atchafalaya, Louisiana	21.3	58	44	150	23
Bäckebo, Sweden	3.4	87	42	57	30
Bogota, Columbia	7-12	90-160	100-170	150-255	35
Champlain sea clays, Québec	—	58-90	17-45	50-290	27-30
Cubzac-les-Ponts, France	4.5-5.5	60-80	40	46-75	32
Dråmmen, Norway	—	52	29	—	30
Favren, Sweden	—	60	—	70	32
México, México	1.7	460	493	71	43
Osaka, Japan	30.0	63	—	330	25
Otaniemi, Finland	2.0	130	63	20	25
Ottawa, Ontario	—	65	36	150	27
Perno, Finland	4.2	100	39	22	23
Pornic, France	1.2-2.0	75-88	40	35-45	29
Riihimäki, Finland	4	55	25	90	27
St. Jean-Vianney, Québec	3.7	41	9	1150	32
St. Louis, Québec	—	67	23	190	25
Winnipeg, Manitoba	8-12	54-63	35-60	190-380	17.5

Table 4.4. Critical embankment height, H_{nc} relation (4.4).

Depth (m)	σ'_{vp} (kPa)	σ'_{vi} (kPa)	$(\sigma'_{vp}-\sigma'_{vi})$	z/D	\bar{B}_1	$1-\bar{B}_1$	I Osterberg	$H_r(1-\bar{B}_1)$	H_{nc} (m)
1	100	17	83	0.11	0.22	0.78	0.95	15	5.5
2	80	23	57	0.22	0.42	0.58	0.92	11.2	5.1
3	60	27	33	0.33	0.51	0.49	0.89	9.1	3.6
4	55	31	24	0.44	0.58	0.42	0.83	7	3.5
5	60	36	24	0.56	0.6	0.40	0.76	6.4	3.6
6	60	41	19	0.67	0.58	0.42	0.70	6	3.1
7	70	46	24	0.78	0.42	0.58	0.70	8.5	2.8
8	75	51	24	0.89	0.22	0.78	0.60	10	2.4
9	90	57	33	1.00	0	1	0.62	13.02	2.5

Table 4.5. Selected values of permeability.

LAYER No.	DEPTH (m)	SELECTED k_x (m/s)	SELECTED k_y (m/s)
1	0-1.0	18.5×10^{-9}	2.5×10^{-9}
2	1.0-2.0	10×10^{-9}	2×10^{-9}
3	2.0-4.0	20×10^{-9}	3×10^{-9}
4	4.0-6.0	12×10^{-9}	3×10^{-9}
5	6.0-8.0	9.5×10^{-9}	3.5×10^{-9}
6	8.0-9.0	9.5×10^{-9}	3×10^{-9}

Table 4.6. Adjusted values of κ_A and λ_A .

LAYER No.	DEPTH (m)	κ_A	λ_A
1	0-1.0	0.015	0.2
2	1.0-2.0	0.03	0.4
3	2.0-4.0	0.085	0.6
4	4.0-6.0	0.05	0.5
5	6.0-8.0	0.05	0.6
6	8.0-9.0	0.05	0.6

Table 4.7. Details of Cubzac-les-Ponts clay anisotropy (Shahanguian, 1981).

σ'_1 (kPa)	σ'_3 (kPa)	ν_{vh}	E_v (kPa)	E_h (kPa)	ν_{vh}
10	4	0.2363	50700	11266.7	0.1217
20	4	0.1953	12680	6337.5	0.1248
30	4	0.2576	5070	3168.7	0.2015
40	4	0.4068	4056	2600	0.2794
50	4	0.6715	2535	388.5	0.3923
60	4	0.387	450.5	226.8	0.4600

Fig 4.1(a). Location of map of France (Muir Wood, 1990).

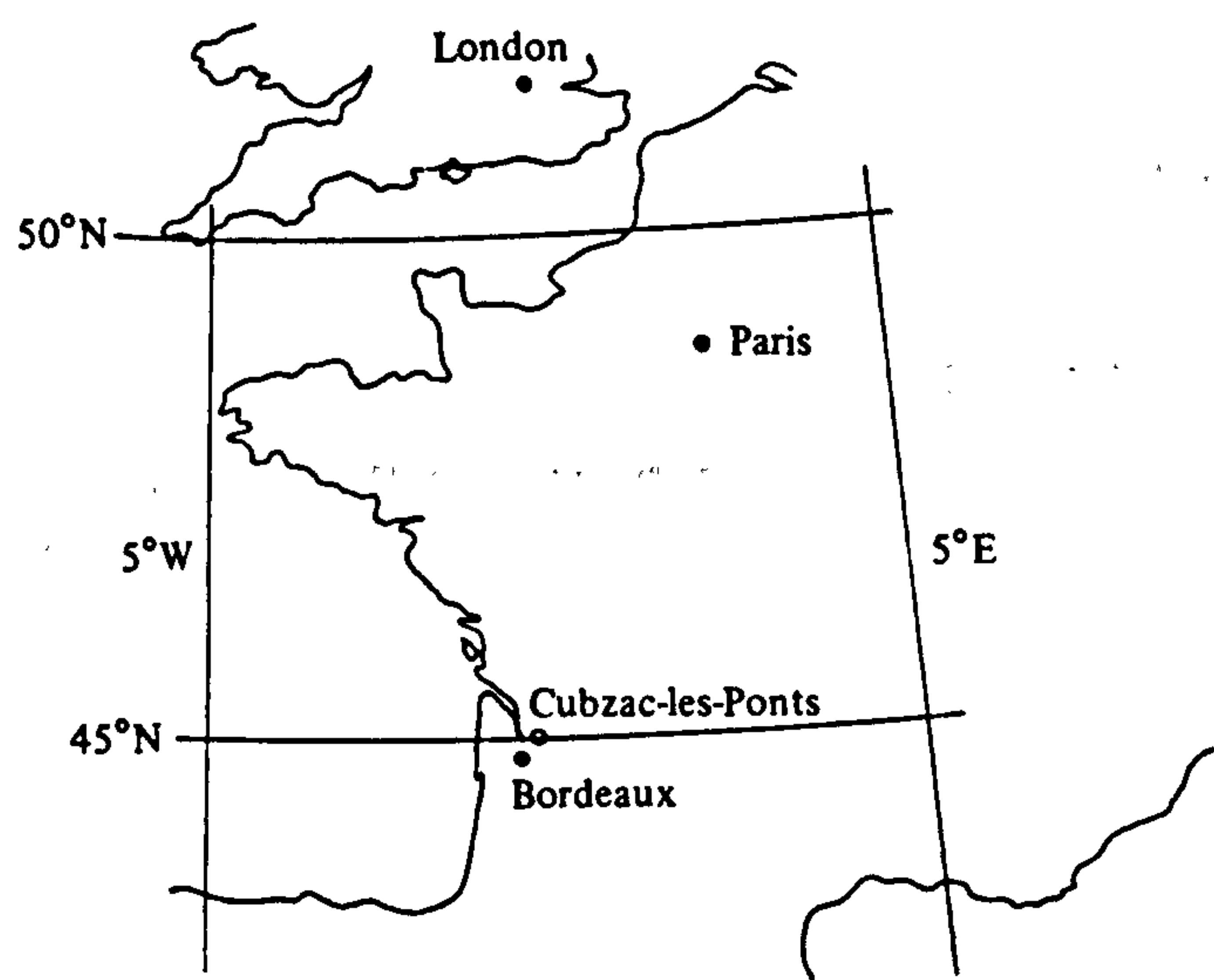


Fig 4.1(b). Section through valley of the Dordogne at Cubzac-les-Ponts (Magnan, Mieussens, and Queyroi, 1983).

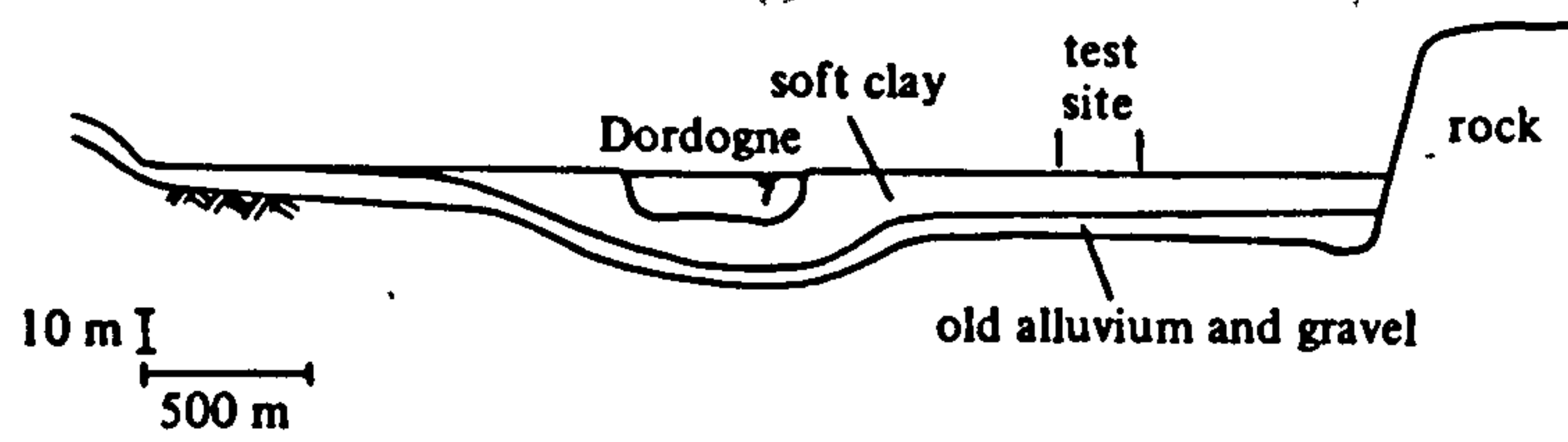


Fig 4.2. Geometry of trial embankment A at Cubzac-les-Ponts.

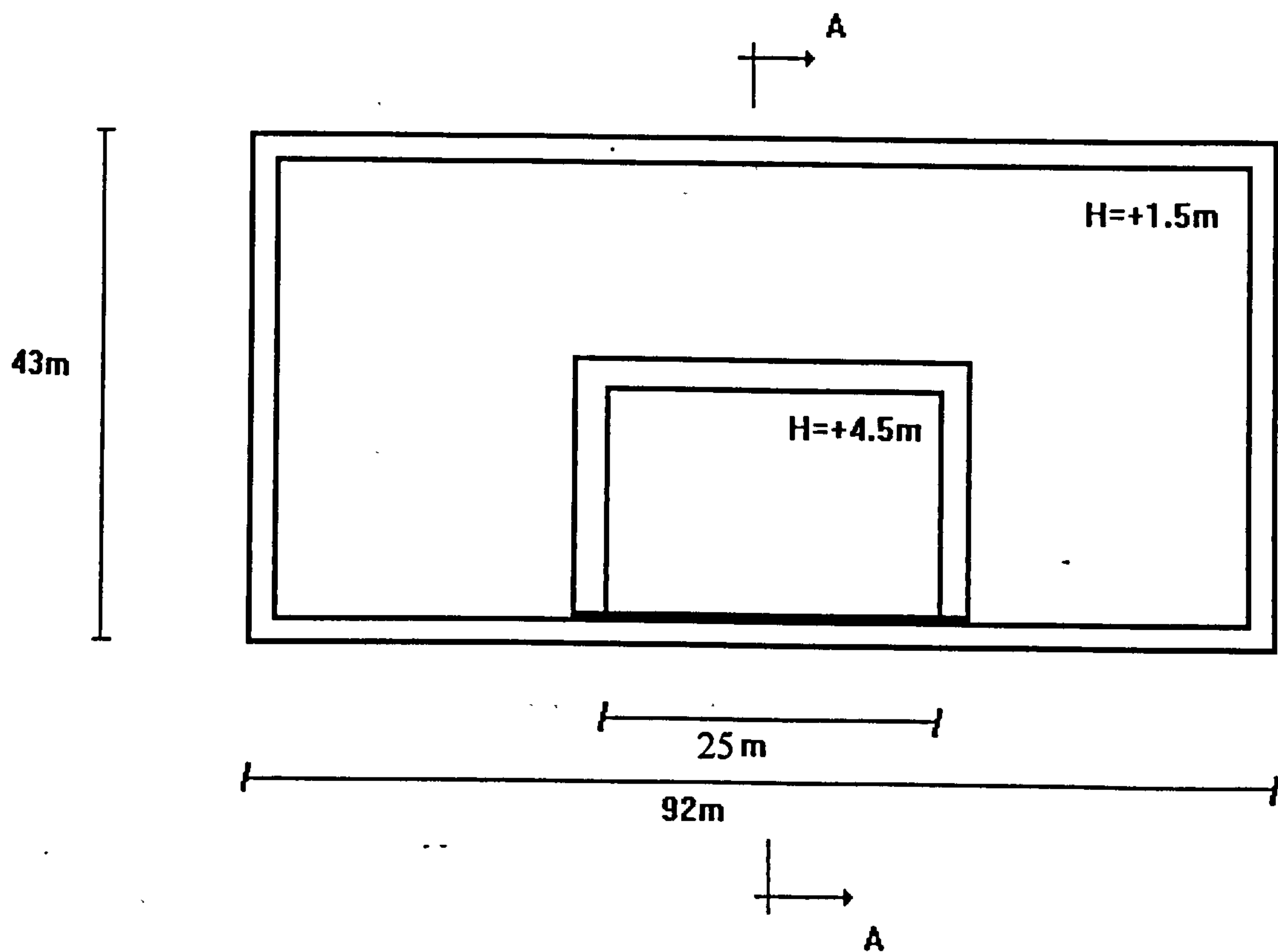
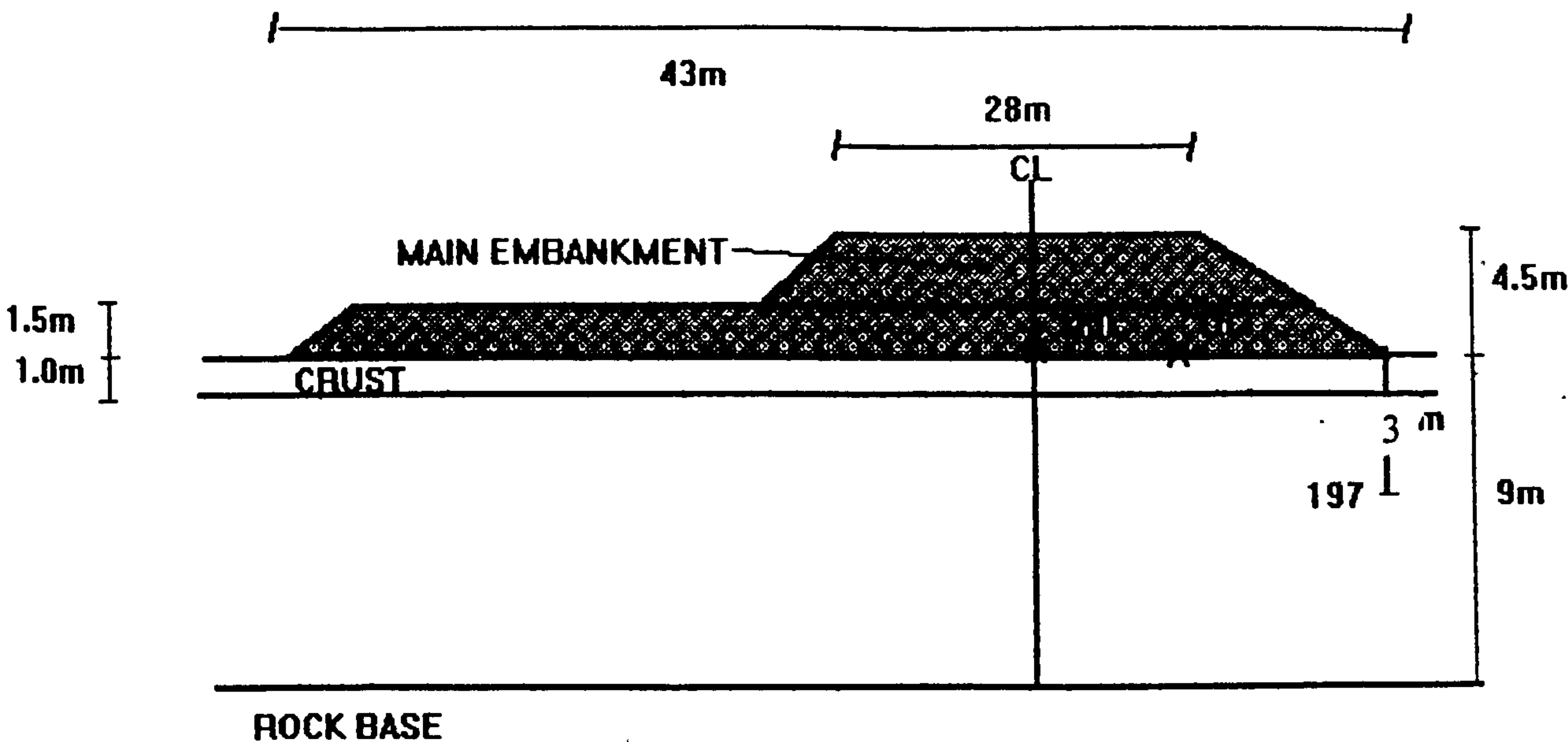


Fig 4.3. Instrumentation section



PIEZOMETERS AT 1.0m INTERVALS FROM 1.0m DEPTH TO 8m DEPTH ON CENTRE LINE OF MAIN EMBANKMENT.

Fig 4.4. Features of MELANIE soil model (Leroueil et al., 1985 and Muir Wood, 1990).

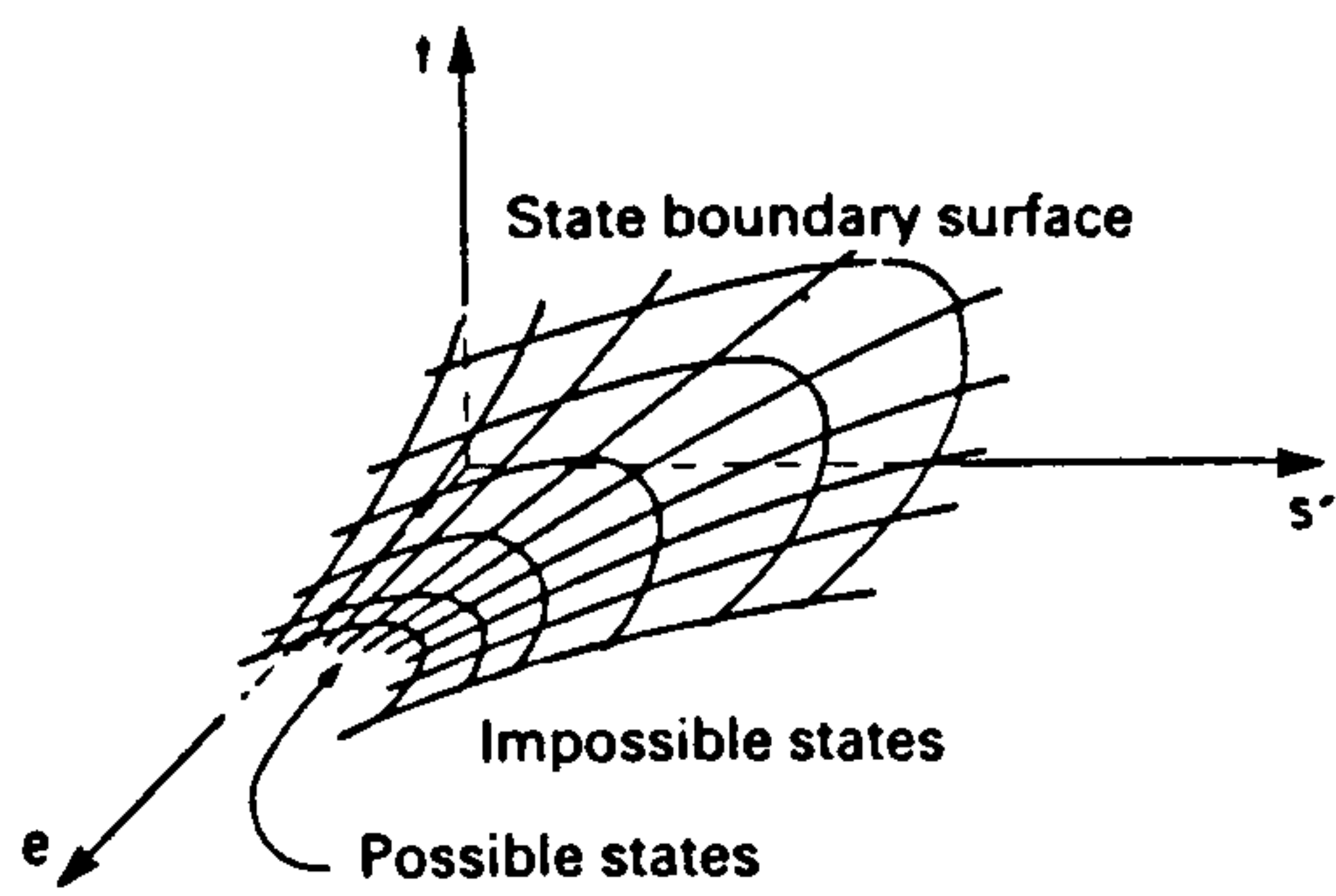


Fig 4.4(a). State boundary surface for natural clays. (Leroueil et al., 1985)

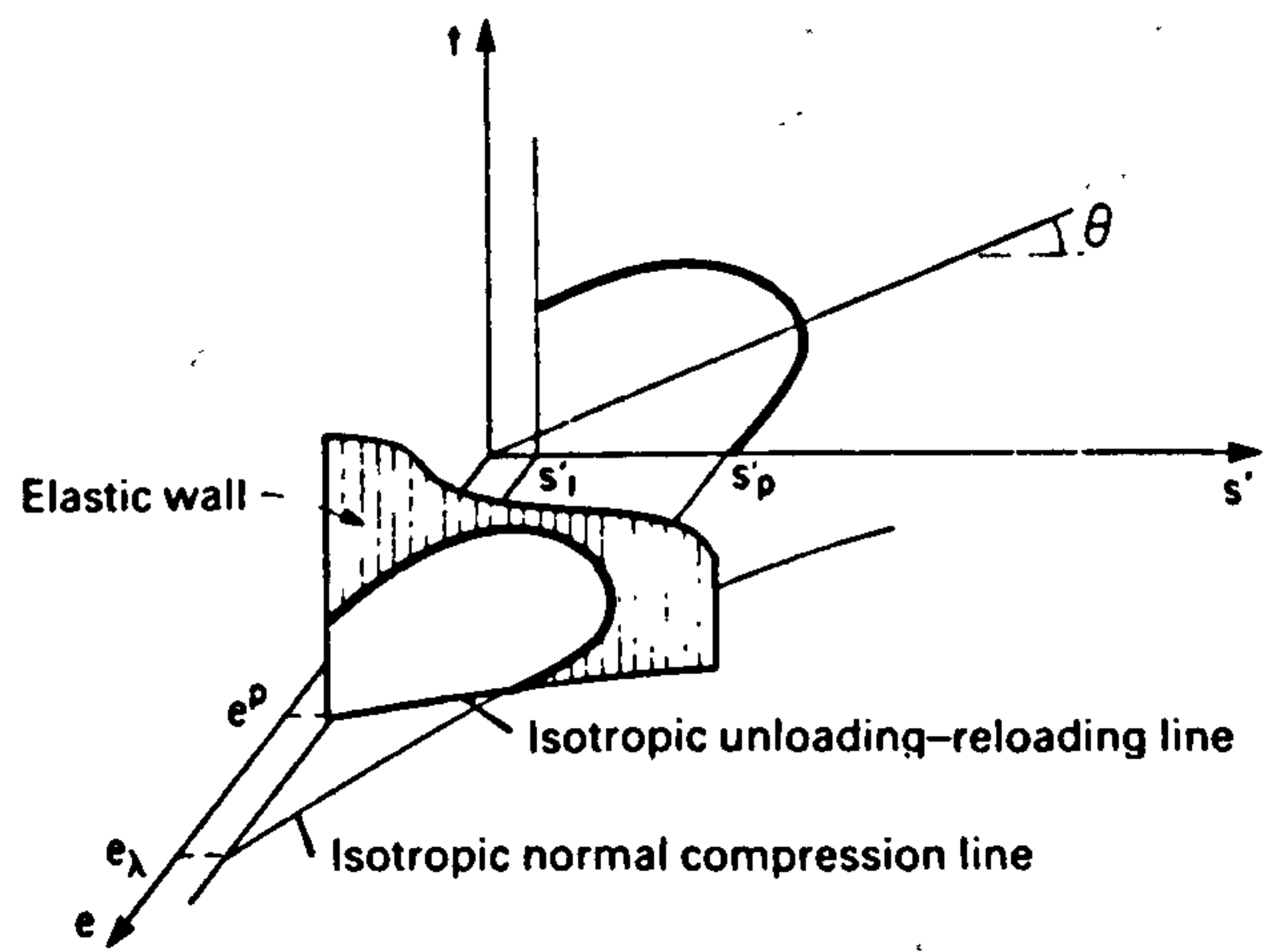


Fig 4.4(b). Description of the state boundary surface. (Leroueil et al., 1985)

Fig 4.4(c). Yield loci (yl) and plastic potentials (pp) assumed for clay at Cubzac-les-Ponts, plotted in s' : t effective stress plane. (Muir Wood, 1990)

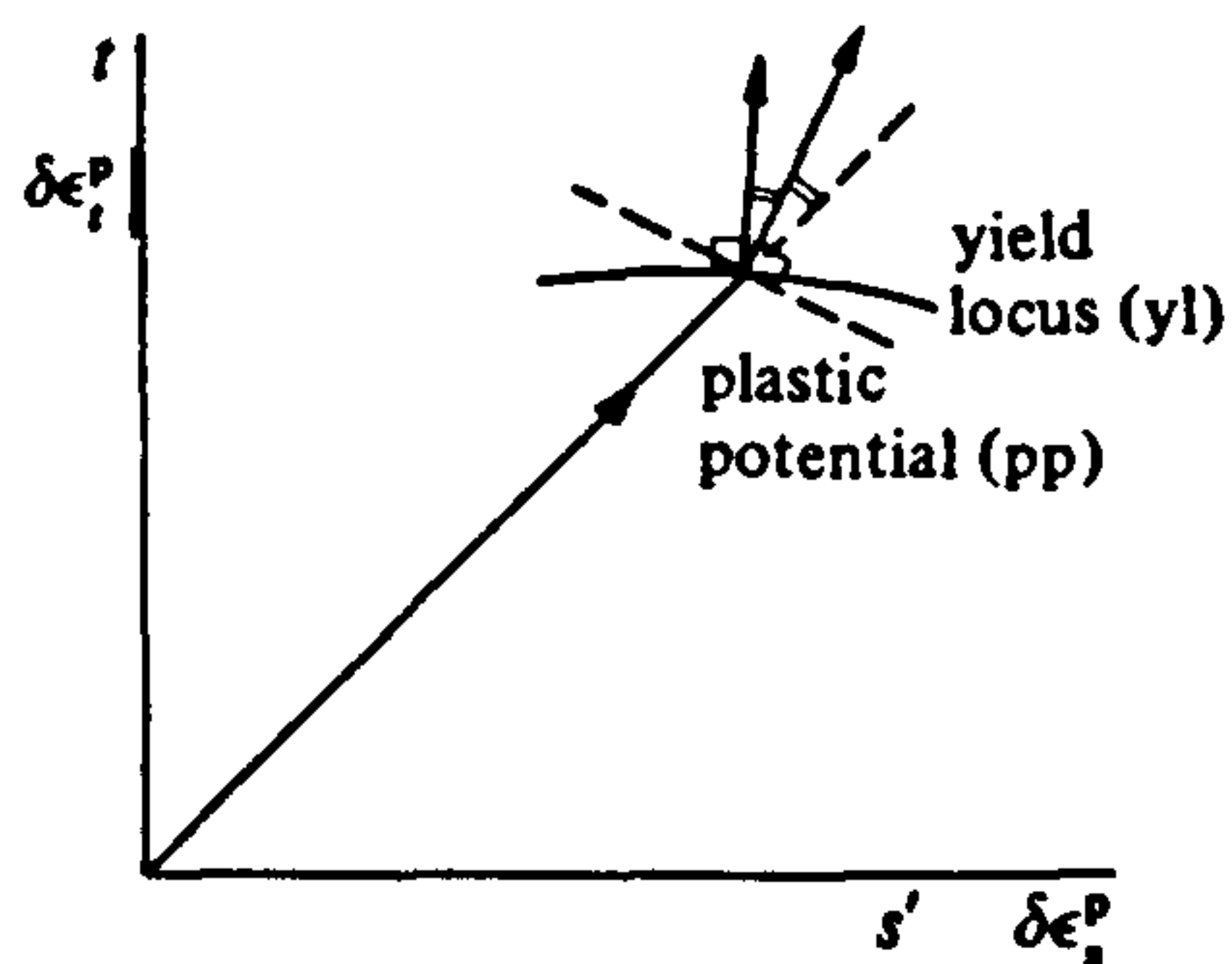
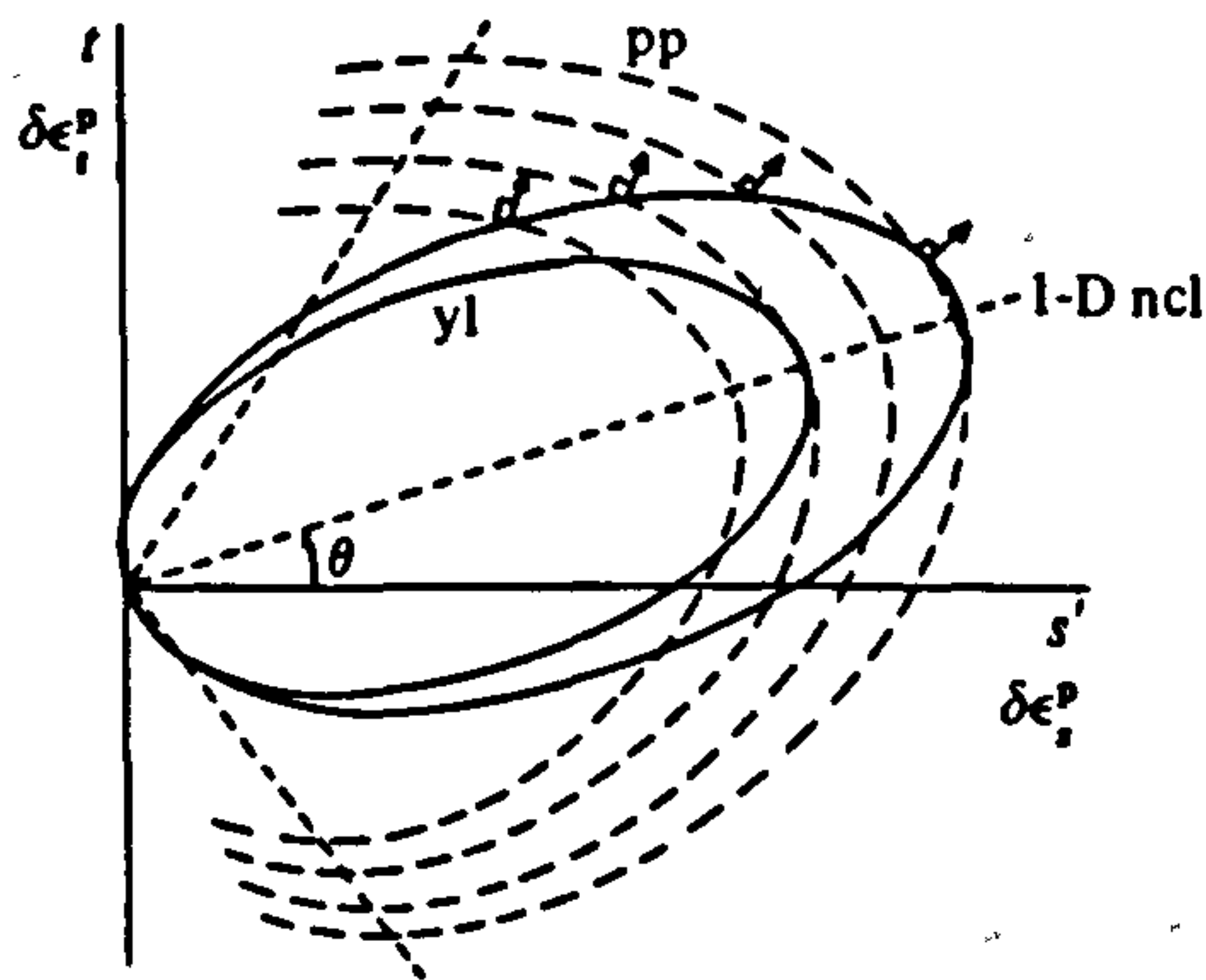


Fig 4.4(d). Direction of plastic strain increment vector stress vector and normal to yield locus. (Muir Wood, 1990)

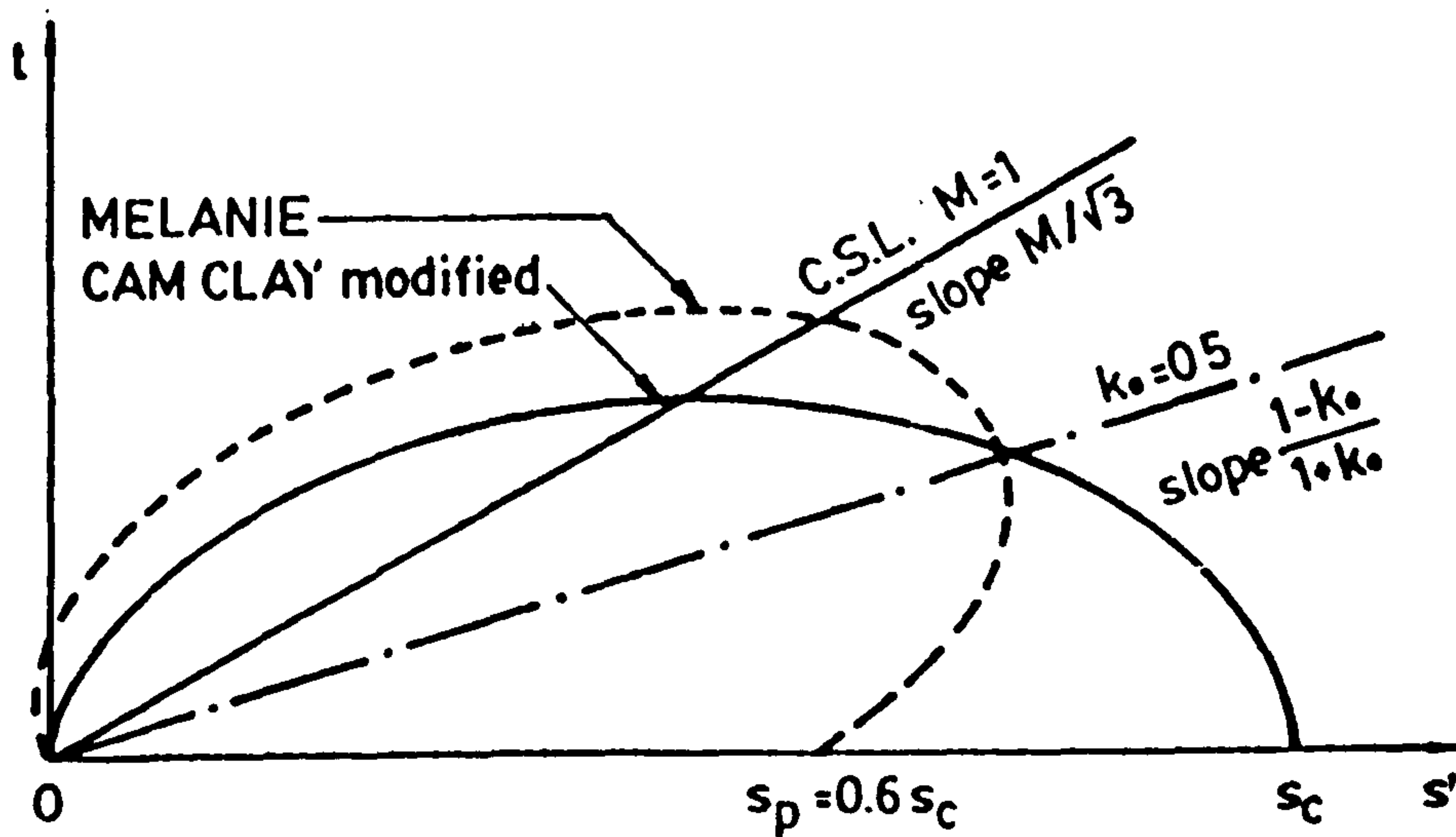


Fig 4.4(e). Comparison of MELANIE and modified Cam clay soil models plotted in s' : t effective stress plane. (Tavenas et al., 1982)

FIGURE 4.5
SOIL INDEX PROPERTIES

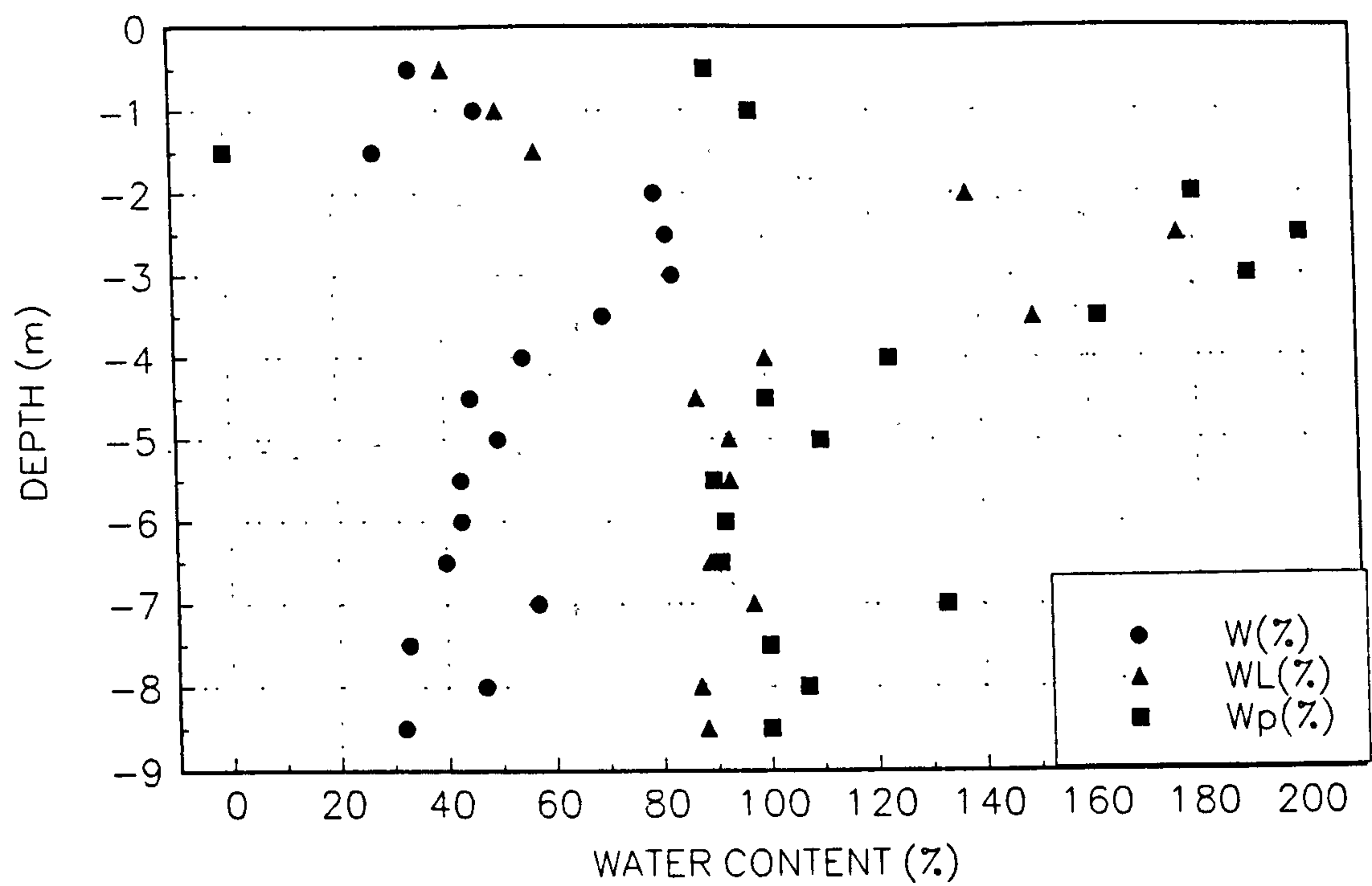


FIGURE 4.6
VARIATION OF UNIT WEIGHT WITH DEPTH

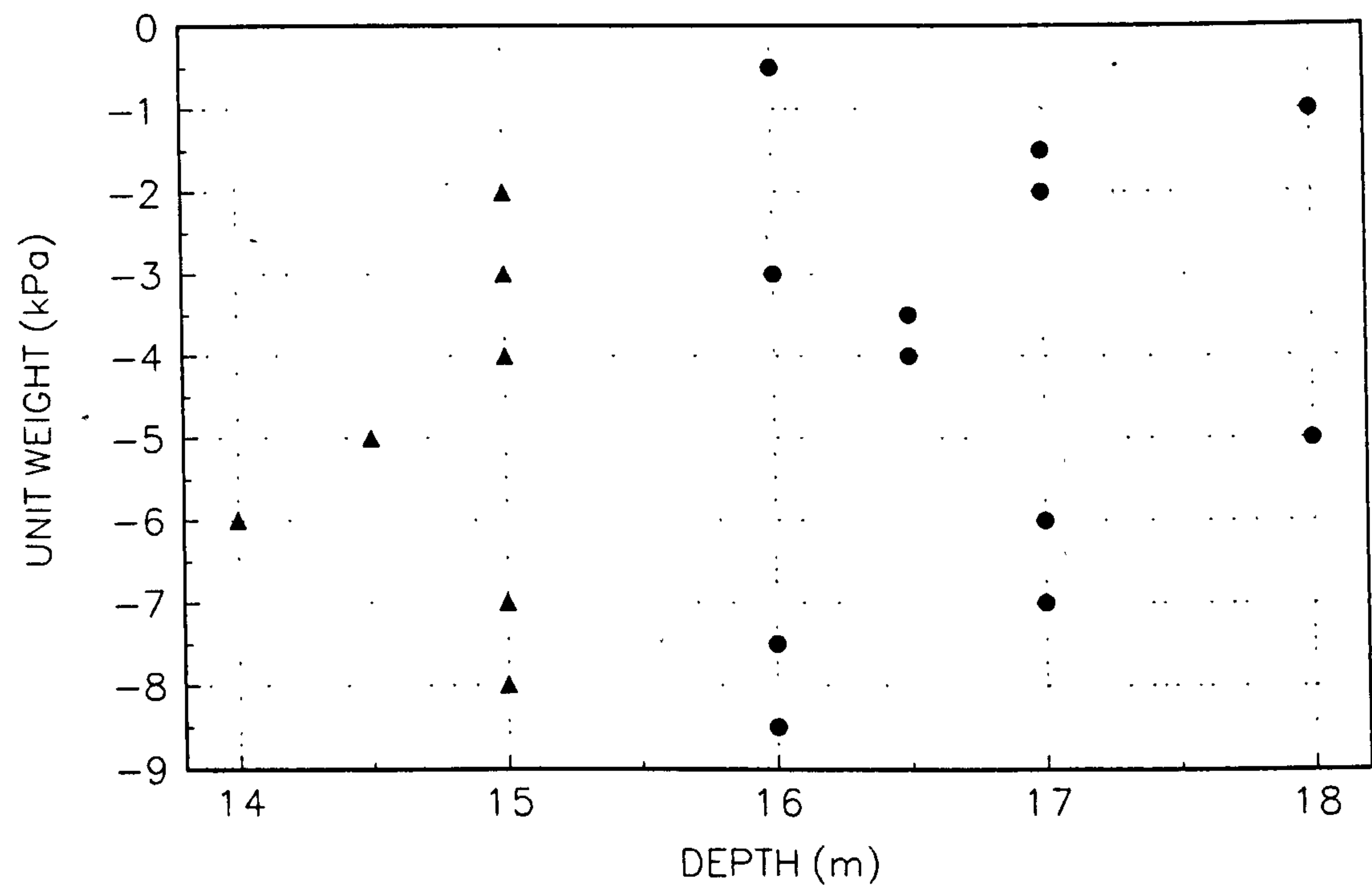


FIGURE 4.7
UNDRAINED SHEAR STRENGTH PROFILE

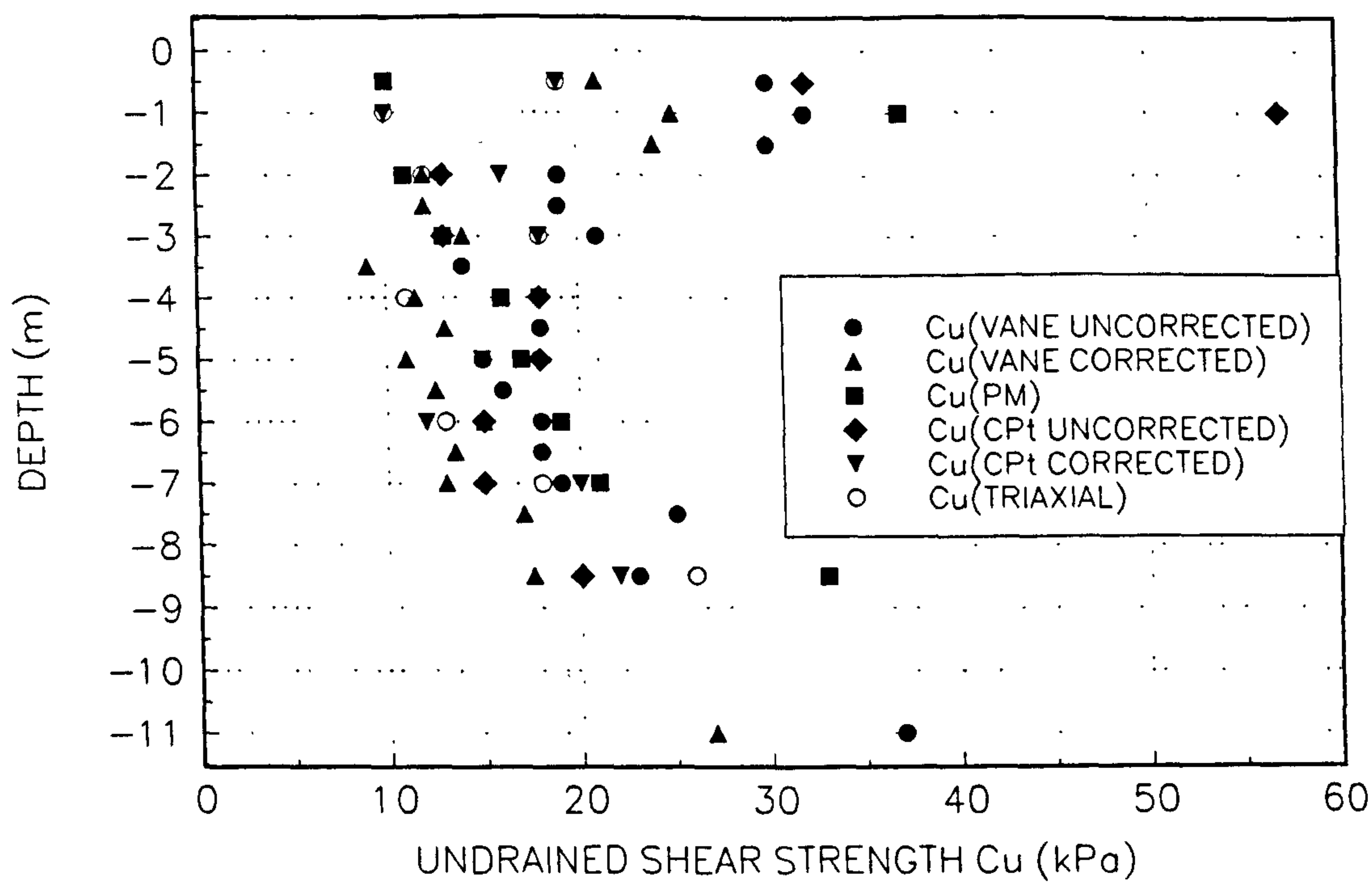


FIGURE 4.8
EFFECTIVE SHEAR STRESS PARAMETERS

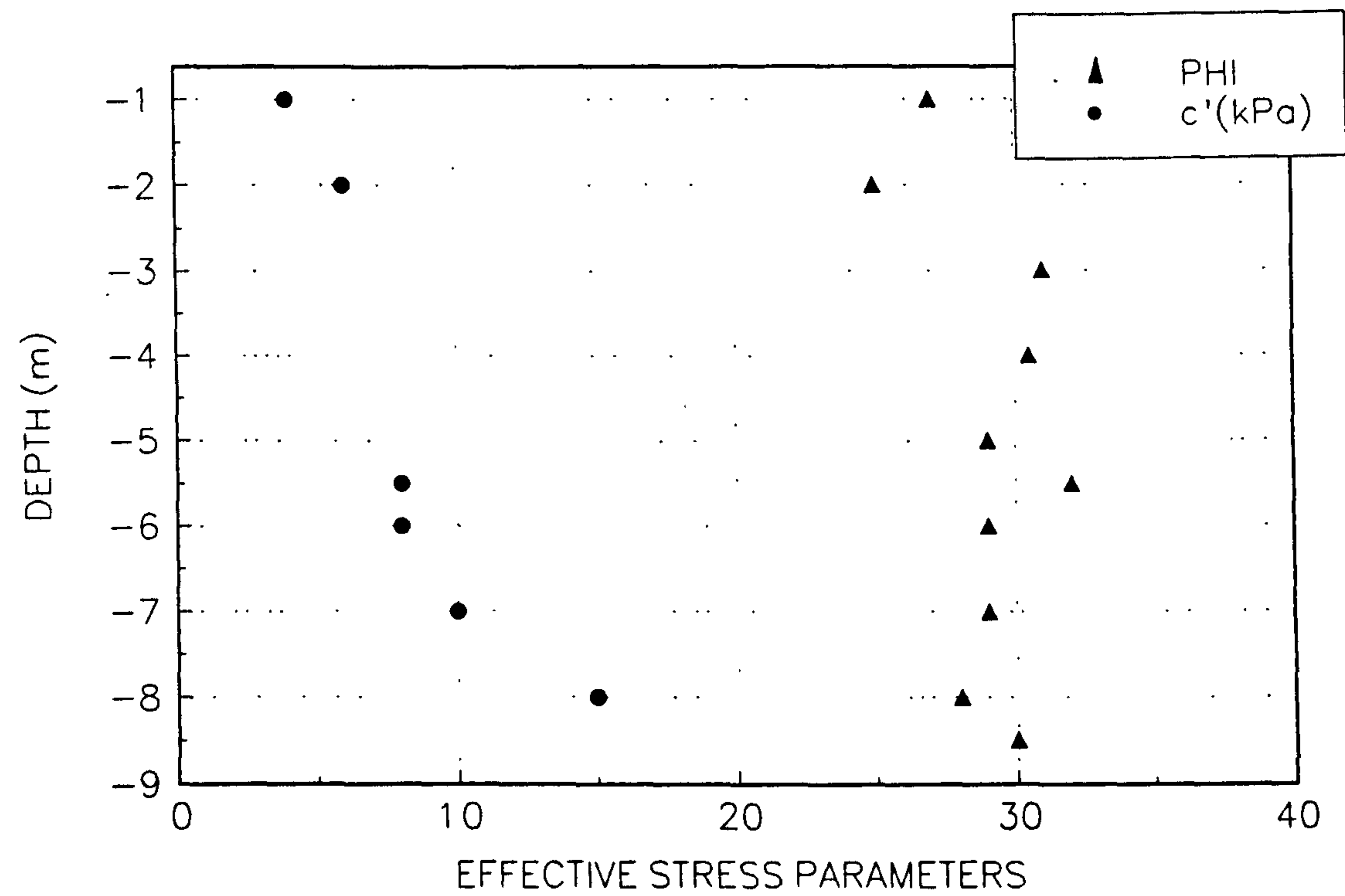


FIGURE 4.9
PRECONSOLIDATION STRESS PROFILE WITH DEPTH

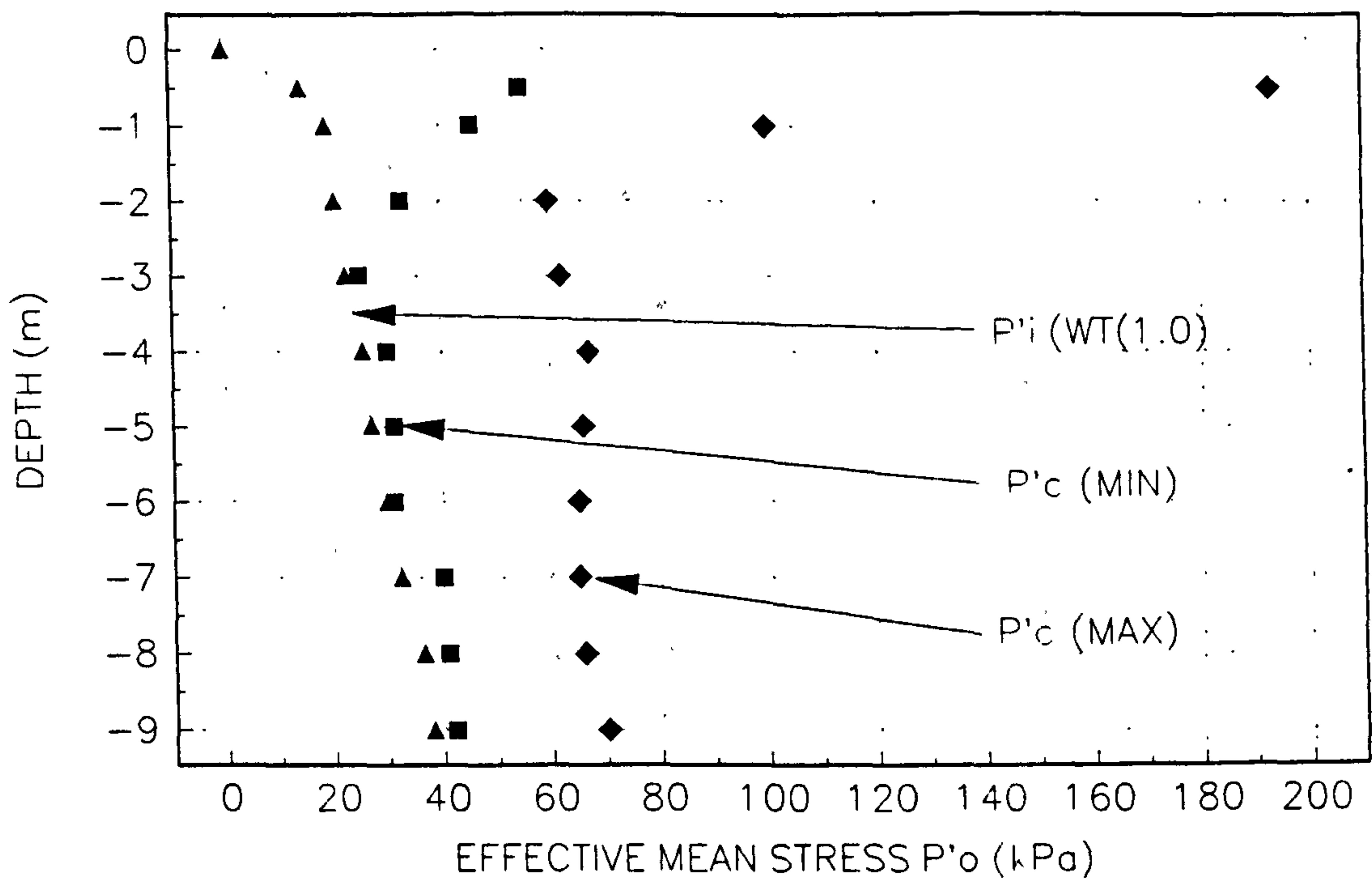


FIGURE 4.10
REFERENCE VALUES OF VOID RATIO

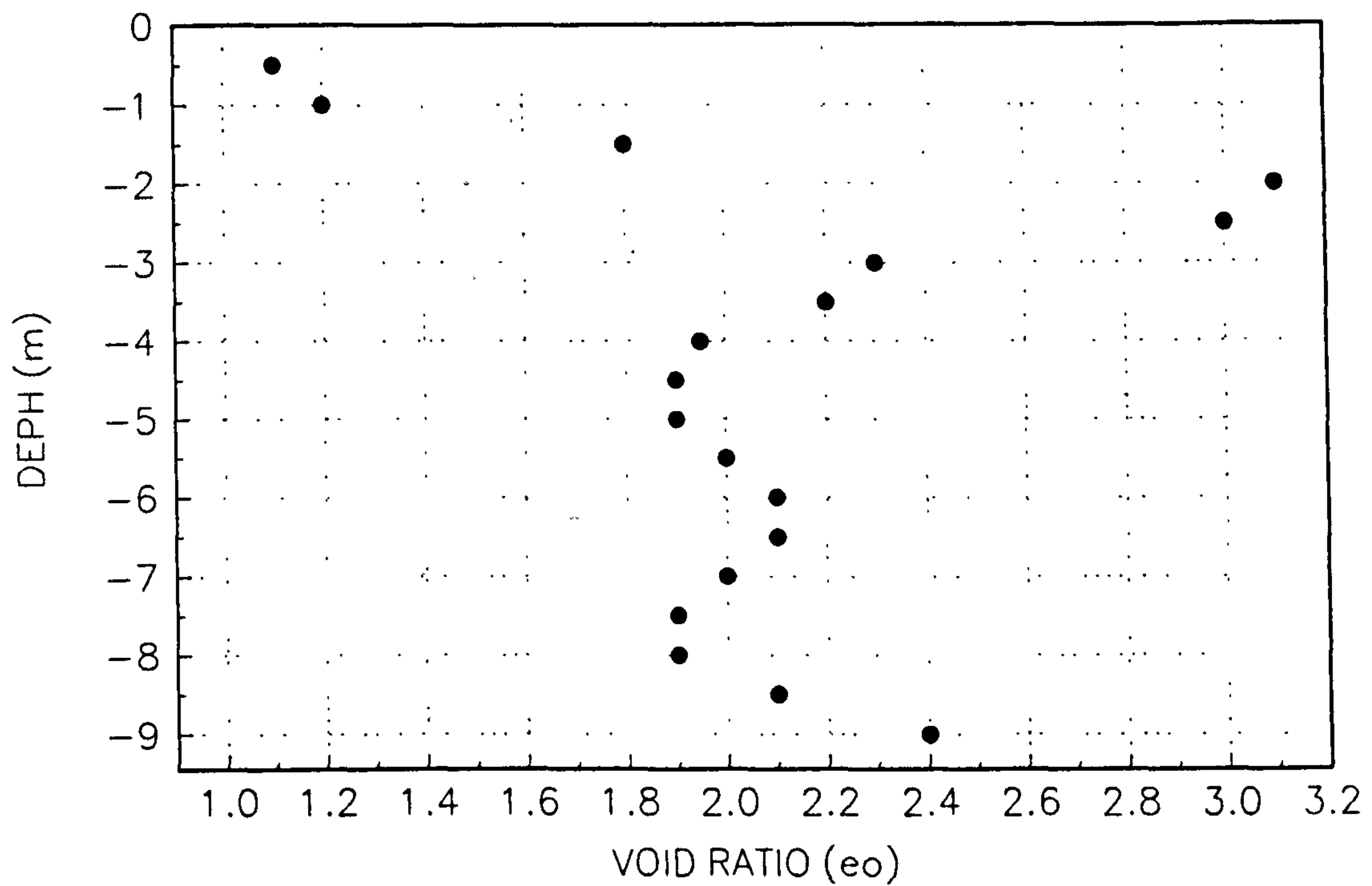


FIGURE 4.11
COMPARISON OF AVERAGE AND MINIMUM VALUES OF KAPPA

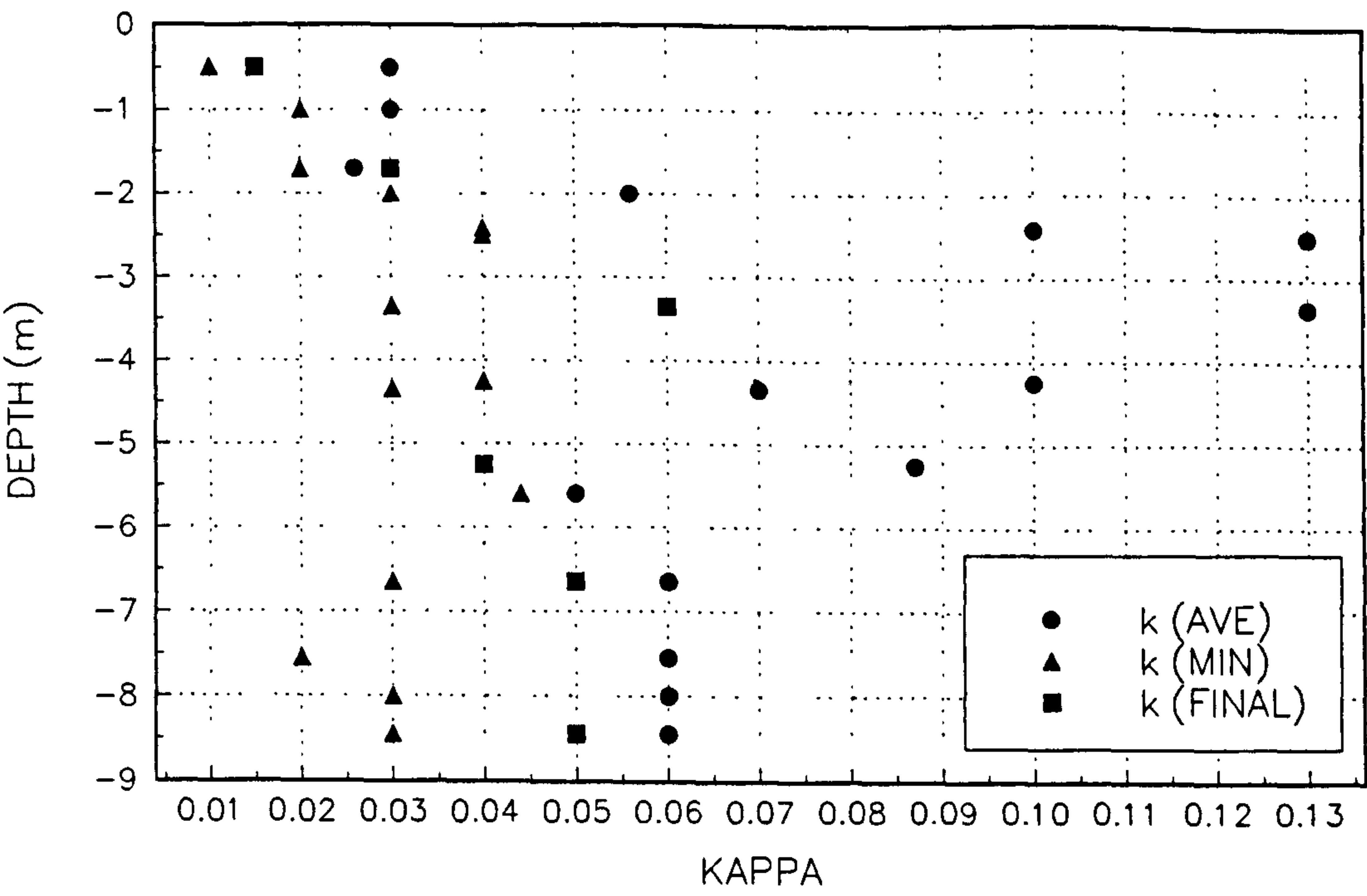
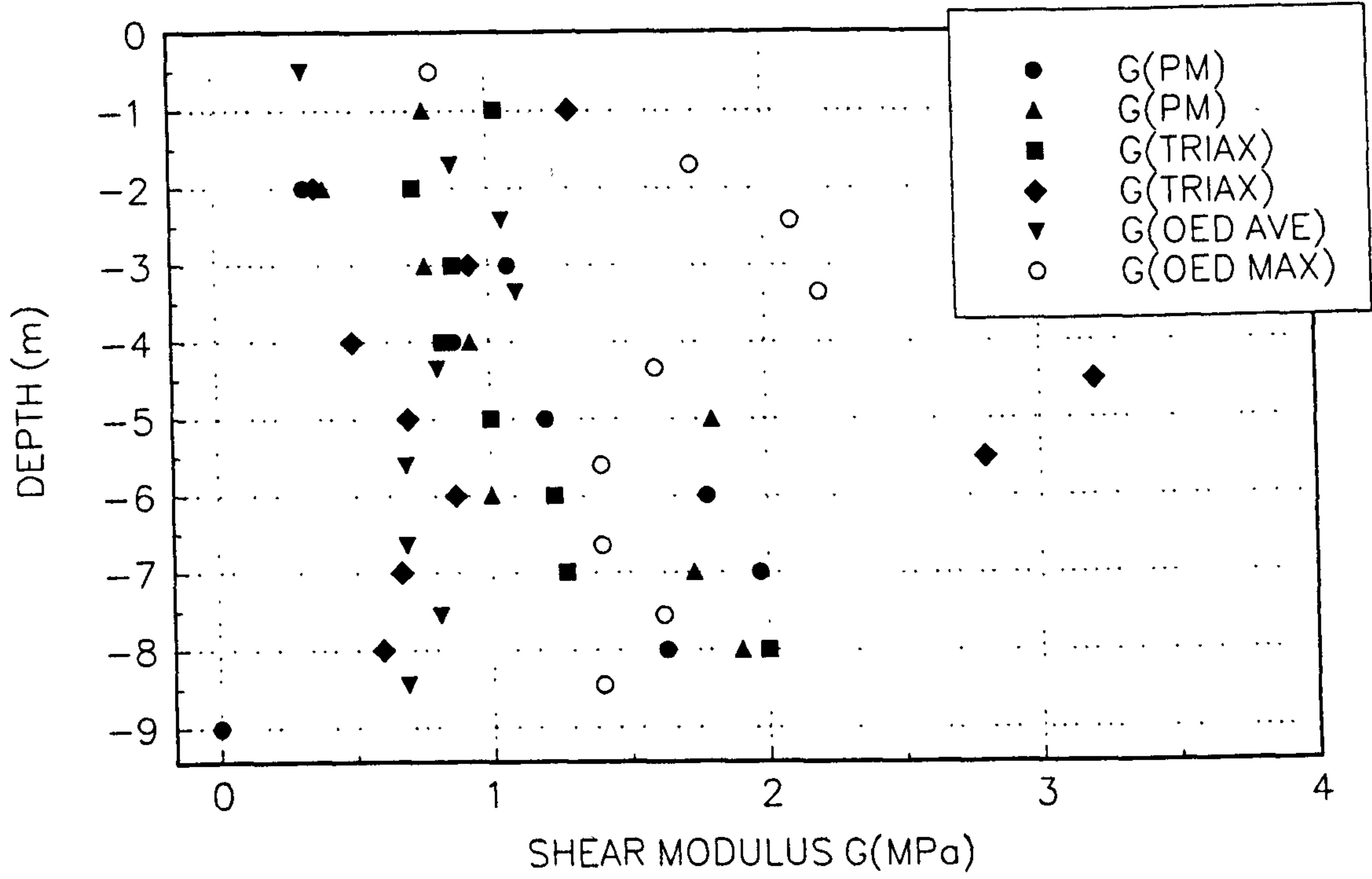


FIGURE 4.12
FOUNDATION ELASTIC STIFFNESS (G)



- Watkins, R. K. (1967), 'Pipeline economy through design of backfill', *Proc. ASCE, Journal of the Pipeline Division*, 93(PL3), 45-57.
- Weaver, W. and Johnston, P. R. (1984), *Finite elements for Structural analysis* (Prentice and Hall, Inc, New York).
- Wroth, C.P. (1972), 'General theories of earth pressure and deformation', in *Proc. 5th European Conf. on Soil Mechanics and Foundation Engineering., Madrid* (Madrid: Sociedad Española de Mecanica del Suelo y Cimentaciones), vol. 2, pp33-52.
- Wroth, C.P. (1975), 'In-situ measurement of initial stresses and deformation characteristics', in *Proc. Speciality Conf. on In-situ Measurement of Soil Properties, Raleigh, North Carolina* (New York: ASCE), vol. 2, pp181-230.
- Youssef, M. S., el Ramli, A. H., and el Demery, M. (1965), 'Relationships between shear strength, consolidation, liquid limit, and plastic limit for remoulded clays', in *Proc. 6th Int. Conf. on Soil Mechanics and Foundation Engineering, Montreal* (Toronto: Toronto University Press), vol. 1, 126-129.
- Zienkiewicz, O.C. (1977), *The finite element method (3rd ed.)* (Maidenhead: McGraw-Hill).
- Zienkiewicz, O.C. (1976), 'Plasticity and some of its corollaries in soil mechanics. Collapse and continuing deformation under load repetition', in *Proc. 2nd Int. Conf. Numerical Methods in ASCE, Blackburg*, Vol. 3, 1275-1303.
- Zienkiewicz, O.C., Humpheson, C. and Lewis, R.W. (1975), 'Associated and non-associated visco-plasticity and plasticity in soil mechanics', *Géotechnique* 25(4), 671-689.
- Zytynski, M., Randolph, M.F., Nova, R., and Wroth, C.P. (1978), 'On modelling the unloading-reloading behaviour of soils', *Int. J. for Numerical and Analytical Methods in Geomechanics* 2, 87-94.

FIGURE 4.1 3
FOUNDATION STIFFNESS RATIOS

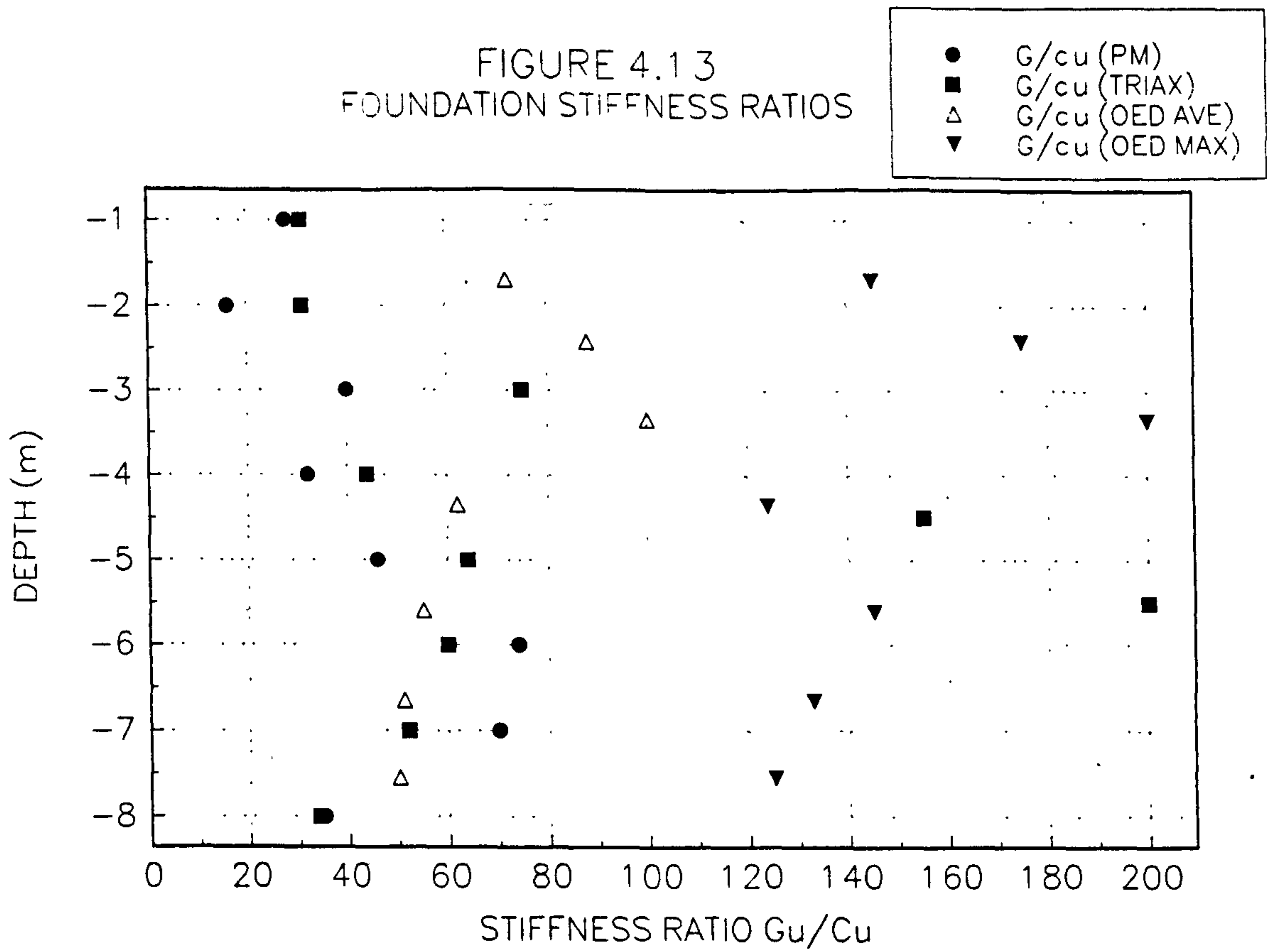


FIGURE 4.1 4
VARIATION OF PLASTICITY INDEX I_p

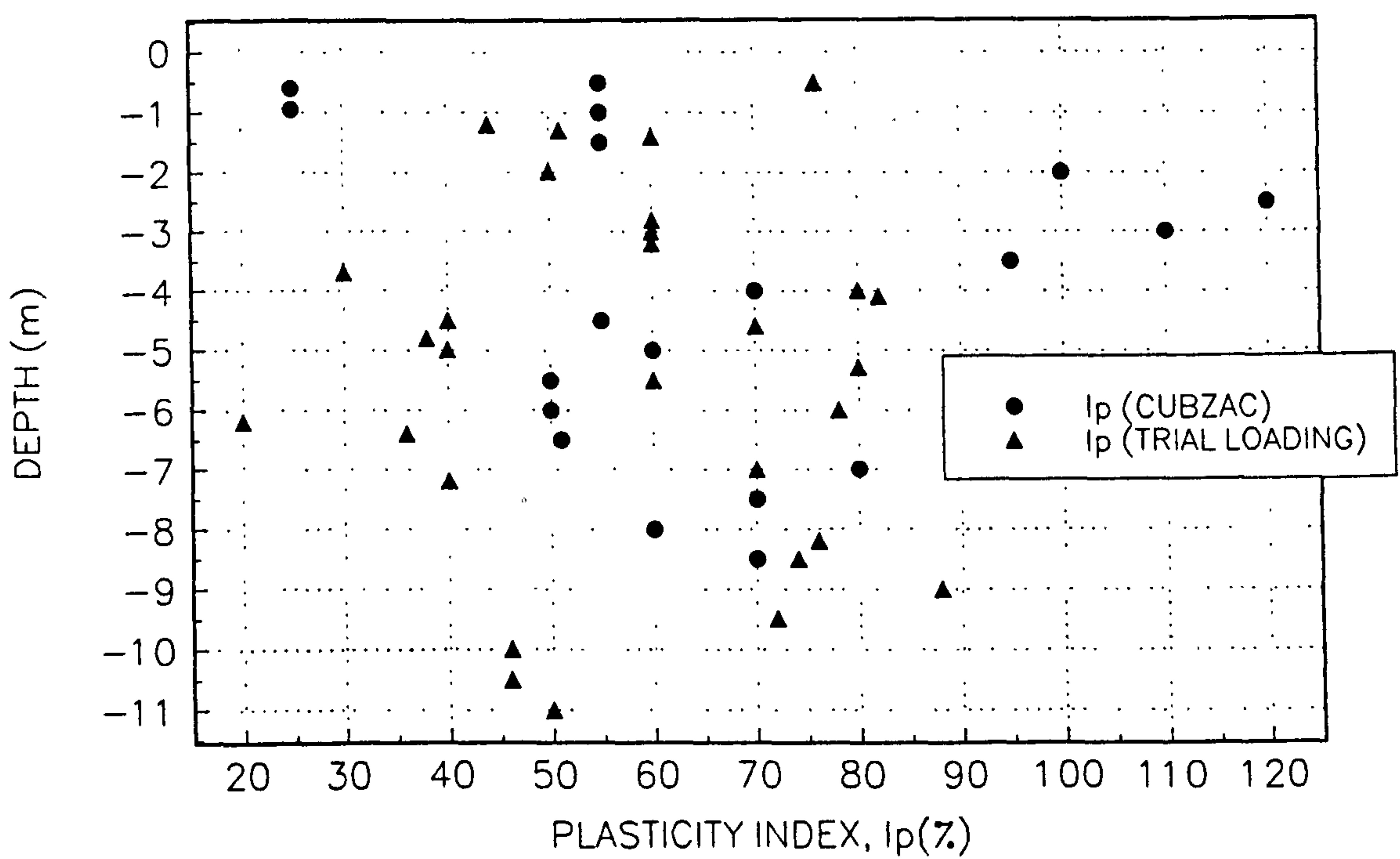


FIGURE 4.15
DEGREE OF OVERCONSOLIDATION n

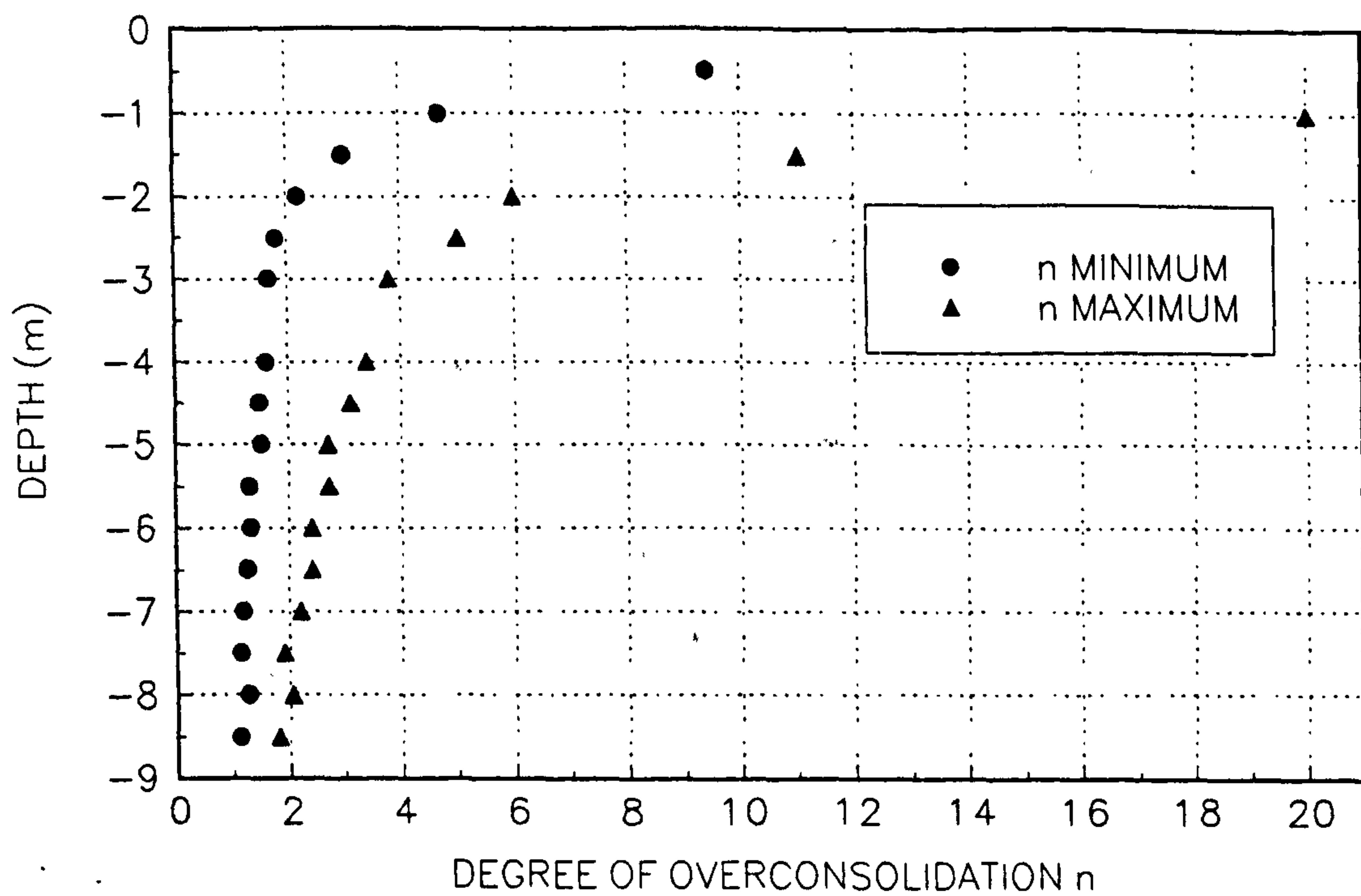


FIGURE 4.16
NORMALISED SECANT MODULUS G/c_u PLOTTED AGAINST SHEAR STRAIN

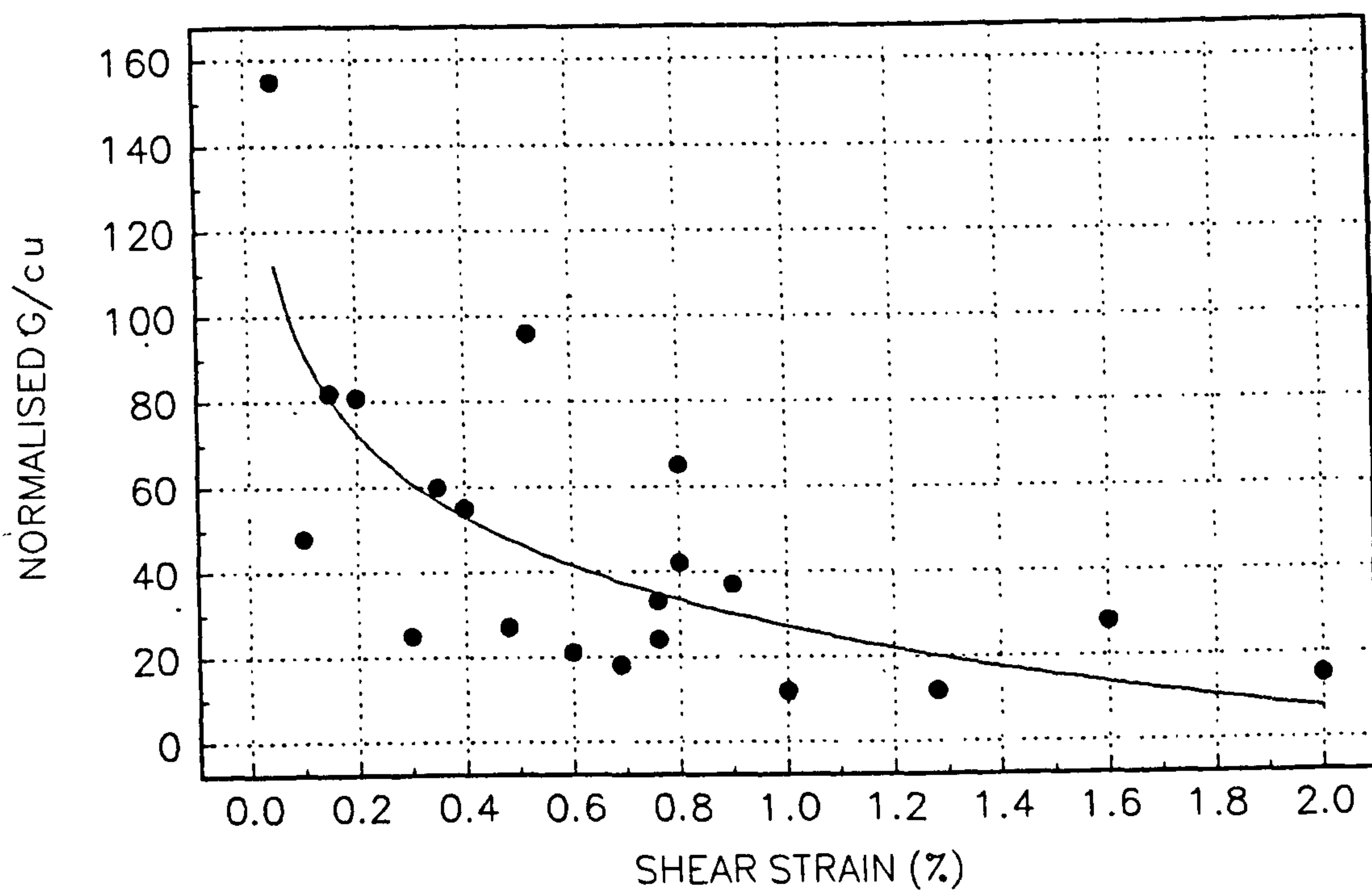


FIGURE 4.17(a)
PLOT OF COMPRESSIBILITY AGAINST PLASTICITY INDEX

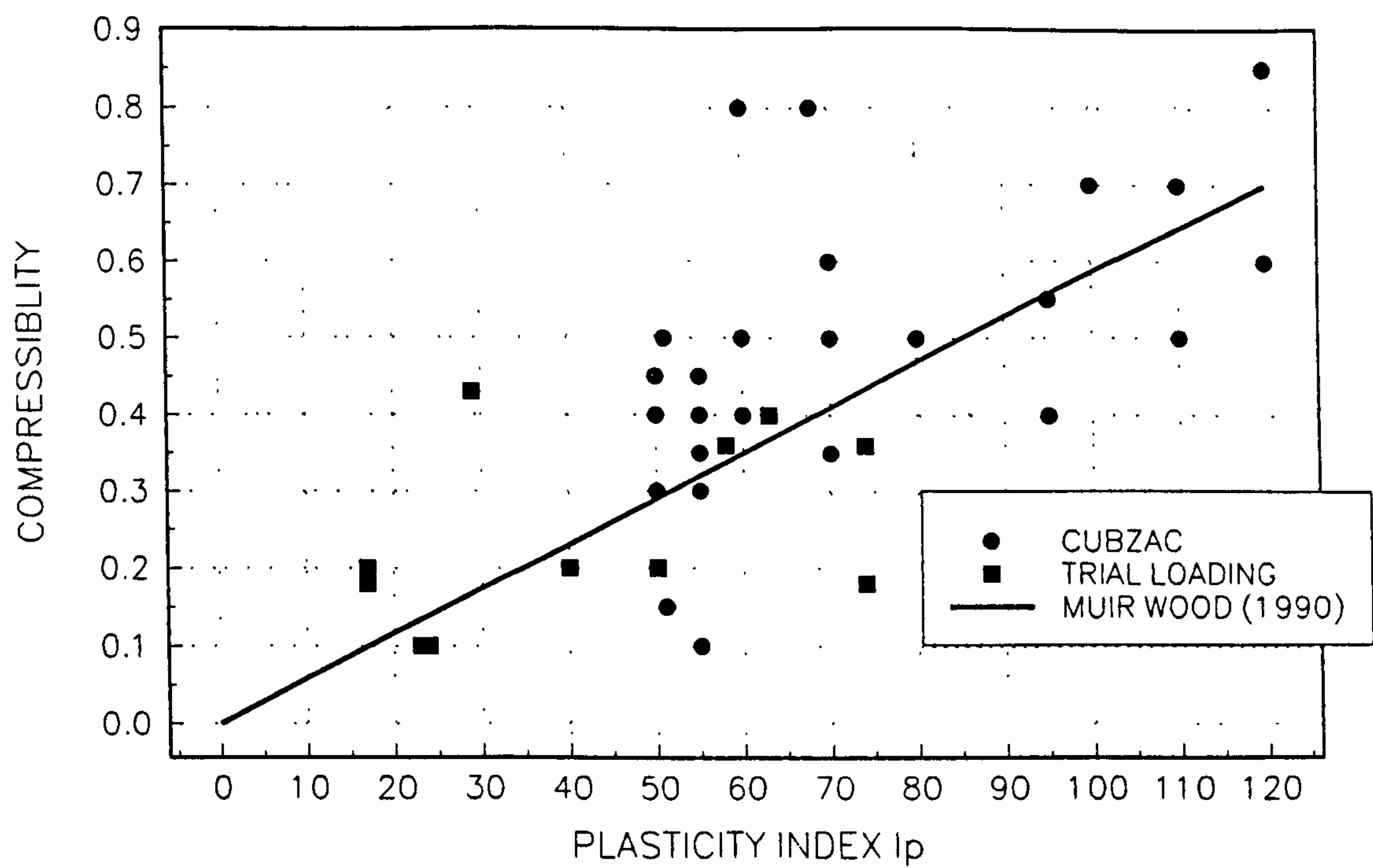


Fig 4.17(b). Data of parameter Λ and plasticity index, I_p (Mayne, 1980 and Muir Wood, 1990)

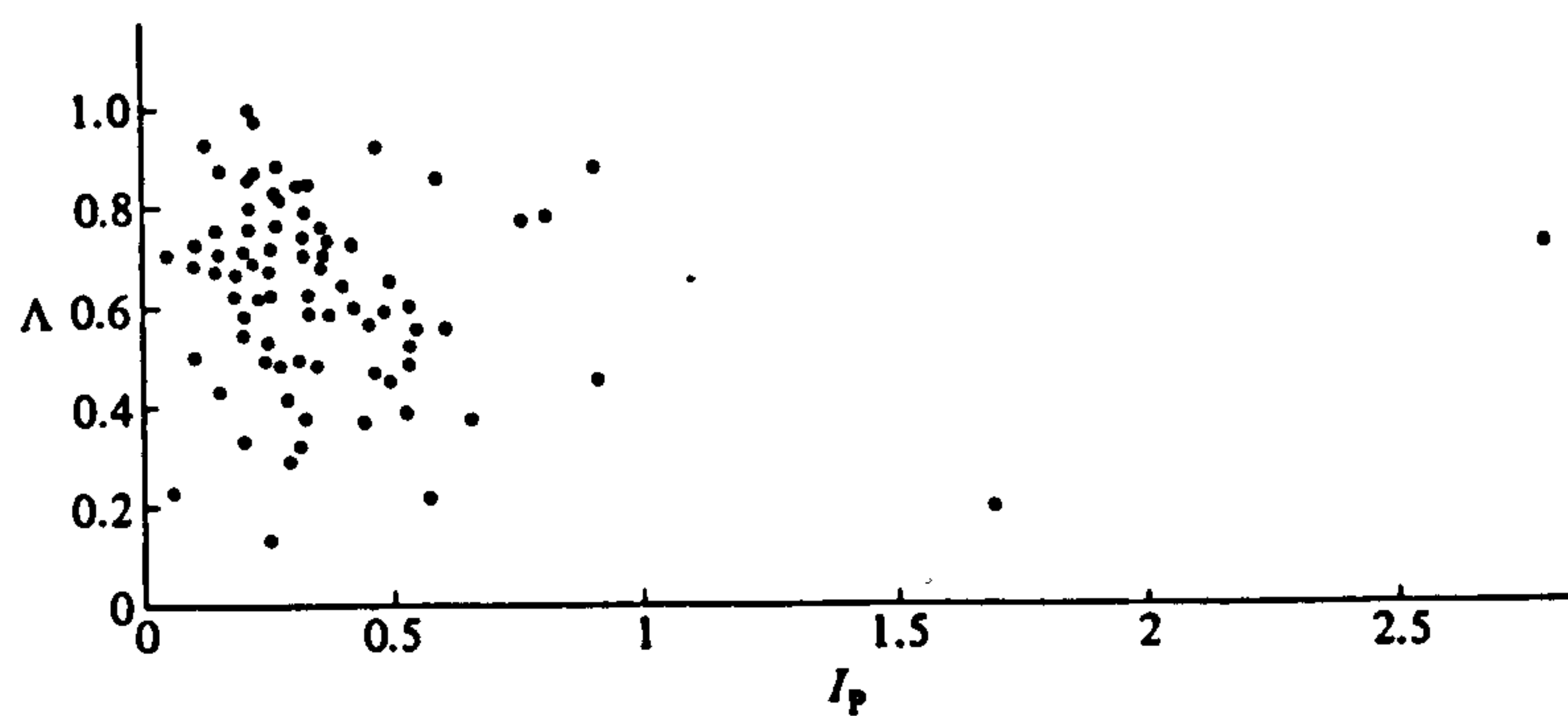


FIGURE 4.18
VARIATION OF PARAMETER PHI

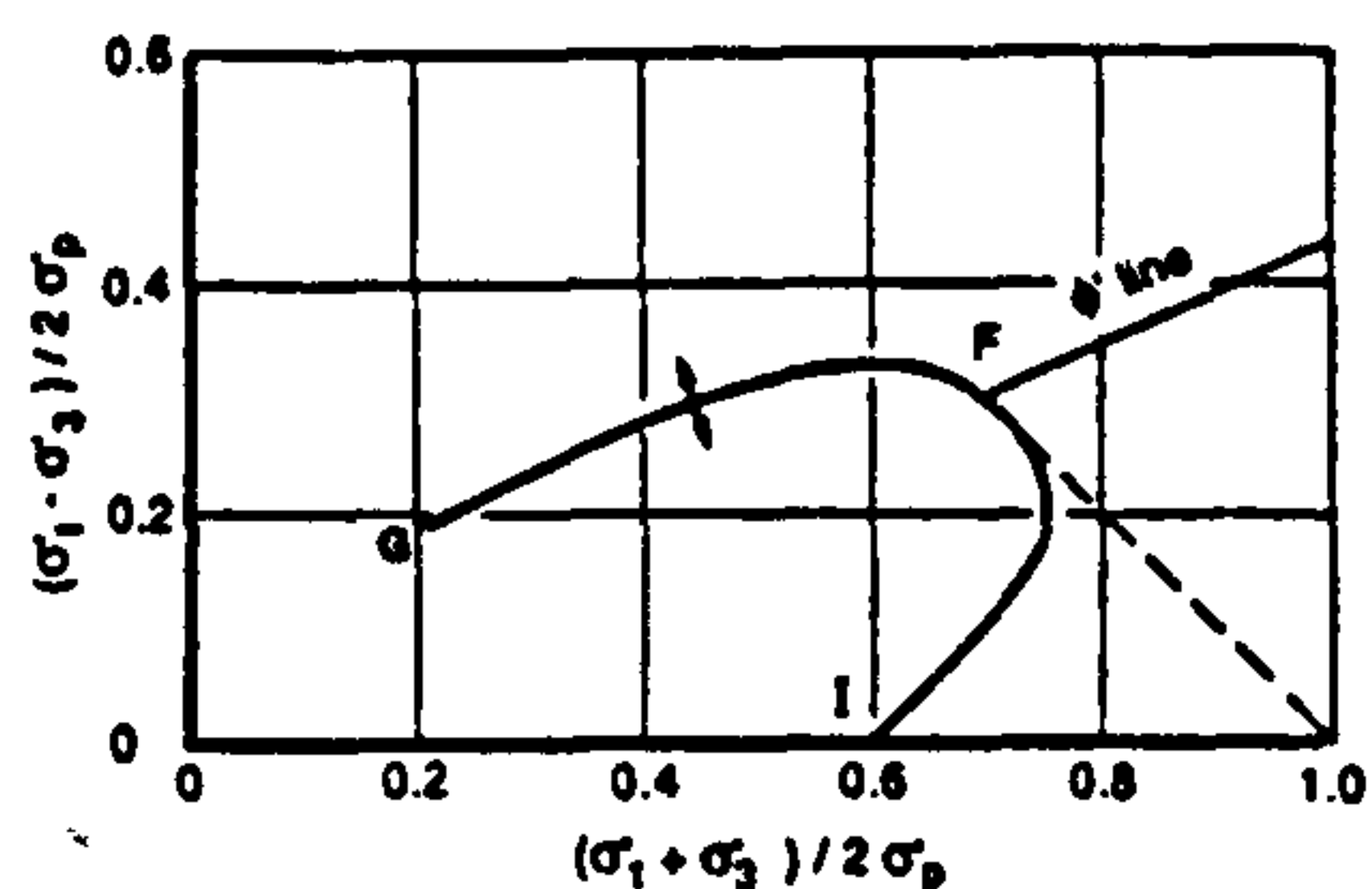
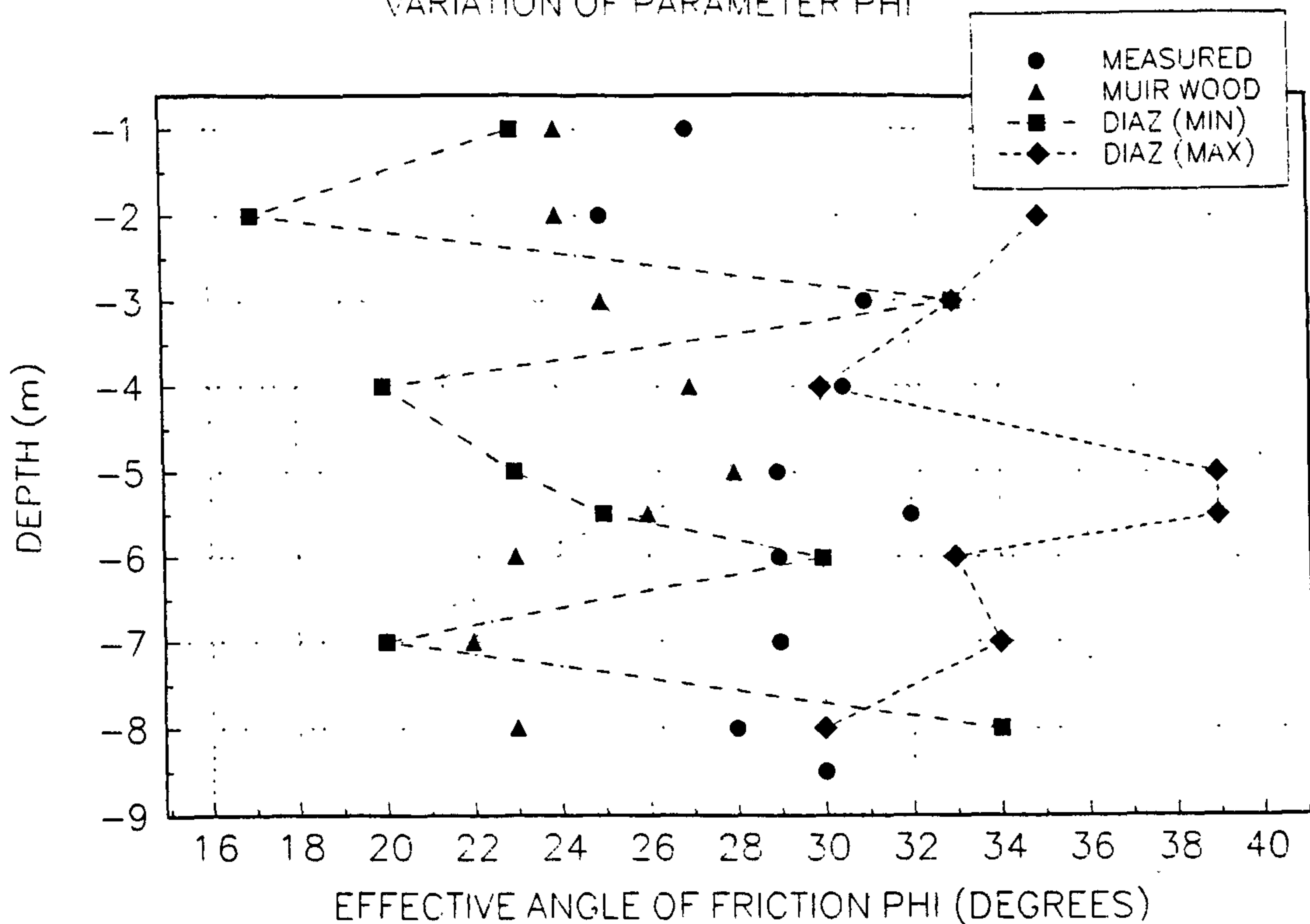


Fig 4.19. Schematic yield curve (Diaz-Rodriguez et al., 1992).

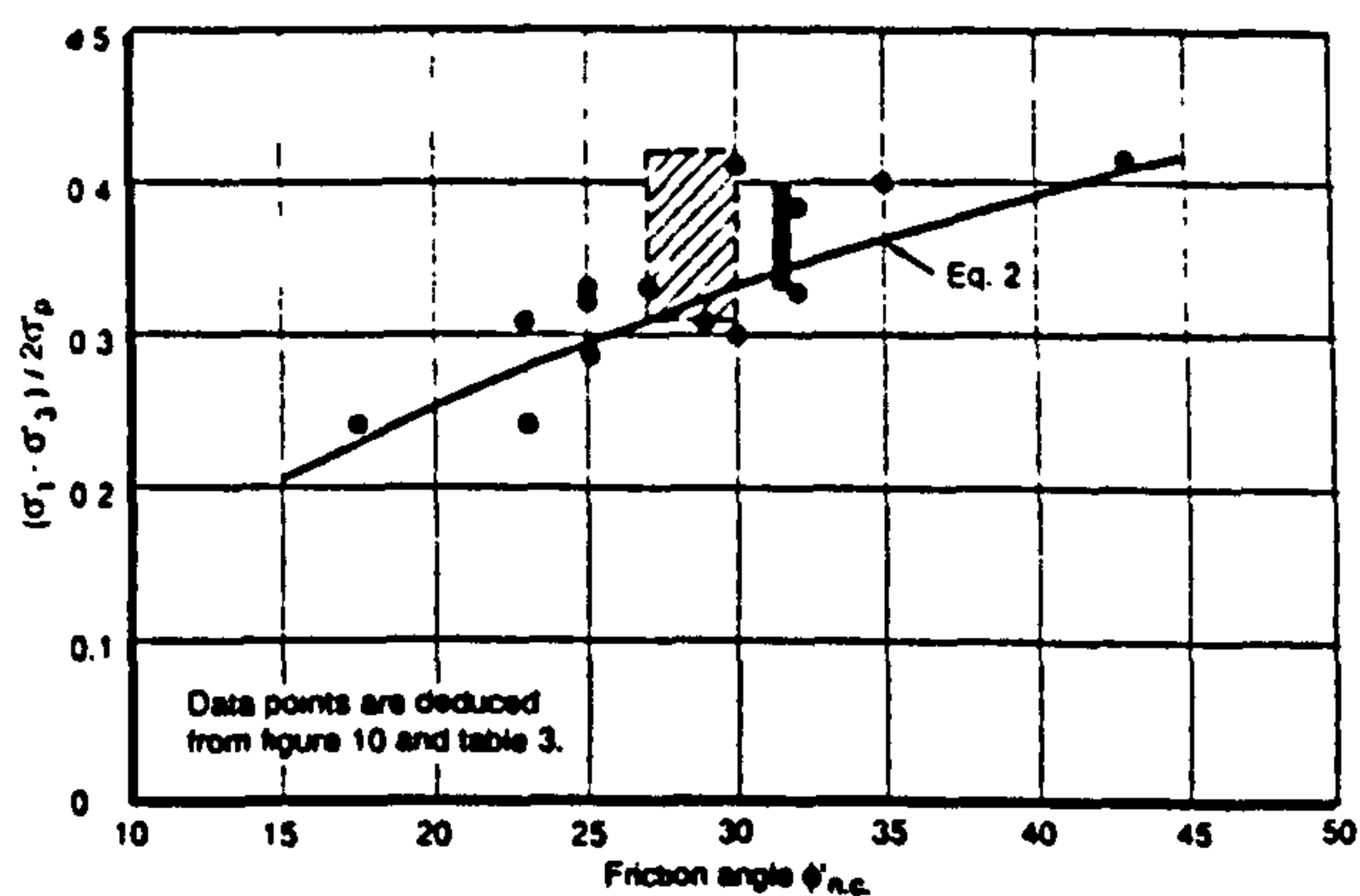


Fig 4.20. Maximum $(\sigma'_1 - \sigma'_3)/2\sigma'_p$ measured values as a function of friction angle in normally consolidated range. Data points are deduced from Table 4.3.

FIGURE 4.21
STRESS HISTORY FOR UNDRAINED ANALYSES

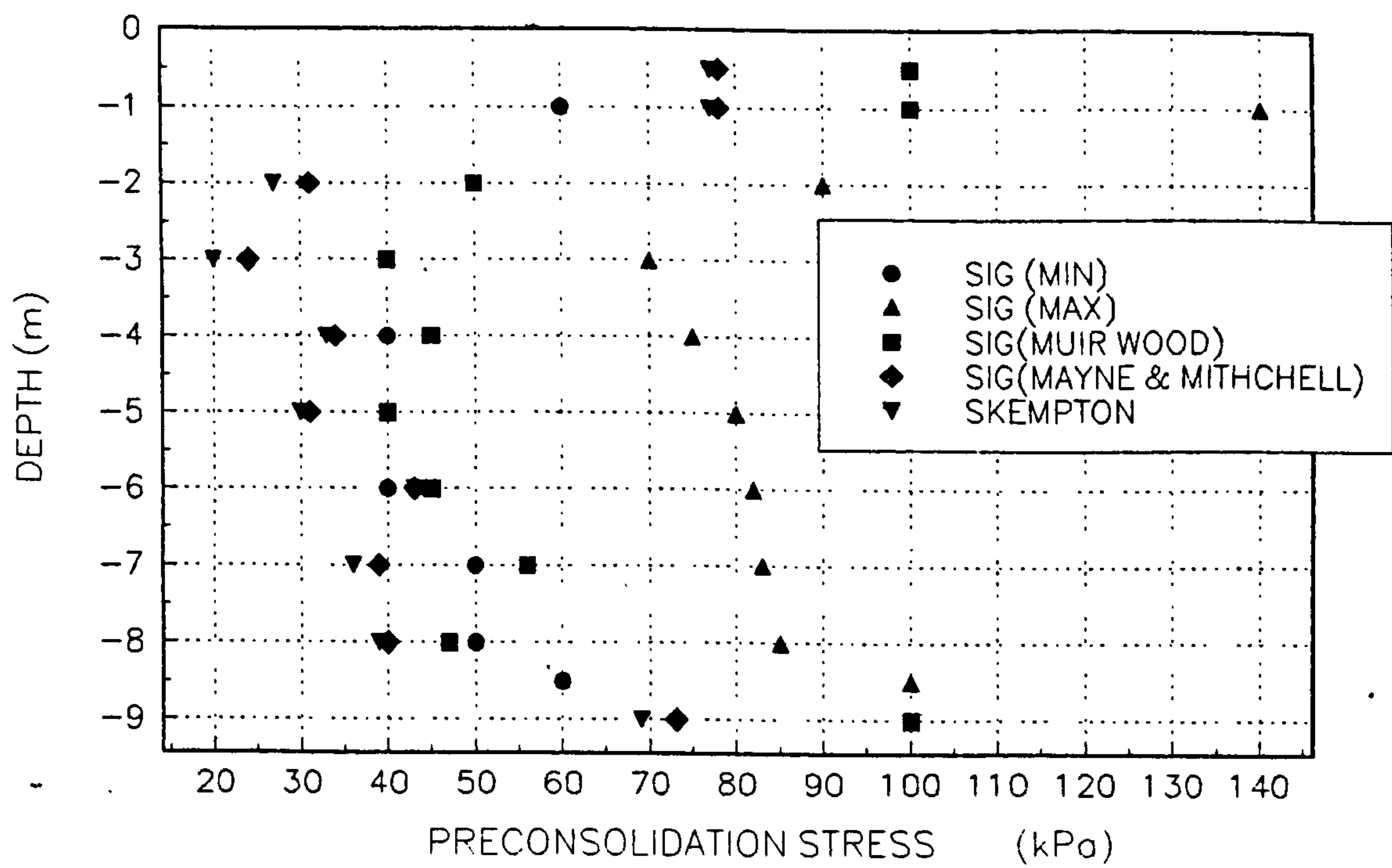
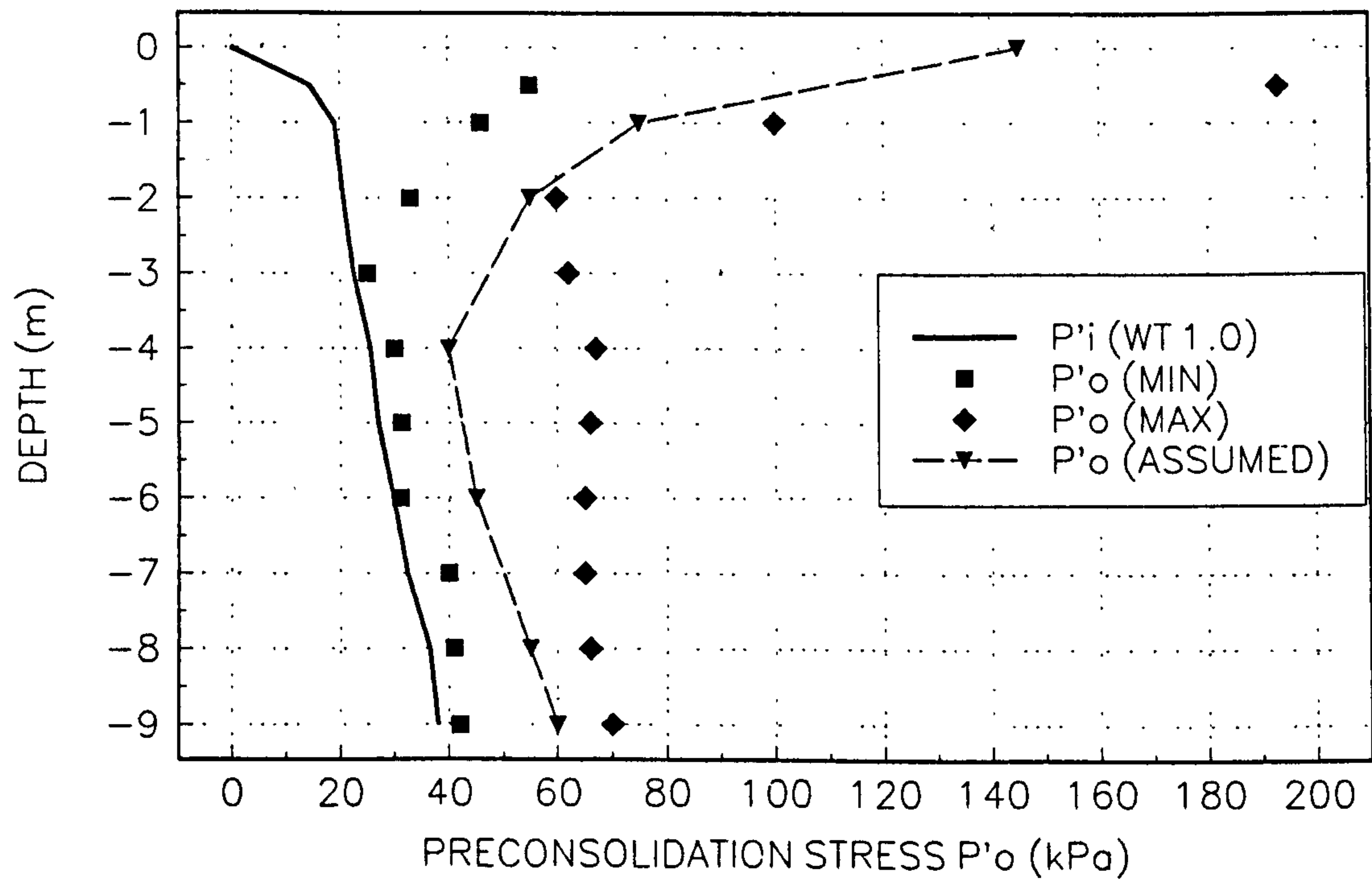


FIGURE 4.22
STRESS HISTORY FOR UNDRAINED ANALYSES



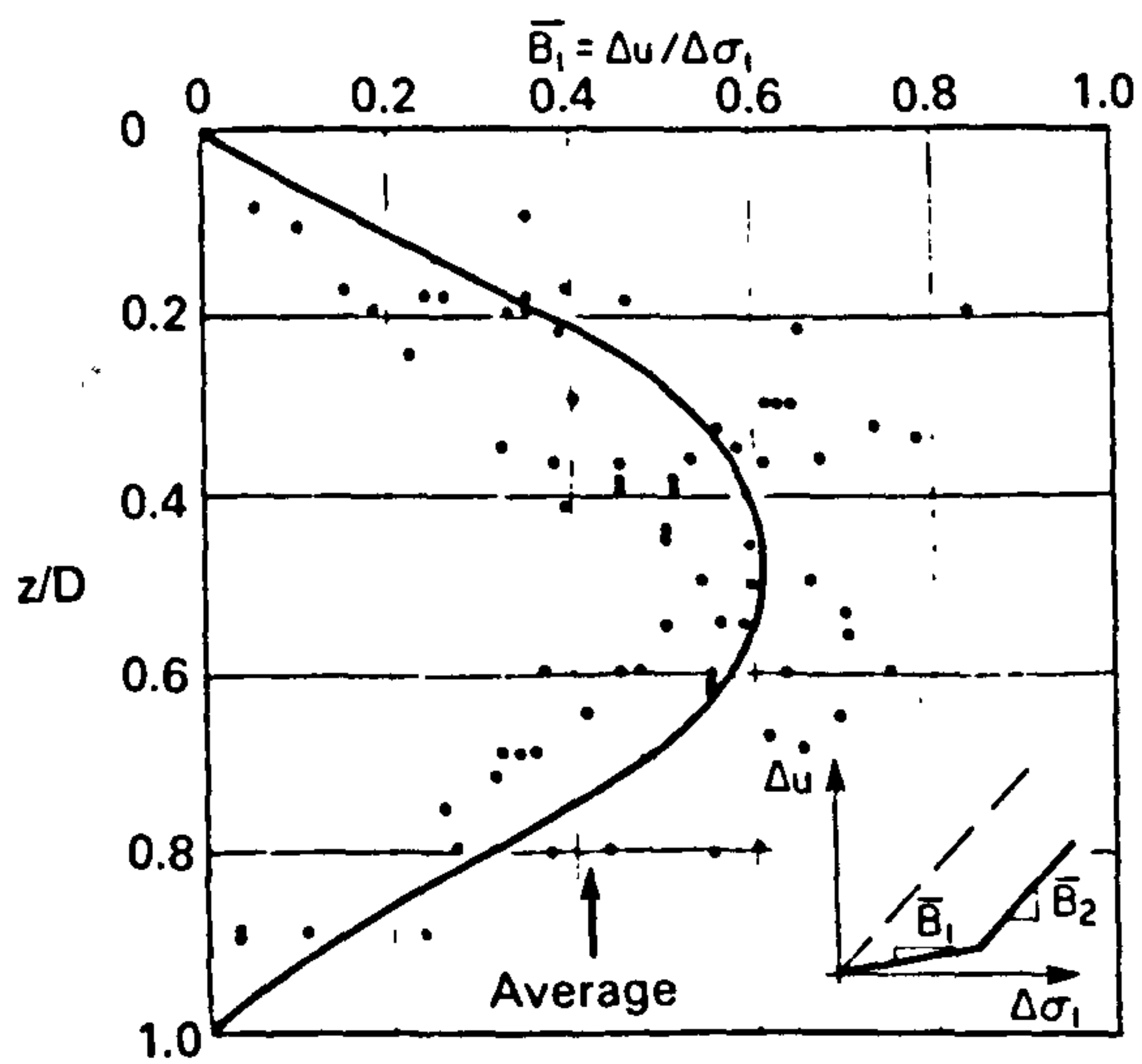


Fig 4.23. Compilation of pore water pressure observed during the first stage of construction of embankments (Tavenas and Leroueil, 1980).

FIGURE 4.24(a)
PERMEABILITY PROFILE

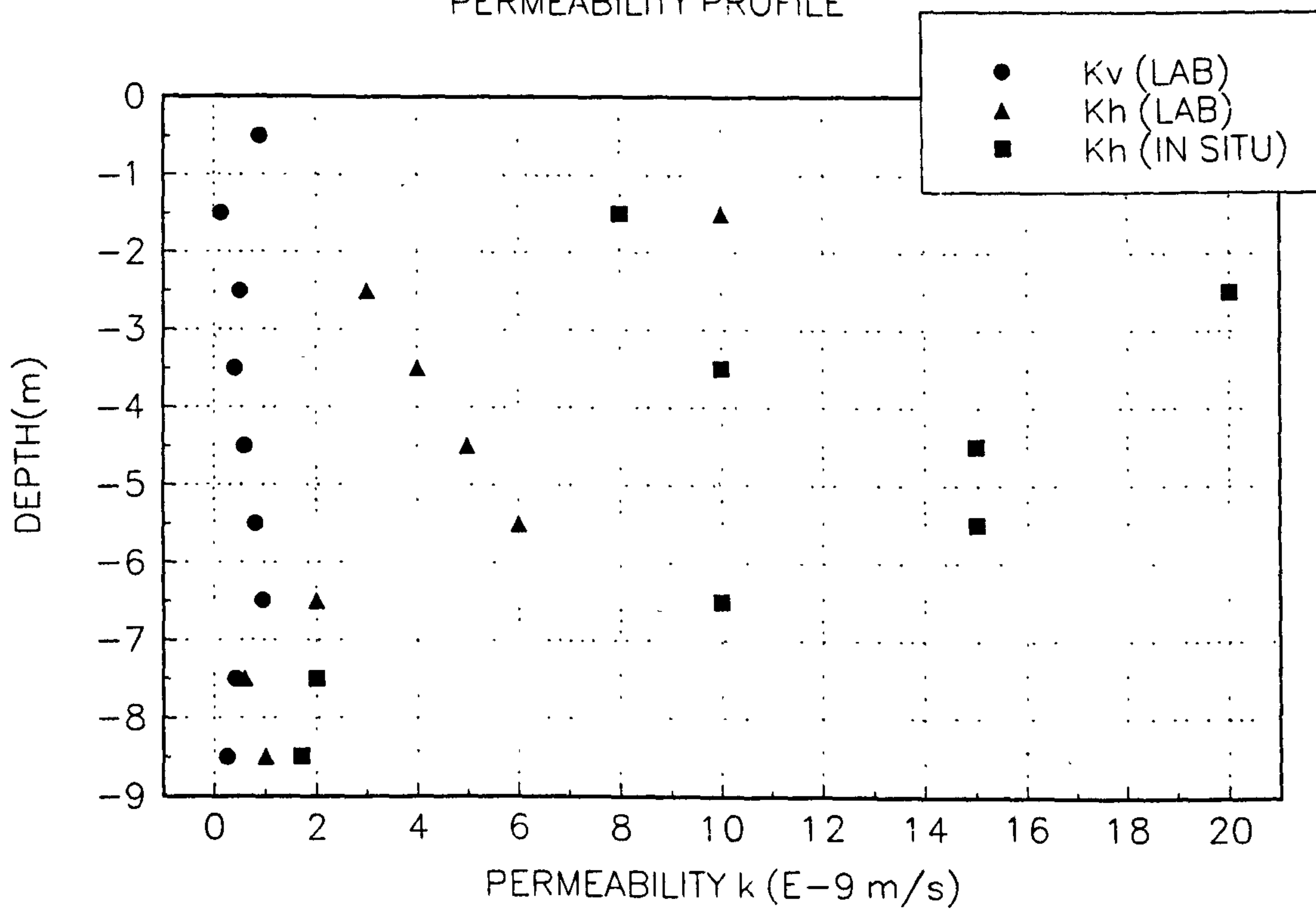


FIGURE 4.24(b)
PERMEABILITY ANISOTROPY PROFILE

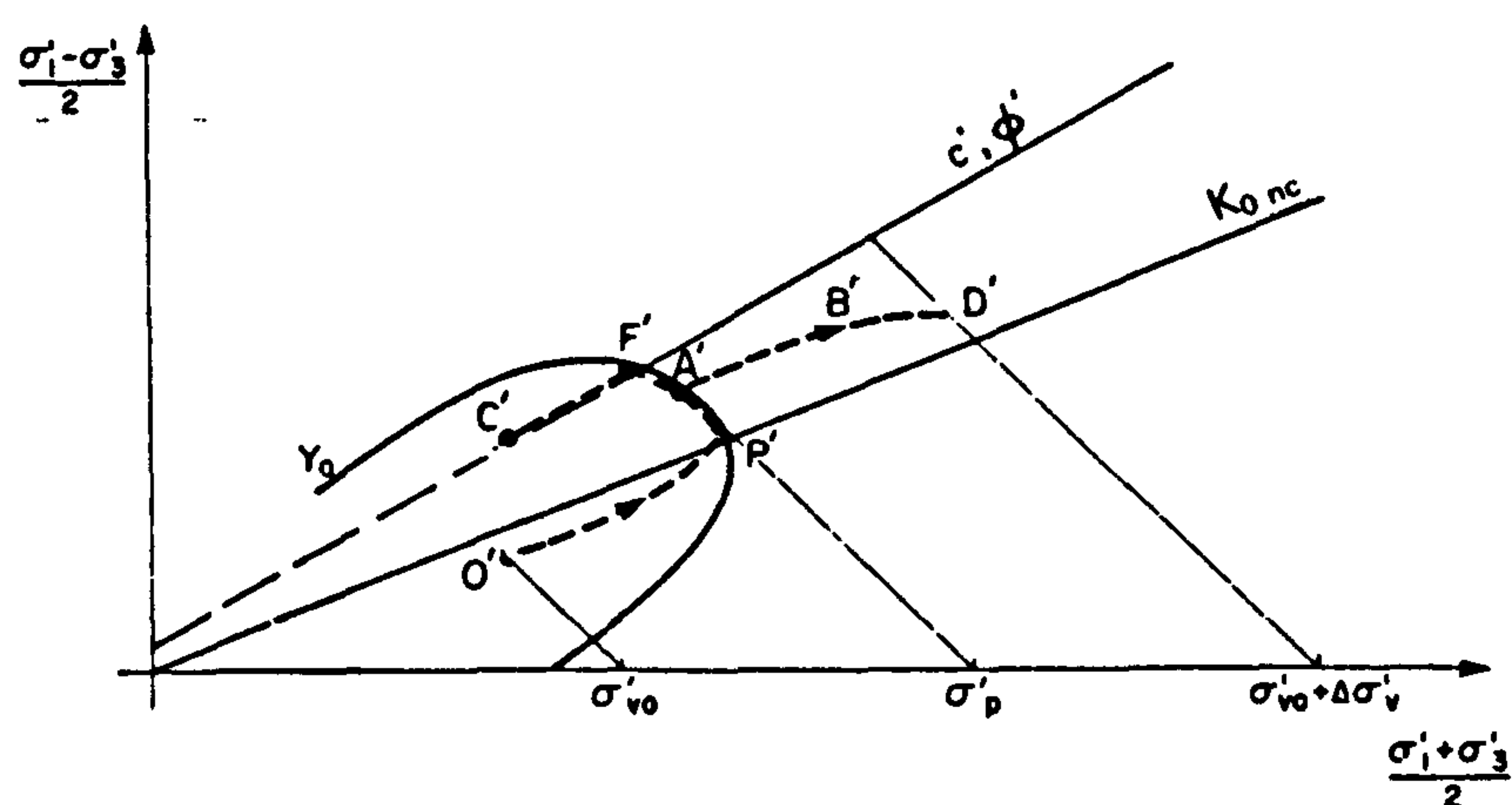
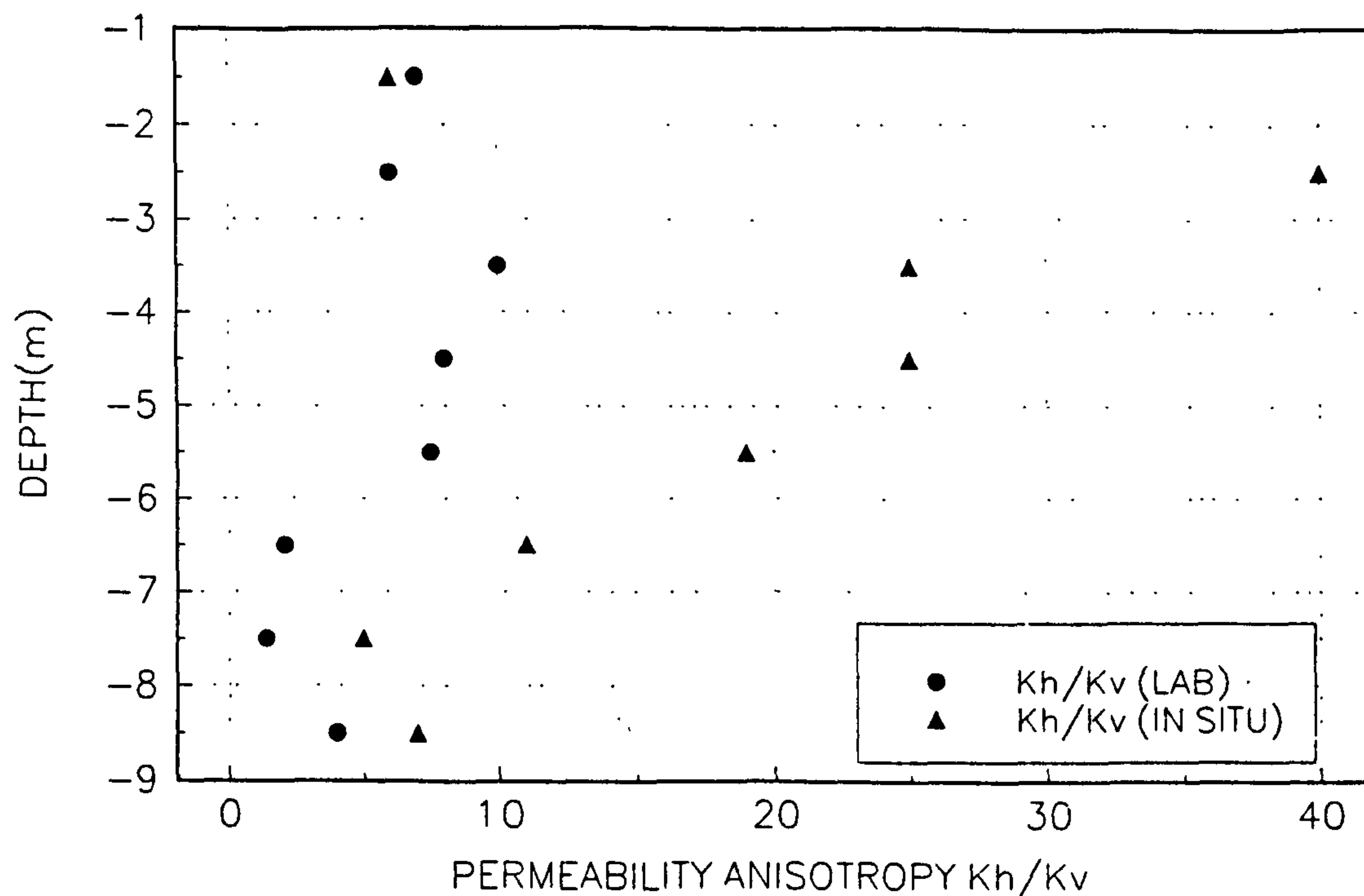


Fig 4.25. Effective stress paths under embankments (Leroueil et al., 1985).

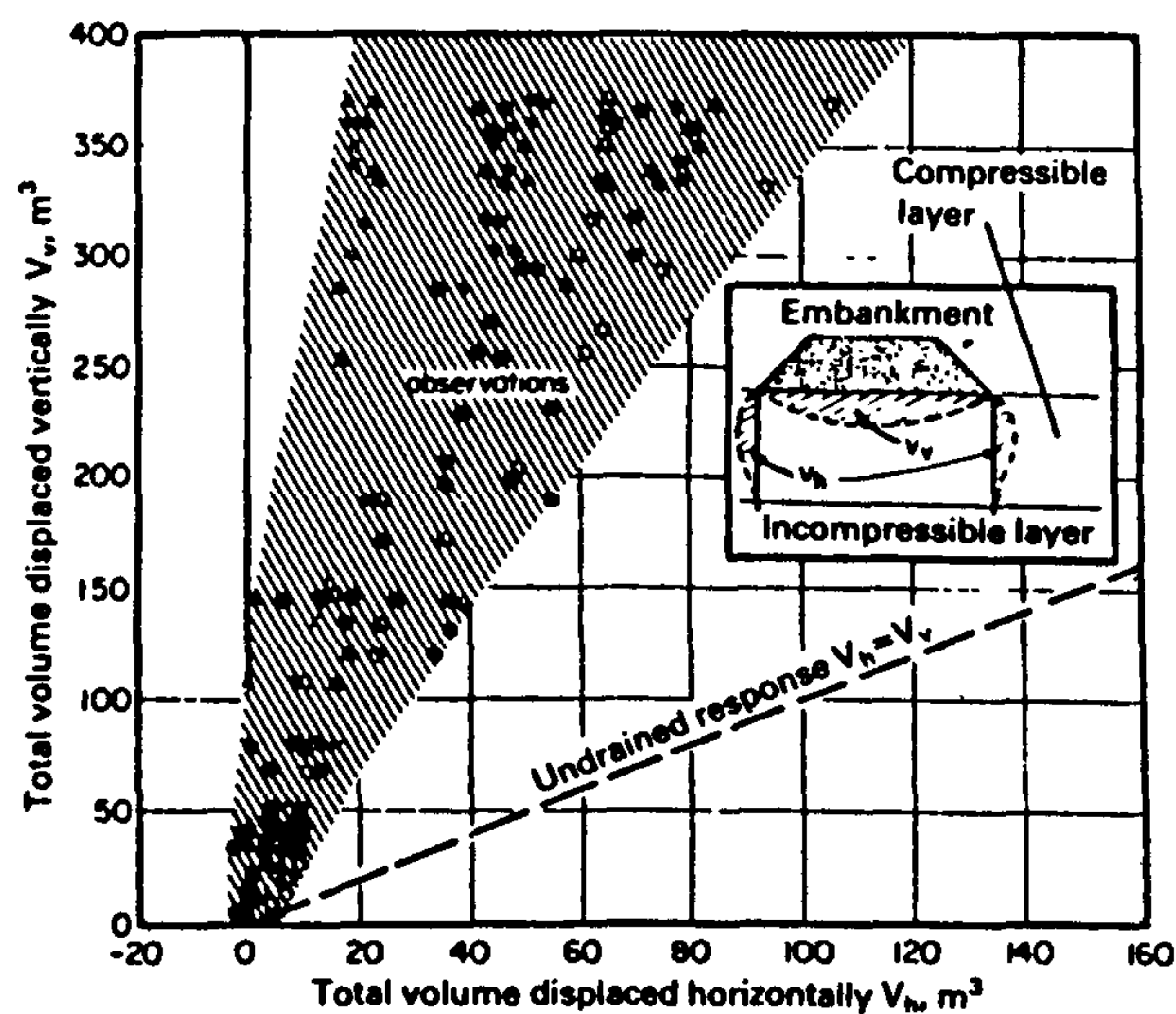


Fig 4.26. Comparison between volumes displaced horizontally and vertically during construction (Johnson, 1973 and Leroueil et al., 1985)

Fig 4.27. Oedometer test on soft marine clay from Belawan, Sumatra, Indonesia (Barry and Nicholls, 1982).

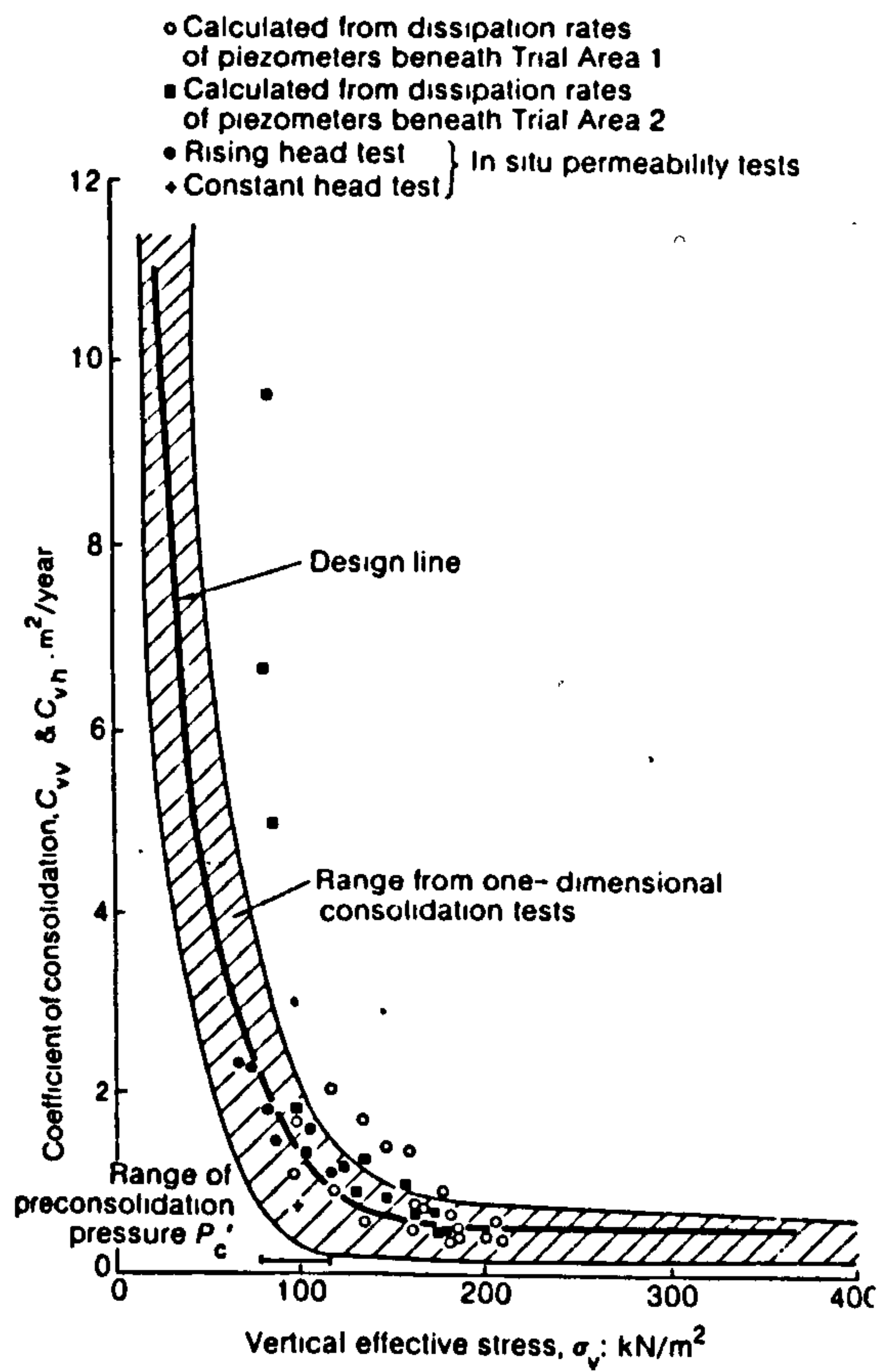
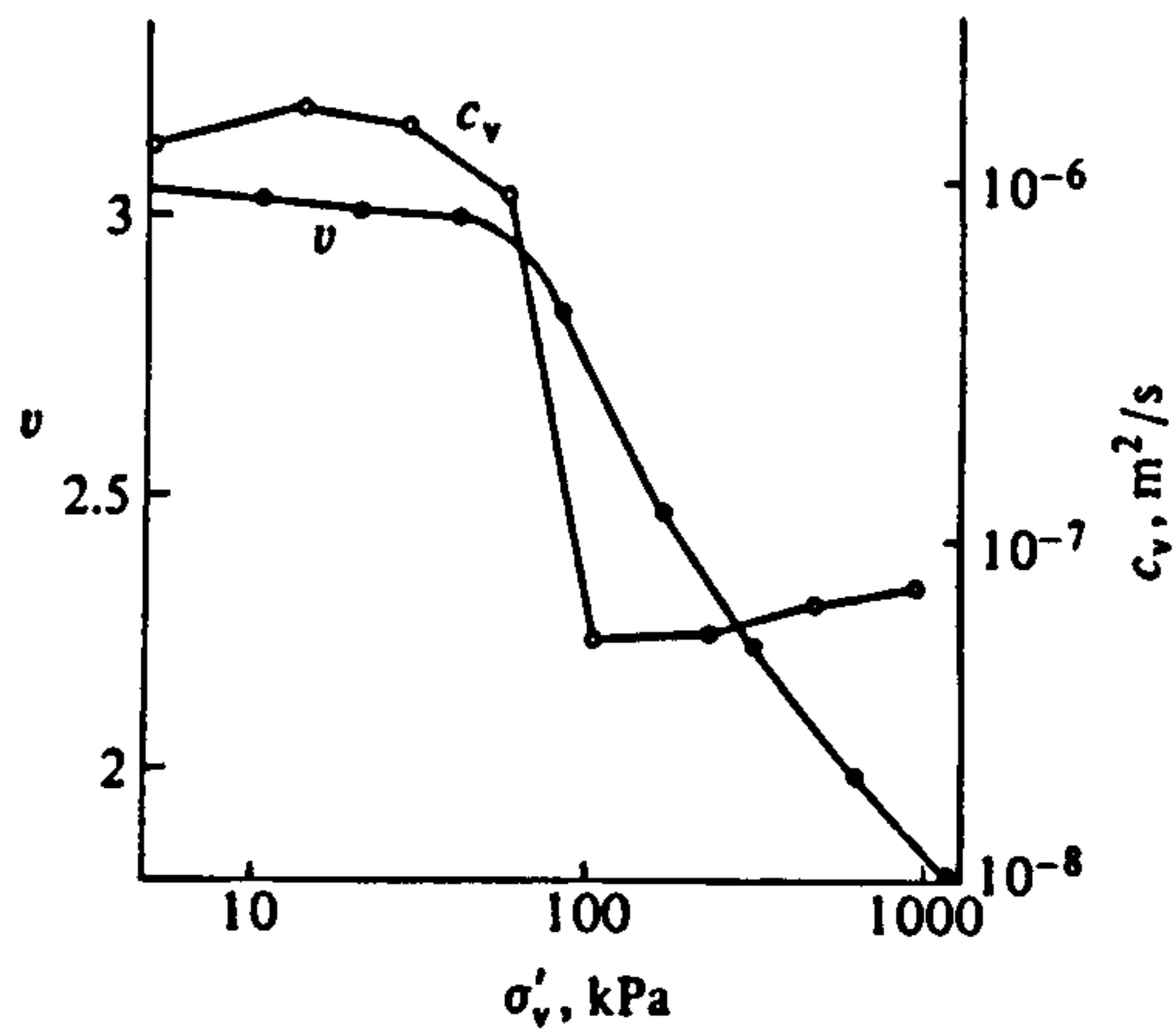


Fig 4.28. Variation of the coefficient of consolidation with vertical effective stress (Davies and Humpheson, 1986).

Fig 4.29. Finite element mesh used to describe embankment A and the foundation soil at Cubzac-les-Ponts.

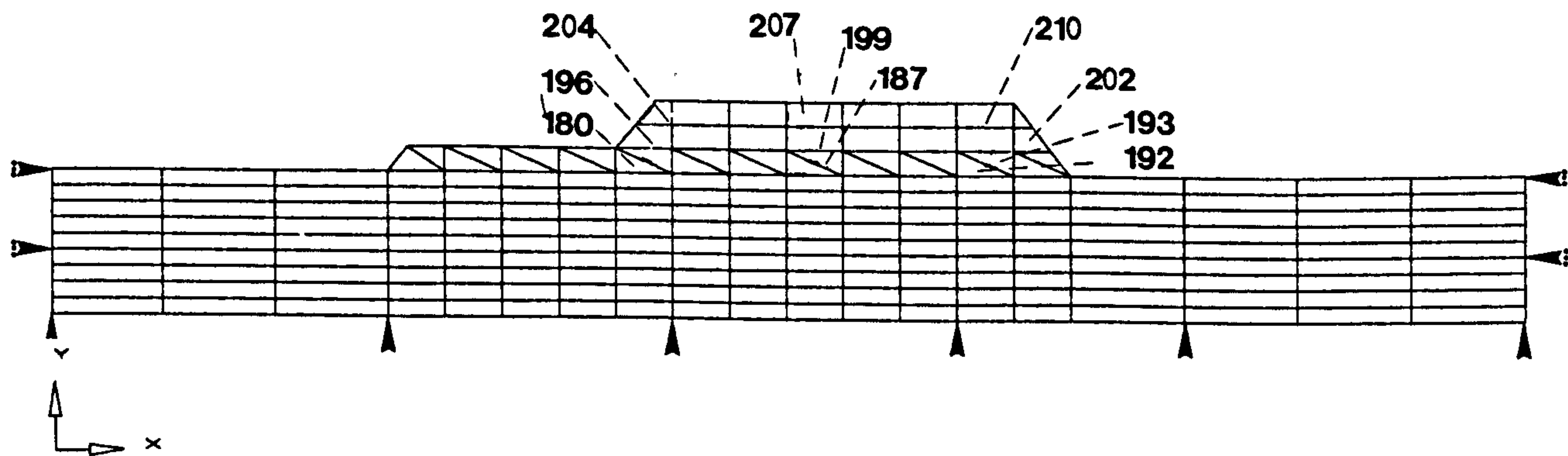


FIGURE 4.30
PREDICTED VERTICAL SURFACE SETTLEMENT PROFILE

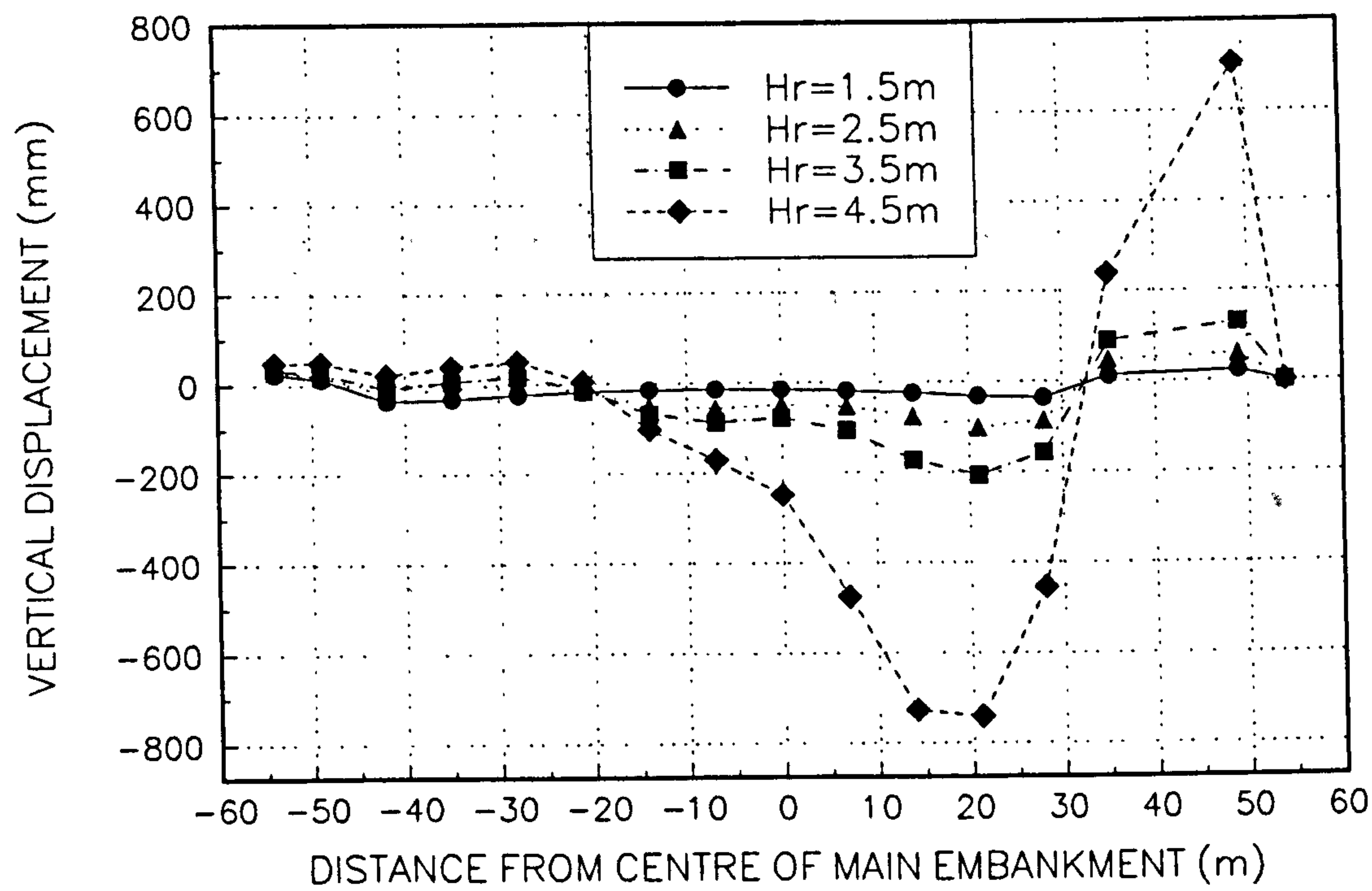


FIGURE 4.31
VERTICAL DISPLACEMENT AT CENTRE LINE. (LOCATION 160)

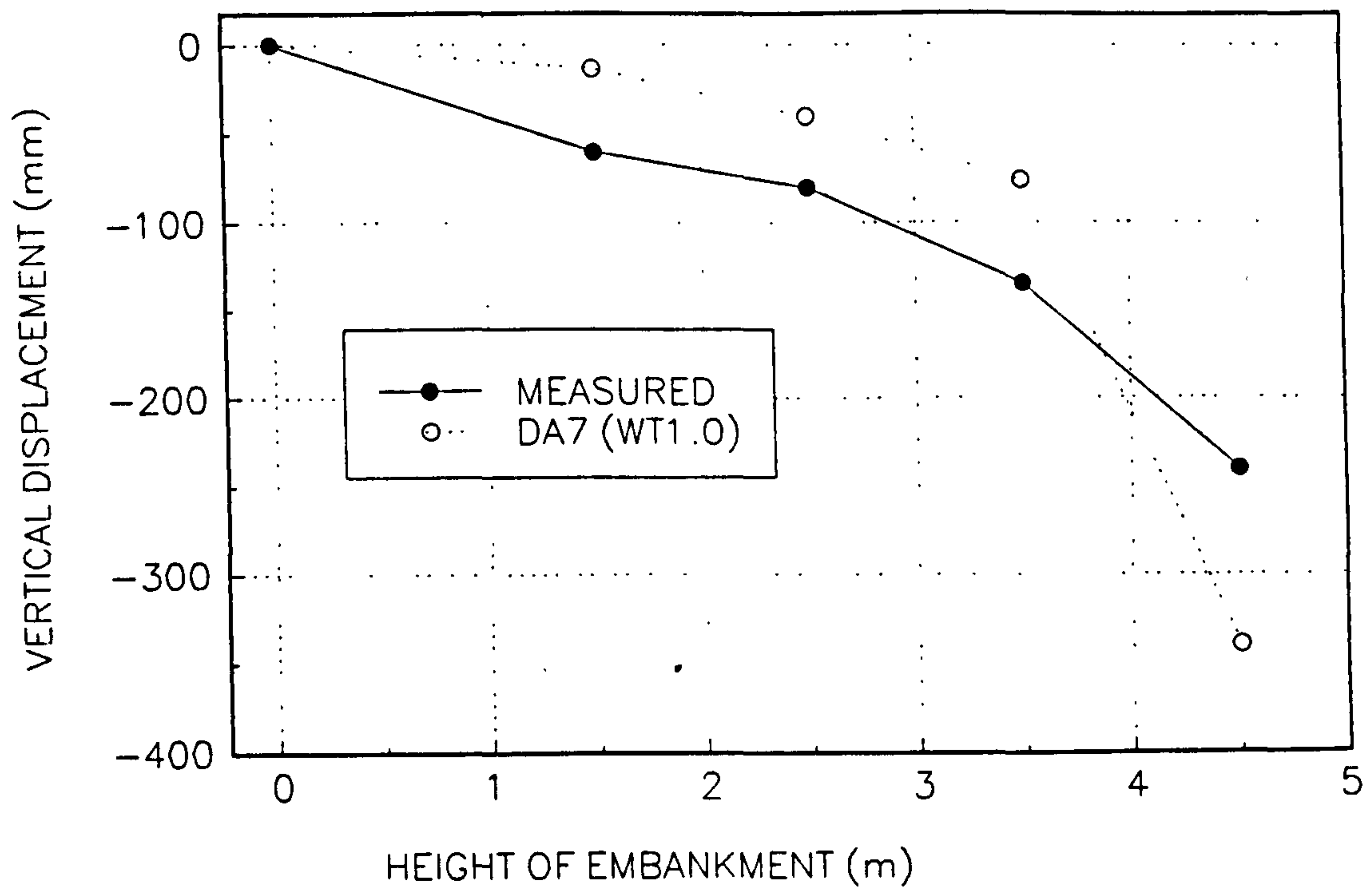


FIGURE 4.32
VERTICAL EDGE DISPLACEMENT. LOCATION 162

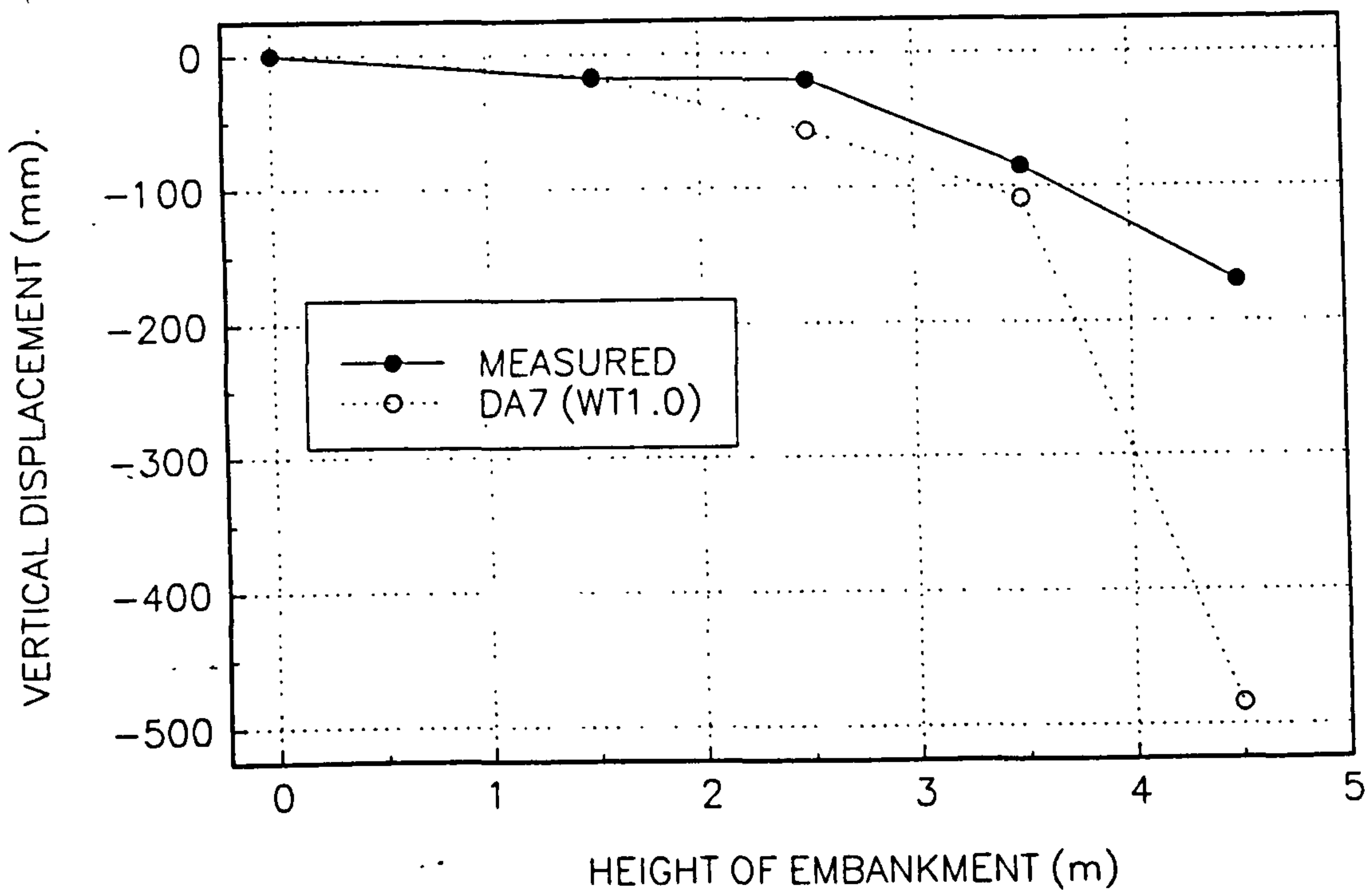


FIGURE 4.33
HORIZONTAL DISPLACEMENT AT LOCATION 197

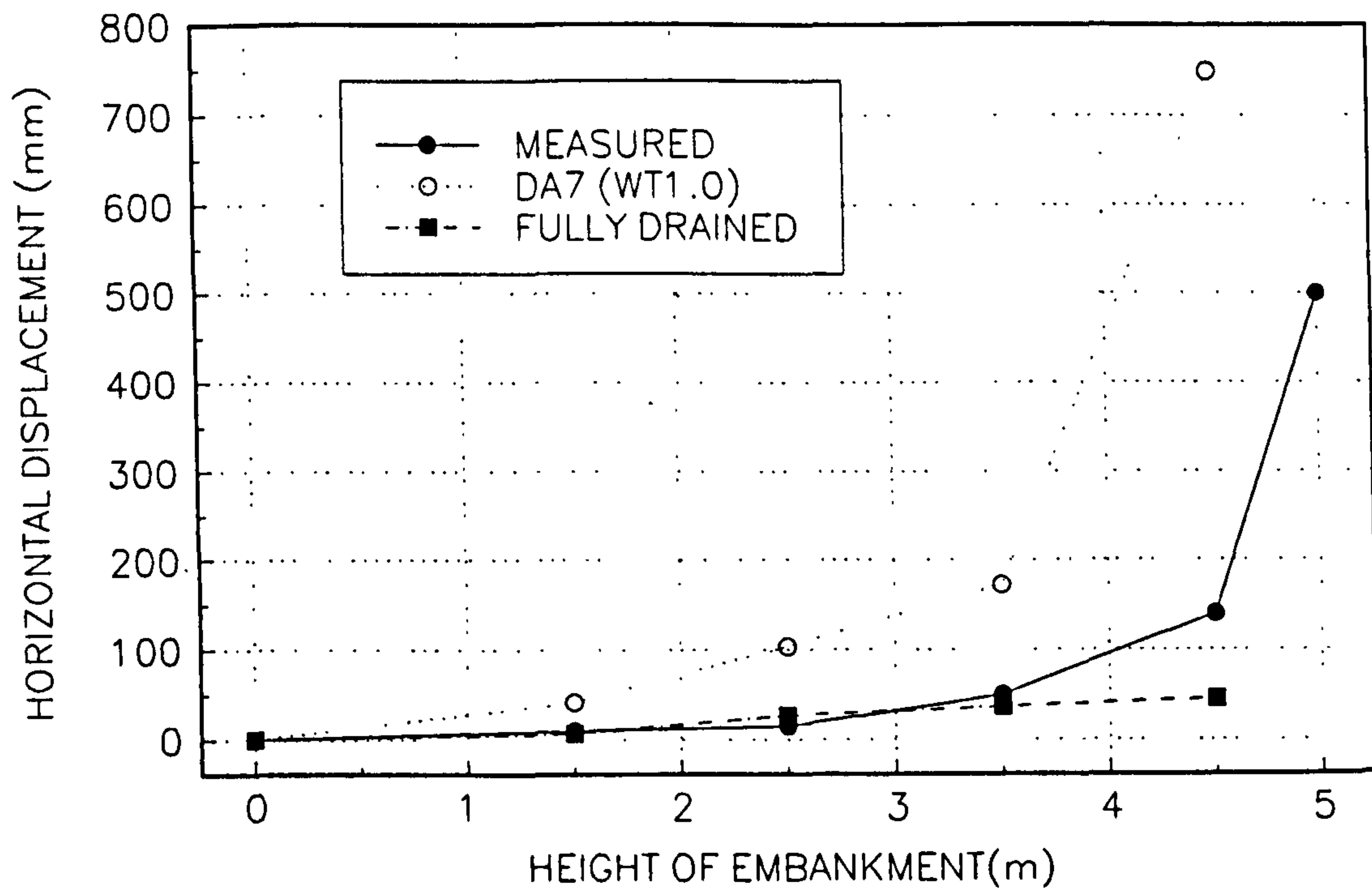


FIGURE 4.34
EXCESS PORE WATER PRESSURE PROFILE FOR AN EMBANKMENT HEIGHT OF 1.5m

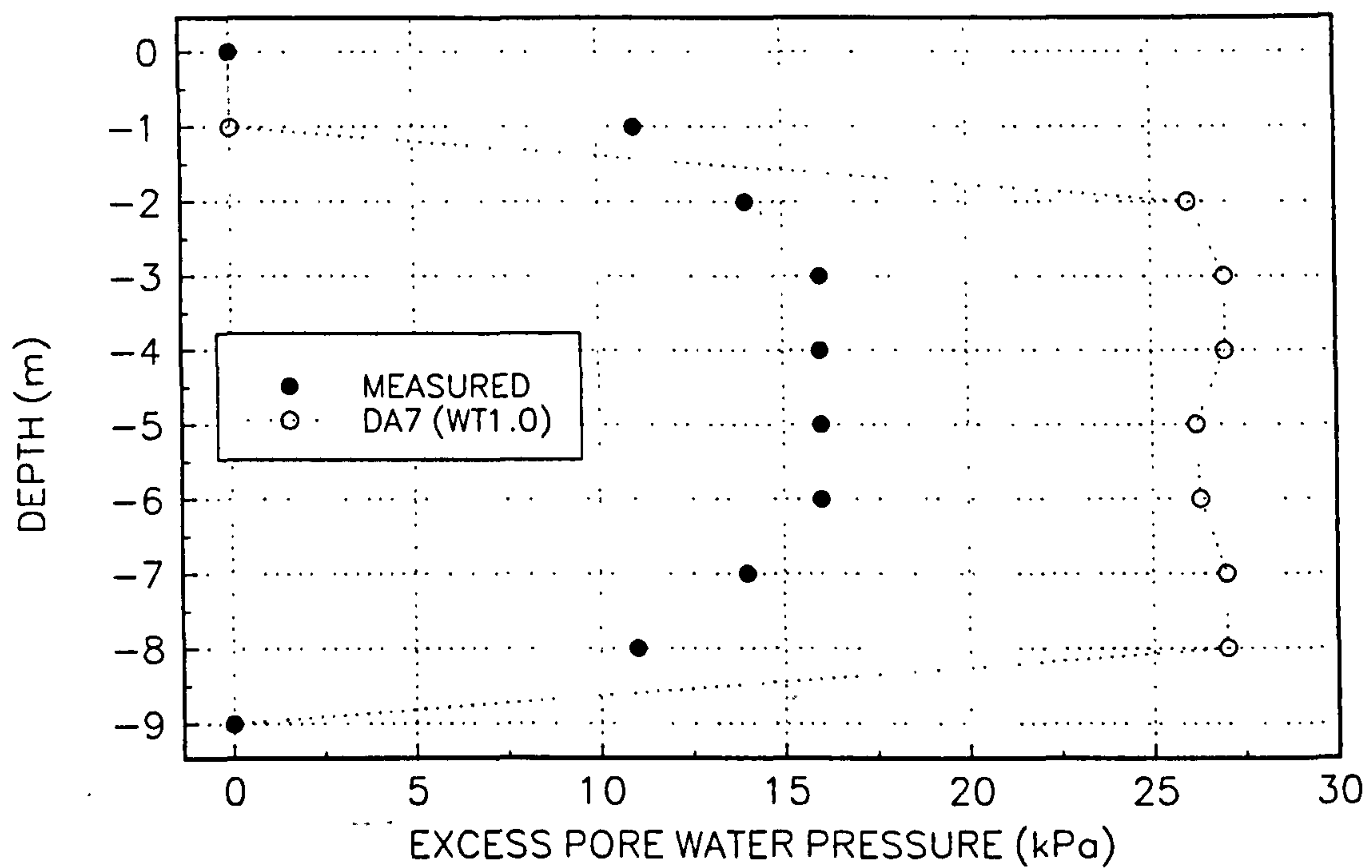


FIGURE 4.35
EXCESS PORE WATER PRESSURE PROFILE FOR AN EMBANKMENT HEIGHT OF 2.5m

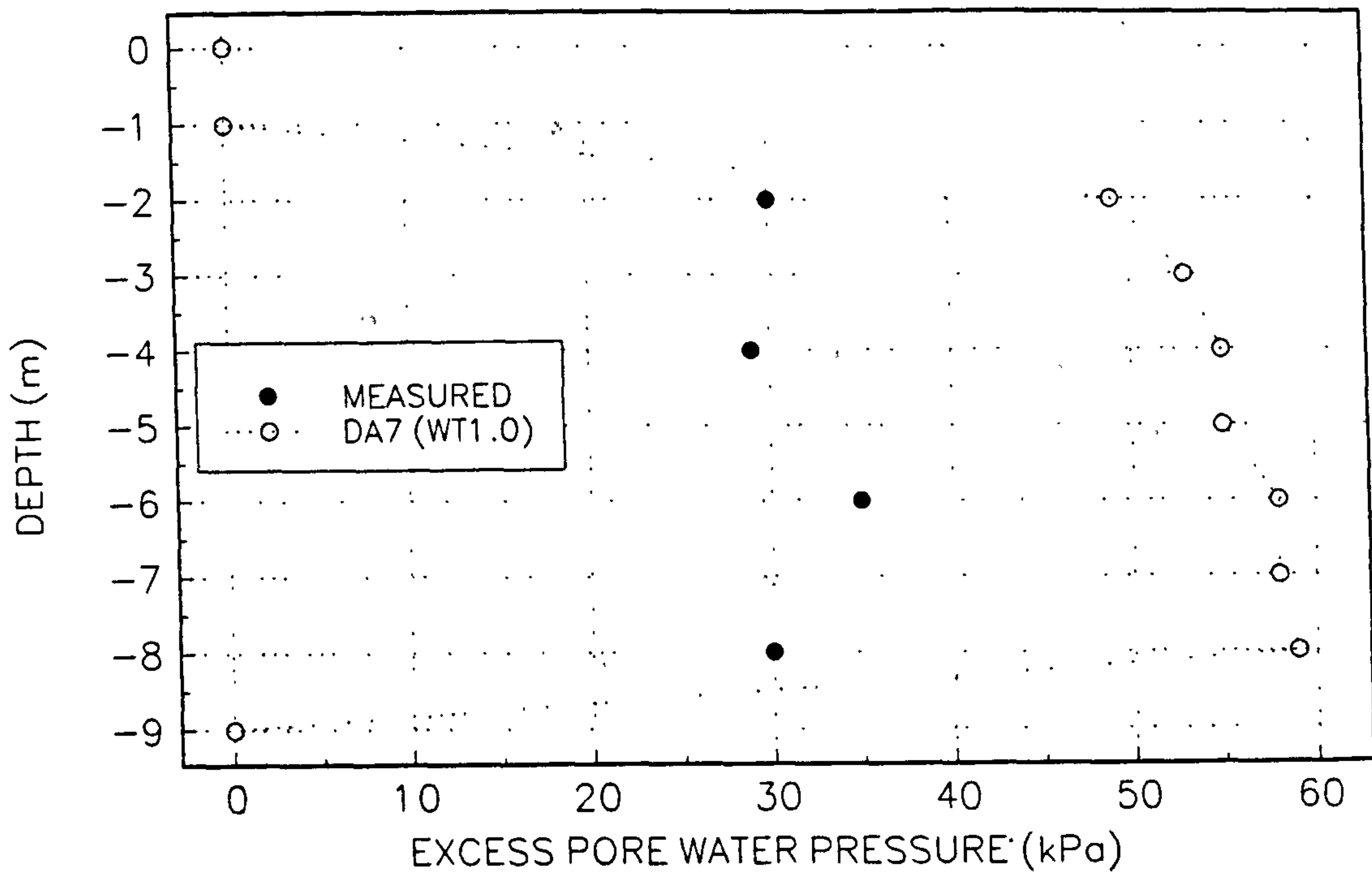


FIGURE 4.36
EXCESS PORE WATER PRESSURE PROFILE FOR AN EMBANKMENT HEIGHT OF 3.5m

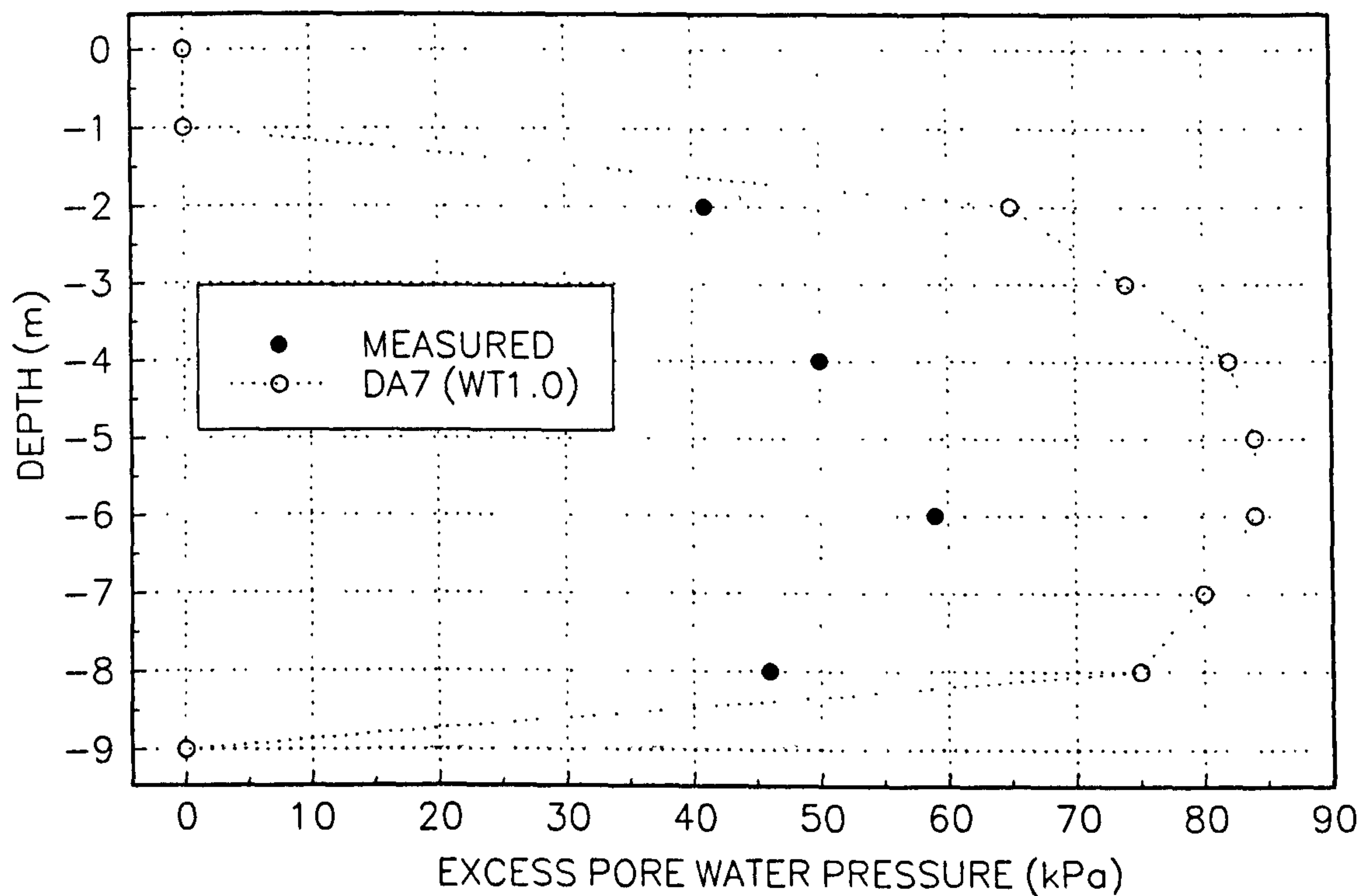


FIGURE 4.37
EXCESS PORE WATER PRESSURE PROFILE AT AN EMBANKMENT HEIGHT OF 4.5m

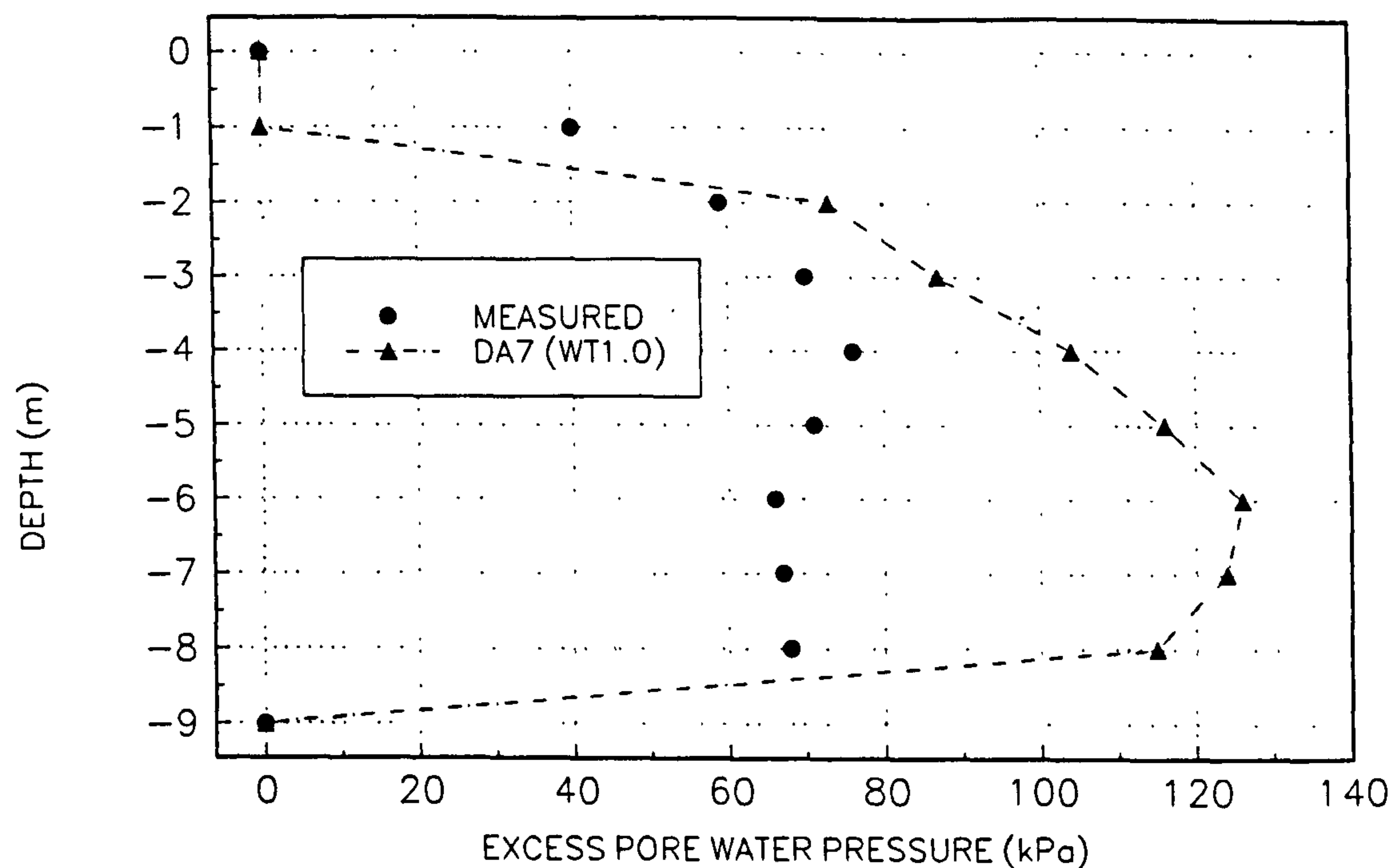


FIGURE 4.38
EXCESS PORE WATER PRESSURE AGAINST EMBANKMENT HEIGHT AT 4m DEPTH.

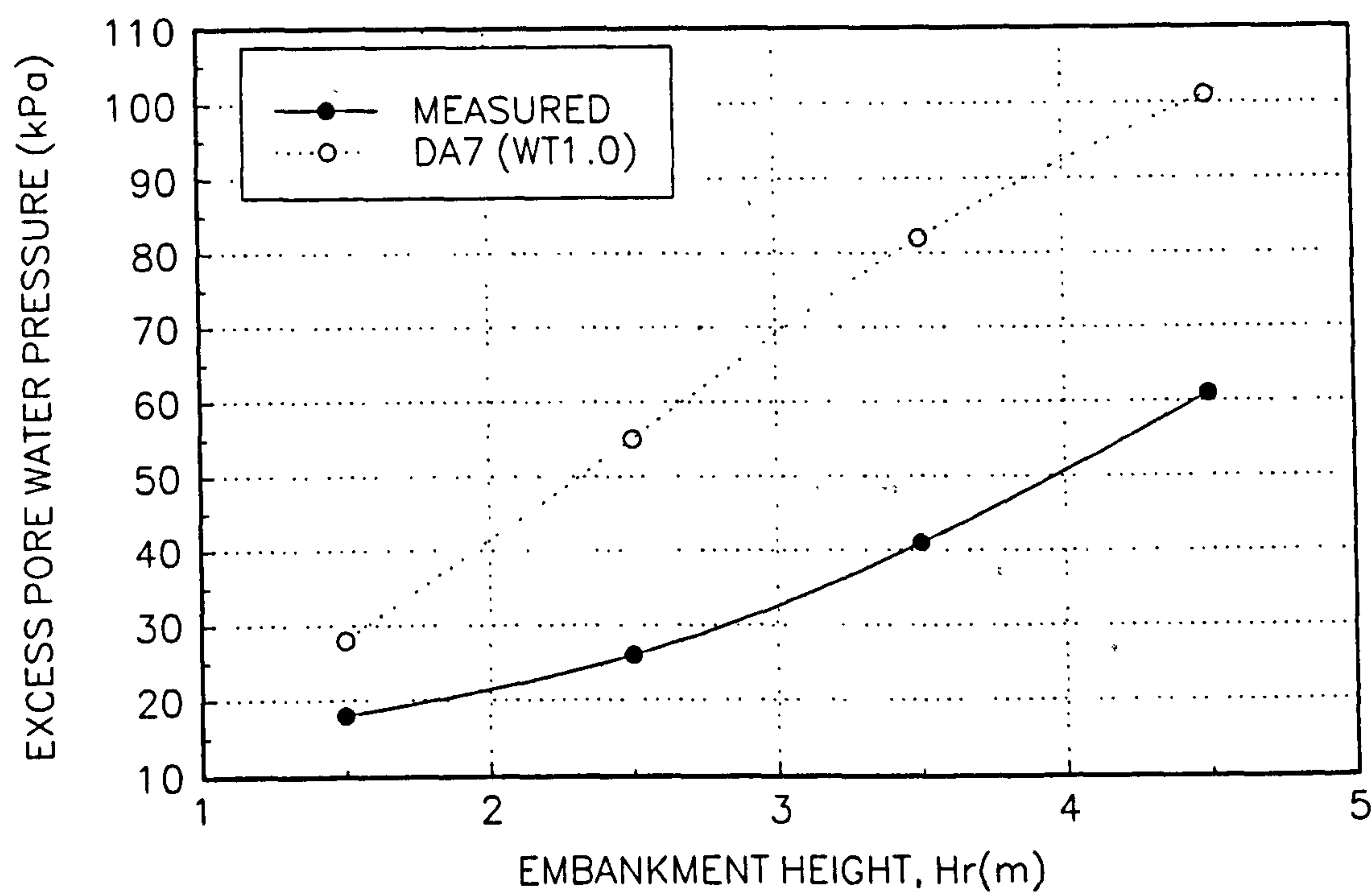


FIGURE 4.39
EXCESS PORE WATER PRESSURE AGAINST EMBANKMENT HEIGHT FOR 6m DEPTH

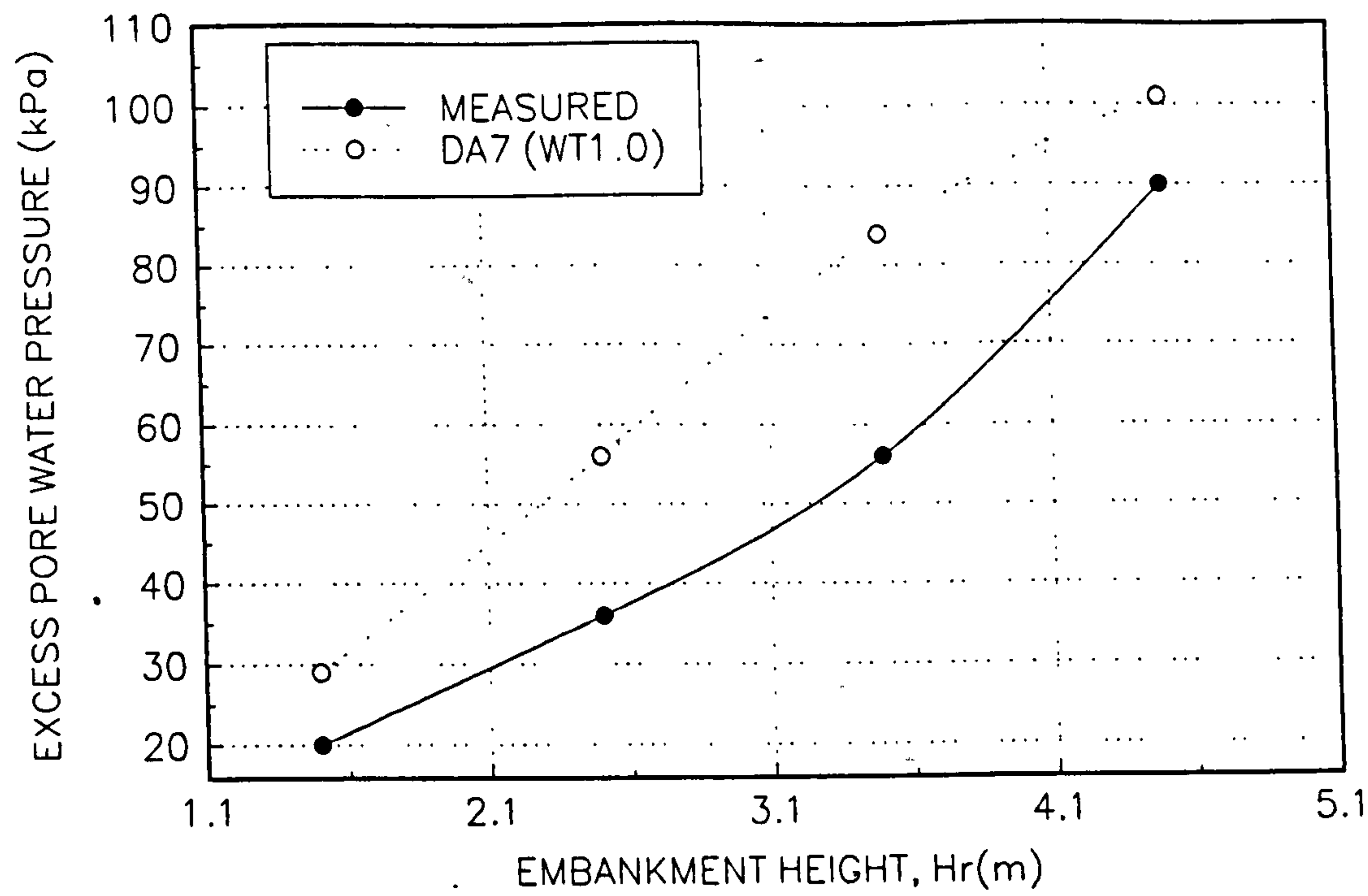


FIGURE 4.40
VARIATION OF LATERAL STRESS UNDER EMBANKMENT

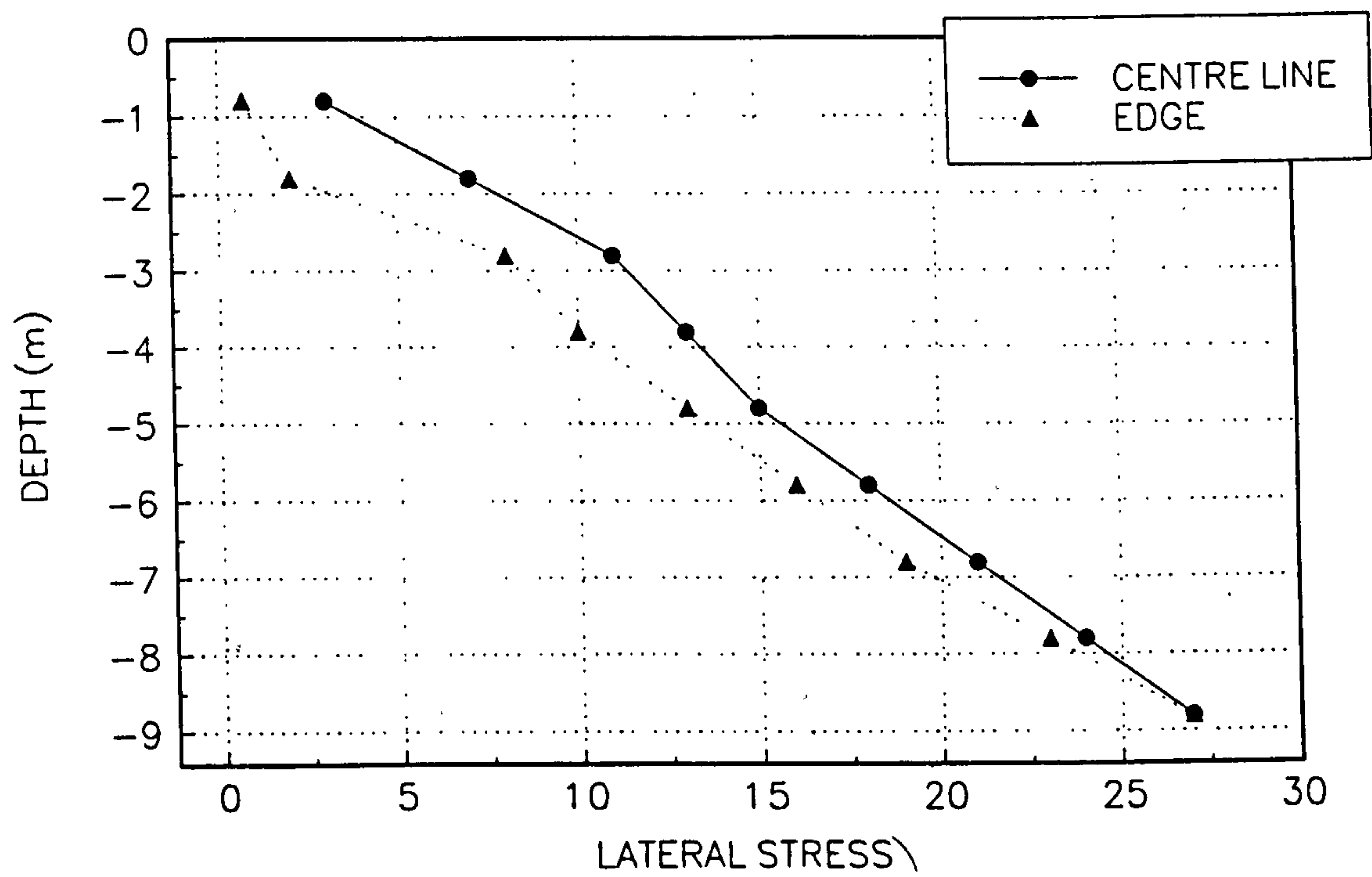


FIGURE 4.41
VARIATION OF SHEAR STRESS UNDER EMBANKMENT

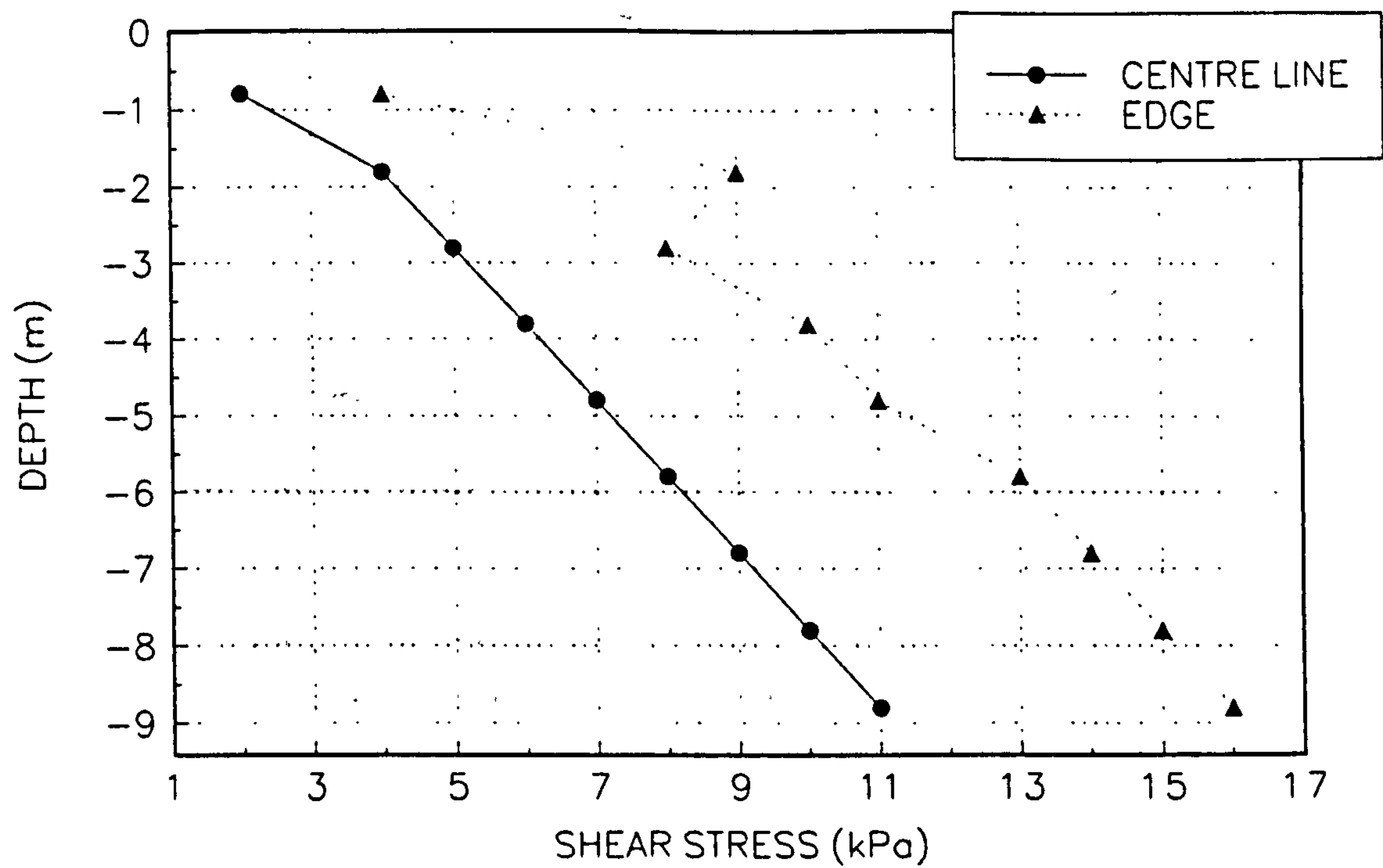
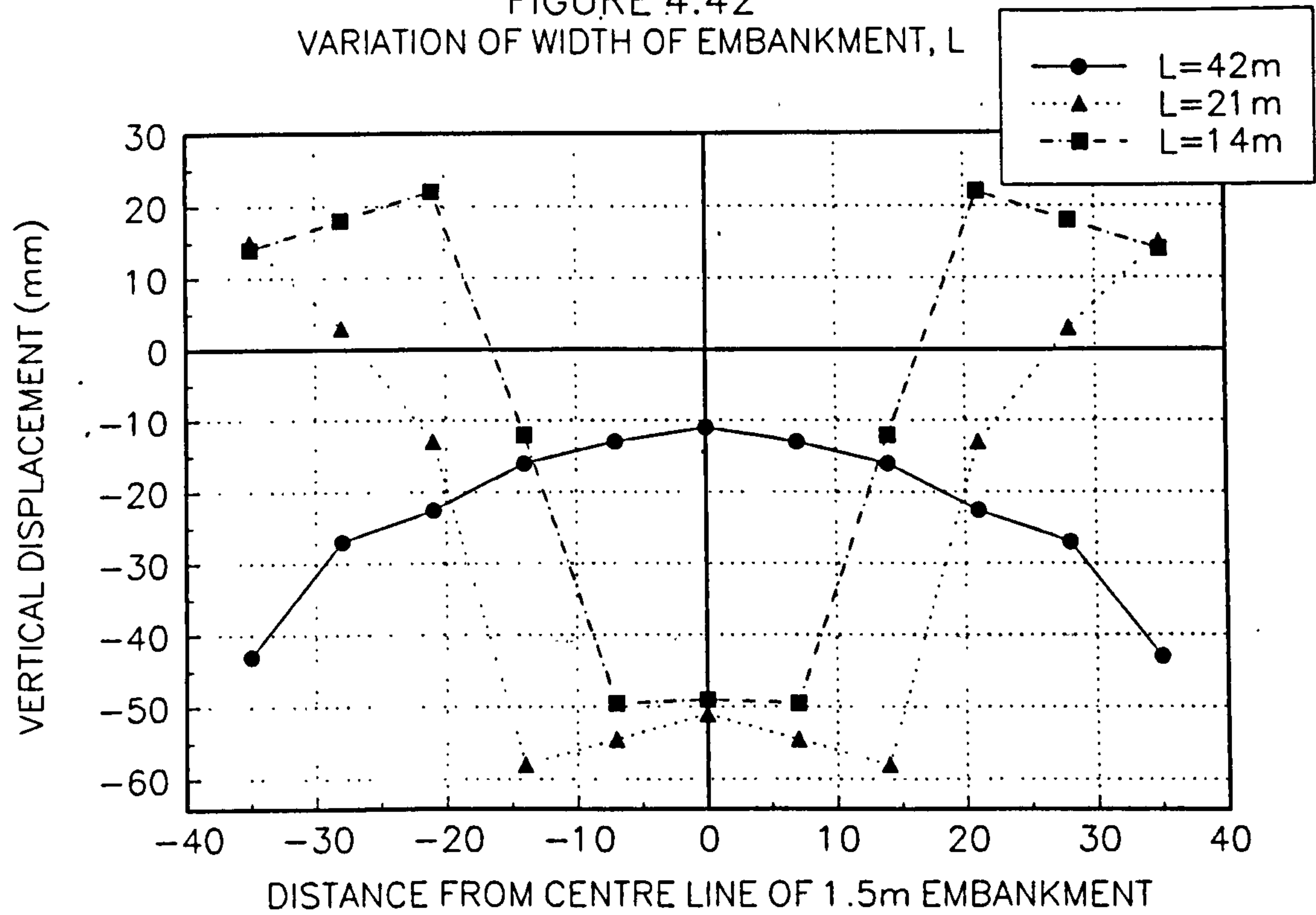


FIGURE 4.42
VARIATION OF WIDTH OF EMBANKMENT, L



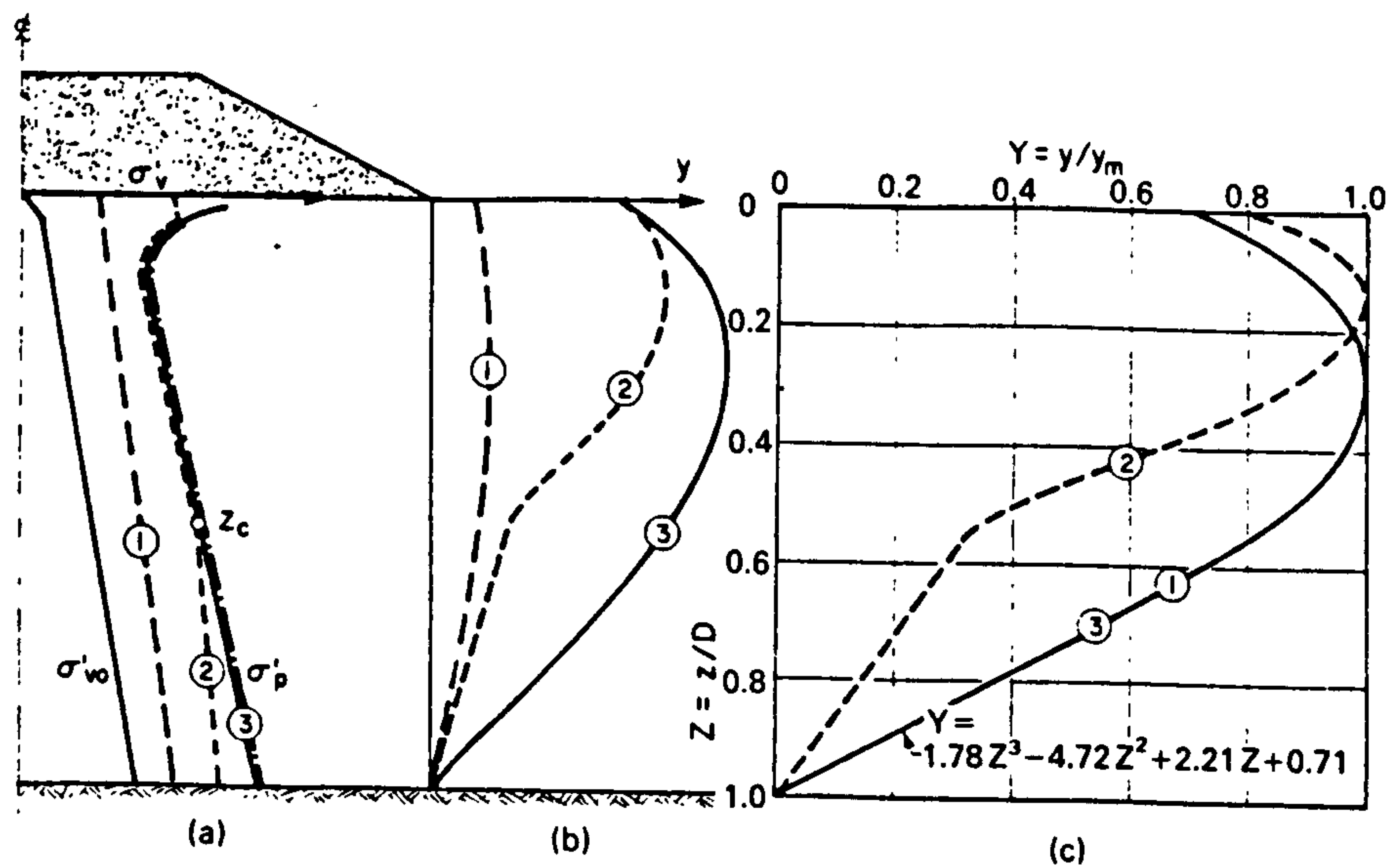


Fig 4.43. Method of estimating the distribution of deformation with depth under toe of slope of embankment (Tavenas et al., 1979).

FIGURE 4.44
VERTICAL DISPLACEMENT AT CENTRE LINE. (LOCATION 160)

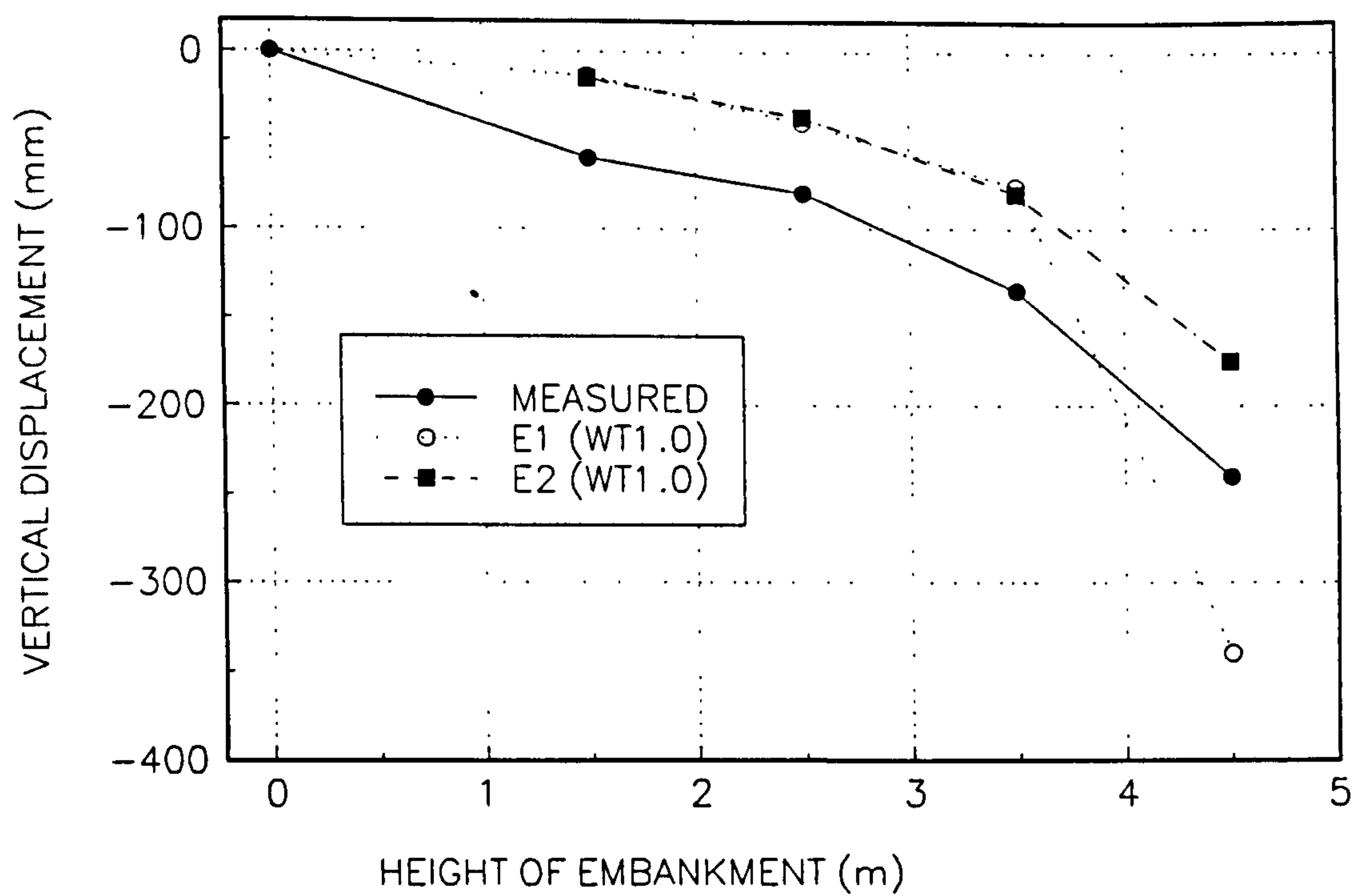


FIG 4.45
VERTICAL EDGE DISPLACEMENT. LOCATION 162

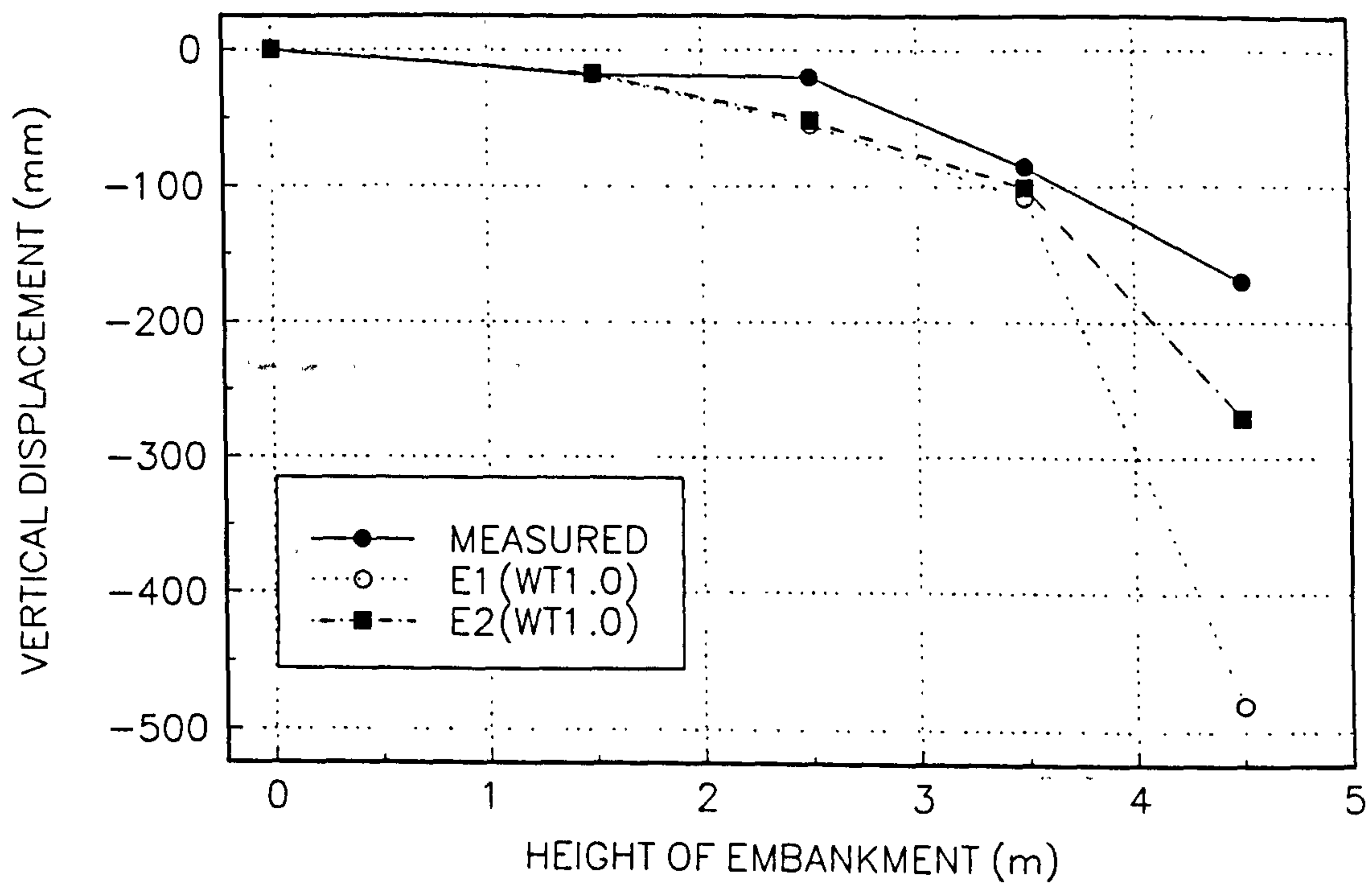


FIGURE 4.46
HORIZONTAL DISPLACEMENT AT LOCATION 197

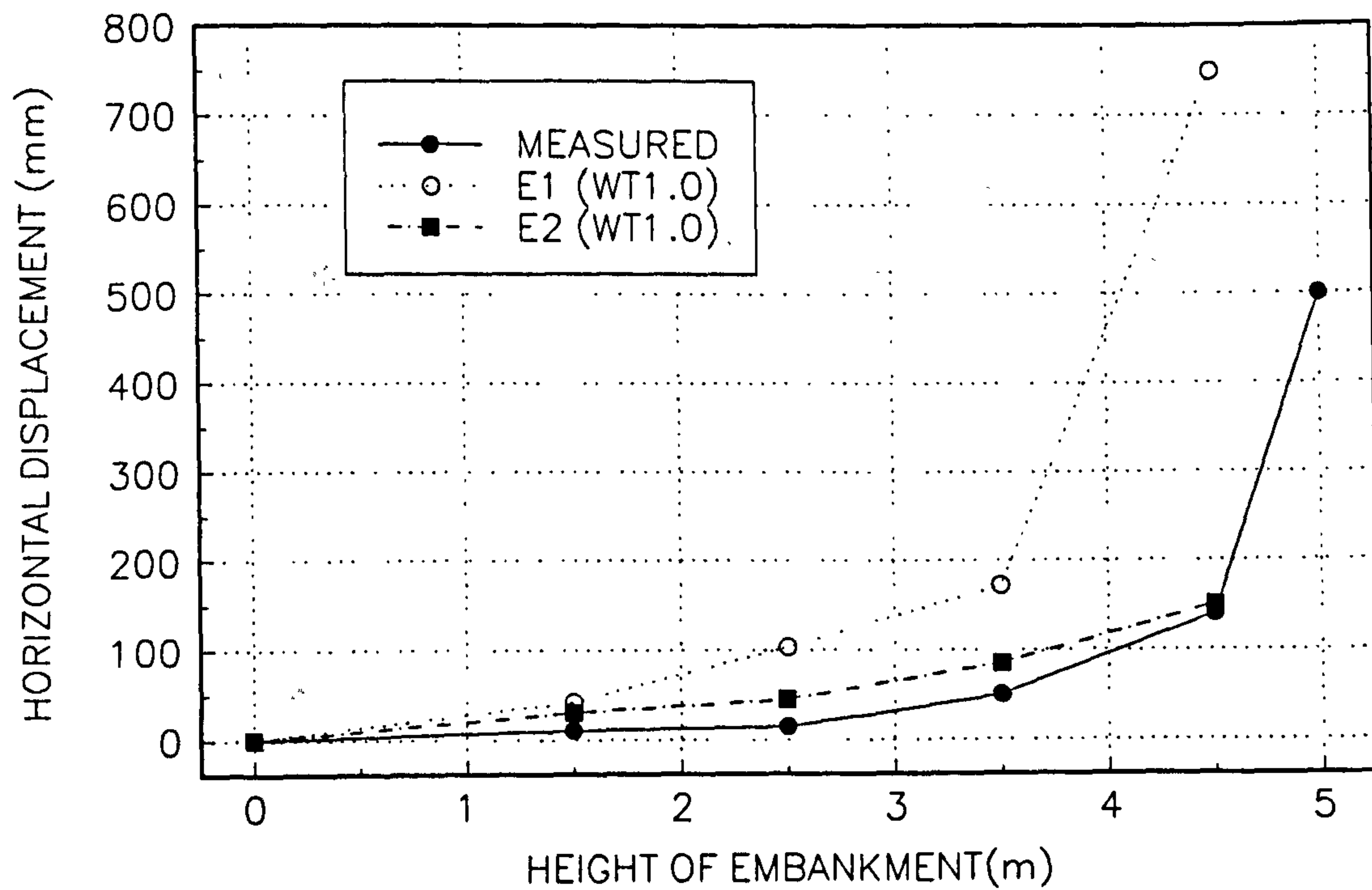


FIGURE 4.47
 VARIATION OF LATERAL STRESS THROUGH MAIN EMBANKMENT. L.H.S EDGE ELEMENTS

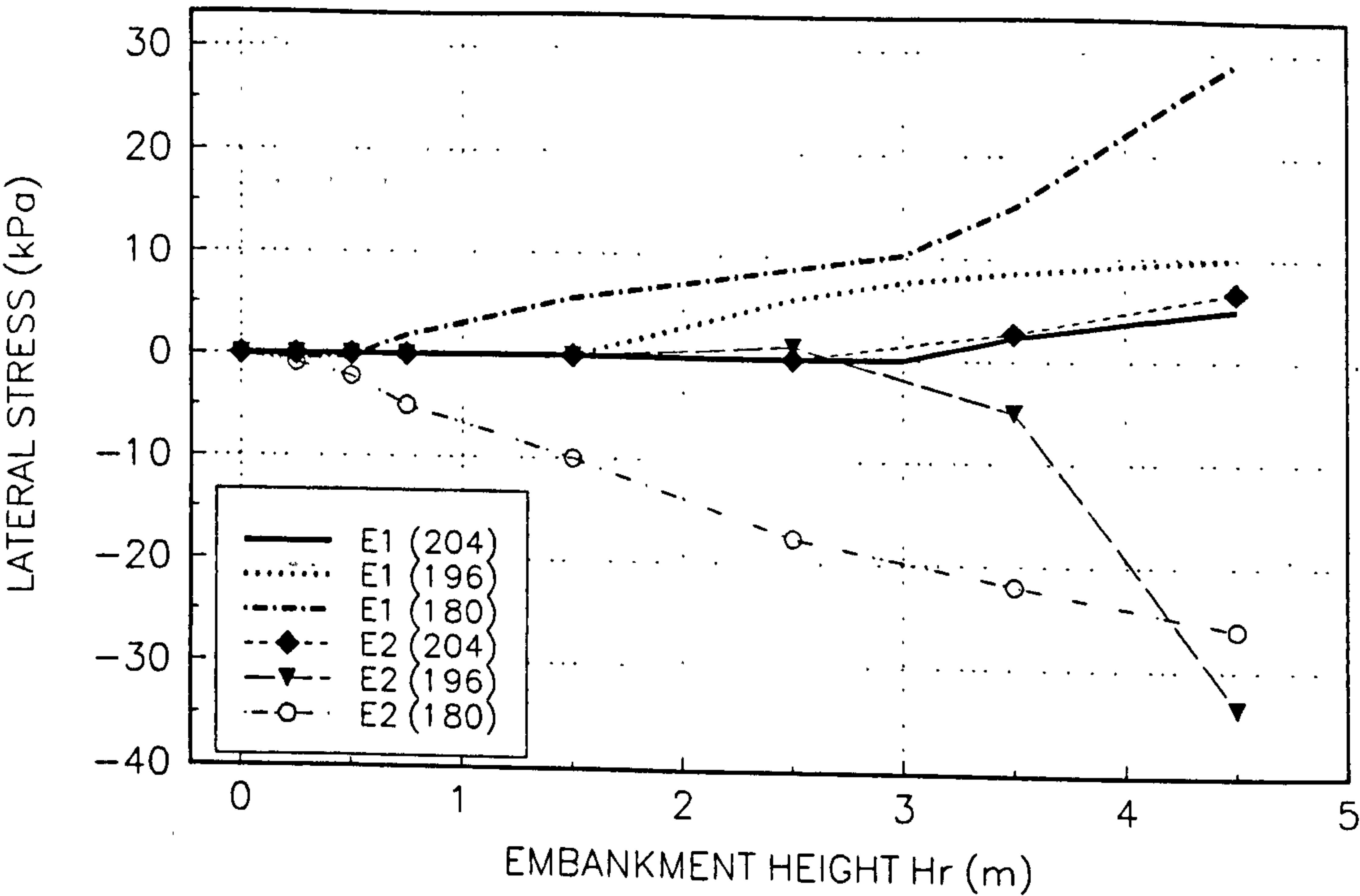


FIGURE 4.48
 VARIATION OF LATERAL STRESS THROUGH MAIN EMBANKMENT. CENTRE ELEMENTS

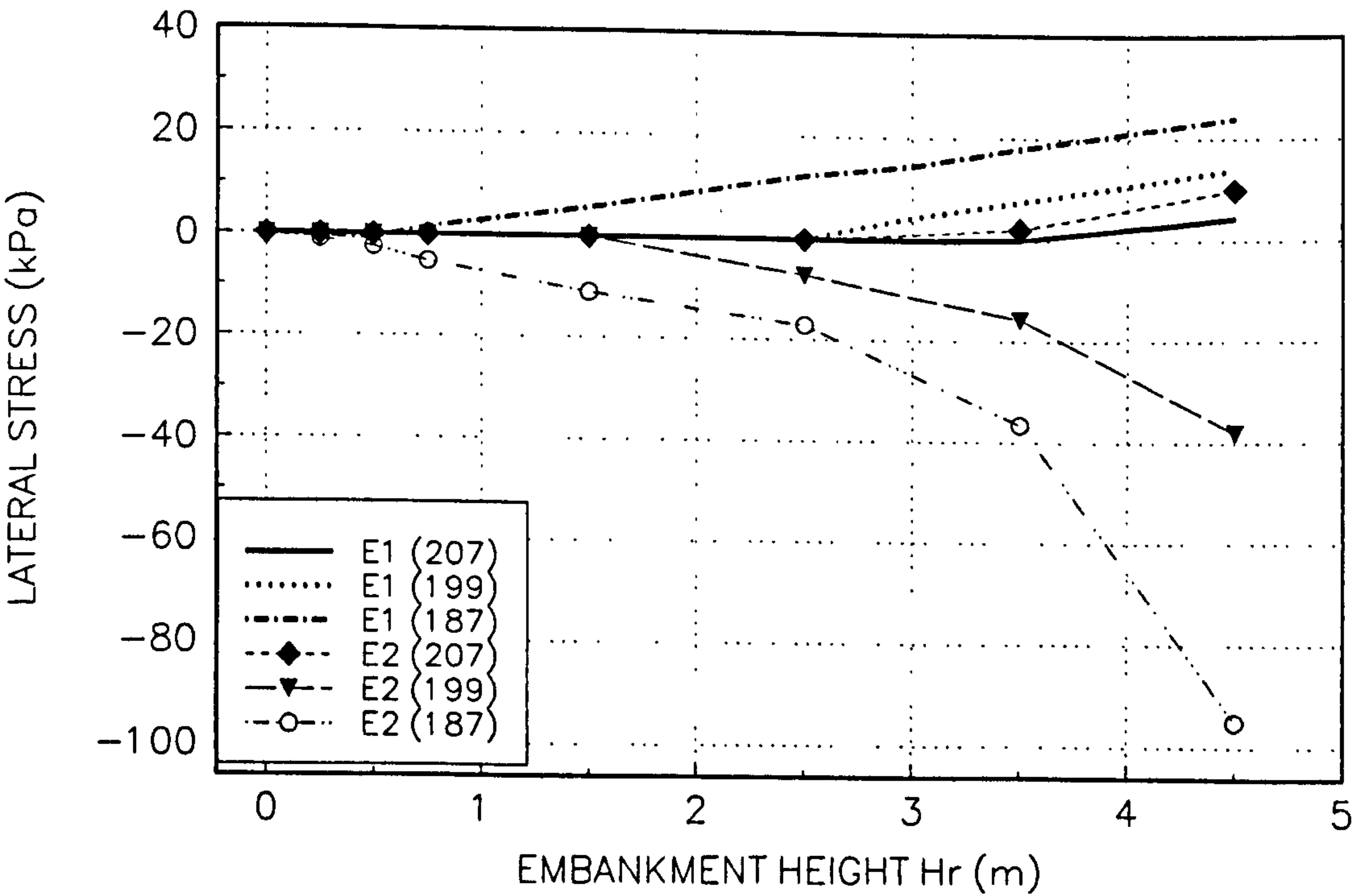


FIGURE 4.49
VARIATION OF LATERAL STRESS THROUGH MAIN EMBANKMENT. R.H.S ELEMENTS

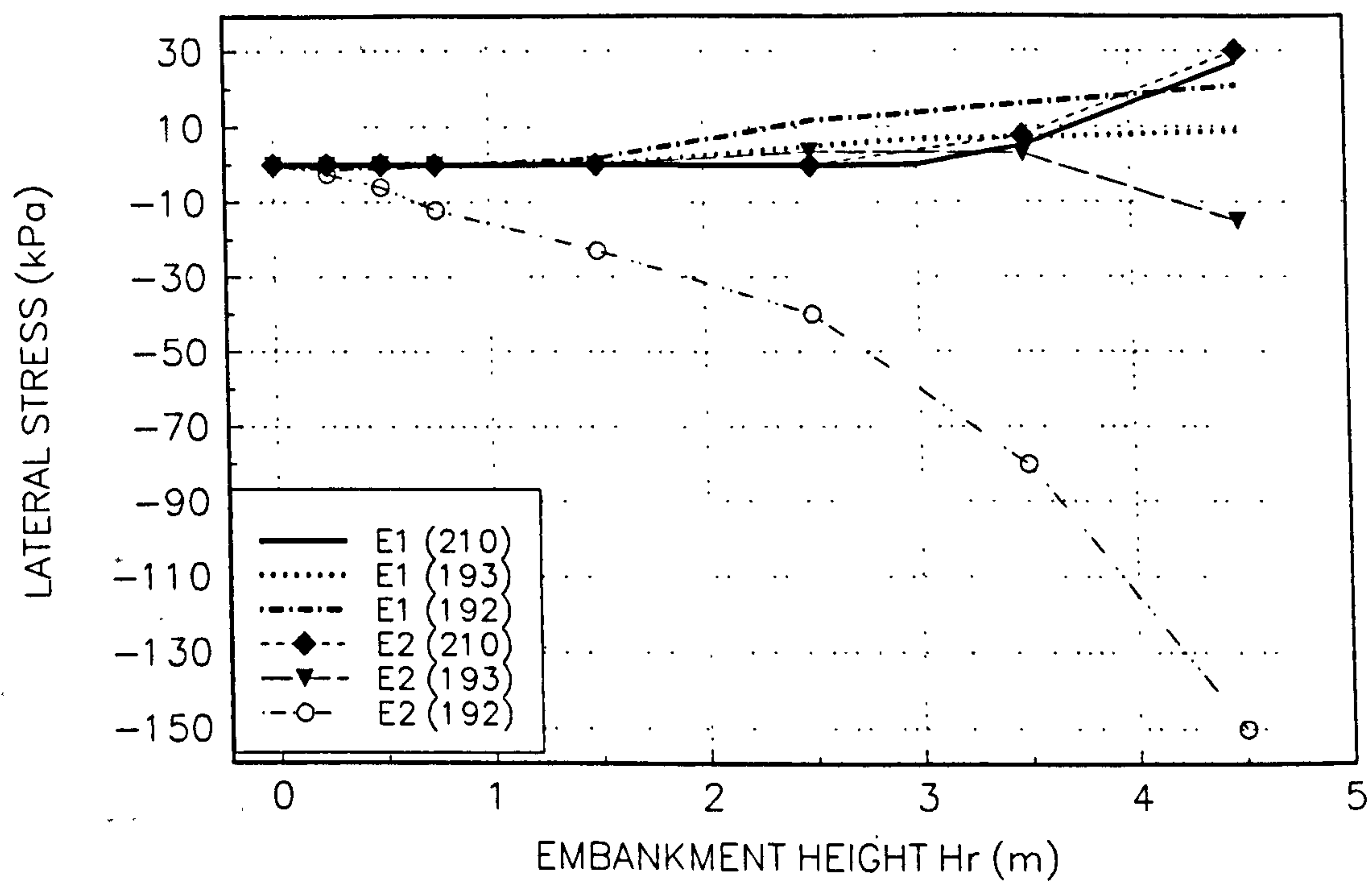


Fig 4.50. Computed displacement vectors obtained using an isotropic elastic, perfectly plastic soil model (Mohr-Coulomb) to describe the embankment. Analysis E1; embankment height of 1.5m. Displacement magnification factor=8

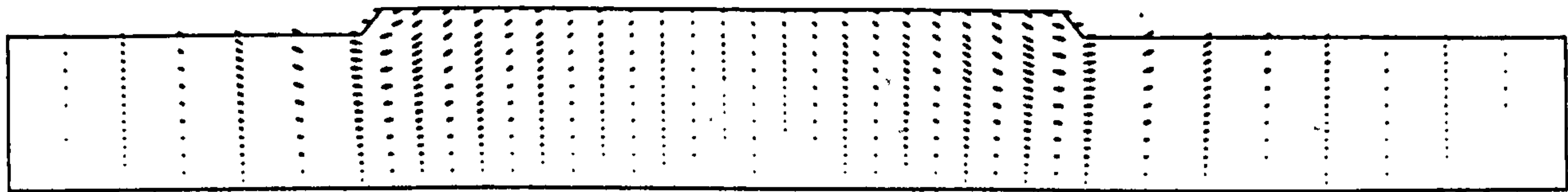


Fig 4.51. Computed displacement vectors obtained using an isotropic elastic soil model to describe the embankment. Analysis E2; embankment height of 1.5m. Displacement magnification factor=8

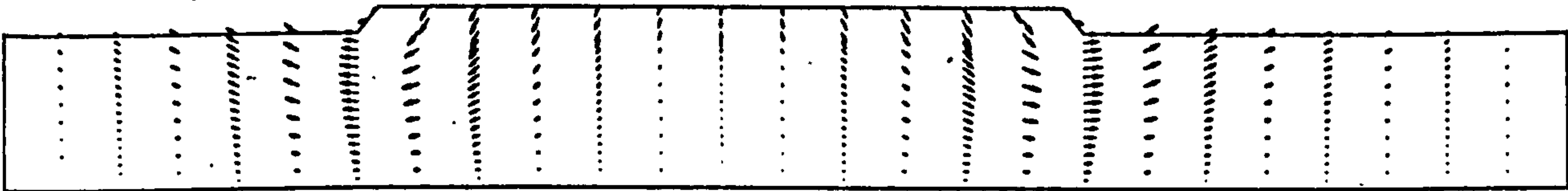


Fig 4.52. Computed displacement vectors obtained using an isotropic elastic, perfectly plastic soil model (Mohr-Coulomb) to describe the embankment. Analysis E1; embankment height of 2.5m. Displacement magnification factor=8

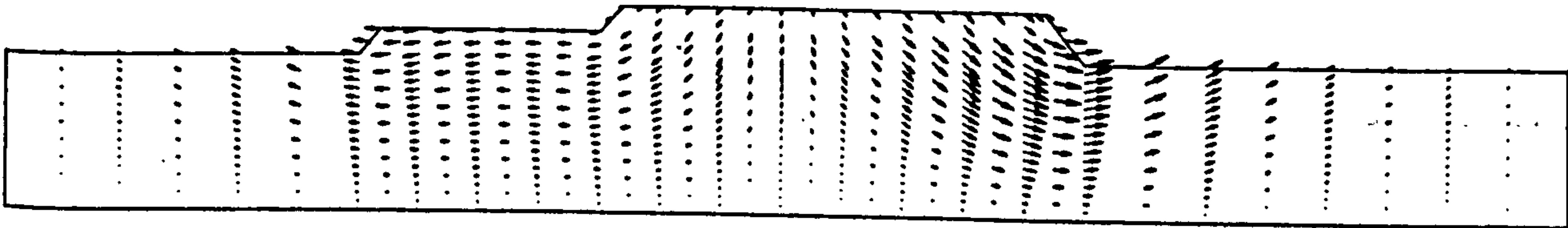


Fig 4.53. Computed displacement vectors obtained using an isotropic elastic soil model to describe the embankment. Analysis E2; embankment height of 2.5m. Displacement magnification factor=8

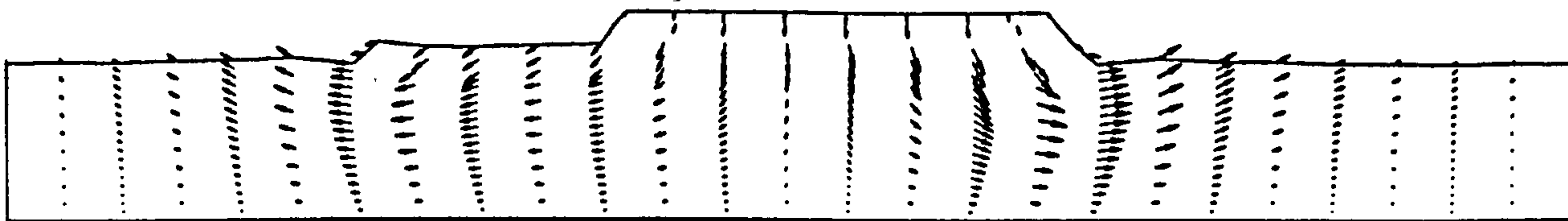


Fig 4.54. Computed displacement vectors obtained using an isotropic elastic, perfectly plastic soil model (Mohr-Coulomb) to describe the embankment. Analysis E1; embankment height of 3.5m. Displacement magnification factor=8

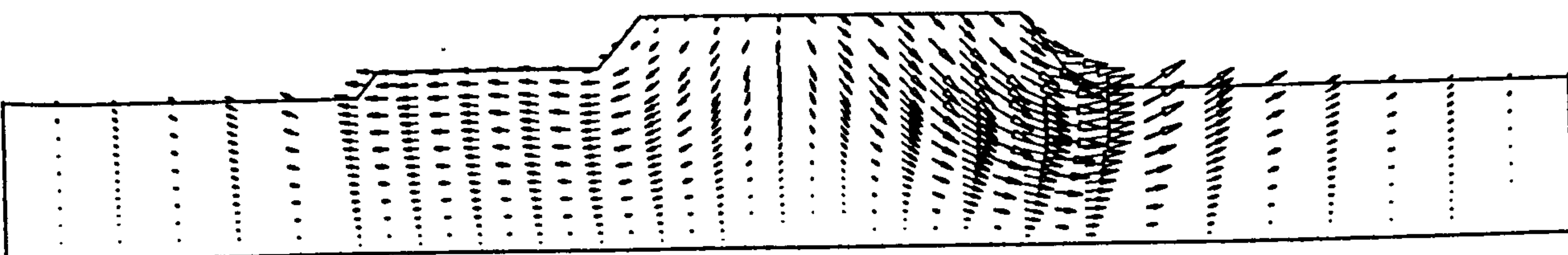


Fig 4.55. Computed displacement vectors obtained using an isotropic elastic soil model to describe the embankment. Analysis E2; embankment height of 3.5m. Displacement magnification factor=8

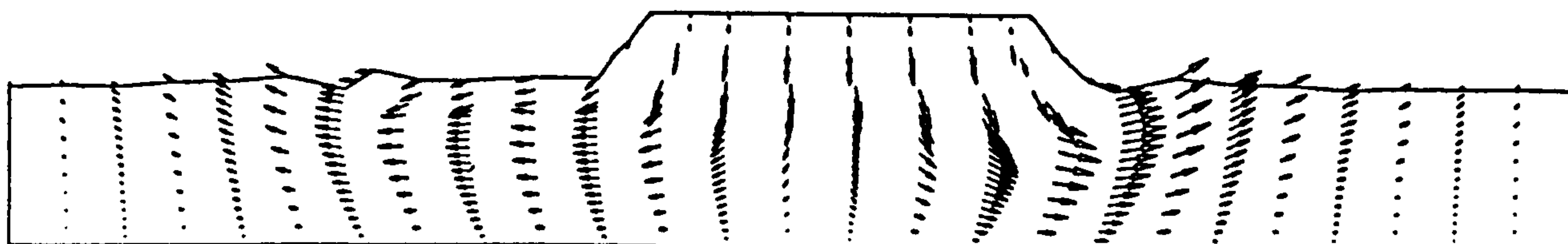


Fig 4.56. Computed displacement vectors obtained using an isotropic elastic, perfectly plastic soil model (Mohr-Coulomb) to describe the embankment. Analysis E1; embankment height of 4.5m. Displacement magnification factor=8

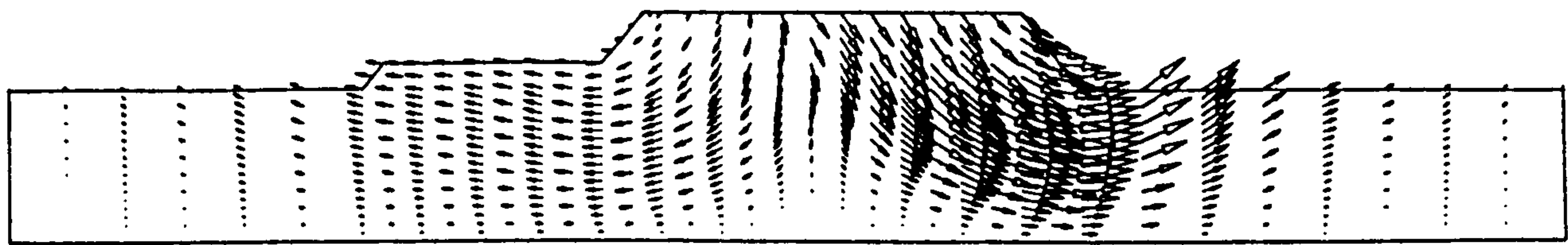


Fig 4.57. Computed displacement vectors obtained using an isotropic elastic soil model to describe the embankment. Analysis E2; embankment height of 4.5m. Displacement magnification factor=8

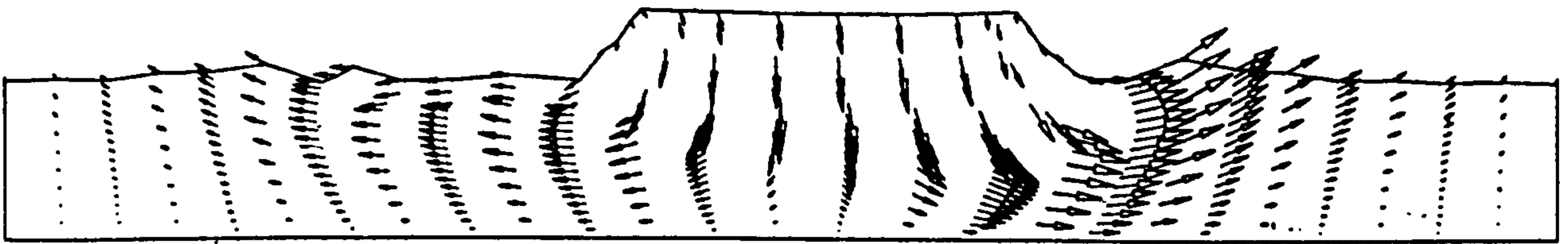


FIGURE 4.58
(IMPROVED) VERTICAL DISPLACEMENT AT CENTRE LINE

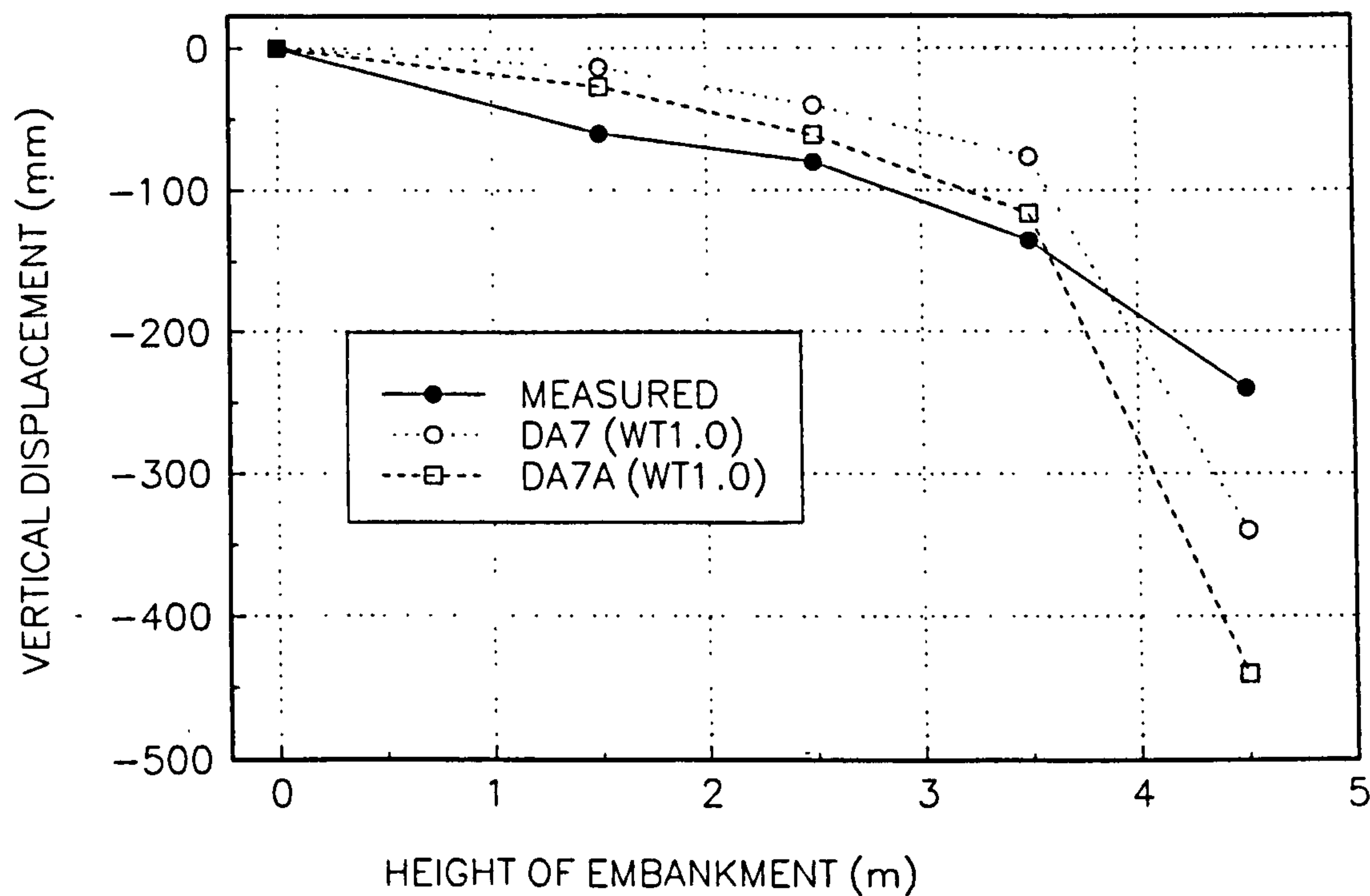


FIGURE 4.59
VERTICAL DISPLACEMENT AT CENTRE LINE

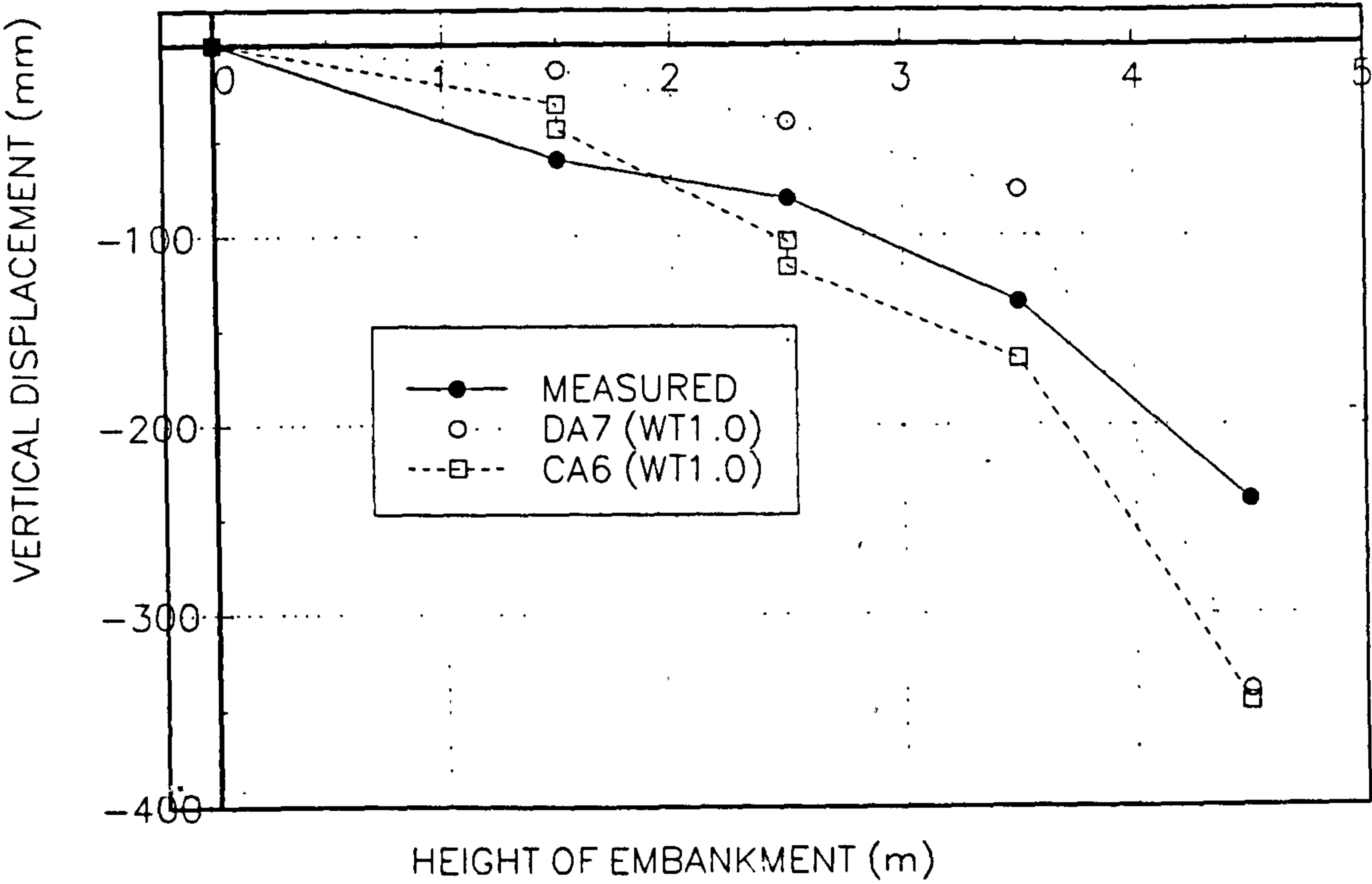


FIGURE 4.60
VERTICAL EDGE DISPLACEMENT. LOCATION 162

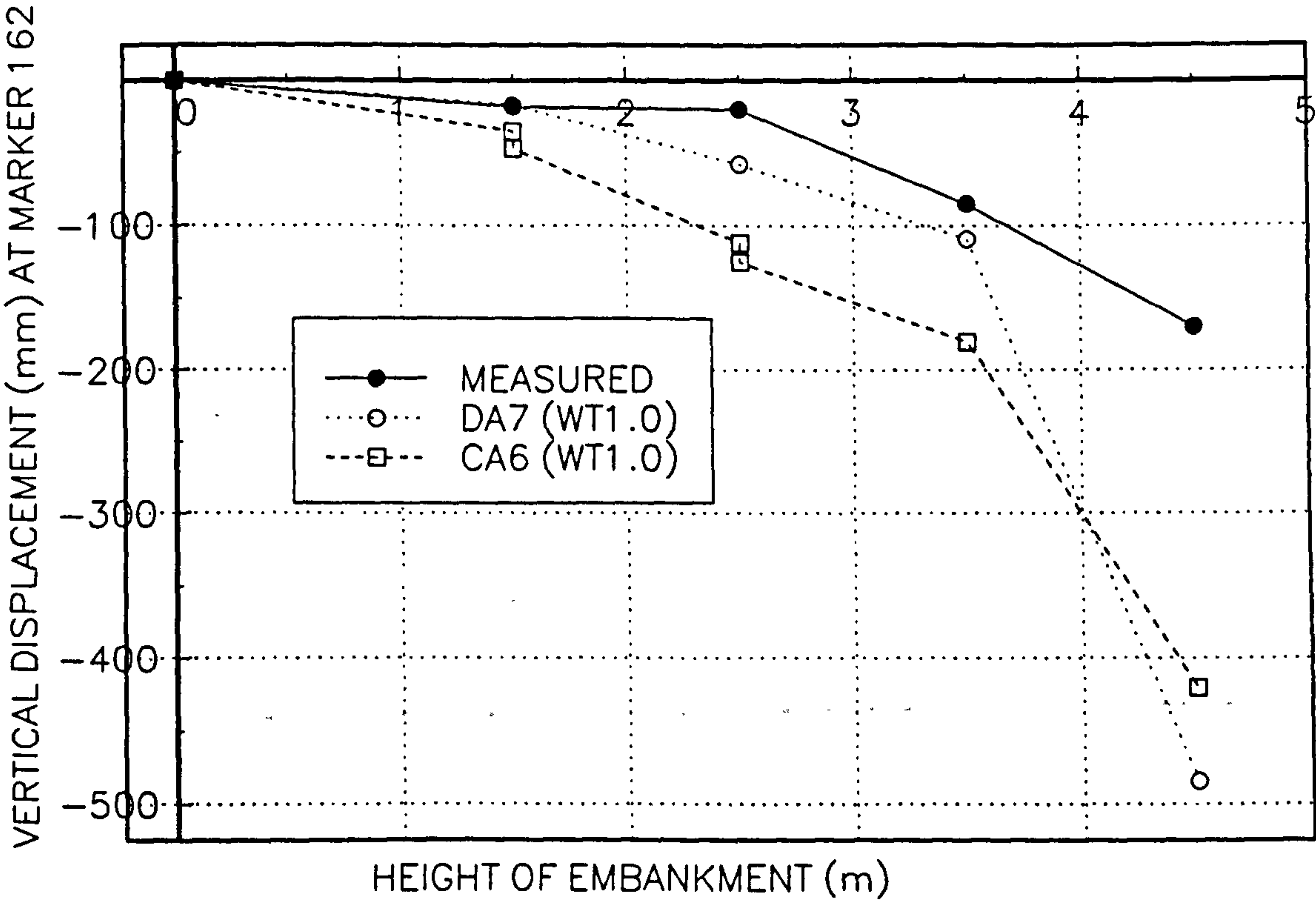


FIGURE 4.61
HORIZONTAL DISPLACEMENT AT 197

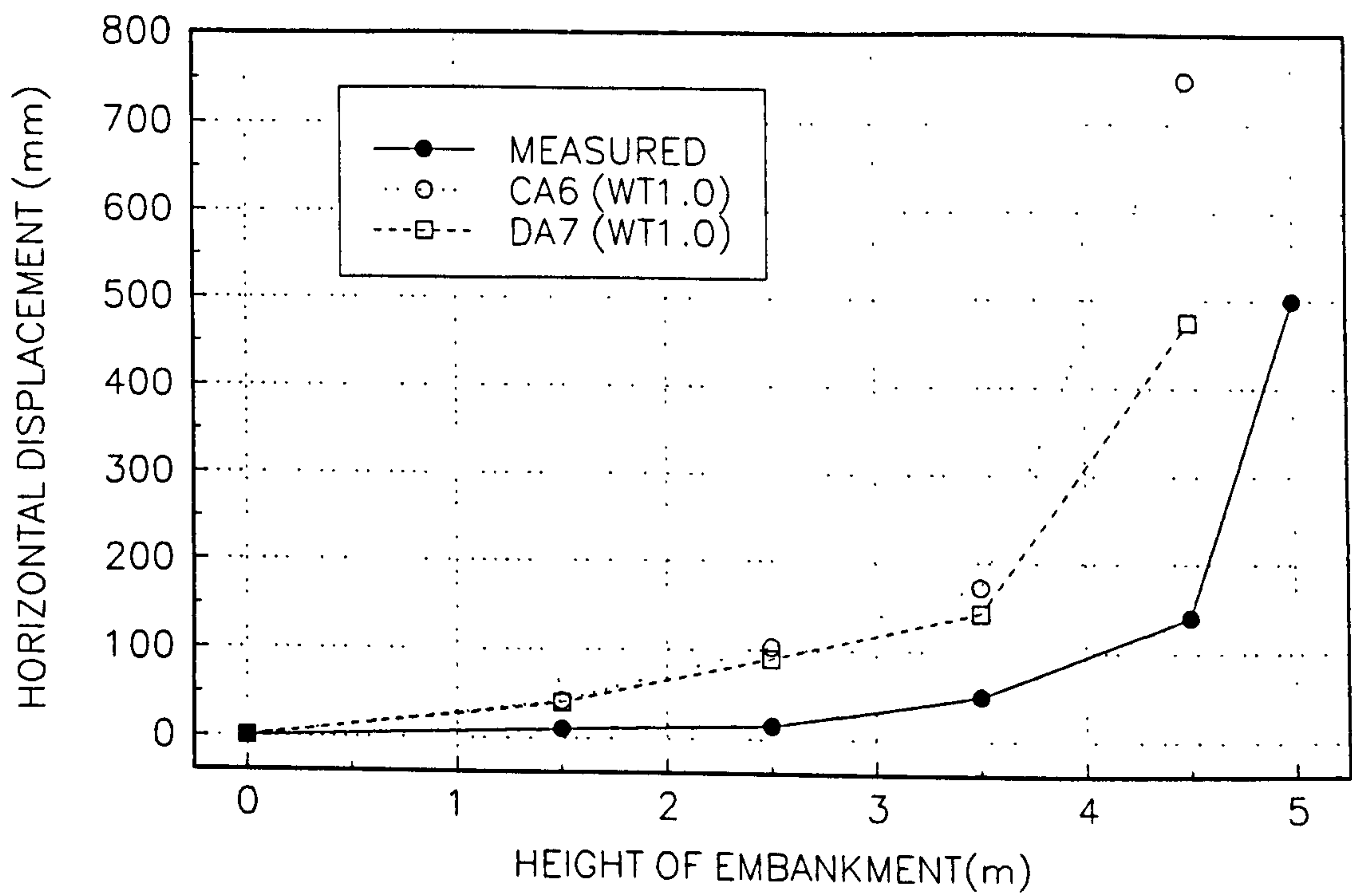


FIGURE 4.62
EXCESS PORE WATER PRESSURE AT EMBANKMENT HEIGHT OF 1.5m

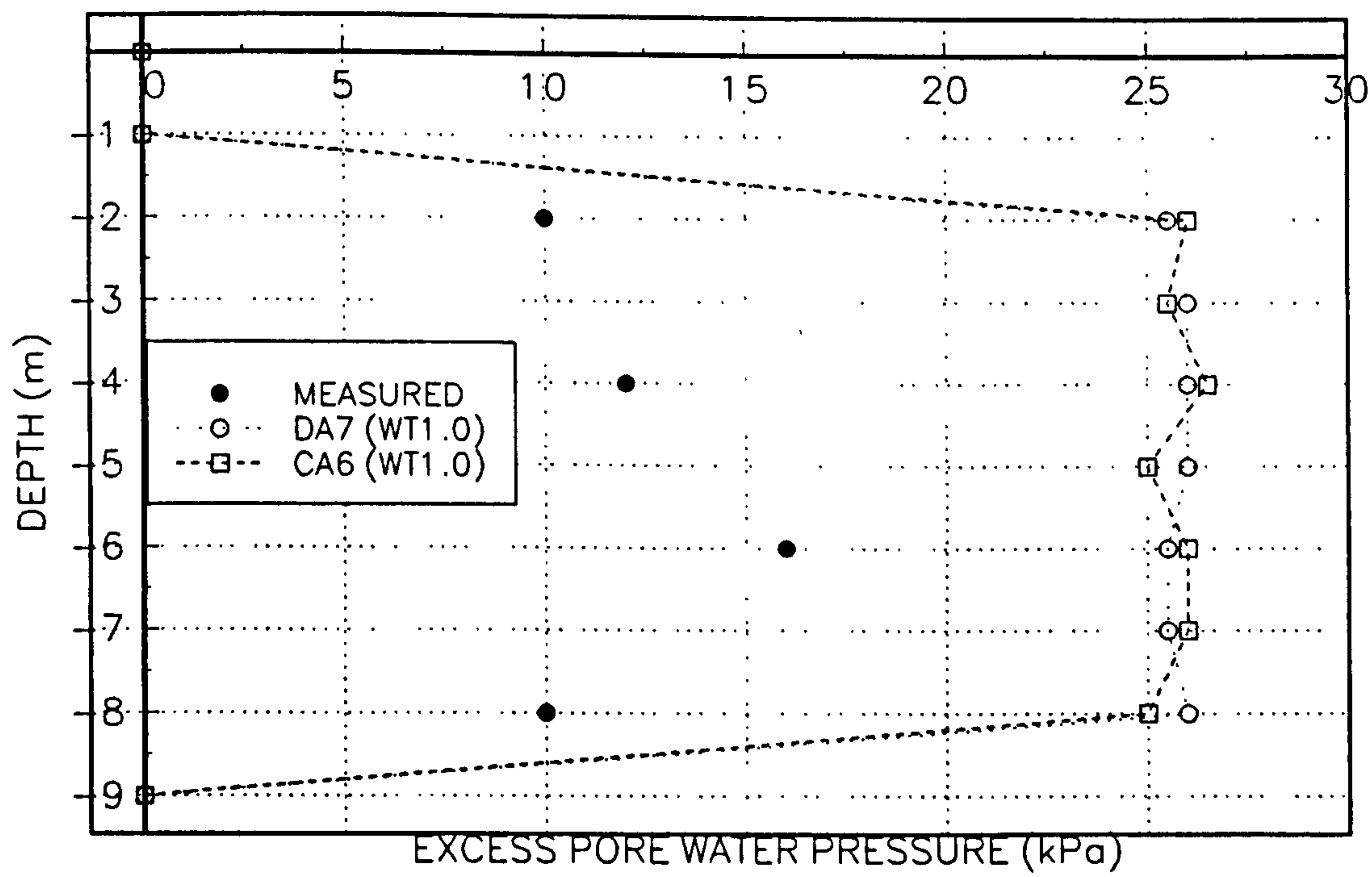


FIGURE 4.63
EXCESS PORE WATER PRESSURE FOR AN EMBANKMENT HEIGHT OF 2.5m

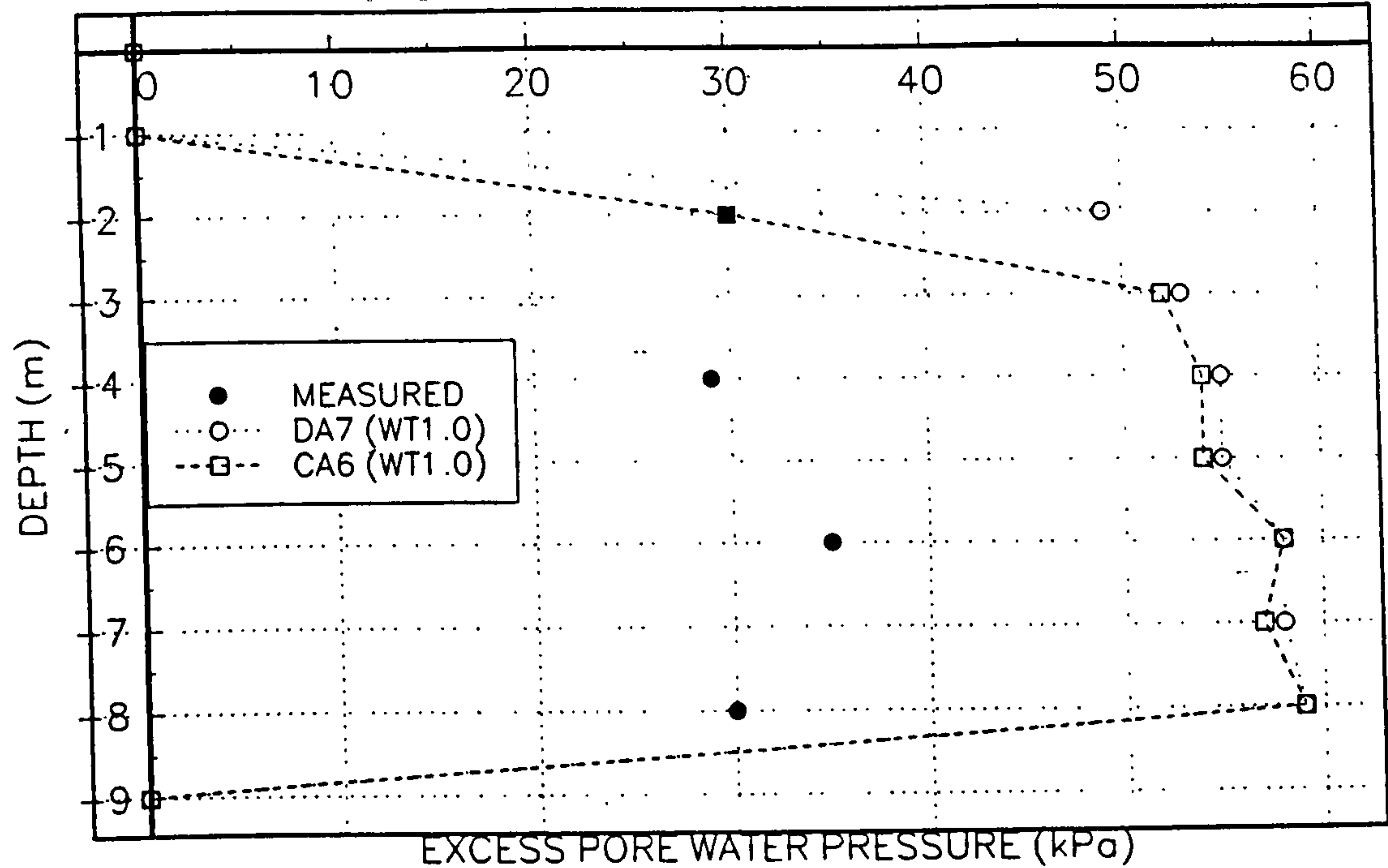


FIGURE 4.64
EXCESS PORE WATER PRESSURE FOR EMBANKMENT HEIGHT OF 3.5m

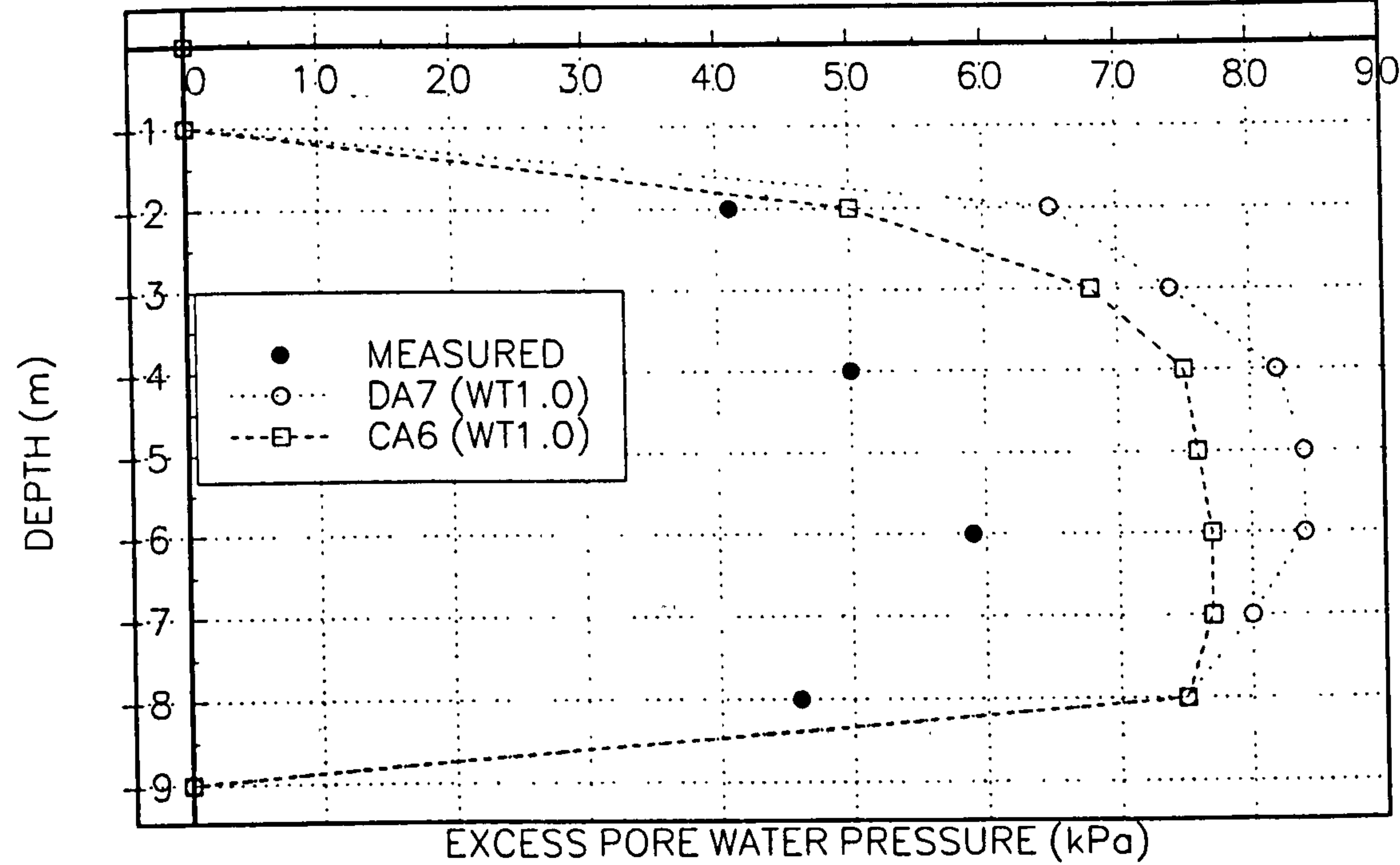


FIGURE 4.65
EXCESS PORE WATER PRESSURE FOR EMBANKMENT HEIGHT OF 4.5m

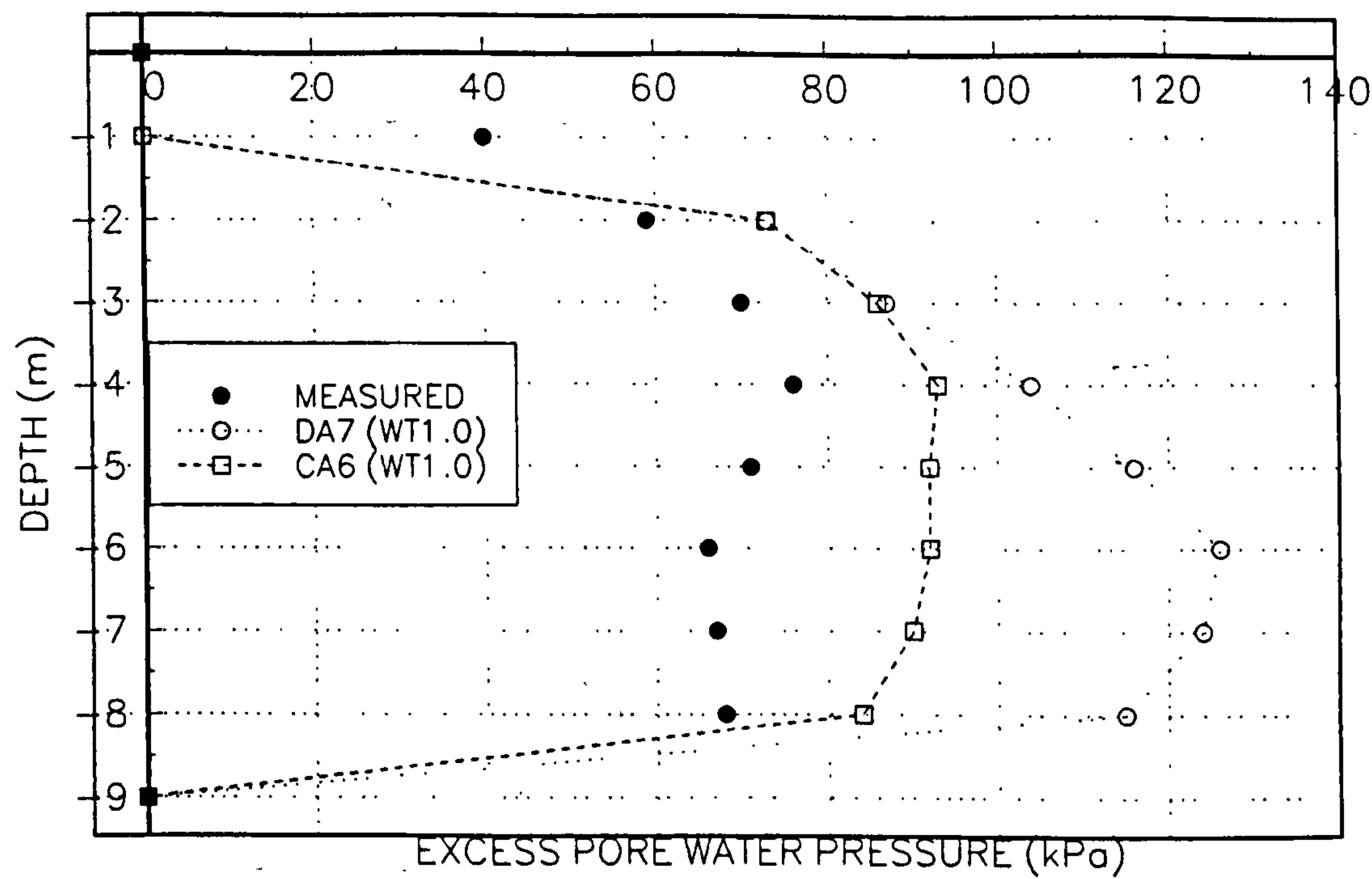


FIGURE 4.66
EXCESS PORE WATER PRESSURE AGAINST EMBANKMENT HEIGHT FOR 4m DEPTH

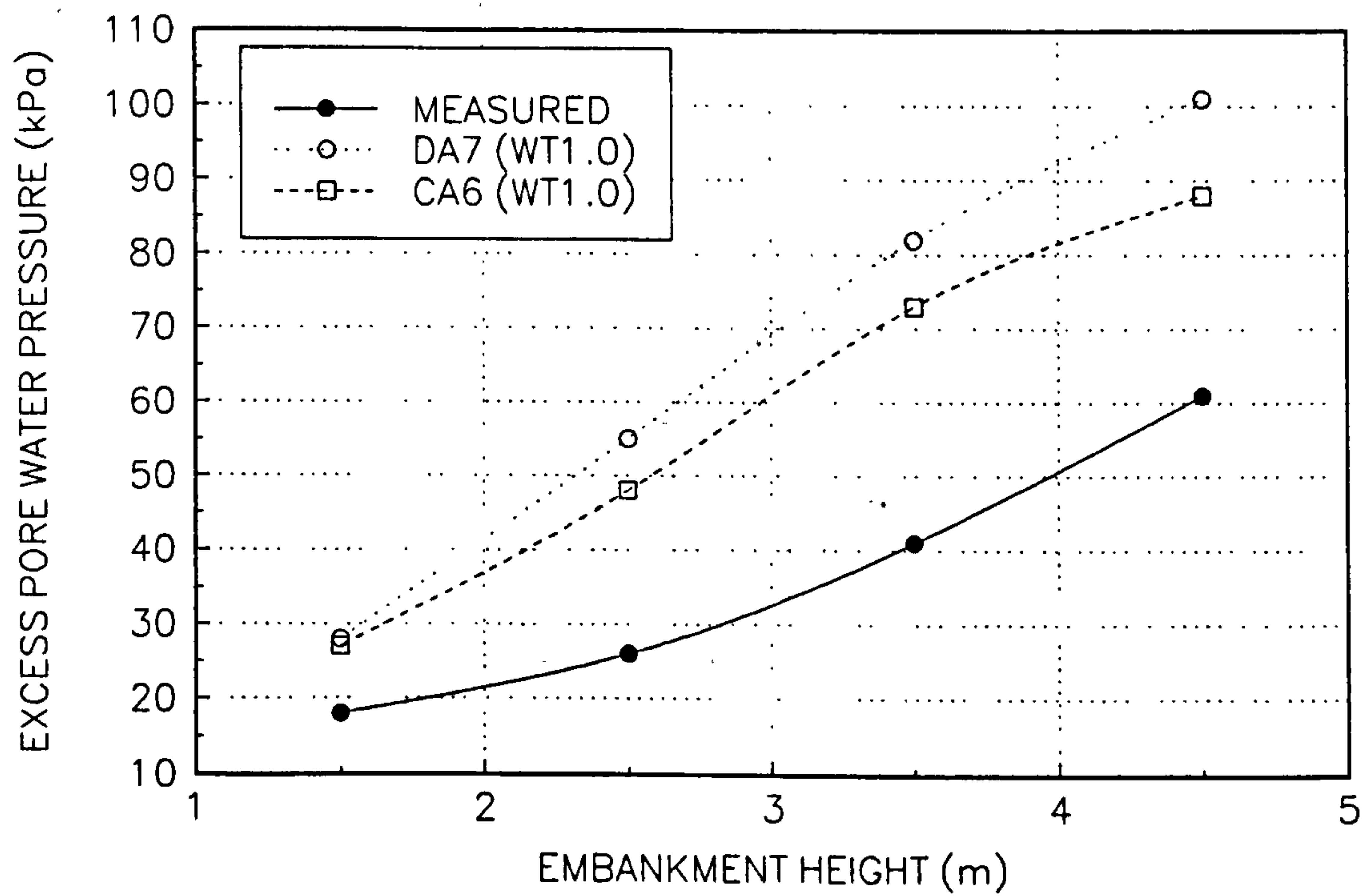


FIGURE 4.67
EXCESS PORE WATER PRESSURE AGAINST EMBANKMENT HEIGHT AT DEPTH OF 6m

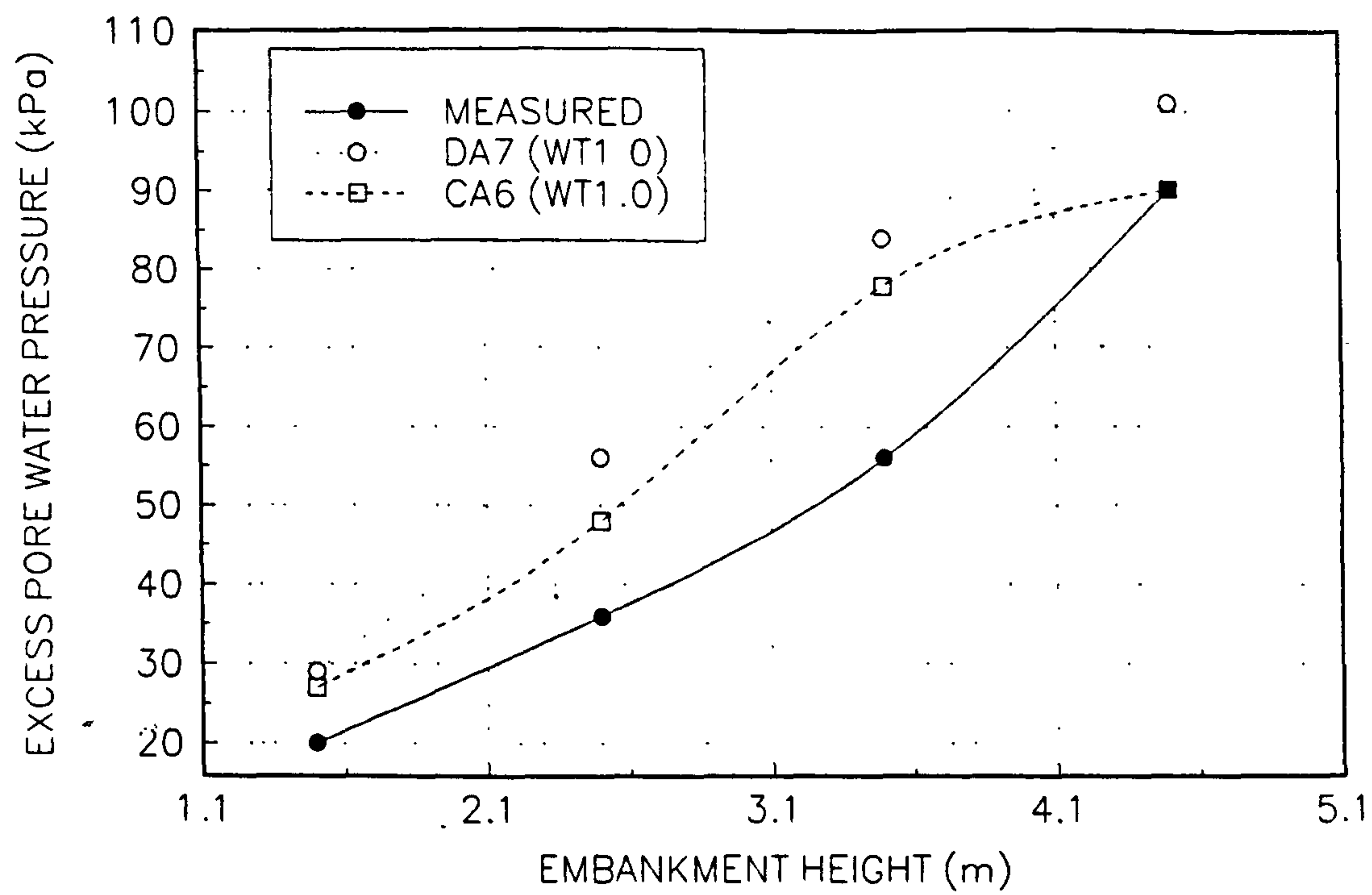


Fig 4.68. Relation between pore water pressure and vertical total stress caused by an embankment. Points OP'A'F' and C' are described in Fig 4.23.

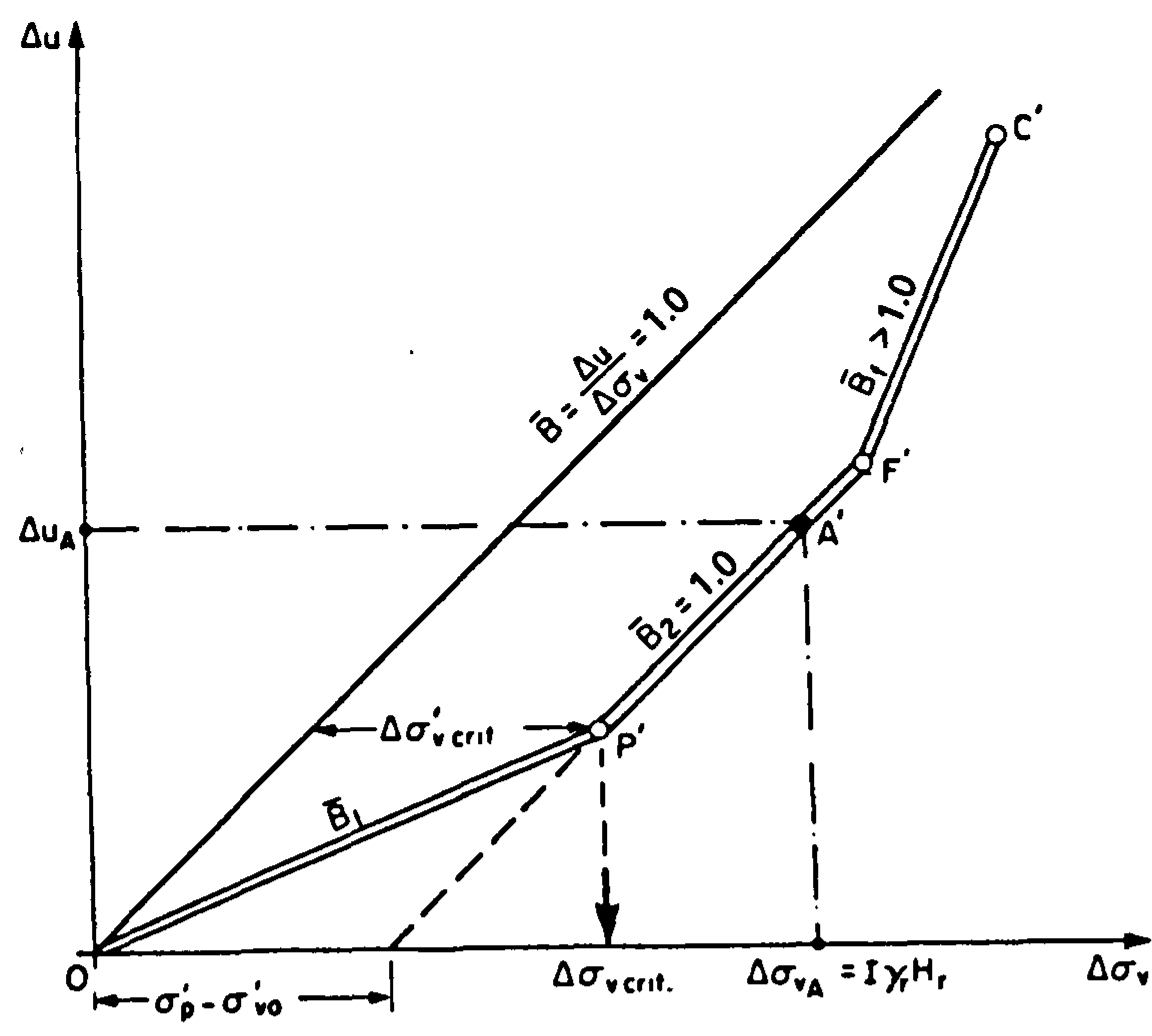


FIGURE 4.69
EXCESS PORE WATER PRESSURE PROFILE FOR AN EMBANKMENT HEIGHT OF 1.5m

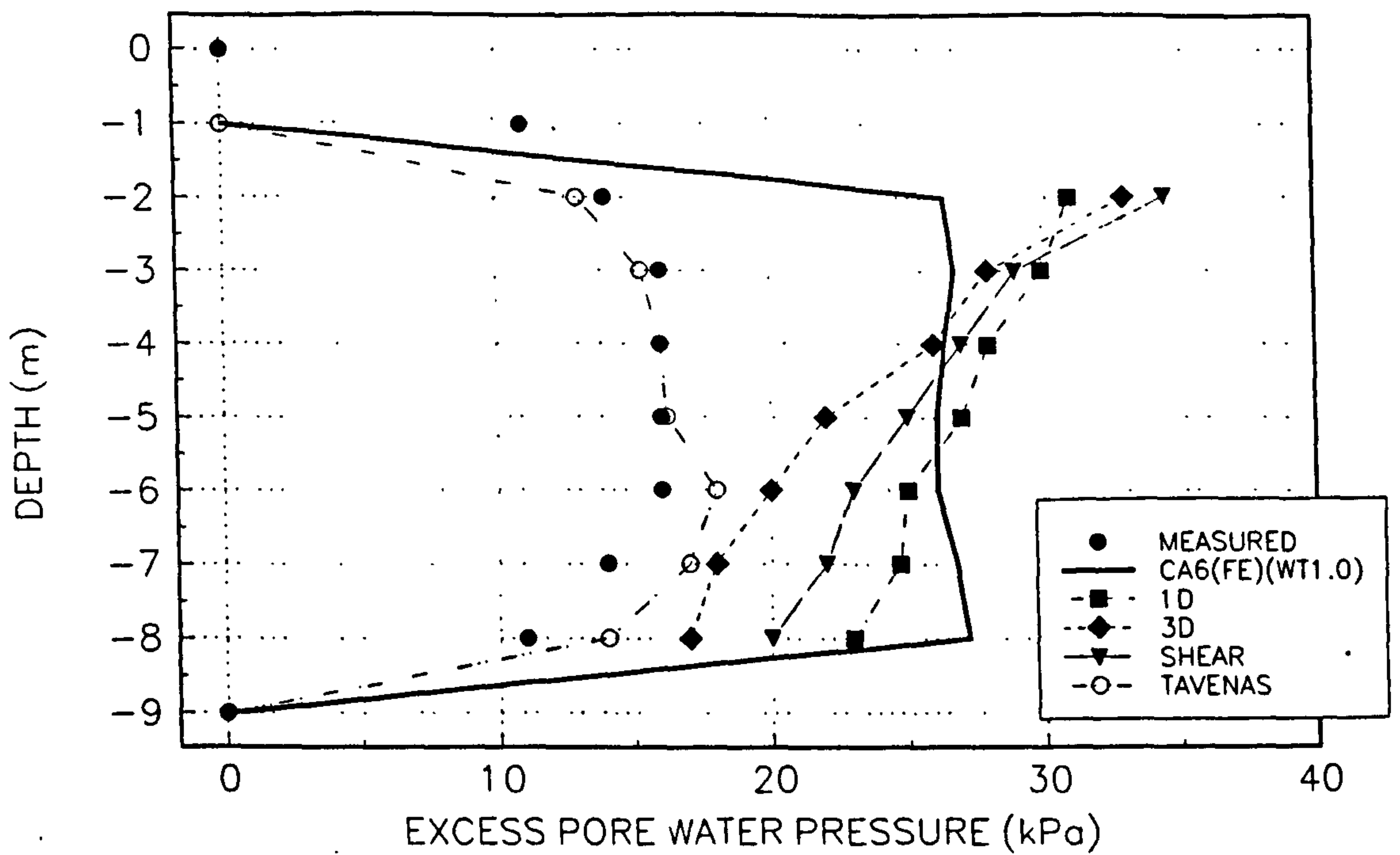


FIGURE 4.70
EXCESS PORE WATER PRESSURE PROFILE FOR AN EMBANKMENT HEIGHT OF 2.5m

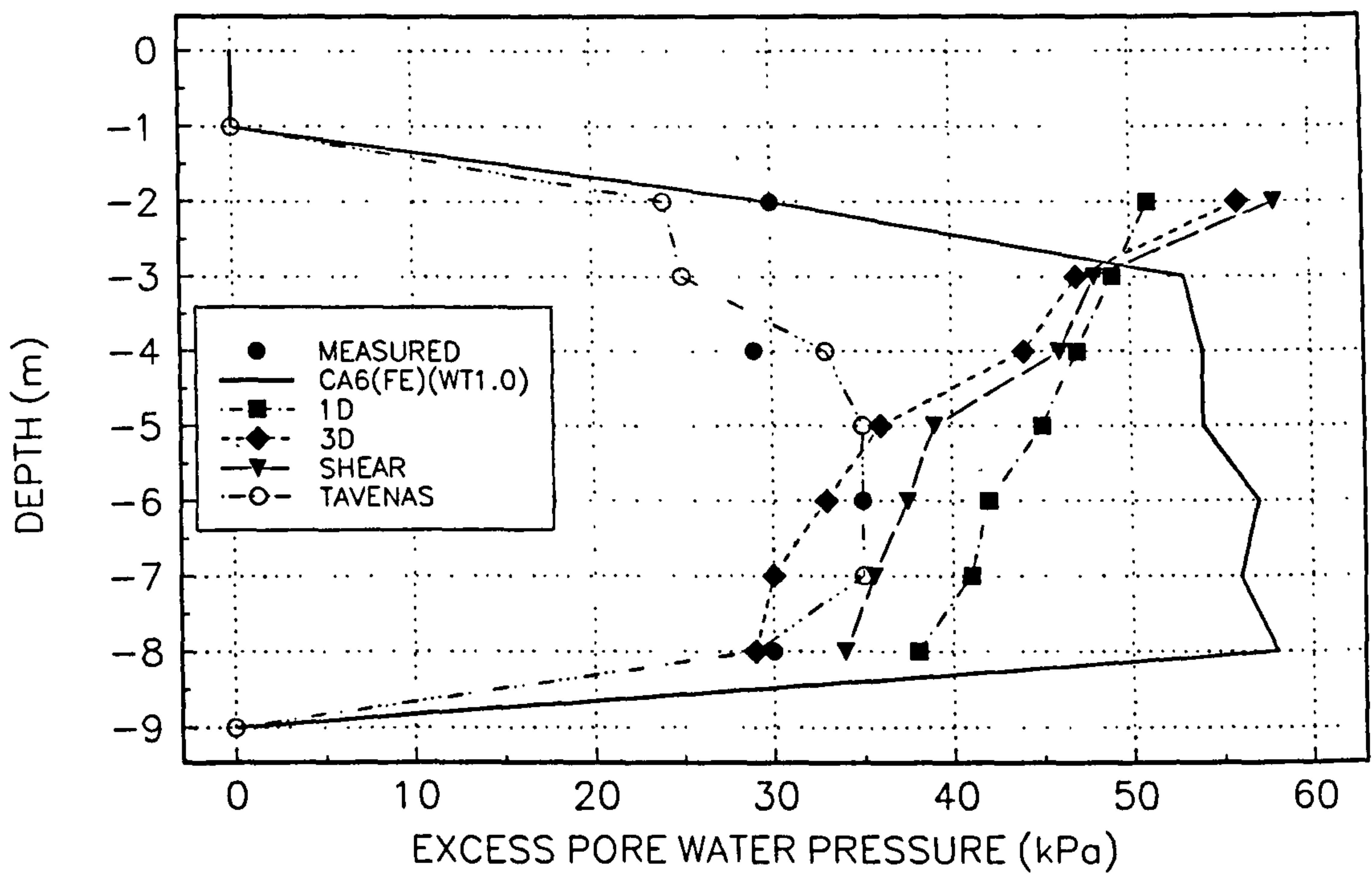


FIGURE 4.71
EXCESS PORE WATER PRESSURE PROFILE FOR AN EMBANKMENT HEIGHT OF 3.5m

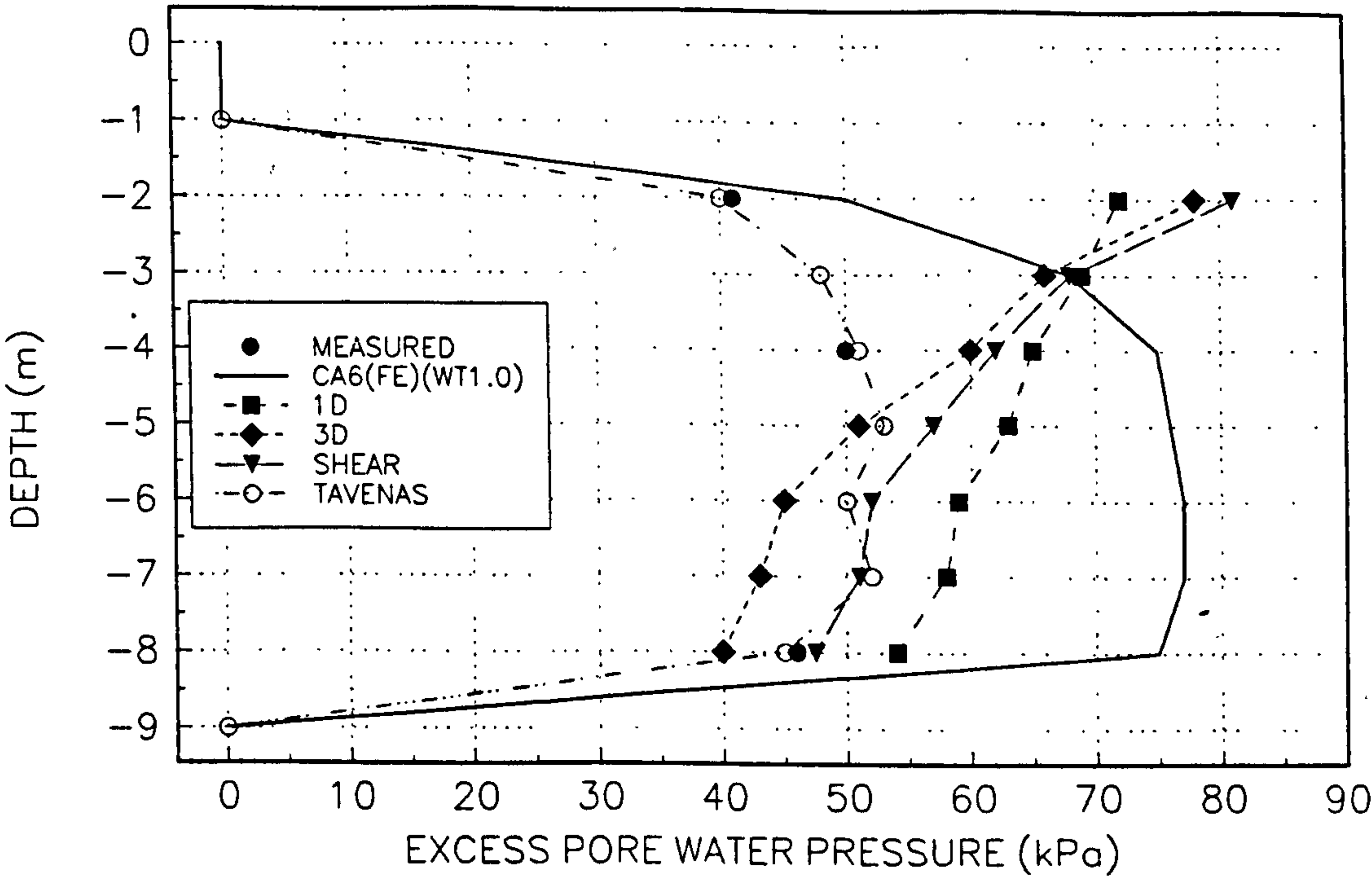


FIGURE 4.72
EXCESS PORE WATER PRESSURE PROFILE FOR AN EMBANKMENT HEIGHT OF 4.5m

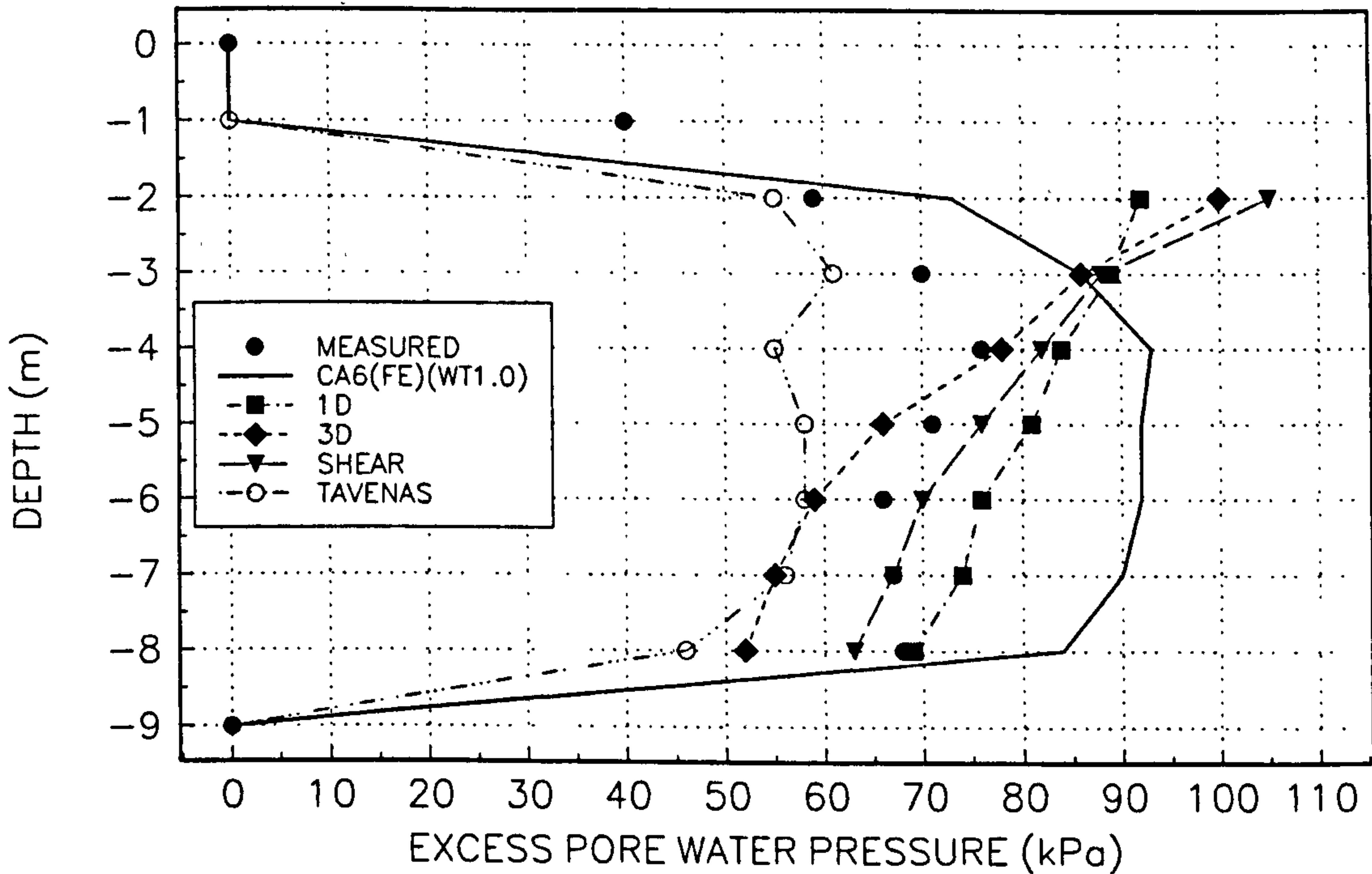


Fig 4.73. Effect of compressibility of pore water pressure on calculations of excess pore water pressure at 4m and 6m depth (Magnan, Mieussens and Queyroi, 1983).

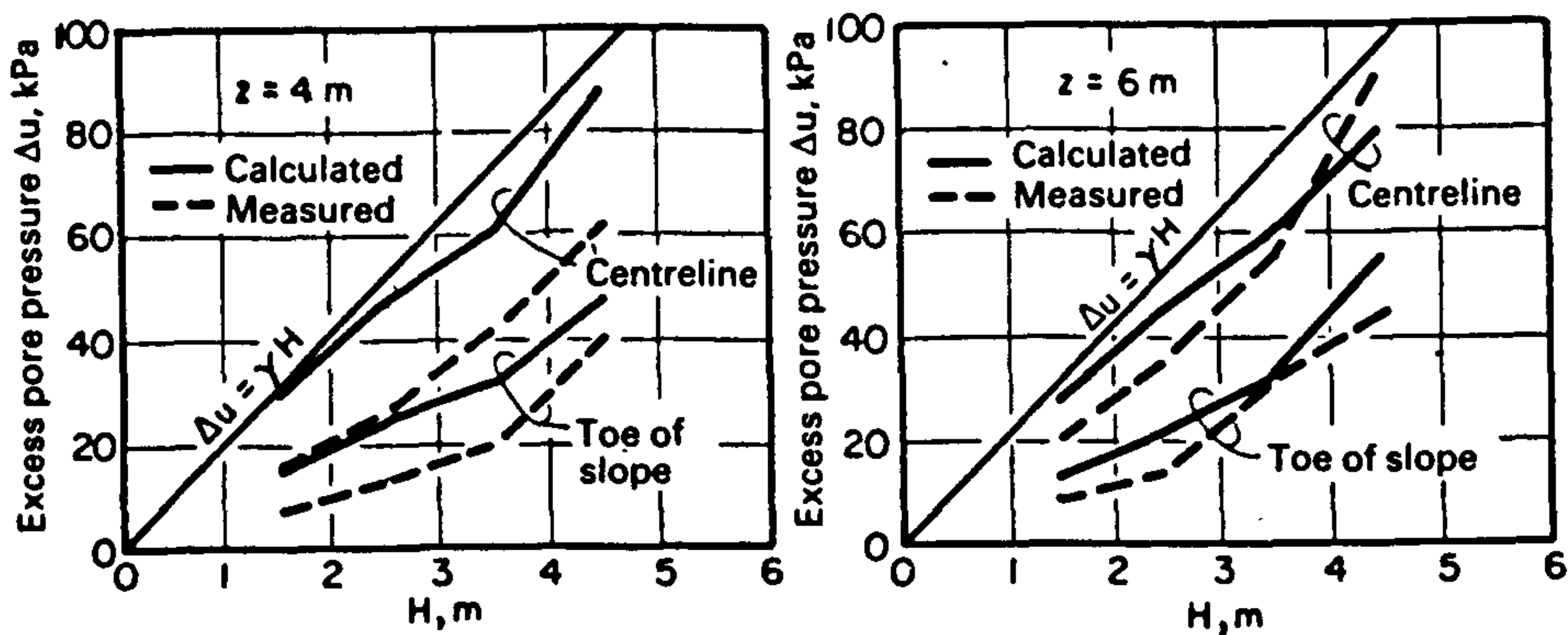


Fig 4.74. Effect of compressibility of pore water pressure on calculations of excess pore water pressures under the centre of embankment at construction heights of 1.5m and 4.5m (Magnan, Mieussens and Queyroi, 1983).

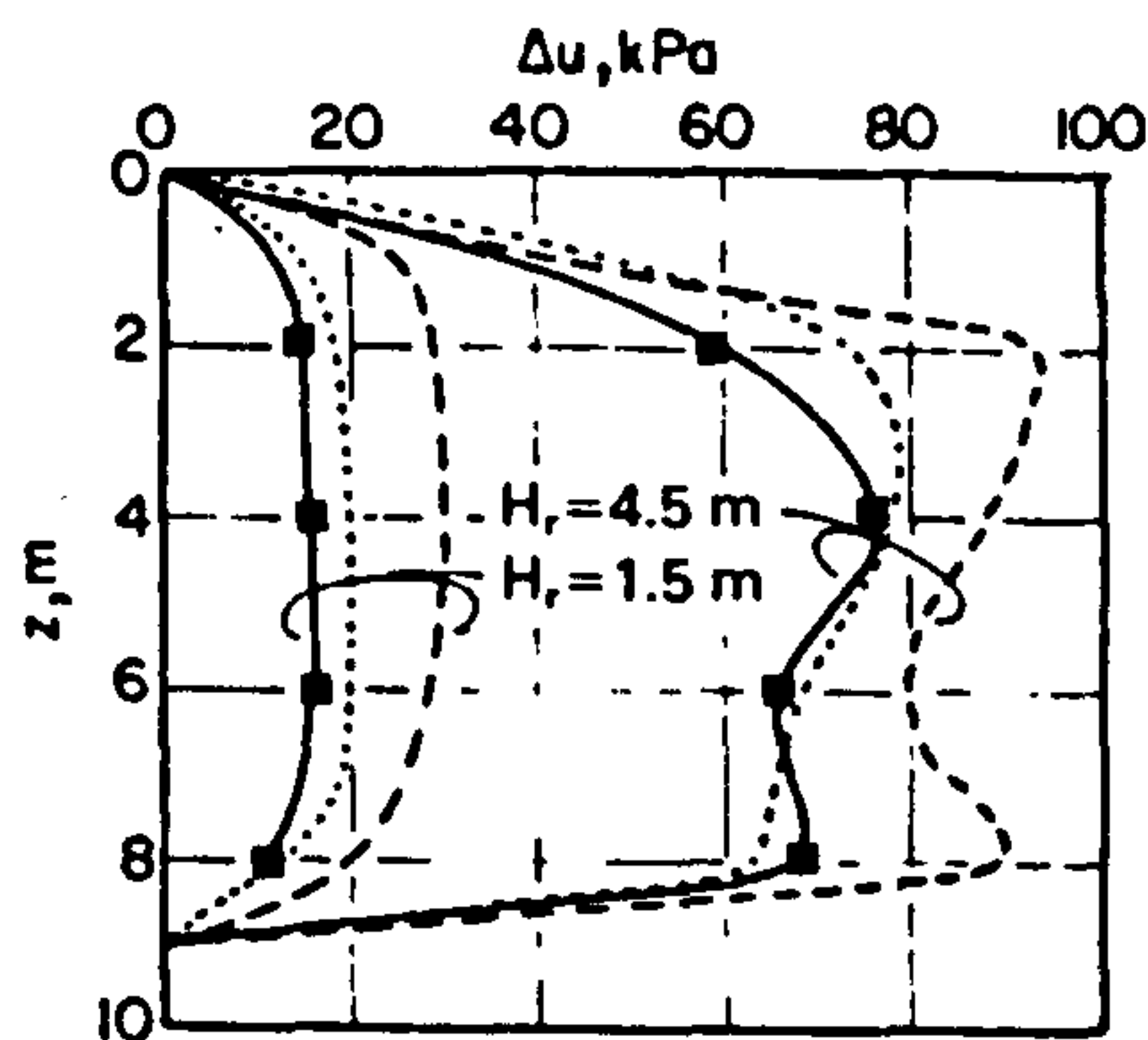


Fig 4.75. Relation between settlement, s , and maximum horizontal displacement, y_{max} , (Magnan, Mieussens and Queyroi, 1983).

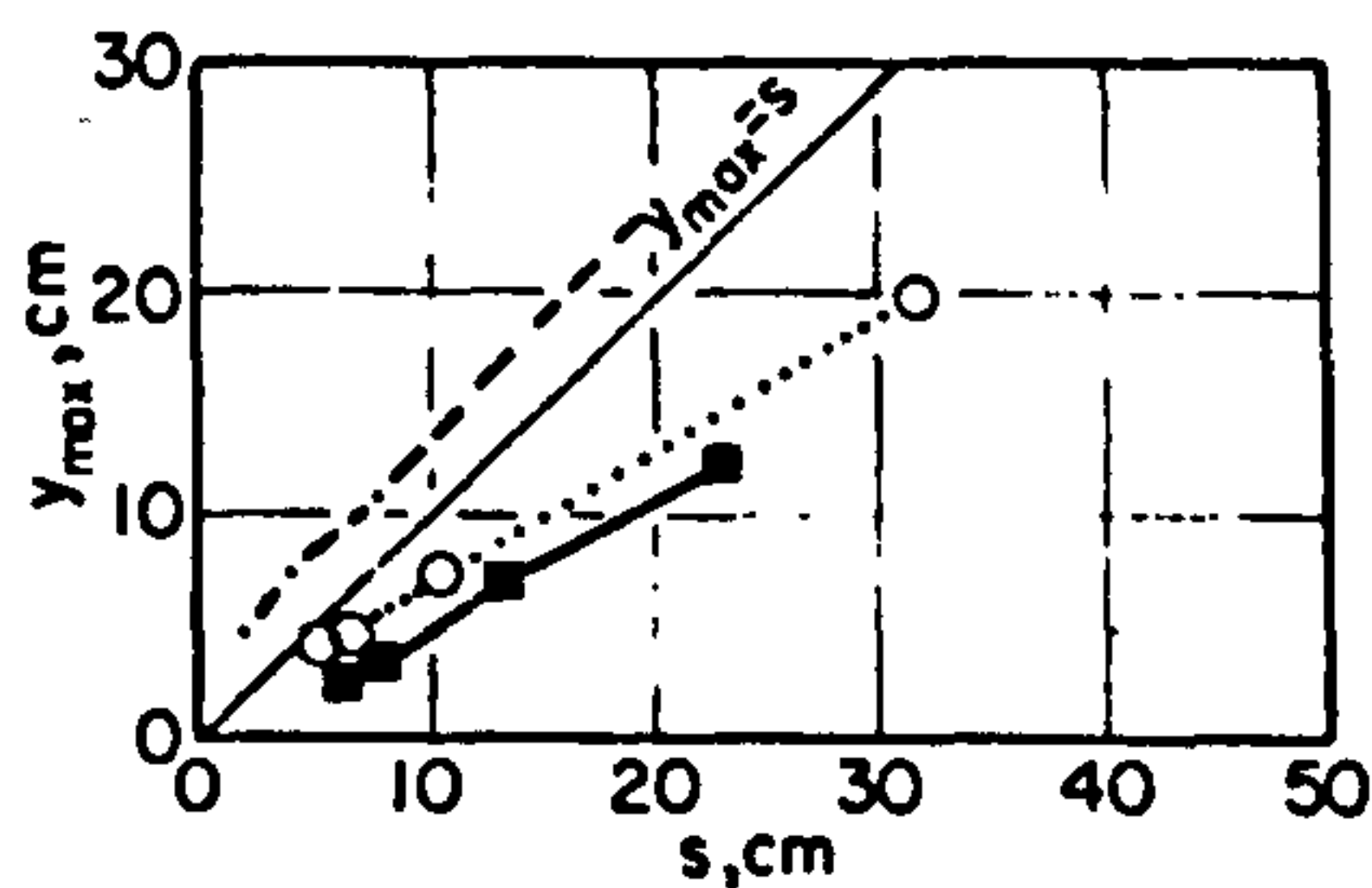
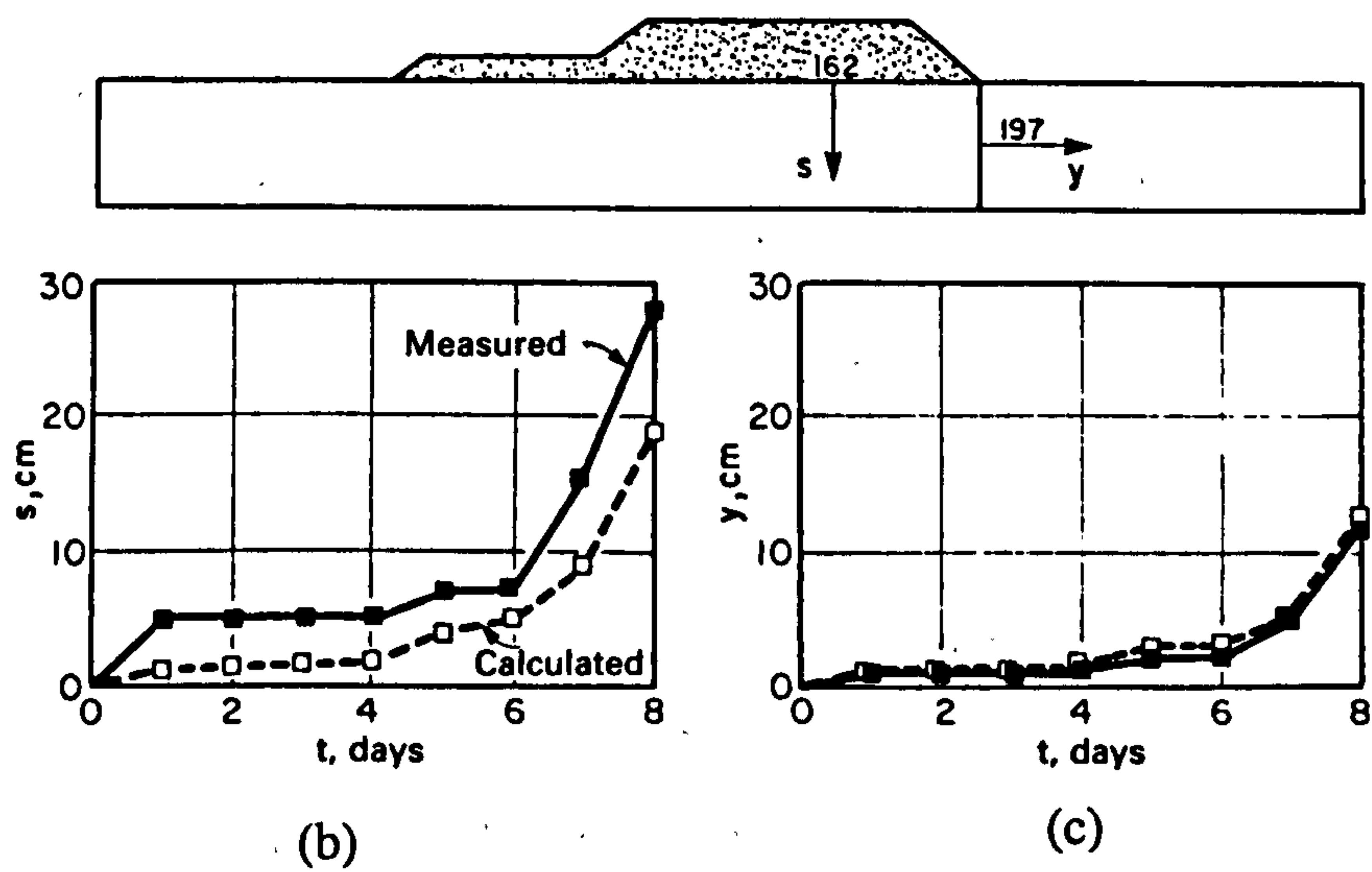
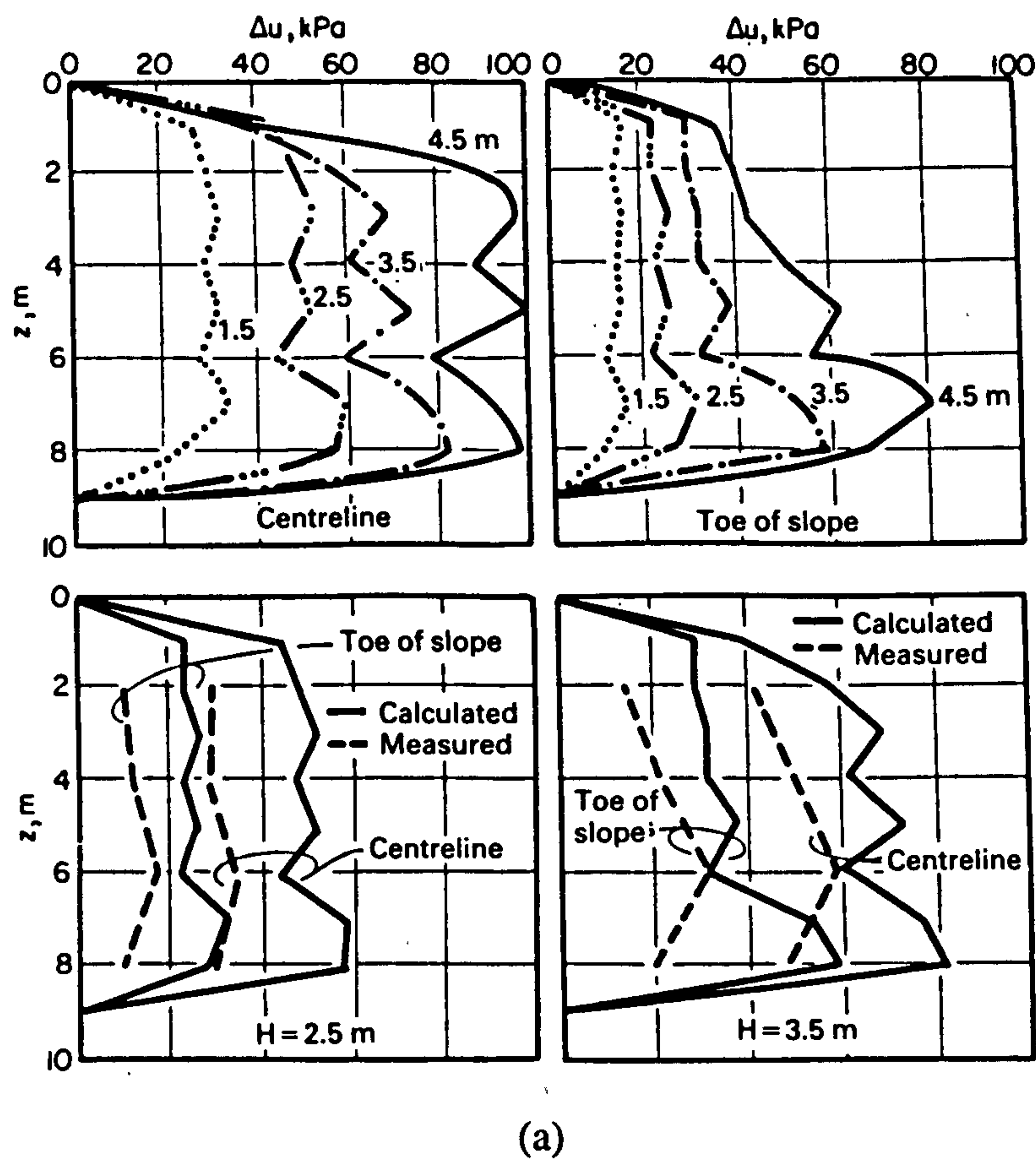


Fig 4.76. Effect of compressibility of pore water pressure on calculations: (a) Excess pore water pressures under the embankment; (b) settlement of point 162 and (c) horizontal displacement of point 197 (Magnan, Mieussens and Queyroi, 1983).



CHAPTER 5

5. Cubzac-les-Ponts embankment B.

5.1 Introduction

In this chapter the long term pre-failure behaviour of a soft clay foundation loaded via a trial embankment has been investigated using finite element analysis. Numerical predictions using the modified Cam clay soil model have been compared with the observed foundation behaviour measured over a period of six years (Magnan, Mieussens and Queyroi, 1983). The predictability of the foundation behaviour has been investigated in detail. However, the main concern of analyses was to determine a set of material parameters that provided a reasonable estimate of the observed behaviour and hence provide a framework of parameter selection for similar loading situations. It is therefore the intent of this chapter to present the main results of the back analyses and discuss the parameter selection process from which a suitable numerical solution was obtained. A hypothetical design situation requiring an estimation of the long term settlements, lateral displacements and excess pore water pressures has been assumed.

The embankment described in this chapter (embankment B) was the second embankment constructed at Cubzac-les-Ponts and was used to study the time-dependent consolidation of the soil under and adjacent to the embankment. Details of embankment B and the trial loading are given in section 5.2. Numerical modelling assumptions of this loading event are also included in section 5.2.

Details of the soft clay research site at Cubzac-les-Ponts are given in chapter 4. Previous analysis of this trial embankment (Magnan et al., 1983) was performed using the MELANIE soil model. The MELANIE soil model is briefly described in chapter 4.

In chapter 4, use of the modified Cam clay soil model to describe the soft clay foundation was of limited success and only served to reproduce reasonably well the observed vertical displacement response. The inability of analyses described in chapter 4 to reproduce the observed behaviour associated with the construction of embankment A is characteristic of simple elasto-plastic soil models (Indraratna et al., 1992). Despite the poor predictions obtained in the chapter 4 numerical analyses performed by Almeida et al. (1985); Chai and Bergado (1992); Brinkgreve and Vermeer (1992); Naatanen and Lojander (1994) and Hird (1994) have demonstrated that for the long term (consolidation) behaviour the modified Cam clay soil model can generally predict reasonable results, particularly for excess pore water pressures and settlements, but not lateral deformations. However, this problem is not only limited to modified Cam clay but also to the more complex elasto-plastic soil models such as MELANIE (Mouratidis and Magnan, 1983) (see section 5.6). It is still not yet fully understood what feature is required in a soil model to accurately obtain lateral displacements (Gens, 1994) however, use of elasto-visoplastic soil models (Sekiguchi and Ohta, 1977 and Miki et al., 1994) provide improved lateral displacement solutions. In practice elasto-visoplastic soil models are not yet widely available nor widely favoured as their use requires further soils testing to determine the greater number of soil parameters associated with their use. Additionally, typical design situations, especially in the UK, do not justify the level of complexity associated with these models. As a result, the simpler modified Cam clay soil model which is widely recognised and used in practice to describe soft clay foundations (Gens, 1994) has been used to re-analyse embankment B. Embankment B is representative of many embankment studies encountered in practice.

Material parameters required for analyses described in this chapter are based on those selected for embankment A. Selected parameters are briefly reviewed and discussed in section 5.3. The results of the consolidation analyses are presented and discussed in section 5.4. In the discussion presented in section 5.4 vertical displacements, lateral displacements and excess pore water pressures are considered separately. Additionally, within each subsection alternative design methods are suggested. For comparison the results of previous analysis (Mouratidis and Magnan, 1983) are briefly

summarised in section 5.5. Conclusions drawn from the discussion are presented in section 5.6.

5.2 Trial loading and numerical modelling.

Embankment B was constructed from coarse sand and gravel (same material as embankment A); $\gamma=21\text{kPa}$ and $\phi'=35$ degrees (Mouratidis and Magnan, 1983 and Magnan et al; 1983), over a period of six days to a height of 2.3m, Fig 5.1, and with a factor of safety against immediate failure of 1.5. Details of the embankment dimensions are shown in Fig 5.2. The instrumentation which consisted mainly of piezometers, settlement gauges and inclinometers, was placed predominantly in one transverse section of the embankment, section k-k. The location of the instrumentation on section k-k is shown in Fig 5.3. Measurements were taken over a period of approximately 2000 days after construction. Numerical predictions were compared with the measurements obtained from the transverse section k-k. It was assumed that this section was sufficiently remote from the ends to be deforming under conditions of plane strain. The plane strain condition was imposed on analyses. The finite element mesh used, symmetric about the centre line, is shown in Fig 5.4. Boundary conditions are the same as were assumed for the consolidation analyses performed in chapter 4. The embankment loading was applied to the foundation by the self weight of the embankment elements when they are introduced into the mesh.

The Mohr-Coulomb soil model was used to describe the embankment. The soft clay foundation was described using the modified Cam clay soil model.

In chapter 4 undrained and consolidation analyses were performed to describe the foundation response to the construction of embankment A. Construction of embankment A took approximately nine days with standing times of 3 and 2 days after placement the first and second lifts. These standing times were sufficiently long to allow consolidation to be included in analyses. Here, embankment B was constructed quicker, in approximately 6 days, with only a single standing time after the first lift of 2 days. Initial analyses of embankment B found that this standing time was not long

enough to allow modelling of consolidation during the construction stage. Consequently, drainage conditions were not introduced to analyses until after construction of the embankment was complete, therefore the construction process was modelled as undrained. A consolidation period of approximately 6 years was modelled in analyses.

As for embankment A the water table was modelled at 1.0m depth.

5.3 Material parameters for embankment B.

The chosen parameters are presented in Table 5.1. Parameters presented in Table 5.1 were derived from slight adjustment of the improved parameter solution obtained from the undrained analyses described in chapter 4 (see section 4.5 and Table 4.6). The undrained parameter solution was chosen rather than the consolidation parameter solution because here the embankment construction is assumed to be undrained. Analyses described in chapter 4 found that the undrained response was less stiff than the corresponding consolidation behaviour.

Only parameters κ and λ , controlling the magnitude of elastic and plastic strains, and the permeability, k_h and k_v were adjusted.

Final values of κ are similar to with values obtained from the average slope of oedometer unload-reload data. The corresponding values of elastic stiffness, G , are similar to values of elastic stiffness obtained from the triaxial test measured at strains of approximately 0.3%, Fig 4.12.

Final values of λ are similar to the maximum values of λ obtained from normal compression data in an oedometer test. Chosen values of λ are not similar to those estimated using Muir Wood's empirical correlation, Fig 5.5. As can be seen from Fig 5.5 the spread of data points is wide, this is due to the high variation of plasticity index of the Cubzac-les-Ponts soft clay.

Plastic strains were found to dominate the foundation behaviour and as a result the predicted displacement solution was significantly influenced by the value of the parameter λ .

Selected values of permeability are lower than those selected previously in chapter 4. Final values selected, shown in Table 5.1, were obtained by repeatedly adjusting initial values to improve the match between computed and observed excess pore water pressure profiles. Final values of horizontal permeability, k_h , are consistent with values measured from in situ testing. Values of the vertical permeability were selected using the permeability anisotropy ratios determined from laboratory testing.

The permeability was found to significantly influence the computed results. The depth profile of preconsolidation stress, p'_o , was unchanged from that determined previously in chapter 4.

Using the parameters shown in Table 5.1 consolidation analyses predicting the observed foundation behaviour over a period of nine years have been performed.

5.4 Results and Discussion

5.4.1 Introduction

The results of the analyses are presented in Fig 5.6 -5.14. All times shown on the figures and described throughout the remainder of this chapter are in days and refer to the period of time which has passed since the end of construction. The end of construction has been assumed as time, $t=0$. For convenience and to keep the amount of graphical presentation to a minimum, predictions have been made and compared with field measurements at times of; $t=0$, $t=57$ days, $t=500$ days, $t=1100$ days (3 years) and $t=2030$ days (5.5 years). For consistency comparison at these time intervals was maintained for settlements, lateral displacements and excess pore water pressures. However, in some instances data at the above time intervals were not available, as a result data at the nearest available time interval were used. The discussion of the current solution has been considered in three parts; settlements, lateral displacements and excess pore water pressures. These are considered separately in subsections 5.4.2, 5.4.3 and 5.4.4 respectively.

5.4.2. Vertical displacements

Predictions of the vertical displacements are shown in Fig 5.6-5.8. Measured vertical displacement data are available for surface settlements and points located at 1, 2, 4, 6 and 8m beneath the centre line of the embankment.

Computed and observed surface settlement profiles are in reasonable agreement for times, $t=0$ (end of construction), which was assumed as undrained, and $500 \leq t \leq 2030$ days. Predictions for $57 \leq t \leq 500$ days do not compare well with those observed and are underestimating observed surface settlements by as much as 150mm. The reason for this is evident from Fig 5.7 and 5.8, which shows settlement rates at locations under the centreline of the embankment. As can be seen from Fig 5.7 the observed settlement over the top 4m of foundation occurred much faster than is predicted in analyses over the time period of 8 days. This indicates that drainage of excess pore water pressures is rapid and the soil has a high permeability over this time period. Computed long-term settlements over the top 4m of foundation are greater than those observed. Computed and observed short-term and long term settlements at 6 and 8m depths below the embankment centre line, Fig 5.8, are in reasonable agreement.

In practice an estimation of the rate of settlement at locations beneath the centre line of the embankment may be necessary in situations where services pass underneath the embankment. Here computed settlements over the top layers of the foundation have underestimated the observed movements, in the short-term, by as much as a factor of 2. To improve the short-term settlement predictions the permeability of the soft clay was increased by a factor of ten. Values of permeability are shown in Table 5.2. For comparison the maximum measured (in situ) horizontal permeability is also shown. As can be seen from Figs 5.15-5.17 increasing the permeability has significantly improved short-term settlement predictions. Predictions of the long-term settlement are over predicted. This result further demonstrates that in the short-term the rate of dissipation of excess pore water pressures is rapid, particularly over the top 3-4m of foundation.

As can be seen from Table 5.2 the adjusted values of permeability exceed available permeability data by as much as 2-3 times. These adjusted values of permeability cannot therefore be reasonably justified. However, these values show that in this case high values of measured in situ permeability are required to reproduce the observed initial behaviour.

For comparison the settlement at the centreline has also been estimated using an empirical method (Leroueil et al., 1985). This empirical method assumes that the total settlement, S_T consists of the reconsolidation settlement, S_r , and the consolidation settlement S_c . Parameters used for this empirical method are given in Table 5.3.

The reconsolidation settlement, S_r , corresponds to the initial phase of drained loading of the clay, stress path OP' Fig 5.18 (Leroueil et al., 1985) and is given by relation (5.1).

$$S_{ri} = \frac{H_i}{1 + e_{oi}} C_{si} \log \left(\frac{\sigma'_{vc}}{\sigma'_{vi}} \right) \quad (5.1)$$

where for the purposes of calculation the clay layer is divided into n layers and H_i is the thickness of a layer of clay; e_{oi} is the initial void ratio; σ'_{vi} is the initial effective stress; σ'_{vc} is vertical preconsolidation pressure and C_{si} ($=\kappa \ln 10$) is the recompression index.

Relation (5.1) is based on many deformation observations (Tavenas and Leroueil, 1980 and Leroueil and Tavenas, 1986). Using this empirical method a surface, centre line, reconsolidation settlement of 155mm was estimated, Table 5.3.

The consolidation settlement, S_d , is the main component of the long-term settlement of a clay embankment foundation and arises from volumetric compression, produced by the increase in effective stresses from σ'_{vc} to $\sigma'_{vi} + \Delta\sigma_v$ (where $\Delta\sigma_v$ is the increase in total vertical stress) following a stress path such as A'B'D', Fig 5.18. As for the reconsolidation settlement the total consolidation settlement of the surface of the clay deposit is obtained by subdividing the deposit into n layers and calculating the settlement S_d of each layer of thickness H_i using relation (5.2).

$$S_{dii} = \frac{H_i}{1 + e_{oi}} C_{ci} \log \left(\frac{\sigma'_{vi} + \Delta \sigma_v}{\sigma'_{vc}} \right) \quad (5.2)$$

where C_{ci} ($=\lambda \ln 10$) is the compression index.

Using relation (5.2) a consolidation settlement of 774mm was estimated, Table 5.4, giving a total surface settlement of approximately 929mm at the centre line. A surface settlement at the centre line of approximately 780mm was observed at $t=2030$ days.

As can be seen from Tables 5.3 and 5.4 use of relations (5.1) and (5.2) to estimate the reconsolidation and consolidation settlements respectively has provided a reasonable estimation of the observed surface settlement. However, both relations are underestimating the short-term vertical displacement over the top 3-4m of foundation. Consequently, for short-term settlement predictions at depth some adjustment of parameters κ , λ and σ'_{vc} is required. It is recommended for design that maximum and minimum values of parameters κ , λ and σ'_{vc} are used to provide upper and lower settlement limits.

5.4.3 Lateral displacement

Predictions of lateral displacements at inclinometer locations T7i, T11i and T15i are shown in Figs 5.9-5.11. As can be seen from Figs 5.9-5.11 predictions do not compare well with observed displacements. Predictions of lateral displacement are typically most inaccurate for the time $t=0$ (end of construction). It is evident from the comparison of the predicted and observed lateral displacements that much of the inaccuracy which has arisen is due to the inability of analyses to accurately reproduce the lateral displacements occurring at the end of construction. In fact predictions of lateral displacement at $t=0$ are closest to observations of lateral displacement arising after 500 days (no lateral displacement data at $t=500$ days are available at T7i).

This behaviour is thought to be due to some overconsolidation and/or incomplete saturation of the clay foundation causing the clay to follow initially a drained response.

The result of this is that the volume of soil displaced vertically, V_v , is considerably greater than the volume of soil displaced horizontally, V_h . For a truly undrained response the displaced volumes are equal, i.e. $V_v=V_h$. The mechanisms of this behaviour have been discussed at length in chapter 4.

Previously in chapter 4 (section 4.6) it was suggested that improved estimates of the end of construction lateral displacements could be obtained by performing drained analyses of the construction procedure or performing undrained analyses with significantly enhanced values of elastic stiffness (or significantly reduced values of κ). Here, back analysed values of elastic stiffness are some 2-3 times larger than maximum values of stiffness obtained from in situ and laboratory testing. These enhanced values of elastic stiffness cannot be justified by available stiffness data and therefore this method was not taken any further.

It is thought that the foundation does not follow an undrained response until yield occurs (or the soil becomes normally consolidated). In chapter 4 (section 4.3) a simple hand calculation was performed which determined that elements of soil beneath the embankment centreline would not start to yield until the embankment reached a height of 2-2.5m, which in this case coincides with the final height of embankment B. Therefore, on the basis of the above discussion performing drained analyses for the entire construction procedure for embankment B is justified. Predictions of the end of construction lateral displacements using drained analyses are shown in Figs 5.19-5.21. As can be seen from Figs 5.19-5.21 predictions of the end of construction lateral displacements are reasonable. However at inclinometer T11i (Fig 5.20) predictions are underestimating lateral displacements by as much as a factor of 2. Despite this, the drained solution has provided a more accurate estimate of the construction lateral displacements. As a result a correction equal to the difference between the drained and undrained end of construction lateral displacement solutions can be applied to subsequent predictions of lateral displacement, therefore removing some of the inaccuracy associated with assuming an undrained response during construction. Using this approach computed lateral displacements at inclinometers T7i, T11i and T15i reduce to those shown in Figs 5.22-5.24. At inclinometers T7i, T11i and T15i the differences between maximum drained and undrained lateral displacements are approximately 50mm, 60mm and 55mm respectively.

As can be seen from Figs 5.22-5.24 the resulting lateral displacement profiles, particularly at $500 \leq t \leq 2030$ days, are in better agreement with those observed.

For comparison the maximum end of construction lateral displacement, y_{mc} , under the embankment toe has been estimated from an empirical correlation, relation (5.3).

$$y_{mc} = 0.2S_r + S_u \quad (5.3)$$

where S_r is the reconsolidation settlement and S_u is the undrained shearing settlement which results from plastic flow of the normally consolidated clay and is given by relation (5.4), also an empirical relation (Leroueil et al., 1985).

$$S_u = (0.07 \pm 0.03)(H_r - H_{nc}) \quad (5.4)$$

where H_r is the height of the embankment and H_{nc} is the critical embankment height.

Relation (5.3) is based on observations assembled by Tavenas et al. (1979) of lateral displacements under the toe of many trial embankments.

The maximum calculated end of construction lateral displacement under the embankment toe, coincident with inclinometer T11i, is approximately 31mm. At inclinometer T11i a lateral displacement of approximately 25mm was observed.

If necessary, using the value of y_{mc} computed, an estimate of the depth profile of the end of construction lateral displacements can be obtained using Fig 4.43. The profile of lateral displacements estimated using this method is shown in Fig 5.25. A consolidation state of 3 has been assumed. As can be seen from Fig 5.25 the computed depth profile of lateral displacement, except over the top 4-5m, is in good agreement with that observed.

Detailed analysis of available observations of lateral displacements (Tavenas et al., 1979 and Bourges and Mieussens, 1979) has shown the distribution of lateral displacements with depth does not change further after the end of construction, Fig 5.26. This observation therefore, enables an estimate of the long-term lateral displacement profile to be obtained given an estimate of the maximum long-term settlement, y_m . Values of y_m can be estimated from relation (5.5) (Tavenas and Leroueil, 1980).

$$\Delta y_m = 0.15 \Delta S_T \quad (5.5)$$

where ΔS_T is the increase in maximum settlement during long-term consolidation.

Relation (5.5) is an empirical relation based on long-term observations of lateral displacements (Tavenas et al, 1979 and Bourges and Mieussens, 1979). Analysis of these lateral displacement and settlement data determined that the ratio between the increase in lateral displacement and increase in settlement remains constant during consolidation. Fig 5.27 illustrates this behaviour. As can be seen relation (5.5) provides a reasonable estimate of the observed behaviour. For the Cubzac embankment B the ratio of the width of the embankment to the thickness of the clay and ratio of the width of slopes to the thickness of the clay are 2.67 and 0.78 respectively. Embankment B was constructed with a factor of safety against immediate failure of 1.5.

Using relation (5.5) gives a long-term lateral displacement, $y_m=155\text{mm}$ under the toe of the embankment (coincident with inclinometer T11i). For the current period for which measurements of lateral displacements are available at inclinometer T11i, approximately 6 years, the observed maximum lateral displacement is approximately equal to 135mm. Using Fig 4.43 the long-term depth profile of lateral displacement is shown in Fig 5.28. As can be seen from Fig 5.28 the computed depth profile of lateral displacement, except over the top 4-5m, is in good agreement with that observed. However, calculated lateral displacements at the ground surface are larger than those observed.

It is evident from comparison of Figs 5.10 and 5.28 that a more accurate estimate of lateral displacement under the embankment toe is obtained using the empirical method than is obtained using finite element analysis.

In practice predictions of lateral displacement are important particularly in situations where there are buried structures close to the embankment. Predictions of lateral displacement solely based on finite element computations will be excessive and may result in extensive and unnecessary remedial measures to protect any buried structures. As a result, it is suggested that more than one method is used to estimate the lateral

displacements so the effects of each can be assessed before considering the extent of remedial works required to protect these structures.

5.4.4 Excess pore water pressures

Predictions of excess pore water pressures have been made at the centreline, 4m from the embankment centre line (approximately half-way between the embankment centreline and toe) and the toe of the embankment. Predictions are shown in Figs 5.12-5.14. As can be seen from Figs 5.12-5.14 predictions of excess pore water pressures over the 2030 day period (approximately 6 years) are in general in reasonable agreement with those observed. Nevertheless differences remain in the current solution. Many analyses were performed to obtain the current solution.

Predictions of excess pore water pressure in the short-term, $0 \leq t \leq 57$ days, are in reasonable agreement with those observed. At $t=0$ predictions at the centreline and 4m from the centreline are typically underestimating observations over the top 4m of foundation but overestimating observations below this depth. Under the embankment toe predictions are in general underestimating those observed, however the difference is small, approximately 5kPa.

At $t=57$ days analyses are overpredicting the rate of dissipation of excess pore water pressure over the top 3-4m of foundation at the centreline and 4m from the centreline. At the centre line at depth analyses are overestimating the observed excess pore water pressure by as much as 20kPa, indicating analyses are underestimating the rate of dissipation of excess pore water pressures. At the toe analyses have not accurately reproduced the observed excess pore water pressures at $t=57$ days. At $t=57$ days analyses are underestimating observed excess pore pressures by some 7kPa at the toe.

Long-term, $500 \leq t \leq 2030$ days predictions of excess pore water pressures at the centreline are in reasonable agreement with observations. However, analyses have overpredicted the rate of excess pore water pressure dissipation over the top 2-3m of foundation.

Predictions of excess pore water pressures for $500 \leq t \leq 2030$ days at 4m from the centre line and at the embankment toe are overestimating those observed by as much as 15-20kPa. It is evident from Fig 5.11-5.12 that the final choice of the values of permeability is inappropriate for these locations. Higher values of permeability at 4m from the centre line and toe are required to improve predictions at these locations. To investigate this further the permeability of the soft clay was increased by a factor of ten (see Table 5.2). The effect of this on the excess pore water pressure predictions is shown in Figs 5.29-5.31. As can be seen from Figs 5.29-5.31 these significantly enhanced values of permeability have provided an improved long-term excess pore water pressure solution at 4m from the centre line and toe but not at the centre line. At the centre line long-term predictions of excess pore water pressure have significantly underestimated those observed.

In CRISP the foundation is divided into several layers to which constant values of horizontal and vertical permeability are assigned. Throughout the analysis the value of permeability assigned to each layer remains constant. It is evident from the above discussion that the permeability of the foundation does not remain constant as assumed.

It has long been recognised that the permeability falls with decreasing void ratio, Fig 5.32 (Magnan, Mieussens and Queyroi, 1983). This implies that the permeability of the soil will change as the volume of the soil changes (Al-Tabba and Wood, 1987), which links changes in permeability to changes in effective stress (Samarasinghe et al., 1982). An example of numerical analyses of stage-constructed embankments on soft clay, incorporating a variable permeability (permeability varies with void ratio) is given in chapter 4 (section 4.3.7.3) (Chai and Bergado, 1983). Studies performed by Chai and Bergado (1993) and others, e.g. Almeida et al. (1986) have shown that allowing the permeability to vary with the void ratio can provide more accurate long-term estimates of excess pore water pressures.

As previously mentioned in chapter 4 an estimate of the excess pore water pressures for stage constructed embankments is important. For embankment B (and similar embankments) predictions of the long-term excess pore water pressure may not be necessary as excess pore pressures generated at the end of construction are

approximately maximum. Consequently, for embankment B predictions of the short-term or end of construction excess pore water pressures are important. The end of construction pore water pressures can be used to assess the stability of the embankment. Here, undrained finite element analyses of embankment B have provided reasonable estimates of the observed pore pressures generated due to construction. Additionally, further estimates of these excess pore pressures can be made using the empirical method described previously in chapter 4 (section 4.6).

However, in situations where excess pore water pressures are required the accuracy of these predictions is significantly influenced by the values of permeability selected. Here, (for embankment B) values of horizontal permeability, k_h , were selected from values of permeability obtained from in situ testing. Final values (subject to some adjustment by trial and error) correspond approximately to the minimum in situ measured permeability or the maximum of horizontal permeability measured in the laboratory. The final values of horizontal permeability were lower than was anticipated in view of the results of consolidation analyses performed for embankment A. However, the effect of incomplete saturation is known to reduce the permeability of the soil (Leroueil et al., 1985) and may account for the lower values of permeability that were estimated from values of permeability anisotropy ratios determined from laboratory testing.

Some check on the selected values of permeability is provided by back analysing estimates of the excess pore water pressure calculated by hand at various times throughout the anticipated life of the embankment. For example, hand calculations can be based on the principle of one-dimensional consolidation (or Tezaghi's theory). However, due to the limitations of Tezaghi's theory of one-dimensional consolidation (Tavenas et al., 1979 and Leroueil et al., 1985) some engineering judgement, based on previous experience or similar loading situations, may be required.

5.5 Previous analysis

5.5.1 Introduction

In this section the results of previous analysis of the embankment B trial loading using the MELANIE soil model are, for comparison, briefly summarised. The results of numerical analyses, employing the MELANIE soil model, have been extracted from Mouratidis and Magnan (1983), Magnan, Mieussens and Queyroi (1983) and Leroueil, Magnan and Tavenas (1985). For clarity the results of the modified Cam clay analyses described in this chapter are not included in the figures associated with this section. The results of analyses using the MELANIE soil model are summarised in Figs 5.33 to 5.37. Figures presented in this section were extracted from Muir Wood (1990).

5.5.2. Results and discussion

It is evident from the results of analyses that the MELANIE soil model has overall, provided a more accurate prediction of the observed foundation response. However, surface settlement predictions using the modified Cam clay soil model, Fig 5.6, are, particularly in the long-term, more accurate. Both the MELANIE and modified Cam clay soil models are unable to predict the initial measured settlement response. The measured initial settlement response is occurring significantly faster, particularly in the top 2-4m of foundation, Figs 5.34 and 5.7, than was computed using the MELANIE and modified Cam clay soil model.

Lateral displacement predictions using the MELANIE soil model Fig 5.36 are after approximately $t=46$ days, significantly more accurate than those obtained using the modified Cam clay analyses, Fig 5.10. In the short-term both MELANIE and modified Cam clay analyses are overpredicting the observed lateral displacements. However, the differences between predicted and observed lateral displacements using the MELANIE soil model are not as acute as was found for the modified Cam clay soil model.

Predictions of excess pore water pressures, Fig 5.37, are approximately similar to those obtained using the modified Cam clay soil model, Fig 5.12. Excess pore water pressure predictions are however in the short-term more accurate using the MELANIE soil model.

Even though some differences remain between the MELANIE soil model solution and observations, introducing a certain amount of compressibility of the pore fluid (corresponding to $S_r=0.98$) has provided a more accurate solution. This is particularly the case for predictions of lateral displacements. Again it is evident that soil characteristics such as anisotropy and the presence of gas within the pores of the soil have a significant influence on the accuracy of the predicted solution.

5.6 Conclusions

The modified Cam clay soil model has provided reasonable predictions of the observed settlements and excess pore water pressures. Accurate simultaneous predictions of observed settlements and lateral displacements was however not possible. Predicted lateral displacements were as much as a factor of two greater than those observed. Greatest discrepancy between computed and observed lateral displacements arose at the end of construction of the embankment.

Values of critical embankment height, H_{nc} , suggest that yield of the soft clay foundation will not start to occur until completion of the embankment. As a result, during construction the foundation will be predominantly following a drained response. Consequently, to improve lateral displacement predictions initial estimates using consolidation analyses were adjusted in relation to the magnitude of lateral displacement arising at the end of construction assuming a fully drained foundation response.

Additional estimates of the end of construction (short-term) and long-term lateral displacements under the toe of the embankment (T11i) were made using empirical correlations (Tavenas and Leroueil, 1980 and Leroueil et al., 1985). The depth profiles of lateral displacement obtained using these methods were in reasonable agreement

with those observed and provided a significant improvement to those estimated using finite element analysis.

For comparison estimates of the surface settlement beneath the centre of the embankment for both the short-term and long-term were performed using empirical correlations (Leroueil et al., 1985). These methods provided reasonable estimates of the observed long-term surface settlement. In the short-term these empirical correlations tended to underestimate the observed settlement. Settlements and excess pore water pressures computed using finite element analysis displayed a similar behaviour. This behaviour is thought to be due to different rates of excess pore water pressure dissipation in the short-term and long-term. Measured settlement and excess pore water pressure data indicate that the permeability of the soil decreases with increasing magnitude of effective stress. Allowing permeability to vary with effective stress (or void ratio) may therefore provide more accurate predictions of settlement and excess pore water pressures (Almeida et al., 1986 and Chai and Bergado, 1993).

Many analyses were performed in order to obtain the presented predictions. The greatest difficulty throughout the study was the selection of values of permeability. The permeability was found to have a significant influence on the predicted results. Here, final values of horizontal permeability are similar (approximately) to minimum values obtained from in situ testing (or maximum values obtained from laboratory testing). This is consistent with initial values of horizontal permeability selected for studies performed by Chai and Bergado (1993) and Indraratna et al. (1992). Values of vertical permeability were selected from ratios of k_x/k_y from laboratory testing. Some check on the selected values of permeability could be provided by back analysing estimates of excess pore water pressure calculated by hand. Alternative methods of estimating excess pore water pressures were discussed in chapter 4.

Plastic strains were found to dominate the foundation behaviour. As a result, accurate selection of values of λ (describing the magnitude of plastic strains) was found to be important. From back analysis optimum values of λ were similar to approximately maximum values of λ obtained from available oedometer normal compression data.

These values of λ were typically larger than those estimated using an empirical link with plasticity index (Muir Wood, 1990), (see section 5.3).

Despite the dominance of plastic strains throughout analyses short-term and long-term settlement predictions were found to be influenced by the magnitude of elastic stiffness. In Cam clay the magnitude of elastic stiffness is influenced by the values of κ . Here, optimum values of κ were selected from values of κ estimated using the average slope of oedometer unload-reload data. Using this method resulting values of elastic stiffness corresponded to a strain level of approximately 0.3-0.4%.

An improved estimate of the lateral displacements (both short-term and long-term) could be achieved using the MELANIE soil model (Mouratidis and Magnan, 1983). Additionally, more accurate predictions of the short term excess pore water pressures was achieved using the MELANIE soil model (Mouratidis and Magnan, 1983). Again the reason for this improved accuracy is thought to be the inclusion of the anisotropic elastic and plastic properties and the presence of gas within the pores (Leroueil et al., 1985).

Neither the modified Cam clay soil model nor the MELANIE soil model (Magnan et al., 1983) were able to accurately reproduce the end of construction lateral displacements. Predictions of the end of construction lateral displacements were least accurate using the modified Cam clay soil model. The elements of a soil model required to accurately model lateral displacements arising due embankment construction are as yet still not fully understood (Gens, 1994). However, good predictions of both short-term (construction induced) and long-term lateral displacements beneath an embankment toe (Yanai city, Japan) were reported by Miki et al. (1994) using Sekiguchi and Ohta's (1977) (also see Sekiguchi et al., 1982) elasto-viscoplastic soil model. Sekiguchi and Ohta's elasto-viscoplastic soil model is an extension of the anisotropic Cam clay soil model developed by Ohta and Wroth (1976). The formulation of these soil models is based on the original Cam clay soil model (Bullet-shaped yield locus) (Roscoe and Schofield, 1963 and Schofield and Wroth, 1968) however the quantity $\eta=q/p'$ in the original formulation is replaced by $\eta=q/p'-q_a/p'_a$ (where q_a and p'_a are the values of q and p' at the end of anisotropic

consolidation) in the anisotropic Cam clay soil model. This causes a rotation of the yield surface around the stress origin resulting in the yield surface shown in Fig 5.38. As can be seen from Fig 5.38 the resulting yield surface has some similarities to that used in the MELANIE soil model.

It has long been recognised that under very rapid loading much higher stresses can be momentarily sustained by soft soils. Studies performed by Ansal et al. (1979) show that the viscoplasticity (time-dependency) of normally consolidated clays is an important aspect of soil behaviour. Consequently, to include the effects of loading rate dependency of soft soils Sekiguchi and Ohta (1977) and Sekiguchi et al. (1982) have extended the anisotropic soil model to include the effects of viscosity. The associated flow rule of the original Cam clay model was maintained. It appears from the results presented by Miki et al. (1994) that the inclusion of viscosity within a soil model may be significant, particularly if accurate predictions of lateral displacements induced beneath embankments are required.

From the above discussion it is evident that anisotropy, the presence of gas within the soil pores and viscosity are important elements of soil behaviour which need to be considered within a numerical framework if accurate predictions of lateral displacements induced beneath an embankment are required. Parameter selection for the resulting soil model may not be straightforward as inclusion of these additional soil characteristics within a numerical framework will require the selection of additional soil parameters which, except for sensitive designs, will not make their introduction into a numerical framework attractive.

Table 5.1. Selected parameters.
+ Mohr-Coulomb soil parameters not modified Cam clay.

LAYER (DEPTH(m))	MODEL	E'(kPa) +	ν'	$\phi' +$ (degrees)	c'(kPa)+	κ	λ	e_{cs}	M	$\gamma(N/m^3)$	$k_x(m/day)$	$k_y(m/day)$
EMBANKMENT	Mohr-Coulomb	15×10^3	0.4	30	1.0	-	0.02	-	-	21	-	-
LAYER 1 (0.0-1.0m)	modified Cam clay	2.3×10^3	0.2	26	-	0.02	0.03	2.08	1.07	17	3.0×10^{-3}	1.5×10^{-3}
LAYER 2(1.0-1.75m)	modified Cam clay	2.6×10^3	0.2	29	-	0.03	0.65	5.24	1.07	15	0.8×10^{-3}	0.35×10^{-3}
LAYER 3(1.75-4.0m)	modified Cam clay	1.1×10^3	0.2	29	-	0.12	0.8	5.16	1.2	15	0.7×10^{-3}	0.2×10^{-3}
LAYER 4(4.0-6.0m)	modified Cam clay	2.2×10^3	0.2	30	-	0.065	0.7	4.19	1.2	15	0.4×10^{-3}	0.09×10^{-3}
LAYER 5(6.0-9.0m)	modified Cam clay	3.4×10^3	0.2	30	-	0.06	0.75	4.68	1.2	15	0.25×10^{-3}	0.088×10^{-3}

Table 5.2. Enhanced values of permeability.

LAYER No	DEPTH (m)	k_x (m/day)	k_y (m/day)	$k_{x \max}$ (m/day)
1	0-1.0	-	-	-
2	1.0-1.75	5.5×10^{-4}	2.6×10^{-4}	6.9×10^{-4}
3	1.75-4.0	2.24×10^{-3}	5.2×10^{-4}	1.73×10^{-3}
4	4.0-6.0	5.2×10^{-3}	8.64×10^{-4}	1.3×10^{-3}
5	6.0-9.0	1.5×10^{-3}	7×10^{-4}	2.0×10^{-4}

Table 5.3. Reconsolidation settlement, S_{ri} .

LAYER H_i (m)	$1+e_{oi}$	C_{si} ($\kappa \ln 10$)	σ'_{vi} (kPa)	$\sigma'_{vi} + \Delta \sigma_v$ (kPa)	$\frac{H_i C_{si}}{1+e_o}$	$\log \left(\frac{\sigma'_{w'} + \Delta \sigma_v}{\sigma'_{w'}} \right)$	S_{ri} (mm)
0-1.0	2.1	0.046	8.5	56.5	0.022	0.823	18
1.0-1.75	3.92	0.069	19.5	65.5	0.013	0.526	7
1.75-4.0	3.86	0.23	27	74.8	0.134	0.443	60
4.0-6.0	3.1	0.15	37	84.8	0.097	0.36	35
6.0-9.0	3.33	0.14	49.5	94.5	0.126	0.281	35

Table 5.4. Primary consolidation settlement, S_d .

LAYER H_i (m)	$1+e_{oi}$	C_i ($\lambda \ln 10$)	σ'_{vi} (kPa)	σ'_{vp} (kPa)	$\frac{H_i C_i}{1+e_o}$	$\log \left(\frac{\sigma'_{p'}}{\sigma'_{w'}} \right)$	S_{di} (mm)
0-1.0	2.1	0.58	8.5	50	0.26	0.77	200
1.0-1.75	3.92	1.5	19.5	43	0.287	0.34	100
1.75-4.0	3.86	1.84	27	41	1.07	0.181	194
4.0-6.0	3.1	1.61	37	57	1.04	0.188	195
6.0-9.0	3.33	1.73	49.5	56	1.56	0.054	85

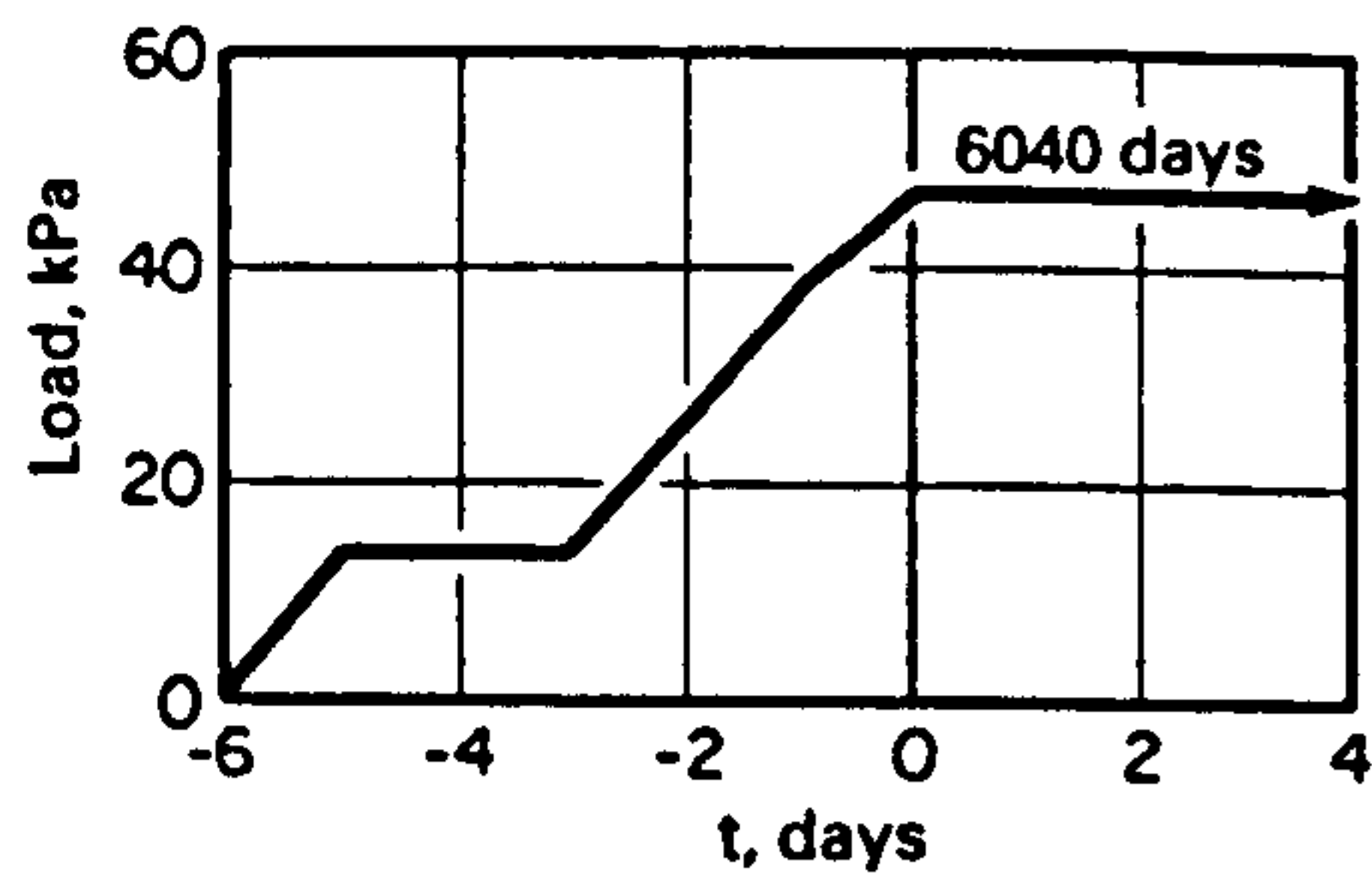


Fig 5.1. Construction sequence for embankment B at Cubzac-les-Ponts (Magnan et al., 1983)

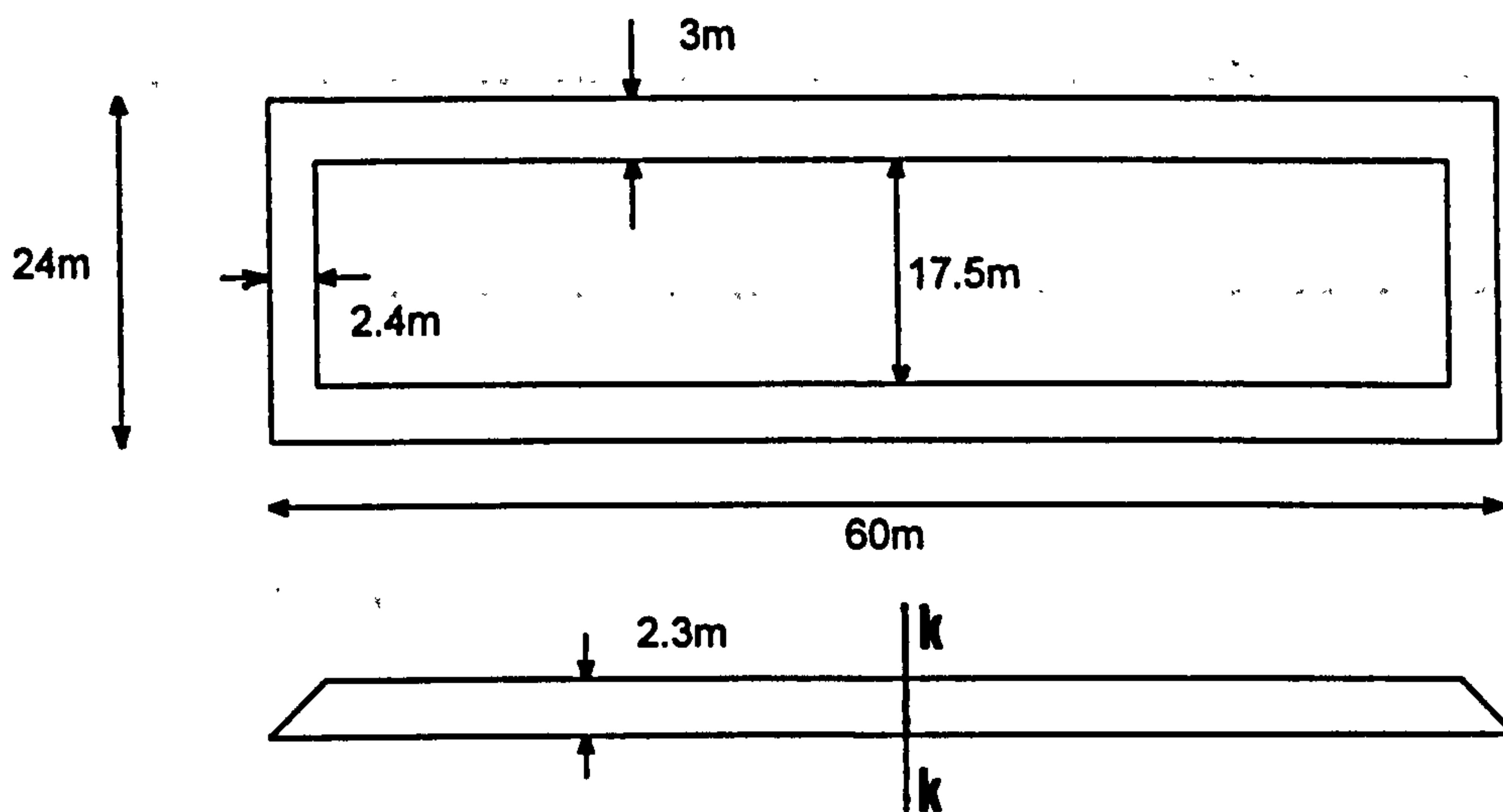
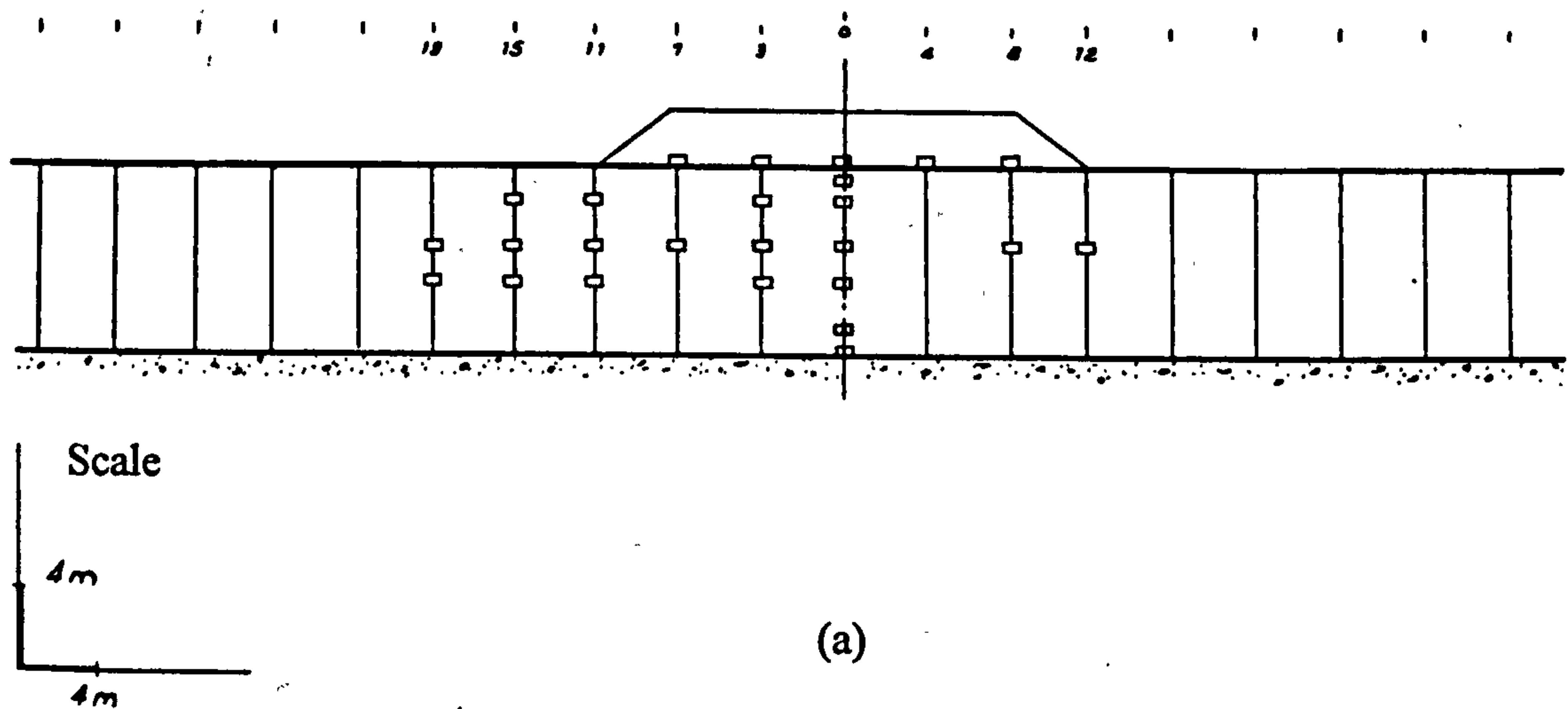


Fig 5.2. Dimensions of embankment B at Cubzac-les-Ponts. (NOT TO SCALE)

Fig 5.3. Instrumentation section K-K showing (a) settlement gauges (b) inclinometer locations and (c) piezometer locations.



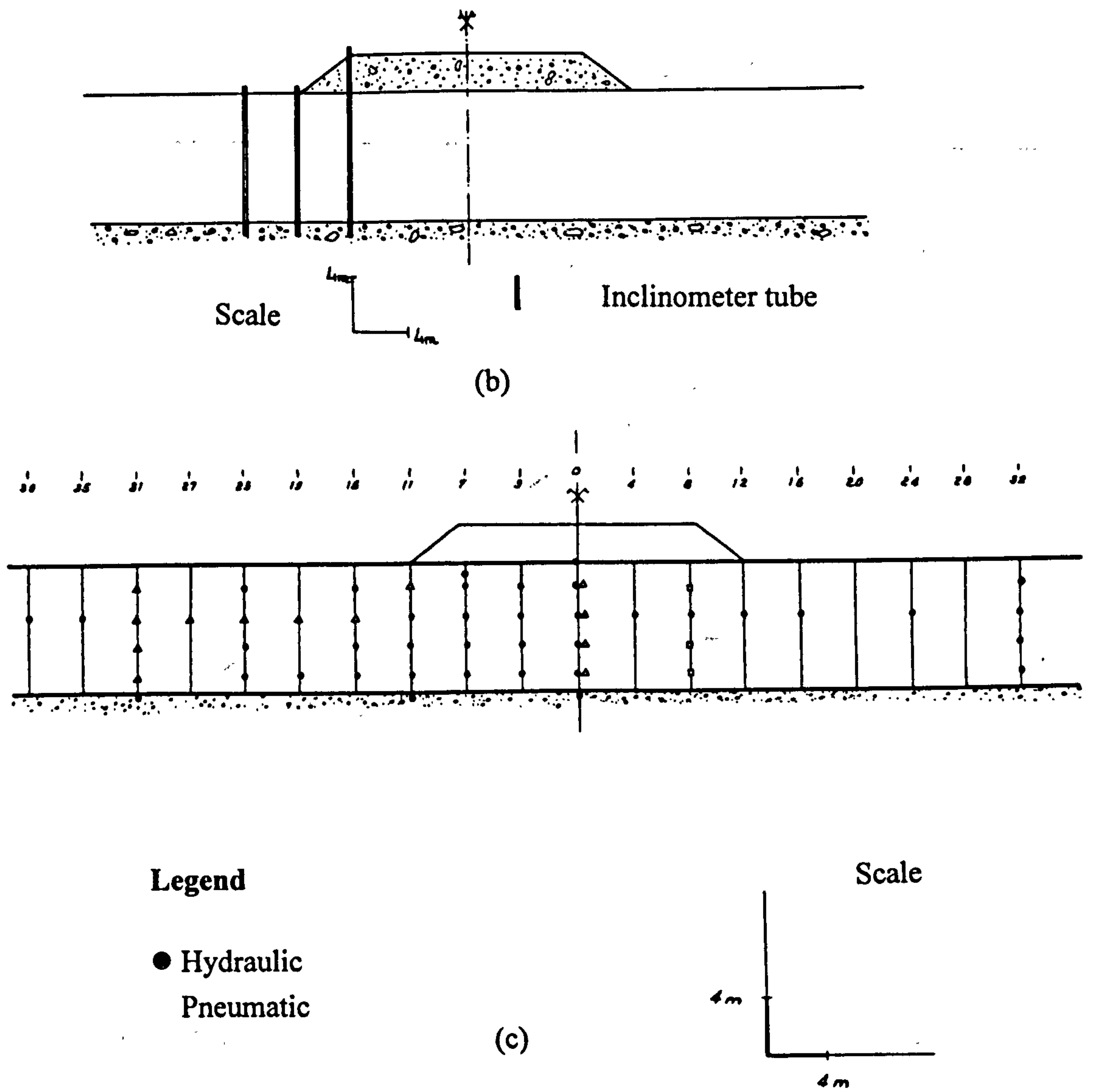


Fig 5.4. Finite element mesh used to describe embankment B and foundation at Cubzac-les-Ponts.

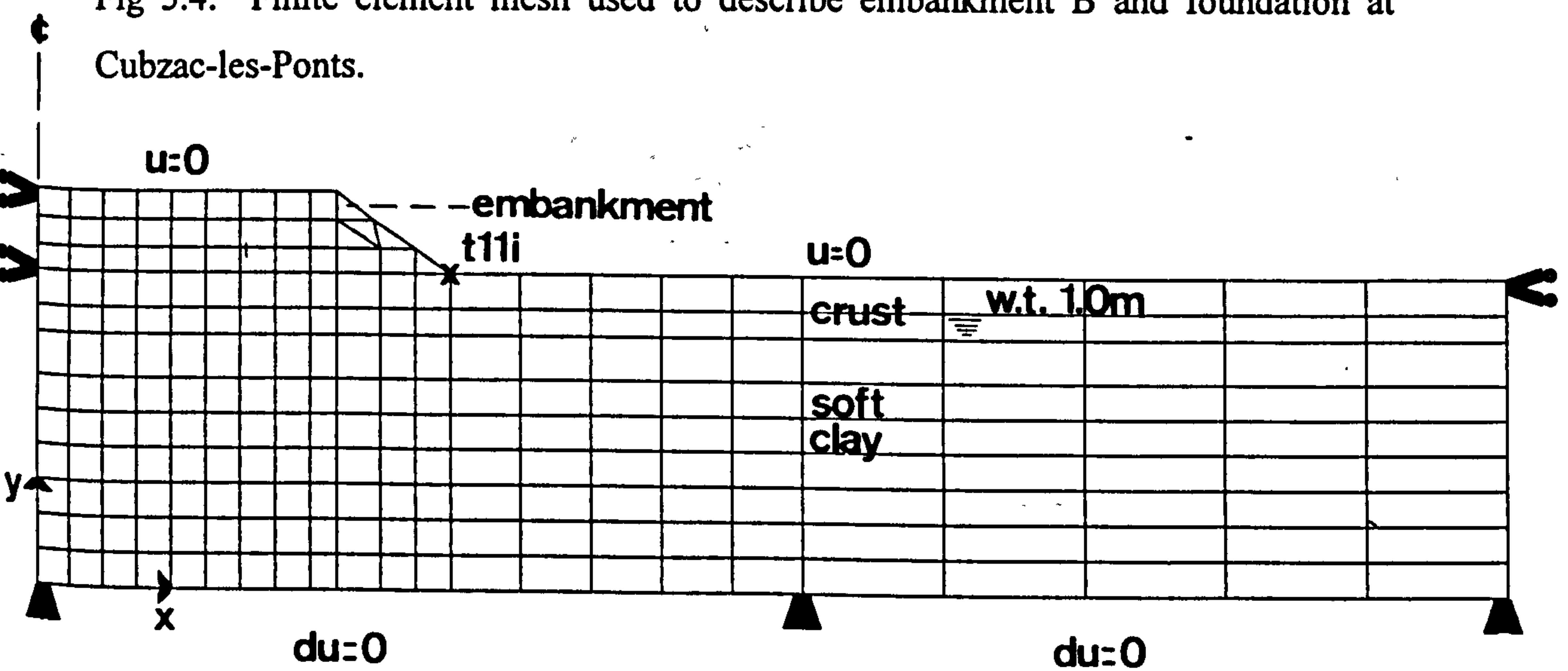


FIGURE 5.5
SELECTED VALUES OF λ COMPARED TO MUIR WOOD'S EMPIRICAL RELATION.

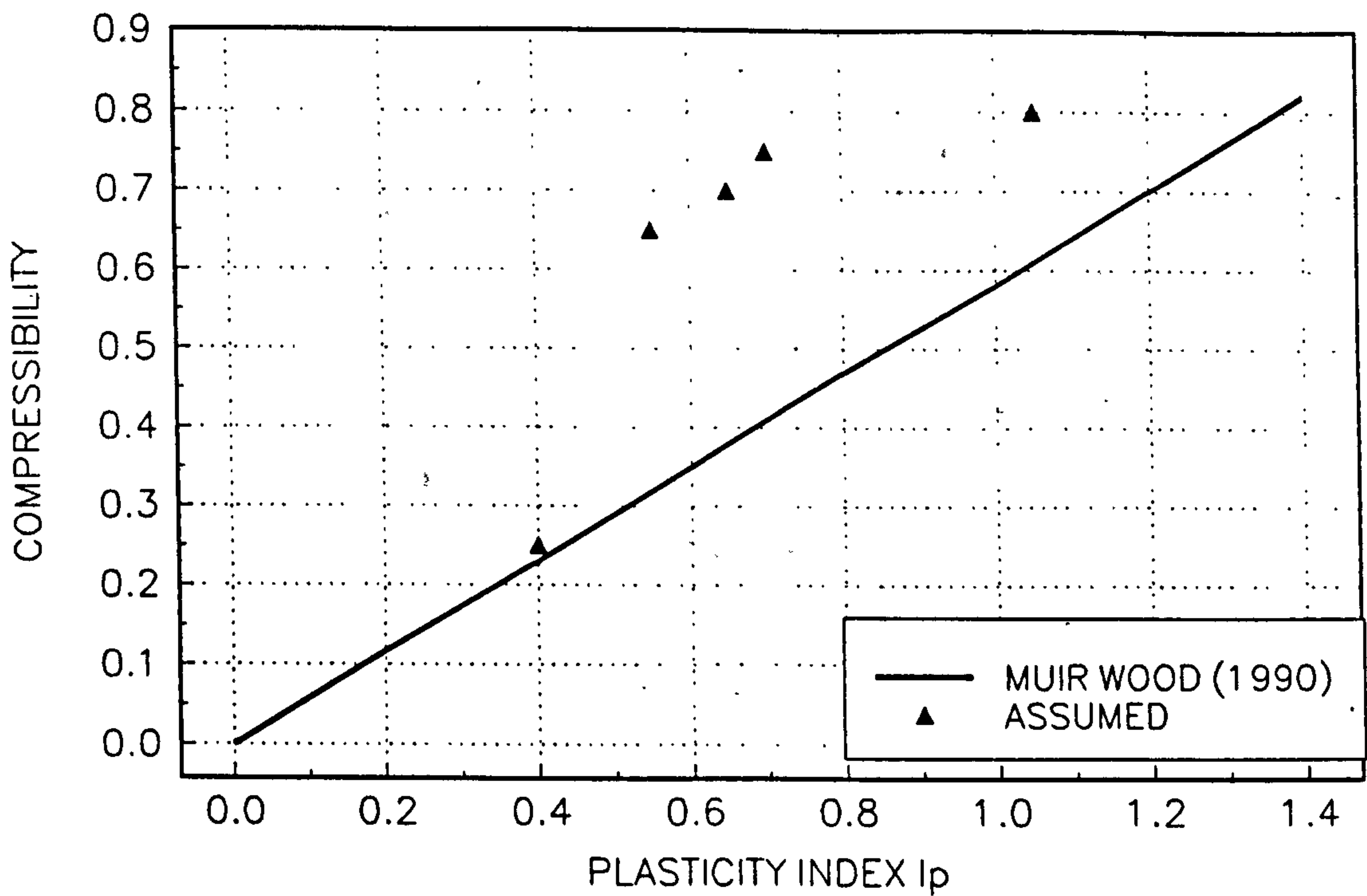


FIGURE 5.6
COMPUTED AND OBSERVED SURFACE SETTLEMENTS BENEATH EMBANKMENT B.

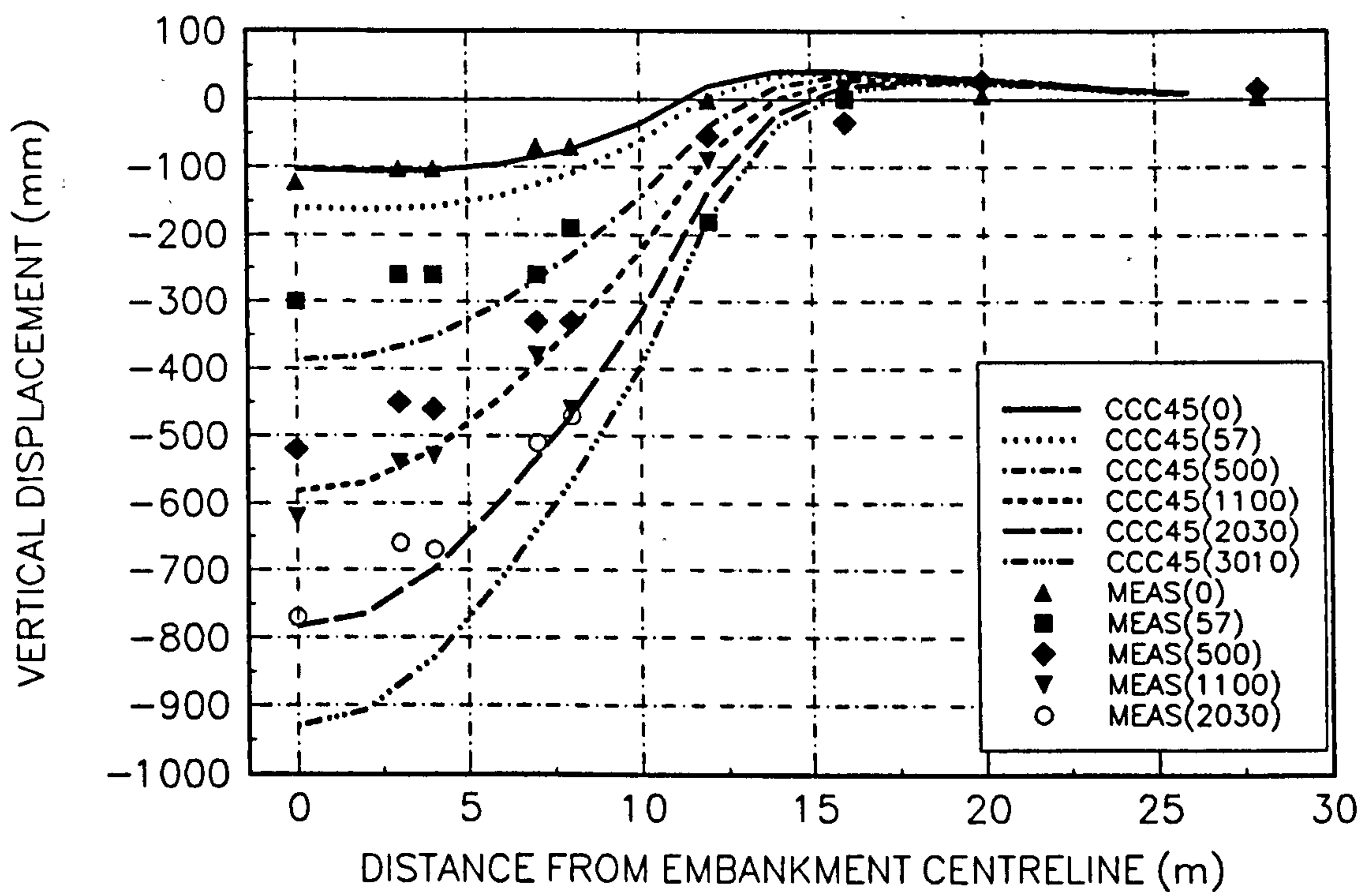


FIGURE 5.7
COMPUTED AND OBSERVED SETTLEMENTS IN SOIL LAYERS BENEATH EMBANKMENT B.

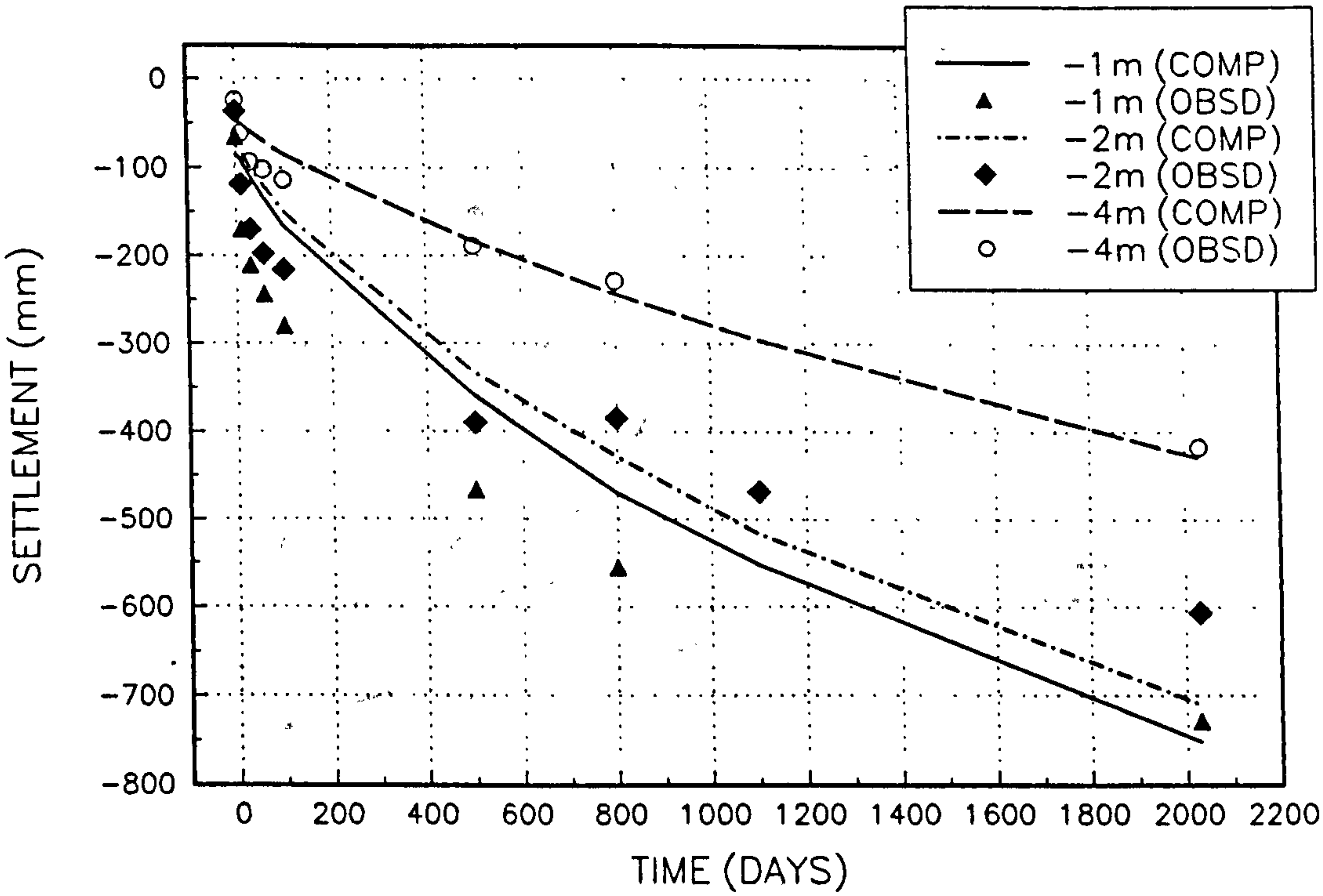


FIGURE 5.8
COMPUTED AND OBSERVED SETTLEMENTS IN SOIL LAYERS BENEATH EMBANKMENT B.

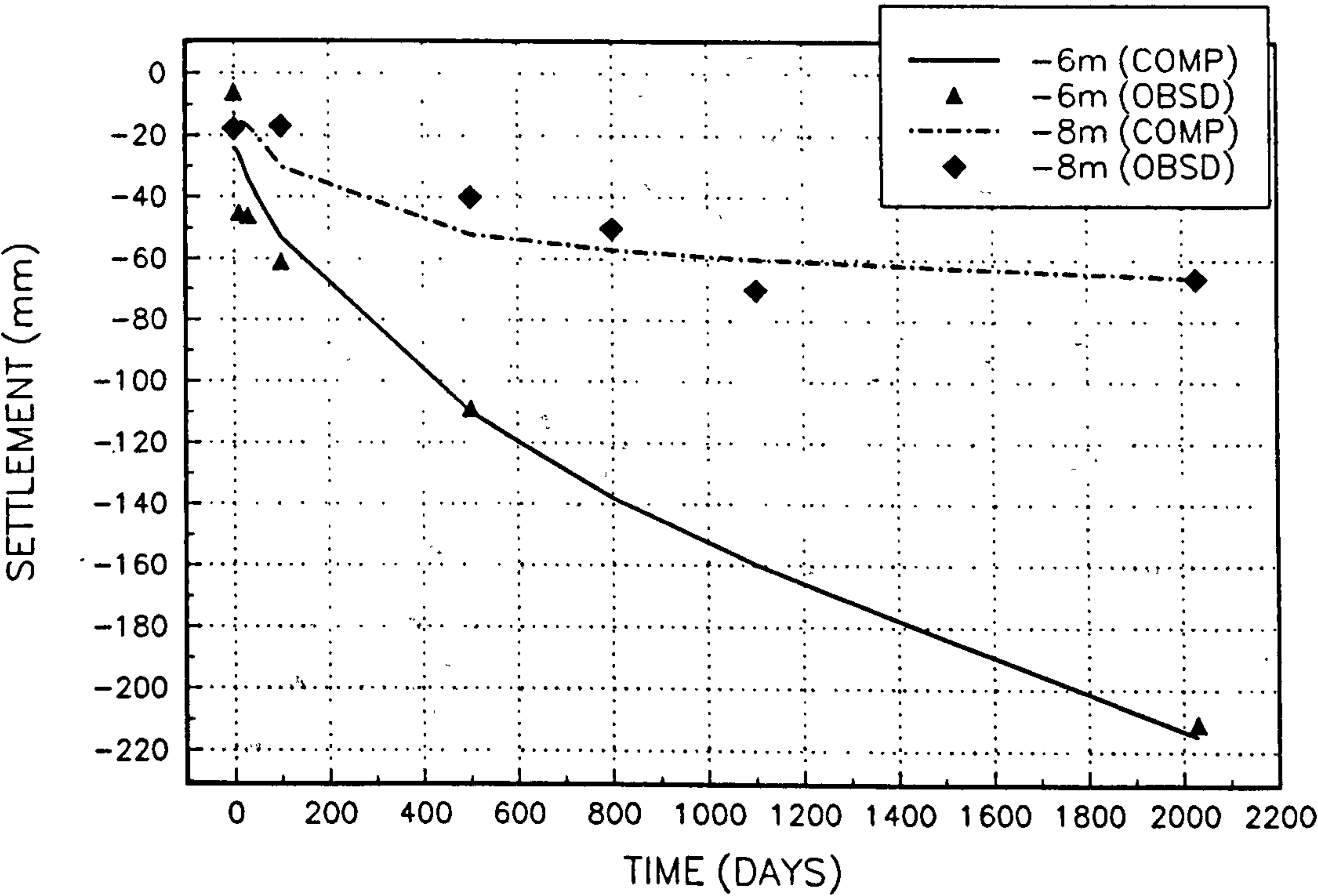


FIGURE 5.9
COMPUTED AND OBSERVED LATERAL DISPLACEMENTS AT INCLINOMETER T7i

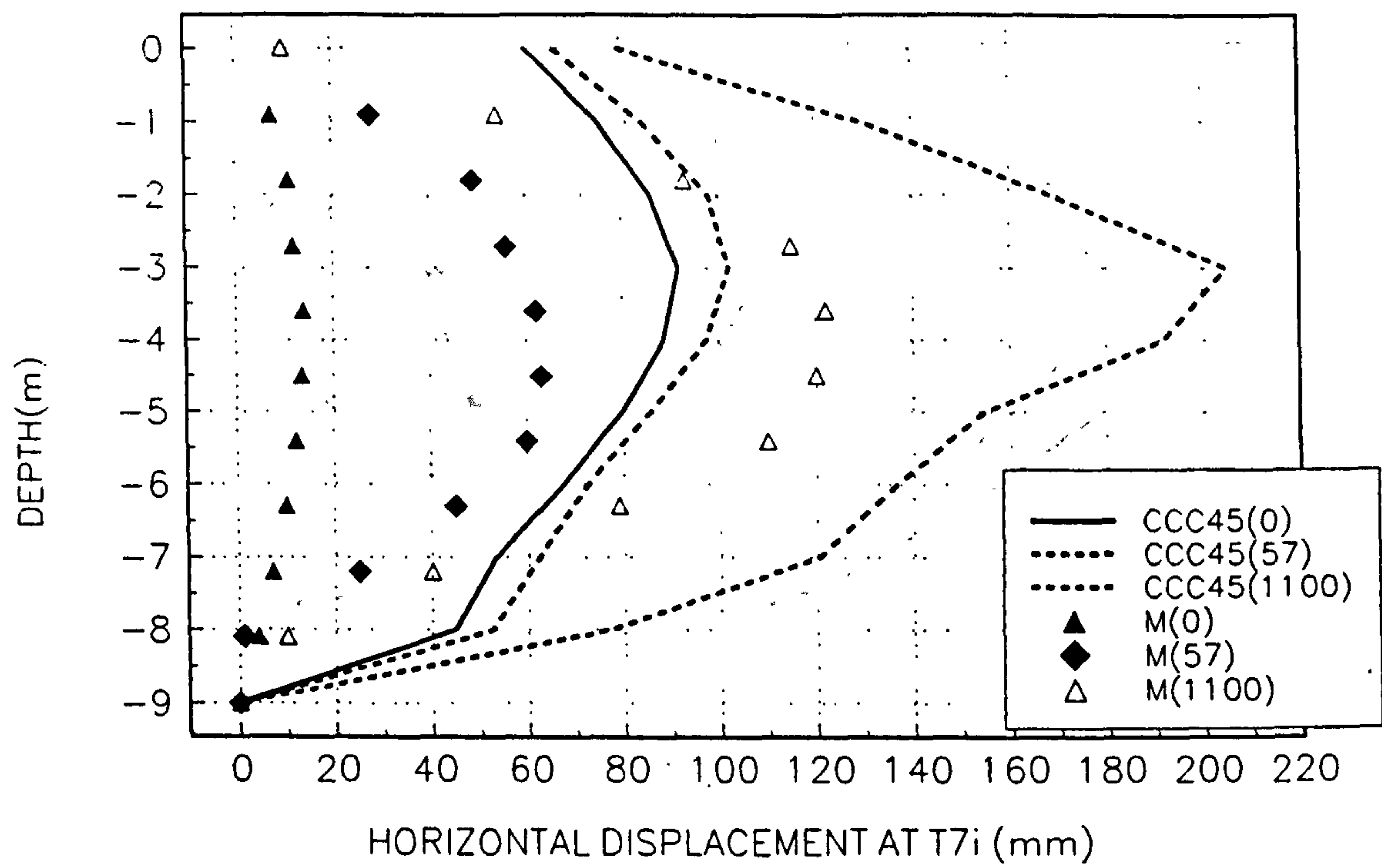


FIGURE 5.10
COMPUTED AND OBSERVED LATERAL DISPLACEMENT AT INCLINOMETER T11i

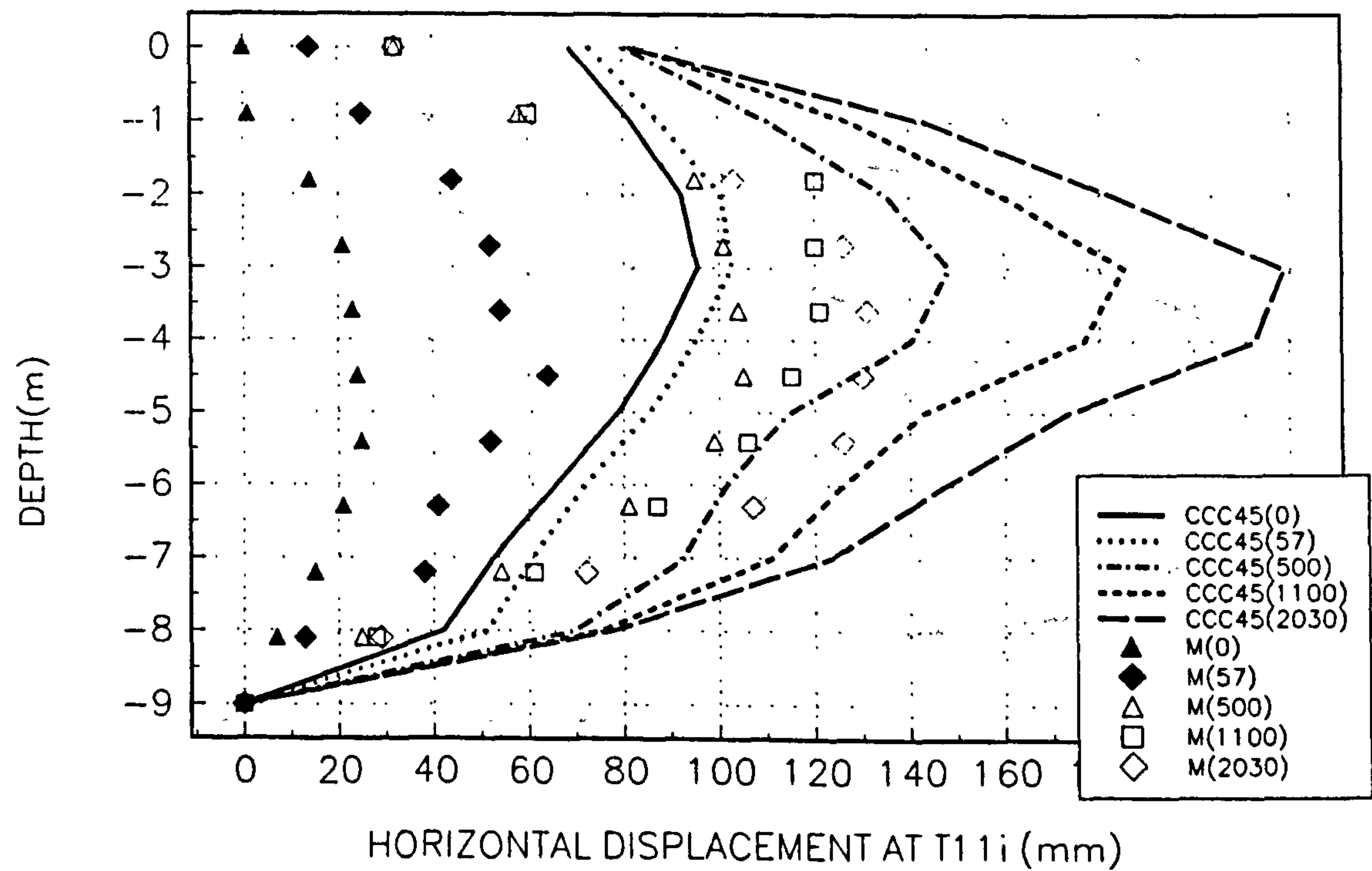


FIGURE 5.11
COMPUTED AND OBSERVED LATERAL DISPLACEMENTS AT INCLINOMETER T1 5i

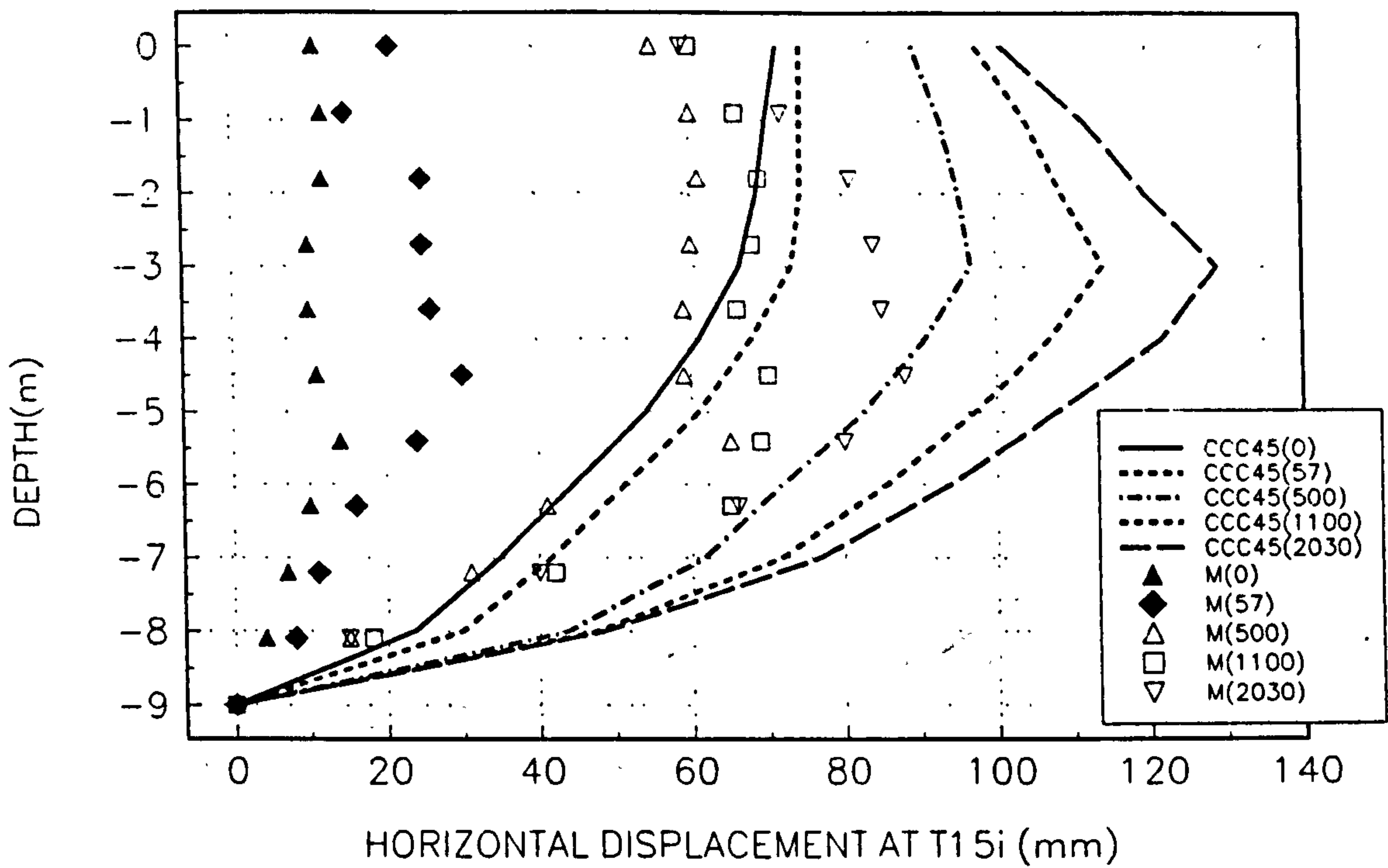


FIGURE 5.12
EXCESS PORE WATER PRESSURES BENEATH CENTRE LINE OF EMBANKMENT B

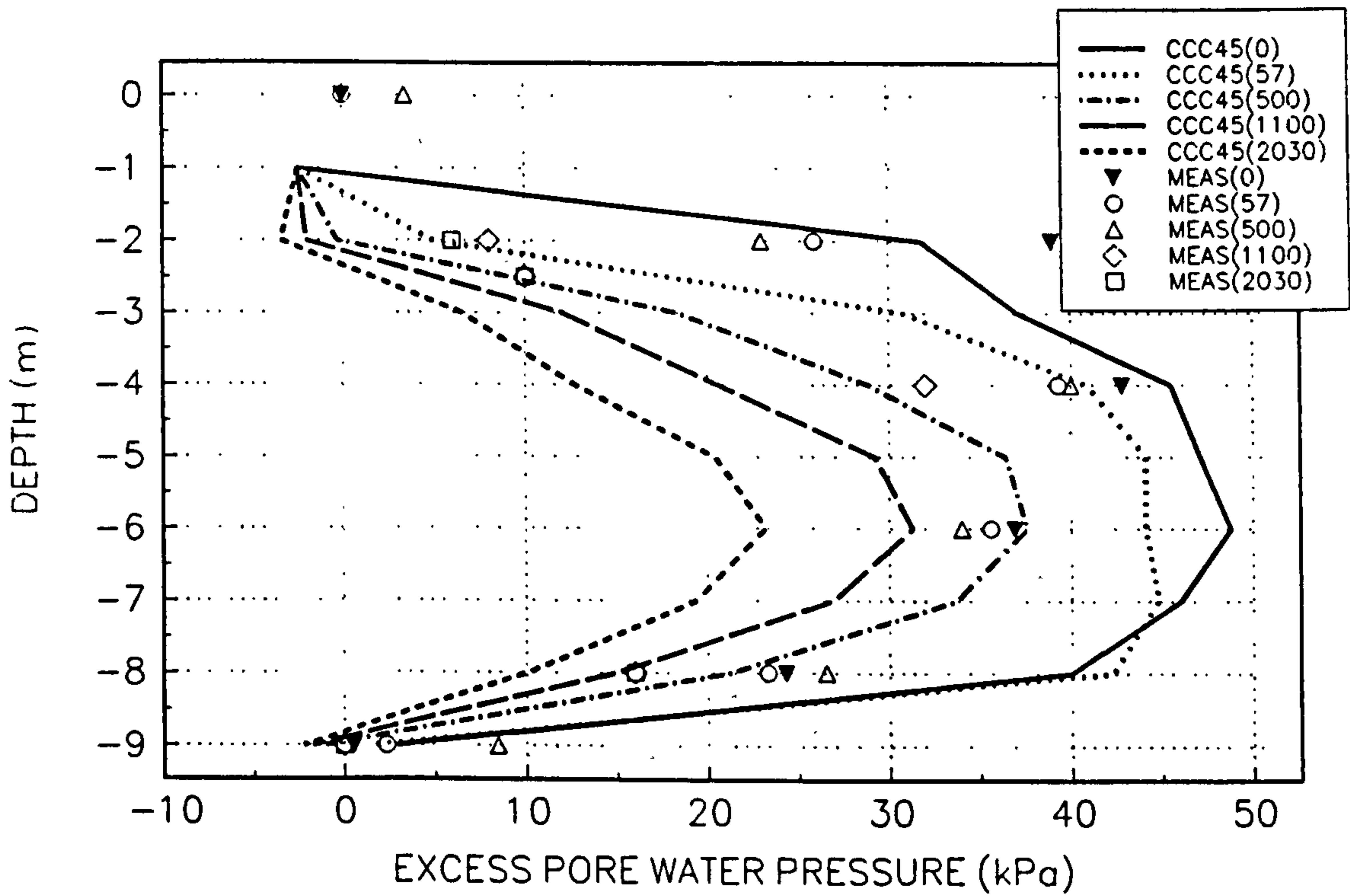


FIGURE 5.13
EXCESS PORE WATER PRESSURES AT 4m FROM CENTRE OF EMBANKMENT B.

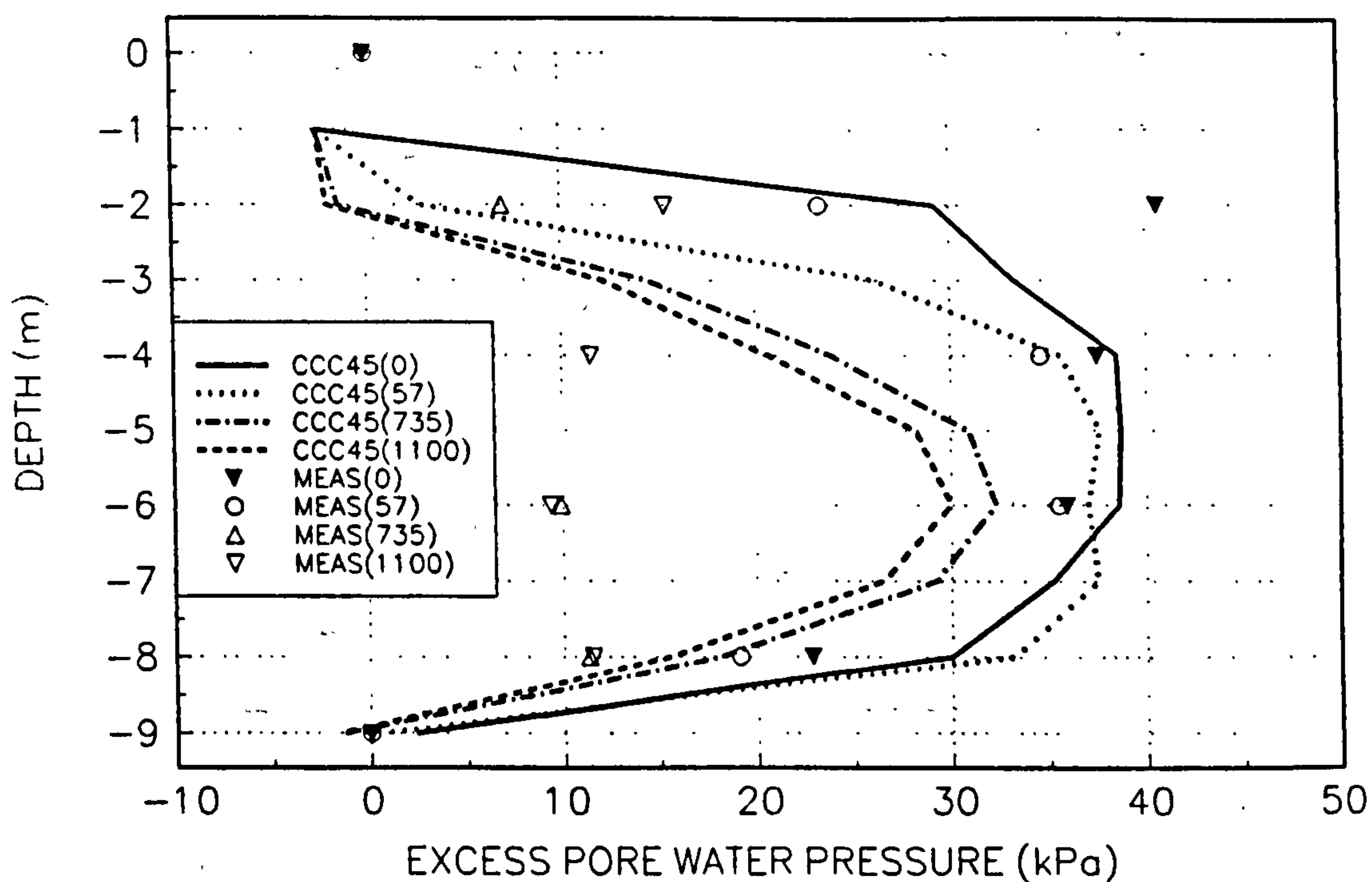


FIGURE 5.14
EXCESS PORE WATER PRESSURE UNDER TOE OF EMBANKMENT B.

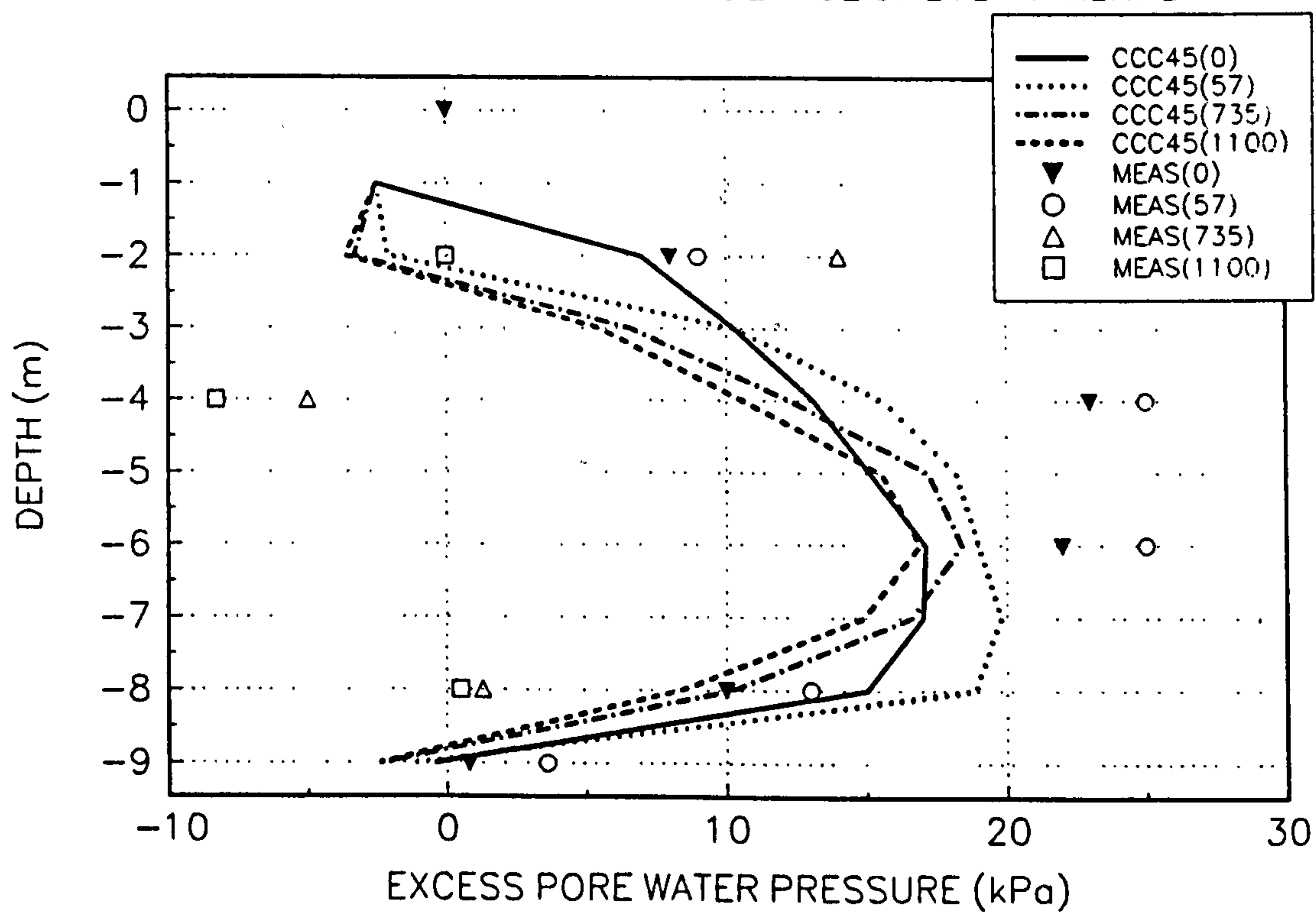


FIGURE 5.15
COMPUTED AND OBSERVED SURFACE SETTLEMENTS BENEATH EMBANKMENT B

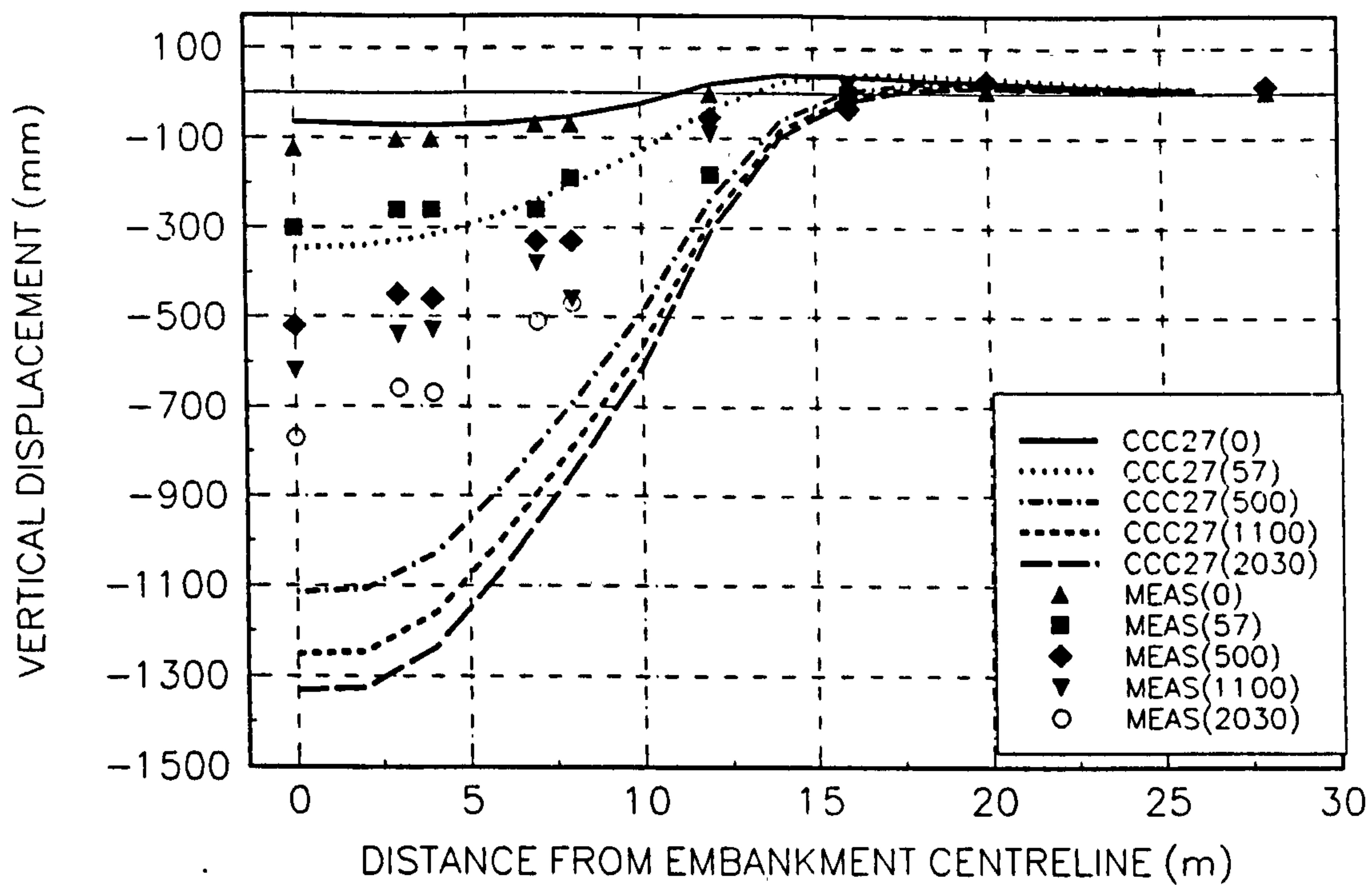


FIGURE 5.16
COMPUTED AND OBSERVED SETTLEMENTS IN SOIL LAYERS BENEATH EMBANKMENT B.

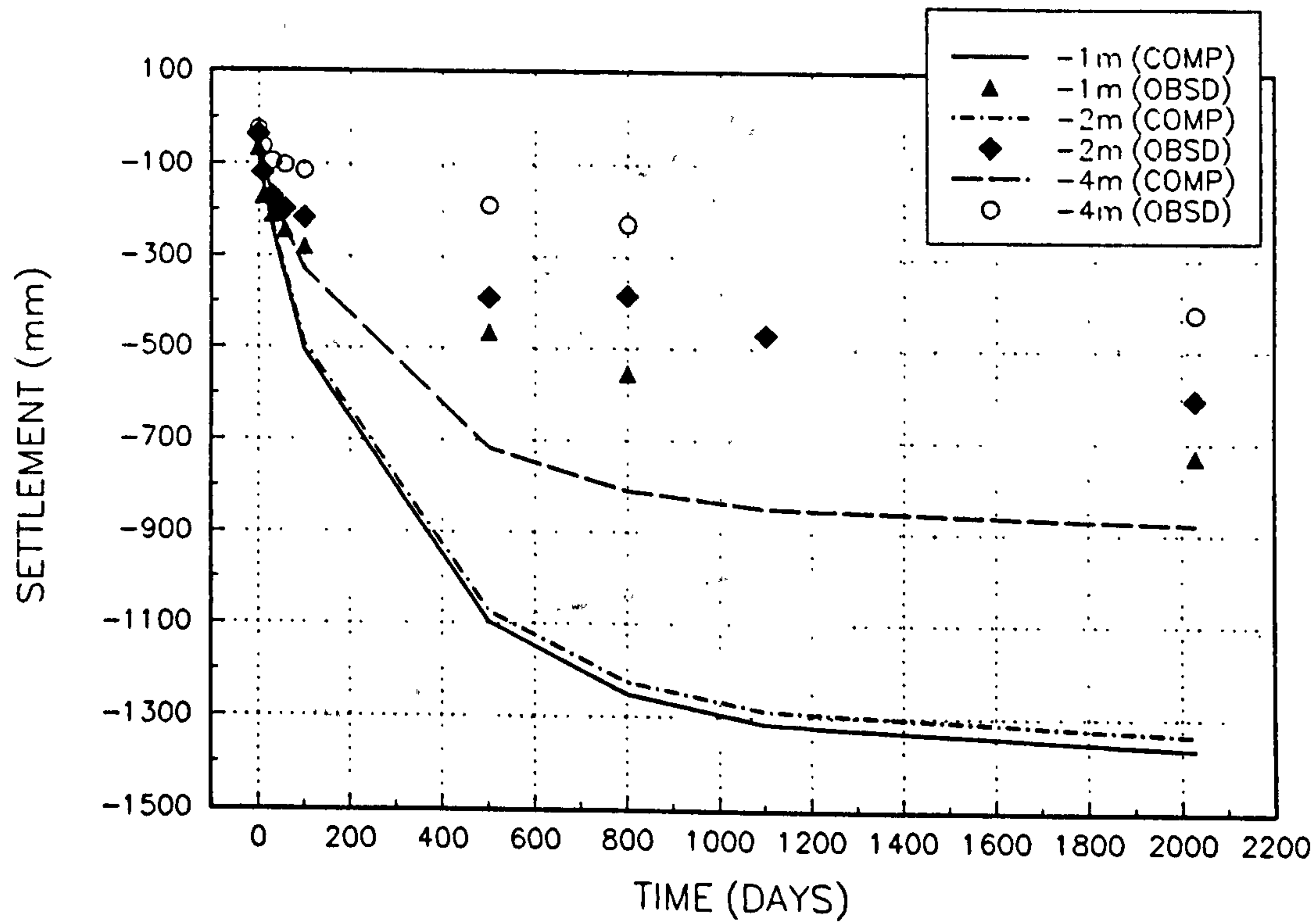


FIGURE 5.17
COMPUTED AND OBSERVED SETTLEMENTS IN SOIL LAYERS BENEATH EMBANKMENT B.

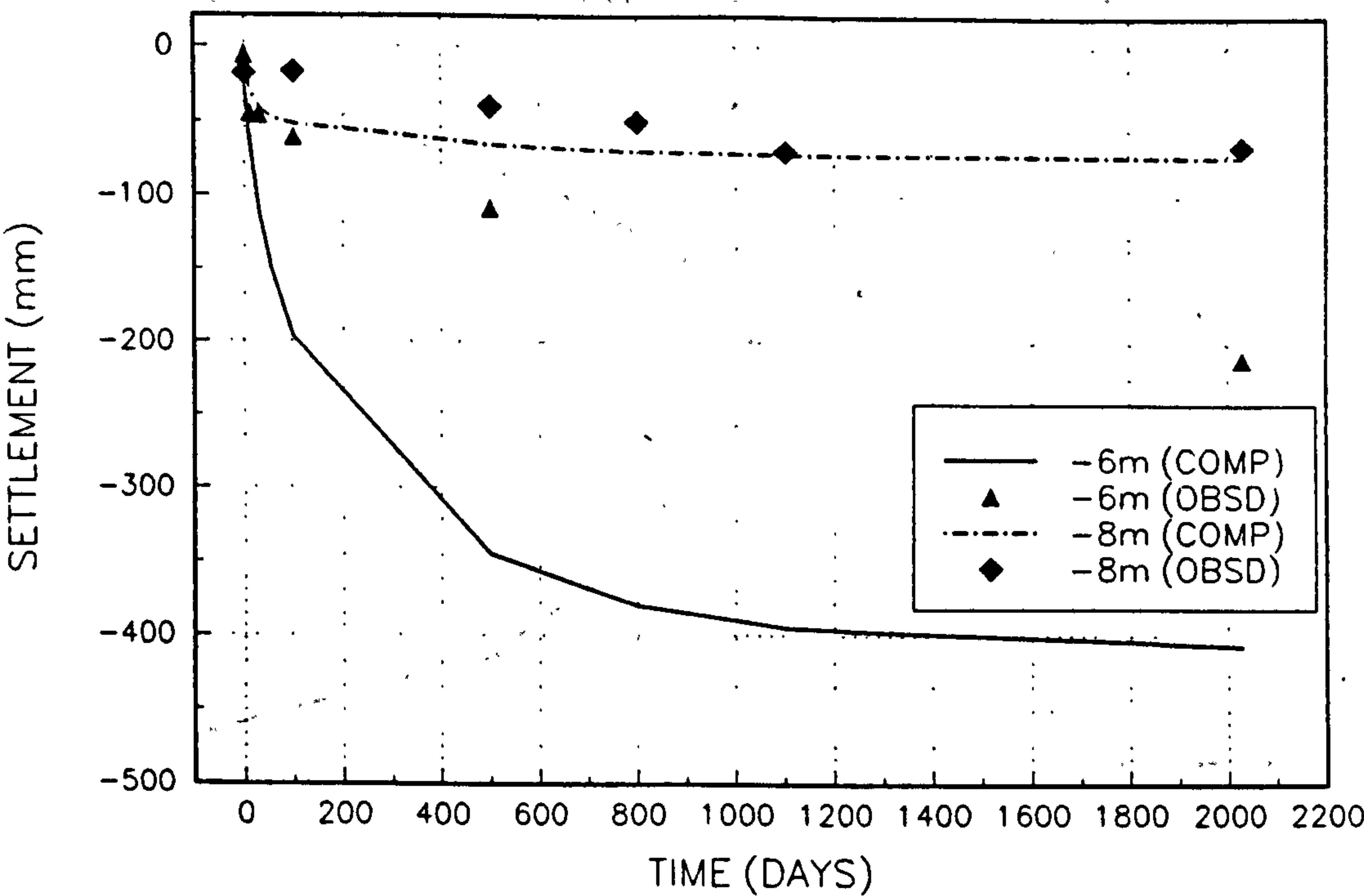


Fig 5.18. Effective stress path and ‘settlement-horizontal displacement’ relationship (Leroueil et al., 1985).

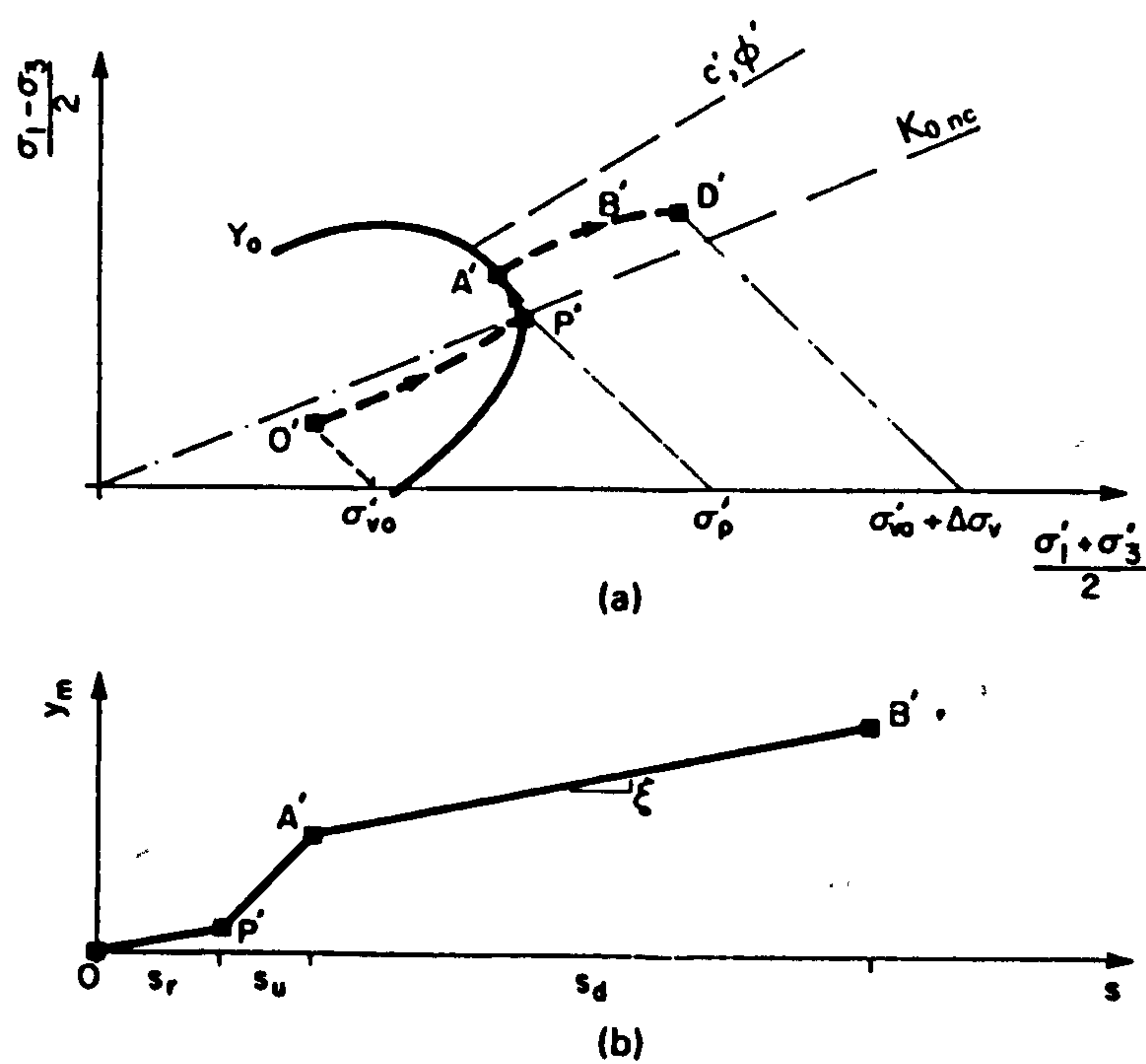


FIGURE 5.19
COMPUTED (DRAINED) AND OBSERVED LATERAL DISPLACEMENTS AT INCLINOMETER T7i

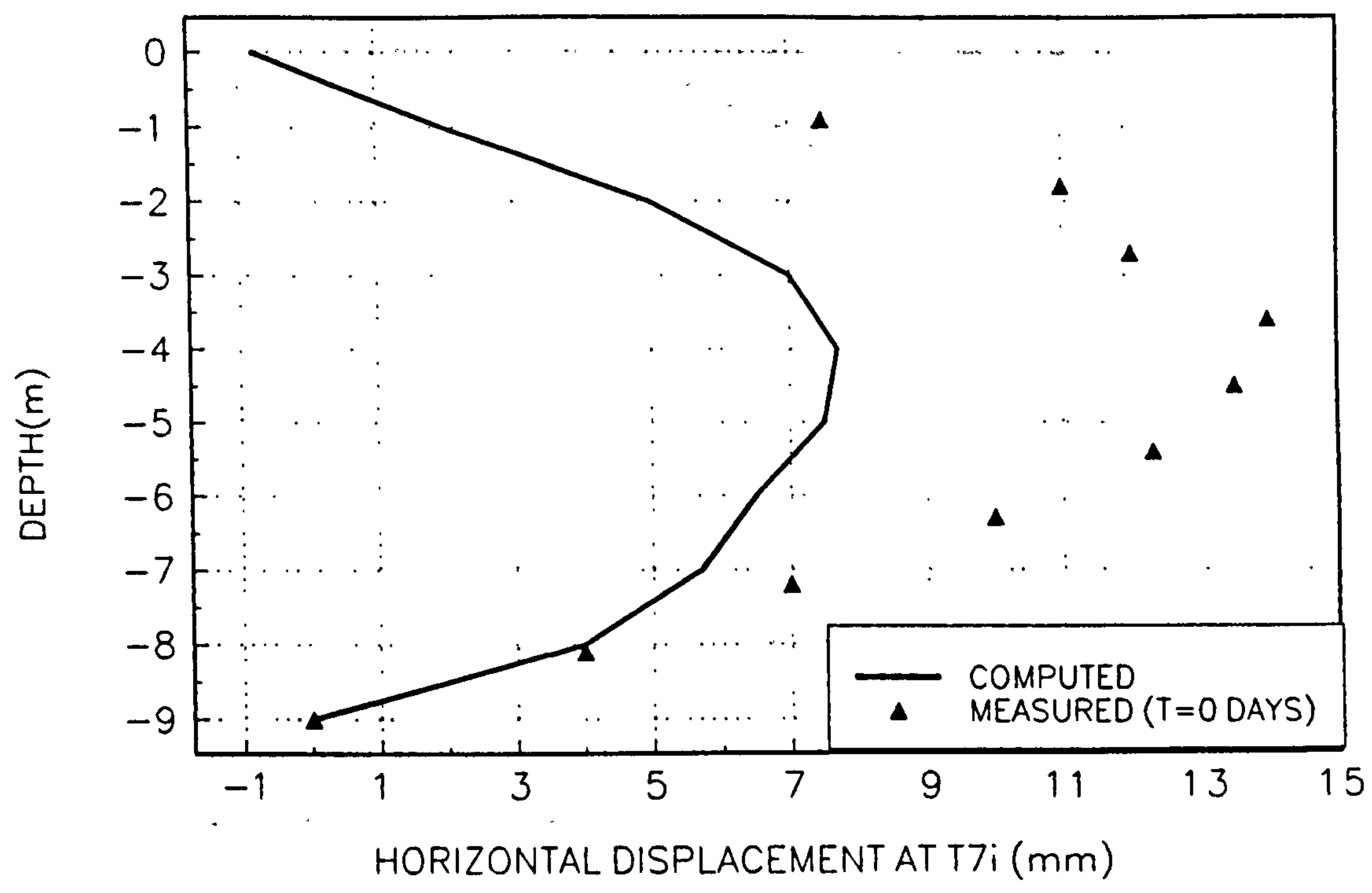


FIGURE 5.20
COMPUTED (DRAINED) AND OBSERVED LATERAL DISPLACEMENT AT INCLINOMETER T11

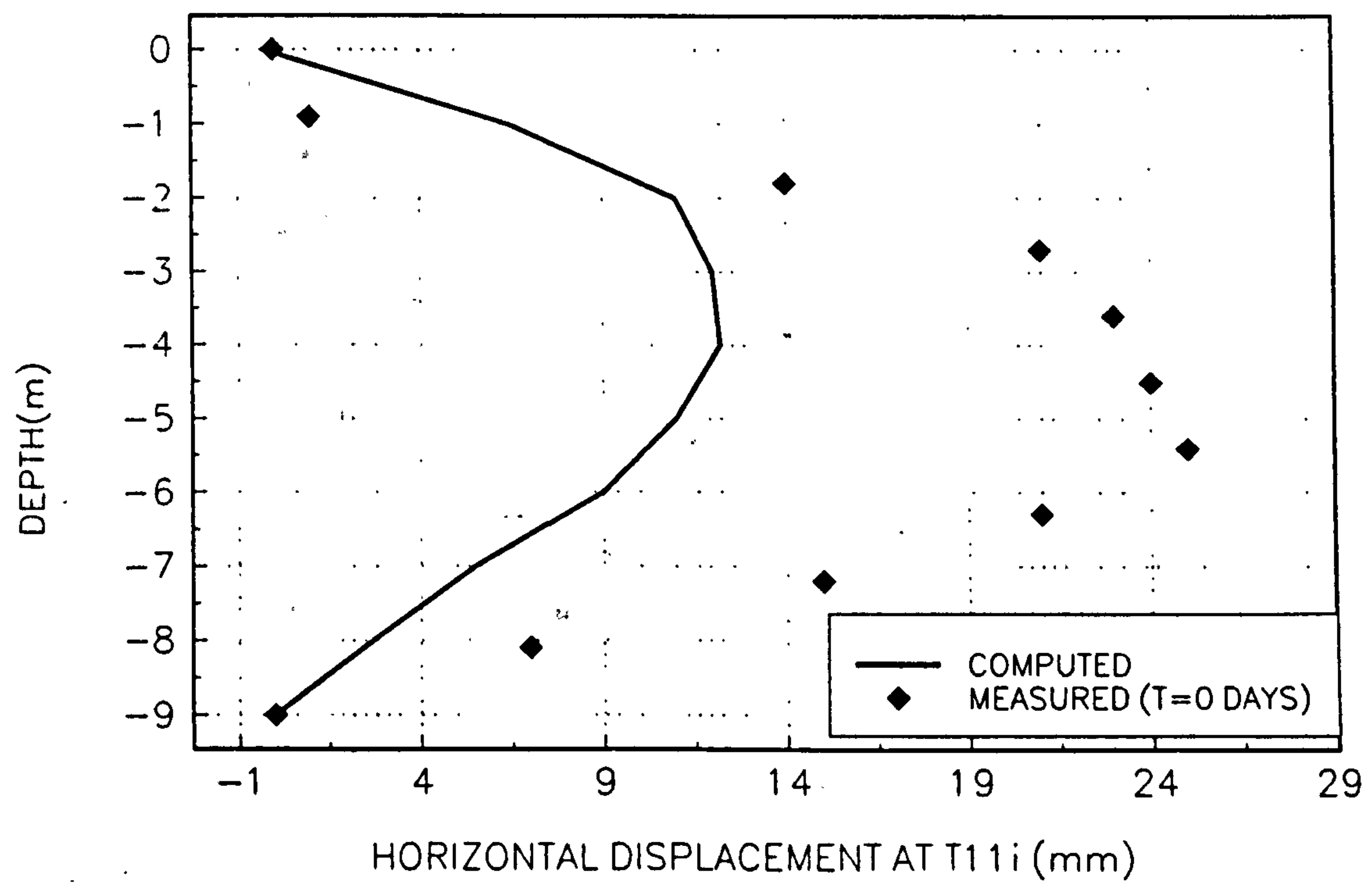


FIGURE 5.21

COMPUTED (DRAINED) AND OBSERVED LATERAL DISPLACEMENTS AT INCLINOMETER T15i

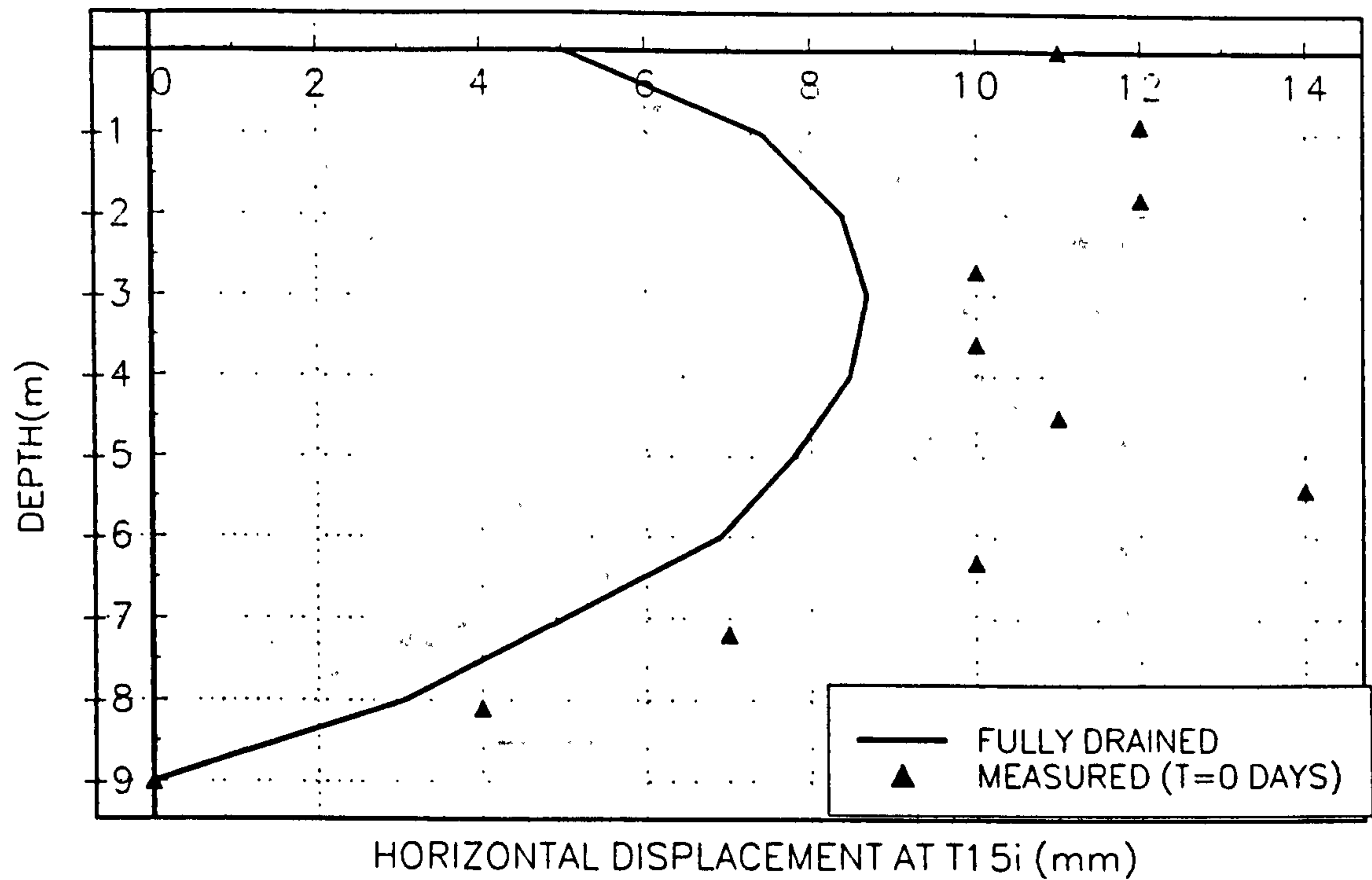


FIGURE 5.22

CORRECTED LATERAL DISPLACEMENT AT INCLINOMETER T7i

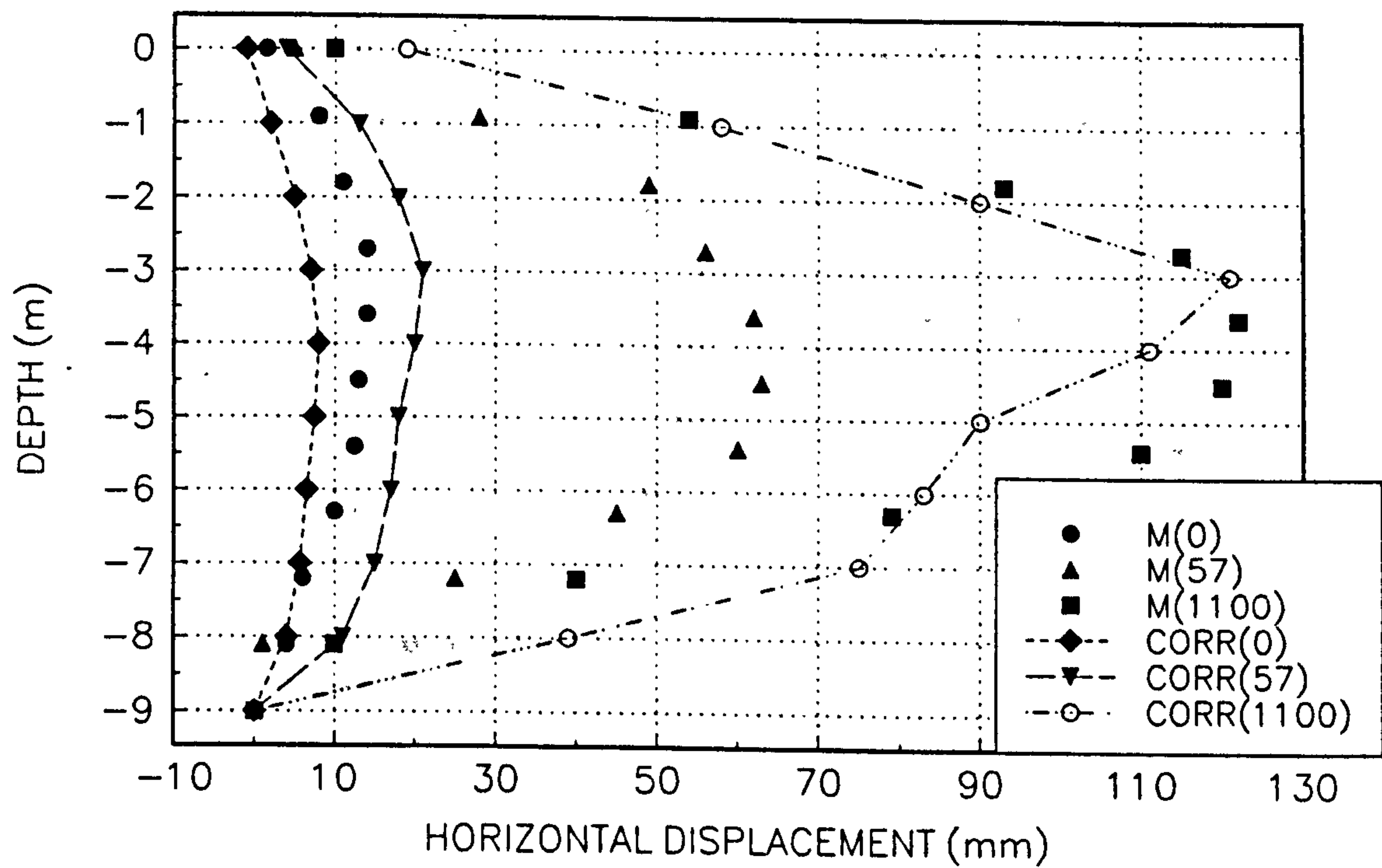


FIGURE 5.23
CORRECTED LATERAL DISPLACEMENT AT INCLINOMETER T11i

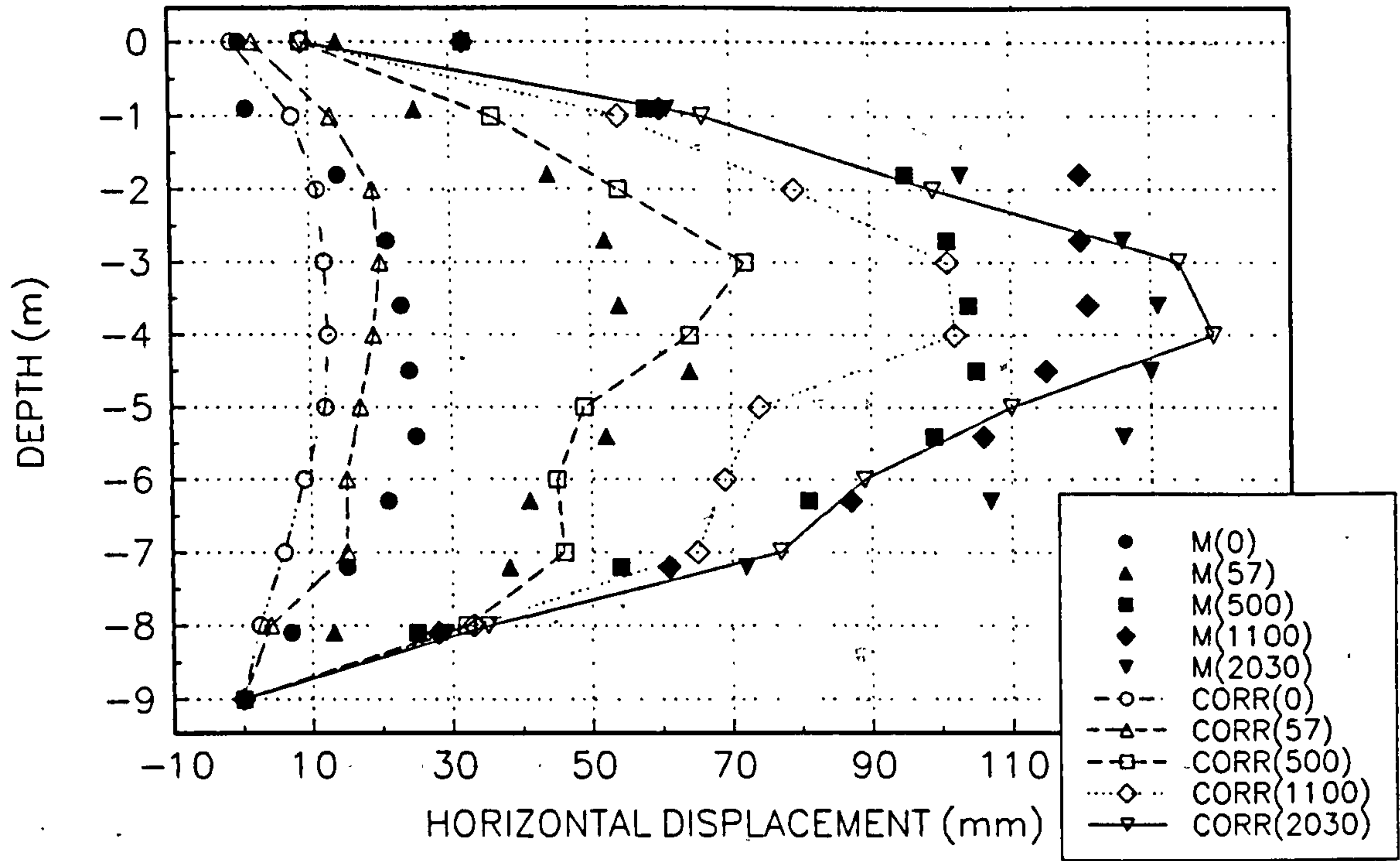


FIGURE 5.24
CORRECTED LATERAL DISPLACEMENTS AT INCLINOMETER T15i

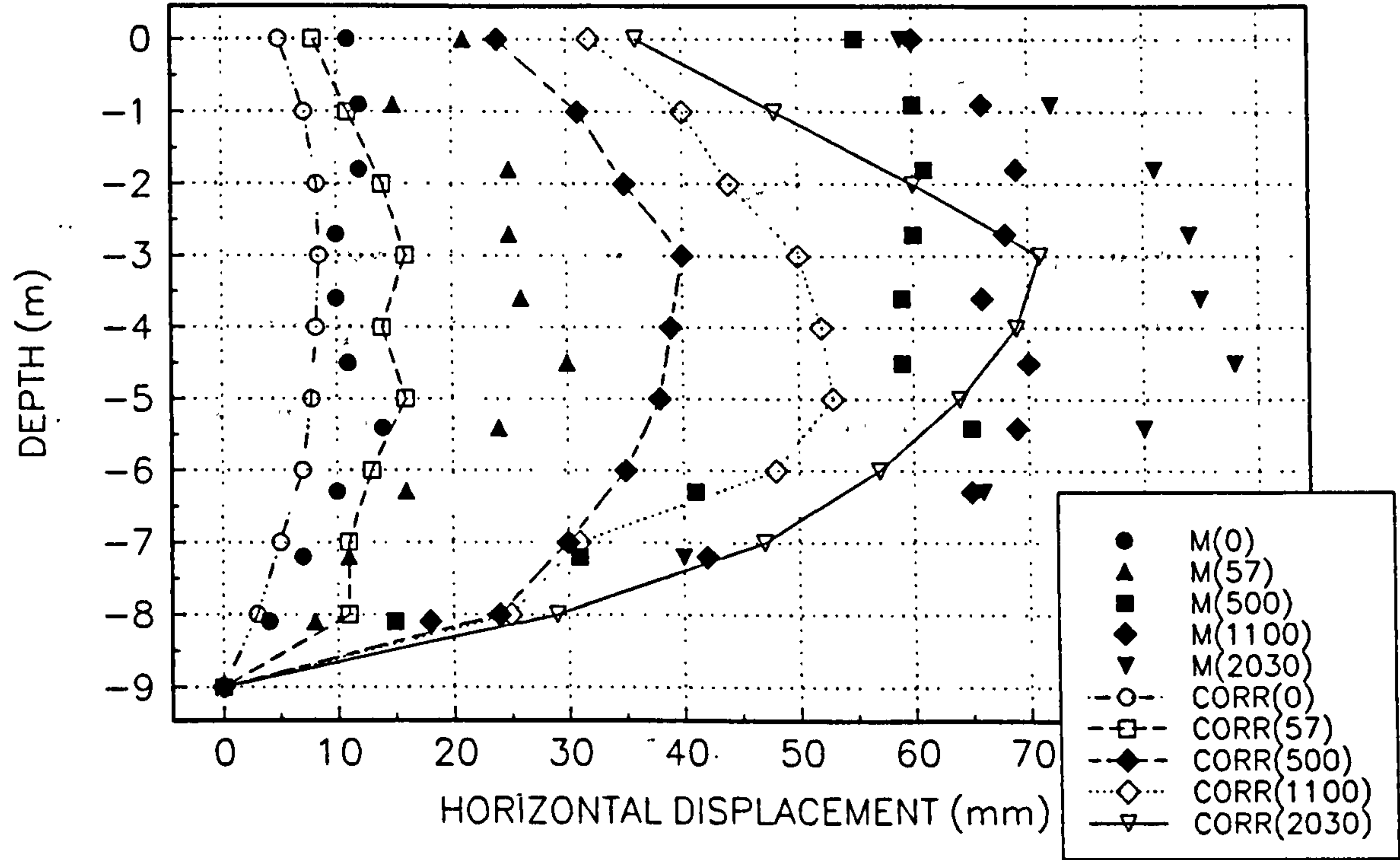


FIGURE 5.25
COMPUTED (RELATION 5.3) AND OBSERVED LATERAL DISPLACEMENTS UNDER TOE

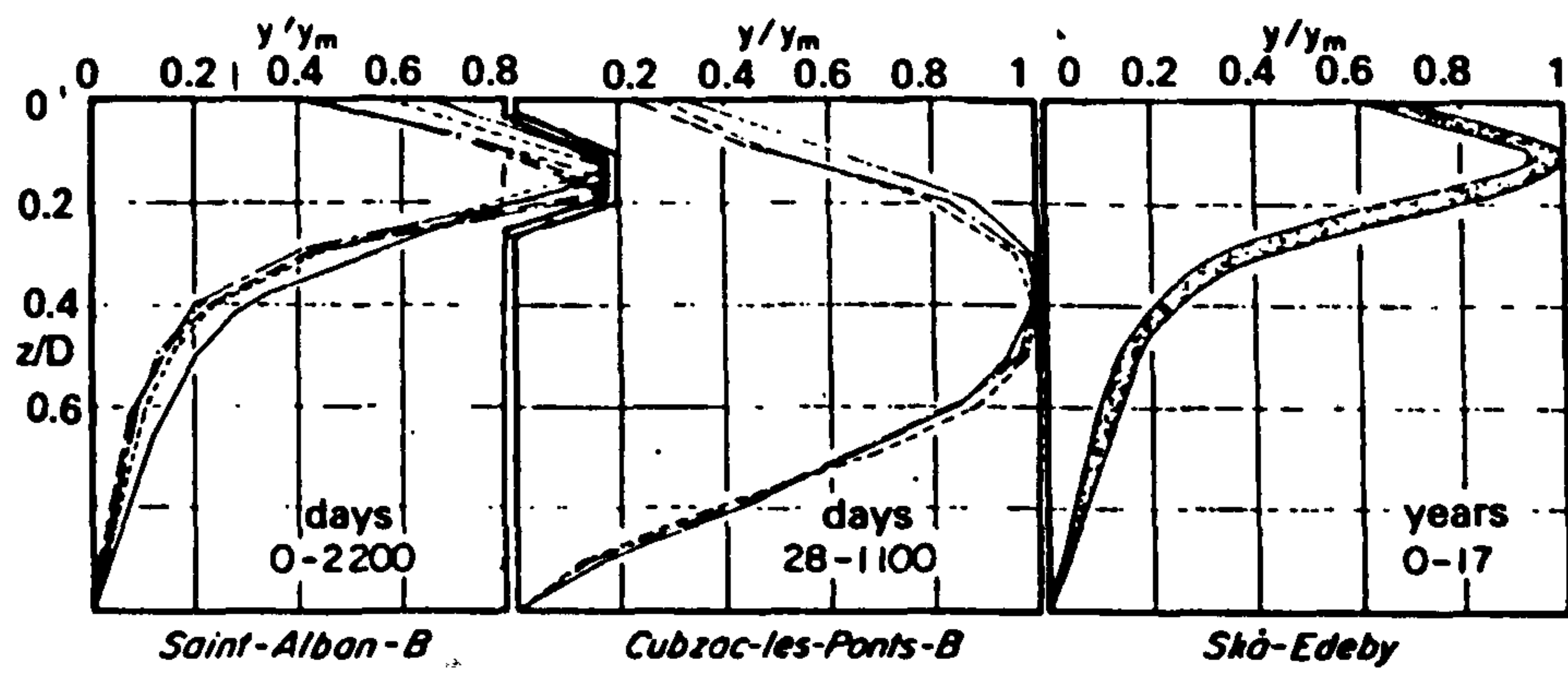
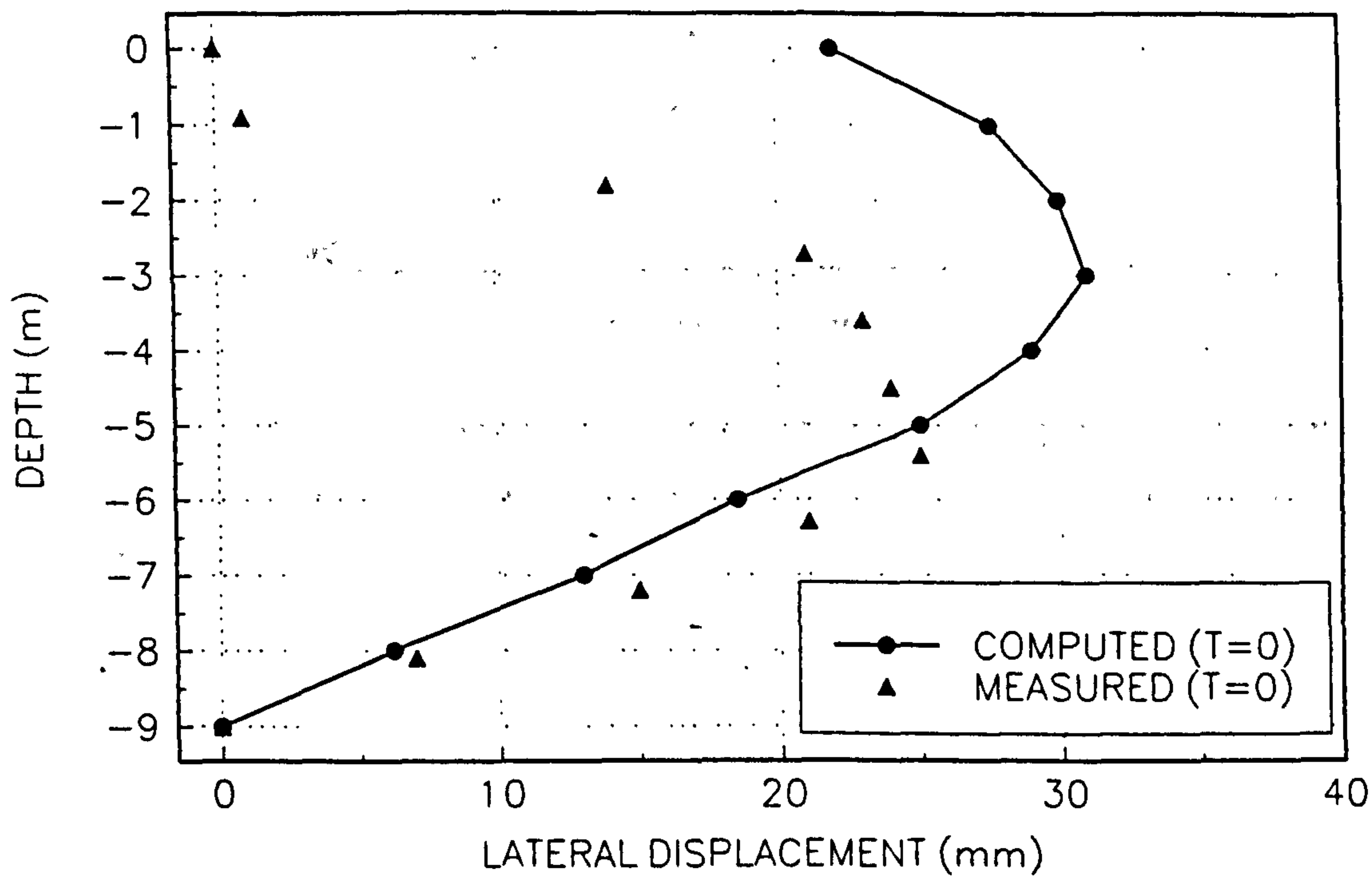


Fig 5.26. Distribution of lateral displacement with depth (Tavenas et al., 1979).

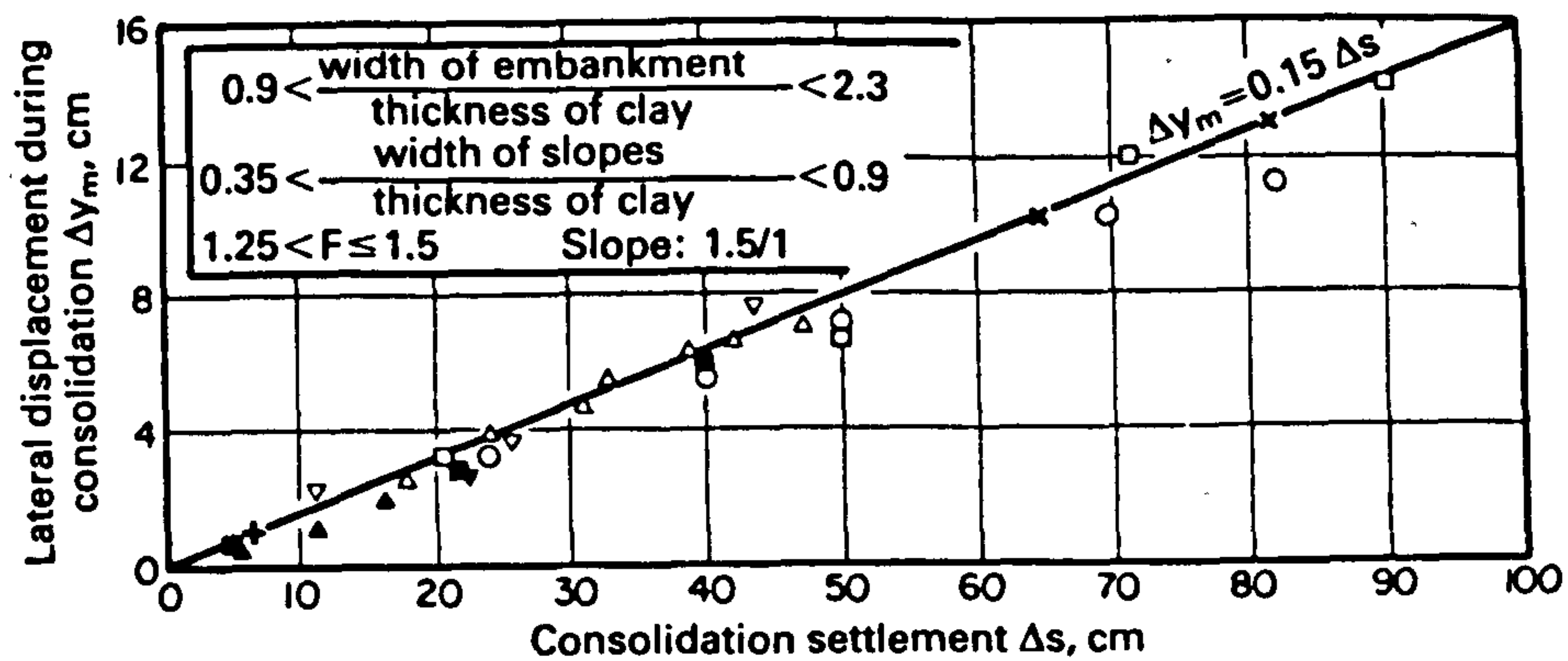


Fig 5.27. Relation between increase in maximum lateral displacement and settlement during long-term consolidation under different embankment on soft clays (Tavenas and Leroueil, 1980).

FIGURE 5.28
COMPUTED (RELATION 5.5) AND OBSERVED LATERAL DISPLACEMENTS UNDER TOE.

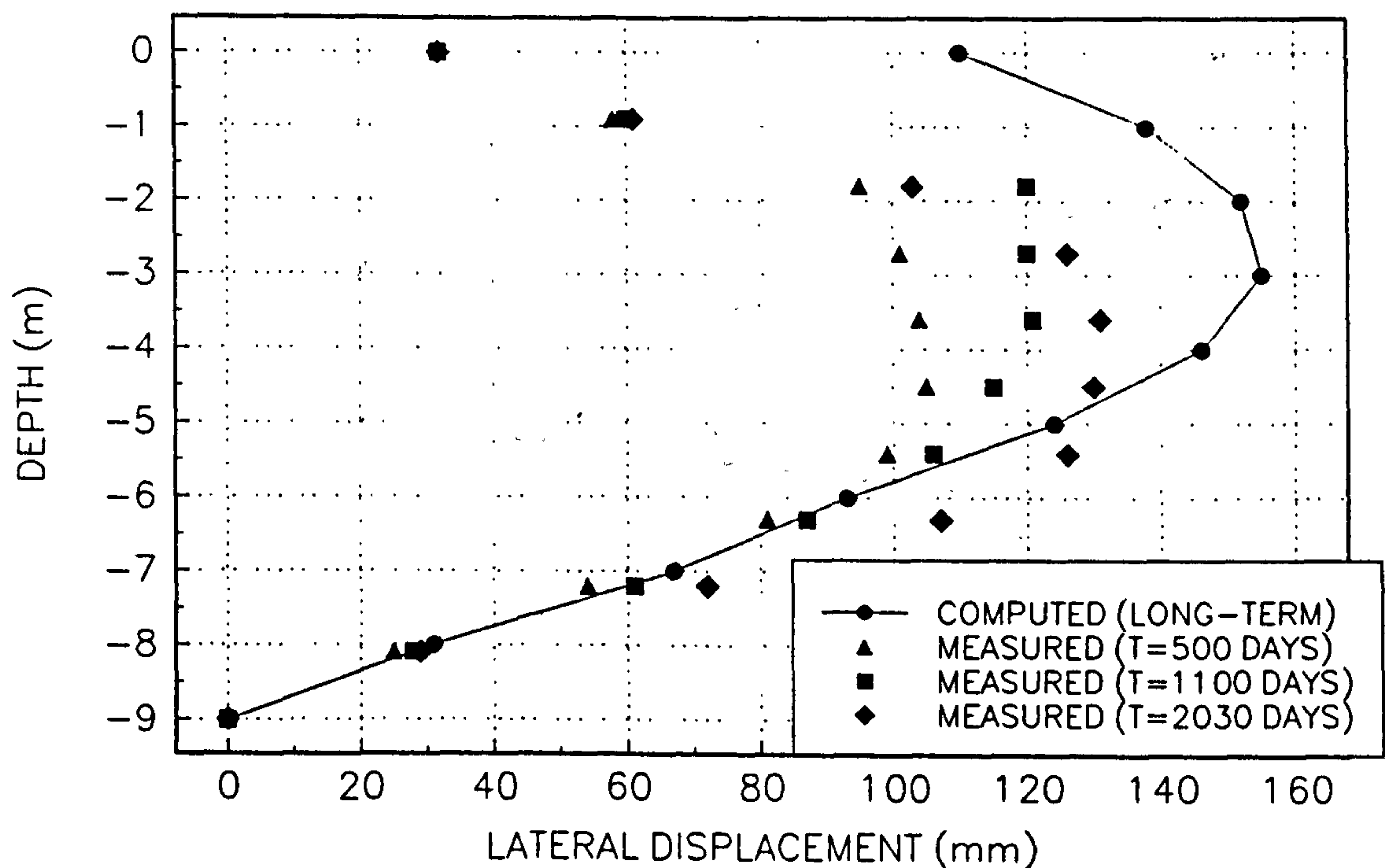


FIGURE 5.29

EXCESS PORE WATER PRESSURE UNDER CENTRE LINE OF EMBANKMENT B.
INCREASE IN PERMEABILITY

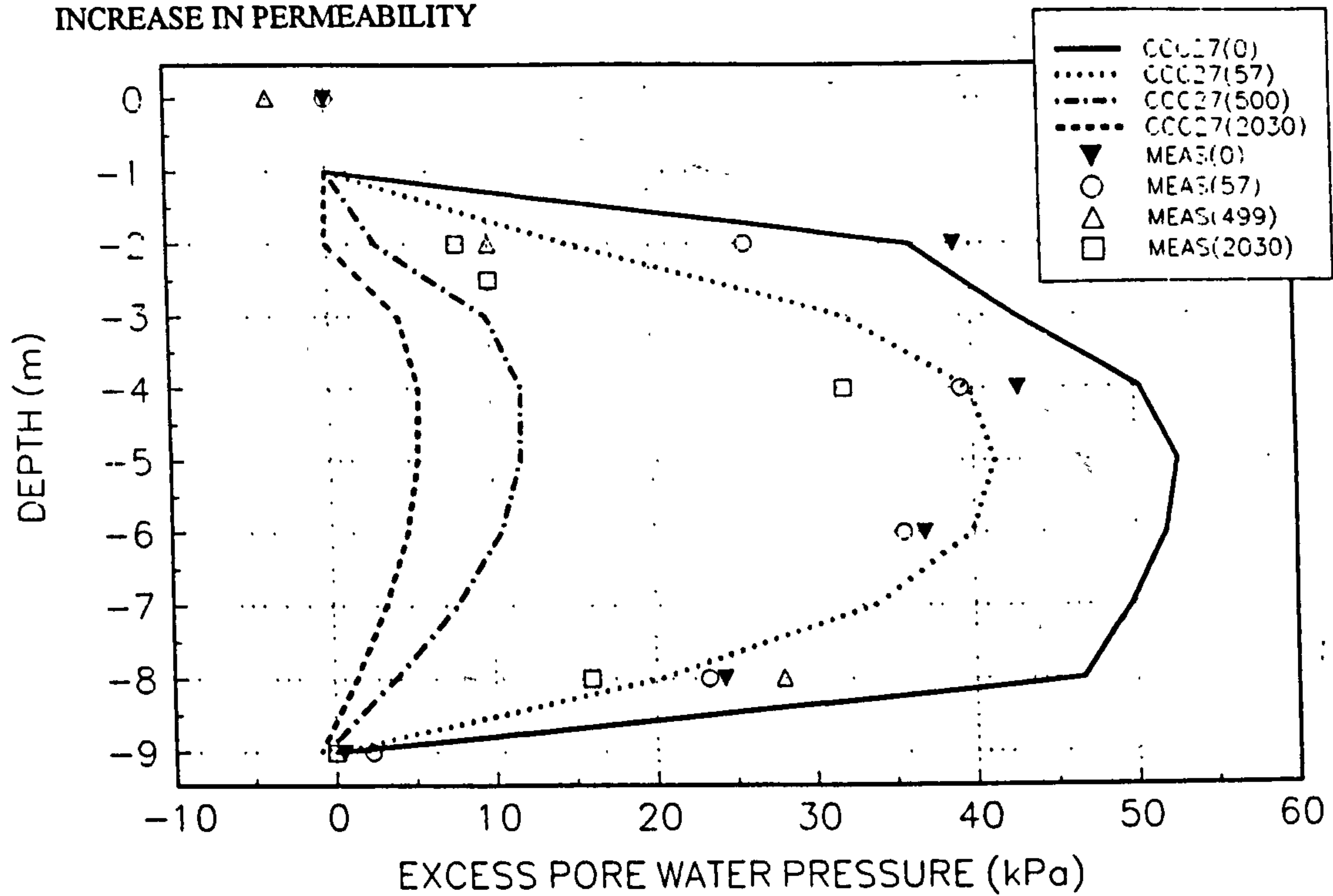


FIGURE 5.30

EXCESS PORE WATER PRESSURE 4m FROM CENTRE OF EMBANKMENT B.
INCREASE IN PERMEABILITY

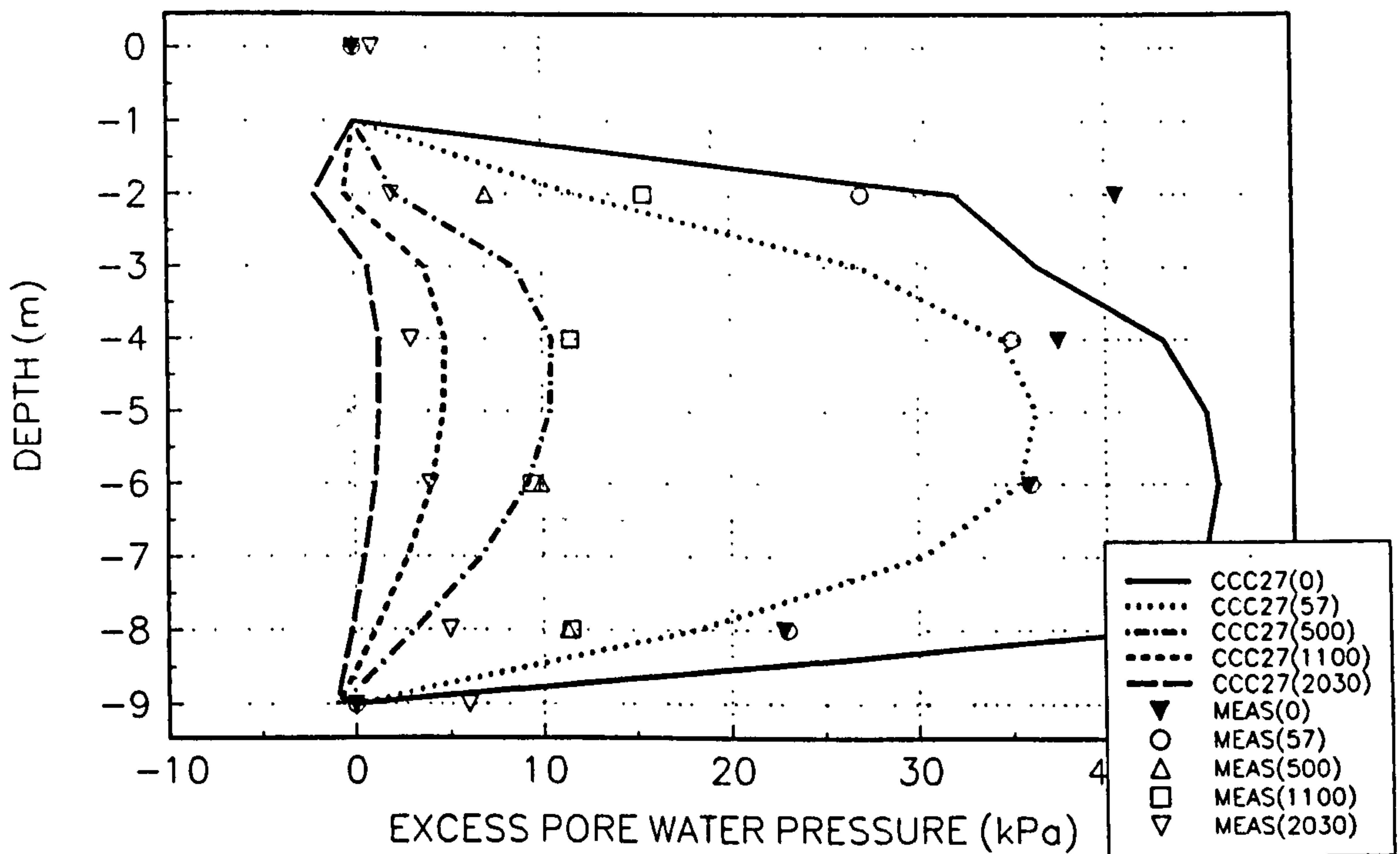


FIGURE 5.31
 EXCESS PORE PRESSURES UNDER TOE OF EMBANKMENT B
 INCREASE IN PERMEABILITY

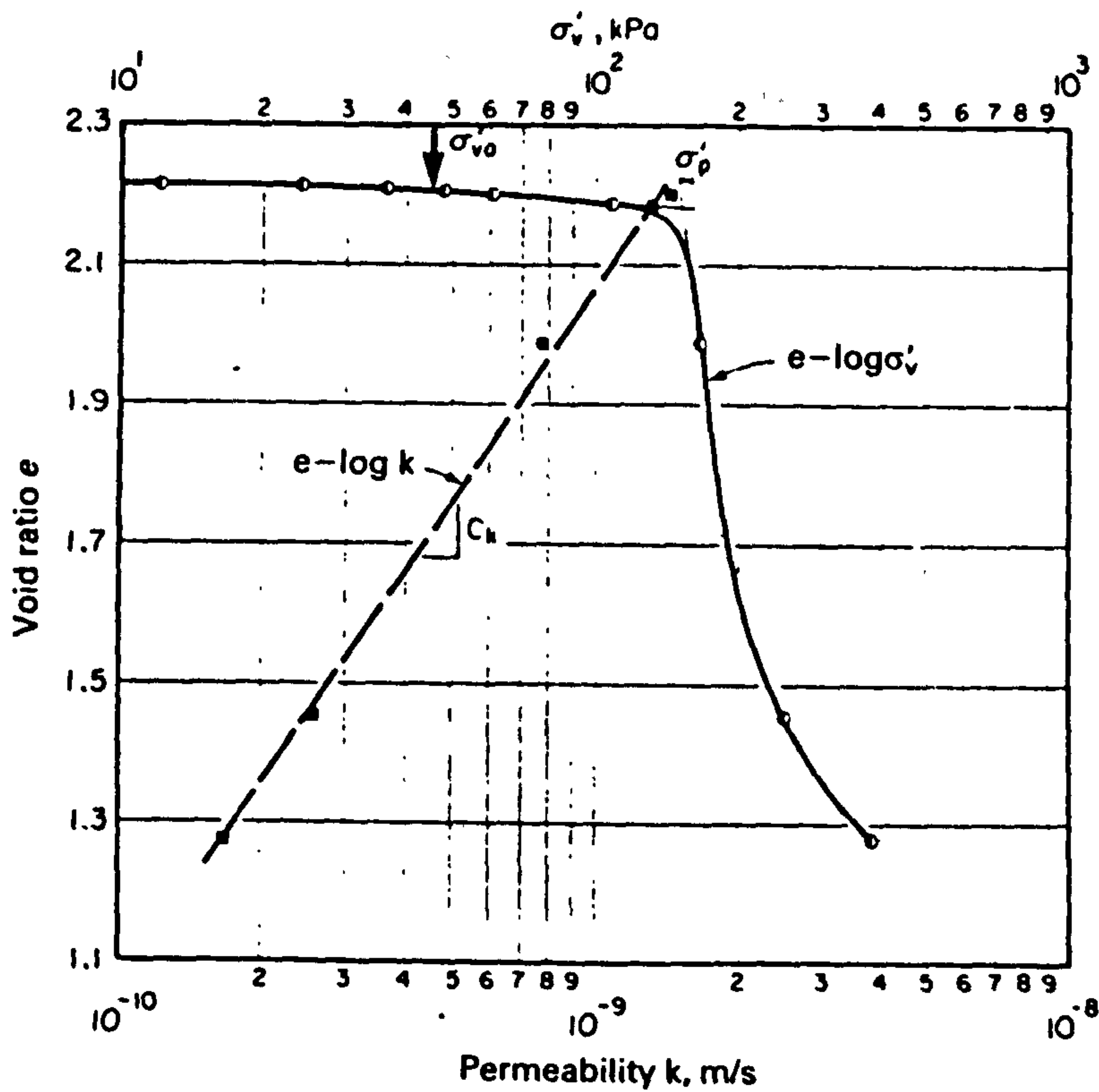
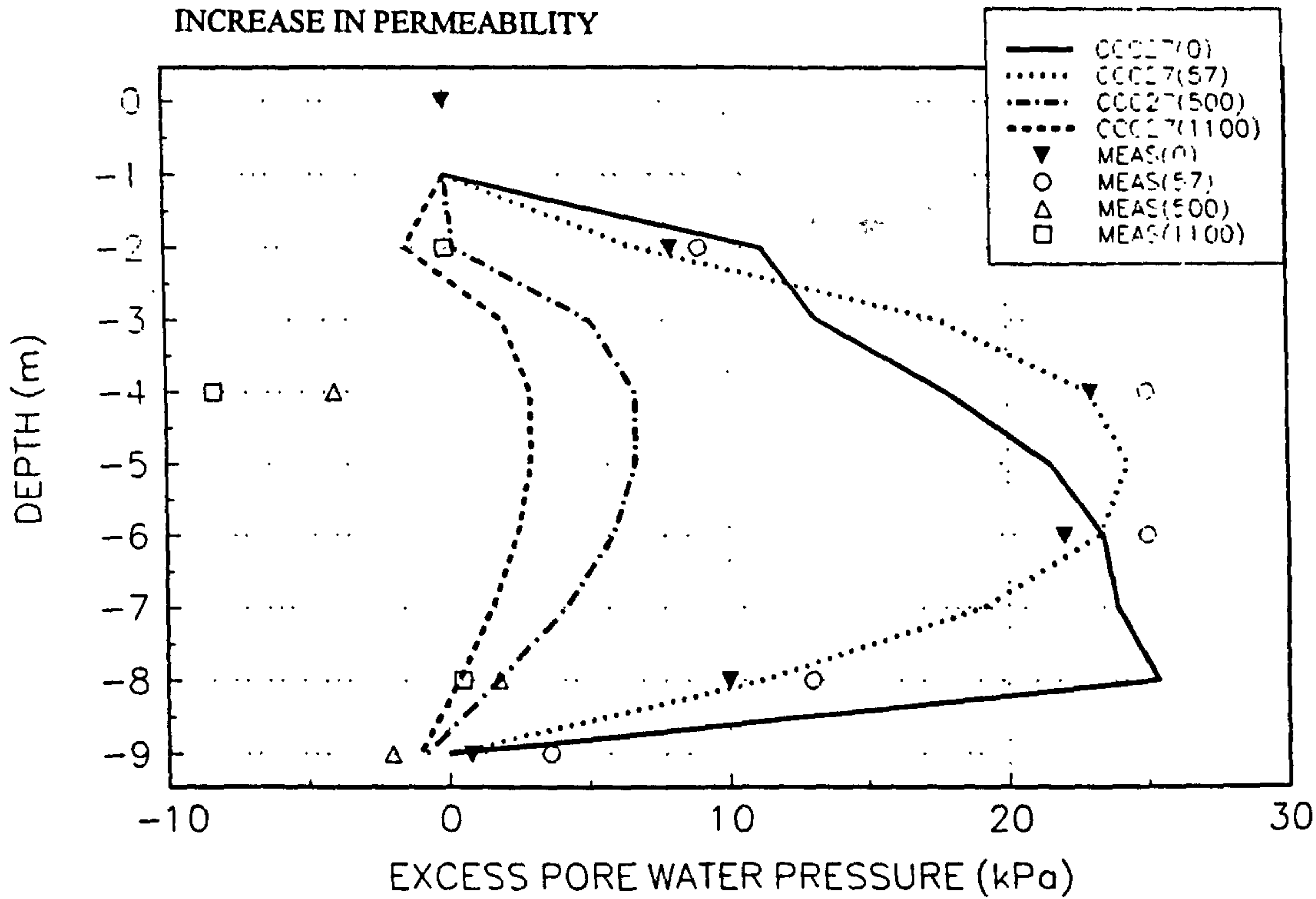


Fig 5.32. Relation between void ratio, e , and permeability, k , obtained in the oedometer (Tavenas et al., 1983b).

Fig 5.33. Computed (MELANIE) (--) and measured (—) settlements at surface of soil beneath embankment B at Cubzac-les-Ponts (Magnan, Mieussens and Queyroi, 1983 and Mouratidis and Magnan, 1983).

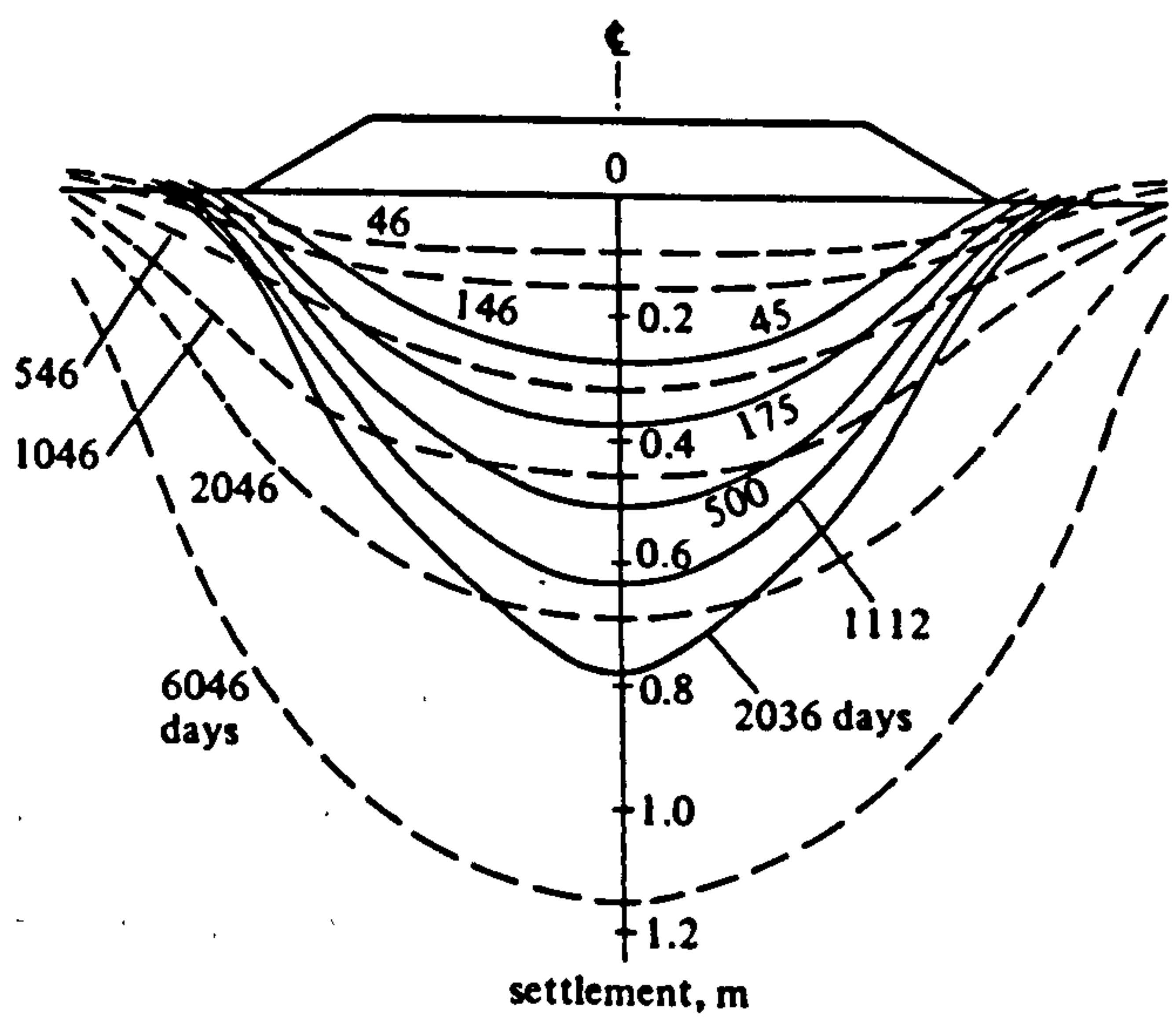


Fig 5.34. Computed (MELANIE) (--) and measured (—) settlements in soil layers beneath embankment B at Cubzac-les-Ponts (a) layers 0-1m,1-2m, 2-4m (Magnan, Mieussens and Queyroi, 1983 and Mouratidis and Magnan, 1983).

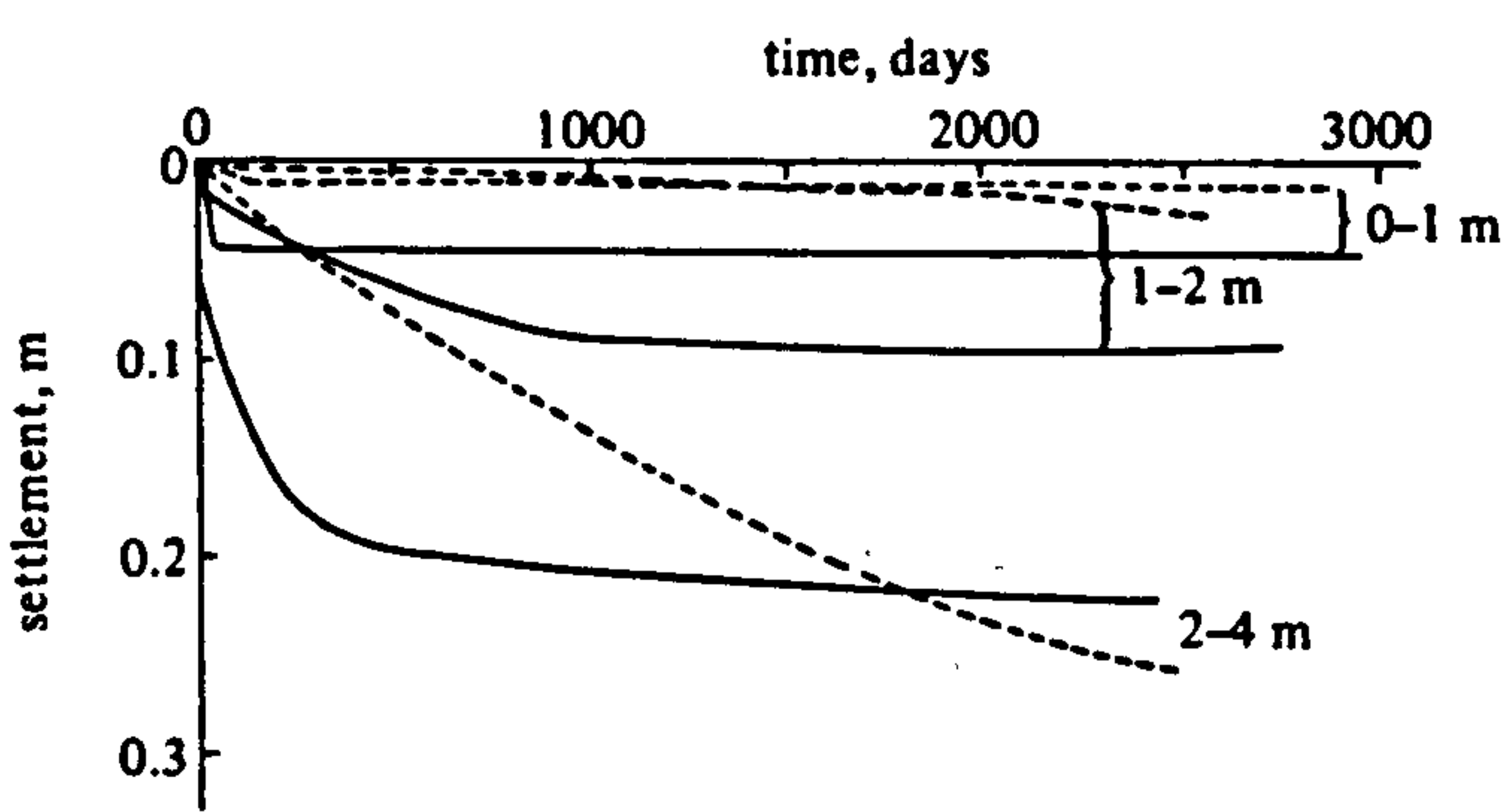


Fig 5.35. Computed (MELANIE) (--) and measured (—) settlements in soil layers beneath embankment B at Cubzac-les-Ponts (a) layers 4-6m and 6-9m (Magnan, Mieussens and Queyroi, 1983 and Mouratidis and Magnan, 1983).

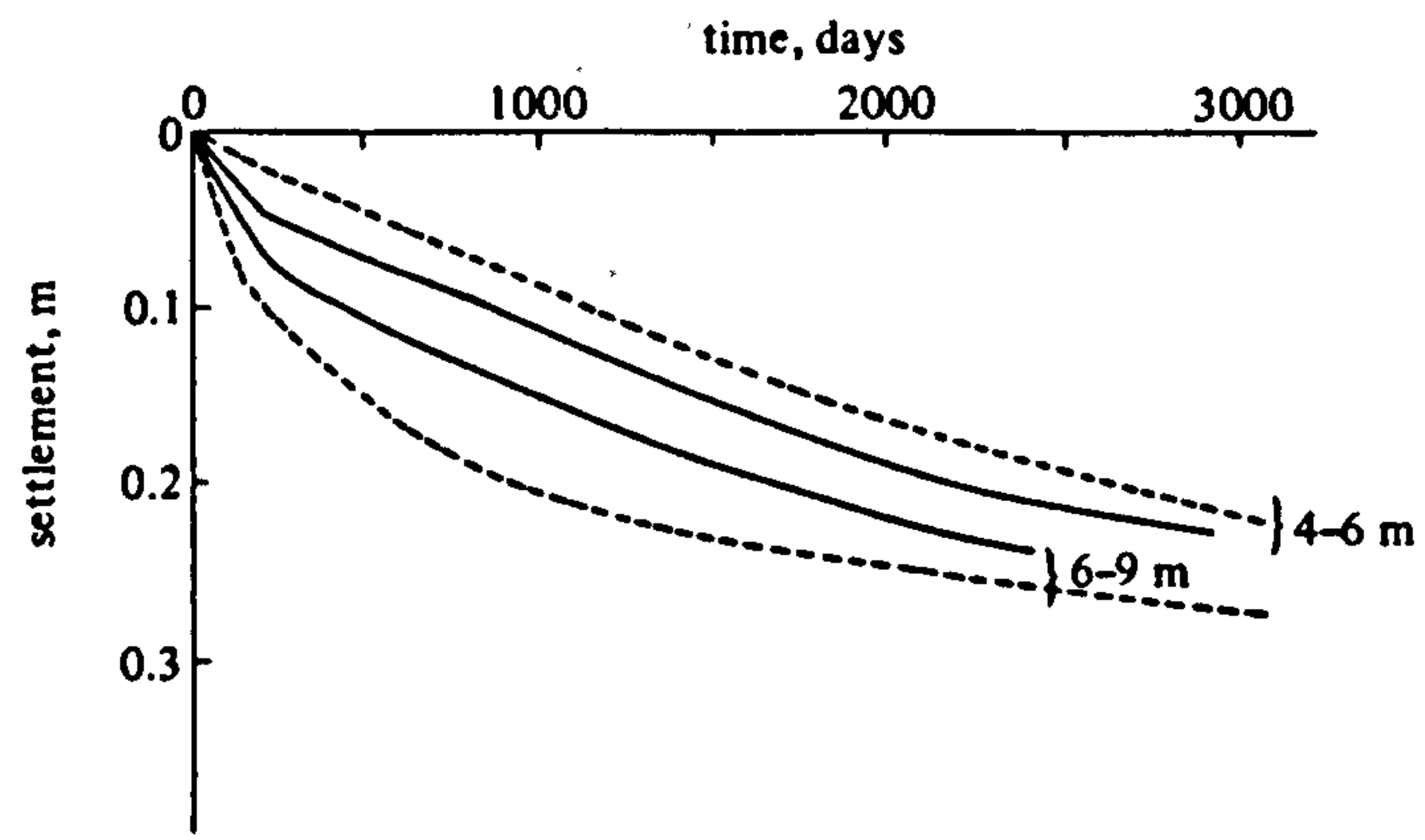


Fig 5.36. Computed (MELANIE) (--) and measured (—) inclinometer profiles for toe (T11i) of embankment B (Magnan, Mieussens and Queyroi, 1983 and Mouratidis and Magnan, 1983).

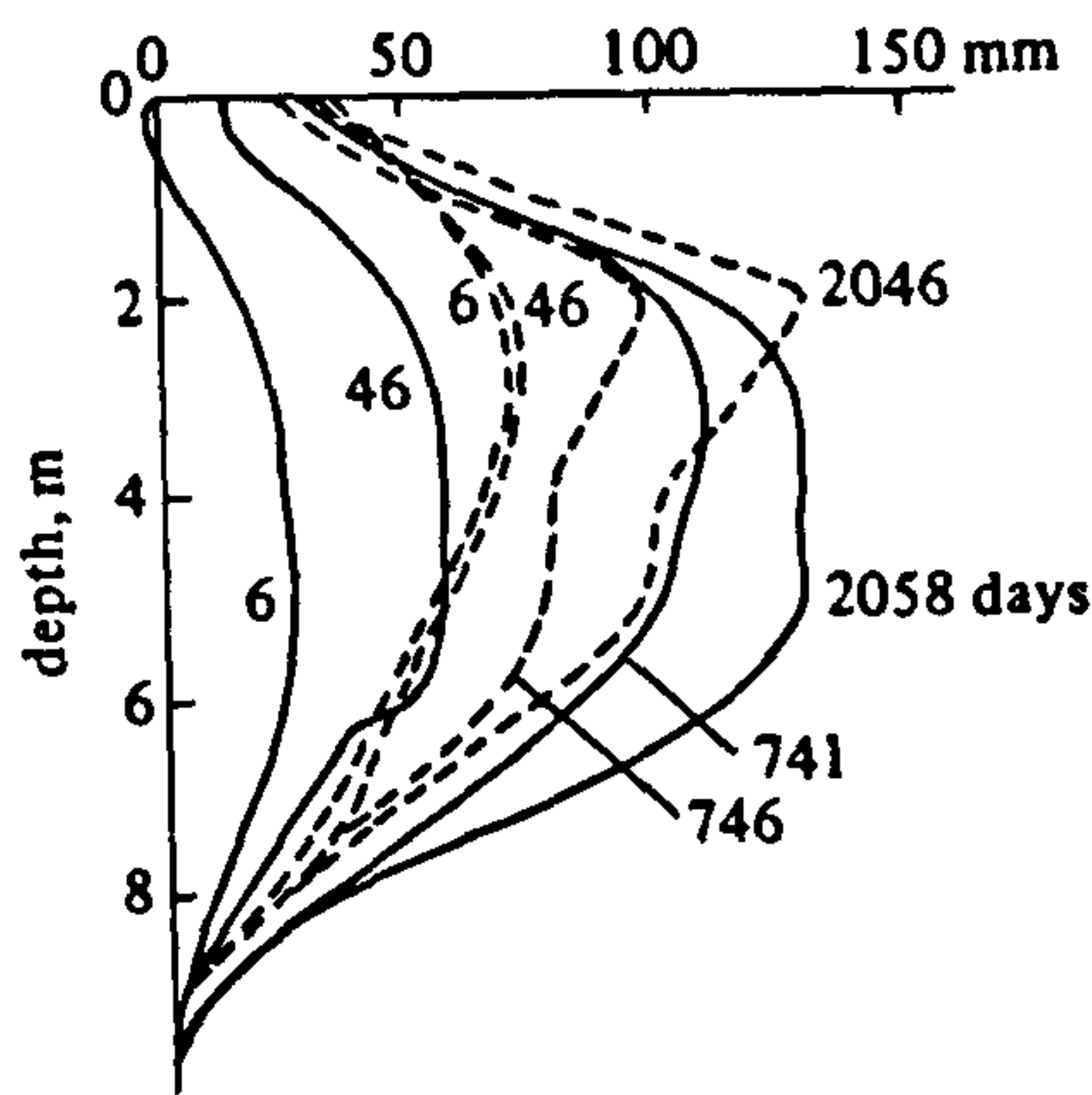


Fig 5.37. Computed (MELANIE) (--) and measured (—) excess pore pressures beneath the centre of embankment B (Magnan, Mieussens and Queyroi, 1983 and Mouratidis and Magnan, 1983).

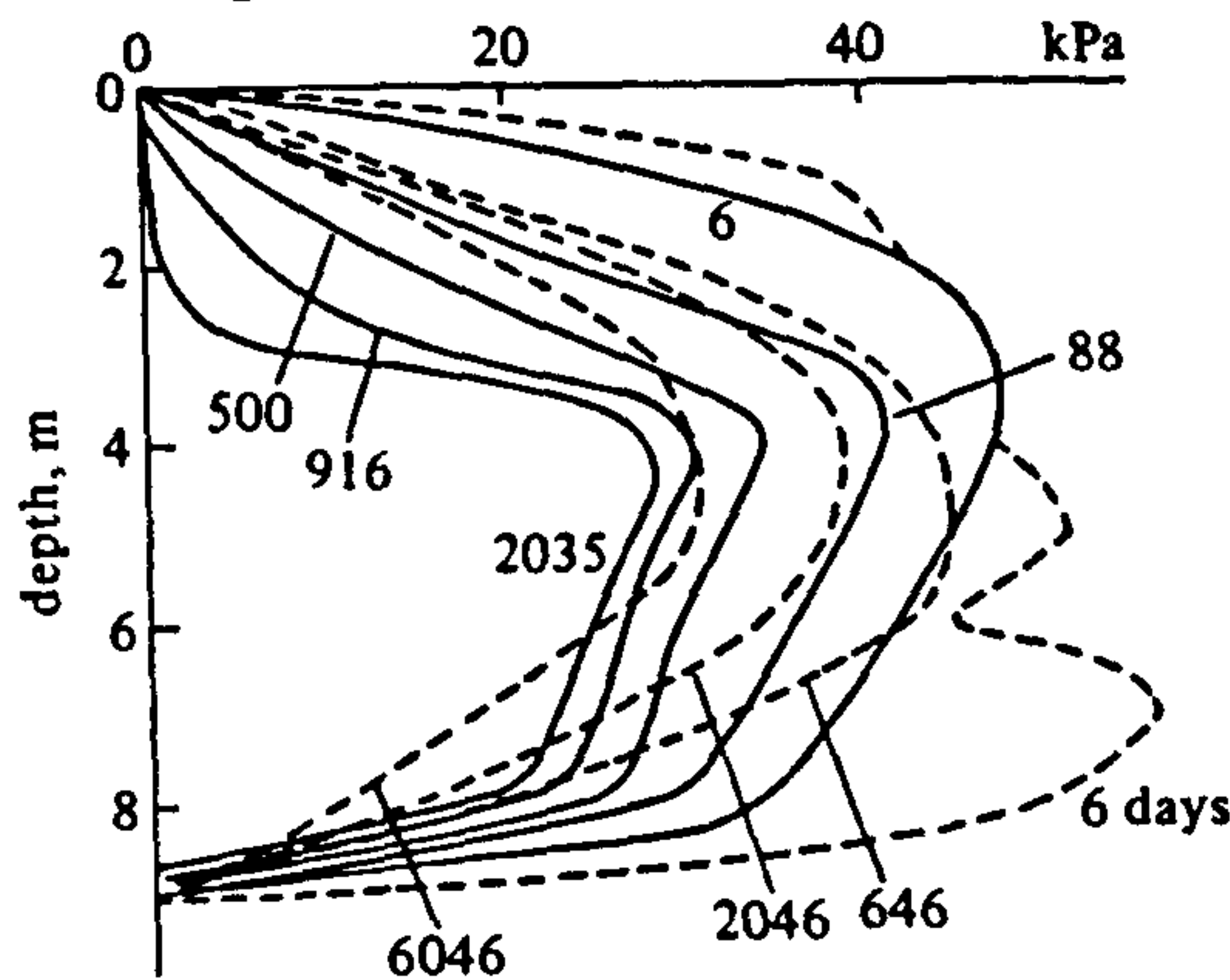
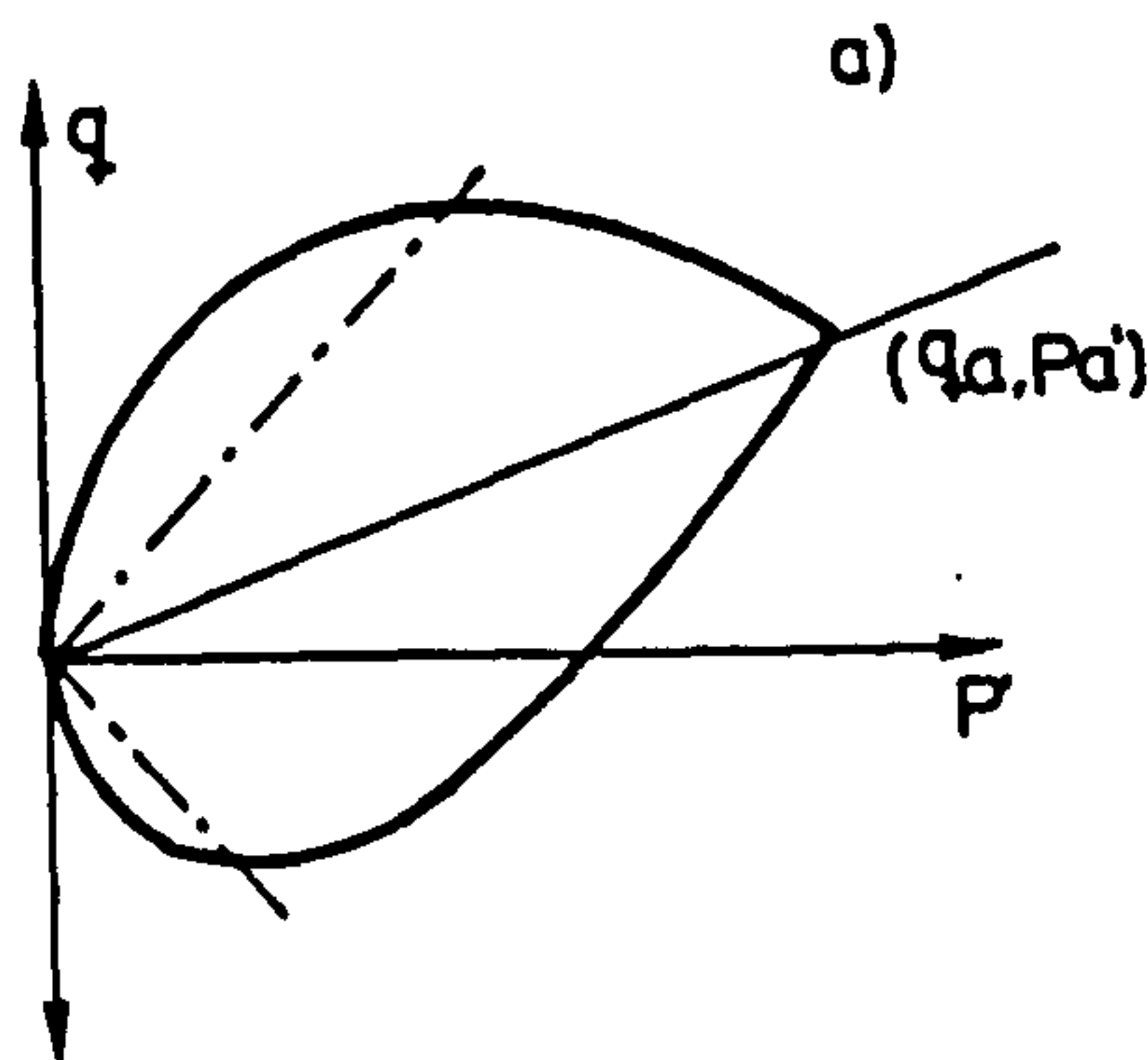


Fig 5.38. Yield surface for K_0 -consolidated soil as described by the anisotropic elastic, viscoplastic soil model (Sekiguchi and Ohta, 1977 and Sekiguchi et al., 1982).



CHAPTER 6

6. Soft clay; conclusions

6.1 Trial loading

Back analyses of the trial loading described in chapter 3 were performed using the isotropic linear elastic, elastic-perfectly plastic Tresca and elasto-plastic modified Cam clay soil models. From comparison of the computed and observed responses the following main conclusions have emerged:

1. During the trial loading the initial settlement response was observed to be stiff (Schnaid et al., 1993). Back analysis of the initial stiff foundation response using the isotropic, linear elastic soil model determined that high values of elastic stiffness were required to accurately model the observed settlement response. Suitable values of elastic stiffness were deduced from a single isotropically consolidated undrained triaxial test performed at low strain ($\epsilon_s < 0.05\%$). Optimum estimates of the elastic stiffness giving the most accurate displacement solution were obtained once parameter selection was performed with an appreciation of the deformation and stress changes expected within the ground.
2. The undrained shear strength of the surface crust was found to significantly influence the bearing capacity of the foundation. Using the linear elastic-perfectly plastic Tresca soil model local failure in the crust was found to be occurring at undrained shear strengths some 1.5-2 times smaller than maximum strength values. Back analysed crust strengths were comparable with strengths estimated from triaxial compression tests. In the modified Cam clay soil model local failure in the crust was modelled by using values of p'_0 estimated from triaxial compression test undrained shear strengths.
3. Back analysis using the Tresca soil model have also shown that the undrained shear strength for the underlying soft clay is most accurately described using the corrected in situ vane.
4. The observed foundation behaviour was most accurately described using the modified Cam clay soil model. However, application of the modified Cam clay soil model was not straightforward but frustrated by sparse soil data from which to select the required material parameters. Available soil data were more suited to the simple Tresca soil model.

5. The reasonable predictions of the observed behaviour using the modified Cam clay soil model indicate that for this trial loading modified Cam clay incorporates the necessary features of soil behaviour. However, differences still remain, particularly between computed and observed lateral displacements. From comparison of published data (Mouratidis and Magnan, 1983; Leroueil et al., 1985 and Poulos, 1972) improvement of the predicted lateral displacement solution may be achieved if anisotropy is also included within the constitutive relation.

6.2 Embankment A

The main conclusions which have emerged from back analysis of embankment A using the modified Cam clay soil model are briefly summarised below.

1. Overall the modified Cam clay soil model has not provided a reasonable description of the observed soil behaviour. However, predicted settlements are reasonable; lateral displacements and excess pore water pressures are not.
2. Reasonable predictions of lateral displacements and excess pore water pressures were made using empirical and semi-empirical hand-calculations (Tavenas et al., 1979 and Tavenas and Leroueil, 1980).
3. Previous analysis of embankment A using the MELANIE soil model (Mouratidis and Magnan, 1983) provided a good description of the observed foundation behaviour. The MELANIE soil model, unlike modified Cam clay, was capable of simultaneously predicting settlements, lateral displacements and excess pore water pressures to a reasonable degree of accuracy. The good comparison between the computed and observed responses provided by the MELANIE soil model indicates that this model incorporates the necessary features of soil behaviour required to accurately describe this type of embankment loading.
4. The inclusion of anisotropy and the ability to vary the degree of saturation of the soft clay within the MELANIE soil model are considered to be the main strengths of this soil model. Additionally, the inclusion of a non-associated flow rule is also thought to provide some improvement to the prediction of lateral displacements induced under embankments (Zienkiewicz, 1976; Leroueil et al., 1985 and Chen and Mizuno, 1990).
5. Like the trial loading described in chapter 3, high values of elastic stiffness were required to match the observed settlement response. Optimum values of elastic stiffness were selected at low strains, $\varepsilon_q \approx 0.1\%$.

6. Low values of Poisson's ratio ($\nu' = 0.2$) were required to ensure a suitably low ratio of maximum lateral movement to maximum vertical movement.

7. For consolidation analyses values of the horizontal permeability, k_h , were selected from self-boring permeameter data. Values of vertical permeability, k_v , were estimated from k_h/k_v ratios estimated from laboratory tests. Consolidation analyses using the modified Cam clay soil model did not improve predictions of excess pore water pressures nor lateral displacements.

6.3 Embankment B

From comparison of the computed and observed responses the following main conclusions have emerged.

1. Overall the modified Cam clay soil model did not provide a good description of the observed foundation behaviour (short term and long term). Lateral displacements were least accurately predicted.
2. Previous analysis of embankment B using the MELANIE soil model (Mouratidis and Magnan, 1983) provided, in general, good predictions of the observed foundation behaviour. However, settlements were more accurately predicted using the modified Cam clay soil model.
3. As mentioned previously the improved accuracy provided by the MELANIE soil model is thought to be the inclusion of the anisotropic elastic and plastic properties and the presence of gas within the pores of the soil (Leroueil et al, 1985). However, despite the inclusion of these properties the depth profile of lateral displacements occurring beneath the embankment toe at the end of construction were overestimated compared to those observed.
4. Back analysis of lateral displacements occurring beneath an embankment using Sekiguchi and Ohta's elasto-viscoplastic soil model (Miki et al., 1994) provided good predictions of the observed short term and long term behaviour. The results presented by Miki et al. (1994) indicate that the inclusion of viscosity may also be an important feature within a numerical framework, particularly if accurate predictions of lateral displacements are required.
5. Reasonable estimates of the end of construction and long term lateral displacements occurring under the embankment toe were made using empirical correlations (Tavenas

and Leroueil, 1980 and Leroueil et al., 1985). Predictions of the lateral displacements using the empirical correlations were more accurate than those using the modified Cam clay soil model.

6. Despite the dominance of plastic strains throughout the analyses, settlement predictions were found to be influenced by the magnitude of elastic stiffness. Here optimum values of elastic stiffness corresponded to a strain level of approximately 0.3-0.4%.

7. Constant values of permeability (isotropic or anisotropic) for all effective stress states are not realistic. Back analysis of observed excess pore water pressure data indicate that allowing the permeability to vary with effective stress (or void ratio) may provide a more accurate description of the foundation behaviour.

6.4 Necessary site investigation requirements for soft clay analyses

6.4.1. Elastic stiffness

Within the soft clay case histories the elastic stiffness has been estimated using triaxial testing with internal and external strain measurement, oedometer tests and the self boring pressuremeter. Ideally, preference should be given to in situ testing to minimise sample disturbance. Consequently, self boring pressuremeter testing is recommended. Measurement of elastic stiffness at small strains ($\varepsilon \approx 0.1\%$) is attainable provided expansion of the cylinder is controlled. In addition to the pressuremeter tests, the elastic stiffness should also be estimated from triaxial tests performed with internal strain measurement on high quality samples (Piston sampler; Gouda or Laval sampler). Triaxial testing, with internal strain measurement has the advantage that the elastic stiffness can be estimated over very small strains and strain rates can be carefully controlled, especially where cycles of unloading and re-loading are necessary. Use of the oedometer test to estimate the elastic stiffness of soil is not recommended. The strain resolution of oedometer tests is rarely small enough to permit accurate measurement of the elastic stiffness over the anticipated strain range.

Values of Poisson's ratio were selected to ensure a low strain ratio of lateral to vertical movement. This approach requires low values of Poisson's ratio. Ideally, the in situ value of Poisson's ratio should be estimated from drained triaxial tests.

6.4.2 Shear strength parameters

The undrained shear strength has been estimated using many different methods. From back analysis the following testing methods were found to provide a reasonable estimate of the in situ undrained shear strength:

1. Undrained triaxial compression tests to describe the strength of an overconsolidated surface crust.
2. Corrected in situ shear vane (Bjerrum, 1973) to describe the strength of soft normally consolidated clays.

Values of undrained shear strength estimated from the self boring pressuremeter tests were considered to be too high for use in the embankment studies. A good estimate of the in situ undrained shear strength was also obtained using the static cone penetrometer. However, the cone factor was estimated using corrected in situ shear vane undrained shear strengths.

An estimate of the drained shear strength parameters, c' and ϕ' , and the critical state parameter M can be accurately estimated from direct shear tests performed using the triaxial apparatus.

6.4.3 Plasticity and preconsolidation parameters

Values of the plasticity parameter λ have been estimated from oedometer and triaxial (constant rate of strain) test normal compression data. Both tests have provided good estimates of λ (see chapters 3 and 4). However, due to the greater testing control associated with the triaxial apparatus this form of test to estimate λ is recommended.

Like the plasticity parameter λ , the preconsolidation pressure should also be estimated from constant rate of strain triaxial tests. This is again due to the greater control associated with triaxial testing, but also the occurrence of yield is better defined (change in slope of the normal compression line) than that observed in a conventional oedometer test.

6.4.4 Permeability

Estimates of the in situ permeability should be made using in situ testing methods. The self boring permeameter was used in chapters 4 and 5 to estimate the in situ horizontal permeability. The self boring permeameter is considered to provide the most accurate estimate of the in situ horizontal permeability (Leroueil et al., 1992). Of the laboratory tests the radial flow cell using large diameter samples (180mm) is considered to provide the most representative estimate of the in situ permeability. In view of this, it is recommended that the horizontal permeability, k_h , is estimated from the self boring permeameter and the vertical permeability, k_v , is estimated from k_h/k_v ratios determined from the radial flow cell.

6.5 Empirical and semi-empirical methods

Throughout the soft clay studies empirical and semi-empirical methods have been used to supplement and check available soils data. The methods which were considered most useful are briefly summarised below.

1. Estimates of elastic stiffness were checked using an empirical link between normalised elastic stiffness (normalised with respect to the undrained shear strength), plasticity index and the overconsolidation ratio (Duncan and Buchigani, 1976).
2. Selected values of Poisson's ratio can be checked using an empirical relationship between Poisson's ratio and plasticity index (Wroth, 1975 and Muir Wood, 1990).
3. Some check on selected values of λ was provided by an empirical link with plasticity index (Muir Wood, 1990).
4. Values of the critical state parameters M were checked using empirical correlations between plasticity index (Mitchell and Muir Wood, 1990) and the undrained shear strength and preconsolidation stress (Diaz-Rodriguez, et al., 1992).
5. Some check on the assumed depth profile of the degree of overconsolidation was obtained from the depth profile of undrained shear strength (chapter 3 section 3.6.4.2); an empirical relation between the preconsolidation pressure, the in situ shear vane and plasticity index (chapter 3 section 3.4.3); and from consideration of the critical embankment height (chapters 4 and 5).

CHAPTER 7

7. Flexible culvert analyses

7.1 Introduction

This chapter serves as an introductory chapter for the flexible culvert finite element studies presented in chapters 8 and 9. The work presented in these chapters forms part of a three year research contracted awarded to Glasgow University, Department of Civil Engineering by the Transport and Road Research Laboratory, (TRRL), to review the design of flexible culverts. To satisfy the requirements of the TRRL contract the original research team (Davies, Chan, Stewart, Muir Wood and Bu, 1993) developed an analytical model to aid flexible culvert design using the finite element method by adapting the general purpose finite element program CRISP, (Britto and Gunn, 1987). CRISP is a well-established analytical design tool used for many geotechnical problems; therefore it was seen as advantageous to further extend the capabilities of CRISP to include the flexible culvert problem. The finite element program CRISP and the adaptations required to model flexible culverts suitably are briefly described in chapter 2. The developed analytical model makes use of the soil models available in the standard version of CRISP and incorporates the backfilling construction sequence. For simplicity, the adopted approach to modelling flexible culvert behaviour incorporates a linear elastic, perfectly plastic soil model with a non-associated Mohr-Coulomb yield criterion used to describe the backfill material. Despite some reservations over the limitations of using a linear elastic soil model (Duncan, 1979, Mohamedzein, 1989) the installation of field culverts typically differs from one to another and the situation during construction is seldom well enough defined or controllable to justify complex numerical analysis (Richards, 1982). This statement is investigated in chapters 8 and 9 by assessing the accuracy with which the developed numerical model is capable of modelling the observed behaviour of two flexible culverts.

Previous studies presented in this thesis were concerned with parameter selection to suitably reproduce the observed foundation response to loading derived from the construction of some surface structure. In this study, the object of performing numerical analyses is quite different. These studies were performed to predict, to a reasonable degree of accuracy, the behaviour of flexible culverts under backfill and live loads. The main concern therefore is the flexible culvert behaviour and not directly that of the foundation. However, the behaviour of flexible culverts is predominantly

dependent on the properties and behaviour of the surrounding backfill (Watkins, 1964; Richards, 1982). The main theme of parameter selection for the foundation soil therefore still applies. However, the parameter selection process is less well defined than that described previously. This is primarily due to the uncertainty and to some extent the uncontrollable nature of the physical properties and behaviour of the backfill material throughout the construction procedure which ultimately influences its final state. Conversely, the behaviour of the culvert can significantly influence the behaviour and distribution of stress throughout the surrounding backfill due to the deformation response of the culvert to imposed loads. Additionally, selected parameters must reflect the certainties and uncertainties of this complex earth pressure problem of soil structure interaction. In this case parameter selection tended to shadow the parametric studies performed to identify the effects of the required model material parameters on the finite element solution. Using this approach and making use of published field and laboratory test data, a framework for parameter selection has been suggested. Implications are drawn concerning the feasibility of using an adapted general purpose finite element program and a linear elastic, perfectly plastic soil model to describe the backfill material as analytical engineering tools with which to analyse and design flexible culverts.

This chapter serves to set the scene for the numerical analyses described in chapters 8 and 9. A brief description of culvert-soil interaction problems and the influence of the construction operations on the interaction is presented in section 7.2. A description of classical and more recent methods used to analyse and design flexible culverts is presented in section 7.3. Additionally, the different constitutive soil models which have been used to describe the backfill material for soil-culvert systems are also discussed at the end of section 7.3. Modelling assumptions required to describe the culvert, backfill material, construction operations, and live loadings are discussed in section 7.4.

7.2 Soil structure interaction; definition of the problem

Flexible culverts isolated from the ground are very flexible and fragile structures with very little strength. Yet when buried within the soil the load carrying capabilities of these simple structures are remarkable. Examples of their use include highway and water way underpasses and even nuclear storage shelters.

Throughout this study the response of the culvert to backfill and live loading has been described in terms of active and passive earth pressures. These terms are most often used to describe the earth pressure conditions leading up to failure behind a retaining wall following Rankine or Coulomb earth pressure analysis. In this study, to some extent, these terms are being used out of their normal context as their use to describe the culvert response primarily refers to the deformation response of the culvert (which is also a retaining structure) in relation to the backfill which is assumed to be on the verge of failure. Consequently for this study an active earth pressure condition may be developed when the culvert is deforming away from the backfill material. Alternatively a passive earth pressure condition may be developed when the culvert deforms towards (or into) the backfill material.

Flexible culverts carry high vertical loads through their ability to mobilise high passive pressures within the soil at the sides of the culvert (Spangler, 1941). The magnitude of the mobilised passive pressures depends on the flexibility of the culvert and its ability to readily deform laterally under the developing active pressures forcing the crown of the culvert downwards, Fig 7.1. The development of active and passive earth pressures causes the applied loads, (dead or imposed loads) to flow through the culvert and into the backfill (Richards, 1982). At the same time there is a second related but distinctly different mechanism for redistribution and reorientation of the stress field around the flexible culvert. This mechanism is called arching and may be either positive or negative depending on the degree of flexibility and axial stiffness of the culvert. Allgood and Takahashi (1972) define arching, A , by relation (7.1)

$$A = 1 - \left(\frac{\sigma_i}{\sigma_y} \right) \quad (7.1)$$

where σ_i is the vertical pressure on the structure at the crown and σ_y is the free-field (no culvert) vertical stress at the elevation of the crown.

If the culvert is flexible and axially less stiff than the surrounding backfill ($\sigma_i < \sigma_y$ and $A > 0$) then load (weight of backfill and applied live loads above the culvert crown) is transferred to the adjoining backfill and away from the culvert (Selig, 1972). This mechanism arises because the contact stresses which form at the culvert-soil interface cannot be supported by the culvert crown which therefore displaces downwards. This displacement causes approximately vertical shear planes to develop within the backfill above the culvert crown, Fig 7.2. However, vertical shear slippage of the backfill above the culvert is prevented by the adjacent unyielded areas of backfill and, as a

result, load is transferred away from the culvert and into the surrounding backfill, Fig 7.3. Alternatively, negative arching ($A < 0$) will occur if the culvert is stiffer than the surrounding backfill ($\sigma_i > \sigma_y$ and $A < 0$) and load will be transferred to the culvert from the surrounding backfill. In flexible culvert design positive arching is promoted, and negative arching can be catastrophic for flexible culverts unless it is anticipated.

For an effective culvert design where the load carrying capabilities of the surrounding backfill are effectively utilised, the response of the culvert should be as shown in Fig 7.1. Active earth pressure is mobilised over the top region of the culvert and the crown is displaced downwards, this forces the culvert sides to push outwards which mobilises passive earth pressure along the culvert sides. The passive earth pressures resist the lateral movement of the culvert and provide the culvert with lateral support. The downward movement of the culvert crown under the mobilised active earth pressures generates the beneficial positive arching mechanism. An effective culvert design therefore, hinges on the mobilisation of active earth pressures above the culvert crown and this itself depends on the ability of the culvert to deform readily. The magnitude of passive earth pressures which can be mobilised along the culvert sides depends primarily on the quality of the backfill and the standard of compaction employed during construction. Ideally a very dense highly compacted fill is required to provide the necessary lateral support. Ideally the culvert should be as flexible as possible in order to utilise effectively the load carrying capabilities of the surrounding backfill (Richards, 1982). The flexible culvert therefore serves only as a liner (Richards, 1982) or reinforcement (Watkins, 1964) to maintain the shape of the passageway and it is the backfill which serves as the main load carrying structure (Watkins, 1964; Richards, 1982).

The flexible culvert soil interaction problem is mainly one of earth pressure. However, other factors such as culvert flexibility and construction quality are also important and cannot be considered separately as these effects interact (Duncan, 1979; Richards, 1982). The construction operations and quality directly affect the soil-culvert behaviour and efficiency to support loads. The construction process generates a stress history within the culvert; therefore if accurate predictions of the behaviour of the culvert-soil system are to be made then the construction process must be simulated in analyses (Duncan, 1979). A brief outline of the accepted correct sequence of construction operations is presented below (Richards, 1982).

7.2.1 Construction sequence

Typically the culvert is fabricated in the field by bolting together curved sections of corrugated steel or aluminium sheet. The backfill is placed in thin layers and compacted, ideally to 90-100% relative compaction. As backfilling progresses the flexible culvert deforms upwards at the crown due to lateral earth pressures (active) mobilised within the fill pushing the culvert sides inwards, Fig 7.4(a) (backfill should be placed simultaneously on both sides of the culvert). If the depth of cover above the culvert crown is large, placement and compaction of fill above the culvert pushes the crown of the culvert back down which in turn forces the culvert sides outwards rendering the culvert in an active earth pressure condition as shown in Fig 7.4(b). Until there is sufficient weight of backfill above the culvert crown to push it downwards the culvert will remain in a passive earth pressure condition. For positive arching to be mobilised an active earth pressure condition must be developed. This can only exist if the culvert crown moves downwards. The upward movement of the culvert crown serves to 'pre-stress' this top region of the culvert, which at low fill depths enables the culvert to safely sustain the weight of construction equipment. For flexible culverts with shallow cover, a cover depth to culvert span ratio of $H/S < 0.25$, this action also serves to provide the culvert with extra flexural stiffness and movement resistance to prevent the culvert collapsing during the action of live loads (Duncan, 1979).

Because of the rigours and uncertainty of the construction procedure culverts typically have a larger flexural and axial stiffness than would usually be required to promote an effective design. For shallow culverts the depth of the backfill, H , and imposed live loads may not be of sufficient magnitude to push the crown of a stiff culvert down and hence unable to mobilise a condition of active pressure. If this condition arises a state of passive pressure will remain and the culvert will carry the weight of the backfill above the crown and possibly any imposed loads. Additionally, if the culvert is axially stiffer than the surrounding soil then the condition of negative arching may occur. Current construction techniques are designed to promote positive arching. Such techniques include decreasing the axial stiffness of the culvert wall by providing slip joints and/or promoting tangential slippage at the interface by lubricating the culvert with grease and placing a plastic sheet over the culvert prior to backfilling. If successful these techniques will generate the required earth pressure condition, Fig 7.1(a).

7.3 Review of flexible culvert design methods

The design of flexible culverts is typically divided into two categories depending on the ratio between the height of cover, H , above the culvert crown and the culvert span, S (Duncan, 1979). If the cover depth to culvert span ratio is less than 0.25 then the culvert design is classed as shallow. Alternatively, if the cover depth to culvert span ratio, H/S , is greater than 0.25 the culvert design is classed as deep.

For deep cover conditions ($H/S > 0.25$) culverts need only be designed for thrust (ring compression forces) and no consideration need be given to bending moments except during backfilling (Peck and Peck, 1948; Duncan, 1979; Richards 1982). Under deep cover conditions a good quality, well compacted backfill will restrain the deformation of the culvert from buckling under imposed loads (Peck and Peck, 1948; Duncan, 1979).

Culverts under shallow cover ($H/S < 0.25$) need to be designed for thrust but must also have sufficient flexural stiffness and moment capacity to prevent excessive deformation and collapse of the culvert. Unlike culverts under deep cover conditions, shallow cover culverts cannot entirely resist imposed live loads through ring compression. As for deep cover conditions separate consideration of buckling in the design need not be considered provided the backfill is of good quality and well compacted. Additionally culvert plate sections are typically much larger than required to allow for durability and loss of capacity due to possible corrosion of the structure. This extra capacity of the structure provides an extra factor of safety against buckling (Richards, 1982). A detailed description of buckling is therefore not presented here.

In this section a description of methods used to analyse and design flexible culverts is presented. Classical methods, closed-form analytical solutions and finite element solutions are considered. Additionally, the different constitutive soil models which have been used to describe the backfill material for soil-culvert systems using finite element analysis are briefly discussed at the end of this section.

7.3.1 Classical concepts

In the previous section it was seen that the magnitude and distribution of earth pressure around the soil-culvert interface are primarily dependent on the deflection of the culvert. Early researchers (Marston and Anderson, 1913; Spangler, 1941) of the flexible culvert problem linked this deformation induced earth pressure behaviour to

Rankine's earth pressure theory. Using this approach the behaviour of flexible culverts was characterised by the active and passive earth pressure conditions, Fig 7.4. The difference in the conditions is determined by the direction of the soil stress produced by culvert-soil deformation.

7.3.1.1.Spangler deflection theory

Spangler (1941) assumed an active soil pressure condition, Fig 7.5, for predicting the deflection of buried flexible culverts, relation (7.2) (IOWA deflection formula)

$$\Delta X = \frac{D_1 K Q_c R^3}{E_c I_c + 0.061 E'_R R^3} \quad (7.2)$$

where ΔX is the horizontal deflection of the culvert, D_1 is the deflection lag factor (see below); K is the bedding constant whose value depends on the bedding angle (see below); Q_c is the vertical load per unit length of the culvert; R is the mean radius of the culvert; ; E'_R is the modulus of soil reaction of the backfill material; E_c is Young's modulus of elasticity of the culvert and I_c is the moment of inertia of the culvert wall.

This concept recognised that passive soil pressure is mobilised at the culvert sides by horizontal expansion of the culvert, which Spangler assumed accounted for the ability of flexible culverts to carry more load than in the unrestrained condition. Spangler proposed that the mobilised passive pressure could be estimated from the computed lateral deflection using relation (7.3).

$$P_h = \frac{E'_R \Delta X}{D} \quad (7.3)$$

where P_h is the maximum pressure at the extreme horizontal diameter; E'_R is the modulus of soil reaction of the backfill material and D is the nominal diameter of the pipe.

The Spangler Iowa formulae has been subject to a wide range of criticism because of the empirical and simplified nature of the deflection expression (7.2). The parameters in this expression which are thought to be most difficult to quantify are discussed below.

The deflection lag factor, D_1 , accounts for soil relaxation with time and is equal to 1.0 immediately after construction and then increases with time. Spangler recommended a maximum value of 2 and an average value of 1.25 for well compacted soil. However, field studies suggest that D_1 may be as high as 6 (Howard, 1977; McVay and Papadopoulos, 1986).

The bedding factor, K , incorporates the effect of the distribution of soil reactions at the base of the culvert. It is assumed that the bedding applies a distributed reaction across the base of the culvert. In this case K is assumed equal to 0.083. For the case of no bedding material, K is assumed equal to 0.11 and the reaction of the invert is a point load.

The modulus of soil reaction, E'_R , is equal to the modulus of passive resistance (unit pressure developed as the side of a culvert moves outward a unit distance against the side fill) multiplied by the radius R of the culvert. Numerical studies have found that E'_R is the most difficult parameter to quantify (Leonards and Roy, 1976; Wu, 1977). The United States Bureau of Reclamation conducted laboratory and field studies to determine values of E'_R for a range of soils in various states of compaction, the main results are shown in Table 7.1 (Howard, 1977; Spangler and Hardy, 1982).

Hartley and Duncan, (1987) suggest that E'_R is approximately equal to the constrained modulus of elasticity, M_f , of the soil. The constrained modulus, M_f , is given by relation (7.4).

$$M_f = \frac{E_f(1 - \nu_f)}{(1 - 2\nu_f)(1 + \nu_f)} \quad (7.4)$$

where E_f and ν_f are the backfill Young's modulus and backfill Poisson's ratio.

Nielson (1967) and Stankowski and Nielson (1969) have found that the modulus of soil reaction, E'_R is of the range between $E'_R = M_f$ and $E'_R = 1.5M_f$. Live load deflections calculated using the IOWA deflection formula agree more accurately with field observations using $E'_R = M_f$ (Hartley and Duncan, 1987).

For design purposes the deflection is required to be less than 5% of the undeformed culvert diameter. Many culverts have been known to deflect up to 20% from their original diameter without structural failure or loss of serviceability (Durazo, 1974). A review of the performance of flexible large diameter pipes (Jeyapalan and Boldon, 1986) determined that the 5% deflection design limit will typically provide a safe and serviceable design for the following reasons.

1. If the pipe is poorly restrained laterally, (poor compaction or weak

embedment material used) failure may occur due to excessive deformation. This will cause the culvert crown to invert, become concave upwards.

2. Flexible pipes/culverts typically continue to deflect with time due to creep. Limiting deflection to 5% helps to prevent excessive deformation over the design life of the culvert.

3. The 5% deflection limit will maintain a substantial factor of safety against structural collapse.

7.3.1.2. Ring compression theory

Unlike Spangler, (1941) White and Layer (1960) assume the failure of buried culverts is dependent on ring compression rather than deflection. White and Layer's theory assumes a uniform normal pressure, p , across a horizontal section above the culvert equal to the density, γ , of the soil times its height, H , Fig 7.6 This pressure produces a compressive force, N , in the culvert equal to the circumferential pressure times the culvert radius, R , relation (7.5).

$$N = pR \quad (7.5)$$

where N is the compressive force or thrust per metre length of culvert at the springline.

This theory assumes that the ring deflection of the structure is negligible and failure occurs by crushing of the culvert walls. No bending moment is assumed to act in the culvert.

The theory was originally developed from extensive field observations of circular culverts. For pipe arch or elliptical culverts the thrust should be calculated using the radius of the top arc, Fig 7.7.

Design of flexible culverts is still very often based on this simple approach. The compressive stress, σ_c , in the culvert wall is compared to the yield stress of the culvert material. The compressive stress is given by relation (7.6).

$$\sigma_c = \frac{N}{A_c} \quad (7.6)$$

where A_c is the cross sectional area of the culvert per metre length. A factor of safety of two is generally applied to yield stress of the culvert material.

This design approach assumes neutral arching at the crown but leads to cross sectional areas of culverts, A_c , larger than required resulting in a culvert that is flexurally and axially stiffer than is necessary (Richards, 1982). Consequently, some negative arching may occur with higher thrusts at the crown than predicted. Finite element solutions (Duncan, 1979) and field measurements for deep and shallow buried culverts (Duncan, 1979; Selig et al., 1979 and Beal, 1982) indicate that some negative arching does develop and pressures and thrusts can be as much as 30-40% greater than those calculated from ring compression theory. Inclusion of a factor of safety of two in design typically compensates for this.

Current design practice for flexible culverts generally uses a combination of the ring compression theory (White and Layer, 1960) and the IOWA deflection formula, (Spangler, 1941). Most design codes require a culvert thick enough to resist the ring compression force (Duane et al., 1986). Using thicknesses established by ring compression theory, deflection is required to be less than 5% (Jeyapalan and Boldon, 1986) as calculated using the IOWA deflection formula.

7.3.2. Closed-form analytical solutions

Many analytical solutions, based on elasticity theory, have been developed to for the culvert problem. In this section only one closed form solution has been considered, namely that of Burns and Richard (1964), which is the most widely used and acclaimed. This methods assumes that the culvert-soil system is an elastic cylinder embedded in an elastic infinite space and subject to a uniform vertical pressure at an infinite vertical distance above the culvert. The soil is assumed to be an isotropic and homogenous continuum and the culvert a thin elastic shell, Fig 7.8. Two interface conditions are considered, bonded and unbonded conditions. The plane strain solutions for the two conditions are presented below. Symbols used are defined at the end of this section.

1. Bonded interface

In the bonded case, shear stress exists at the interface between the culvert and backfill. For the bonded case the interaction pressures are

$$P = P_o (B(1 - a_o^+) - C(1 - 3a_2^+ - 4b_2^+) \cos 2\theta) \quad (7.7)$$

The culvert displacements are given by relation (7.8).

$$U = \frac{1}{2} \left(\frac{P_o r}{M_s} \right) \left(\left(1 + \left(\frac{B}{C} \right) a_o^+ \right) - \left(1 + a_2^+ + \left(\frac{2}{B} \right) b_2^+ \right) \cos 2\theta \right) \quad (7.8)$$

The culvert thrust and moment are given by relations (7.9) and (7.10)

$$N_o = P_o r (B(1 - a_o^+) + C(1 + a_2^+) \cos 2\theta) \quad (7.9)$$

$$M_o = P_o r^2 \left(\left(\frac{CUF}{6VF} \right) (1 - a_o^+) + \frac{1}{2} C(1 - a_2^+ - 2b_2^+) \cos 2\theta \right) \quad (7.10)$$

2. Unbonded case

In the unbonded case, shear stress is zero at the culvert soil interface. For the unbonded case, the interaction pressures are

$$P = P_o (B(1 - \bar{a}_o) - C(1 - 3\bar{a}_2 - 4\bar{b}_2) \cos 2\theta) \quad (7.11)$$

The culvert displacements are given by relation (7.12)

$$U = \frac{1}{2} \left(\frac{P_o r}{M_s} \right) \left(\left(1 + \left(\frac{B}{C} \right) \bar{a}_o \right) - \left(1 + \bar{a}_2 + \left(\frac{2}{B} \right) \bar{b}_2 \right) \cos 2\theta \right) \quad (7.13)$$

The culvert thrust and moment are

$$N_o = P_o r \left(B(1 - \bar{a}_o) + \frac{1}{3} C(1 + 3\bar{a}_2 - 4\bar{b}_2) \cos 2\theta \right) \quad (7.14)$$

and

$$M_o = P_o r^2 \left(\left(\frac{CUF}{6VF} \right) (1 - \bar{a}_0) + \frac{1}{3} C (1 + 3\bar{a}_2 - 4\bar{b}_2) \cos 2\theta \right) \quad (7.15)$$

The uniform pressure, P_o , is computed as the equivalent overburden pressure of the fill above the culvert. Parameter θ is the rotation angle with reference to the culvert springline.

The soil parameters are as follows,

M_f =constrained modulus of elasticity, given by relation (7.4)

E_f =Young's modulus of elasticity

ν_f =Poisson's ratio

K =earth pressure coefficient given by relation (7.16)

$$K = \frac{\nu_f}{1 - \nu_f} \quad (7.16)$$

The culvert parameters are as follows,

R =mean radius

D =diameter of the culvert

E_c =Young's modulus of the culvert material

A_c =cross sectional area of the culvert wall per unit longitudinal length

I_c =moment of inertia of the culvert wall per unit longitudinal length

The load parameters are as follows,

$$B = \frac{1}{2}(1 + K), \text{ uniform pressure component}$$

$$C = \frac{1}{2}(1 - K), \text{ variational pressure component}$$

$$UF = \frac{M_f DB}{E_c A_c}, \text{ relative extensional flexibility}$$

$$VF = \frac{2M_f D^3 C}{48E_c I_c}, \text{ relative bending flexibility}$$

The dimensionless constants for the bonded culvert are,

$$a_0^+ = \frac{UF - 1}{UF + \left(\frac{B}{C}\right)}$$

$$a_2^+ = \frac{C(1 - UF)VF - \left(\frac{C}{B}\right)UF + 2B}{\left((1 + B)VF + C\left(VF + \left(\frac{1}{B}\right)\right)UF + 2(1 + C)\right)}$$

$$b_2^+ = \frac{(B + CUF)VF - 2B}{\left((1 + B)VF + C\left(VF + \left(\frac{1}{B}\right)\right)UF + 2(1 + C)\right)}$$

The dimensionless constants for the unbonded culvert are as follows,

$$\bar{a}_0 = \frac{UF - 1}{UF + \left(\frac{B}{C}\right)}$$

$$\bar{a}_2 = \frac{(UF - 1)}{\left(UF + \left(\frac{B}{C}\right)\right)}$$

$$\bar{b}_2 = \frac{(2VF - 1)}{\left((2VF - 1) + \left(\frac{3}{B}\right)\right)}$$

The simplifying assumptions of this model, that the soil is linear, isotropic elastic, homogenous infinite in extent, have made this method impractical as a design tool (Duane et al., 1986) particularly for shallow buried culverts as elements of the backfill above the crown have been found to yield on application of compaction and/or live loads (Katona et al., 1976). However, this method is of interest because it provides a limiting case check for either empirical models or analytical models based on numerical methods of solution (Duane et al., 1986).

7.3.3. Duncan's design method

The third design method considered here is a semi-empirical analytical method proposed by Duncan (1979) which can be used to design long-span culverts for both deep and shallow cover conditions. This method is based on finite element studies (Duncan, 1979) and field and laboratory studies (Duncan, 1979; Allgood, 1964; Luscher, 1964 and Bartkus and Vey, 1956) and assumes that negative arching will occur over the entire width of the culvert crown irrespective of the cover depth.

Maximum thrust, N , in the culvert is given by relation (7.17)

$$N = K_{p1}\gamma S^2 + K_{p2}\gamma HS + K_{p3}LL \quad (7.17)$$

where N is the thrust in the culvert; K_{p1} is a coefficient for axial force due to backfill up to the culvert crown; K_{p2} is a coefficient for axial force due to cover over the crown; K_{p3} is a coefficient for axial force due to the live load; γ_f is the soil density; S is the culvert span; H is the height of cover above the culvert crown and LL is the live load.

Axial force coefficients are shown in Fig 7.9.

Maximum bending moment, M_B in the culvert due to backfill loads, is given by relation, (7.18).

$$M_B = R_B (K_{M1}\gamma S^3 - K_{M2}\gamma S^2 H) \quad (7.18)$$

where R_B is a moment reduction factor for backfill moments that varies with the culvert rise, R , to span, S , ratio, R/S , Fig 7.10; K_{M1} is a moment coefficient that varies with the flexibility number, N_f of the culvert, Fig 7.11(a); K_{M2} is a moment coefficient which varies with the culvert flexibility number, Fig 7.11(b).

The flexibility number, N_f , given by relation (7.19), describes the stiffness of the backfill relative to the culvert in the form of a dimensionless ratio.

$$N_f = \frac{E_s S^3}{E_c I_c} \quad (7.19)$$

where E_s is the secant modulus of the backfill soil; S is the culvert span; E_c is the Young's modulus of the culvert material and I_c is the moment of inertia of the culvert pre metre length.

Field studies for conditions of shallow cover indicate that the effects of the backfill and applied live loads above the culvert combine to produce a moment at the quarter point that is larger than the moment at any other point on the culvert. The magnitude of the change in quarter point moment, ΔM_L , due to imposed live loads can be calculated from relation, (7.20).

$$\Delta M_{LL} = R_L K_{M3} SLL \quad (7.20)$$

where R_L is a reduction factor for the live load moment, which varies with cover depth and flexibility number, Fig 7.13.; K_{M3} is a live load moment coefficient which varies with flexibility number, Fig 7.12.

For the purposes of design, Duncan (1979) recommends that shallow flexible culverts should have a factor of safety of 1.65 or more against the development of a plastic hinge, considering both the thrust and the bending moment (backfill and live load moments combined). The factor of safety F_p , can be calculated using relation (7.21).

$$F_p = 0.5 \frac{N_p}{N} \left(\sqrt{\left(\left(\frac{M}{M_p} \right)^2 \left(\frac{N_p}{N} \right)^2 + 4 \right)} - \left(\left(\frac{M}{M_p} \right) \left(\frac{N_p}{N} \right) \right) \right) \quad (7.21)$$

where N_p is the fully plastic thrust with no moment; M is the combined backfill and live load bending moment and M_p is the fully plastic bending moment, with no axial force.

The factor of safety, F_p equal to 1.65 is thought to be suitable for design (Richards, 1982) because the margin of safety in terms of additional load required to cause collapse will be greater than 1.65. Duncan outlines three reasons why this should be .

1. For an arch structure the formation of a single plastic hinge will not result in the formation of a failure mechanism. Four plastic hinges are required to initiate failure in an arch structure.
2. Even after sufficient hinges have developed in the structure to form a failure mechanism, the soil will continue to restrain the deformations of the structure.
3. Both aluminium and steel harden when deformed plastically. Therefore, use of N_p and M_p based on minimum values of yield stress, provides a conservative estimate of the ultimate resistance of the culvert metal.

On the basis of experimental and theoretical evidence, Duncan (1979) does not consider buckling to be a problem provided the backfill is of good quality and is well compacted.

The design procedure proposed by Duncan (1979) was used to estimate the forces in an 8.7m span, 3.6m rise (spring line to crown) pipe arch culvert (Beal, 1982). The height of cover above the culvert crown was 0.6m, giving a H/S ratio of approximately 0.07 (< 0.25 , shallow cover conditions). Calculated values of bending moment using Duncan's method underestimated the observed bending moments by nearly 100%. Conversely, calculated values of thrust overestimated the observed thrusts by as much as 100%. Observed values of thrust at the spring line were some 30-40% less than those estimated using ring compression theory (White and Layer, 1960), which assumes a condition of neutral arching. From this Beal, (1982), concluded that a positive arching mechanism had developed rather than the negative arching mechanism as assumed by Duncan's design procedure.

7.3.4 Constitutive soil models used to describe soil-culvert systems

7.3.4.1 Introduction

In this section the different constitutive soil models which are more commonly used to describe the backfill material surrounding a culvert are discussed. Full mathematical descriptions of the models included in this discussion are not presented here but can be found in texts such as and Chen and Mizuno (1990).

7.3.4.2 Constitutive soil models

In practice flexible culverts are typically designed to the serviceability limit state (strictly elastic behaviour) and as a result linear or non-linear elastic soil models are most used. Plasticity is very seldom included in the design process.

Linear elasticity is the simplest soil model used to describe soil behaviour and is still widely used in situations where the culvert design is straightforward and an insight into the possible culvert deflection behaviour may be required. The main advantage of this model is that it is completely defined by two elastic parameters, Young's modulus E , Poisson's ratio ν . The elastic shear modulus G can be obtained from E or ν . Simple tests can be performed to estimate E , ν or G , however in practice these parameters are

typically selected from a data base compiled from material properties of similar backfills.

In numerical modelling of soil-culvert systems constant elastic stiffness within the linear elastic soil model poses a particular problem as experimental observations have found that the stress-strain behaviour of a soil is dependent largely on the strain/stress level within the soil mass (Seed and Duncan, 1986). During construction compaction of the backfill may significantly increase the stress within the backfill and consequently will induce a gradient of elastic stiffness within the soil mass. In view of this there is really no basis for selection of single values of the elastic parameters, E , ν or G to describe an entire range of stress conditions induced within the backfill. Studies performed by Nayak et al. (1977) and Duane et al. (1986) using the linear elastic soil model have found that culvert displacements and normal soil pressures on the culvert underestimate those observed from experimental and full-scale field studies. Many researchers (Duncan, 1979; McVay and Selig, 1982; Leonards et al., 1985 and Seed and Duncan, 1986) describe predictions using the linear soil model as erratic and do not recommend its use in flexible culvert design. Despite the shortcomings of this soil model it is still widely used, particularly in Britain. However, designs based on this model typically incorporate high factors of safety of 3 or more. Additionally studies by Rude (1982) found that numerical predictions using this model are very sensitive to the value of Poisson's ratio selected and as will be shown later, any inaccuracy associated with the constant elastic stiffness can be compensated for by performing predictions with low values of Poisson's ratio.

A more detailed analysis of the backfill elastic behaviour can be performed using a non-linear elastic soil model. Such soil models are significantly more complex than the linear elastic soil models and require a greater number of soil material parameters in order to describe the response. These soil models are not often used in the Great Britain as typically required culvert designs are rarely complex enough to warrant their use. In the United States of America where soil-culvert systems are routinely complex these types of models are frequently used. The non-linear Duncan-Chang soil model (Duncan and Chang, 1970) is perhaps the most frequently used and accepted soil model. The reason for the wide acceptance of this model is primarily the good predictions of soil-culvert behaviour for situations where the loading is monotonically increasing in the absence of plastic deformations in the soil (Leonards et al., 1985 and Seed and Duncan, 1986).

The Duncan-Chang soil model is a hypoelasticity model within which the stress and strain increments are linearly related through variable tangent moduli, which are functions of stress and strain. As a result this model is stress (strain)-path dependent. It is this aspect of this model which makes it particularly advantageous when using it

to describe the soil-culvert response as variations of the backfill stiffness following application of compaction pressures can be suitably modelled.

The Duncan-Chang model is described in terms of the tangent Young's modulus, E_t and the tangent Poisson's ratio, ν_t . The tangent Young's modulus is given by relation (7.22)

$$E_t = \left(1 - \frac{R_f(\sigma_1 - \sigma_3)(1 - \sin \phi)}{2c \cos \phi + 2\sigma_3 \sin \phi} \right)^2 K P_a \left(\frac{\sigma_3}{P_a} \right)^n \quad (7.22)$$

The tangent Poisson's ratio is expressed by relation (7.23)

$$\nu_t = \frac{G - F \log \left(\frac{\sigma_3}{P_a} \right)}{\left(1 - \frac{D(\sigma_1 - \sigma_3)}{\left(1 - \frac{R_f(\sigma_1 - \sigma_3)(1 - \sin \phi)}{2c \cos \phi + 2\sigma_3 \sin \phi} \right) K P_a \left(\frac{\sigma_3}{P_a} \right)^n} \right)^2} \quad (7.32)$$

where σ_1 and σ_3 are the major and minor principal stresses; P_a is the atmospheric pressure; ϕ and c are the Mohr-Coulomb shear strength parameters; K , n , R_f , G , F and D are model parameters to be determined experimentally. The wide use of this model has enabled an extensive data base for these material parameters to be compiled for a wide range of backfill types and loading conditions.

Experimental studies have shown that, particularly for culverts under shallow cover conditions, local shear failure can develop in the backfill surrounding the culvert (Dessouki and Monforton, 1986; Duane et al., 1986 and Mohamedzein, 1989). Consequently to suitably model this behaviour models incorporating plasticity will need to be used.

The simplest models incorporating plasticity are the traditional linear elastic, perfectly plastic soil models with the onset of failure described by the Von Mises, Mohr-Coulomb or Drucker-Prager failure surfaces. Use of these models in soil-culvert interaction has largely been avoided because these models cannot simulate the non-linear behaviour of the backfill during compaction. As a result researchers of the flexible culvert problem, particularly in the United States of America, have focused on the development of soil models which incorporate more of the important factors

affecting the soil-culvert system. Despite this, these models have helped the understanding of the propagation of failure within the backfill surrounding the culvert (Valliappan et al., 1977 and Dessouki and Monforton, 1986).

The most detailed study incorporating plasticity into soil-culvert interaction has been performed by Mohamedzein (1989) using a non-linear elastic-perfectly plastic soil model incorporating an elasto-plastic cap hardening surface, Fig 7.14. The onset of failure was described using the Drucker-Prager failure surface. In Mohamedzein's study non-linear elasticity was described using the Duncan-Chang soil model. An associative flow rule was assumed throughout. This soil model is complex and is not often used in practice except in special circumstances, i.e. multiple culvert installations, where a more rigorous and detailed design is required. Use of this model requires the selection of thirteen material parameters, eight to describe the non-linear elastic Duncan-Chang soil model, two to describe the Drucker-Prager soil model and three to describe the cap hardening surface. In the absence of published field data for a particular project, detailed soils laboratory testing is required to determine these parameters.

Mohamedzein (1989) has demonstrated the ability of this soil model to provide accurate predictions of soil-culvert behaviour using several case histories, the most noted of which was the Tice Valley culvert, which is an 8m span, elliptical flexible culvert embedded under shallow cover conditions, $H/S=0.15$. This culvert was previously analysed by Duncan (1979) and Duncan and Jeyapalan (1982) using the non-linear Duncan-Chang soil model. Better agreement of the observed behaviour was obtained using the non-linear elastic cap model. This was attributed to the more accurate representation of plastic compression of the backfill (Mohamedzein, 1989). However the difference between the predicted solutions was small.

7.3.4.3 Discussion

Selection of a suitable method of analysis for a particular soil-culvert system depends on the complexity of the system, the sensitivity of the structure in relation to existing structures and perhaps the most important factor, the time available for the design. In most flexible culvert design problems the empirical and semi-empirical methods of analysis described in section 7.2, used in conjunction with a suitable factor of safety, will suffice. However design situations do arise where a more detailed design study is required and finite element analysis is often used to provide the necessary information. The decision to use finite element analysis then requires judgement as to the appropriate level of complexity of analyses and consequently selection of an

appropriate soil model with which to describe the problem. Ideally the selected soil model should be capable of reproducing the essential elements of soil-culvert behaviour, such as the complex non-linear elastic and non-linear elastic, elasto-plastic, cap hardening soil models described latterly in section 7.3.4.2. However as noted previously these models require a greater number of material parameters which will require careful selection from a data base compiled from laboratory testing. The gains associated with the use of the simpler linear elastic, perfectly plastic soil models are self-evident. Despite the shortcomings of the linear elastic assumption, these models require fewer material parameters and are typically less time consuming to use for analysis. Additionally, the sensitivity of analyses to Poisson's ratio and the angle of internal friction and angle of dilation (see chapter 8) may be advantageous as performing analyses with extreme quantities of these parameters may ensure that the most adverse design condition has been considered.

In this study a linear elastic, perfectly plastic soil model with the onset of failure described using the Mohr-Coulomb criterion has been used. Additionally the soil model is assumed to have a non-associated flow rule. Incorporation of a non-associated flow rule is known to significantly improve displacement predictions of granular materials (Graham et al., 1983). This feature is thought to improve estimation of compaction induced displacements and consequently compensates to some degree for the absence of stress-strain path dependency of the soil elastic parameters.

Successful use of the simpler linear elastic, perfectly plastic soil model may provide a half-way house between the very simple and more complex soil models and therefore assist the engineer with the decision of whether or not a more complex method of analysis is required for a particular design problem.

7.4 Finite element modelling

In this section the modelling assumptions required to define the culvert-soil interaction problem are briefly described. This discussion includes the culvert and backfill modelling assumptions as well as the modelling of the construction process and representation of applied live loadings.

7.4.1. Modelling the culvert and backfill

Two dimensional plane strain finite element analyses have been performed to represent a slice of unit thickness through the culvert and backfill. In analyses it is assumed that the slice analysed is representative of any section along the length of the culvert. The culvert was modelled using eight isoparametric linear strain quadrilateral elements, the backfill was modelled using a combination of isoparametric linear strain quadrilateral and linear strain triangular elements. The geometry and loading of the flexible culverts described in this thesis are essentially symmetric, therefore only half of the system was modelled.

The actual culvert cross-sections described in this thesis are not rectangular but rippled because of the corrugated steel sections used to construct the culvert. As already noted the culvert is modelled using smooth rectangular elements. To ensure that the model culvert elements have the same deformation characteristics, i.e. same axial stiffness and flexible rigidity, as the original corrugated culvert sections, an equivalent thickness, T^* , and Young's Modulus, E^* , must be determined for the model culvert. The equivalent culvert thickness is given by relation (7.22)

$$T^* = \sqrt{\frac{12I_c}{t}} \quad (7.22)$$

where I_c is the second moment of area of the culvert per unit length and t is the actual corrugated plate thickness.

The equivalent Young's modulus, E^* is given by relation (7.23),

$$E^* = \frac{Et}{T^*} \quad (7.23)$$

where E is the value of Young's modulus for steel, assumed equal to $205 \times 10^6 \text{ kPa}$.

7.4.2 Modelling of soil-culvert interface

The buried culvert problem involves the interaction between two different materials each of very different material properties, gravel and metal. In numerical analysis of soil-structure interaction such as the culvert problem, an interface element can be introduced into the finite element mesh between the culvert and backfill to bridge the boundary between the two materials and therefore allow the actual relative movement to occur between the soil and culvert. Three types of movement have been identified

to occur at the culvert-soil interface: debonding, rebonding and slip (Leonards et al, 1982). Debonding is the separation of the soil and culvert normal to the interface element typically arising due to tension developing in the soil above the culvert. Rebonding is the opposite movement and typically arises due to the development of compressive contact stresses at the interface. Slip relates to tangential movement between the culvert and the soil and is characterised by concentrations of shear displacements once certain shear stress levels are reached.

In this study, as with most problems of soil-structure interaction (Griffiths, 1988) it is assumed that the stresses at the soil-culvert interface are compressive, therefore no separation of the culvert and soil can occur. The only movement between the culvert and soil considered was interface slip. The interface behaviour was modelled by refining the finite element mesh in the vicinity of the soil-culvert interface and introducing a thin quadrilateral element, of the same shape and dimensions as the culvert elements, to model the interfacial fill region, Fig 7.15. These elements can be prescribed reduced frictional shear strength parameters to model some degree of interface slip. This simple approach is believed to be adequate for most culvert design problems (Griffiths, 1988; Davies et al., 1993). Studies show that interfacial shear stresses are substantially lower than those required to mobilise the full frictional strength of the backfill material, therefore it can be assumed that for design unless the interface is perfectly smooth, as with some aluminium culverts, interface slip is not significant (Duncan, 1979; Davies et al., 1993).

In these studies the soil-culvert interface was modelled as rough and the interface elements were assumed to have the same properties as the surrounding backfill. Consequently, failure or slip will occur not at the interface itself but at the nearest stress point in the weaker of the two materials sandwiching the interface, (Griffiths, 1988). The method used to model the interface behaviour in this study is simple and assumes the culvert and soil are continuously in contact. For more complex problems of soil-structure interaction, where debonding and rebonding will occur readily under working loads and therefore cannot be neglected, more specialised interface elements and advanced modelling techniques will need to be used. Examples of such complex interaction problems are described by Goodman et al. (1988); Ghaboussi et al. (1973); Mohamedzein (1989).

7.4.3 Modelling the construction sequence

An outline of the modelled construction sequence is presented below.

- 1 Place and compact bedding layer elements.
- 2 Construct culvert
- 3 Place and compact backfill around culvert in thin layers of approximately 0.5-0.7m thick

CRISP is particularly situated to modelling the required sequence of construction as it is straightforward to add elements to the mesh as they are required.

To simulate compaction of the backfill, a pressure loading was applied to the surface of each layer. The pressure loading (compacting pressure) was removed by applying an equal and opposite pressure loading to the surface layer in the next increment block.

The proper magnitude of the compaction pressure used in each of the case studies presented is not known. An appropriate magnitude of compaction pressure for each case was primarily determined by trial and error. However, some indication of the required magnitude of compaction pressure was obtained from work reported by previous researchers of the flexible culvert problem. In each case selection of the final magnitudes of compaction pressure shown below was arbitrary.

Chang et al., (1980)	35kPa (solutions for 0, 21 and 35kPa)
Selig and Musser, (1985)	105kPa
Sharp et al., (1985)	70kPa

7.4.4 Representation of live loads

Imposed live loads, applied above the culvert crown on the top of the backfill, represent traffic loading. To perform two-dimensional analyses of live load effects it is necessary to represent the actual three-dimensional traffic load by an equivalent loading that is continuous along the length of the structure. Values of equivalent continuous loading were determined by calculating the intensity of a continuous live load, $Q(kN/m)$, that produces the same peak vertical stress, σ_v , on the crown of the culvert as does the loading trailer using Boussinesq's elasticity solution. Boussinesq's

solution assumes that the soil mass is semi-infinite, homogenous, isotropic and has a linear stress-strain relationship. This approach to estimating the equivalent loading is similar to that used by Katona et al. (1976). The loading trailer is of dimensions shown in Fig 7.16, with a single axle of weight equivalent to the revised HB load defined in BS 5400 Part 2: 1978. Referring to Fig 7.17, the vertical stress, σ_v , at point X on the culvert crown due to the weight of the loaded trailer is given by relation (7.24).

$$\sigma_v = 2 \left(\frac{3P_{1/4}}{2\pi H^2} \left(\frac{1}{1 + \left(\frac{r_2}{H} \right)^2} \right)^{5/2} \right) + 2 \left(\frac{3P_{2/3}}{2\pi H^2} \left(\frac{1}{1 + \left(\frac{r_1}{H} \right)^2} \right)^{5/2} \right) \quad (7.24)$$

where P is the wheel point load; H is the cover depth and r is the perpendicular distance from point X to the applied wheel load.

Again using Boussinesq's elasticity solution the equivalent line load Q per unit length on the surface is given by relation (7.25)

$$Q = \frac{H\pi\sigma_v}{2} \quad (7.25)$$

The load acts on the surface of the backfill.

7.4.5 Determination of stresses around culvert

As noted earlier flexible culvert design requires a description of the thrust (ring compression forces) and bending moments induced within the culvert, in addition to an estimate of the radial, σ_{rr} and tangential shear, $\tau_{r\theta}$, stresses which develop around the soil-culvert interface. These quantities are not readily obtained from general purpose finite element programs such as CRISP. To obtain these variables directly from CRISP an extra subroutine was added (Davies et al., 1993). A brief outline of the main assumptions and operations performed to determine the required quantities is presented below.

The radial stress, σ_{rr} , and tangential shear stress, $\tau_{r\theta}$, induced around the soil-culvert interface were obtained by sampling the Cartesian stresses, σ_x , σ_y , and τ_{xy} , at the nine Gauss integration points within the eight interface elements located around the culvert. The stresses σ_{rr} , and $\tau_{r\theta}$ are polar stresses and were converted from the Cartesian

stresses using the usual transformation as a function of rotation angle θ . Where θ is the angle between the normal to the culvert element (NN) and the horizontal (xx), Fig 7.18. The stresses σ_{rr} and $\tau_{r\theta}$ are calculated using relations (7.26) and (7.27).

$$\sigma_{rr} = \sigma_x \cos^2 \theta + \sigma_y \sin^2 \theta + \tau_{xy} \sin 2\theta \quad (7.26)$$

$$\tau_{r\theta} = \frac{1}{2}(\sigma_y - \sigma_x) \sin 2\theta + \tau_{xy} \cos 2\theta \quad (7.27)$$

The average radial and tangential shear stress, $\bar{\sigma}_{rr}$ and $\bar{\tau}_{r\theta}$, induced at the soil-culvert interface were calculated as a weighted average of the radial and tangential shear stress at each of the nine Gauss integration points.

The sign convention for radial stress, σ_{rr} , is that compressive stress is positive; for shear stresses, $\tau_{r\theta}$, downdrag (shear stress trying to pull the culvert downwards) is positive.

Thrust, N , and bending moment, M , induced within the culvert were determined from considerations of simple stress and beam bending theory. Consider first the stress distribution within the culvert, Fig 7.8. As can be seen from Fig 7.8 the thrust and bending moment are functions of the circumferential hoop stress, $\sigma_{\theta\theta}$, induced within the culvert wall. The circumferential hoop stress, $\sigma_{\theta\theta}$, is a polar stress and was converted from the Cartesian stresses, σ_x , σ_y , and τ_{xy} , using relation (7.28).

$$\sigma_{\theta\theta} = \sigma_y \cos^2 \theta + \sigma_x \sin^2 \theta - \tau_{xy} \sin 2\theta \quad (7.28)$$

The derivation of transformation relations (7.26), (7.27) and (7.28) is not presented here, but can be found from classical elasticity texts (Timoshenko and Goodier, 1970 and Saada, 1974).

The Cartesian stresses, σ_x , σ_y , and τ_{xy} , were sampled from the three Gauss integration points located across the centre section of the culvert element, Fig 7.19.

The average thrust, \bar{N} , within a culvert element was estimated using relation (7.29).

$$\bar{N} = \bar{\sigma}_{\theta\theta} A_c \quad (7.29)$$

where $\bar{\sigma}_{\theta\theta}$ is the average circumferential hoop stress induced within the culvert element calculated as a weighted average of the circumferential hoop stress, $\sigma_{\theta\theta}$, estimated at each of the three Gauss integration points. Parameter A_c is the cross sectional area per metre length of the culvert wall.

The bending moment is estimated using the average circumferential hoop stress, $\sigma_{\theta\theta}$, obtained at the two extreme centre line Gauss integration points, relation (7.30), Fig 7.20,

$$M = (\sigma_{\theta\theta_1} - \sigma_{\theta\theta_2}) \frac{I_c}{2y} \quad (7.30)$$

where I_c is the second moment of area per metre length of culvert wall and y is the depth to the neutral axis, assumed equal to half the distance between the two extreme integration points, Fig 7.20.

The sign convention assumed for bending moments is hogging moments (tension on the outside of the culvert element) are positive and sagging moments (tension on the inside of the culvert element) are negative (Burns and Richard, 1964).

Measurements of load thrusts (ring compression forces) and bending moments observed for each of the culvert case histories are presented in terms of strains. These quantities, as required for design, were converted to their usual force units.

Ring compression strains were converted to thrusts using simple stress-strain theory given by relation (7.31).

$$N = E_c \varepsilon_T A_c \quad (7.31)$$

where N is the thrust; E_c is Young's modulus of the culvert material, assumed equal to $205 \times 10^3 \text{ MPa}$ for steel; ε_T is the ring compression strain and A_c is the cross sectional area of the culvert wall per metre length.

Bending moments are calculated from bending strains (where bending strain is the strain that arises when only the effects of bending moments are considered) using simple beam bending theory, relation (7.32)

$$M = \frac{E_c \varepsilon_b I_c}{y} \quad (7.32)$$

where M is the bending moment; E_c is Young's modulus of the culvert wall material assumed equal to $205 \times 10^3 \text{ MPa}$; ε_b is the bending strain; I_c is the second moment of area of the culvert wall material per metre length and y is the depth to the neutral axis, which assuming simple beam bending theory is equal to half the distance between the extreme Gauss integration points.

Table 7.1. Values of E'R for 18 flexible steel pipe culverts (Spangler and Hardy, 1982)

Item	Location	Pipe Diam.		Soil Type ^a	Fill Height		Passive Resist., e		Value of $\frac{E'}{R} = e_r$	
		mm	(in.)		m	(ft)	MPa/m	(lb/in. ² /in.)	MPa	(lb/in. ²)
1 ^b	Ames, Iowa	1067	42	Loam top soil (U)	4.6	15	3.80	14	2.03	294
2 ^b	Ames, Iowa	1067	42	Well-graded gravel (U)	4.9	16	8.69	32	4.63	672
3 ^b	Ames, Iowa	914	36	Sandy clay loam (T)	4.6	15	7.60	28	3.46	502
4 ^b	Ames, Iowa	914	36	Sandy clay loam (U)	4.6	15	3.53	13	1.61	234
5 ^b	Ames, Iowa	1067	42	Sandy clay loam (T)	4.6	15	6.79	25	3.62	525
6 ^b	Ames, Iowa	1067	42	Sandy clay loam (U)	4.6	15	4.07	15	2.17	315
7 ^b	Ames, Iowa	1219	48	Sandy clay loam (T)	4.6	15	7.87	29	4.80	696
8 ^b	Ames, Iowa	1219	48	Sandy clay loam (U)	4.6	15	3.80	14	2.32	336
9 ^b	Ames, Iowa	1524	60	Sandy clay loam (T)	4.6	15	7.06	26	5.38	780
10 ^b	Ames, Iowa	1524	60	Sandy clay loam (U)	4.6	15	3.26	12	2.48	360
11 ^c	Chapel Hill, N.C.	762	30	Sand	3.7	12	6.79	25	2.59	375
12 ^c	Chapel Hill, N.C.	800	31.5	Sand	3.7	12	15.20	56	6.08	882
13 ^c	Chapel Hill, N.C.	762	30	Sand	3.7	12	21.72	80	8.27	1200
14 ^c	Chapel Hill, N.C.	508	20	Sand	3.7	12	9.50	35	2.41	350
15 ^c	Chapel Hill, N.C.	533	21	Sand	3.7	12	22.26	82	5.94	861
16 ^d	Culman Co., Ala.	2134	84	Crushed sandstone (C)	41.8	137	51.58	190	55.02	7980
17 ^d	McDowell Co., N.C.	1676	66	Clayey sandy silt (C)	51.8	170	10.86	40	9.10	1320
18 ^d	Wolf Creek, Mont. (reconstructed)	5486	216	Graded crushed gravel (C)	25.3	83	15.74	58	43.44	6300

^a U—untamped; T—tamped, C—compacted.
^b Side pressure and pipe deflections measured.
^c Side pressures estimated, pipe deflections measured.
^d Load and pipe deflections measured.

1 (a) ACTIVE SOIL PRESSURE CONDITION FIG 7.1 (b) PASSIVE SOIL PRESSURE CONDITION
(LINGER, 1972)

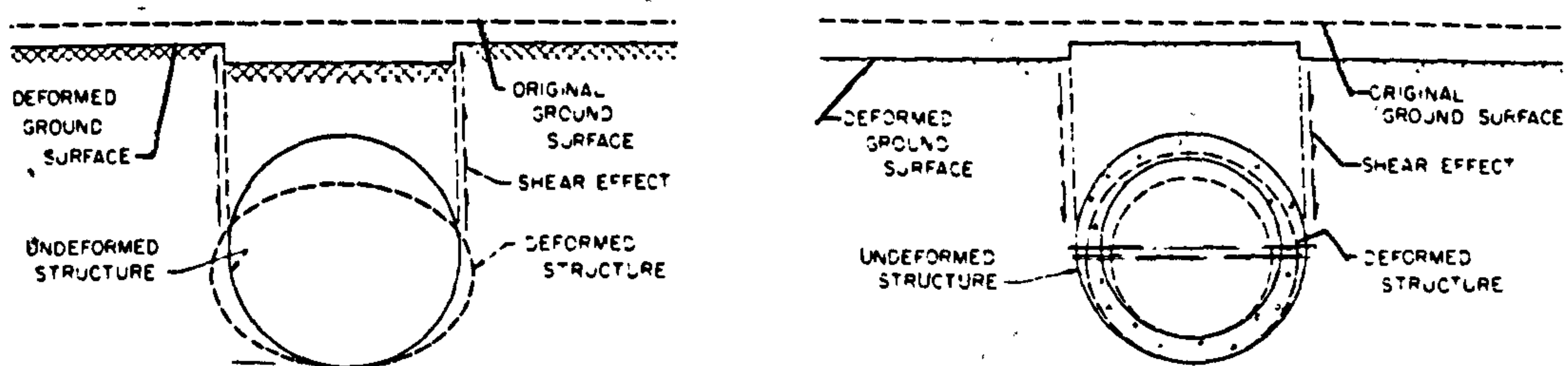


FIG 7.2 FORMATION OF ARCHING STRESSES (LINGER, 1972)

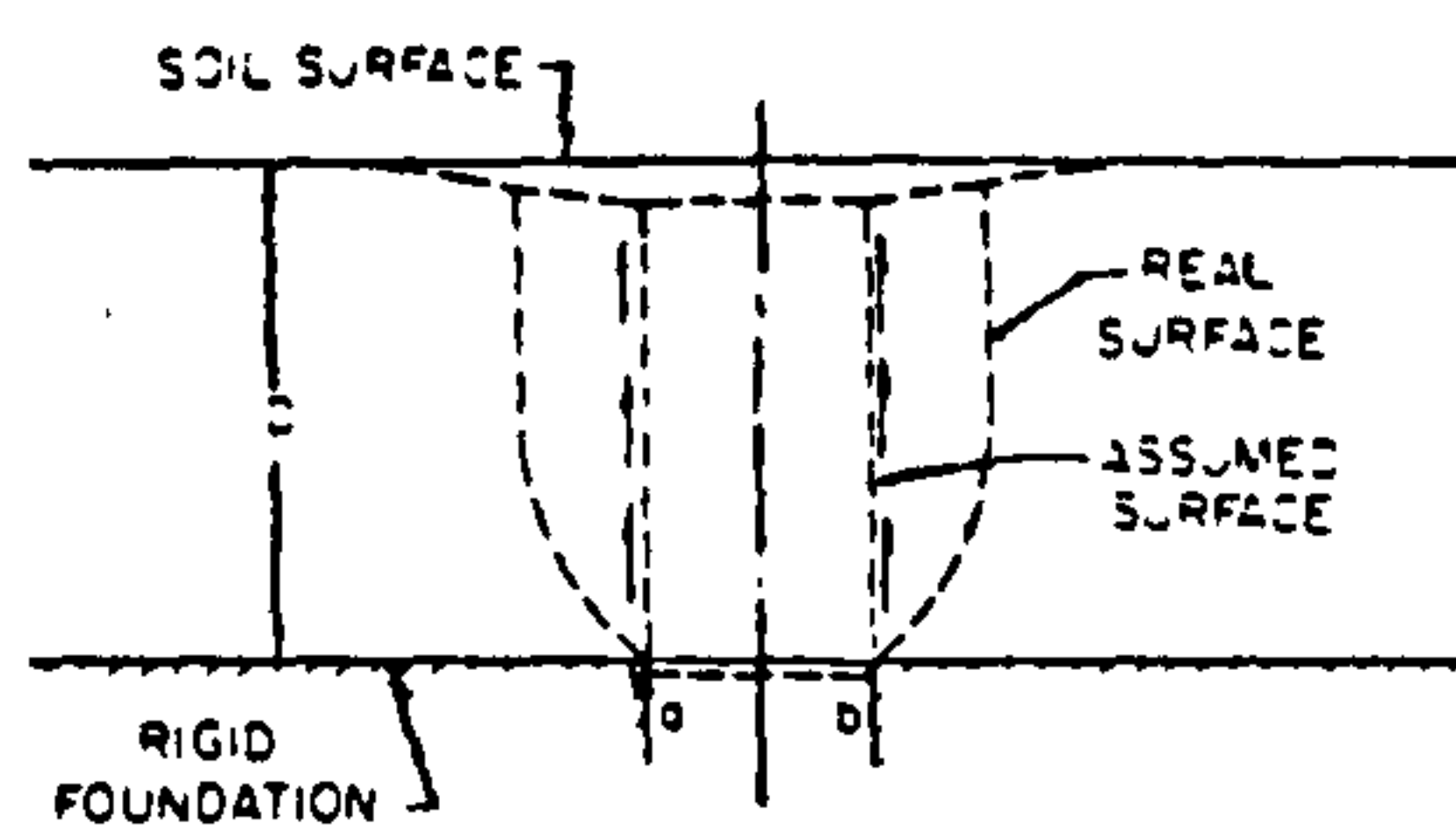
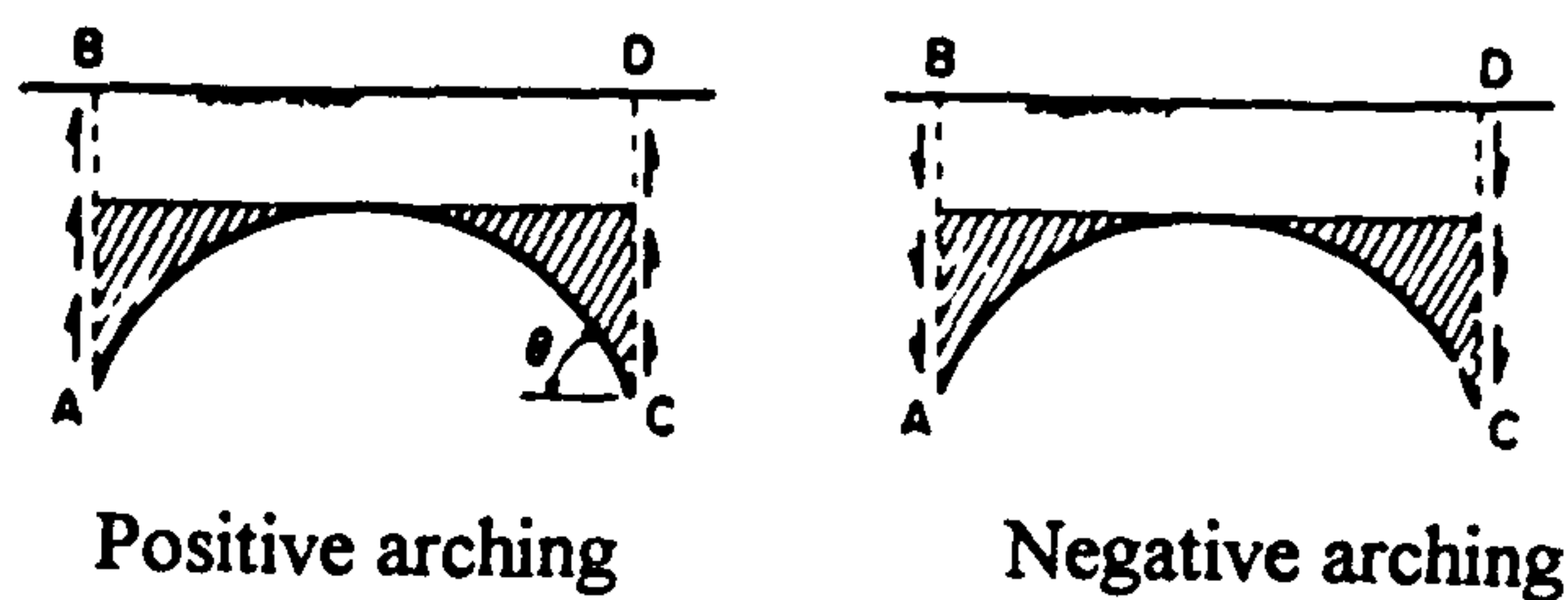


FIG 7.3 SHOWING POSITIVE AND NEGATIVE ARCHING
(DUNCAN, 1979).



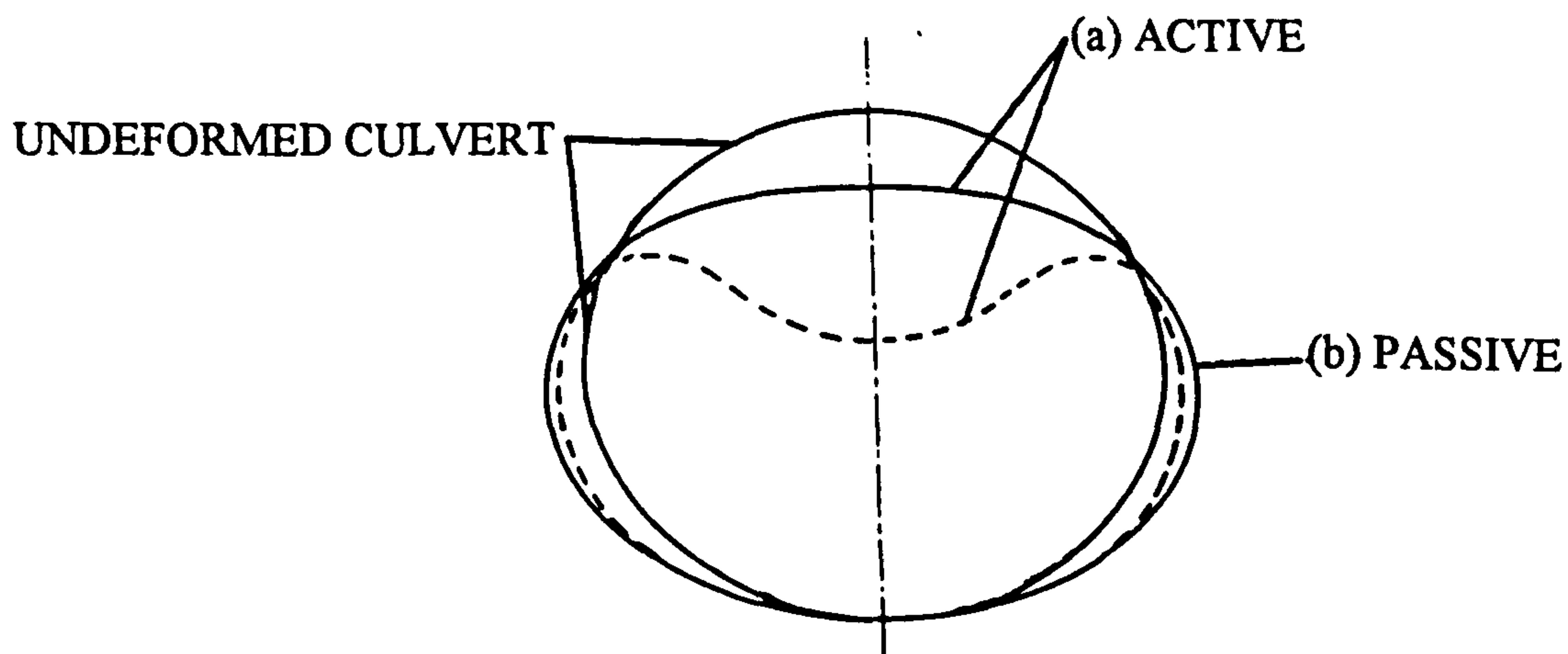


FIG 7.4 (a) & (b) SHOWING STAGES OF DEFLECTION OF A FLEXIBLE CULVERT

FIG 7.5 LOADING ASSUMPTIONS FOR THE IOWA FORMULA (SPANGLER, 1941)

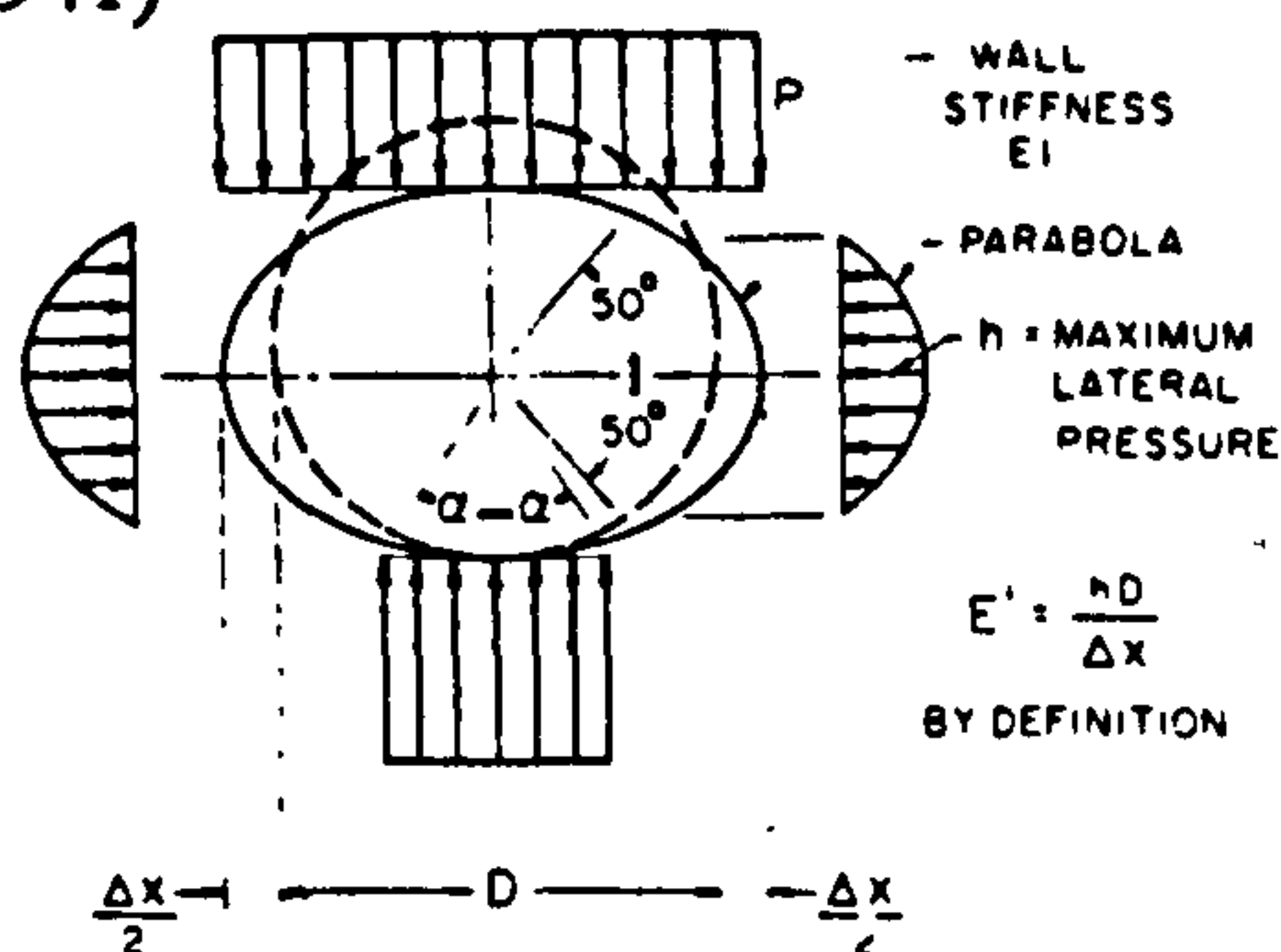


FIG 7.6 RING COMPRESSION THEORY (WHITE AND LAYER, 1960)

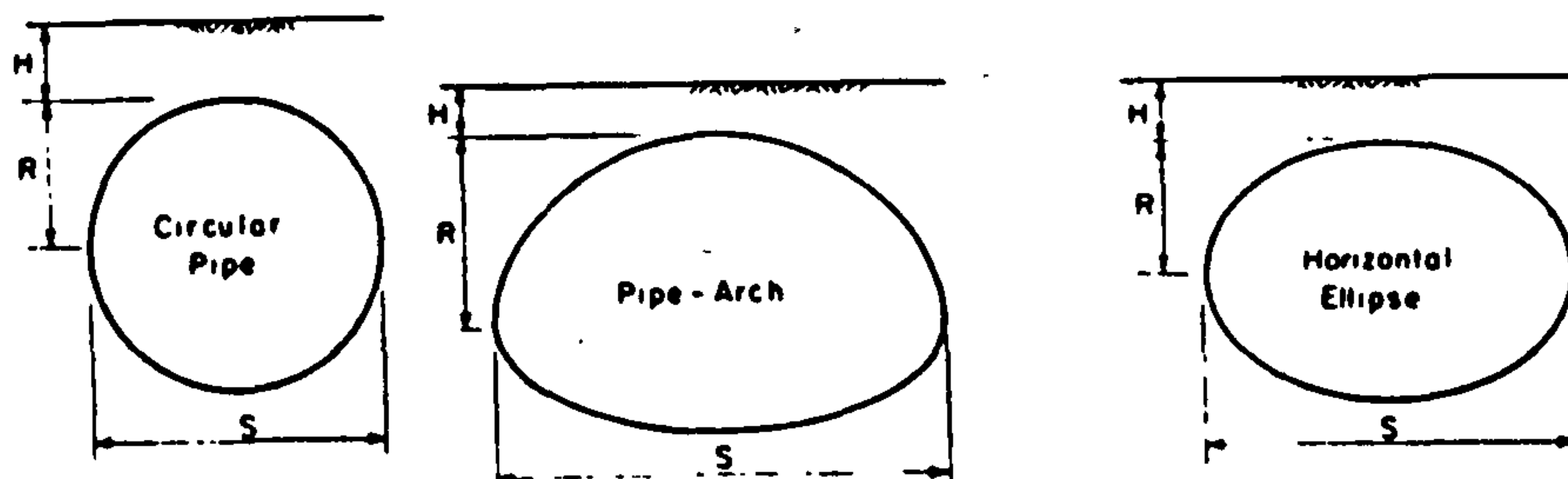
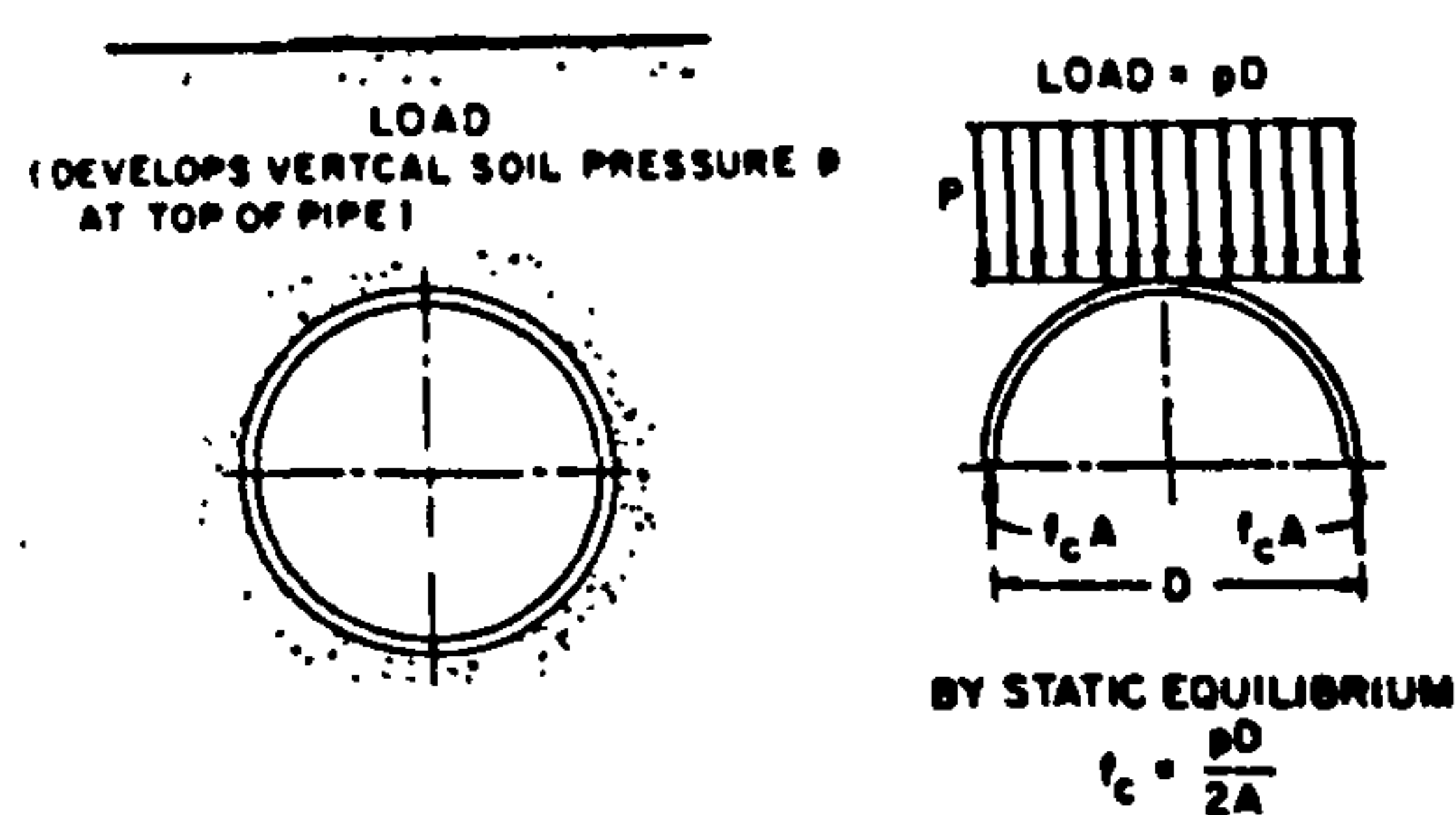


FIG 7.7 TYPES OF LONG SPAN METAL CULVERT STRUCTURES (DUNCAN, 1979)

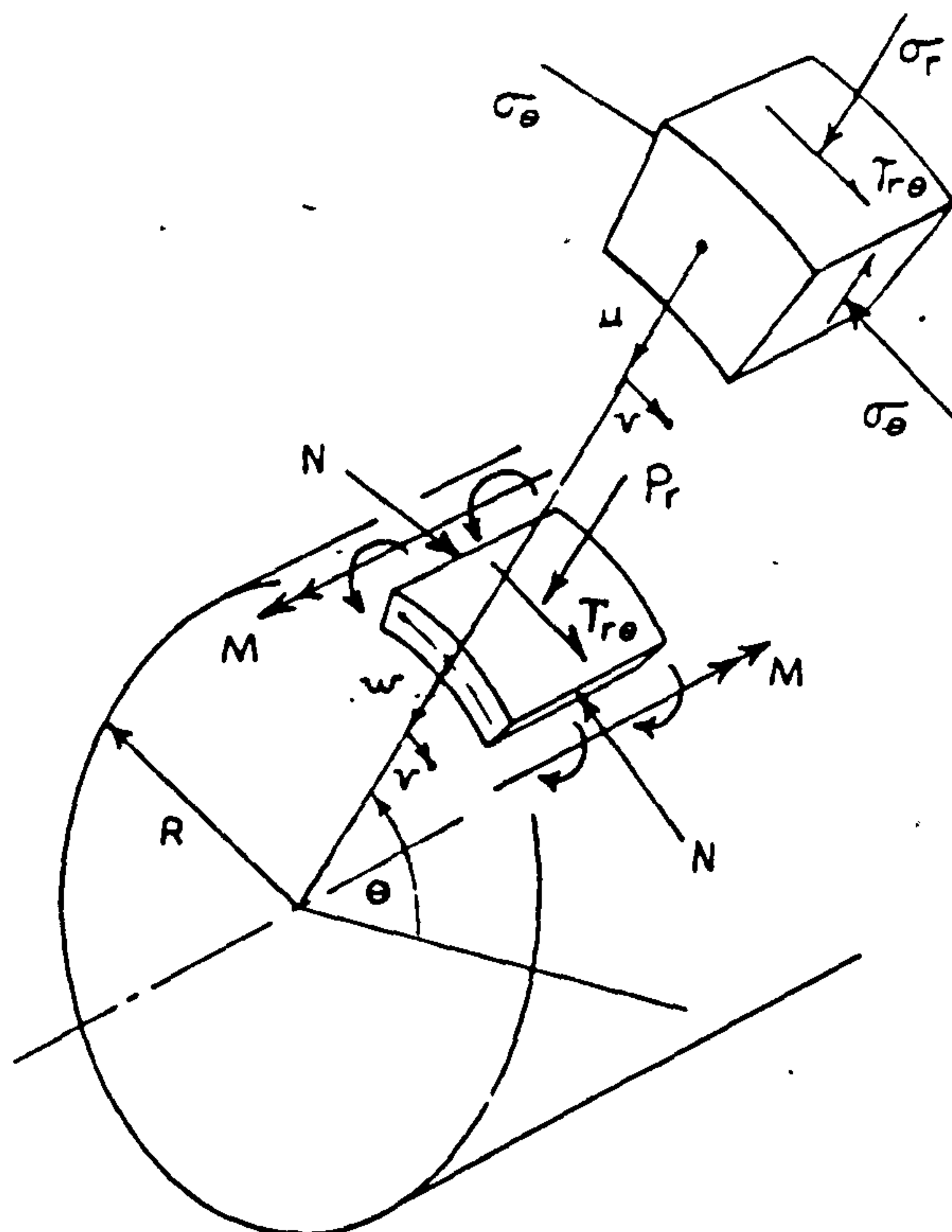


FIG 7.8 NOTATION FOR BURNS AND RICHARD'S SOLUTION (BURNS AND RICHARD, 1964).

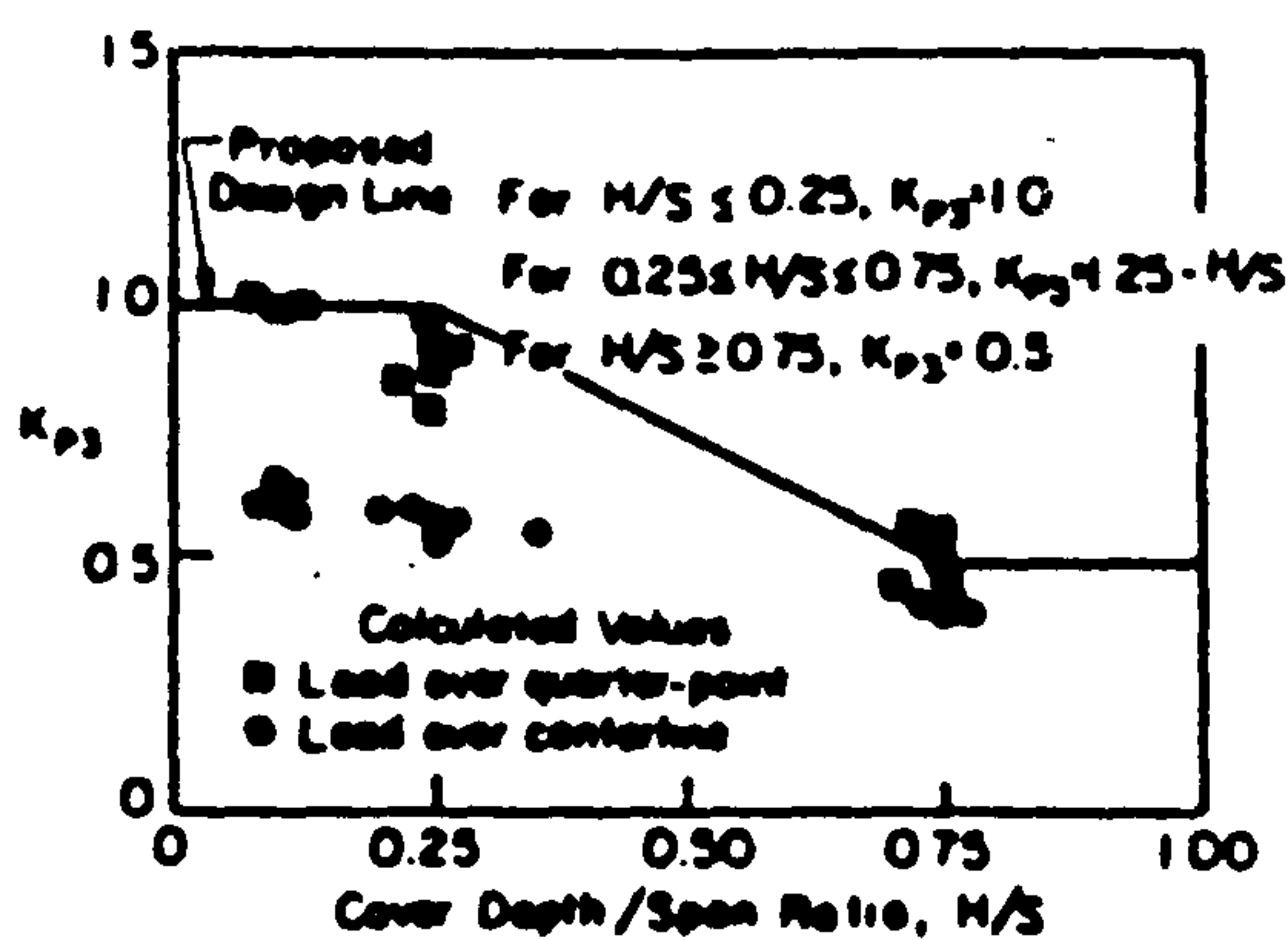
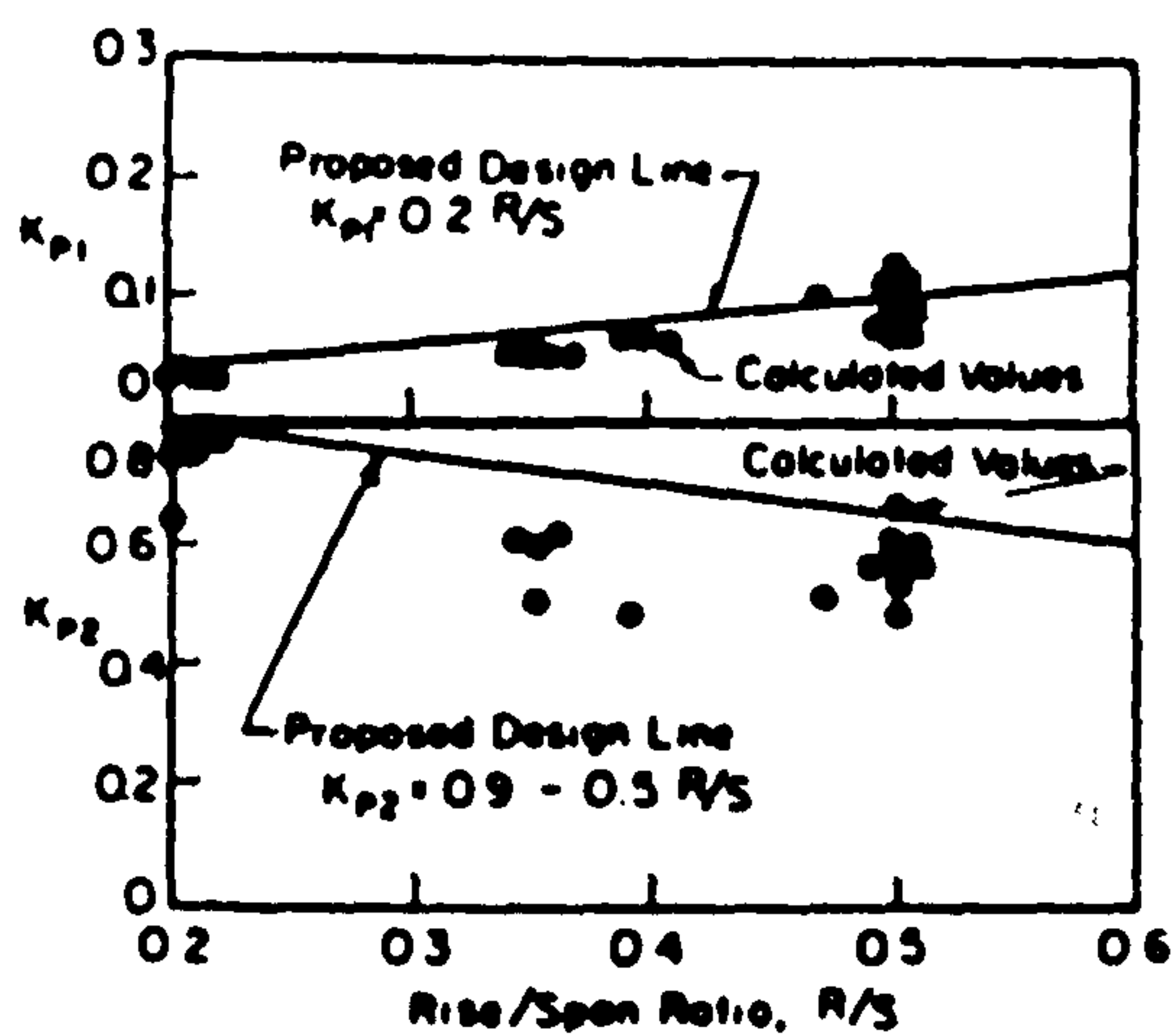


FIG 7.9 AXIAL FORCE COEFFICIENTS (DUNCAN, 1979).

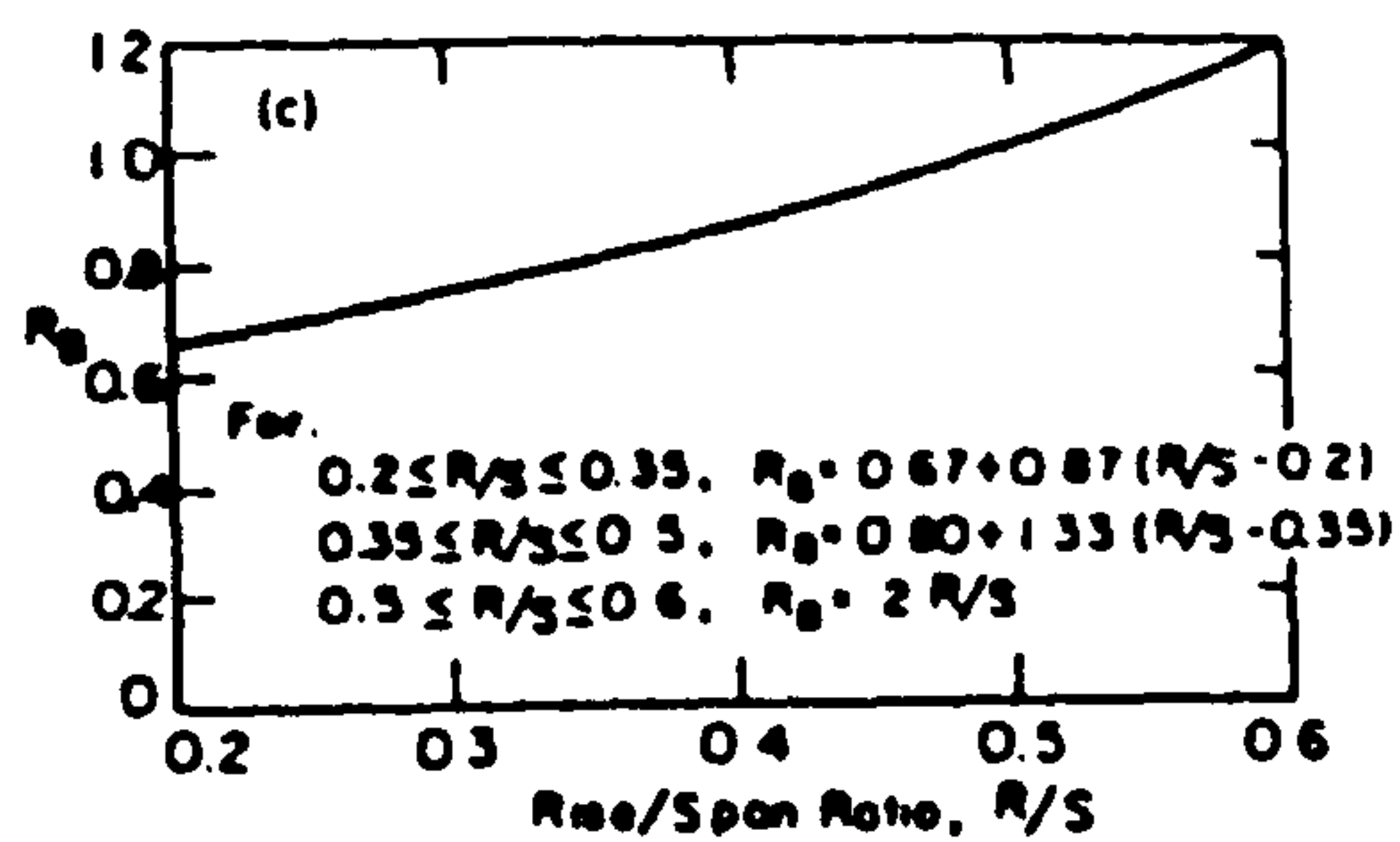


FIG 7.10 R_B AGAINST R/S ; COEFFICIENT FOR BACKFILL MOMENTS (DUNCAN, 1979).

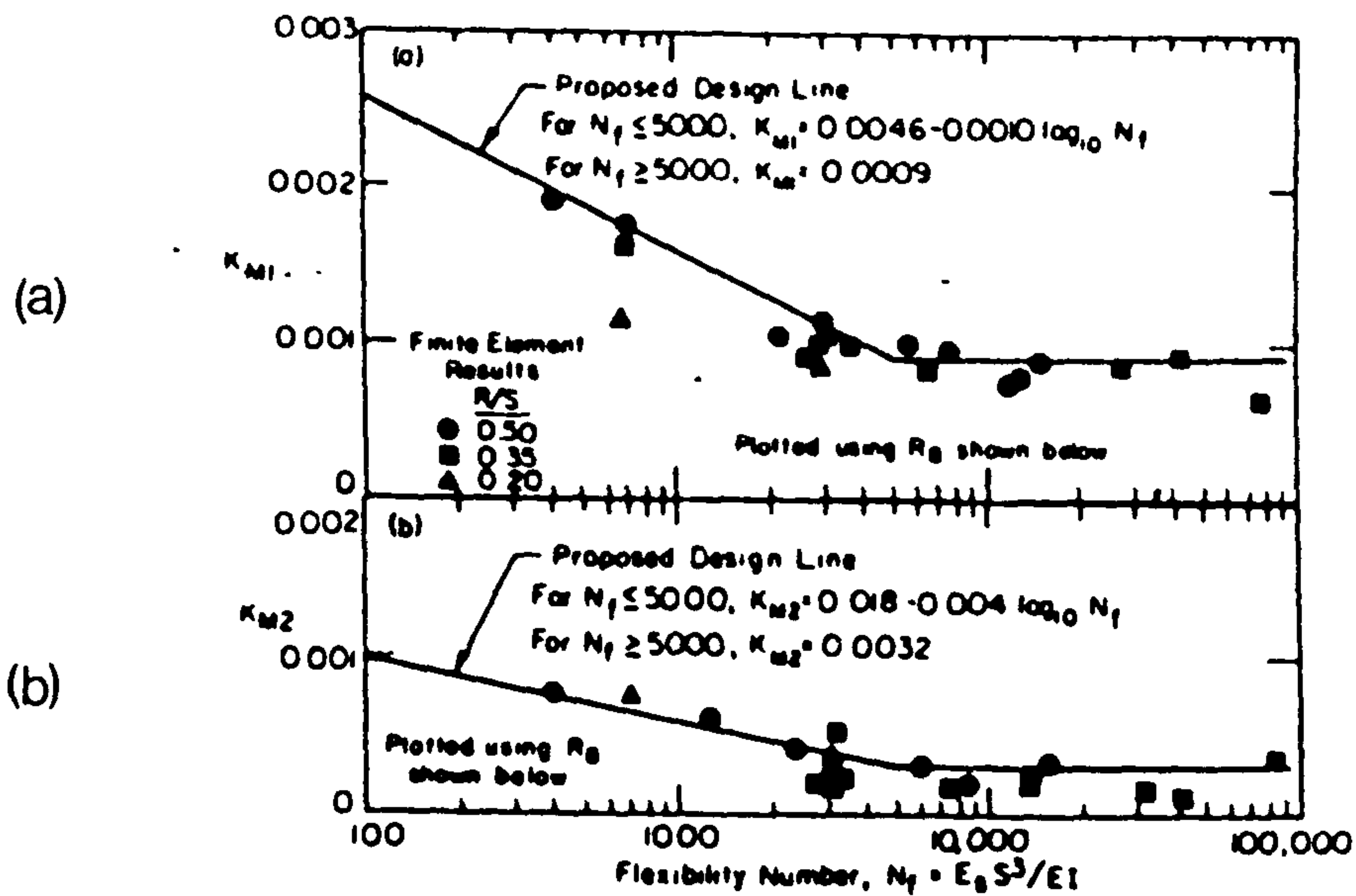


FIG 7.11(a) K_{M1} ; COEFFICIENT FOR BACKFILL MOMENTS (DUNCAN, 1979).

FIG 7.11(b) K_{M2} ; COEFFICIENT FOR BACKFILL MOMENTS (DUNCAN, 1979).

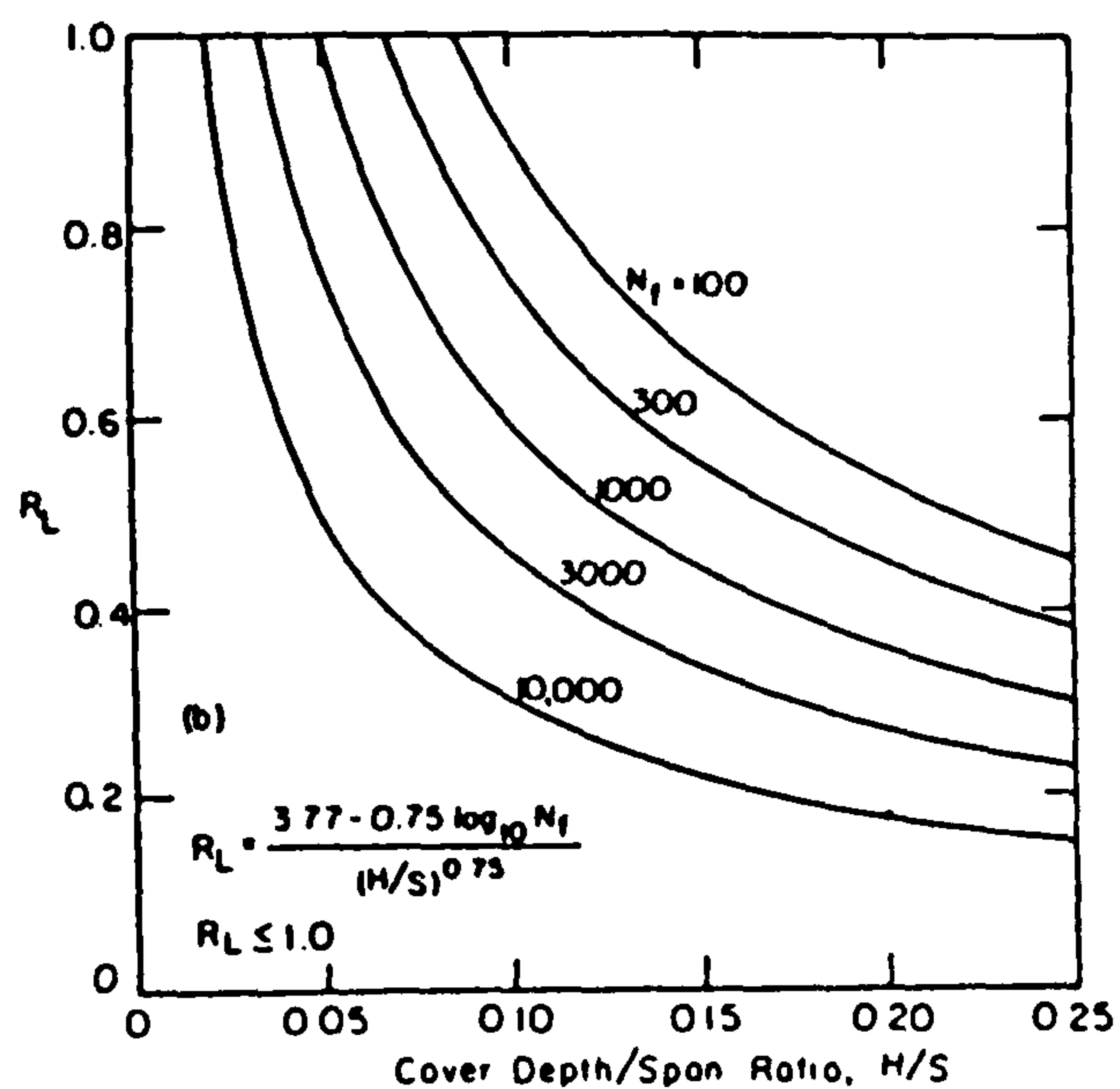


FIG 7.12 R_L AGAINST H/S ; COEFFICIENT FOR LIVE LOAD MOMENTS (DUNCAN, 1979).

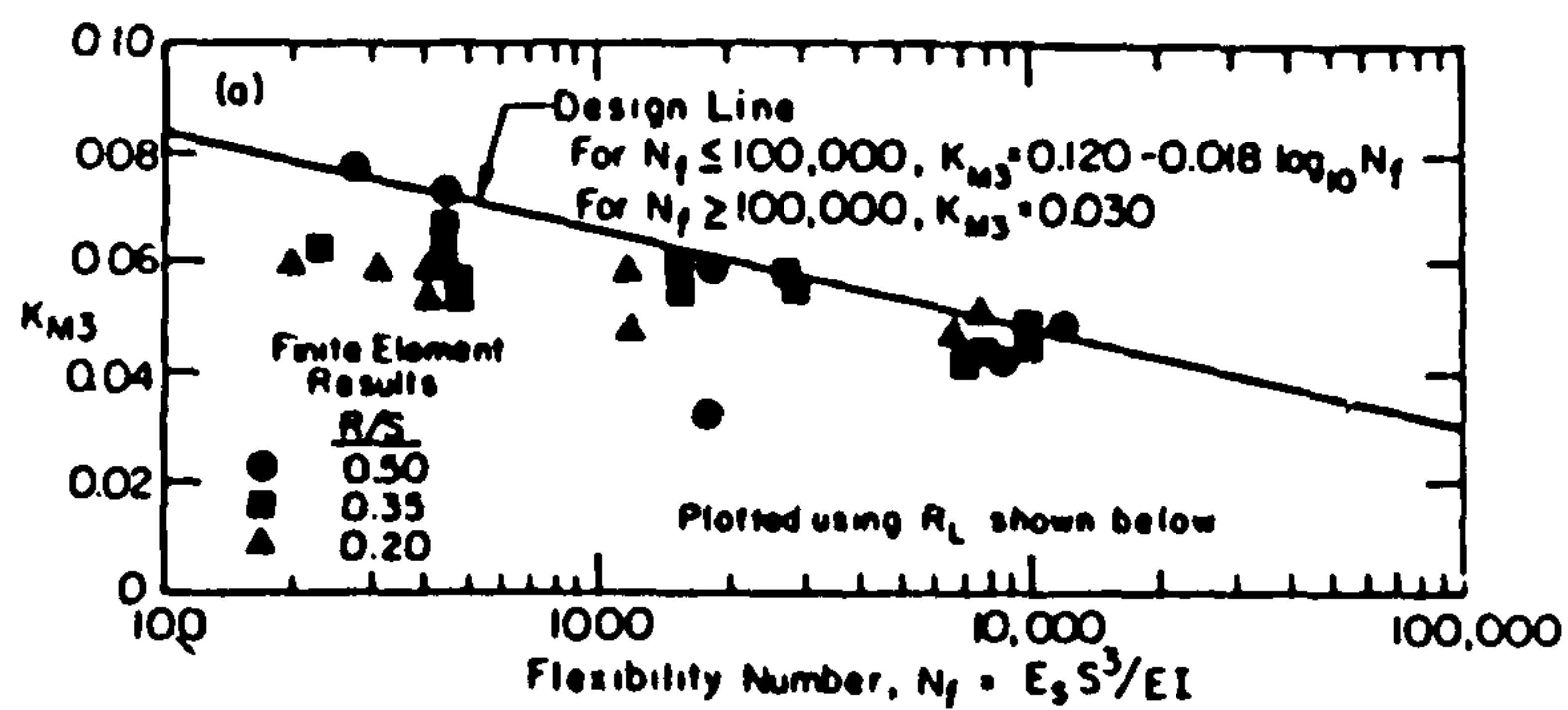


FIG 7.13 K_{M3} ; COEFFICIENT FOR LIVE LOAD MOMENTS (DUNCAN, 1979).

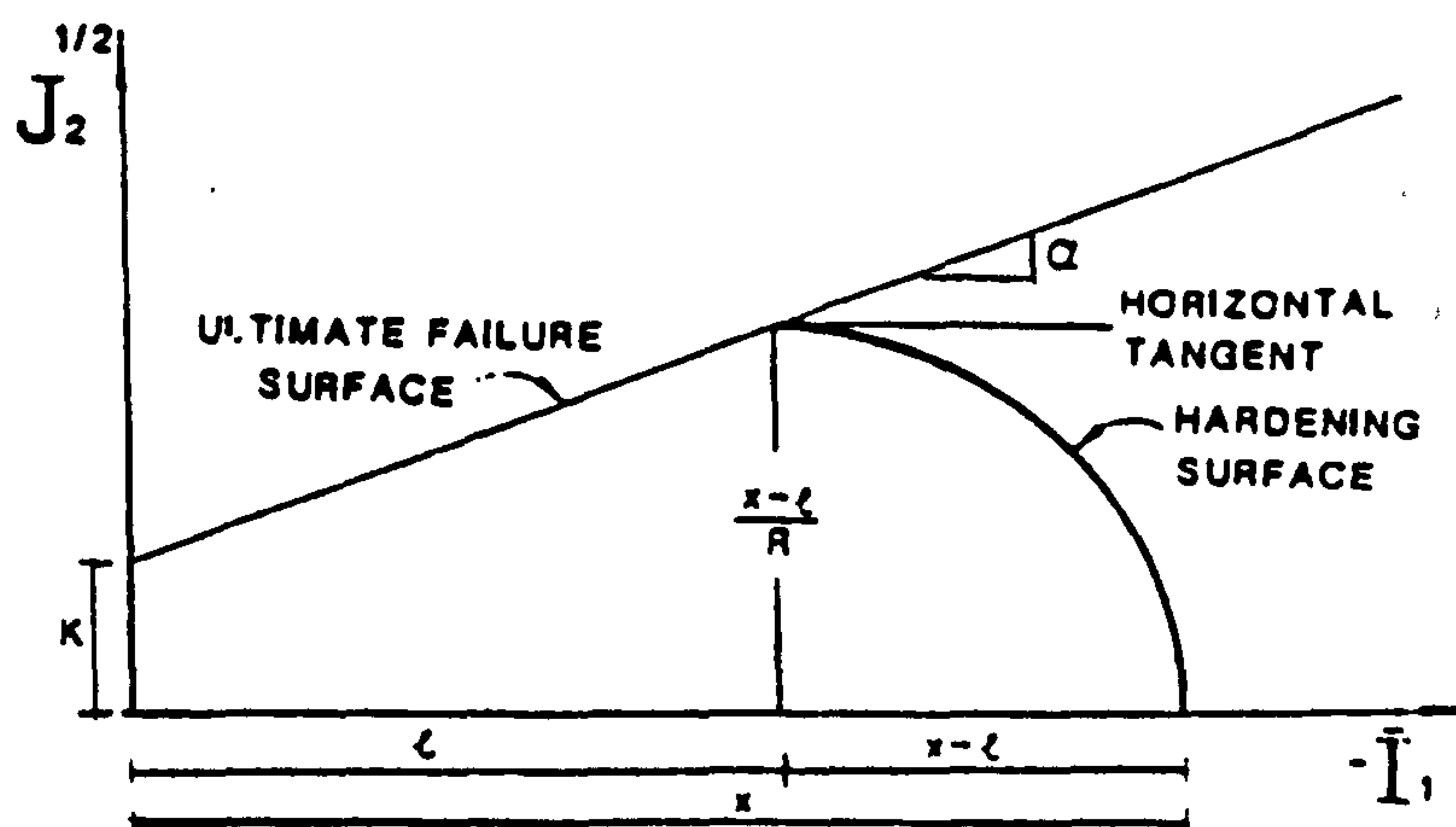


Fig 7.14 NON-LINEAR ELASTIC, PERFECTLY PLASTIC SOIL MODEL WITH CAP HARDENING SURFACE (MOHAMEDZEIN, 1989)

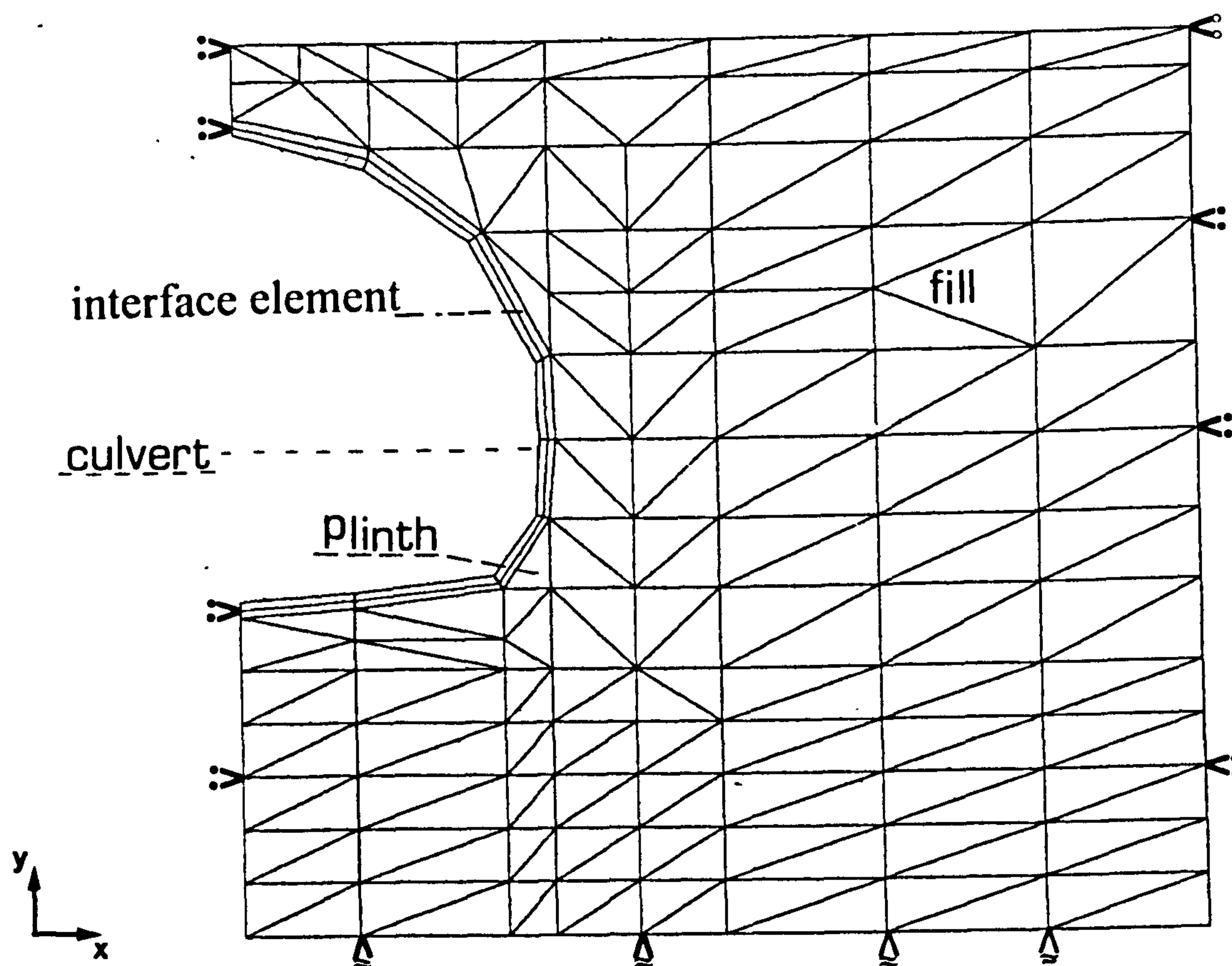


Fig 7.15 SHOWING MODELLING OF CULVERT-BACKFILL INTERFACE

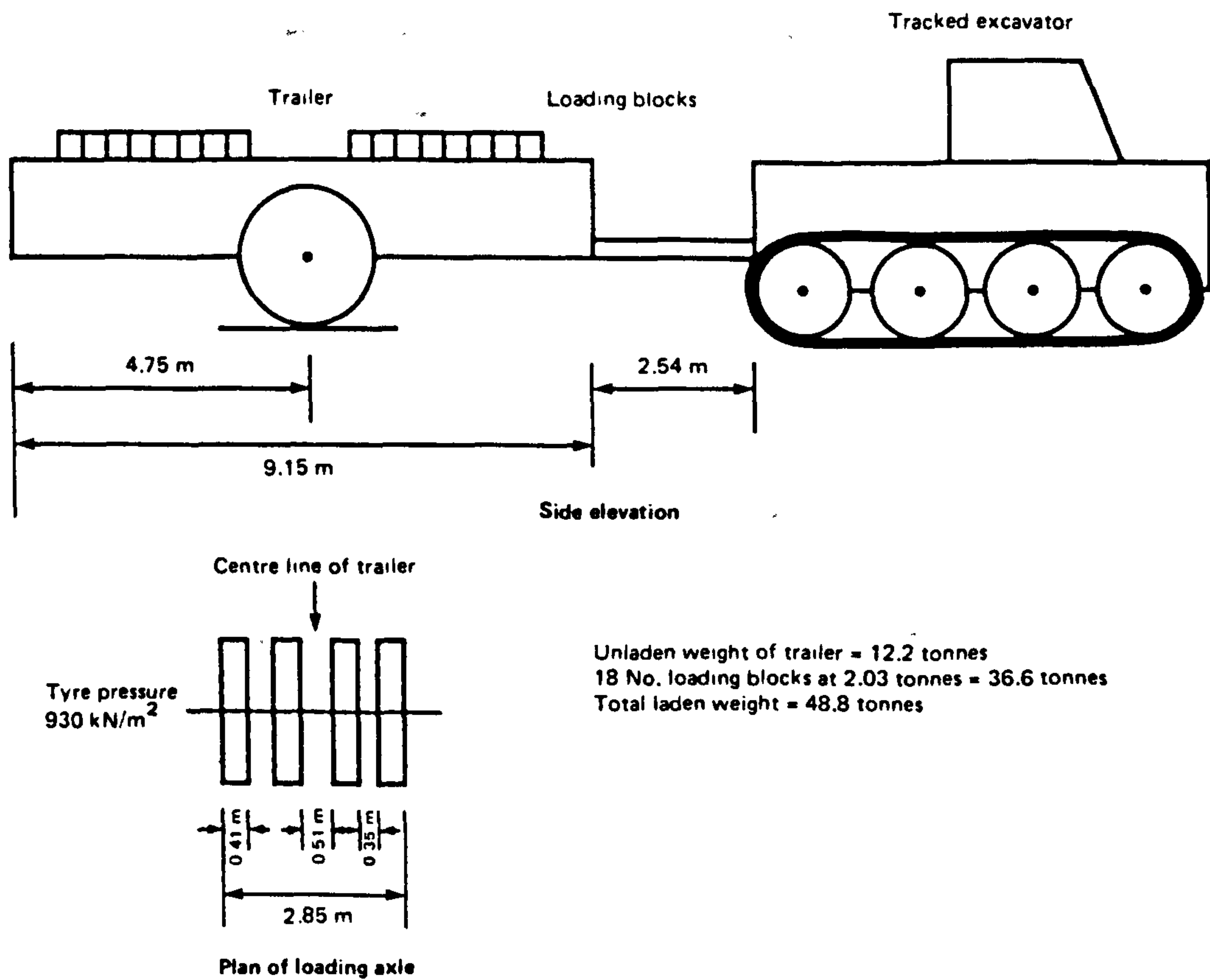


Fig 7.16 LAYOUT OF LOADING TRAILER (Temporal et al., 1985)

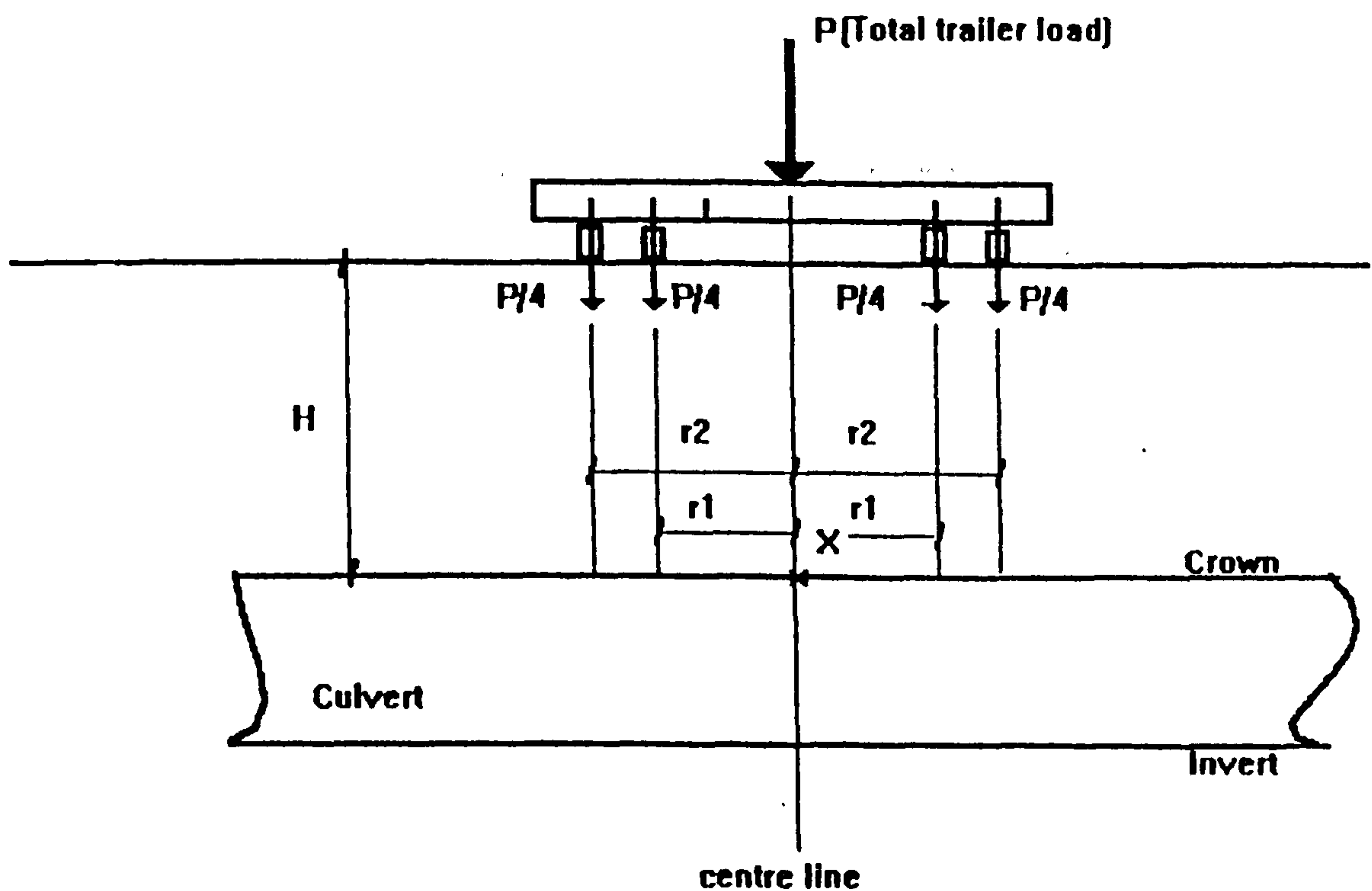


FIG 7.17 REPRESENTATION OF LIVE LOADS (LONGITUDINAL SECTION)

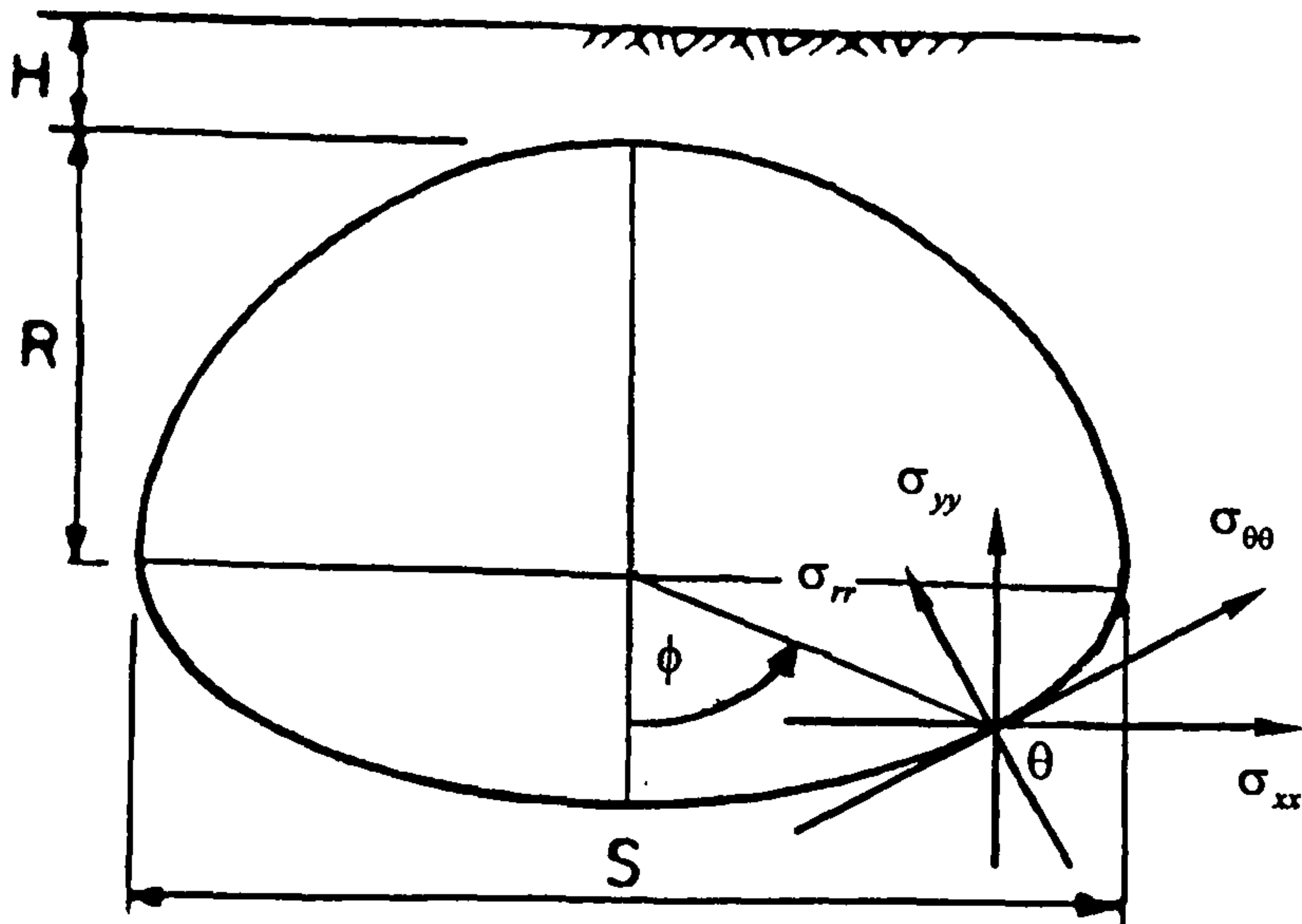


FIG 7.18 SHOWING TRANSFORMATION ANGLE θ

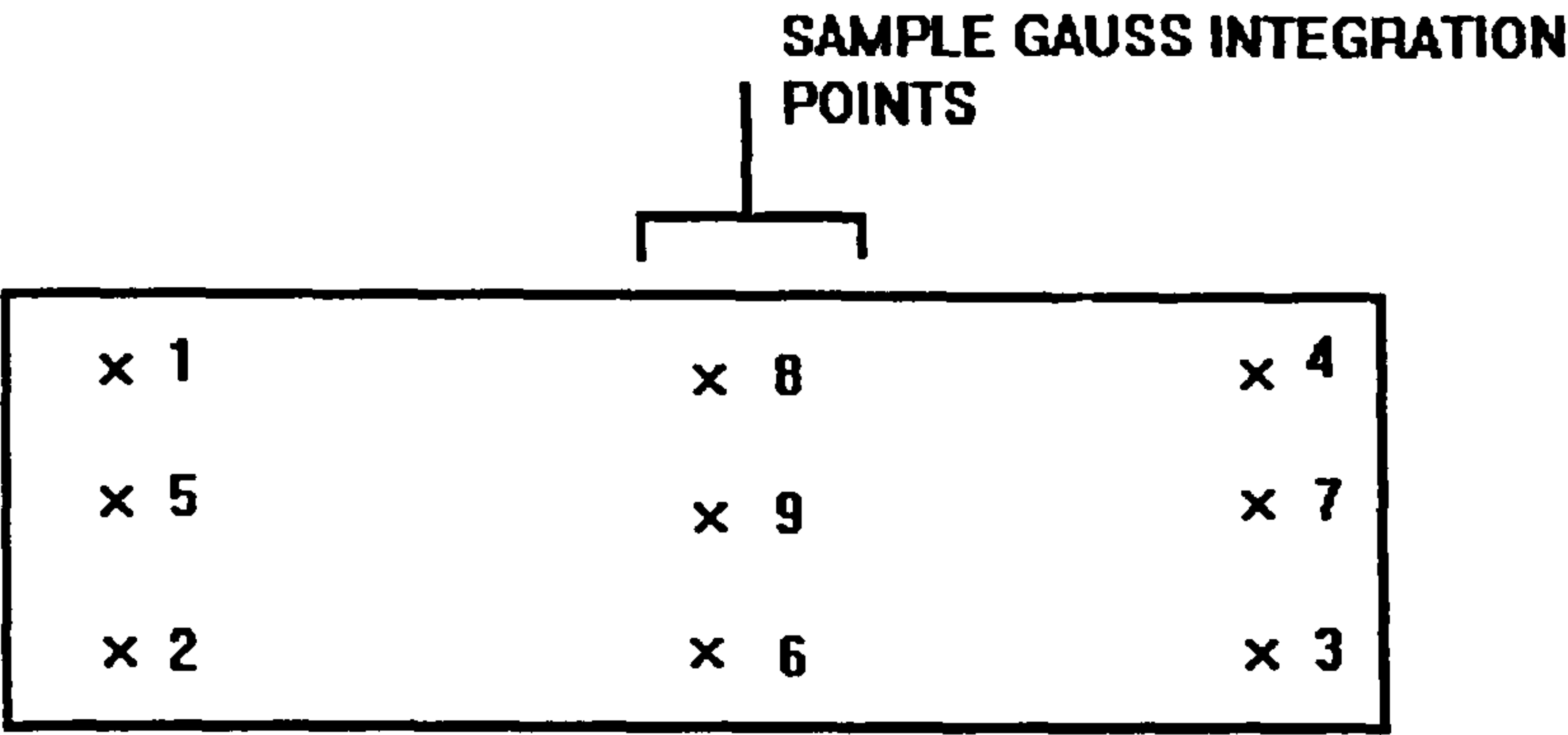


FIG 7.19 CENTRE GAUSS INTEGRATION POINTS USED TO SAMPLE STRESSES

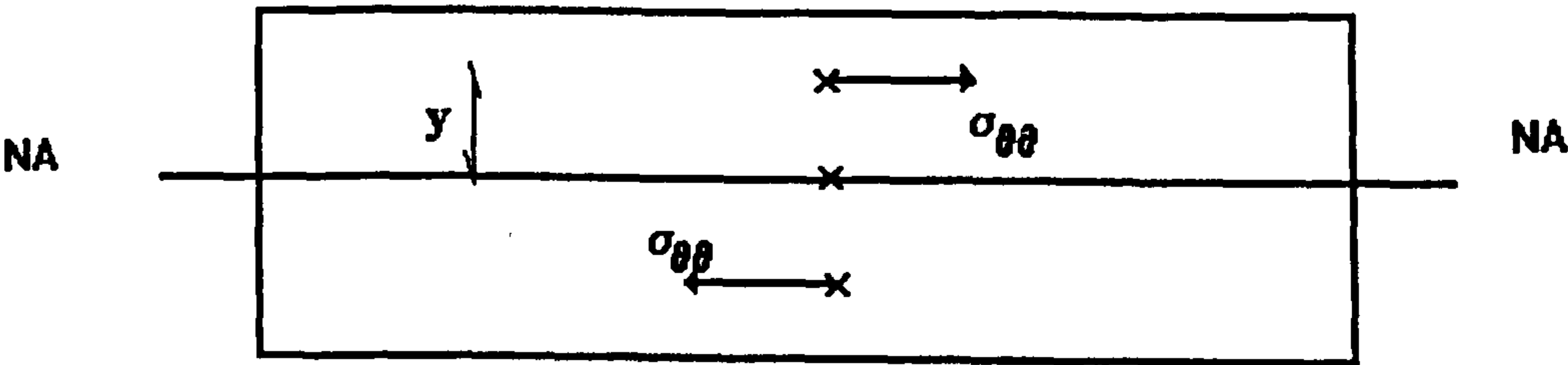


FIG 7.20 SHOWING CULVERT ELEMENT NEUTRAL AXIS AND HOOP STRESS AT CROSS SECTION

CHAPTER 8

8. Mytholmroyd culvert

8.1 Introduction

In this chapter the first of two case histories is used to assess the ability of the developed soil model to predict flexible culvert behaviour. The case history used reports a trial loading test performed on a high profile pipe arch culvert, of span $S=5.95\text{m}$, using a single axle load up to 455kN . Three loading tests were performed (presented as cases A, B and C) all under conditions of shallow cover, $H/S < 0.25$ (Duncan, 1979). The trial loadings were performed to determine the effect of pavement layers on the behaviour of corrugated steel culverts under live loadings (Johnson et al., 1989). Full details of the live loading are given in section 8.2.

Given measurements of live load culvert deflections, ring compression and bending strain, parametric and back analysis studies were performed to assess the developed approach to modelling culvert behaviour and determine a set of material parameters which give a reasonable estimate of the observed live load behaviour. Parameter selection tended to shadow the parametric studies and was predominantly a process of trial and error. No measured data were available for the construction process.

Parametric and back analysis parameter selection studies for each of the three trial loadings have been considered separately. Additionally, within each of the three trial loadings for this study the parametric and back analysis (parameter selection) studies are also considered separately. This procedure was adopted due to differing heights of backfill above the culvert crown. For each loading case initial, first estimate model material parameters were obtained from available site and laboratory data (Johnson et al., 1989). Using this initial set of parameters, parametric studies have been performed where each of the soil model parameters have been varied in turn. The effects of varying the model material parameters were noted and were used to re-examine and improve the selected model material parameters. To obtain a better set of material parameters several empirical and semi-empirical methods have been used. Studies for the first loading, case A ($H/S=0.12$, no pavement present) are described in section 8.3. Case B, ($H/S=0.2$, no pavement) and Case C, ($H/S=0.2$, pavement present) are considered in sections 8.4 and 8.5 respectively. Comparison of case studies B and C is considered in section 8.5 to demonstrate the effect of the pavement layers on the culvert behaviour. The results of each of the load cases are discussed at the end of each

of the relevant sections. Conclusions drawn from the results are reviewed and presented in section 8.6.

8.2 Mytholmroyd flexible culvert trial loading

The Mytholmroyd culvert was a 5.95m span high profile pipe arch culvert, constructed in 1986 to carry an access road over the Rochdale canal at Moderna Bridge, Mytholmroyd, West Yorkshire. The culvert was installed as part of a refurbishment of the canal to return it to a navigable state. The culvert consisted of 5.5mm thick structural plates with a corrugation of 200x55mm. The geometry of the culvert is shown in Fig 8.1 and further details are given in Table 8.1 (Johnson et al., 1989). No-fines concrete plinths were introduced at the corner plates, where high bearing pressures were anticipated to provide necessary backfill support.

The culvert was backfilled with a well graded crushed sandstone which was compacted to a high density (90-100% relative compaction). The particle size distribution of the backfill is shown in Fig 8.2 and the density and moisture content are given in Table 8.2 (Johnson et al., 1989). The constrained modulus, M_f of the backfill material was determined from plate loading tests. Values of constrained modulus equal to 42MPa and 93MPa were determined from the first and subsequent load cycles respectively. Previous researchers of this loading event (Johnson et al., 1989) using the design method of Kloppel and Glock (Kloppel and Glock, 1970) recommend a constrained modulus of $M=52\text{MPa}$. The backfill material extended to approximately one span of the culvert on each side of the structure.

Three loading tests were performed at Mytholmroyd each with differing cover conditions above the culvert crown. The first test (case A) was performed with a cover depth, H equal to 0.7m ($H/S=0.12$) of crushed sandstone. The depth of cover was then increased to 1.2m ($H/S=0.2$) the final cover depth for case B. For case C the depth of crushed sandstone backfill above the crown was reduced from 1.2m to 0.7m and pavement layers were constructed to return the total cover depth to 1.2m. The pavement consisted of a 300mm thick layer of Type 1 gravel (crushed Limestone) overlain by a 100mm thick layer of dense bitumen road base course and a 40mm thick layer of hot rolled asphalt wearing course. After completion of the pavement the third test, case C, was performed.

Loading was applied to the culvert through the loading trailer previously described in chapter 7, section 7.4.4 and shown in Fig 7.17. The trailer was pulled across the culvert using an attachment boom and a tracked excavator, which was thought to be sufficiently remote from the loading trailer to have little effect on the loading

(Temporal et al., 1985 and Johnson et al., 1989). Measurements of the live load culvert displacements, ring compression (thrusts) and bending strains were measured at the measuring positions as shown in Fig 8.3. Full details of the results of these test are described by Johnson et al. (1989), however, for this study only, the loading position of the trailer directly above the culvert crown was considered. The displacements are presented in centimetres (cm), ring compression (thrusts) in kN/m and bending moments in kNm/m. The original study (Johnson et al., 1989) presented the response of the culvert in terms of ring compression and bending strain. For this study these quantities were converted to their usual force units, using the method described in section 7.4.5.

8.3 Loading case A

This part of the trial loading was performed when the depth of crushed sandstone backfill cover was 0.7m above the culvert crown. The trial loading was performed as previously described in section 8.2. Using the loading trailer the culvert was loaded up to a maximum load of 455kN, however, owing to some initial confusion over the fill height above the culvert for this loading case, much of this study has been performed for a loading of 300kN.

8.3.1 Modelling of the soil-structure system

Analysis for loading case A was performed using the finite element mesh shown in Fig 8.4. Only half of the system was modelled as the geometry and loading are essentially symmetric. The culvert and interface elements were modelled using eight isoparametric linear strain, quadrilateral elements and the backfill was modelled using isoparametric linear strain triangular elements. The no-fines concrete plinths were included in analyses. The right hand boundary was located at a distance of 1.5 times the culvert span, S from the culvert centre line (Davies et al., 1993). The bottom boundary was located at a depth of half the culvert span, S beneath the culvert invert. This was considered to be sufficiently far away to ensure that the boundary did not significantly influence the soil-culvert behaviour (Ng et al., 1994). The vertical boundaries were constrained in the horizontal direction (x-axis) but free to move in the vertical direction (y-axis). Displacement was assumed to be fully constrained in both vertical and horizontal directions at the bottom boundary.

The construction process was modelled and the live load was applied as a point load at the surface corner node directly above the centre line of the culvert. Throughout the construction process no compaction pressure was applied to the backfill elements immediately adjacent to the culvert. The backfill was placed in layers of approximately 0.5-0.7m thick.

8.3.2 Initial parameter selection and analyses

Drained analyses were performed using the non-associated Mohr-Coulomb soil model to describe the backfill material and the isotropic elastic model to describe the culvert and no-fines concrete plinths located at the culvert corner plates. Full details of these models are given in chapter 2.

The non-associated Mohr-Coulomb soil model requires the selection of six material parameters, effective stress Young's modulus, E'_f , effective stress Poisson's ratio, ν'_f , effective stress shear strength parameters, c'_f and ϕ'_f , the unit weight γ_f of the backfill material and the angle of dilation, ψ'_f . Initial values of these parameters are presented in Table 8.3 and were obtained from available data (Temporal et al., 1985 and Johnson et al., 1989).

Initial values of Young's modulus of the backfill material, E'_f were estimated from values of constrained modulus, M_f obtained from in situ plate loading tests performed at the end of construction. Values of E' were estimated using the first cycle value of M_f and using relation (8.1).

$$E'_f = \frac{(1-2\nu'_f)(1-\nu'_f)M_f}{(1-\nu'_f)} \quad (8.1)(7.4bis)$$

where ν'_f is Poisson's ratio of the backfill material, and was initially assumed equal to 0.2 (Chang et al., 1980 and Mohamedzein, 1989). A Poisson's ratio equal to 0.2 reduces relation (8.1) to relation (8.2).

$$E'_f = 0.90M_f \quad (8.2)$$

From the first cycle of loading value of M_f was found equal to 42MPa, (Johnson et al., 1989).

The backfill material was assumed to have zero drained cohesion, $c'_f=0.0$. The second shear strength parameter required by the soil model, ϕ'_f was assumed to be equal to 35 degrees. A ϕ'_f equal to 35 degrees was assumed from published data (Chang et al.,

1980; Mayne and Kulhawy, 1982 and Craig, 1987). No data were available from which ϕ'_f could be selected.

The unit weight of the backfill material, γ_f was determined from laboratory testing (Test 14, BS 1377:1975) and found approximately equal to 20kN/m³. This parameter was unchanged throughout the analyses and was not included in the parametric studies.

Based on studies performed by Davies et al. (1993) an initial value of -5 degrees was assumed for the angle of dilation of the backfill material, ψ'_f . Negative values of dilatancy were input to represent the contractant behaviour of the backfill material during the construction procedure.

Initial parameters required to describe the culvert and plinths using the isotropic elastic model are shown in Table 8.4.

The equivalent Young's modulus of the culvert E_c was determined using the method described in chapter 7. Poisson's ratio for the culvert, ν_c , based on published data (Chang et al., 1980 and Mohamedzein, 1989) was assumed equal to 0.3. In CRISP the 'D' matrix (see chapter 2) is expressed in terms of G (shear modulus) and K (bulk modulus). Elastic parameters G and K are calculated automatically within CRISP using relations (8.2a) and (8.2b).

$$G_c = \frac{E_c}{2(1 + \nu_c)} \quad (8.2a)$$

$$K_c = \frac{E_c}{3(1 - 2\nu_c)} \quad (8.2b)$$

Elastic parameters, E_p and ν_p , Young's modulus and Poisson's ratio for the plinths, were obtained from published data (Chang et al., 1980).

Although not a material parameter, an assumption of the magnitude of compaction pressure applied during placement of the backfill is also required. As noted earlier, from previous analysis of the flexible culvert problem (Chang et al., 1980 and Selig and Musser, 1985) selection of an appropriate magnitude of compaction pressure is an arbitrary process. However, for this study, case A, an initial estimate of the compaction pressure was assumed equal to 25kPa. No information of the actual magnitude of compaction pressure applied is given. The compaction pressure of 25kPa is of similar magnitude to that used by Chang et al. (1980). Typically a compaction pressure some 3-4 times higher than that assumed here is used (Selig and Musser, 1985 and Mohamedzein, 1989). However a compaction pressure of 25kPa was thought to be

reasonable for a first estimate. The effect of variation of the compaction pressure has also been included in the back analysis study.

8.3.3 Results, initial analysis

Output manipulated from CRISP has concentrated on extracting culvert thrusts, bending moments, radial (normal) and tangential (shear) stress and culvert crown and springline movements.

Results of the initial analysis are shown in Fig 8.5-8.10. Throughout this study, unless otherwise stated, the computed construction and live load behaviours are shown graphically as (○) and (●) respectively. Computed and measured culvert behaviours are presented in Table 8.5 for comparison. The position of sampling points (or any position) around the culvert are described as an angle ϕ (degrees) referenced from the culvert invert as shown in Fig 8.11. The invert, springline, quarter-points and crown of the culvert are therefore located at 0, 90, 120 and 180 degrees respectively. The no-fines concrete plinths are located at approximately 70 degrees.

8.3.3.1 Thrust (ring compression forces)

The distribution of computed construction and live load thrust around the culvert is shown in Fig 8.5. As can be seen maximum computed construction thrusts (compressive) occur at the culvert invert and at the centre-line of the no-fines concrete plinths, 0 and 70 degrees. Maximum combined construction and live load thrusts occur at 140 degrees. From Table 8.6 the measured data suggest a maximum combined construction and live load thrust occurs at 160 degrees.

From simple equilibrium theory, which automatically assumes neutral arching, the maximum construction thrust is given by relation (8.3).

$$N_{\text{con}} = N_1 + N_2 \quad (8.3a)$$

$$N_{\text{con}} = \frac{\gamma_f S H}{2} + \frac{\gamma_f S (H^* - H)}{4} \quad (8.3b)$$

where N_{con} is the construction thrust; N_1 is the thrust induced from fill area A1; N_2 is the thrust induced from area A2, Fig 8.12; γ_f is the unit weight of the backfill material; H is the height of the backfill above the culvert crown and H^* is the height of fill above the springline being considered to compose area A2.

Relation (8.3) is similar to that used in ring compression theory (White and Layer, 1960). However, ring compression theory does not include the effect of area A_2 at the sides of the culvert on the thrust.

Simple equilibrium theory, relation (8.3), estimates a maximum construction thrust of approximately 75kN/m at the springline for a H^* equal to 1.7m. Finite element analysis estimated the springline construction thrust equal to approximately 90kN/m. For comparison, ring compression theory estimates the springline construction thrust equal to approximately 45kN/m. The construction thrust estimated using simple equilibrium theory is some 1.7 times larger than that estimated using ring compression theory. Studies performed by Duncan (1979) determined that the difference between thrusts estimated using simple equilibrium theory and ring compression theory can be significant for culverts with a low ratio of culvert rise (or top radius) to span (R/S) typically $R/S > 0.35$ is considered as high. Here, the Mytholmroyd culvert has $H/b = 0.12$ and $R/S = 0.5$. Comparing the finite element thrust with that obtained from equilibrium theory indicates that a condition of approximately neutral arching exists at the end of construction. However, comparing the finite element results with that obtained from ring compression theory assumes a state of negative arching has developed.

Application of the live load (160kN/m) significantly increases the thrust between the culvert springline and crown, Fig 8.5(a). Thrusts between the culvert invert and springline, including the plinths are decreased on application of the live load, however the difference between construction and live load thrusts is small, maximum 15kN/m at the culvert invert. It is evident therefore, that the applied load is predominantly sustained over the upper region of the culvert, between the springline and crown.

Again applying simple equilibrium theory and incorporating the live load thrusts of approximately 165kN/m are calculated, or 80kN/m for the live load only. Finite element analysis gives a combined thrust of 115kN/m or 22kN/m for the live load only. Ring compression theory gives a combined thrust of 125kN/m. From comparison of these results it is evident that some positive arching has occurred in the finite element analysis.

Previous researchers of long span pipe arch flexible culverts using finite element analysis (Duncan, 1979 and Davies et al., 1993) found that under conditions of shallow cover negative arching would prevail. However, experimental studies performed by Abel et al. (1973) and Beal (1982) found that positive arching rather than negative arching would occur.

No measured data from the trial loading are available for the springline behaviour. The nearest measuring point was located at 110 degrees, which gives a live load thrust of 40kN/m. Detailed measurements of live load induced thrusts, reported by Beal

(1982) and Temporal et al. (1985), found that variations of the live load thrust within the springline region were small.

It is evident from Table 8.5(a) that computed (analysis MA1) and measured live load thrusts compare reasonably well at measuring points 3 and 4, 140 and 110 degrees respectively. However, in each case the computed thrusts underestimate those observed by 15kN/m at 140 degrees and 5kN/m at 110 degrees.

Analyses estimated that the maximum live load thrust would occur at 140 degrees, measurements indicate that the maximum live load thrust did in fact occur at 160 degrees, measuring point 2. Numerical analyses significantly underestimated the observed thrust at this position by approximately 40kN/m. At the crown the observed live load thrust is overpredicted by approximately 24kN/m. This suggests that in the field a much larger degree of positive arching has occurred over the culvert crown region and consequently increased the observed thrust at measuring points 2 and 3, located at 160 and 140 degrees respectively. Numerical analyses have not reproduced this arching behaviour well, therefore observed thrusts over the top of the culvert at positions 2 and 3 are also not accurately predicted.

8.3.3.2 Bending moment

The distribution of construction and live load induced bending moments around the culvert are shown in Fig 8.6, hogging moments are positive (tension on the outer surface of the culvert). Maximum hogging construction induced bending moments were found to occur at the crown and the springline, the magnitude was approximately 6kNm/m. Conversely, the maximum sagging construction induced bending moment of -5.5kNm/m occurred at the culvert quarter-points. This pattern of behaviour is similar to that observed by Beal (1982) for full-scale trial loading tests performed on shallow cover, long span flexible culverts.

Live load bending moments between the culvert invert and quarter-points are approximately equal to zero. As was observed for the live load thrusts, the computed bending moments over the top region, between the quarter-points and the crown, are most influenced by the application of the live load. The maximum computed hogging and sagging live load moments were observed to occur at the crown and at 140 degrees. In the field the maximum sagging moment was observed to occur at approximately 160 degrees, Table 8.5(b).

Comparison of magnitudes of maximum computed and observed live load bending moments are in reasonable agreement, Table 8.5(b), however as already noted the

location of the occurrence of the maximum sagging moment was not accurately predicted. This difference may be attributed to the occurrence of positive arching over the culvert crown. In the field larger thrusts at measuring points 2 and 3, (location 160 degrees and 140 degrees) were induced.

Computed and observed live load bending moments at the remaining measuring positions, 3 and 4, located at 140 and 110 degrees, are in reasonable agreement and of compatible sign.

8.3.3.3 Radial stress.

No measured data for the radial stress distributions around the culvert for either the construction or live loadings are available. However, for data corroboration and to demonstrate that the developed numerical model is providing reasonable results, radial stresses, σ_{rr} computed by the finite element numerical model are compared with radial stresses estimated using the method proposed by Burns and Richard (1964). Details of this method are given in chapter 7.

Maximum construction and combined construction and live load radial stresses, σ_{rr} occur at the no-fines concrete plinths located at 70 degrees, Fig 8.7. It is evident that this stiffer area has resulted in an area of stress concentration. Application of the live load results in a small decrease in σ_{rr} of 10kPa at the plinths. The construction induced radial stress around the culvert, between the invert and plinths is largely unchanged by application of the live load. Application of the live load has greatest influence on the culvert region between the springline and crown. The maximum live load radial stress occurs within the crown region, magnitude of 30kPa. However, in the field the actual radial stress above the culvert crown will have been less due to the occurrence of positive arching, as indicated by the magnitude of observed thrust levels.

Construction radial stress at the culvert springline and crown calculated using the method of Burns and Richard (1964) for the fully bonded and unbonded conditions are 17kPa and 14kPa and 10kPa and 14kPa respectively. These values of radial stress, especially for the crown, compare reasonably well with values of radial stress estimated from the finite element analyses.

Using the same method for the live load induced radial stress gives 71kPa and 55kPa at the springline for the bonded and unbonded conditions, and 40kPa and 56kPa at the culvert crown. These values are larger than those obtained from analyses, particularly at the springline.

8.3.3.4 Shear stress

No measured shear stress data are available for the distribution of shear stress around the culvert. As with the radial stress, shear stress data have been calculated using the method after Burns and Richard to permit some corroboration of the analyses.

The distribution of shear stress around the culvert, calculated from analyses are shown in Fig 8.8. As can be seen the maximum construction and combined construction and live load shear stress is located at the plinths. This behaviour has arisen because in analyses no movement between the culvert and plinths was allowed to occur. As a result this tangentially stiff area will result in a concentration of shear stress as shown. In the field some movement between the culvert and plinths may have occurred as the plinths are not set rigidly against the culvert. Consequently, finite element analyses may be overestimating the magnitude of shear stress in this region. However, in the absence of measured shear stress data no firm conclusions can be drawn. Application of the live load has caused a reduction in the shear stress at the plinths from approximately 55kPa to 30kPa, a reduction of 25kPa. The shear stress between the culvert invert and plinth is only slightly reduced on application of the live load.

Between the springline and the 140 degree position application of the live load has caused an increase in magnitude and change in sign of the shear stress. This has arisen due to the change in the deformation response of the culvert in this region. The shear stress over the crown region of the culvert, (140-180 degrees) is increased in magnitude and of the same sign. This has occurred due to the increased vertical deformation of the culvert crown. This response is unchanged from the construction procedure.

The maximum construction shear stress τ_{θ} is typically assumed to occur at the culvert quarter-point (120 degrees) (Burns and Richard, 1964). Using their method gives a maximum shear stress of $\pm 8\text{kPa}$. Additionally, the shear stress induced by the live load is approximately $\pm 65\text{kPa}$. In both cases the fully bonded condition was assumed.

The method of Burns and Richard does not incorporate the effect of the plinths. Therefore an estimate of the maximum construction shear stress which is induced at the plinths is not possible using this method. However, the construction shear stresses estimated by the two methods at the quarter-points are in reasonable agreement. Live load shear stress estimated by Burns and Richard overestimates that obtained from analyses.

8.3.3.5 Culvert displacements

The displacement histories of the culvert crown and springline, from the start of the construction sequence through to the application of the live load, are shown in Fig 8.9 and Fig 8.10. The displacement history of the culvert invert is also shown in Fig 8.9. Measured culvert displacement data are only available for the vertical displacement of the culvert crown. At the current applied load level, 160kN/m or 300kN, a vertical crown deflection of -0.8cm was observed in the field. Note the sign convention being used for displacements: any displacements causing a reduction in the radial dimension of the culvert are negative. The original culvert shape, i.e. original crown and springline levels, is the zero or the undeformed position. The stages of construction history shown in Fig 8.9 and Fig 8.10 are: stages 3 and 4 correspond to placement of the fill up to the culvert springline. Stages 5, 6 and 7 correspond to placement of backfill just above the culvert quarter-points. Construction stage 8 corresponds to placement of the backfill level with the culvert crown and stage 9 corresponds to placement of the backfill above the culvert crown to the required fill height. Stage 10 coincides with the application of the live load.

Placement of backfill layers around the base of the culvert and plinths, construction stages 3 and 4, has caused a small inward (negative) deflection of the culvert crown of -2cm and an outward deflection of the culvert springline of 0.02cm. This pattern of behaviour has arisen because placement of the backfill and subsequent compaction has caused the culvert base and plinths to rotate clockwise, pulling the culvert crown downwards and pushing the sides outwards. Placement of the first layer of backfill above the culvert springline (stage 5) has arrested the downward crown movement and reversed the direction of movement at the springline. Placement and compaction of subsequent layers of backfill up to the quarter-point level further pushes the culvert sides inwards which in turn forces the culvert crown to rise upwards or 'peak'. Continued construction above the culvert quarter-points and subsequently above the culvert crown reverses this behaviour and the crown is pushed downwards under the imposed compacting pressures and increasing weight of backfill, which in turn forces the side walls to push outwards. This deformation behaviour, provided deformations are small, has been found to be desirable as it tends to "pre-stress" the culvert crown and makes it less susceptible to buckling particularly under low cover conditions (Duncan, 1979 and Richards, 1982).

Application of the live load above the culvert crown further pushes the culvert crown downwards, forcing the culvert sides outwards. In this case the final culvert crown position is beneath its original zero, undeformed position.

Finite element analysis computed a live load crown displacement of -1.0cm. In the field a crown displacement of -0.8cm was observed.

No measured data for the springline displacements are available, however for corroboration of data finite element displacements are compared with springline displacements estimated from the method of Burns and Richard (1964) and the IOWA deflection formula (Spangler, 1941). Finite element analysis estimated the live load springline displacement equal to 1.1cm.

Using the method of Burns and Richard gave springline displacements of 4.5cm and 6cm for the fully bonded and unbonded conditions respectively.

The IOWA deflection formula, assuming a deflection lag factor of 2 (Spangler and Hardy, 1982) and a modulus of soil reaction E'_R of 55kPa (Howard, 1977 and Spangler and Hardy, 1982) gave a live load springline displacement of approximately 1cm.

As can be seen the IOWA deflection formula produces a result similar to that obtained from the finite element analysis. However, the parameters, D_L (deflection lag factor) and E'_R (modulus of soil reaction) are ambiguous parameters: as a result the accuracy of this method is questionable.

8.3.3.6 Discussion

In summary the initial set of parameters has provided a reasonable first estimate of the observed culvert behaviour. However, as noted previously some differences and discrepancies between the measured and predicted responses still remain. These differences will be examined in the parametric studies described in the following section.

From the results of the initial analysis it is evident that predominantly all of the applied load is sustained by the top region of the culvert, $180 \geq \theta \geq 90$ degrees. Consequently, the parametric studies and subsequent analyses will primarily concentrate on this region of the culvert.

It is evident from comparison with the observed data and limited comparison with alternative, but proven methods of analysis, that the developed numerical model has reproduced the essential elements of the culvert behaviour. However, this statement will be further investigated in the following sections.

8.3.4. Parametric and back analysis studies

8.3.4.1. Introduction

In this section parameter studies have been performed to identify the influence and effects of the soil model material parameters on the finite element solution. Measured data are available for the culvert live load thrusts, bending moments and crown displacement, the parametric study has therefore tended to concentrate on the effect of model parameter variation on these measured quantities. The results of the analysis described in the previous section form the 'base-line' for the parametric study. Model parameters, except the drained shear strength, c'_f and the unit weight of the backfill, γ_f , were varied in turn. The compaction pressure, although not a model material parameter was also included in the parametric studies. The presence of the no-fines concrete plinths on the culvert behaviour is also investigated. The parametric studies are presented in the following section (8.3.4.2). Full results and details of the finite element parametric studies for this case study are presented in Tables 8.6-8.9. Tables 8.6-8.9 include both the construction and live load behaviour.

Using the results of the parametric studies the selected model parameters have been re-evaluated and justifiable improvements, based on published empirical and experimental data, have been made. Using this diagnostic approach a framework of parameter selection for similar loading situations is described (section 8.3.4.3.). The results of the optimum finite element solution are also compared with the alternative methods of analysis described in chapter 7.

8.3.4.2. Variation of the backfill modulus,

The order in which each of the soil model parameters is considered in this study follows the order in which they are entered into CRISP (E'_f , ν'_f , c'_f , ϕ'_f and ψ'_f).

Variation of the backfill Young's modulus did not have a significant effect on the construction thrust behaviour, Table 8.6, analyses MA5-MA9. As can be seen an increase in E'_f from 20MPa to 70MPa has resulted only in an increase in the construction thrusts of 2-3kN/m. A similar magnitude of increase was observed for the radial and shear stresses, Table 8.8, induced over the top region (180-190 degrees) of the culvert. A larger increase of approximately 10kPa in the construction induced radial and shear stress was observed at the no-fines concrete plinths. The increase in

construction induced bending moments, Table 8.7, was again small, approximately 1-2kN/m.

The effect of the variation of the backfill modulus, E'_f on the culvert live load behaviour is shown in Figs 8.13-8.17 in terms of the culvert quantities, thrust, bending moment, radial and shear stress, and displacements (crown and springline).

Consider first the displacement response of the culvert under the varying backfill modulus E'_f .

As can be seen from Fig 8.17 monotonic variation of the backfill Young's modulus, E'_f results in a non-monotonic displacement response (crown and springline). The crown displacement response in the range of $35\text{MPa} \leq E'_f \leq 70\text{MPa}$ is approximately similar to that inferred from the analytical method after Burns and Richard (1964). In the range of $E'_f < 35\text{MPa}$ the computed finite element behaviour is very different and displays a decrease in the crown displacement. The crown displacement computed using the Burns and Richard methods gives -4.1cm, a continued increase.

In the range of $50\text{MPa} \leq E'_f \leq 70\text{MPa}$ the computed finite element crown displacements are larger than those computed using the analytical method after Burns and Richard. For $E'_f < 50\text{MPa}$ approximately the computed finite element crown displacements are less than those computed using the analytical method. This suggests a decrease in the rate at which the culvert crown live load displacements are generated. A similar form of behaviour is observed for the culvert springline displacements, Fig 8.17(b).

The computed displacement behaviour between, $35\text{MPa} \leq E'_f \leq 70\text{MPa}$ was as expected from classical solutions (Spangler, 1941 and Burns and Richard, 1964) however the behaviour resulting for $E'_f < 35\text{MPa}$ was surprising. Explanation of this behaviour can be obtained from consideration and comparison of the culvert deformation response through construction and application of the live load for backfill moduli 70MPa and 10MPa.

Experimental studies performed by Shmulevich et al. (1986) to determine the soil stress distribution around buried flexible metal pipes, found that the horizontal to vertical load ratio, C_H at the sides of the culvert was a function of the pipe-soil stiffness ratio, S_R , Fig 8.18. From Fig 8.18 it is evident that increasing the backfill stiffness will increase the horizontal to vertical load ratio, C_H and consequently increase the horizontal force on the sides of the pipe. This behaviour is reflected in the finite element studies investigating the variation of E'_f . Consider the behaviour resulting from placement and loading of a backfill of $E'_f=70\text{MPa}$.

Placement and compaction of a high stiffness backfill around the culvert will, due to the higher magnitude of mobilised horizontal force, F_H (Shmulevich et al., 1986) associated with a high stiffness fill, cause the culvert sides to be pushed inwards and the crown forced upwards more than is induced when a low stiffness fill is placed. This behaviour is reflected in Table 8.9 (analyses MA5, MA8 and MA9).

On application of the live load the increase in the crown and springline displacement is larger than that anticipated from consideration of classical solution methods. Finite element analysis computed a culvert crown to springline displacement ratio of approximately 6, however a displacement ratio of 1.1 was obtained using the method of Burns and Richard and additionally a ratio of 4.5 was obtained using Burns and Richard to compute the crown displacement but using the Iowa deflection formula to compute the springline deflection. Both methods, Burns and Richard and the Iowa deflection formula make no allowance for the presence of the no-fines concrete plinths, which will to some extent (see later) restrict the lateral movement of the culvert, forcing the displacement ratio to be higher. The live load displacement ratio is plotted against the backfill modulus and is shown in Fig 8.17(c), for comparison the combined construction and live load displacement ratios are also shown. As can be seen the two behaviours are very different, however both curves display a marked decrease in the slope at low backfill moduli owing to the decrease in the rate of culvert displacement. This slowdown in the displacement ratio may be attributed to the end of construction position of the culvert crown in relation to the initial undeformed culvert position.

Observations by Spangler and Hardy (1982) determined that continued deflection of the culvert past its initial undeformed position will eventually cause the culvert crown to flatten, with curvature approaching zero. Further deflection beyond this position will cause the curvature of the culvert crown to reverse, becoming concave upwards. When this occurs the side of the culvert will pull inward which will gradually eliminate the soil support of the culvert sides.

Flattening of the culvert crown will result in a decrease towards zero of the culvert crown bending moment but an increase in the quarter-point bending moment, as it is at this position that the culvert crown is bending. This behaviour is exhibited by the finite element live load bending moments at $E'_f=10\text{MPa}$, Fig 8.14. Therefore, as the culvert flattens there is a decrease in the rate of increase of the culvert crown deflection (further deflection will be resisted at the quarter-points) and subsequently a decrease in the springline movement. The reduction in springline movements will be further exaggerated due to the presence of the no-fines concrete plinths.

The flattening behaviour of the crown is further described by the radial and shear stresses at the culvert crown, Figs 8.15 and 8.16. As can be seen both quantities show a decrease at low backfill stiffness. The decrease in the radial and shear stress is due to

the culvert starting to pull away from the soil. This decrease is also evident at the culvert sides, where due to the culvert starting to pull away from the surrounding backfill the lateral support is diminishing. Without the necessary backfill support the culvert cannot carry any further load through ring compression, hence the marked decrease in thrust in the culvert, Fig 8.13.

It is evident from the above discussion that the backfill should be of a high quality and stiffness to provide the necessary lateral restraint to the culvert and consequently enable the culvert to sustain high ring compression forces, but also maintain the displacements within reasonable safe limits. This study has demonstrated that allowing the culvert crown to displace beneath its original undeformed position (through embedment in a low stiffness fill) can lead to the development of a potentially dangerous culvert displacement mechanism. To avoid this problem note needs to be taken of the culvert displacement during construction and subsequent placement of any live loads. Ideally, what is required is a large, positive displacement ratio $(\frac{\Delta y}{\Delta x})$ (where y and x are the crown and springline displacement respectively) for the combined construction and live loads displacement as described in Fig 8.17(c). Similarly, the live load displacement ratio arising due to application of the live load should be of a high magnitude, typically $\frac{\Delta y}{\Delta x} < -8$ (negative because of the assumed displacement convention; inward displacement is negative). However, these displacement ratios are also likely to be functions of the compaction effort employed during placement of the backfill which will influence the magnitude of construction displacement ratios (Duncan, 1979; Richards, 1982 and Spangler and Hardy, 1982). The influence of the compaction pressure is considered in section 8.3.4.6.

Experimental studies performed on metal pipes embedded in non-cohesive backfill material (Jeyapalan and Abdel-Magid, 1984 and Jeyapalan and Bolden, 1986) determined that the magnitude of the pipe displacement ratio, ratio of pipe crown and springline displacement, varied inversely with the pipe-soil stiffness factor, S_K , Fig 8.19. The pipe-soil stiffness factor is defined by relation (8.4).

$$S_K = \frac{E_p I_p}{R_p^3 M_f} \quad (8.4)$$

where E_p and I_p are Young's modulus and the second moment of area per metre length of the pipe wall material; R_p is the radius of the pipe and M_f is the constrained modulus of the backfill material and is given by relation (8.7). The constrained modulus M_f is directly proportional to the soil stiffness, E'_f .

Re-plotting Fig 8.17(c), live load behaviour only, in terms of the magnitude of the pipe displacement ratio against the pipe-soil stiffness ratio, Fig 8.20, reveals a similar trend of behaviour to that observed by Jeyapalan and Boldon (1986). The radius R_p was assumed to be equal to the radius of the top section, crown to quarter-points, of the culvert.

Comparison of the live load springline ring compression strains, ϵ_r plotted against the pipe-soil stiffness ratio obtained from experimental studies (Jeyapalan and Abdel-Magid, 1984 and Jeyapalan and Boldon, 1986) and finite element analysis also displays a similar trend in behaviour, Fig 8.21. Finite element ring compression strains ϵ_{rfe} were converted from computed thrusts using relation (8.5), assuming a Young's modulus of 205GPa for the steel culvert, E_c .

$$\epsilon_{rfe} = \frac{NA_c}{E_c} \quad (8.5)$$

where N is the computed live load culvert thrust and A_c is the culvert cross-sectional area per unit length of culvert.

The comparisons with published work demonstrate that the results obtained from the developed finite element soil model are consistent with experimental observations.

For comparison the springline live load thrusts were calculated from simple equilibrium theory and Duncan's design method (Duncan, 1979). Simple equilibrium theory gave a live load thrust of 40kN/m and Duncan's method (independent of soil stiffness) gave a live load of 44kN/m, using the live load factor, K_{p3} data relating to the application of the live load above the culvert crown. Using a live load factor K_{p3} as recommended by Duncan (1979), $K_{p3}=1.0$ for a cover depth to span ratio of less than 0.25 based on the live load applied at the culvert quarter point, gives a live load thrust of 80kN/m. Within the range of values of the backfill Young's modulus used in this parametric study the finite element computed springline live load thrusts are always smaller. This suggests that positive arching is occurring across the full width of the culvert. Duncan's method (Duncan, 1979) assumes that negative arching will occur across culverts under shallow cover conditions. However finite element predictions of arching behaviour are consistent with the experimental observations reported by Beal (1982) for flexible, low span metal culverts under shallow cover conditions.

The trend of finite element computed live load springline thrusts in Fig 8.13 suggests that increasing the backfill modulus beyond 70MPa will further increase the live load thrust towards that computed previously using simple equilibrium theory.

8.3.4.3 Variation of Poisson's ratio

The effect of the variation of the backfill Poisson's ratio on the culvert live load behaviour is shown in Figs 8.22-8.26. The influence on construction induced effects is presented in Table 8.6-8.9, analyses MA1 and MA14-MA18.

Except for culvert displacements, variation of Poisson's ratio does not have as significant influence on the construction behaviour as the live load behaviour.

As can be seen from Table 8.6, construction thrusts at the culvert crown tend to decrease with increasing Poisson's ratio, however between the culvert quarter-points and springline the construction thrust increases with increasing Poisson's ratio. This trend is less evident at the springline, where the thrust behaviour is quite erratic. A combination of the low cover height and inclusion of the no-fines concrete plinths may account for this behaviour. Construction thrusts at the culvert invert increase by some 50-60kN/m for an increase in Poisson's ratio from 0.0 to 0.4. This increase in construction thrust experienced at the culvert invert is due to the greater inward movement of the culvert sides during construction forcing the culvert crown and invert outwards (inducing the shape of an oval).

As noted previously the thrust induced at the culvert springline calculated from simple equilibrium theory is approximately 85kN/m. Using ring compression theory gives a springline thrust of approximately 45kN/m, however this theory does not take into account the weight of the backfill at the culvert sides. Finite element computed springline thrusts are in the range of 80-90kN/m suggesting that a condition of neutral arching has developed, compared to thrust determined from equilibrium theory. Comparison with thrusts determined from ring compression theory (White and Layer, 1960) suggests that a condition of negative arching has developed and the culvert is carrying loads in excess of the weight of backfill above it. Duncan's design method, which assumes that negative arching will develop, estimates the construction thrust at the culvert springline equal to 126kN/m, some 35-45kN/m greater than that obtained from the finite element analyses.

The main effect of varying Poisson's ratio of the backfill material is evident from relation (8.6) from which the initial in situ horizontal stress are estimated.

$$\sigma_{hi} = \left(\frac{\nu_f}{1 - \nu_f} \right) \sigma_{vi} \quad (8.6)$$

where σ_h and σ_v are the in situ horizontal and vertical stress; $\left(\frac{\nu_f}{1-\nu_f}\right)$ is equal to K_0 the coefficient of earth pressure at rest.

It is evident from relation (8.6) that decreasing ν_f towards zero reduces the in situ horizontal stress to zero. High in situ horizontal stress can be obtained by using $\nu_f=0.4$. Using progressively lower values of Poisson's ratio therefore gradually eliminates the horizontal contact stresses which also provide some restraint to the movement of the soil mass between soil particles and consequently removes the arching support within the soil mass.

Applying this to the culvert problem for $\nu_f=0.0$, initial in situ horizontal stresses within the soil mass are zero. Horizontal stresses induced by the compaction process are small and offer little restraint between adjacent soil particles. Consequently, the soil mass is unrestricted from bearing directly down onto the culvert, hence the observed increase in crown thrusts at the expense of the springline thrust as Poisson's ratio is reduced towards zero, Table 8.6. Additionally, the lateral restraint offered by the soil at the sides of the culvert for low values of ν_f will be lower. Conversely, for high Poisson's ratio fills, high pressures will exist within the soil providing large scale arching support. Therefore, the full weight of the soil mass is prevented from bearing directly onto the culvert by this arching action. In this situation positive arching would be expected to occur at the culvert springline. This behaviour is not truly reflected in the results for Case A.

Variation of the backfill Poisson's ratio had a significant influence on the computed live load thrusts, Fig 8.22. As can be seen the live load thrust varies inversely with Poisson's ratio, a decrease in Poisson's ratio from 0.3 to 0.0 increases the live load thrust on the culvert approximately by a factor of ten. The live load thrusts for $\nu_f=0.3$ and 0.4 are approximately equal. The decrease in arching support within the soil is evident as Poisson's ratio tends towards zero and the culvert springline line thrust (which tends to 80kN/m) is approximately equal to that implied from simple equilibrium theory.

Duncan's design method (Duncan's, 1979) gives a maximum live load thrust of approximately 90kN/m, at the culvert springline. This is approximately equal to the springline thrust determined from finite element analysis for a Poisson's ratio of 0.0.

The presence of high overlying stresses within the soil at $\nu_f=0.3$ and 0.4 has transferred much of the applied load away from the culvert. This behaviour is evident from the

variation of radial and shear stress induced around the culvert, following variation of Poisson's ratio, Figs 8.23-8.24. Both the radial and shear stress display a behaviour similar to that of the live load thrusts, increasing live load radial and shear stress with decreasing Poisson's ratio, induced due to the removal of the arching support within the soil causing the soil to bear directly onto the culvert subsequently increasing the radial stress around the culvert. The increase in shear stress follows from the increased settlement of the soil around the culvert, at low values of ν'_f . At higher values of ν'_f the development of arching support sustains the soil and prevents it from bearing directly onto the culvert, which results in low radial and shear stresses around the culvert.

Using relation (7.1) (Allgood and Takahashi, 1964) the degree of arching A , occurring above the culvert crown can be obtained. Using the computed crown radial stress the variation of the degree of arching occurring at the culvert crown following variation of Poisson's ratio can be computed, Fig 8.27. The degree of arching is shown for both the end of construction and after application of the live load. As can be seen from Fig 8.27 at the end of construction negative arching is occurring at low values of Poisson's ratio but the degree of negative arching is decreasing with increasing Poisson's ratio. At Poisson's ratio of $\nu'_f=0.4$ approximate neutral arching is occurring. On application of the live load the behaviour is very different and positive arching is occurring. As can be seen the degree of positive arching is increasing with increasing value of Poisson's ratio.

This arching behaviour is similar to that observed by Beal (1982) from field tests on long-span, shallow cover, flexible culverts for the behaviour following construction and after application of a live load.

The effect of variation of Poisson's ratio on the culvert crown and springline displacements is evident from Fig 8.25. At high values of Poisson's ratio, $0.3 \leq \nu'_f \leq 0.4$, high lateral soil pressures are induced at the culvert sides which during the construction process push the culvert sides inwards, forcing the culvert crown upwards by approximately -0.17cm and 1.3cm respectively. Further placement of fill around and above the culvert crown recovers only approximately 0.3cm of the initial crown rise and 0.06cm of the initial inward movement of the culvert springline. In this case application of the live load does not significantly alter or affect the magnitude or sign of the culvert crown and springline displacements. As a result live load bending moments around the culvert, Fig 8.26 are small. This is due to the presence of high soil pressures at the culvert sides, supporting the culvert.

For low values of Poisson's ratio ($0.0 \leq \nu'_f \leq 0.1$) the situation is reversed. Placement of fill around the culvert during the construction procedure results in small inward movement of the culvert springline and consequently a small rise in the culvert crown,

Figs 8.25(a) and 8.25(b). Placement of fill above culvert crown recovers this small rise and at the end of construction the culvert has displaced some -0.5cm beneath its original undeformed position. The magnitude of horizontal soil pressure at the culvert sides is insufficient to support the culvert sides without large lateral displacement occurring. The end of construction springline displacement is approximately 0.35cm. Application of the live load significantly increases the culvert crown and springline displacement, Figs 8.25(a) and 8.25(b). Again the springline must displace significantly in order to mobilise sufficient lateral restraint to support the culvert. In this case, due to the large scale culvert displacement, the live load bending moments Fig 8.6 around the top region of the culvert ($180 \leq \theta \leq 90$ degrees) are large, maximum of -11kNm/m at the culvert crown. Bending moments at the culvert quarter-points indicate a change of sign and hogging moments (positive moments) are occurring.

Duncan's design method (Duncan, 1979) estimates a maximum construction bending moment of approximately 4.5kNm/m. The maximum construction bending moment obtained from the finite element analysis was 6.5kNm/m for a $\nu'_f=0.4$. The maximum construction bending moment has arisen at this value of Poisson's ratio because of the large magnitude of construction displacements at the culvert crown and springline combining to induced a large positive moment at the culvert crown.

The maximum live load induced bending moment determined from finite element analysis, is approximately -11kNm/m obtained for a $\nu'_f=0.0$. Duncan's method gives a live load bending moment of approximately 13kNm/m using the smallest value of R_L available given the limit of flexibility numbers, N'_f in Fig 7.13.

Ideally, a Poisson's ratio of $\nu'_f \geq 0.3$ for the backfill makes most efficient use of the flexible culvert soil interaction as the backfill material is the main load carrying structure and the culvert serves as a liner or reinforcement to maintain the shape of the hole. To achieve this level of efficiency between the culvert and soil will require a high quality, highly compacted backfill. However in practice the high quality required to achieve this level of efficiency cannot be guaranteed owing primarily to the uncertainty of the construction process and Poisson's ratio is known to vary extensively within the backfill (Dalton and Hawkins, 1982 and Britto and Gunn. 1989).

From the results of this study, Poisson's ratio equal to 0.0 gave the most adverse culvert behaviour. A value of $\nu'_f=0.0$ in relation (8.6) implies a stress ratio $\sigma'_h/\sigma'_v=0.0$ (or $K_0=0.0$). Clearly, this is unrealistic and use of $\nu'_f=0.0$ cannot be justified. Back analyses, performed by Seed and Duncan (1986), of compaction induced lateral stress adjacent to a flexible metal retaining wall determined that for a granular backfill (clean

sand) K_{onc} was approximately 0.37 ($\nu'_f=0.27$ using relation 8.6)). Additionally, K_o data reported by Mayne and Kulhawy (1982) for sands and gravels are of the range $0.36 \leq K_o \leq 0.5$ giving a range of Poisson's ratio of $0.26 \leq \nu'_f \leq 0.333$. In view of this use of $\nu'_f < 0.2$ for a compacted granular material is unrealistic and not consistent with experimental observations.

Duncan's design method (Duncan, 1979) gives results similar to those obtained from the finite element analysis assuming a $\nu'_f=0.0$. Duncan's method is independent of Poisson's ratio. In this method negative arching is assumed to occur: as a result high thrusts are estimated.

8.3.4.4 Variation of the angle of internal friction, ϕ'_f

The effect of varying the angle of internal friction is to alter the shearing resistance of the backfill material. A direct relationship exists between the angle of internal friction and the shearing resistance of the backfill, such that the larger the angle ϕ'_f the higher is the shearing resistance of the backfill material.

During construction the backfill material is being continuously worked (sheared) by the construction compaction stresses to force the soil particles to arrange themselves into a tight matrix around the culvert. To achieve this the compaction pressures must be of sufficient magnitude to overcome the shearing resistance of the soil and consequently force the soil particles to move around each other to form a tight, interacting structure. The effect of driving the soil particles together is to increase the contact stresses between the soil particles which on a global scale will increase the lateral stress throughout the soil mass. The effect of these lateral stresses on the side of the culvert during construction is to induce an active pressure on the culvert sides which in effect is a retaining structure.

As can be seen from Fig 8.28(a) and (b), for a low frictional fill ($\phi'=20$ degrees) the forced inward and upward movement of the culvert springline and crown is larger than that induced during the placement of a high frictional fill. The reason for this behaviour is evident from Fig 2.2 as a high ϕ' fill has a higher ratio of σ'_v/σ'_h (or $1/K_o$) than a low ϕ' fill. Consequently high ϕ' fills can sustain higher stress before shearing will occur.

As can be seen from the construction induced radial stresses, Table 8.8 (analyses MA10-MA13) at the culvert crown and construction thrusts at the culvert springline, at the end of construction the condition of negative arching has developed across the culvert. At the end of construction the culvert crown radial stress, σ_{rr} will be approximately equal to the vertical stress, σ_{yy} or overburden pressure, $\sigma_{rr}=\sigma_{yy}$.

Arching therefore, is approximately zero. For low frictional fill ($\phi'_f=20$ degrees) the end of construction radial stress is approximately 21kPa, some 6kPa larger than the overburden pressure, implying negative arching has developed. Additionally, as noted previously the thrust at the springline, assuming neutral arching, estimated from simple equilibrium theory is 85kN/m, finite element analysis for low frictional fills ($\phi'_f=20$ degrees) calculated a springline thrust of 92kN/m, Table 8.6. These differences in radial stress and thrust imply a condition of negative arching has developed for the low frictional fill. This condition has arisen because placement of the backfill above the culvert crown has not significantly recovered the initial upward movement of the culvert. The change in crown displacement between placement of the first and last layer of fill above the crown is approximately -0.01cm, Table 8.9. This magnitude of displacement is not sufficient to cause yielding within the soil above the crown and has consequently induced a condition of positive arching. The crown displacement induced by the live load is large enough to cause shearing of the soil immediately above the culvert crown, inferred from the low live load radial and shear stresses over the crown (Figs 8.29-8.30), and consequently mobilised a condition of positive arching across the full width of the culvert. The live load thrust at the culvert springline, Fig 8.31, for this condition is considerably lower than that implied from equilibrium theory of 40kN/m.

Live load culvert displacements for the low frictional fills, ($\phi'_f=20$ degrees) are lower than those arising from the high frictional fill ($\phi'_f=45$ degrees). This has arisen because of the lower compacted state of the backfill associated with the high frictional fills, and the culvert will displace under the increasing live load mobilising sufficient lateral restraint at the culvert sides to support the culvert. The large displacements of the culvert crown and springline associated with the high frictional fills have resulted in significantly increased bending moments at the culvert crown, Fig 8.32.

At the culvert crown the radial stress is approximately equal to the vertical stress in the soil assuming a condition of neutral arching is occurring. Using Boussinesq's elastic theory relation (8.8) the live load vertical stress, σ_{yy} is approximately 75kPa.

$$\sigma_{rr} = \sigma_{yy} = \frac{2Q}{\pi H} \quad (8.8)$$

where Q is the applied line load per metre length and H is the depth of cover above the culvert crown.

Finite element analyses for $\phi'_f=45$ degrees computed live load radial stress at the crown of approximately 60kPa, some 15kPa less than that calculated from elastic theory, suggesting that some positive arching is still occurring above the culvert crown.

From the results presented it is evident that for the given soil parameters and construction conditions the low friction fill, $\phi'_f=20$ degrees has produced the most efficient system, such that the backfill material and not the culvert is carrying the load. The results also suggest that use of too high a backfill frictional resistance may not be advantageous. Additionally the results demonstrate that some upward movement of the culvert crown of 2-3cm, due to the forced inward movement of the culvert during construction may be beneficial to the overall performance (through the development of positive arching) and efficiency of the flexible culvert system. However, a ϕ'_f of 20 degrees is very low for a granular fill. Data reported by Mayne and Kulhawy give ϕ'_f for sands and gravels of 30-50 degrees. In view of this recommendation of $\phi'_f=20$ degrees for a granular fill is unrealistic, reflecting only numerical convenience (value which gives the best numerical solution) rather than the physical properties of granular material.

8.3.4.5 Variation of the angle of Dilation, ψ'_f .

The shearing of a granular material can be illustrated by soil particles sliding over one another on planes inclined at an angle to the horizontal equal to the angle of dilatancy, ψ'_f , Fig 8.33. This shearing process is associated with yielding or failure of granular soils, dilatancy therefore describes the ratio of plastic strain increments $\delta\epsilon_v^p / \delta\epsilon_s^p$ (where $\delta\epsilon_v^p$ and $\delta\epsilon_s^p$ are increments of plastic volumetric and plastic shear strain respectively for situations of plane strain). In analyses the angle of dilatancy is used to define the direction and magnitude of plastic strain increment vectors, Fig 8.34. For a soil model incorporating an associated flow rule the angle of dilatancy is equal to the angle of friction ϕ' . The Mohr-Coulomb soil model used throughout the flexible culvert analyses employs a non-associated flow rule and therefore requires a description of the plastic strain increment ratio $\delta\epsilon_v^p / \delta\epsilon_s^p$ to define plastic strain vectors.

On placement of the backfill material the material is in a loose state. Subsequent compaction results in a decrease in volume of the material (contraction) as the soil particles are forced together and the material is converted to a dense state. It is this process which is being modelled in the finite element analyses and the angle of dilation input is negative to represent this contractant behaviour during compaction. The angle of dilation remains constant throughout the analysis. In hindsight this approach is not entirely reasonable. The magnitude of compaction pressure used ($25\text{kPa} < \text{CP} < 125\text{kPa}$) which for a granular fill is low, produced construction induced stress states which were typically entirely elastic. On application of the live load some local yielding above the

culvert crown did occur. It is recognised that the culvert behaviour would have been more accurately modelled had positive values of dilatancy been input to represent shearing of a compressed material. However, for completeness the results of the dilatancy study have been included here.

In this study the angle of dilation, ψ_f has been varied between -20 degrees (highly contractant material) and 0.0 degrees, which represents shearing at zero plastic volume change, $\delta\epsilon_s^p=0$. The effect of variation of the angle of dilation on the culvert behaviour is shown in Figs 8.35-8.38.

Construction induced thrusts around the culvert, especially at the culvert invert, are larger for the highly contractant backfill ($\psi_f=-20$ degrees) than for non-dilatant fill ($\psi_f=0.0$ degrees), Table 8.6 analyses MA27 and MA28. The difference however is small. In each case the construction crown radial stress and springline thrusts indicate that a condition of negative arching exists at the end of construction. Computed crown radial stresses are 20 and 16kPa for $\psi_f=-20$ and 0.0 degrees respectively. The overburden pressure at the culvert crown (γH) is approximately 15kPa. Additionally, simple equilibrium theory gives a springline thrust of approximately 85kPa. Analyses for $\psi_f=-20$ degrees and $\psi_f=0.0$ degrees gave springline thrusts of 93kN/m and 91kN/m respectively. In each case the computed quantities are larger indicating the condition of negative arching. The magnitudes of construction thrusts and degree of negative arching are larger for the contractant fill. Compaction of a contractant fill results in a decrease in volume $\delta\epsilon_s^p=-ve$, arising due to soil particles being pressed tightly together. This process causes an increase in the angle of friction and consequently a decrease in the earth pressure coefficient K_0 , Fig 2.2, which also implies a decrease in the horizontal stress generally within the soil. However, adjacent to culvert the contractant behaviour is causing the backfill to locally press up against the culvert inducing higher thrusts and generating larger crown displacement. As was seen previously for the variation of parameters, E'_f and ν'_f , large scale upward movement of the culvert crown is associated with the development of negative arching. As a result of the larger construction displacements induced by the more contractant fill, larger construction bending moments are induced around the culvert.

On application of the live load the culvert behaviour is reversed. For the dilatant fill the thrust has not been significantly increased and comparison of crown radial stress and springline thrusts with equivalent qualities determined from equilibrium theory, $\sigma_{rr}=74\text{kPa}$ and $N_{LL}=80\text{kN/m}$, indicates that a condition of positive arching has developed with the backfill. Application of the live load has significantly increased the

culvert thrust for the non-dilatant fill, Fig 8.35. For the same fill the radial stress is also increased, however the magnitude of crown radial stress indicates the development of some positive arching within the backfill. Live load displacements for the non-dilatant fill, Fig 8.38 are increased and significantly larger than that arising for the highly contractant fill. This behaviour has arisen because with the highly contractant behaviour (increased ϕ' giving a lower K_0 and a higher value of K_p) during construction high lateral soil pressures supporting the culvert were mobilised. However, for the non-dilatant fill these forces are lower and subsequently the culvert needs to displace more to mobilise the necessary backfill support.

The results indicate, as was noted previously, that to obtain an efficient soil-culvert system the backfill should be compacted to a high standard, which as described within the results for $\psi'_f = -20$ degrees, causes the backfill material to be the main load carrying structure and not the culvert as was seen for the non-dilatant fill.

8.3.4.6 Variation of the compaction pressure

Compaction of the backfill is necessary to provide a stiff, tightly compact material surrounding the culvert which will sustain the anticipated loads safely. In practice selection of a suitable magnitude of compaction pressure depends primarily on the backfill material such that the selected magnitude of compaction pressure is not sufficiently large to cause yielding or failure of the backfill or culvert, but also must be large enough to adequately compact the backfill material to render it capable of supporting any applied loads. In this case the actual magnitude of compaction pressure is unknown. An initial estimate of 25kPa has been selected, however it is recognised that this pressure loading is small and does not necessarily reflect that typically used in practice. Although compaction pressure is not a material parameter it is an essential part of the soil-culvert interaction problem. Therefore to determine its influence on the culvert behaviour and possibly obtain a more accurate magnitude, variation of the compaction pressure from 25kPa to 150kPa has been included in this study. The effect of variation of the compaction pressure on the culvert behaviour is shown in Figs 8.39-8.43.

As can be seen from Table 8.6, the construction thrusts vary directly with the increasing compaction pressure. From the range of compaction pressures studied greatest increase in the construction thrust is observed at the culvert invert and at the no-fines concrete plinths. Increasing the compaction pressure from 25kPa to 150kPa increased

the construction thrust at the invert and plinths from 90kN/m to 125kN/m respectively. This behaviour has arisen because with increasing compaction pressure the culvert sides are pushed further inwards forcing the culvert invert and crown to push outwards, making the shape of the culvert more oval. The larger displacements Table 8.9 associated with the high compaction pressures account for the higher construction induced bending moments. For a compaction pressure of 150kPa a maximum bending moment of 16kNm/m was obtained at the culvert crown, Table 8.7.

Construction radial stresses display a behaviour similar to the thrusts. From simple equilibrium theory, assuming a condition of neutral arching, a radial stress at the culvert crown of 14kPa was calculated. As can be seen from Table 8.8 computed construction radial stresses increase away from 14kPa with increasing compaction pressure, indicating the development of negative arching above the culvert crown. At low compaction pressures, CP=25kPa, the radial stress at the crown is 14kPa, increasing the compaction pressure to CP=150kPa increases the crown radial stress to 26kPa .

Construction shear stress, like radial stress, increases with increasing compaction pressure.

For compaction pressures, $25 \leq CP \leq 90\text{kPa}$, application of the live load causes an increase in the live load thrust around the culvert, Fig 8.39. The increase in live load thrust between 90kPa and 150kPa is very much smaller, maximum approximately 2kN/m. This behaviour is also observed in the live load bending moments and radial and shear stresses, Figs 8.40-8.42. Comparison of culvert crown live load radial stresses and springline live load thrust with similar quantities calculated from simple equilibrium theory indicates that a condition of positive arching has developed. This is common to all compaction pressures studied.

Live load crown displacements are not significantly influenced by the magnitude of construction pressure, Fig 8.43. However, the overall magnitude, under construction and live load combined, increases with increasing compaction pressure. This follows as the construction induced displacements are significantly influenced by the magnitude of compaction pressure. A similar behaviour is observed for the computed springline displacements.

The effect of varying the magnitude of the compaction pressure was not as significant as initially anticipated. Perhaps the most significant effect is the shape of the post-construction culvert. Low compaction pressures do not exert significant lateral soil

pressures on the culvert sides. The final end of construction shape is not significantly different from the initial undeformed shape. However, typically the culvert crown will have displaced beneath the original crown level. Increasing the compaction pressure renders the culvert more oval. Further increasing the compaction pressure further exaggerates this oval shape.

As noted previously this 'prestresses' the culvert crown region to further loading. Additionally significant upward movement can significantly benefit the development of positive arching across the culvert.

8.3.4.6 Effect of no-fines concrete plinths

The effect of the no-fines concrete plinths on the culvert behaviour was investigated by replacing the plinths by an equivalent area of backfill. In the field the no-fines concrete plinths were included in the design to reduce the bearing pressure at the corner joint of the culvert, where bearing pressures were expected to be high. The results of this study are presented in Figs 8.44-8.49. These results are compared with the results of the initial study presented previously in Figs 8.5-8.10.

As can be seen from Fig 8.44, the magnitude and distribution of the construction thrusts around the culvert are not significantly affected by omission of the plinths, except over the invert region ($0.0 \leq \theta \leq 40$ degrees), however even here the difference is small. A similar pattern of behaviour is observed for the construction bending moments, Fig 8.45, however over the invert region the bending moment is of different sign indicating a differing displacement behaviour when the plinths are omitted.

The most evident influence of omission of the plinths is on the construction radial and shear stress distributions between the culvert invert and springline ($0.0 \leq \theta \leq 90$ degrees), Figs 8.46-8.47. The construction radial stress distributions between the culvert springline and crown ($90 \leq \theta \leq 180$ degrees) for the two cases, with and without plinths are approximately equal. The occurrence of the maximum radial stress is still at $\theta=70$ degrees, location of the plinths, however omission of the plinths has reduced the magnitude of this maximum to approximately 45kPa from 100kPa with plinths. The occurrence of negative radial stress at $\theta=40$ degrees (indicating tension in the backfill) is eliminated when the plinths are omitted. For the same case the radial stress over the base of the invert ($0.0 \leq \theta \leq 20$ degrees) are small, maximum 5kPa. A similar form of behaviour is observed for the shear stress distribution around the culvert for the two plinth conditions. However, in this case for the condition of no plinths the

magnitude of the maximum shear stress is approximately -12kPa, reduced from 55kPa. The location of this maximum is still at $\theta=70$ degrees. The change in sign of the shear stress in this region for the no plinths condition indicates that the backfill in this region is trying to push the culvert upwards

The magnitudes of construction crown and springline displacements (construction stages 1-9) are significantly larger for the case of no plinths Fig 8.48 and Fig 8.49. It is evident from this that the plinths are restricting the construction induced lateral displacements and subsequently restricting the movement of the culvert crown.

Omission of the plinths has not resulted in any significant change in the live load thrust nor live load radial shear stress distributions (Figs 8.44, 8.46 and 8.37 and Figs 8.5, 8.7 and 8.8). Culvert live load displacements are approximately the same at the crown for both plinth conditions. The live load springline displacements are also similar, however as anticipated the springline displacement is larger for the no plinths condition. The difference however is small.

Examination of the culvert springline thrust and the culvert crown radial stresses at the end of construction and after application of the live load for both plinth conditions indicate that the developed arching conditions, negative arching at the end of construction and positive arching after application of the live load, remain unchanged.

As can be seen from the results no adverse condition has arisen from exclusion of the plinths, e.g. reversal of arching action. It has been shown that the radial and shear stresses imposed on the culvert are reduced if the plinths are omitted. Therefore for the height of fill considered, the plinths may not be beneficial to the culvert behaviour.

8.3.4.7 Discussion

Soil model material parameters have been varied and their influence on the culvert behaviour has been identified. Additional factors (not material parameters) such as the compaction pressure and effect of inclusion of the no-fines concrete plinths on the culvert behaviour have also been investigated.

From the study it was found that each of the material parameters varied had an influence on the culvert behaviour, however the degree of significance of each parameter on the culvert behaviour varied. Poisson's ratio of the backfill material was found to be the most significant material parameter on the culvert behaviour, as even small changes in the magnitude of Poisson's ratio were significant. For example a

decrease in ν_f from 0.3 to 0.0 was found to increase the culvert thrusts and bending moments by a factor of ten. The sensitivity of the culvert behaviour to even small changes in Poisson's ratio of the backfill significantly outweighed the influence on the culvert behaviour following variation of the remaining material parameters.

Parameters, angle of internal friction, ϕ'_f , and the angle of dilation, ψ_f , were also found to have significant effect on the culvert behaviour, however their influence on the computed solution was not as significant as Poisson's ratio. Nevertheless, a change of $\phi'_f=5$ degrees (increasing ϕ'_f from 35 degree to 40 degrees) was found to increase the live load thrust by approximately a factor of 2. A similar result was observed for an increase in ψ_f from -5 degrees to 0.0 degrees.

In this study the initial value of Young's modulus of the backfill was obtained indirectly from plate loading tests performed on the backfill material immediately after construction. Typically, values of the angle of internal friction ϕ'_f , and angle of dilation, ψ_f of a granular backfill can be reasonably well estimated using the conventional shear box test. Given the sensitivity of the culvert behaviour to changes in Poisson's ratio of the backfill, which in practice is typically estimated from past experience of similar material, the accuracy with which these tests can estimate the required material parameters may be sufficient and more complex and costly testing procedures may not be necessary.

From the parametric study performed and comparison of the results with estimate of the culvert behaviour using simple equilibrium theory it was found that typically negative arching occurred at the end of construction. The amount of this may be directly proportional to the magnitude of the culvert displacements (crown and springline) occurring at the end of construction. Positive arching developed on application of the live load. The degree of the positive arching above the culvert was found to depend on the magnitude of the live load culvert displacements, such that the smaller the crown displacement the larger the degree of arching. It has been shown previously that the magnitudes of displacements arising at either the end of construction or after application of the live load are a function of the magnitude of the lateral soil pressures induced within the backfill. The greater the lateral soil pressures induced during construction the larger are the culvert displacements. Conversely, live load displacements are smaller the greater the magnitude of the soil lateral pressures. Therefore, it follows that the degree and sign of arching (negative or positive) is also a function of the magnitude of the lateral soil pressures present within the backfill.

From the parametric study it was found that the compaction pressure was of influence on the culvert behaviour, particularly the culvert construction displacements. However, the significance of the compaction pressure was overshadowed by the sensitivity of the culvert behaviour to variation of the backfill value of Poisson's ratio.

The influence of the no-fines concrete plinths on the culvert behaviour was also investigated. It was found that the plinths were of no significant use to the culvert behaviour. Therefore, for this culvert cover depth the benefit of inclusion of such a structure within a culvert design is questionable.

A review of the results of the parametric studies with the observed data indicates that the initial finite element prediction can be suitably improved by increasing the compaction to 100kPa or alternatively by simply further reducing the value of Poisson's ratio to either 0.0 or 0.1. These low values of Poisson's ratio are considered to be unrealistic. A review of compaction pressures used in similar flexible culvert studies does suggest that the initial estimate of 25kPa is low and a compaction pressure of the order of 100kPa is more realistic. A compaction pressure of this magnitude was found to give a good comparison with the observed behaviour, however the observed thrust at the culvert crown is still significantly overestimated.

The computed culvert crown displacements after application of the live load for this magnitude of compaction pressure are slightly larger, -0.87cm compared to a value of -0.8cm, obtained for a compaction pressure of 25kPa. The measured crown displacement in the field was approximately -0.8cm. As can be seen the difference is very small and further demonstrates that the magnitude of compaction pressure used during construction does not have a significant effect on the live load behaviour.

The observed magnitude of live load thrust at the culvert crown was only reproduced for a backfill value of friction $\phi'_f=20$ degrees, however the thrusts at the remaining positions around the culvert were poorly reproduced. Additionally, the culvert bending moments and displacements for this analysis were also significantly underestimated. As mentioned previously, a $\phi'_f=20$ degrees is not considered to be reasonable nor representative of granular backfills used in practice. In practice granular backfills typically have $\phi'_f=40-45$ degrees.

The live load bending moments are more accurately reproduced for values of ϕ'_f equal to 40 or 45 degrees. However, for these values the live load thrust and live load crown displacements are significantly overestimated. For example the live load thrust at the culvert crown for $\phi'_f=40$ degrees is overestimated by approximately a factor of 8. The maximum live load thrust is overestimated by a factor of 1.5. Live load crown

displacements are overestimated by approximately a factor of 2. A similar result as that obtained for $\phi'_f=40$ and 45 degrees was obtained by increasing ψ'_f towards 0.

From comparison with the observed data it was considered that the initial parameter set selected previously was sufficient to describe the foundation soil provided the compaction pressure was increased to 100kPa analysis (MA3). Unfortunately this increase in compaction pressure cannot be corroborated due to the absence of construction data. A further check on the suitability of the selected material parameters can be made by plotting the computed culvert live load crown thrusts and crown displacement against increasing applied live load and comparing the resulting profiles with those observed, Fig 8.50. Computed results are for a compaction pressure of 100kPa (analysis MA3). As can be seen from Fig 8.50(a) computed and observed crown thrusts are in reasonable agreement up to an applied live load of approximately 200kN. At applied live loads greater than 200kN predicted thrusts are overpredicting those by as much as 3-4 times. This suggests that for applied loads greater than 200kPa, analysis are underestimating the degree of positive arching occurring within the backfill and therefore inaccurately modelling the redistribution of stress within the culvert.

Computed and observed displacement responses over the range of available data are in reasonable agreement, Fig 8.50(b). This suggests that the developed method is more accurate at predicting culvert crown displacements than thrusts.

Throughout the parametric study use was made of Duncan's design method (Duncan, 1979) to check the finite element results. During the course of these comparisons it was found that Duncan's method provided a good estimate of the culvert behaviour. Culvert thrusts however were typically overestimated but culvert bending moments, particularly live load moments were reasonably well reproduced. This is similar to the findings of Duncan (1979) and Beal (1982), however Beal (1982) found that the culvert bending moments were not well predicted using Duncan's method.

8.4 Loading case B

8.4.1 Introduction

This part of the load test was performed when the depth of cover to the culvert crown was increased to 1.2m. As in case A, the backfill material like consisted of crushed sandstone. A full description of this part of the trial loading is given in section 8.2. As with the previous load test the trial loading was performed up to a maximum trailer load of 455kN.

In this study analyses have been performed using the maximum trailer load of 455kN, which for the given depth of cover depth the culvert crown is equivalent to a live load of 160kN/m.

Analyses have been performed using the basic finite element mesh developed for case A, however for this study the height of elements above the culvert crown was increased to give a total height of 1.2m to model the required cover depth. The finite element mesh is shown in Fig 8.51.

The study for this load test has been performed in a similar way to that for case A, where the same initial parameter set was used but a compaction pressure of 100kPa has been used to provide an initial first estimate of the observed live load behaviour. The results of this initial analysis are presented in section 8.4.1. Available measured data for this load test are only available for the maximum applied live loading of 455kN. Parametric studies have also been performed to assess the influence of each of the material parameters on the culvert behaviour at this fill depth. As with case A the effects of the compaction pressure and no-fines concrete plinths at this cover depth have also been included. The results of these studies are briefly described in section 8.4.3.

8.4.2 Initial analysis

The initial backfill and culvert material parameters are unchanged from those used previously to describe the culvert and backfill in case A. In this case however the compaction pressure is 100kPa. The results of this analysis are presented in Figs 8.52-57. The main results of this analysis are also shown in Table 8.11, analysis MB3/MY4..

8.4.2.1 Culvert thrusts

The distribution of thrust around the culvert is of similar form to that described previously in case A. The magnitudes of construction thrusts around the culvert are higher than in case A due to the greater height of backfill above the culvert crown. However, construction thrusts at the culvert springline for cases A and B are approximately equal. This has arisen because for case B a condition of positive arching has developed within the backfill transferring some of the load away from the culvert. From simple equilibrium theory the construction thrust at the springline is estimated at 110kN/m, which is greater than that computed from analyses. For case A, negative arching was found to have developed.

Finite element analysis estimated the end of construction crown radial stress, σ_{rr} to be equal to approximately 40kPa, some 15kPa larger than that estimated from equilibrium theory. This suggests that negative arching ($A=-0.4$) has developed in the backfill. However, the springline thrusts (see above) indicate positive arching. The high crown pressure, indicating negative arching, is thought to be a local effect resulting from the magnitude of the culvert stiffness assumed in analyses. In analyses the culvert stiffness is assumed to be the same in both bending and ring compression. As a result, the culvert as modelled is stiff in bending and can therefore support high fill thicknesses above the crown. It has been long been recognised that in the field culverts are weak in bending but stiff in ring compression (Richards, 1982). As a result, in situ measurements of culvert springline thrusts indicate negative arching for the structure as a whole due to their high ring compression stiffness (Selig et al., 1979 and Richards, 1982). Low crown pressures, indicating the local occurrence of positive arching, typically develop due to the low bending stiffness of flexible culverts which significantly reduces the heights of backfill which can be supported above the culvert crown (Selig et al., 1979). Therefore, to improve the match between the observed culvert behaviour (generally) and that computed some reduction of the culvert stiffness over the crown region may be required.

As for case A the maximum live load thrust was found to occur at the culvert quarter-points. Using equilibrium theory the live load springline thrust and crown radial stress are estimated to be approximately 80kN/m and 43kPa respectfully. Finite element analysis determined the live load springline thrust and crown radial stress to be equal to 38kN/m and 14kPa. This implies that a degree of positive arching of approximately 0.67 has developed. This behaviour is similar to that observed for loading case A.

Computed and observed live load thrusts, Table 8.11, do not compare well, particularly over the crown of the culvert, $140 \leq \theta \leq 180$ degrees. The computed and observed live

load thrust in the vicinity of the springline do however compare well. This indicates that the development of positive arching in this region has been accurately reproduced in analyses. Computed live load thrusts over the crown region of the culvert suggest that the degree of positive arching is overpredicted in analyses.

Using Duncan's method of design (Duncan, 1979) gives a maximum live load thrust of 160kN/m, calculated from K_{p3} data obtained for the load applied over culvert quarter-points. However using K_{p3} data for the load applied over the crown gives a thrust of 96kN/m, which is approximately equal to that observed. Clearly, using Duncan's method as recommended gives a factor of safety of approximately 1.5-1.7 on the maximum culvert live load thrust.

For comparison the live load thrust calculated from ring compression theory (White and Layer, 1960) gives a thrust of 80kN/m, some 16kN/m lower than that observed. Additionally, using the method of Burns and Richard (1964) gives a live load thrust of 215kN/m for the condition of no slippage and 260kN/m for the full slip condition. Live load thrust estimated using the method of Burns and Richard are significantly larger than those computed in analyses.

8.4.2.2 Bending moment distributions

The distribution and magnitude of bending moments around the culvert are similar for cases A and B. For case B the maximum construction bending moment occurs at approximately the springline, previously for case A the maximum was observed to occur at the culvert crown. Live load bending moments for case B, particularly over the top region of the culvert, $90 \leq \theta \leq 180$ degrees, are smaller than those computed for case A. This behaviour has arisen because for case B the magnitudes of culvert displacements are smaller than those computed for case A due to the development of positive arching from the culvert.

Computed and observed live load bending moments are not accurately predicted for $140 \leq \theta \leq 180$ degrees, but are reasonably well reproduced for $90 \leq \theta \leq 140$ degrees. In the absence of measured construction data, the reason for this is uncertain particularly as the observed crown live load displacement (-0.75cm) is predicted reasonably well (-0.7cm). It may be attributed to the overpredicted degree of positive arching occurring after application of the live load.

Bending moments estimated using Duncan's design method, of 4kNm/m and 9kNm/m, underpredict the maximum finite element construction bending moments by a factor of three and overpredict the computed live bending moment also by a factor of three. The

live load bending moment computed using Duncan's method (9kNm/m) compares well with that observed in the field.

Using the Burns and Richard's method gives a maximum live load bending moment of 2.5kNm/m and 3kNm/m for the conditions of no slippage and full slippage respectively.

8.4.2.3 Radial stress

The distribution of radial stress around the culvert is similar to that observed for case A with the maximum construction stress occurring at the no-fines concrete plinths, $\theta=70$ degrees. The free-field vertical stress, σ_{yy} at the culvert crown for case B is 25kPa. The finite element analysis predicts a vertical stress at the culvert crown of 41kPa at the end of construction, indicating negative arching is occurring. The magnitude of negative arching which is occurring can be defined using relation (7.1) (Allgood and Takahashi, 1964). Using relation (7.1) gives a degree of arching equal to -0.64. Applying relation (7.1) to case A to define the degree of negative arching occurring at the end of construction gives -0.71. This shows that the degree of negative arching is less for case B. This follows as the height of backfill for case B is larger. In analyses a degree of positive arching was observed for both case histories, however direct comparison of live load effects is not possible due to the different magnitudes of live load in each case.

No measured radial stress data are available for this trial loading. Therefore the accuracy of the model to predict the stress distribution around the culvert cannot be properly assessed.

Using Burns and Richard's method (Burns and Richard, 1964) to determine the live load radial stress at the culvert crown and springline, gives 64kPa and 90kPa for the conditions of no slippage and full slippage respectfully at the crown. Similarly, the analysis giving 114kPa and 92kPa at the springline for the conditions of no slip and full slip. These values are significantly larger than those determined using the finite element analysis.

8.4.2.4. Shear stress

The distribution of radial stress around the culvert is similar to that computed for case A. The magnitudes of construction shear stresses due to the greater height of backfill bearing down on the culvert are larger for case B than case A. Maximum construction shear stress occurs at the culvert plinths. Maximum live load shear stress (30kPa) occurs over the top region of the culvert at $\theta=160$ degrees.

Using Burns and Richard's method, to provide some check on the computed shear stress, gives a maximum shear stress of 51kPa (condition of no slip).

8.4.2.5 Culvert displacements

The magnitude of computed crown live load displacements (-0.8cm) compares well with that observed (-0.75cm). Using the method of Burns and Richard to determine live load crown displacements gave -0.8cm and -0.91cm for the conditions of no slip and full slip. In this case the computed values compare well with those observed in the field.

Computed live load springline displacements are 0.22cm. Using Burns and Richard's method the springline displacement is 0.7cmm and 0.82cm for no slip and full slip. The IOWA deflection formula (Spangler and Hardy, 1982) gave a live load springline displacement of 1cm. However, as noted previously in section 8.3.3.5 for case A this method is very sensitive to the chosen magnitude of the deflection lag factor and modulus of soil reaction, E'_R . Using a lower drag factor of 1.25 (as recommend for design) gives a springline deflection of 0.6cm, which is closer to that computed using finite element analysis.

8.4.2.6 Discussion

From the results of the analysis presented it is evident that the initial parameter set have not provided a good estimate of the observed behaviour for this load test. The only reasonable predictions, for the live load culvert crown displacement, are overshadowed by the poor predictions of the culvert live load thrusts. Clearly some improvement to the material parameters is required if more accurate predictions of this load test are to be made. As for case A improvements to the material parameters are considered in the form of a parametric study in the following section.

The most accurate predictions of the live load thrust and bending moment were obtained using Duncan's method. Estimation of these quantities using Burns and Richard's method significantly overestimated the thrusts and significantly underestimated the bending moments. The reason for this is thought to be due to the omission of the construction procedure on culvert behaviour in the Burns and Richard method. Estimates of the crown displacement were made using finite element analysis and the analytical method of Burns and Richard. Both methods provided reasonable estimates of the observed behaviour. The finite element analysis was however the most accurate.

Comparison of the computed finite element culvert crown radial stress with that computed from simple equilibrium theory, indicated that at the end of construction negative arching was occurring. However, comparison of springline thrusts indicated the occurrence of positive arching. The development of high crown pressures suggesting negative arching are thought to be a local effect resulting from inaccurate modelling of the culvert bending stiffness over the culvert crown. After application of the live load a state of positive arching was found to have developed. This behaviour is similar to that found for case A after application of the live load. However, at the end of construction springline thrusts indicate negative arching for the structure as a whole. The degree of arching induced within the soil will be investigated further in the parametric studies.

8.4.3 Case B; parametric study

8.4.3.1 Introduction

The outline of the parametric study is similar to that performed for case A, where each of the soil model material parameters is varied in turn and their effect on the behaviour of the culvert is noted. The effects of the no-fines concrete plinths and magnitude of the compaction pressure are also included.

The parametric study follows the same order as the soil material parameters are required by CRISP. Assessment and subsequent adjustment of the soil material parameters is included in the discussion presented in section 8.4.3.7. The main results of analyses are shown in Tables 8.12 to 8.16.

8.4.3.2. Effect of backfill Young's modulus, E'_f

The effect of varying the backfill Young's modulus on the culvert behaviour is shown in Fig 8.58. Young's modulus of the backfill, E'_f has been varied between 20 and 120kPa. As can be seen from Fig 8.58(a) the construction thrust varies directly with the backfill Young's modulus, i.e. increasing E'_f increases the construction thrust however the variation is typically small. For case A the construction thrust remained approximately constant through variation of E'_f . Variation of E'_f has little effect on the construction induced thrusts over the culvert crown region, $180 \geq \theta \geq 140$ degrees. Variation of E'_f becomes significant in the vicinity of the springline where an increase in E'_f to 120MPa from 20MPa increases the construction thrust at the springline by approximately 20kN/m. From consideration of simple equilibrium theory, the construction thrust at the culvert springline is approximately 110 kN/m. For the range of backfill Young's modulus studied, $20\text{MPa} \leq E'_f \leq 120\text{MPa}$, the range of springline construction thrust is, $77 \leq N_{\text{con}} \leq 95\text{kN/m}$. In each case the computed thrust is less than that calculated using equilibrium theory and assuming neutral arching. This implies that positive arching is occurring at the end of construction. As can be seen from Fig 8.59(a) the magnitude of crown rise at the end of construction varies directly with the backfill Young's modulus up to approximately $E'_f=80\text{MPa}$. End of construction crown arising at values of $E'_f > 80\text{MPa}$ are approximately constant. Inward movement of the culvert springline at the end of construction, Fig 8.59(b) varies approximately directly with the backfill modulus up to $E'_f=80\text{MPa}$, beyond this the springline displacement is approximately constant.

The end of construction culvert displacement behaviour is not immediately obvious from Figs 8.59(a) and 8.59(b). As a result the displacement histories at the culvert crown and springline for $E'_f=20\text{MPa}$ and 120MPa (analyses MB8 and MB6 respectively) are also shown, Fig 8.59(c) and 8.59(d). As can be seen from Fig 8.59(c) crown displacements up to construction stage 7 are greater for the low stiffness fill ($E'_f=20\text{MPa}$; analysis MB8). This behaviour has arisen because the low E'_f will displace more (vertically and laterally) under compaction loads therefore pressing the culvert inwards. The lateral displacement of the springline during construction is shown in Fig 8.59(d) and as can be seen the inward movement of the springline is largest when the culvert is embedded in a low E'_f backfill. The maximum construction crown displacement arising at construction stage 7 is approximately equal for the both the low stiffness and high stiffness backfills. The reason for this behaviour is the different displacement responses of the two backfills considered. The low stiffness backfill, as mentioned previously, is displacing more around the culvert therefore inducing a different culvert displacement response. This is most evident from Fig 8.59(d) between

construction stages 6 and 7. As can be seen from Fig 8.59(d) between construction stages 6 and 7 the springline displacement associated with the stiff backfill displays a small increased inward movement of -0.061cm, however springline displacement associated with the low stiffness backfill show an outward displacement of 0.03cm. This has arisen because the low stiffness fill is displacing more around the culvert and pressing on different areas of the culvert, giving the different culvert displacement responses. Following placement of backfill above the culvert crown (construction stages 7-9), associated crown and springline displacements are significantly larger for the low stiffness backfill than those arising for the high stiffness backfill. This is because under the weight of the backfill above the crown the low stiffness backfill cannot generate the necessary lateral support to sustain the outward movement of the culvert springline. The higher stiffness backfill can generate greater resistance to the outward movement of the culvert and consequently end of construction crown displacement (Fig 8.59(a)) are of greater magnitude than those associated with a low stiffness backfill. This argument also applies to the end of construction springline displacements.

The behaviour described above is similar to that reported by Shmulevich et al., (1986) investigating stress distributions around cylinders buried in sand.

As can be seen from Fig 8.58(b) the live load thrust varies inversely (except at the crown) with the backfill Young's modulus, E'_f . The thrust behaviour at the culvert crown appears erratic, but increases with increasing E'_f up to $E'_f=80\text{MPa}$ then decreases to $E'_f=120\text{MPa}$. The reason for this behaviour is unclear. The inverse relationship displayed is very different from that described by case A, where the live load thrust was found to vary approximately directly with the backfill Young's modulus, E'_f . The reason for this difference in behaviour may be attributed to the smaller cover depth to culvert span ratio, H/S . For case A, on application of the live load the low cover depth is initiating failure of elements directly above the culvert crown, which may be exaggerating the degree of positive arching. As a result computed live load thrusts at low values of E'_f are smaller. For case B the variation of springline live load thrusts decreases with increasing E'_f , indicating that the magnitude of positive arching (equilibrium gives a live load thrust at the springline of 80kN/m) is increasing with increasing E'_f . This is attributed to the increased horizontal force within the backfill associated with higher values of E'_f (Shmulevich et al., 1986). The degree of positive arching occurring locally above the culvert crown is evident from consideration of the live load crown radial stresses. Using relation (7.1) this local degree of arching is shown in Fig 8.60(a). The degree of arching occurring locally above the culvert crown at the end of construction is also shown. As can be seen this local degree of arching at

the of construction is negative and remains approximately constant with varying E'_f . This behaviour is also reflected in Fig 8.60(b) showing end of construction crown radial stress, σ_{rr} with varying E'_f .

Variation of E'_f does not have a significant influence on either the construction or the live load induced bending moments, Fig 8.61. Over the range of values of E'_f studied the maximum difference in construction and live load bending moments is 4kNm/m. For $E'_f=20\text{MPa}$ the maximum construction bending moment occurs at the culvert springline, whereas for $E'_f=120\text{MPa}$ the maximum construction bending moment occurs at the culvert crown. In each case the magnitude of the maximum construction moments is the same, 12kNm/m. The reason for this behaviour is the higher end of construction crown displacement, Fig 8.59(a), inducing larger hogging (positive) moments over the culvert crown region, associated with the higher values of E'_f . As described previously the higher crown construction displacements are due to the larger lateral soil pressures induced at the culvert sides. For a culvert embedded in a high E'_f fill, $E'_f=120\text{MPa}$, these high lateral soil pressures are restraining the culvert side walls from pushing outwards as the fill is placed above the culvert crown and consequently inhibiting the development of bending moment around the culvert sides. For culverts embedded in low stiffness fills, e.g. $E'_f=20\text{MPa}$, the magnitude of lateral soil restraint at the culvert sides is less than that for a high E'_f fill and consequently the end of construction culvert crown displacement is considerably lower. As a result of this, crown bending moments are lower. Additionally, the lower backfill restraint at the culvert sides cannot prevent the culvert sides from pushing outwards under the increasing weight of backfill above the culvert crown. As can be seen from Fig 8.59(b) this outward movement for low E'_f backfills can be substantial and accounts for the maximum construction bending moment occurring at the culvert springline.

Live load bending moments, Fig 8.61 decrease with increasing E'_f . This behaviour reflects the increasing magnitude of positive arching or decreasing crown pressure occurring locally above the culvert crown with increasing magnitude of E'_f . The occurrence of positive arching for the structure as a whole, transferring load away from the culvert, also accounts for the live load bending moment being zero at the culvert springline.

The final property to be considered here is the shear stress distribution. As can be seen from Fig 8.62 the construction and live load shear stress vary inversely (except at the quarter points) with E'_f . The change in shear stress for the range of E'_f values considered is not significant for the effects of construction or live load.

8.4.3.3 Variation of Poisson's ratio

As described previously the effect of variation of Poisson's ratio is to alter the magnitude of the in situ horizontal stress, σ_{xx} and subsequently vary the degree of arching support within the backfill. The degree of arching support decreases with decreasing value of Poisson's ratio. For $\nu'_f=0.4$ arching support in the backfill is maximum and conversely for $\nu'_f=0.0$ arching support in the backfill is minimum. The effect of Poisson's ratio on the degree of arching support is best shown through description of the culvert thrust and radial stress. Variations of the culvert thrust and radial stress are shown in Figs 8.63 and 8.64, the degree of arching, A (Allgood and Takahashi, 1964) is shown in Fig 8.65 obtained from the radial stress at the culvert crown.

As can be seen from Fig 8.63 the culvert construction thrusts at the quarter points and springline vary directly with Poisson's ratio. Construction thrusts at the crown vary approximately inversely with Poisson's ratio. Live load thrusts at the culvert crown, quarter points and springline follow a similar pattern of behaviour as found previously for case A and vary approximately inversely with Poisson's ratio. From comparison of springline thrusts obtained from consideration of equilibrium, construction thrusts for $0.0 \leq \nu'_f \leq 0.2$ indicate positive arching and for $0.3 \leq \nu'_f \leq 0.4$ negative arching is occurring as a whole for the structure. On application of the live load the behaviour changes and positive arching is occurring at all values of Poisson's ratio studied. The degree of arching is however decreasing with decreasing Poisson's ratio as the computed springline live load thrust is tending towards that calculated from equilibrium theory (assuming neutral arching) of 80kN/m.

The end of construction radial stress Fig 8.64(a) the culvert crown and springline display a similar behaviour to the construction thrust. At the quarter points the end of construction radial stress up to $\nu'_f=0.2$ varies inversely with ν'_f . At $\nu'_f>0.2$, the radial stress increases to 54kPa for a $\nu'_f=0.4$. This local change in behaviour at culvert quarter points has arisen due to the decrease in the magnitude of degree of negative arching, Fig 8.65, occurring locally at the culvert crown. This is causing soil pressure at the crown, at values of Poisson's ratio $\nu'_f=0.3-0.4$, to be redistributed around the top region of the culvert.

The radial stress displays a similar behaviour to the thrust for the live load behaviour. As can be seen from Fig 8.65 the degree of arching, A , occurring at the culvert crown due to a local increase in crown soil pressure, is negative at the end of construction. The degree of negative arching is decreasing with increasing Poisson's ratio, as Poisson's ratio tends towards $\nu'_f=0.4$ the degree of arching tends towards neutrality, i.e. $A=0$. On application of the live load positive arching exists for all values of Poisson's

ratio locally above the culvert crown. The degree of arching is again increasing with increasing Poisson's ratio.

Variation of Poisson's ratio was not found to have a significant influence on the construction induced bending moments at crown, quarter points or springline, Fig 8.66(a). A similar behaviour was found at the culvert quarter points and springline after application of the live load. Crown live load bending moments between $0.0 \leq \nu' \leq 0.2$ vary approximately inversely with ν'_f . At $\nu'_f > 0.2$ the crown live load bending moments are approximately equal. The reason for this behaviour is due to the deformation response of the culvert to the applied construction and live loading. As described previously (section 8.4.3.2) the culvert displacements are a function of the earth pressures generated within the backfill and the displacement response of the backfill against the culvert sides. Culvert crown and springline displacements are shown in Figs 8.66(a) and 8.66(b). The effect of variation of ν'_f on both the culvert bending moment and displacement responses is similar to that described previously for variation of E'_f .

Shear stress, except at the quarter points, varies approximately inversely with Poisson's ratio, Fig 8.68, and as can be seen from Fig 8.68 the magnitude of shear stress, particularly live load shear stress, is a function of the degree and condition of arching which exists within the backfill.

8.4.3.4 Variation of the angle of internal friction, ϕ'_f

The effect of varying the angle of friction, ϕ'_f , on the culvert behaviour is shown in Fig 8.69-8.74. It was shown previously that altering the angle of internal friction influences the magnitude of active earth pressure mobilised at the culvert springline during construction. The active earth pressure mobilised at the culvert sides during placement of a low ϕ'_f backfill ($\phi'_f = 20$ degrees) is larger than that for a high ϕ'_f backfill ($\phi'_f = 45$ degrees). The most significant influence of this is evident from the construction induced culvert displacements, Fig 8.69. The larger active earth pressures induced during the construction process for a low ϕ'_f backfill have driven the culvert sides inwards resulting in significant upward movement of the culvert crown. As a result of this, the construction induced bending moments for this type of backfill are significantly larger than for a high ϕ'_f backfill, Fig 8.70. The large displacements associated with low ϕ'_f backfills tend to increase the degree of positive arching which will occur at the culvert springline, and decrease the degree of negative arching occurring locally at the culvert crown, Fig 8.71. As can be seen from Fig 8.71 this local degree of arching tends towards neutrality as the angle of internal friction is decreased.

The construction shear stress distribution around the culvert is typically higher for a low ϕ'_f backfill because the backfill has been compacted around the culvert, against which the culvert must move, Fig 8.72.

For a low ϕ'_f backfill on application of the live load subsequent culvert displacements are small, Fig 8.69. This is due to the high magnitude of positive arching which is occurring for the culvert as a whole. Computed (finite element) springline thrusts are approximately 5kN/m for $\phi'_f=20$ degrees, some 16 times smaller than that obtained considering equilibrium, Fig 8.73. Additionally, for $\phi'_f=20$ degrees the crown pressure increased by some 3kPa after application of the live load, Fig 8.74(b). As can be seen from Fig 8.71 this implies a local degree of positive arching at the crown of approximately 0.95. This magnitude of positive arching indicates that in analyses a considerable amount of redistribution of load away from the culvert and into the backfill is occurring. In this case the degree of positive arching which is occurring may be being amplified by the occurrence of failure within elements of soil above the culvert crown. The degree of arching associated with a culvert embedded within a high ϕ'_f soil ($\phi'_f>40$ degrees) is lower than that discussed previously. As a result, a smaller amount of redistribution of load away from the culvert is occurring and consequently live load culvert displacements are larger. Live load bending moments for the high ϕ'_f fill are also higher, Fig 8.70, due to the larger culvert displacements.

8.4.3.5 Effect of compaction pressure

The effect of the magnitude of compaction pressure on the culvert behaviour has been briefly considered previously during the parametric study for case A. In this case the effect of the compaction pressure has been investigated more closely.

As can be seen from Fig 8.75, the increased compaction effort at the culvert sides during construction has increased the inward movement of the culvert sides and consequently increased the culvert vertical movement. Placement and compaction of fill above the culvert crown has recovered much of this initial distortion of the culvert using a low compaction pressure. This is because during construction a low compaction pressure did not cause any significant rise (or 'peaking') of the culvert crown; for a compaction pressure of 25kPa a maximum crown rise of approximately 1.1cm was computed. For high compaction pressures much of the initial distortion (maximum 4cm) remains at the end of construction. This behaviour has arisen because the backfill material is of sufficient stiffness to restrict any further lateral movement of

the culvert. The increased compaction effort has also increased the construction bending moments induced around the culvert due to the larger culvert displacements associated with the use of higher compaction pressures, Fig 8.76. The greater movement of the culvert against the backfill, associated with the use of higher compaction pressures has resulted in increased shear stress distributions around the culvert, Fig 8.77.

Increased forced lateral displacement of the culvert sides typically results in a higher degree of positive arching at the culvert springline. This behaviour is evident from Fig 8.78. At low compaction pressures, $CP < 50\text{kPa}$ negative arching has developed at the culvert springline. This behaviour is attributed to the outward movement of the culvert springline following the completion of the construction procedure.

The magnitude and condition of arching occurring above the culvert crown at the end of construction can be examined from consideration of the radial stress, Fig 8.79. As can be seen from Fig 8.78 at the end of construction, following the use of high compaction pressures, a condition of negative arching exists locally, indicating high soil pressures above the culvert crown. This follows as with a high compaction effort greater soil pressures have been locked into the backfill. As the compaction effort is reduced the degree of negative arching decreases. At a $CP = 25\text{kPa}$ an approximate condition of neutrality exists.

Previously for case A the effects of the magnitude of compaction pressure did not have a significant effect on the culvert live load displacement. In this case however the effects of varying the magnitude of compaction are significant on the magnitude of the live load displacement. As can be seen from Fig 8.75 the live load displacements at the culvert crown and springline increase with increasing magnitude of compaction pressure. At a compaction pressure of 25kPa the resulting live load displacements at the crown and springline are some 25 and 40 percent lower than those occurring following compaction of the backfill using 125kPa . The reason for this may be the presence of the no-fines concrete plinths. In the case of the low compaction pressure, at the end of construction crown displacement has been recovered, $\Delta y = 0.093\text{cm}$, the springline displacement is 0.17cm outwards or beyond the original undeformed culvert position. On application of the live load the springline displacement was only increased to 0.25cm , an increase of 0.08cm . The concrete plinths therefore may be restricting any further lateral movement of the culvert beyond the undeformed culvert position. As a consequence of the small culvert live load displacement for this case the live load bending moments are also small.

Live load bending moments induced around the culvert are small and do not exhibit any significant variation following variation of the compaction pressure, Fig 8.76. A

similar behaviour is displayed by the live load shear stresses induced around the culvert, Fig 8.77.

Live load radial stress and live load thrusts are shown in Fig 8.79 and Fig 8.80. As can be seen, increasing the compaction pressure from 20kPa to 120kPa does result in a significant increase in the thrust or radial stress. Greatest increase occurs at the springline and for each case the increase is approximately 50%. It is evident from the springline thrust and crown radial stress that a condition of positive arching exists across the full width of the culvert. The degree of arching however increases with decreasing compaction pressure.

8.4.3.6 Effect of no-fines concrete plinths

To determine the effect of the concrete plinths on the culvert behaviour at this increased cover depth, the initial analysis has been re-run and the concrete plinths replaced by equivalent backfill parameters. The results of this analysis are presented in Fig 8.81-8.86. For comparison the result of the initial solution, plinths included, is also shown.

From the results it is evident that the concrete plinths do not have a significant influence on culvert thrusts and bending moments. However exclusion of the plinths has reduced the culvert construction bending moment at the culvert springline. The reason for this is the significantly increased inward lateral movement of the culvert sides during construction. Removal of the plinths has significantly increased the culvert displacements, indicating that the plinths are restricting the deformation response of the culvert.

The most significant result arising from the removal of the plinths is the significant reduction of the radial and shear stress at the plinths location, approximately 70 degrees.

It is evident from the results that exclusion of the plinths does not have an adverse effect on the culvert behaviour. As was found for case A inclusion of the plinths in the culvert design does not appear to be significantly beneficial to the overall performance of the culvert.

8.4.3.7 Discussion

From the parametric study it has been shown that the culvert behaviour is most sensitive to variations of Poisson's ratio, ν'_f and the angle of internal friction, ϕ'_f . Variation of the parameter ψ'_f was not included in this study, however previously for case A it was found that increasing this parameter towards zero was significant. The similarity of the culvert behaviour for each of the case studies suggests that variation of ψ'_f would also be significant in this case. As for case A, the optimum set of material parameters most accurately describing the observed culvert behaviour are not considered to be entirely realistic nor descriptive of the backfill material.

In section (8.4.3.2) it was shown that the initial set of backfill material parameters did not provide a reasonable estimate of the observed culvert behaviour. Previously in case A it was found that reducing the value of Poisson's ratio to 0.0 or 0.1 significantly improved the accuracy of the predictions, however for this study, although analyses are sensitive to Poisson's ratio, decreasing Poisson's ratio to $\nu'_f < 0.2$ does not have as significant effect on the accuracy of the predicted result. The magnitude of the maximum live load thrust is reproduced, however the magnitude of thrust over the culvert crown is underestimated by approximately a factor of 1.5. Additionally, live load bending moments are underestimated by a factor of 2. However, the observed crown displacement is reasonably well reproduced. It should be noted that reducing Poisson's ratio to less than 0.2 is unreasonable and not descriptive of typical engineering fills.

Greatest improvement to the accuracy of the analyses was achieved from increasing the value of ϕ'_f to 40 degrees. The increase in the culvert live load thrust and bending moment given the small increase in ϕ'_f , 5 degrees, demonstrates that analyses are sensitive to variations of ϕ'_f . With ϕ'_f equal to 40 degrees the observed culvert live load thrusts and bending moments are reasonably well reproduced. The live load crown displacement is overpredicted by approximately a factor of 2.

Previously for case A it was found that reducing ψ'_f towards zero degrees gave a similar result to increasing ϕ'_f to 40 degrees. Given the similarity between the result of the two parametric studies it is likely that reducing ψ'_f to 0.0 degrees in this case will also provide a similar result to ϕ'_f equal to 40 degrees.

The influence of Young's modulus, E'_f , of the backfill and the compaction pressure for case B is less than that found previously for case A. This suggests that the significance of E'_f and the compaction pressure is dependent on the cover depth, H and diminishes with increasing cover depth.

From the results available from the parametric study, it is evident that the observed culvert behaviour can be more accurately predicted by simply altering a single parameter, ϕ'_f to 40 degrees, an increase of 5 degrees. However for this analysis the observed crown displacement is overestimated by a factor of 2.

Inclusion of the concrete plinths within the culvert design was found not to have a significant influence on the culvert behaviour, except that it restricted the culvert displacements, which have been beneficial to the culvert behaviour at low compaction pressures, following application of the live load. Removal of the concrete plinths from the design did not result in any adverse condition for the culvert.

From the parametric studies it was found that the degree and condition of arching, positive or negative, occurring at the end of construction and after application of the live load, is primarily dependent on the magnitude of lateral earth pressures induced at the culvert sides during construction. Parameters ν'_f and ϕ'_f significantly influenced the degree and condition of arching at both the end of construction and after application of the live load. The magnitude of compaction pressure applied during construction also has a significant influence on the degree and condition of arching occurring at the end of construction; however, it does not significantly influence the degree of arching after application of the live load. Throughout the parametric study for case B it was found that positive arching occurred after application of the live load, above the culvert crown and at the springline.

Finally, the results of the parametric studies have shown that the developed approach to model the culvert can provide reasonable predictions of the culvert behaviour. Careful consideration to parameter selection is required and the parametric study has shown that parameters ν'_f , ϕ'_f and ψ'_f require the most careful selection. The sensitivity of analyses to these parameters does show that complex testing to determine values of the backfill modulus may not be necessary.

8.5 Trial loading, case C

8.5.1 Introduction

Immediately after completion of load test, case B the backfill material (crushed sandstone) was excavated and re-constructed to a height of approximately 0.7m above the culvert crown. The backfill material was then overlain by a 0.3m thick layer of type 1 sub-base (coarse gravel) material and pavement layers consisting of approximately

0.2m of bituminous-bound materials. The pavement layer comprised a 0.1m thick layer of dense bitumen road base, a 0.06m thick dense bitumen base course and a 0.04m thick hot rolled asphalt wearing course. The fill cover depth above the culvert crown was approximately 1.2m. This load test was performed to determine the effect of the pavement layers on the culvert behaviour by direct comparison with load test case B.

The load test was performed in the same way as for cases A and B. As for case B measured data are only available for a maximum loading of 455kN or an equivalent line load of 160kN/m applied above the culvert crown. Measured data include culvert live load thrusts, bending moments and crown deflection. No measured data are available for the construction procedure.

Comparison of the measured results of load tests B and C (Johnson et al., 1988) found that inclusion of the pavement reduced the maximum crown deflection by approximately 30% and bending moments by approximately 50%. The culvert thrust was observed to increase by as much as 25% over the top region of the culvert, $180 \geq \theta \geq 90$ degrees.

Load test C has been included to provide an additional case history with which to further assess the chosen method of analysis and approach to the flexible culvert problem. In this case only three predictions, using finite element analysis, were performed to provide a reasonable estimate of the observed behaviour. No further parametric studies were performed.

Details of the finite element mesh, backfill and pavement material parameters are given in section 8.5.2. The results of the analyses are presented in section 8.5.3 and the main findings of this study are discussed in section 8.5.4.

8.5.2 Description of analysis and parameters

The finite element mesh used to describe the culvert and foundation is shown in Fig 8.87. The mesh is the same as that used to describe case A; however, the sub-base and pavement layers have been added to give the required height above the crown. The bituminous pavement was described using the isotropic elastic soil model. Both the backfill and gravel sub-base were modelled using the elastic, perfectly plastic Mohr-Coulomb soil model.

The backfill (crushed sandstone) material parameters were taken to be equal to those used to describe the backfill in case A. The height of backfill above the culvert crown for cases A and C is the same, 0.7m. For this height of backfill the initial set of parameters selected for case A provided a reasonable estimate of the observed

behaviour using a compaction pressure of 100kPa. Therefore for a suitable first approximation these parameters were considered appropriate, and therefore also used to describe the backfill present in load case C. A compaction pressure of 100kPa was used to compact the backfill and granular sub-base. The compaction pressure was also applied to the top of the bituminous pavement layer to represent the weight of construction traffic used to press the completed pavement layers.

The material parameters used to describe the granular sub-base (crushed limestone) are shown in Table 8.17. As can be seen the parameters c'_{sb} (cohesion) and Poisson's ratio ν_{sb} are equal to those assumed for the backfill material. The value of the sub-base Young's modulus, E'_{sb} was selected from published data (Temporal et al., 1985 and Temporal and Johnson, 1988) describing plate loading tests performed on similar backfill material (crushed limestone) prior to flexible culvert testing. A value of angle of internal friction of $\phi'_{sb}=35$ degrees was also selected from published data (Temporal and Johnson 1988; Craig 1987 and Mayne and Kulhawy, 1982).

The pavement was described using the isotropic elastic soil model, material parameters used to describe this model are shown in Table 8.18. A value of the pavement Young's modulus, E_{pav} , was assumed equal to 600MPa and was selected from published plate loading test data (Croney, 1977; Powell et al., 1984 and Temporal and Johnson, 1988). A value of Poisson's ratio for the pavement, $\nu_{pav}=0.35$ was also selected from published data (Powell et al., 1984 and Temporal and Johnson, 1988).

8.5.3 Results of analyses

This section is divided into two sub-sections. The first section 8.5.3.1 compares the results of the initial analysis of case C with the measured data. The second section 8.5.3.2 compares the results of case C and the results of corresponding analyses from case B.

The results of the initial analysis for case C are presented in Figs 8.88-8.93. For comparison with the observed data the main results of this analysis are shown in Table 8.19. Also shown are the corresponding results for case B. Measured data are only available for the culvert behaviour after application of the live load.

8.5.3.1 Case C; results

As can be seen from Table 8.19 computed live load thrusts compare reasonably with those observed. Over the region of $180 \geq \theta \geq 160$ degrees the computed live load thrusts underestimate those observed, however the difference is small, maximum 10%. Computed live load thrusts overestimate those observed by a maximum of 12% over the region of $140 \geq \theta \geq 90$ degrees. From comparison of the computed live load springline thrust (71kN/m) with that estimated from equilibrium theory (80kN/m) it is evident that some degree of positive arching is occurring as a whole for the culvert. However, measured thrust data from the springline region ($\theta=110$ degrees) suggest that the degree of positive arching predicted here is smaller than that occurring in the field. Similarly, comparing the computed crown radial stress (35kPa) with that estimated from equilibrium theory (43kPa) also indicates that positive arching is occurring locally above the culvert crown. Relation (7.1) suggests a degree of arching, A equal to 0.2.

Predicted live load bending moments compare well with those observed, particularly at the culvert crown. Overall the computed bending moments are overpredicting those observed, however the difference is small.

The computed live load crown displacement (-1.05cm) overpredicts that observed (-0.52) by approximately a factor of 2. Previous predictions of the live load crown displacement for cases A and B were more accurate. From parametric studies performed for cases A and B it was found that increasing Poisson's ratio towards 0.4 decreased the culvert displacements. Therefore, some improvement to the predicted crown displacement can be made by increasing the value of Poisson's ratio of the backfill. However, this will also reduce the accuracy of the predicted thrust and bending moments.

Finite element analysis computed a live load springline deflection of 0.18cm. Using the principle of superposition and applying the IOWA deflection formula (Spangler, 1941 and Spangler and Hardy, 1982) gives a maximum springline deflection of 0.413cm. In this case a drag factor D_L of 1.25 (recommended) was used and values of the modulus of soil reaction E'_R for the sub-base and pavement layers were determined using the ratio of Young's modulus of these layers with that of the backfill material. A modulus of soil reaction of $E'_R=55\text{MPa}$ was assumed for the backfill material.

Previously for cases A and B, for all the alternative analytical methods used to analyse the flexible culvert behaviour described here, it has been found that Duncan's design method (Duncan, 1979) gives the most accurate results. Applying this method here for case C gives a maximum live load thrust and bending moment of 96kN/m and

8kN/m respectively. These values are very similar to those observed however the live load thrust has underestimated that observed by approximately 10%.

8.5.3.2. Comparison of case B and C

In this section the results of case C are compared with those obtained from the corresponding analysis from case B.

As can be seen from Fig 8.94 the distribution and form of construction thrusts for case C are similar to those of case B. Over the region of $180 \geq \theta \geq 90$ degrees the construction thrusts for case C are larger by 10%. The construction thrust over the region $140 \geq \theta \geq 90$ degrees are larger for case B by approximately 20%. The lower springline thrusts for case C indicate that a greater degree of positive arching is occurring for this case than for case B, when compared to the springline thrust obtained from simple equilibrium theory (110kN/m). Ring compression theory (White and Layer, 1960) which only takes into account the area of backfill directly above the culvert crown, gives a springline thrust of approximately 80kN/m. Comparison of the finite element computed thrust with that of ring compression theory would suggest that negative arching is occurring.

Construction radial stress distribution for cases C and B, Fig 8.95, are also similar, however the construction radial stresses for B are typically smaller than that for case C. Additionally, radial stress at the culvert crown suggests a higher degree of negative arching is occurring locally for case C (-0.76) than for case B (-0.64), however the difference is small.

On application of the live load the thrusts induced within the culvert for case C are approximately twice as large as those for case B. Analyses have provided a more accurate description of the live load thrusts for case C than for case B. Live load springline thrusts for case B and C are 38kN/m and 71kN/m respectively. Equilibrium theory gives a springline thrust of 80kN/m. This suggests that overall a higher degree of positive arching is occurring for case B than for case C. Similarly, from crown live load radial stress, a higher degree of positive arching is occurring locally at the culvert crown (as a result of a local decrease in crown pressure) for case B ($A=0.67$) than for case C ($A=0.18$). The degree of arching occurring above the culvert crown for case C is similar to that computed for case A ($A=0.11$). The lower degree of positive arching occurring within the backfill around the culvert for case C does suggest that addition of the pavement layers is causing the culvert to attract more load, giving rise to the higher live load thrusts and radial stress distributions. It is evident from comparison of

measured live load thrust data for case C (Table 8.19) and case B (Table 8.11(a)) that this behaviour is the same as that observed.

Construction bending moments Fig 8.96 for cases B and C are approximately equal, for the springline moments, where the moment for case B is some 1.5 times greater than that for case C. This is due to the larger inward construction springline displacement for case C (-0.32cm) which has reduced the curvature of the culvert in this region. Live load bending moments for the case C are typically larger than those computed for case B, however the difference is small.

Live load crown displacement for case C is some 0.3cm larger than that for case B. This is the opposite behaviour to that observed in the field. The live load springline displacement for case B (-0.22cm) is larger than that for case C (-0.18cm). The larger crown displacement for case C may suggest that the degree of arching occurring locally above the culvert crown is significantly underestimated (or overestimating the magnitude of radial stress at the culvert crown).

8.5.4 Discussion

From comparison of the computed and observed results it is evident that the selected material parameters have provided a reasonable estimate of the observed culvert live load behaviour. However, the optimum set of parameters which has emerged is considered not to be entirely descriptive of the actual physical behaviour of the backfill. Values of E'_f were estimated from in situ plate loading tests data (Johnson et al., 1989). These values of E'_f modulus have provided a reasonable description of the backfill, however in the absence of more detailed soils testing for E'_f , no firm conclusions can be drawn. It is recognised that the plate loading test is only reliable if the backfill is known to be reasonably uniform over the depth of the foundation. Consequently, minor local weaknesses near the surface of the foundation can significantly influence the results of the test and hence influence the perceived foundation behaviour.

An alternative to the plate loading test is the standard penetration test performed down percussion drilled boreholes or hand-probing equipment at various depths through the foundation. The resulting standard penetration test resistance, N , can then be correlated to Young's modulus using some empirical relation.

In this study (Mytholmroyd) low values of Poisson's ratio ($\nu'_f=0.2$) were required to ensure a reasonable prediction of the live load thrusts. From relation (8.6) $\nu'_f=0.2$ implies a low earth pressure coefficient, K_0 of 0.25 or alternatively from Fig 2.2 a high angle of shearing resistance, $\phi'_f=50$ degrees (approximately). This is not consistent

with the value of ϕ'_f assumed ($\phi'_f=35^\circ$). As can be seen from Fig 2.2, the resulting value of K_o associated with $\nu'_f=0.2$ is outwith the trend of available experimental data. Additionally, the Mohr-Coulomb soil model provides a further constraint (or limit) on the chosen value of Poisson's ratio, relation (8.10).

$$\frac{\nu'_f}{1 - \nu'_f} = \frac{1 - \sin \phi'_f}{1 + \sin \phi'_f} \quad (8.10)$$

Where $\left(\frac{\nu'_f}{1 - \nu'_f}\right) = K_o$ and $\frac{1 - \sin \phi'_f}{1 + \sin \phi'_f} = K_A$, the active earth coefficient.

In the Mohr-Coulomb soil model K_A is a limiting earth pressure coefficient, as a result, values of $K_o < K_A$ cannot be stably sustained. This condition therefore, imposes a lower limit on the value of Poisson's ratio. For a $\phi'_f=35^\circ$ the limiting value of Poisson's ratio, ν'_{fl} , is approximately 0.21, which is approximately consistent with the value assumed in analyses. However, reducing ν'_f to less than ν'_{fl} is not consistent with the Mohr-Coulomb limiting condition. In sections 8.3.4.3. and 8.4.3.3. the value of ν'_f was reduced to 0.0 to illustrate the influence of ν'_f on analyses. However, in view of relation (8.10) reducing $\nu'_f < \nu'_{fl}$, for a Mohr-Coulomb soil is not realistic. Consequently the influence of varying Poisson's ratio on the predicted results (Figs 8.22-8.27 and Fig 8.63-8.68) is not as significant as was first thought. As can be seen from the above figures, variation of ν'_f only becomes significant as ν'_f approaches the Mohr-Coulomb limit, ν'_{fl} .

Except for case B, resulting values of ϕ'_f which have emerged from the analyses in order to provide reasonable results are low. Optimum values of ϕ'_f for cases A and C are considered not to be realistic nor descriptive of the backfill described in this study. Typical values of ϕ'_f for engineering granular fills associated with culvert construction are of the range 40-45 degrees.

In practice the shear box test is typically used to estimate the angle of dilation, ψ , of granular soils. A typical direct shear test result (shear box) for dense and loose Ottawa sand (Taylor, 1948) is shown in Fig 8.97, where P is the normal load; Q is the shear load and corresponding displacements x and y of the boundaries of the shear box, Fig 8.97(c). Using the shear box the angle of dilatancy is given by relation (8.11).

$$\psi = \tan\left(\frac{-\partial y}{\partial x}\right)^{-1} \quad (8.11)$$

where upward movement of the shear box top boundary is defined as negative.

As can be seen from Figs 8.97(a) and 8.97(b) failure of both the dense and loose sand samples is associated with a rise (-ve y) of the shear box top boundary. This behaviour arises because as the sand is sheared it expands to overcome the interlocking of the sand particles therefore, from Fig 8.33 implying a positive angle of dilation.

In analyses it is assumed that the backfill is placed in a loose state and is compressed (by the action of the compaction pressure) to a dense state. Comparison of Figs 8.97(a) and 8.97(b) suggests that during the process of compacting the backfill should failure occur (either local or global) then an expansion of the backfill will occur. Therefore, specifying negative values of the angle of dilatancy to describe the plastic deformation response of the backfill is unrealistic and is not consistent with the observed response of granular soils during shearing.

Previously numerical predictions of the live load behaviour for cases A and B were most accurate for predictions of the culvert crown displacement, predictions of the thrust and bending moment were less accurate. Parametric studies performed for these studies indicated that the accuracy of predictions could be suitably improved through small adjustment of soil material parameters. Poisson's ratio, ν'_f , the angle of internal friction, ϕ'_f , and the angle of dilation, ψ'_f . Therefore, in this case if predictions of displacement were important, a more accurate prediction of the crown displacement could be made through increasing the value of Poisson's ratio towards 0.4 or decreasing either the value of ϕ'_f or ψ'_f . In each case this will reduce the accuracy of the predictions of thrusts and bending moments. Therefore, simultaneous accurate prediction of the main elements of the culvert behaviour (thrusts, bending moments and displacements) may not be possible.

The arching behaviour for case C is similar to that for case B at the end of construction; however, the degree of arching is typically larger for case B. For case C after application of the live load negative arching was found to occur locally at the culvert crown. Positive arching was found to occur for case B after application of the live load. Therefore, incorporation of the pavement layers to the problem has altered the distribution of load to the culvert and subsequently induced the culvert to attract more load. This may be attributed to the smaller springline displacement for case C which suggests that higher lateral restraint within the backfill material has been induced causing the culvert to attract more load.

Predictions of the culvert live load behaviour, thrusts and bending moments, have also been made using Duncan's design method (Duncan, 1979). Predictions using this method compare well with those observed, particularly for the live load bending moment. Predictions of live load bending moments induced on shallow cover culverts are important (Duncan, 1979 and Beal, 1982) as the transient live loads (not considered here) induced by construction traffic can induce high bending moments within the culvert causing it to buckle and possibly collapse. Duncan's method as well as the finite element analysis, in this case, indicate that prior warning of possible adverse bending within the culvert can be given by using these methods. The finite element analysis and Duncan's design method have provided reasonable predictions of the culvert behaviour and used together may provide a reasonable design.

8.6 Conclusions

A back analysis study of a pipe arch culvert under different cover conditions has been performed using finite element analysis. From comparison of the observed and computed culvert response conclusions can be drawn on the ability of the developed approach to model flexible culvert behaviour and, in general, the behaviour and design of flexible culverts under shallow cover conditions.

From back analysis of the trial loading an optimum set of parameters has emerged which provides a reasonable estimate of the observed behaviour. However, the resulting parameters, particularly ν'_f and ϕ'_f , are considered to be unrealistic and consequently are providing an inaccurate description of the backfill. This implies that in this case the Mohr-Coulomb soil model is inappropriate for describing the backfill behaviour. The simplicity of the Mohr-Coulomb soil model may therefore be causing inaccurate soil parameters to emerge.

The Mohr-Coulomb soil model is typically classified as a first-order approximation of soil behaviour (Brinkgreve and Vermeer, 1992). The pre-failure behaviour is described using Hooke's law of elasticity. This law is fully described by two soil parameters E'_f and ν'_f , which for all pre-failure stress states remain constant. In view of the discussions presented in chapters 3-6, this description of the pre-failure behaviour of soils, even for simple loading situations, is unrealistic. The backfill surrounding a flexible culvert has a complex loading history; the complexity emerging due to the compaction process. The compaction process, which should be considered as a transient, surficial load of finite lateral extent (Seed and Duncan, 1986) can impose significant stress/strain variations throughout the backfill. It has been discussed at

length in chapters 3-6 that the magnitude of elastic stiffness mobilised is a function of the strain induced within the soil, consequently, the variations of strain induced by the compaction process will give rise to gradients of elastic stiffness within the backfill surrounding the culvert. This behaviour has important implications for the choice of soil model used to describe the backfill material. Evidently, a soil model incorporating non-linear elasticity is an obvious improvement to the simple Mohr-Coulomb soil model.

The dependency of elastic stiffness on the level of stress/strain within the backfill requires an accurate description of the stresses and strains within the backfill, in particular those induced during the compaction process. During the compaction process the backfill is undergoing multiple cycles of loading and unloading. A standard feature of loading and unloading cycles of soils is hysteresis (reloading and unloading stress paths are not coincident). Studies performed by Seed and Duncan (1986) have found that the degree of hysteresis occurring, even on pre-yield stress paths, can be significant. The influence of the hysteretic behaviour is to cause residual (or locked-in) stresses to be induced within the backfill following each cycle. The complex hysteretic behaviour of soils cannot possibly be modelled in a simple linear elastic soil model.

The significant variations of stress which can be induced during the construction procedure, through relation (8.6), implies that v'_f should also vary with stress level. The Duncan-Chang and Seed and Duncan soil models both include a non-linear variation of v'_f with stress level.

Soil models incorporating stress/strain dependent elastic stiffness and/or Poisson's ratio which are used to describe flexible culvert behaviour could be further enhanced if the hysteretic behaviour is also included. The Seed and Duncan soil model (Seed and Duncan, 1986) is an example of a soil model which incorporates hypoelasticity and the hysteretic behaviour associated with the compaction process. Using this soil model the observed behaviour of the Tice Valley (flexible) culvert (Duncan and Jeyaplan, 1982) was predicted reasonably well. Despite the good agreement between the computed and observed responses, the Seed and Duncan soil model only considers pre-failure stress states. Consequently, local failure within the backfill and its subsequent influence on the predicted results cannot be modelled. Back analysis of flexible culverts under backfill (compaction) and live loads (Mohamedzein, 1989 and Dessouki and Monforton, 1986) indicate that the effects of local failure on the flexible culvert behaviour can be significant. In the analyses described in this chapter local failure was found to occur; the significance of which was not clearly quantified. However, the occurrence of local failure of the backfill adjacent to the flexible culvert was found to give rise to small localised areas over which positive arching was occurring. The

degree of arching occurring in these areas was typically the opposite to that occurring overall.

The Mohr-Coulomb soil model incorporates a failure criterion which for generalised stress paths induced during the compaction process (volumetric deformations are dominant, $\delta s > \delta t$) is not considered to be appropriate. Stress paths describing loading where the volumetric response is dominant are following a response which is entirely elastic. This description of soil behaviour is unrealistic and consequently a mean stress cap should be introduced to limit the magnitude of elastic volumetric strains. Numerical studies performed by Mohamedzein (1989) using the Seed and Duncan soil model, modified to include a mean stress cap yield surface, indicate that inclusion of the mean stress cap can provide improved predictions of flexible culvert behaviour.

Soil models incorporating, non-linear elasticity, hysteresis and a mean stress cap yield surface, are complex and require many soil parameters. The modified Duncan soil model with a cap yield surface requires 12 soil parameters. Except for very complex flexible culvert designs, this number of soil parameters is typically higher than that which is tolerated in practice. Additionally, flexible culvert designs in Great Britain are rarely of sufficient complexity to justify the use of higher-order soil models. However, where the complexity arises, then the elements of soil behaviour discussed previously may be necessary to provide the required accuracy of numerical predictions.

Throughout this study (Mytholmroyd) plane strain analyses were performed. Imposing the condition of plane strain on analyses implies that the ends of the culvert are sufficiently remote to ensure that the culvert deformation response at mid-section is predominantly in the plane of the culvert cross-section. Deformations perpendicular to this plane (along the culvert length) are assumed to be negligible. Additionally, in analyses the longitudinal stiffness has also been ignored. In view of the transient and finite extent of the compaction loading (only a small area of backfill is compacted at any one time) the longitudinal behaviour of the culvert may be significant, particularly on the culvert deformations and thrusts. Additionally, along the length of the culvert the interface conditions will also be significant. Consequently, minor slippage (arising due to temperature gradients and/or inadequate compaction) between the culvert and backfill will also be significant particularly on the culvert thrusts. In view of this, the flexible culvert behaviour may be more accurately modelled if the original three dimensional problem is maintained. Adopting three dimensional modelling of the culvert should enable the compaction process to be modelled more accurately. The transient and finite extent (in three dimensions) of the compaction loads could be modelled by an element by element compaction process. Additionally, three

dimensional modelling will enable a more accurate representation of the applied live loading.

Throughout this study the main concern of analyses was to reproduce the observed live load behaviour of the culvert. However, as previously discussed the behaviour of flexible culverts is significantly influenced by its loading history, and consequently an accurate description of the construction behaviour is required. Here, no data for the construction behaviour are available therefore, the accuracy of the developed approach at describing the construction behaviour cannot be assessed.

Previous studies performed by Davies et al. (1993) of the construction behaviour of the Newport (Armco) culvert (Temporal et al., 1985) provided a reasonable estimate of the observed behaviour. However, as was found in the study described in this chapter, selected material parameters, particularly Poisson's ratio ($\nu'_f=0.2$), are not thought to be entirely descriptive of the backfill material (crushed limestone fill). Despite the comprehensive and detailed measurement of stresses and strains induced within the culvert and backfill, analyses concentrated on reproducing culvert crown and springline displacements, thrusts and bending moments. This approach was also adopted (primarily due to the lack of field data) in the study described in this chapter (Mytholmroyd). In view of the complex interaction behaviour of the culvert and backfill, judging the ability of the developed approach to describe the construction and live load behaviour on the basis of limited data may not be reasonable. Culvert deformations and thrusts are end-products following the response of the backfill to an applied loading. Within the numerical framework the development of the culvert response and how accurately it has been modelled, has not been properly assessed. A more accurate assessment of the modelled culvert/backfill behaviour should involve a comparison of computed and observed stress paths at key positions within the backfill. Key stress/strain measuring positions within the backfill are considered to be adjacent to the crown, quarter points and springline (Selig et al., 1979 and Byrne et al., 1993). Additionally, these measuring positions should be located at varying distances from the culvert to enable accurate monitoring of the developing degree of arching. With these data a more accurate assessment of the developed approach to modelling flexible culvert behaviour should be able to be made.

Comparison of the computed and observed culvert response indicates that the adopted approach to modelling flexible culvert behaviour is capable of providing reasonable results. However, uncertainties remain and further work is required before any firm conclusions can be made. As was found previously for the soft clay analyses,

simultaneous prediction of the main elements of the culvert behaviour (thrusts, bending moments and displacements) was not possible.

Parametric studies determined that the predicted solution was dominated by the value of Poisson's ratio selected for the backfill material. The sensitivity of the culvert behaviour to even small changes in Poisson's ratio significantly outweighed the influence on the culvert behaviour following variations of the remaining model parameters. Parameters ϕ'_f , angle of internal friction and ψ'_f , angle of dilation, were also found to have a significant effect on the predicted culvert behaviour. The current modelling approach requiring specification of negative values of the angle of dilatancy is not considered to be reasonable. A more accurate approach to modelling the dilatant behaviour of the backfill would be to specify positive values of ψ'_f , therefore, reflecting published experimental data.

For the culvert as a whole negative arching was found to develop at the end of construction. After application of the live load positive arching was found to develop. Local variations of the overall degree of arching was found to occur at the culvert crown. This behaviour was found to be a result of a local increase or decrease in soil pressure over the top of the culvert. From the parametric studies it was found that the degree and condition of arching (positive or negative) occurring at the end of construction and after application of the live load is primarily dependent on the magnitude of lateral earth pressure induced at the culvert sides during construction. Typically, except for case B the resulting local degree of arching was the opposite to that which had developed globally.

Predictions of the culvert behaviour have also been made using traditional methods (hand calculations). Of the methods used Duncan's design method (Duncan, 1979) was found to provide the most accurate description of the culvert construction and live load behaviour. Given the complexity of most flexible culverts installed in practice it is thought that designs based on this method would be sufficient and the added complexities of finite element modelling may not be necessary. However, designs do arise where a more complex method of analysis is required. In these situations Duncan's method could be used to check the results of finite element analysis or alternatively be used to provide estimates of thrust and bending moment from which a suitable value of Poisson's ratio could be back analysed.

Table 8.1 Details of Mytholmroyd culvert (Johnson et al., 1989)

CULVERT PROPERTY	MYTHOLMROYD CULVERT
CULVERT PROFILE	HIGH PROFILE ARCH
SPAN, S(m)	5.95
TOP RADIUS, R(m)	3.01
DEPTH OF COVER, H(m)	0.7/1.2
PLATE THICKNESS, t(mm)	5.5
CORRUGATIONS (mm)	200x55
MOMENT OF INERTIA (mm ⁴ /mm)	2506
AREA OF SECTION (mm ² /mm)	6.51
LONGITUDINAL SEAMS	2
CULVERT MATERIAL	STEEL
YOUNG'SMODULUS, E(GPa)	205
YIELD STRESS, σ (kPa)	215

Table 8.2 Details of backfill material (Johnson et al., 1989)

PROPERTY	BACKFILL
BACKFILL MATERIAL	CRUSHED SANDSTONE
IN SITU BULK DENSITY (Mg/m ³)	2.20
IN SITU DRY DENSITY (Mg/m ³)	2.05
IN SITU MOISTURE CONTENT (%)	8.2
MAXIMUM DRY DENSITY (Mg/m ³)	2.15
OPTIMUM MOISTURE CONTENT (%)	8.4
IN SITU DRY DENSITY (Mg/m ³)	0.95

Table 8.3 Initial values of backfill material parameters (non-associated flow Mohr-Coulomb)

SOIL MODEL PARAMETER						
STRUCTURE	E' _f (kPa)	v' _f	c' _f (kPa)	ϕ' _f (degrees)	γ _f (kN/m ³)	ψ' _f (degrees)
BACKFILL	35x10 ³	0.2	0.2	35	21	-5

Table 8.4 Culvert and plinth material parameters (isotropic linear elastic soil model)

STRUCTURE	E (kPa)	ν	γ (kN/m ³)
CULVERT	15x10 ⁶	0.3	-
PLINTH	20x10 ⁶	0.2	24

Table 8.5 Initial analysis main results. Comparison of computed and observed data.

Table 8.5(a) Thrust behaviour

Measuring position on culvert (degree)	180	160	140	120	110	90	Details of material parameters used in numerical analyses
Observed live load thrust (kN)	12	95	85	-	40	-	
Analysis name							
MAI	120 67	55 67	133 66	152 70	125 84	122 94	
Fill Mohr-Coulomb model. $E'_f=35\text{MPa}$, $\nu'_f=0.3$ $c'_f=0.2$, $\phi'_f=35$, $\gamma_f=20\text{kPa}$, $\psi_f=-5$ Compaction pressure 25kPa. Rigid base at -3m below invert.							

Table 8.5(b) Bending moment behaviour

Measuring position on culvert (degree)	180	160	140	120	110	90	Details of material parameters used in numerical analyses
	Observed live load bending moment (kNm)	-10.0	4.0	2.0	-	-0.35	
Analysis name							
MA1	-0.4 6.3	1.1 3	-2.9 -3.5	1.5 -4.9	5 -5.0	0.1 -3	

(Combined construction and live load behaviour)
(Construction behaviour only)

(live load behaviour only)

Table 8.6 Parametric studies; Thrust

Measuring position on culvert (degree)	180	160	140	120	110	90	Details of material parameters used in numerical analyses
Observed live load thrust (kN)	12	95	85	-	40	-	
Analysis name							
MA1	120 67	55 67	133 66	152 70	80 77	125 84	Fill Mohr-Coulomb model. $E'_f = 35\text{MPa}$, $v'_f = 0.2$ $c'_f = 0.2$, $\phi'_f = 35$, $\gamma_f = 20\text{kPa}$, $\psi_f = -5$ Compaction pressure 25kPa. Rigid base at -3m below invert.
MA2	142 80	62 80	160 80	170 76	70 70	132 80	
MA3	155 95	60 92	172 82	180 78	66 69	130 82	
MA5	68 65	3 68	74 68	80 67	10 76	8 84	Same as MA1 but $E'_f = 20\text{MPa}$
MA8	118 65	53 66	130 66	142 68	49 76	36 84	Same as MA1 but $E'_f = 50\text{MPa}$
MA9	125 67	58 67	140 73	155 69	58 76	42 84	Same as MA1 but $E'_f = 70\text{MPa}$
MA10	96 80	13 81	100 81	102 74	20 71	16 82	Same as MA1 but $\phi'_f = 20$
MA12	158 62	96 63	182 63	211 68	95 77	74 84	Same as MA1 but $\phi'_f = 40$
MA13	157 59	98 60	180 60	211 65	96 77	79 81	Same as MA1 but $\phi'_f = 45$

Table 8.6 continued

Measuring position on culvert (degree)	180		160	140	120	110	90	Details of material parameters used in numerical analyses	
Observed live load thrust (kN)	12		95	85	-	40	-		
Analysis name									
MA14	146 76	70	173 73	196 68	167 71	189 78	114 85	29 85	Same as MA1 but $v'_f = 0.0$
MA15	143 74	69	162 70	185 68	158 73	145 80	131 85	46 85	Same as MA1 but $v'_f = 0.1$
MA16	74 69	5	79 70	85 71	86 76	93 85	90 83	7	Same as MA1 but $v'_f = 0.3$
MA18	74 70	4	79 71	86 71	86 76	93 86	90 83	7	Same as MA1 but $v'_f = 0.4$
M26	103 66	37	122 69	141 83	124 77	122 86	105 85	20	Same as MA1 but no plinths present
M27	160 64	86	182 69	214 72	175 82	156 87	138 91	46	Same as MA1 but $\psi_f = -0.0$ degrees
M28	72 68	4	78 70	86 72	90 78	98 78	99 93	6	Same as MA1 but $\psi_f = -20.0$ degrees

Table 8.7 Bending moment behaviour

Measuring position on culvert (degree)	180	160	140	120	110	90	Details of material parameters used in numerical analyses	
Observed live load bending moment (kNm)	-10.0	4.0	2.0	-	-0.35	-		
Analysis name								
MA1	-0.5 6.0	-5.5 2.6	1.8 -2.9	1.0 -3.7	4.7 0.3	-3.7 -0.4	4.50 -0.10 4.60	Fill Mohr-Coulomb model. $E'_f = 35\text{MPa}$, $\nu'_f = 0.2$ $c'_f = 0.2$, $\phi'_f = 35$, $\gamma_f = 20\text{kPa}$, $\psi_f = -5$ Compaction pressure 25kPa. Rigid base at -3m below invert.
MA2	3.3 10.4	-7.1 6	4.5 -2.5	1.4 -4	5.4 0.4	-8.5 -0.5 -8	9.6 -0.1 9.7	Same as MA1 but compaction pressure 90kPa
MA3	8 16	-8 9	7.5 -1.5	0 -5	5 0.4	-3 0 -3	13 0 13	Same as MA1 but compaction pressure 150kPa
MA5	4.7 5.5	-0.8 5.5	2.2 -0.5	-2.4 -3	0.6 0.17	-3 0 -3	6 0 6	Same as MA1 but $E'_f = 20\text{MPa}$
MA8	1.4 6.5	-5.1 6.5	2.0 -1.0	0.4 -3.7	4.1 0	-3.1 -0.3 -2.8	4.85 -0.16 5.01	Same as MA1 but $E'_f = 50\text{MPa}$
MA9	2.1 5.5	-3.4 5.5	2.5 -0.6	-1.0 3.8	2.8 0.25	-3.3 -0.4 -2.9	5 0 5	Same as MA1 but $E'_f = 70\text{MPa}$
MA10	9 10.8	-1.8 10.8	5.6 -0.4	-2.8 -4	1.2 0	-9 0 -9	9 0 9	Same as MA1 but $\phi'_f = 20$
MA12	-5.8 5.1	10.9 5.1	0 2.3	5.4 -3	8.4 0.2	-2 -1 -1	4 -0.6 4.6	Same as MA1 but $\phi'_f = 40$
MA13	-6.5 4.5	-11.0 4.5	-0.4 1.8	5.5 -3	8.5 0.28	-1.6 -1.0 -0.6	3.8 0.56 3.24	Same as MA1 but $\phi'_f = 45$

Table 8.7 continued

Measuring position on culvert (degree)	180	160	140	120	110	90	Details of material parameters used in numerical analyses						
Observed live load bending moment (kNm)	-10.0	4.0	2.0	-	-0.35	-							
Analysis name													
MA14	1.1 4	-3.9 2	1.4 2	-0.6 -2.4	-0.3 -2.4	2.1 -4.16	-4.06 -4.16	0.1 -3	-3 -3	0 7	7 7	-1.4 -0.3	Same as MA1 but $v'_f = 0.0$
MA15	-3.5 4.9	-8.4 0.5	2.5 0.5	-2.0 -2.8	3.7 -2.8	6.5 -4.6	-4.3 -4.6	0.3 -3.0	-3.4 -3.0	-0.4 5.7	5.7 5.7	-0.3	
MA16	4.8 5.4	-0.6 2.5	2.5 2.5	0 -3.2	-2.8 -3.2	0.4 -5.12	-5.0 -5.12	0.12 -3.5	3.5 -3.5	0 5.3	5.3 5.3	0	Same as MA1 but $v'_f = 0.3$
MA18	6 6.6	-0.6 3	3 3	0 -3.85	-3.4 -3.85	0.45 -5.4	-5.4 -5.4	0 -3.5	-3.5 -3.5	0 4.4	4.4 4.4	0	
MA26	1.4 6.7	-5.4 -3.3	2.4 -3.3	-0.79 -3.4	1.05 -3.4	4.6 -3.4	-5.6 -5.9	0.3 -4	-4.6 -4	-0.6 1.4	1.4 1.4	0	Same as MA1 but no plinths present
MA27	-5.7 5.75	-11.4 2.6	0.6 2.6	-2 -3.3	6 -3.3	9.3 -3.3	-4.4 -5.25	0.8 -3.3	-4.1 -3.3	-0.8 4	4.6 4	-0.6	
MA28	5.7 6.3	-0.6 3	2.9 3	-0.1 -3.6	-3 -3.6	0.6 -6.2	-6.2 -6.3	0.1 -4	-4 -4	0 5.6	5.6 5.6	0	Same as MA1 but $\psi_f = -20.0$ degrees

Table 8.8 Radial and shear stress

Parameter	Radial Stress (kPa)				Shear Stress (kPa)		Details of material parameters used in analyses					
Measuring position on culvert (degree)	180	120	90	Maximum	120	90						
Analysis name												
MA1	43 14	29 33	17	29 22	7	114 101	-12 5.0	-17 -14 -11.3 -2.7	31 53	-22	Fill Mohr-Coulomb model. $E'_f = 35\text{MPa}$, $\nu'_f = 0.2$ $c'_f = 0.2$, $\phi'_f = 35$, $\gamma_f = 20\text{kPa}$, $\psi_f = -5$ Compaction pressure 25kPa. Rigid base at -3m below invert.	
MA2	56 24	32 43	64 43	25 18	7	88 103	-26.6 1.6	-28 -13 -13 0	15 45	-30		Same as MA1 but compaction pressure 90kPa
MA3	56 26	30 46	69 46	21 13	8	100 110	-31 -5	-26 -18 -10	26 55	-29		Same as MA1 but compaction pressure 150kPa
MA5	20 16	4 37	3 34	25 23	2	102 105	2.4 5	-2.6 -5 -2.4 -2.6	55 58	-3		Same as MA1 but $E'_f = 20\text{MPa}$
MA8	45 15	30 33	50 33	28 21	7	80 93	-14 6	-20 -12 -10 -2	21 44	-23	Same as MA1 but $E'_f = 50\text{MPa}$	
MA9	50 17	33 33	52 33	28 21	7	81 98	-17 6	-22.5 -12.5 -10 -2.5	21 49	-28	Same as MA1 but $E'_f = 70\text{MPa}$	
MA10	31 21	10 40	47 40	27 24	3	114 120	-4.5 2	-6.5 -10 -6	60 69	-9	Same as MA1 but $\phi'_f = 20$	
MA11	27 19	8 37	43 37	25 22	3	96 100	-1.25 4	-5.25 -7.5 -4	40 47	-7	Same as MA1 but $\phi'_f = 28$	
MA12	74 14	60 30	63 30	36 24	12	75 100	-30 4	-34 -20 -18.3 -1.7	10 56	-46	Same as MA1 but $\phi'_f = 40$	
MA13	73 14	59 30	60 30	40 25	15	80 104	-30 4	-34 -20 -21 1	17 64	-47	Same as MA1 but $\phi'_f = 45$	

Table 8.8 continued

Parameter	Radial Stress (kPa)				Shear Stress (kPa)			Details of material parameters used in analyses		
Measuring position on culvert (degree)	180		120		90		Maximum			
Analysis name										
MA14	39	15	60	30	40	15	80	-24	-30 -34 -20 -21 17 -47 5 -1.6 35	Same as MA1 but $\nu'_f = 0.0$
	24		32		30		75			
MA15	66	43	63	31	38	9	54	-15	-32.4 -28 -15 -12 -8 -38 4.4 -3 30	Same as MA1 but $\nu'_f = 0.1$
	23		32		29		69			
MA16	22	2	35	4	30	4	80	-1	2.5 -0.5 -5.6 -1.9 27 -4 3 -3.7 31	Same as MA1 but $\nu'_f = 0.3$
	20		31		26		81			
MA18	22	4	34	3	23	2	101	-2	5.0 -2 -3.5 -1.8 46 -4 7 -1.7 50	Same as MA1 but $\nu'_f = 0.4$
	18		31		21		103			
MA26	45	30	48	16	36	8	46	4	-13.7 -18 -2 -15 -137 -18 4.3 -17 4.3	Same as MA1 but no plinths present
	15		32		28		42			
MA27	80	64	69	36	37	14	115	16	-30 -25 -20 -17.3 10 -45 5 -2.7 55	Same as MA1 but $\psi_f = 0.0$ degrees
	16		33		23		99			
MA28	23	2.7	37	4	24	2.4	105	2	4.3 -3 -6.4 -2 40 -4 7.3 -4.5 44	Same as MA1 but $\psi_f = -20.0$ degrees
	20		33		21.6		103			

Table 8.9 Displacement behaviour

Construction stage	End of construction	Live load and end of construction	Live load only	Measuring location on culvert	Details of material parameters used in numerical analyses
Observed in situ displacement (cm)	-	-	(crown) -0.8		
Analysis name					
MA1	0.65	-0.15	-0.80	Crown	Fill Mohr-Coulomb model. $E'_f = 35\text{MPa}$, $\nu'_f = 0.2$ $c'_f = 0.2$, $\phi'_f = 35$, $\gamma_f = 20\text{kPa}$, $\psi_f = -5$ Compaction pressure 25kPa. Rigid base at -3m below invert.
	-0.035	-0.029	0.006	Invert	
	0.0098	0.117	0.107	Springline	
MA2	1.8	0.93	-0.87	Crown	Same as MA1 but compaction pressure 90kPa
	0	0	0	Invert	
	-0.27	-0.13	0.14	Springline	
MA3	3.1	2.4	-0.7	Crown	Same as MA1 but compaction pressure 150kPa
	0.038	0.054	0.016	Invert	
	-0.68	-0.57	0.11	Springline	
MA5	0.15	-0.015	-0.165	Crown	Same as MA1 but $E'_f = 20\text{MPa}$
	-0.06	-0.06	0	Invert	
	0.156	0.188	0.034	Springline	
MA8	1.0	0.25	-0.75	Crown	Same as MA1 but $E'_f = 50\text{MPa}$
	-0.095	-0.01	0.005	Invert	
	-0.061	0.031	0.092	Springline	
MA9	1.20	0.68	-0.52	Crown	Same as MA1 but $E'_f = 70\text{MPa}$
	-0.021	-0.014	0.007	Invert	
	0.028	0.06	0.032	Springline	

Table 8.9 continued

Construction stage	End of construction	Live load and end of construction	Live load only	Measuring location on culvert	Details of material parameters used in numerical analyses
Observed in situ displacement (cm)	-	-	(crown) -0.8		
Analysis name					
MA10	2.34	2.07	-0.27	Crown	Same as MA1 but $\phi'_f = 20$
	0.027	0.031	0.004	Invert	
	-0.46	-0.42	0.04	Springline	
MA11	1.35	1.08	-0.27	Crown	Same as MA1 but $\phi'_f = 28$
	0.021	-0.019	0.002	Invert	
	-0.15	-0.11	0.04	Springline	
MA12	0.44	-1.5	-1.69	Crown	Same as MA1 but $\phi'_f = 40$
	-0.033	-0.02	0.013	Invert	
	0.073	0.275	0.20	Springline	
MA13	0.17	-1.5	-1.67	Crown	Same as MA1 but $\phi'_f = 45$
	-0.043	-0.021	0.022	Invert	
	0.131	0.340	0.21	Springline	
MA14	-0.566	-1.07	-0.504	Crown	Same as MA1 but $v'_f = 0.0$
	-0.166	-0.167	-0.001	Invert	
	0.335	0.416	0.081	Springline	
MA15	0	-1.39	-1.39	Crown	Same as MA1 but $v'_f = 0.1$
	-0.097	-0.092	0.005	Invert	
	0.190	0.388	0.198	Springline	
MA16	0.3	0.20	-0.1	Crown	Same as MA1 but $v'_f = 0.3$
	-0.05	-0.06	-0.01	Invert	
	0.084	0.103	0.019	Springline	

Table 8.9 continued

Observed in situ displacement (cm)	-	-	(crown) -0.8	on culvert	numerical analyses
Analysis name					
MA18	1.05	0.90	-0.15	Crown	Same as MA1 but $\psi_f = 0.4$
	0.05	0.05	0	Invert	
	0.480	0.585	0.105	Springline	
MA26	-1.1	0.3	-0.8	Crown	Same as MA1 but no plinths present
	-0.034	-0.035	-0.01	Invert	
	-0.3	-0.185	0.115	Springline	
MA27	0.61	-1.07	-1.68	Crown	Same as MA2 but $\psi_f = 0.0$ degrees
	0.01	0.225	0.215	Invert	
				Springline	
MA28	0.84	0.73	-0.11	Crown	Same as MA2 but $\psi_f = -20.0$ degrees
				Invert	
	-0.032	0.012	0.02	Springline	

Table 8.10. Initial values of backfill material parameters (non-associated flow Mohr-Coulomb).

SOIL MODEL PARAMETER						
STRUCTURE	E' _f (kPa)	ν _f	c' _f (kPa)	φ' _f (degrees)	γ _f (kN/m ³)	ψ' _f (degrees)
BACKFILL	35x10 ³	0.2	0.2	35	21	-20

Table 8.11 Comparison of computed and observed data

Table 8.11(a) Thrust

Measuring position on culvert (degree)	180	160	140	120	110	90	Details of material parameters used in numerical analyses	
Observed live load thrust (kN)	45	90	95	-	45	-		
Analysis name							Fill, M-C model. E' _f =35MPa, ν' _f =0.2, c' _f =0.2, φ' _f =35 Compaction pressure 100kPa. Rigid base at -3.00m.	
MB3/MY4	141	27	157	46	170	70		
	114		111		100			
					133	45	120	40
					88		80	

Table 8.11(b) Bending moment

Measuring position on culvert (degree)	180	160	140	120	110	90	Details of material parameters used in numerical analyses
Observed live load bending moment (kNm)	-8	2	2.5	-	0	-	
Analysis name							
MB3	6.5	-3.8	5	-0.8	-1.63	-10.4	Fill, M-C model. $E'_f=35\text{MPa}$, $\nu'_f=0.2$, $c'_f=0.2$, $\phi'_f=35$ Compaction pressure 100kPa. Rigid base at -3.00m.
	10.3		5.8		2.67	0.3	
					-8.4	12	
					0.2	0	
					-8.6	12	

(Combined construction and live load behaviour)
(Construction behaviour only)

(Live load behaviour only)

Table 8.11(c) Radial stress and shear stress

Parameter	Radial Stress (kPa)			Shear Stress (kPa)			Details of material parameters used in analyses
Measuring position on culvert (degree)	180	120	90	120	90	Maximum	
Analysis name							
MB3	55	14	64	19	35	11	7
	41		35		24	93	

Table 8.11(d). Displacement; crown, invert and springline.

Construction stage	End of construction	Live load and end of construction	Live load only	Measuring location on culvert	Details of material parameters used in numerical analyses
Observed in situ displacement (cm)	-	-	(crown) -0.75		
Analysis name					
MB3	0.01	-0.8	-0.81	Crown	Fill, M-C model. $E'_f=35\text{MPa}$, $\nu'_f=0.2$, $c'_f=0.2$, $\phi'_f=35$ Compaction pressure 100kPa. Rigid base at -3.00m.
	-0.05	-0.1	-0.05	Invert	
	-0.11	0.035	0.145	Springline	

Table 8.12 Parametric studies; Thrust

Measuring position on culvert (degree)	180	160	140	120	110	90	Details of material parameters used in numerical analyses
Observed live load thrust (kN)	45	90	95	-	-	-	
Analysis name							
MB1	168 30 138	188 60 128	203 100 103	160 87 73	151 77 74	130 62 68	Fill, M-C model. $E'_f = 35\text{MPa}$, $\nu'_f = 0.0$, $c'_f = 0.2$, $\phi'_f = 35$ Compaction pressure 100kPa. Rigid base at -3.00m.
MB2	154 27 127	173 51 122	189 84 105	155 85 84	146 58 88	130 50 80	
MB3	141 27 114	157 46 111	170 70 100	141 58 83	133 45 88	120 40 80	Same as MB1 but $\nu'_f = 0.1$
MB4	103 3 100	108 6 102	112 11 101	111 9 102	120 6 114	136 6 130	Same as MB1 but $\nu'_f = 0.2$
MB5	105 3 102	112 8 104	116 10 106	111 11 100	120 7 113	131 6 125	Same as MB1 but $\nu'_f = 0.3$
MB6	138 19 119	150 36 114	155 52 103	134 38 96	130 30 100	119 24 95	Same as MB3 but $E'_f = 120\text{MPa}$
MB7	151 33 118	166 53 113	177 76 101	146 57 89	138 49 89	124 35 89	Same as MB3 but $E'_f = 80\text{MPa}$
MB8	136 22 114	150 42 108	170 70 100	143 60 83	135 49 86	118 41 77	Same as MB3 but $E'_f = 20\text{MPa}$
MB9	166 66 100	193 93 100	226 130 96	200 100 100	183 76 107	156 57 99	Same as MB3 but $\phi'_f = 45$
MB10	172 63 109	200 95 105	229 129 100	192 97 95	175 75 100	154 57 97	Same as MB3 but $\phi'_f = 40$

(Combined construction and live load behaviour)

(Live load behaviour only)

(Construction behaviour only)

Table 8.12 continued

Measuring position on culvert (degree)	180	160	140	120	110	90	Details of material parameters used in numerical analyses
Observed live load thrust (kN)	45	90	95	-	45	-	
Analysis name							
MB11	138 128	10 124	154 108	127 88	127 94	116 90	Same as MB3 but $\phi'f = 30$
MB12	149 146	3 140	124 114	89 79	100 92	96 89	Same as MB3 but $\phi'f = 20$
MB13	108 88	20 90	142 94	144 104	145 117	142 120	Same as MB3 but compaction pressure 25kPa
MB14	118 101	17 100	148 98	140 100	140 108	132 108	Same as MB3 but compaction pressure 50kPa
MB15	136 111	25 108	170 100	150 89	140 94	124 86	Same as MB3 but compaction pressure 75kPa
MB16	150 125	25 136	182 108	146 86	140 90	123 79	Same as MB3 but compaction pressure 125kPa
MB17	141 119	22 116	175 105	142 85	131 97	108 69	Same as MB3 but no plinths present at the corner plates
MB18	143 116	27 115	182 106	158 96	153 100	149 111	Same as MB3 but -1.00m to rigid base.
MB19	138 113	25 111	176 102	155 90	150 100	137 97	Same as MB3 but -6.00m to rigid base

Table 8.13 Parametric studies; Bending moment

Measuring position on culvert (degree)	180	160	140	120	110	90	Details of material parameters used in numerical analyses
Observed live load bending moment (kNm)	-8	2	2.5	-	0	-	
Analysis name							
MB1	4 8	5 -0.95 4.05	-0.41 2.44 -2.85	-9.5 0.7 -10.2	-8.86 0.47 -9.33	13.2 0 13.2	Fill, M-C model. $E'_f=35\text{MPa}$, $\nu'_f=0.0$, $c'_f=0.2$, $\phi'_f=35$ Compaction pressure 100kPa. Rigid base at -3.00m.
MB2	5.8 9.3	4.75 -0.95 5.7	-1.58 1.9 -3.48	-10 0.9 -10.9	-9 0.5 -9.5	12 0 12	
MY3	6.5 10.3	5 -0.8 5.8	-1.63 2.67 -4.3	-10.4 0.3 -10.7	-8.4 0.2 -8.6	12 0 12	Same as MB3 but no compaction to elements above the crown
MB3/MY4	6.5 10.3	5 -0.8 5.8	-1.63 2.67 -4.3	-10.4 0.3 -10.7	-8.4 0.2 -8.6	12 0 12	Same as MB1 but $\nu'_f=0.2$
MB4	10 10.5	5.8 -0.1 5.9	-4.1 0.2 -4.3	-10 0 -10	-8.2 0 -8.2	9.3 0 9.3	Same as MB1 but $\nu'_f=0.3$
MB5	11.4 11.8	6.1 -0.1 6.2	-5.3 0.2 -5.5	-10.5 0.1 -10.6	-8.0 0 -8.0	7.8 0 7.8	Same as MB1 but $\nu'_f=0.4$
MB6	11 12	5.4 -0.2 5.6	-5.5 0.5 -6.0	-9.3 0 -9.3	-5.6 0 -5.6	8.2 0 8.2	Same as MB3 but $E'_f=120\text{MPa}$
MB7	8.4 12	5 -1.0 6	-3 2.8 -5.8	-10 0 -10	-7.3 0 -7.3	8 0 8	Same as MB3 but $E'_f=80\text{MPa}$
MB8	2.7 7.7	1.35 -3.3 4.6	0.3 -3.3 -3.0	-8.1 0.8 -8.9	-8.1 0.4 -8.5	12 0 12	Same as MB3 but $E'_f=20\text{MPa}$
MB9	-1.1 7	-1.7 -1.7 3.6	2.5 5.8 -3.3	-6.6 0.3 -6.9	-5 0 -5	8.2 0 8.2	Same as MB3 but $\phi'_f=45$

Table 8.13 continued

Measuring position on culvert (degree)	180	160	140	120	110	90	Details of material parameters used in numerical analyses
Observed live load bending moment (kNm)	-8	2	2.5	-	-0	-	
Analysis name							
MB10	0 8.4	-8.48 2.8 4.6	-1.8 2.3 3.8	6.1 -8.1 -8.5	0.4 -6.8 -6.8	0 8.7 8.7	Same as MB3 but $\phi'f = 40$
MB11	10.6 12.4	-1.8 7.0 7.6	-0.6 3.2 4.76	1.56 -13 -13.7	0.7 0.3 -11.9	0 13.6 13.6	Same as MB3 but $\phi'f = 30$
MB12	18 18.6	-0.6 11.9 11.9	0 -4.5 -4.5	0 -21 -21	0 -20.5 -20.5	0 15.2 15.2	Same as MB3 but $\phi'f = 20$
MB13	2 5	-3 2.4 3.1	-0.6 -0.6 -2.8	2.2 -4.7 -4.7	0 -3.18 -3.0	0 6.3 6.3	Same as MB3 but compaction pressure 25kPa
MB14	5 7.6	-2.6 3.3 3.86	-0.56 -1.9 -2.4	0.5 -7.2 -7.2	0 -5 -5	0 8.6 8.6	Same as MB3 but compaction pressure 50kPa
MB15	4.6 8.65	-4.0 3.9 14.9	-1.0 -0.5 -3.5	-4 -8.6 -9	0 -7.7 -7.7	0 9.6 9.6	Same as MB3 but compaction pressure 75kPa
MB16	9.5 12.6	-3.1 6.8 7.6	-0.8 -2.5 -4.7	2.2 -13 -13.5	0.5 -11.4 -11.8	0 13 13	Same as MB3 but compaction pressure 125kPa
MB17	8.1 12.4	-4.3 6.3 7.3	-1.0 -1.6 -2.9	1.3 -11.2 -11.7	0 -8.9 -8.9	0 1.6 1.6	Same as MB3 but no plinths present at the corner plates
MB18	6.5 10.2	-3.7 5.1 6.0	-0.9 -1.35 -4.05	2.7 -10.5 -10.8	0.3 -8.21 -8.43	0 -9.5 9.5	Same as MB3 but -1.00m to rigid base.
MB19	4.76 8.22	-3.46 4.4 5.4	-1.0 0 -2.54	0.1 -10 -10.1	0 -9.5 -9.5	0 10 10	Same as MB3 but -6.00m to rigid base

Table 8.14 Parametric studies; Radial and shear stress

Parameter	Radial Stress (kPa)				Shear Stress (kPa)				Details of material parameters used in analyses					
Measuring position on culvert (degree)	180	120	90	PLINTH	120	90	PLINTH							
Analysis name														
MB1	66	21	74	26	35	18	126	6	-33	-16	-24	-14	41	-36
	45		48		17		120		-17		-10		77	
MB2	61	17	69	24	36	16	108	5	-14	16	-20	-10	-30	-15
	44		45		20		103		-30		-10		-15	
MY3	57	16	68	18	32	10	89	-7	-30	-14	-19	-10	24	-27
	41		50		22		96		-16		-9		51	
MB3 / MY4	55	14	64	19	35	11	100	7	-25	-16	-19	-7	22	-25
	41		35		24		93		-9		-12		47	
MB4	35	1	54	3	31	2	120	1	1.1	-1.2	-4.9	-1.5	44	-4
	34		51		29		119		2.3		-3.4		48	
MB5	29	4	57	3	25	2	176	2	-4	-2	-8	-2	89	-5
	25		54		23		174		-2		-6		94	
MB6	45	5	56	11	38	8	84	3	-21	-12	-16	-6	19	15
	40		45		30		81		-9		-10		34	
MB7	63	22	66	11	40	12	90	4	-30	-20	-23	-15	11	-32
	41		45		28		86		-10		-8		43	
MB8	59	19	66	19	34	11	90	-8	-29	-14.0	-14	-7	28	-27
	40		47		23		98		-15		-21		55	
MB9	74	33	74	41	51	16	81	18	-33	-30	-28	-14	-5	-46
	41		33		35		63		-3		-14		41	

Table 8.14 continued

Parameter	Radial Stress (kPa)				Shear Stress (kPa)		Details of material parameters used in analyses		
Measuring position on culvert (degree)	180	Stress		Maximum	Stress				
		120	90		120	90			
								Maximum	
Analysis name									
MB10	75	35	71	40	42	15	84	11	Same as MB3 but $\phi'f = 40$
	40		31		27		73		
MB11	50	8	63	13	28	8	118	3	Same as MB3 but $\phi'f = 30$
	42		50		20		115		
MB12	42	3	76	4	16	7	193	1	Same as MB3 but $\phi'f = 20$
	39		72		9		192		
MB13	44	16	53	12	46	6	81	10	Same as MB3 but compaction pressure 25kPa
	28		41		40		71		
MB14	45	9	56	14	42	7	87	8	Same as MB3 but compaction pressure 50kPa
	36		42		35		79		
MB15	55	18	66	18	34	11	90	10	Same as MB3 but compaction pressure 75kPa
	37		47		23		80		
MB16	58	13	65	19	33	14	110	3	Same as MB3 but compaction pressure 125kPa
	45		46		19		107		
MB17	51	13	53	15	40	17	67	5	Same as MB3 but no plinths present at the corner plates
	38		38		23		62		
MB18	54	16	66	21	26	7	94	6	Same as MB3 but -1.00m to rigid base.
	38		45		19		88		
MB19	56	13	67	20	37	9	105	8	Same as MB3 but -6.00m to rigid base
	43		57		28		97		

Table 8.15 Parametric study; Displacement

Construction stage	End of construction	Live load and end of construction	Live load only	Measuring location on culvert	Details of material parameters used in numerical analyses
Observed in situ displacement (cm)	-	-	(crown) -0.75		
Analysis name					
MB1	0.036	-0.8	-0.836	Crown	Fill, M-C model. $E'_f=35\text{MPa}$, $\nu'_f=0.0$, $c'_f=0.2$, $\phi'_f=35$ Compaction pressure 100kPa. Rigid base at -3.00m.
	-0.15	-0.17	-0.02	Invert	
	0.28	0.43	0.15	Springline	
MB2	0.93	0.15	-0.78	Crown	Same as MB1 but $\nu'_f=0.1$
	-0.064	-0.077	-0.013	Invert	
	-0.05	0.21	0.16	Springline	
MY3	1.49	0.78	-0.71	Crown	Same as MB3 but no compaction to elements above the crown
	-0.0034	-0.0052	-0.0018	Invert	
	-0.114	0.005	0.119	Springline	
MB3 / MY4	0.01	-0.8	-0.81	Crown	Same as MB1 but $\nu'_f=0.2$
	-0.05	-0.1	-0.05	Invert	
	-0.11	0.035	0.145	Springline	
MB4	1.95	1.87	-0.08	Crown	Same as MB1 but $\nu'_f=0.3$
	-0.0107	-0.013	-0.004	Invert	
	-0.27	-0.25	0.02	Springline	
MB5	2.48	2.39	-0.09	Crown	Same as MB1 but $\nu'_f=0.4$
	0.083	0.074	0.001	Invert	
	-0.37	-0.35	0.02	Springline	
MB6	2.23	2.08	-0.17	Crown	Same as MB3 but $E'_f=120\text{MPa}$
	0.015	0.014	0.001	Invert	
	-0.27	-0.24	0.03	Springline	

Table 8.15 continued

Construction stage	End of construction	Live load and end of construction	Live load only	Measuring location on culvert	Details of material parameters used in numerical analyses
Observed in situ displacement (cm)	-	-	(crown) -0.75		
Analysis name					
MB7	2.25	1.67	-0.56	Crown	Same as MB3 but $E'_f = 80\text{MPa}$
	2.09	1.95	-0.14	Invert	
	-0.26	-0.18	0.08	Springline	
MB8	0.367	-0.73	-1.10	Crown	Same as MB3 but $E'_f = 20\text{MPa}$
	-0.063	-0.072	-0.009	Invert	
	0.157	0.367	0.21	Springline	
MB9	0.55	-0.81	-1.36	Crown	Same as MB3 but $\phi'_f = 45$
	-0.0281	-0.0297	-0.0016	Invert	
	0.13	0.36	0.23	Springline	
MB10	1.0	-0.44	-1.44	Crown	Same as MB3 but $\phi'_f = 40$
	-0.031	-0.083	-0.052	Invert	
	0.028	0.270	0.242	Springline	
MB11	2.26	1.86	-0.40	Crown	Same as MB3 but $\phi'_f = 30$
	0.016	0.012	-0.004	Invert	
	-0.32	-0.24	0.08	Springline	
MB12	4.58	4.50	-0.08	Crown	Same as MB3 but $\phi'_f = 20$
	0.108	0.107	-0.001	Invert	
	-1.21	-1.20	0.01	Springline	
MB13	0.093	-0.43	-0.523	Crown	Same as MB3 but compaction pressure 25kPa
	-0.053	-0.047	0.006	Invert	
	0.17	0.25	0.08	Springline	

Table 8.15 continued

Construction stage	End of construction	Live load and end of construction	Live load only	Measuring location on culvert	Details of material parameters used in numerical analyses
Observed in situ displacement (cm)	-	-	(crown) -0.75		
Analysis name					
MB14	0.73	0.26	-0.47	Crown	Same as MB3 but compaction pressure 50kPa
	-0.0265	-0.0262	0.0003	Invert	
	0.073	0.15	0.077	Springline	
MB15	1.21	0.47	-0.74	Crown	Same as MB3 but compaction pressure 75kPa
	-0.011	-0.012	-0.001	Invert	
	-0.056	0.07	0.126	Springline	
MB16	2.26	1.55	-0.71	Crown	Same as MB3 but compaction pressure 125kPa
	0.042	0.032	-0.010	Invert	
	-0.28	-0.15	0.13	Springline	
MB17	2.41	1.57	-0.84	Crown	Same as MB3 but no plinths present at the corner plates
	0.072	0.074	0.002	Invert	
	-0.82	-0.67	0.15	Springline	
MB18	2.30	1.64	-0.66	Crown	Same as MB3 but -1.00m to rigid base.
	0.041	0.043	0.002	Invert	
	-0.29	-0.16	0.13	Springline	
MB19	0.58	-0.14	-0.72	Crown	Same as MB3 but -6.00m to rigid base
	-0.335	-0.376	-0.041	Invert	
	-0.052	0.073	0.125	Springline	

Table 8.16. Initial values of backfill material parameters (non-associated flow Mohr-Coulomb).

SOIL MODEL PARAMETER						
STRUCTURE	E _f (kPa)	ν _f	c _f (kPa)	φ _f (degrees)	γ _f (kN/m ³)	ψ _f (degrees)
BACKFILL	35x10 ³	0.2	0.2	35	21	-20

Table 8.17 Material parameters for pavement sub-base

STRUCTURE	E _{sb} (kPa)	ν _{sb}	c _{sb} (kPa)	φ _{sb} (degrees)	γ _{sb} (kPa)
SUB-BASE (TYPE 1 GRAVEL)	150x10 ³	0.3	0.2	35	21

Table 8.18 Material parameters for pavement surface layers

STRUCTURE	E _{pav} (kPa)	ν _{pav}	G _{pav} (kPa)	γ _{pav} (kPa)
PAVEMENT SURFACE LAYER	600x10 ³	0.35	222x10 ³	22

Table 8.19 Main data for load case C; Thrusts

Measuring position on culvert (degree)		180											Details of material parameters used in numerical analyses
Observed live load thrust (kN)		60											
Analysis name													
MC2	186 130	56	212 128	84	234 110	124	188 80	108	169 79	90	158 87	71	Pavement I.E, Ep=600MPa, v'p=0.35: Fill and Sub-base M-C E'f=35MPa, v'f=c'f=0.2, $\phi'_f=35$; E _{sb} =150MPa, v' _{sb} =0.3, c' _{sb} =0.2, $\phi'_{sb}=45$
	MC3	258 135	123	300 131	169	343 112	231	198 82	116	253 82	171	222 87	
MC5	189 120	69	214 116	98	233 106	127	196 91	105	184 97	87	156 87	69	Same as MC2 but E _{sb} = 125MPa Same as MC2 but v'f=0.1

(Combined construction and live load behaviour)

(Construction behaviour only)

(Live load behaviour only)

Table 8.20 Bending moments

Measuring position on culvert (degree)	180	160	140	120	110	90	Details of material parameters used in numerical analyses				
Observed live load bending moment (kNm)	-4	-0.6	2.4	-	-0.05	-					
Analysis name											
MC2	4 9	-5 6	4.9 6	-1.1 -2.9	4 -2.9	-11 -11.4	0.5 -9.5	8.4 8.4	0	Same as MC1 but $E_p=600\text{MPa}$	
MC3	-2.8 8.8	-11.6 6	3 6	-3 -2.8	-5.8 -2.8	-9.6 -11.8	2.2 -10	0 -10	8 9		Same as MC2 but $E_{sb} = 125\text{MPa}$
MC5	5.3 11	-5.7 6.7	5.1 6.7	-1.6 -3.7	4 -3.7	-11 -11.6	0.6 -11.3	0.3 -11.3	9.4 9.4	0	Same as MC2 but $v'_f=0.1$

Table 8.21 Radial and shear stress

Parameter	Radial Stress (kPa)				Shear Stress (kPa)			Details of material parameters used in analyses
Measuring position on culvert (degree)	180	120	90	Maximum	120	90	Maximum	
Analysis name								
MC2	79 44	35 41	54 36	140 156	-35 -17	-10.5 7.5	63 110	
MC3	122 48	74 43	75 35	126 152	-46 -18	33 6.5	20 106	
MC5	74	38	58	100	-34	26.4	33	
				-12		-26.5 -16.5	-43	

Table 8.22 Displacement

Construction stage	End of construction	Live load and end		Measuring location on culvert	Details of material parameters used in numerical analyses
		of construction	only (crown)		
Observed in situ displacement (cm)	-	-	-0.52		
Analysis name					
MC2	1.66	0.61	-1.05	Crown	Pavement I.E, Ep=300MPa, vp=0.35: Fill and Sub-base M-C E'f= 35MPa, v'f= c'f = 0.2, ϕ' f= 35; E _{sb} = 150MPa, v' _{sb} = 0.3 , c' _{sb} = 0.2, ϕ' sb = 45
	-0.019	-0.026	-0.007	Invert	
	-0.11	-0.14	0.18	Springline	
MC3	1.69	-0.63	-2.32	Crown	Same as MC2 but E _{sb} = 125MPa
	-0.0186	-0.0325	-0.0139	Invert	
	-0.33	0.042	0.372	Springline	
MC5	1.00	0.15	-1.15	Crown	Same as MC2 but v'f=0.1
	-0.024	-0.02	0.004	Invert	
	-0.02	-0.32	-0.3	Springline	

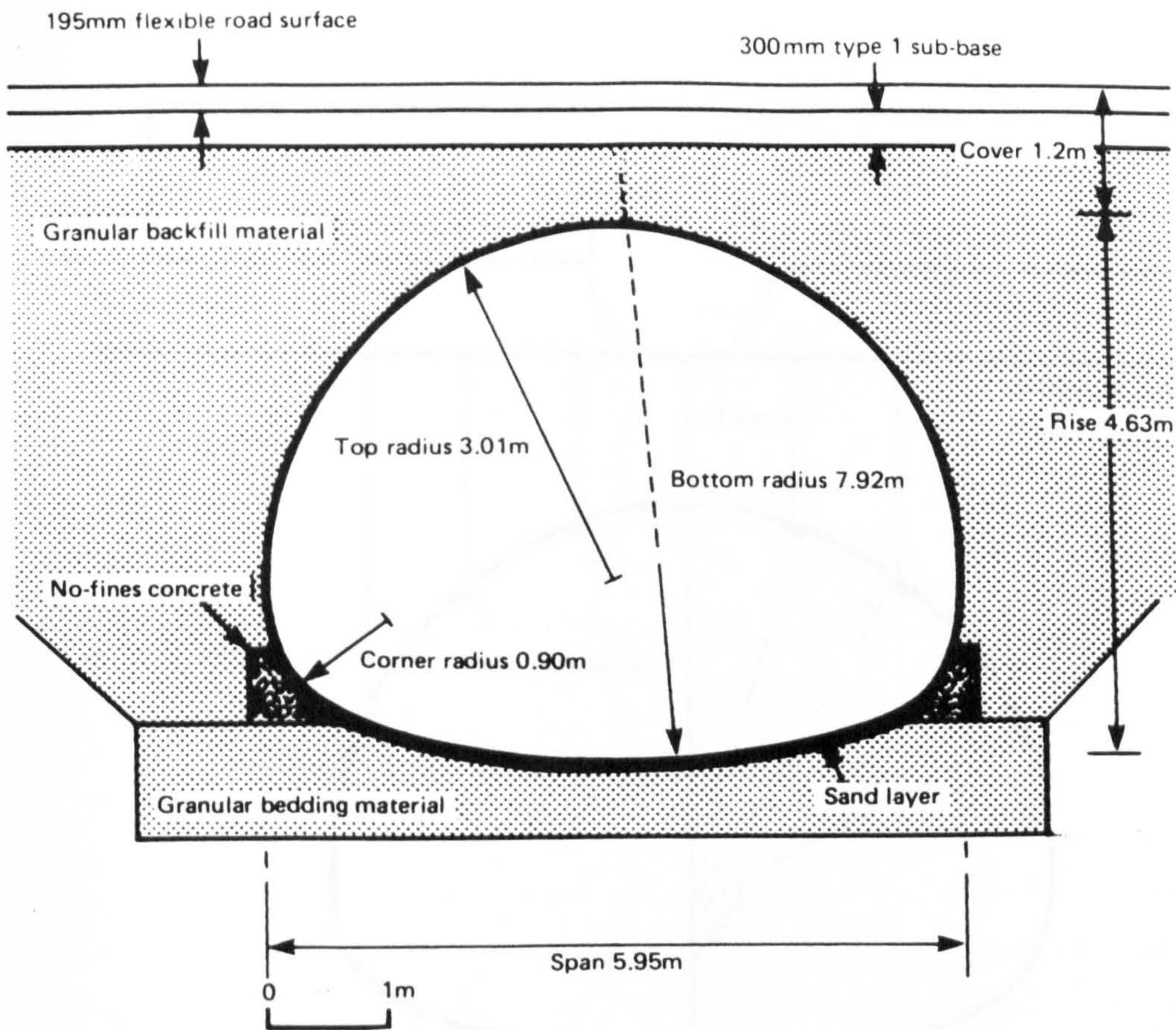


Fig 8.1 Geometry of Mytholmroyd culvert (Johnson et al., 1989)

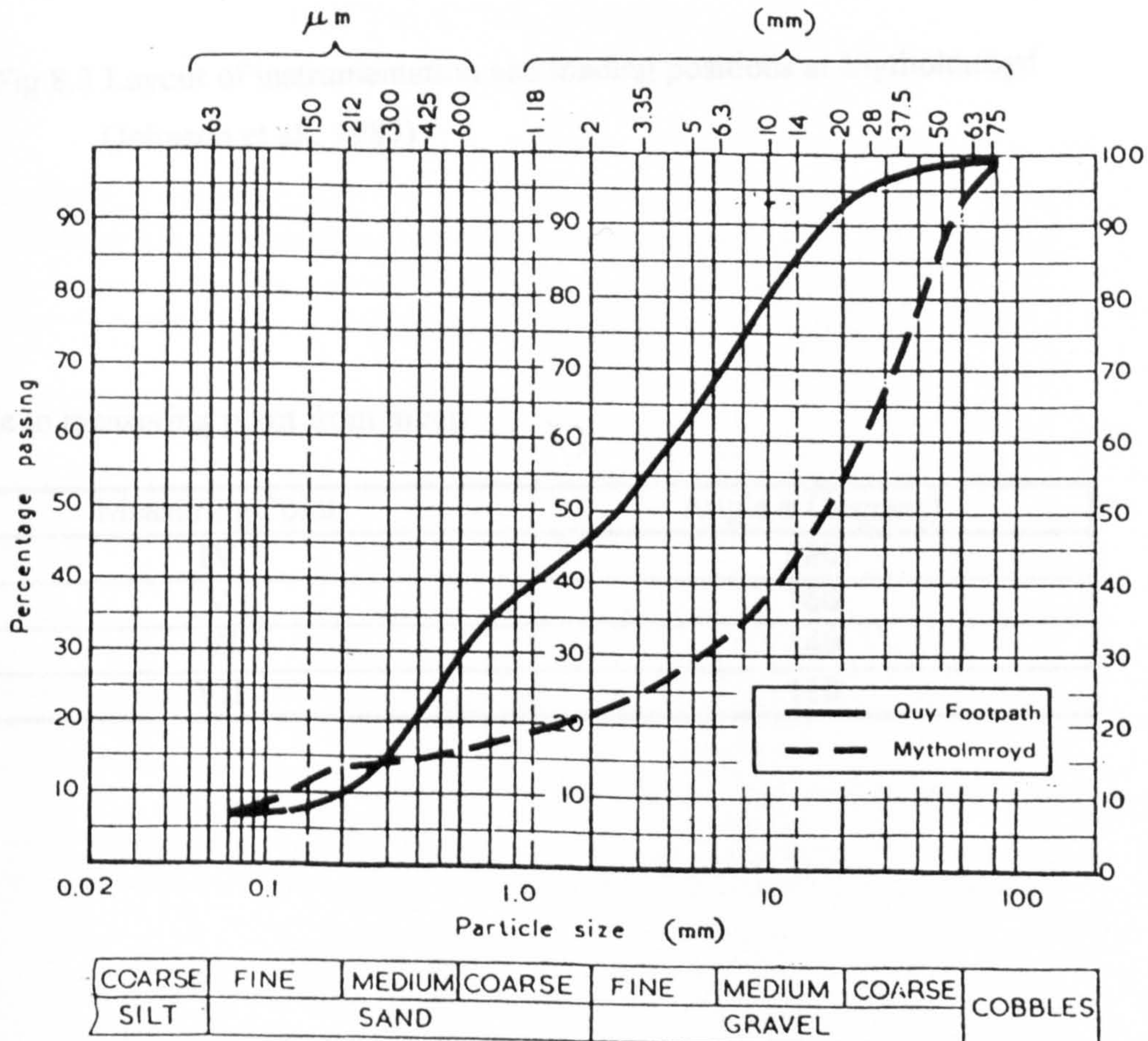


Fig 8.2 Particle size distribution for backfill material (Johnson et al., 1989)

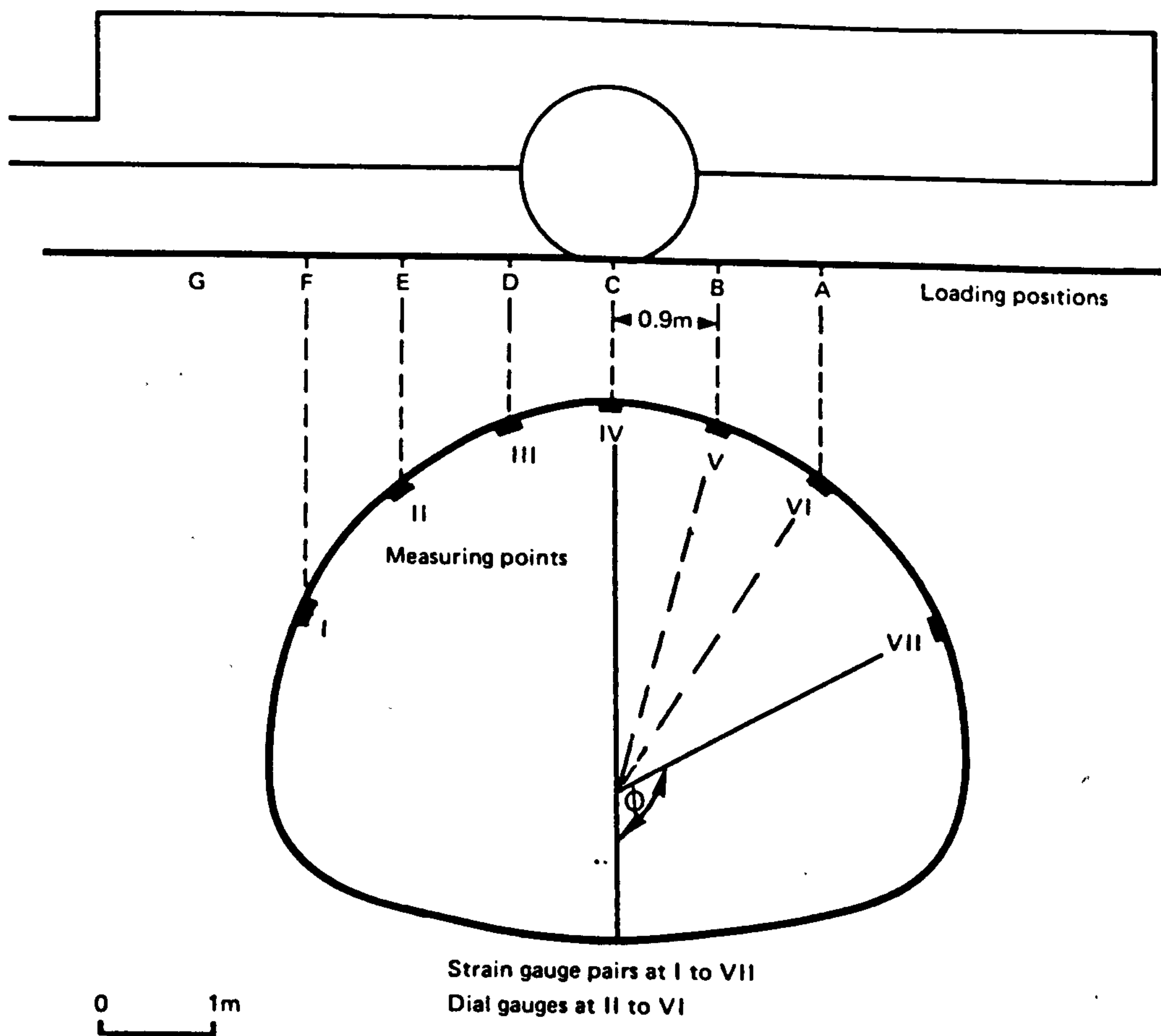


Fig 8.3 Layout of instrumentation and loading positions at Mytholmroyd
(Johnson et al., 1989)

ϕ =angle to measuring point from invert

Measuring Point	Angle ϕ (degrees)
IV	180
V	160
VI	140
VII	110

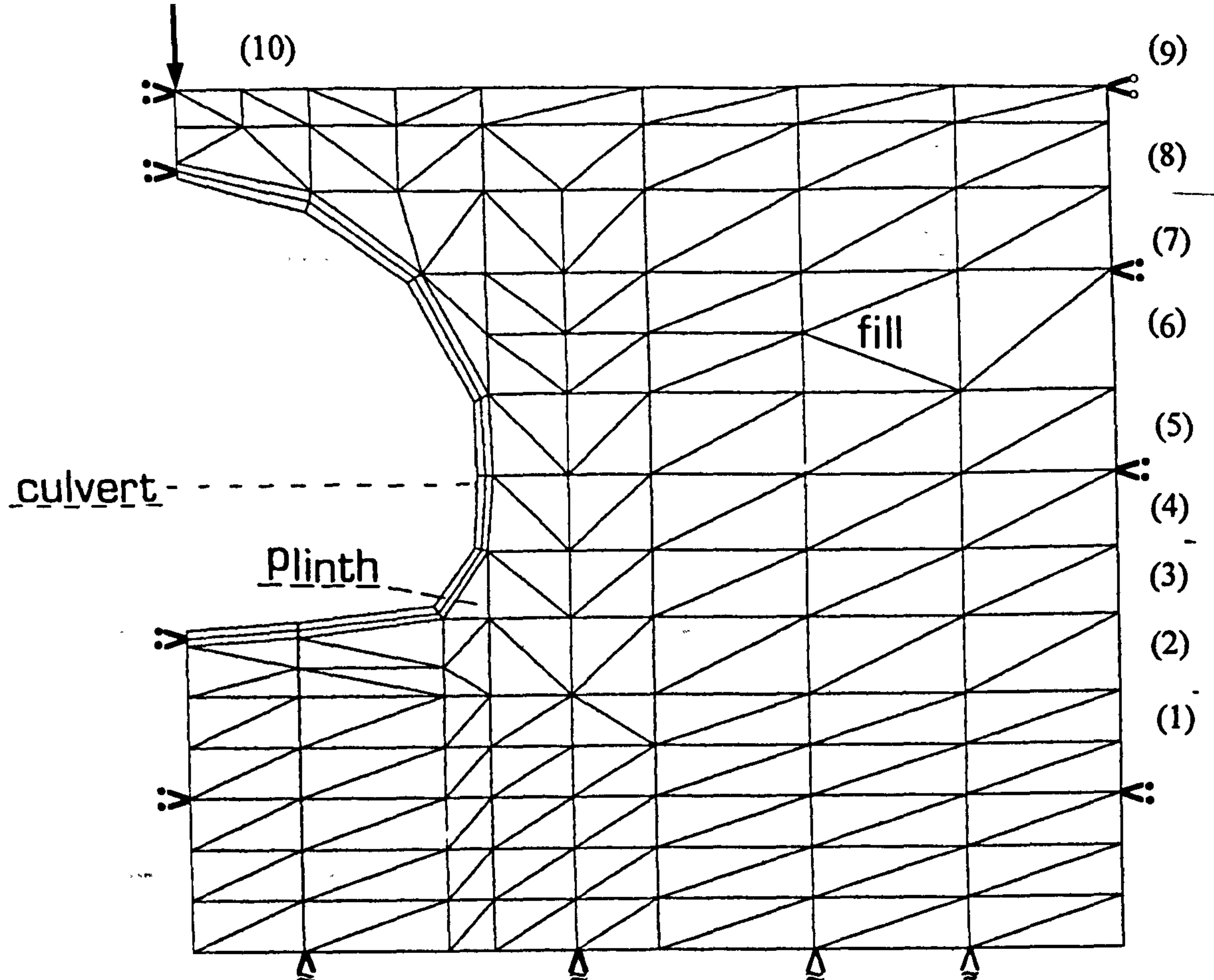


Fig 8.4 Finite element mesh for loading case A.

CONSTRUCTION STAGE ()

CONSTRUCTION STAGE	DESCRIPTION
1	COMPACT EXISTING FOUNDATION SOIL
2	PLACE AND COMPACT BASAL LAYER
3	PLACE BACKFILL AND PLINTH , COMPACT BACKFILL
4	PLACE AND COMPACT BACKFILL UP TO SPRINGLINE
5	PLACE AND COMPACT BACKFILL TO BELOW QUARTER POINTS
6	PLACE AND COMPACT BACKFILL UP TO QUARTER POINTS
7	PLACE LEVEL WITH CROWN AND COMPACT
8	PLACE BACKFILL ABOVE CROWN AND COMPACT
9	PLACE TO FINAL FILL HEIGHT AND COMPACT
10	APPLY LIVE LOAD

Fig 8.5 Initial analysis; Thrust

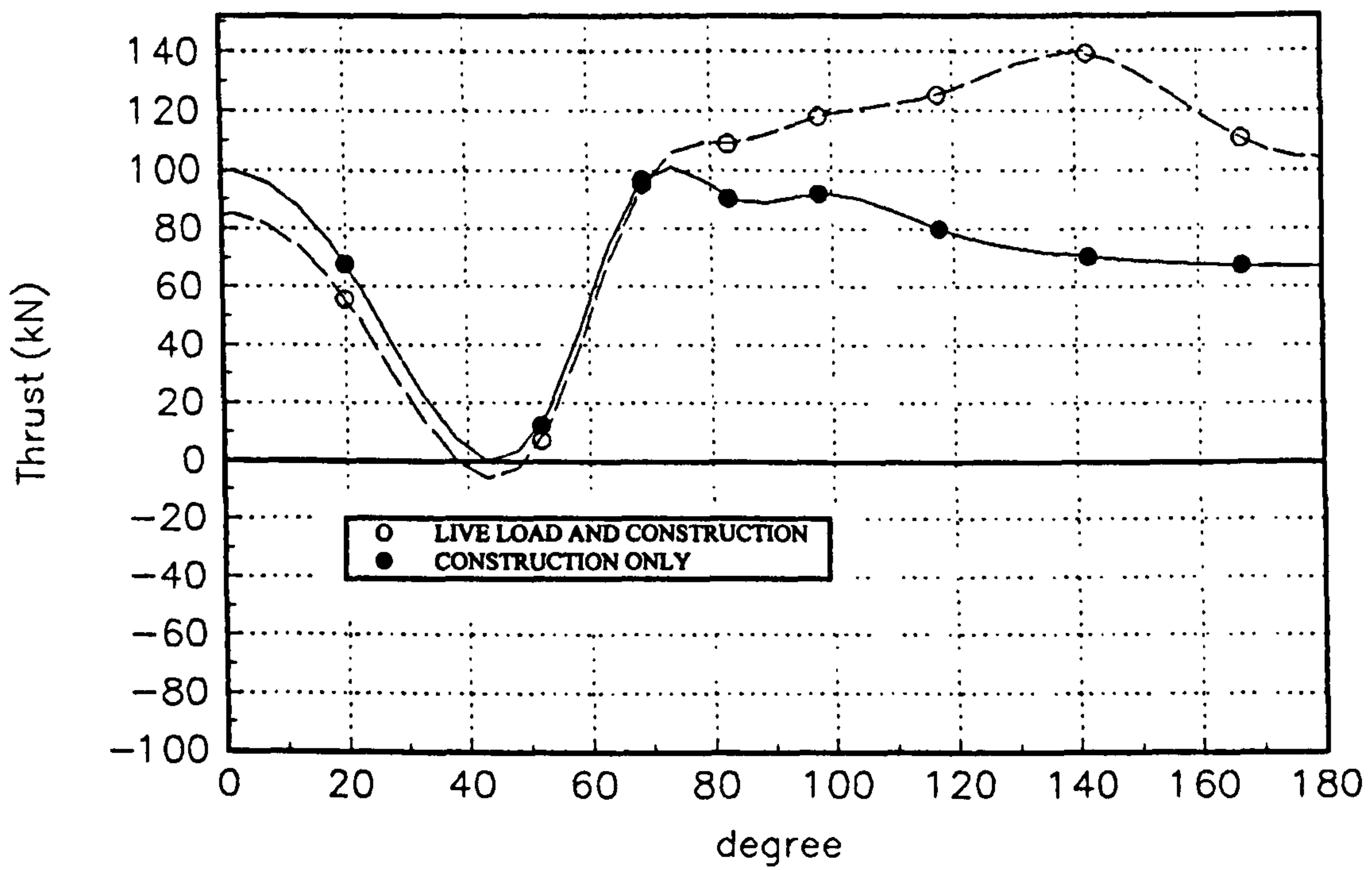


Fig 8.6 Initial analysis; Bending moment

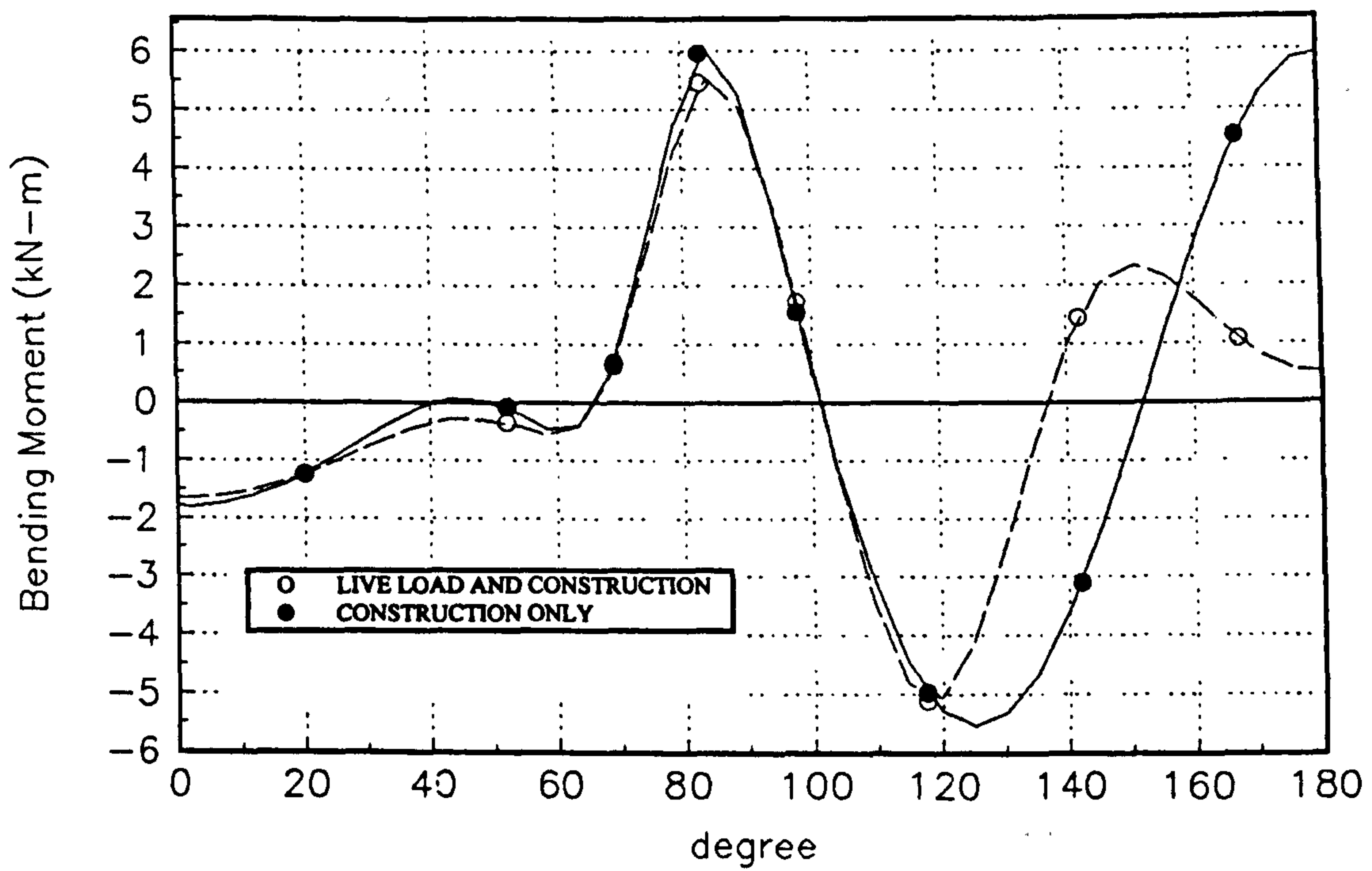


Fig 8.7 Initial analysis; Radial stress

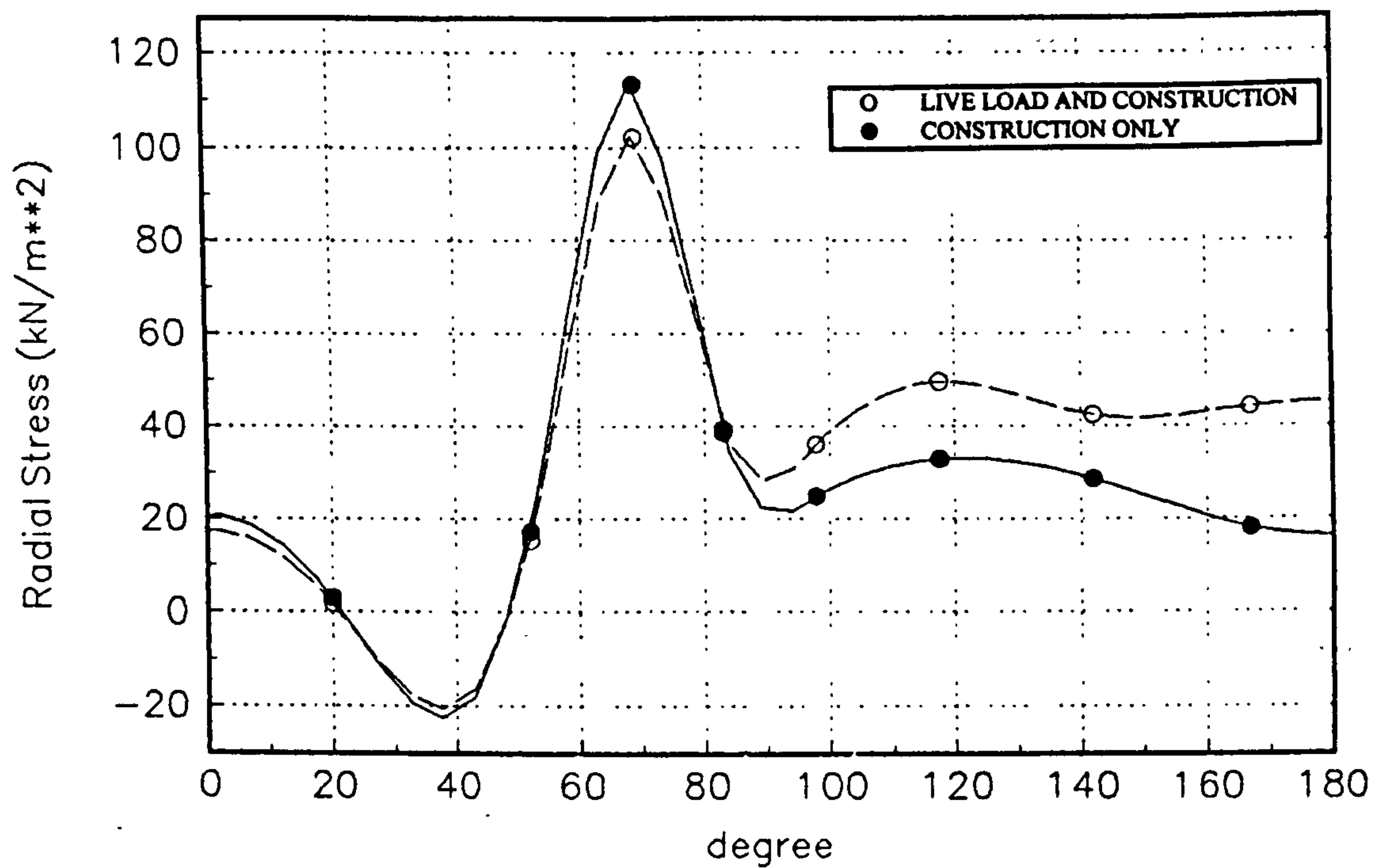


Fig 8.8 Initial analysis; Shear stress

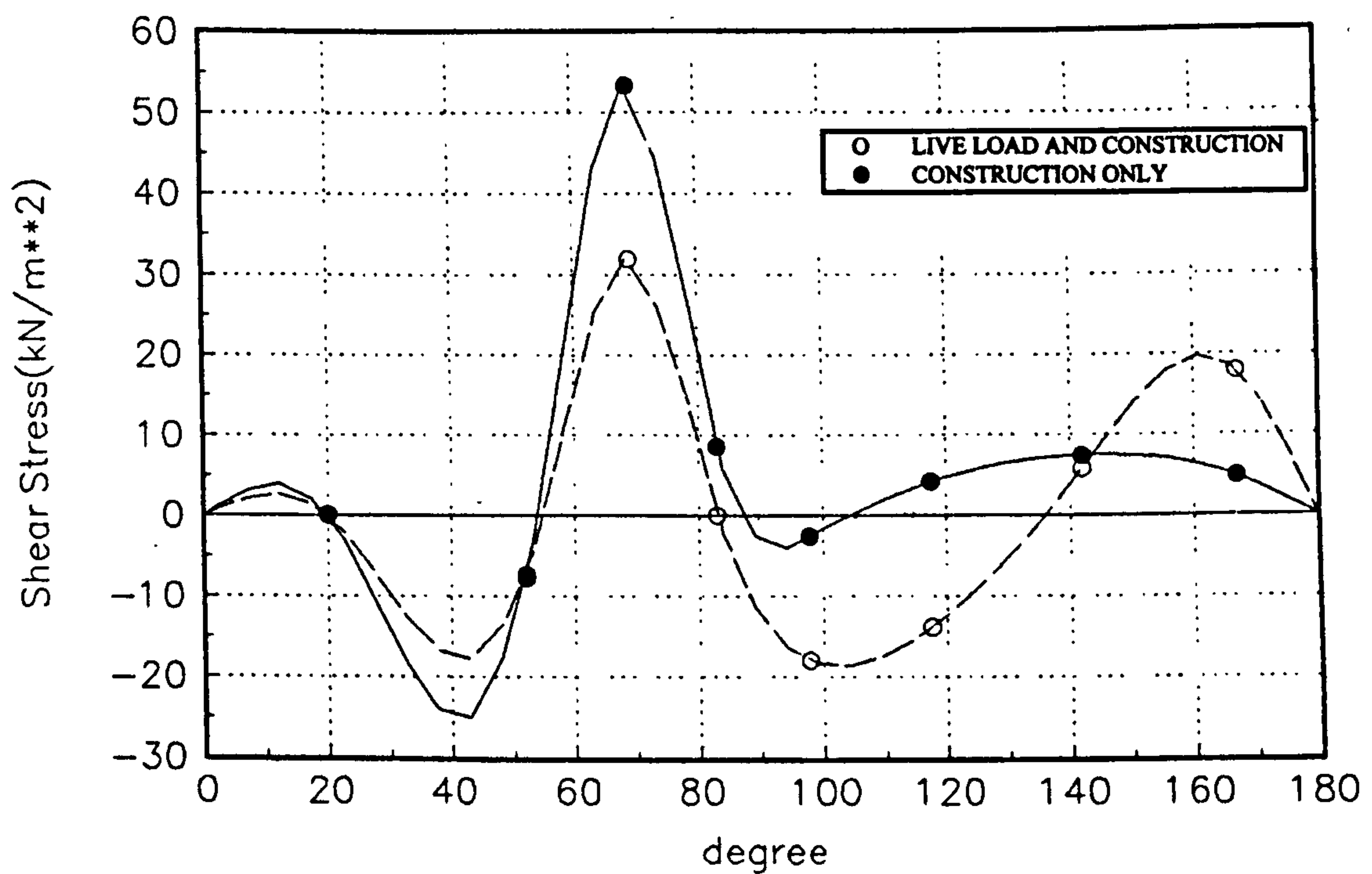


Fig 8.9 Initial analysis; Crown displacement

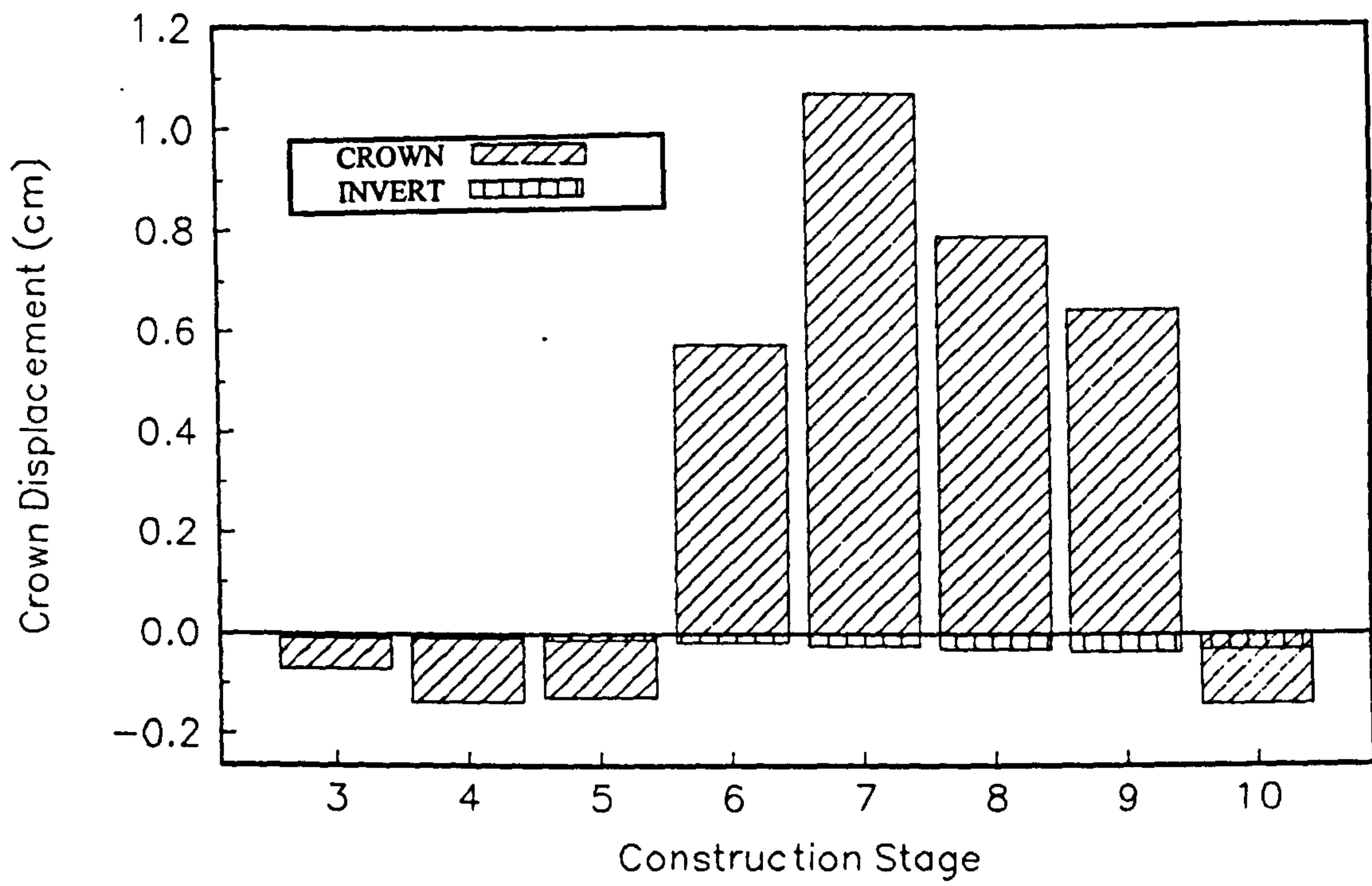
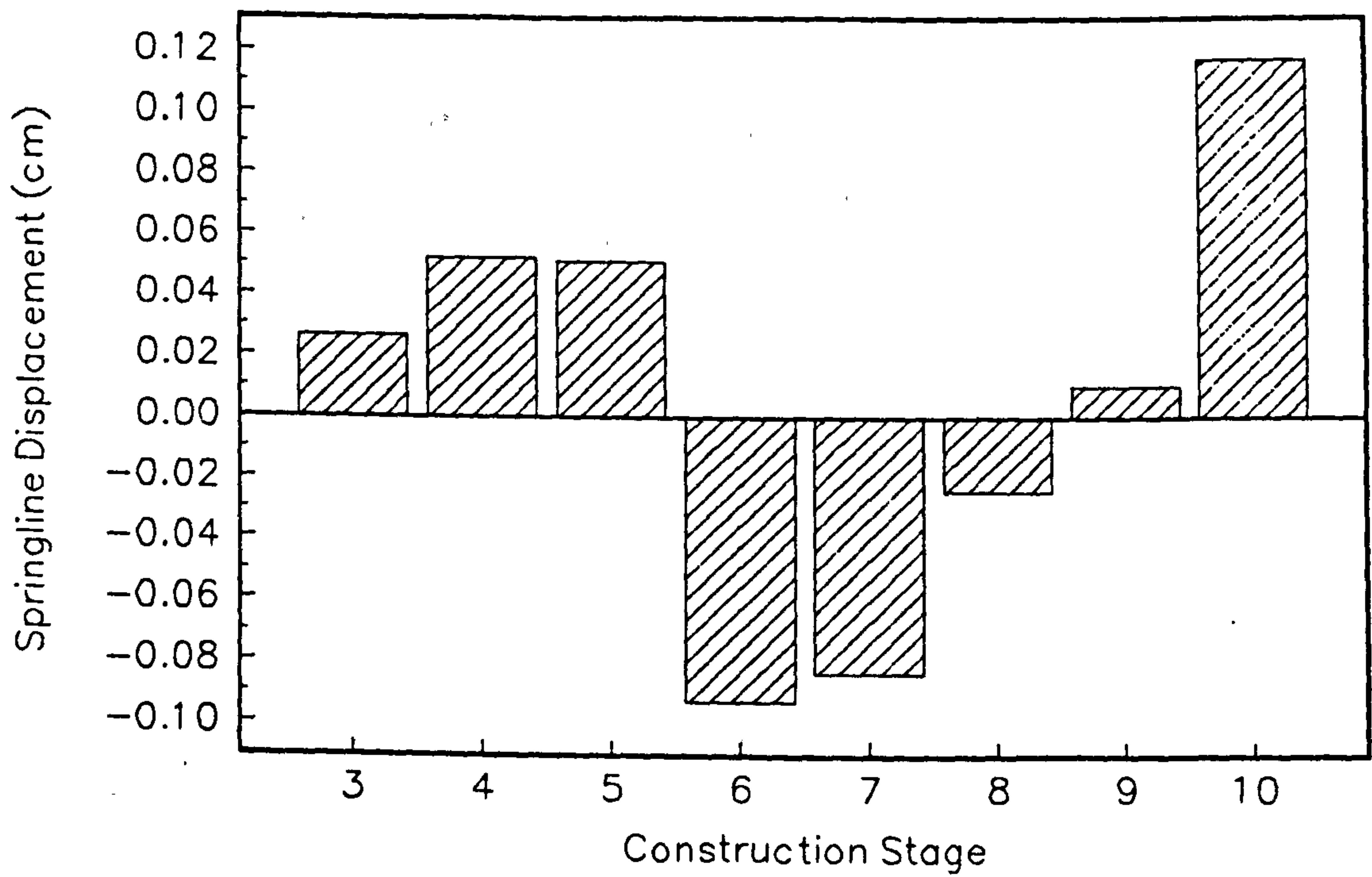


Fig 8.10 Initial analysis; Springline displacement



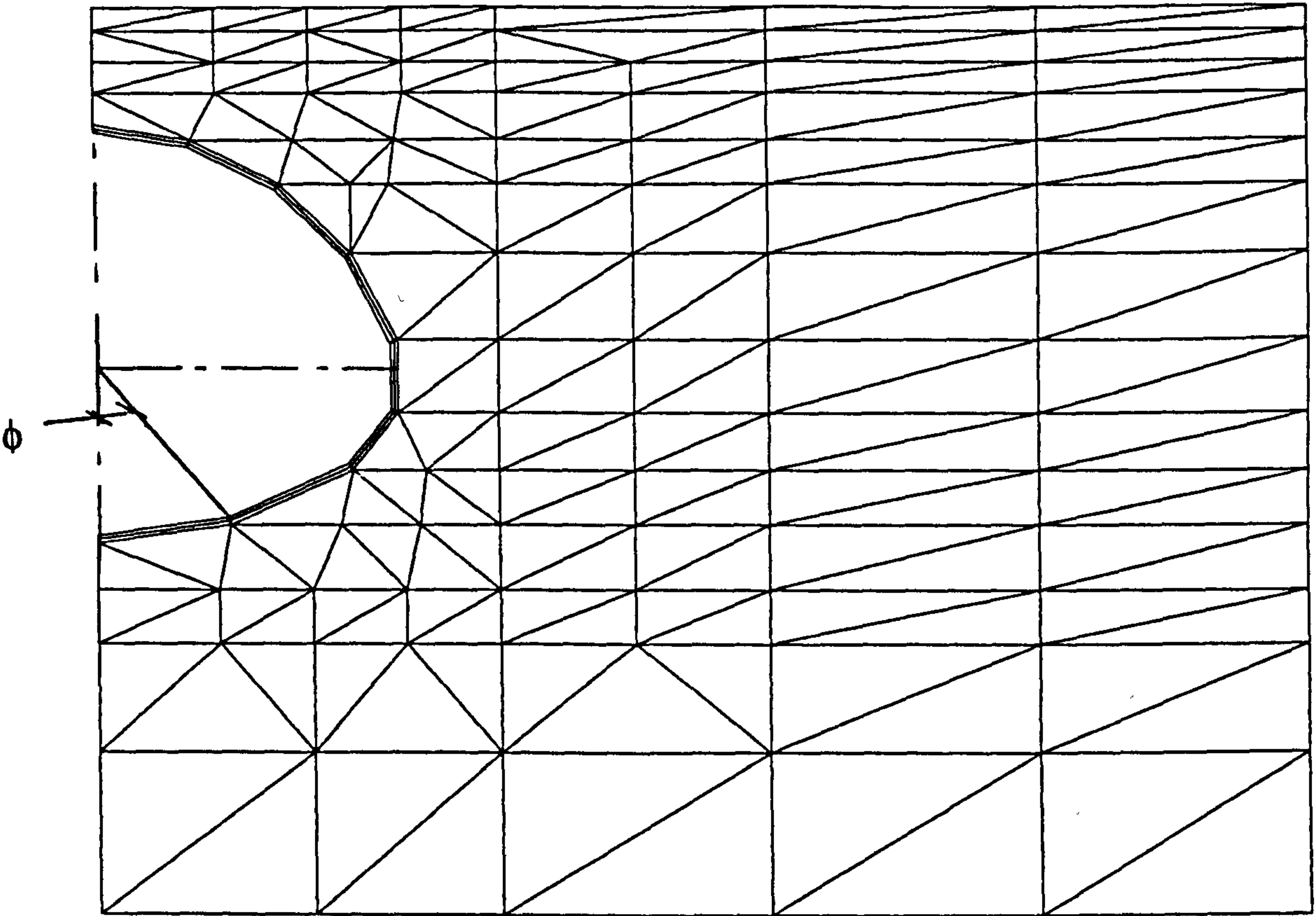


Fig 8.11 Location of culvert origin and position of measuring ϕ

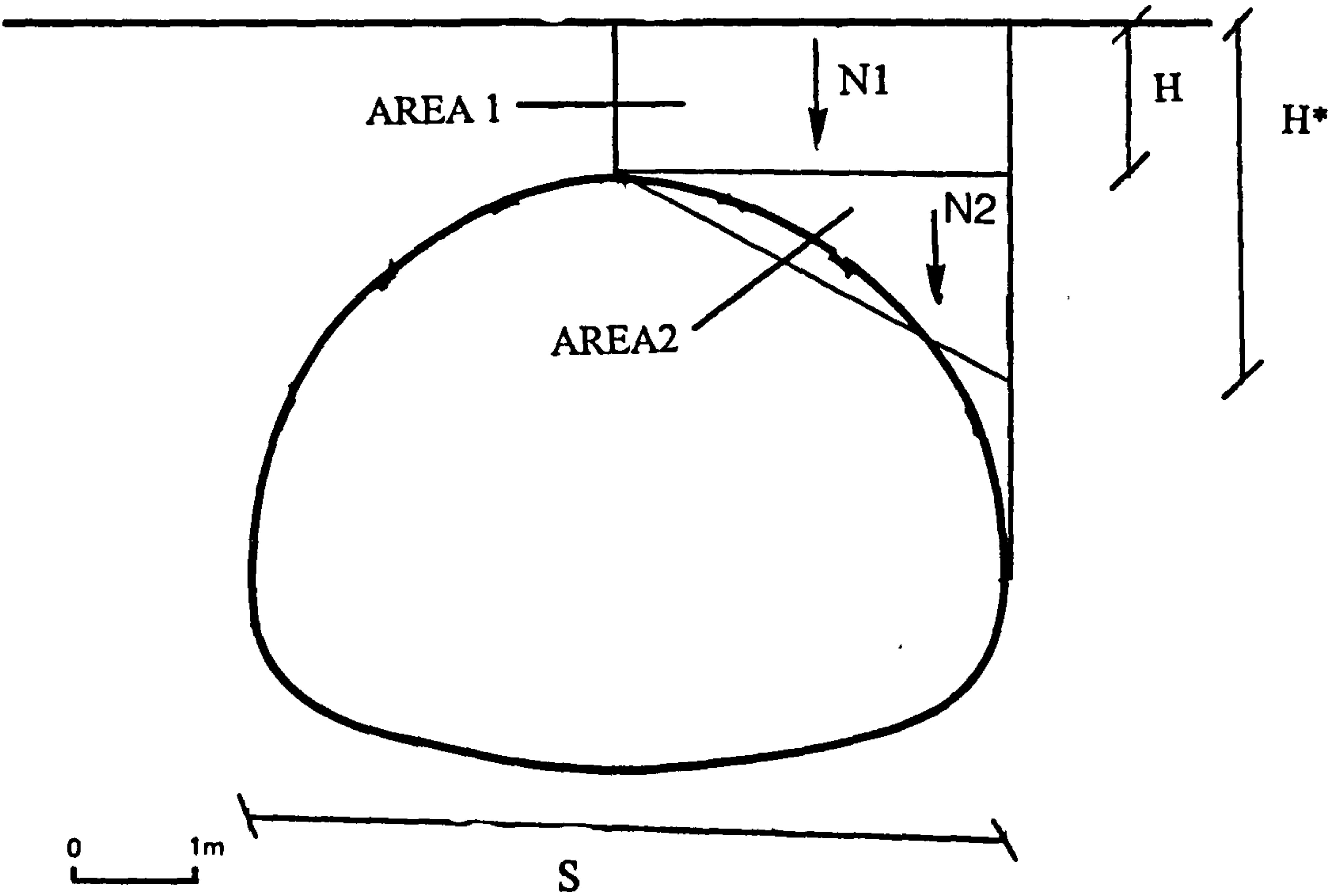


Fig 8.12 Diagram describing equilibrium theory to estimate thrusts

FIGURE 8.13 LIVE LOAD THRUST AGAINST BACKFILL STIFFNESS

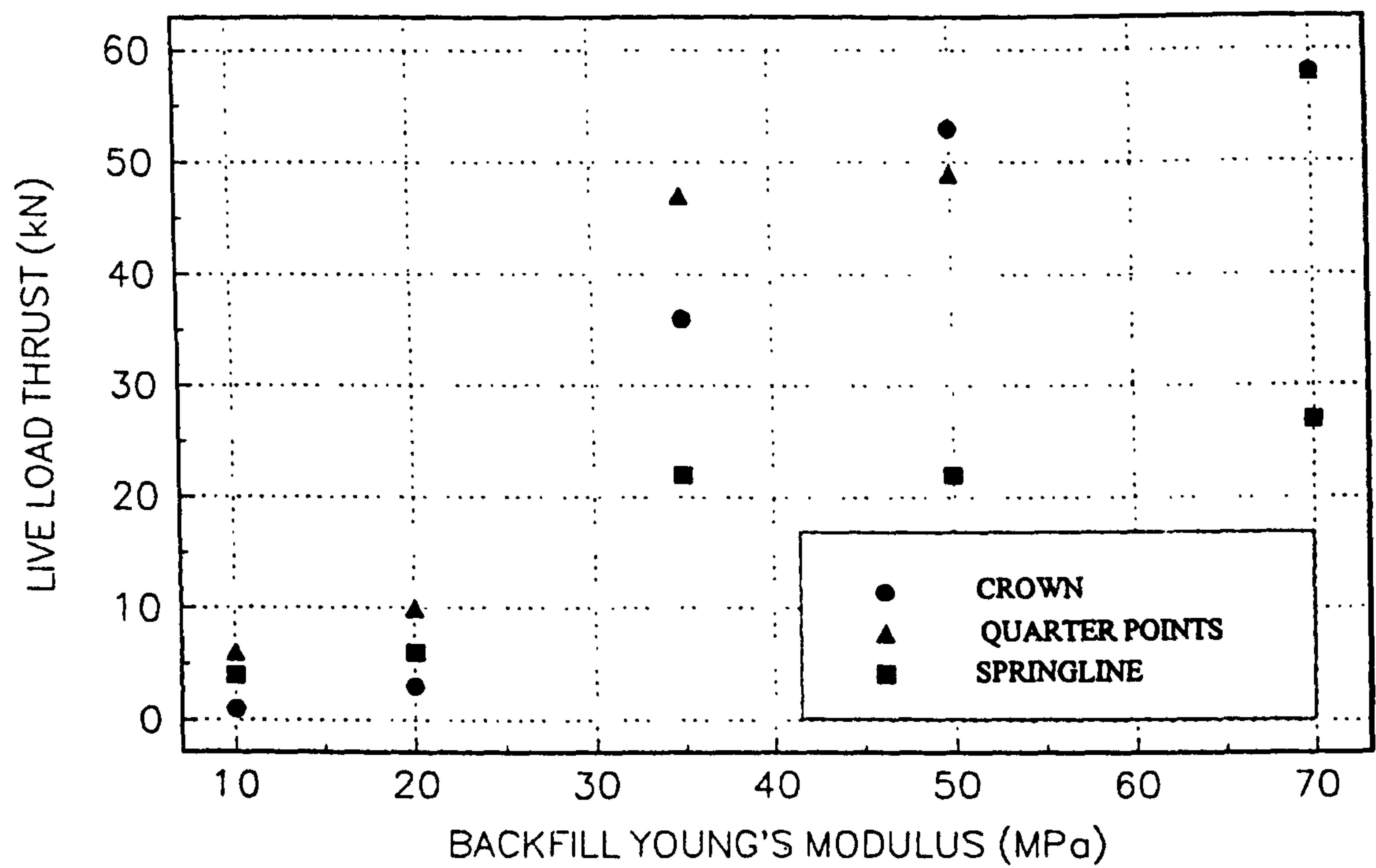


FIGURE 8.14 LIVE LOAD BENDING MOMENT AGAINST BACKFILL STIFFNESS

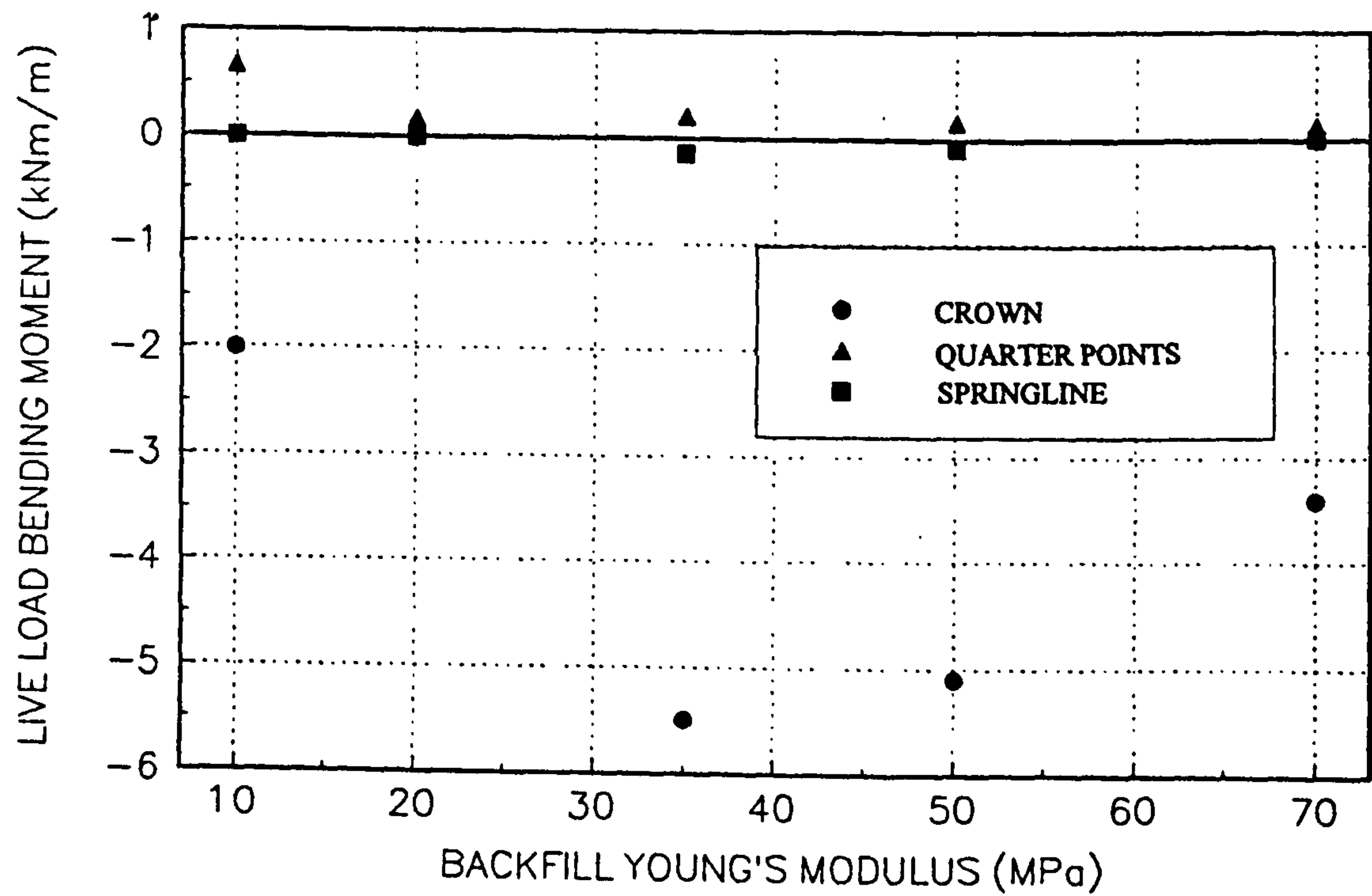


FIGURE 8.15 LIVE LOAD RADIAL STRESS AGAINST BACKFILL STIFFNESS

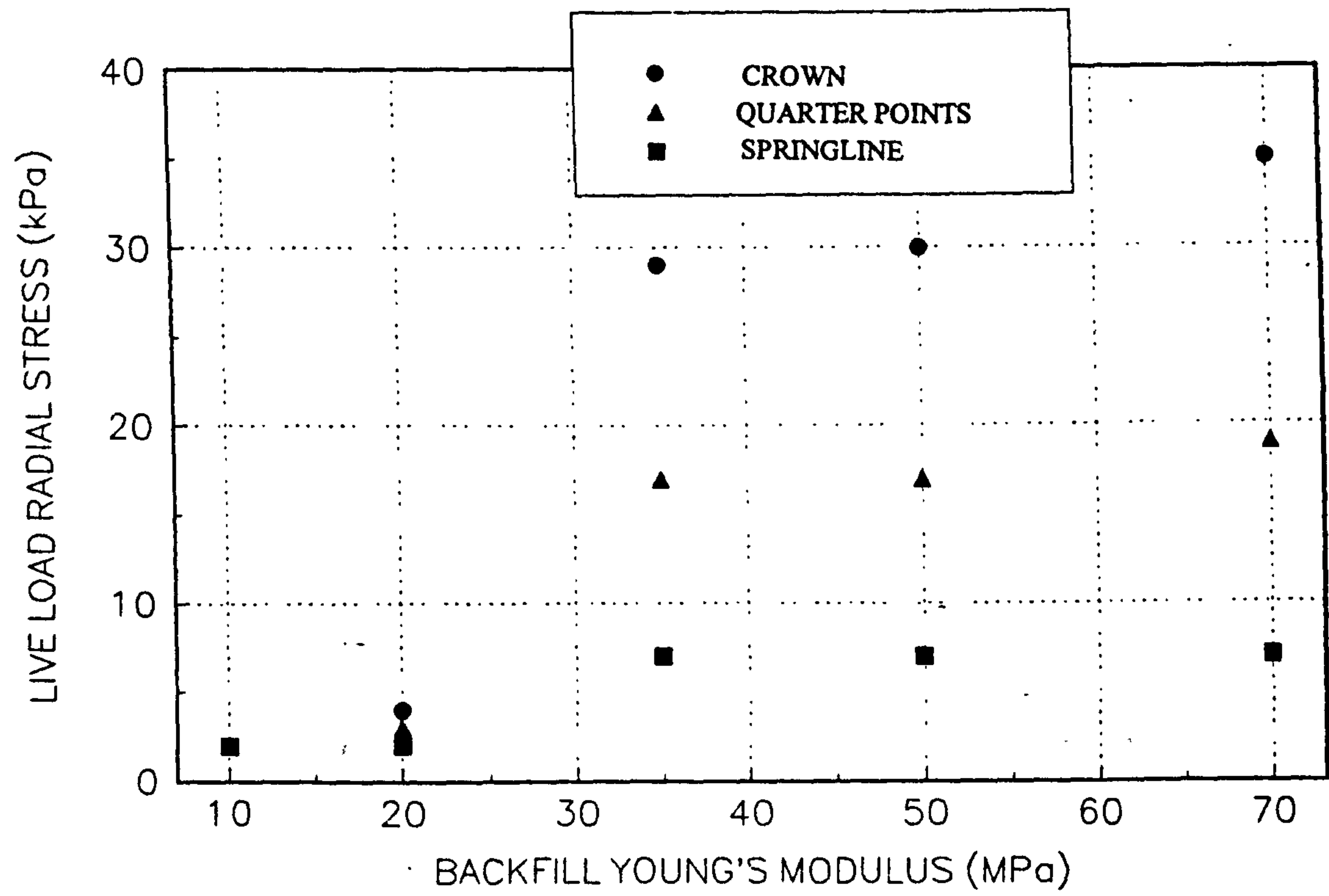


FIGURE 8.16 LIVE LOAD SHEAR STRESS AGAINST BACKFILL STIFFNESS

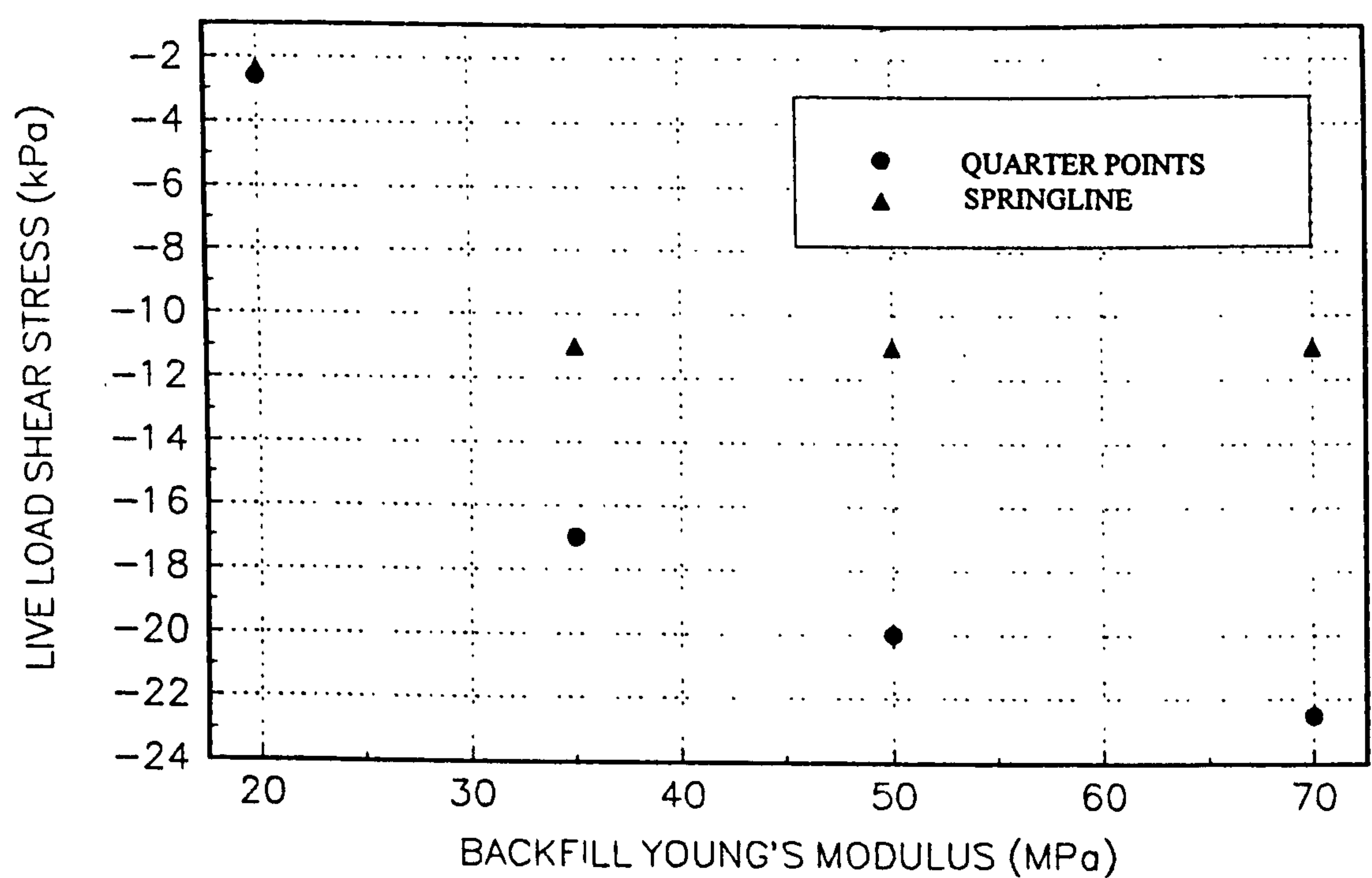


FIGURE 8.17(a) LIVE LOAD CROWN DISPLACEMENT AGAINST BACKFILL STIFFNESS

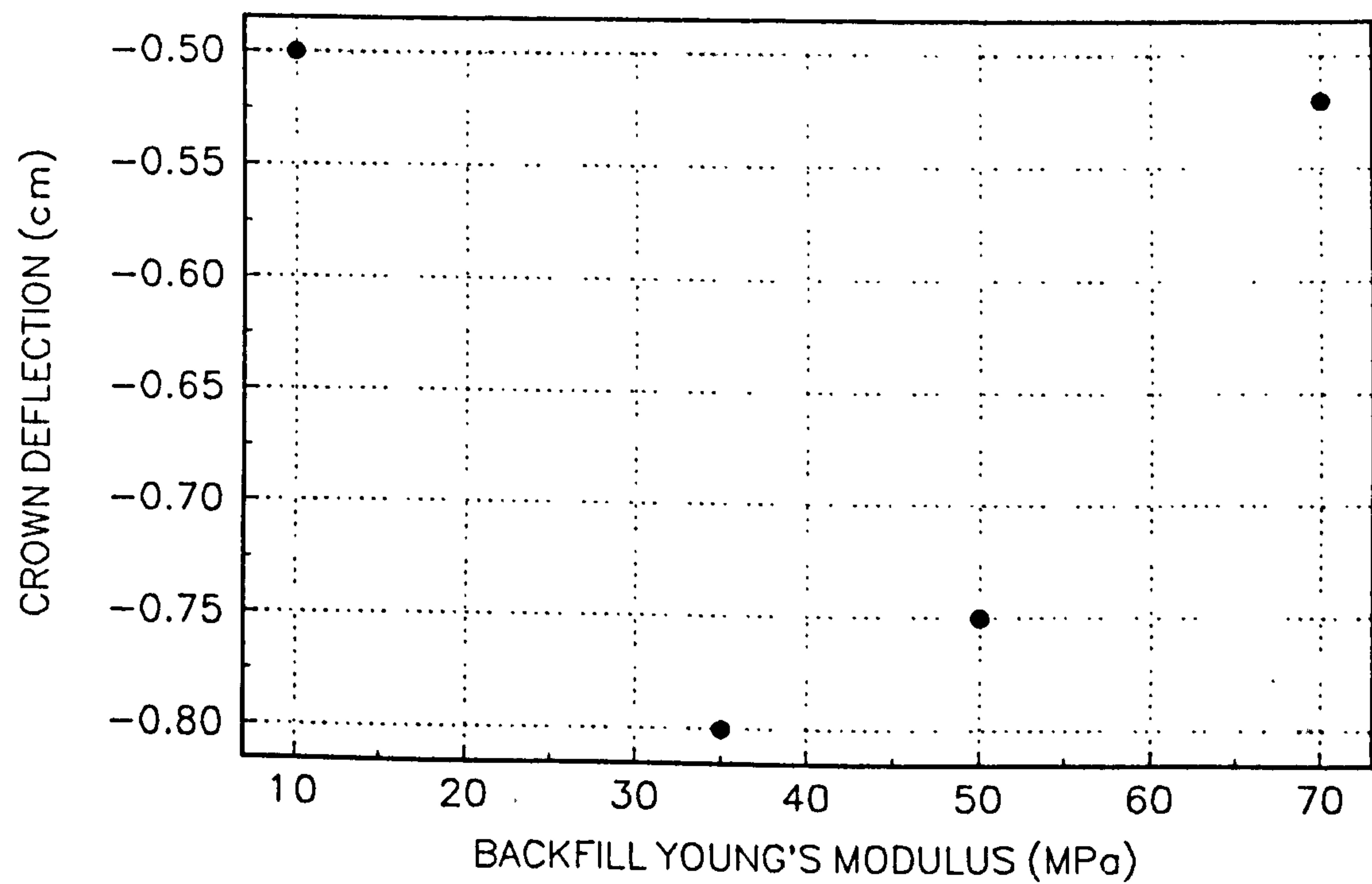


FIGURE 8.17(b) LIVE LOAD SPRINGLINE DISPLACEMENT AGAINST BACKFILL STIFFNESS

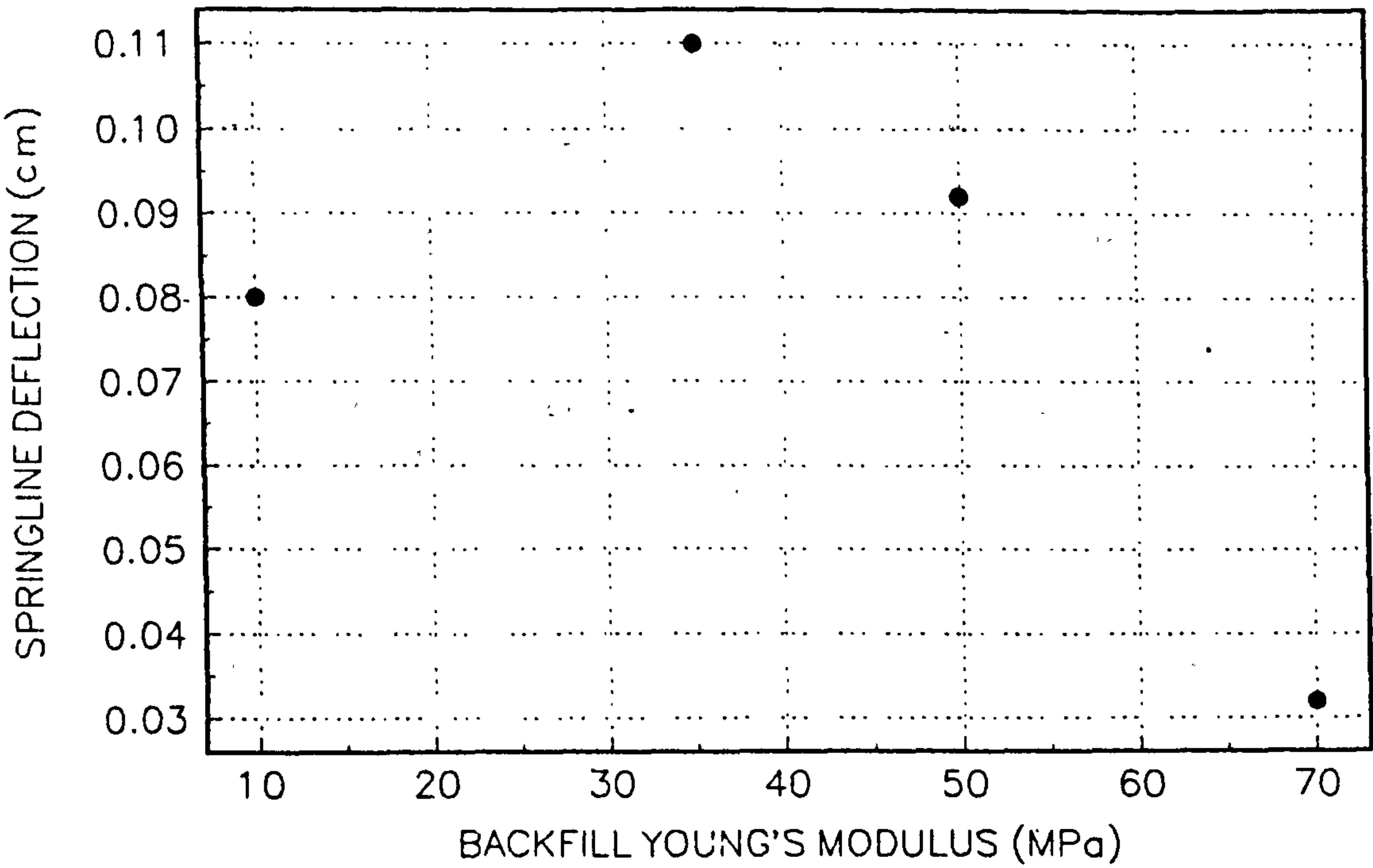
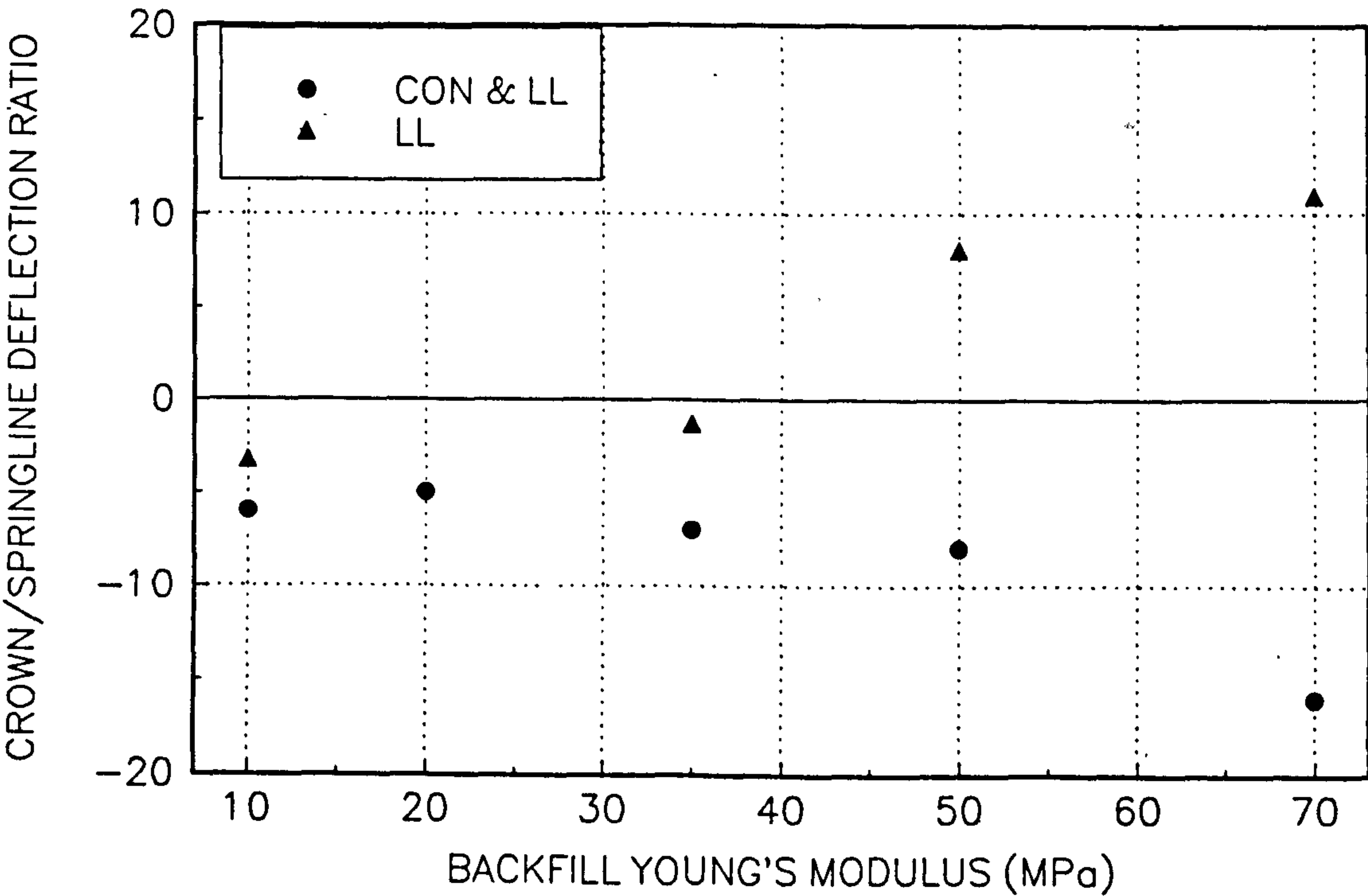


FIGURE 8.17(c) LIVE LOAD DISPLACEMENT RATIO AGAINST BACKFILL STIFFNESS



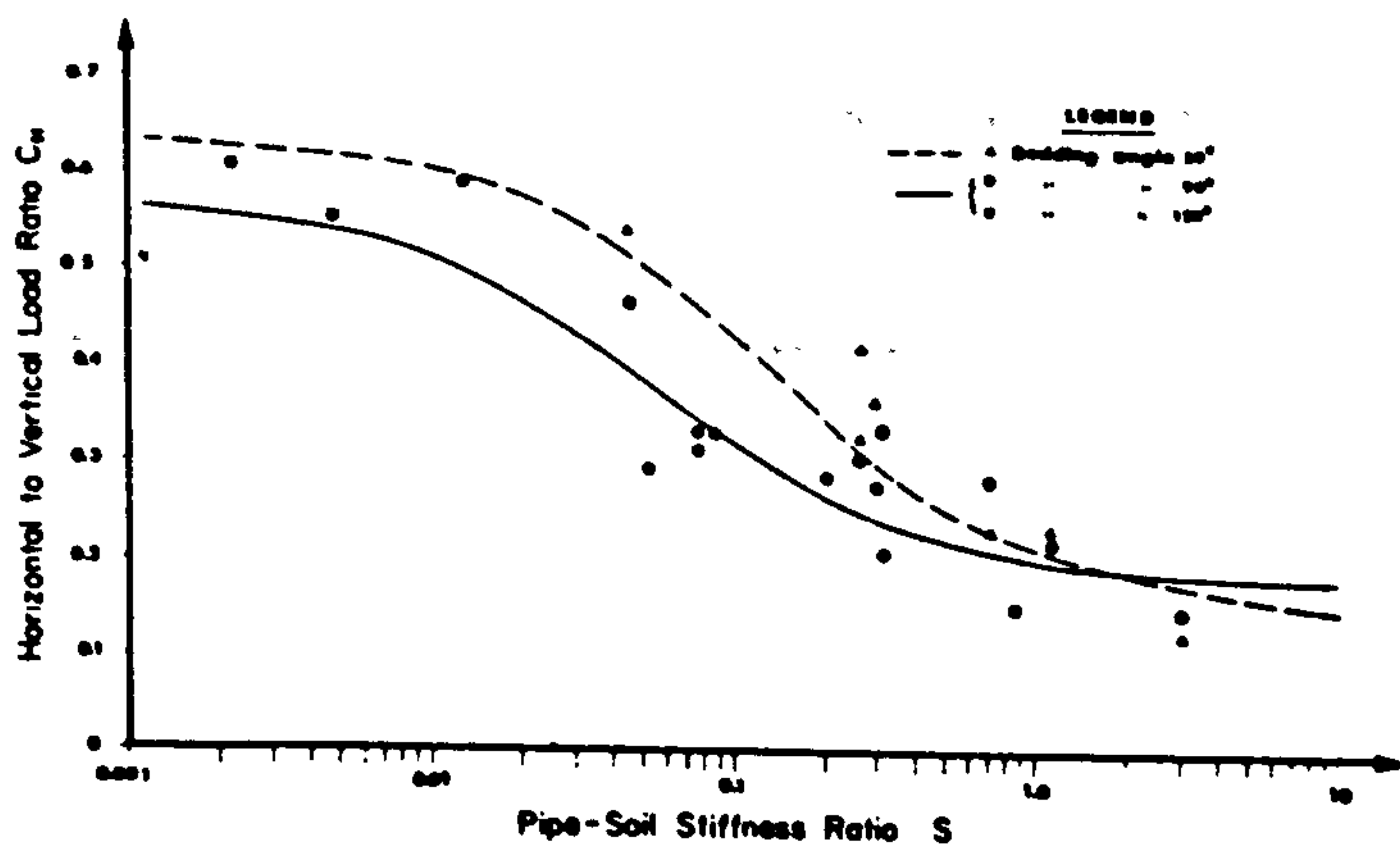


Fig 8.18 Horizontal to vertical soil load ratio C_H against Pipe-Soil stiffness (Shmulevich et al., 1986)

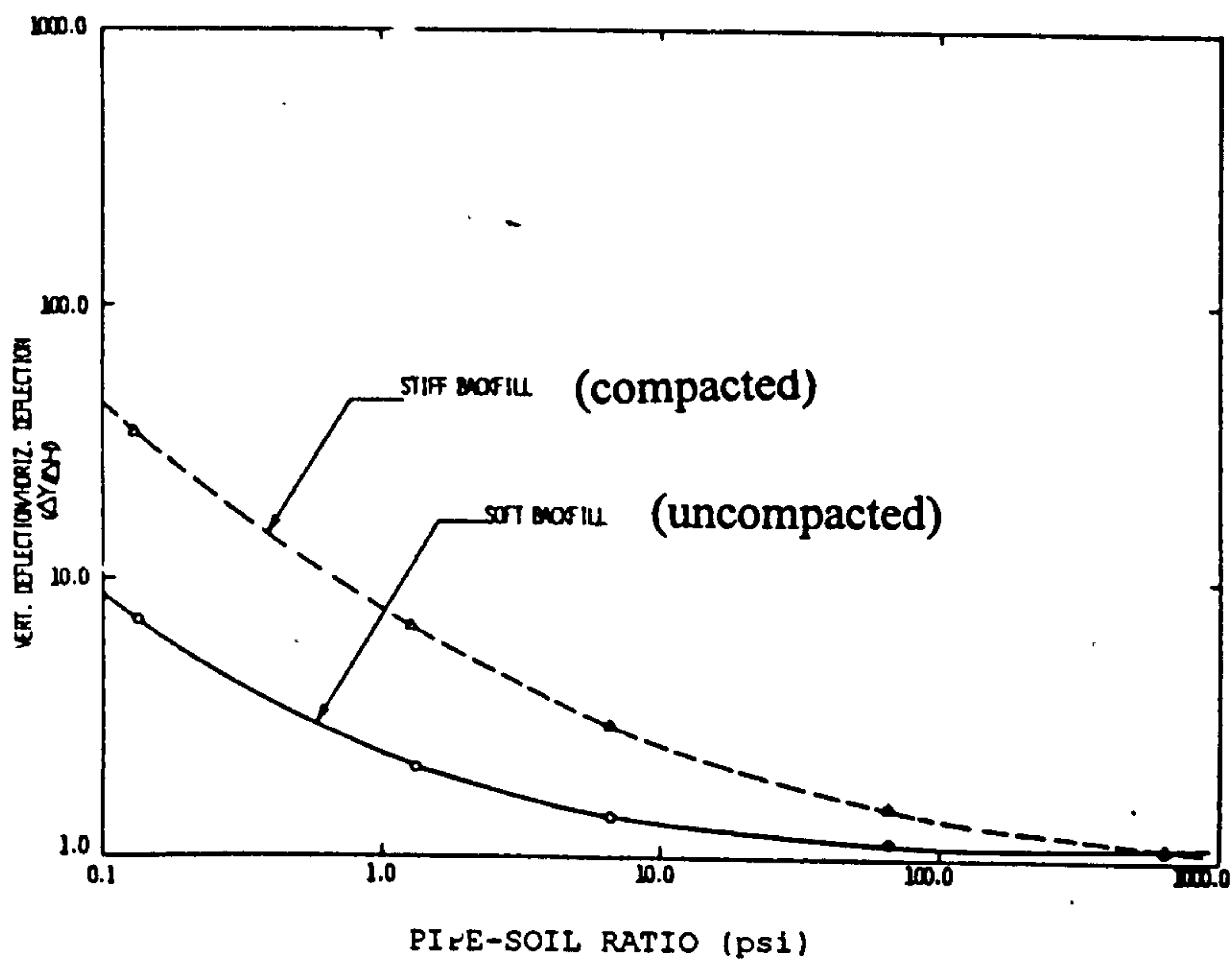


Fig 8.19 Variation of Ratio of vertical to horizontal deflection with Pipe-Soil stiffness ratio (Jeyapalan and Boldon, 1986)

FIG 8.20 DISPLACEMENT RATIO AGAINST PIPE-SOIL STIFFNESS RATIO

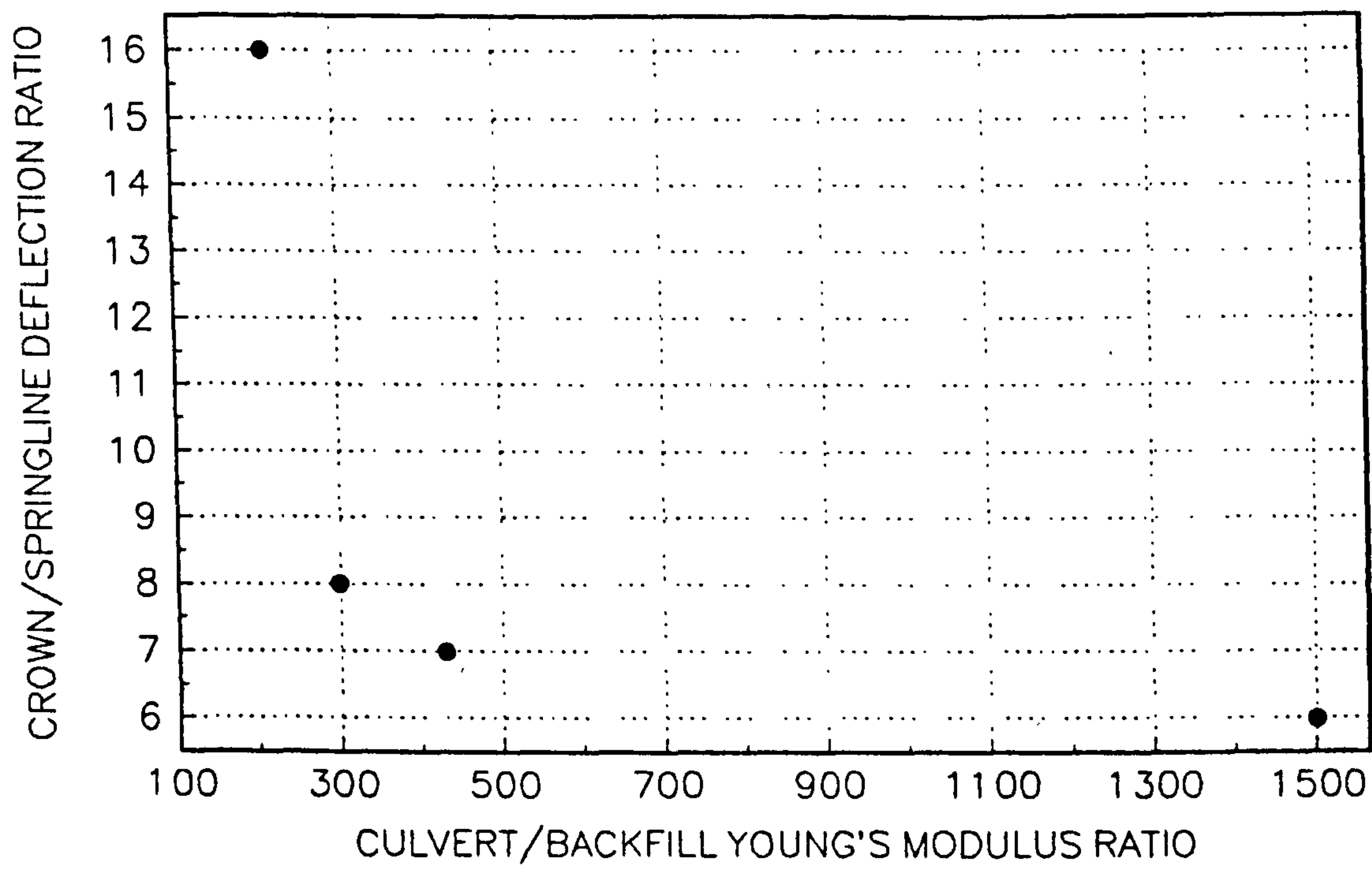


FIG 8.21 RING COMPRESSION STRAIN AGAINST PIPE-SOIL STIFFNESS RATIO

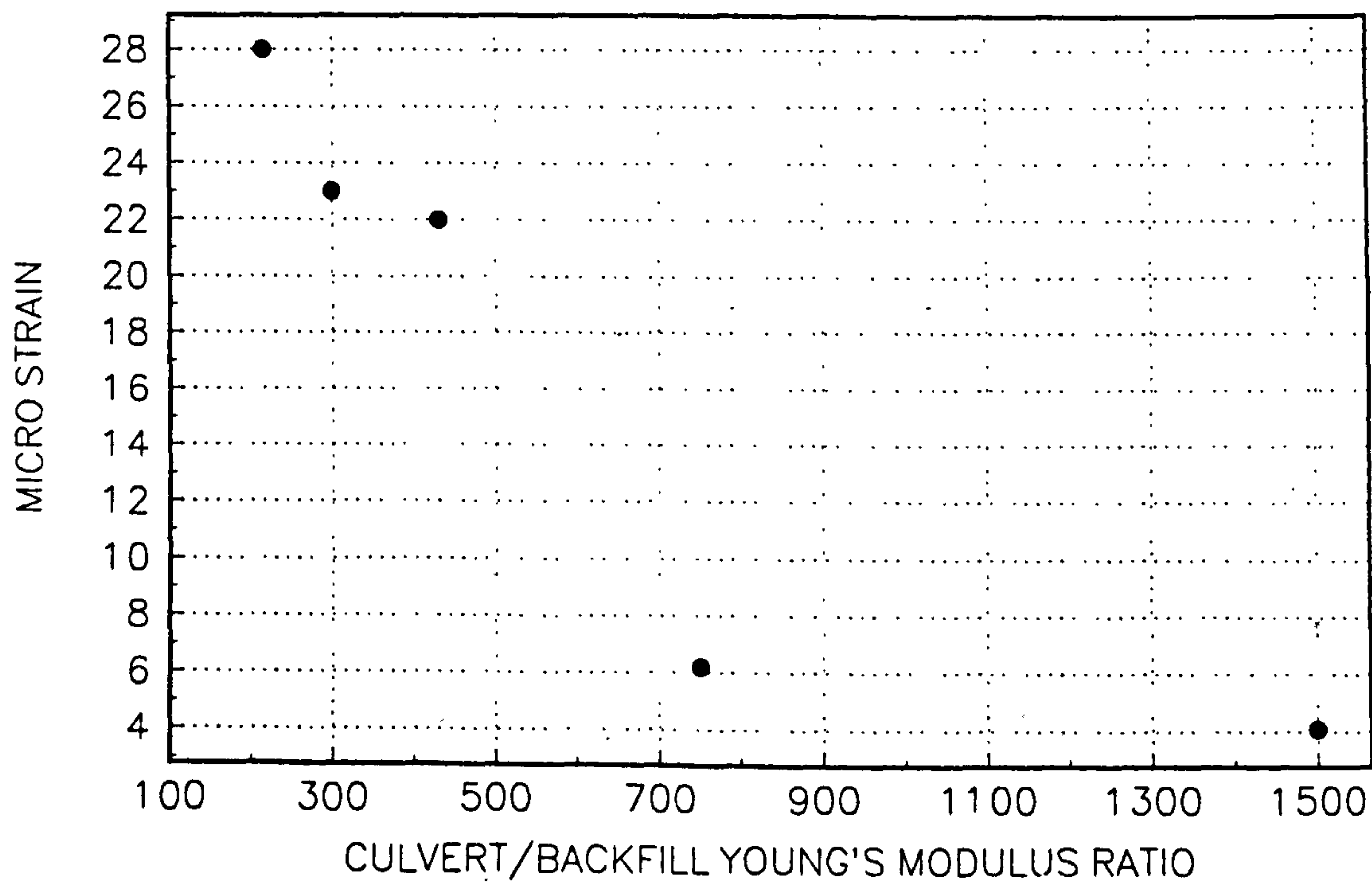


FIG 8.22 VARIATION OF LIVE LOAD THRUST WITH POISSON'S RATIO

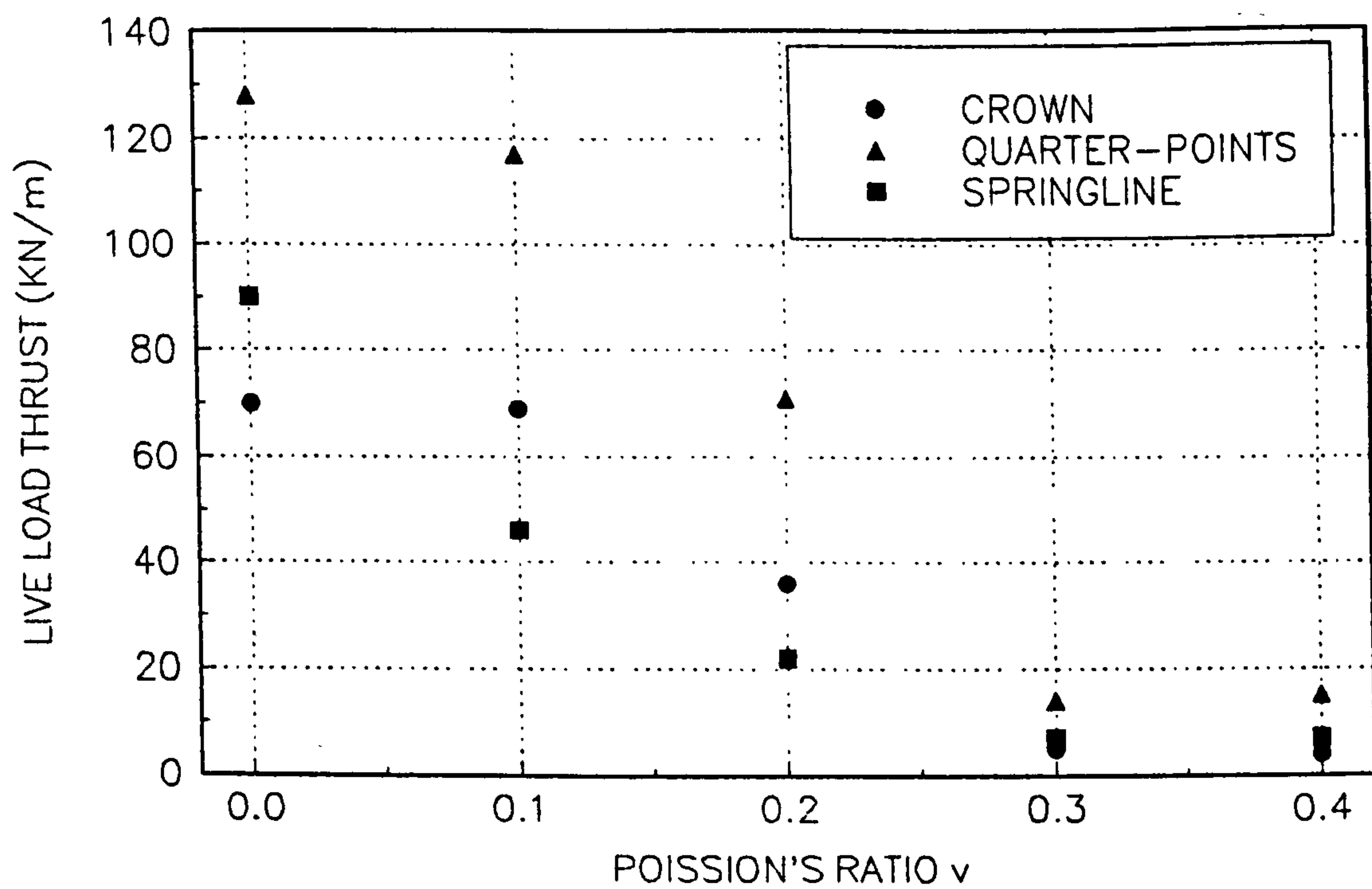


FIG 8.23 VARIATION OF LIVE LOAD RADIAL STRESS WITH POISSON'S RATIO

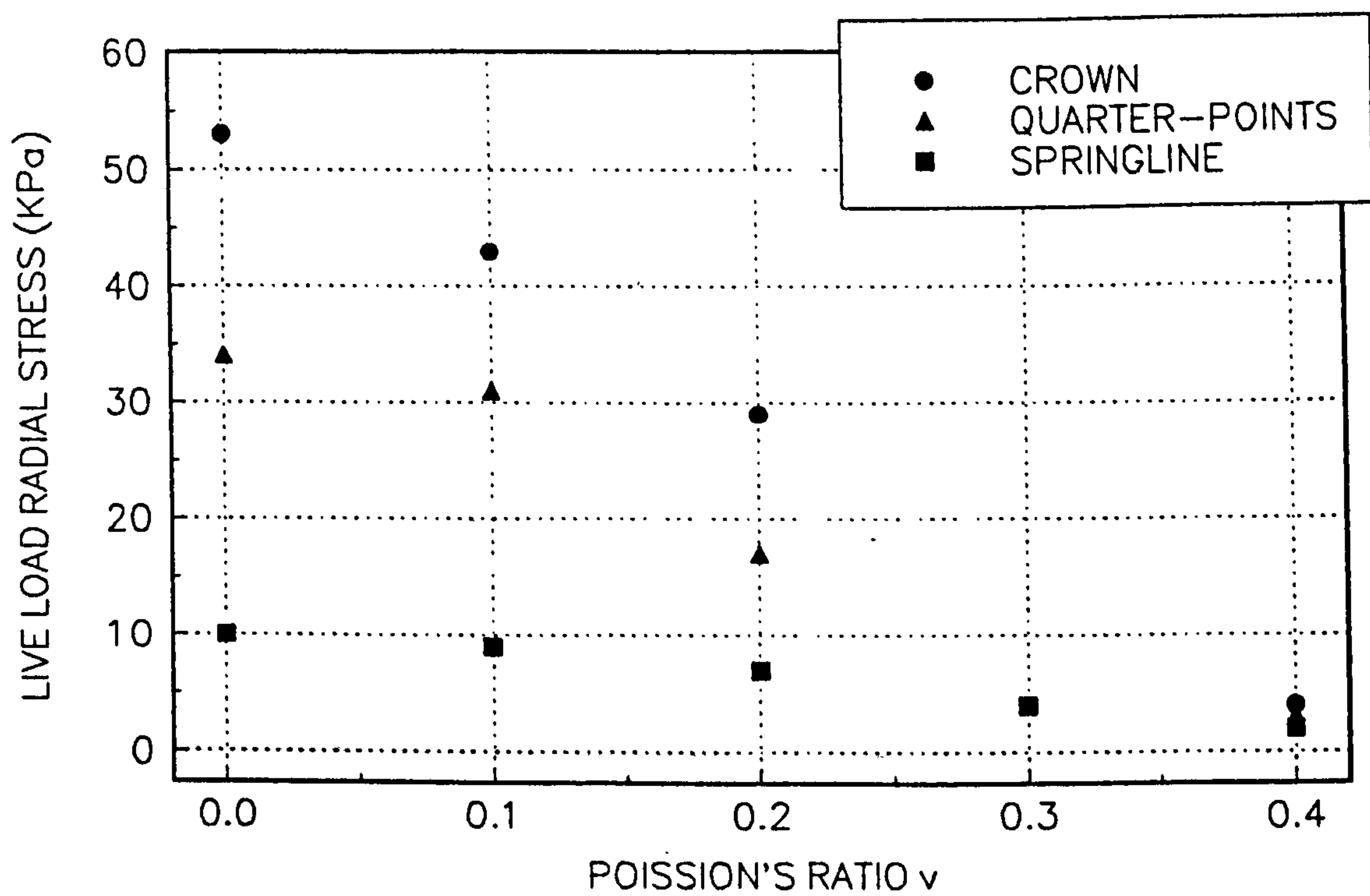


FIG 8.24 VARIATION OF LIVE LOAD SHEAR STRESS WITH POISSON'S RATIO

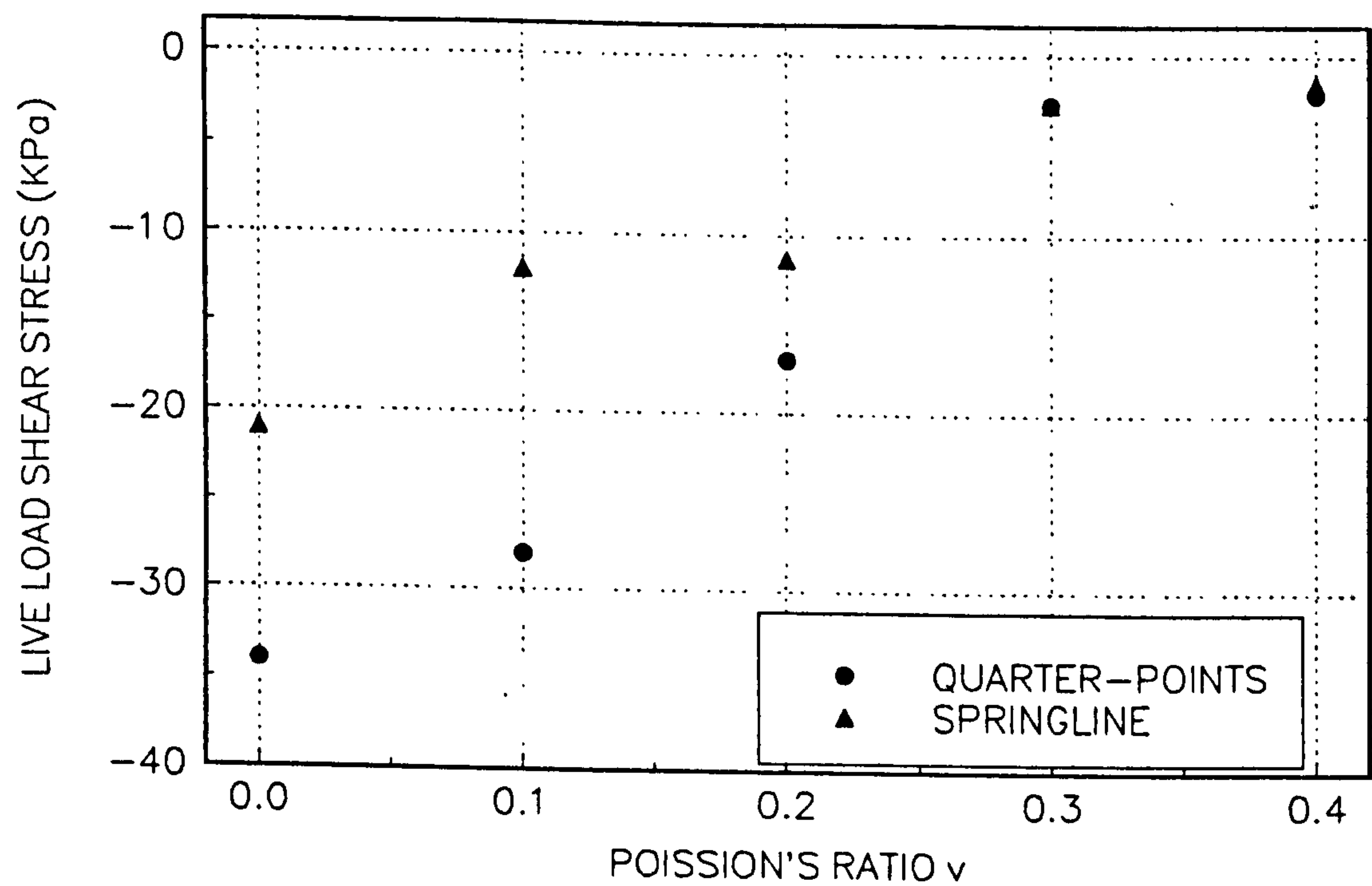


FIG 8.25(a) VARIATION OF LIVE LOAD CROWN DISPLACEMENT WITH POISSON'S RATIO

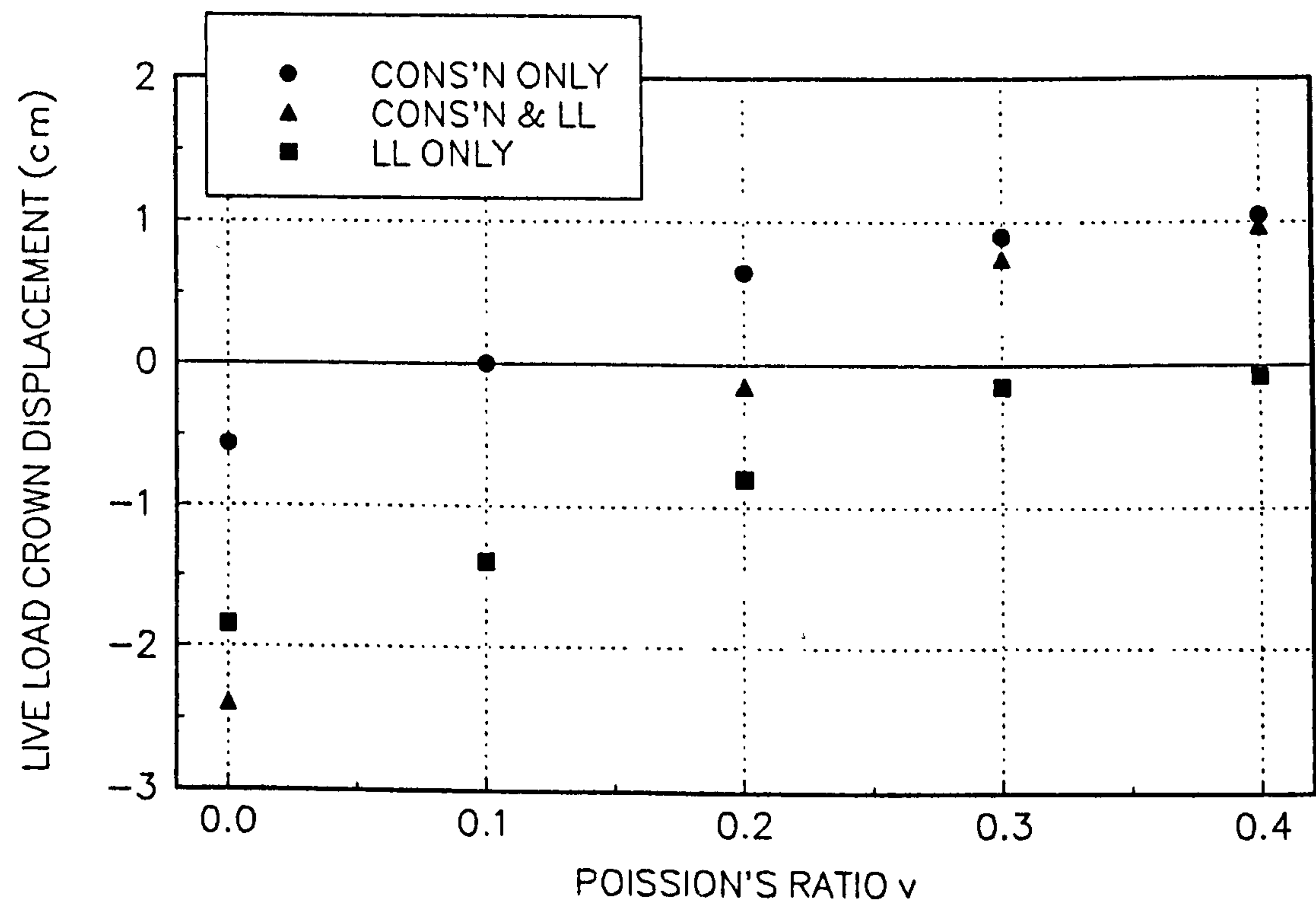


FIG 8.25(b) VARIATION OF LIVE LOAD SPRINGLINE DISPLACEMENT WITH POISSON'S RATIO

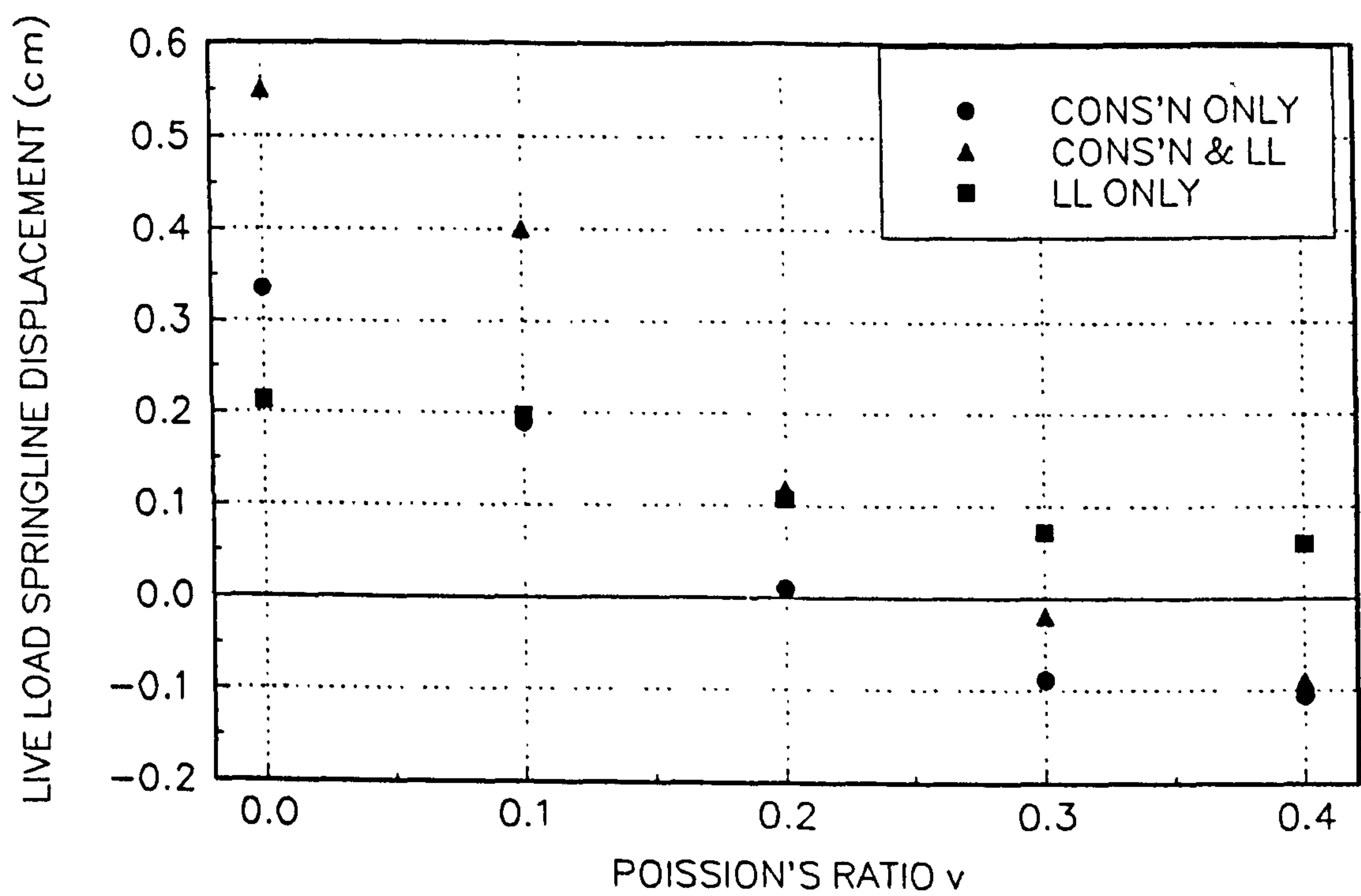


FIG 8.26 VARIATION OF LIVE LOAD BENDING MOMENT WITH POISSON'S RATIO

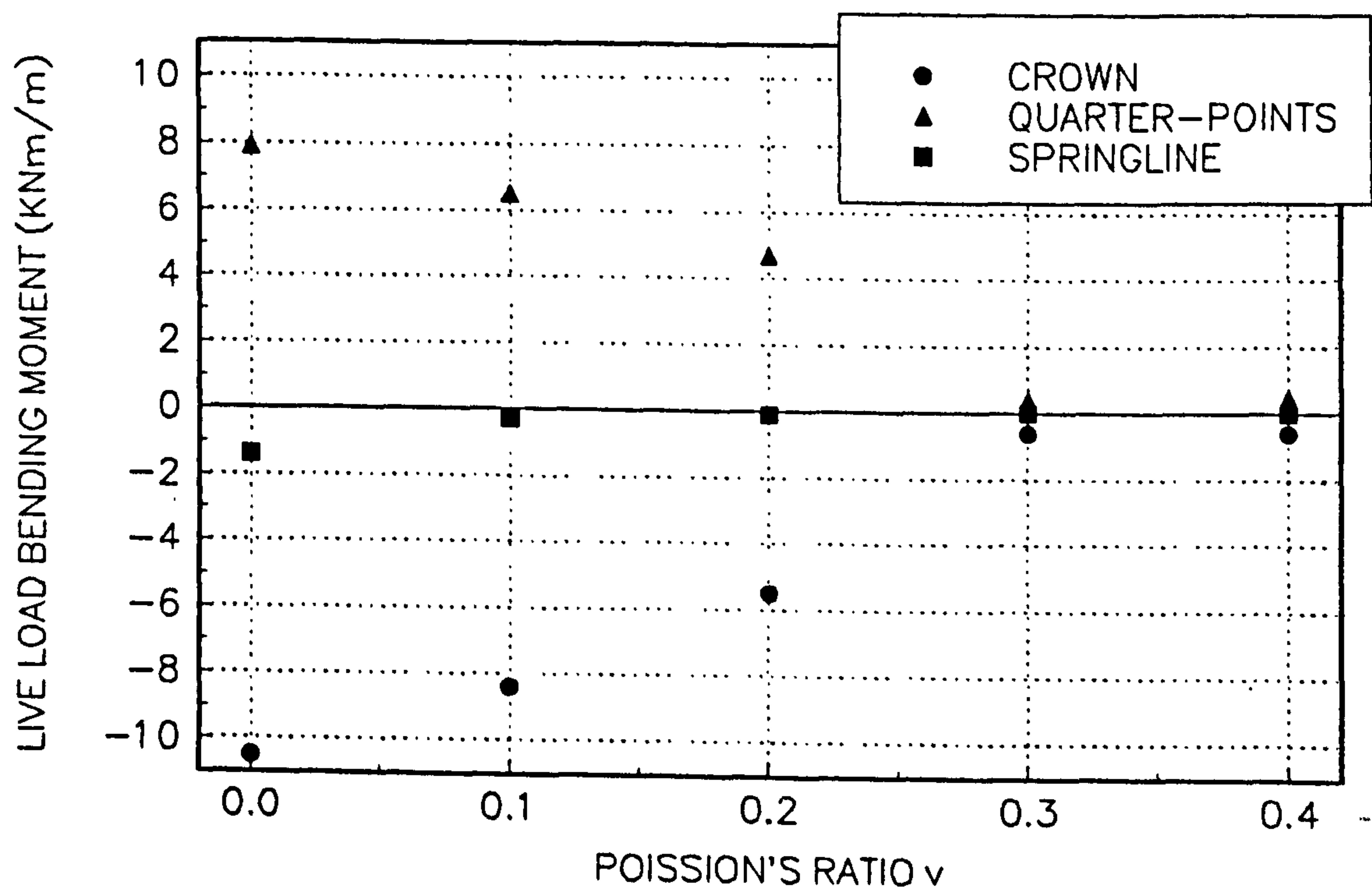


FIG 8.27 VARIATION OF THE DEGREE OF ARCHING WITH POISSON'S RATIO

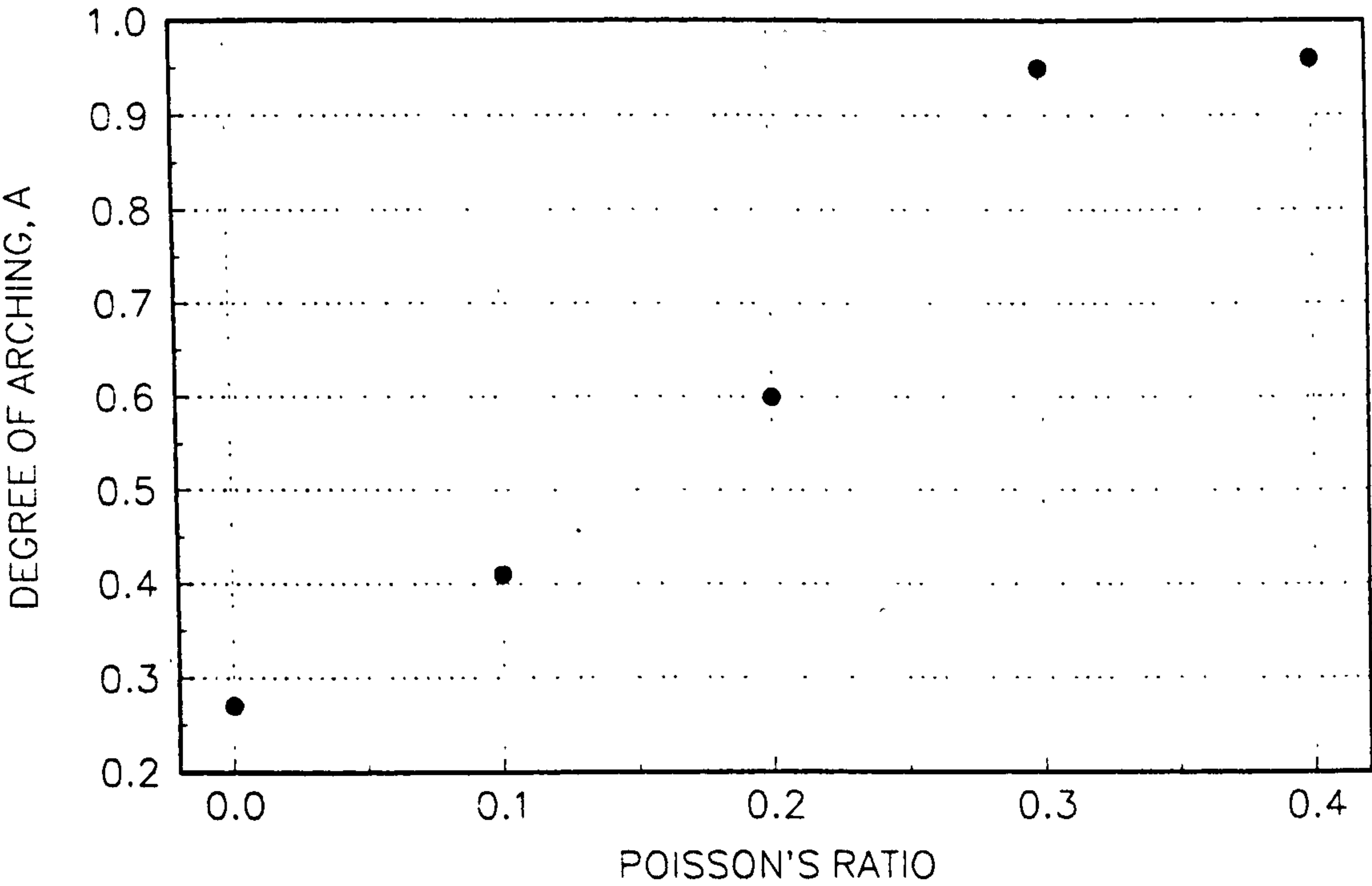


FIG 8.28(a) VARIATION OF LIVE LOAD CROWN DISPLACEMENT WITH ϕ_f

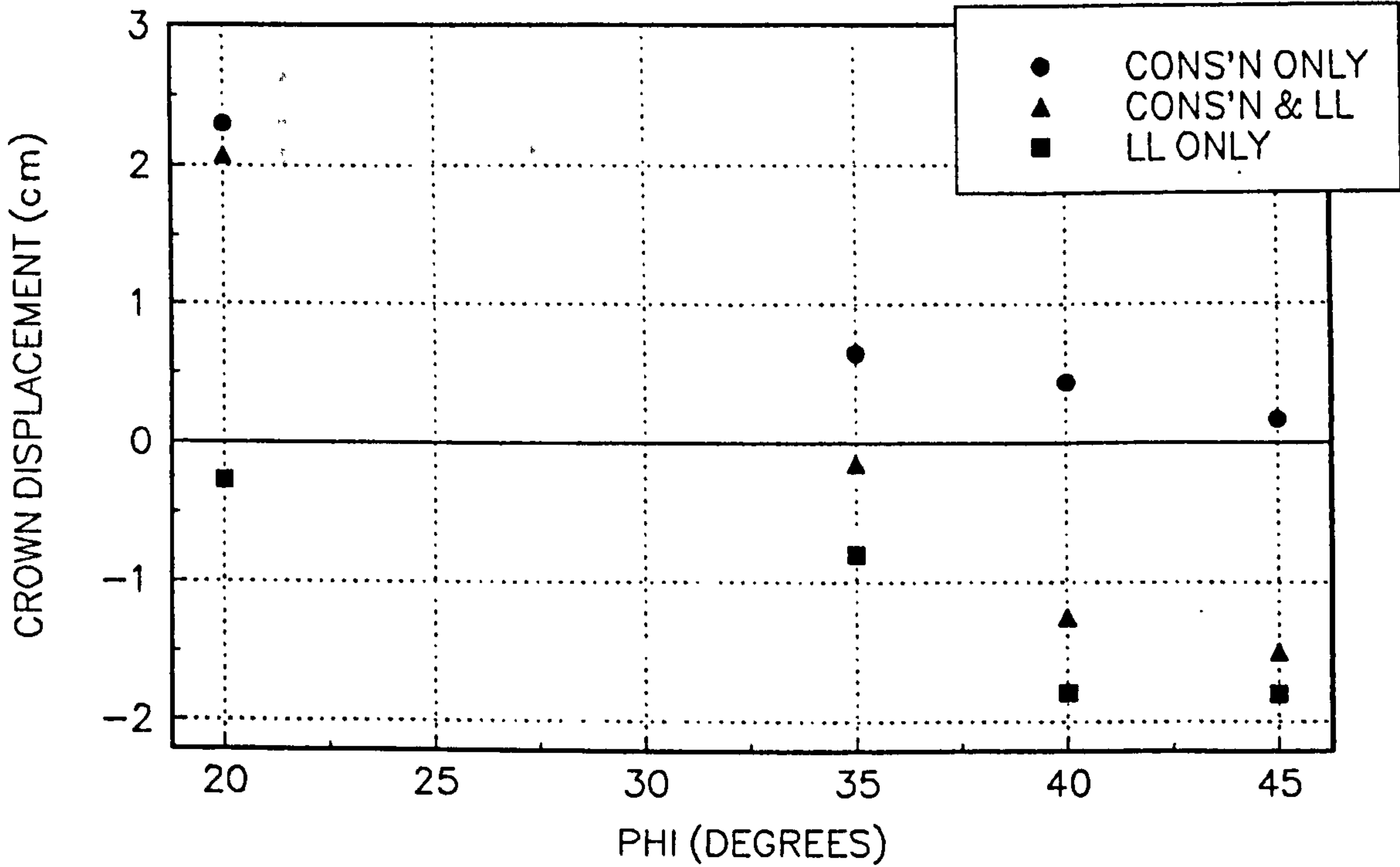


FIG 8.28(b) VARIATION OF LIVE LOAD SPRINGLINE DISPLACEMENT WITH ϕ_f

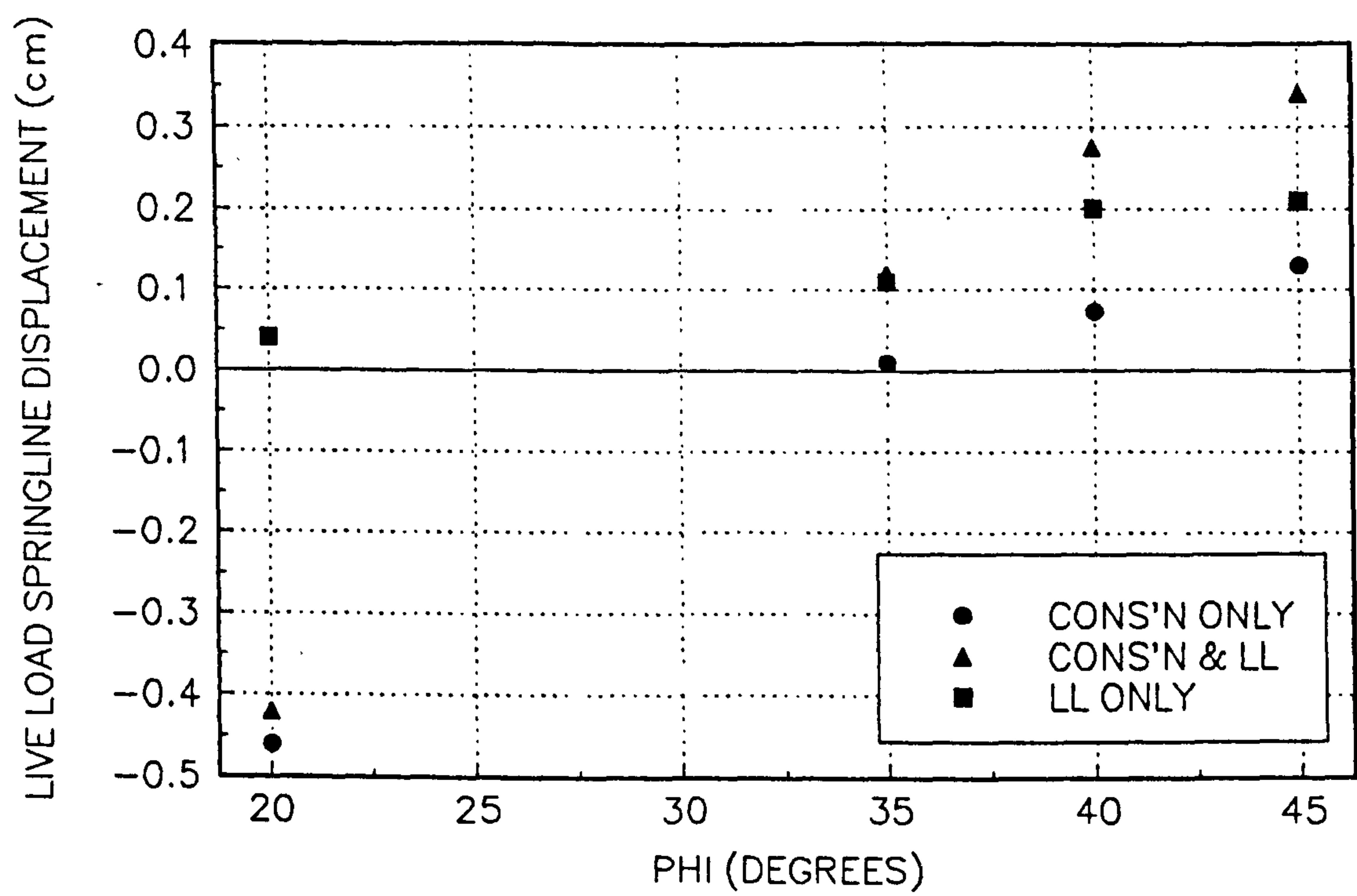


FIG 8.29 VARIATION OF LIVE LOAD RADIAL STRESS WITH ϕ_f

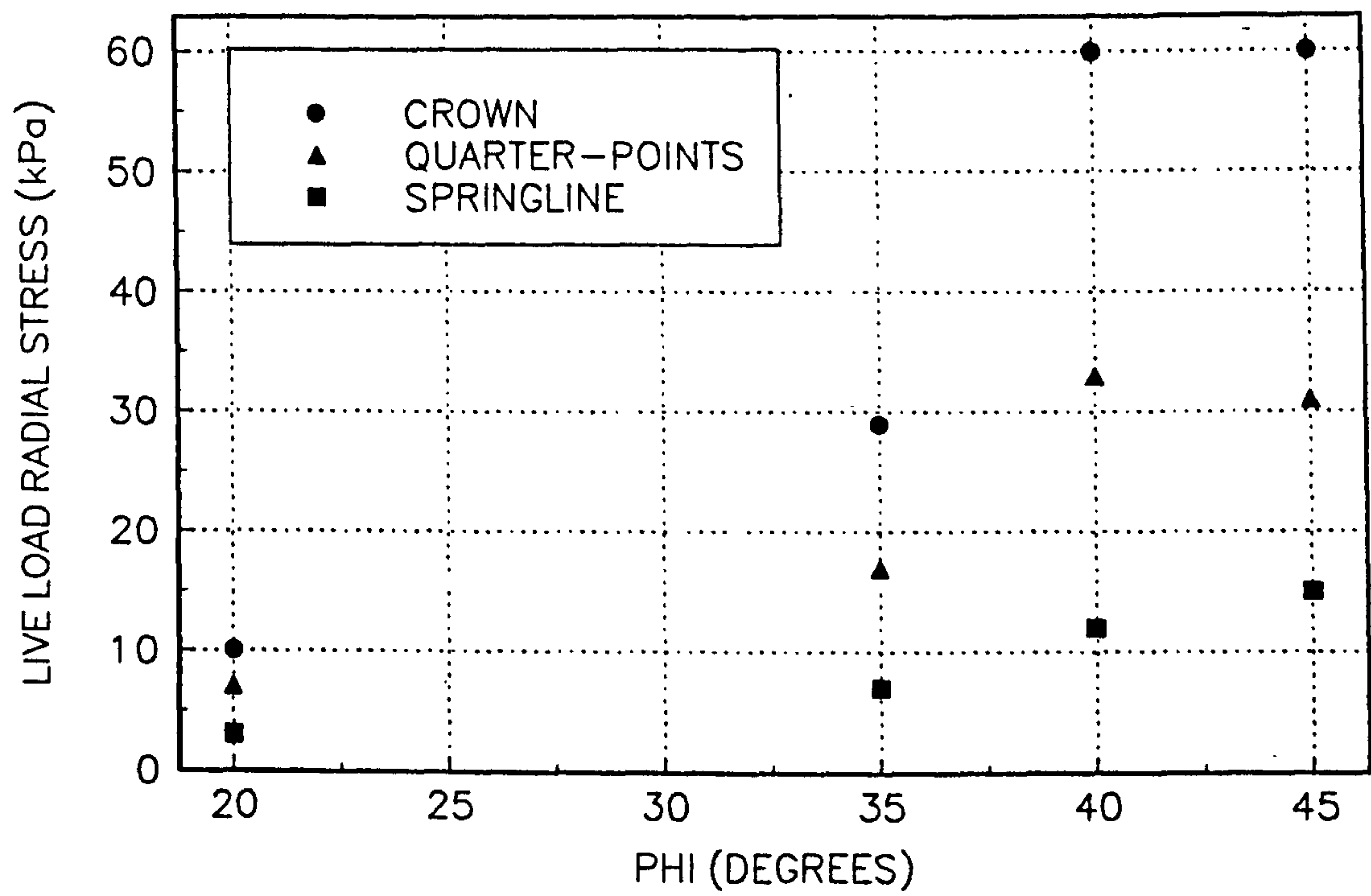


FIG 8.30 VARIATION OF LIVE LOAD SHEAR STRESS WITH ϕ_f

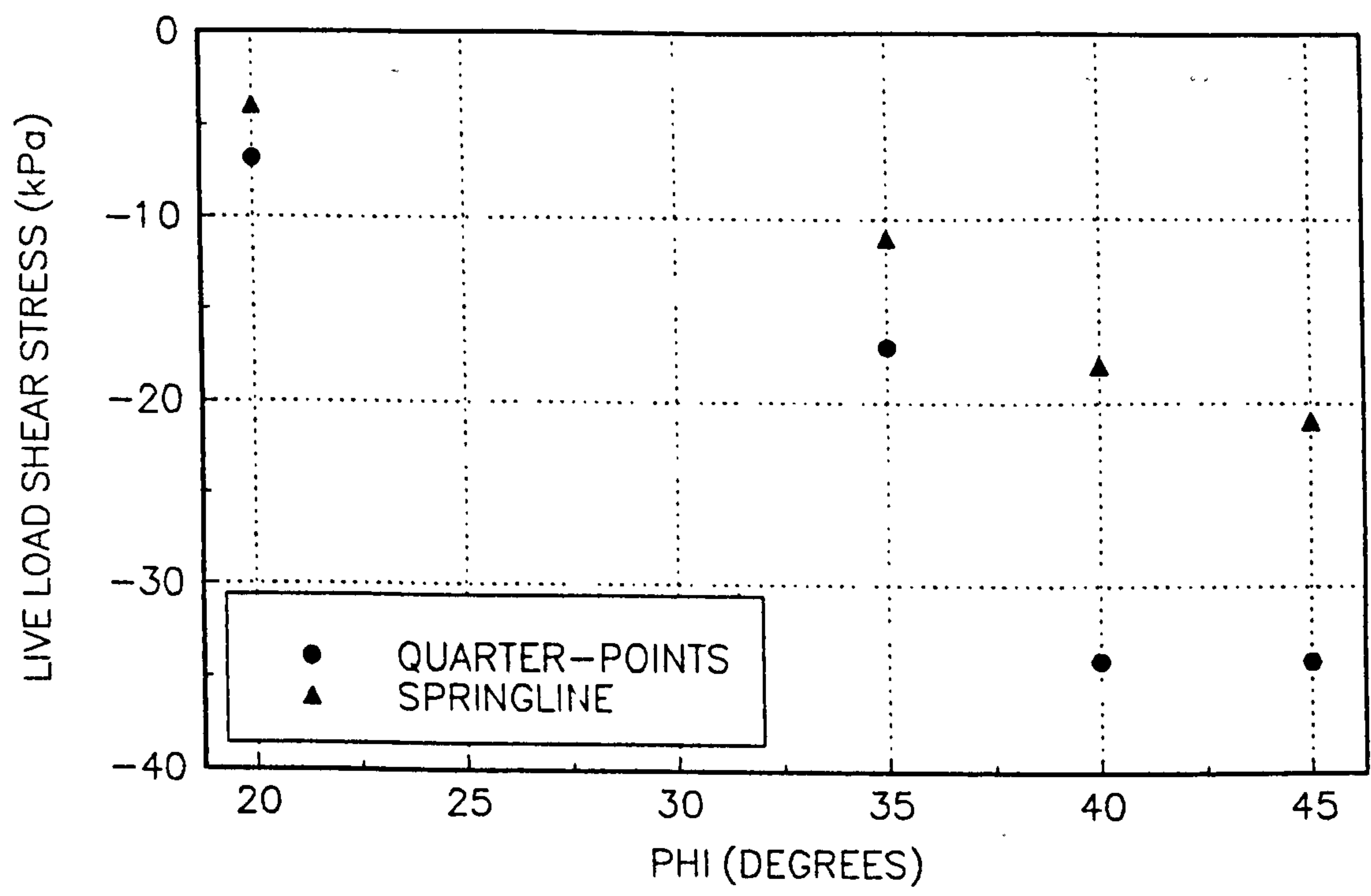


FIG 8.31 VARIATION OF LIVE THRUST WITH ϕ_f

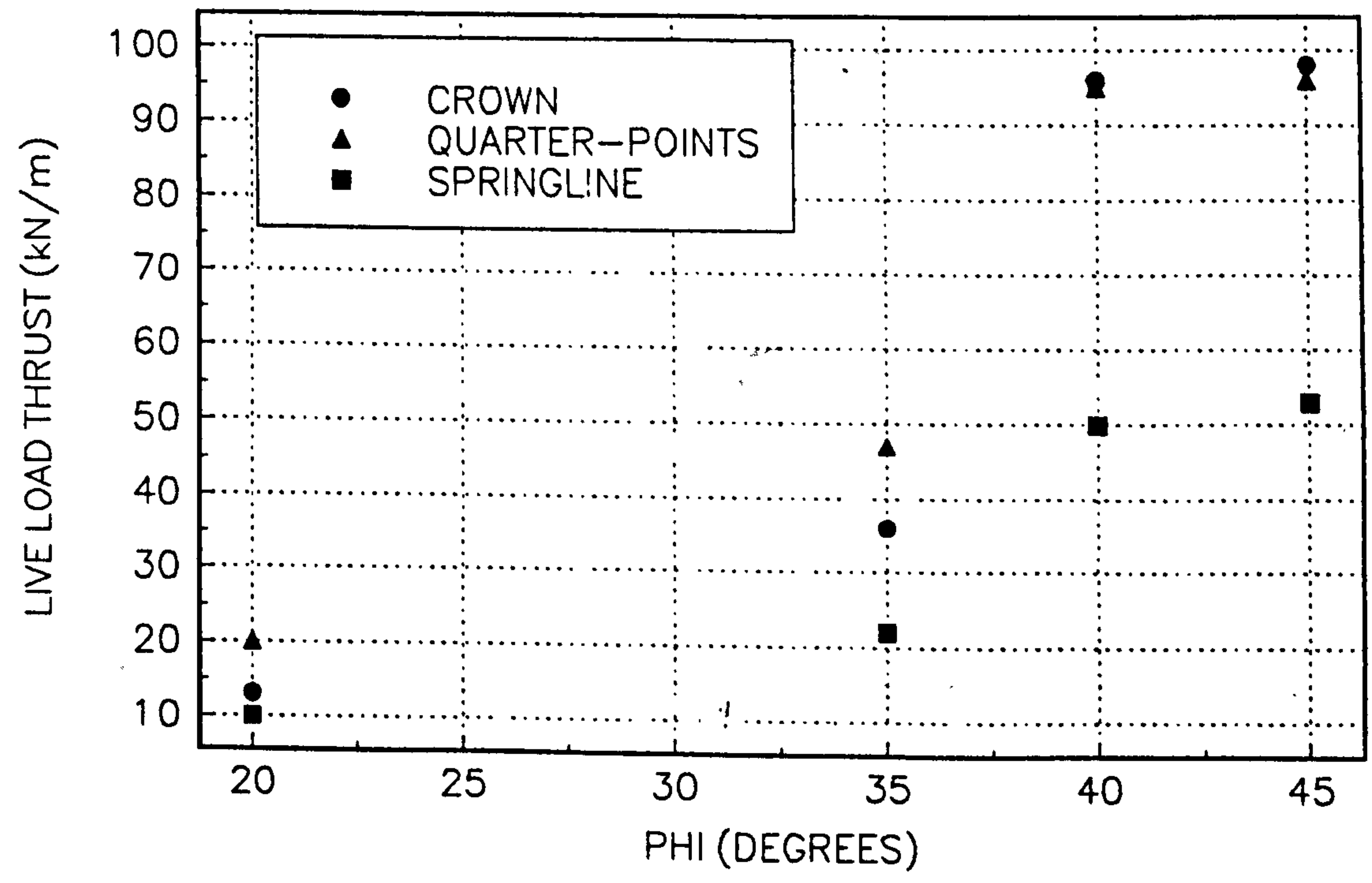
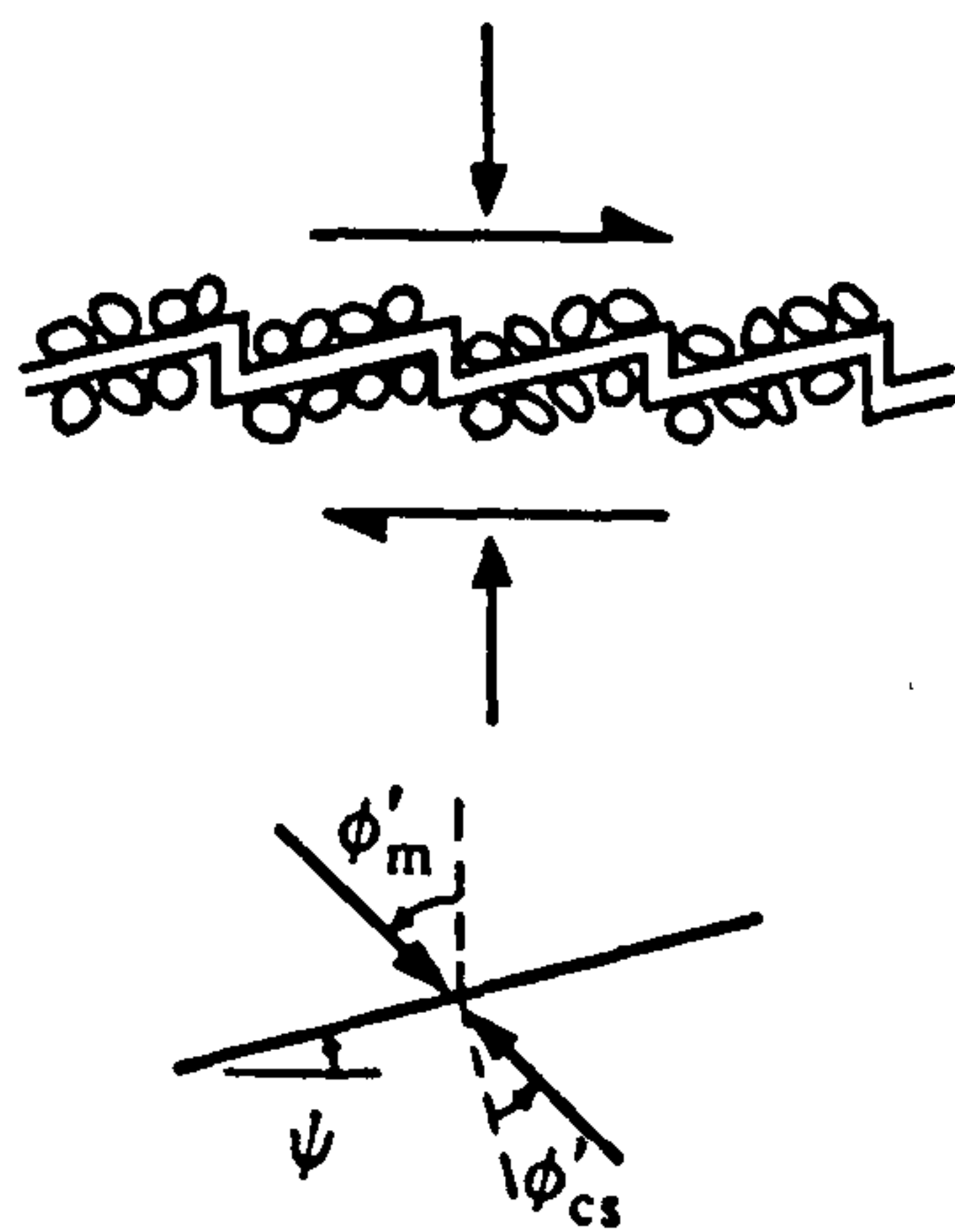
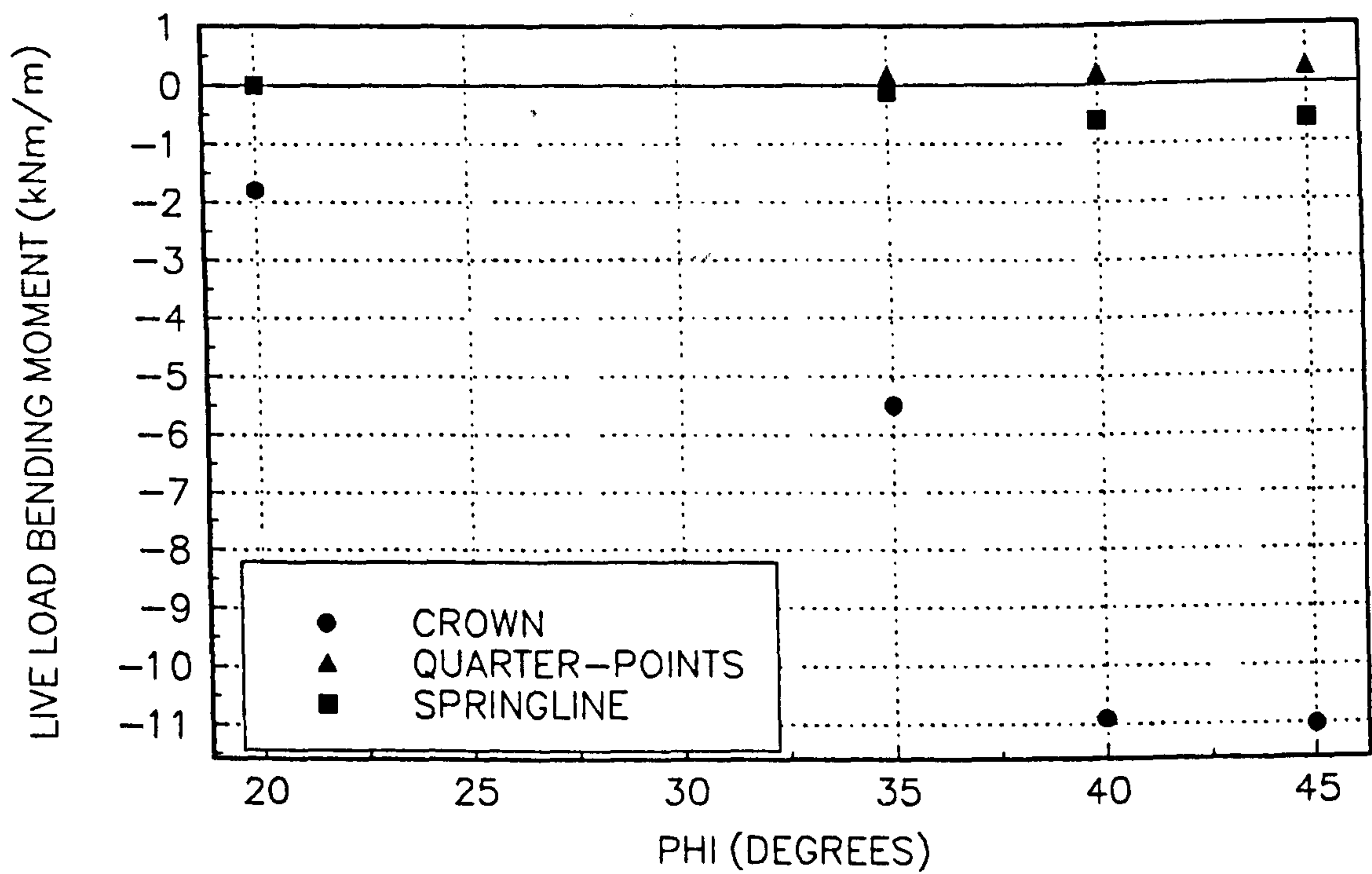


FIG 8.32 VARIATION OF LIVE LOAD BENDING MOMENT WITH ϕ_f



Where ϕ'_m is the the mobilised angle of friction on horizontal planes; ϕ'_{cs} angle of friction resisting sliding on the inclined planes.

FIG 8.33 SLIDING OF SOIL PARTICLES ON INCLINED PLANES AND
RESULTANT FORCES ON AN INCLINED SURFACE
(MUIR WOOD, 1990)

Fig 8.34 (a) and (b) Definition of angle of dilation ψ (Muir Wood, 1990).

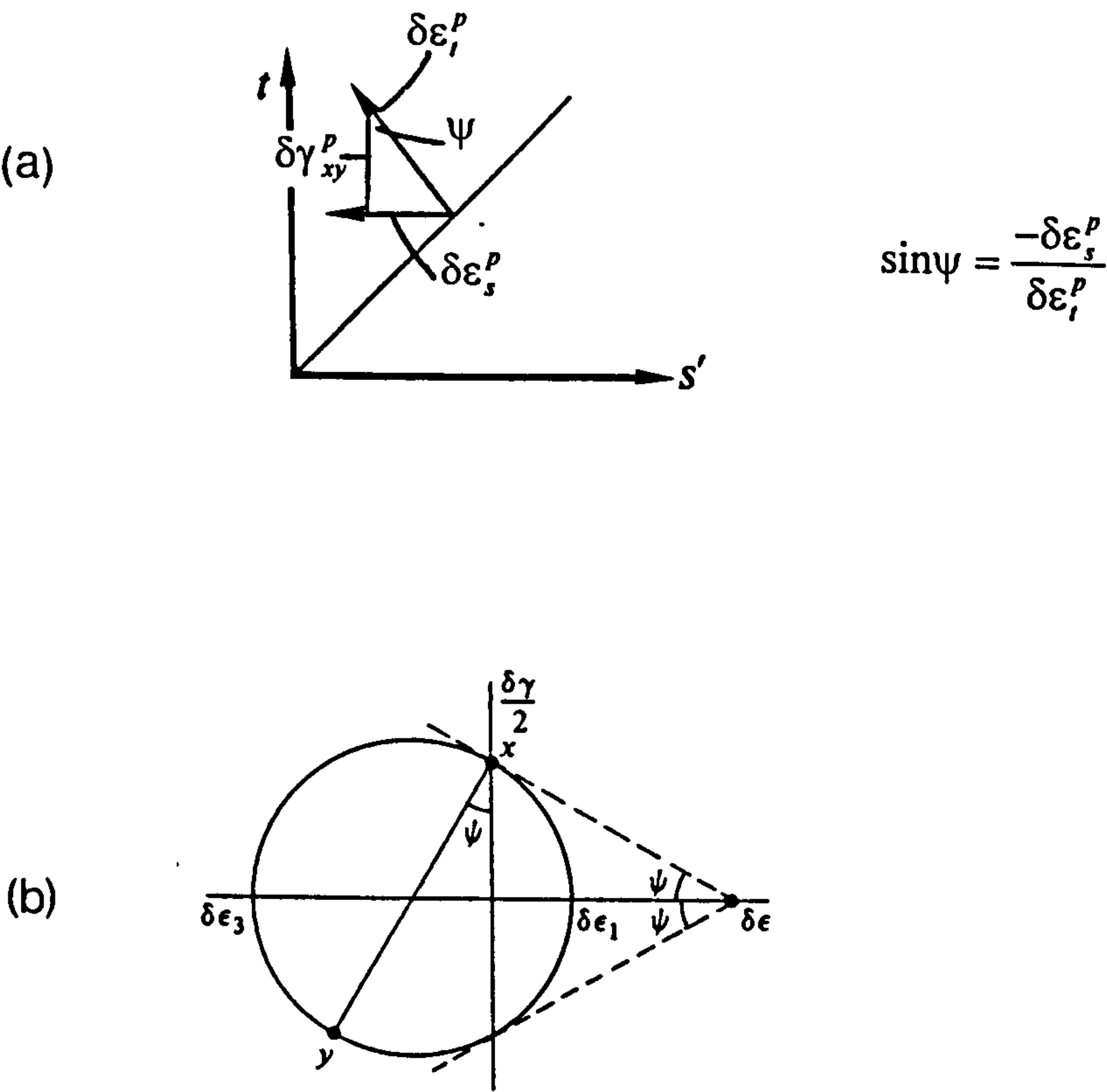


FIG 8.35 VARIATION OF LIVE THRUST WITH ψ_f

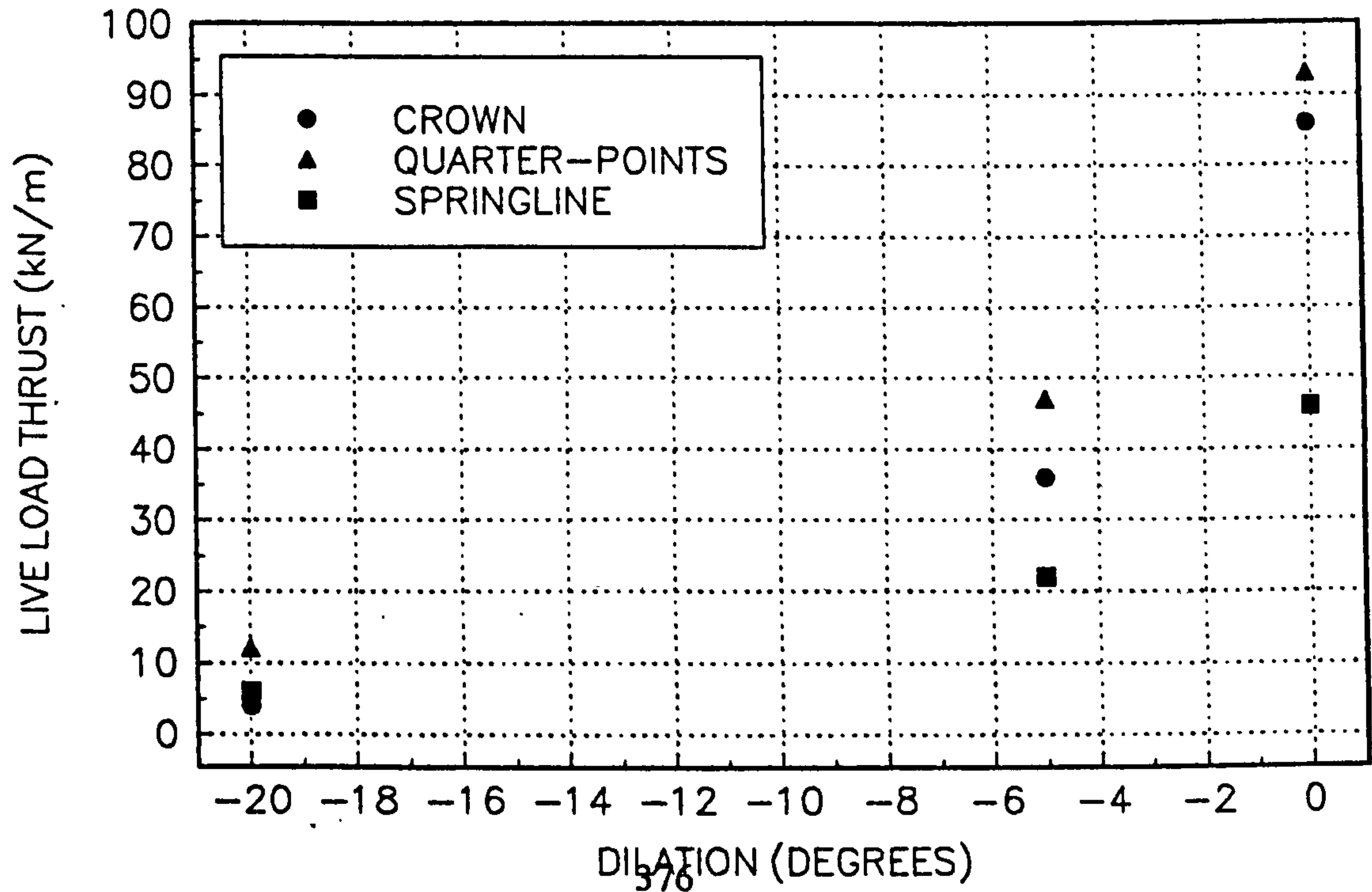


FIG 8.36 VARIATION OF LIVE LOAD BENDING MOMENT WITH ψ_f

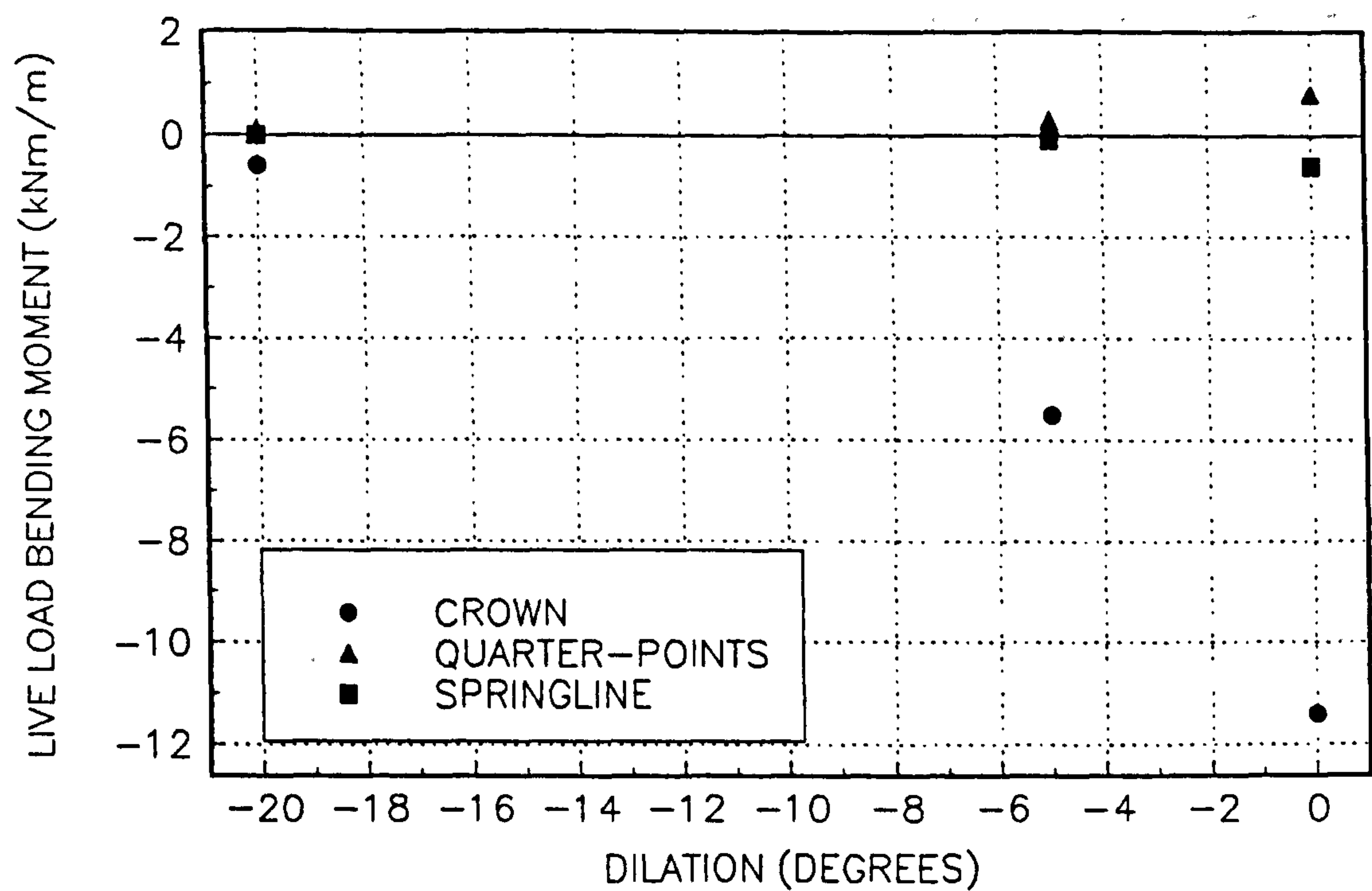


FIG 8.37(a) VARIATION OF LIVE LOAD RADIAL STRESS WITH ψ_f

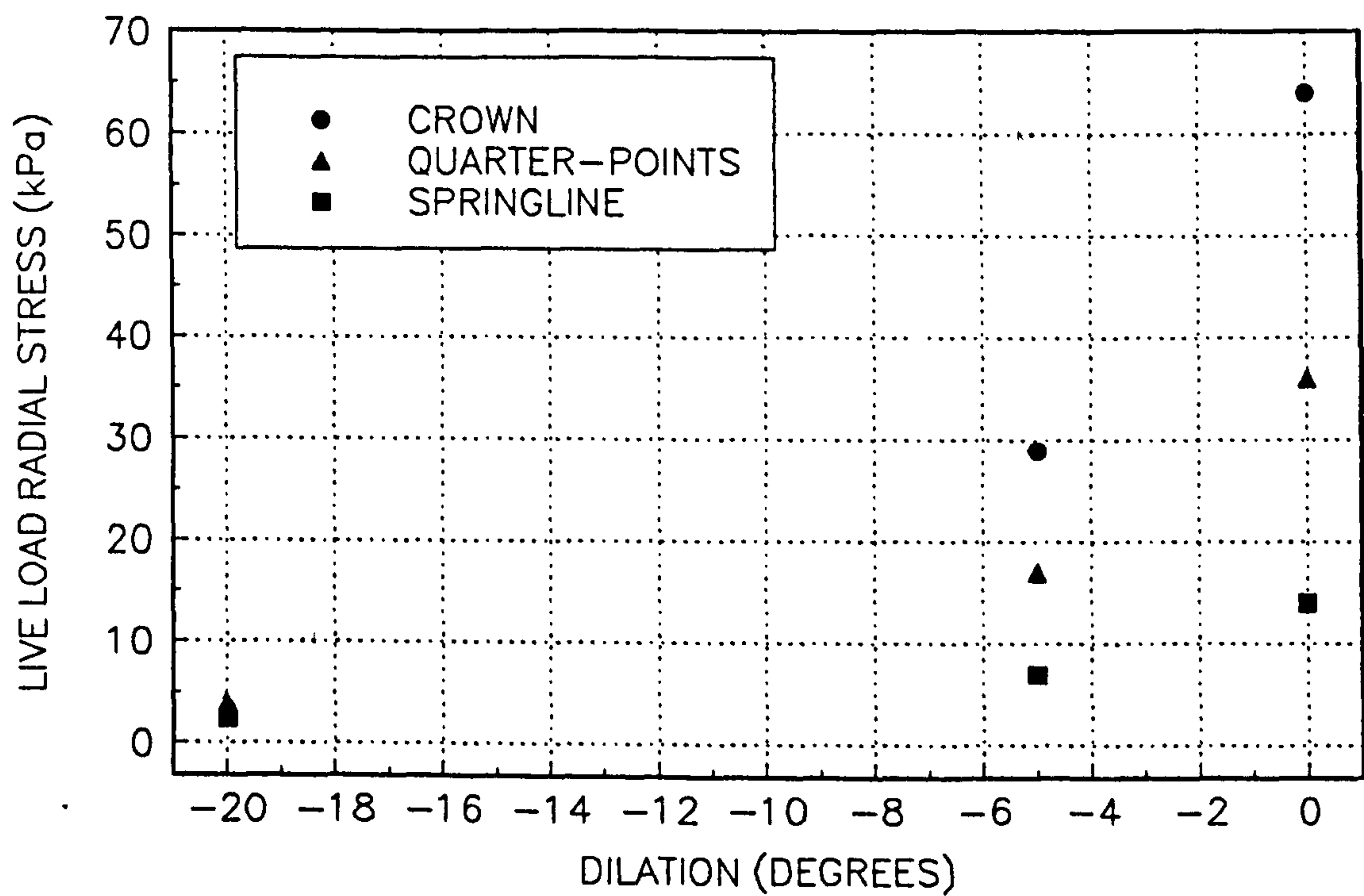


FIG 8.37(b) VARIATION OF LIVE LOAD SHEAR STRESS WITH ψ_f

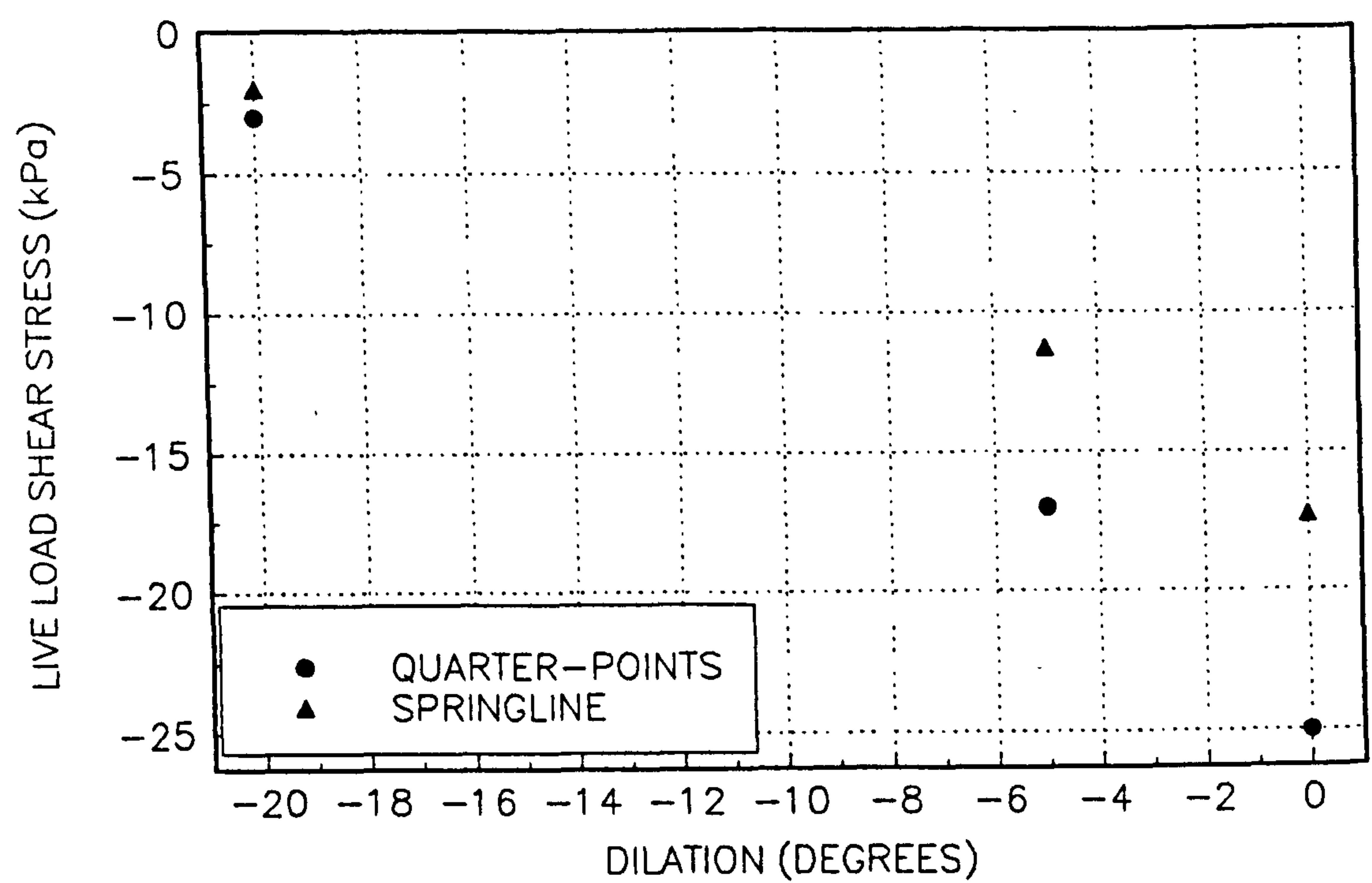


FIG 8.38(a) VARIATION OF LIVE LOAD CROWN DISPLACEMENT WITH ψ_f

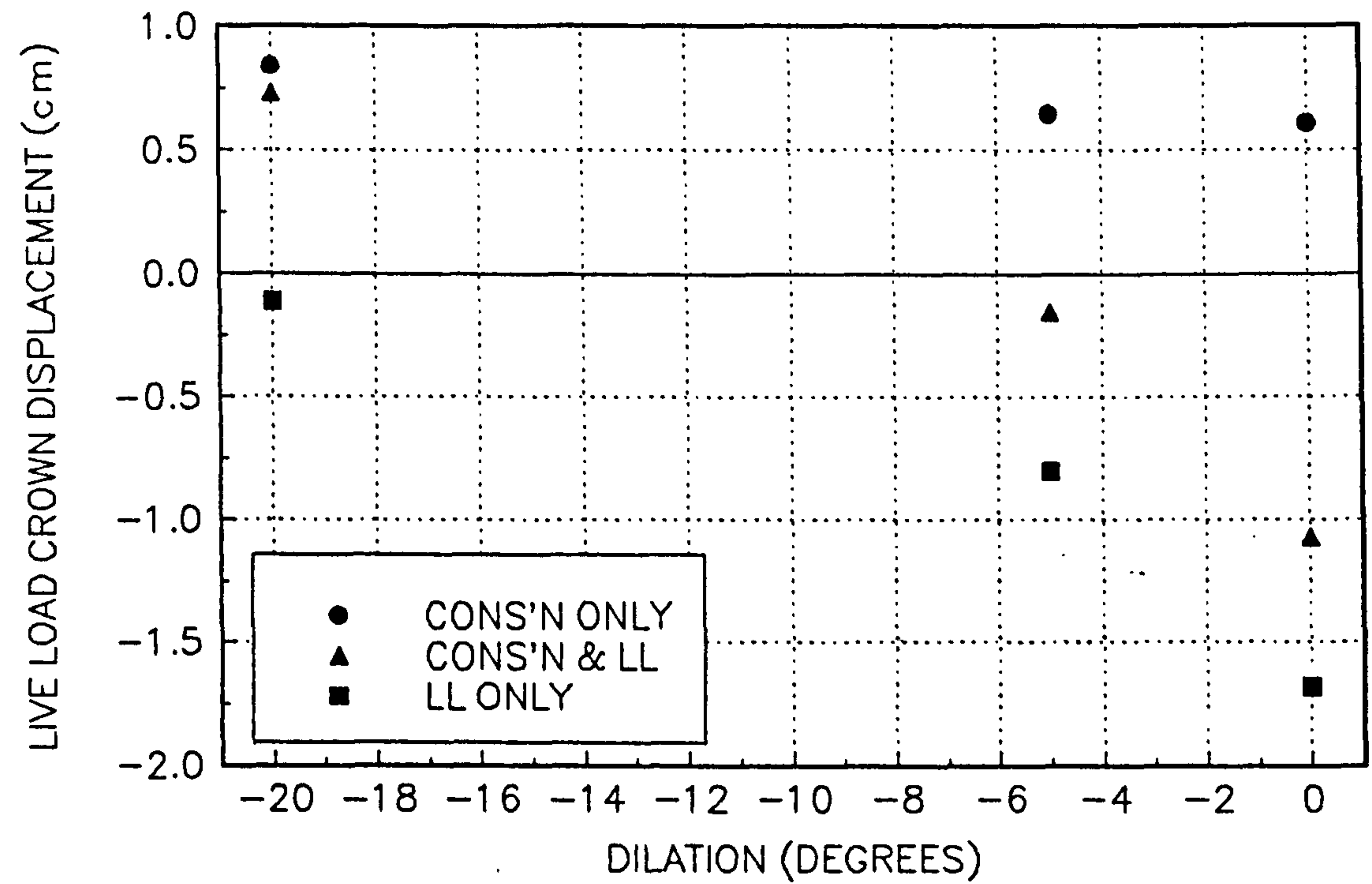


FIG 8.38(b) VARIATION OF LIVE LOAD SPRINGLINE DISPLACEMENT WITH ψ_f

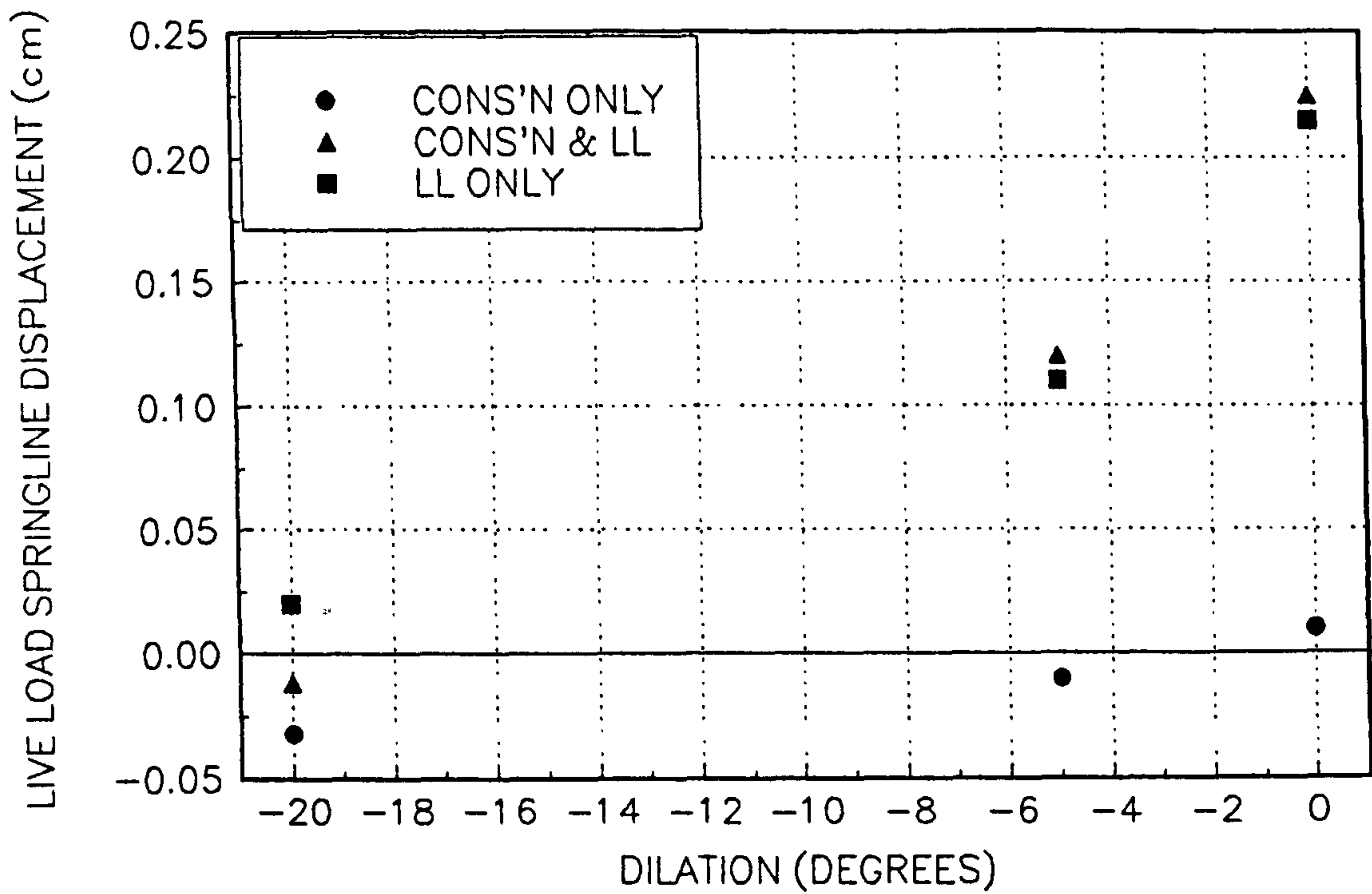


FIG 8.39 VARIATION OF LIVE LOAD THRUST WITH COMPACTION PRESSURE

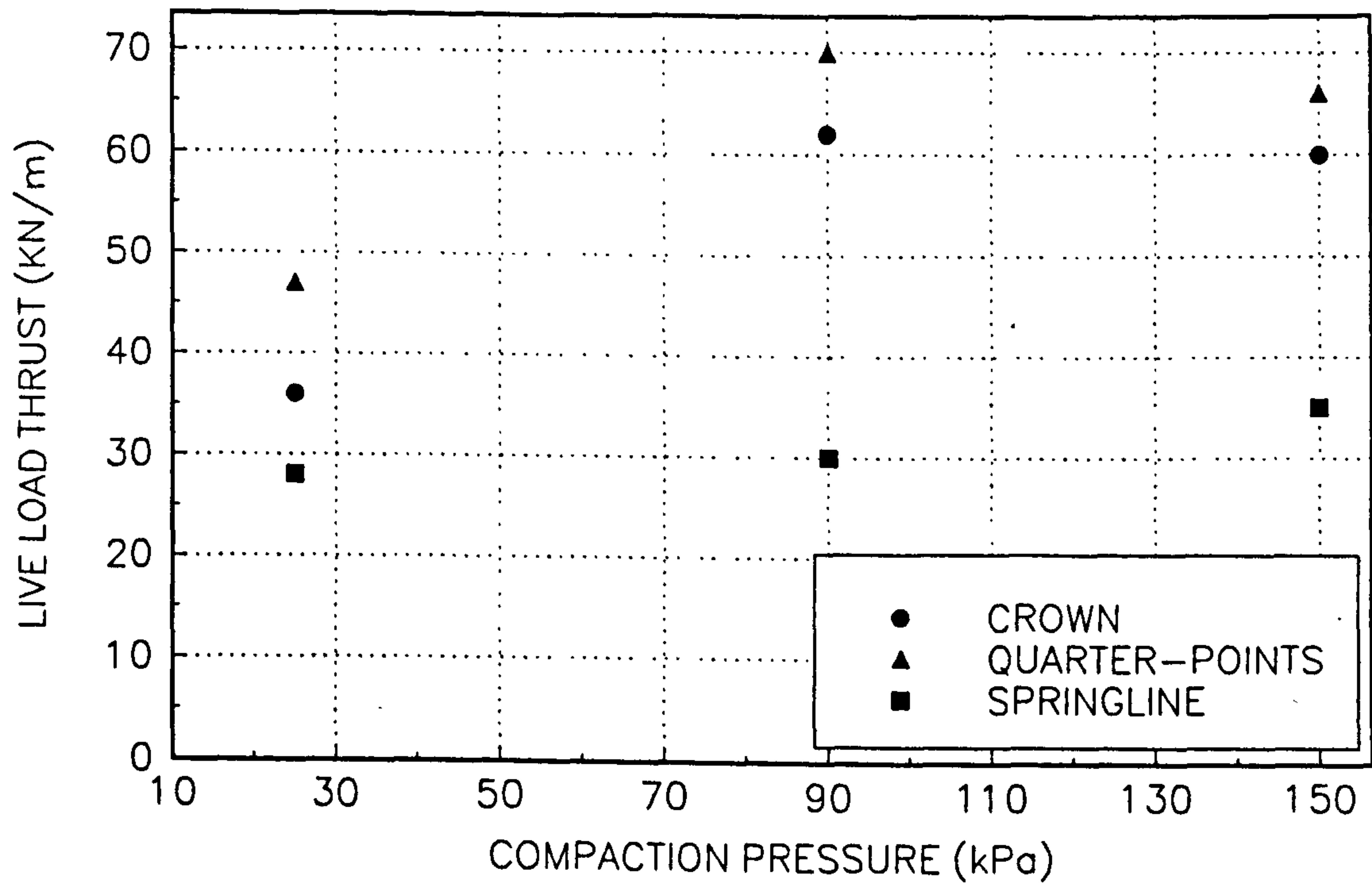


FIG 8.40 VARIATION OF LIVE BENDING MOMENT THRUST WITH COMPACTION PRESSURE

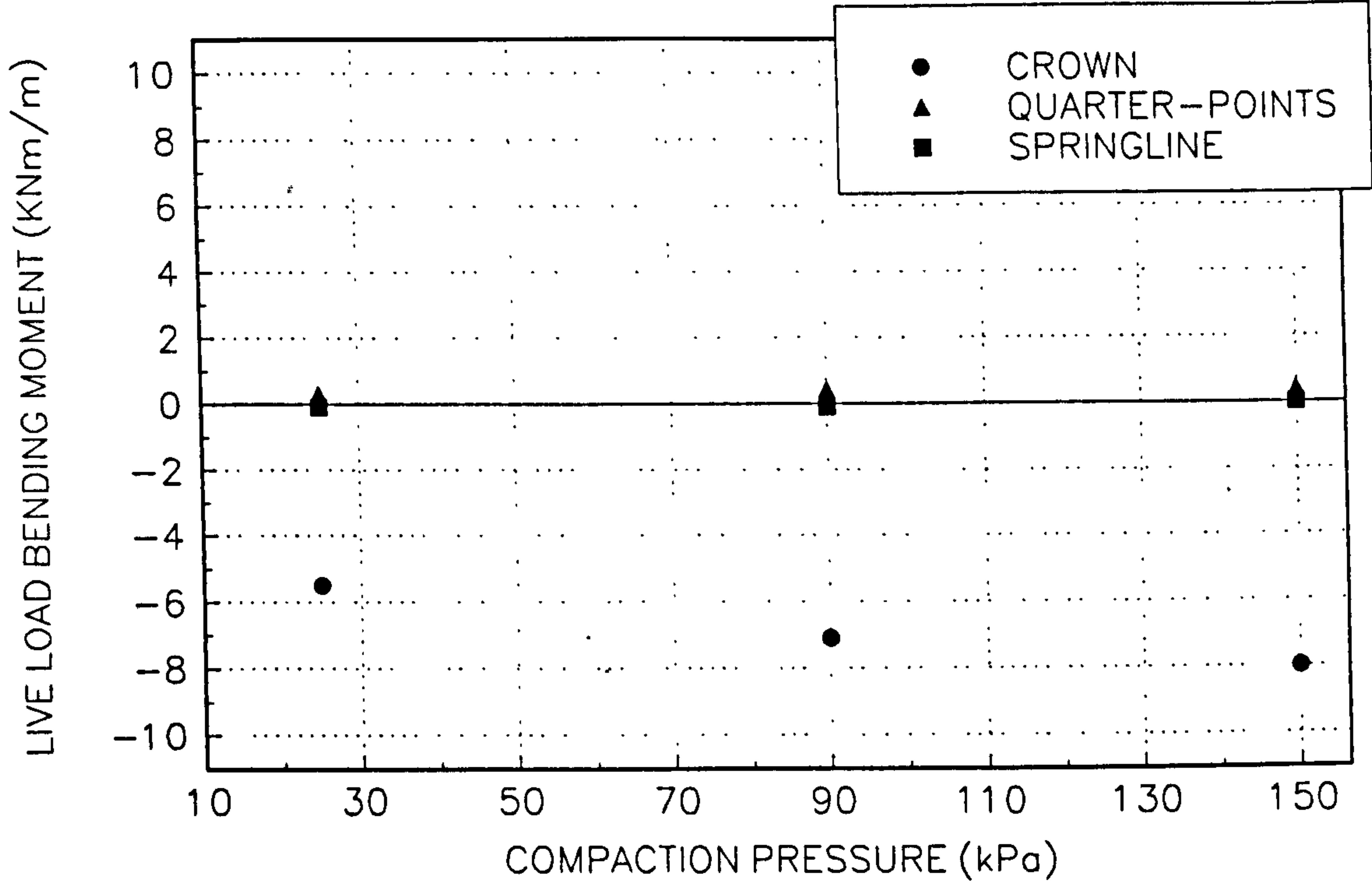


FIG 8.41 VARIATION OF LIVE LOAD RADIAL STRESS WITH COMPACTION PRESSURE

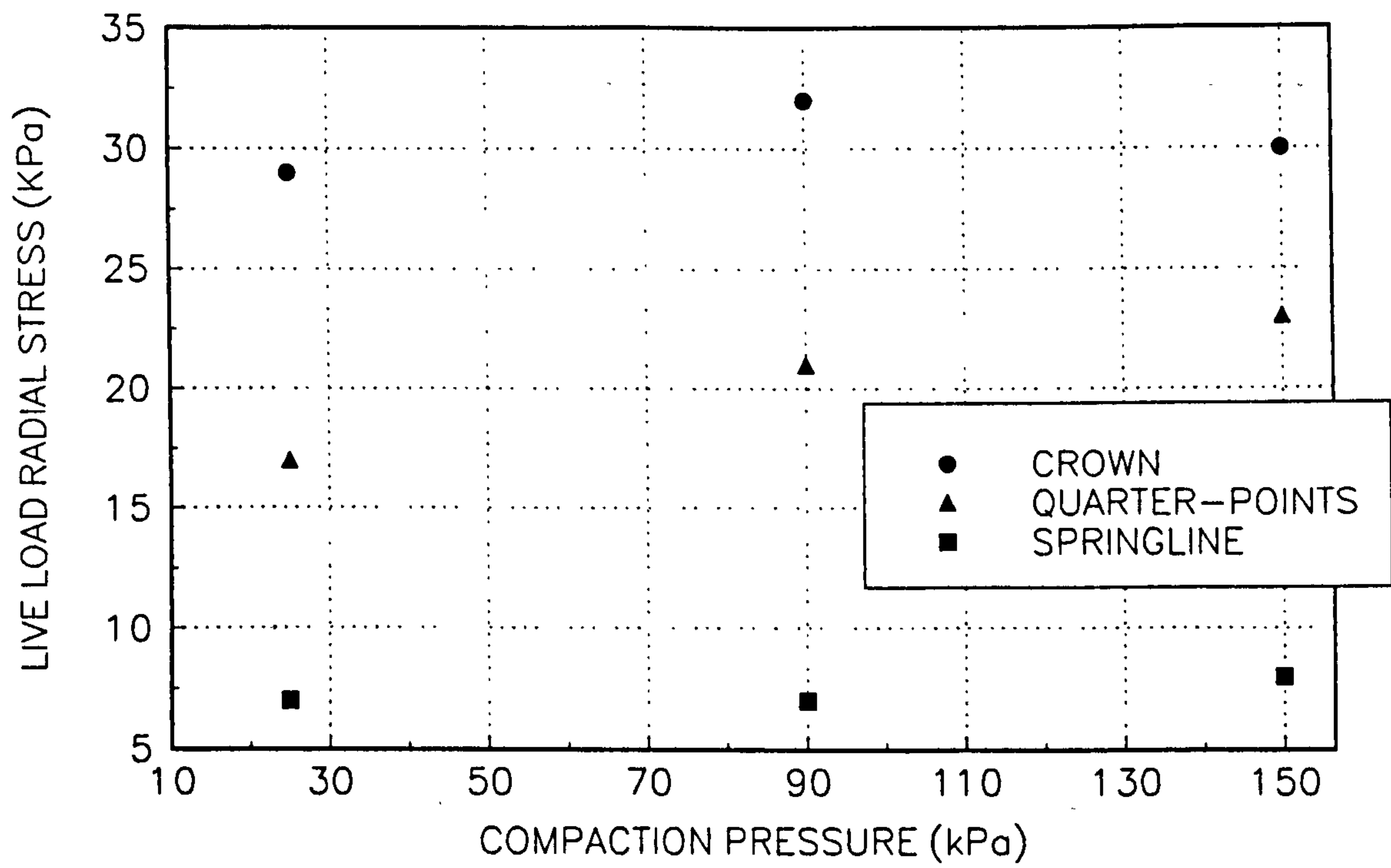


FIG 8.42 VARIATION OF LIVE LOAD SHEAR STRESS WITH COMPACTION PRESSURE

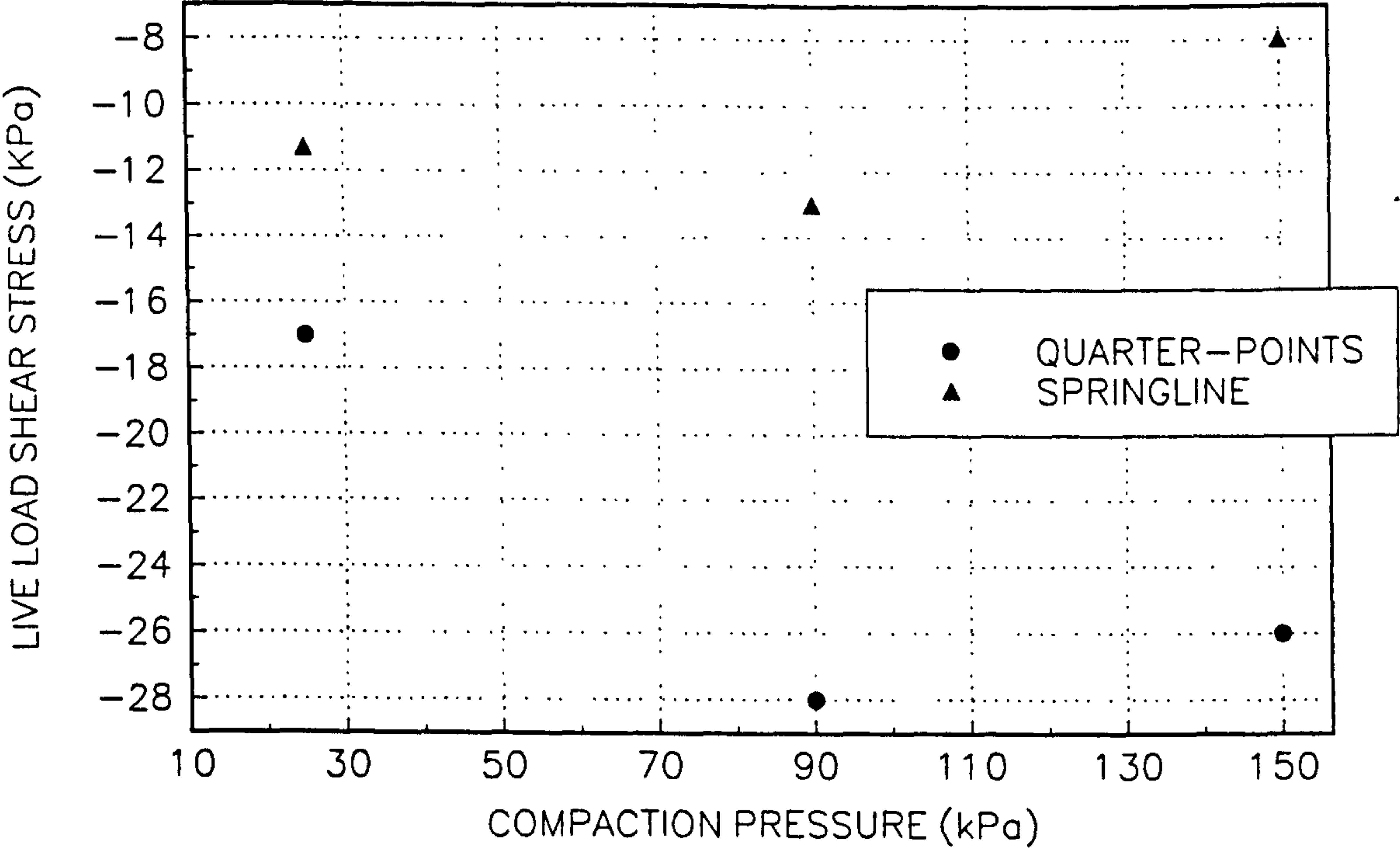
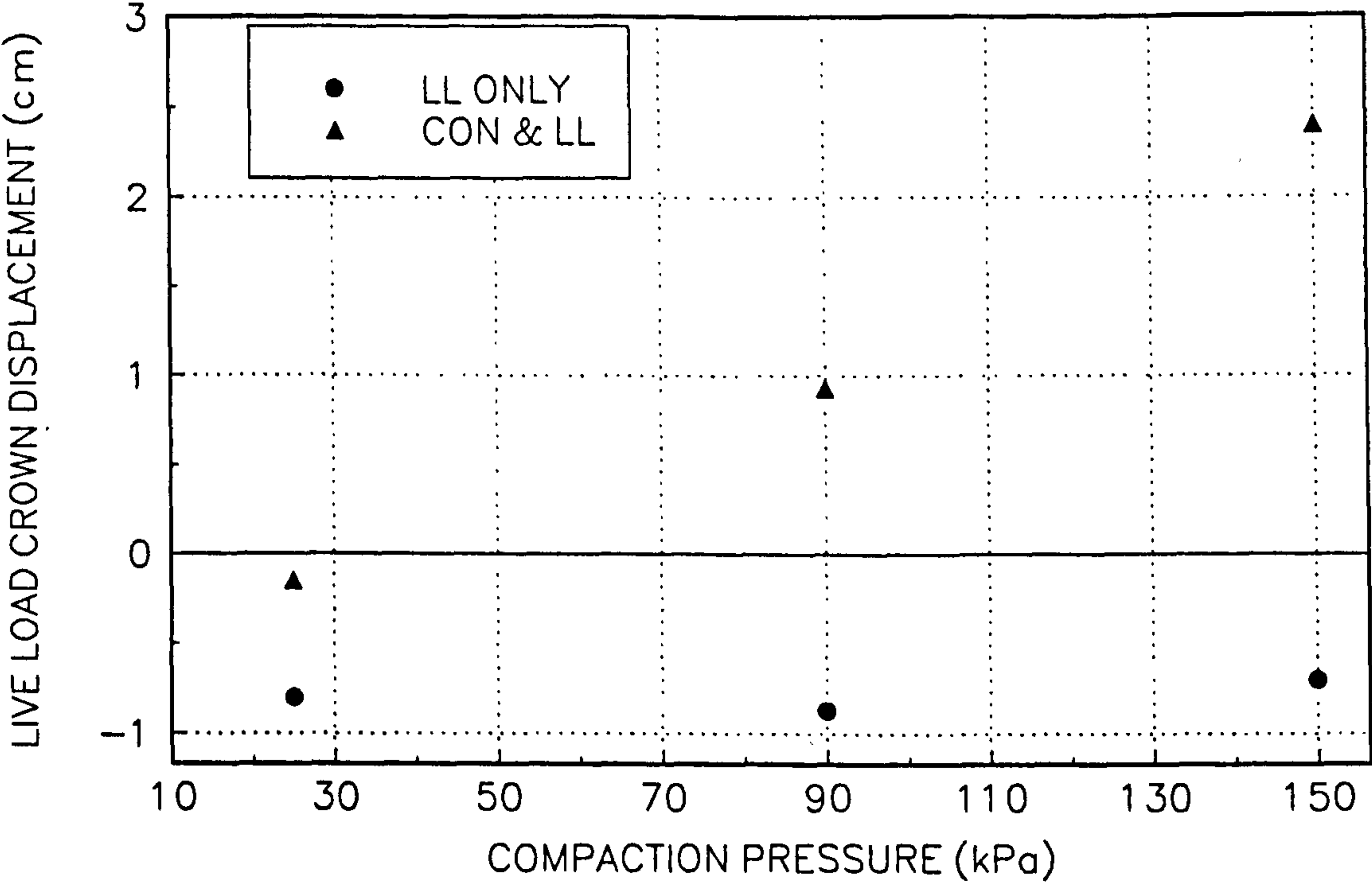


FIG 8.43(a) VARIATION OF LIVE LOAD CROWN DISPLACEMENT WITH COMPACTION PRESSURE



G 8.43(b) VARIATION OF LIVE LOAD SPRINGLINE DISPLACEMENT WITH COMPACTION PRESSURE

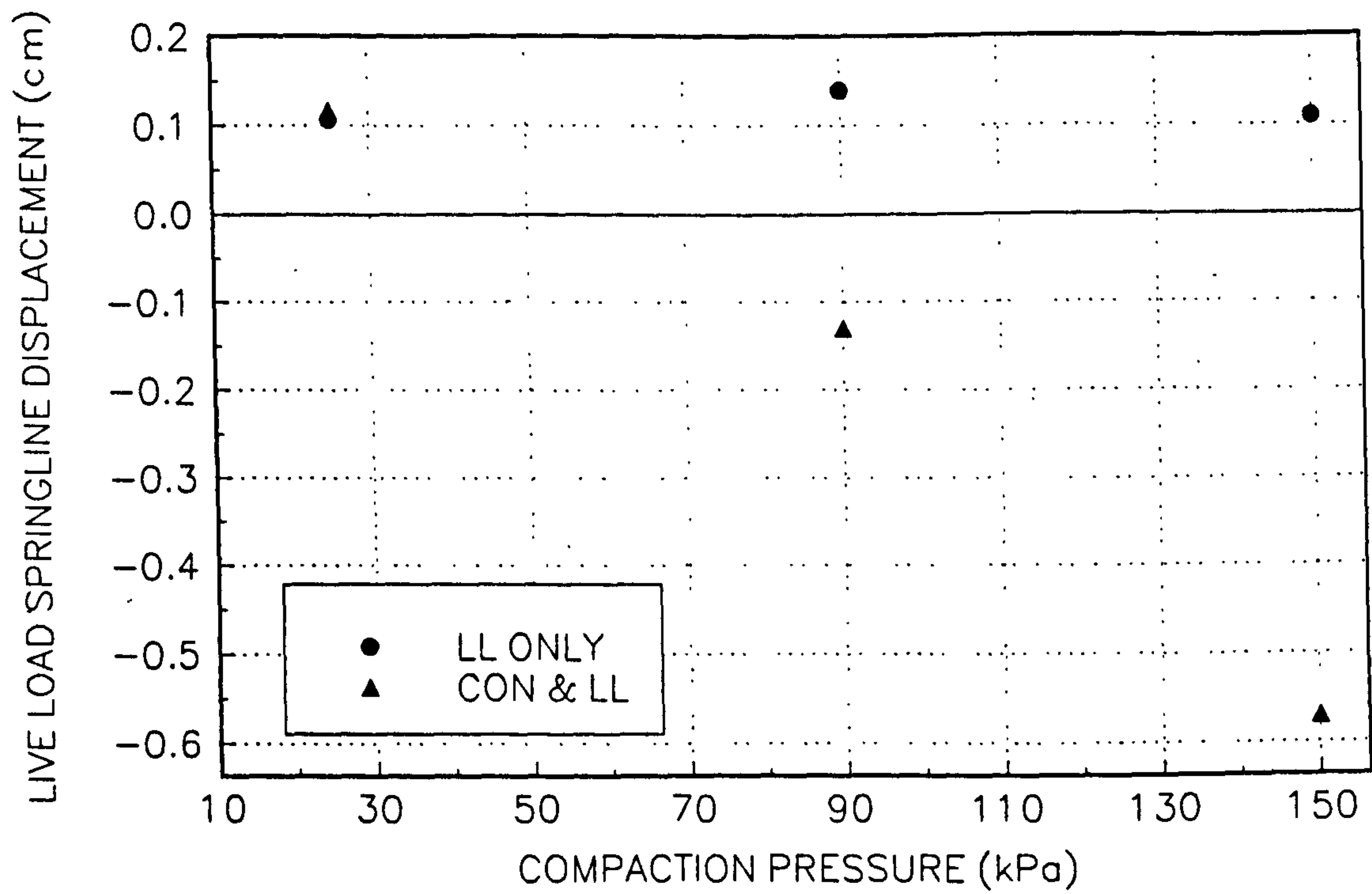


FIG 8.44 NO PLINTHS; THRUST BEHAVIOUR

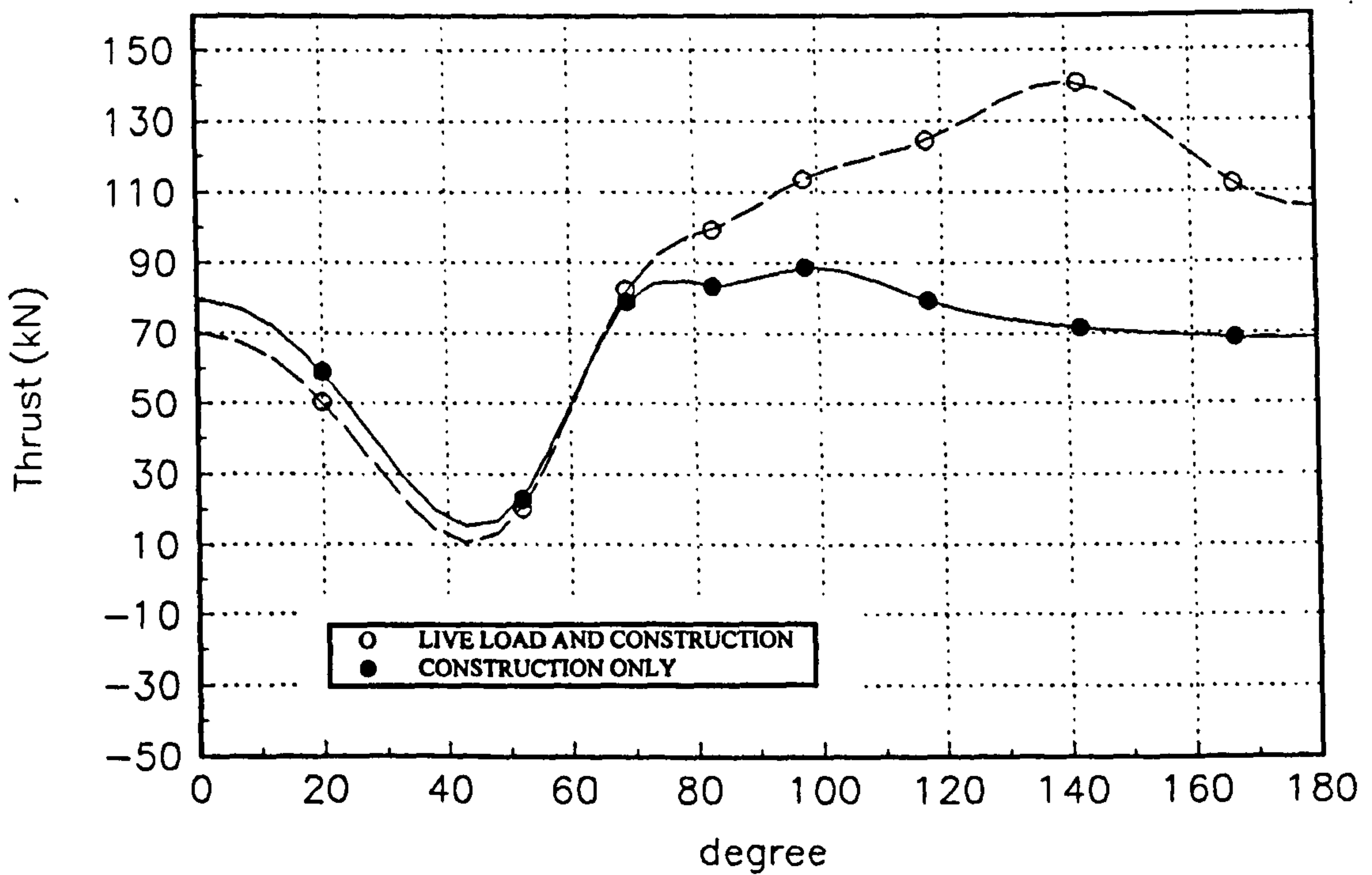


FIG 8.45 NO PLINTHS; BENDING MOMENT BEHAVIOUR

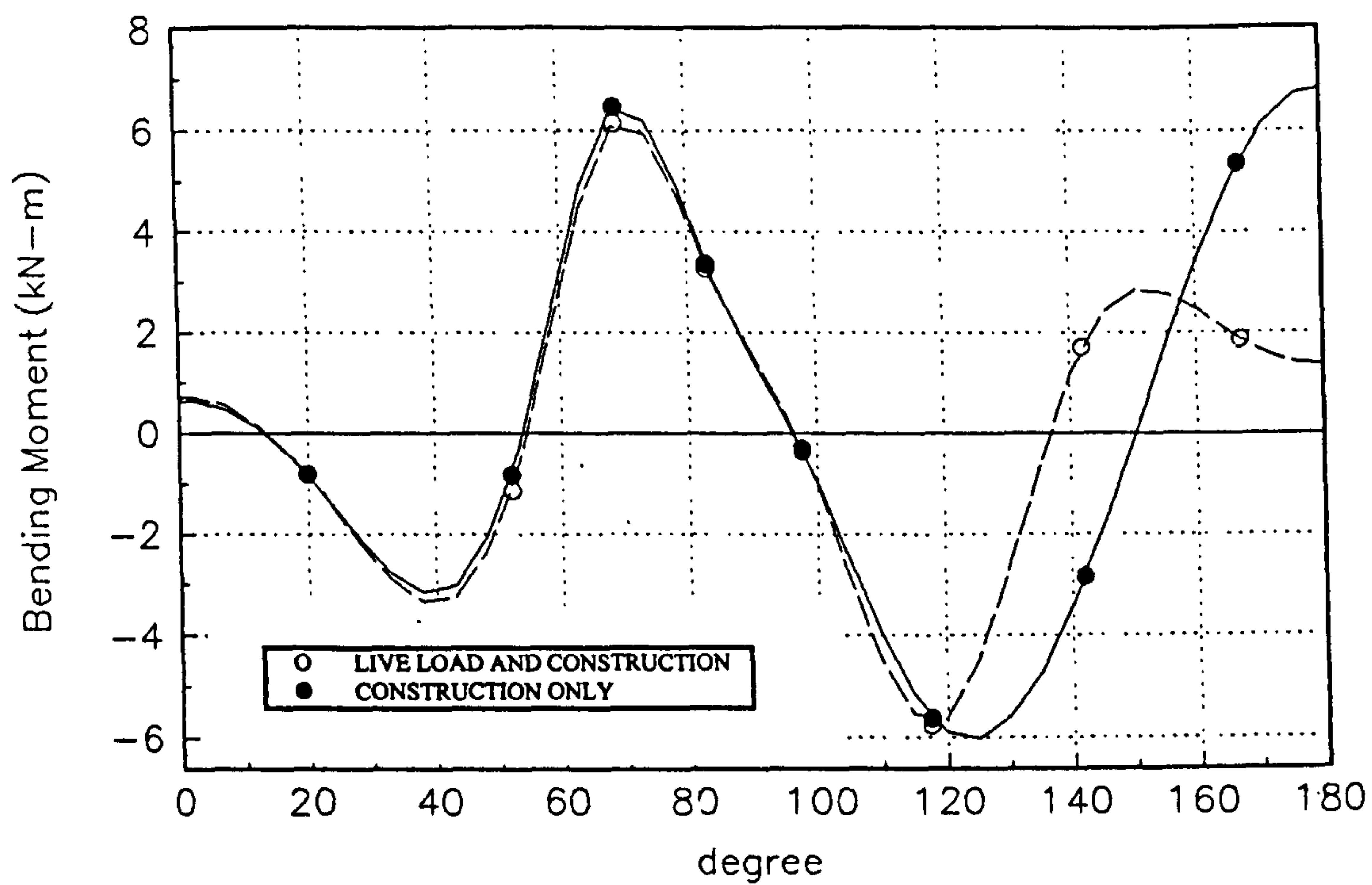


FIG 8.46 NO PLINTHS; RADIAL STRESS BEHAVIOUR

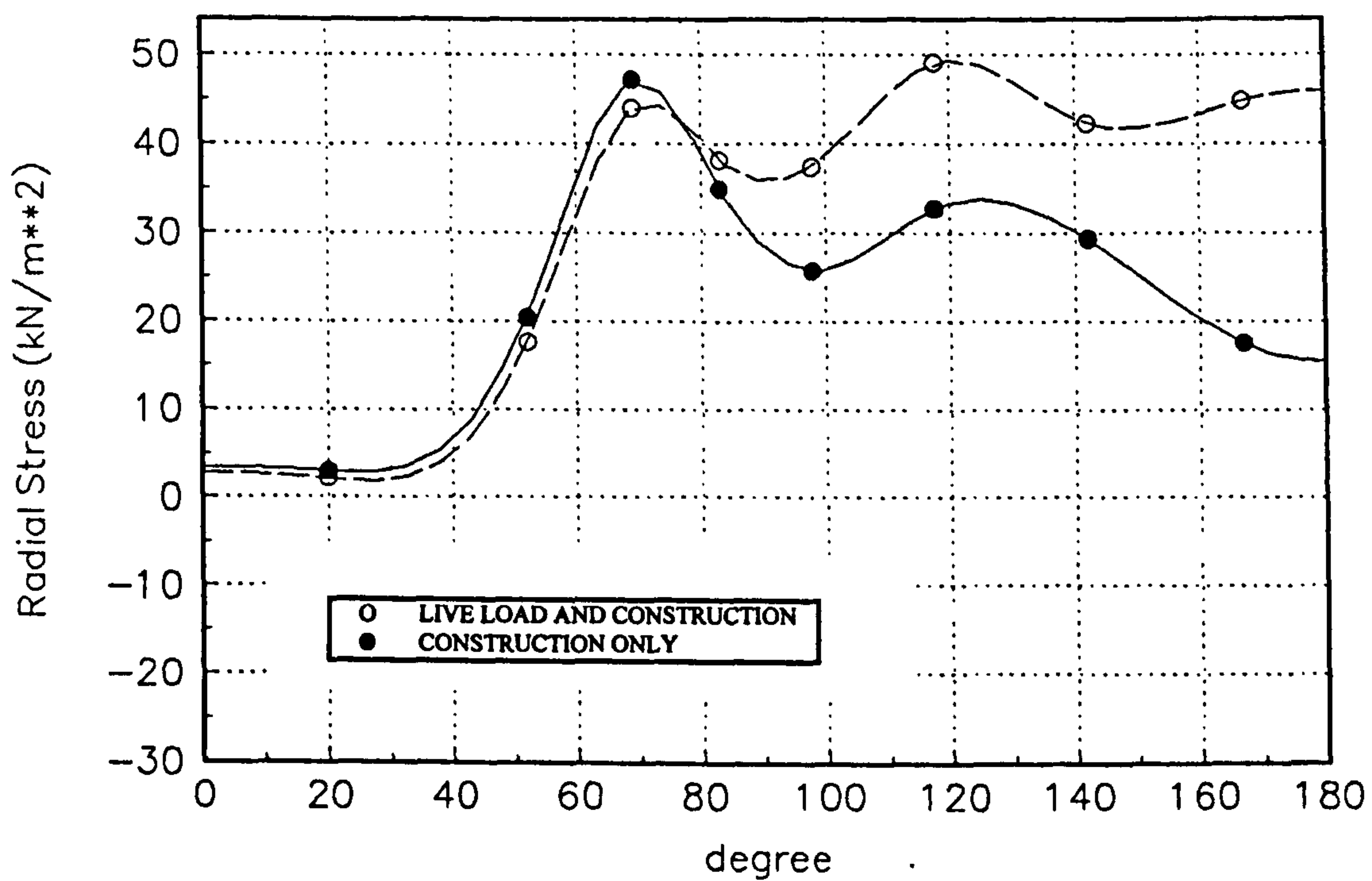


FIG 8.47 NO PLINTHS; SHEAR STRESS BEHAVIOUR

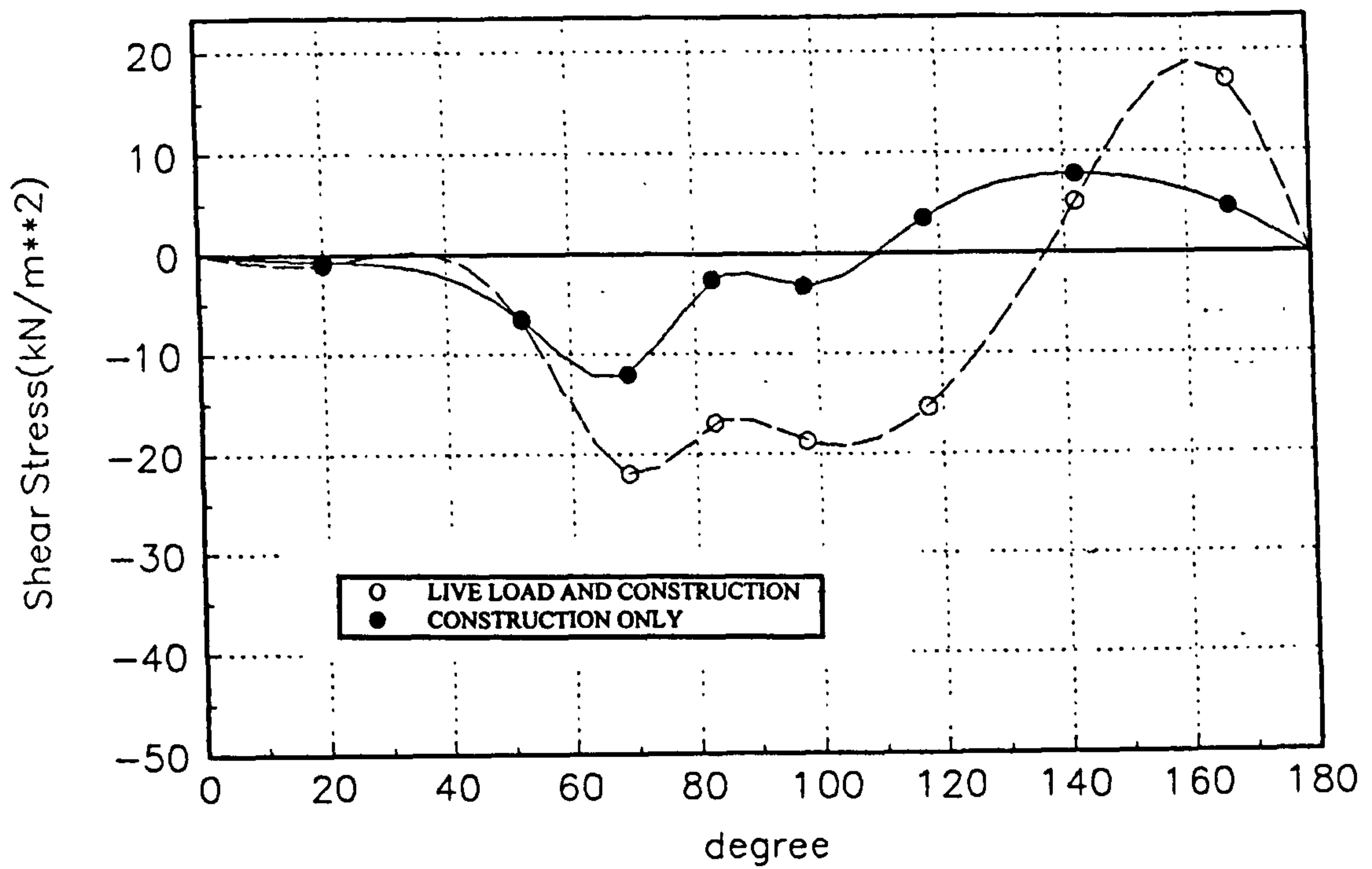


FIG 8.48 NO PLINTHS; CROWN DISPLACEMENT

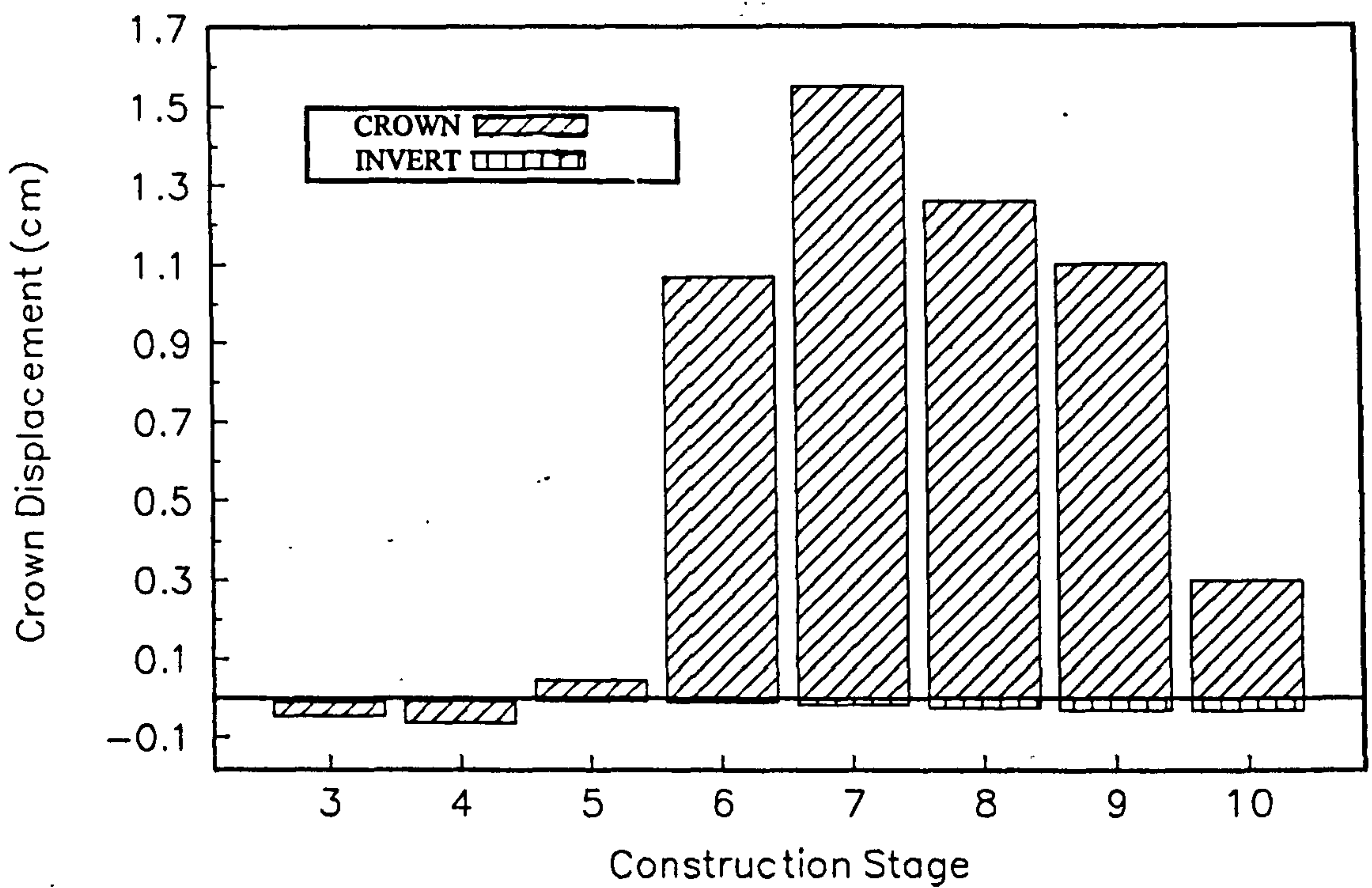


FIG 8.49 NO PLINTHS; SPRINGLINE DISPLACEMENT

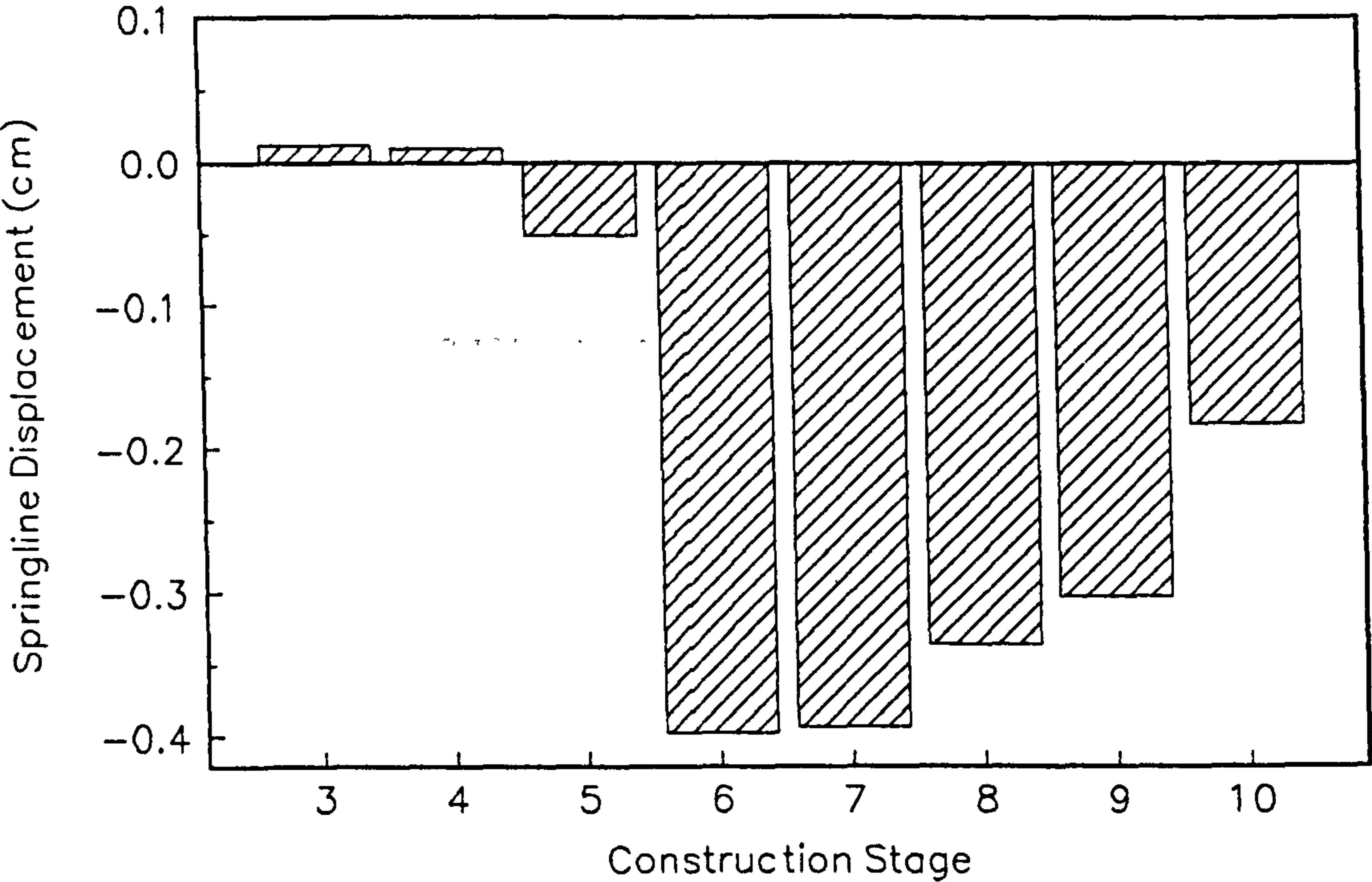


FIGURE 8.50(a)
APPLIED LOAD vs COMPUTED AND OBSERVED CROWN LIVE LOAD THRUST

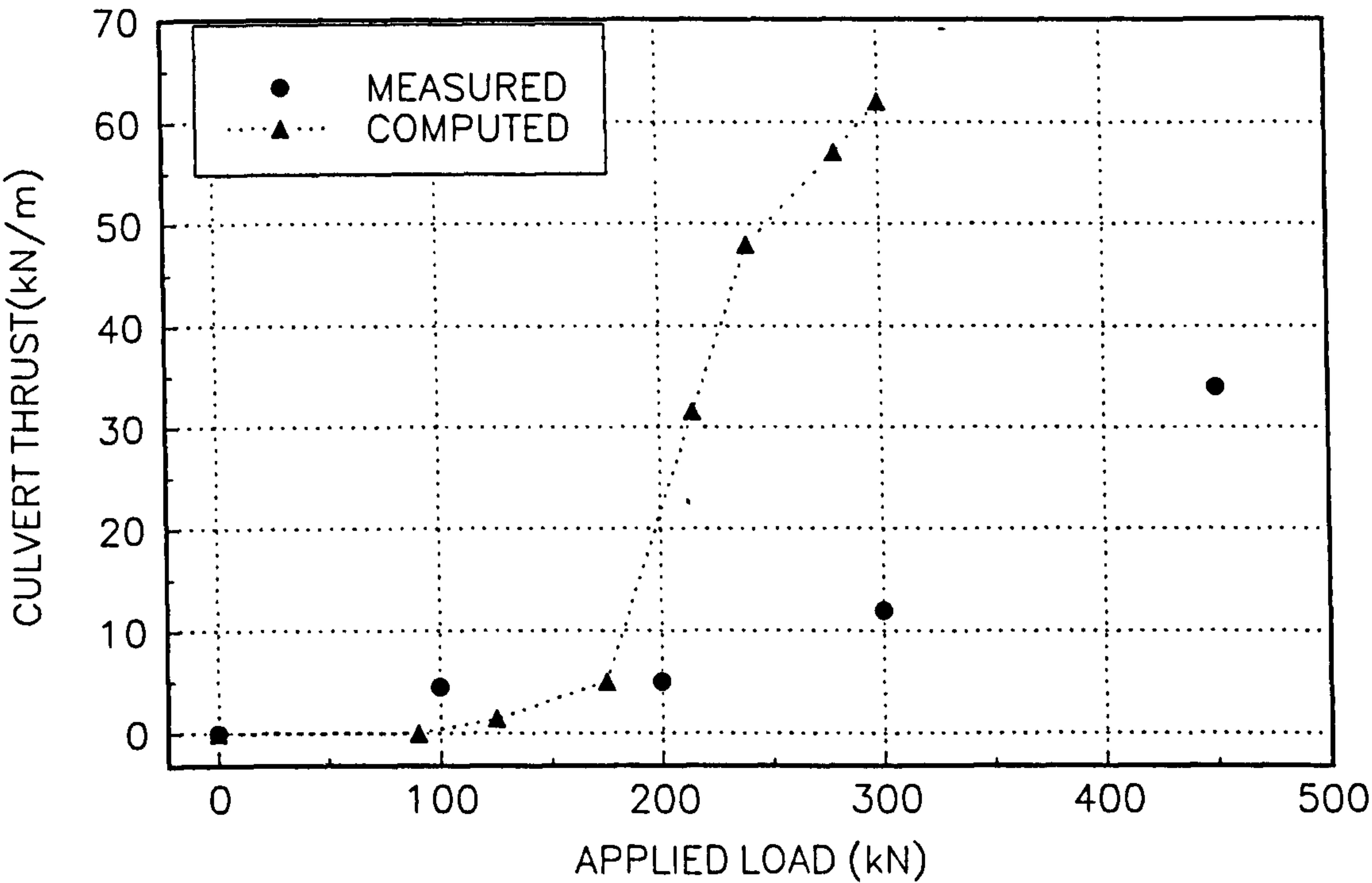
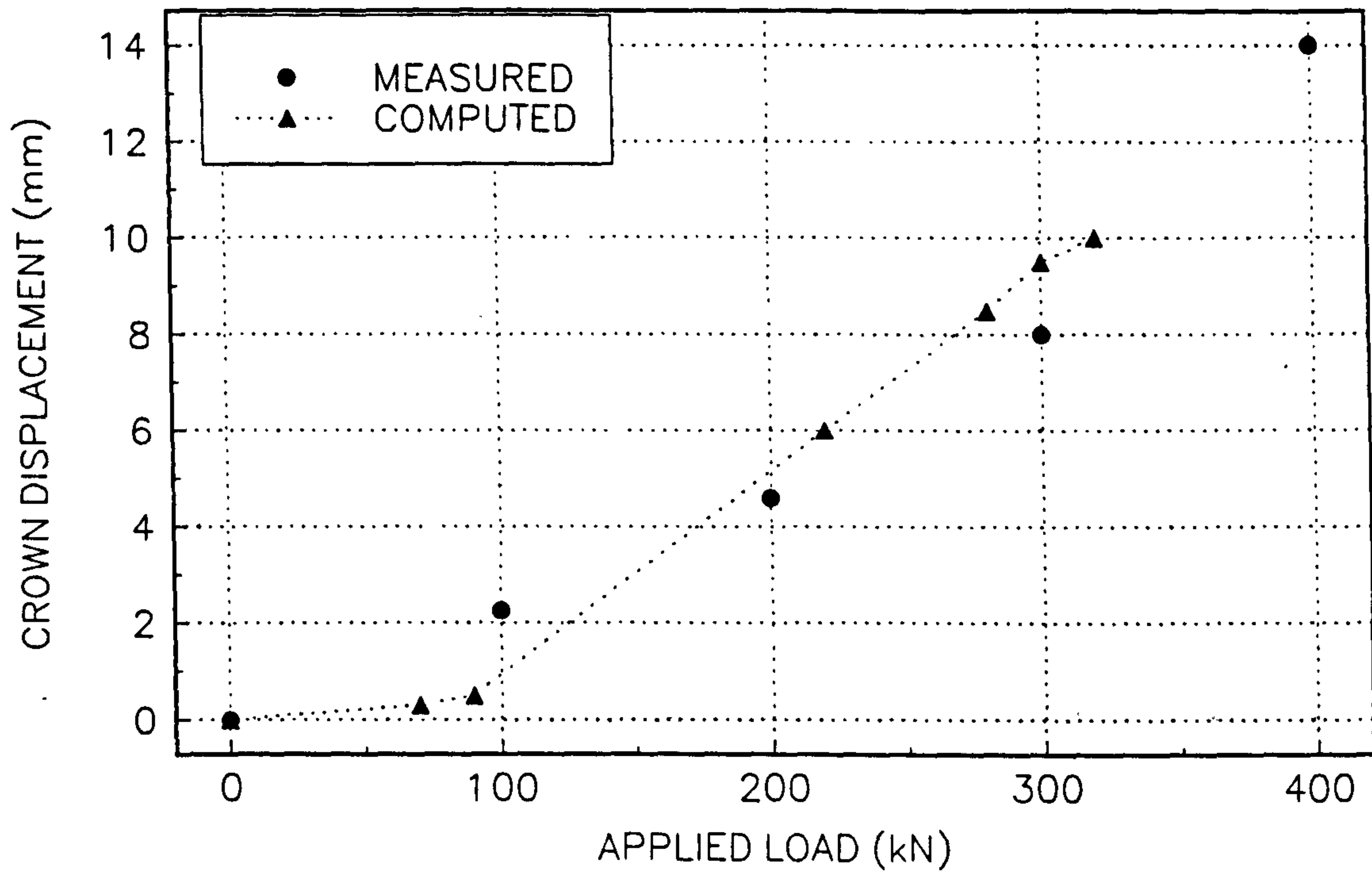


FIGURE 8.50(b)

APPLIED LOAD vs COMPUTED AND OBSERVED CROWN LIVE LOAD DISPLACEMENT



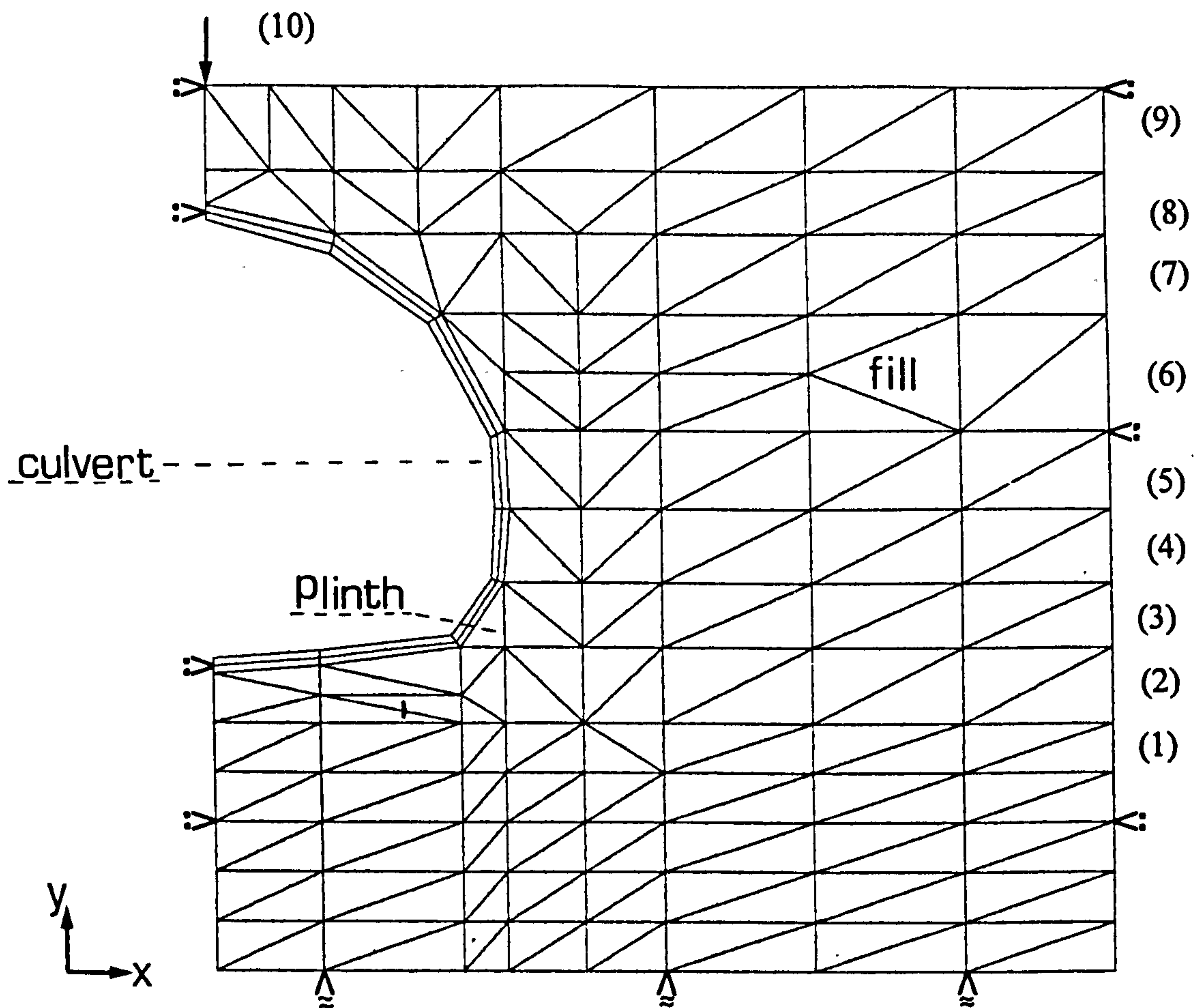


FIG 8.51 FINITE ELEMENT MESH FOR LOADING CASE B
CONSTRUCTION STAGE ()

CONSTRUCTION STAGE	DESCRIPTION
1	COMPACT EXISTING FOUNDATION SOIL
2	PLACE AND COMPACT BASAL LAYER
3	PLACE BACKFILL AND PLINTH , COMPACT BACKFILL
4	PLACE AND COMPACT BACKFILL UP TO SPRINGLINE
5	PLACE AND COMPACT BACKFILL TO BELOW QUARTER POINTS
6	PLACE AND COMPACT BACKFILL UP TO QUARTER POINTS
7	PLACE LEVEL WITH CROWN AND COMPACT
8	PLACE BACKFILL ABOVE CROWN AND COMPACT
9	PLACE TO FINAL FILL HEIGHT AND COMPACT
10	APPLY LIVE LOAD

FIG 8.52 LOADING CASE B; THRUST

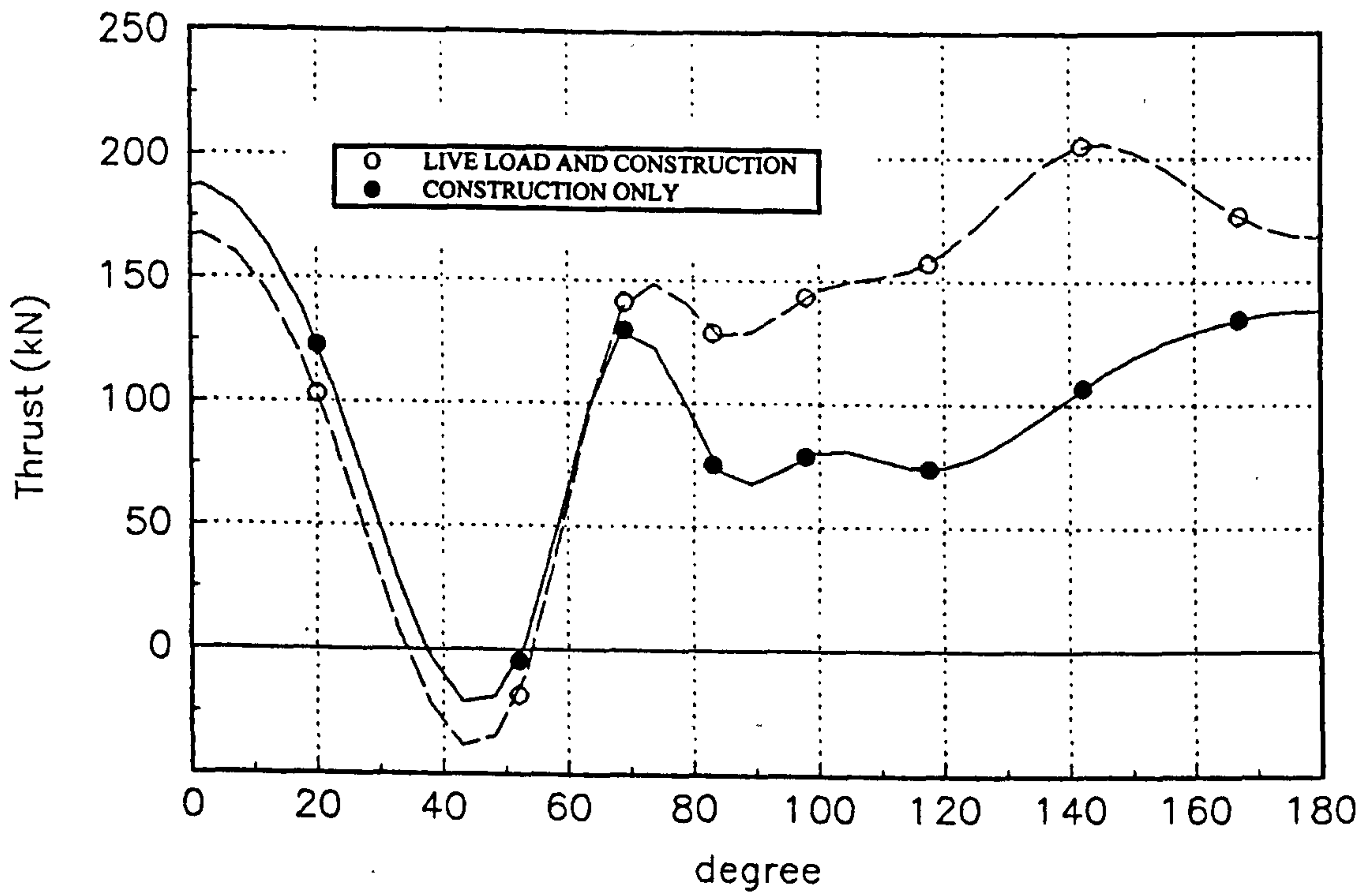


FIG 8.53 LOADING CASE B; BENDING MOMENT

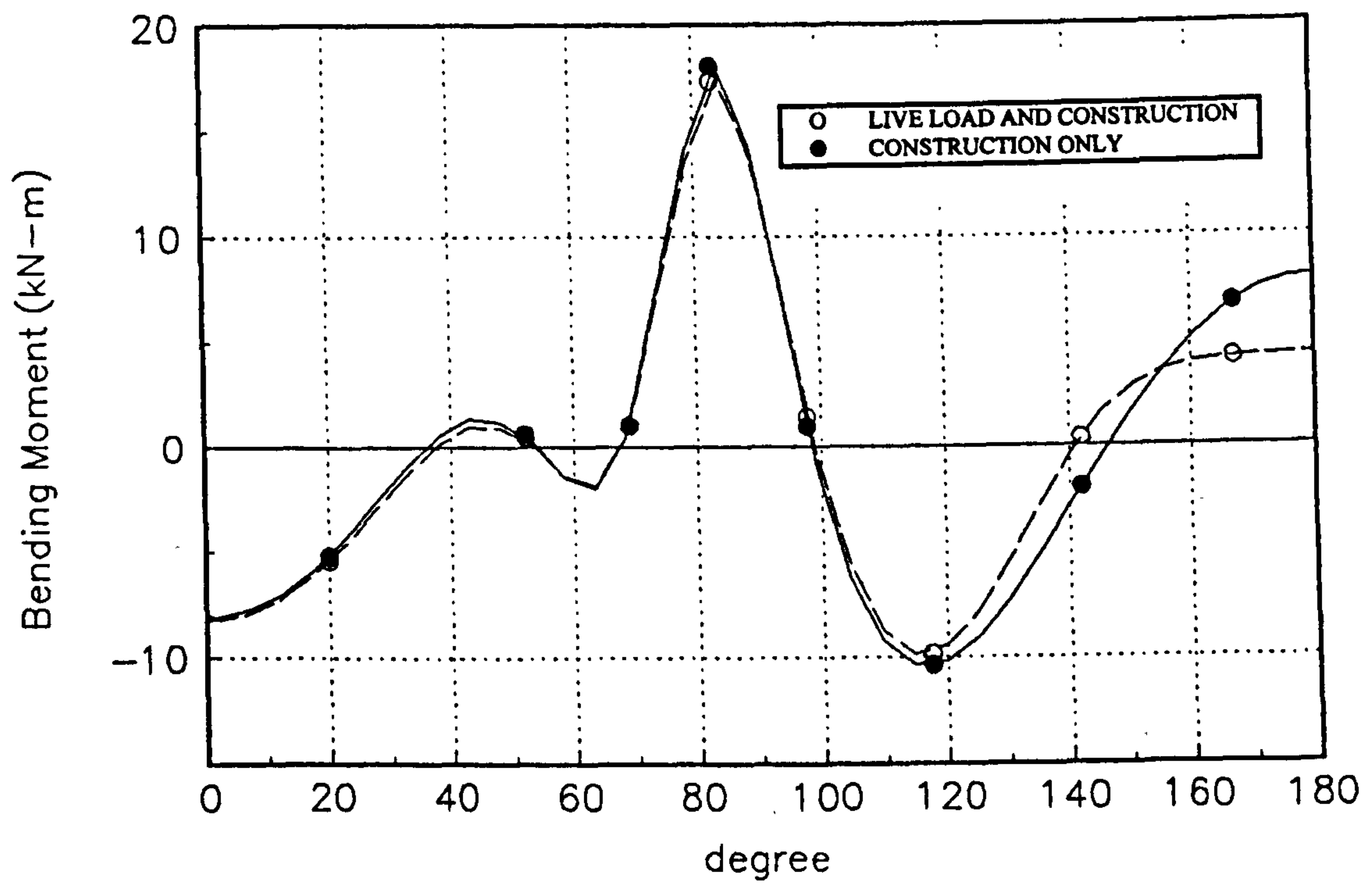


FIG 8.54 LOADING CASE B; RADIAL STRESS

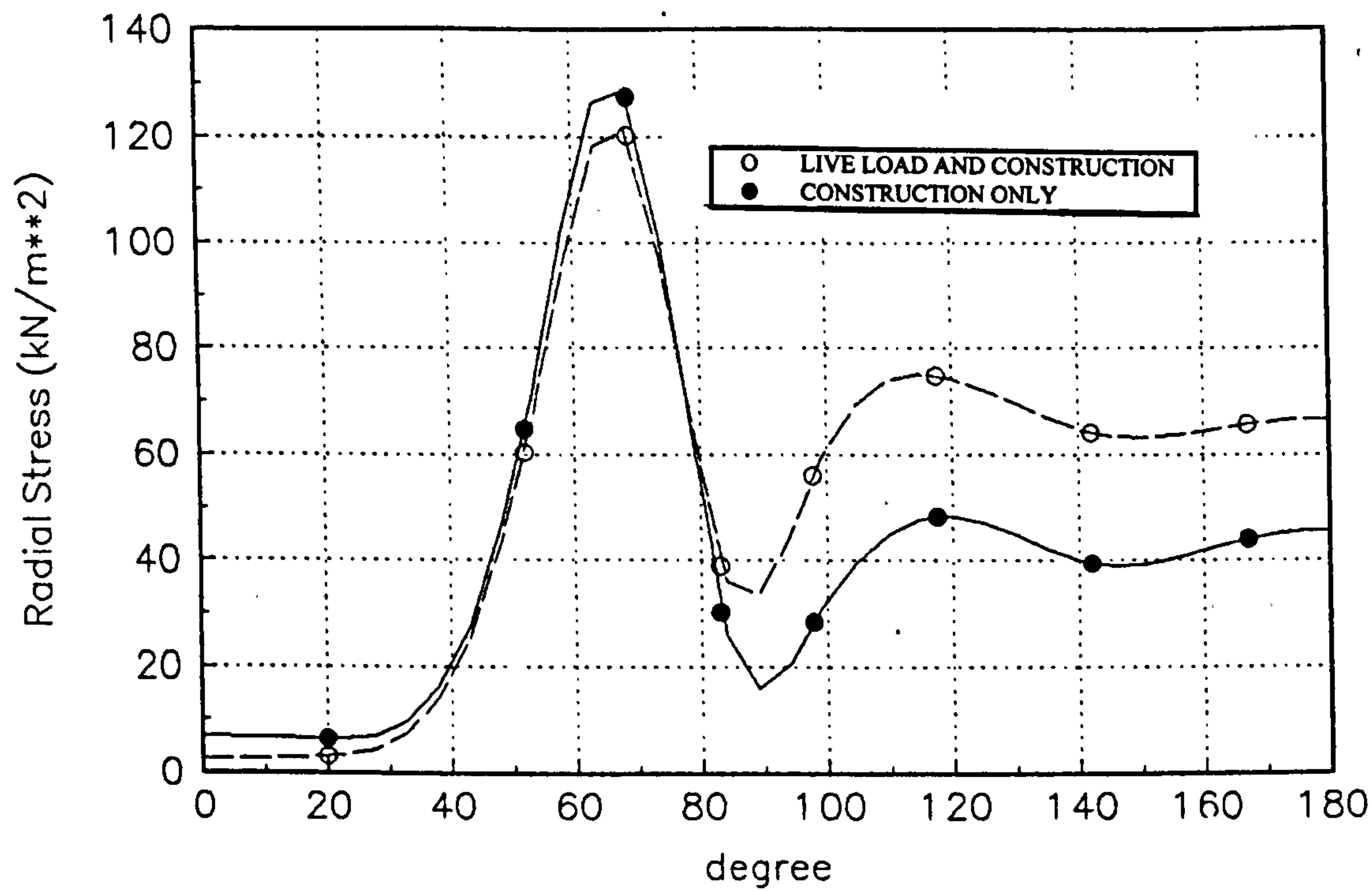


FIG 8.55 LOADING CASE B; SHEAR STRESS

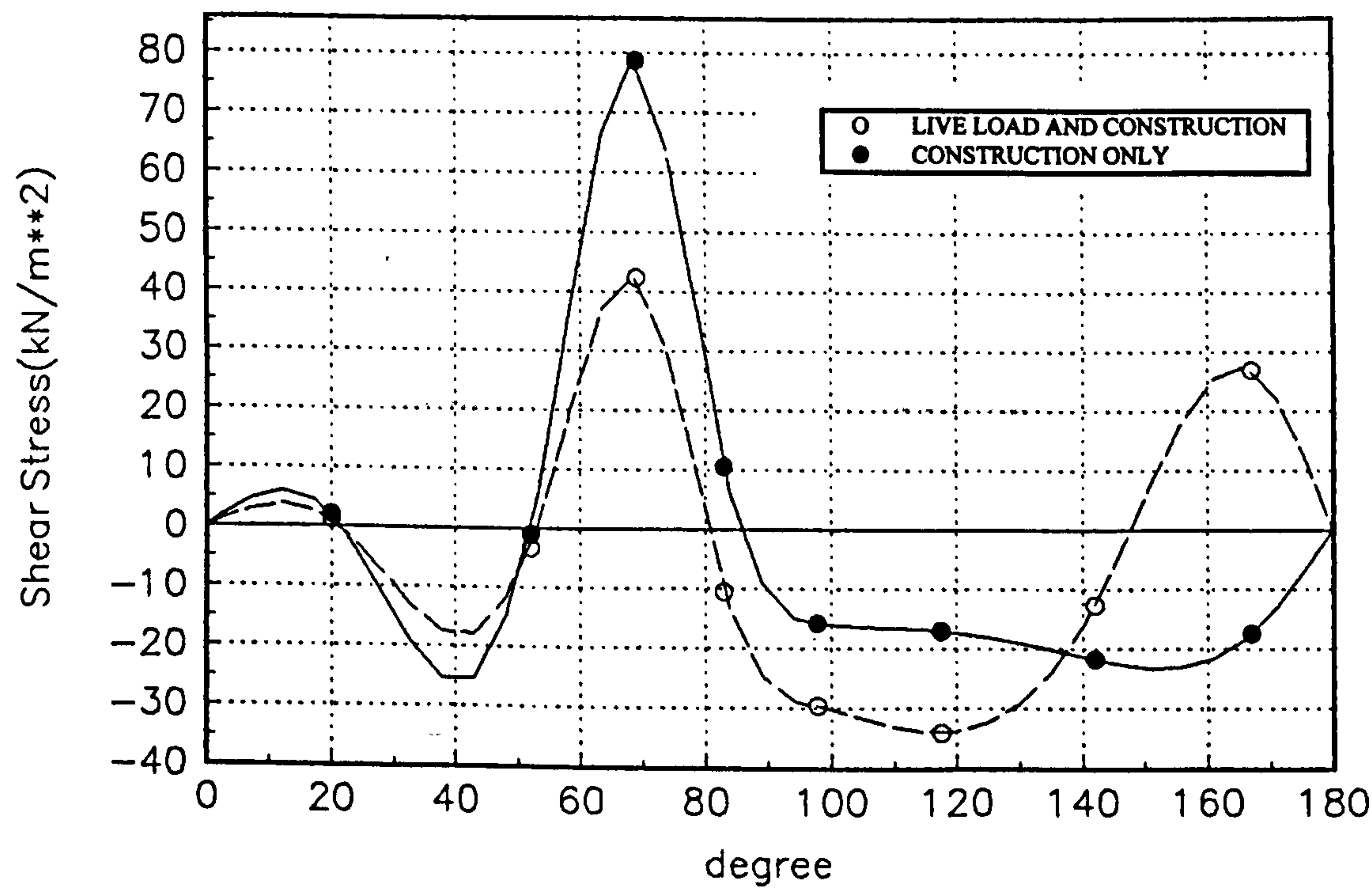


FIG 8.56 LOADING CASE B; CROWN DISPLACEMENT

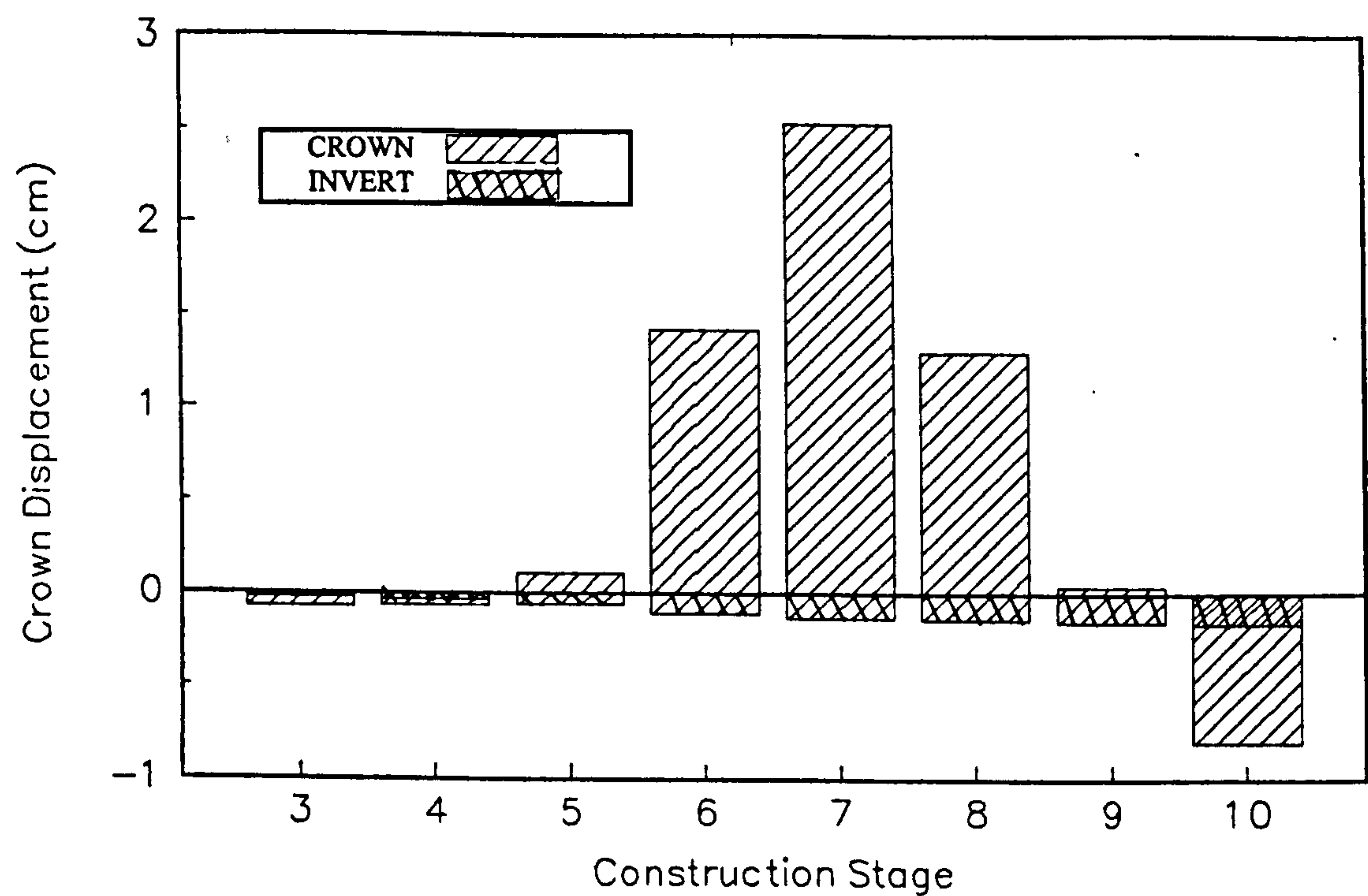


FIG 8.57 LOADING CASE B; SPRINGLINE DISPLACEMENT

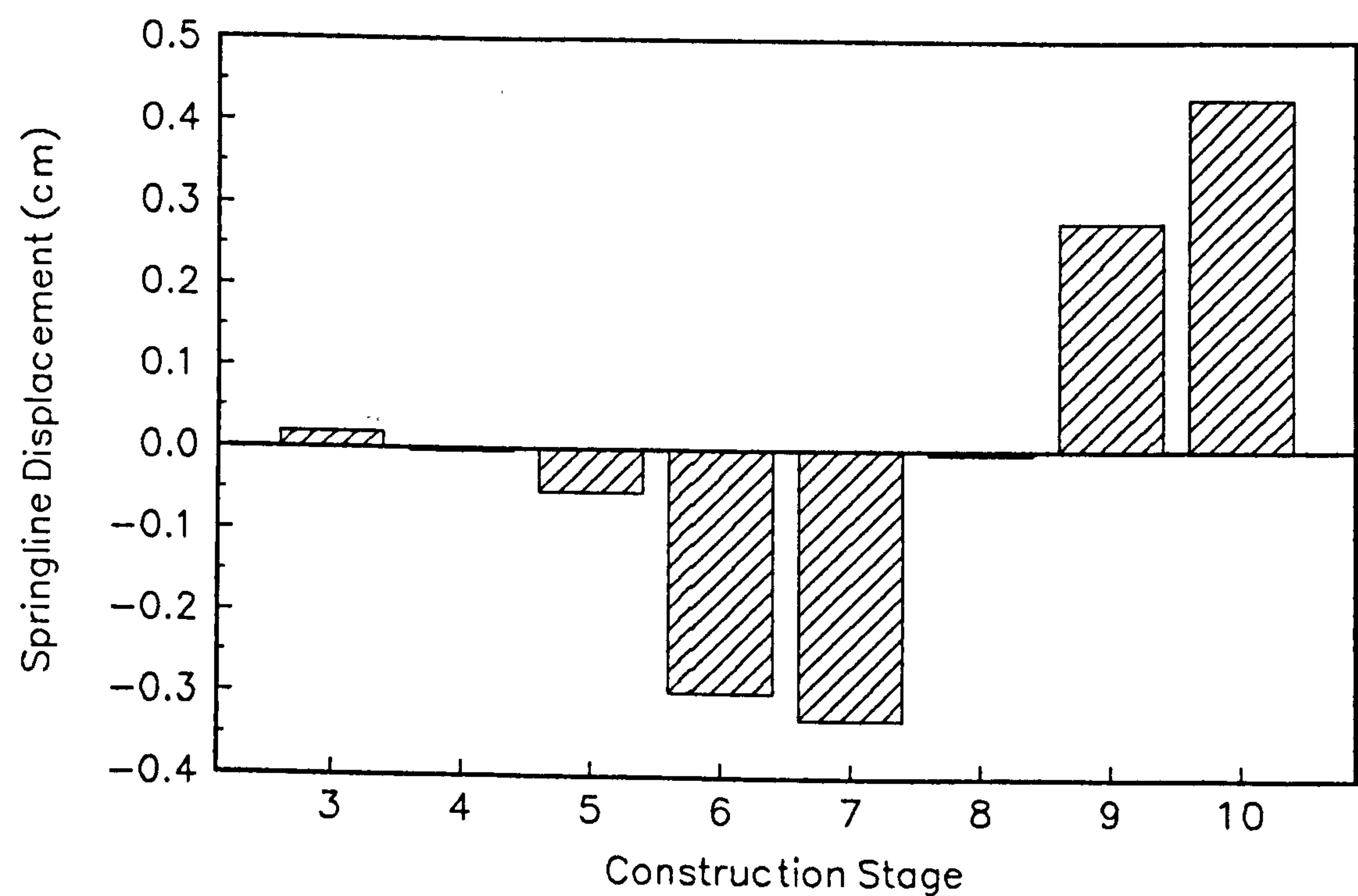


FIGURE 8.58(a)
VARIATION OF CONSTRUCTION THRUST WITH BACKFILL YOUNG' MODULUS

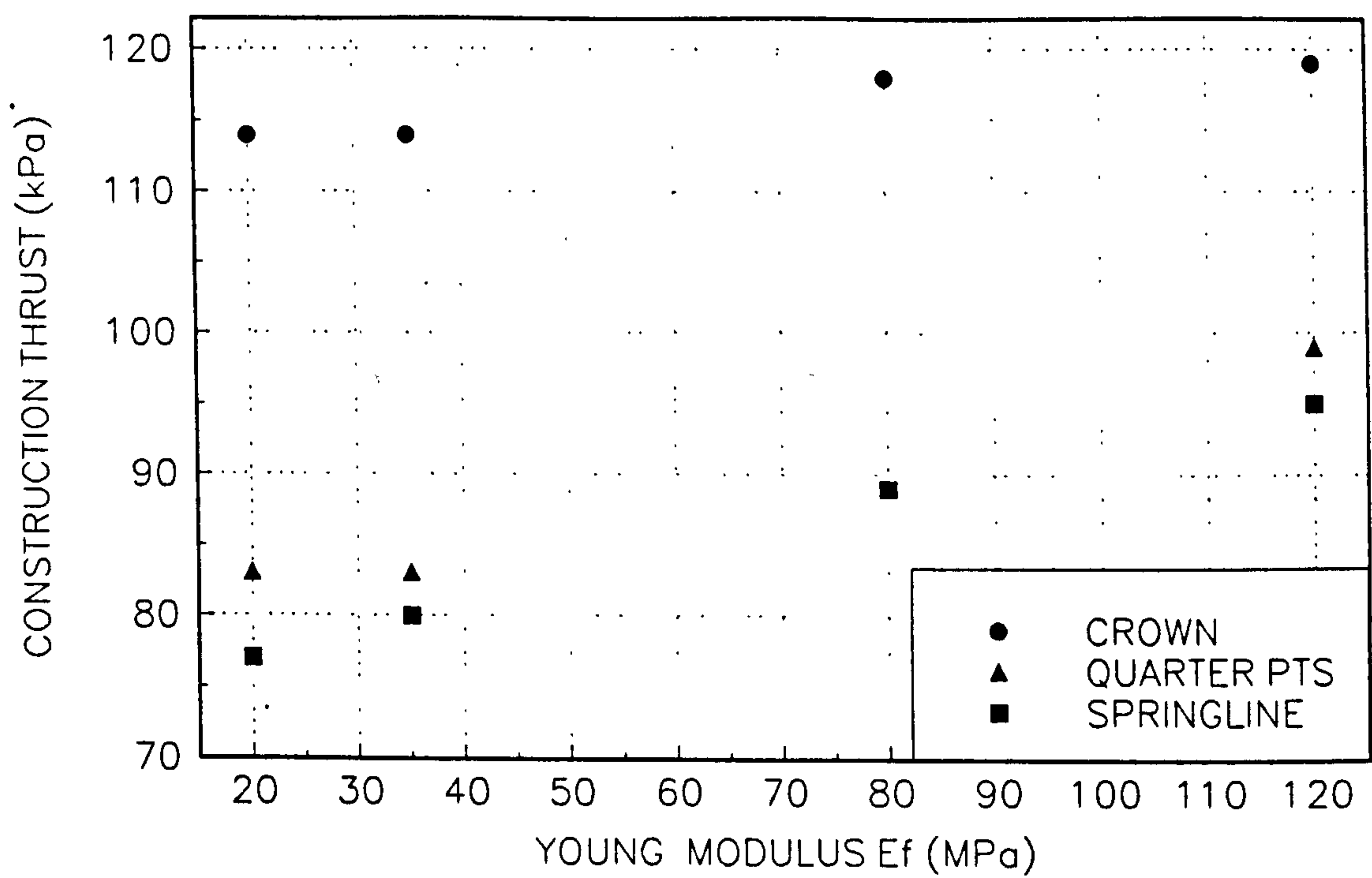


FIGURE 8.58(b)
VARIATION OF LIVE LOAD THRUST WITH BACKFILL YOUNG' MODULUS

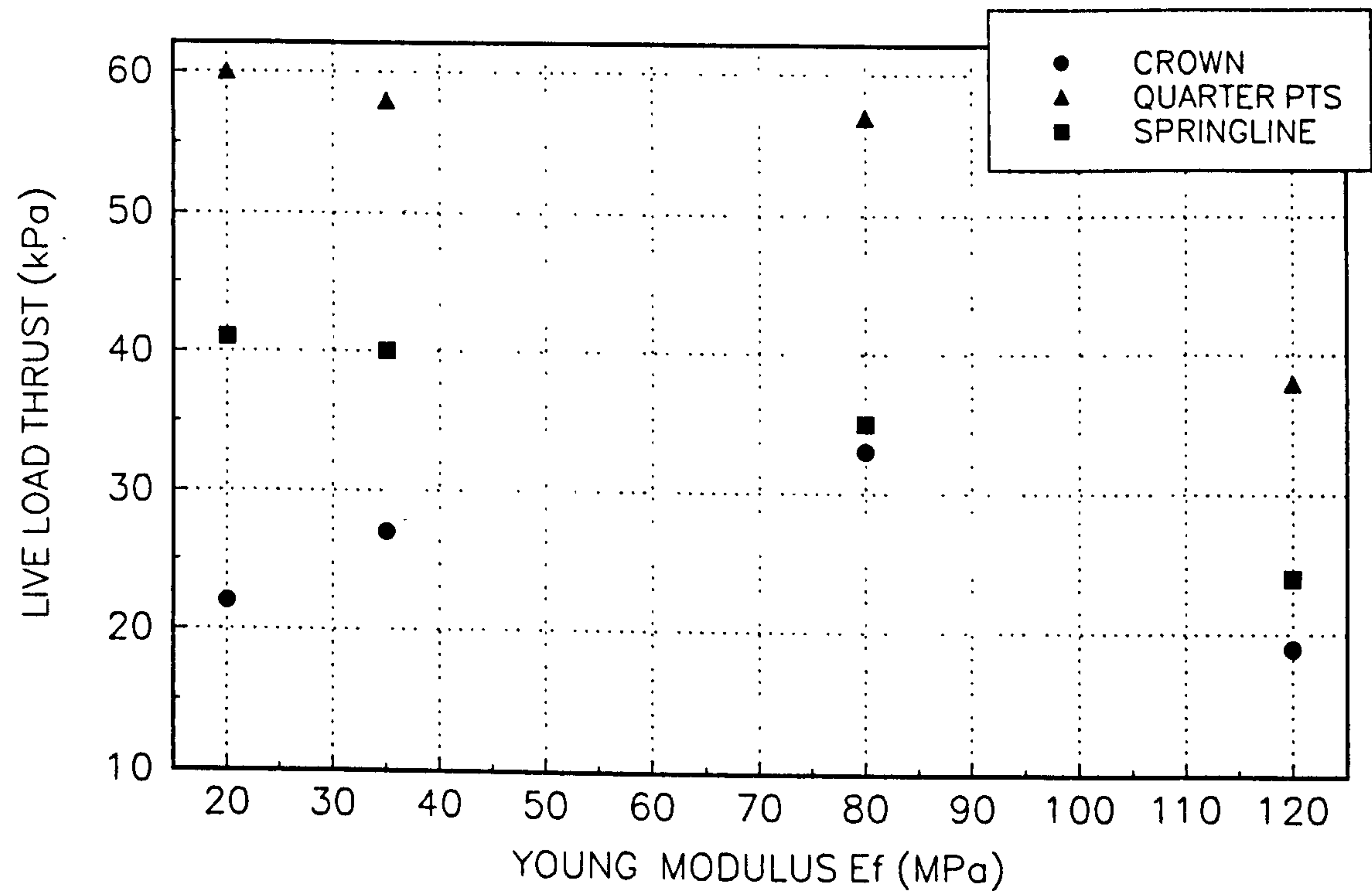


FIGURE 8.59(a)
 VARIATION OF CROWN DISPLACEMENTS WITH BACKFILL YOUNG'S MODULUS

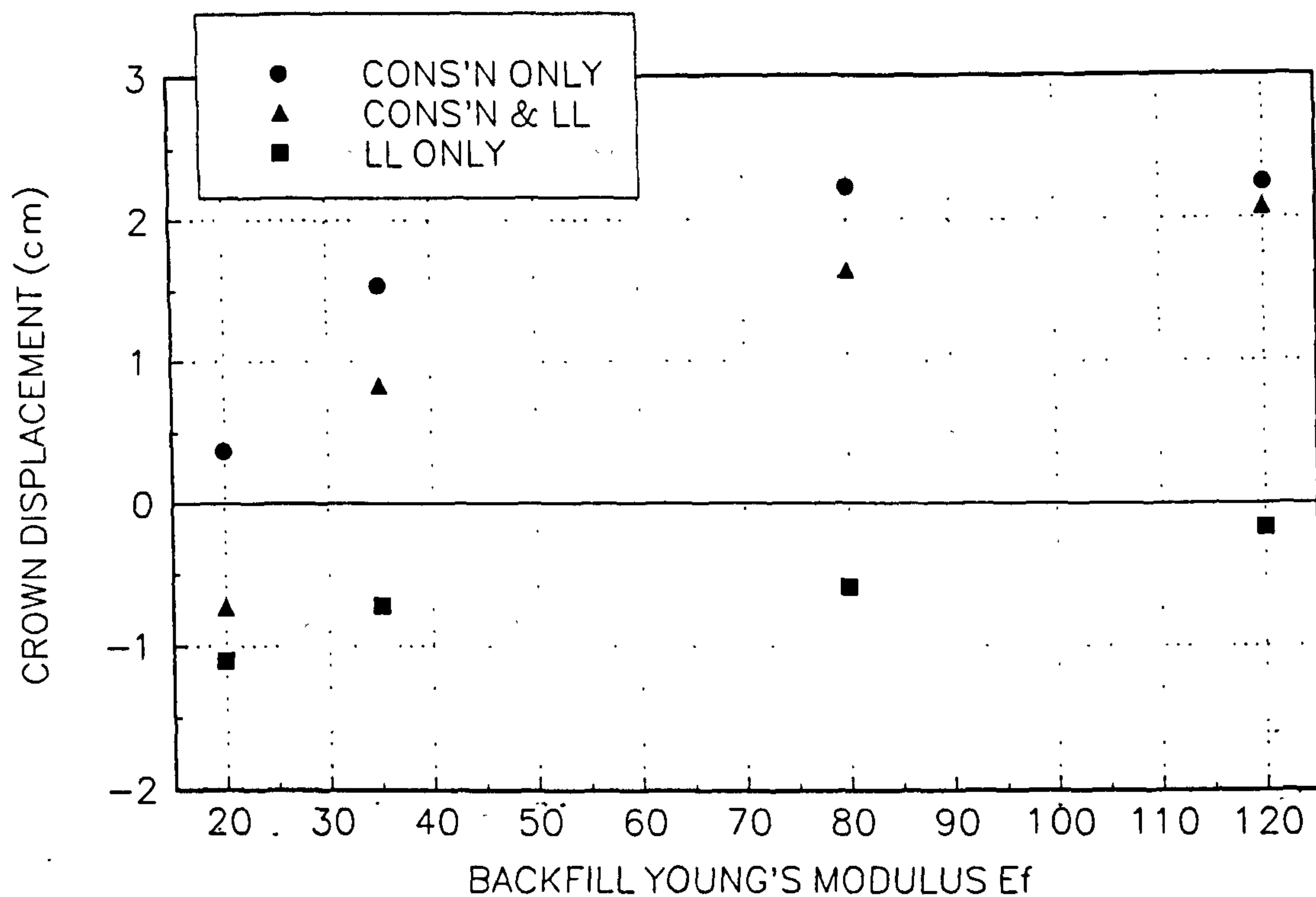


FIGURE 8.59(b)
 VARIATION OF SPRINGLINE DISPLACEMENTS WITH BACKFILL YOUNG'S MODULUS

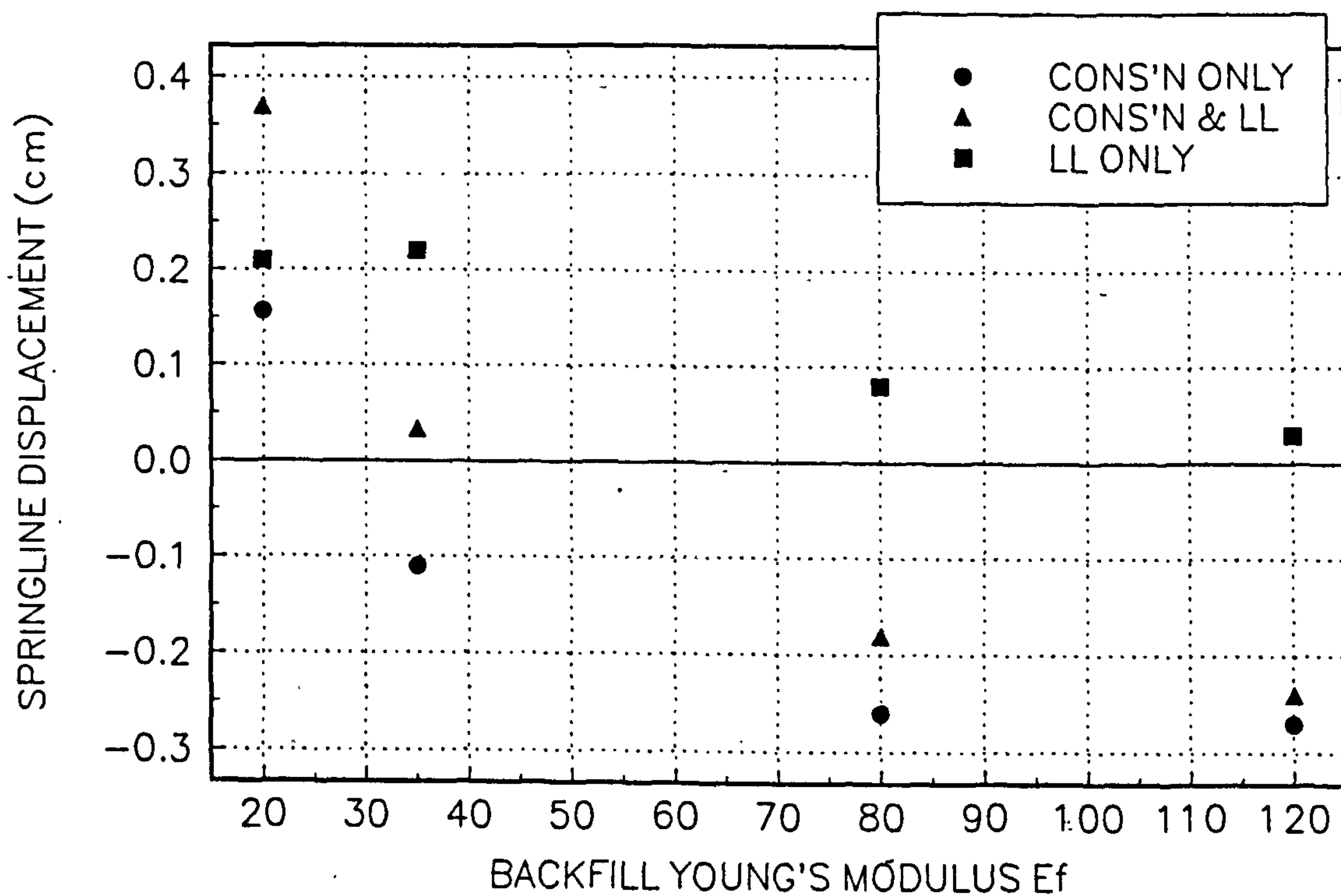


FIG 8.59(c)-(i) CROWN AND INVERT DISPLACEMENT; $E_f=20\text{MPa}$

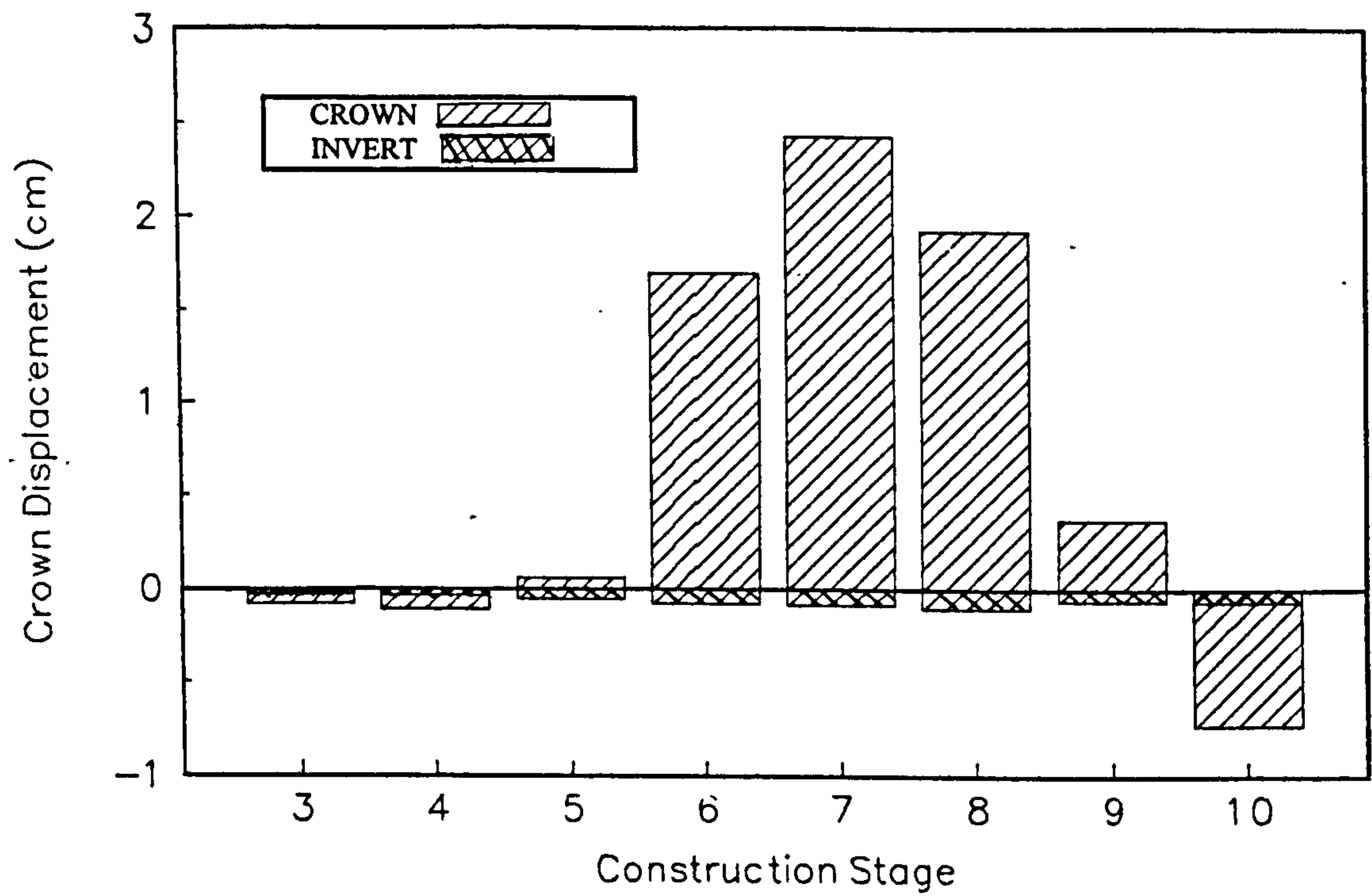


FIG 8.59(c)-(ii) CROWN AND INVERT DISPLACEMENT; $E_f=120\text{MPa}$

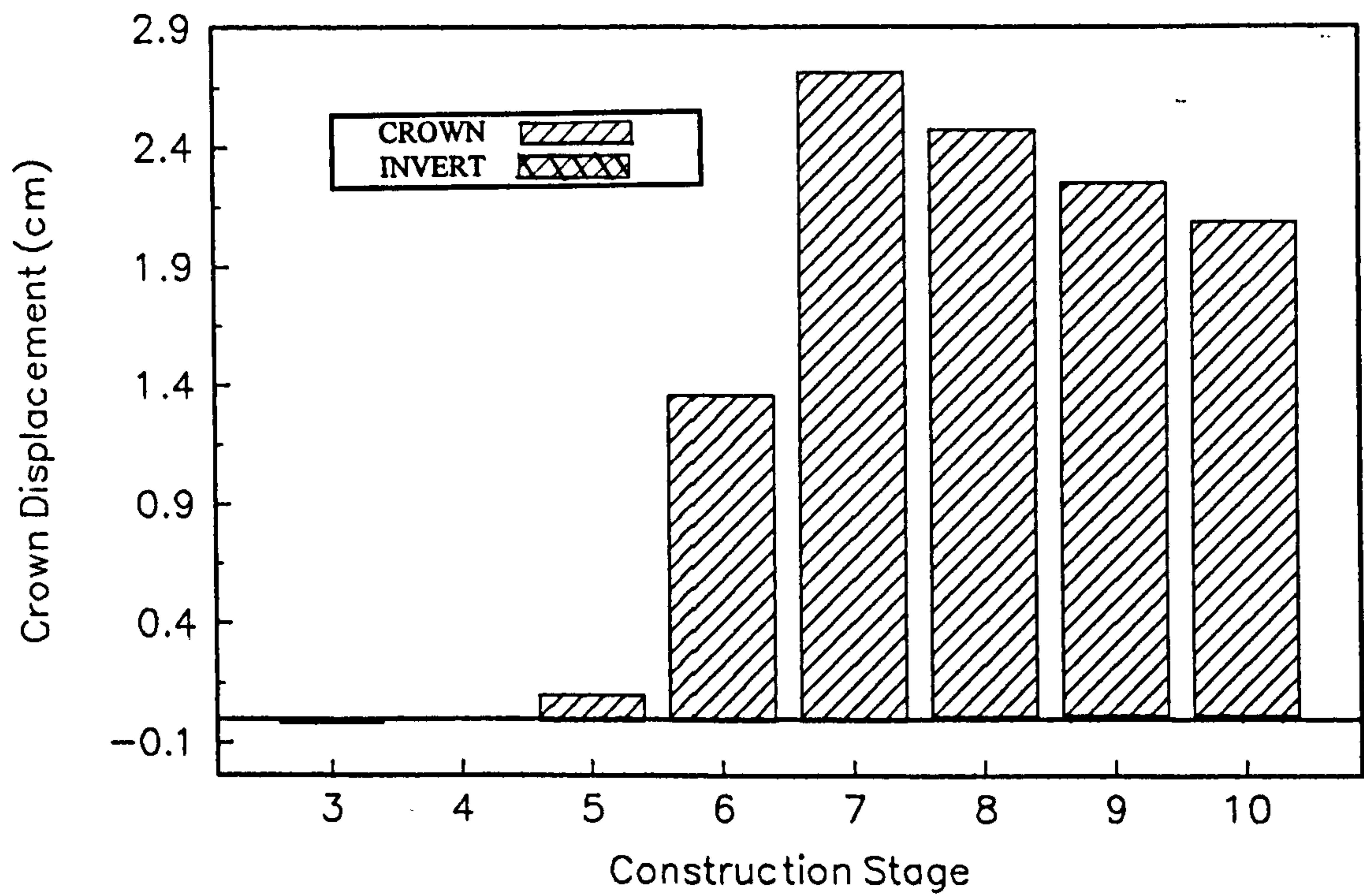


FIG 8.59(d)-(i) SPRINGLINE DISPLACEMENT; $E_f=20\text{MPa}$

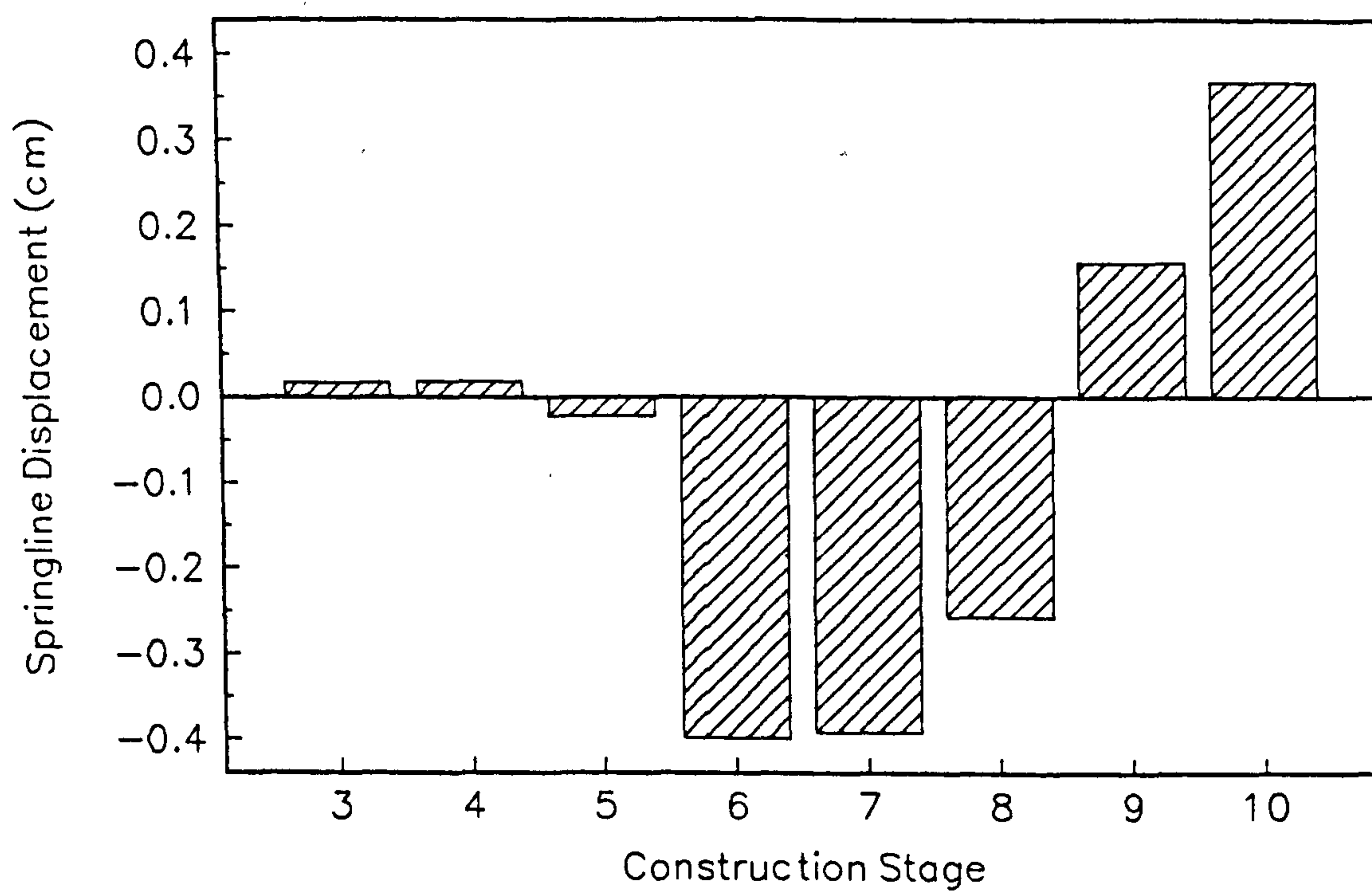


FIG 8.59(d)-(ii) SPRINGLINE DISPLACEMENT; $E_f=120\text{MPa}$

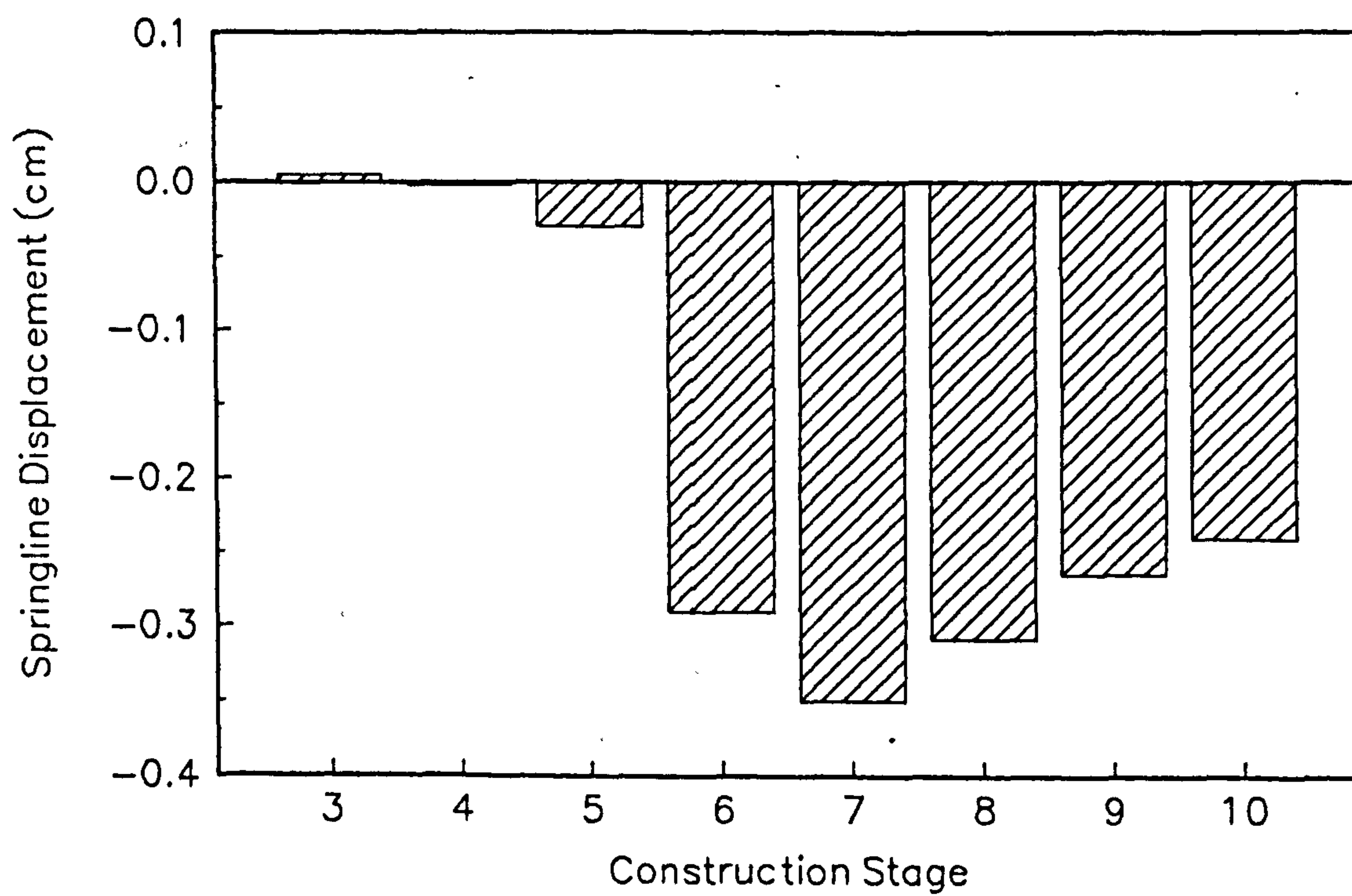


FIGURE 8.60(a)
VARIATION OF DEGREE ARCHING WITH BACKFILL YOUNG'S MODULUS

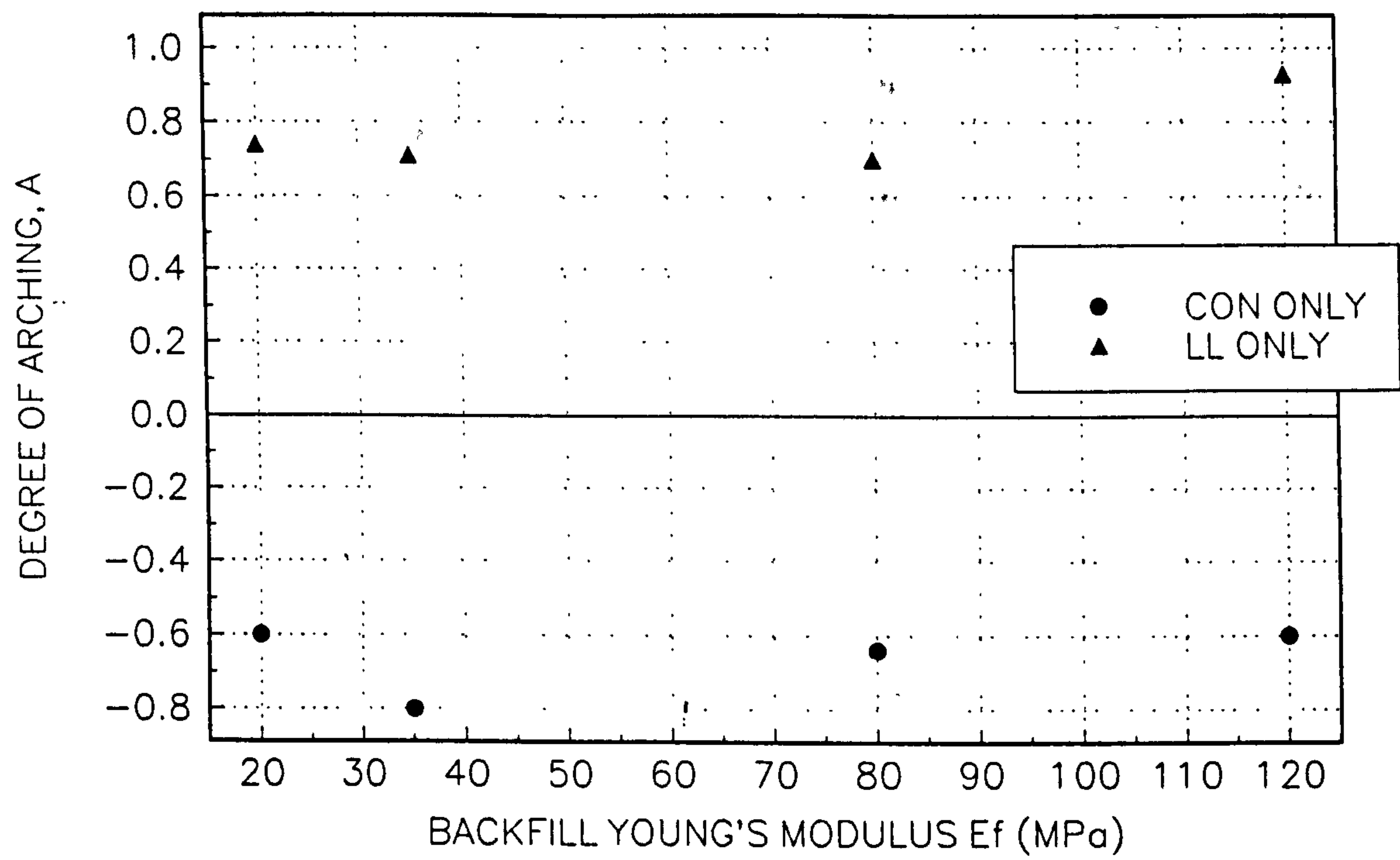


FIGURE 8.60(b)
VARIATION OF RADIAL STRESS WITH BACKFILL YOUNG' MODULUS

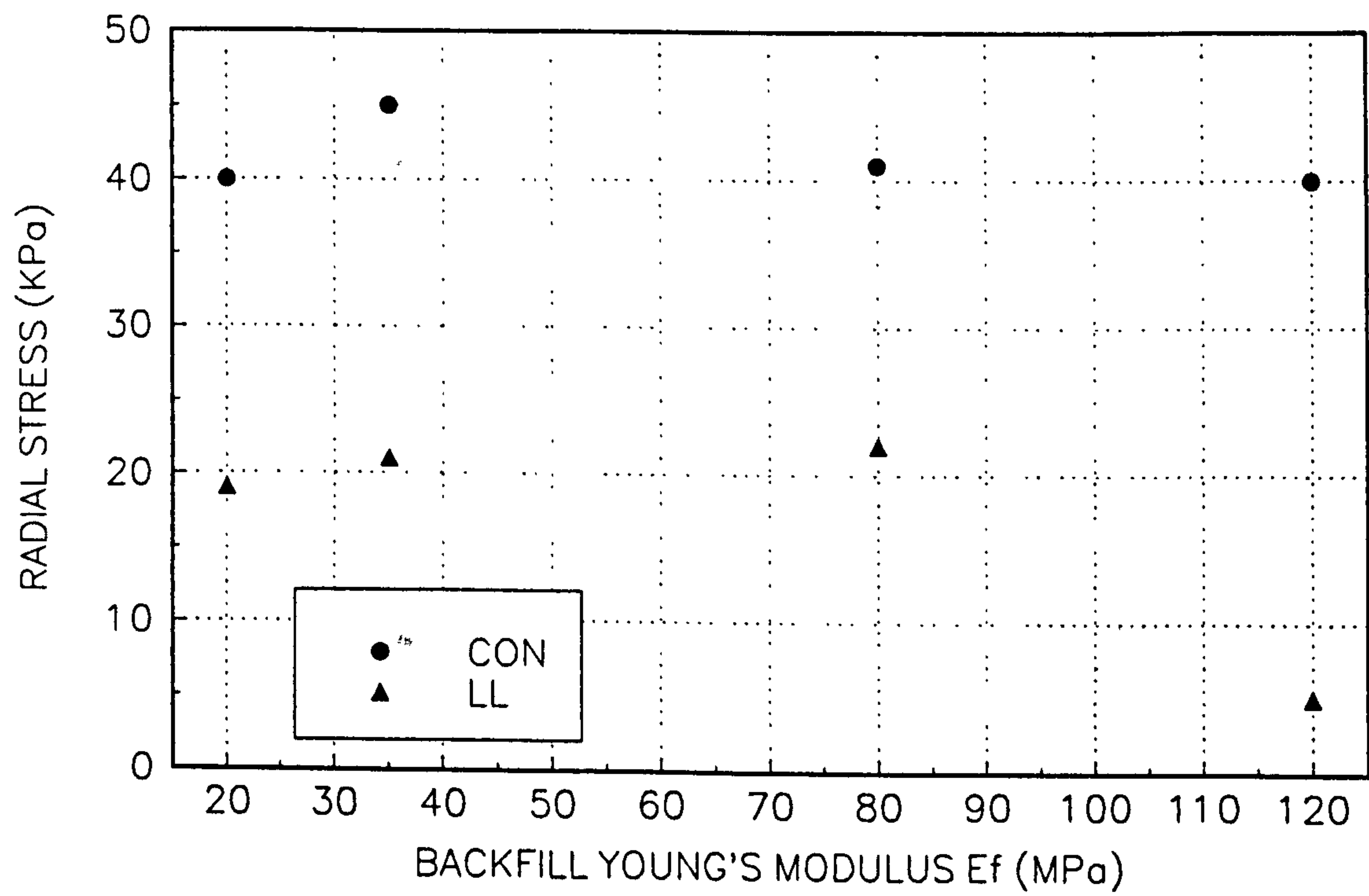


FIGURE 8.61 (a)

VARIATION OF CONSTRUCTION BENDING MOMENT WITH BACKFILL YOUNG'S MODULUS

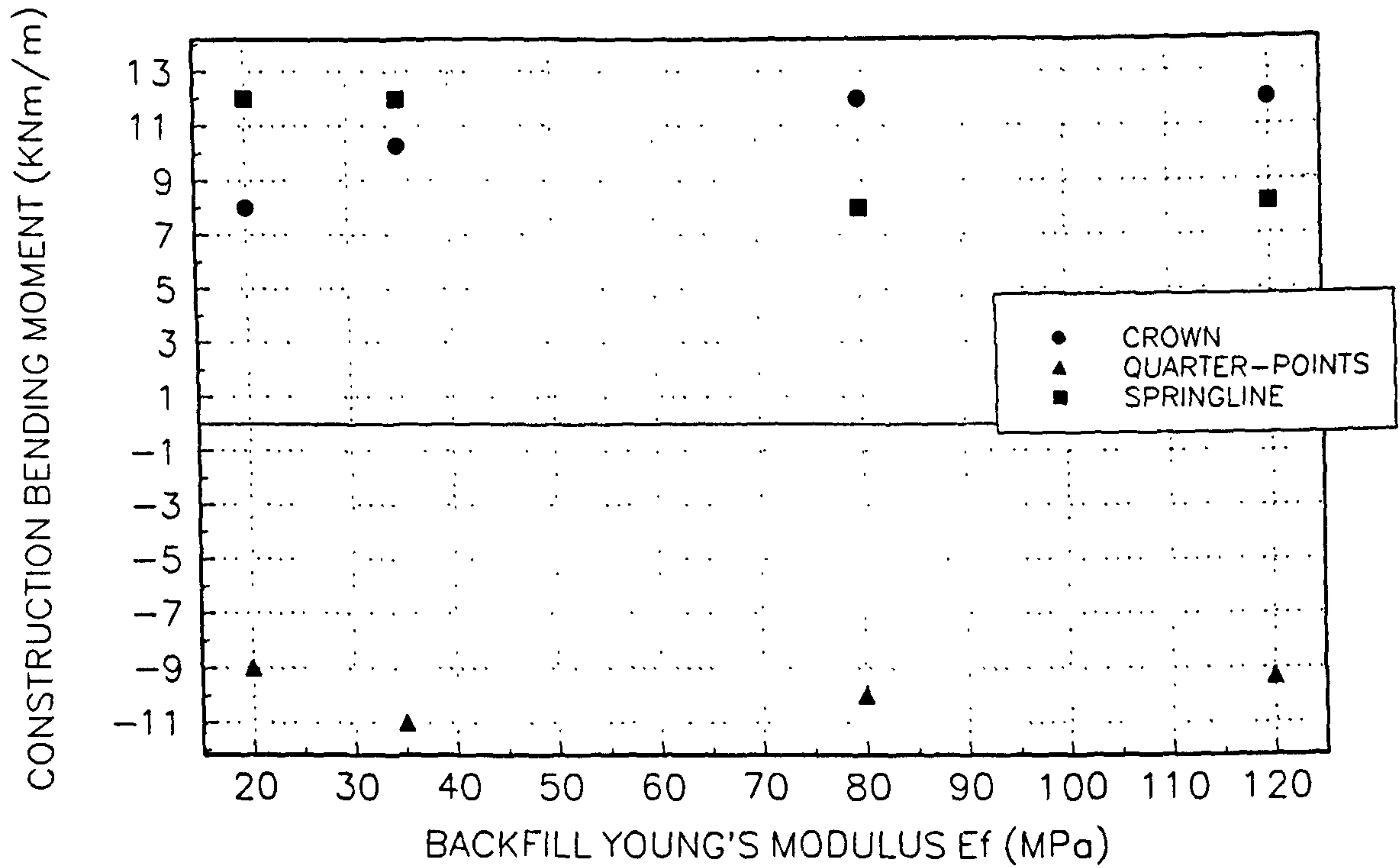


FIGURE 8.61 (b)

VARIATION OF LIVE LOAD BENDING MOMENT WITH BACKFILL YOUNG'S MODULUS

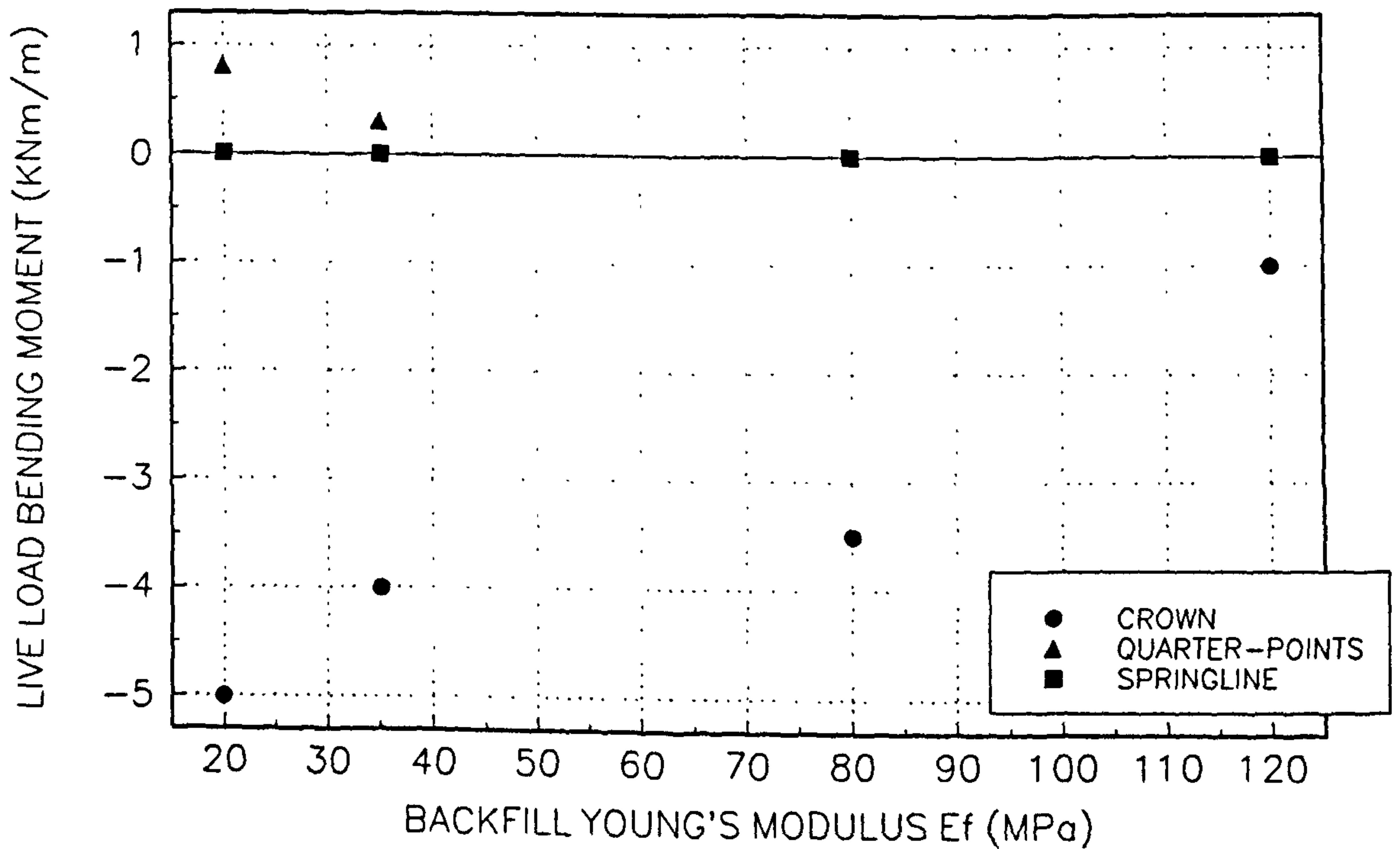


FIGURE 8.62(a)
VARIATION OF CONSTRUCTION SHEAR STRESS WITH BACKFILL YOUNG' MODULUS

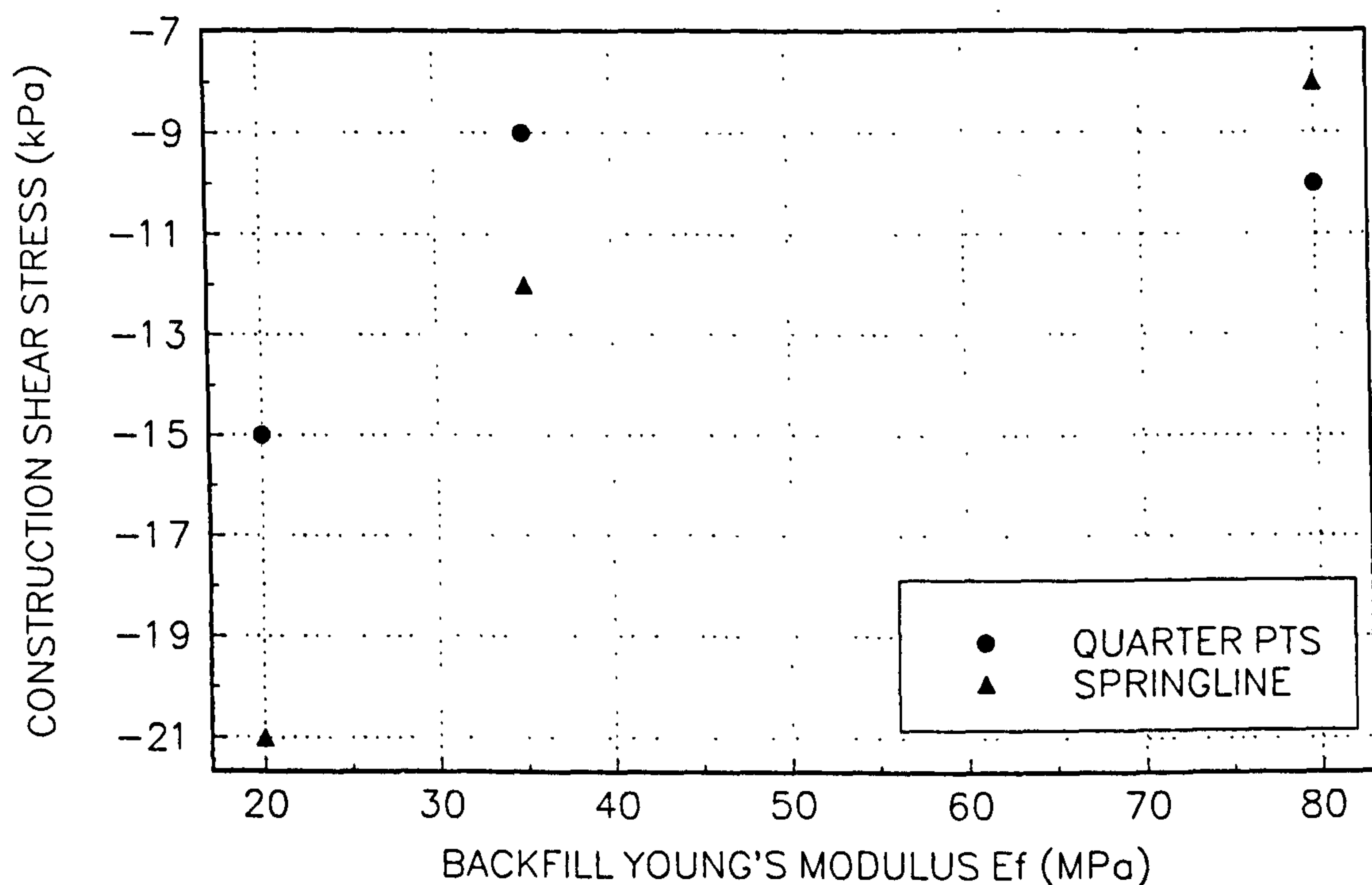


FIGURE 8.62(b)
VARIATION OF LIVE LOAD SHEAR STRESS WITH BACKFILL YOUNG' MODULUS

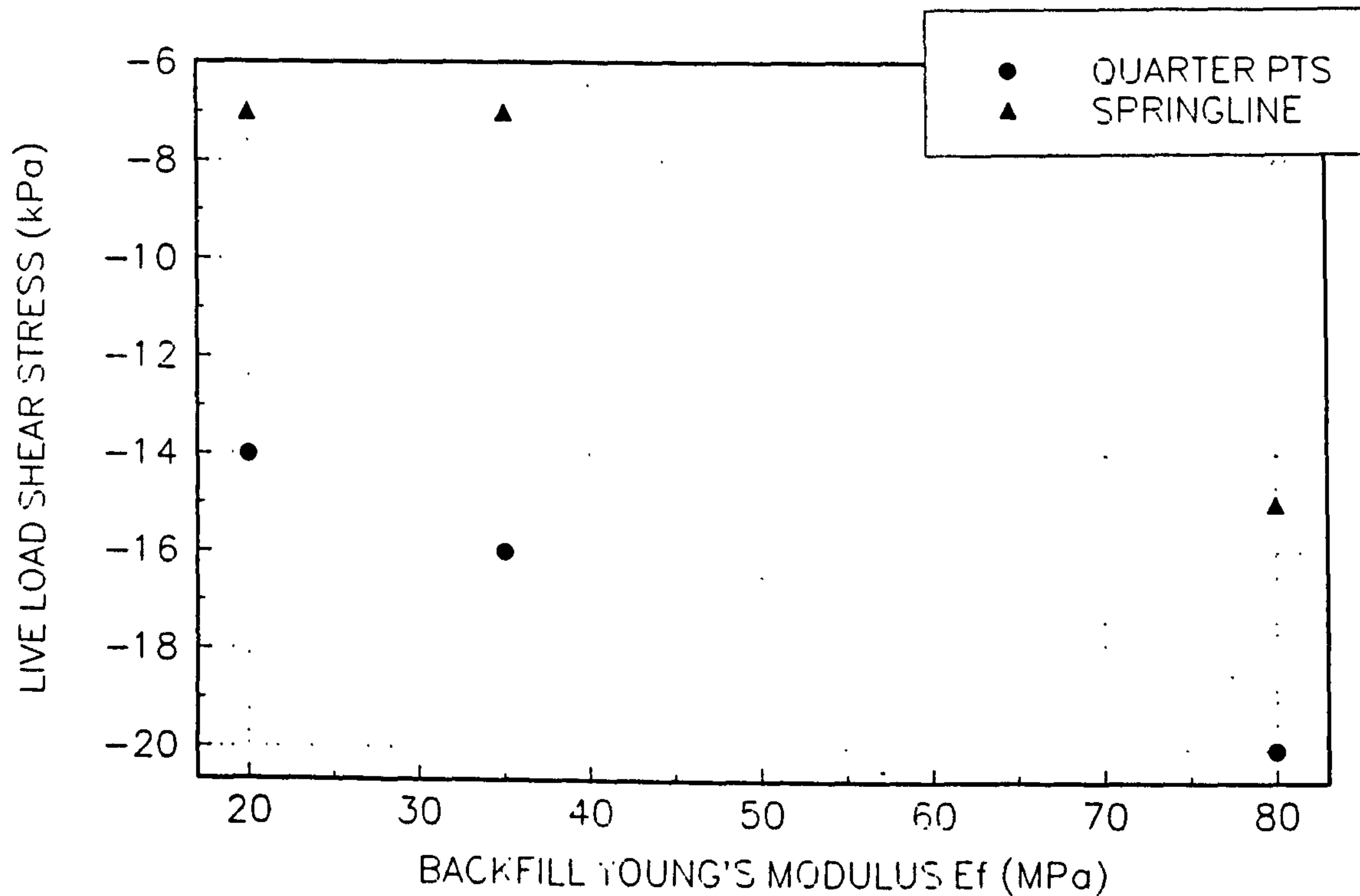


FIGURE 8.63(a)
VARIATION OF CONSTRUCTION THRUST WITH POISSON'S RATIO

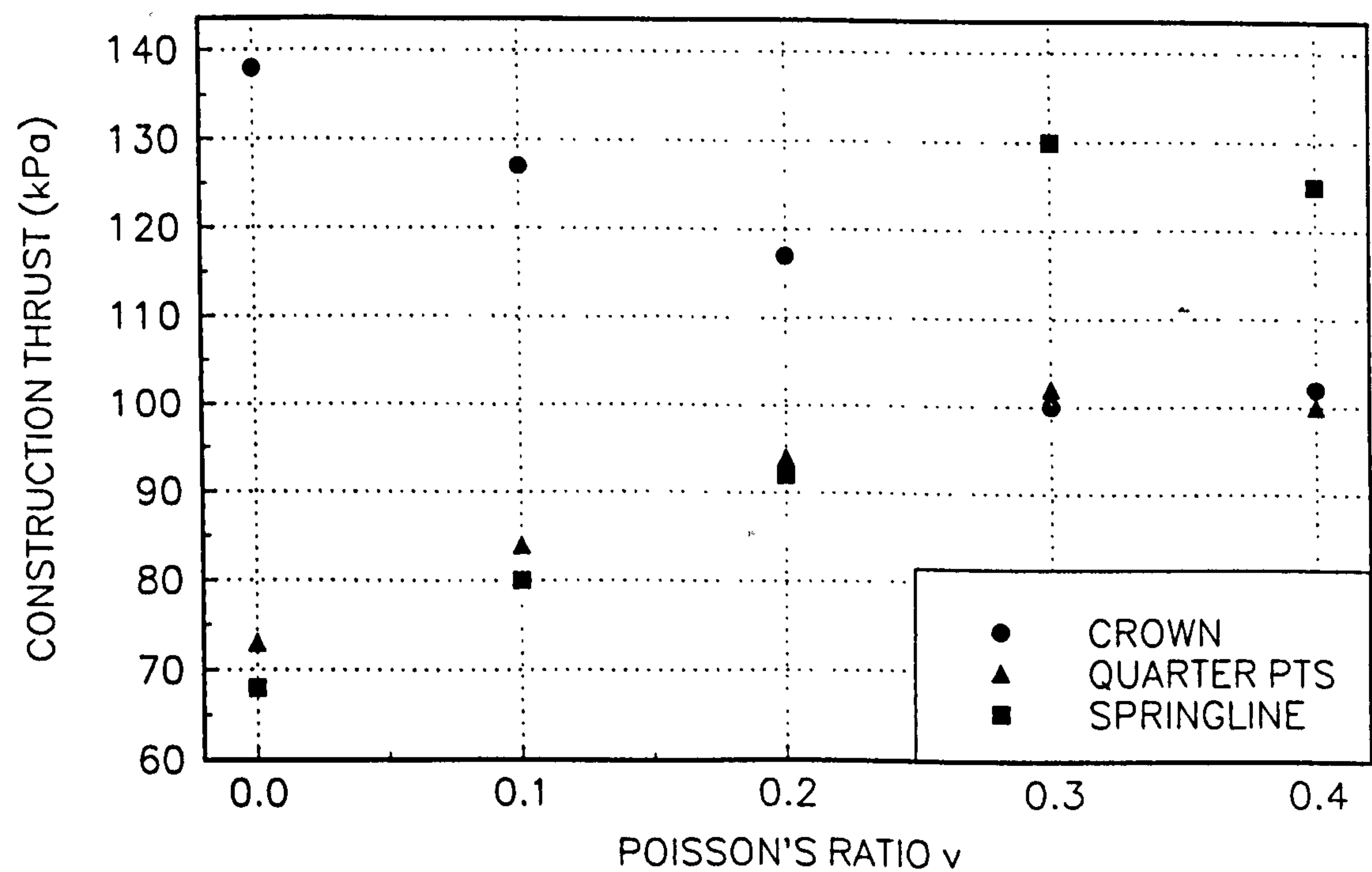


FIGURE 8.63(b)
VARIATION OF LIVE LOAD THRUST WITH BACKFILL POISSON'S RATIO

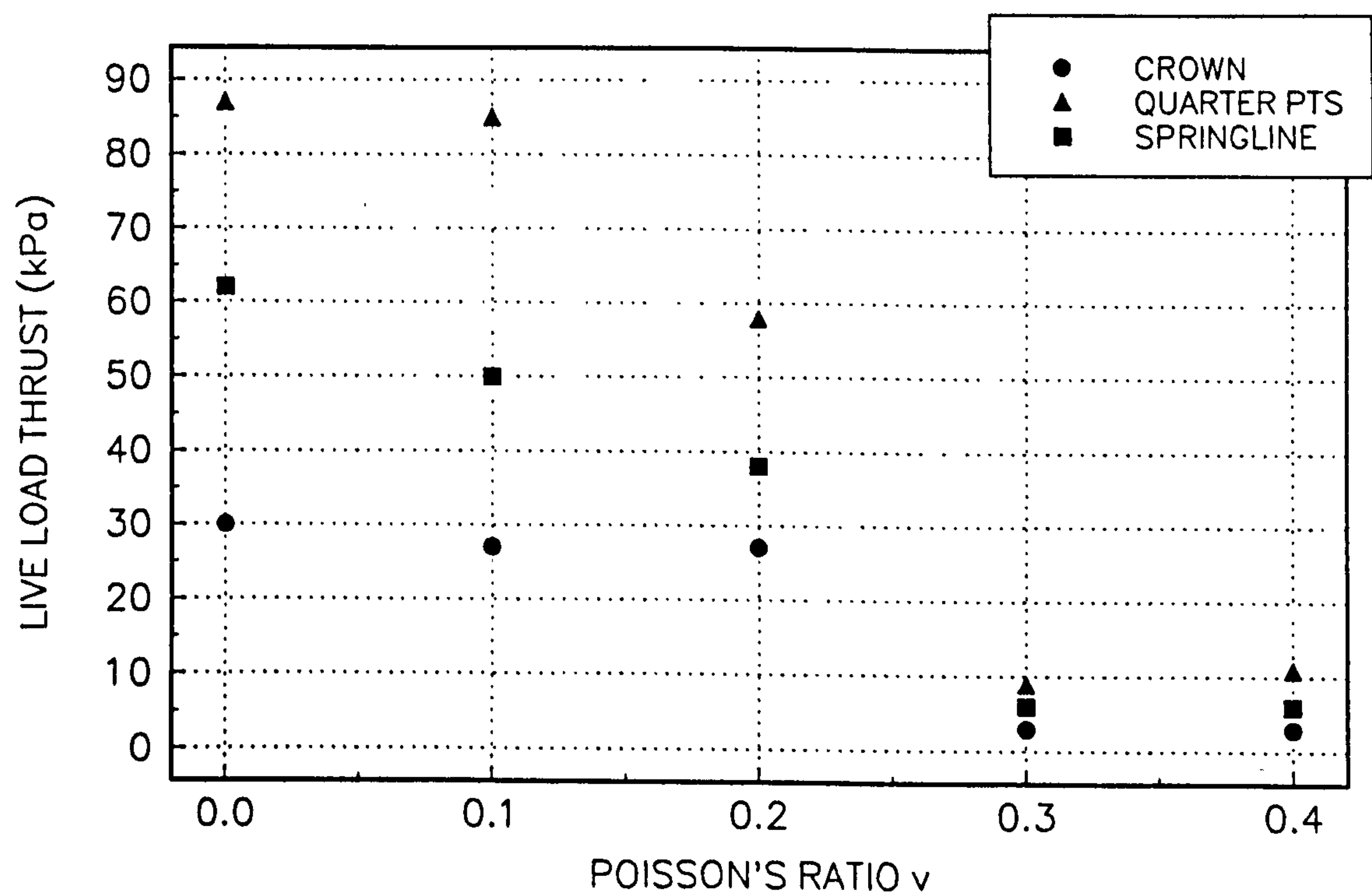


FIGURE 8.64(a)

VARIATION OF CONSTRUCTION RADIAL STRESS WITH BACKFILL POISSON'S RATIO

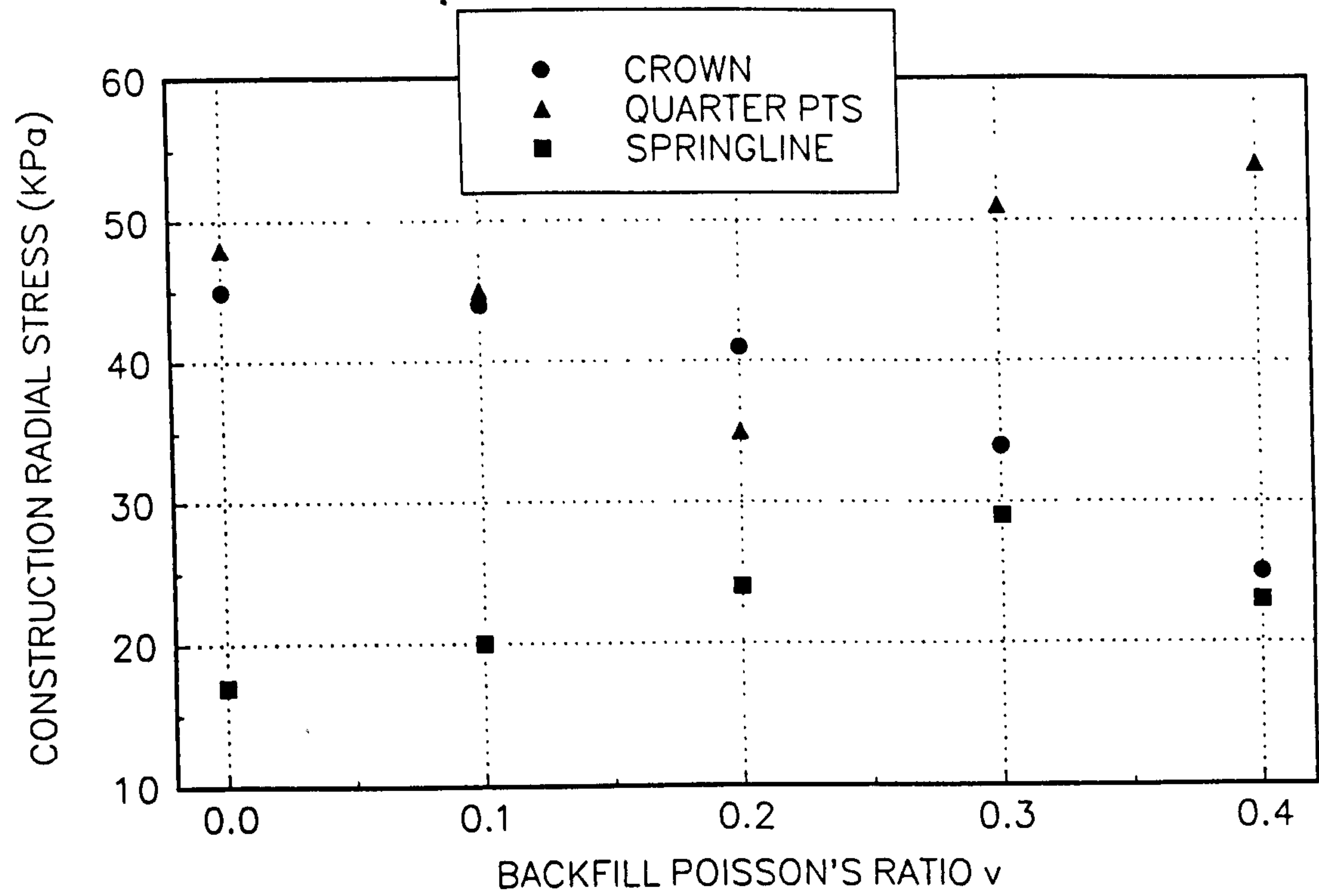


FIGURE 8.64(b)

VARIATION OF LIVE LOAD RADIAL STRESS WITH BACKFILL POISSON'S RATIO

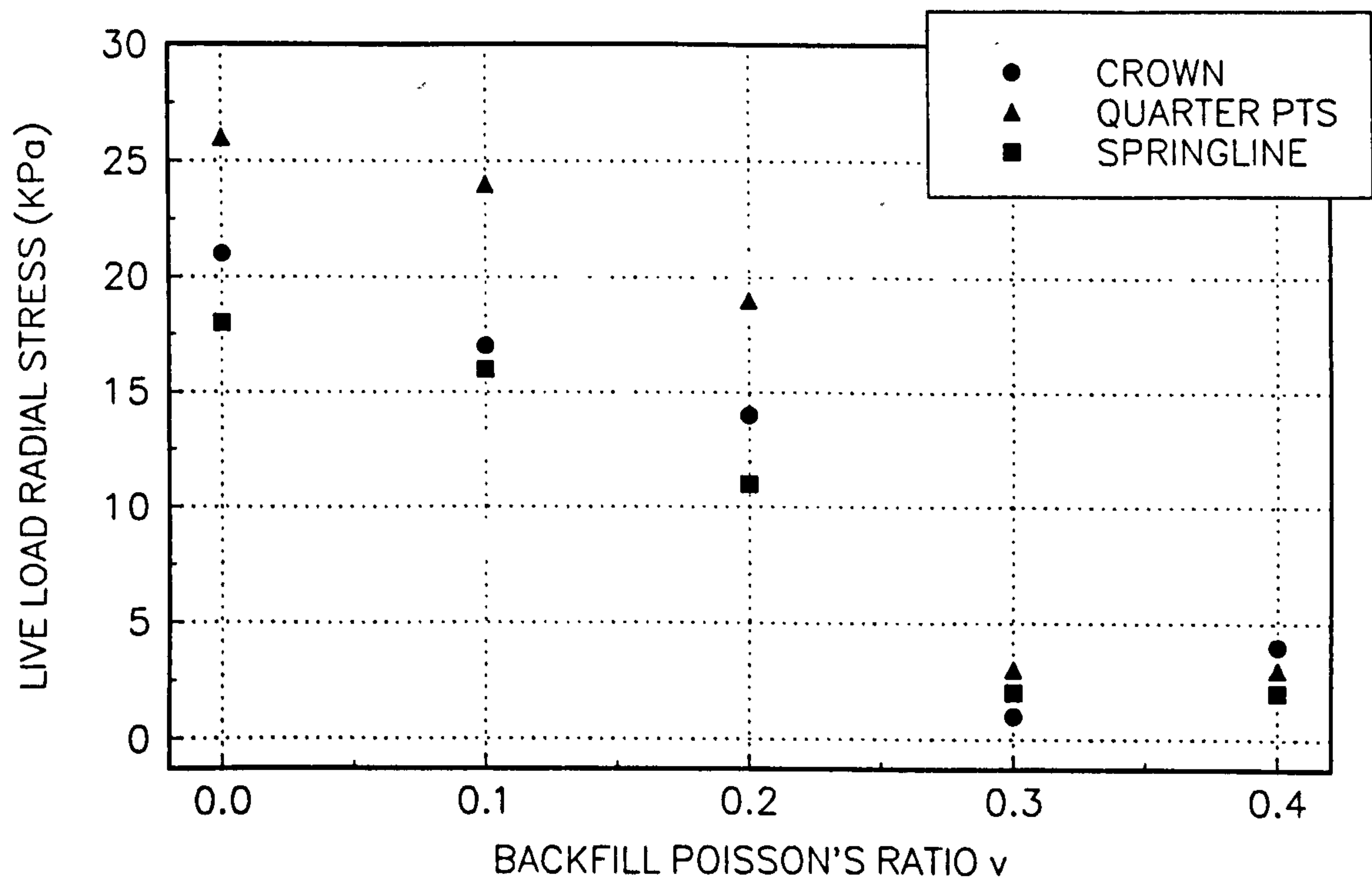


FIGURE 8.65
VARIATION OF DEGREE ARCHING WITH BACKFILL POISSON'S RATIO

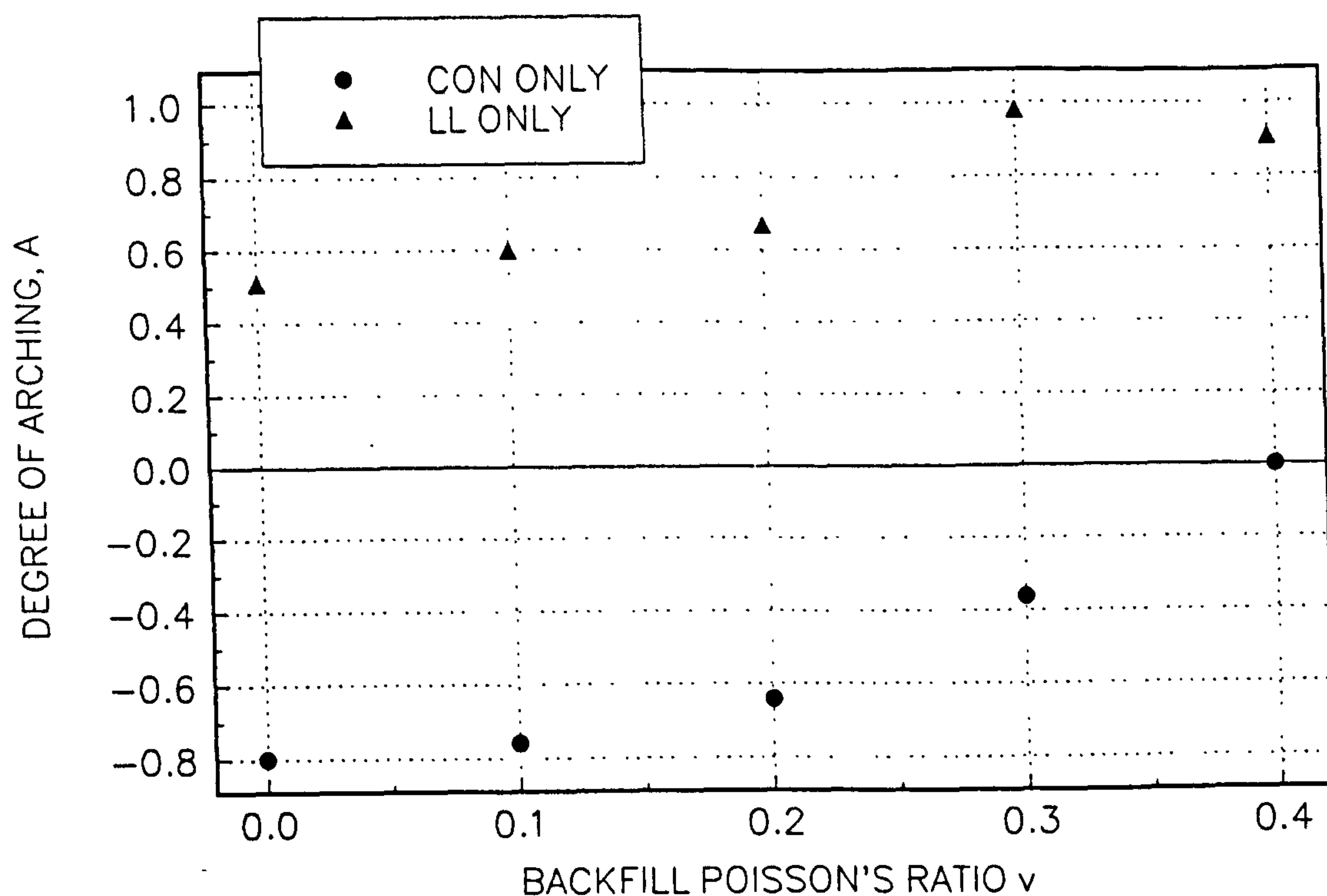


FIGURE 8.66(a)
VARIATION OF CONSTRUCTION BENDING MOMENT WITH BACKFILL POISSON'S RATIO

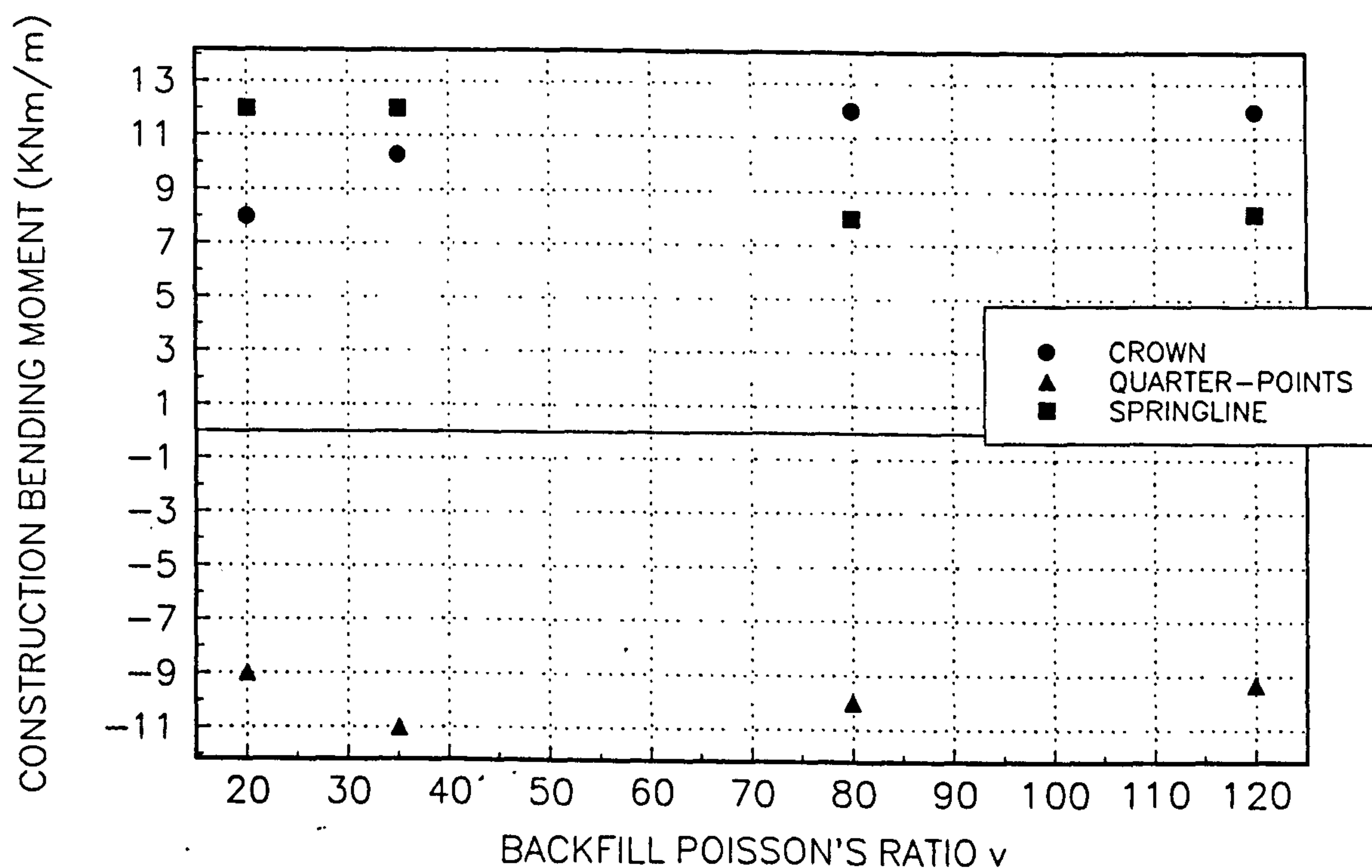


FIGURE 8.66(b)
 VARIATION OF LIVE LOAD BENDING MOMENT WITH BACKFILL POISSON'S RATIO

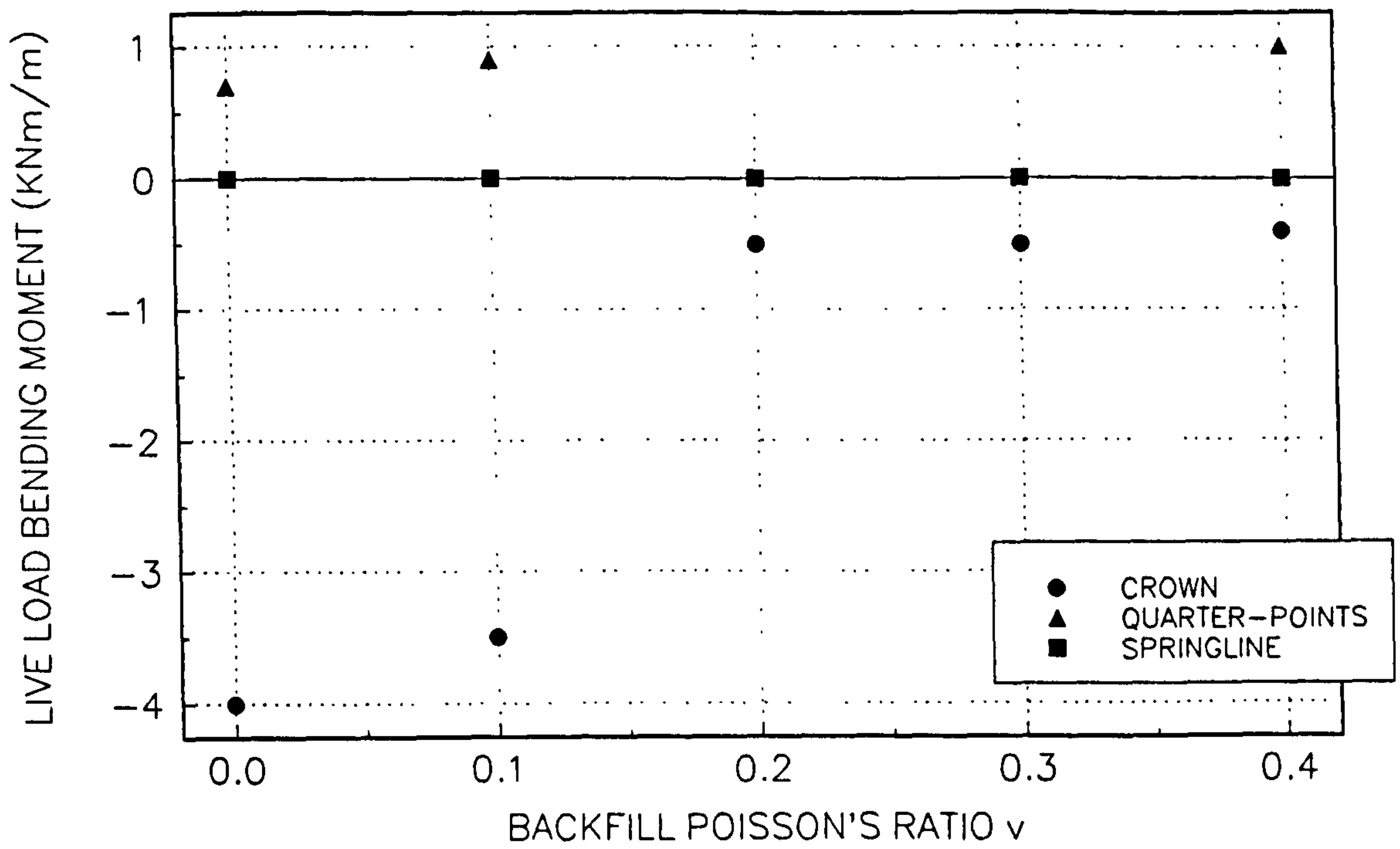


FIGURE 8.67(a)
 VARIATION OF CROWN DISPLACEMENTS WITH BACKFILL POISSON'S RATIO

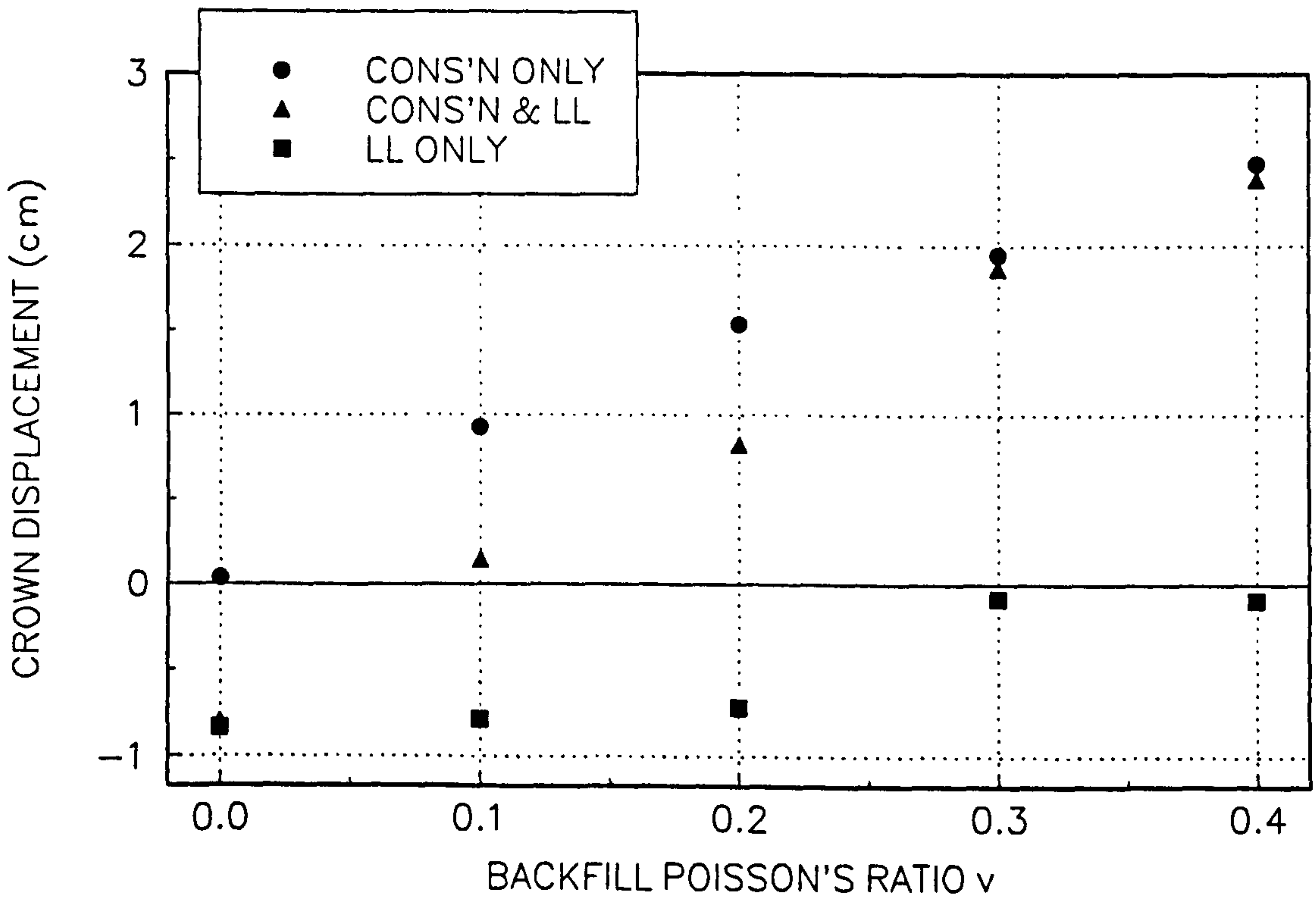


FIGURE 8.67(b)
VARIATION OF SPRINGLINE DISPLACEMENTS WITH BACKFILL POISSON'S RATIO

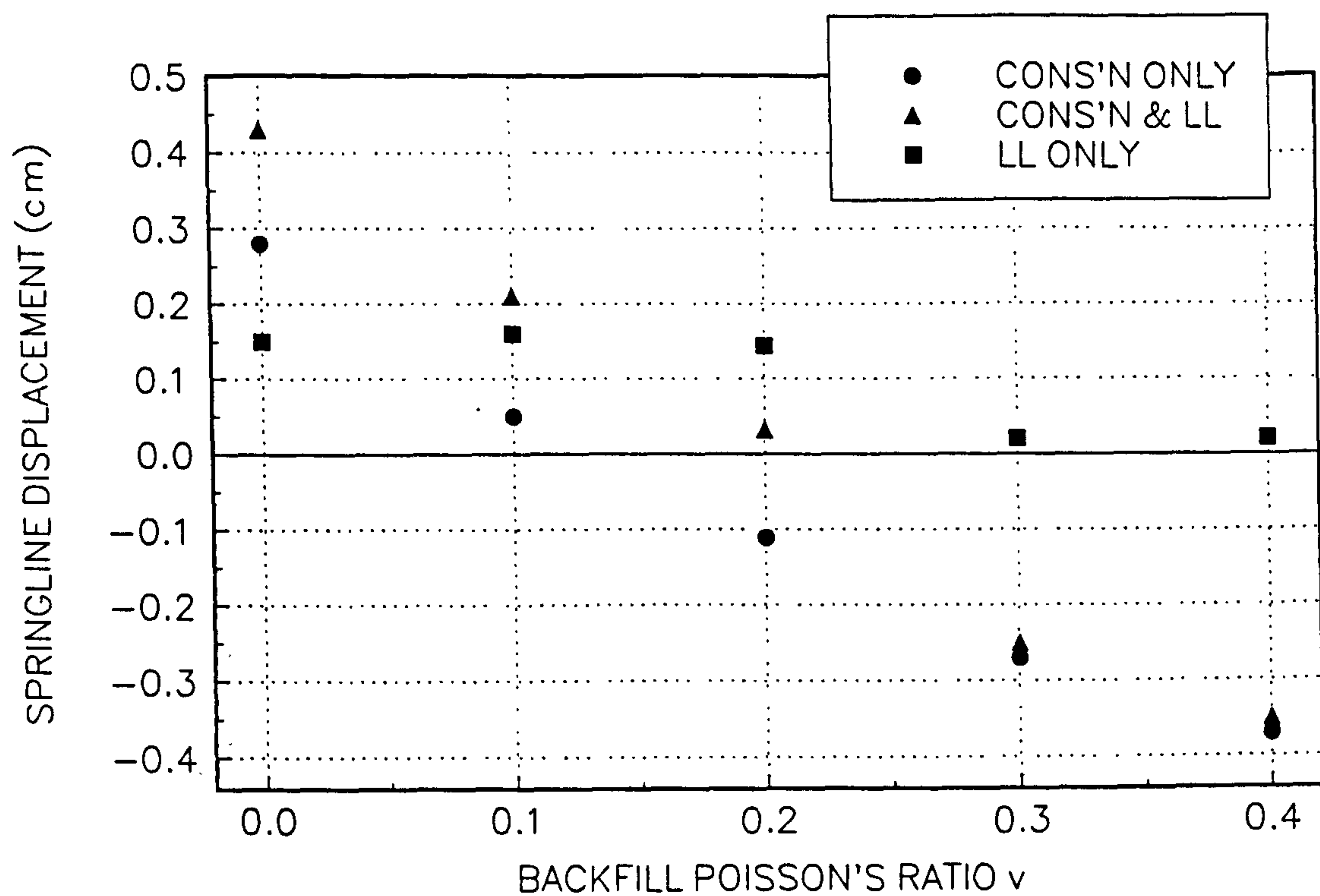


FIGURE 8.68(a)
VARIATION OF CONSTRUCTION SHEAR STRESS WITH BACKFILL POISSON'S RATIO

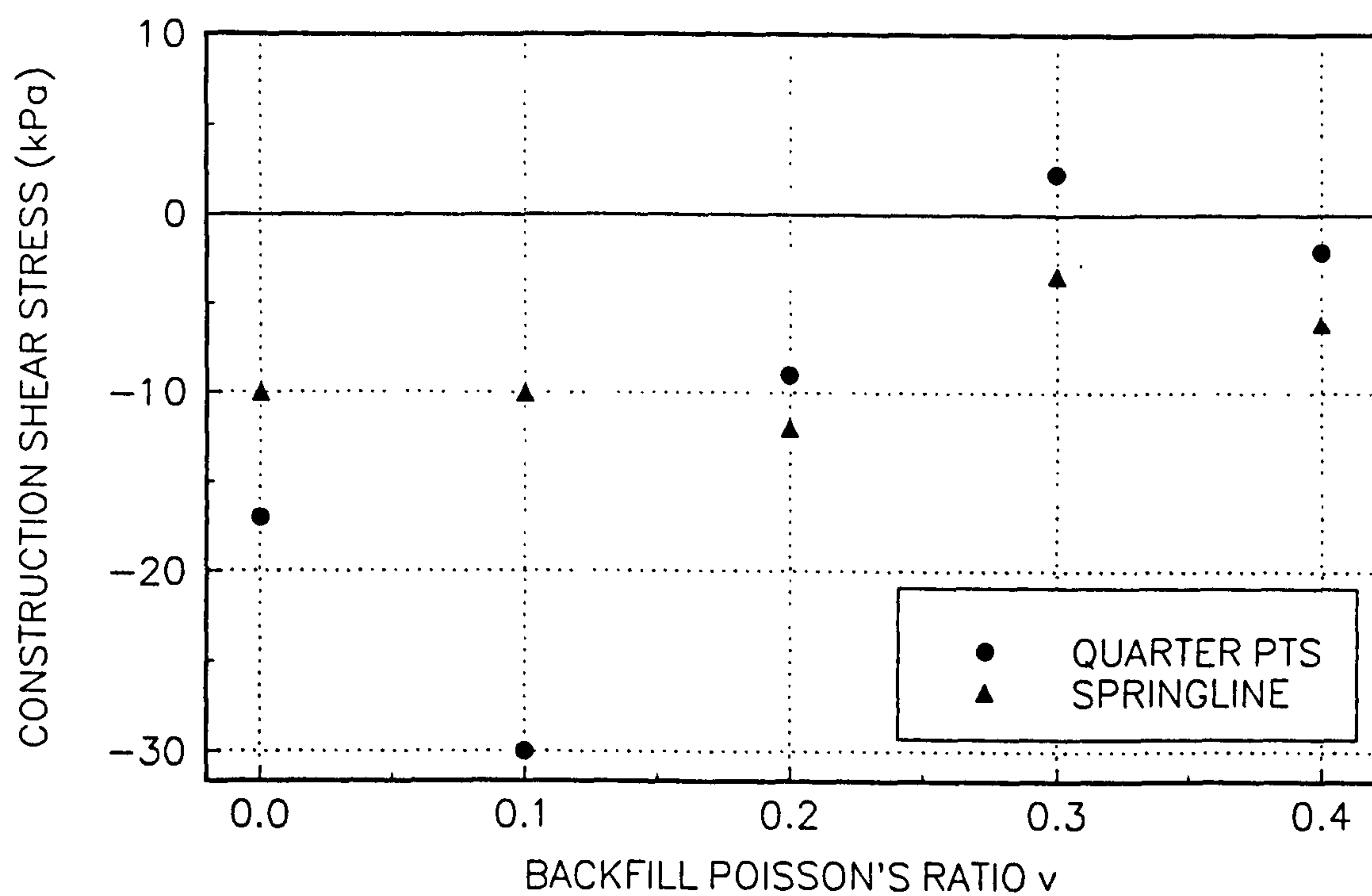


FIGURE 8.68(b)
VARIATION OF LIVE LOAD SHEAR STRESS WITH BACKFILL POISSON'S RATIO

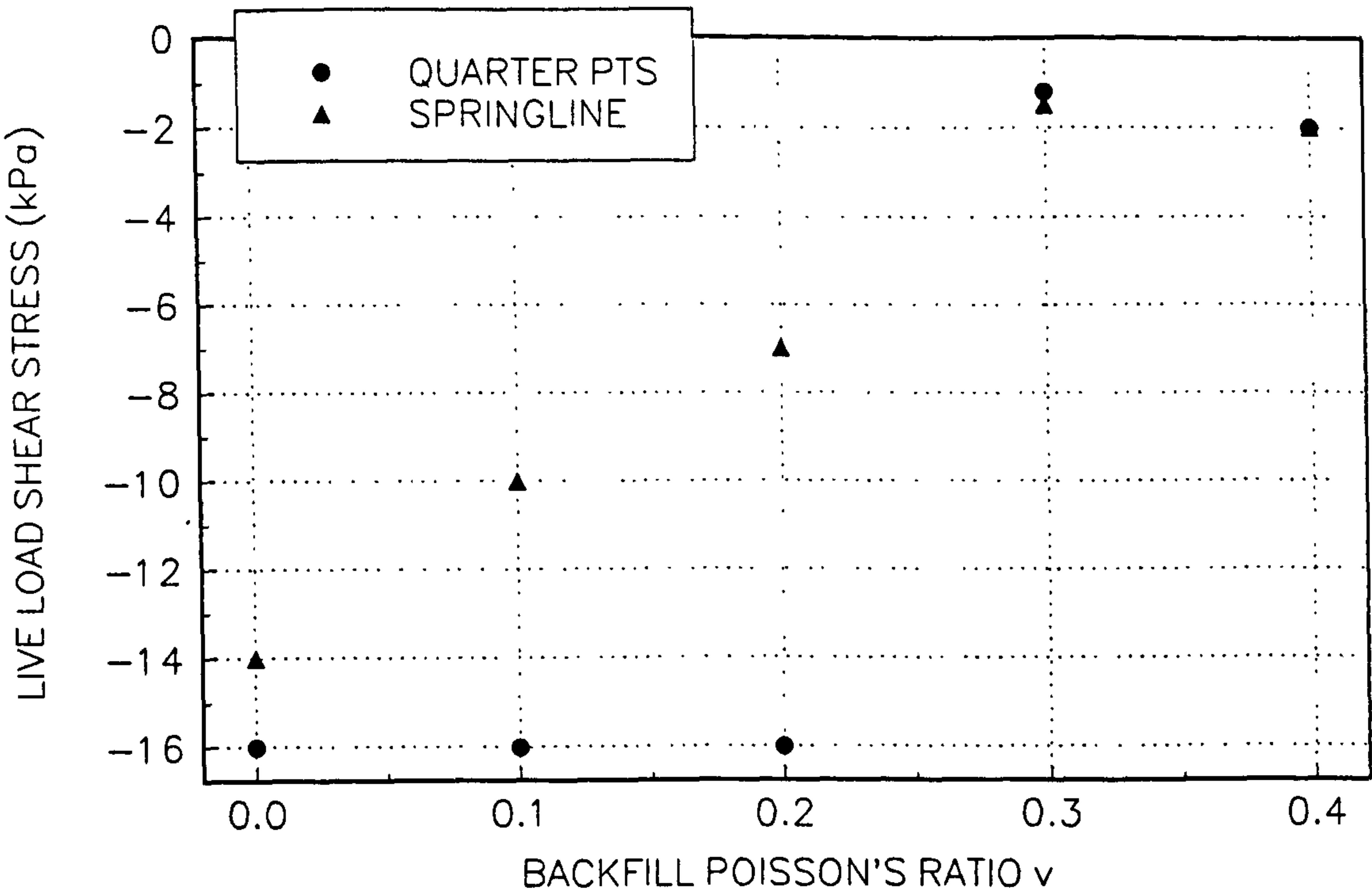


FIGURE 8.69(a)
VARIATION OF CROWN DISPLACEMENTS WITH BACKFILL ANGLE OF FRICTION

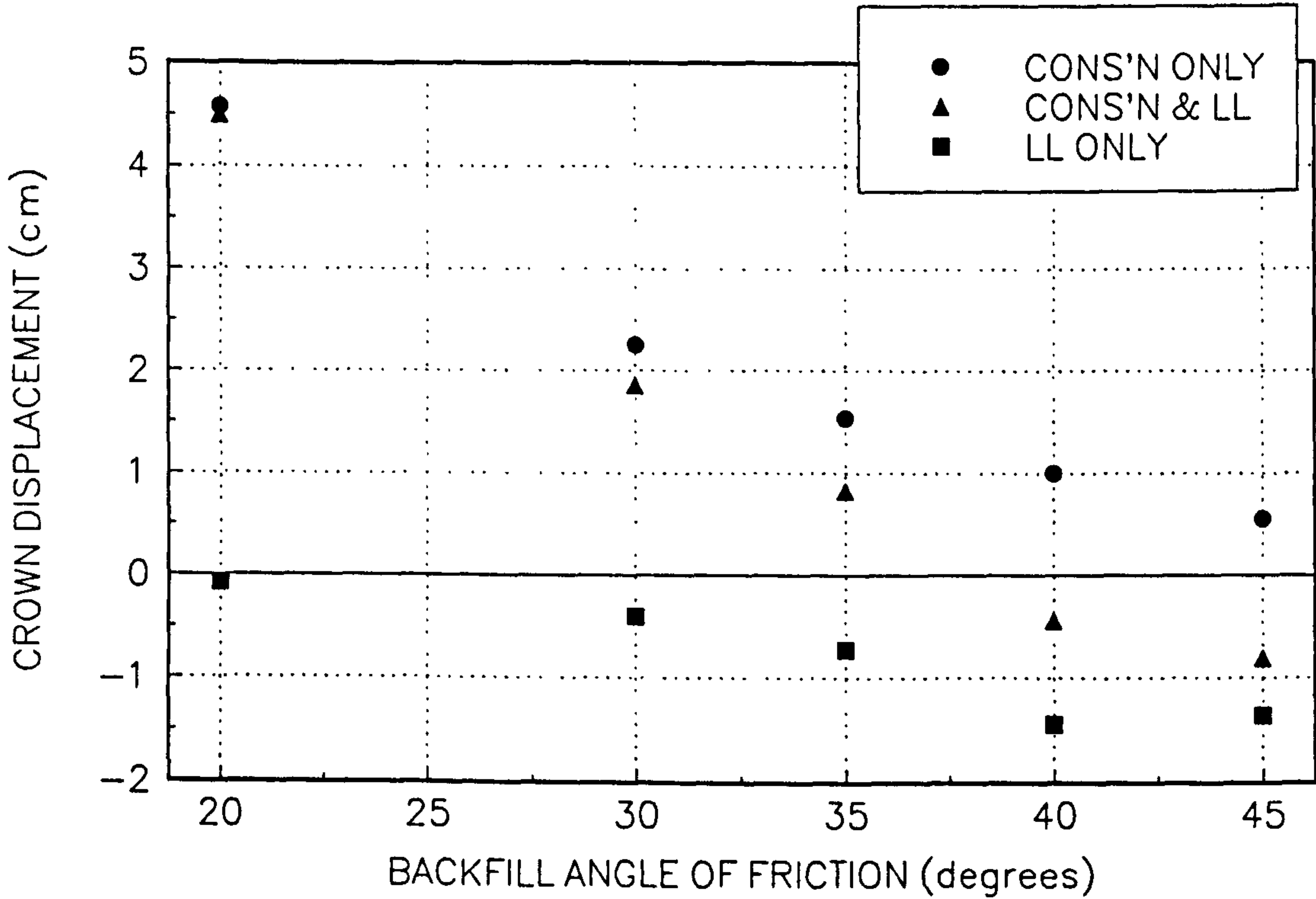


FIGURE 8.69(b)
VARIATION OF SPRINGLINE DISPLACEMENTS WITH BACKFILL ANGLE OF FRICTION

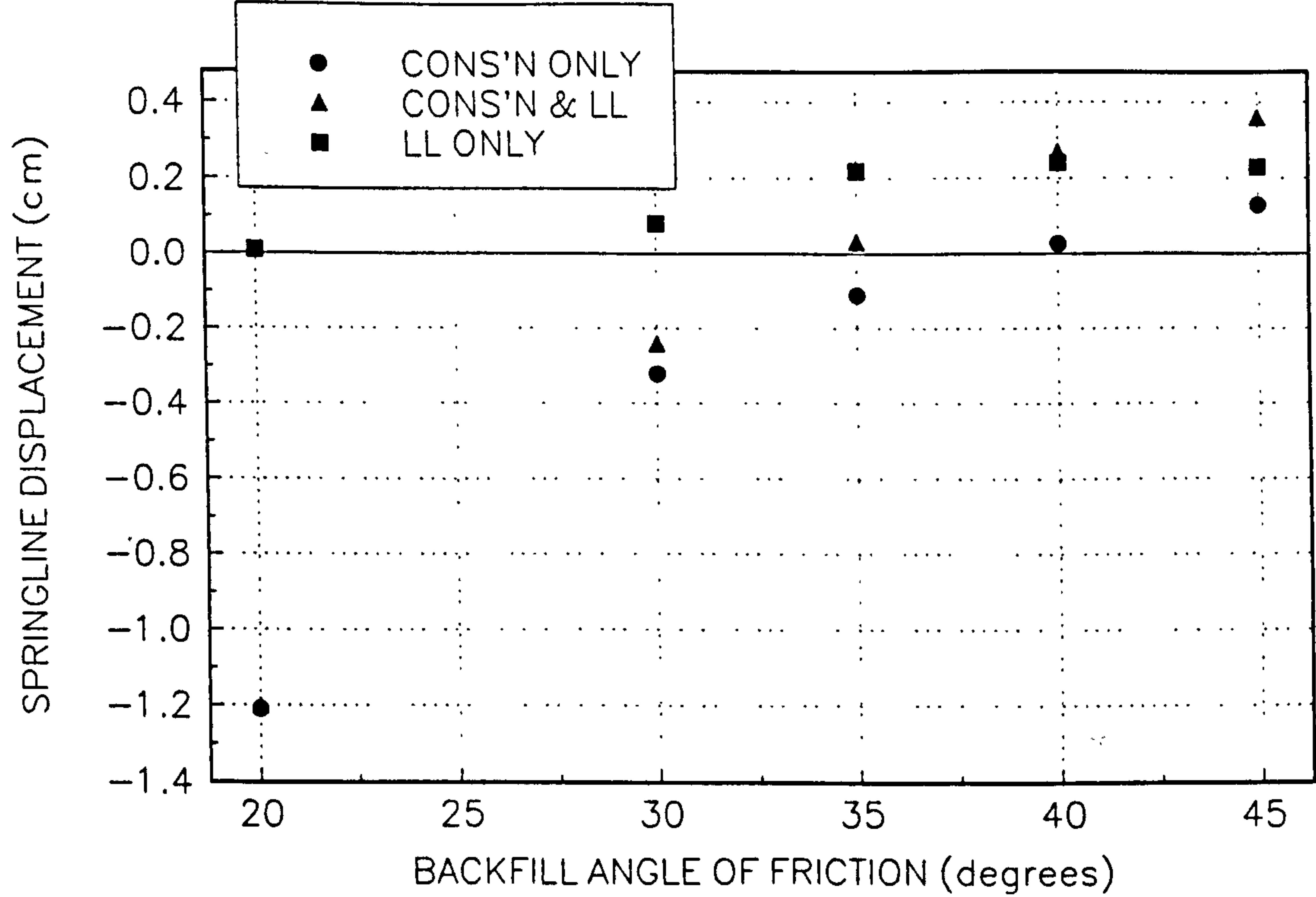


FIGURE 8.70(a)
VARIATION OF CONSTRUCTION BENDING MOMENT WITH BACKFILL ANGLE OF FRICTION

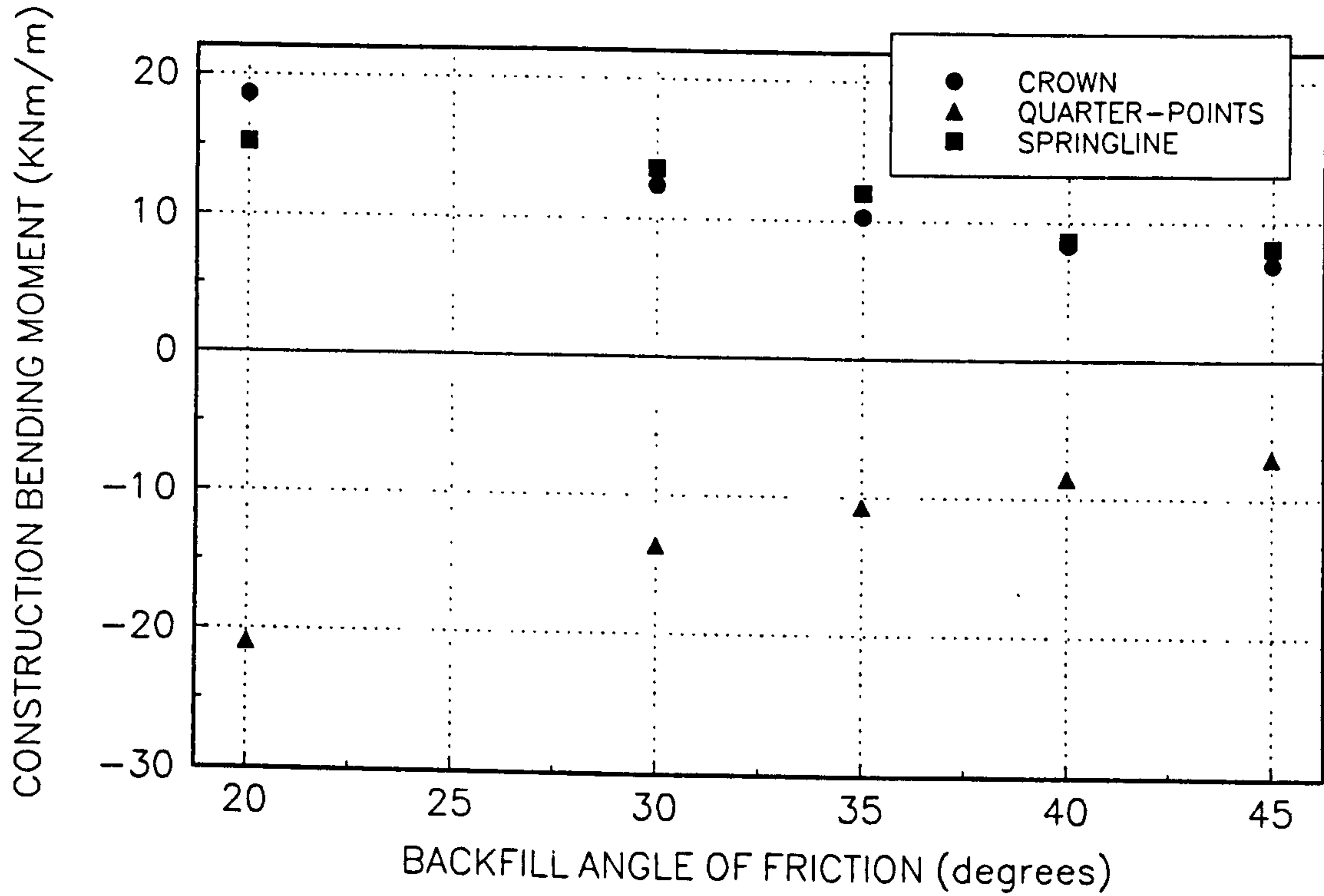


FIGURE 8.70(b)
VARIATION OF LIVE LOAD BENDING MOMENT WITH BACKFILL ANGLE OF FRICTION

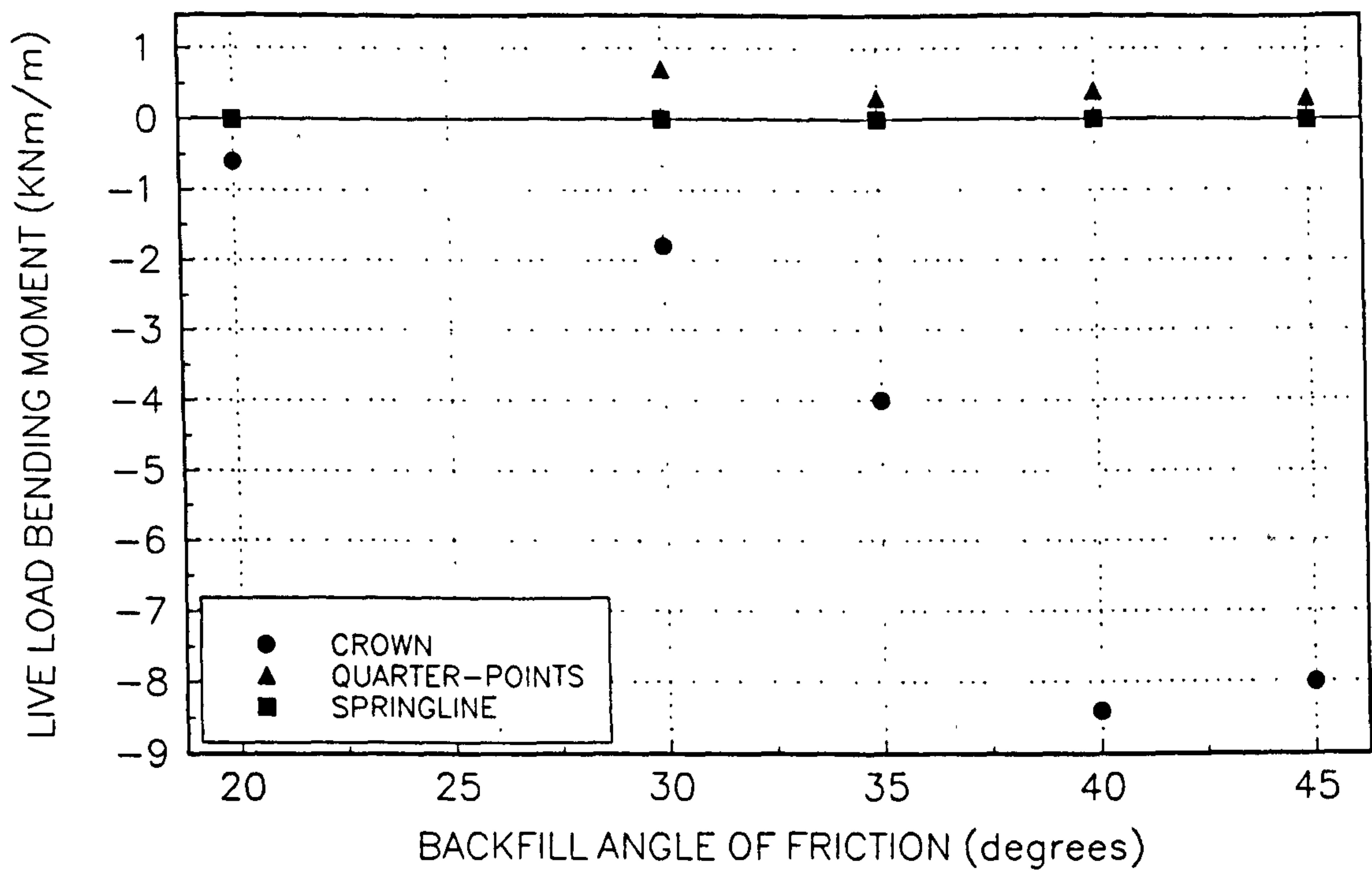


FIGURE 8.71
VARIATION OF DEGREE ARCHING WITH BACKFILL ANGLE OF FRICTION

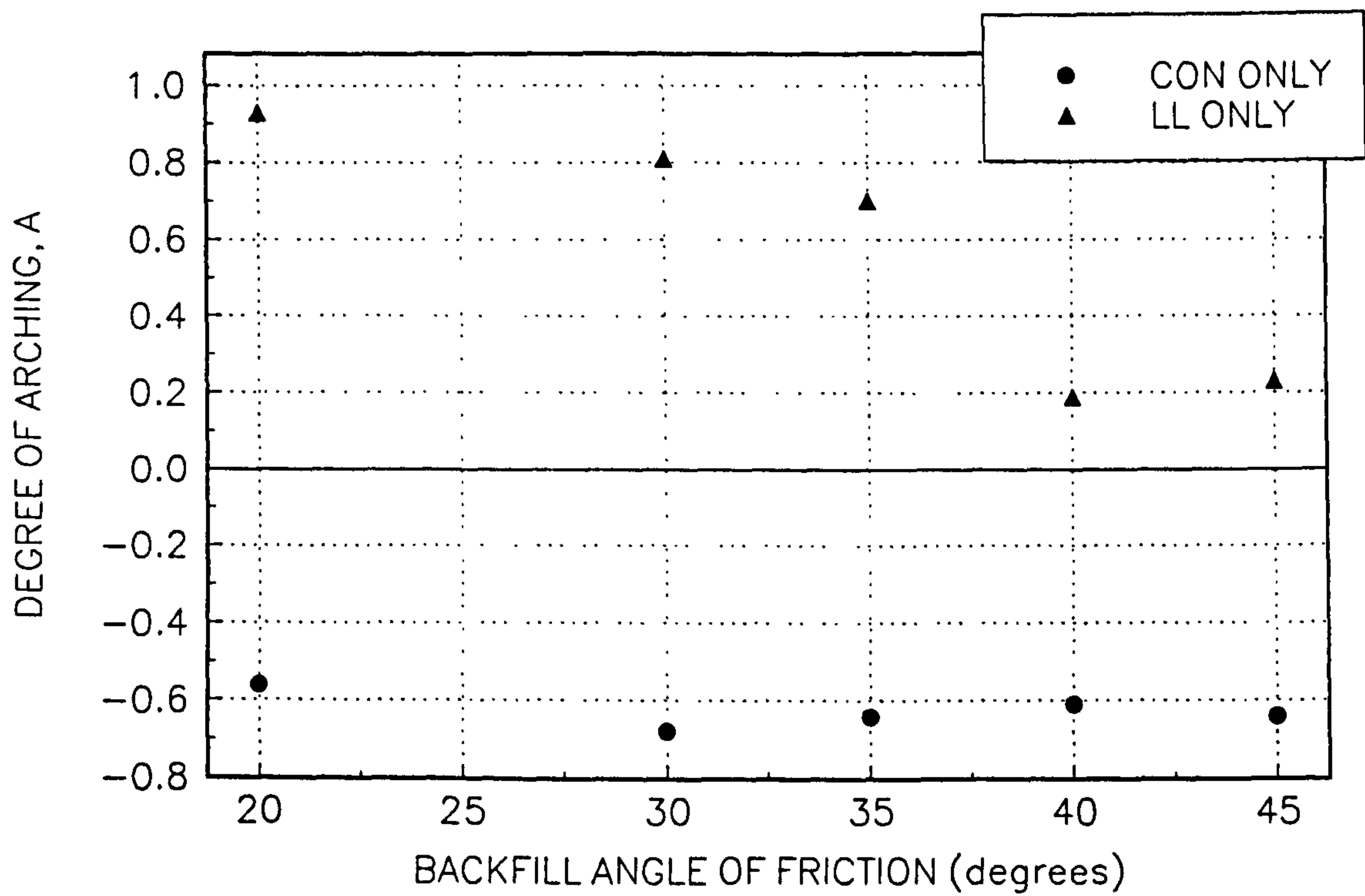


FIGURE 8.72(a)
VARIATION OF CONSTRUCTION SHEAR STRESS WITH BACKFILL ANGLE OF FRICTION

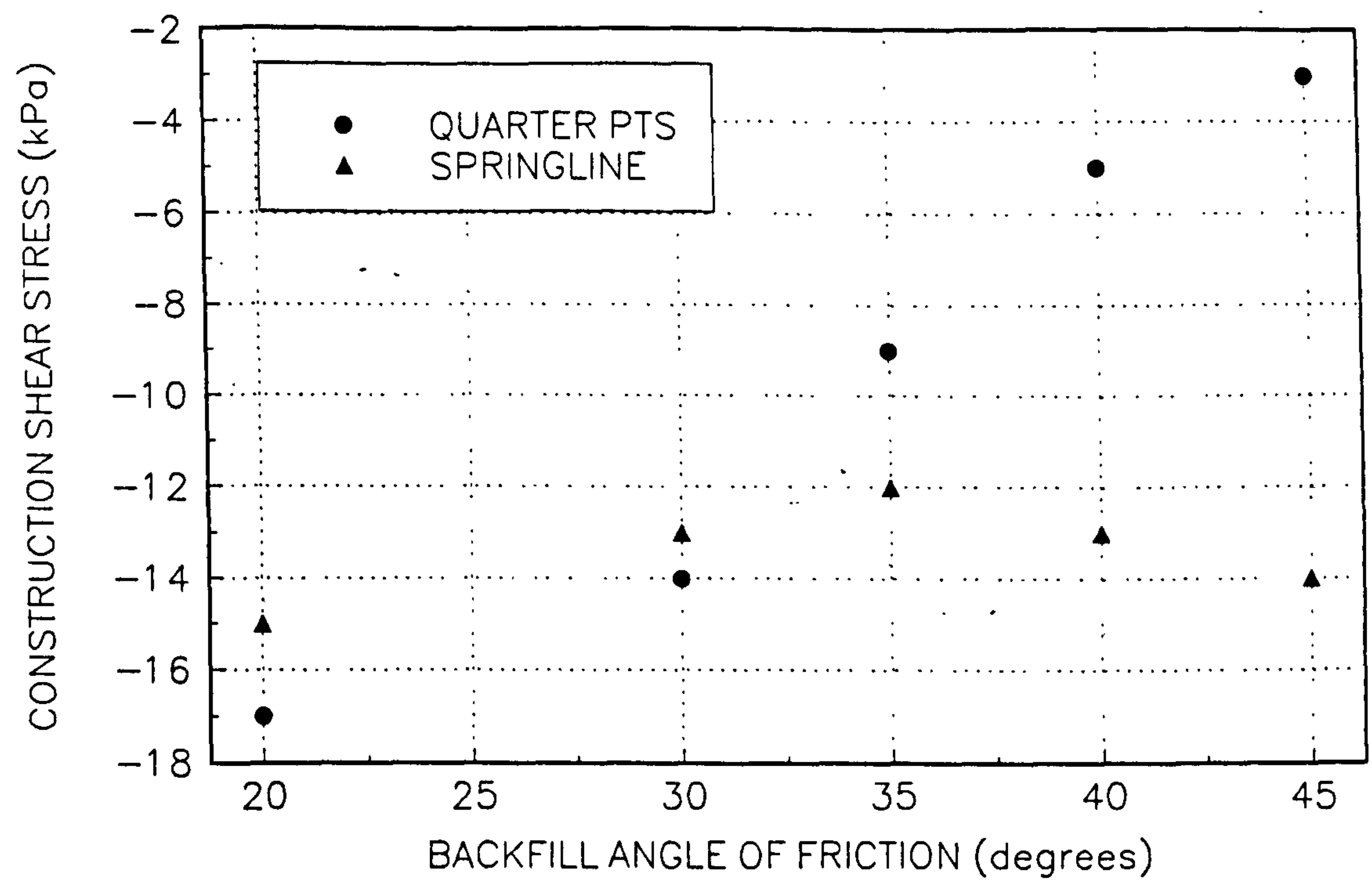


FIGURE 8.72(b)
VARIATION OF LIVE LOAD SHEAR STRESS WITH BACKFILL ANGLE OF FRICTION

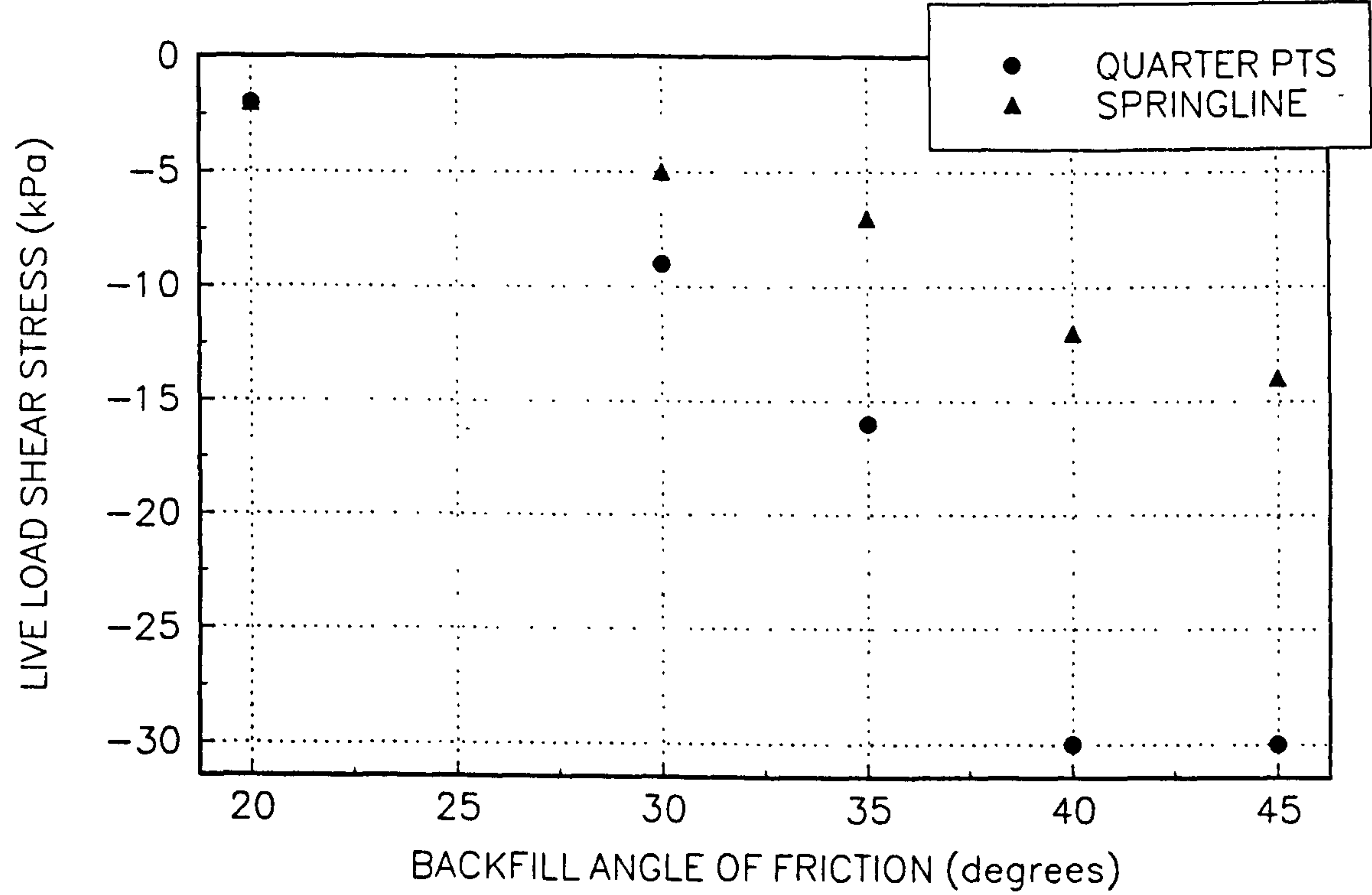


FIGURE 8.73(a)
VARIATION OF CONSTRUCTION THRUST WITH BACKFILL ANGLE OF FRICTION

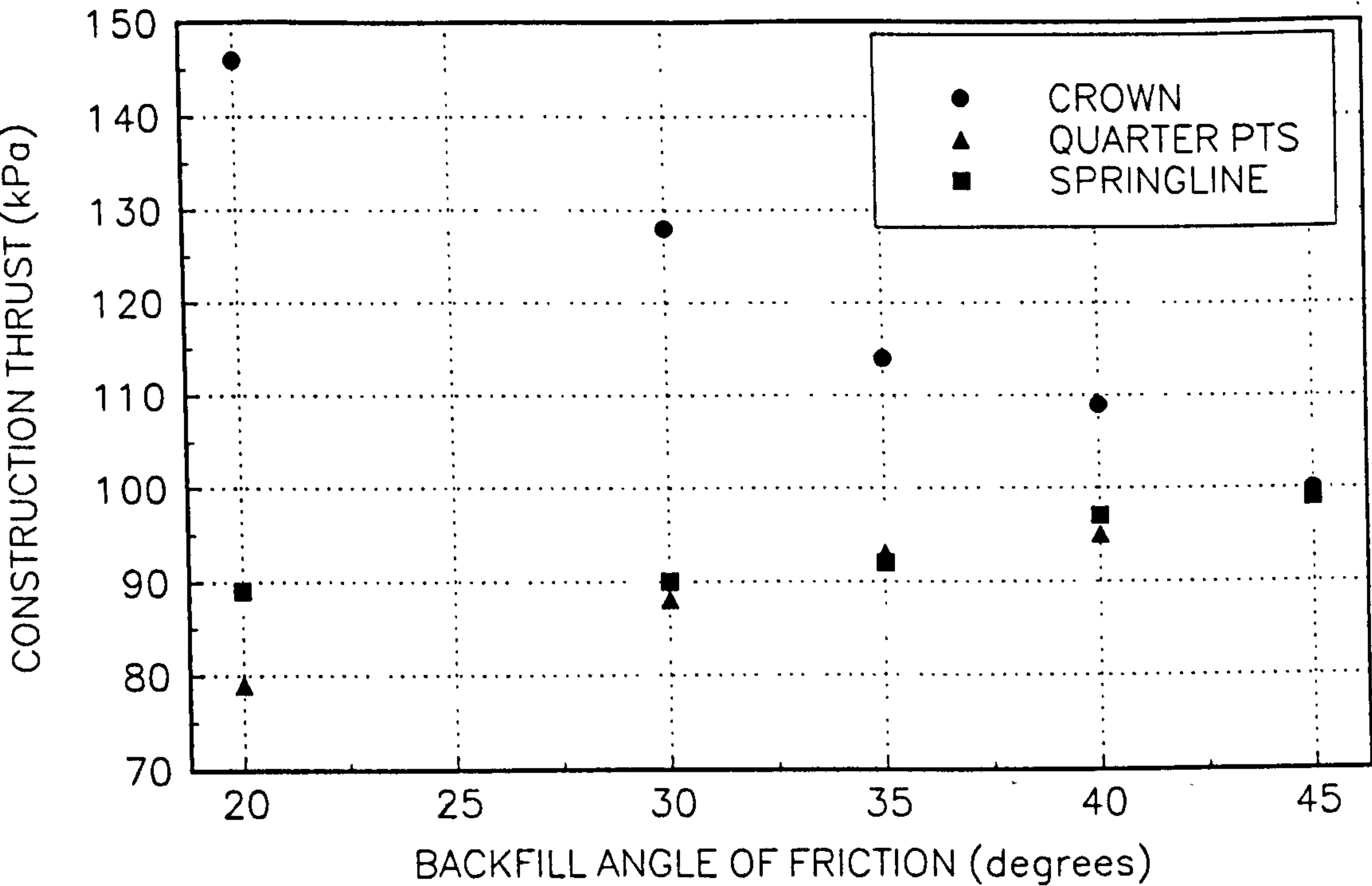


FIGURE 8.73(b)
VARIATION OF LIVE LOAD THRUST WITH BACKFILL ANGLE OF FRICTION

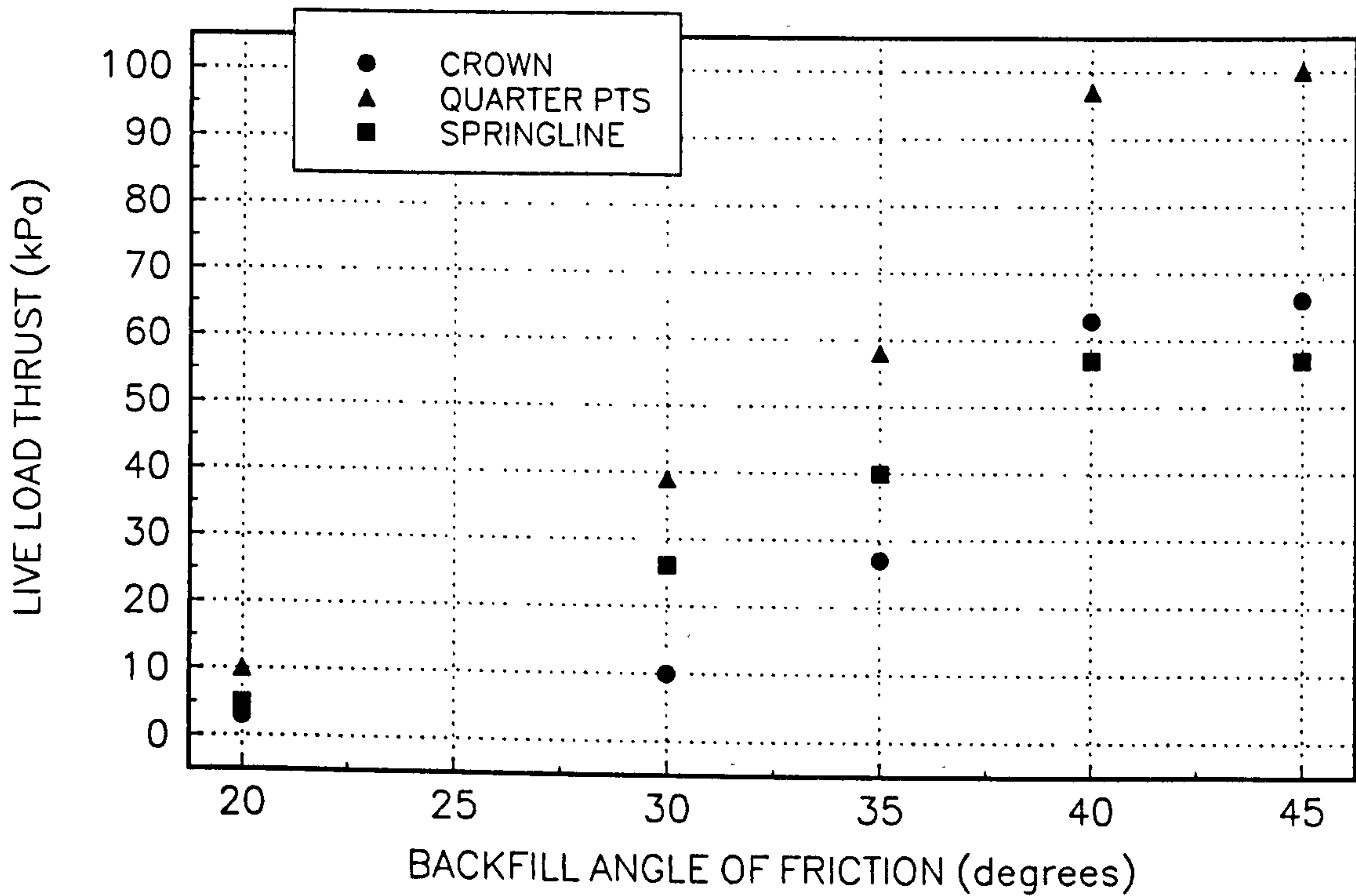


FIGURE 8.74(a)
 VARIATION OF CONSTRUCTION RADIAL STRESS WITH BACKFILL ANGLE OF FRICTION

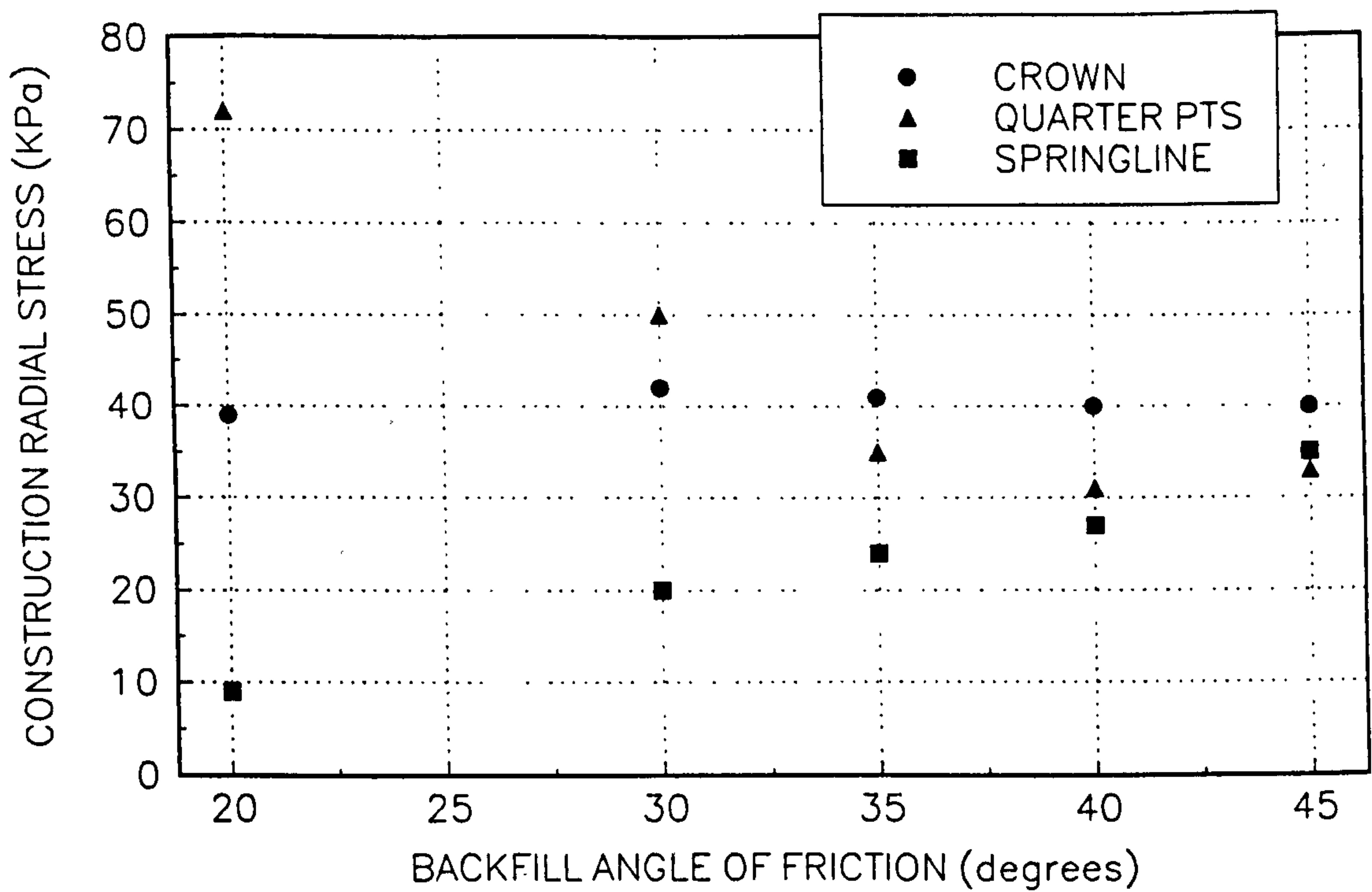


FIGURE 8.74(b)
 VARIATION OF LIVE LOAD RADIAL STRESS WITH BACKFILL ANGLE OF FRICTION

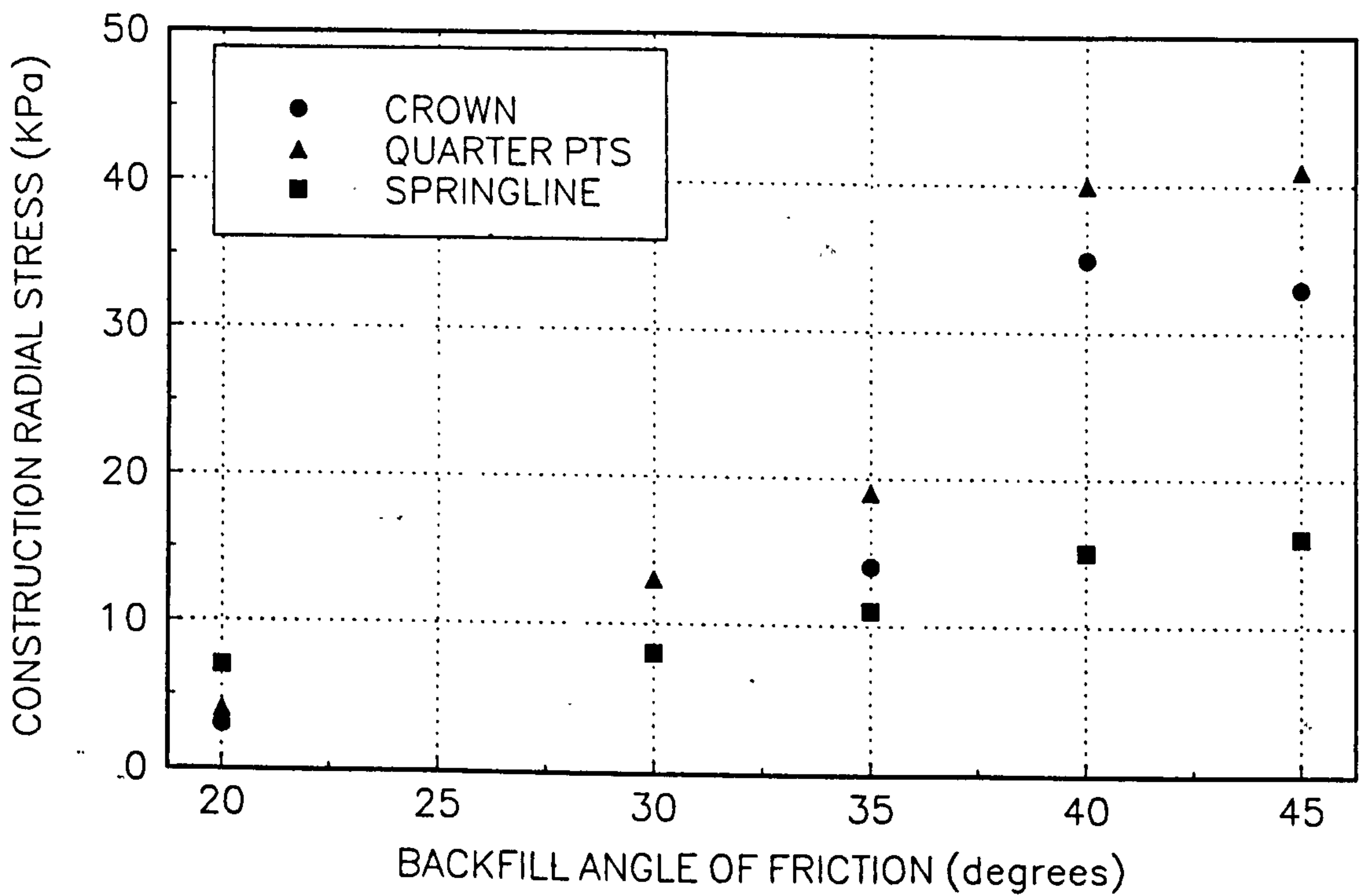


FIGURE 8.75(a)
VARIATION OF CROWN DISPLACEMENTS WITH COMPACTION PRESSURE

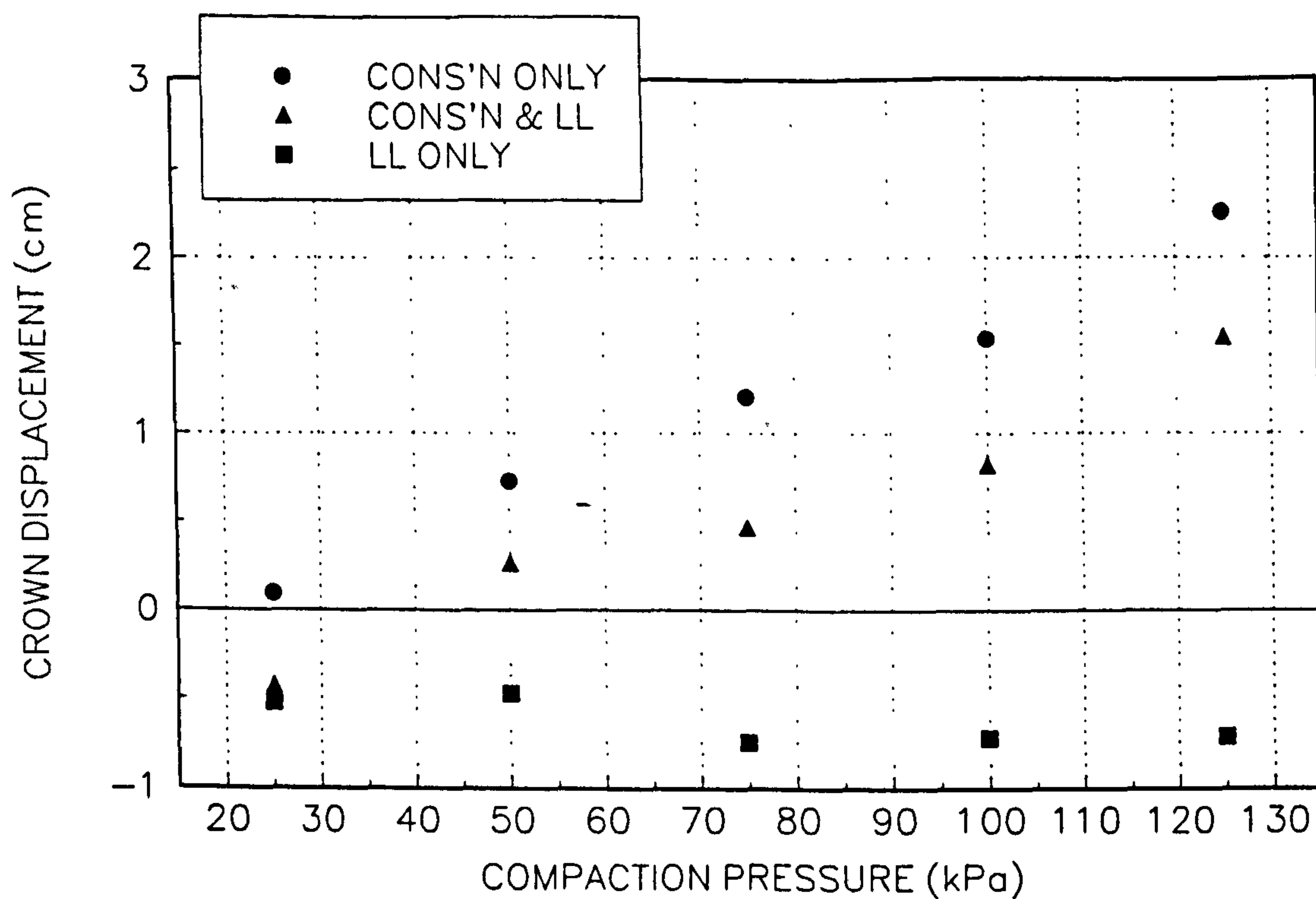


FIGURE 8.75(b)
VARIATION OF SPRINGLINE DISPLACEMENTS WITH COMPACTION PRESSURE

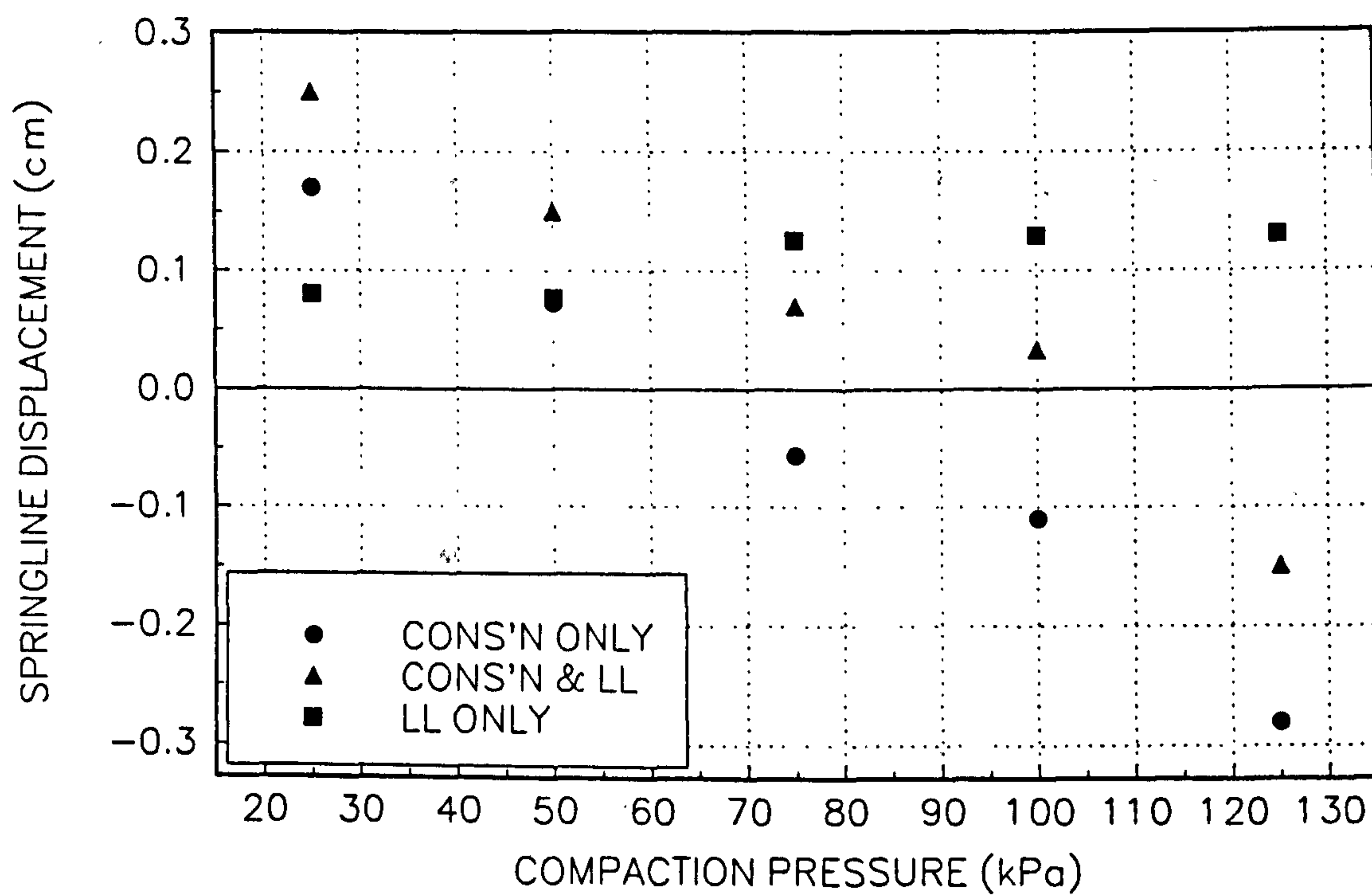


FIGURE 8.76(a)
VARIATION OF CONSTRUCTION BENDING MOMENT WITH COMPACTION PRESSURE

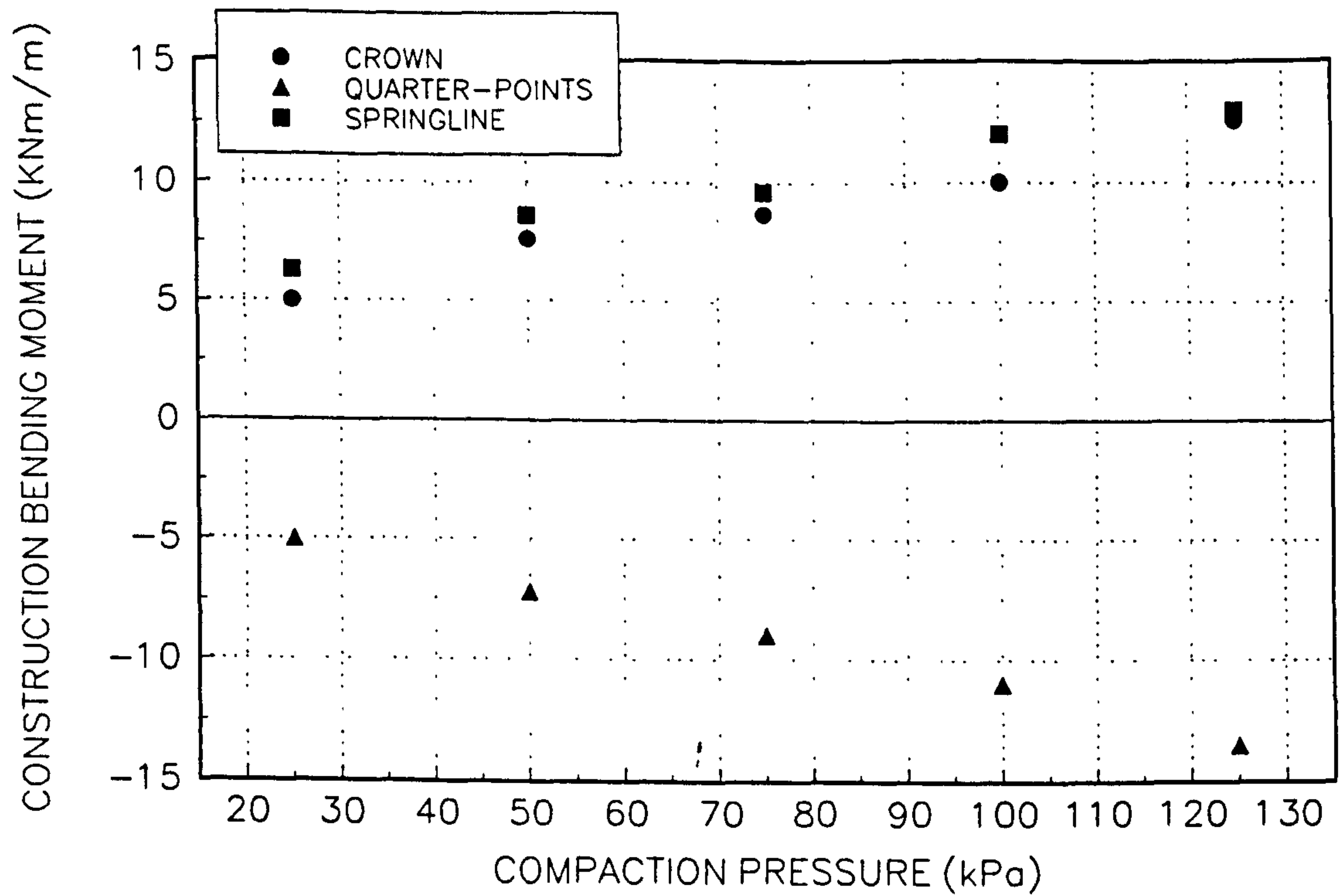


FIGURE 8.76(b)
VARIATION OF LIVE LOAD BENDING MOMENT WITH COMPACTION PRESSURE

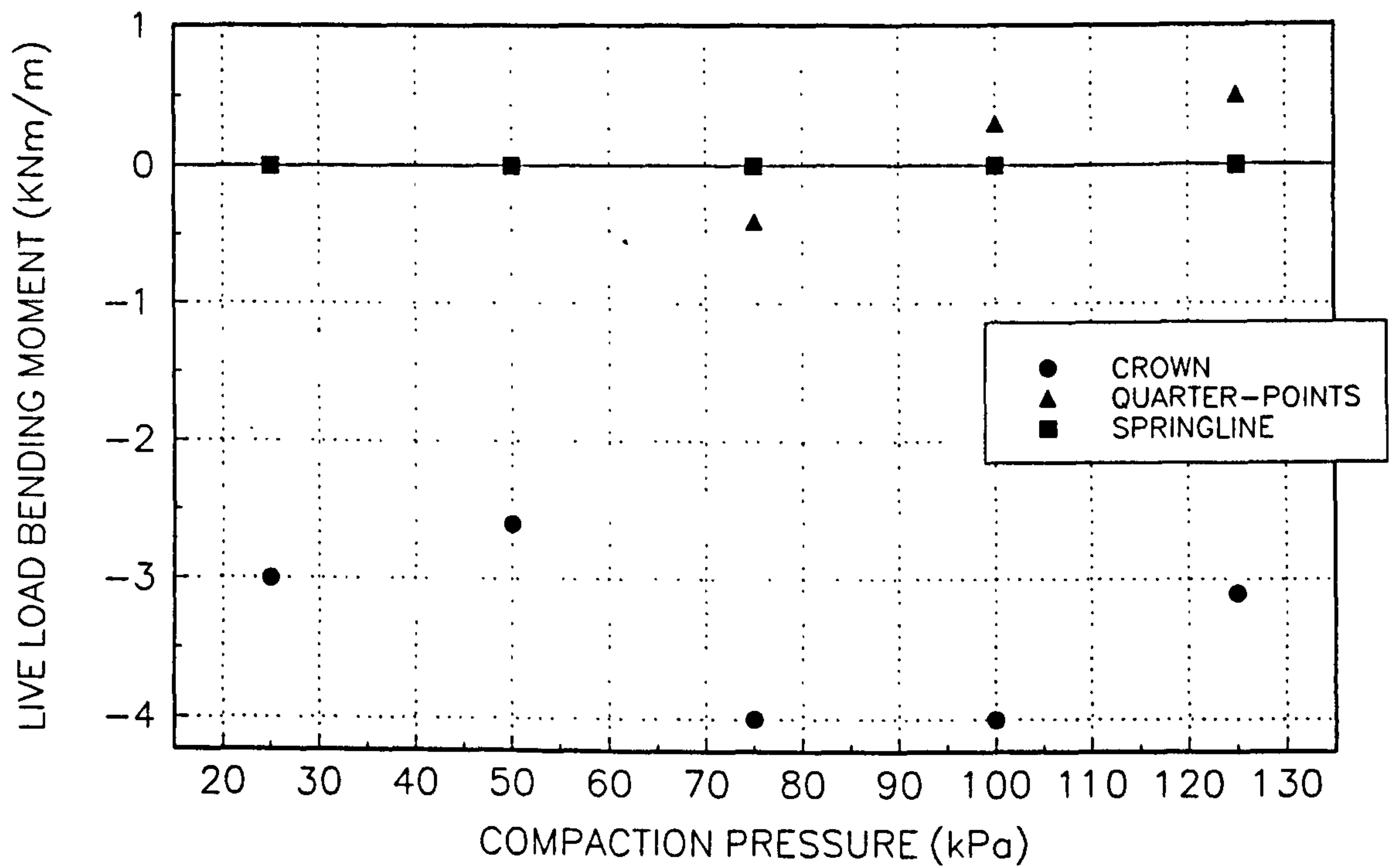


FIGURE 8.77(a)
VARIATION OF CONSTRUCTION SHEAR STRESS WITH COMPACTION PRESSURE

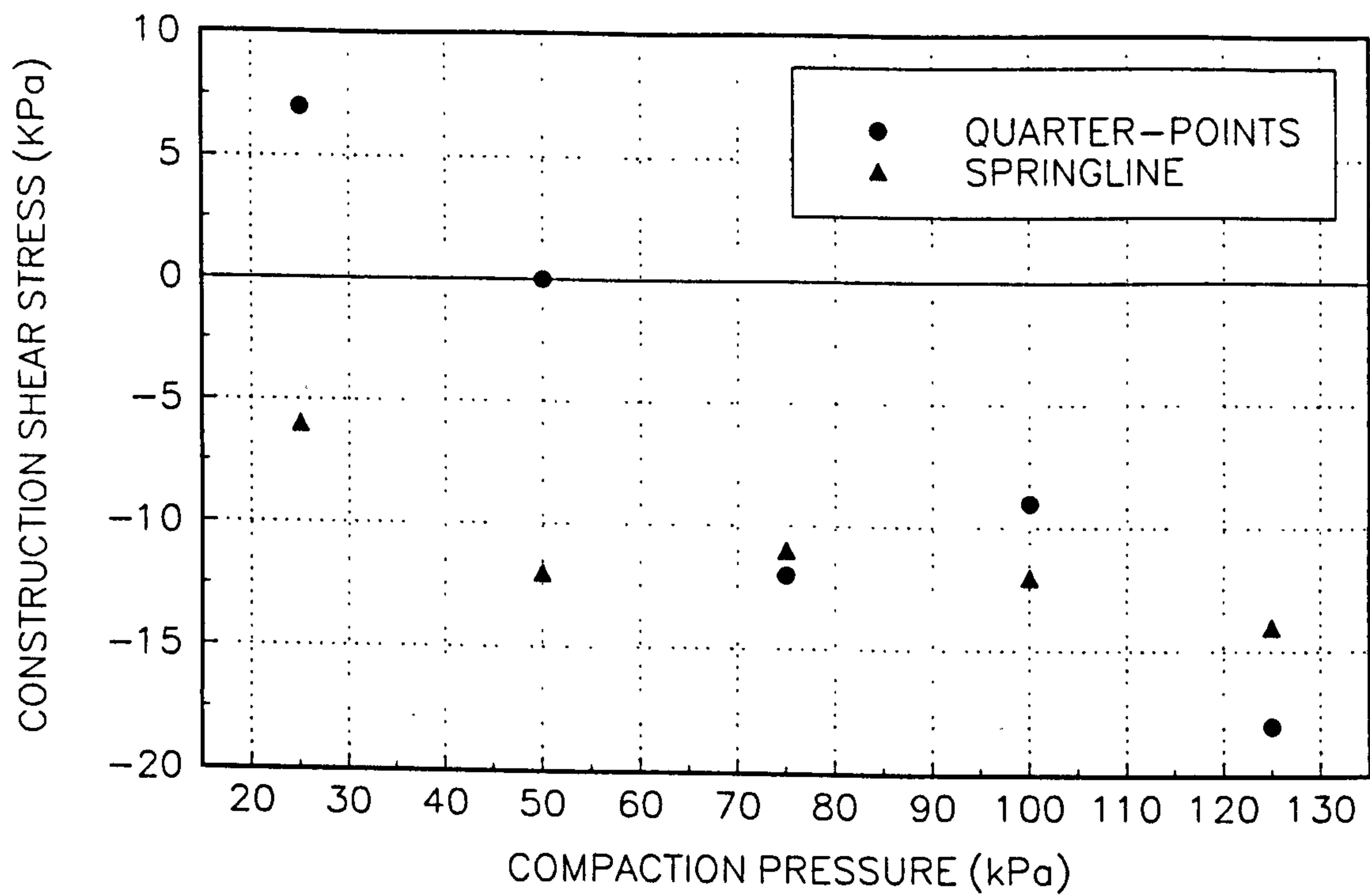


FIGURE 8.77(b)
VARIATION OF LIVE LOAD SHEAR STRESS WITH COMPACTION PRESSURE

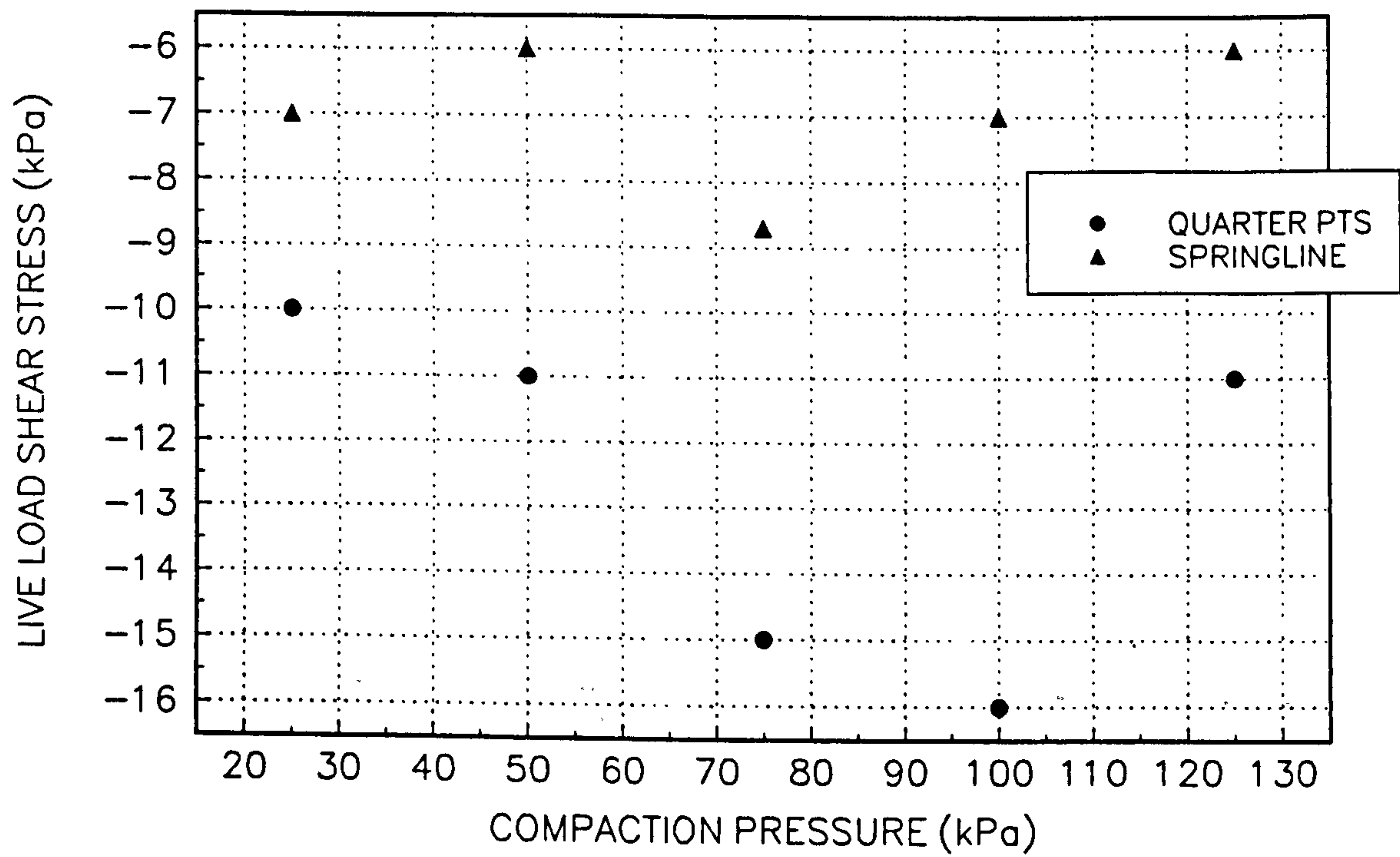


FIGURE 8.78
VARIATION OF DEGREE ARCHING WITH COMPACTION PRESSURE

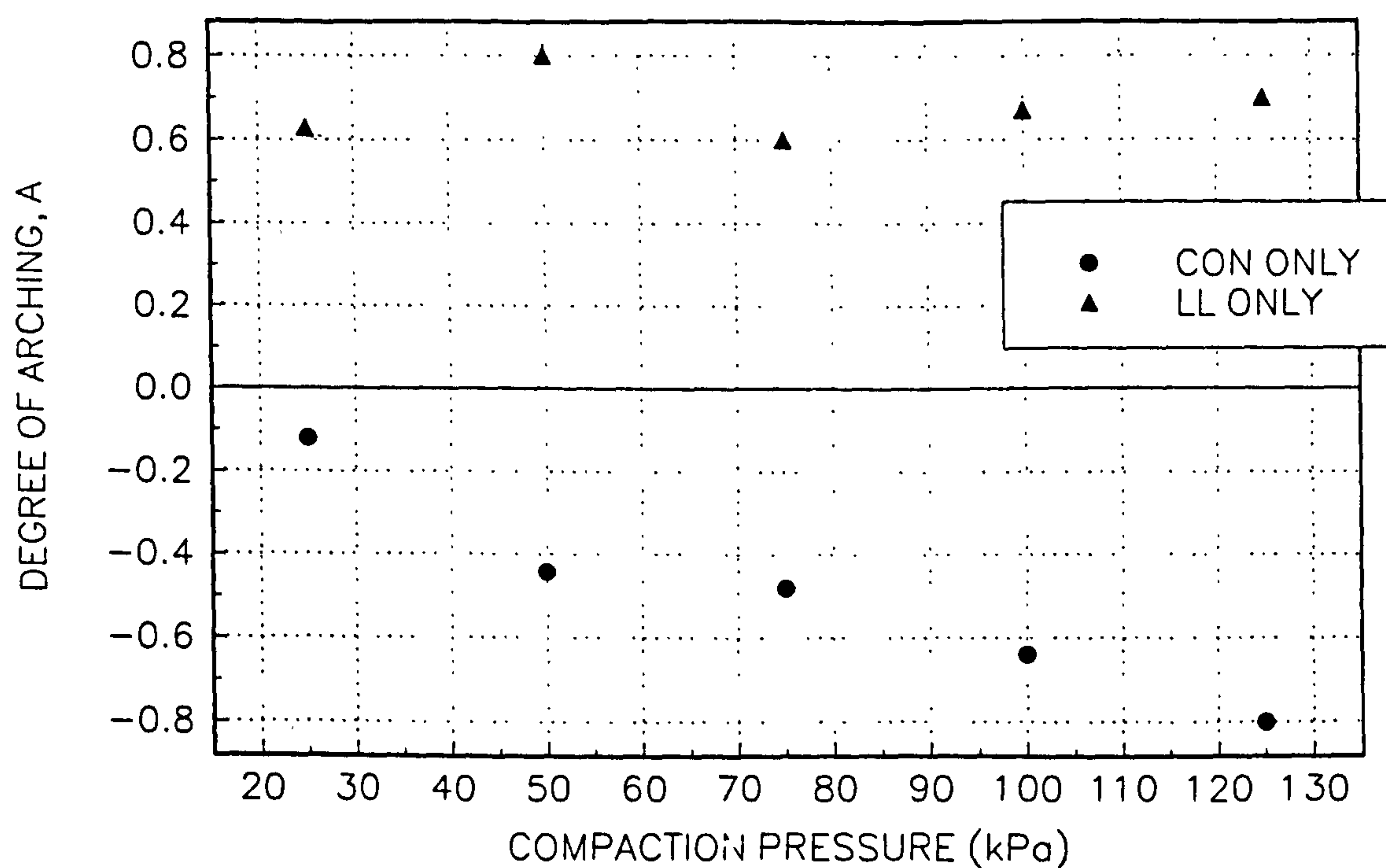


FIGURE 8.79(a)
VARIATION OF CONSTRUCTION RADIAL STRESS WITH COMPACTION PRESSURE

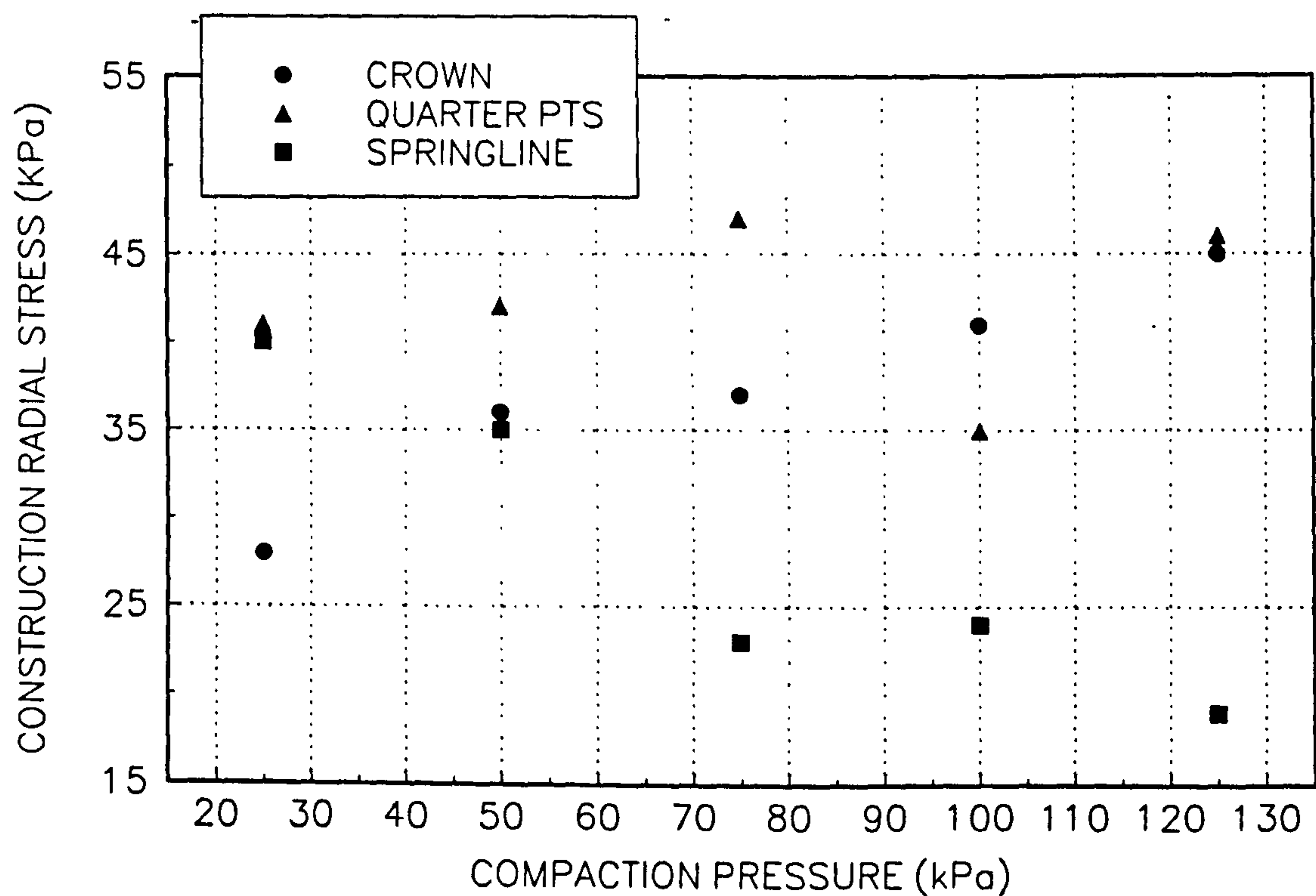


FIGURE 8.79(b)
VARIATION OF LIVE LOAD RADIAL STRESS WITH COMPACTION PRESSURE

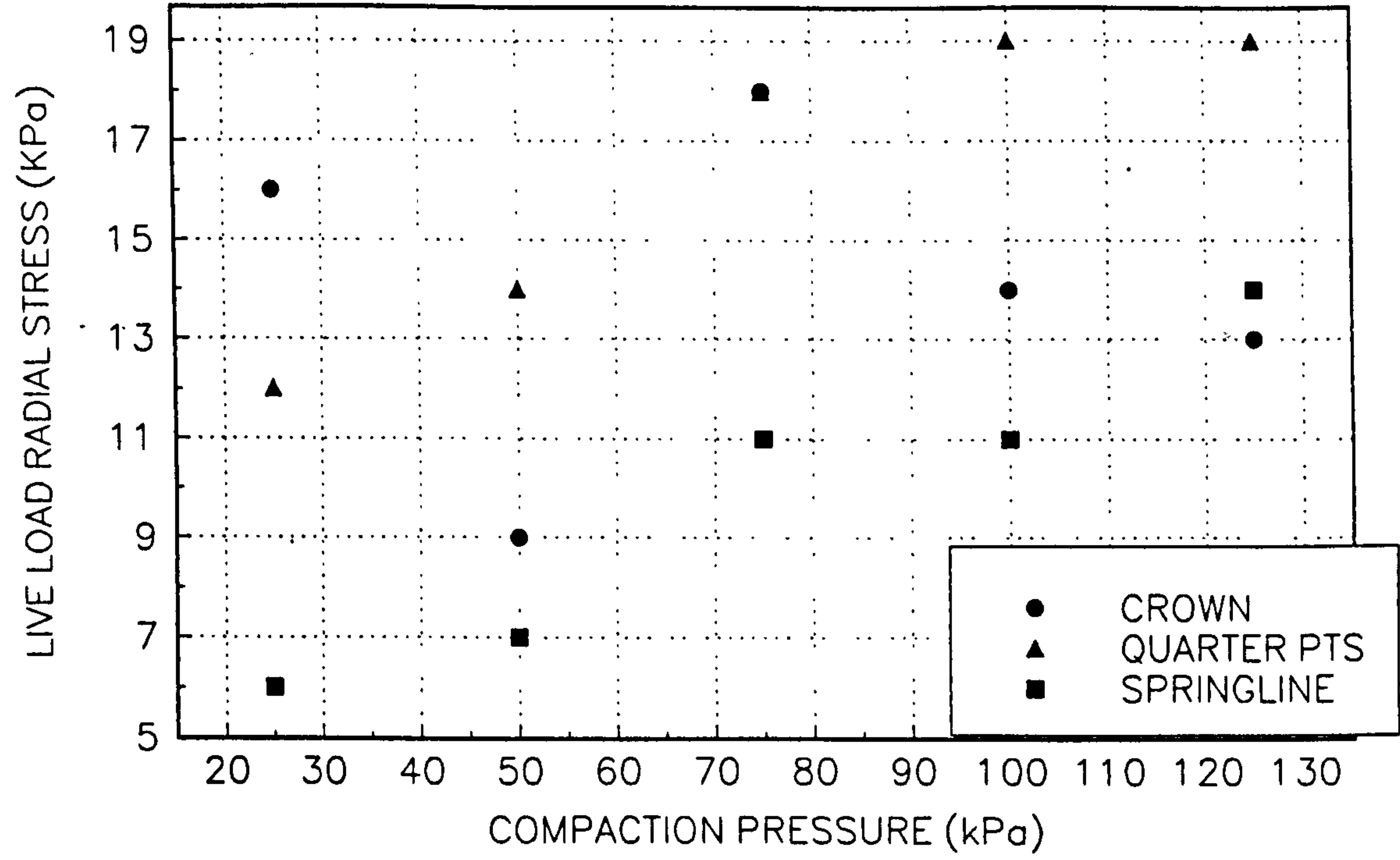


FIGURE 8.80(a)
VARIATION OF CONSTRUCTION THRUST WITH COMPACTION PRESSURE

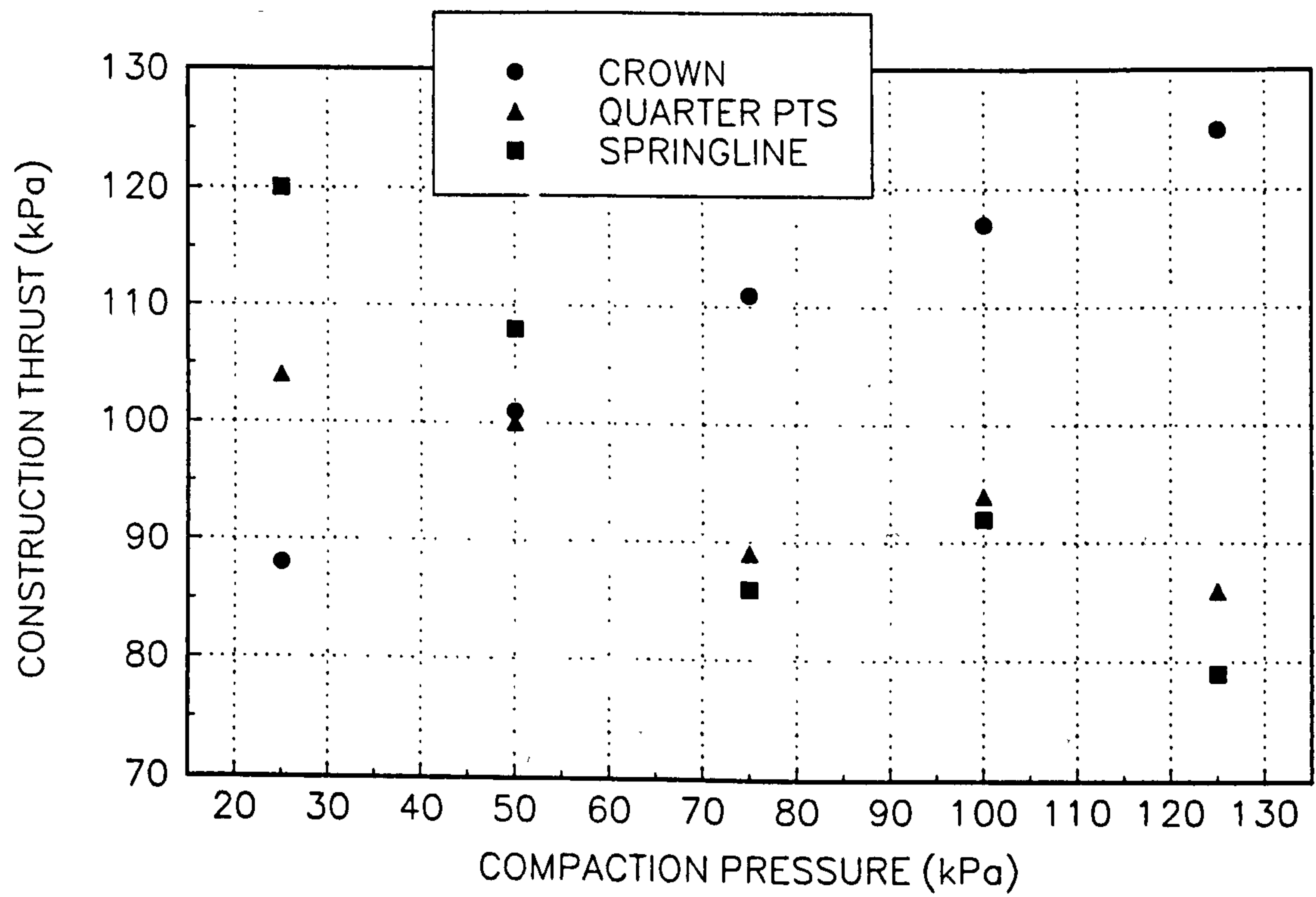


FIGURE 8.80(b)
 VARIATION OF LIVE LOAD THRUST WITH COMPACTION PRESSURE

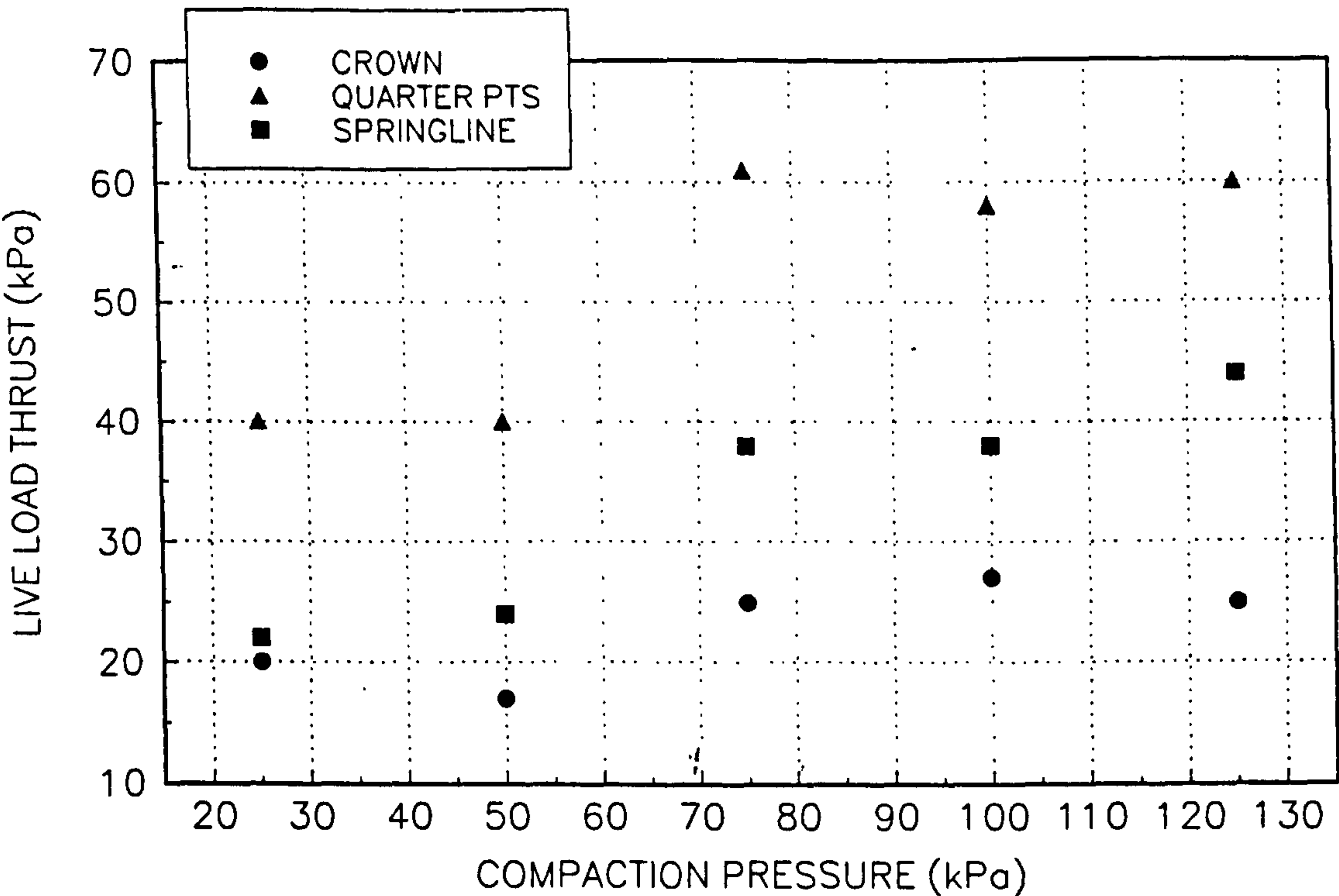


FIG 8.81 NO PLINTHS; THRUST BEHAVIOUR

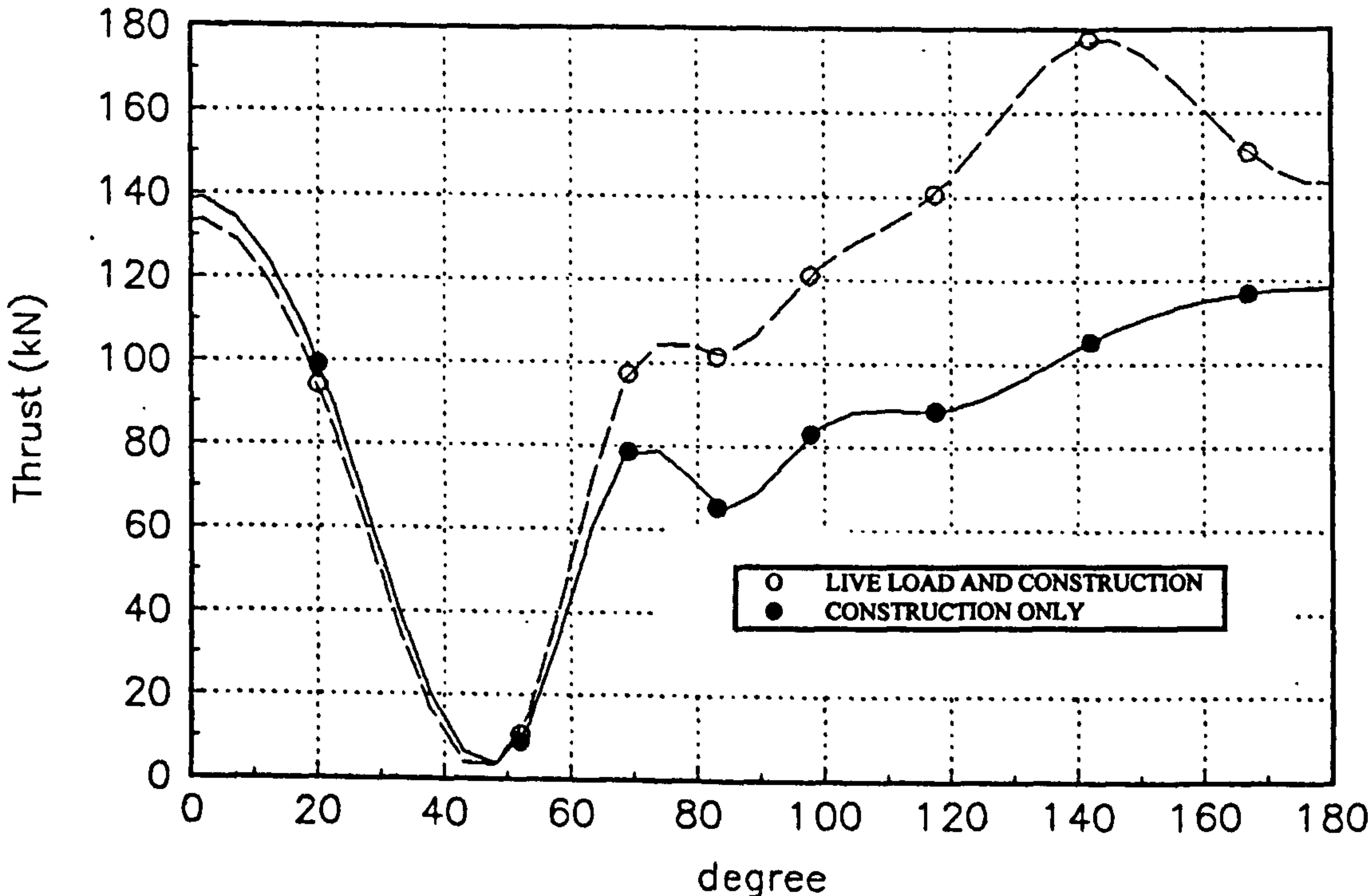


FIG 8.82 NO PLINTHS; BENDING MOMENT BEHAVIOUR

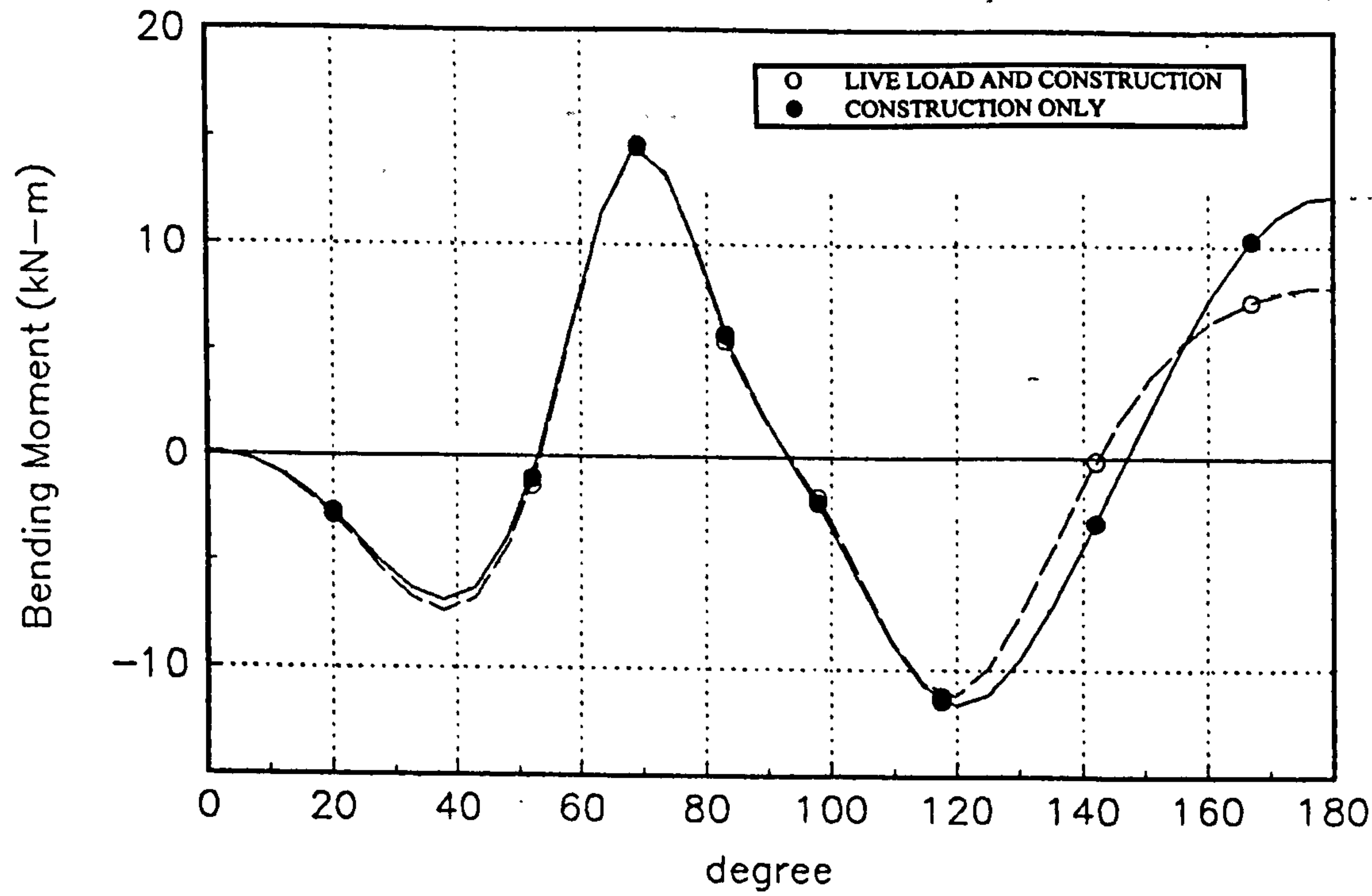


FIG 8.83 NO PLINTHS; RADIAL STRESS BEHAVIOUR

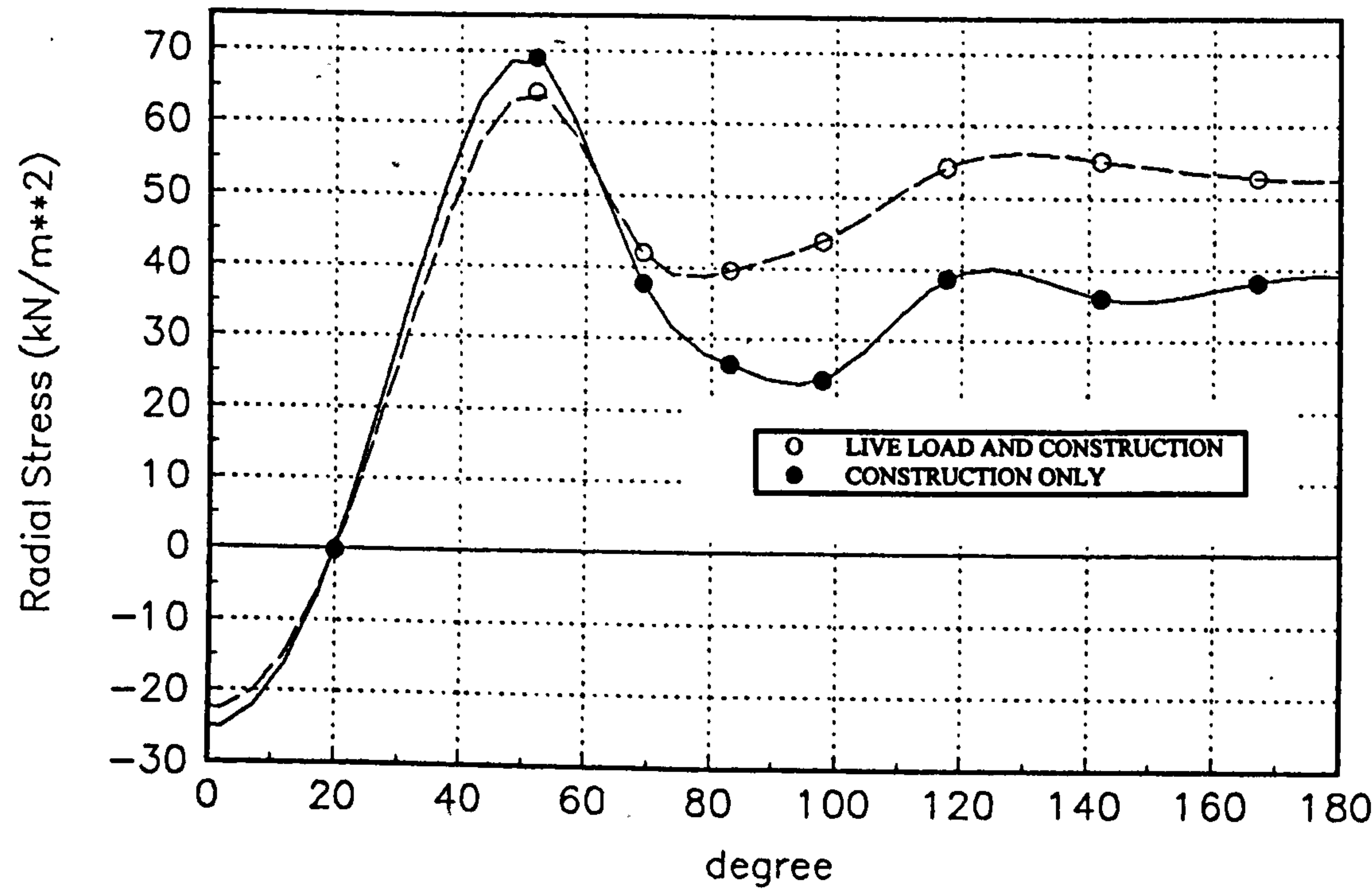


FIG 8.84 NO PLINTHS; SHEAR STRESS BEHAVIOUR

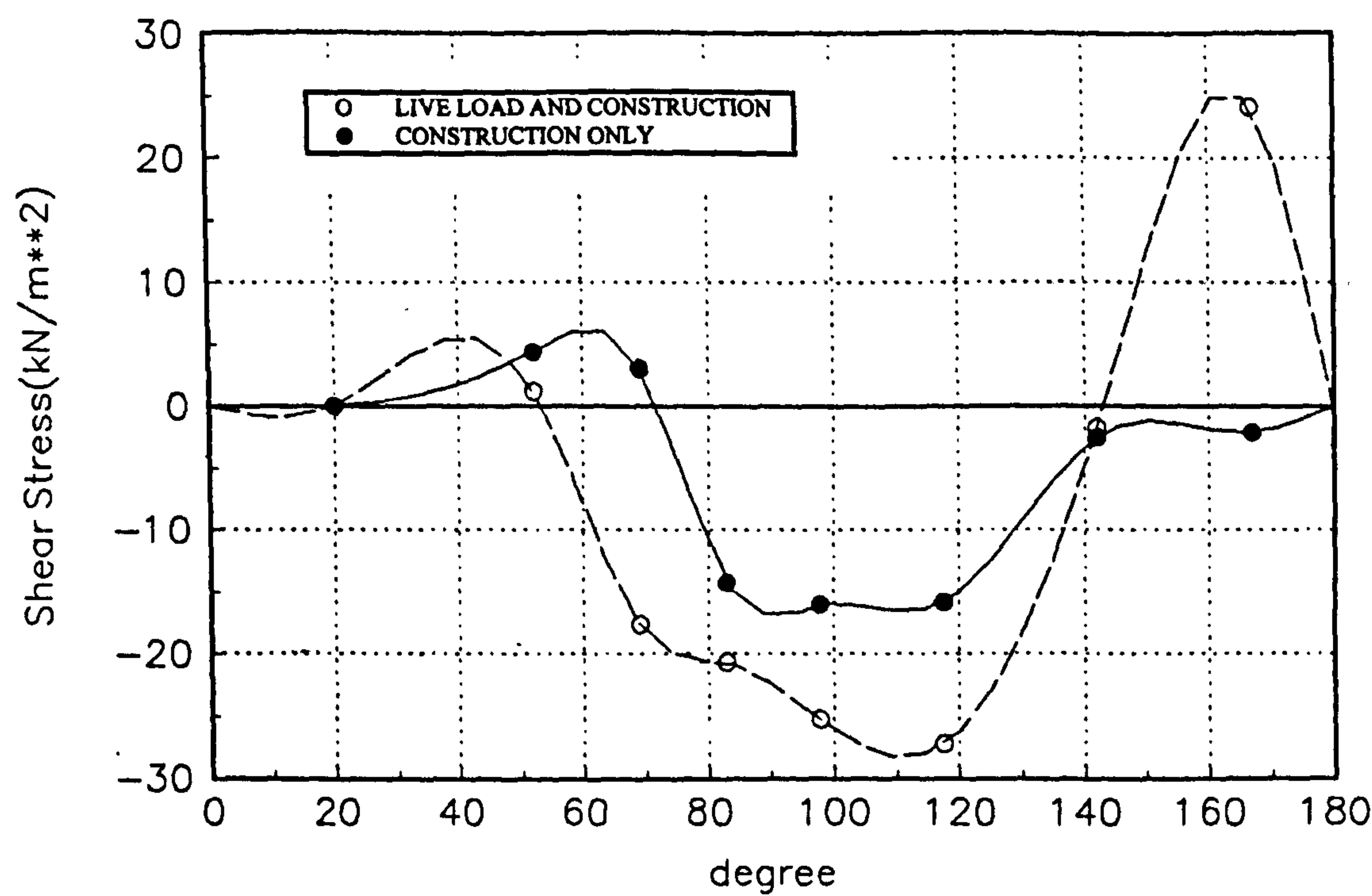


FIG 8.85 NO PLINTHS; CROWN DISPLACEMENT

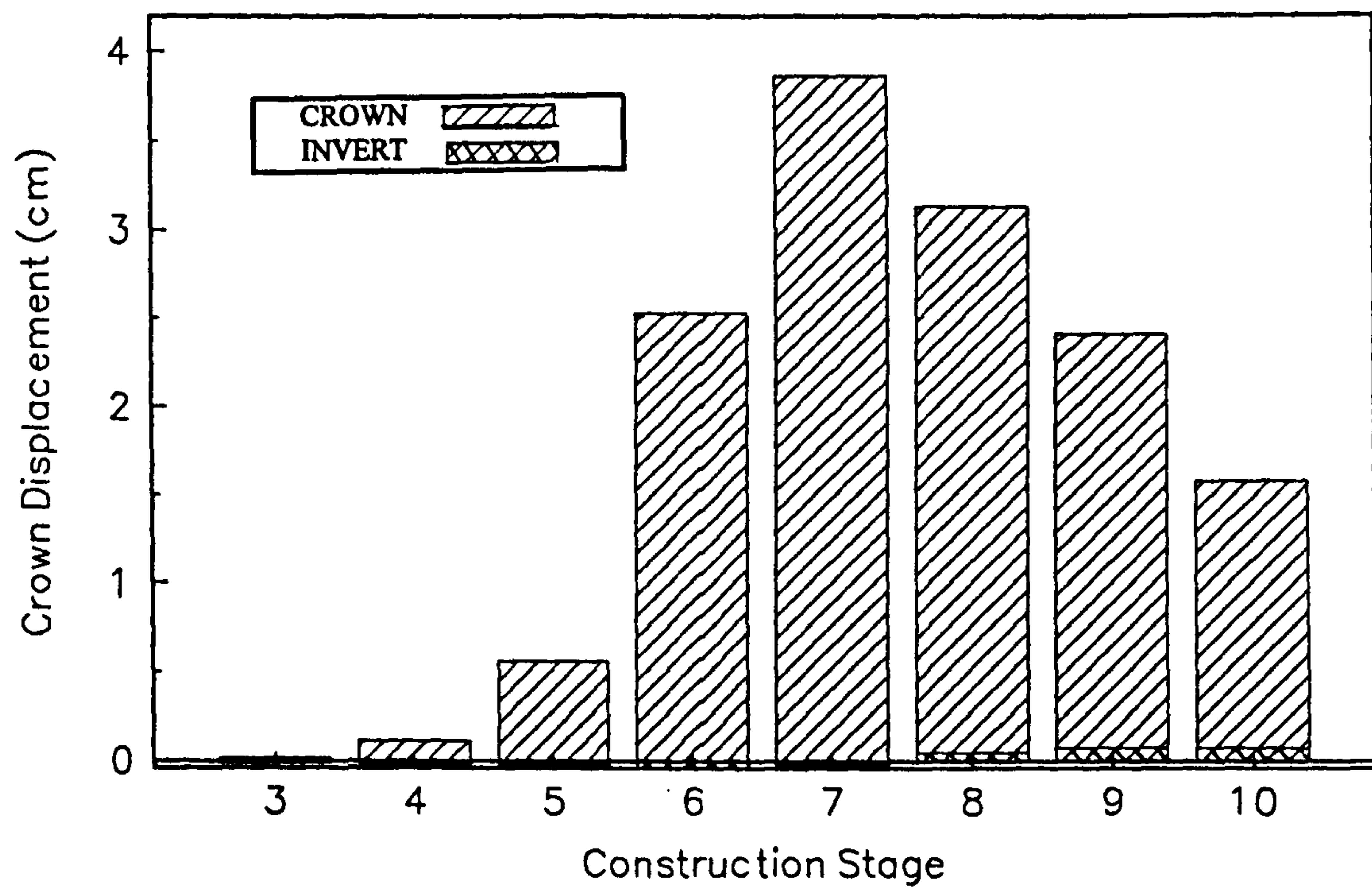
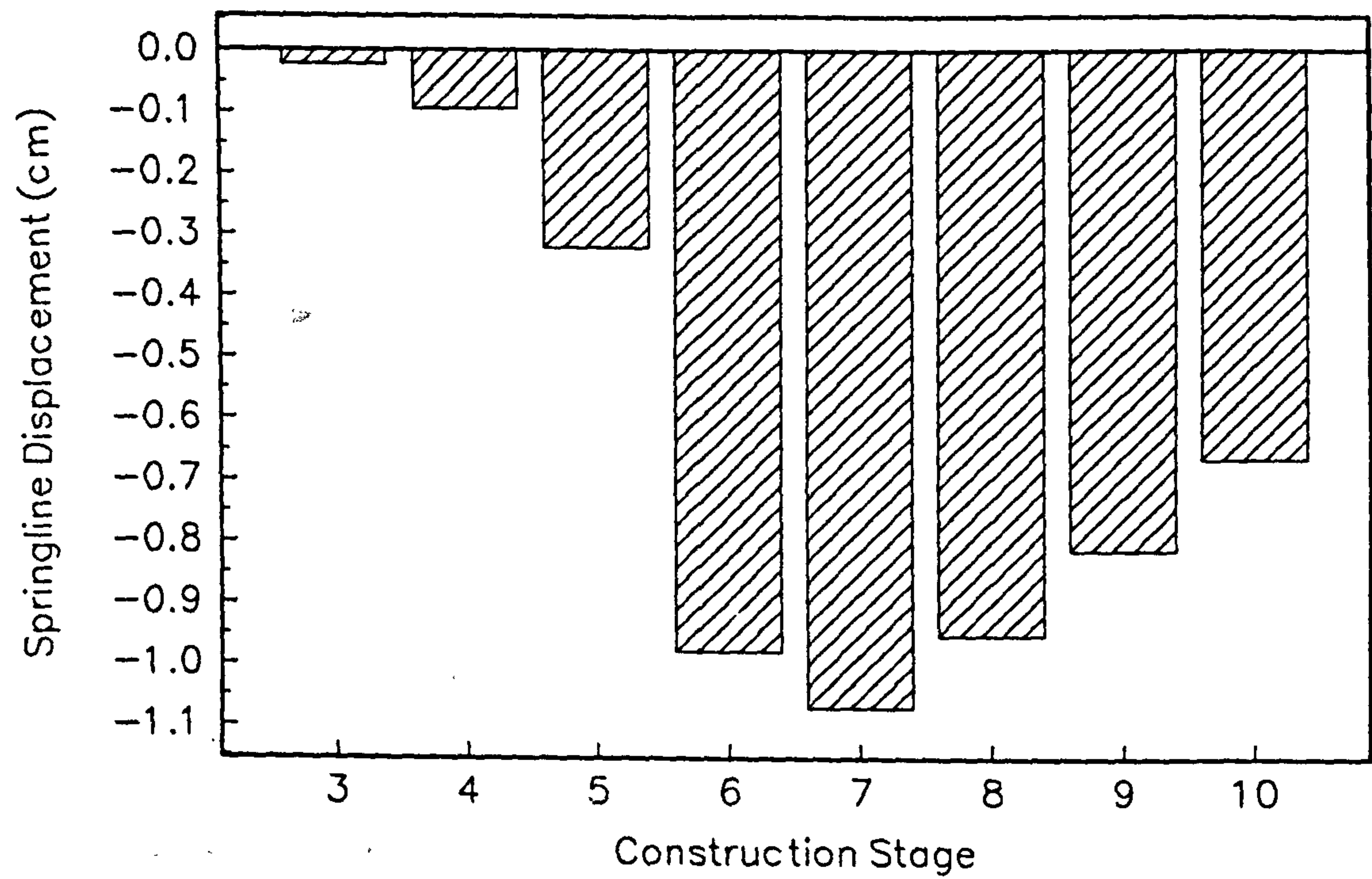


FIG 8.86 NO PLINTHS; SPRINGLINE DISPLACEMENT



**TEXT BOUND
INTO
THE SPINE**

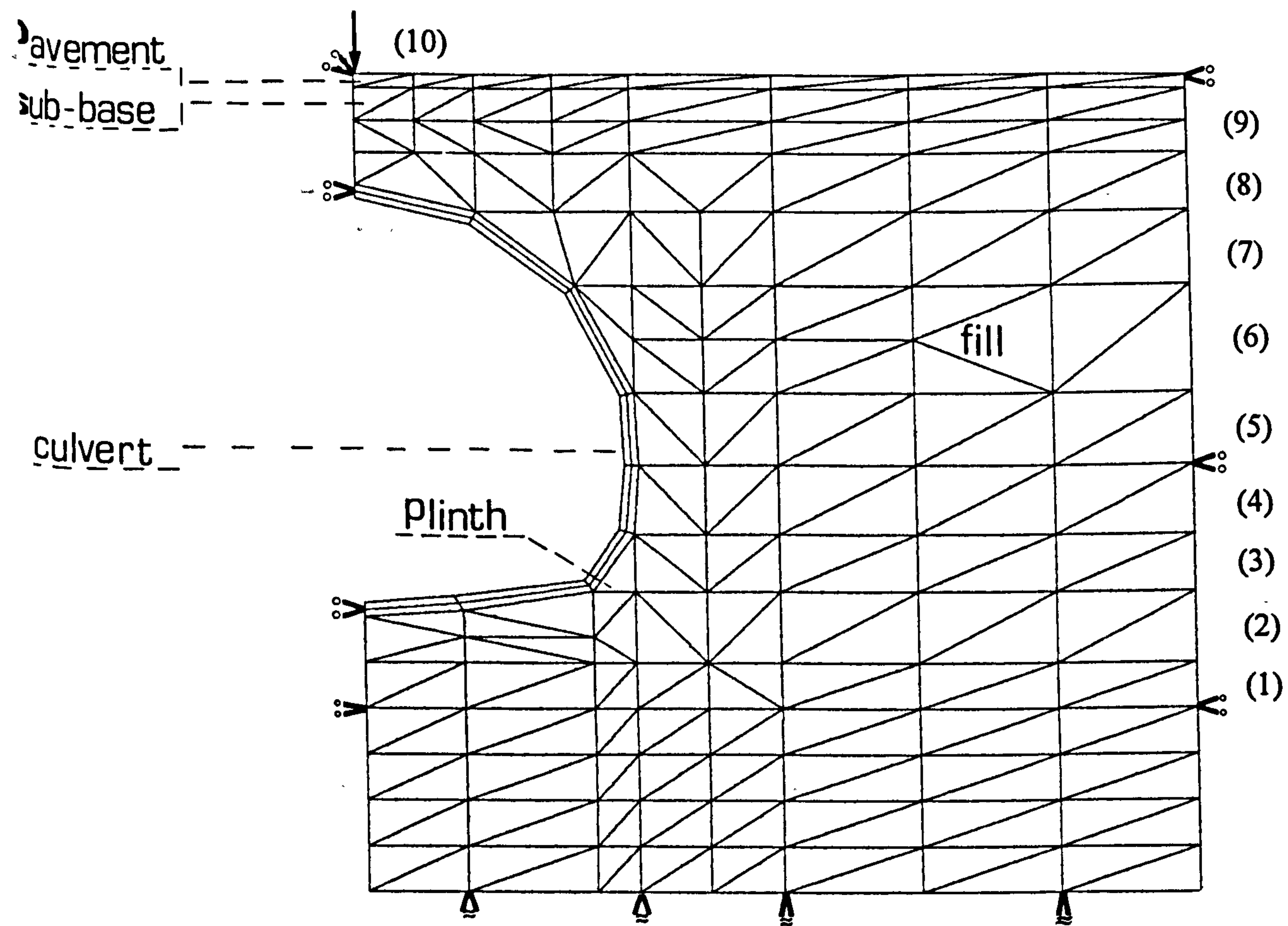


FIG 8.87 FINITE ELEMENT MESH FOR LOADING CASE C
CONSTRUCTION STAGE ()

CONSTRUCTION STAGE	DESCRIPTION
1	COMPACT EXISTING FOUNDATION SOIL
2	PLACE AND COMPACT BASAL LAYER
3	PLACE BACKFILL AND PLINTH , COMPACT BACKFILL
4	PLACE AND COMPACT BACKFILL UP TO SPRINGLINE
5	PLACE AND COMPACT BACKFILL TO BELOW QUARTER POINTS
6	PLACE AND COMPACT BACKFILL UP TO QUARTER POINTS
7	PLACE LEVEL WITH CROWN AND COMPACT
8	PLACE BACKFILL ABOVE CROWN AND COMPACT
9	PLACE TO FINAL FILL HEIGHT AND COMPACT
10	APPLY LIVE LOAD

FIG 8.88 THRUST BEHAVIOUR

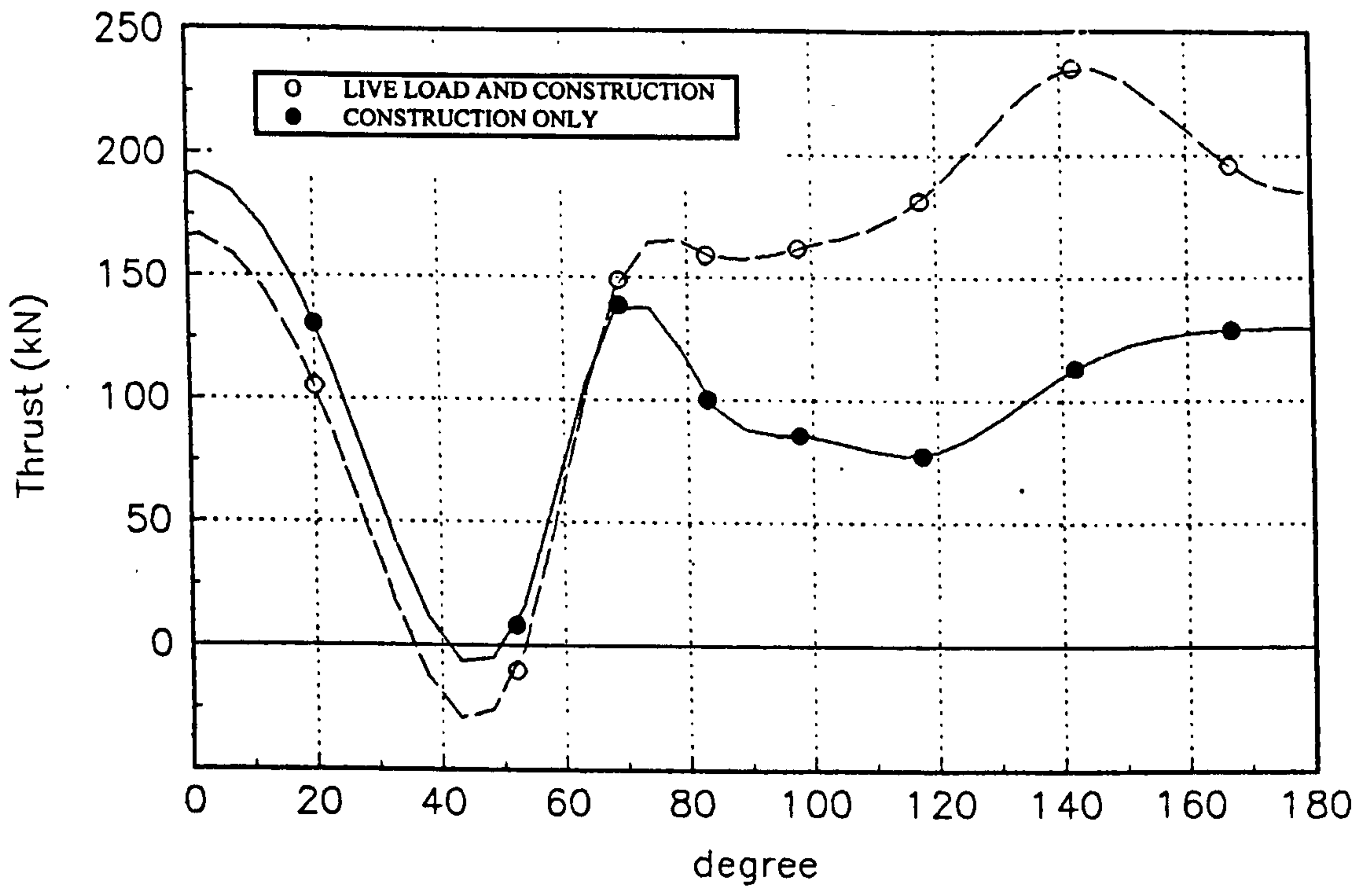


FIG 8.89 BENDING MOMENT BEHAVIOUR

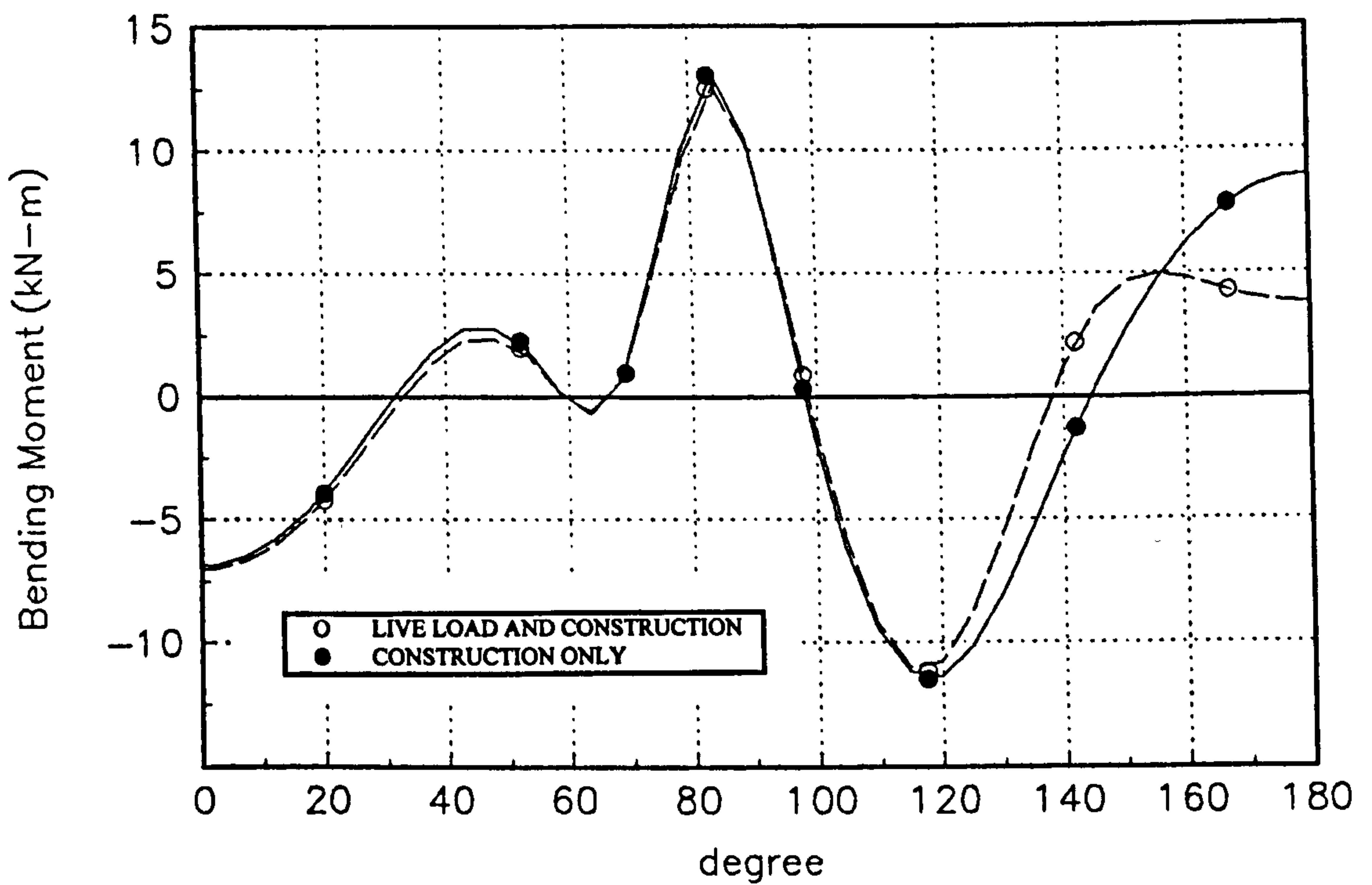


FIG 8.90 RADIAL STRESS BEHAVIOUR

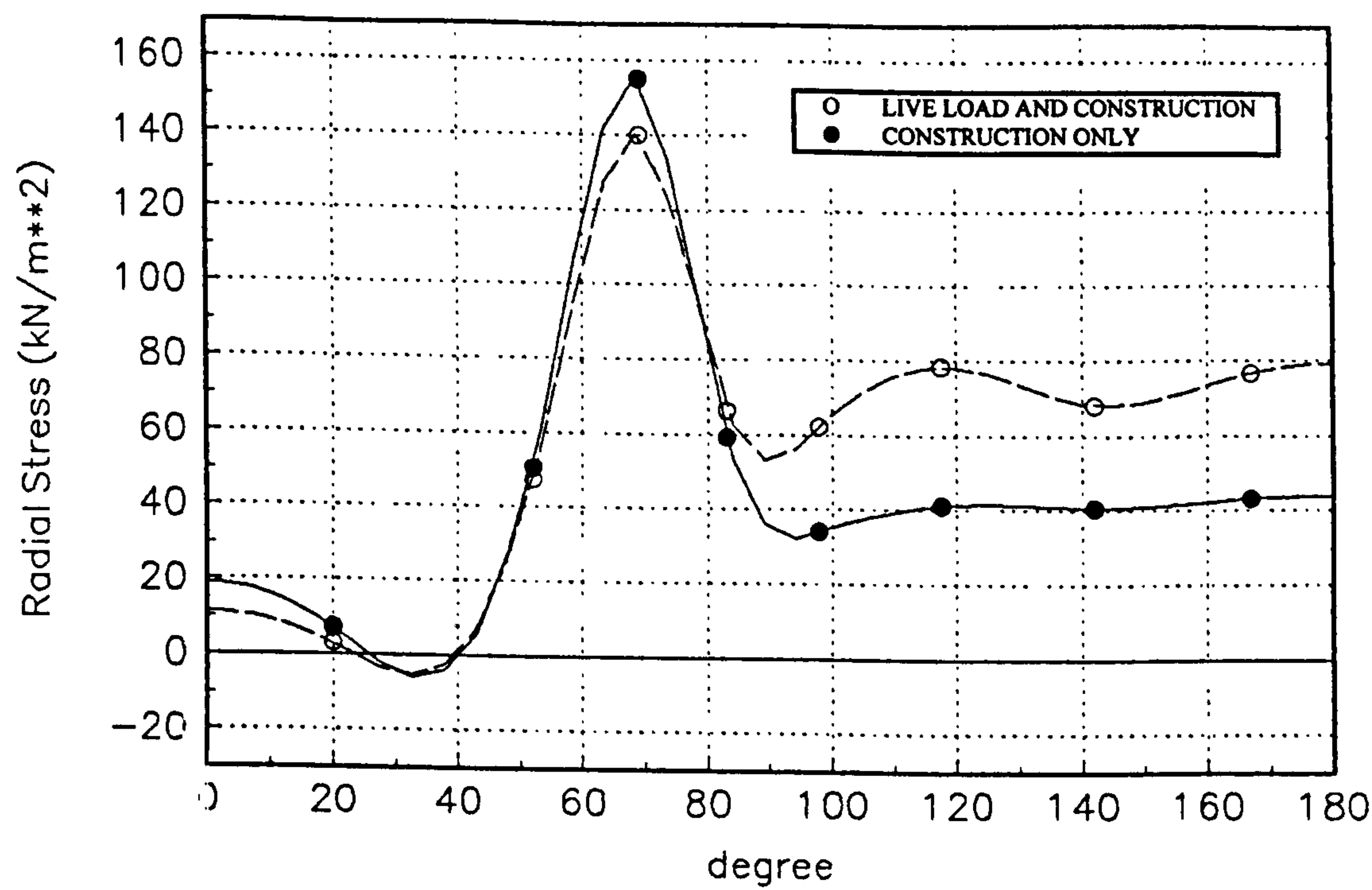


FIG 8.91 SHEAR STRESS BEHAVIOUR

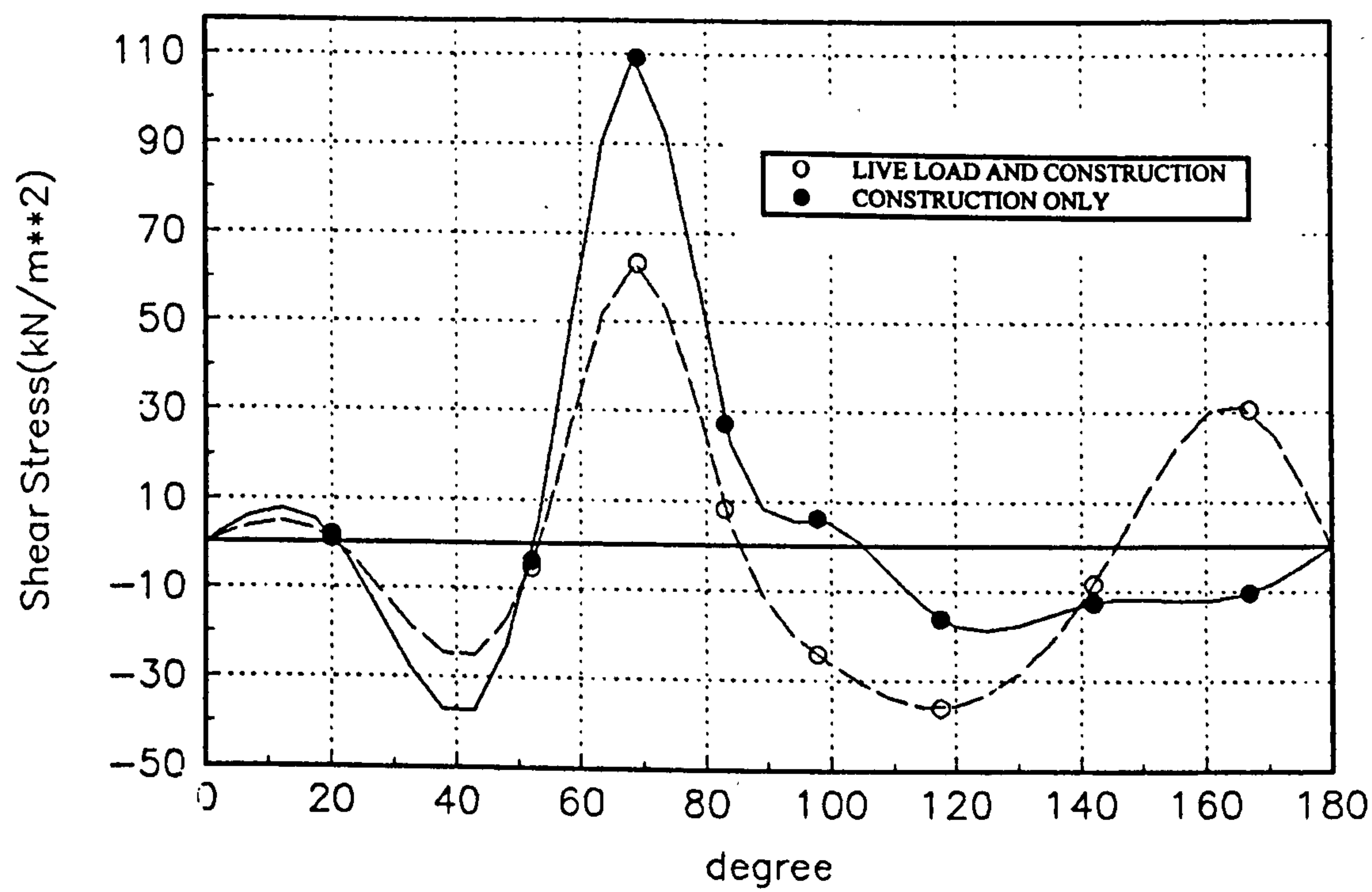


FIG 8.92 CROWN DISPLACEMENT

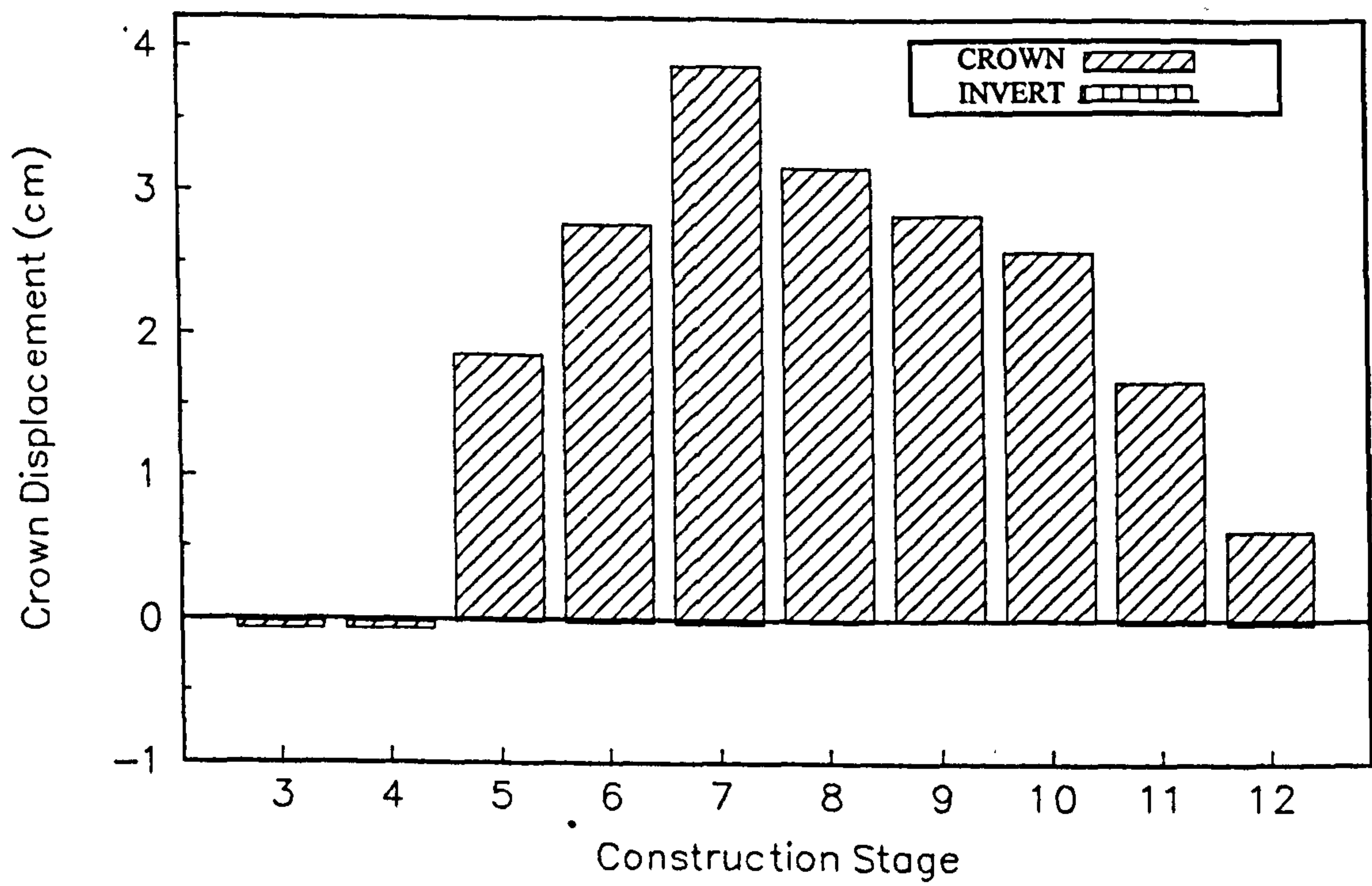


FIG 8.93 SPRINGLINE DISPLACEMENT

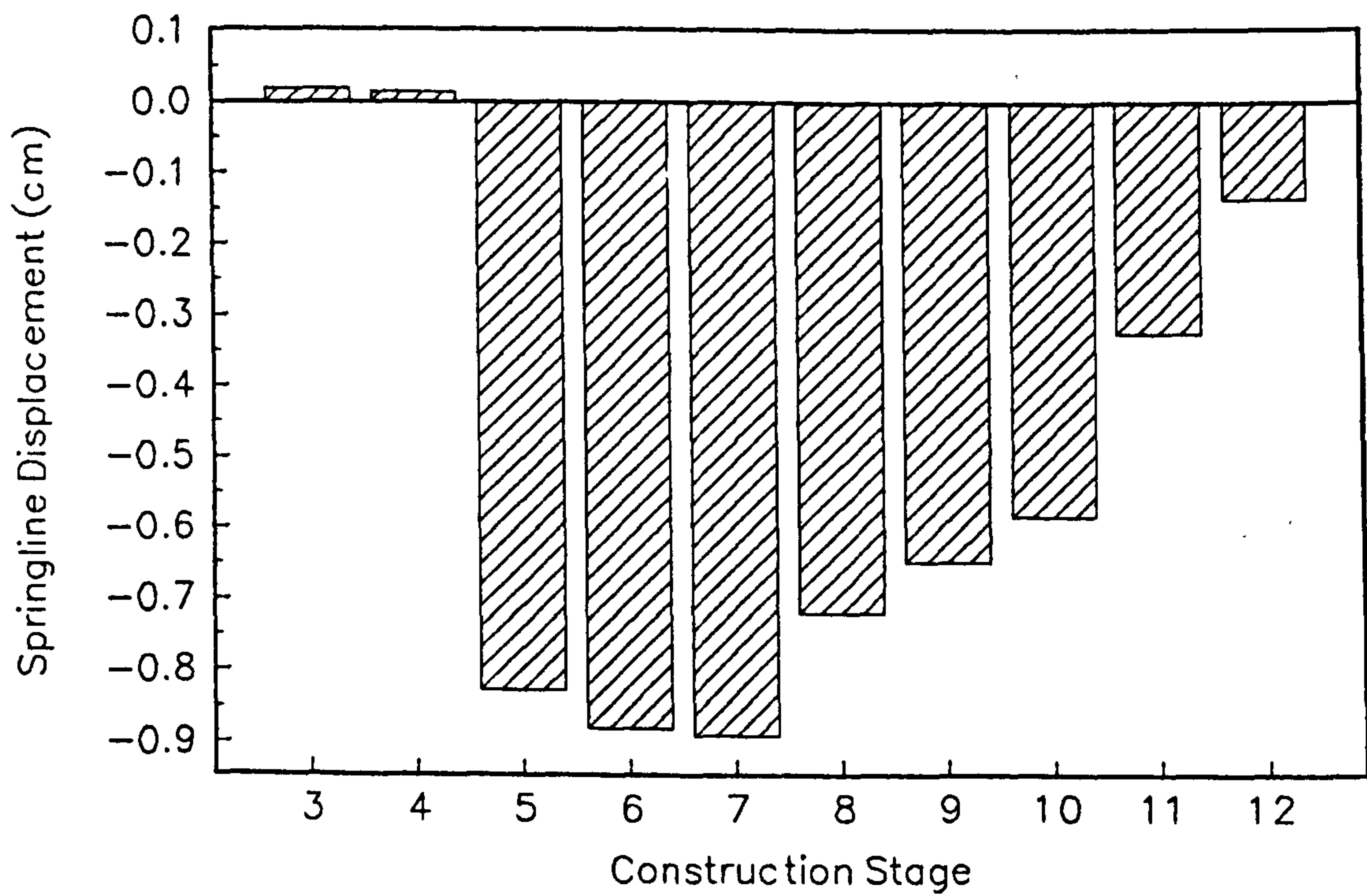


FIGURE 8.94
COMPARISON OF LOAD CASES B AND C; THRUST BEHAVIOUR

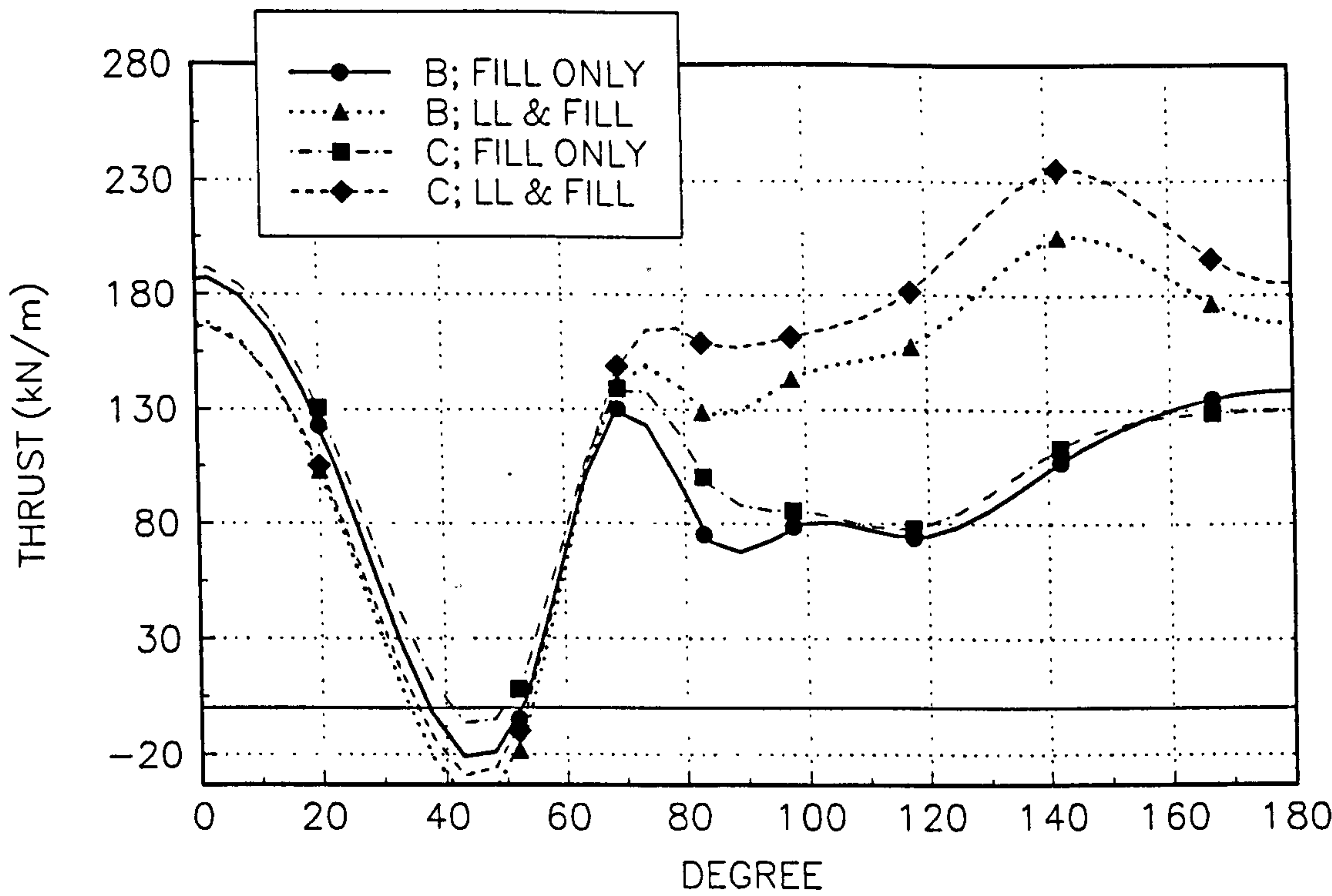


FIGURE 8.95
COMPARISON OF LOAD CASES B AND C; RADIAL STRESS BEHAVIOUR

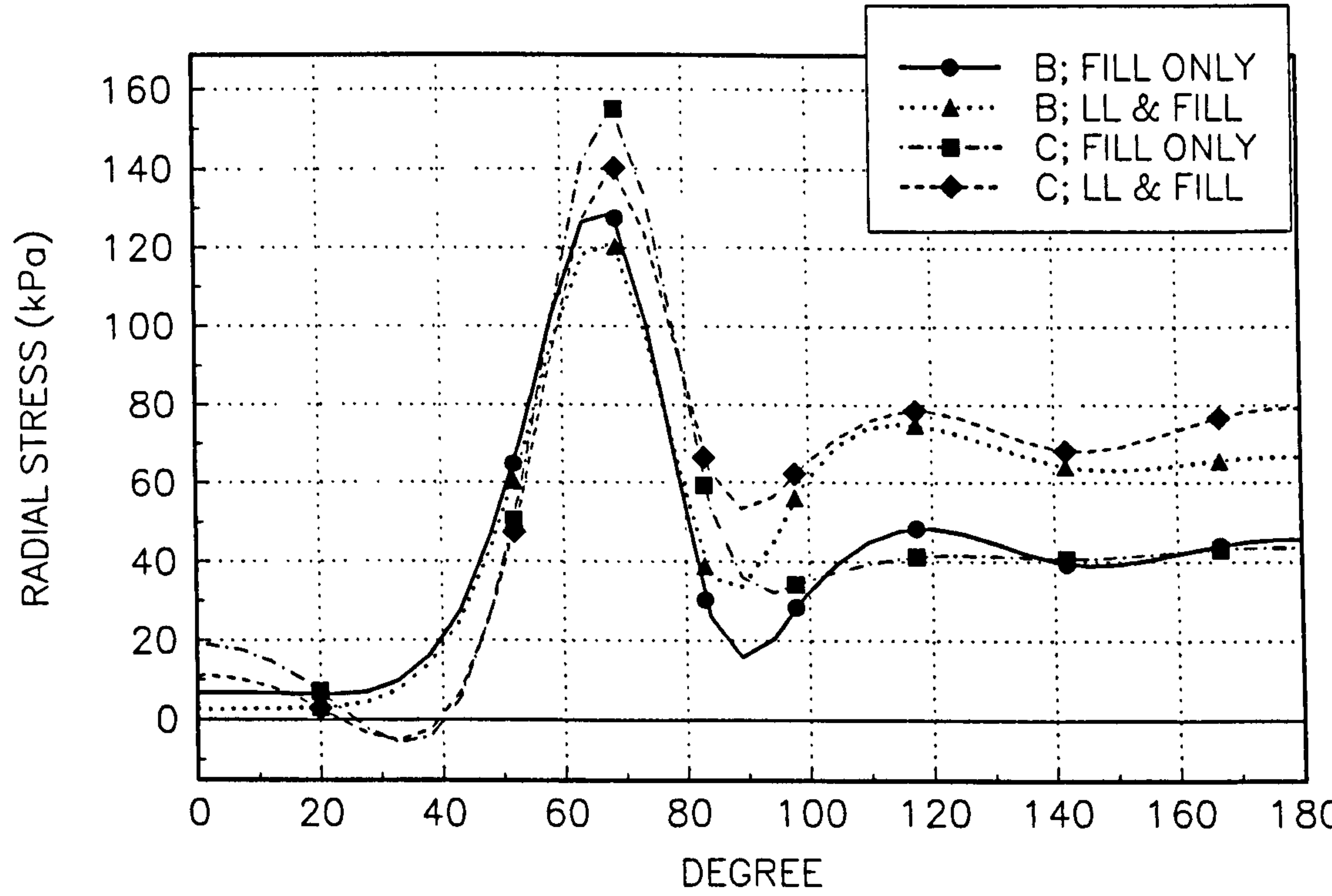


FIGURE 8.96
COMPARISON OF LOAD CASES B AND C; BENDING MOMENT BEHAVIOUR

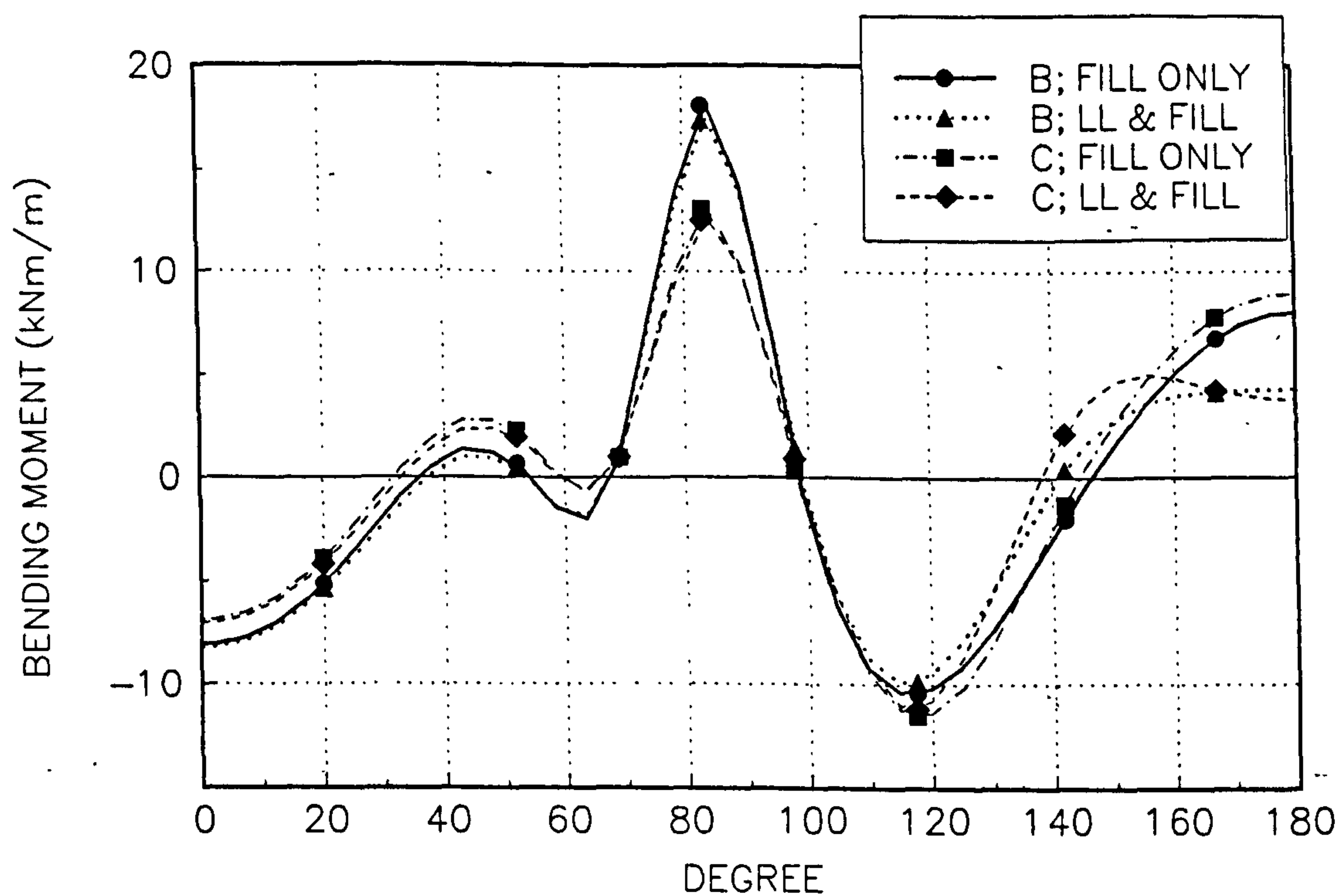
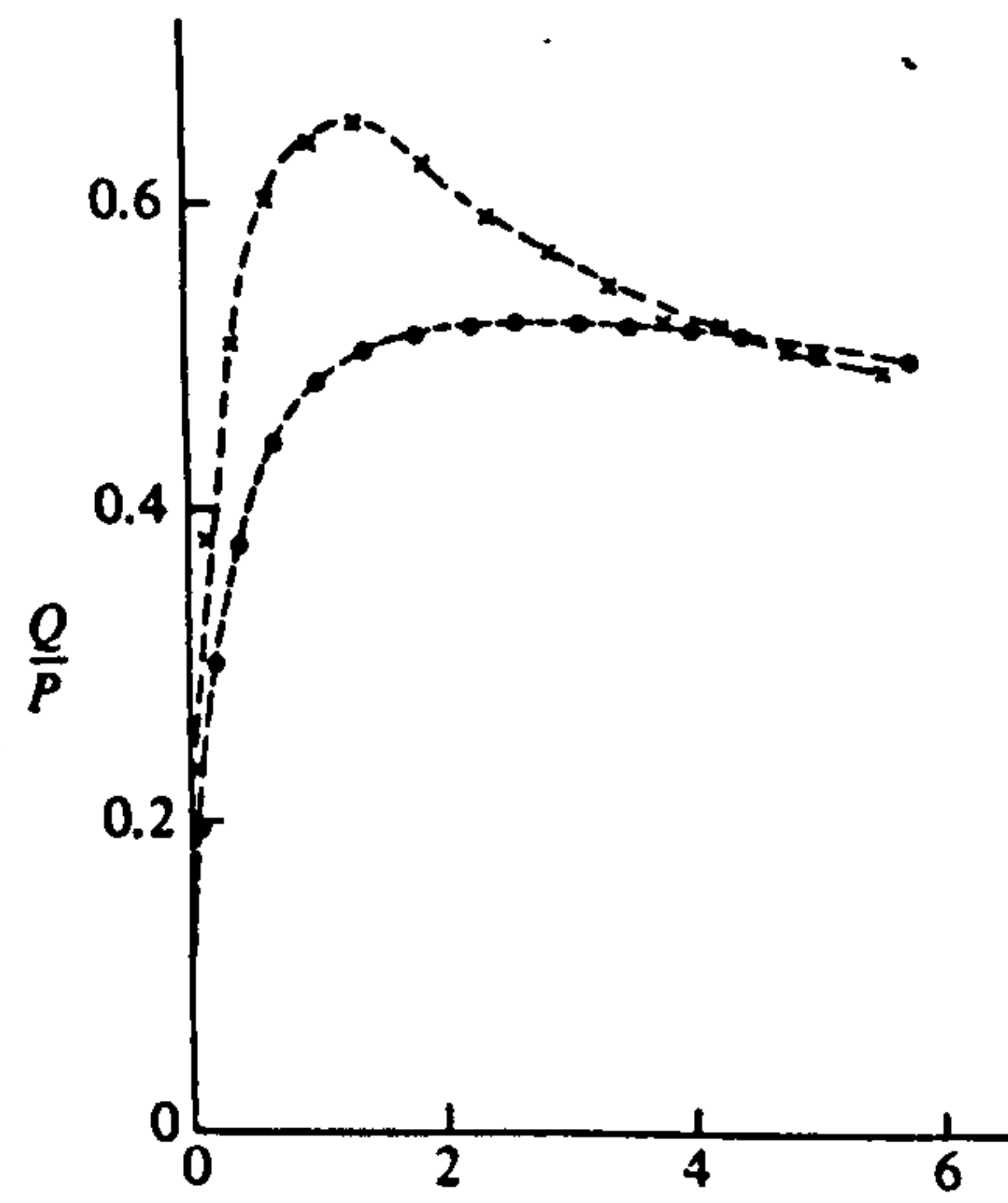
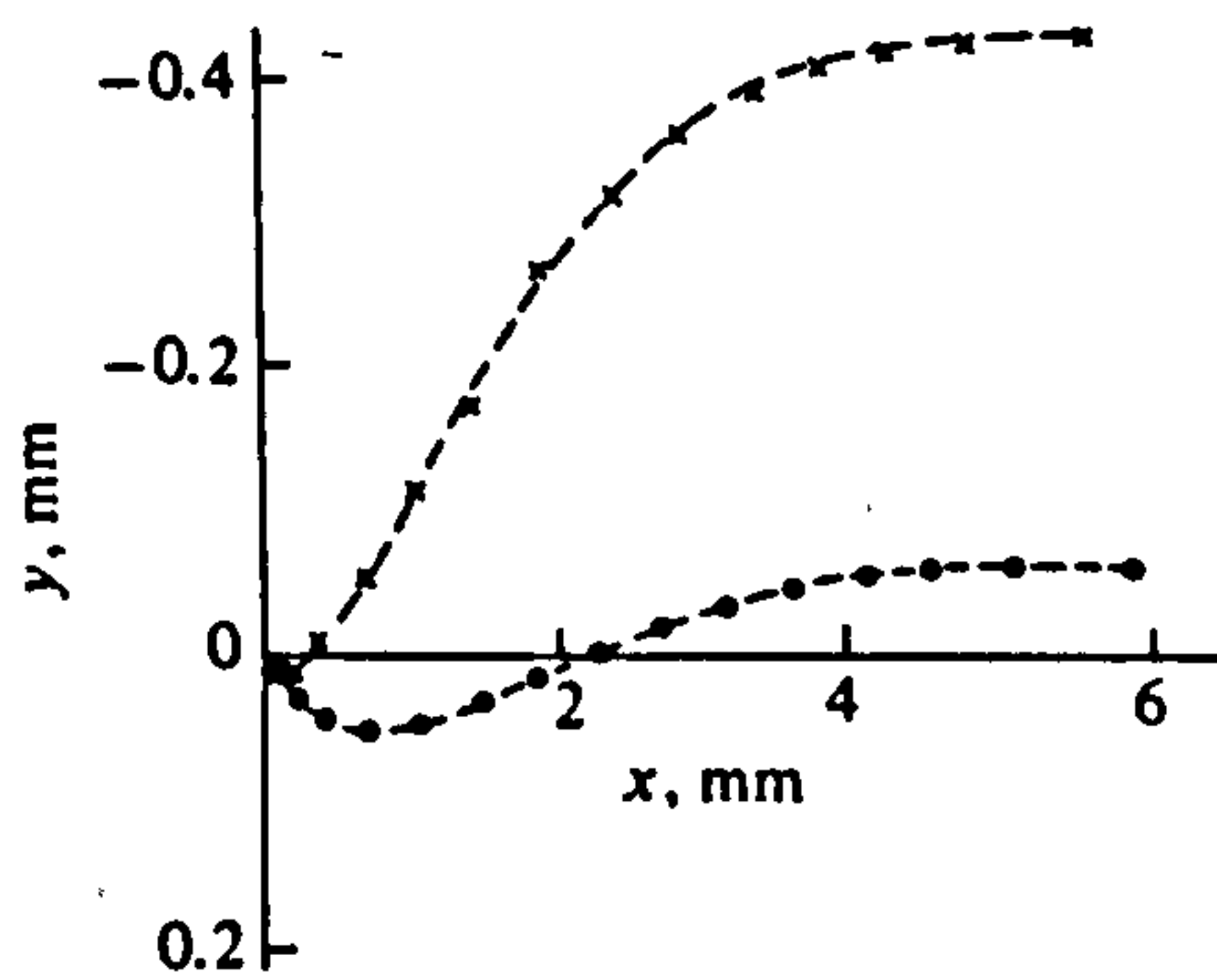


Fig 8.97 DIRECT SHEAR TESTS ON OTTAWA SAND (x DENSE, o LOOSE): (a) MOBILISED FRICTION Q/P ON HORIZONTAL PLANE AND SHEAR DISPLACEMENT x ; (b) VERTICAL DISPLACEMENT y AND SHEAR DISPLACEMENT x (TAYLOR, 1948).

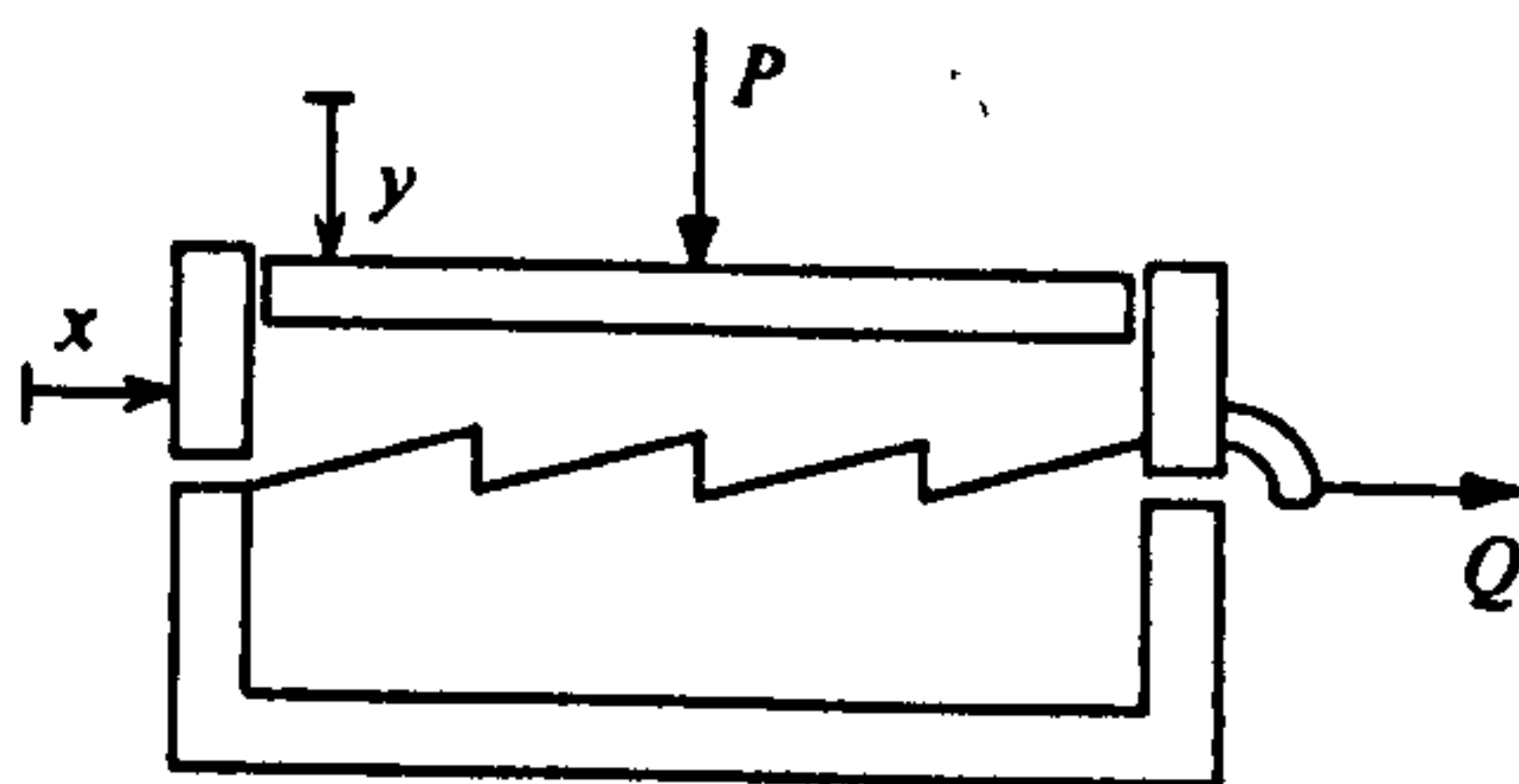


(a)



(b)

FIG 8.97(c) SCHEMATIC DIAGRAM OF THE SHEAR BOX TEST.



CHAPTER 9

Quy Water culvert

9.1 Introduction

In highway projects, because of increasing construction costs, flexible culverts are increasingly being used as short span bridges. Typically these structures are embedded under shallow cover conditions and can be of spans of up to 14m (Byrne et al., 1993). Previous analysis of flexible culvert behaviour under shallow cover using the developed modelling approach (Davies et al., 1993) has tended to concentrate on shorter culvert spans, e.g. Mytholmroyd culvert (chapter 8) 6m span and, Newport (Armco) culvert 3m span (Davies et al., 1993). Therefore, in this chapter the ability of the chosen approach to predict the live load behaviour of longer span, shallow cover culverts has been assessed. To do this a case history describing a trial loading of a long span ($S=10\text{m}$) elliptical flexible culvert embedded under shallow cover ($H/S=0.19$) has been used. The height of cover above the culvert crown includes the thickness of a flexible pavement (0.4m).

A brief description of the culvert and trial loading is given in section 9.2. Full details can be found from Temporal and Johnson (1988).

The structure of this chapter is similar to that adopted for chapter 8. Discretisation of the problem and selection of an initial first estimate set of material parameters from available in situ and laboratory data (Temporal and Johnson, 1988) are considered in section 9.3. The predicted culvert behaviour is presented and discussed in section 9.4. In this case the predictions of the culvert behaviour are less accurate than those presented previously in chapter 8 and variation of the material parameters, to improve the predicted result, was not successful. Therefore through a process of trial and error (section 9.4) the main inaccuracy was identified and determined to be the culvert finite element discretisation assumptions. The developed approach to modelling the culvert (Davies et al., 1993) currently limits the number of culvert elements to eight rectangular, isoparametric elements. For the flexible culvert considered here the curvature of the side walls is significant and is modelled more accurately using isoparametric elements with curved sides. Using elements with curved sides the initial analysis was re-run and a significantly more accurate prediction of the culvert live load behaviour was obtained. The results of this analysis are presented and discussed in section 9.5. Conclusions drawn from the results of this study are presented in section 9.6.

9.2 Description of case history; Quy Water

This culvert is a 9.83m span horizontal ellipse which carries a stream known as Quy Water under a section of the A45, Cambridge Northern bypass. The structural plates of the culvert are 7mm thick with a corrugation of 152.4mm x 50.8mm. The geometry of the culvert is shown in Fig 9.1 and further details of the culvert are given in Table 9.1. Reinforced concrete thrust beams were incorporated into the structure at each of the shoulders (quarter-points) at locations approximately 120 degrees. The thrust beams act as longitudinal stiffeners and are also considered to assist compaction of the backfill within these areas.

The culvert was backfilled with a well-graded sand and gravel fill which was well compacted. The sand and gravel backfill extended to approximately one span of the culvert on each side of the culvert and to a depth of 1.53m above the culvert crown. The particle size distribution of the backfill is shown in Fig 9.2. The unit weight of the backfill material, γ_f , was found to be approximately 20kN/m³.

A pavement consisting of 0.21m of lean mix concrete overlaid by 0.16m of bituminous-bound material was constructed on top of the backfill, giving a total cover depth of 1.90m above the culvert crown.

The culvert was loaded to a maximum load of 450kN using a loading trailer similar to that described previously in chapters 7 and 8. The response of the culvert to the applied loading (representative of a live loading) was monitored using strain gauges installed within the culvert which measured the vertical displacement and ring compression and bending strain induced within the culvert. The layout of the instrumentation and loading positions relative to the culvert is shown in Fig 9.3. In this case analyses are only concerned with predictions of the culvert live load behaviour for application of the maximum loading (455kN) directly above the culvert crown (corresponds to loading position number 1). Using the method described previously in chapter 7, ring compression strains and bending strains were converted to thrusts and bending moments for direct comparison with the finite element analysis output.

At Quy Water, the culvert was skewed at 15 degrees relative to the carriageway as shown in Fig 9.4. Insufficient space at the test location did not permit the loading to be performed in the same plane as the culvert. Previous researchers of this loading event (Temporal and Johnson, 1988) found that the presence of the skew did not have a significant influence on the results. As can be seen from Fig 9.4, for the worst loading condition (load directly above the culvert crown) the effect of the degree of skew is minimised as the centre line of the loading trailer is directly over the culvert crown.

9.3 Modelling of soil-culvert system

Drained plane strain finite element analyses have been performed using the finite element mesh shown in Fig 9.5 to predict the behaviour of the Quy water culvert. Because of the symmetry of the problem only half of the soil-culvert system was modelled. The corrugated metal culvert was modelled using eight rectangular linear strain, isoparametric elements. Equivalent elastic material properties of the rectangular culvert sections were determined using the method described in chapter 7. The culvert was described using the isotropic elastic model.

The backfill material was modelled using triangular linear strain, isoparametric elements and described using the elastic, perfectly plastic Mohr-Coulomb soil model and a non-associated flow rule. Full details of this model are given in chapter 2.

The interface elements were of similar form and shape to those used to describe the flexible culvert. The interface elements were given the same material properties as the backfill material and also modelled using the Mohr-Coulomb soil model. The pavement was modelled as a single layer using triangular, linear strain isoparametric elements and was described using the isotropic elastic model.

The reinforced concrete thrust beams located at the culvert quarter-points were also modelled and were described using the isotropic elastic model.

The vertical boundaries of the mesh were fixed horizontally (x-axis) but free to move vertically (y-axis). The right-hand side boundary of the mesh was positioned at a distance of approximately 1.5 times the culvert span, S . The bottom boundary was located at a distance approximately equal to the span of the culvert beneath the invert. No movement in either the horizontal or vertical directions was permitted at the bottom boundary.

The construction process was modelled and the live loading was applied as an equivalent line load (see chapter 7) at the surface corner node, directly above the culvert crown. No compaction pressure was applied to elements immediately adjacent to the culvert.

Material parameters selected for the backfill material, pavement and culvert are shown in Table 9.2 and 9.3. As previously noted the backfill material is determined using the elastic, perfectly plastic Mohr-Coulomb soil model. The pavement, culvert and thrust beams are described using the isotropic elastic model. The Mohr-Coulomb soil model requires the selection of six material parameters; E'_f , ν'_f , c'_f , ϕ'_f , γ_f and ψ_f (symbols have their usual meaning). The backfill Young's modulus E_f , was obtained indirectly from values of constrained moduli, M_f , obtained from plate loading tests, performed in situ at Quy water. Using relation (9.1) and assuming a M_f equal to 180MPa,

determined from the first load cycle tests, a value of E'_f equal to 175MPa was obtained.

$$E'_f = \frac{M_f(1-2\nu_f)(1+\nu_f)}{(1-\nu_f)} \quad (9.1)(7.4\text{bis})$$

A value of Poisson's ratio of the backfill was assumed equal to 0.2. The backfill material was assumed to have zero drained cohesion, i.e. $c'_f=0.0$. The second shear strength parameter, ϕ'_f (angle of internal friction) was determined from published data (Chang et al., 1980; Mayne and Kulhawy, 1982 and Craig, 1987). A value of ϕ'_f equal to 40 degrees was assumed for the backfill material.

The unit weight of the backfill material, γ_f was determined from available laboratory test data and was found to be approximately 20kN/m³.

Parameter ψ_f which describes the angle of dilatancy of the backfill material is an extra material parameter and was added (Davies et al., 1993) to represent the contractant behaviour of the backfill material during the construction procedure. Consequently the value of ψ_f input is of negative sign and remains constant throughout the analysis. Values of ψ_f were determined from previous analysis of the flexible culvert problem using this soil model (Davies et al., 1993). A value of ψ_f equal to -10 degrees was assumed for the backfill material.

The isotropic elastic model requires the selection of two material parameters; Young's modulus, E , and Poisson's ratio, ν .

The culvert Young's modulus E_c was determined using the method described in chapter 7. Poisson's ratio ν_c was assumed equal to 0.3 (Chang et al., 1980).

The pavement Young's modulus, E_{pav} was assumed equal to 540MPa and was determined from plate load tests performed on the pavement surface, which determined that the pavement Young's modulus was some three times larger than that determined for the backfill. A Poisson's ratio of 0.35 was assumed for the pavement layer (Temporal and Johnson, Temporal and Watts, 1989).

Elastic parameters required to describe the reinforced concrete thrust beams were determined from published data (Chang et al., 1980). Values of 25GPa and 0.2 were assumed for Young's modulus and Poisson's ratio of the thrust beams. The unit weight of the thrust beams was assumed equal to 24kN/m³.

To model the construction process a compaction pressure of magnitude of 100kPa was used. The magnitude of compaction pressure was chosen based on the results of the Mytholmroyd culvert study. Compaction pressure was applied to the top of the pavement layer to represent pressing of the surface layers.

Using the chosen parameter set (Tables 9.2 and 9.3) an initial, first-estimate analysis has been performed. The results of this analysis are presented and discussed in the next section.

9.4 Initial analysis and results

9.4.1 Introduction

The main concern of the analyses is to predict to a reasonable degree of accuracy the observed live load behaviour of the flexible culvert. However, for convenience the discussion commences with the construction induced behaviour (section 9.4.2). No measured data are available for the construction procedure, therefore corroboration of this part of the analysis has been made using alternative methods of flexible culvert analysis. In section 9.4.3 the discussion progresses onto the live load behaviour and the results of the finite element analysis are compared with observed data and alternative methods of analysis. The main findings of the results are summarised and discussed in section 9.4.4.

9.4.2 Results, construction behaviour

The results of the initial, first-estimate analysis of the Quay Water culvert behaviour are presented in Figs 9.6-9.11.

The distribution of construction induced thrusts is similar to that observed by Abel et al. (1973) following scaled laboratory studies performed to determine the stress distribution around flexible, metal elliptical culverts. However, the decrease in thrust at the thrust beam, approximately 120 degrees, Fig 9.6(a) is greater in these analyses than was observed by Abel et al. (1973). Exclusion of the thrust beams from the analysis and replacement by an equivalent area of backfill, significantly increase the thrust in the culvert within this region, Fig 9.6(b). Therefore, it is evident that the thrust beams, which are assumed stiffer than the culvert, are attracting the thrust in this region and as a result the thrust in the culvert is significantly lower. Reducing the stiffness of the thrust beams to less than or equal to that of the culvert will increase the culvert thrust in this region and also smooth the predicted thrust distribution at this location.

Analyses computed a springline thrust of approximately 245kN/m. Using simple equilibrium theory, relation (9.2) and Fig 9.12, gives a construction springline thrust of approximately 360kN/m.

$$N_{\text{CON}} = \frac{\gamma_f S H}{2} + \frac{\gamma_f S (H^* - H)}{4} \quad (9.2)$$

Ring compression theory (White and Layer, 1960) gives a springline thrust of approximately 205kN/m. As noted previously ring compression theory does not take account of the weight of backfill at the culvert sides above the springline. As was found for the Mytholmroyd case studies the springline thrusts calculated from ring compression theory and equilibrium theory are lower and higher than that obtained from analyses.

Comparison of finite element springline thrusts with that calculated from equilibrium theory suggests that positive arching is occurring at the culvert springline and consequently load is being transferred away from the culvert in this region. This trend of behaviour is similar to that found by Beal (1982).

An estimation of the degree of arching, A , occurring at the culvert crown can be obtained from the computed crown radial stress, σ_{rr} , and relation (7.1) (Allgood and Takahashi, 1964).

Computed radial stress at the culvert crown, at the end of construction is equal to 50kPa, giving a negative degree of arching of -0.25. As was found for the Mytholmroyd culvert, the degree of arching varies around the culvert from negative at the crown to positive at the springline. However, comparison with finite element thrusts at the culvert springline with that calculated from ring compression theory implies that negative arching occurs at the springline. This behaviour is similar to the findings of Duncan (1979); however, Duncan compared the results of his finite element analysis with those obtained from ring compression theory and did not include the weight of soil above the culvert springline.

Using Duncan's method (Duncan, 1979), which assumes negative arching, gives a maximum thrust in the culvert of approximately 415kN/m. The maximum construction thrust obtained from analyses is approximately 260kN/m and was found to occur at approximately 150 degrees. Duncan's method is predicting a culvert thrust some 1.6 times larger than that obtained from the finite element analysis.

The distribution of computed construction bending moment around the culvert is shown in Fig 9.7. As can be seen the maximum bending moment occurred at the culvert crown and is a hogging moment (tension on the outside surface of the culvert). Maximum sagging moment (tension inside the culvert) is occurring in the region of the

culvert springline. Bending moments around the base of the culvert are small and diminish to zero at the invert. This form of behaviour is similar to that observed by Beal (1982) from full-scale field studies performed on long span, shallow cover, flexible pipe-arch culverts.

The decrease in bending moment to zero at the thrust beams is due to the positioning of the culvert and thrust beam elements at this location on the culvert. As can be seen from Fig 9.5 the culvert and thrust beam elements are the same length, therefore the stiffer thrust beam element is resisting the culvert element from deforming, consequently the bending moment is zero. The marked decrease in bending moment observed in analysis at the thrust beams location is not observed in the field (Byrne et al., 1992 and Lefebvre et al., 1976).

Using Duncan's method the maximum end of construction bending moment is estimated to be approximately 5kNm/m. This is approximately 3-4 times lower than that estimated from finite element analysis. A similar trend of behaviour was found by Beal (1982) following comparison of field construction bending moments with those obtained from Duncan's design method.

The distribution of radial (normal) stress around the culvert is shown in Fig 9.8. As can be seen the maximum radial stress is occurring at approximately 70 degrees and is of magnitude 175kPa. The radial stress distribution also displays a small increase at the quarter-points to $\sigma_{rr}=95\text{kPa}$ due to the presence of the thrust beams at this location. This distribution is more representative of a pipe-arch culvert (Richards, 1982) than an elliptical culvert (Richards, 1982 and Beal, 1982). This is not surprising as the chosen finite element mesh is of a form more representative of a pipe-arch culvert than an ellipse. This form of mesh for the culvert was not intentional and arose from the need to avoid sharp corners in the culvert mesh. The presence of sharp corners in such numerical problems can result in shear locking of elements adjacent to the corner (Britto and Gunn, 1987). Refining the mesh with elements with curved sides (see section 9.7) or a greater number of rectangular elements to model the actual culvert shape more accurately will provide a more accurate representation of the radial stress distribution. The anticipated radial stress distribution around a long span, shallow cover, elliptical culvert is shown in Fig 9.8(b) (Abel et al., 1982). As can be seen the maximum radial stress should occur between the culvert quarter-points and springline. Beneath the culvert springline the radial stress should tend towards zero. As can be seen from Fig 9.8(a) the computed radial stress distribution does not compare well with that obtained from observations (Abel et al., 1982). This implies that in design situations where accurate predictions of the radial stress distributions are required the shape of the culvert must be accurately reproduced within the finite

element mesh. Currently the adopted approach to numerical modelling of the culvert only allows the use of eight elements to model the culvert. For predictions of the performance of such long span culverts more elements are required to accurately model the culvert shape. The effect of modelling the culvert shape is considered in more detail in section 9.7.

The distribution of shear stress around the culvert is shown in Fig 9.9. As can be seen the maximum shear stress is occurring at the thrust beam and is of magnitude -300kPa. This high magnitude of shear stress has arisen at the thrust beam-culvert interface because under the increasing weight of backfill over the culvert crown the culvert is being forced outwards, this in turn is causing the thrust beam to bear into the backfill as shown in Fig 9.13. The backfill material has a high angle of friction, ϕ_f and consequently can mobilise a high magnitude of passive earth pressure to resist any movement of the culvert sides and thrust beam into the backfill. The earth pressure distribution developing at the side of the thrust beams is similar to that mobilised behind a retaining wall. The presence of the thrust beams may also be helping to resist the lateral displacement of the culvert under backfill and live loads.

The distribution of computed shear stress around the culvert is similar to that observed by Abel et al., (1982). However the magnitude of shear stress observed by Abel et al., (1982) at the thrust beams was considerably smaller than that computed here. Additionally, the computed shear stress distribution is of a similar form to that observed by Shumlevich et al. (1986) following investigations into the distribution of soil stresses around buried flexible pipes, Fig 9.9(c). Thrust beams were not present in the study performed by Shmulevich et al. (1986).

The histories of culvert crown and springline displacement throughout the construction process are shown in Fig 9.10 and Fig 9.11. The form of displacements is similar to that presented previously for the Mytholmroyd case study. As can be seen the construction displacements are dominated by high upward crown and inward springline displacements following the mobilisation of high lateral earth pressures at the sides of the culvert during the construction process. In each case (crown and springline) the initial construction displacement is only slightly recovered as the construction process progresses above the culvert crown. This is due to the presence of high lateral earth pressures at the culvert sides. As noted previously the thrust beams may also be assisting to resist any lateral movement of the culvert as the construction process progresses above the culvert crown.

9.4.3 Results, live load behaviour

Numerical (finite element) predictions of the culvert live load behaviour are compared with observations in Tables 9.4-9.7. Observed data are only available for the top region of the culvert, $180 \geq \theta \geq 135$ degrees.

As can be seen from Table 9.4 predictions of the culvert live load thrust are inaccurate and do not compare with those observed. Analyses predict zero change in the culvert thrust at the crown following application of the live load at the culvert crown. At the remaining sampling positions analyses are underpredicting the observed thrusts by as much as a factor of 15.

Using simple equilibrium theory, which assumes neutral arching, gives a live load thrust of 60kN/m at the culvert springline. Alternatively using Duncan's method (Duncan, 1979), which assumes negative arching, gives a live load thrust of 72kN/m at the springline. No measured data are available for the thrust behaviour at the springline. The nearest measuring location is at $\theta=135$ degrees, which gave a live load thrust of 30kN/m. The measured thrust data (Table 9.4) follow a similar trend to that observed for the Mytholmroyd load test. Observed thrusts increase with increasing circumferential distance away from the crown moving in an anti-clockwise direction) up to $\theta=150-140$ degrees, thereafter the thrust decreases towards the culvert springline. Given the magnitude of observed live load thrust at $\theta=135$ degrees of 30kN/m for the Quay water culvert, and assuming that the observed trend in data for the Mytholmroyd culvert applies, culvert thrusts are lower than that calculated from equilibrium theory suggesting that positive arching, due to a locally low crown pressure is occurring at the culvert springline. Analyses are also predicting positive arching as a whole for the culvert (thrust equal to 7kN/m) however the degree of arching does appear to be unrealistic.

Computed live load radial stress at the culvert crown is zero which indicates that analyses are significantly overpredicting the degree of arching occurring in the backfill. Computed live load radial stress at the culvert quarter-points and springline are also very small, less than 5kPa.

The alternative methods of analysis, equilibrium theory and Duncan's method, are providing better estimates of the culvert live load thrust behaviour than the finite element analyses.

Analyses did not predict any increase in the bending moment on application of the live load. Observed bending moments are small, maximum 0.1kNm/m. Reproduction of such a small magnitude may be difficult.

Duncan's design method gives a maximum live load bending moment of 7kNm/m, this is approximately a factor of ten greater than that observed. A similar trend was observed by Beal (1982).

The magnitude of crown displacement is small, approximately -0.1cm. Analyses predicted a crown displacement of -0.04cm. Given the magnitude of displacement, computed and observed crown displacement are in reasonable agreement.

Observations of the crown displacement and bending moments are very small and insignificant to the magnitude of the observed thrusts. Consequently further predictions of the culvert behaviour will concentrate on improving the accuracy of thrust predictions.

9.4.4. Discussion

Numerical predictions of the culvert live load behaviour are inaccurate and not representative of that observed. The main failing of the predictions is the inability to reproduce even reasonably the observed live load thrust. As noted previously, the reason for this is that the predictions significantly overestimate the observed degree of positive arching. Previously for the Mytholmroyd load test (chapter 8) these inaccuracies were overcome by suitably adjusting the backfill material input parameters, backfill Poisson's ratio, ν'_f and angle of internal friction, ϕ'_f . Analyses were found to be most sensitive to these (backfill) parameters. In this study (Quy Water) these parameters, particularly Poisson's ratio, were chosen such that the 'sensitivity' was maximised and predictions would tend to overpredict the observed behaviour. However, as shown previously in section 9.4.3 this is not the case and despite the selection of adverse parameters (parameters which will give the worst result for design), analyses have significantly underestimated the observed thrusts. Therefore variation of the backfill material parameters will not improve predictions.

The previous load test (Mytholmroyd) determined that incorporation of the pavement layers significantly reduced the live load bending moments and culvert displacements, however it did not reduce the live load thrust. Given the magnitude of the live loading and the shallow cover height above the culvert crown, the magnitudes of the culvert crown displacement and live load bending moments also demonstrate the influence of the pavement layer. As can be seen from Table 9.8 (analysis Q1_17) replacing the pavement layer with an equivalent layer of backfill significantly increases the live load

thrust on the culvert. However, maintaining the pavement layer and reducing the stiffness to 360MPa, which is approximately twice the stiffness of the backfill, does not have any influence on the culvert live load thrust.

These results suggest that modelling the pavement as isotropic elastic is causing nearly all of the applied live load to be transferred into the surrounding backfill and away from the culvert. Alternatively using the Mohr-Coulomb soil model to describe the pavement and introducing a degree of yielding in the elements beneath the applied loading is causing a different load path through the backfill material to develop and consequently load is now being shared between the culvert and backfill. During the course of the load test no distress to the pavement layer through the action of the applied loading was observed (Temporal and Johnson, 1988). Therefore, it is unlikely that any significant degree of yielding (particularly the degree of yielding required to give the magnitude of live load thrusts described above) would have occurred. The selected pavement stiffness is considered to be at the lower end of the range of stiffness values. The pavement stiffness was measured using the plate load test and was found to be in excess of a constrained modulus of 600MPa, which is approximately four times greater than the backfill stiffness. A pavement stiffness of 540MPa was used in analyses, this is three times greater than the backfill stiffness. In the field the actual stiffness of the pavement layer may be larger as the plate test is not particularly accurate for pavement design (Temporal and Johnson, 1985). Therefore it is apparent that realistic variation of the pavement parameters will also not significantly improve the live load thrust predictions.

The poor live load thrust predictions may be attributed to the assumed discretisation of the culvert which was highlighted previously during consideration of the radial stress. Currently the culvert is modelled using eight rectangular isoparametric elements. As noted previously limiting the number of elements to eight for such a long span culvert is not accurately modelling the culvert shape. In this case the resulting shape is more representative of a pipe-arch culvert than that of an ellipse. To reproduce the elliptical shape within the analyses eight isoparametric elements with curved sides were used, Fig 9.14. As can be seen from Fig 9.14 using curved elements has significantly improved the modelling of the culvert-shape, given the limitation of the number of elements which can be used. The benefits of using curved elements are most evident at the culvert sides where the curvature is high.

Re-modelling the culvert using more rectangular elements will improve the accuracy however this would have required changes to the subroutines added to CRISP to analyse the culvert problem and due to time restrictions this was not feasible. Use of the curved elements within analyses significantly improved the predictions of the live

load thrust. Full details of using curved elements to model the culvert are given in section 9.5.

Throughout the previous section some empirical and semi-empirical methods have also been used to estimate the maximum live load thrust. All methods used (simple equilibrium theory, ring compression theory and Duncan's method) overpredicted the maximum observed live load thrust (40kN/m) by as much as a factor of 2 (Duncan's Method). Despite the degree of overestimation of the thrust associated with these methods, they provide a better estimate of the maximum culvert live load thrust than the finite element analyses.

9.5 Curved culvert elements

9.5.1 Introduction

The remaining sections of this chapter are concerned with using elements with curved sides to model the shape of the elliptical culvert. Application of these refined elements to the culvert was not straightforward but required careful consideration of the curvature and thickness of the culvert to avoid numerical problems. Details of how these elements were described and input into CRISP are given in section 9.5.2. The results of numerical analyses incorporating the curved element sides are presented in section 9.5.3. The results of analyses are discussed and compared with the results of previous analyses using rectangular culvert elements in section 9.5.4. Conclusions drawn from these results are presented in section 9.6.

9.5.2 Discretisation of the culvert using curved elements

In CRISP elements with curved sides are specified by highlighting within the geometry program input data the elements to have curved sides and specifying the co-ordinates of the nodes which lie along the curved sides. Throughout this study linear strain elements were used, therefore the co-ordinates of only one mid-side node per side were required to be specified, Fig 9.15. Both the culvert and slip elements were specified to have curved element sides. To avoid numerical problems both sides of the slip element were specified as curved. Having one element side curved and the other straight, is not feasible for either the culvert or slip element in order to maintain a constant element thickness, Fig 9.16. The curvature of both the culvert and slip element must be accurately reproduced within the mesh as the elements are so thin that

elements within areas of high displacement can deform sufficiently to allow opposite sides of the element to touch, Fig 9.17. If this occurs the analysis will fail. To avoid this problem great care was taken to ensure that all the culvert and slip element nodes accurately reproduced the required degree of curvature and thickness at each element. This was done using a computer program which translated the known element edge and mid-side nodes of the previous rectangular culvert mesh onto the required ellipse. The co-ordinates of the rectangular elements were translated in the direction of the radius drawn from the culvert 'origin' to the element node in question, Fig 9.18. The slope of this radius was determined from the known rectangular element co-ordinates. For this part of the operation the culvert origin was centred on the Cartesian origin allowing the radius to be described using a simple straight line relation, relation (9.3).

$$y = mx + c \quad (9.3)$$

where y and x are the y -axis and x -axis Cartesian co-ordinates; m is the slope (or gradient) of the radius and c is the intercept of the radius with the y -axis, in this case $c=0.0$.

The position of the translated node on the elliptical culvert is therefore defined by the point of intersection of the chord and the ellipse. The equation of an ellipse (centre at the origin) is given by relation (9.4).

$$y^2 = \left(1 - \frac{x^2}{a^2}\right)b^2 \quad (9.4)$$

where a and b are the lengths of the major and minor axes of the ellipse, Fig 9.18. Solving relations (9.4) and (9.5) for the Cartesian ordinates x and y will give the co-ordinates of the node position on the culvert. Using the above procedure the nodes of the inner culvert surface were defined. The outer culvert surface nodes (inner surface for the slip element) and outer surface nodes of the slip elements were defined by increasing the lengths of the major and minor axes of the ellipse by the required culvert and slip element thickness and re-solving relations (9.3) and (9.4).

In this case the above method was used to define the co-ordinates of the culvert using curved elements; this method could also be used to model the culvert using rectangular elements.

Axial forces (thrusts) and bending moments in the culvert were estimated at the centre of the culvert elements using the method described previously in chapter 7.

Using curved elements to describe the culvert and slip elements the main analysis has been re-run using material parameters as defined previously in section 9.4. The finite element mesh used in analyses is shown in Fig 9.19. As can be seen from Fig 9.19 the shape of the modelled culvert is more representative of the actual culvert shape than the mesh previously used (Fig 9.5). Analyses performed using the curved elements are described in the next section.

9.5.3 Result with curved elements

In this section the results of the analysis incorporating elements with curved sides to model the culvert shape are presented and discussed. The results are also compared with the solution obtained using rectangular culvert elements. In the absence of measured construction data, the main concern of analyses is to reproduce the observed live load behaviour. Therefore, the discussion in this section will tend to concentrate on the live load behaviour.

Using culvert and slip elements with curved sides, the initial analysis has been re-run. The results of this analysis are shown in Figs 9.20-9.25. Computed thrusts and bending moments are compared with those observed in Table 9.4.

As can be seen from Figs 9.20-9.25 and Figs 9.6-9.11 the resulting solution obtained from using elements with curved sides to model the culvert is different, particularly for thrust, bending moments and displacements. However the computed live load thrusts, Table 9.4, are in good agreement with those observed. Computed bending moments are of similar order of magnitude to those observed. However comparison of quantities of such a small magnitude is difficult. The predicted live load crown displacement is in reasonable agreement with that observed, however, as with bending moments the magnitude of displacement is very small (-0.01cm observed, -0.195cm predicted).

9.5.3.1. Thrust behaviour

Using elements with curved sides has altered the distribution of thrust around the culvert, Fig 9.20 and Fig 9.6. The resulting distribution is typically of a higher magnitude. The maximum thrust, occurring at the culvert crown is nearly 1.5 times higher than that observed previously. The most marked differences between the two solutions are the thrusts around the culvert base, $0 \leq \theta \leq 60$ degrees. Over the base of

the culvert the thrust decreases from 200kN/m at the invert becoming negative at $\theta=40$ degrees. At the springline a double-peak behaviour is observed. Both these behaviours are eliminated by increasing the value of Poisson's ratio of the backfill material, Fig 9.26 ($\nu_f=0.4$). Experimental studies by Beal (1982) have shown that negative hoop stress develops in the culvert suggesting the backfill is in tension when slippage between the culvert and surrounding backfill is allowed to occur. For this condition the interface shear stress will tend towards zero. As can be seen from Fig 9.23, the interface shear stress over this region of the culvert is approximately equal to zero. For $\nu'_f=0.4$, the shear stress over the base region Fig 9.29 is approximately constant at -15kPa. Consequently, as can be seen from Fig 9.26, the thrust over this region is also constant and of magnitude 120kN/m (compressive).

The thrust at the culvert springline ($\theta=90$ degrees), Fig 9.20 may be attributed to some local yielding of the backfill elements adjacent to the culvert at the springline, which is initiating a degree of positive arching. Comparison of calculated end of construction thrust and live load thrust (255kN/m and 20kN/m respectively) with those obtained from equilibrium theory (365kN/m and 60kN/m respectively) suggests that a high degree of positive arching is occurring. The double-peaks occurring at $\theta=70$ degrees and 100 degrees may indicate that the load from the springline is being transferred to these adjacent areas.

The increase in the thrust within the culvert after application of the live load is small, maximum 50kN/m at $\theta=140$ degrees, and is typically confined to the top region, $120 \leq \theta \leq 180$ degrees, of the culvert. Using Boussinesq's elastic theory gives a crown live load radial stress, σ_{rr} equal to 40kPa, analyses estimate the live load σ_{rr} at the crown is equal to 10kPa, implying a degree of arching, A , equal to 0.75 (Allgood and Takahashi, 1964). At the end of construction a degree of negative arching, A , equal to -0.79, is occurring locally at the culvert crown.

Duncan's method estimates the maximum thrusts at the end of construction and after application of the live load to be 435kN/m and 72kN/m. These maximum values of thrust are similar to those estimated from analyses.

9.5.3.2 Radial stress, σ_{rr}

The distribution of radial stress around the culvert is shown in Fig 9.22. As can be seen the stress distribution is different from that obtained previously, Fig 9.8(a), and the occurrence of the maximum radial stress is at the quarter-points. This distribution of radial stress is consistent with experimental observations performed to determine the

stress distribution around elliptical culverts (Abel et al., 1973 and Richards, 1982). Evidently using elements with curved sides to more closely model the culvert shape has significantly improved predictions of radial stress. Additionally, this solution highlights the importance of accurately modelling the given culvert shape.

9.5.3.3 Shear stress, $\tau_{r\theta}$

The shear stress distribution around the culvert, Fig 9.23 is similar to that obtained previously using rectangular culvert elements, Fig 9.9(a). The magnitude of shear stress at the culvert quarter-points ($\theta=120$ degrees) and over the top region of the culvert, $140 \leq \theta \leq 160$ degrees is larger using culvert elements with curved sides. This behaviour may be attributed to the different culvert displacement responses for the curved sided and rectangular culvert elements.

9.5.3.4 Bending moments and displacements

The distribution of bending moment around the culvert, obtained using elements with curved sides, is shown in Fig 9.21. As can be seen from comparison of Figs 9.21 and 9.7 this distribution is significantly lower than that obtained previously using rectangular culvert elements. Previously the maximum bending moment 15kNm/m (Fig 9.7) was located at the culvert crown, however for curved culvert elements the maximum bending moment (-11.0kNm/m) is located at $\theta=50$ degrees. The reason for the marked difference between the two bending moment distributions is the different displacement responses of the culverts, Fig 9.24 (previously Fig 9.10) and Fig 9.25 (previously Fig 9.11), which have given rise to very different hoop stress distributions within the culvert, Fig 9.32.

As can be seen from Figs 9.24 and Fig 9.25 the displacement response of the culvert using curved culvert elements indicates that the culvert is being squashed (culvert crown pushed downwards, forcing the sides outwards) under the weight of the backfill and applied live load. Some peaking of the culvert (culvert sides pushed inwards forcing the crown to rise upwards) is occurring at construction stages 7 and 8, however the magnitude of crown rise is small, approximately 0.7cm. The rise in the crown is recovered entirely in the next construction stage (stage 9). Successive culvert crown and springline displacements are describing a behaviour which has previously been discussed for stages 1-6. As can be seen from Fig 9.32 this behaviour has resulted in a compressive hoop stress distribution throughout the cross-section of the

entire culvert. The displacement response obtained using rectangular elements to model the culvert, Fig 9.10 and Fig 9.11, is very different from that obtained using curved elements. As can be seen, typically throughout construction and after application of the live load the culvert displacement response is describing a behaviour previously described as peaking. Initial placement of fill around the culvert sides (construction stages 7 and 8) resulted in a significant inward movement of the culvert sides and rise of the crown, approximately -1.5cm and 6cm respectfully. Placement of successive layers of fill and application of the live load only recovered some 2.5cm of this rise at the crown. Approximately only 0.2cm of the initial inward movement of the culvert crown was recovered. Using rectangular culvert elements a hoop stress distribution across the culvert which varies between compressive and tensile was obtained, Fig 9.32.

For the culvert modelled using rectangular elements the reason for such a difference in the culvert displacements and bending moments is the greater magnitude of radial stress around the region of the springline. This has arisen mainly from the shape of the culvert in the mesh for this case. In this case the resulting culvert shape is similar to that of a pipe-arch culvert (Mansfield, 1953 and Richards, 1982). For this shape the maximum radial stress, σ_{rr} is located approximately between the culvert invert and springline. Therefore, for such a culvert shape the high magnitude of radial stress around the base and springline of the culvert will cause the culvert to peak. The above discussion would suggest that the difference in the radial stress behaviour, Fig 9.8 and 9.22, is attributed to the poor modelling of the culvert rather than using curved elements to model the culvert. To investigate this behaviour further analysis CQ1_26 was re-run using a crude approximation of the elliptical culvert using rectangular elements, Fig 9.33. The results of this analysis are shown in Figs 9.34 to 9.39, and as can be seen the bending moment and displacement solutions are similar to that obtained previously for the pipe arch culvert rather than the ellipse. The magnitudes of bending moments and displacements for this crude mesh are however smaller. The radial stress distribution obtained for this mesh is similar to that obtained using curved elements with the maximum radial stress occurring at the culvert springline. The magnitude of radial stress in the vicinity of the springline, $60 \leq \theta \leq 90$ degrees, however is larger. This implies that use of rectangular elements will induce a larger radial stress distribution in this region than curved elements. This difference in behaviour has arisen from the different shape or interpolation functions associated with the rectangular and curved slip elements adjacent to the culvert.

In a displacement method finite element program like CRISP the stiffness matrix, K is a function of the shape functions. Therefore the stiffness matrices of the rectangular and

curved elements are different and will give rise to different stress and displacement solutions. The different shape functions and hence stiffness matrices associated with the curved culvert and slip elements are the main reason for the markedly different culvert hoop stress and to a lesser extent the radial stress distributions.

As previously described elements with curved sides were used to improve the numerical modelling of the culvert through an improved shape function. Given the limitations of the chosen method used to discretise the culvert it was considered that this method would result in greater accuracy than that achieved using rectangular culvert elements. Therefore this would suggest that the resulting bending moment and displacement solutions obtained using curved elements are closer to the actual solution than obtained using rectangular elements. Using rectangular elements to model the culvert did not result in any increase in the bending moment after application of the live load. Using curved culvert elements a small change was observed which was in good agreement with that observed. In the absence of any information concerning the construction induced bending moments little can be said of the predicted bending moments during construction for either the curved or rectangular culvert elements.

9.5.4 Discussion

Based on available field data numerical analyses using culvert elements with curved sides are a significant improvement on the previous solution and has provided a good estimate of the observed live load behaviour. The curved elements appear to have resulted in better numerical modelling of the culvert shape through improved shape or interpolation functions describing the culvert element behaviour. It is from these functions that the culvert element stiffness matrices are obtained.

The difference between numerical solutions provided by curved and rectangular elements is significant and may indicate that switching to curved elements has indirectly altered some other aspect of the mesh and/or analyses. Numerical studies performed by Sloan and Randolph (1982) to determine collapse loads using an elastic, perfectly plastic soil model and quadrilateral elements, have found that 'locking-up' of elements can occur due to stress concentrations in areas of the mesh where the change of shape is significant and produces an edge (or discontinuity). Using curved culvert elements has effectively eliminated edges with the culvert mesh and as a result a more even and realistic stress distribution around the culvert may have developed. This behaviour may be implied from Fig 9.32, which illustrates the hoop stress distribution at the centre of curved and rectangular culvert elements. As can be seen from Fig 9.32 the hoop stress distribution for the curved elements is less erratic and describes a more

even distribution of hoop stress than that described for the rectangular culvert elements. Further investigations of this behaviour are recommended.

Computed values of culvert bending moment are small, typically less than 2kNm/m, except $\theta < 50$, degrees, for the construction and live load behaviour combined. This magnitude is not consistent with experimental observations obtained from field studies performed on flexible culverts at similar cover depths (Beal, 1982). Beal reports a maximum bending moment of 24kNm/m for a cover depth of 1.8m, however in this field study no pavement layers were present. Johnson et al. (1988) report that the presence of pavement layers reduced the maximum bending moment by approximately 50%. Applying this to the observations reported by Beal gives a maximum moment of 12kNm/m which is still significantly larger than that obtained from numerical analyses described in this section.

In numerical analyses bending moments are estimated from the hoop stress, $\sigma_{\theta\theta}$, distributions sampled at the three Gauss integration points located across the centre cross-section of the culvert element. It was shown previously that the hoop stress distribution throughout the culvert was compressive and variation of the hoop stress across the culvert cross-section was small. Computed culvert displacements were also small. Direct comment on the method of analysis to describe flexible culvert behaviour is difficult in the absence of construction data. However, comparison with observations reported by Beal (1982) suggests that in analyses the resulting culvert stiffness matrices for the curved elements are unrepresentative of the culvert and are predicting an over stiff culvert response to the loading. The effect of this could be compensated by reducing the value of Young's modulus for the culvert, E_c . This will reduce the value of the "D" matrix, elastic stress-strain matrix, and consequently through relation (9.5) reduce the magnitude of the element stiffness matrix, K.

$$K = \int_V (B^T D B) d(vol) \quad (9.5)$$

where B is the strain matrix (or more simply the 'B' matrix) and is obtained by differentiating the shape function matrix, N and B^T is the transpose of the strain matrix.

The culvert Young's modulus or stiffness, E_c was not altered following the use of curved sided elements to model the culvert shape. The culvert stiffness was estimated previously using the method described in chapter 7, assuming an equivalent rectangular culvert element. Some reduction in the culvert stiffness, E_c may be required if the culvert is to be modelled using curved sided elements. However, further work needs to be performed in order to define the influence of the culvert stiffness on the predicted solution.

Reducing the culvert stiffness will increase the strains, both bending and ring compression strain, induced in the culvert during construction and after application of the live load (Jeyapalan and Boldon, 1986).

Use of this case history has highlighted many of the deficiencies associated with the chosen method used to describe flexible culvert behaviour. Curved-sided culvert elements were used because it was recognised that the current use of a maximum of eight rectangular elements to discretise the culvert was inadequate for the long span culvert described in this study. As previously noted a better discretisation technique would be to use 16 or more rectangular elements to describe the culvert. Katona et al. (1976) suggest the use of at least ten elements to describe the culvert. This would also provide a check on the performance of the curved-sided culvert elements used here.

An estimation of bending moments is important for long span flexible culverts under shallow cover conditions, particularly during the early stages of construction (Duncan, 1979 and Beal, 1982). Throughout this study bending moments have been estimated indirectly using the hoop stress distributions across the centre of a culvert element. Culvert elements are linear strain, eight noded isoparametric elements and do not allow direct estimation of bending moment (or rotation) within the element. Such an element has only two degrees of freedom, described by vertical and horizontal movements u and v , Fig 9.40. Using these elements to estimate the bending moment throughout the culvert can introduce inaccuracies, particularly if the aspect ratios of the elements are large. A better approximation of bending within the culvert could be achieved through the use of a beam element which has three degrees of freedom described by u , v , and θ , Fig 9.41, where θ is the rotational degree of freedom. Rotations and consequently bending moments across a culvert element can then be obtained directly from analyses. Beam elements were used successfully by Britto (1990) to model flexible culvert behaviour under deep cover conditions. Fig 9.42-Fig 9.44.

An alternative to the beam element is a multi-node isoparametric element which has as many degrees of freedom as the beam element and may be either curved or straight. Use of this element type to describe culvert behaviour is described by Mohamedzein (1989). Full details of the finite element formulation of this element is found in Bathe (1982); Weaver and Johnston (1984) and Mohamedzein (1989). It is not known if this element has been implemented in CRISP.

Throughout the flexible culvert study (chapters 8 and 9) the main concern of analyses has been to reproduce the live load behaviour. Consequently, analyses have concentrated on the end of construction and combined end of construction and live load results. Neither of these results necessarily constitutes a worst-case solution for

design. In design the distress caused to the culvert during the construction procedure is of most concern. The influence of any live loads on the culvert is typically very small compared with the effect of the construction procedure. As can be seen from Fig 9.45 the maximum construction thrust developed in the culvert which coincides with application of the compaction pressures (100kPa) and occurs at the culvert springline, is approximately 2.5-3.0 times larger than that induced by the live load. From analyses the maximum thrust imposed on the culvert is approximately 1075kN/m and occurs during the compaction or pressing of the pavement bituminous layer, construction stage 12. Clearly the selection and design of a suitable culvert must be based on these maximum thrusts. Ring compression theory (White and Layer, 1960) and Duncan's design method (Duncan, 1979) give maximum thrusts, taking into account the compaction pressures, of 700kN/m and 600kN/m respective.

As for the thrusts, maximum displacements and consequently bending moments are occurring during the construction process. In this case maximum culvert displacements (crown and springline) are occurring at approximately construction stage 8, which coincides with placement of the backfill up to the level of the culvert quarter-points. Maximum bending moment is occurring at construction stage 12, during the compaction of the pavement layers.

Therefore, in order to determine the most adverse effects on the culvert, the design process needs to follow the behaviour of the culvert through construction and up to the completed structure. Of all the methods used to analyse the culvert behaviour the finite element approach has provided the most comprehensive design approach. However, the overall accuracy of the finite element approach, in the absence of observed construction data, cannot be properly assessed. If the maximum thrust computed using analyses is representative of the in-field culvert behaviour then empirical methods, ring compression theory and Duncan's design method, underestimate the maximum thrust behaviour in the absence of a factor of safety of two or more. As has been shown here live load effects are small and may not require rigorous analysis to determine their effects.

9.6 Conclusions

Using the adopted method of flexible culvert analysis a long span flexible culvert under low cover conditions has been analysed. Predictions of the culvert live load behaviour have been compared with measured data. No data were available for the construction procedure. From comparison of the computed and observed responses conclusions have been drawn which have implications for the method used to describe flexible culvert behaviour.

Based on available field data the adopted approach used to discretise the culvert using eight rectangular elements was found to be inaccurate. An improved solution, in this case, was obtained using curved-sided culvert elements which resulted in better numerical modelling of the culvert through improved shape or interpolation functions describing the culvert element behaviour. The inaccuracy associated with using rectangular elements to model the culvert was identified by comparing predictions of the culvert radial stress distribution with data available from published culvert case histories (Abel et al., 1973 and Beal, 1982).

Using curved-sided culvert elements predicted values of the construction bending moments were significantly reduced from that obtained previously using rectangular elements. Due to the absence of observed construction data no conclusion can be drawn from this result. However, comparison with observations reported by Beal (1982) suggests that in numerical analyses the stiffness matrices for the curved-sided culvert are unrepresentative and are predicting an over stiff culvert response to the loading.

A more accurate approach to modelling the culvert, and which would give a more accurate description of culvert bending moments, is to use a beam element (Britto, 1990) and/or a multi-noded isoparametric element (Mohamedzein, 1989). Each of these elements includes a rotational degree of freedom, θ , which will allow direct estimation of bending moments generated within the culvert.

The improvements associated with the use of curved-sided culvert elements may have significant implications on the results of the culvert analyses described in chapter 8. The Mytholmroyd culvert described in chapter 8 was not described using curved-sided elements. The problems associated with the discretisation of the culvert described in chapter 9 were not encountered in chapter 8. In chapter 8 adjustment of the backfill parameters was sufficient to generate the observed magnitude of thrust and displacements. This may imply that the adopted approach used to discretise the culvert (eight rectangular elements) is reasonable for short to medium span culverts, $S < 10$. However, in chapter 8 the resulting optimum set of material parameters is considered

to be unrealistic and not entirely descriptive of the backfill material. Re-modelling the Mytholmroyd culvert with curved-sided elements may amend this problem.

Analyses have identified that the finite element discretisation of the culvert is important and has a significant influence on the predicted solution. Consequently, further investigation into the finite element modelling of the culvert is required. The main points which need to be considered are the number and type of elements required to accurately describe the culvert.

Analyses have determined that the main concern of flexible culvert design should be the construction procedure and not the effect of the live load. During construction the induced thrusts were found to be some 2.5-3.0 times greater than those induced within the culvert after application of the live load. As a result, rigorous finite element analysis of the influence of the live load on the culvert behaviour may not be necessary. Additionally, Duncan's design method (Duncan, 1979) provided a good description of the culvert live load behaviour.

Back analyses have been performed with limited observed culvert data. Observed data are limited to the live load behaviour and include thrusts, bending moments and displacements. As mentioned previously in chapter 8 (section 8.6) given the complexity of culvert/soil interaction and scale of problems which have arisen the available data may be insufficient to suitably assess the accuracy of analyses. More appropriate trial loading data should include the construction behaviour of the culvert and an accurate description of the stress history induced within the backfill. The construction behaviour is important and as a result, the success of a developed modelling approach should be assessed on this behaviour.

As in chapter 8 values of Young's modulus of the backfill were estimated from in situ plate loading test data. Values of Young's modulus for the pavement layers were selected from published data which describe in situ plate load tests performed on similar backfill material.

A value of Poisson's ratio for the backfill material was selected on the basis of the results of parametric studies performed previously in chapter 8. A value of $\nu'_f=0.2$ was used. As discussed previously, this value of Poisson's ratio is not entirely consistent for a Mohr-Coulomb soil nor with that which would be obtained using relation (8.6) and Fig 2.2.

Table 9.1 Details of Quay Water culvert (Temporal and Johnson, 1988)

CULVERT PROPERTY	QUY WATER CULVERT
CULVERT PROFILE	HORIZONTAL ELLIPSE
SPAN, S(m)	9.83
TOP RADIUS, R(m)	6.27
DEPTH OF COVER, H(m)	1.90
PLATE THICKNESS, t(mm)	7.0
CORRUGATIONS (mm)	152.4x50.8
MOMENT OF INERTIA (mm ⁴ /mm)	2718
AREA OF SECTION (mm ² /mm)	8.17
LONGITUDINAL SEAMS	2
CULVERT MATERIAL	STEEL
YOUNG'SMODULUS, E(GPa)	205
YIELD STRESS, σ (kPa)	215

Table 9.2 Details of backfill material (Temporal and Johnson, 1988)

PROPERTY	BACKFILL
BACKFILL MATERIAL	SAND AND GRAVEL
IN SITU BULK DENSITY (Mg/m ³)	2.08
IN SITU DRY DENSITY (Mg/m ³)	1.99
IN SITU MOISTURE CONTENT (%)	4.7
MAXIMUM DRY DENSITY (Mg/m ³)	2.21
OPTIMUM MOISTURE CONTENT (%)	7.5
IN SITU DRY DENSITY (Mg/m ³)	0.9

Table 9.2(b) Initial values of backfill material parameters

SOIL MODEL PARAMETER						
STRUCTURE	E' _f (kPa)	ν'_f	c' _f (kPa)	ϕ'_f (degrees)	γ_f (kN/m ³)	ψ_f (degrees)
BACKFILL	180x10 ³	0.2	0.2	40	20	-10

Table 9.3 Culvert, Thrust beams and pavement layer material parameters

	ISOTROPIC	LINEAR	ELASTIC	PROPERTIES
STRUCTURE	E (kPa)	ν	G (kPa)	γ (kN/m ³)
CULVERT	20.5x10 ⁶	0.3	7.7x10 ⁶	-
THRUST BEAMS	25x10 ⁶	0.2	10.4x10 ⁶	21
PAVEMENT	540x10 ³	0.35	200x10 ³	22

Table 9.4 Comparison of computed and observed data; Thrust

Measuring position on culvert (degree)	180	165	150	135	120	90	Details of material parameters used in numerical analyses
	Observed live load thrust (kN)	.					
		25	30	40	30	-	
Analysis name							
Q1_14.QW (rectangular elements)	265	0	281	1	300	5	Fill, M-C model. $E'_f=180\text{MPa}$, $\nu'_f=0.2$, $c'_f=0.2$, $\phi'_f=40$ Compaction pressure 100kPa. Rigid base at -6.00m. Rectangular elements
	265		280		295	92	
CQ1_26 (curved elements)	415	25	390	35	321	49	Same as Q1_14.QW but curved culvert elements
	390		355		272	134	
				173	39	93	15
				82	3	234	6
				78		228	
						279	20
						259	

Table 9.5 Bending moment

Measuring position on culvert (degree)		180	165	150	135	120	90	Details of material parameters used in numerical analyses						
Observed live load bending moment (kNm)		-8	2	2.5	-	0	-							
Analysis name														
Q1_14.QW		16	0	11	0	5.4	0	6	0	-1	0	4	0	Fill, M-C model. $E'_f=180\text{MPa}$, $\nu'_f=0.2$, $c'_f=0.2$, $\phi'_f=40$ Compaction pressure 100kPa. Rigid base at -6.00m. Rectangular elements
(rectangular elements)		16		11		5.4		6		-1		4		
CQ1_26.QW		0.36	-0.36	0.36	-0.36	0.29	-	0.07	0.002	0	0	-0.36	0	Same as Q1_14.QW but curved culvert elements
(curved elements)		0.72		0.72		0.36		0.07		0		-0.36		

**PAGE
NUMBERING
AS ORIGINAL**

Table 9.8 Summary of main results. Thrust. (C=curved culvert elements)

Measuring position on culvert (degree)	180	166	15	135	120	90	Details of material parameters used in numerical analyses
Observed live load thrust (kN)	25	30	40	30	-	-	
Analysis name							
Q1_15	304 266	38 0	343 283	60 0	403 297	106 0	Fill & Pavement, M-C model. $E'_f=E_{pav}=180\text{MPa}$. $v'_f=v'_{pav}=0.2$, $c'_f=c'_{pav}=0.2$, $\phi'_f=\phi'_{pav}=40$. Compaction pressure 100kPa. Rigid base at -6.00m.
Q1_16	197 197	0 0	220 220	0 0	251 245	6 0	
Q1_17	310 281	29 0	345 294	51 0	391 311	80 0	
Q1_18	265 265	0 0	284 281	3 0	300 294	2 0	Same as Q1_15 but $E_{pav}=360\text{MPa}$. Pavement modelled as isotropic elastic
Q1_20	272 272	0 0	290 288	2 0	309 304	6 0	Same as Q1_15 but $E'_f=90\text{MPa}$
Q1_21	289 246	43 0	323 254	69 0	371 266	105 0	Same as Q1_17 but $E_{pav}=360\text{MPa}$ and $v'_{pav}=0.1$ Pavement modelled as elastic perfectly plastic (M-C)
CQ1_22	485 398	60 0	473 366	107 0	633 266	140 80	Same as Q1_15 but curved culvert elements
CQ1_23	300 275	25 0	310 280	30 0	346 252	20 0	Fill M-C model $E'_f=90\text{MPa}$; $v'_f=0.1$. Pavement isotropic elastic see Table 9.3. Curved culvert elements
CQ1_24	336 320	16 0	328 316	12 0	308 300	2 0	All backfill no pavement. $E'_f=E_{pav}=180\text{MPa}$ $v'_f=v'_{pav}=0.3$, $c'_f=c'_{pav}=0.2$, $\phi'_f=\phi'_{pav}=40$
CQ1_25	468 400	68 0	525 373	152 0	623 288	45 100	Same as CQ1_24 but $v'_f=v'_{pav}=0.3$ All backfill

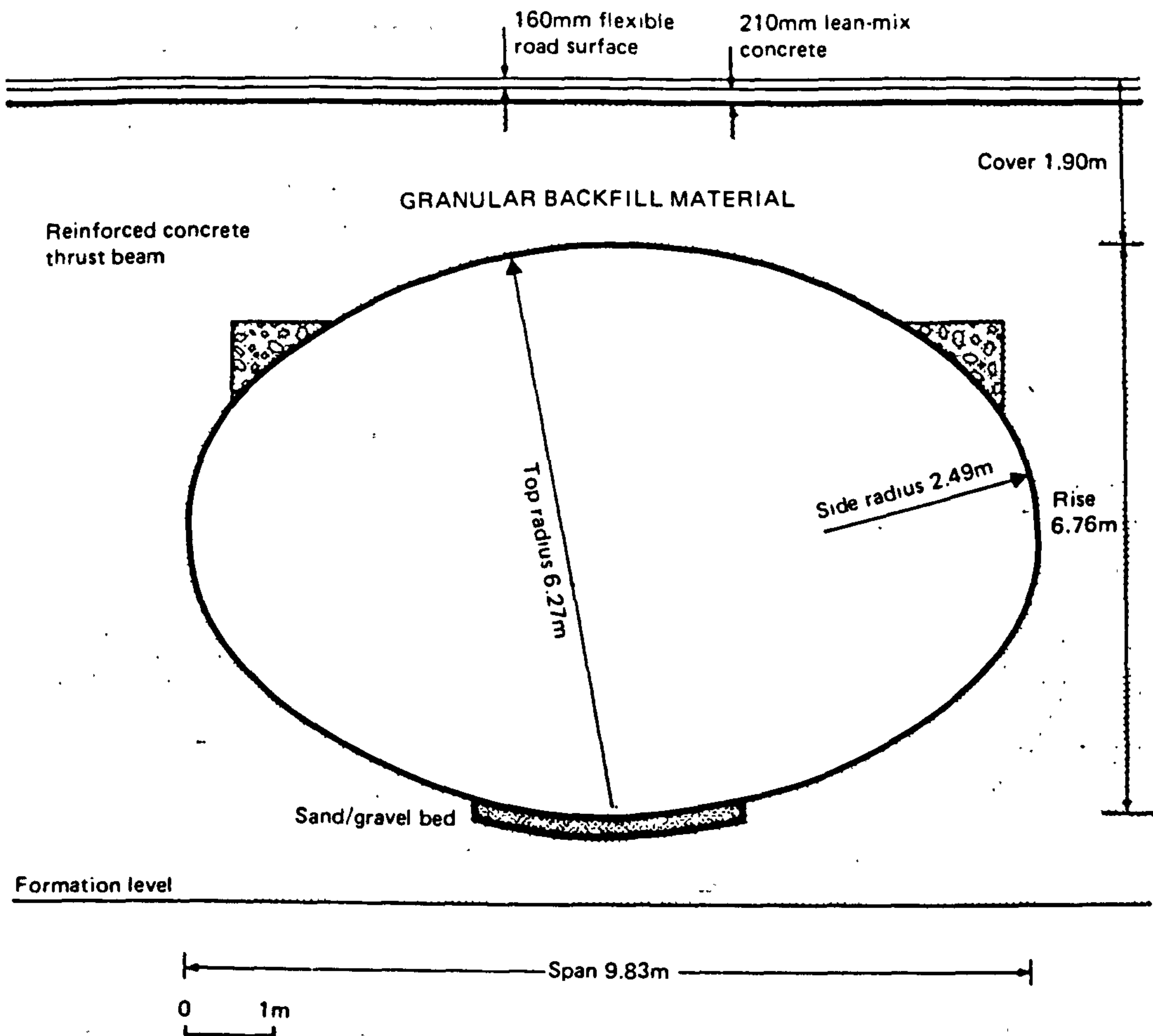


FIG 9.1 GEOMETRY OF QUAY WATER CULVERT (TEMPORAL AND JOHNSON, 1988)

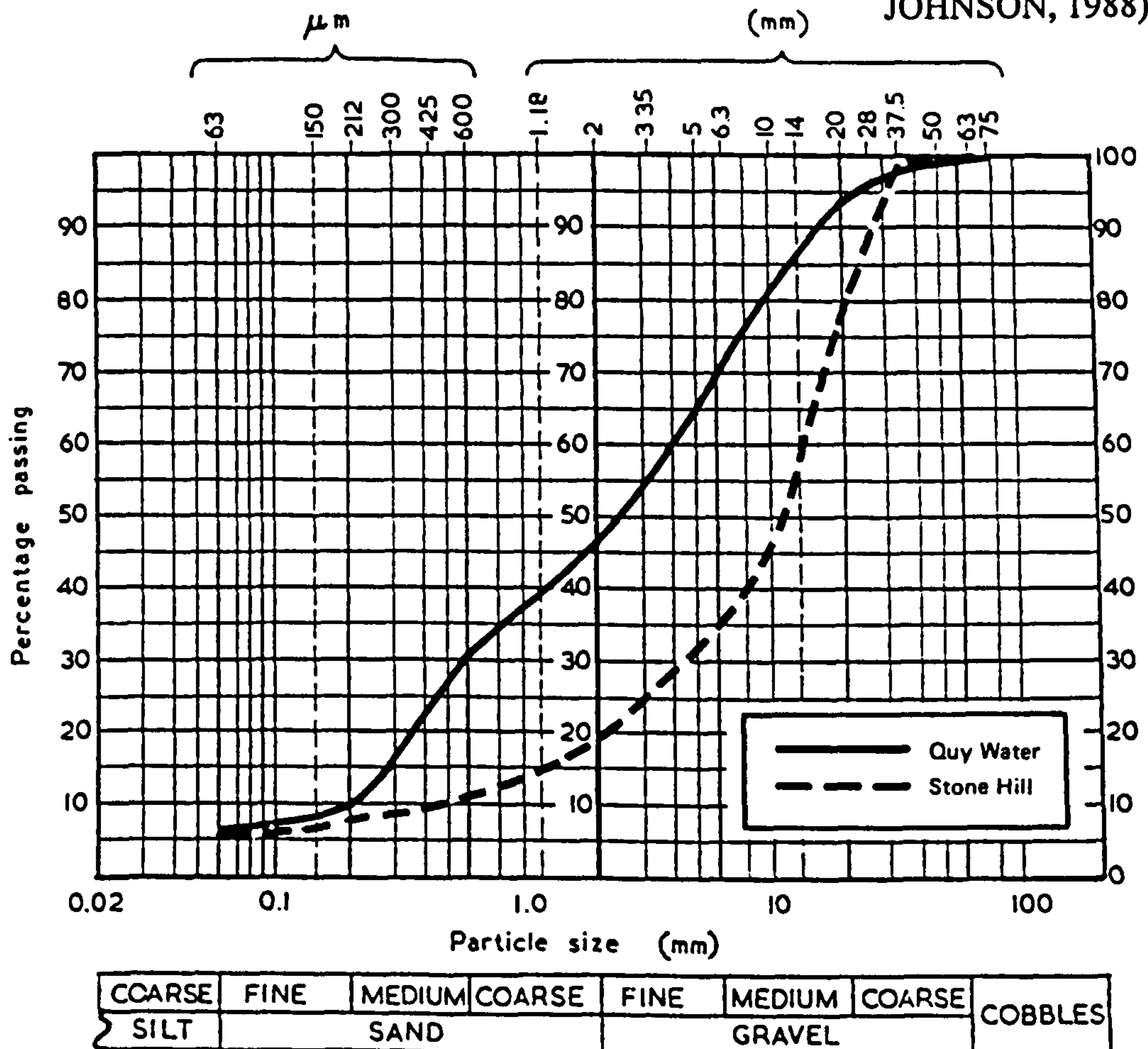


FIG 9.2 PARTICLE SIZE DISTRIBUTION FOR BACKFILL MATERIAL (TEMPORAL AND JOHNSON, 1988)

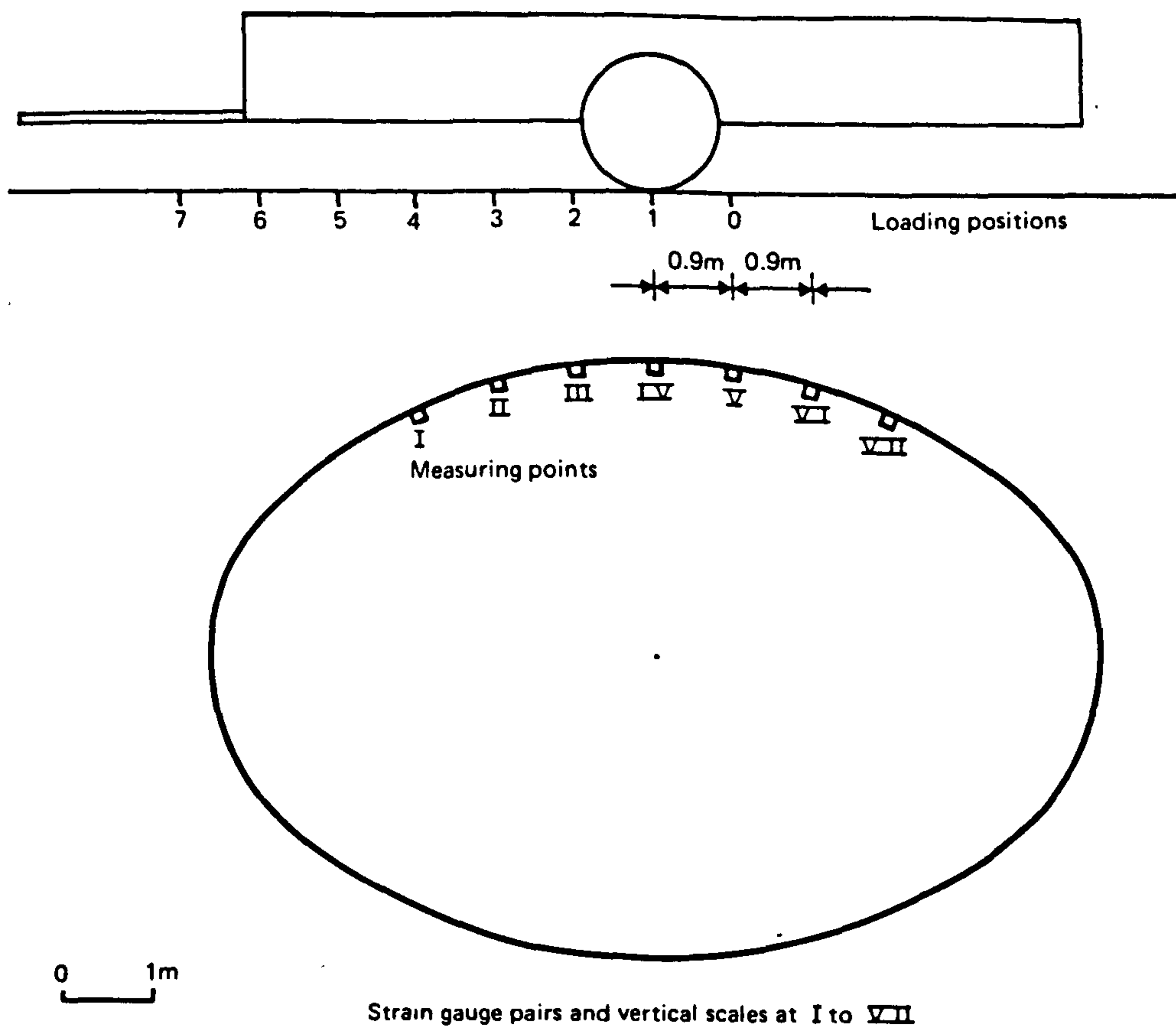


FIG 9.3 CROSS SECTION OF QUY WATER CULVERT SHOWING INSTRUMENTATION LOCATIONS (TEMPORAL AND JOHNSON, 1988)

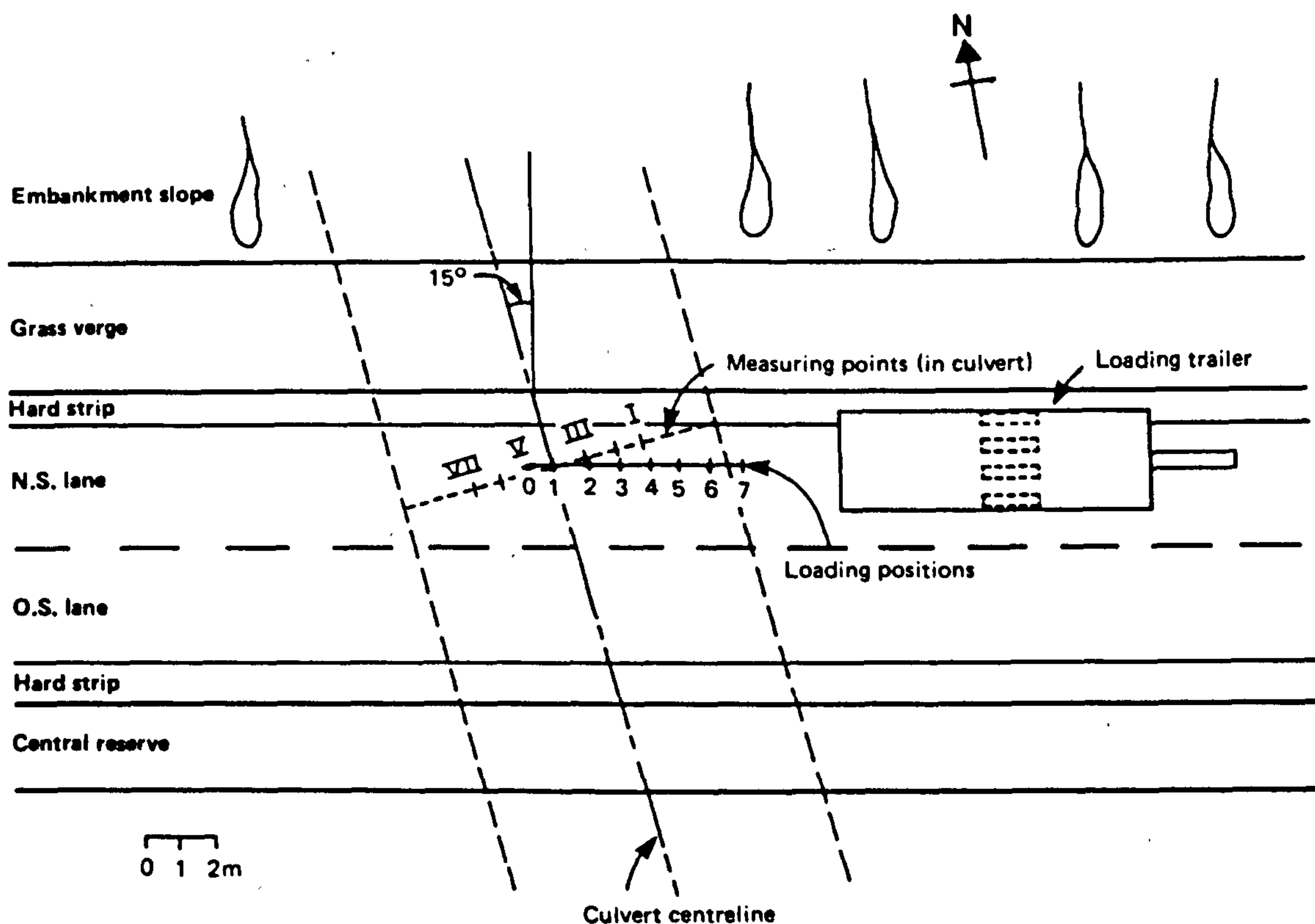


FIG 9.4 PLAN VIEW OF QUY WATER SITE SHOWING POSITION OF CULVERT RELATIVE TO CARRIAGEWAY (TEMPORAL AND JOHNSON, 1988)

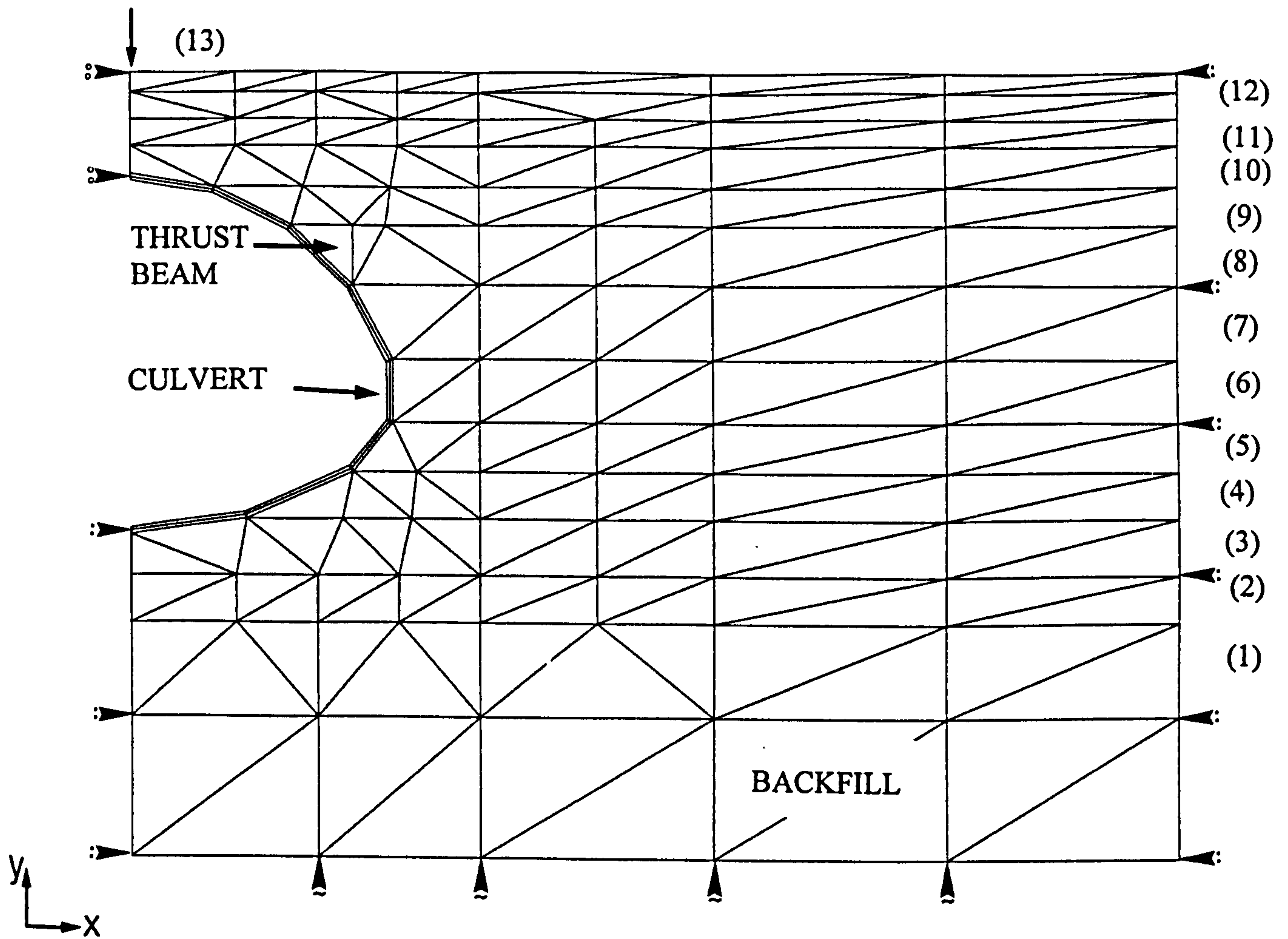


FIG 9.5 FINITE ELEMENT MESH FOR QUY WATER CULVERT
CONSTRUCTION STAGE ()

CONSTRUCTION STAGE	DESCRIPTION
1	COMPACT EXISTING FOUNDATION SOIL
2	PLACE AND COMPACT BASAL LAYER
3	PLACE BACKFILL AND COMPACT LAYER 2
4	PLACE AND COMPACT LAYER 3
5	PLACE AND COMPACT LAYER 4
6	PLACE AND COMPACT LAYER 5
7	PLACE AND COMPACT LAYER 6
8	PLACE AND COMPACT LAYER 7
9	PLACE AND COMPACT LAYER 8
10	PLACE AND COMPACT LAYER 9
11	PLACE AND COMPACT LAYER 10
12	PLACE AND COMPACT PAVEMENT LAYERS
13	APPLY LIVE LOAD

FIG 9.6(a) INITIAL ANALYSIS; THRUST BEHAVIOUR

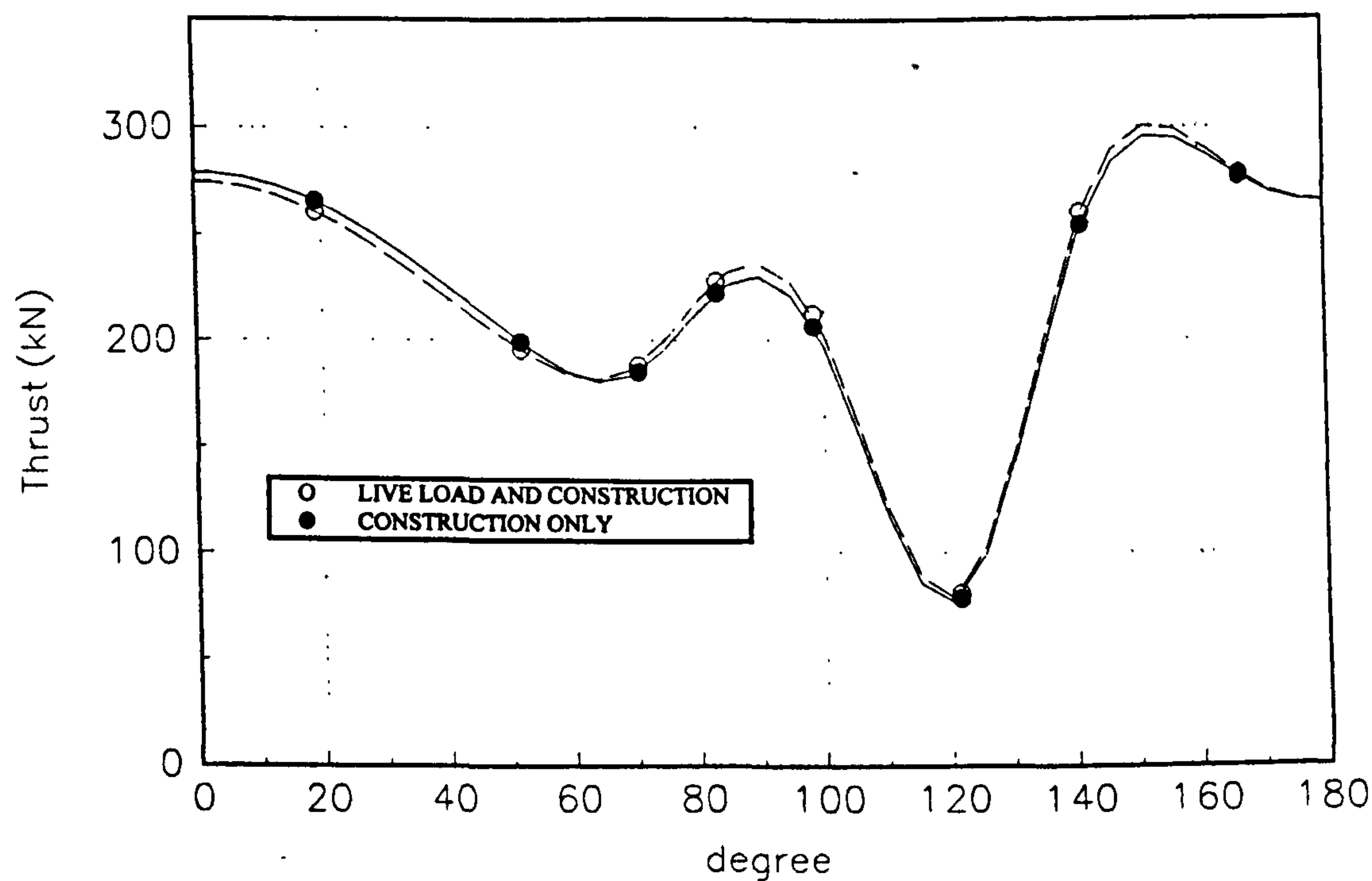


FIG 9.6(b) THRUST BEHAVIOUR; NO THRUST BEAMS PRESENT

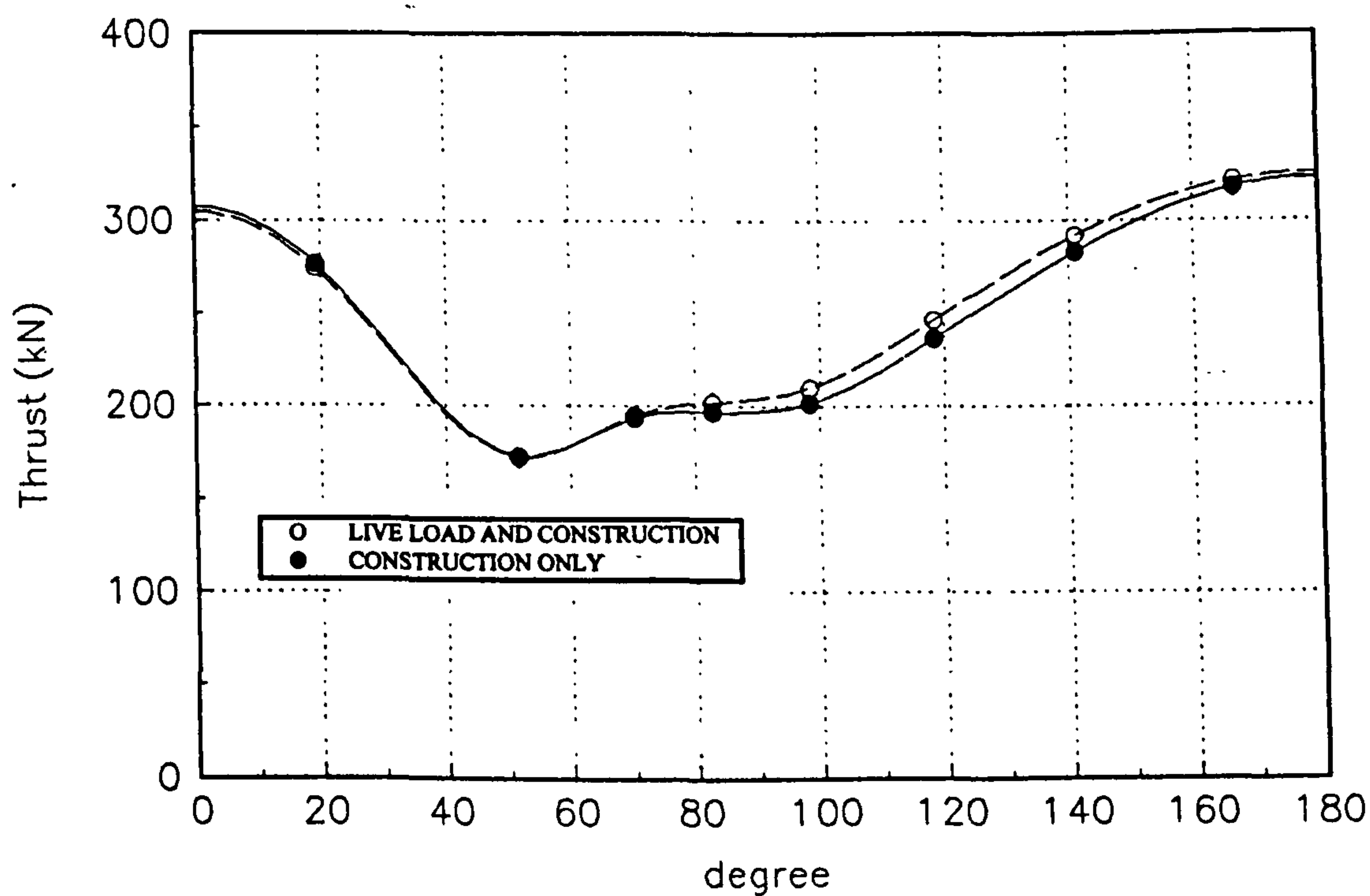


FIG 9.7 INITIAL ANALYSIS; BENDING MOMENT BEHAVIOUR

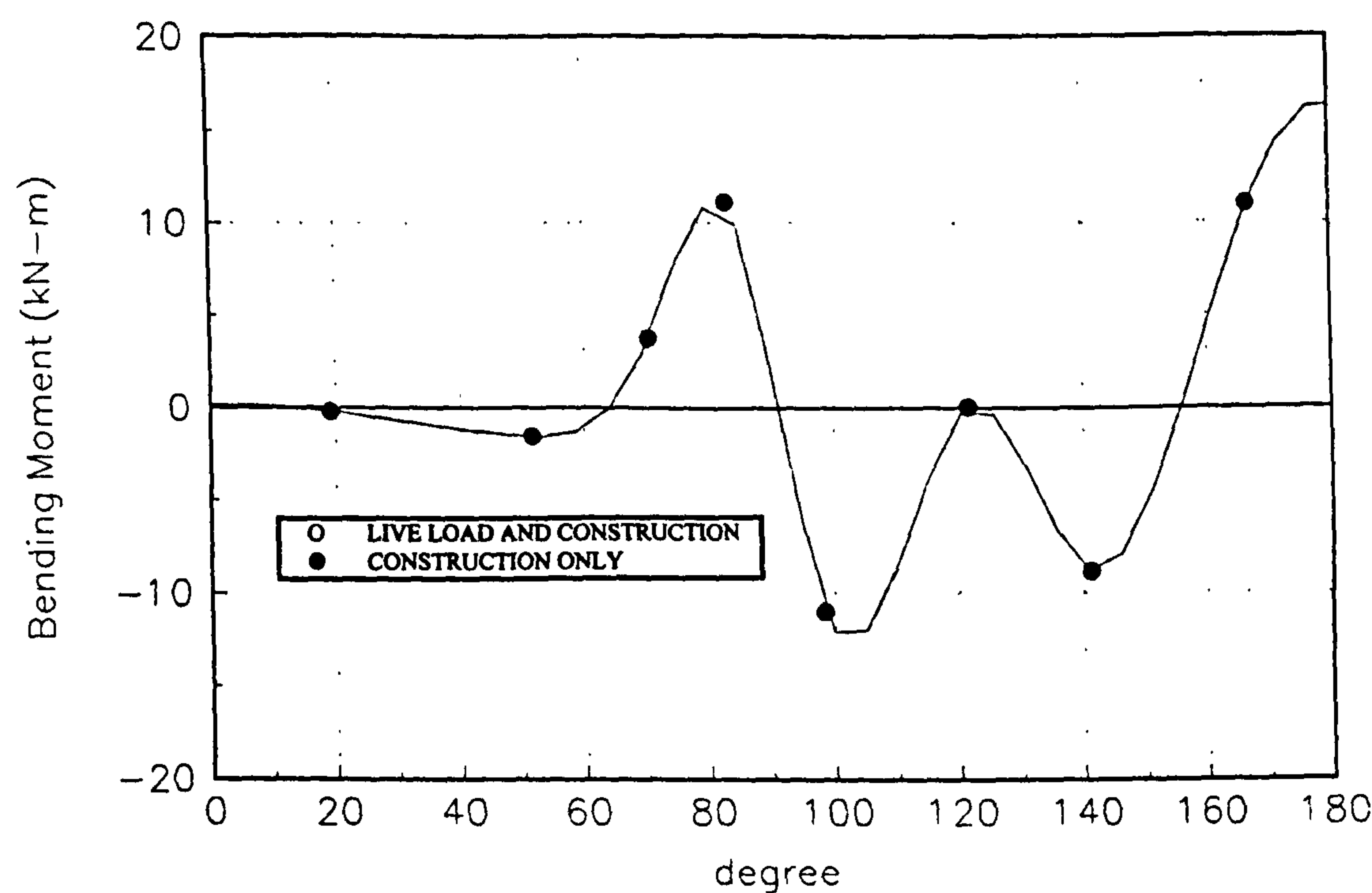
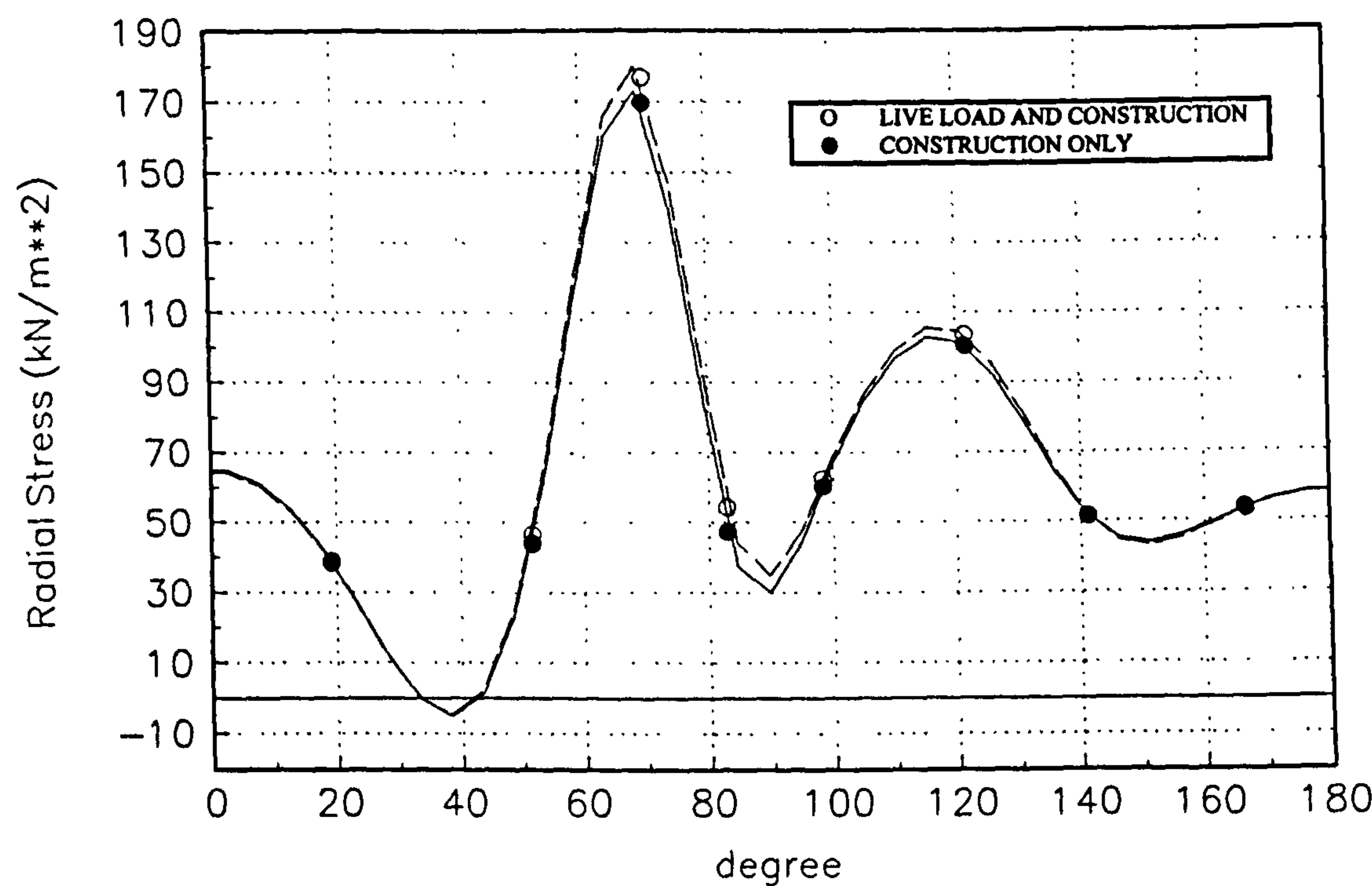


FIG 9.8(a) INITIAL ANALYSIS; RADIAL STRESS BEHAVIOUR



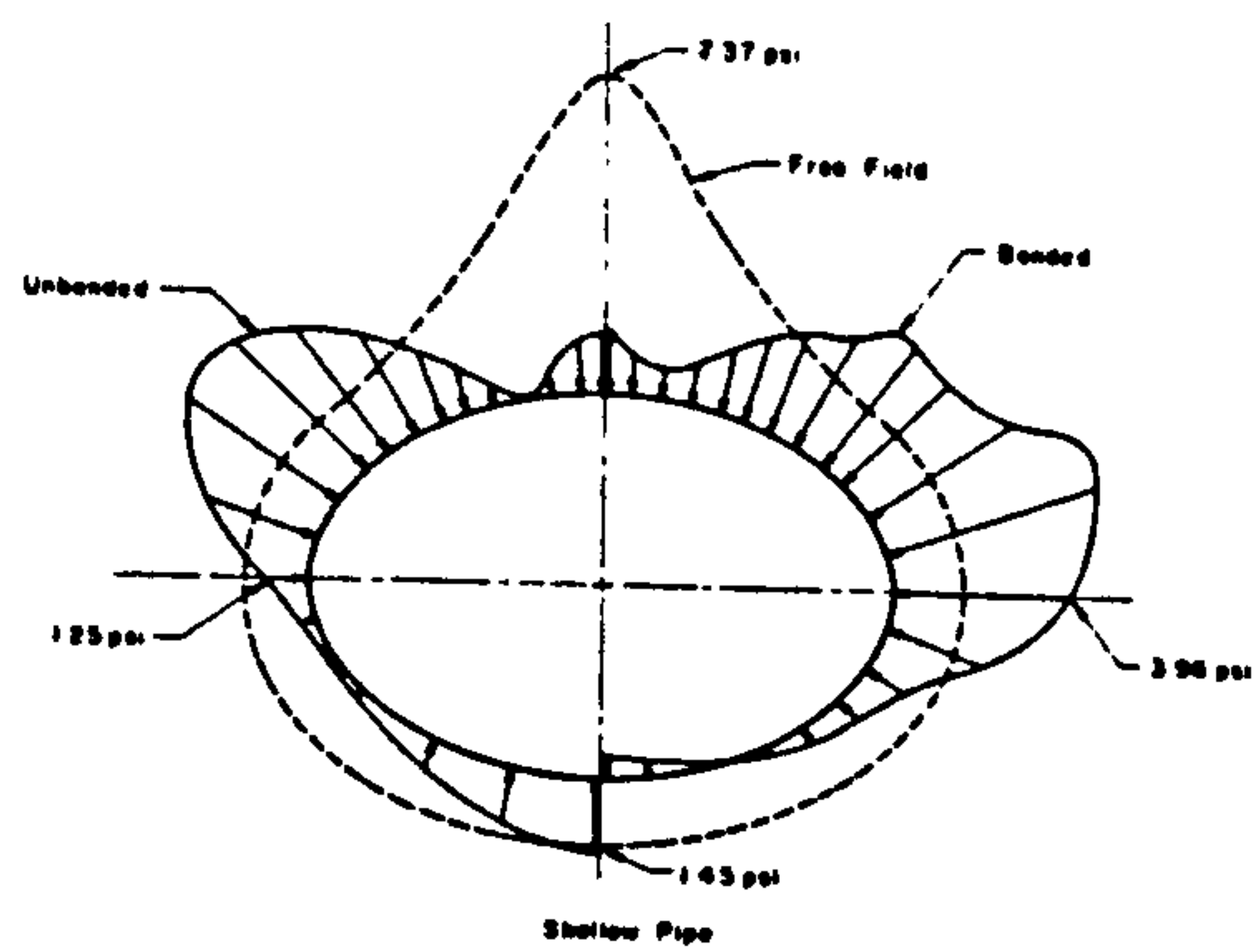
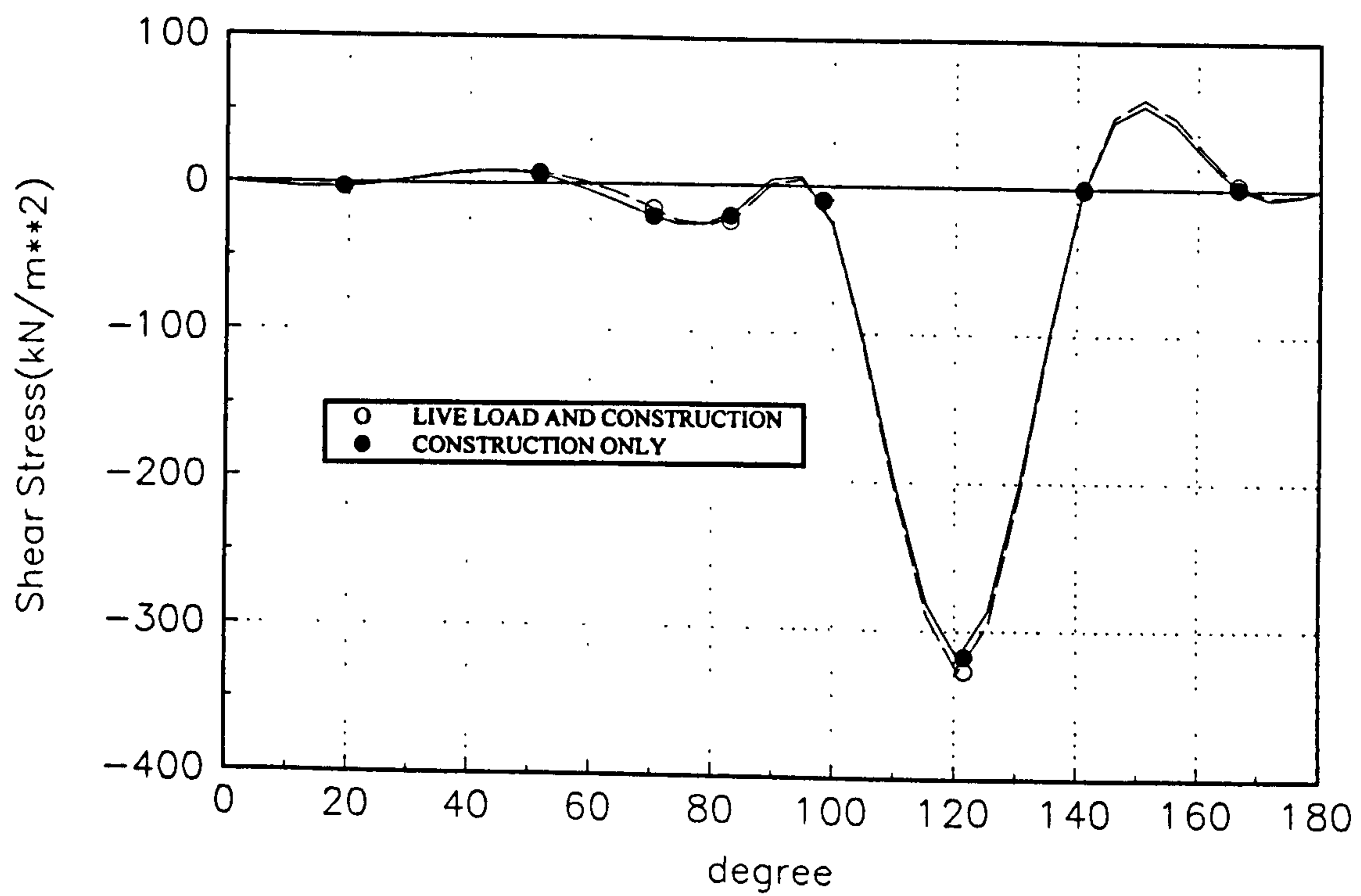


FIG 9.8(b) RADIAL STRESS DISTRIBUTION AFTER ABEL ET AL. (1982)

FIG 9.9(a) INITIAL ANALYSIS; SHEAR STRESS DISTRIBUTION



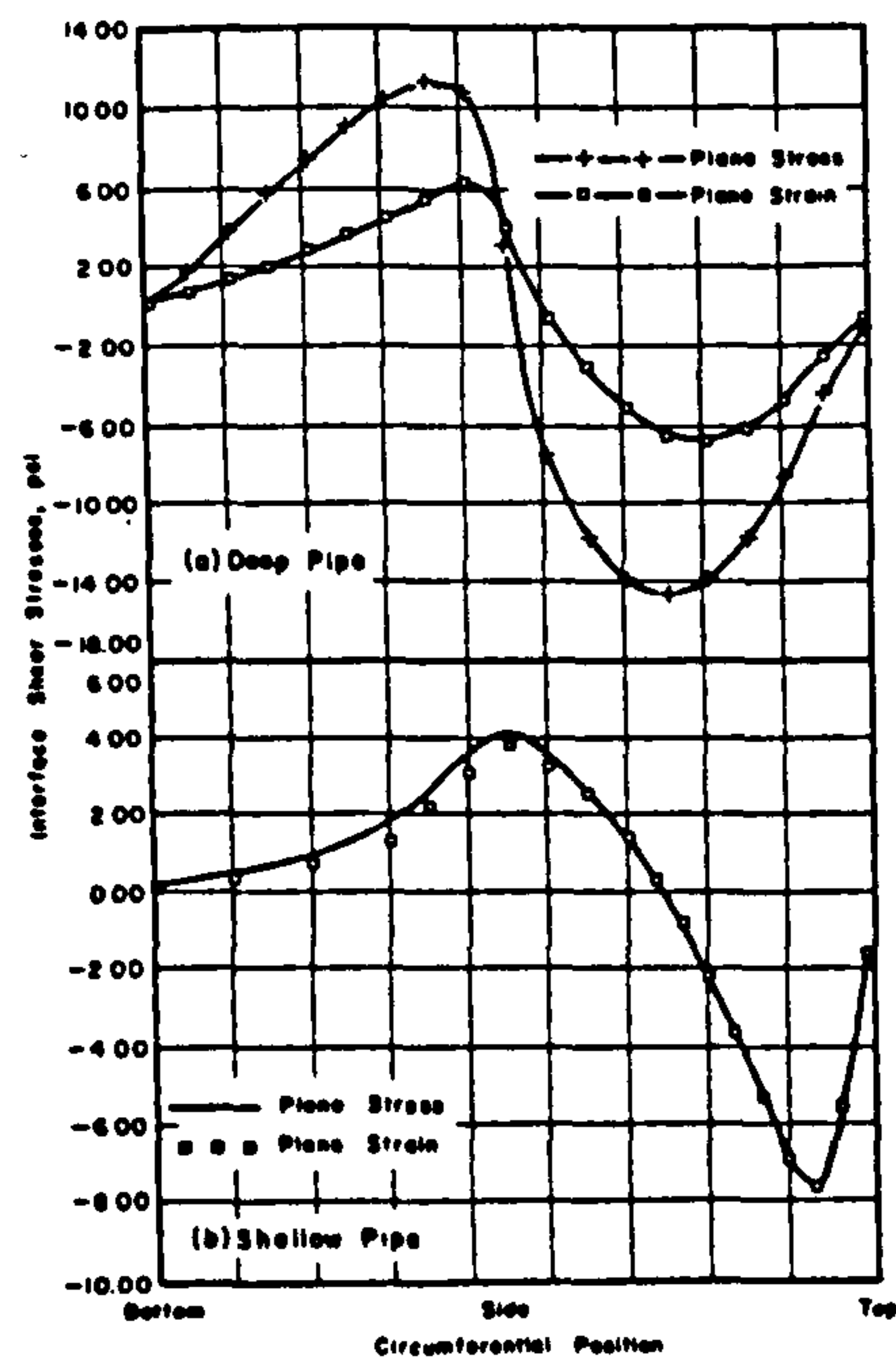


FIG 9.9(b) SHEAR STRESS DISTRIBUTION AFTER ABEL ET AL. (1982)

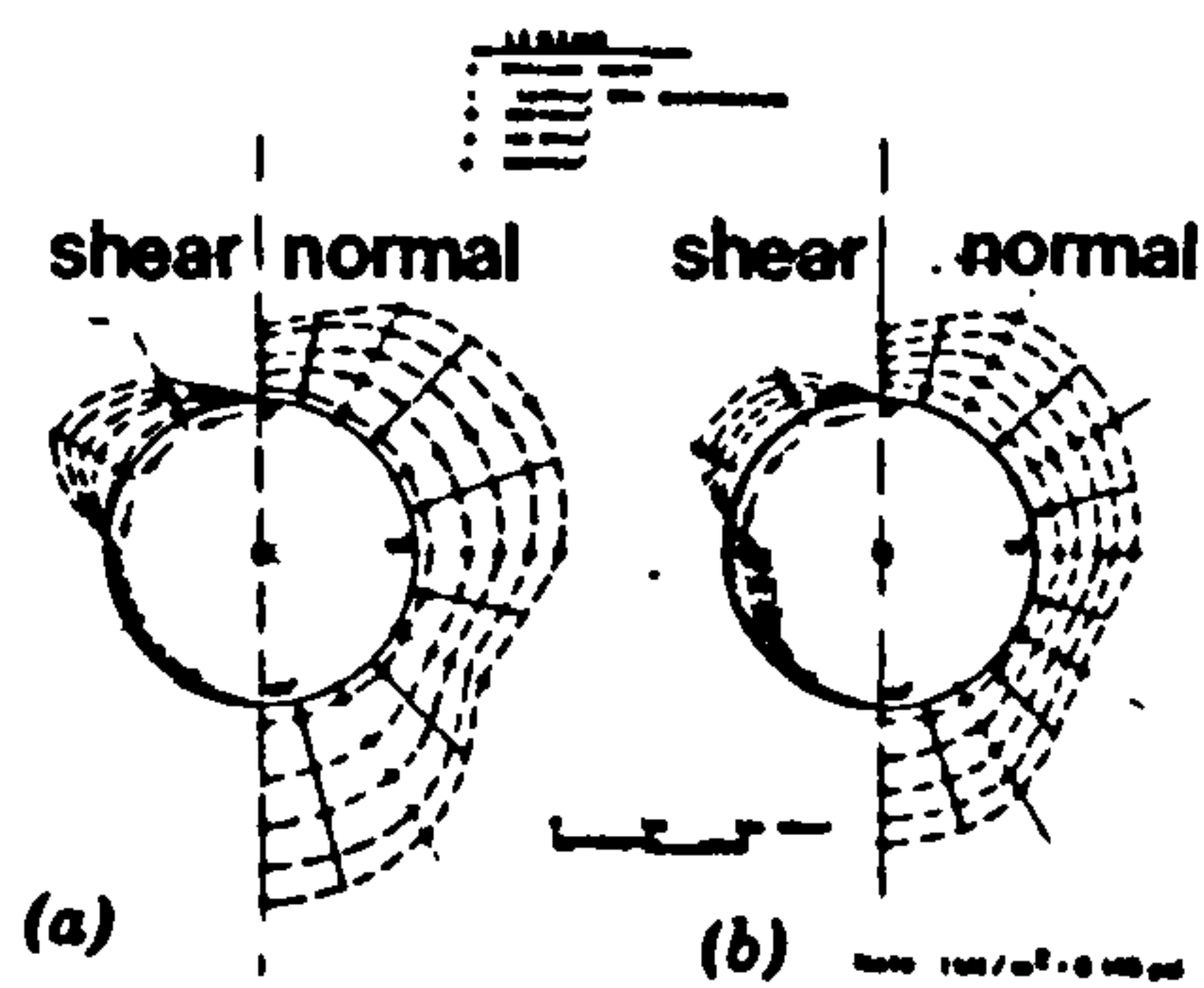


FIG 9.9(c) SHEAR STRESS DISTRIBUTION AFTER SHMULEVICH ET AL. (1986)

FIG 9.10 INITIAL ANALYSIS; CROWN DISPLACEMENT

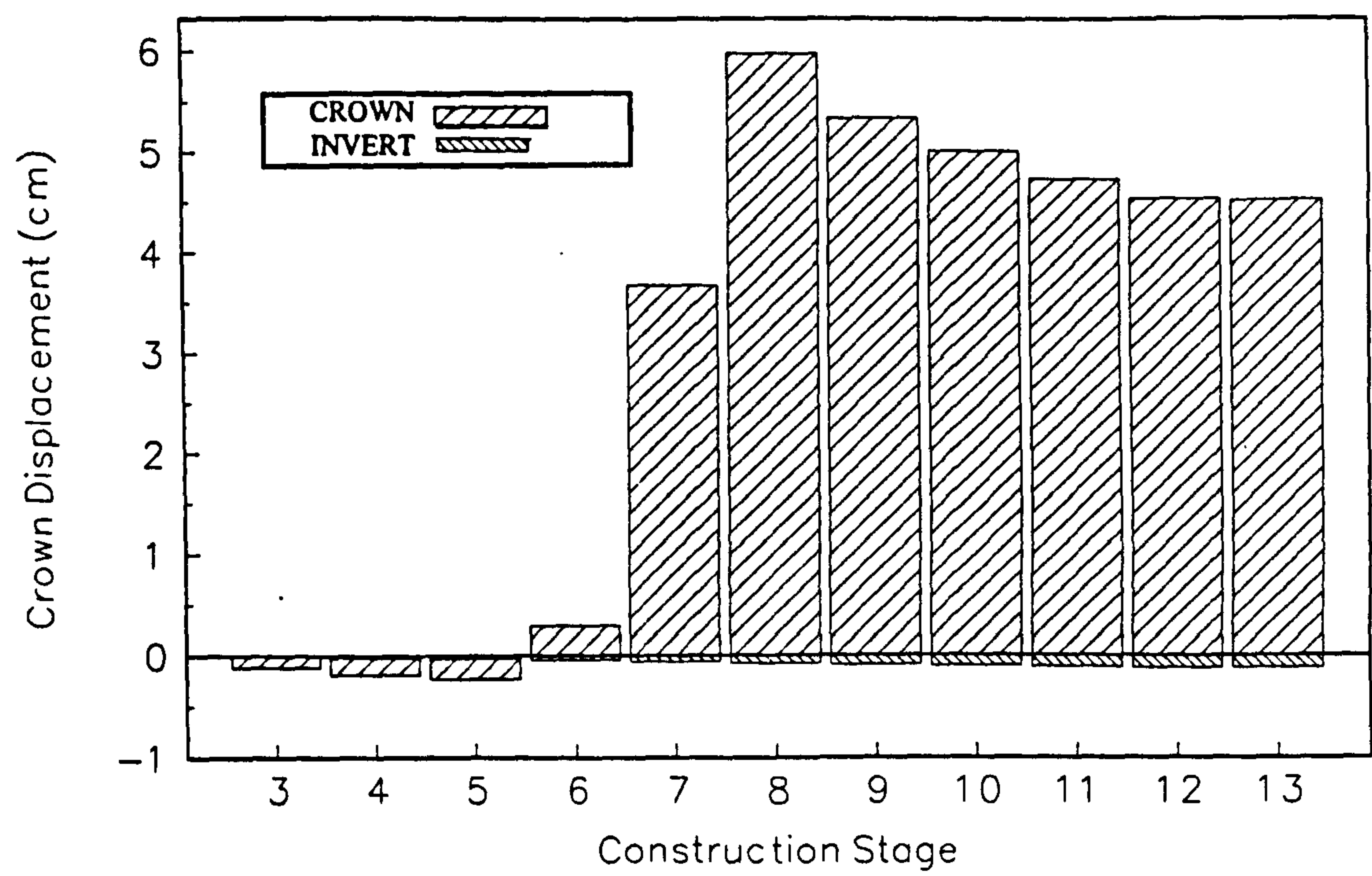
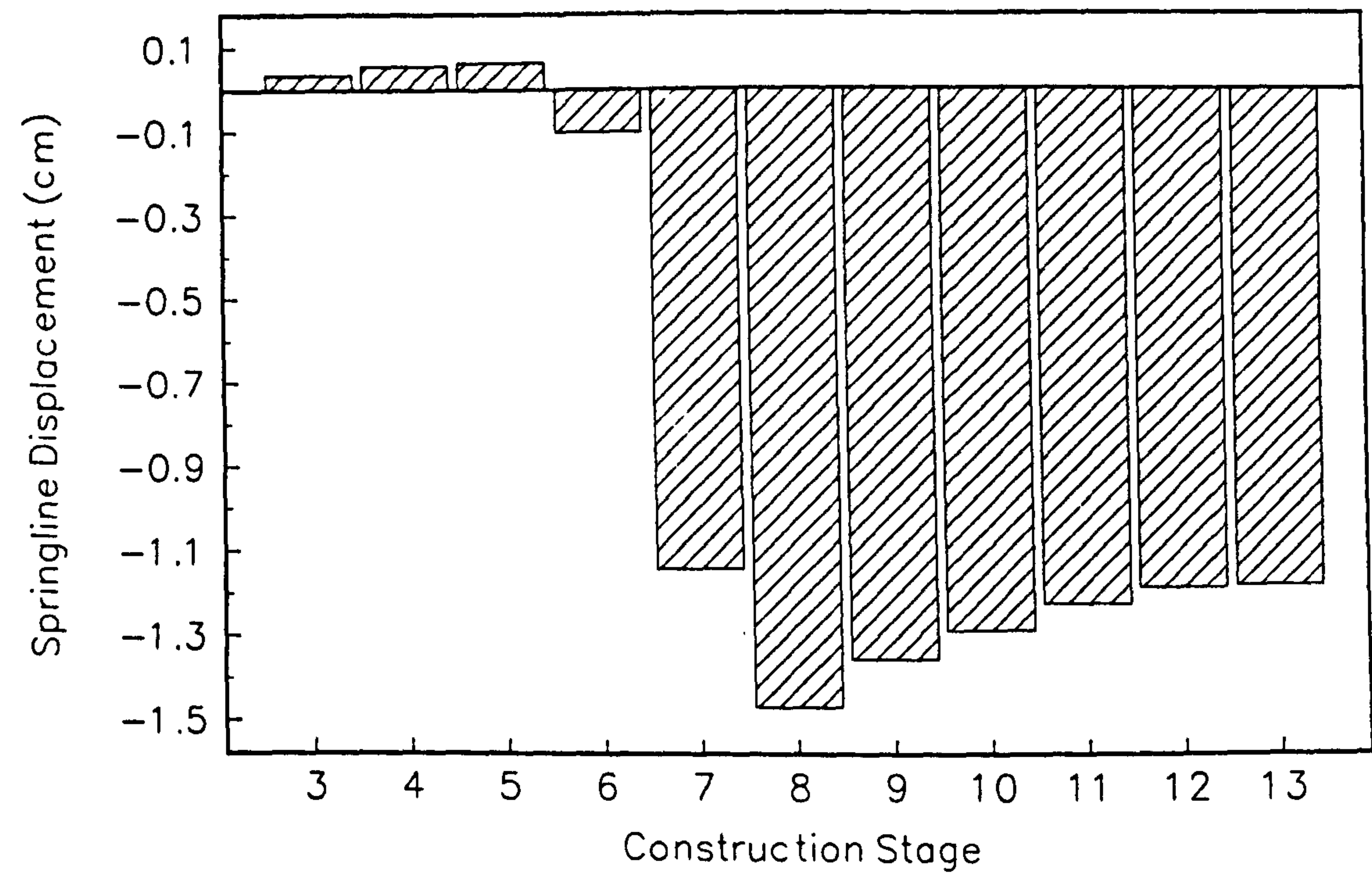


FIG 9.11 INITIAL ANALYSIS; SPRINGLINE DISPLACEMENT



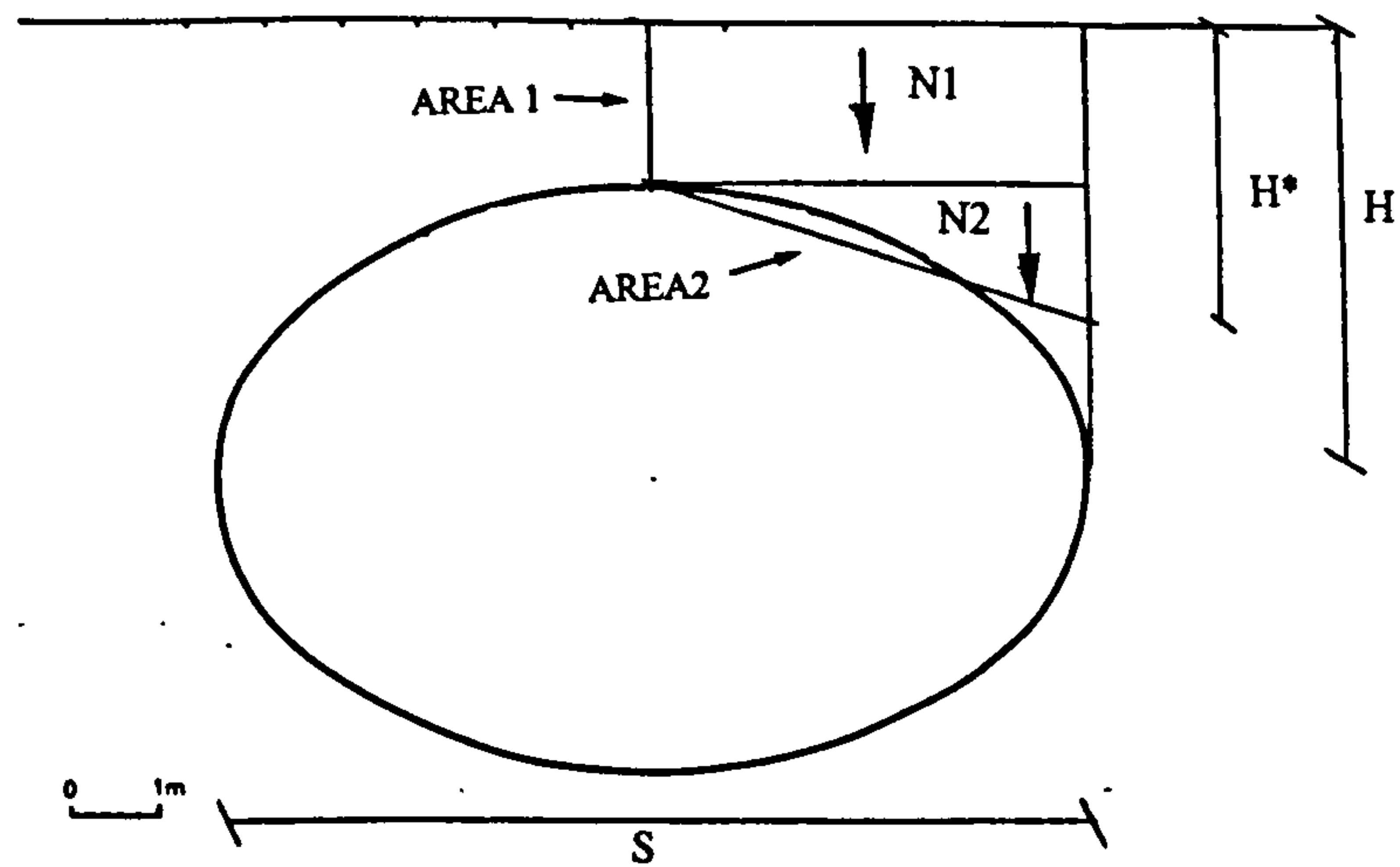


FIG 9.12 DIAGRAM DESCRIBING EQUILIBRIUM THEORY USED TO ESTIMATE CULVERT THRUSTS

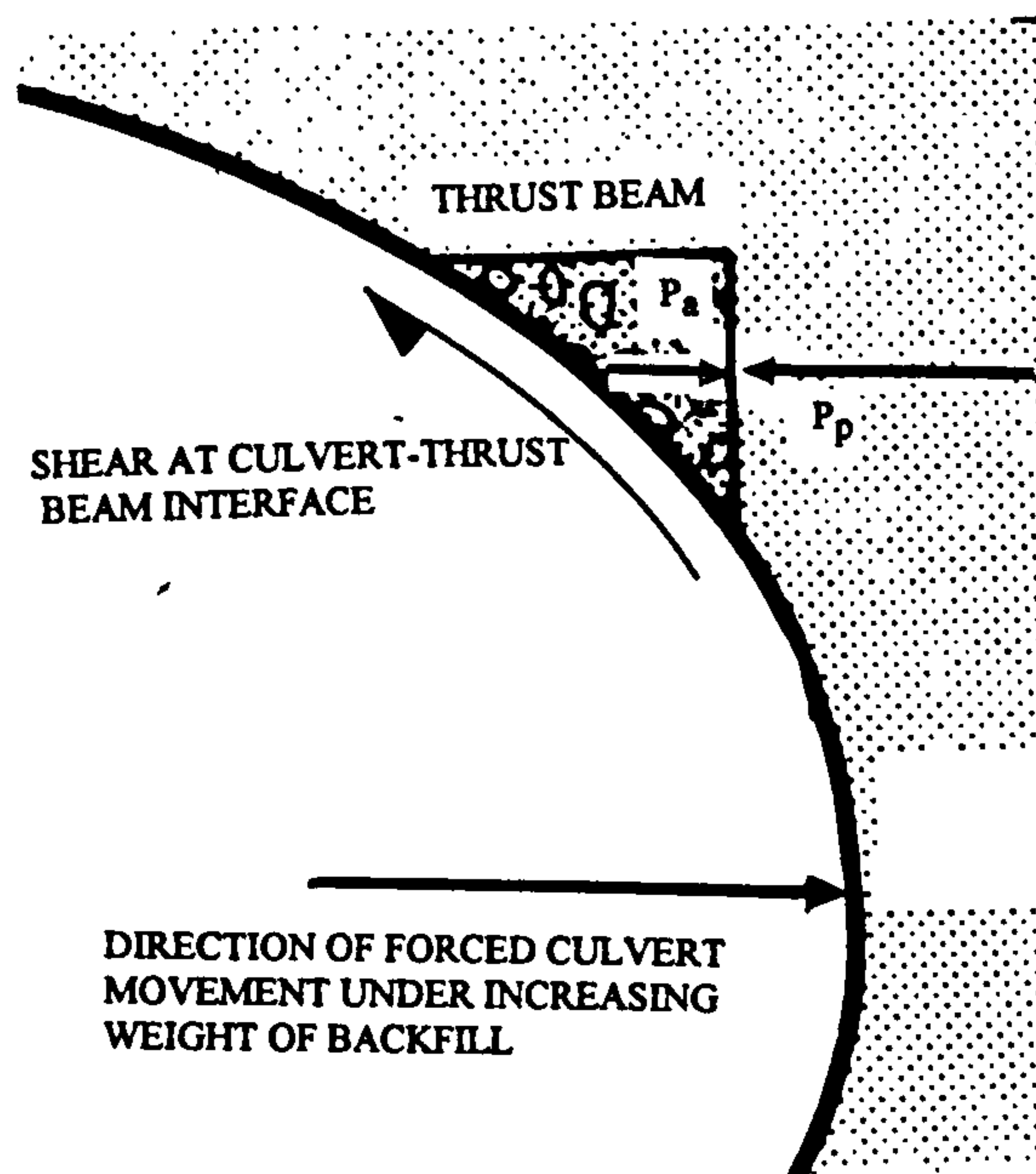


FIG 9.13 DIAGRAM SHOWING THRUST BEAM BEARING INTO BACKFILL

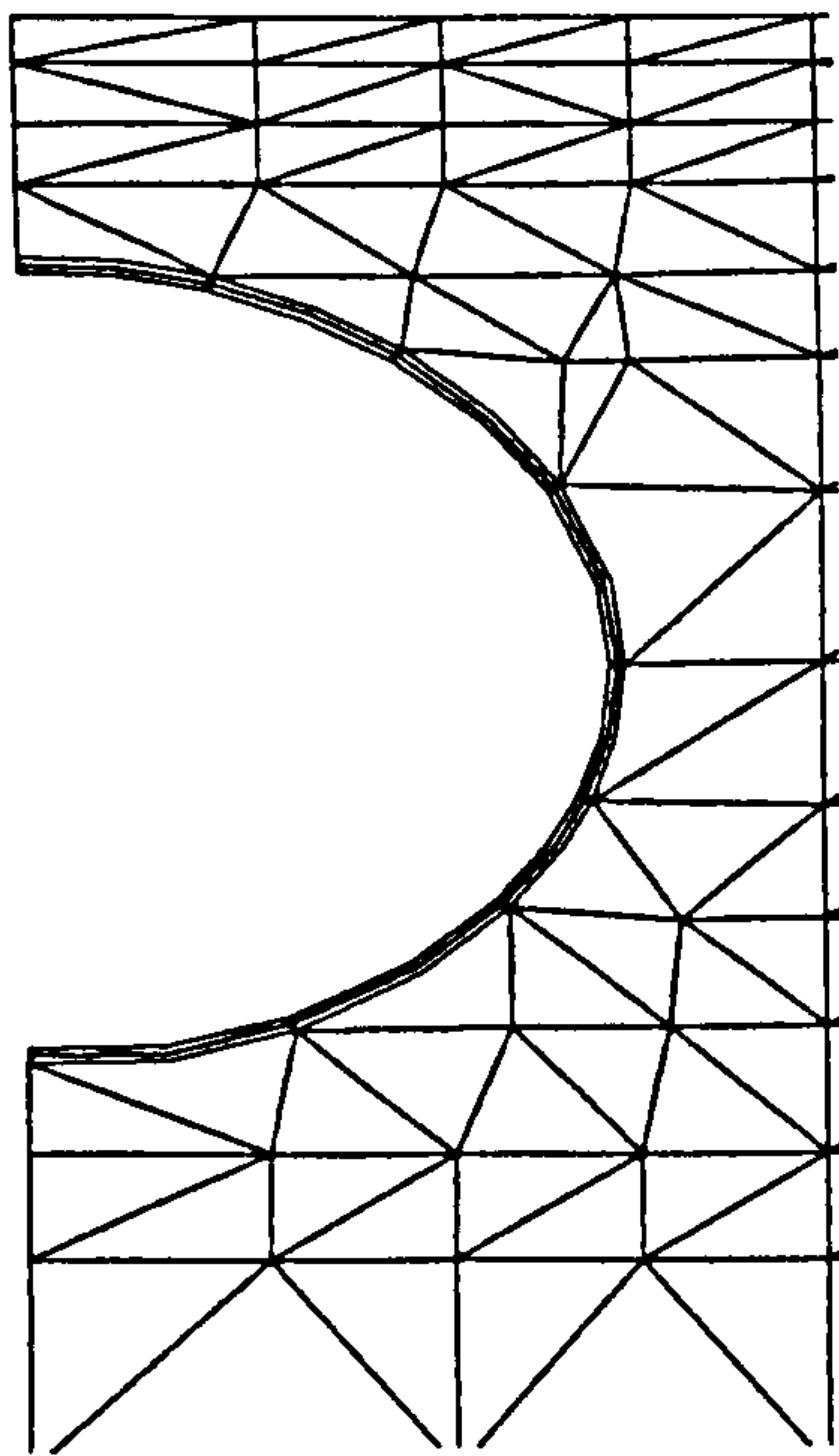


FIG 9.14 FINITE ELEMENT MESH WITH CURVED CULVERT ELEMENTS

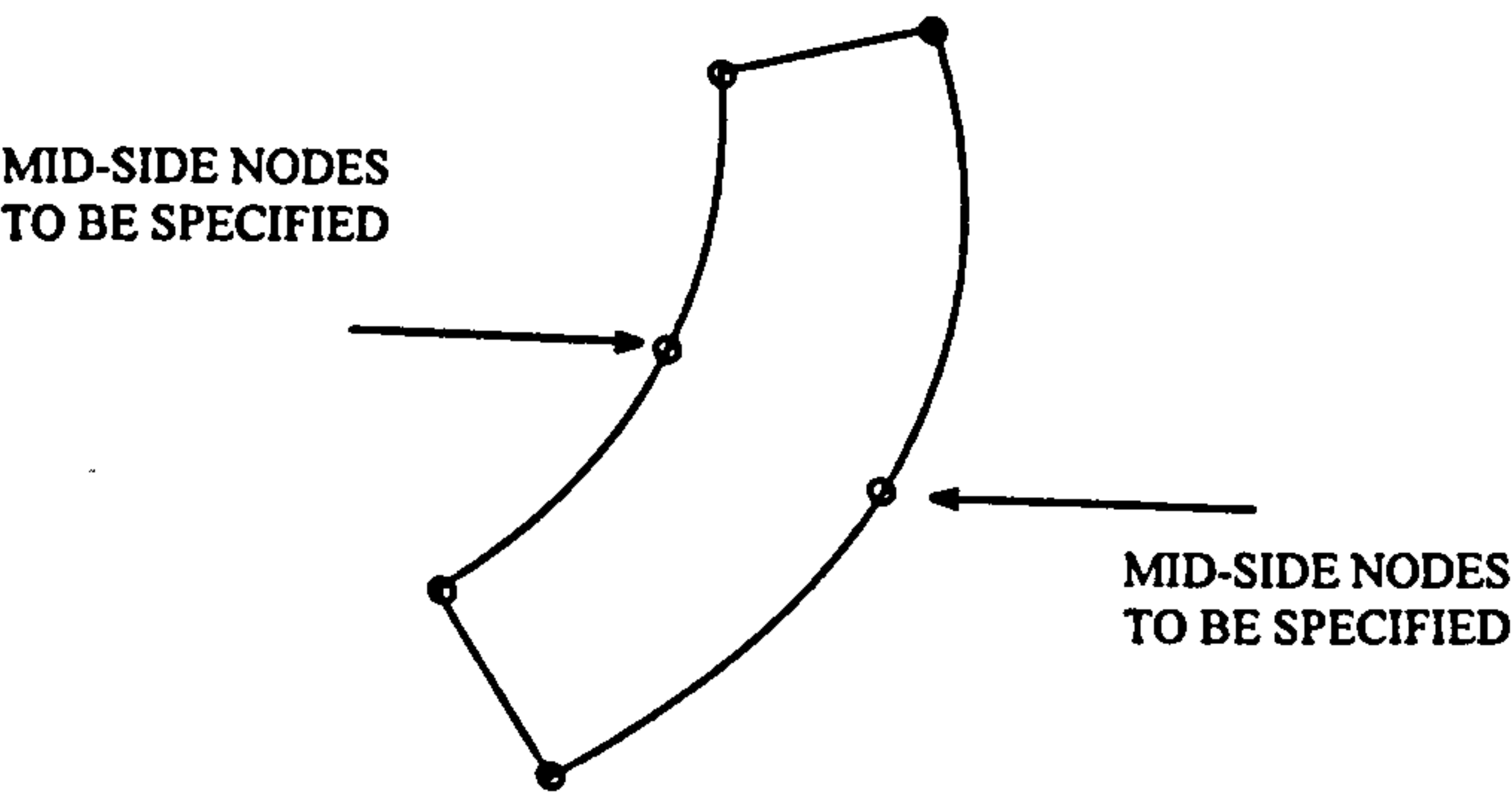


FIG 9.15 SHOWING CURVE-SIDED ELEMENT

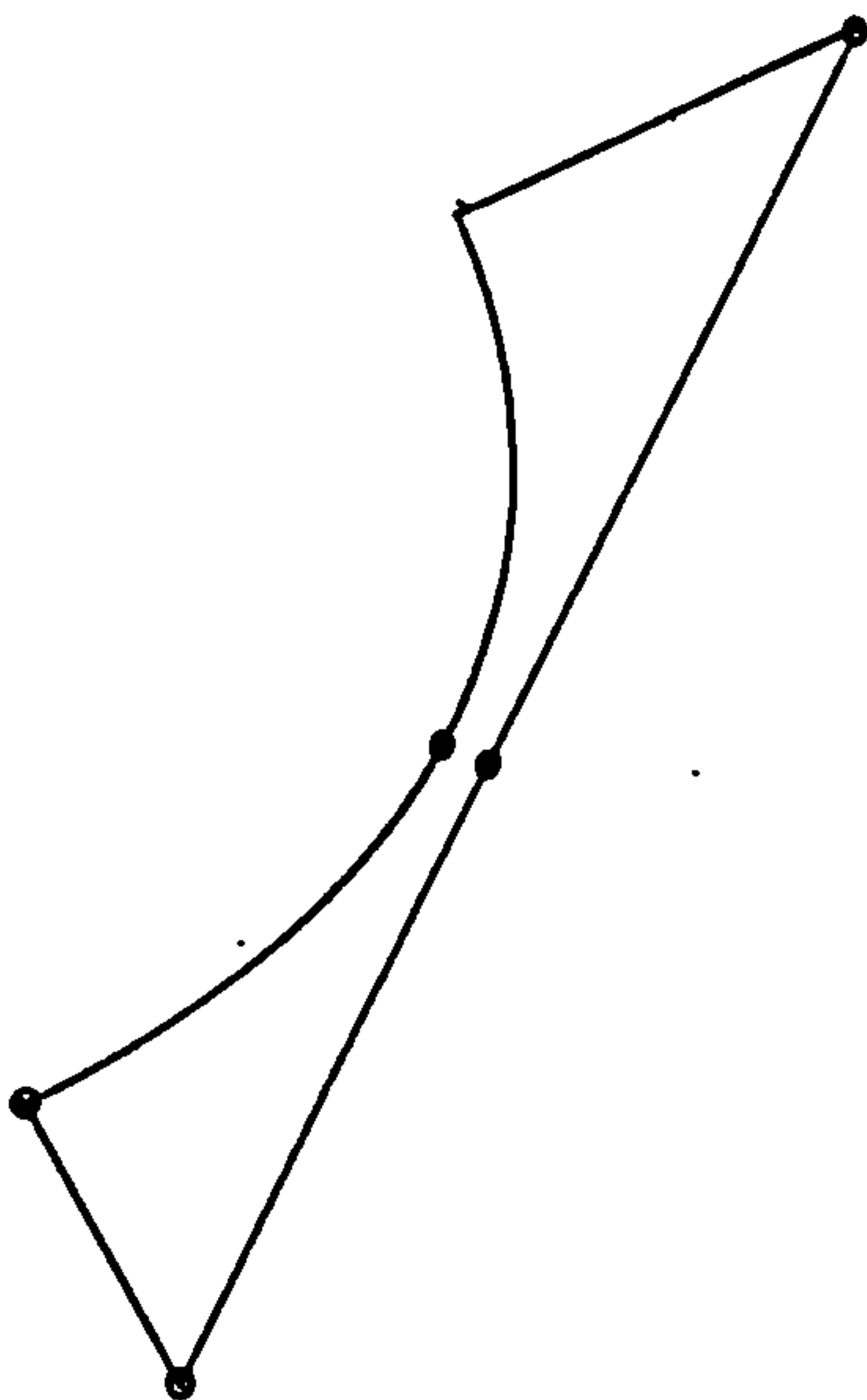


FIG 9.16 SHOWING MODELLING DETAIL FOR ELEMENTS WITH CURVED SIDES

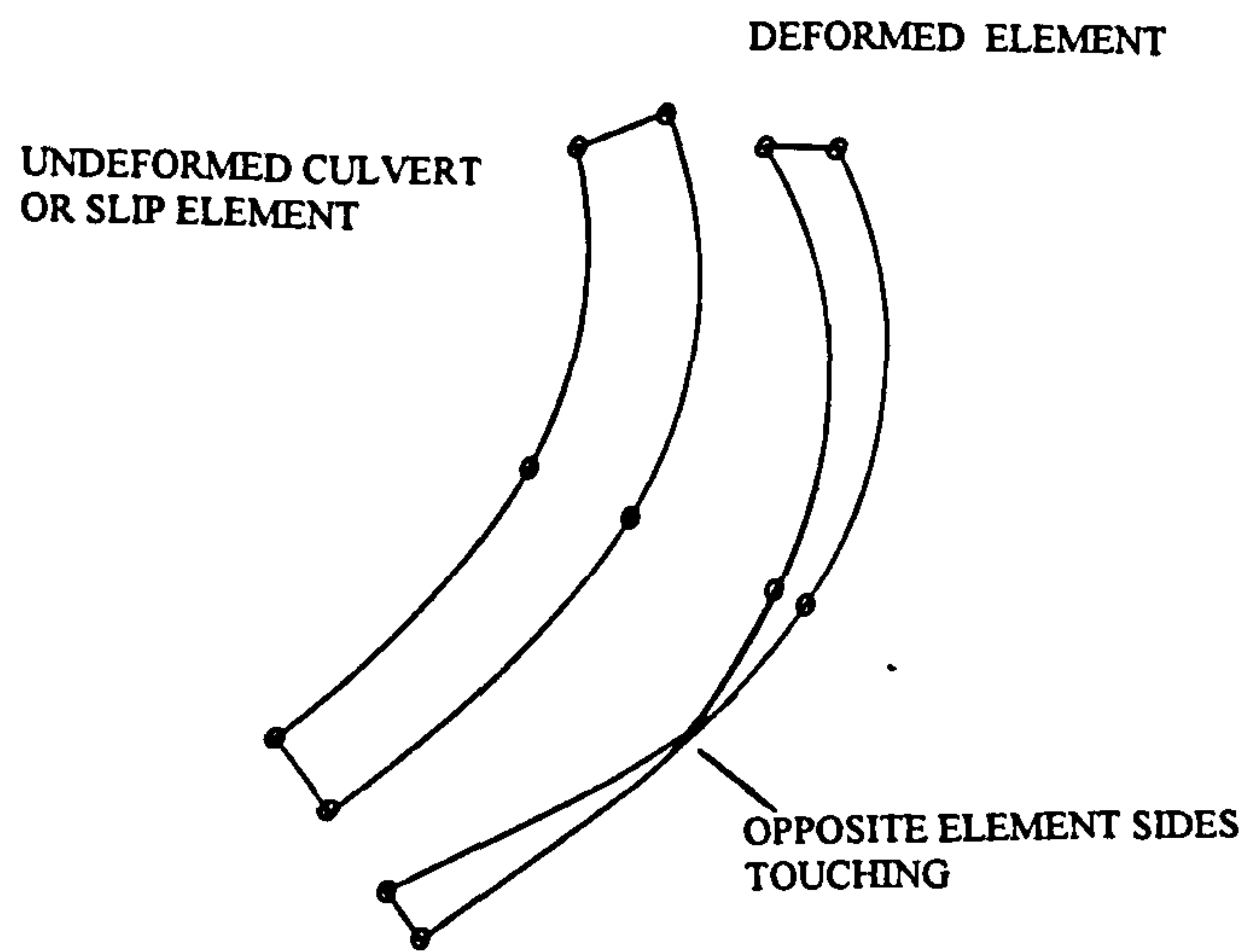
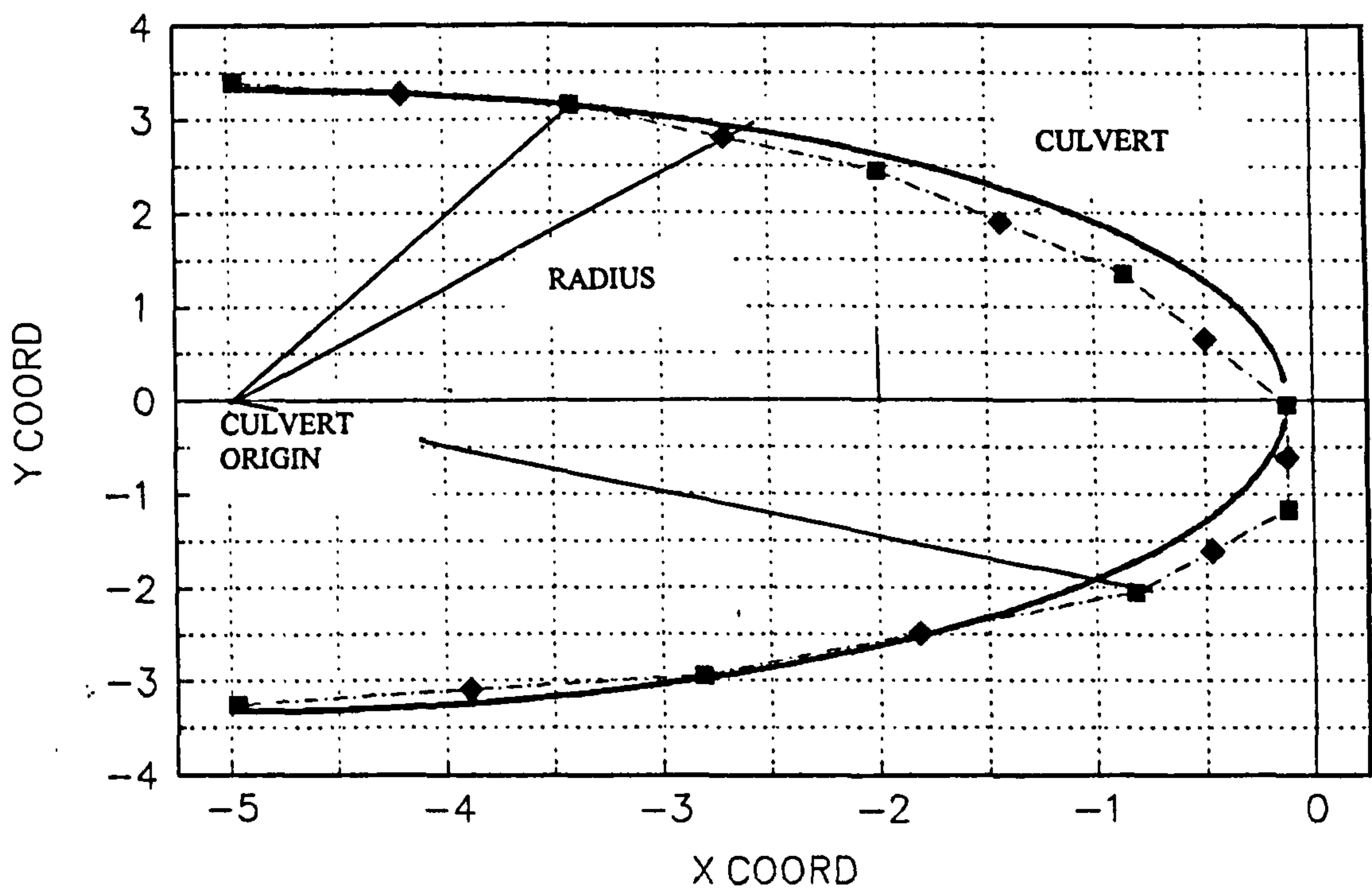


FIG 9.17 MODELLING DETAIL FOR ELEMENTS WITH CURVED SIDES

FIG 9.18 TRANSLATION OF RECTANGULAR CULVERT ELEMENT MESH TO A CURVED CULVERT ELEMENT MESH.



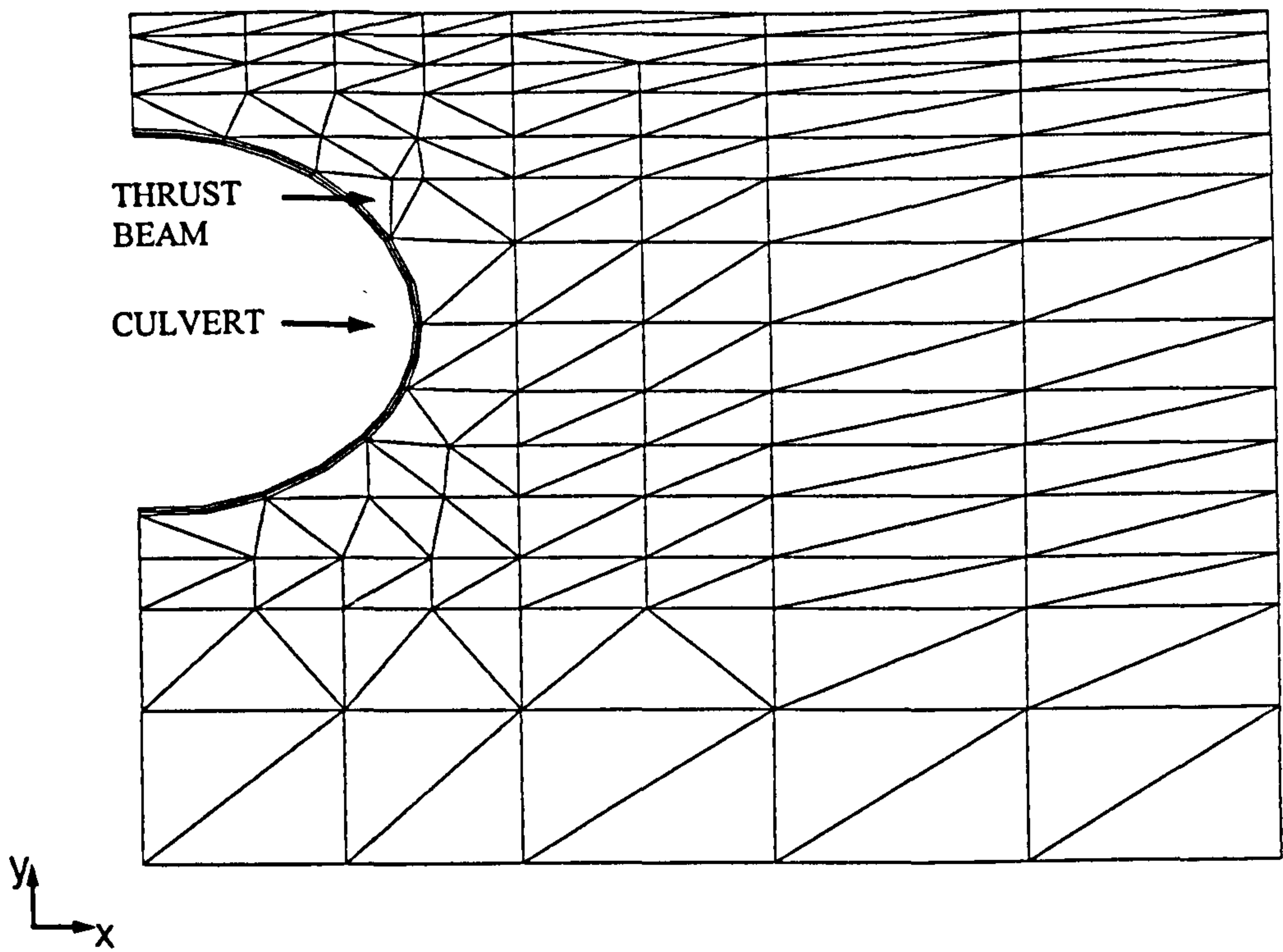


FIG 9.19 FINITE ELEMENT MESH USED WITH CURVED CULVERT ELEMENTS

FIG 9.20 CURVE-SIDED CULVERT ELEMENTS; THRUST

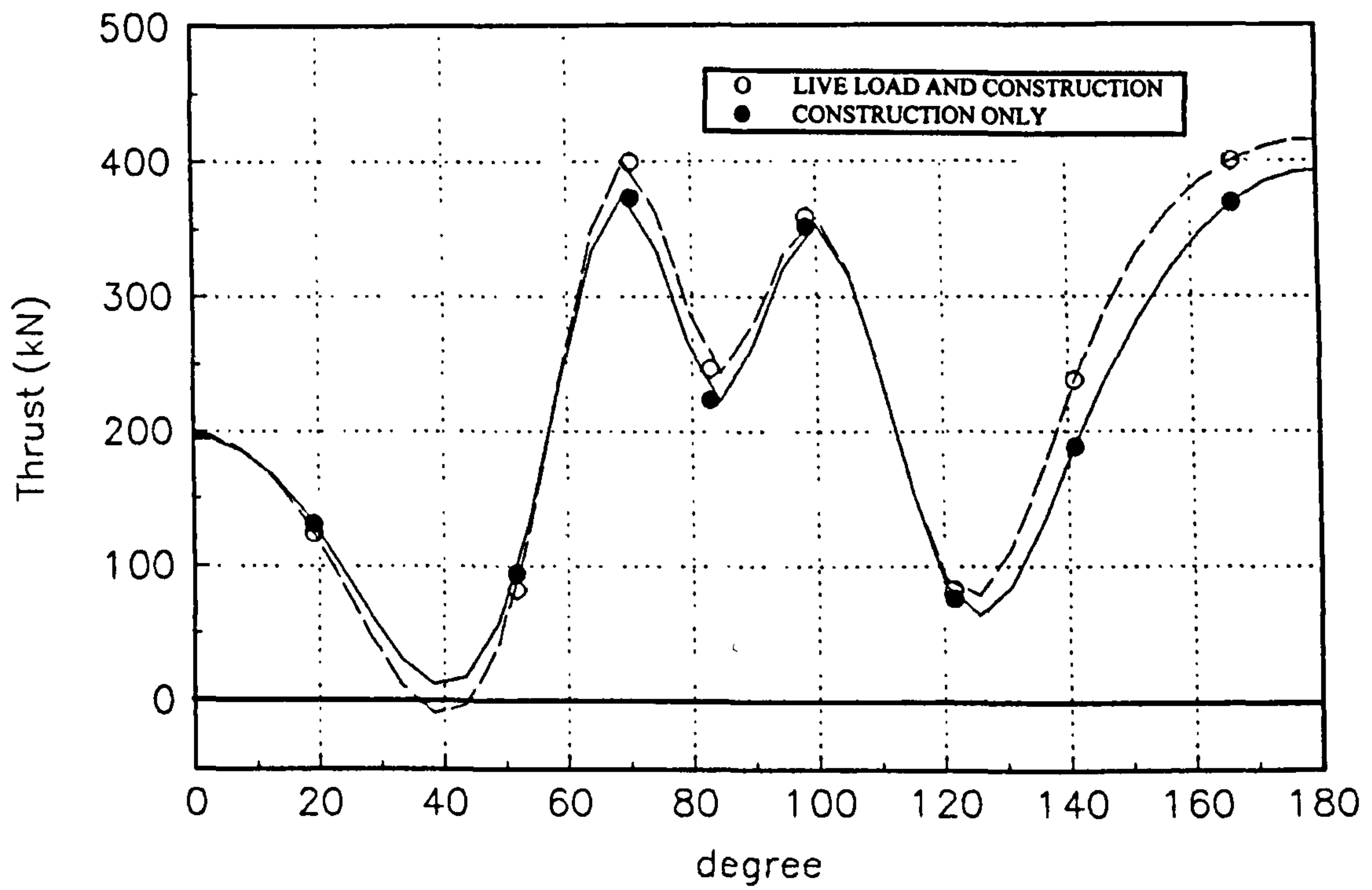


FIG 9.21 CURVE-SIDED CULVERT ELEMENTS; BENDING MOMENT

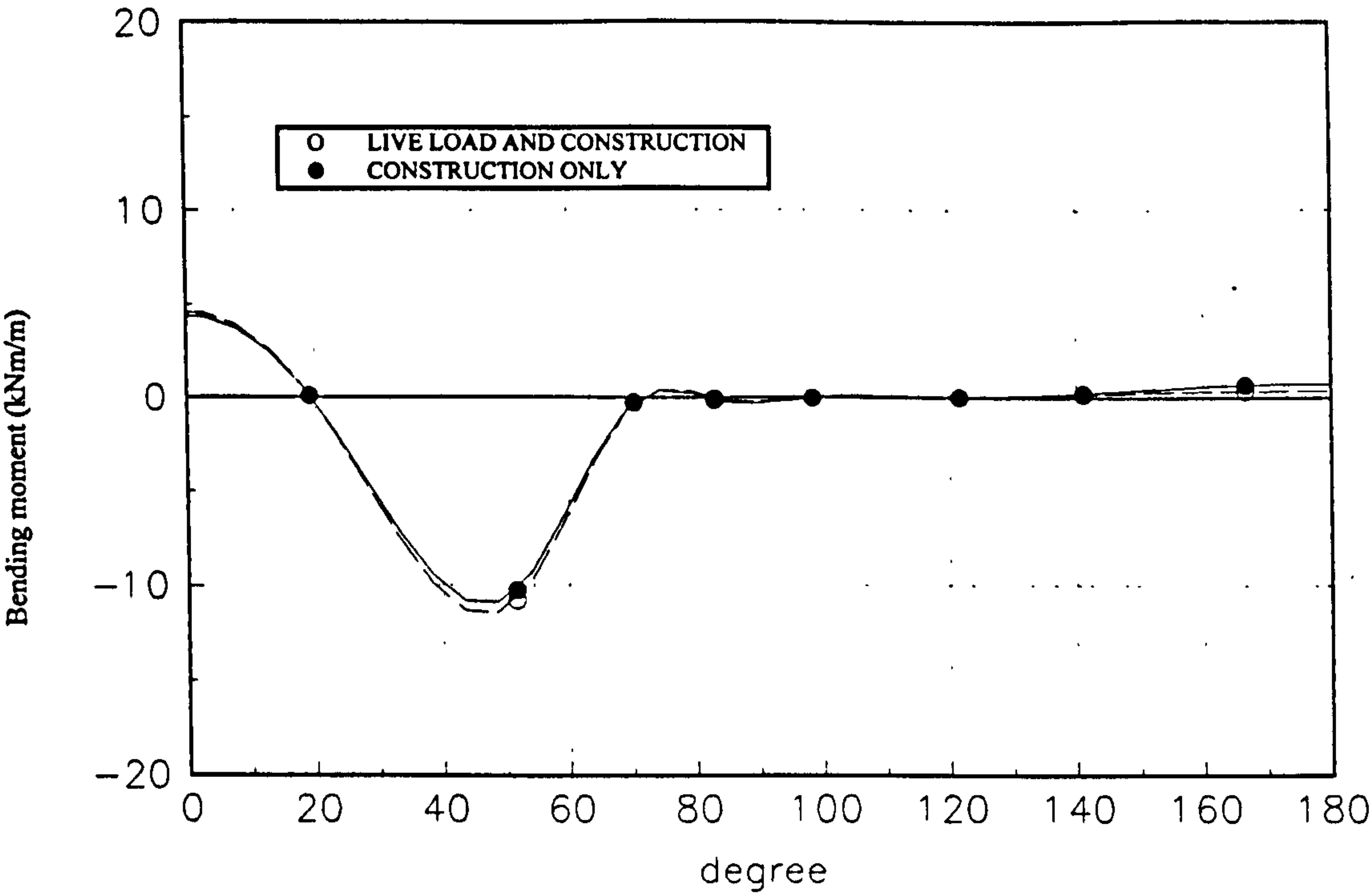


FIG 9.22 CURVE-SIDED CULVERT ELEMENTS; RADIAL STRESS

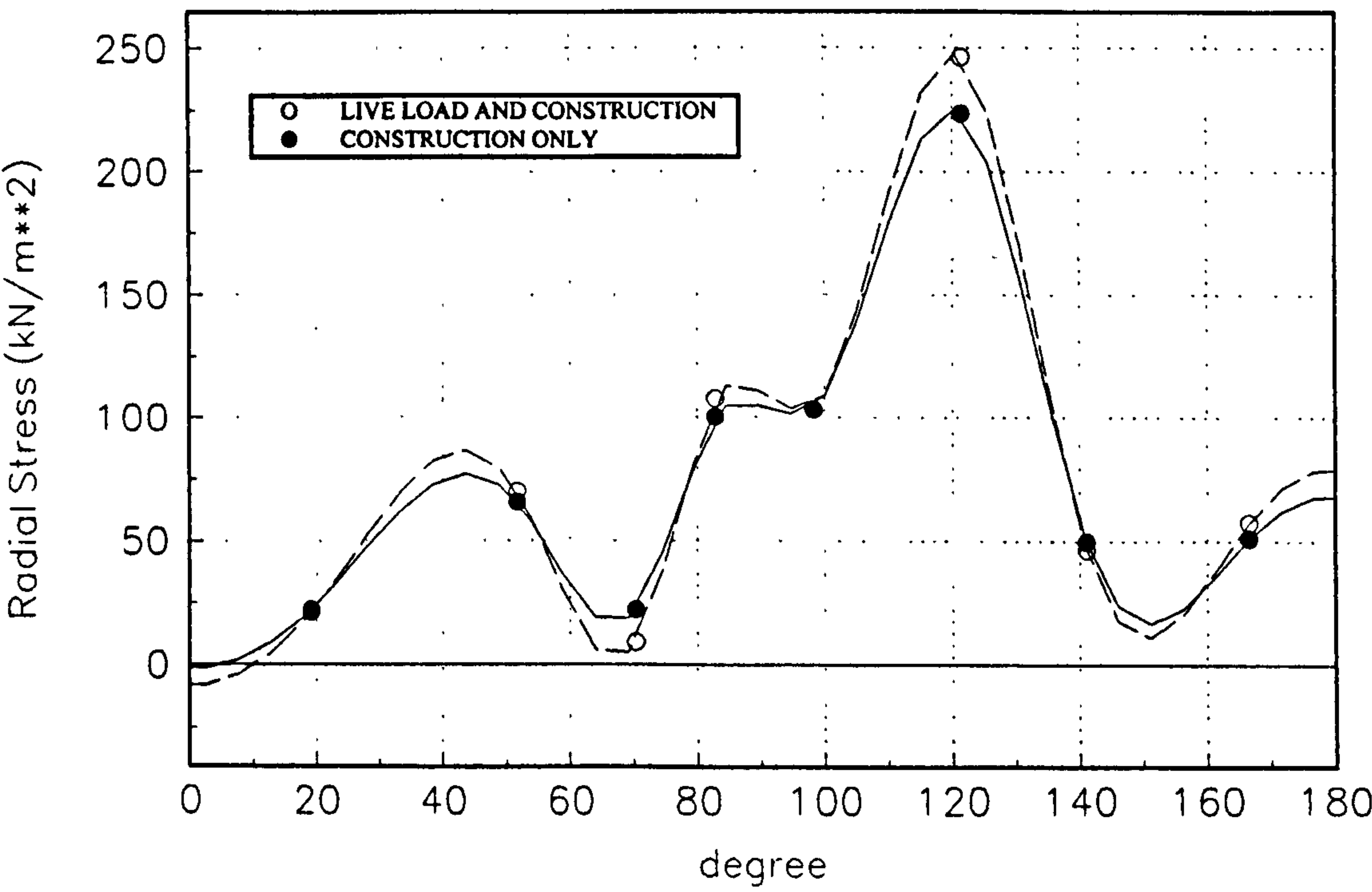


FIG 9.23 CURVE-SIDED CULVERT ELEMENTS; SHEAR STRESS

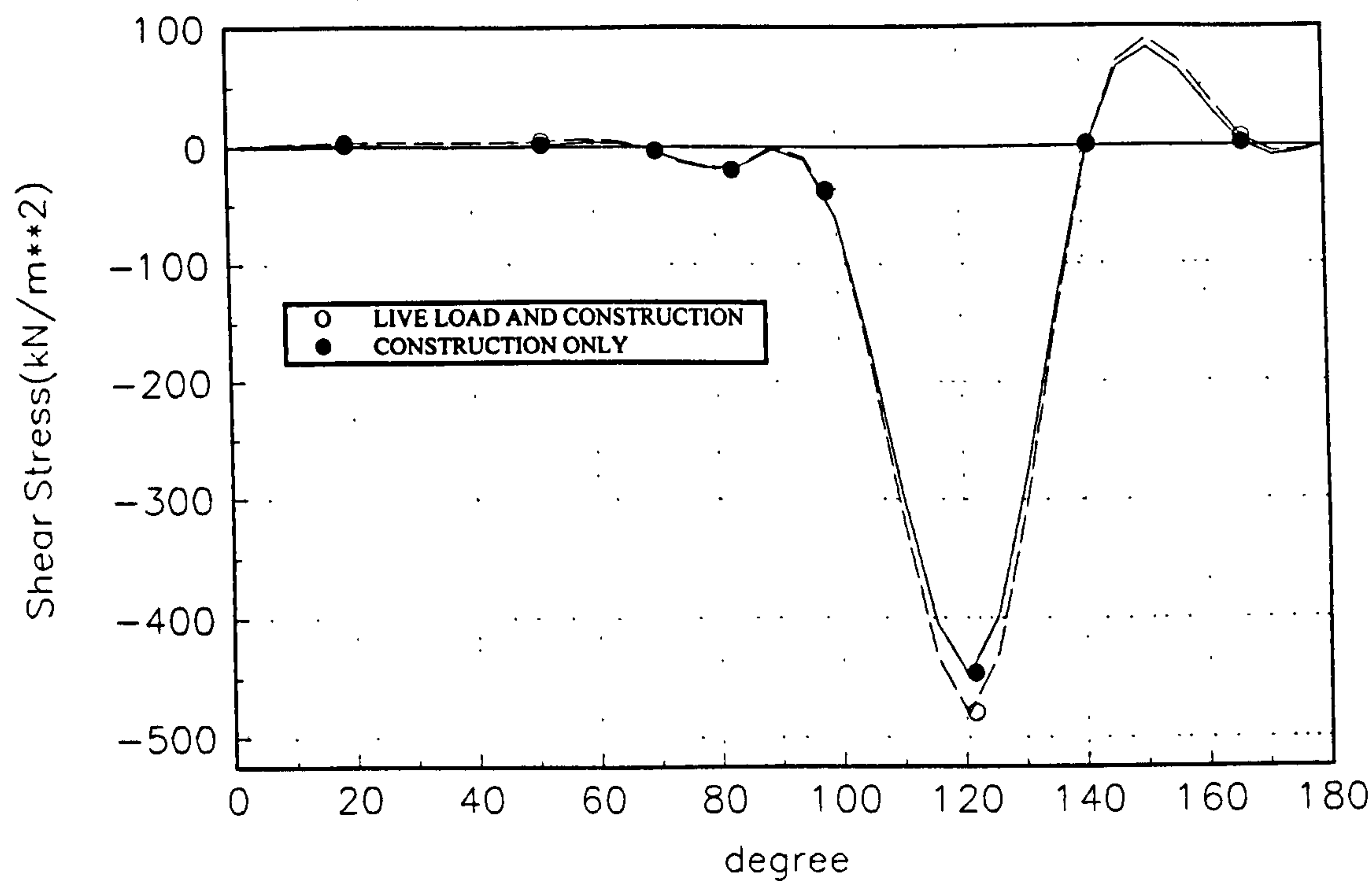


FIG 9.24 CURVE-SIDED CULVERT ELEMENTS; CROWN DISPLACEMENT

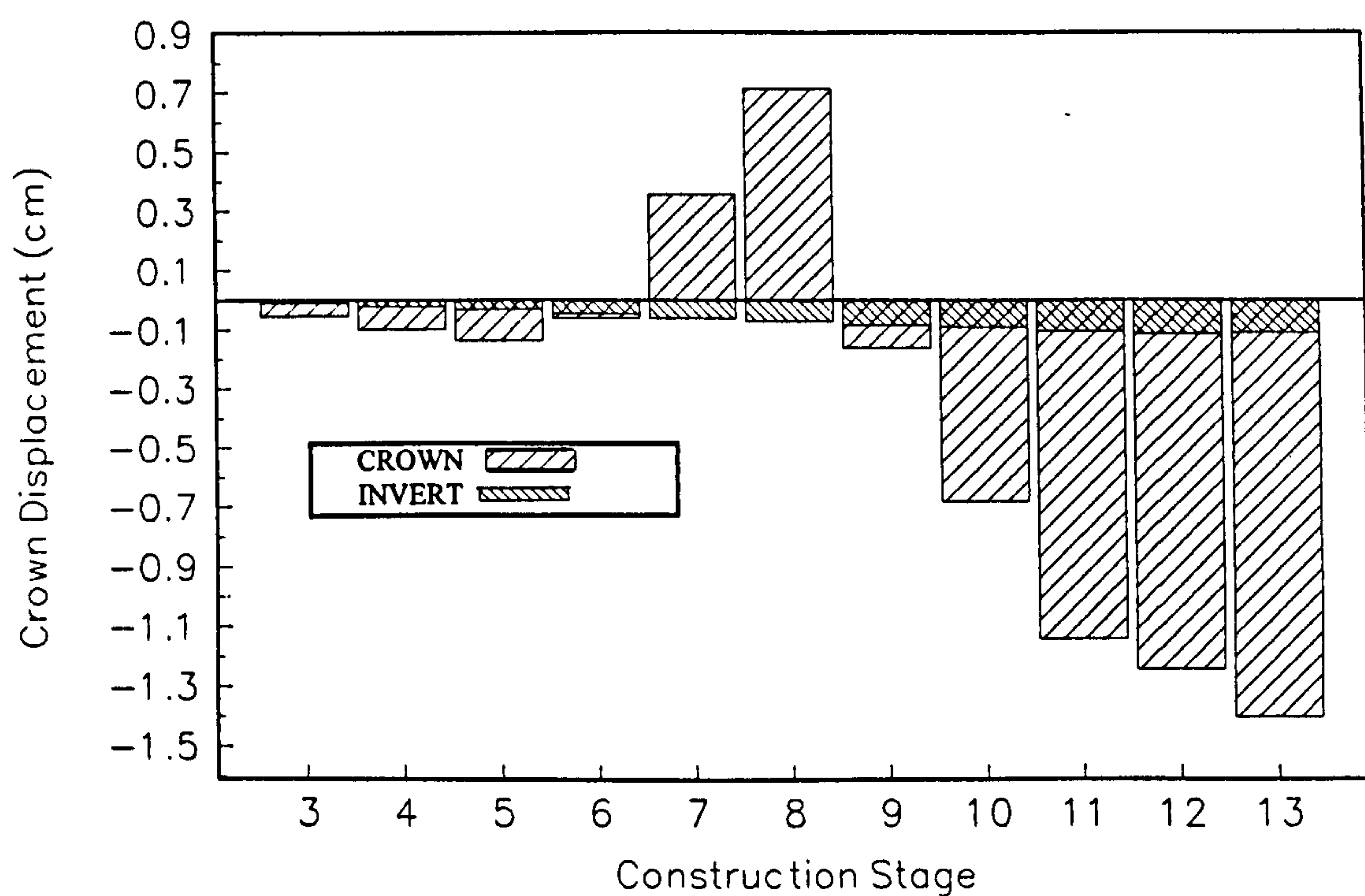


FIG 9.25 CURVE-SIDED CULVERT ELEMENTS; SPRINGLINE DISPLACEMENT

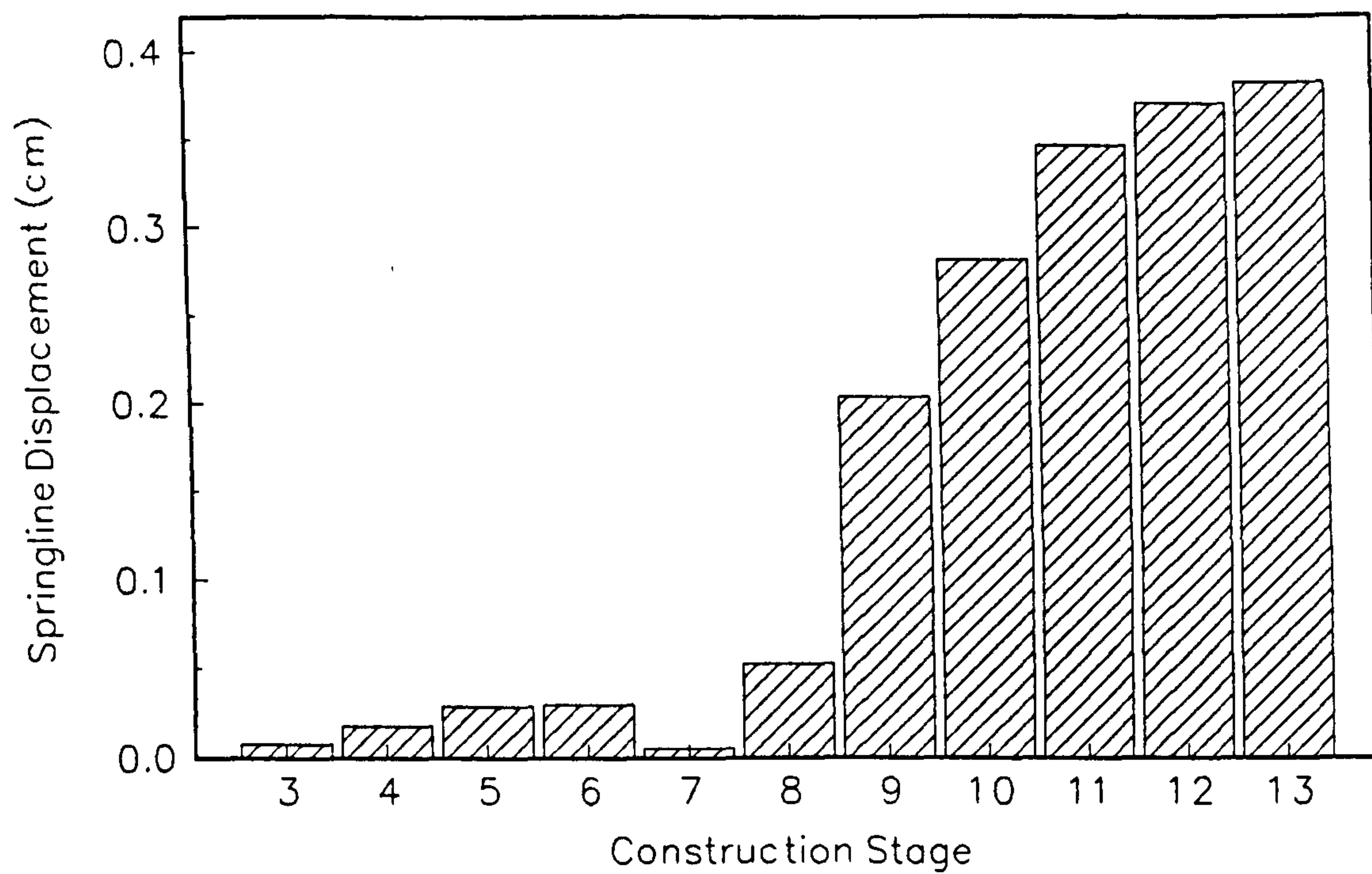


FIG 9.26 THRUST ($\nu_f=0.4$)

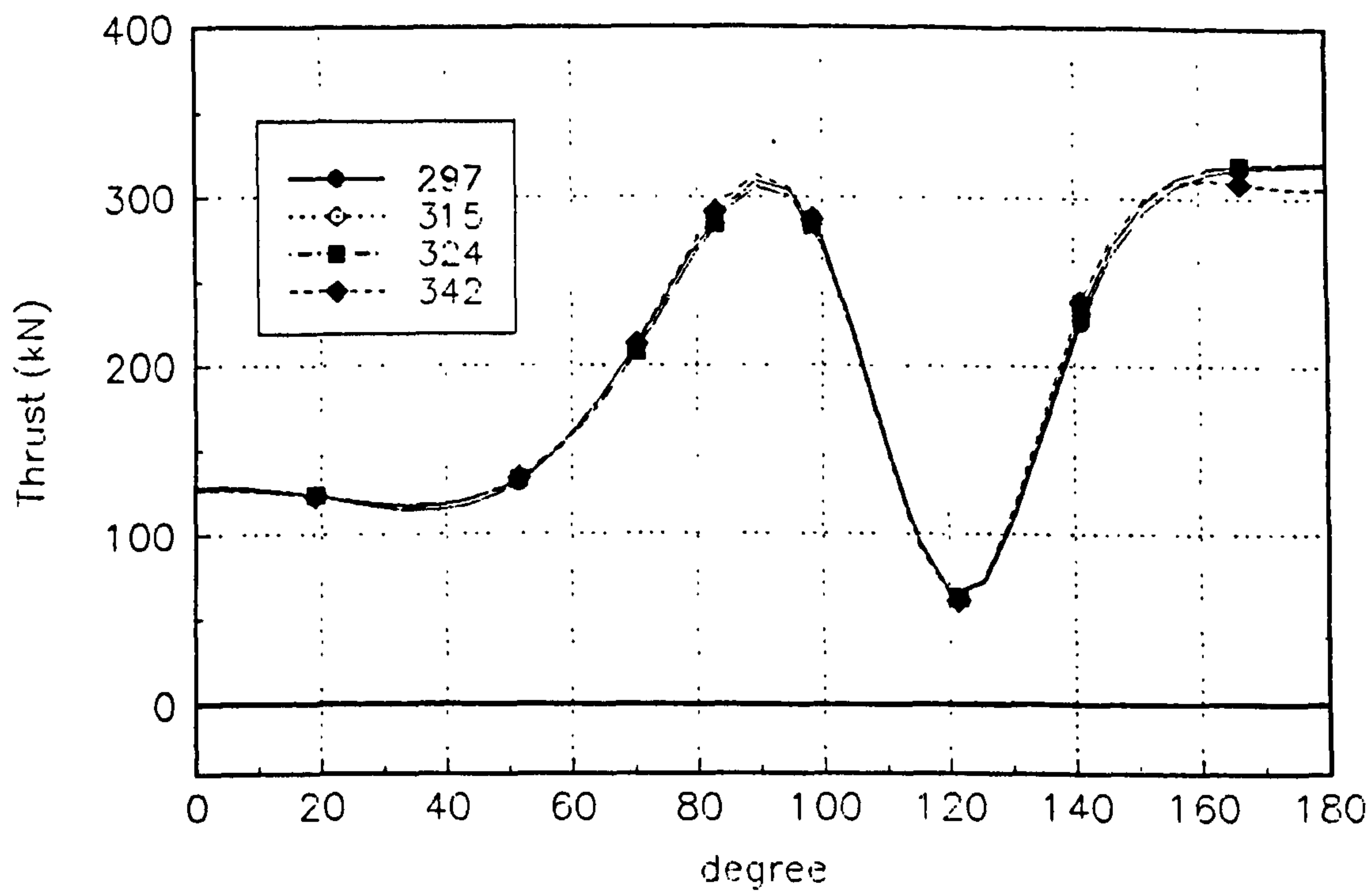


FIG 9.27 BENDING MOMENT ($\nu_f=0.4$)

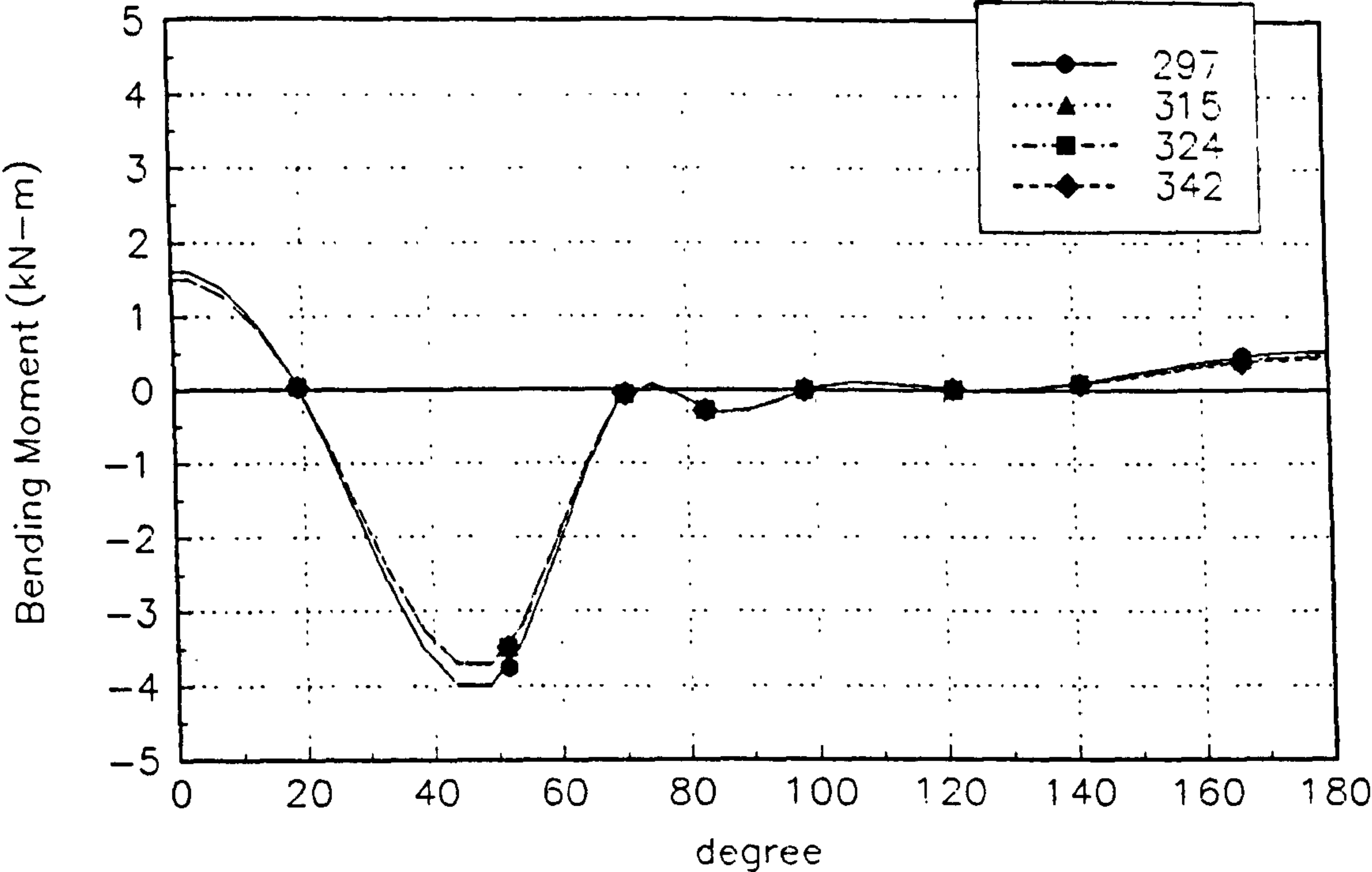


FIG 9.28 RADIAL STRESS ($\nu_f=0.4$)

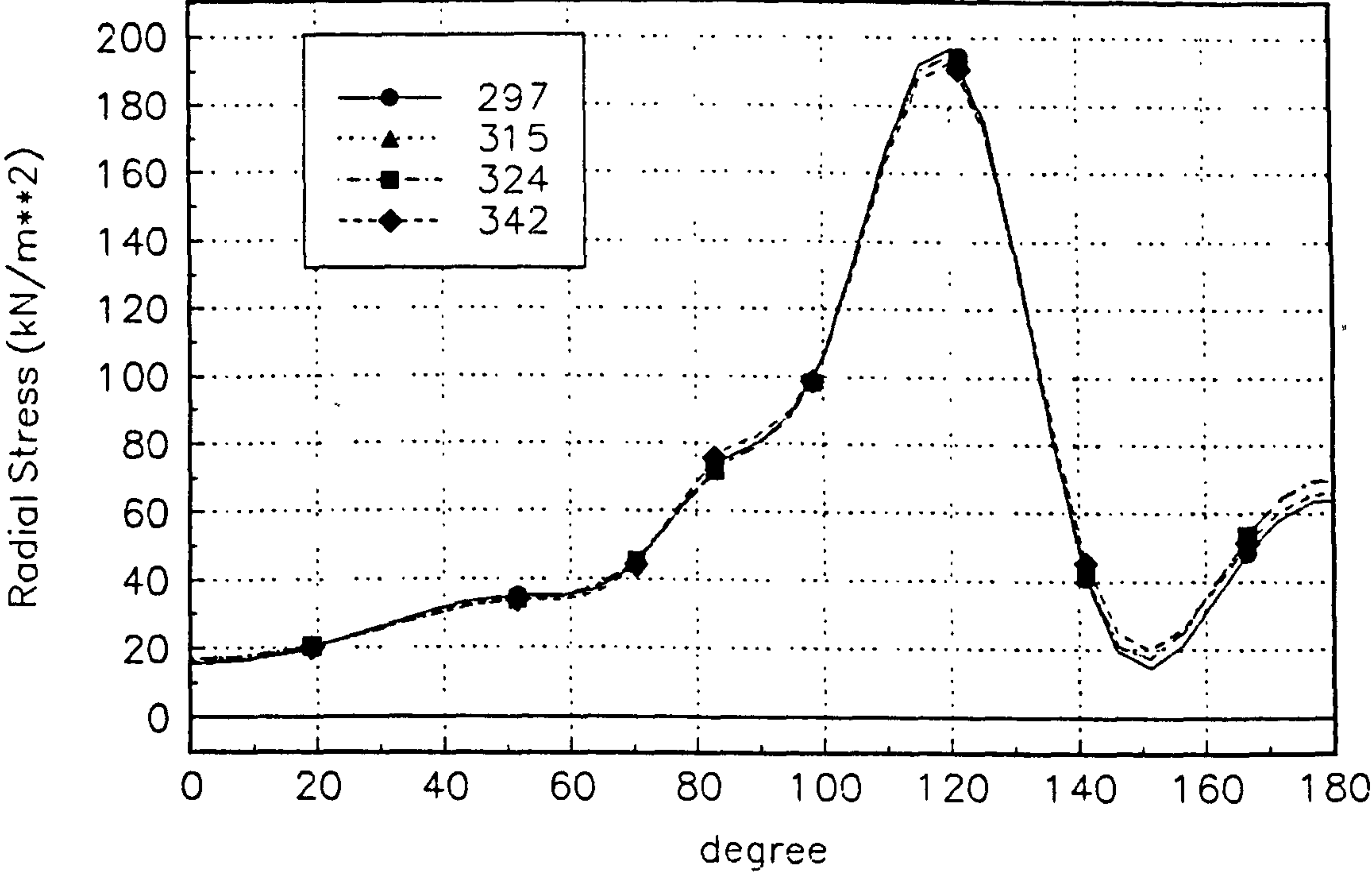


FIG 9.29 SHEAR STRESS ($v_f=0.4$)

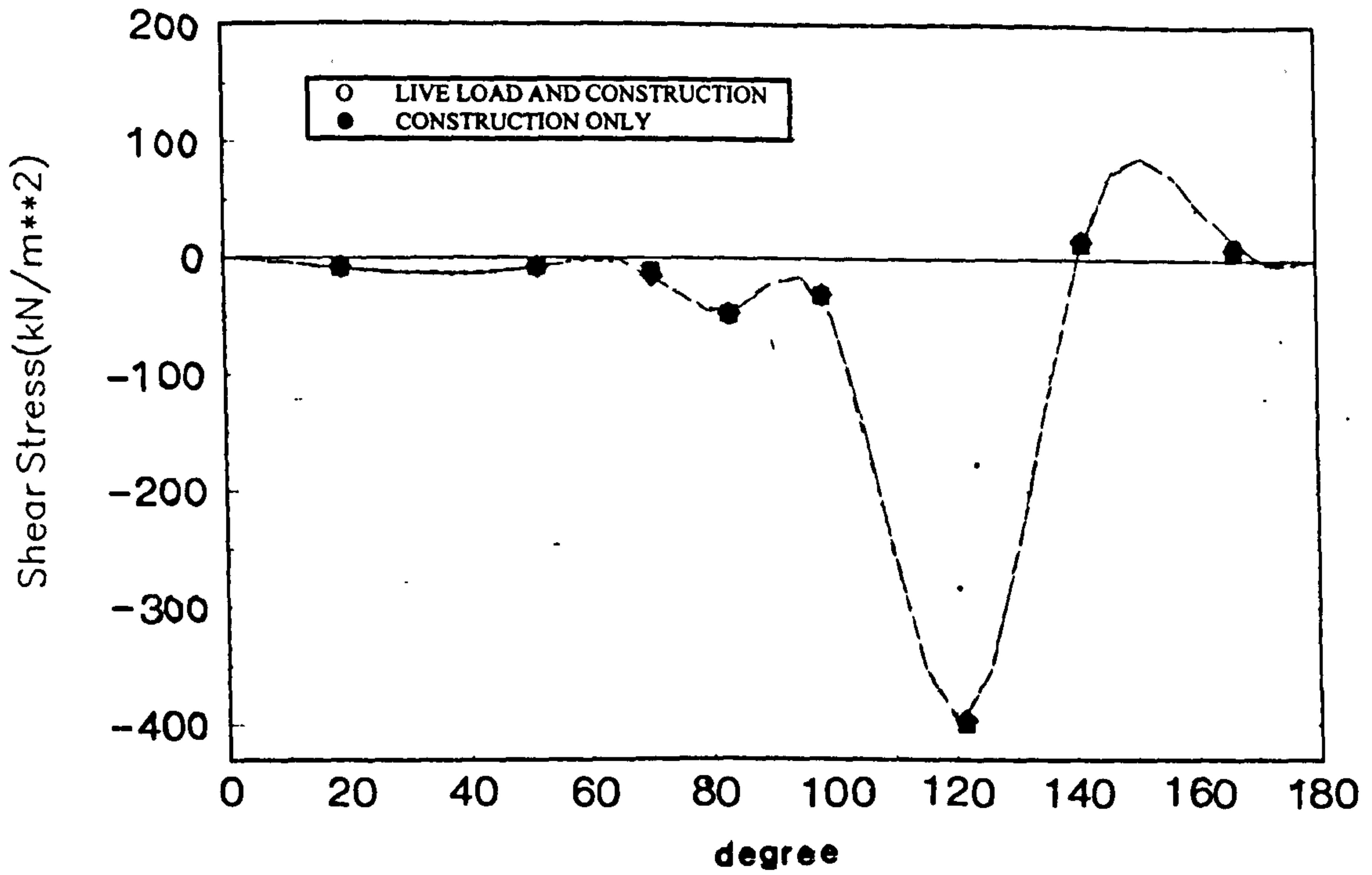


FIG 9.30 CROWN DISPLACEMENT ($v_f=0.4$)

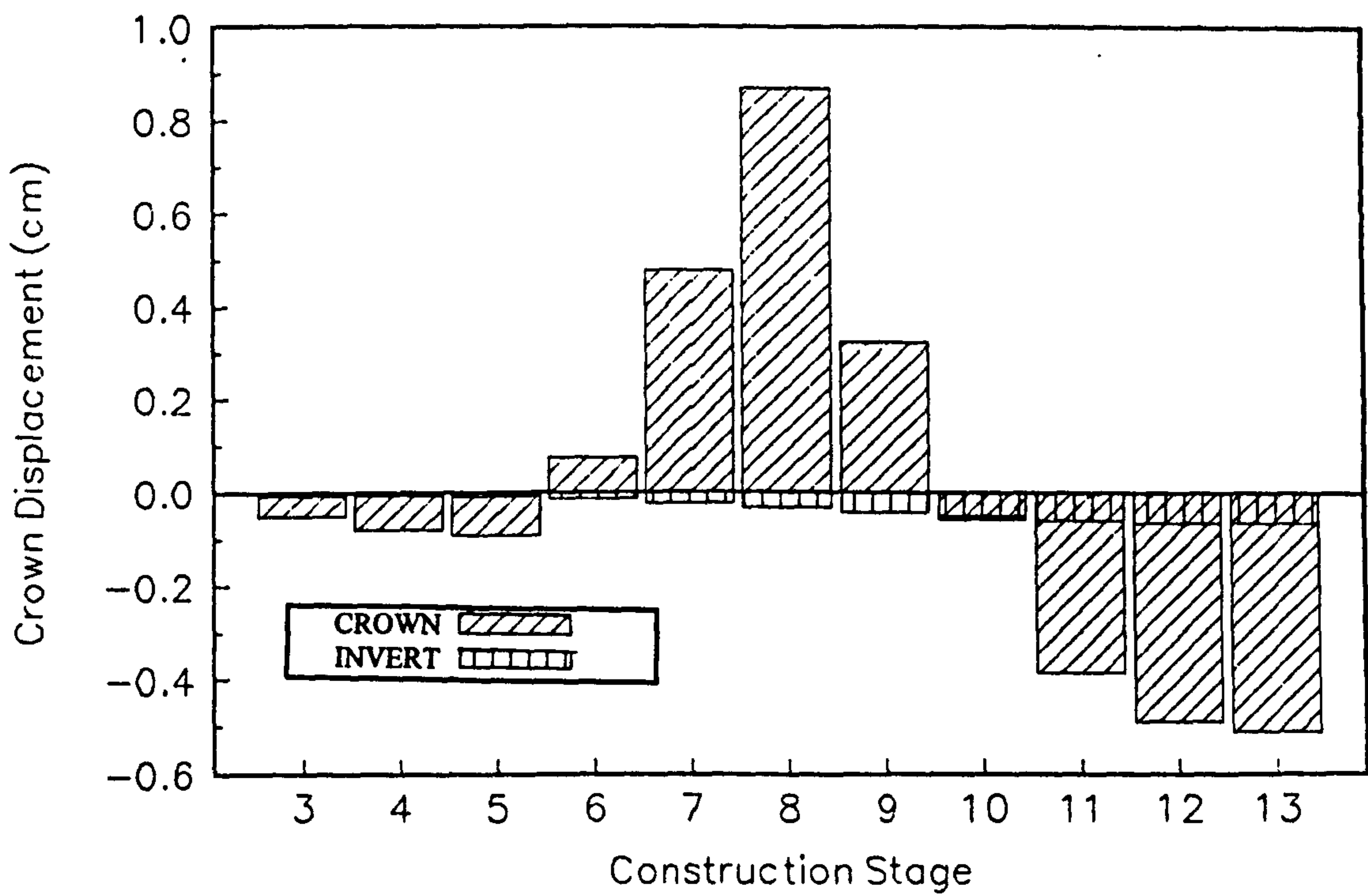


FIG 9.31 SPRINGLINE DISPLACEMENT ($\nu_f=0.4$)

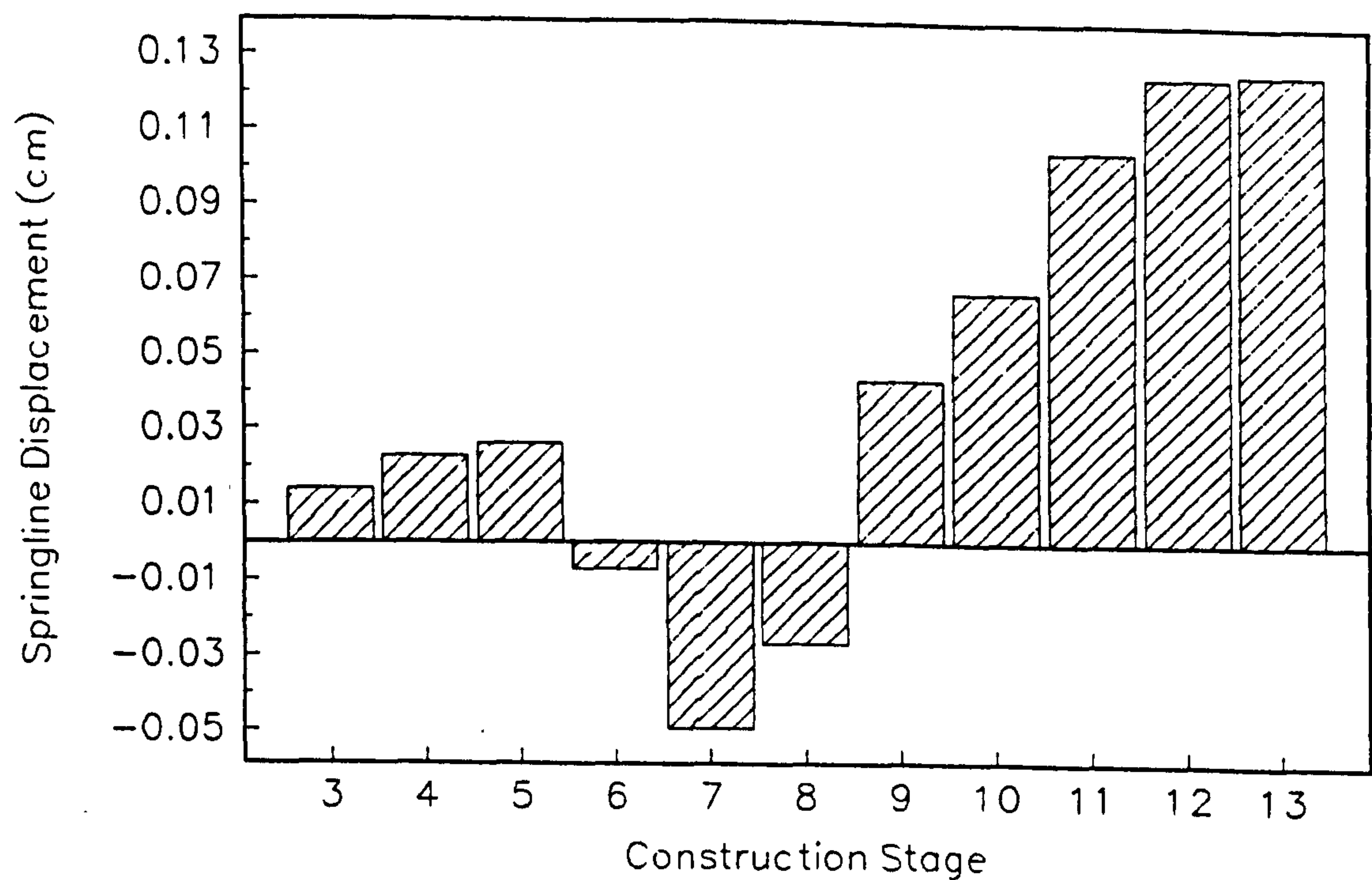
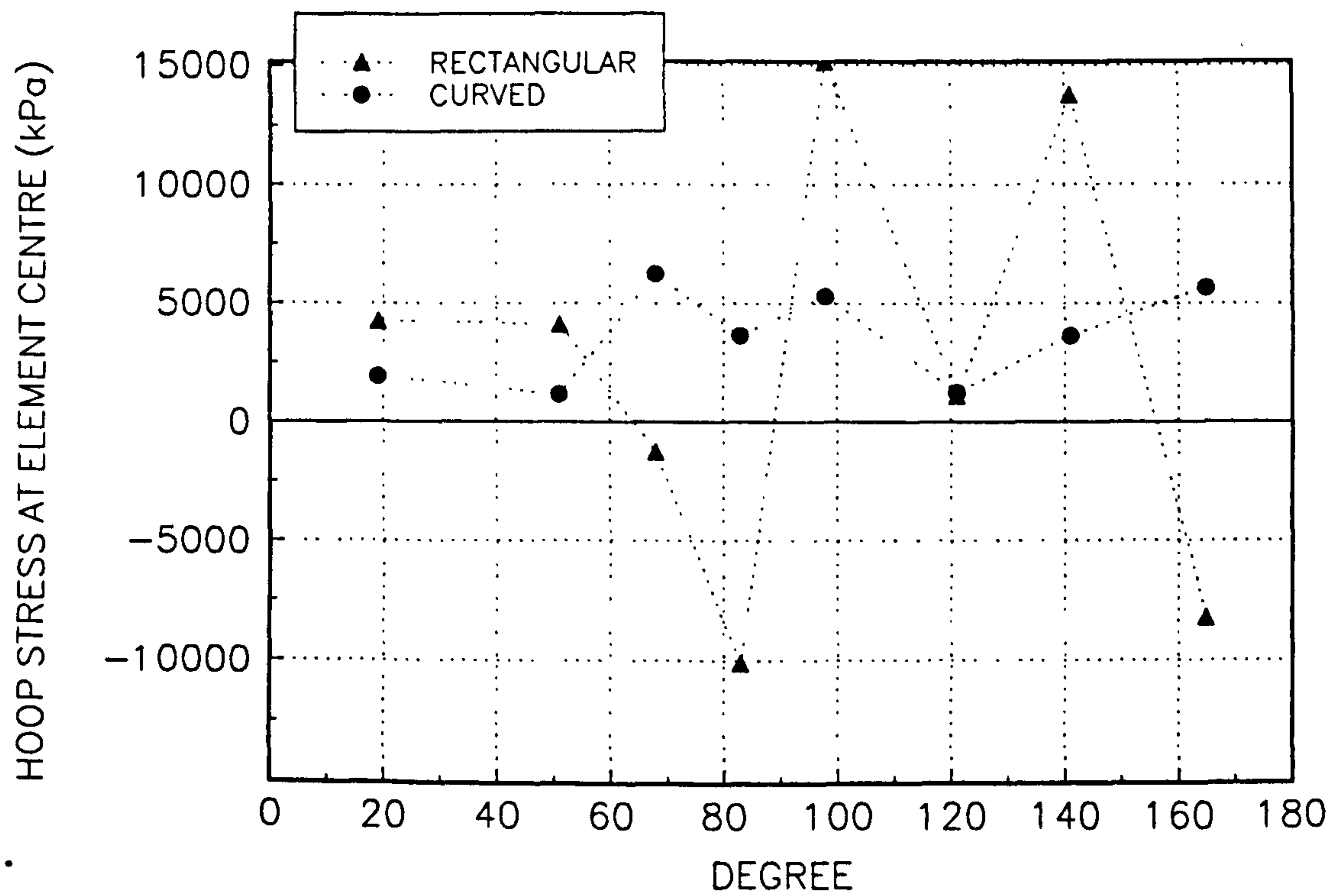


FIGURE 9.32
HOOP STRESS DISTRIBUTIONS IN RECTANGULAR AND CURVED CULVERT ELEMENTS



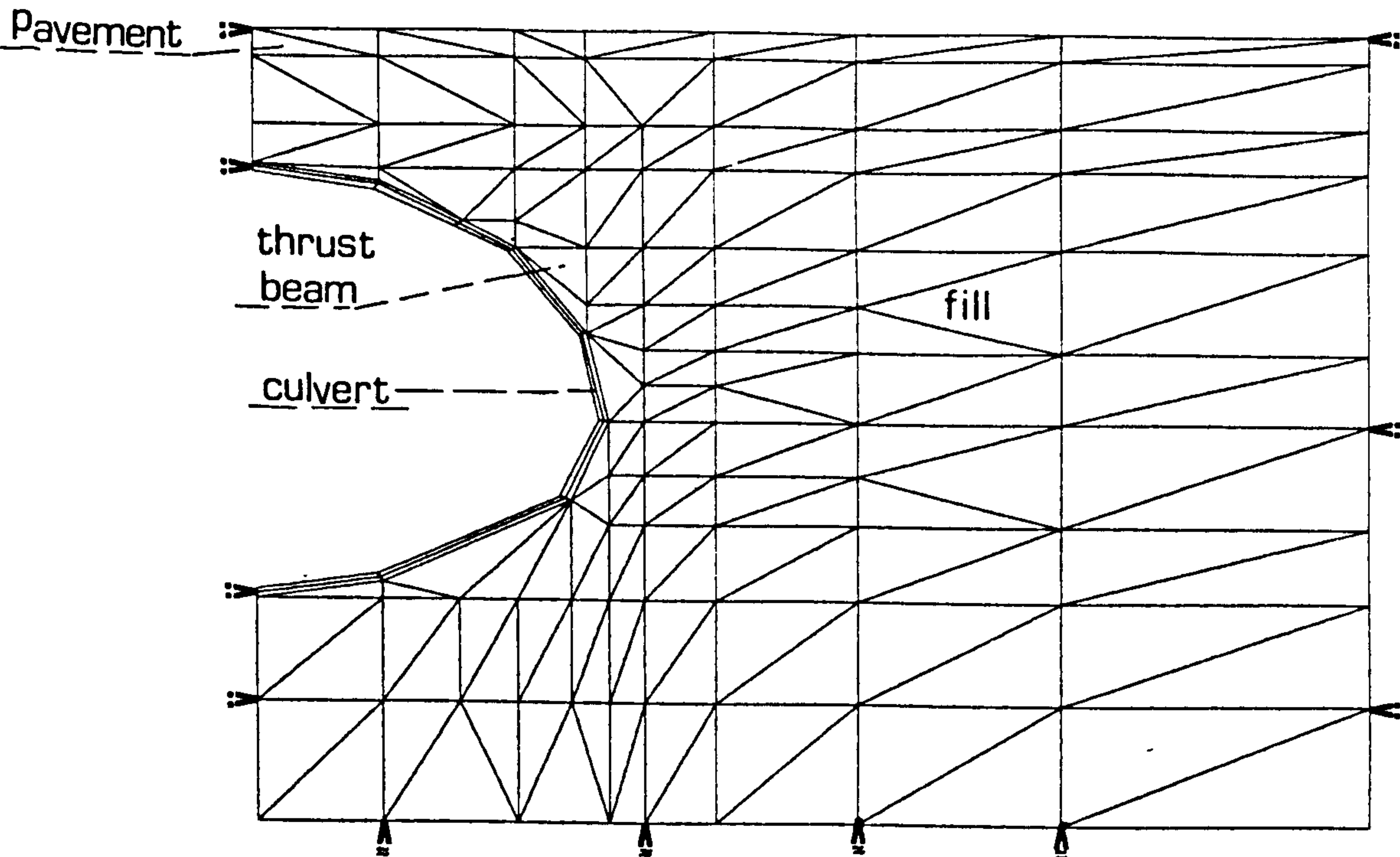


FIG 9.33 CRUDE CULVERT MESH MODELLING CULVERT USING RECTANGULAR ELEMENTS

FIG 9.34 THRUST BEHAVIOUR

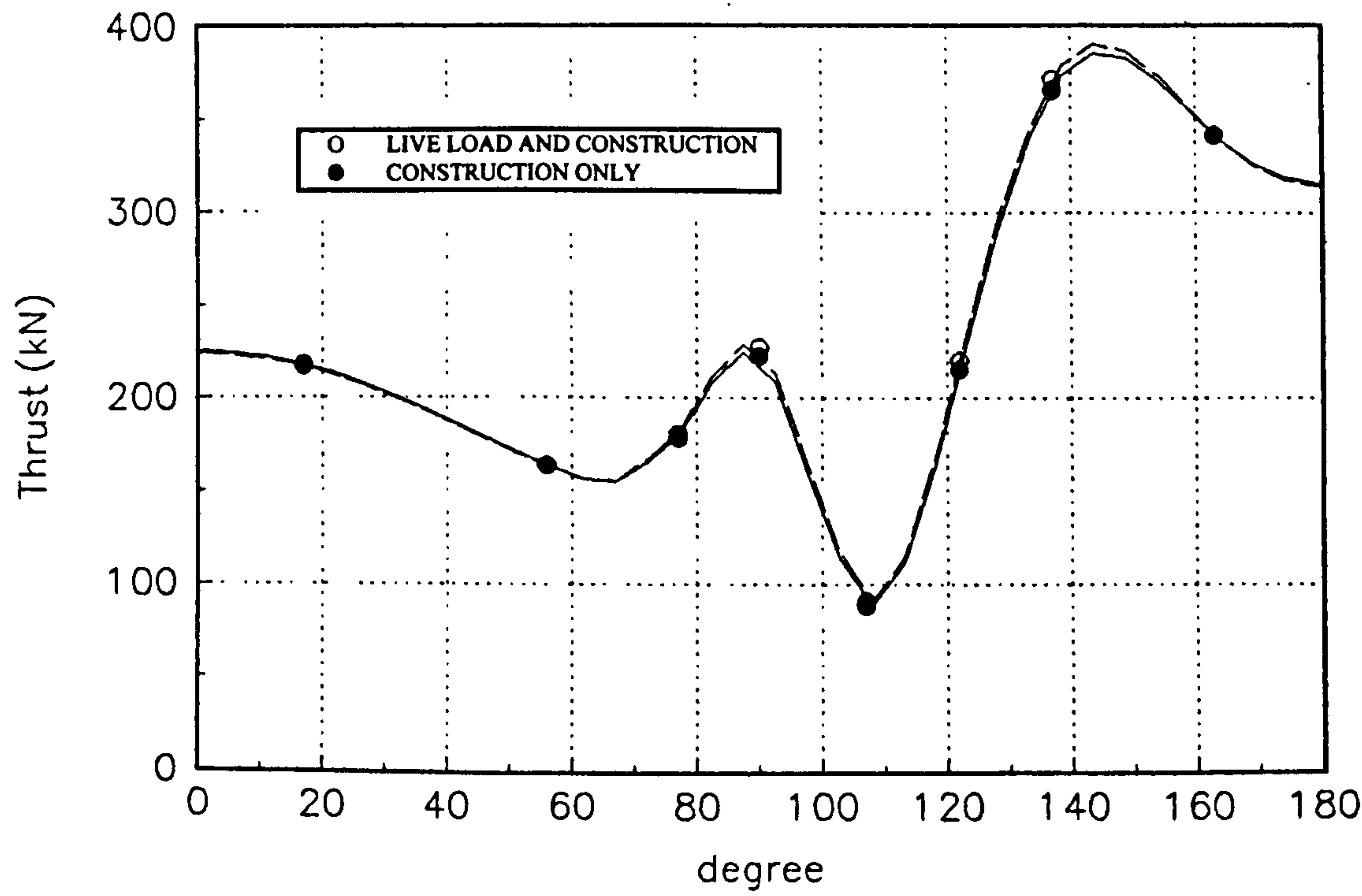


FIG 9.35 BENDING MOMENT BEHAVIOUR

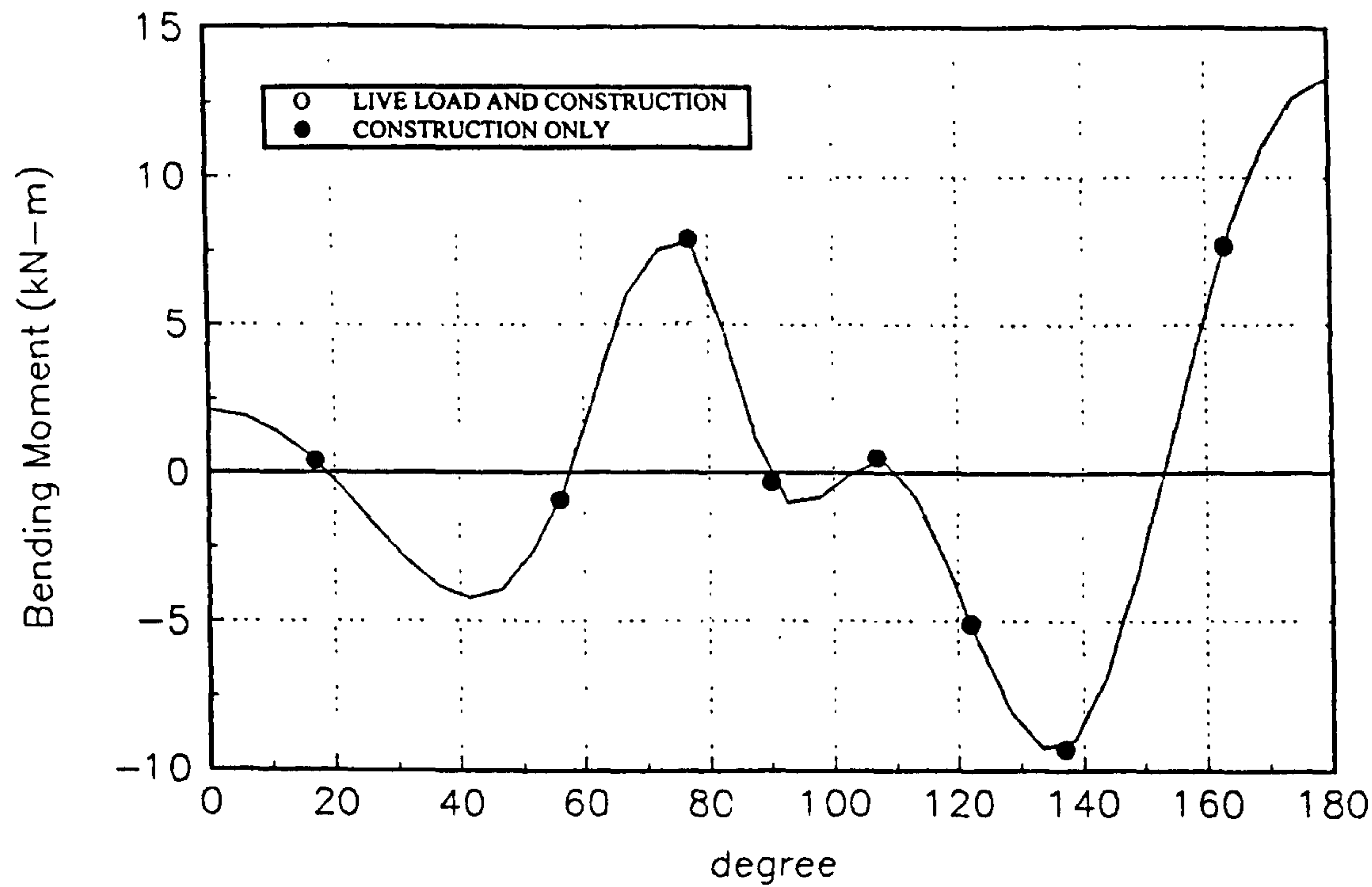


FIG 9.36 RADIAL STRESS BEHAVIOUR

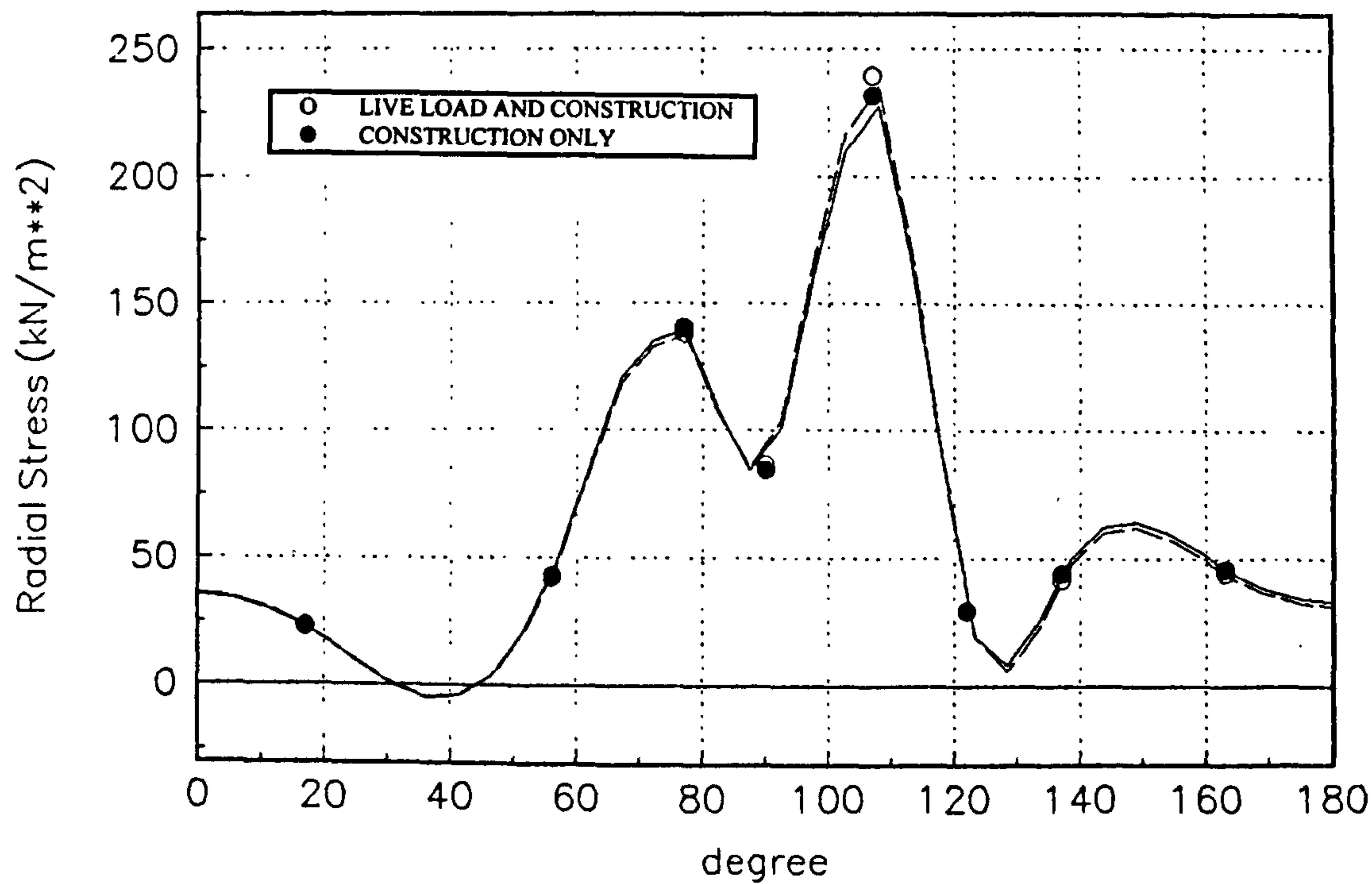


FIG 9.37 SHEAR STRESS BEHAVIOUR

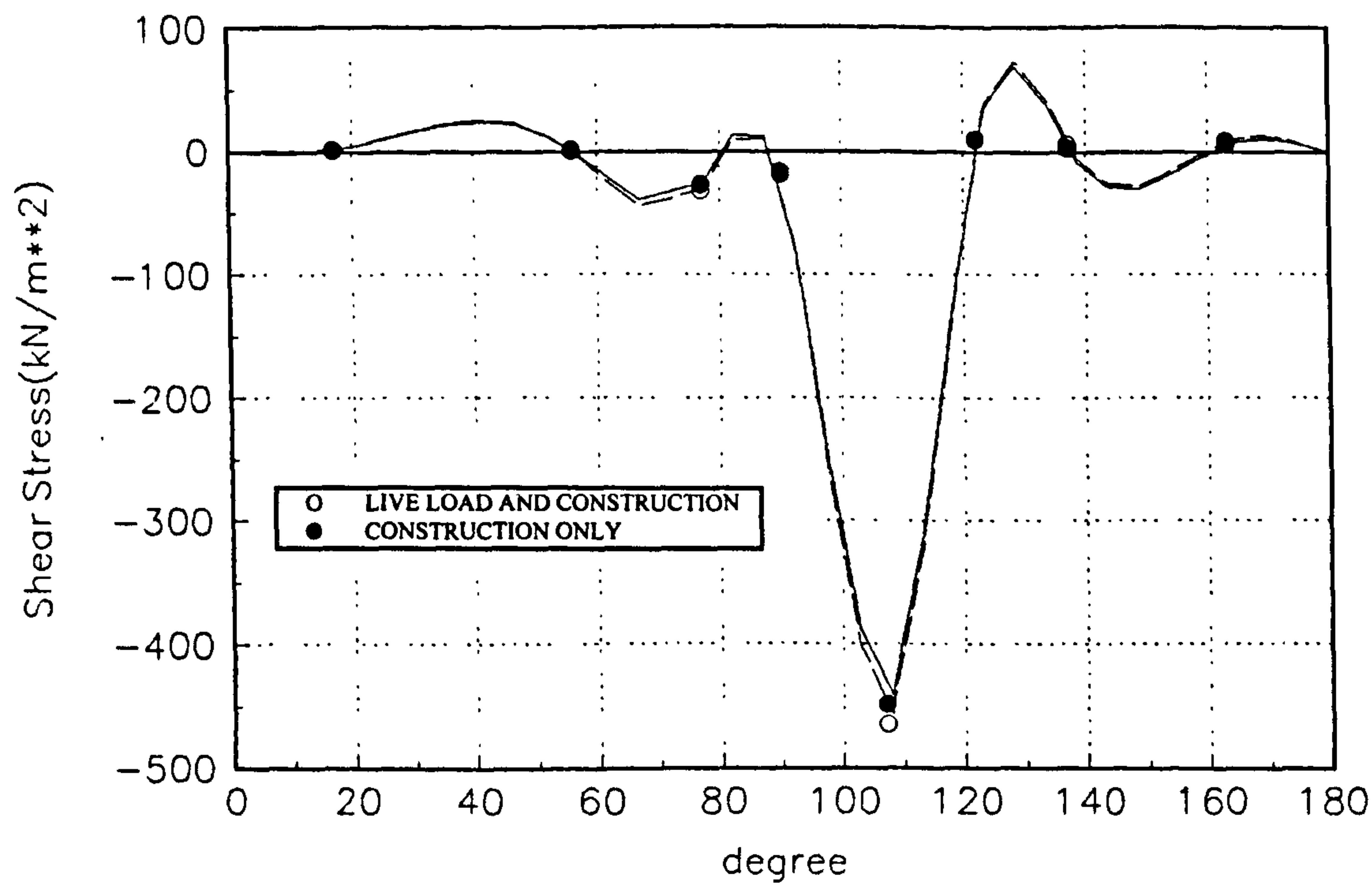


FIG 9.38 CROWN DISPLACEMENT

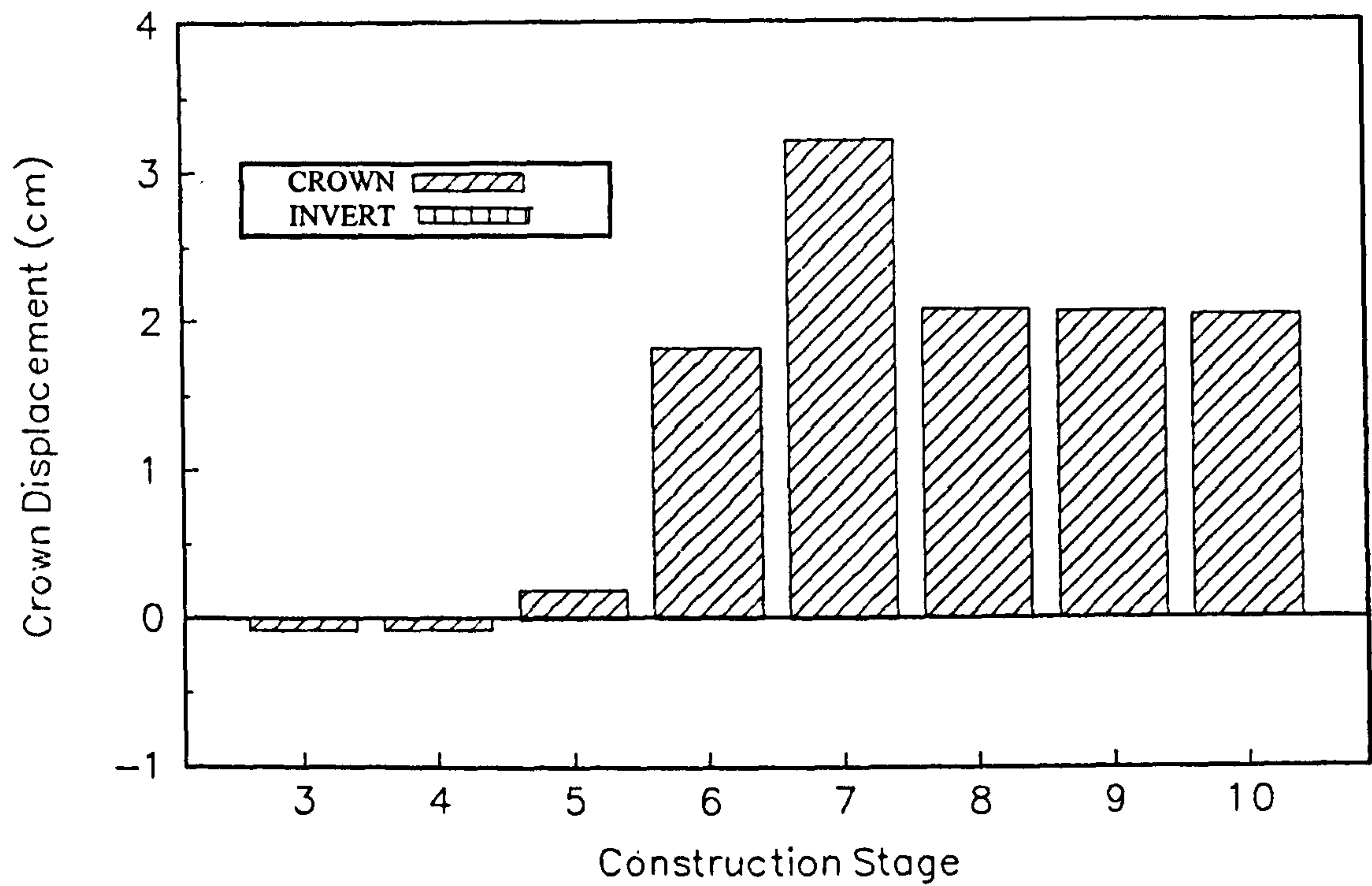


FIG 9.39 SPRINGLINE DISPLACEMENT

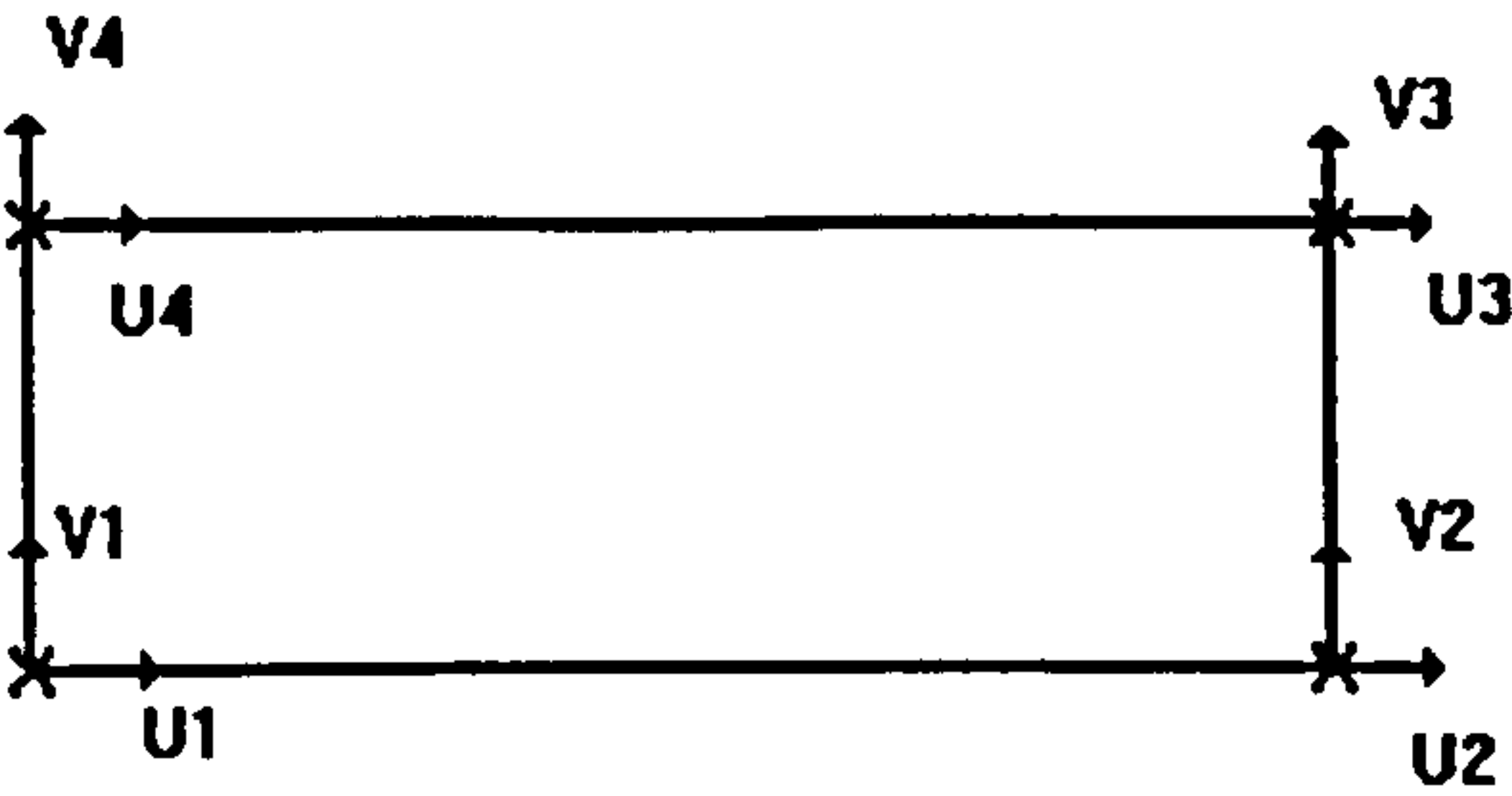
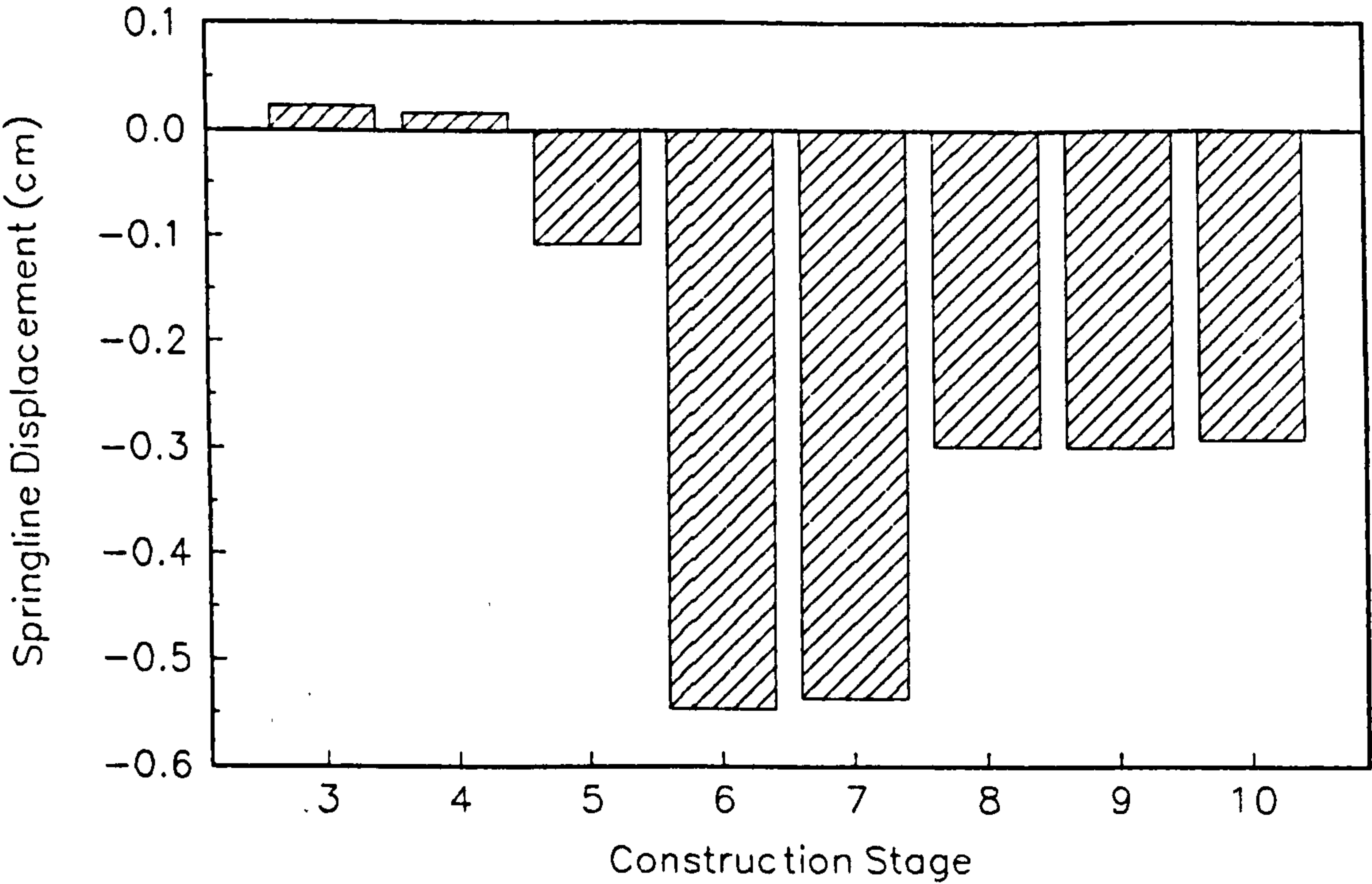


FIG 9.40 SHOWING DEGREES OF FREEDOM FOR AN ISOPARAMETRIC ELEMENT

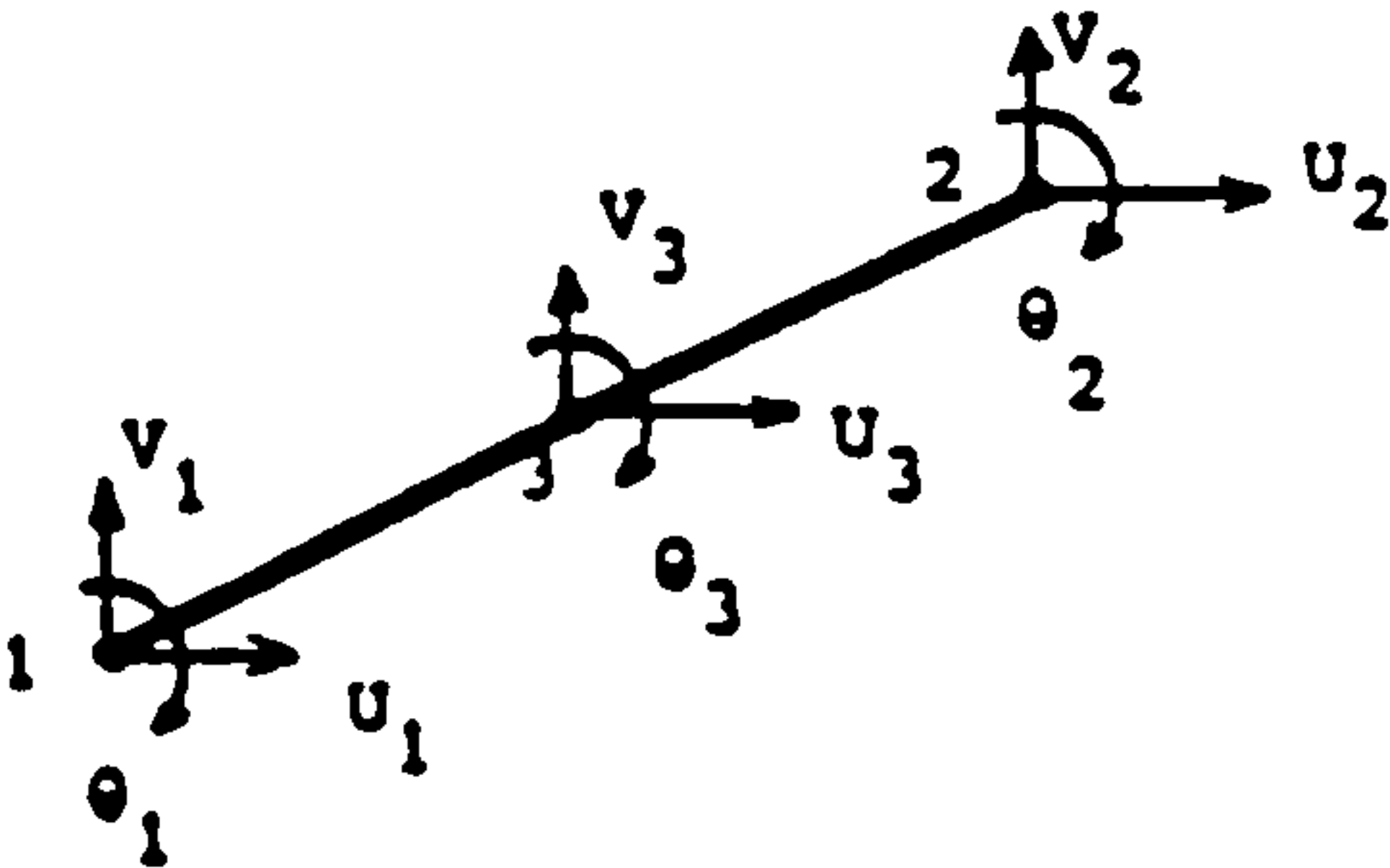


FIG 9.41 SHOWING DEGREES OF FREEDOM FOR A BEAM ELEMENT

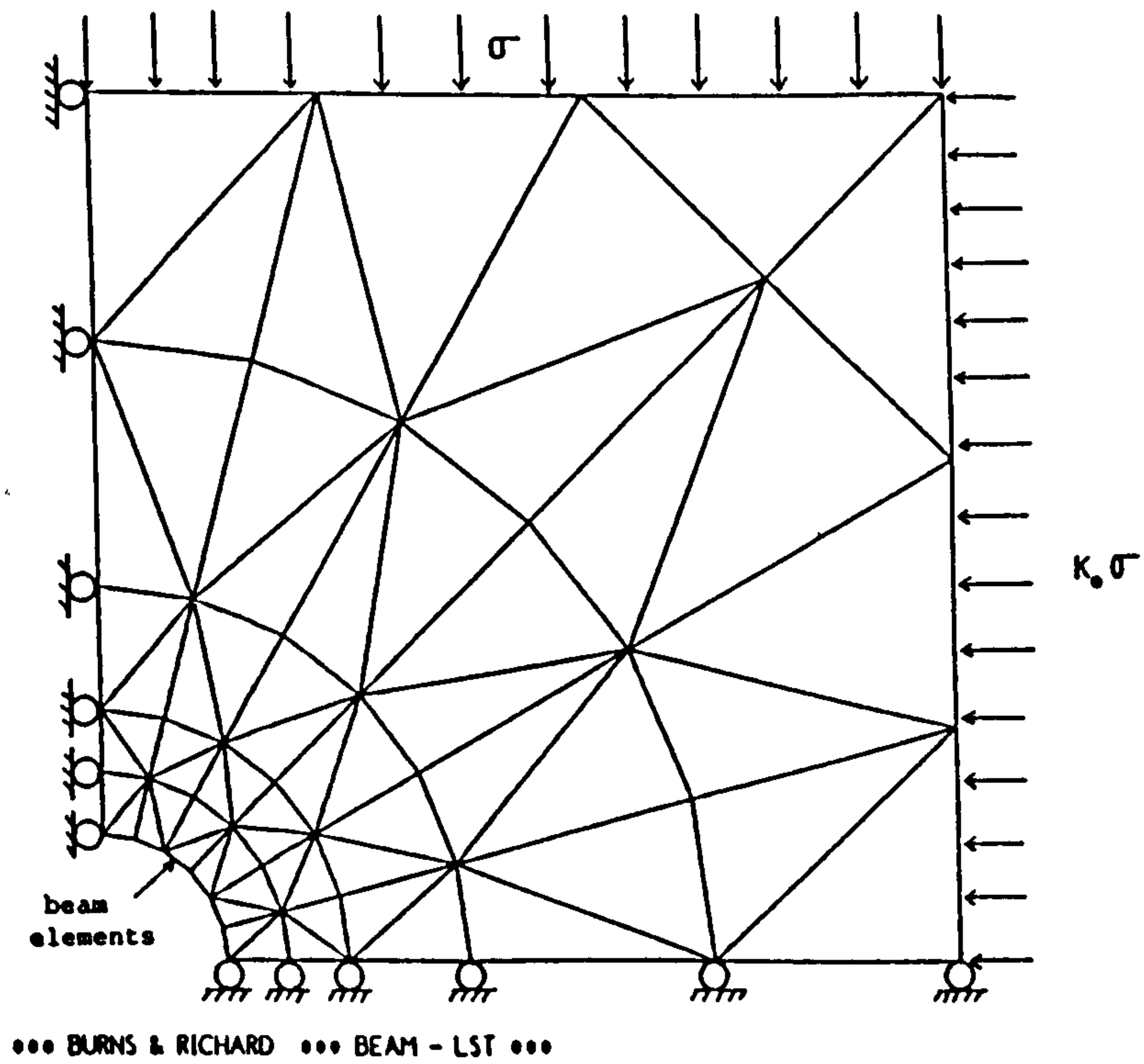


FIG 9.42 FINITE ELEMENT MESH AND BOUNDARY CONDITIONS (BRITTO, 1990)

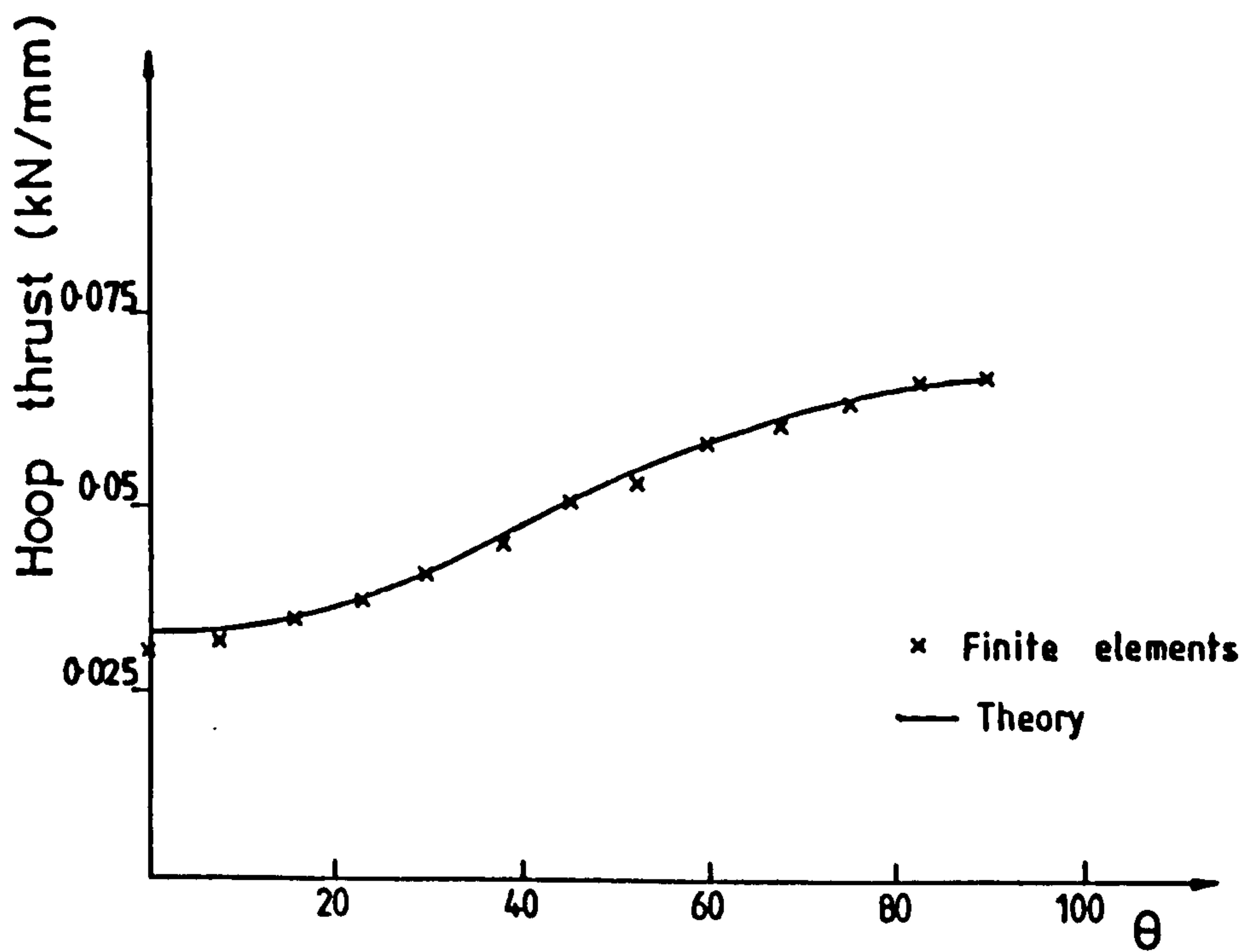


FIG 9.43 COMPARISON OF THRUST (NO SLIPPAGE) (BRITTO, 1990)

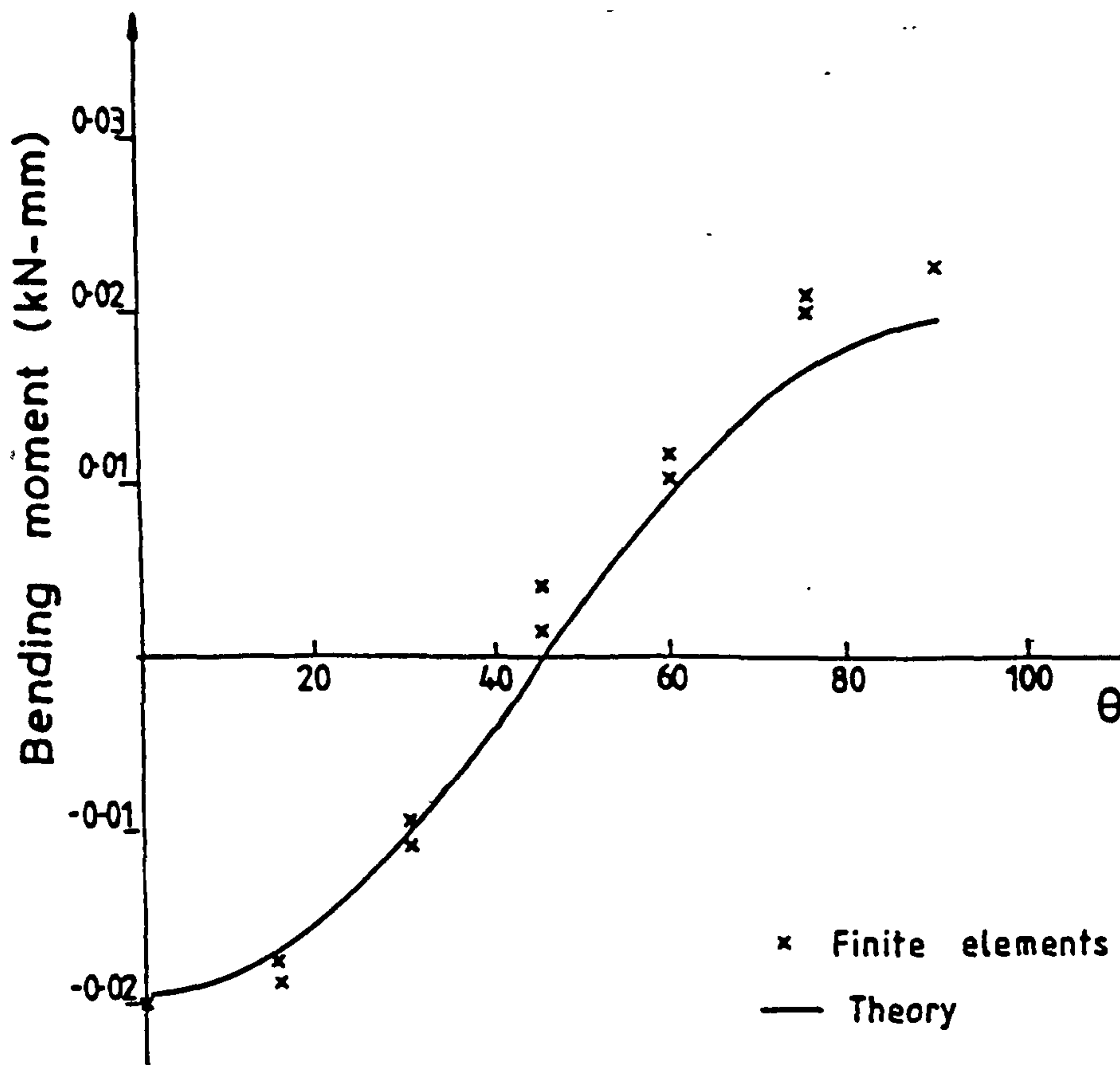
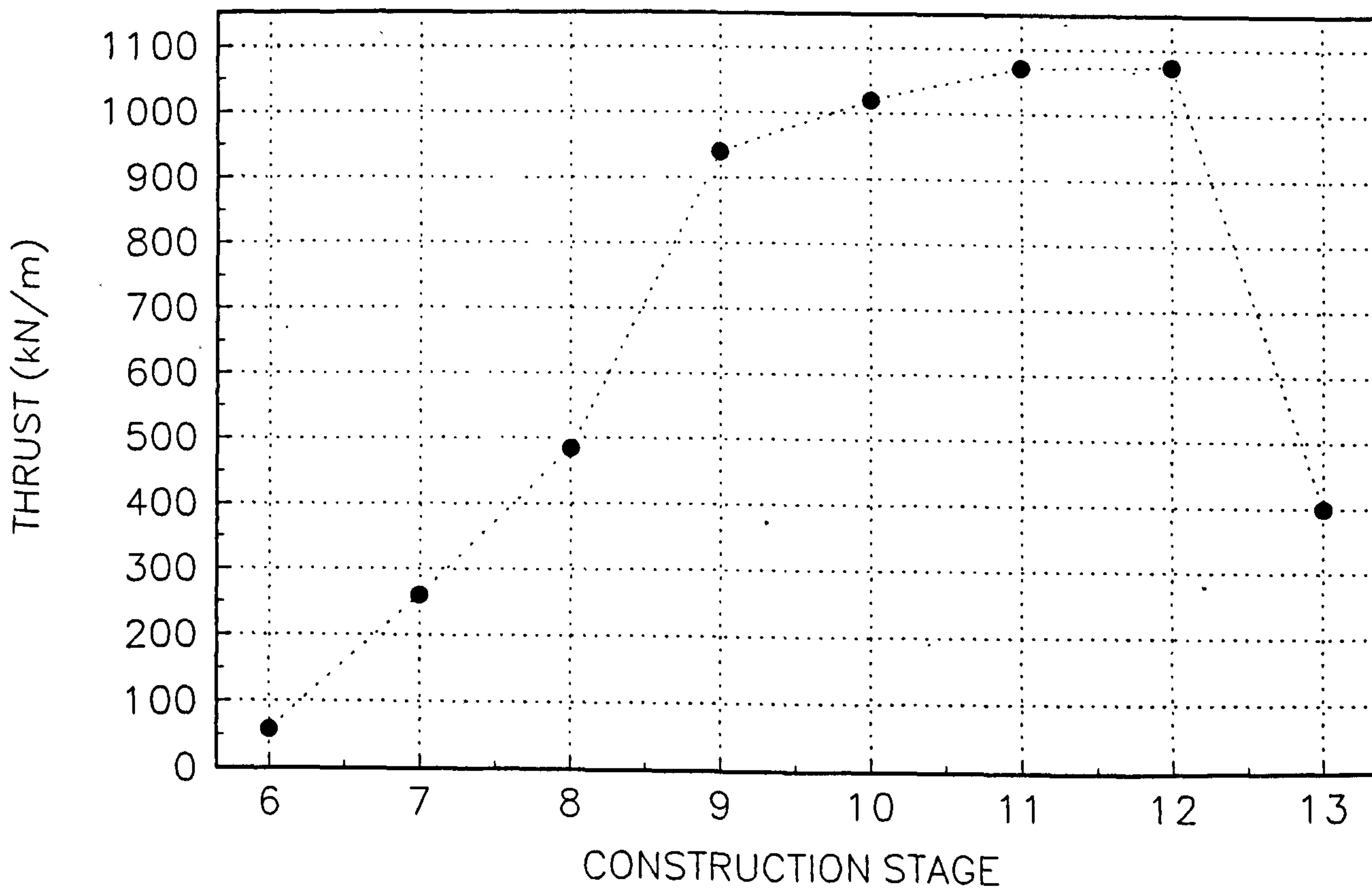


FIG 9.44 COMPARISON OF BENDING MOMENT (NO SLIPPAGE)
(BRITTO, 1990)

FIGURE 9.45
MAXIMUM CULVERT THRUSTS



CHAPTER 10

10. Conclusions

10.1 Introduction

From the work presented in this thesis conclusions have arisen which are common to both the soft clay and flexible culvert analyses. These conclusions are presented and briefly discussed in this chapter (section 10.2). Additionally, recommendations for future improvements to modelling problems of soil/structure interaction are also presented (section 10.3).

10.2 Conclusions

Conclusions can be drawn which have implications for the general application of finite element analysis to geotechnical problems; parameter selection for numerical analyses; and the role and requirements of the soil model for predicting soil behaviour.

10.2.1. General application of finite element analysis and modelling assumptions

The application of finite element analysis to geotechnical problems is not straightforward, but requires an understanding of: the physical problem being analysed; the finite element method; and the constitutive soil model being used to describe the problem. The learning curve is steep and in a commercial environment time constraints very often compel users to treat finite element systems as a “black box”. During the initial stages of this thesis it was found that this approach is potentially disastrous. Consequently, it is urged that every effort is made by the user to at least gain an appreciation of finite elements prior to embarking on any analyses.

Throughout this study the back analyses have been performed following the prediction process outlined by Lambe (1973). However, for each of the case histories described, the geometric modelling of the trial loadings has not been discussed in

detail. Omission of the modelling stage from the main discussion was not intended to relegate its importance. This stage of the predictive process is important and care should be taken to ensure that the chosen geometry and detail of the finite element mesh is sufficient to provide accurate results. This, requires that particular attention is given to the number (and type) of elements used to describe the foundation, and the distance to the boundaries of the mesh in relation to the imposed loadings. Minimising the influence of these aspects on the results is an iterative process which depending on the complexity of the geometry of the problem can also be time consuming.

In this study the trial loadings have been modelled using plane strain analyses. Imposing the condition of plane strain on analyses was a convenient assumption which reduces the problem to two dimensions, therefore removing the complexities associated with three dimensional modelling. Based on available trial loading data plane strain analyses describing the soft clay studies provided reasonable results. As a result, more complex three dimensional modelling of these loadings was considered to be unnecessary. The assumption of plane strain may be too simplistic for the flexible culvert analyses, particularly in view of the complex behaviour induced within the backfill during the compaction procedure. Restricting the compaction process to two dimensions is not an accurate representation of this process. Consequently, modelling the culvert behaviour and the compaction procedure in three dimensions may have provided more accurate results.

10.2.2. Soft clay; necessary requirements of a soil model

Full conclusions for the soft clay studies were presented in chapter 6, therefore only a brief summary of the main conclusions is presented below.

In chapters 3, 4 and 5 (soft clay) the modified Cam clay soil model was used to provide predictions of the essential elements of the observed behaviour which comprised: settlements; horizontal deformations; and excess pore water pressures. The features of the modified Cam clay soil model were sufficient to provide reasonable predictions of the observed foundation behaviour described in chapter 3. However, in chapters 4 and 5 (Cubzac-les-Ponts trial embankments) horizontal

displacements and excess pore water pressures were not accurately predicted, suggesting that for embankment type loads the modified Cam clay soil model is not appropriate if reasonable simultaneous prediction of the essential elements of the foundation behaviour is required. The elements of soil behaviour thought necessary to be included within a numerical model to provide reasonable predictions of soft clay foundation behaviour under embankment loads are: anisotropy; viscosity; and degree of saturation (Gens, 1994). Non-linear elasticity, is also thought to be a necessary ingredient (Jardine et al., 1984 and 1986 and Al-Tabba and Wood, 1989).

10.2.3. Site investigation and laboratory test data

In chapter 3 the exercise of applying finite elements to the trial loading was further complicated by sparse site investigation and laboratory test data which were insufficient to meet the demands of the soil model used (modified Cam clay). The extent of site investigation and laboratory testing conducted at the trial loading site was probably greater than average. Consequently, the detail of the site investigation and laboratory testing should reflect the demands of the soil model chosen to describe the foundation behaviour. This approach will therefore require that from the outset the complexity of the intended analyses is clearly defined. For example, analyses using the Cam clay soil model require accurate estimates of the soil parameters describing the elastic and plastic behaviour. Additionally, transition of elastic to plastic strains (yield) also requires an accurate description, particularly for normally consolidated soils where plastic strains were found to dominate the behaviour. The Cam clay soil model also requires an accurate description of the initial in situ soil stresses. In Cam clay the elastic stiffness is stress dependent, therefore an accurate estimate of the in situ stresses is required to define, as accurately as possible, the initial elastic stiffness of the soil. Additionally, for a normally consolidated soil the initial stress state will lie on or close to the yield locus, therefore to avoid overestimating or underestimating the magnitude of plastic strains the initial stresses should be accurately defined.

10.2.4. Flexible culvert analyses

In chapters 8 and 9 the simple linear elastic, perfectly plastic Mohr-Coulomb soil model has been used to describe the behaviour of granular backfill surrounding flexible culverts. Using this soil model reasonable estimates of the observed culvert behaviour have been obtained. These predictions, however, were based on soil parameters which were considered to be unrealistic and not descriptive of the backfill material. The simple Mohr-Coulomb soil model is, therefore, considered to be inappropriate for describing the culvert/backfill behaviour. Much of the inadequacy of the Mohr-Coulomb soil model is thought to emerge from the simple description of soil elasticity (Hooke's Law); for all pre-yield stress states the elastic stiffness remains constant. It has long been recognised that elastic stiffness (described through E'_f and ν'_f) varies with stress level. Further inadequacy of the Mohr-Coulomb soil model is thought to emerge due to the absence of a mean stress cap yield surface. During the construction process volumetric strains dominate, consequently in the absence of a mean stress cap unlimited elastic volumetric strains occur.

During the construction process the backfill is undergoing many cycles of loading and unloading. A standard feature of a loading and unloading cycles (even on elastic load cycles) is hysteresis. Studies of compaction induced stresses within backfills surrounding flexible culverts (Seed and Duncan, 1986) indicate that to provide an accurate description of the stresses induced within the backfill during the construction procedure hysteresis should be considered. Inclusion of this feature of soil behaviour within a numerical framework becomes especially important if non-linear elasticity (both E'_f and ν'_f varying with stress level) is also incorporated.

In summary the necessary elements of soil behaviour required within a soil model to simultaneously predict the essential elements of flexible culvert behaviour (thrusts, bending moments and displacements) are thought to be: non-linear elasticity (both E'_f and ν'_f varying with stress level); a mean stress cap yield surface; and the inclusion of hysteresis.

Back analysis of the flexible culvert behaviour has been performed with limited data. Data were only available for the live load behaviour. As previously discussed in chapter 8 (section 8.6), assessing the ability of the developed approach on these data

may not be reasonable, particularly in view of the dominance of the construction behaviour on the flexible culvert.

10.2.5. Empirical and semi-empirical hand calculation methods

In chapters 4 and 5 accurate estimates of the observed horizontal displacements and excess pore water pressures were obtained by using empirical, hand calculation methods (Leroueil et al., 1986). These methods are based on the observed behaviour of many trial embankments on soft clay foundations. Using the empirical methods, predictions of horizontal movements and excess pore water pressures were more accurate than those obtained from analyses.

In chapters 8 and 9 (flexible culverts), hand calculations performed using a semi-empirical method (Duncan, 1979) provided reasonable predictions of the maximum observed live load thrust and bending moment generated within the culvert. For the Quay water culvert (chapter 9), the semi-empirical method was initially significantly more accurate than analyses.

It is recognised that in Great Britain flexible culvert design is very rarely performed using finite element analysis. A typical design follows a standard hand-calculation which assumes that a condition of negative arching will develop, and such a design is liked, to be conservative. However given the level of complexity required to provide a more economic design using finite element analysis, engineers are unlikely to favour the adoption of finite elements in culvert design.

In view of the above discussion, established hand calculations, particularly those based on experimental observations, remain powerful design tools. For the studies presented in this thesis, the accuracy of these methods does question the need for detailed finite element analysis. Additionally, for most designs the accuracy provided by the hand calculations described would be sufficient.

10.3 Recommendations for future work

In this section recommendations for future work which are thought to be required to improve predictions of soil behaviour using finite element analysis are briefly discussed.

10.3.1. Soft clay

Back analyses of trial loading data for two common geotechnical structures on soft clay foundations have been performed. Similar studies should be extended to include other geotechnical structures such as retaining structures, piles and buried structures (culverts, pipes and tunnels), constructed on soft clay foundations, therefore constructing a data base for; parameter selection techniques for a particular problem (using an optimisation procedure), and identifying the necessary requirements of soil models to provide accurate predictions. Additionally, further studies should be performed using soil models incorporating anisotropic elasticity, degree of saturation, and elastic non-linearity (especially for the flexible culvert studies), and viscosity.

Anisotropic elasticity, degree of saturation and elastic non-linearity are elements of soil behaviour considered to be most useful for describing the initial (construction stage) behaviour of a soft clay foundation. Inclusion of these elements of soil behaviour within a numerical framework should provide improved predictions of horizontal displacement and excess pore water pressures in the short term. Viscosity is unlikely to be useful within a numerical framework until plastic strains are occurring. Consequently, viscosity is a feature of soil behaviour which should be included if predictions of the long term (consolidation) behaviour are required.

Inclusion of these elements of soil behaviour within a numerical framework will result in additional soil parameters. As a result, available soil data will need to be sufficiently detailed from which to select the necessary soil parameters. The level of soils data required should be similar to that obtained for the trial embankments constructed at Cubzac-les-Ponts (Shahanguian, 1980). Additionally, in order to accurately assess the influence of the inclusion of the elements of soil behaviour described above, trial loading data will need to be detailed, similar to that obtained at

Cubzac-les-Ponts. Available data obtained from the trial loading described in chapter 3 are considered to be insufficient to properly assess the influence of the more complex aspects of soil behaviour.

10.3.2. Flexible culverts

Further back analysis of flexible culvert trial loading data using the method of analysis described in this thesis is considered to be unnecessary given the problems which have been encountered. However, given the general acceptance of using the Mohr-Coulomb soil model to describe soil plasticity, adaptation of the method to incorporate the features described previously is recommended. The main concern of improving the current method of analysis should be to provide a reasonable description of the culvert construction behaviour. Consequently, inclusion of a mean stress cap yield surface, non-linear elasticity and inelasticity (or kinematic plasticity) are important. However, to limit the complexity of the developed method the first two features, mean stress cap and non-linear elasticity may be considered as a first-estimate of the culvert/backfill behaviour.

Further improvements of the developed approach may be achieved through modelling of the interaction problem in three dimensions. This will enable the compaction process to be more accurately modelled. In three dimensional analyses the compaction loading can be applied consecutively to backfill elements, therefore representing the transient and finite extent of the compaction loading. Using this modelling approach the influence of the longitudinal behaviour of the culvert can also be properly assessed. However, three dimensional modelling does introduce complications into the numerical analyses, mainly in relation to the type of finite element required to describe the culvert. In three dimensions the culvert is now a shell structure, consequently, a higher-order finite element (shell element) is required. These types of element are not available in the standard version of CRISP, therefore an alternative finite element program which can accommodate these higher order elements will need to be used. A further restriction associated with three dimensional modelling is the significant increase in computational time.

REFERENCES

- Abel, J. F., Mark, R., and Richards, R. (1973), 'Stresses around flexible elliptical pipes', *Proc. ASCE, Journal of Soil Mechanics and Foundation Engineering*, 99(SM7), 509-526.
- Adachi, T. and Oka, F. (1982), 'Constitutive equations for normally consolidated clays based on elasto-viscoplasticity', *Soil and Foundations* 24(4), 57-70.
- Allgood, J. R. (1964), 'The behaviour of shallow-buried cylinders', *Proc. Symp. Soil Structure Interaction*, (Tucson: University of Arizona), 189-210.
- Allgood, J. R., and Takahashi, S.K. (1972), 'Balanced design and finite element analysis of culvert', *Highways Research Board*, Record 413.
- Almagor, G.(1967), 'Interpretation of strength and consolidation data from bottom cores off Tel-Aviv, Polmakim coast, Israel', in A. F. Richards (ed.), *Marine Geotechnique* (Urbana: University of Illinois Press), 131-153.
- Almeida, M. S. S., Britto, A. M. and Parry, R. H. G. (1986), 'Numerical modelling of a centrifuged embankment on soft clay', *Canadian Geotechnical Journal* 23, 103-114.
- Al-Tabba, A. and Wood, D.M. (1989), 'An experimentally based 'bubble' model for clay', in S. Pietruszczak and G.N. Pande (eds.), *Numerical models in geomechanics NUMOG III* (London: Elsevier),pp. 91-99.
- Andresen, A., Berre, T., Kleven, A., and Lunne, T. (1979), 'Procedures used to obtain soil parameters for foundation engineering in the North sea', *Marine Geotechnology* 3(3), 201-266.
- Ansal, A. M., Bazant, Z. P., and Krizek, R. J. (1979), 'Viscoplasticity of normally consolidated clays', *Proc. ASCE, Journal of the Geotechnical Engineering Division*, 105(GT4), 519-537.
- Babchia, M. (1984), *Analyse nume'rique du comportement des massifs de sols argileux*, The'se de Docteur - Inge'nieur, Ecole Nationale des Ponts et Chausse'es, Paris, 118 pages.
- Balachandran, S. (1990), 'Simulation of a test embankment failure (Muar flood plain, Malaysia) using finite element techniques coupled with critical state soil mechanics', thesis presented to the Asian Institute of Technology, Bangkok, Thailand, in partial fulfilment of the requirement for the degree of Master of Science.

- Balasubramaniam, A. S., Phien-wej, N., Indraratna, B., and Bergado, D. T. (1989), 'Predicted behaviour of a test embankment on a Malaysian marine clay', in *Int. Symp. on Trial Embankments on Malaysian Marine Clays*, Kuala Lumpur, Malaysia, vol. 2, 1-1-1-18.
- Barry, A. J., and Nicholls, R. A. (1982), 'Discussion', in *Vertical drains* (London: Thomas Telford), 143-146.
- Bartkus, E. A. and Vey, E. (1956), 'Granular earth pressure on steel tunnel lining', *Bulletin 141, Highway Research Board*, Washington, D. C, 26-43.
- Bathe, K. J. (1982), *Finite Element Procedures in Engineering Analysis*, (Prentice and Hall Inc, New York).
- Beal, D. B. (1982), 'Field tests on long-span aluminum culvert', *Proc. ASCE, Journal of Geotechnical Engineering Division*, 108(GT6), 873-890.
- Beer, G. and Swoboda, G. (1985), 'On the efficient analysis of shallow tunnels', *Computers and Geotechnics* 1, 15-31.
- Bjerrum, L. (1972), 'Embankments on soft ground', in *Proc. Specialty Conf. on Performance of Earth and Earth-Supported Structures, Purdue* (New York: ASCE), vol. 2, 1-54.
- Bjerrum, L. (1973), 'Problems of soil mechanics and construction of soft clays and structurally unstable soils', in *Proc 8th Int. Conf. on Soil Mechs. and Foundation Eng., Moscow* (Moscow: USSR National Society for Soil Mechanics and Foundation Engineering), vol. 3, 111-159.
- Bourges, F., and Mieussens, C. (1979), 'De'placements late'raux 'a proximite' des remblais sur sols compressibles, me'thode de pre'vision', *Bulletin de Liaison des Laboratoires des Ponts et Chausse'es*, Paris No. 101, 73-100.
- Bowey, A. W. and Muir Wood, D. (1994). 'Back analysis of a trial loading on soft clay', in *Proc. Int. Symp. on Pre-failure Deformation Characteristics of Geomaterials, Sapporo, Japan*, 559-565.
- Brinkgreve, R. B. J. and Vermeer, P. A. (1992), 'On the use of Cam-clay models', in G.N. Pande and S. Pietruszczak (eds.), *Numerical models in Geomechanics* (London: Balkema), 557-565.
- Britto, A. M. and Gunn, M. J. (1987) *Critical state soil mechanics via finite elements* (Chichester: Ellis Horwood Ltd).
- Britto, A. M. (1990), 'Advanced Geotechnical analysis: Advanced use of CRISP', in Lecture notes given for a course, *CRISP: Advanced Programme for Industry*, on 11th July 1990.

- Burland, J.B. (1990), 'On the compressibility and shear strength of natural clays,' *Géotechnique* 40(3), 329-378.
- Burns, J. Q., and Richard, R. M. (1964), 'Attenuation of stresses around buried cylinders', *Proc. Symp. on Soil Structure Interaction, Arizona*, 378-392.
- Byrne, P. M., Srithar, T., and Kern, C. B. (1993), 'Field measurements and analysis of a large-diameter flexible culvert', *Canadian Geotechnical Journal*, 30, 135-145.
- Carter, J.P., Small, J.C. and Booker, J.R. (1977), 'A theory of finite elastic consolidation', *Int. J. Solids and Structures*, 13, 467-478.
- Casagrande, A. (1936), 'The determination of the preconsolidation load and its practical significance', *Proc. 1st Int. Conf. Soil Mech.*, Cambridge, Mass., 3, 60-64.
- Chai, A. J. C., and Bergado, D. T. (1993), 'Some techniques for finite element analysis of embankments on soft ground', *Canadian Geotechnical Journal* 30, 710-719.
- Chan, A.H.C. (1988), *User manual for DIANA SWANDYNE II*, Institute for Numerical Methods in Engineering, University College of Swansea.
- Chang, C. S., Espinoza, J. M., and Selig, E. T. (1980), 'Computer analysis of Newton Creek Culvert', *Proc. ASCE, Journal of Geotechnical Engineering*, 106(GT5), 531-556.
- Chen, W. F. and Mizuno, E. (1990), *Nonlinear analysis in soil mechanics; Theory and implementation*. (Amsterdam: Elsevier Science Publishers).
- Clausen, C-J. F., Graham, J., and Wood, D. M. (1984), 'Yielding in soft clay at Masteymr, Norway', *Géotechnique* 34(4), 581-600.
- Clayton, C. R. I. and Khatrush, S. A. (1986), 'A new device for measuring local axial strains on triaxial specimens', *Géotechnique* 36(4), 593-598.
- Cook, R.D. (1981), *Concepts and applications of finite element analysis, (2nd ed.)*, Wiley, New York.
- Craig, R. F. (1987), *Soil Mechanics (4th ed.)*, (Van Nostrand Reinhold, (UK) Berkshire, England).
- Croney, D. (1977), *The design and performance of road pavements*, HMSO, London.
- Crooks, J. H. A., Becker, D. E., Jefferies, M. G., and McKenzie, K. (1984), 'Yield behaviour and consolidation 1: pore pressure response,' in *Proc. ASCE, Symp. on Sedimentation consolidation models: predictions and validation*, 356-381.

- Dalton, J.C.P. and Hawkins, P.G. (1982), 'Fields of stress- some measurements of the *in situ* stress in a meadow in the Cambridgeshire countryside', *Ground Engineering*, 15, 15-23.
- D'Appolonia, D. J., Lambe, T. W., and Poulos, H. G. (1971), 'Evaluation of pore pressures beneath an embankment', *Proc. ASCE, J. Soil Mechs. and Foundation Div.* 97(SM6), 881-898.
- Davies J. A., and Humpheson, C. (1986), 'A comparison between the performance of two types of vertical drain beneath a trial embankment in Belfast', *Vertical drains*, London: Thomas Telford.
- Davies. T, G., Chan. A. H. C., Stewart, W. M., Muir Wood, D. and Bu, S. (1993), 'Review of the Design of Flexible Culverts-Interim Report (July 1993)', *Transport Research Laboratory*, (University of Glasgow).
- Dessouki, A. K. and Monforton, G. R. (1986), 'Effect of soil failure on soil-steel structures', *Proc. ASCE, Journal of Geotechnical Engineering*, 112(GT5), 522-536
- Diaz-Rodriguez, J. A., Leroueil, S. and Aleman, J. D. (1992), 'Yielding of Mexico City clay and other natural clays', *Proc. ASCE, Journal of Geotechnical Engineering*, 118(GT7), 981-995.
- Duane, J., Robinson, R., and Moore, C. A. (1986), 'Culvert-soil interaction finite element analysis', *Proc. ASCE, Journal of Transportation Engineering*, 112(3), 250-263.
- Duncan, J, M. and Chang, C. Y. (1970), 'Nonlinear analysis of stress and strain in soil', *Proc. ASCE, Journal of Soil Mechanics and Foundation Engineering*, 96(SM5), 1629-1653.
- Duncan, J, M. and Buchignani, A. L. (1973), 'Failure of underwater slope in San Francisco Bay', *Proc. ASCE, Journal of Soil Mechanics and Foundations Division*, 99(SM9), 687-704.
- Duncan, J, M. (1979), 'Behaviour and design of long-span metal culverts', *Proc. ASCE, Journal of Geotechnical Engineering*, 105(GT3), 399-418.
- Duncan, J, M. and Jeyapalan, J. K. (1982), 'Deflection of flexible culverts due to backfill compaction', *Transport Research Board*, 878, 10-16
- Drucker, D. C. (1966), 'Concepts of path independence and material stability for soils', in J. Kravtchenko and P. M. Sirieys (eds.), *Proc. IUTAM Symp. on Rheology and Soil Mechanics, Grenoble* (Berlin: Springer-Verlag), 23-46.
- Fraser, R. A., and Wardle, L. J. (1976), 'Numerical analysis of rectangular rafts on layered foundations,' *Géotechnique* 26(4), 613-630.

- Gens, A. (1994), 'Session 3: Prediction, Performance and Design. General Report', in *Proc. Int. Symp. on Pre-failure Deformation Characteristics of Geomaterials, Sapporo, Japan*, 421-444.
- Ghaboussi, J., Wilson, E.L., and Isenberg, J.(1973), 'Finite element for rock joints and interfaces', *Proc. ASCE, Journal of Soil Mechanics and Foundation Engineering Division*, 99(SM10), 833-848.
- Gibson, R. E. (1950), 'Discussion on the bearing capacity of screw piles and screwcrete cylinders', *Journal of the Institution of Civil Engineers*, 34, 382-383
- Goodman, R. E., Taylor, R. L., and Brake, T. L. (1968), 'A model for the mechanics of jointed rock', *Proc. ASCE, Journal of Soil Mechanics and Foundation Engineering Division*, 94(SM3), 637-659.
- Graham, J., Crooks, J. H. A., and Bell, A. L. (1983), 'Time effects on the stress-strain behaviour of natural soft clays', *Géotechnique* 33(3), 327-340.
- Graham, J., and Houlsby, G. T. (1983), 'Yielding states and stress-strain relationships in a natural plastic clay', *Géotechnique* 33(2), 165-180.
- Graham, J., Noonan, M. L., and Lew, K. V., (1983), 'Yield states and stress-strain relationships in a natural plastic clay', *Canadian Geotechnical Journal* 20(3), 502-516.
- Griffiths, D. V. (1982), 'Computation of bearing capacity factors using finite elements', *Géotechnique* 32(3), 195-202.
- Griffiths, D. V. (1988), 'Numerical studies of soil-structure interaction using a simple interface model', *Canadian Geotechnical Journal* 25, 158-162
- Hansbo, S. (1957), *A new approach to the determination of the shear strength of clay by the fall-cone test* (Stockholm: Royal Swedish Geotechnical Institute), *Proceedings* 14.
- Hartley, J. D. and Duncan, J. M. (1987), 'E', and its variation with depth', *Proc. ASCE, Journal of Transportation Engineering Division*, 113(5), 538-553.
- Henkel, D.J. (1956), 'The relationships between the strength pore-water pressure, and volume-change characteristics of saturated clays', *Géotechnique* 9(2), 119-135.
- Hird, C.C., and Kwok, C.M. (1986), 'Predictions for the Stanstead Abbots trial embankment based on the finite element method', in *Proc. Prediction symposium on a Reinforced Embankment on Soft Ground*, King's College, London.
- Hird, C.C., Pyrah, I.C., and Russell, D. (1990), 'Finite element analysis of the collapse of reinforced embankments on soft ground', *Géotechnique* 40(4), 633-640.

- Hird, C.C., Pyrah, I.C., and Russell, D. (1992), 'Finite element modelling of vertical drains beneath embankments on soft ground', *Géotechnique* 42(3), 499-511.
- Hird, C.C. (1994), 'Numerical Modelling of a Reinforced Embankment at the Willow Plantation (A414)', *Department of Transport, TRRL Research Report 92*, Transport and Road Research Laboratory, Crowthorne.
- Hight, D. W., Bond, A. J., and Legge, J. D. (1992), 'Characterisation of the Bothkennar clay: an overview', *Géotechnique* 42(2), 303-347.
- Hooper, J. A. (1974), 'Analysis of a circular raft in adhesive contact with a thick elastic layer,' *Géotechnique* 24(4), 561-580.
- Houlsby, G. T. (1985), 'The use of a variable shear modulus in elastic-plastic models for clays', *Computers and Geotechnics* 1, 3-13.
- Howard, A. K. (1977), 'Modulus of soil reaction, E', values for buried flexible pipes', *Report, Rec-ERC-77-1*, Engineering and Research Centre, Bureau of Reclamation, Denver, Colorado.
- Indraratna, B., Balasubramaniam, A. S. and Balachandran, S. (1992), 'Performance of test embankment constructed to failure on soft marine clay', *Proc. ASCE, Journal of Geotechnical Engineering*, 118(GT1), 12-33.
- Jáky, J. (1944), 'A nyugalmi nyomás te'nyeezője' ('The coefficient of earth pressure at rest'), *Magyar Mérnök és Építész-Egylet Közlönye (J. of the Union of Hungarian Engineers and Architects)*, 355-358.
- Jardine, R.J., Symes, M.J., and Burland, J.B. (1984), 'The measurement of soil stiffness in the triaxial apparatus', *Géotechnique* 34(3), 323-340.
- Jardine, R.J., Potts, D.M., Fourie, A.B., and Burland, J.B. (1986), 'Studies of the influence of non-linear stress-strain characteristics in soil-structure interaction', *Géotechnique* 36(3), 377-396.
- Jeyapalan, M. and Abdelmagid, A. M. (1984), 'Importance of pipe soil stiffness ratio in plastic pipe design', in *ASCE Convention*, San Francisco, California.
- Jeyapalan, M. and Boldon, B. A. (1986), 'Performance and selection of rigid and flexible pipes', *Proc. ASCE, Journal of Transportation Engineering*, 112(5), 507-524.
- Johnson, P. E., Temporal, J. and Watts, G. R. A. (1989), 'The effect of pavement layers on the behaviour of corrugated steel culverts', *Department of Transport, TRRL Research Report 209*, Transport and Road Research Laboratory, Crowthorne.
- Johnston, I. W. (1973), *Discussion, session 4. In Field Instrumentation in Geotechnical Engineering* (Halsted Press Book: John Wiley, New York), 700-702.

- Katona, M. G., Smith, J. M., Odello, R. S., and Allgood, J. R., (1976), 'CANDE-a modern approach for structural design and analysis of buried culverts', *Engineering report, User manual, system manual, reports FHWA-RD-77-5, 77-6, 77-7*, U.S. Naval Civil Engineering Laboratory, Port Hueneme, California.
- Klöppel, K. and Glock, D. (1970). 'Theoretische und experimentelle untersuchungen zu den Traglastproblemen biegeeweicher, in die Erde eingebetteter Rohre.' Veröffentlichung des Institutes für Statik and Stahlbau der Technischen Hochschule Darmstadt, Heft 10.
- Konrad, J. M. and Law, K. T. (1987), 'Preconsolidation pressures from piezocone tests in marine clays', *Géotechnique* 37(2), 177-190.
- Kulhawy, F. H. and Mayne, P. W. (1990), 'Manual on estimating soil properties for foundation design', *Rept. EL-6800*, Electrical Power Research Inst. Palo Alto, 306 pages.
- Ladd, C.C. (1965), 'Stress-strain behaviour of anisotropically consolidated clays during undrained shear', in *Proc. 6th Int. Conf. on Soil Mechanics and Foundation Eng., Montreal* (Toronto: University of Toronto Press), vol. 1, pp. 282-290.
- Ladd, C.C., Foott, R., Ishihara, K., Schlosser, F., and Poulos, H. G. (1977), 'Stress-deformation and strength characteristics', in *Proc. 9th Int. Conf. on Soil Mechanics and Foundation Engineering, Tokyo* (Tokyo: Japanese Society of Soil Mechanics and Foundation Engineering), vol. 2, pp. 421-494.
- Lade, P.V. (1977), 'Elasto-plastic stress-strain theory for cohesionless soil with curved yield surfaces', *Int. J. Solids and Structures* 13(11), 1019-1035.
- Lambe, T.W. (1964), 'Methods of estimating settlement', *Proc. ASCE, Journal of Soil Mechanics and Foundations Division* 90(SM5), 43-67.
- Lambe, T.W. (1967), 'Stress path method', *Proc. ASCE, Journal of Soil Mechanics and Foundations Division* 93(SM6), 309-331.
- Lambe, T.W. (1973), 'Predictions in soil engineering', *Géotechnique* 23(2), 149-202.
- Larsson, R. (1980), 'Undrained shear strength in stability calculation of embankments and foundations on soft clays,' *Canadian Geotechnical Journal* 17(4), 591-602.
- Lefebvre, G., Laliberte', M., Lefebvre, L. M., Lafleur, J, and Fisher, C. L. (1976), 'Measurement of soil arching above a large diameter flexible culvert', *Canadian Geotechnical Journal*, 13, 58-71.
- Lefebvre, G., Pare', J. J., and Dascal, O. (1987), 'Undrained shear strength in the surficial weathered crust', *Canadian Geotechnical Journal*, 24(1), 23-34.

- Leonards, G. A., Wu, T. H., and Juang, C. H. (1982), 'Predicting performance of buried conduits', *Report FHWA/IN/JHRP-81-3*, School of Civil Engineering, Purdue University.
- Leonards, G. A., Juang, C. H., Wu, T. H., and Stetkar, R. E. (1985), 'Predicting performance of buried metal conduits', *Transport Research Board*, **1008**, National Research Council, Washington D. C., 42-45.
- Leroueil, S., and Tavenas, F. (1981), 'Pitfalls of back-analyses', in *Proc. 10th Int. Conf. on Soil Mechanics and Foundation Engineering, Stockholm* (Rotterdam: A.A. Balkema), vol. 1, pp. 189-190.
- Leroueil, S., Kabbaj, M., Tavenas, F., and Bouchard, R. (1985), 'Stress-strain-strain rate relation for the compressibility of sensitive natural clays', *Géotechnique* **35**(2), 159-180.
- Leroueil, S., Magnan, J-P., and Tavenas, F. (1985), *Remblais sur argiles molles* (Paris: Technique et Documentation, Lavoisier) English translation D.M. Wood (1990) *Embankments on soft clays* (Chichester: Ellis Horwood Ltd.).
- Leroueil, S. and Tavenas, F. (1986), Discussion on 'Effective stress paths and yielding in soft clays below embankments' by D. J. Folkes and J. H. A. Crooks. *Canadian Geotechnical Journal*, **23**(3), 410-413.
- Leroueil, S. (1988), 'Recent developments in consolidation of natural clays: 10th Canadian Geotechnical Colloquium,' *Canadian Geotechnical Journal*, **25**(1), 85-107.
- Leroueil, S., Diene, M., Tavenas, F., Kabbaj, M., and La Rochelle, P. (1988), 'Direct determination of the permeability of clay under embankment,' *Proc. ASCE, Journal of the Geotechnical Engineering Division*, **116**(GT6), 645-657.
- Leroueil, S., Kabbaj, M., and Tavenas, F. (1988), 'Study of the validity of a $\sigma'_v - \epsilon_v - \dot{\epsilon}$ model in *in situ* conditions,' *Soils and Foundations*, **28**(3), 13-25.
- Leroueil, S., Lerat, P., Hight, D. W., and Powell, J. J. M. (1992), 'Mechanical properties of reconstituted Bothkennar soil', *Géotechnique* **42**(2), 275-288.
- Lunne, T. and Kleven, K. (1981), 'Role of CPT in North Sea foundation engineering' in G. M. Norris and R. D. Holtz, *Cone penetration testing and experience*, Proc. Session sponsored by Geotechnical Engineering Division at ASCE National Convention, St. Louis (Missouri), 76-107.
- Luscher, U. (1966), 'Buckling of soil-surrounded tubes', *Proc. ASCE, Journal of the Soil Mechanics and Foundation Engineering Division*, **92**(SM6), 211-228.

- Magnan, J-P., Belkeziz, A., Humbert, P. and Mouratidis, A. (1982), 'Finite element analysis of soil consolidation with special reference to the case of strain hardening elastoplastic stress-strain models', in *Proc. 4th Int. Conf. Num. Meth. Geomech, Edmonton*, vol. 1, 327-336.
- Magnan, J-P., Mieussens, C., and Queyroi, D. (1983), *E'tude d'un remblai sur sols compressibles: Le remblai B du site expe'rimental de Cubzac-les-Ponts* (Paris: Laboratoire Central des Ponts et *Chausse'es*), Rapport de recherche LPC 127.
- Magnan, J-P. (1984) *Mode'lisation nume'rique du comportement des argiles molles naturelles*, Th`ese de Doctorat `es Sciences, Universite' Paris VI, Paris, 262 pages.
- Mansfield, E. H. (1953), 'Neutral holes in plane sheet-reinforced holes which are elastically equivalent to the uncut sheet', *Quarterly Journal of Mechanics and Applied Mathematics*, 6(Pt3), 370-378.
- Marsland, A. and Powell, J. J. M. (1977), 'The behaviour of a trial bank constructed to failure on soft alluvium of the River Thames', in *Proc. Int. Symp. of Soft Clay, Bangkok, Thailand* (Bangkok: Asian Institute of Technology), vol. 1, 505-525.
- Marston, A., and Anderson, A. O. (1913), 'The theory of loads on pipes in ditches and tests on cement and clay drain tile and sewer pipe', *Eng. Exp. Sta., Iowa State College, Bull*, 31.
- Mayne, P. W. (1980), 'Cam-clay predictions of undrained strength', *Proc. ASCE, Journal of the Geotechnical Engineering Division* 106(GT11), 1219-1242.
- Mayne, P. W. and Swanson, P. G. (1981), 'The critical-state pore pressure parameter from consolidated-undrained shear tests, in R. N. Yong and F. C. Townsend (eds.), *Laboratory shear strength of soil*, Spt740 (Philadelphia: American Society for testing and Materials), 410-430.
- Mayne, P. W. and Kulhawy. F, H. (1982), 'Ko-OCR relationships in soil', *Proc. ASCE, Journal of the Geotechnical Engineering Division* 108(GT6), 851-872
- Mayne, P. W., and Mitchell, J. K. (1988), 'Profiling of overconsolidation in clays by field vane', *Canadian Geotechnical Journal* 25, 150-157.
- Mayne, P. W. (1993), 'In situ determination of clay stress history by piezocone model', in G.T. Houlsby and A.N. Schofield (eds.), *Predictive soil mechanics (Proc. Wroth Memorial Symp.)* 483-495. London: Thomas Telford.
- McClelland, B. (1967), 'Progress of consolidation in delta front and prodelta clays of the Mississippi River', in A.F. Richards (ed.), *Marine Geotechnique* (Urbana: University of Illinois Press), pp.22-40.

- McVay, M. and Papadopoulos, P. (1986), 'Long-term behaviour of buried large span culverts', *Proc. ASCE, Journal of Geotechnical Engineering Division*, 112(GT3), 23-29.
- McVay, M. and E. T. (1982), 'Performance and analysis of a long-span culvert', *Transport Research Board*, 878, National Research Council, Washington D. C, 23-29.
- Meigh, A. C., (1987), *Cone penetration testing: methods and interpretation*, CIRIA Ground Engineering Report: In-situ testing (London and Sevenoaks: CIRIA and Butterworths).
- Mesri, G. (1975), 'Discussion: New design procedure for stability of soft clays', *Proc. ASCE, Journal of the Geotechnical Engineering Division* 101(GT4), 409-412.
- Mesri, G., and Godlewski, P. M. (1977), 'Time-and stress-compressibility interrelationship', *Proc. ASCE, Journal of the Geotechnical Engineering Division* 103(GT5), 417-430
- Mesri, G. (1989), 'A re-evaluation of S_u (mob) = $0.22 \sigma'_p$ using laboratory shear tests', *Canadian Geotechnical Journal*, 26, 162-164
- Meyerhof, G.G. (1976), 'Bearing capacity and settlement of pile foundations', 11th Terzaghi Lecture, *Proc. ASCE, Journal of the Geotechnical Engineering Division* 102(GT3), 197-228.
- Miki, H., Kohashi, H., Asada, H. and Tsuji, K. (1994), 'Deformation-pore pressure behaviours measured and analysed for a trial embankment', in *Proc. Int. Symp. on Pre-failure Deformation Characteristics of Geomaterials, Sapporo, Japan*, 547-552.
- Mitchell, J.K. (1976), *Fundamentals of soil behaviour* (New York: John Wiley and Sons).
- Mohamedzein, Y. E-A. (1989), *Non-linear finite element analysis of soil-culvert interaction*, Ph.D. thesis, Purdue University.
- Morin, P., Leroueil, S., and Samson, L. (1983), 'Preconsolidation pressure of Champlain clays. Part I. In-situ determination,' *Canadian Geotechnical Journal*, 25, 150-157.
- Mouratidis, A., and Magnan, J-P. (1983), *Mode'le e'lastoplastique anisotrope avec e'crouissage pour le calcul des ouvrages sur sols compressibles* (Paris: Laboratoire Central des Ponts et Chausse'es), Rapport de recherche LPC 121.
- Muir Wood, D. (1990), *Soil behaviour and critical state soil mechanics* (Cambridge: Cambridge University Press).

- Muir Wood, D., MacKenzie, N.L. and Chan, A.H.C. (1993), 'Selection of parameters for numerical predictions', in G.T. Houlsby and A.N. Schofield (eds.), *Predictive Soil Mechanics (Proc. Wroth Memorial Symp.)* 496-512. London: Thomas Telford.
- Näätänen, A. and Lojander, M. (1994), 'The selection of the parameters for the modified Cam clay analysis', in Smith (ed.), *Numerical Methods in Geotechnical Engineering*, 105-110.
- Nash, D. F. T., Powell, J. J. M., and Lloyd, I. M. (1992), 'Initial investigations of the soft clay test site at Bothkennar', *Géotechnique* 42(2), 163-181.
- Nayak, G. C., Prakash, S., and Gupta, R. (1977), 'Finite element analysis of ditch conduits', in *Int. Symp. on Soil Structure Interaction*, University of Roorkee, India.
- Ng, C. F., Pyrah, I. C. and Anderson, W. F. (1994), 'Lateral soil restraint of a buried pipeline', in *Proc. of the 3rd European Conf. on Numerical Methods in Geotechnical Engineering, Manchester*, 215-220.
- Nielson, F. D. (1972), 'Design of circular soil-culvert systems', *Highways Research Board*, Record 413.
- Nicholson, D. P. and Jardine, R. J. (1982), 'Performance of vertical drains at Queenborough bypass', *Vertical drains*, 67-90. London: Thomas Telford.
- Ohta, H. and Wroth, C.P. (1976), 'Anisotropy and stress reorientation in clay under load', in *Proc. 2nd Int. Conf. Numerical Methods in Geomechanics, ASCE, Blackburg*, Vol. 1, 319-328.
- O'Riordan, N. J., Davies, J. A, and Dauncey, P. C. (1982), 'The interpretation of static cone penetrometer tests in soft clays of low plasticity', in *Proc. 2nd Eur. Symp. on Penetration testing, Amsterdam*, 755-760.
- Osterberg, J. O. (1957), 'Influence values for vertical stresses in a semi-infinite mass due to an embankment loading', in *Proc. 4th Int. Conf. on Soil Mechanics and Foundation Eng.*, London, vol. 1, 393-394.
- Owen, D. R. J. and Hinton, E. (1980), *Finite elements in plasticity: theory and practice* (Pineridge Press: Swansea).
- Parry, R. H. G. (1970), 'Overconsolidation in soft clay deposits', *Géotechnique* 20(4), 442-446.
- Peck, O. K. and Peck, R. B. (1948), 'Experience with flexible culverts through railroad embankments', in *Proc. 2nd Int. Conf. on Soil Mechanics and Foundation Engineering*, vol. 2, 95-98

- Poorooshasb, H.B., Holubec, I., and Sherbourne, A.N. (1966), 'Yielding and flow of sand in triaxial compression: Part I', *Canadian Geotechnical Journal*, 3(4), 179-190.
- Poorooshasb, H.B., Holubec, I., and Sherbourne, A.N. (1967), 'Yielding and flow of sand in triaxial compression: Parts II and III', *Canadian Geotechnical Journal*, 4(4), 376-397.
- Potts, D. M. and Gens, A. (1984), 'The effect of the plastic potential in boundary value problems involving plane strain deformations', *Int. J. Numerical and Analytical Methods in Geomechanics* 8, 259-286.
- Potts, D.M., and Ganendra, D. (1991), 'Discussion on finite element analysis of the collapse of reinforced embankments on soft ground', *Géotechnique* 41(4), 627-630.
- Poulos, H. G. (1967), 'Stresses and displacements in an elastic layer underlain by a rough rigid base', *Géotechnique* 17, 378-410.
- Poulos, H. G. (1972), 'Difficulties in prediction of horizontal deformations of foundations', *Proc. ASCE, Journal of Soil Mechanics and Foundations Division* 98(SM8), 843-848.
- Poulos, H.G., and Davis, E.H. (1974), *Elastic solutions for soil and rock mechanics* (New York: John Wiley and Sons).
- Poulos, H.G., Lee, C. Y., and Small, J. C. (1989), 'Prediction of embankment performance on Malaysian marine clays,' in *Int. Symp. on Trial Embankments on Malaysian Marine Clays*, Kuala Lumpur, Malaysia, vol. 2, 1-22-1-31.
- Powell, W. D., Potter, J. F., Mayhew, H. C. and Nunn, M. E. (1984), 'The structural design of bituminous roads', *Department of Transport, TRRL Report LR1132*, Transport and Road Research Laboratory, Crowthorne.
- Powrie, W and Li, E. S. F. (1991), 'Finite element analyses of an in situ wall propped at formation level', *Géotechnique* 41(4), 499-514.
- Ramalho-Ortigão, J. A., Werneck, M. L. G., and Lacerda, W. A. (1983), 'Embankment failure on clay near Rio de Janeiro', *Proc. ASCE, Journal of Geotechnical Engineering Division*, 109(GT11), 1460-1479.
- Rankine, W. J. H. (1895), *Applied Mechanics*, (4th ed.), Arts.
- Richards, R. (1987), 'Buried Structures' in F. G. Bell (ed.), *Ground Engineer's Reference Book*, Butterworths, London.
- Robertson, P. K. and Campanella, R. G. (1983), 'Interpretation of cone penetration tests: Part II, clay', *Canadian Geotechnical Journal*, 20, 734-745.

- Roscoe, K. H., Schofield, A. N., and Wroth, C. P. (1958), 'On the yielding of soils', *Géotechnique* 8(1), 22-52.
- Roscoe, K. H. and Schofield, A. N. (1963), 'Mechanical behaviour of an idealised 'wet' clay', *Engineering Plasticity*, Cambridge University Press.
- Roscoe, K. H., Schofield, A. N., and Thurairajah, A. (1963), 'Yielding of clays in states wetter than critical', *Géotechnique* 13(3), 211-240.
- Roscoe, K. H. and Burland, J. B. (1968), 'On the generalised stress-strain behaviour of 'wet' clay', in J. Heyman and F. A. Leckie (eds.), *Engineering plasticity* 535-609. Cambridge: Cambridge University Press.
- Rude, L. C. (1982), 'Measured performance of a laboratory culvert', *Proc. ASCE, Journal of the Geotechnical Engineering Division*, 108(GT12), 1624-1641.
- Saada, A. S. (1974), *Elasticity: Theory and Applications*, (Pergamon Press, Inc., New York).
- Samarasinghe, M. A., Huang, H. Y., and Drnevich, P. V. (1982), 'Permeability and consolidation of normally consolidated soils', *Proc. ASCE, Journal of the Geotechnical Engineering Division*, 108(GT6), 835-850.
- Samson, L. and Garneau, G. (1973), 'Settlement performance of two embankments on deep compressible soils', *Canadian Geotechnical Journal*, 10, 211-225.
- Schmidt, B. (1966), 'Discussion: Earth pressures at rest related to stress history', *Canadian Geotechnical Journal*, 3(4), 239-242.
- Schnaid, F., Wood, W. R., Smith, A. K. C. and Jubb, P. (1993), 'An investigation of bearing capacity and settlements of soft clay deposits at Shellhaven', in G.T. Houlsby and A.N. Schofield (eds.) *Predictive soil mechanics (Proc. Wroth Memorial Symp.)* 609-627. London: Thomas Telford.
- Schofield, A.N., and Wroth, C.P. (1968), *Critical state soil Mechanics* (London: McGraw-Hill).
- Seed, R. B., and Duncan, J. M. (1986), 'Finite element analysis: Compaction-induced stresses and deformations', *Proc. ASCE, Journal of the Geotechnical Engineering Division*, 112(GT1), 23-43.
- Sekiguchi, H. and Ohta, H. (1977), 'Induced anisotropy and time dependency in clay', in *Proc. 9th Int. Conf. Soil Mechanics and Foundation Engineering, Speciality Session 9, Tokyo*, 163-175.
- Sekiguchi, H., Nishida, Y., and Kanai, F. (1982), 'A plane-strain viscoplastic constitutive model for clay', in *Proc. 37th Annual Convention of the Japanese Society of Civil Engineers, Nagoya*, 181-182.

- Selig, E. T. (1972), 'Subsurface soil-interaction: a synopsis', *Highways Research Board*, 413.
- Selig, E. T., Lockhart, C. W. and Lautensleger, R. W. (1979), 'Measured performance of Newton Creek Culvert', *Proc. ASCE, Journal of the Geotechnical Engineering Division*, 105(GT9), 953-966.
- Selig, E. T. and Musser, S. C. (1985), 'Performance evaluation of a rib-reinforced culvert,' *Transport Research Board*, 1008, 117-122.
- Shahangiuan, S. (1981), *De'ter mination expe'rimentale des courbes d'e'tat limite de l'argile organique de Cubzac-les-Ponts*. (Paris: Laboratoire Central des Ponts et Chausse'es), Rapport de recherche LPC 106.
- Sharp, K. D., Anderson, L. R., Moser, A. P., and Bishop, R. P. (1985), 'Finite element analysis applied to the response of buried FRP pipe under various installation conditions', *Transport Research Board*, 1008, 63-72
- Shmulevich, I., Galli, N., and Foux, A. (1986), 'Soil Stress distribution around buried pipes', *Proc. ASCE, Journal of the Transportation Division*, 112(GT5), 481-494.
- Simpson, B., O'Riordan, N.J. and Croft, D.D. (1979), 'A computer model for the analysis of ground movements in London clay', *Géotechnique* 29(2), 149-175
- Simpson, B. (1993), 'Development and application of a new soil model for prediction of ground movements', in G.T. Houlsby and A.N. Schofield (eds.) *Predictive soil mechanics (Proc. Wroth Memorial Symp.)* 495-509. London: Thomas Telford.
- Skempton, A. W. (1944), 'Notes on the compressibility of clays', *Quarterly Journal Geological Soc. of London* 125(3), 373-411.
- Skempton, A. W., and Henkel, D. J., (1953), 'The post-glacial clays of the Thames estuary at Tilbury and Shellhaven', in *Proc. 3rd Int. Conf. on Soil Mechanics and Foundation Engineering, Zurich* (Zurich: organising committee ICOSOMEF), vol. 3, pp 302-308.
- Skempton, A. W., and Northey, R.D. (1953), 'The sensitivity of clays', *Géotechnique* 3(1), 30-53.
- Skempton, A. W. (1954), 'The pore pressure coefficients A and B', *Géotechnique* 4(4), 143-147.
- Skempton, A. W., and Bjerrum, L. (1957), 'A contribution to the settlement analysis of foundations on clay', *Géotechnique* 7(4), 168-178.

- Sloan, S. W. and Randolph, M., F.(1982), Numerical prediction of collapse loads using finite element methods', *Int. J. Numerical and Analytical methods in Geomechanics*, 6, pp 47-76.
- Smith, P.R., Jardine, R.J. and Hight, D.W. (1992), 'The yielding of Bothkennar clay,' *Géotechnique* 42(2), 257-274.
- Spangler, M. G. (1941), 'The structural design of flexible pipe culverts', *Iowa State College Engineering Experimental Sta. Bulletin*.
- Spangler, M. G. and Handy, R. L. (1982), *Soil Engineering (4th ed.)* (New York: Harper and Row).
- Stankowski, S. and Nielson, F. D, 'An analytical-experimental study of under-ground structural cylinder systems', *Eng. Exp. Sta.*, New Mexico State University, Las Cruces.
- Tavenas, F., and Leroueil, S. (1977), 'Effects of stresses and time on the yielding of clays,' in *Proc. 9th Int. Conf. on Soil Mechanics and Foundation Engineering, Tokyo*, vol. 1., 319-326.
- Tavenas, F., Leroueil, S., LaRochelle, P., and Roy, M. (1978), 'Creep behaviour of an undisturbed lightly overconsolidated clay', *Canadian Geotechnical Journal*, 153, 402-423.
- Tavenas, F., Blanchette, G., Leroueil, S., Roy, M., and La Rochelle, P. (1975), 'Difficulties in the *in situ* determination of K_0 in soft sensitive clays', in *Speciality Conf. on In situ measurement of Soil Properties, ASCE, Raleigh, NC*, vol. 1., 450-476.
- Tavenas, F., Mieussens, C., and Bourges, F. (1979), 'Lateral displacements in clay foundations under embankment', *Canadian Geotechnical Journal*, 16(3), 532-550.
- Tavenas, F., and Leroueil, S. (1979), 'Clay behaviour and the selection of design parameters', in *Proc. 7th European Conf. on Soil Mechanics and Foundation Engineering, Brighton, England*, vol. 1., 281-291.
- Tavenas, F., and Leroueil, S. (1980), 'The behaviour of embankments on clay foundations', *Canadian Geotechnical Journal*, 17(2), 236-260.
- Tavenas, F., Trak, B., and Leroueil, S. (1980), 'Remarks on the validity of stability analyses', *Canadian Geotechnical Journal*, 17(1), 61-73.
- Tavenas, F., Leblond, P., Jean, P., and Leroueil, S. (1983), 'The permeability of natural clays, Part I: methods of laboratory measurement', *Canadian Geotechnical Journal*, 20(4), 629-644.
- Tavenas, F., Jean, P., Leblond, P., and Leroueil, S. (1983), 'The permeability of natural clays, Part II: permeability characteristics', *Canadian Geotechnical Journal*, 20(4), 645-660.

- Tavenas, F., Tremblay, M., Larouche, G., and Leroueil, S. (1986), 'In situ measurement of permeability in soft clays', in *ASCE Speciality Conf. In Situ 86*, Blacksburg, VA, 1034-1048.
- Taylor, D.W. (1948), *Fundamentals of soil mechanics* (New York: John Wiley).
- Temporal, J., Barratt, D. A. and Hunnibell, B. E. F. (1985), 'Loading tests on a Armco pipe arch culvert', *Department of Transport, TRRL Research Report 32*, Transport and Road Research Laboratory, Crowthorne.
- Temporal, J. and Johnson, P. E. (1988), 'Loading tests on two long span corrugated steel culverts,' *Department of Transport, TRRL Research Report RR141*, Transport and Road Research Laboratory, Crowthorne
- Terzaghi, K., and Peck, R.B. (1948), *Soil Mechanics in engineering practice* (New York: John Wiley).
- Timoshenko, S. (1934), *Theory of elasticity* (New York: McGraw-Hill).
- Trak, B., LaRoche, P., Tavenas, F., Leroueil, S., and Roy, M. (1980), 'A new approach to the stability analysis of embankments on sensitive clays', *Canadian Geotechnical Journal*, 17(4), 526-544.
- Valliappan, S., Matsuzaki, K., and Rajasekar, H. L. (1977), 'Nonlinear stress analysis of buried pipes', in *Proc. Int. Symp. on Soil Structure Interaction*, University of Roorkee, India.
- Van Langen, H. and Vermeer, P.A. (1991), 'Interface elements for singular plasticity points', *Int. J. Numerical and Analytical Methods in Geomechanics* 15, 301-315.
- Vermeer, P. A. (1984), 'A five-constant model unifying well-established concepts', in G. Gudehus, F. Darve, and I. Vardoulakis (eds.), *Constitutive Relations for Soils* (Rotterdam: A. A. Balkema), 175-197.
- Vesic, A. S., and Clough, G. W. (1968), 'Behaviour of granular materials under high stresses', *Proc. ASCE, Journal of the Soil Mechanics and Foundations Division* 94(SM3), 661-688.
- Vesic, A. S. (1977), *Design of pile foundations*, National Co-operative Highways Research Program, Transportation Research Board, National Research Council, Washington (DC), Synthesis Of Highway Practice, 42, 1977.
- White, H. L. and Layer, J. P. (1960), 'The corrugated metal conduit as a compression ring', *Proc. Highway Research Board*, 39, 389-397.
- Watkins, R. K. (1964), 'Structural design trends in buried flexible conduits', *Proc. Symp. Soil Structure Interaction* (Tucson: University of Arizona) 246-255.